ANL-81-62
CONF-810607

(2) Ch. 389

ANL-81-62
CONF-810607--

I-2355

174
4-5-82

THE PROCEEDINGS OF THE 1981 SYMPOSIUM ON INSTRUMENTATION AND CONTROL FOR FOSSIL-ENERGY PROCESSES

June 8-10, 1981

Sheraton-Palace Hotel
San Francisco, California

MASTER

ARGONNE NATIONAL LABORATORY

ARGONNE NATIONAL LABORATORY, ARGONNE, ILLINOIS

Prepared for the U. S. DEPARTMENT OF ENERGY
under Contract W-31-109-Eng-38

Distribution Category:
Coal Conversion Demonstration
Plants (UC-89)

ANL-81-62
CONF-810607

ARGONNE NATIONAL LABORATORY
9700 South Cass Avenue
Argonne, Illinois 60439

THE PROCEEDINGS OF THE 1981 SYMPOSIUM ON INSTRUMENTATION AND CONTROL FOR FOSSIL-ENERGY PROCESSES

June 8-10, 1981
Sheraton-Palace Hotel
San Francisco, California

ANL--81-62

DE82 011969

Sponsored by

U. S. Department of Energy
Office of Fossil Energy

Argonne National Laboratory

Society for Control and Instrumentation
of Energy Processes

January 1982

Prepared for the

U. S. Department of Energy
Task 49626

ACKNOWLEDGMENTS

The U.S. Department of Energy, Argonne National Laboratory, and the Society for Control and Instrumentation of Energy Processes, sponsors of the 1981 Symposium on Instrumentation and Control for Fossil Energy Processes, thank the 1981 Symposium Committee for organizing and presenting this Symposium. The Symposium Committee members, listed on the following page, acknowledge the many persons who contributed to the success of the Symposium: speakers presenting papers, luncheon and banquet speakers, session chairs, and the organizations participating in the Show and Tell hardware display.

Special recognition and thanks are due Richard Greene of Trade Associates for presenting the commercial instrumentation exposition concurrent with the Symposium.

Funding of this Symposium by the U.S. Department of Energy - Fossil Energy is gratefully acknowledged.

The many organizations, including private industry, universities, national laboratories, and government are thanked for the numerous contributions by their employees. Their investment of time and effort led to a successful Symposium, furthering the solution of instrumentation and control problems in fossil energy processes.

Future Symposia are planned for June 7-9, 1982, in Houston, Texas, and June 20-22, 1983, in San Diego, California. Additional information will be sent to people on the printed distribution list and will be available from Argonne National Laboratory, Conference Planning and Management, 9700 South Cass Avenue, Argonne, Illinois 60439.

* * * * *

Proceedings of previous Symposia are also available from NTIS:

1977 The Proceedings of the 1977 Symposium on Instrumentation and Process Control for Fossil Demonstration Plants, held July 13-15, 1977, Chicago, IL (ANL-78-7/CONF-770729)

1978 The Proceedings of the 1979 Symposium on Instrumentation and Control for Fossil Demonstration Plants, held June 19-21, 1978, Newport Beach, CA (ANL-78-62/CONF-780656)

1979 The Proceedings of the 1979 Symposium on Instrumentation and Control for Fossil Energy Processes, held August 20-22, 1979, Denver, CO (ANL-79-62/CONF-790855)

1980 The Proceedings of the 1980 Symposium on Instrumentation and Control for Fossil Energy Processes, held June 9-11, 1980, Virginia Beach, VA (ANL-80-62/CONF-800602)

SYMPOSIUM COMMITTEE

General Chair:
C. L. Merzenberg, Argonne National Laboratory

Program Chair:
W. R. Miller, Ashland Synthetic Fuels, Inc.

Vice Program Chair:
J. V. Walsh, Jet Propulsion Laboratory

Exposition Liaison:
H. C. March, Procon, Inc.

Conference Arrangements:
M. L. Holden, Argonne National Laboratory

Secretary:
R. W. Doering, Argonne National Laboratory

Sponsor Liaison, DOE:
T. K. Lau, U.S. Department of Energy
Office of Advanced Research and Technology

Sponsor Liaison, ANL, and Vice General Chair:
N. M. O'Fallon, Argonne National Laboratory

Industrial Sponsor Liaison:
H. Kaplan, President, SCIEP, Inc.

Control Elements Session Organizer:
T. Carroll, Foster Wheeler Energy Corporation

Temperature and Special Topics Session Organizer:
G. Burns, National Bureau of Standards

Analysis and Control Session Organizer:
J. Williams, Stearns-Roger Engineering Corp.

Flow Session Organizer:
M. A. Scott, University of Tennessee Space Institute

Industrial Hygiene-Health and Safety Session Organizer:
D. R. Telesca, Enviro Control, Inc.

Analysis and Sampling Session Organizer:
F. T. Finch, Los Alamos National Laboratory

Process Control Session Organizer:
R. Shah, Rockwell International

TABLE OF CONTENTS

TABLE OF CONTENTS (cont'd)

TABLE OF CONTENTS (cont'd)

TABLE OF CONTENTS (cont'd)

TABLE OF CONTENTS (cont'd)

TABLE OF CONTENTS (cont'd)

TABLE OF CONTENTS (cont'd)

TABLE OF CONTENTS (cont'd)

OPENING REMARKS

THE FEDERAL ROLE IN SUPPORT OF FOSSIL I & C

John J. Roberts
Argonne National Laboratory

I am pleased to welcome you on behalf of Argonne National Laboratory to the Fifth Annual Symposium on Instrumentation and Control for Fossil Energy. The year since we last met at Virginia Beach has been a successful one - in terms of advances in the state-of-the-art (as will be covered in depth via our ambitious agenda), increased professional interaction fostered by SCIEP, and the increased recognition by DOE of the importance of I&C to the success of a synthetic fuels industry. Evidence of the latter is clear when one looks at the I&C portions of an austere FY82 President's Budget: for gasification and liquefaction $1.7 million compared to $0 in FY81; for Advanced Research and Technology Development, a new $2.2 million line item.

Of course with congressional action underway the last word has yet to be said regarding the FY82 funding of fossil I&C.

In order to establish and maintain such funding for I&C, however modest compared to the total fossil budget, it has been necessary to argue two points in succession: (1) the need for I&C research and development in support of emerging fossil conversion and utilization technologies, and (2) the appropriateness of federal spending for such activity. The first of these two questions is answered clearly in the affirmative, and in some detail, by recent survey studies by ANL on FBC instrumentation and on instrumentation for the entire spectrum of advanced fossil technologies. The second deserves our attention, especially as the new administration seeks to reshape the role of the federal government in energy R&D.

To what extent should the federal government invest our tax dollars in fossil I&C developments? An examination of this matter, however brief, entails four essential logical elements: a federal mission, a measure for levels of investment, a model of the process which translates an idea at an early stage of research into a commercially available technology, and finally a definition of the federal role in that process.

We recognize that imports of oil impose on U.S. society at large costs which are not captured directly in the price per barrel, that is, costs reflective of incremental increases in inflation and unemployment and a weakening of national security. That there is an energy-related mission for the federal government which goes beyond reliance on normal private sector market incentives seems clear - and for both Carter and Reagan administrations, domestic coal plays a key strategic role.

If some federal involvement in energy is appropriate, a difficult question remains: "How much?" A measure of the return on any such investment is required, if not used in a detailed cost/benefit calculation then certainly to suggest an appropriate order of magnitude. As an engineer, I tend to favor establishing a range of prudent federal investment by estimating upper and lower bounds for the discounted social (i.e., incremental) cost of imported oil. Such an approach suggests energy-related federal expenditures could reasonably fall within the range of $10-15 billion per year to reduce imports by 3 million barrels per day. The Federal R&D budget plus various tax incentives lie at the low end of this range. Annualized capital expenditures under PURPA and the Fuel Use Act could well exceed the upper limit.

Given that the federal government has a role in support of the development of technologies for coal conversion and utilization, what might that role be? As appealing as the phrase "R&D in high risk, high pay-off technologies" may be, I find it insufficient as the primary guide for determining the appropriate federal role. Rather, that role must be understood in the context of the process from basic and applied research, through engineering development and demonstration, to commercialization. And, as suggested in Figure 1, which lays out this process in a somewhat simplistic form, I feel that one very important area for federal involvement is to provide the more generic scientific and engineering underpinning to families of coal technologies, even during the latter stages where the lion's share of funding comes directly from and by initiative of the private sector.

Fossis I&C, as well as materials and component R&D, falls in this all important and highly cost-effective support category. The debates in Congress and elsewhere understandably focus on the big ticket items. Unfortunately, there is substantial risk that less dramatic yet essential activities such as

I&C get squeezed out. I therefore took our time this morning to present, albeit hastily, a formalized structure for characterizing the federal role in energy R&D so that we can turn that debate wherever possible into a more rational evaluation of the federal role in R&D, and most particularly, to recognize the exceptional value received through support activities such as fossil I&C.

A DEVELOPING AWARENESS OF THE INSTRUMENTATION ROLE IN SYNFUEL APPLICATIONS

John Notestein, Director
Technology Development & Engineering Division
U.S. Department of Energy
Morgantown, West Virginia

I would like to take this opportunity to welcome our colleagues who have again joined with us and extend a warm welcome to those who are participating in this symposium for the first time.

As many of you know, Mr. Ed Lievens has been a significant force behind this symposium from its inception and was anticipated to speak in this slot on the agenda. Unfortunately a schedule conflict arose and he had to keep a DOE commitment in Germany and, consequently, I will attempt to fill in for him.

As mentioned in the introduction, I am from the Morgantown Energy Technology Center. The Morgantown, West Virginia, Center is one of five such DOE field organizations and is charged with implementation of categories of DOE projects and development of centers of expertise. As a result we see instrumentation and control technology and, more significantly, the associated problems from a very tangible point-of-view. I will come back to this point-of-view later in this discussion, but right now I would like to summarize by saying that it is quite gratifying to note that the fossil energy community is beginning to recognize the need for advances in instrumentation and control technology, especially in coal conversion applications.

At this point I would like to utilize a considerable fraction of the speech Ed Lievens would have presented because the philosophy provides a synfuel equivalent to the punch line from a frequent TV commercial -- "You've come a long way baby" and, more specifically, because many of you have contributed directly to the day-to-day solutions involved in the design, construction, and operation of our pilot plants and other facilities. You can take justifiable pride in your contributions.

The perception of the people of this country is interesting. A Harris poll taken 2 years ago showed that a majority of Americans supported the creation of a synthetic fuels industry. And a more recent Gallup/Newsweek survey showed that more than 70 percent of the people interviewed continued to approve our movement toward a synfuels industry. So, instead of a debate on whether or not we need synthetic fuels, discussions will center on establishing the most effective roles for Government and industry in supporting the development of a successful synfuels programs. One clear signal emerging from the Reagan Administration is that industry must assume the leading role in this development.

I am sure that most of you have asked the question, "How much synthetic fuel will industry be producing during this decade or by the year 2000?" or "Can we really make a dent in our level of imports?"

These are perhaps the most difficult of questions to answer in the synfuels area. Many analysts view the goals established for the Synthetic Fuels Corporation of 500,000 barrels of oil equivalent per day by 1987 and 2 million barrels per day by 1992 as optimistic at best. When the Chairman of the Board of Exxon told a group of securities analysts in the fall of 1979 that synthetic fuels had the potential of meeting a healthy share of U.S. energy needs for 150 years, almost no one noticed. But last spring, when Exxon published a white paper suggesting that synthetic fuels could fill a projected 15 million barrel-per-day gap between domestic demand for oil and gas and expected production early in the next century, a lot more people suddenly became interested.

The truth is that no one really knows what the production levels will be. We have never built a full-size synthetic fuel plant in this country. Without experience in actually constructing such facilities, it is hard for anyone to assess with any degree of certainty what the time scale will be for building the first commercial plants or how many will be on-line in the next 10 to 20 years. It's difficult to assess, for example, what potential shortages might arise in such high-demand construction items as compressors, pumps, and heat exchangers -- and what the impact might be on construction schedules and costs.

Building a synfuels industry is a unique experience for this nation in many respects. In the past, major undertakings have had some depth of experience behind them. We could draw a comparison from an experience in the early 1940's. Some historians claim that this nation was unprepared when it entered World War II with about a dozen B-17's. The fact is, that those 12 aircraft represented more than a decade of experience in assembling, testing, fitting frames to power systems, in developing armament, the flight controls, and the like. When the need arose we were able to replicate those 12 airplanes quickly and efficiently.

Today, this country does not yet have the B-17 equivalent in synthetic fuels. But we have taken significant steps in that direction. As you know, we have brought two large-scale coal liquefaction pilot plants on stream. The experience we are gaining from these plants has moved us substantially up the learning curve. The success which has been experienced with processes such as Ashland's H-Coal and Exxon's EDS process point to our ability to solve complex problems on a broad front and that industry is willing to marshall its talents to deal with each problem as it arises. Moreover, the information generated in the designs of the five major demonstration plants in our program comprises the most detailed descriptions yet of the requirements for an advanced commercial-scale synfuels plant.

From these efforts, we have a much better -- not an exact -- but a much better picture of what the prototype synthetic fuel plant will look like. We have a better idea of the special requirements for equipment and manpower, for plant construction, and for siting.

As a backdrop for this discussion, let me recap briefly the status of these efforts:

The Exxon Donor Solvent pilot plant is one of our two large-scale coal liquefaction pilot plants which began operations last summer. At maximum capacity, it processes 250 tons of coal per day to produce between 500 and 600 barrels of oil. The plant was designed and built under a 50/50 co-funded cooperative agreement between DOE and a group of industrial sponsors headed by Exxon Research and Engineering Company. The detailed engineering and procurement for the facility was handled by the firm of Arthur McKee, Inc., and the plant constructor was the Daniel Construction Company.

In May of 1980, we achieved mechanical completion of the plant and began start-up operations in June. From that point until we brought it down to prepare for the initial long-term test run, the facility was onstream 50 percent of the time -- a factor which I believe is extremely significant given the advanced state of technology and the experimental nature of much of the process equipment.

The key feature of the Exxon process is the use of a separate vessel to bring the solvent made in the process into contact with hydrogen in the presence of a catalyst. The solvent then flows into the liquefaction vessel where, at temperatures of 800 to 880 degrees F and pressures of 1500 to 2000 psi, it "donates" the hydrogen to the incoming coal -- hence, the name.

The second major pilot plant, currently in operation, is the H-Coal facility outside Catlettsburg, Kentucky. Like the Exxon Donor Solvent facility, this unit also began its start-up operations last summer, but as many of you know, we experienced mechanical problems which hampered the early operation. Our primary problems centered in the pressure letdown valves which are required to operate in the 3000 psi range. During the fall of last year, we undertook an extensive evaluation of this problem, and benefitting considerably from the technical "cross-pollination" with other valve testing and operational experiences, we believe the problems have essentially been overcome. As evidence of this, the H-Coal plant recently completed a continuous 43-day test run with no breaks in the coal feed. This achieved the design objective for the first series of operations.

The H-Coal process was developed by Hydrocarbon Research, Inc., now a subsidiary of the Dynalectron Company. It is based on the addition of a catalyst directly into a reactor vessel operating at a temperature of about 850 degrees F and, as I indicated, pressures approaching 3000 psi. The Catlettsburg plant is designed to operate in either of two modes -- processing up to 200 tons per day of coal to produce about 600 barrels of a distillate synthetic crude suitable for refining; or up to 600 tons per day of coal to produce 1800 barrels of a heavier boiler fuel. While the pilot plant has the flexibility of producing either product, we anticipate that future H-Coal commercial sponsors will utilize the data generated by this facility and opt for one or the other in the design of their full-size plant.

The third of our major liquefaction technology efforts -- the solvent-refined-coal program -- has followed somewhat of a different development path.

Solvent refining is based on the fact that certain portions of the coal ash have a natural catalytic effect for coal liquefaction. Two variations of the solvent-refined-coal technology have emerged from our program -- the SRC-I technology which produces a clean-burning solid fuel, or if a second hydrogenation step is added, a liquid fuel; and the SRC-II technology which converts coal directly into a liquid in a single process step.

In the 1970's, the technology had progressed to the pilot plant stage, but at this point there is a marked difference between the SRC program and the later Exxon donor solvent and H-Coal programs. The SRC pilot plants are an order of magnitude smaller in scale -- owing to the state of knowledge at the time they were completed in 1974. The Government-owned pilot plant in Ft. Lewis, Washington, which operates in both the SRC-I and SRC-II modes, processes from 25 to 50 tons per day. A second plant is an industry-owned plant in Wilsonville, Alabama, which operates only in the SRC-I mode and processes 6 tons of coal per day.

Unlike the Exxon donor solvent and H-Coal projects, a single step directly from the comparatively smaller scale SRC pilot plants to full-size commercial plants entails too great a technical risk. Consequently, an intermediate step was needed which we call the "demonstration" plant.

A demonstration plant might be viewed as the final stage of the development program - or alternatively as the precursor of a commercial facility. It is typically a module of a full-size plant -- one that uses essentially full-scale, commercial components. To go from a demonstration plant to a commercial plant, therefore, one need only replicate the module, not increase the size of the process equipment.

In 1978, we began a multi-phase SRC demonstration program involving two major projects. Air Products & Chemicals and Wheelabrator-Frye are working with us to design a 6000-ton per day SRC-I demonstration plant proposed for Newman, Kentucky. A subsidiary of Gulf Oil is our domestic partner in the design of a similar-sized SRC-II demonstration plant proposed for Morgantown, West Virginia. The SRC-II project is unique in that it involves both governments and industries from the Federal Republic of Germany and Japan.

These demonstration projects have been a focal point of the new administration's restructuring of the Federal synthetic fuels effort -- it is here where the major shift has occurred in the roles of the Federal Government and private industry.

These projects -- as I mentioned -- were started in 1978. Since that time, the domestic and international energy and economic situation has changed substantially. Oil prices doubled in 1979 following the Iranian revolution. The Synthetic Fuels Corporation was created in July of 1980 with the passage of the Energy Security Act. And most recently, the Reagan Administration has taken steps to restore a free market environment through the decontrol of oil.

These latter actions should be read as a clear signpost that we are looking to the private sector to seize the initiative in making commercial synfuel decisions -- including demonstration plants. And to ensure that we have an efficient, streamlined Federal program acting as a "safety net" for the first-of-a-kind

ventures, we have proposed to consolidate all large-scale construction projects in the synthetic fuels corporation. We in DOE will continue funding design efforts for these demonstration efforts through most of this fiscal year, giving our industrial partners opportunity to prepare proposals to the synfuels corporation.

Regardless of the outcome of this new course of action, we believe the money spent to date in both the SRC-I and SRC-II projects has been money well spent.

Engineering teams in both projects have completed conceptual designs of the demonstration modules. Both are now working on process designs. This information has given us a much better picture of the engineering requirements -- and of the costs -- for these very complex plants. Much of this information will be useful in other synthetic fuel projects regardless of the specific process employed.

Both projects have moved through a significant portion of the Environmental Impact Statement (EIS) procedure required by the National Environmental Policy Act. In January we published the final EIS for the SRC-II project and expect a similar document to be issued early this summer for the SRC-I project.

Together, these documents represent the most extensive analysis ever done of the environmental, health, and safety effects of a large coal liquids plant. Coupled with the process designs being developed, they also serve as a valuable source of information for estimating manpower and equipment needs in the construction and operation of these large, complex facilities.

These activities and many others which could be cited are examples of significant technical progress to be sure. However, they also appear to have triggered the development and dissemination of an awareness which is both significant in itself and applicable to this gathering. This is the awareness that the instrumentation and control needs of the developing synfuel processes are:

- in many cases unlike previous applications and experience, and

- are capable of having major effects, both positive and negative, on plant performance (including such basic attributes as the financial attractiveness of the plant).

In addition, the need to make instrumentation an integral part of the total "system" is also beginning to be recognized. This latter need requires understandings of the often conflicting interrelationship between achievable instrumentation accuracy and reliability and the role to be accomplished; detailed performance evaluation or a process control function. We at Morgantown work with many of you in a highly tangible R&D arena and I am sure you share my enthusiasm at seeing the development of these understandings in the technical community dealing with synfuels.

This symposium is an example of DOE's commitment to the transfer of useful information and technology and we are glad to have had a role in supporting its efforts. During the rest of this symposium the basic aspects of instrumentation -- sensing/sampling, information processing, and control/response --

will be addressed in various presentations. It is hoped that the participants will take home additional insights and assist in continuing the development and dissemination of these necessary understandings.

I wish you all a successful meeting and I am sure that your contributions will find reward in the success of our collective efforts.

OVERVIEW OF INSTRUMENTATION NEEDS FOR ADVANCED FOSSIL ENERGY PROCESSES

Nancy M. O'Fallon
Argonne National Laboratory

Several years ago I spoke at the first Symposium on Instrumentation and Control for Fossil Energy Processes. At that time I expected the job of developing needed instruments to be nearly finished by now, but we have had several lean and hungry years. The situation appears to be much better now and funding is becoming available.

A 1975 study published in 1976 by Argonne[1] was the starting point of the present program. This study identified four areas of instrumentation need for fluidized bed combustion, liquefaction, and gasification. Those four areas were, very broadly, measurement of mixed-phase mass flow, measurement of levels, measurement of temperatures, and on-line analysis. The 1975 study is being updated in a series of reports. The first report, which has already been published,[2] dealt with available process control instruments. It surveyed the range of applicability of these instruments and helped to pinpoint areas in which available instruments could not function in fossil energy processes. Other reports, which are now in preparation, deal with a survey of problem areas in fossil energy processes and with potential solutions to these problems. Additional reports will be written as appropriate on new developments in instrumentation and control, operating experience with these instruments, and test results.

I would like to summarize for you this morning the report on the survey of problem areas in advanced fossil energy processes.[3] This report contains brief descriptions and schematics of all the processes surveyed in order to facilitate understanding of where the problems occur. These process descriptions are followed by data sheets on which individual instrumentation needs are noted along with all information available on the conditions at that point in the process.

The processes surveyed included the SRC-I, SRC-II, H-COAL, EDS, and Synthoil liquefaction processes. Gasification processes included HYGAS, BI-GAS, CO_2 Acceptor, Synthane, Rockwell Flash Hydrogasification, Westinghouse, Combustion Engineering, Rockwell Molten Salt, Bell HMF, Lurgi dry bottom, Slagging Lurgi, U-Gas, Texaco, and COED/COGAS. In the fluidized-bed combustion area, a recent study was completed at Argonne[4] in which all known coal fluidized-bed combustion installations in the world were surveyed for their instrumentation needs. In the present report, therefore, only a representative sample of processes was included. These are Exxon, Combustion Power, Argonne National Laboratory, Pope, Evans and Robbins,and Fluidyne. In the area of oil shale processing, we were unable to aquire any data. In the magnetohydrodynamics area we obtained information from Rockwell, Avco, and TRW. We also obtained some information on coal preparation needs.

The purpose of the survey was to identify needs in instrumentation for process control and safety in the advanced fossil energy processes. The format of the report, in which the instrumentation needs are put onto specification sheets, was intended to be useful as a reference for instrument manufacturers.

The report pinpoints area where government sponsorship of instrument development is appropriate because of the lack of a demonstrated market of sufficient size to interest instrument manufacturers. Since the survey is intended to be an ongoing one it will provide a focus for collecting operating experiences with instruments in the advanced fossil energy process plants. The sources of information for this report were primarily visits to operating pilot plant. In addition A&E process designers who are concerned with the design of large scale plant were consulted. Government program managers provided valuable input on their individual programs. Finally, the SCIEP workshops were extremely valuable in providing a consensus on the instrumentation needs.

The report in draft form has been sent for review to those from whom information was collected in order to verify its accuracy before publication. It is in the final stages of preparation for printing at this time. There are still many blanks and there are other processes which should be added, but we felt it important to get the report published with the information now available and to update it as necessary. We solicit your help in making future reports more complete by sending us new information and corrections to the information we now have.

The results of the survey provided no surprises. There is a great need for a way or ways to measure mixed-phase mass flow. This seems to be everybody's number one priority. The measurement of particulate loading in nominally clean gas streams is important. There are many problems remaining in temperature measurement. Level and pressure measurements are problematical. There is a great need for real-time on-line analysis suitable for process control. The report is organized so that the data sheets are gathered into these categories as well as a final miscellaneous category.

There were 22 cases of a need for the measurement of solids mass flow in solid-liquid streams. Some limited amount of success was reported with quadrant edge orifice meters, but lifetimes are still severely limited. Recent success with a high temperature Doppler flowmeter developed at Argonne National Laboratory will be reported later in this meeting. Also a capacitive flowmeter has been demonstrated successfully for solid-liquid flows. While the need is primarily one of liquefaction processes, there are a number of gasification processes which also have a need for slurry flow measurement.

There were 36 cases in which the measurement of the flow of solids being conveyed by gas was a requirement. Approximately half of these were required in gasification systems. Fluidized-bed combustion feedlines need this measurement in order to balance the feed between multiple injection points. In MHD there is a need not only for the measurement of the flow but for a very rapid (millisecond) response.

There were even a few instances in which the flow of solids mixed with both liquids and gases was required. Some success has been reported by one liquefaction plant using a segmental wedge type of flowmeter.

Seventeen data pages were developed on particulate loading in nominally clean gas streams. This need is particularly important in pressurized fluidized-bed combustion and in gasifier combined cycle systems where the gas is expanded through a turbine. The turbine, of course, cannot tolerate particulate loadings above a certain level without deterioration. Even the development

of hot gas cleanup systems suitable for integration into these turbine installations requires the availablilty of a particulate loading monitor.

Temperature measurement is a crucial need in almost all kinds of processes. There were 20 instances cited by the processes surveyed for the study. The measurement of slurry temperatures in liquefaction processes is a problem. In gasification systems there is a need to know the temperature and the temperature profile across the bed, the temperature of the particles in the bed, and the temperature of the walls. Similar requirements occur in fluidized bed combustion. Magnetohydrodynamics has very severe instrumentation requirements for temperature and some progress has been in this area in the development of sodium line reversal techniques and optical pyrometry. The most promising areas for development appear to be optical and acoustic techniques.

Eighteen cases were found in which a level measurement of one kind or another was required. Oil-water interface detection is frequently given as a need. Capacitive instruments appear to be workable in this situation. The location of ash-char interfaces within a vessel is rather difficult but appears to be amenable to solution by neutron probing. Slurry levels can probably be measured using high temperature acoustic transducers. Catalyst levels within a bed could be monitored using neutron techniques. The measurement of char levels within vessels requires the technique to integrate over the surface rather than probe in a single location. Similar consideration apply in measurement of the level of fluidized beds. The differential pressure measurement most often used now is felt by most operators to be less desirable than a more direct measurement.

The need for on-line analysis of dense systems was given in 30 different cases. The most common measurements required are the hydrogen to carbon ratio, sulfur content, iron content, chlorine content, water content, and concentration of catalyst poisons such as nickel, iron, and vanadiam. Gas composition measurements were given as needed 17 cases. The main problem here is the sampling problem with the time lag involved and the question of the representativeness of the samples. Alkali detection is a big problem, particularly in the pressurized fluidized-bed combustion processes.

There were, in addition, 15 cases of miscellaneous needs including viscosity, location of plugs in pipes, monitoring pipe wear, and characterization of beds.

During the next few days we will hear about new developments in the instrumentation to meet the needs verified in the survey. Reports from the SCIEP miniworkshops will further define the needs. The final report of the survey will be mailed in the near future. We ask your help in feeding information back to us to help complete and make current the data base represented in the report. In return we will be able to provide you with information on availability of instrumentation and on the operating experiences with these instruments. Thank you.

REFERENCES

1. N. M. O'Fallon, R. A. Beyerlein, W. W. Managan, H. B. Karplus, and T. P. Mulcahey, "A Study of the State-of-the-Art of Instrumentation for Process Control and Safety in Large-Scale Coal Gasification, Liquefaction, and Fluidized-Bed Combustion Systems," ANL-76-4, January 1976.

2. B. G. Liptak and C. P. Leiter, "Overview of Coal Conversion Process Instrumentation," ANL-FE-49628-TM01, May 1980.

3. N. M. O'Fallon, R. W. Doering, and C. P. Leiter, "Review of Instrumentation Needs for Process Control and Safety in Advanced Fossil Energy Processes," ANL-FE-49628-TM02, to be published.

4. C. L. Herzenberg, K. E. Griggs, R. F. Henry, and J. F. Podolski, "A Study of Instrumentation Needs for Process Control and Safety in Coal Fluidized-Bed Combustion Systems," ANL-CEN-FE-80-15, February 1981.

AN OVERVIEW OF INSTRUMENTATION, CONTROL AND DIAGNOSTICS TECHNOLOGY BASE FOR THE ADVANCED RESEARCH AND TECHNOLOGY ACTIVITIES

T. K. Lau
U. S. Department of Energy

I am very pleased that so many of you have found the time in your busy schedules to join us here in San Francisco. I am sure that having so many of you here is rewarding to those who worked so hard and worried so much organizing this symposium. These next few days should be rewarding to all of us.

As all of you are well aware, the need for an intensified effort in the area of advanced instrumentation, control and diagnostics has been recognized by most of us for a number of years. I am happy to report that a new major thrust for this effort in advanced research and technology activities will begin in FY 1982. This new research effort will be aimed at developing new instruments capable of functions in the harsh environments of many coal processes. This work will also establish the foundation for advanced generic control systems, and provide the research tools for diagnostic techniques.

Consistent with the refocused Federal energy policy, the advanced research and technology development activity plays an important role in the Department's Fossil Energy program by developing a sound technology base for coal processes. Through applied and exploratory research at DOE's field centers, at universities, and industrial laboratories, this long-term high-risk activity with a potentially high payoff, will provide momentum for new processes, improve the fundamental understanding of coal characteristics and reactions and hold the potential for significant improvements or breakthroughs in the use of coal.

This morning however, I would like to discuss in some detail the effort in the area of advanced instrumentation which is of interest to those of us gathered here. DOE has been involved in instrumentation and control activities for a number of years. As a matter of fact, this is our fifth Annual I&C Symposium. For the most part this activity has been one based on responding to specific needs as they arose. We are also aware that many I&C requirements which were identified over the years are still problems and continue to be a concern. The rate of progress in finding solutions has been frustrating to many of us.

This continuing problem has been recognized and has resulted in a new DOE program element - instrumentation, control and diagnostics. The principle purpose of this new technology thrust is to insure a healthy fundamental technology base for instrumentation and control systems for advanced fossil energy processes. The overall objective of this program is to achieve the goal which has been stated at these meetings many times -- the safe, reliable, economic and environmentally acceptable operation of fossil energy processes.

We have identified the need for research to achieve a basic understanding of process dynamics which will allow us to interpret measurements and provide the basis for intelligent process design and scale-up.

Also identified is the need not only for the improvement of existing sensors but also for the exploratory development of sensors systems, and techniques which may be applied to emerging needs.

As these processes become more complex we realize the need for research in the area of control strategies for unit operations, and ultimately, integrated fossil energy processes.

This program also recognizes the need for the formulation of application guidelines in order that all elements of the government and private sector may apply their skills in a well-ordered and efficient manner. These guidelines will involve both general and specific needs.

These are the specific objectives which have been folded to include those identified by many of you during previous symposia and workshops. By their very nature, these objectives encompass both theoretical and experimental work on instrument development and an understanding of control phenomena. The results of these efforts should find application to the wide range of fossil energy process applications.

Through the efforts of a great many people from all sections of the fossil energy I&C community, many present here today, technology transfer has had real meaning. There has been established a free flowing exchange of ideas, opinions, requirements and, at times, complaints. With few exceptions, the inputs have been positive and meaningful. As a result of these numerous studies, workshops, large and small, and symposia, there has been developed a general consensus of instrumentation and control needs as they relate to fossil energy processes. It is clear that as a minimum we must be able to measure:

- multiphase flow and interface level
- perform on-line chemical and thermal analysis
- real-time control processes
- monitor combustion

- o provide a clean and safe environment
- o provide diagnostic measurements
- o model effectively and establish and maintain a working data base
- o insure the availability of instrumentation which can effectively provide data involving flames, flows, temperature, viscosity, pressure and level

I would like to outline for you some areas which have been identified and suggested as part of the long-term program.

In the area of polyphase flow, current techniques involve the use of empirical approximations that yield marginally acceptable results which are limited to two-phase flow. Coal processes requires that three-phase flow systems be amenable to accurate flow predictions. In addition, the behavior of multicomponent flow, its patterns, concentration, size, shape & velocity are not yet understood. Initial task will undertake to provide the data necessary for the development of multiphase flow models; devise experimental techniques to acquire kinetic and transient data; and to establish a means of making the polyphase flow data available on a broad base.

Effective process control requires accurate information from on-line real time measurements. Aided by advanced electronics and micro-processors, in-situ analysis of gas/solid and slurry streams can be performed. Examples of such research projects include optical and infrared techniques; neutron-induced prompt gama spectrometry for elemental and molecular composition analysis; laser absorption spectroscopy; tunable atomic absorption spectroscopy; chirp sonar application and evaluation; and development of dynamic models for integrated control schemes.

The exploratory development of instrumentation for emerging and novel fossil technologies will include new sensors, preferably function in a non-instrusive manner. Measurement techniques can be developed to permit function in previously unworkable types of configurations. These techniques will include acoustic, electronmagnestic, nuclear, and optical concepts. Let us take a closer examination on each of these techniques.

Acoustic (and ultrasonic) techniques has been used successfully in several flow measuring applications in coal conversion systems. A high temperature doppler slurry flowmeter is operating at the SRC pilot plant in Ft. Lewis, Washington. Passive acoustic flow/no-flow indicators are operating in the 800 F char injection lines at the BI-GAS pilot plant in Pennsylvania. Active acoustic cross-correlation was demonstrated in a slurry line at the HYGAS pilot plant in Chicago.

While some work has been done to relate acoustic signal attenuation to coal concentration in slurries, future work will include studies on the effects

of particle size, particle size distribution, scattering, temperature, pressure, fluid viscosity, particle/fluid velocity difference, and flow of entrained liquid droplets in gases. The strengths and weaknesses of different acoustic configurations and geometrics need to be defined for a range of slurry characteristics. Particle concentration measurement will be explored. The effects of viscosity and flow profiles will be determined.

In addition, the feasibility of acoustics for measurement of other parameters such as level and temperature will be looked into. Development of high temperature transducers will be addressed. In each of the instruments and applications studied, attention will be given to the questions of rangeability. sensitivity, accuracy, repeatibility, and scale up potential.

In the electromagnetic technique area, sensing of parameters of coal process media via their electrical properties has been possible in a number of cases. Capacitive sensing of solid/fluid ratio and solid velocity (via cross-correlation) was demonstrated in the HYGAS pilot plant. Capacitive monitoring of liquid/liquid interfaces and solids levels is also done successfully. Of course, the contrast in dielectric properties of the two components is critical. Similar success can be expected using conductive or inductive sensing if the conductivity or magnetic properties show the appropriate degree of contrast.

Microwave probing of slurry streams has been used in the laboratory for flow velocity measurements. Density sensing should also be a possibility. Further explorations in these techniques will include the same set of considerations listed under acoustics.

For the nuclear measuring technique, the use of penetrating radiation, primarily neutrons and gamma rays, provides a means of interrogating the process media without physical introduction of a probe or extraction of a sample -- thus providing a clear advantage in high temperature, high pressure fossil energy processes.

The analysis of prompt gamma rays emitted from the process material following neutron capture has been used to monitor the elemental composition of process streams in-situ. In addition to the advantage of not needing to extract a sample, another plus for the technique is that it inherently averages over a large volume of the material. Use of delayed gamma rays following neutron capture permits measurement of flow velocity since the portion of material which has been activated can be detected downstream. This technique will provide a means of gathering fundamental data on multiphase flow characteristics since suitably chosen elements of the different phases can be activated and detected as they arrive at the downstream detector at different times.

Other neutron induced reactions and inelastic scattering also can be explored for possible composition information. The same considerations regarding the tradeoffs among various configurations, types of neutron sources, and types of detectors will apply.

In the area of optical measurement technique, spectrographic and laser diagnostic techniques offer non-intrusive methods of determining the critical fossil process parameters with both temporal and spacial resolution. Integration of these optical techniques with advanced micro- and mini-computers can result in real-time, on-line analysis.

Some optical research applications have been demonstrated. In the MHD application, both the Mississippi State University and Stanford University -- have been actively developing optical diagnostic techniques. They have adapted optical techniques for determination of the plasma-flow interior of the MHD power train. A sodium line reversal system and a two-color pyrometer to provide measurements of the operating variables such as average gas temperatures and slag temperature and emissity have been used. A microprocessor based optical system developed by MSU for the detection of nitric oxide (NO) is on display for the "Show and Tell" exposition.

The Combustion Research Facility -- at Sandia Laboratories in Livermore, California is providing accurate spectrographic data, and developing new non-linear optical diagnostic systems for applications to general combustion problems. An optical particle sizing technique developed by Sandia Livermore will also be on display for the "Show and Tell" session of the exposition.

Examples of other novel optical techniques which arise as potentially fruitful areas are hetrodyne laser absorption spectroscopy, multispectral pollution sensors and image based data systems. We can explore further in the optical research for fossil energy process application.

Fluidic sensors, as an instrument and control device offer the potential benefit of high reliability, long life and insensitive to vibration, temperature and EMI. Exploring this technology and adapting it to the hostile fossil energy environment will have a long range beneficial effect. Examples of fluidic cappillary pryometry and fluidic gas concentration sensing and control will be exhibited during the show and tell session.

The assessment of carcinogenic and other pollutants escaping from smoke stacks and those circulating inside plants requires constant monitoring of extremely low air velocities. Fluidic anemometry with its attendant high resolution and extreme reliability can be used in both an alarm and a closed loop control mode.

Fluidics can also be utilized effectively in those applications where electronic controls fail due either to environmental or radiative effects or when the reliability or maintainability requirement precludes use of electrical and/or mechanical components either because of accessibility restrictions or because of wear.

Adequate control and instrumentation for Fossil Energy requires solutions for several serious materials problems, that probably will take more than a couple of years. However, these issues are of such overriding importance in a number

of fossil energy and other high-temperature technologies, that further neglect cannot be tolerated.

The number one problem is erosion-and-corrosion. These two phenomena are the major source of materials degradation and, therefore, strongly contribute to the deterioration of many instruments: thermocouples, flowmeter, pressure-measuring devices, straingauges, analytical instruments, etc. Erosion and corrosion should be broadly investigated, each by itself as well as in combination. Most important is to find reliable erosion and corrosion sensors for those regimes where electrochemical devices cannot be used.

Another subject of high priority in material consideration is coatings and thin films. Thin film sensors (for temperature, strain, corrosion, etc.) and coatings as protection for thermocouples, detectors, etc. Research must include the strength and adhesion of coatings and films.

At this point I would like to point out that the I&C progrms undertaken by DOE Fossil Energy are still being continued. The near term needs are real and have not been diminished. Their support will fall within the guidelines developed during the restructuring of the synfuels program. On the other hand, we will support the long-term high-risk research and development efforts that are not currently appropriate nor desirable for the private sector. In general, we will continue projects through "proof of concept."

This brings me to an essential point. I have already made reference to the effective communication that has been developed in the past few years. There appears to be little argument that this should continue and be expanded as long as it contributes to improving the effectiveness of all of us. This means that all of you must continue to support our technology transfer activity. There is always the threat that we will find ourselves spending our resources, both public and private, solving the wrong problems. This is a constant risk as any instrument manufacturer can attest.

The response to this years symposium, as evidenced by both the number and quality of the presentations and the attendance, points to be the growing interest in our I&C activity. Our activity is growing also. It is now I C and D, Instrumentation Control and Diagnostics. We are looking to the future with great hope and expectation. In spite of recent restructuring effort, the excitement of our challenge has not diminished.

We hope that we can all share in this excitement at this meeting as well as in the months and years ahead. I look forward in meeting with many of you individually during the next few days and hope that you find your experience here both enjoyable and worthwhile.

MONITORING TEMPERATURES IN COAL CONVERSION AND COMBUSTION PROCESSES VIA ULTRASOUND

N. Gopalsami, A. C. Raptis and T. P. Mulcahey
Argonne National Laboratory

Abstract

A study of the state-of-the-art of instrumentation for monitoring temperatures in coal conversion and combustion systems is presented first. The instrumentation types studied are limited to thermocouples, radiation pyrometers, and ultrasonic thermometry. Some of the capabilities and limitations of each type are examined. The study identifies that the ultrasonic thermometry has the potential of providing viable instrumentation under the hostile atmospheres prevailing in the coal conversion sytems.

A feasibility study of the ultrasonic thermometry is carried out next. This entails developing a mathematical model of a pulse-echo measurement system and devising a suitable signal processing technique for the estimation of propagation delays. Computer simulations are made to test the efficacy of the measurement technique under noise-free as well as noisy conditions.

INTRODUCTION

Instrumentation deficiencies for monitoring temperatures have been reported in the reactors or combustors of many small-scale coal conversion systems such as HYGAS, BI-GAS, Exxon, Pope, Evans and Robbins.[1] Difficulties in measurement occur for temperatures above 1500°F, especially when the temperature fluctuations must be followed and controlled rapidly. The presence of erosive and corrosive atmospheres at high pressures precludes the applicability of most conventional instruments. Detecting fast transients in the process conditions, while protecting the sensing element from the hostile environment is a challenging problem. New techniques and devices are required to adequately meet the challenge.

The objectives of this paper are (i) to identify a viable instrumentation technique for the coal conversion/combustion systems by surveying the recent advancements in thermometry and (ii) to investigate its feasibility.

SURVEY OF HIGH TEMPERATUPE THERMOMETRY

For the temperature range of interest (1500 to 3000°F), the applicable instrumentation techniques include thermocouples, radiation pyrometry, and ultrasonic thermometry. A brief account of these techniques in light of their applicability to coal conversion processes is given below.

Thermocouple

The thermocouple is based on the principle that when two dissimilar metals are joined together at one end, an emf is developed at the other end depending on the temperature difference between the two ends.

Figure 1 shows a simple thermocouple circuit. In practice, the circuit may have extension wires for remote measurement, compensating devices for the reference temperature variations, and multiple elements for increased sensitivity.

Because of the simplicity and relative ease of application, the thermocouple is widely used in process measurements. It generates output signals in the order of 0 to 50 mV without the need for any external excitation power. The typical sensitivities range from 0.005 mV/°F to 0.03 mV/°F. Several types of thermocouples with different material compositions are commercially available. The type J or K thermocouples are commonly used in the small-scale combustion/conversion systems. Since the instrument has to operate under a hostile environment, the thermocouple should be sheathed, insulated and encased in a thermowell. This precludes the realization of a quick response to changing temperatures. Also, it is reported that most thermocouples suffer drift in calibration over a period of time at elevated temperatures.[2]

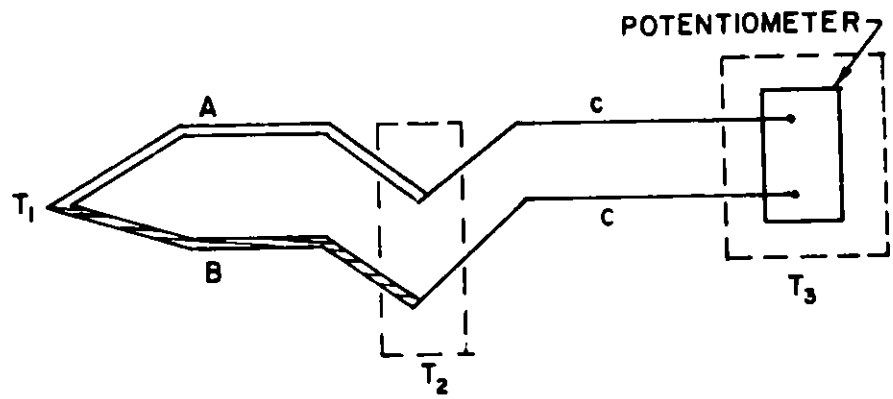

Fig. 1 A simple thermocouple circuit.

Radiation Pyrometry

Radiation pyrometry permits the temperature of an object to be monitored without any physical contact. It is based on the principle that all objects emit radiant energy and that the intensity of emitted radiation is a function of temperature. The radiation emitted by a hot object is stronger in the infrared region than in the visible spectrum.

Figure 2 shows a basic radiometer block diagram consisting of (1) an optical system, which determines the combination of receiving aperture and angular field of view; (2) a detector element, which converts the changes in incident radiant energy into an electrical signal; and (3) an amplifier and recorder.[3] The radiation detectors are either of quantum or energy types. The quantum detectors are preferable for high temperature application, and for the most part silicon or lead sulfide detectors are suitable. Silicon detector instruments especially require no recalibration for prolonged periods, and the response time is fast enough for most industrial needs. The instrument accuracy is reasonably good ($\pm$ 1 per cent).

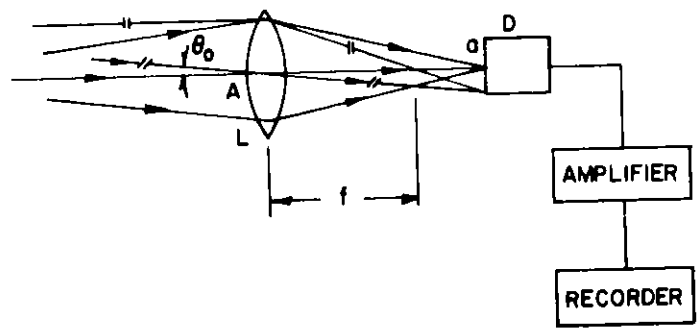

L = COLLECTING OPTICS WITH APERATURE STOP OF AREA A

D = DETECTOR ELEMENT WITH FIELD STOP OF AREA a

θ_0 = HALF ANGLE MEASURED IN RADIANS

f = FOCAL LENGTH

Fig. 2 A basic radiometer.

However, a major practical problem in the application of radiation pyrometry is the establishment of an optical path. The transmission of infrared radiation requires the use of a sighting tube and an infrared window. The transmission losses in the window may change with time during exposure to high temperatures and chemically active environments. Char particles could also enter the sighting tube and block the optical path, and the tube should often be purged with some spectrally transparent gas.

Ultrasonic Thermometry

Ultrasonic thermometry is based on the principle that the velocity of sound in a medium is a function of its temperature. Figure 3, for example, shows the velocity changes of sound in several media with temperature. Intrusive (solid) probes are suitable for process applications. A common method of measurement consists of propagating short pulses of ultrasonic waves in a sensor and of measuring the time taken for the pulses to travel through a known length of the sensor. Multiple temperature measurements along the length of the sensor can be made by providing a number of acoustic reflectors in the sensor.

One of the potential features of ultrasonic thermometry is the greater choice of sensor materials available to it than to alternative devices. Any refractory or ceramic material with a high melting point and good corrosion resistant properties can be employed. Rhenium is a widely used sensor material for thermometric applications. It has a good sensitivity, and provides an accuracy of less than 1 percent at 2000°C. Much higher temperatures may be measured using tungsten, but the sensitivity is low compared to rhenium. Single crystal aluminum oxide (Sapphire) has a melting point of 2505°C, is oxidation resistant, and provides an accuracy of $\pm$ 2°C at 1900°C.

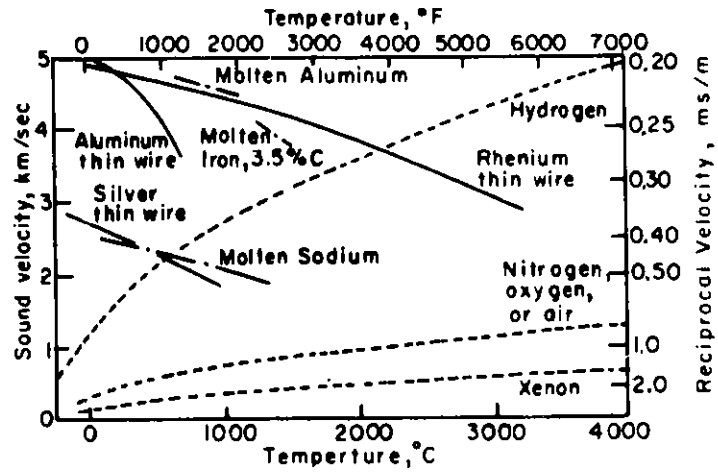

Fig. 3 Velocity of sound with respect to temperature.

FEASIBILITY STUDY OF AN ACOUSTIC TEMPERATURE MEASUREMENT SYSTEM

A pulse-echo type of measurement system as shown in Fig. 4 is considered for the feasibility study. The pulser sends out a narrow pulse p(t) which excites the transducer producing an ultrasonic signal x(t) of short duration. This signal is transmitted through the lead-in to the sensor. The sensor, for simplicity, is assumed to have two zones of equal length. Part of the signal x(t) gets reflected backward at each of the boundaries. The reflected signals, called echoes, trace back the path and generate an electrical signal r(t) at the transducer. The signal processor estimates the propagation delays in each zone from the received signal.

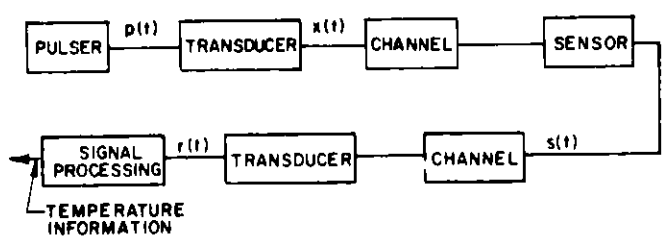

Fig. 4 Block diagram representation of a pulse-echo measurement system.

Mathematical Model

Each of the blocks in the measurement system is assumed to be linear, which is justifiable in the case of low intensity ultrasound. If p(t) is idealized to a delta function, x(t) then represents the impulse response of the transducer. The lead-in is assumed to cause no distortion to the transmitted pulse.

Modeling of the sensor is based on the reflection theory of sound waves.[4] For a forward traveling acoustic wave, the sound pressure reflection and transmission coefficients R and T are given by

$$R = \frac{(Z_2/Z_1) - 1}{(Z_2/Z_1) + 1}$$

$$T = \frac{2\,(Z_2/Z_1)}{(Z_2/Z_1) + 1} \qquad (1)$$

$$T - R = 1$$

where Z_1 and Z_2 are the characteristics impedances of the materials. For a backward traveling wave, the reflection and transmission coefficients R' and T' are given by

$$R' = -R$$

$$T' = 1 + R' = 1 - R \qquad (2)$$

Consider Fig. 5 which shows the echo paths in a two-zone sensor. Suppose the reflection coefficients at the boundaries are equal except at the end where R = 1. Let α represent the attenuation coefficient and L the length of each sensor zone. Traversing the echo paths as shown in Fig. 5 and using the expressions for the reflection and transmission coefficients, the combined output resulting from all the echoes may be represented by

$$s(t) = C_o\, x\,(t) + C_1\, x\,(t - T_1) + C_2\, x\,(t - T_1 - T_2) + n(t) \qquad (3)$$

where,

C_o = R

C_1 = $R\,(1 - R^2)\exp(-2\,\alpha\,L)$

C_2 = $(1 - R^2)^2 \exp(-4\,\alpha\,L)$

T_i = proporgation delay in the ith zone,

and n(t) = noise, representing the model error and noise background. The echo signal equation in the form given above lends itself to a tapped delay line representation as shown in Fig. 6. The transduction of s(t) into r(t) is a convolution operation given by

$$r(t) = \int_0^t h(\tau)\, s(t - \tau)\, dt \qquad (4)$$

where $h(\tau)$ is the impulse response of the transducer, and is equal to $x(\tau)$ under the assumption of impulse input.

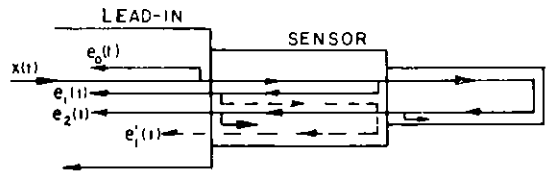

Fig. 5 Echo paths.

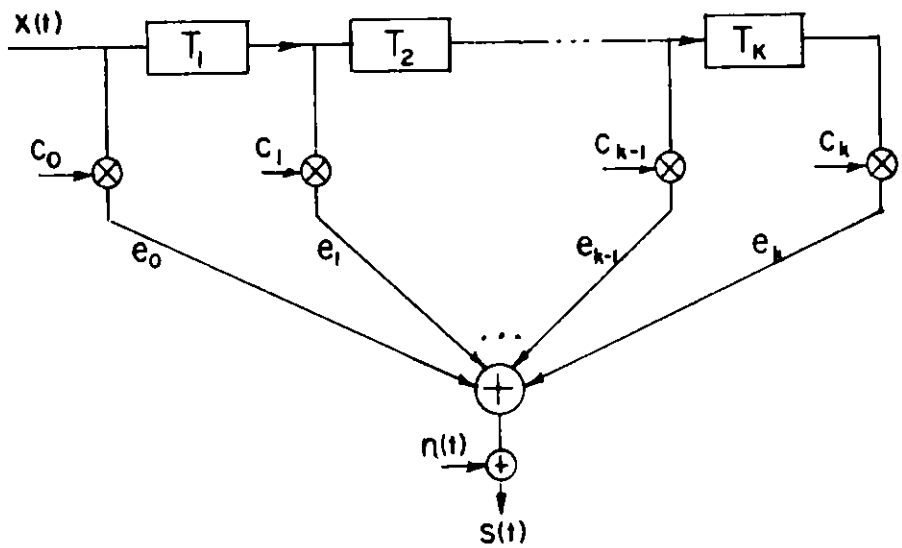

Fig. 6 Tapped delay line representation of the sensor.

Design Considerations

Given the values of α and L, the echo signal amplitudes in Eq. 3 depend on the value of R. For easy identification of the individual echoes, the value of R must be chosen in such a way that the echo signal amplitudes are on the same order of magnitude. This enables even distribution of the input pulse energy among the echoes.

The attenuation coefficient α of a material varies with the frequency of operation and temperature. In the frequency range of interest (below 10 MHz), α is sensitive mainly to temperature. For lack of adequate theory, the dependence of α on temperature is often determined experimentally. For design purposes, the peak value of α may be used.

The sensor zone length L should be small so as to provide a good spatial resolution. But, for easy echo separation L should be at least (3/2) times the wavelength. The phenomenon of Raleigh scattering, however, sets a lower limit on wavelength ($\gtrsim$ 10 MHz).

Signal Processor

In the past, correlation techniques have been successfully applied to single path time delay estimation problems.[5] However, the success of these methods to multipath problems is impaired by the interpath signal interference. In what follows, the use of a generalized correlation technique[6] is considered for the estimation of multiple time delays.

Considering the transfer function representations of the measurement system as shown in Figs. 7a and 7b, the expression for the received signal may be written in a standard form as:

$$r(t) = C_o\, y(t) + C_1\, y(t-T_1) + C_2\, y(t-T_1-T_2) + v(t) \tag{5}$$

where y(t) is the source signal which is assumed to be known, and v(t) is the noise which is assumed to be incoherent with y(t).

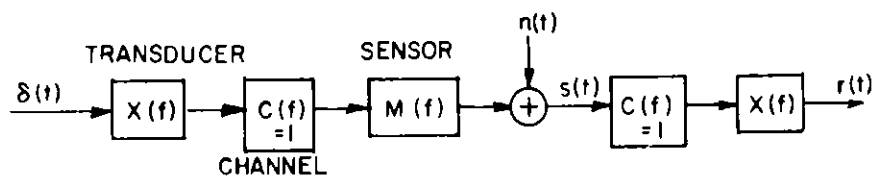

(a)

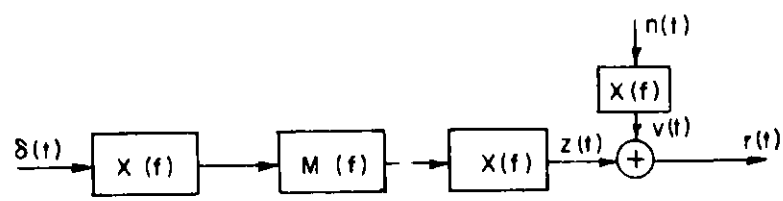

(b)

Fig. 7 Transfer function representations.

The cross correlation function between y(t) and r(t) is defined as:

$$\begin{aligned} R_{yr}(\tau) &= \lim_{T\to\infty} \int_{-T/2}^{T/2} y(t)\, r(t+\tau)\, dt \\ &= C_o\, R_{yy}(\tau) + C_1\, R_{yy}(\tau-T_1) \\ &\quad + C_2\, R_{yy}(\tau-T_1-T_2) \end{aligned} \tag{6}$$

where $R_{yr}(\tau)$ represents the cross-correlation function, and $R_{yy}(\tau)$ the autocorrelation function. The Fourier transforms of Eq. 6 gives the energy spectral densities as:

$$\begin{aligned} G_{yr}(f) &= \{C_o + C_1 \exp(-j\,2\pi f\, T_1) \\ &\quad + C_2 \exp[-j\,2\pi f\,(T_1+T_2)]\}\, G_{yy}(f) \end{aligned} \tag{7}$$

Because of the finite observation time, $R_{yr}(\tau)$, $G_{yr}(f)$ and $G_{yy}(f)$ in practice can only be estimated. For this, a gneralized correlator is defined as:

$$\hat{R}_{yr}(\tau) = \int_{-\infty}^{\infty} \psi_g(f)\, G_{yr}(f) \exp(j\, 2\pi\, f\tau)\, df \qquad (8)$$

where $\psi_g(f)$ represents the generalized filter function.

Many known estimators can be derived from Eq. 8 by a proper selection of the filter functions. Three useful estimators and their associated filter functions are listed below:[7]

(1) Basic correlator: $\psi_g(f) = 1$

(2) Impulse Reponse Estimator: $\psi_g(f) = \dfrac{1}{G_{yy}(f)}$

(3) Maximum Likelihood (ML) Estimator: $\psi_g(f) = \dfrac{1}{G_{vv}(f)}$

The effectiveness of these estimators is tested by using the model Eq. 3.

Numerical Results

The following specifications for an ultrasonic thermometer are assumed:

sensor material = rhenium,
sensor length = 50-mm/zone,
sensor size = 4-mm,
frequency = 200 kHz,
type of wave = extensional,
α = 0.03 Np/cm, R = 0.4.

Based on these constants, Eq. 3 becomes

$$s(t) = 0.4\, x(t) + 0.25\, x(t-T_1) + 0.39\, x(t-T_1-T_2) + n(t) \qquad (9)$$

Suppose that the time delays T_1 and T_2 are 24 μs and 26 μs respectively.

For simulation, a test signal for x(t) is selected as

$$x(t) = \frac{\sin \pi t/\tau}{\pi t/\tau}$$

where τ = 4 μs. It may be noted that the above test signal resembles the impulse response of a typical transducer.[4]

The generalized correlator is simulated using the Fast Fourier Transform techniques.[8] Corresponding to a sampling time of 2/3 μs, 128 samples were obtained from the output signal in Eq. 9. Pseudo-random numbers of normal distribution with zero mean and specified variance were used for the noise term. The output data were zero padded with 384 zeros to avoid circular effect and time aliasing in the cross-correlation computation. Ten averagings were used to obtain smoothed spectral estimates.

For the noise-free case, an efficient technique is the impulse response filter which yields sharp spikes as shown in Fig. 8. For the noisy signal with a signal-to-noise ratio of 1.75, the results of basic cross-correlator, impulse response estimator, and ML estimator are respectively as shown in Fig. 9a, b, and c. Although each of the estimators correctly identifies the peaks, the ML estimator appears to be more robust than the other estimators.

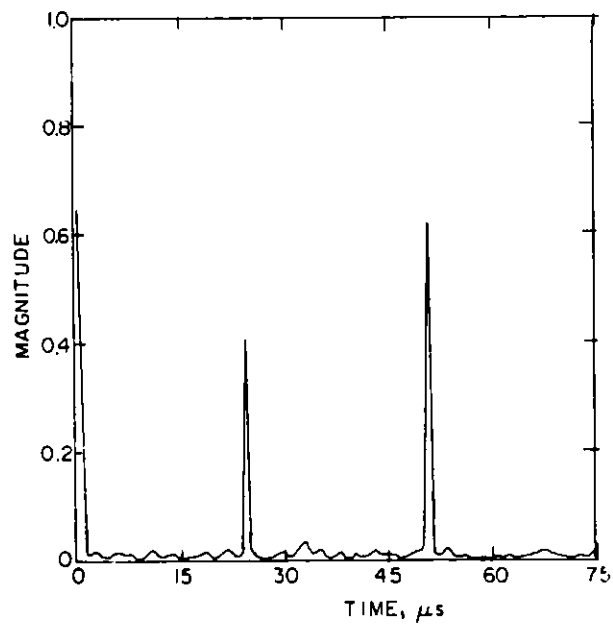

Fig. 8 Impulse response method for the noise-free case.

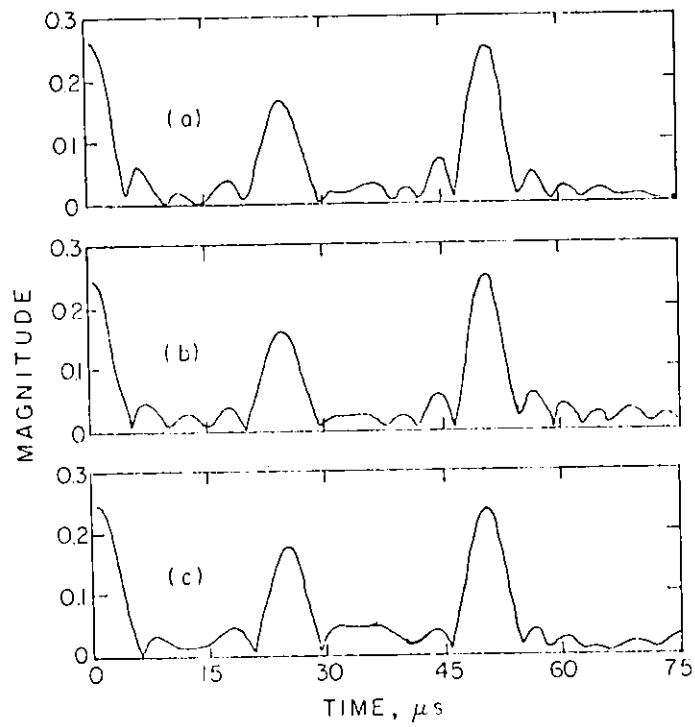

Fig. 9 Time delay estimation:

a) Basic cross-correlator
b) Impulse response estimator
c) Maximumlikelihood estimator

CONCLUSIONS

A study of the high temperature instrumentation techniques comprising thermocouples, radiation pyrometry and ultrasonic thermometry has been made in the light of their applicability to coal conversion systems. The study shows that the ultrasonic thermometry has the potential of providing viable instrumentation in the coal process environment.

A theoretical analysis of a pulse-echo type acoustic measurement system has been carried out to assess its feasibility. Based on a mathematical model, the trade-offs involved in the determination of the design parameters such as the sensor length, reflection and attenuation coefficients, and the frequency of operation have been discussed. The simulation results show that the signal processor based on a generalized correlation technique could provide reliable temperature estimates. The proposed measurement system will be especially useful for temperature profiling.

REFERENCES

1. N. M. O'Fallon, R. A Beyerlein, W. W. Managan, H. P. Karplus, and T. P. Mulcahey, "A Study of the State-of-the-Art of Instrumentation for Process Control and Safety in Large-Scale Coal Gasification, Liquefaction, and Fluidized-Bed Combustion Systems," ANL-76-4 (Jan 1976).

2. J. F. Schooley, "State-of-the-Art of Instrumentation for High Temperature Thermometry," Proc. of 1977 Symp. on Instrumentation and Process Control for Fossil Demonstration Plants, Chicago, Illinois (1977).

3. G. F. Warnke, "Industrial Radiation Pyrometers: A Guide to Performance Parameters," Instrumentation Technology (Sept 1971).

4. L. C. Lynnworth and D. R. Patch, "New Sensors for Ultrasound: Measuring Temperature Profiles," Materials Research and Standards, pp. 6-11 (Aug 1970).

5. J. S. Bendat and A. G. Piersol, Engineering Applications of Correlation and Spectral Analysis, New York: John Wiley (1980).

6. C. H. Knapp and G. C. Carter, "The Generalized Correlation Method for Estimation of Time Delay," IEEE Trans. Acoust., Speech, Signal Processing, ASSP-24, pp. 320-26 (1976).

7. N. Gopalsami, A. C. Raptis and T. P. Mulcahey, "Monitoring Temperatures in Coal Conversion and Combustion Systems via Ultrasound," ANL Tech. Memo. ANL-FE-49622-TM09 (1980).

8. L. R. Rabiner and B. Gold, Theory and Application of Digital Signal Processing, Prentice-Hall, 1975.

ULTRASONIC THERMOMETRY IN OIL SHALE RETORTS*

Joseph J. Ronchetto
Lawrence Livermore National Laboratory

ABSTRACT

A relatively novel instrumentation system was recently applied to the detection of the high temperatures (up to 1000°C) observed in in situ oil-shale retorts.

The instrumentation system operates on the principle that the speed of sound in a medium is affected by the temperature of the medium. The method relies on the principles of ultrasonic reflectometry to locate and determine temperatures within zones of a slender-rod-sensing element installed in the retort bed. The measurement technique consists of sending an ultrasonic pulse down an element containing n zones spaced along its length. The zone boundaries are defined by n+1 discontinuities within the element. The time intervals between pairs of returning echoes, caused by reflections from these discontinuities, are measured electronically. These measured time intervals are then related to the average temperature of the corresponding zones.

Our preliminary results have been very encouraging, and it appears that the ultrasonic thermometer can be a useful in situ instrument. Further development is needed to optimize the sensor material and sensor design for practical in situ use.

In this report, we describe the approach and apparatus used and the results obtained from our tests. We also mention our current projects and future plans.

INTRODUCTION

In oil shale retorting, one of the most vital process parameters requiring continuous monitoring is the temperature profile within the retort. Although sheathed thermocouples are currently being used for this purpose, they exhibit a high failure rate and are expensive, particularly for the in situ case. The environment experienced by the instrumentation needed for in situ processes is extremely hostile. Not only are there rigorous thermal, chemical, and mechanical stresses acting on these instruments once they are in

*This work was performed under the auspices of the U.S. Department of Energy by Lawrence Livermore National Laboratory under Contract W-7405-Eng-48.

place, but the emplacement process itself may also produce severe stresses on the instrumentation. Because of this environment, very rugged in situ instruments are needed. Also, because of the size and general characteristics of in situ retorts, long cable lengths are required for instrumentation. Therefore, a minimum number of cables must be used in order to meet economic constraints.

The temperature and positional accuracy needed for in situ retorting is only moderate; temperatures within 25 to 50°C at the retorting temperature and positions within 1.5 to 3 m are sufficient.

The ultrasonic thermometer is a good candidate for this in situ service. The sensor itself is an inexpensive, small-diameter rod. Though the rod must be isolated from external forces by a sheath, it is rugged and may be bent or curved without affecting its performance. The single transducer that drives this sensor rod is also capable of surviving a moderately hostile environment. The sensor rod may have up to 16 temperature zones along its length. Therefore, a 16-region profile of the temperature distribution within a retort could be obtained from a single coaxial cable. The ultrasonic thermometer in its present form is capable of better than a $\pm 50^{\circ}C$ measurement accuracy. Thus, the detector system is simple, inexpensive, rugged, minimizes the number of cables needed, and has sufficient accuracy for in situ measurements.

ULTRASONIC THERMOMETRY TECHNIQUE

The technique uses the principle that the velocity of sound in a medium is a function of the temperature of the medium. In most solids, as the temperature increases, the velocity decreases--primarily because the modulus of elasticity decreases.[1] A nondispersive extensional wave propagates down an elastic waveguide at a wave velocity, V, that is proportional to $(E/\rho)^{1/2}$, where E is Young's modulus and ρ is the density. Both E and ρ are functions of temperature. One can determine the temperature of a length of waveguide from a transit-time measurement by simply having calibrated the waveguide previously.

The pioneering work on ultrasonic thermometry was performed in the late 1950s by Bell[2] and his co-workers in the United Kingdom. Parametrics, Inc. of Waltham, Mass. extended the concept to its patented multiple zones, and has been developing and producing commercial versions of ultrasonic thermometry systems since the late 1960s. L. C. Lynnworth, Head of the Ultrasonics

Department for Panametrics, Inc. has made many contributions and authored numerous papers on the subject.[3-5]

The multiple zone technique operates in the following manner: low reflectivity discontinuities are placed along the total waveguide path of the sensor, typically at regular intervals. The time intervals between the successive echoes can then be interpreted in terms of a temperature profile along the waveguide path. This temperature profile represents the average temperature of each zone.

The detector used for this multiple-zone ultrasonic pulse thermometry technique consists of two basic elements (Fig. 1): the sensor and the transducer.

The Sensor

The sensor is the element in which the velocity of sound as a function of temperature is measured. This element is typically notched at the desired zone boundaries creating the discontinuities in this sonic waveguide. When the acoustic pulse is transmitted, these notches cause reflections to echo down the element toward the transmitted end. Since the signal must make a round trip through the zone, the time intervals between these reflected signals are equal to twice the transit time of the ultrasonic pulse in the specific zone.

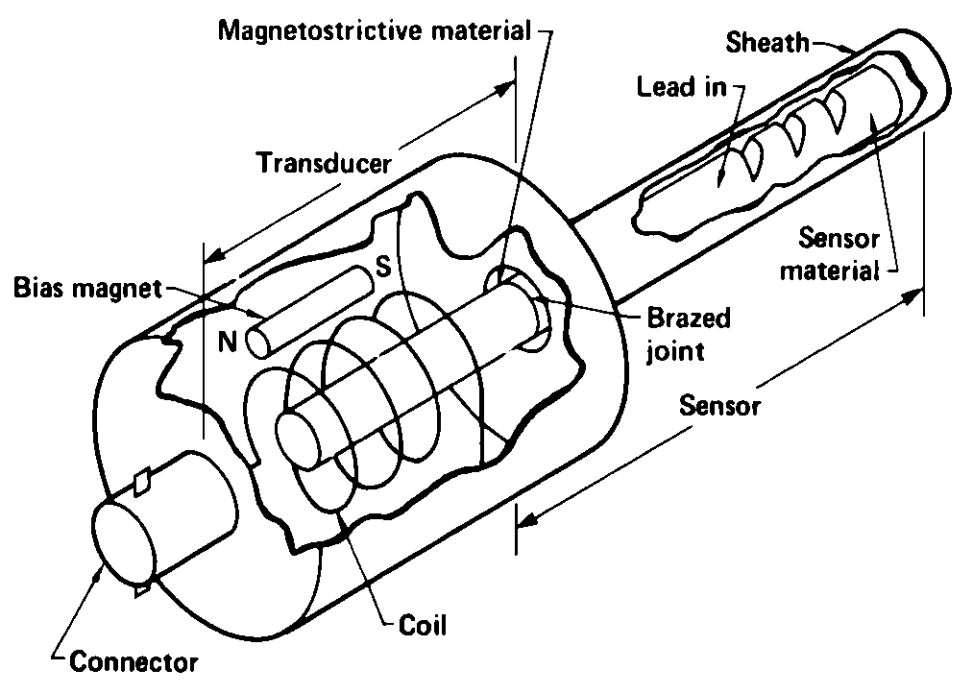

Fig. 1. Features of the magnetostrictive, ultrasonic temperature detector.

The sensor material may also be used as a lead-in element to transfer acoustic pulses between a remote transducer and the active area of the sensor. Other material may be used for this lead-in function depending upon the specific arrangement.

Transducer

The transducer is an electro-acoustic converter. When electrically energized, it acts as a transmitter and sends an acoustic pulse down the sensor. The reflected acoustic echoes return to the transducer, which now acts as a receiver and converts them back into electrical signals.

The transducer consists of three major components:

- The solenoidal coil, which converts the electrical current into a magnetic field during transmission and vice versa during reception.
- The ferromagnetic magnetostrictive material, in this case Remendur 27,* a cobalt-iron alloy that deforms when subjected to a magnetic field.
- A permanent magnet, which emphasizes the extensional mode of the magnetostrictive material.

The electronics for an ultrasonic thermometer consists of 1) a pulse generator to interrogate the transducer by sending the ultrasonic pulse down the sensor, 2) a receiver that amplifies and filters the reflected signals, and 3) a measurement scheme to determine the time interval between these reflected signals. This measurement scheme can be as simple as an oscilloscope readout or as sophisticated as a computer-controlled digital time intervalometer.

This temperature measuring technique has some important features:

- The sensor rod must be acoustically isolated from surrounding material. If not, extraneous echoes can be created that make zone delineations very difficult.
- Attenuation in the sensor and lead-in element increases with temperature. Therefore, if a very long acoustic waveguide is at elevated temperatures, the reflected signals may become indistinct as the signal-to-noise ratio decreases.
- The temperature measurement is an average temperature over the entire length of the zone and not a point temperature, as is the case with thermocouples.

*Amax Speciality Metals, Orangeburg, SC.

- In many cases, particularly for higher temperature operation, the sensor material may have to be tempered before it can be calibrated and used.
- Some of the most desirable sensor materials from a temperature standpoint exhibit a hysteresis-like effect of the transit time-temperature curve when going to very high temperatures. (This problem is discussed below.)

INSTRUMENTATION

The experimental setup we used contains three major components (Fig. 2): the detector, the signal processor, and a standard oscilloscope.

Detector

Two different detectors were employed in the experiments we performed. The first detector (304SS) was a commercial unit manufactured by Panametrics, Inc. of Waltham, Mass. It consisted of their transducer housing #5010E5, which drove a 2-cm long, Remendur, magnetostrictive stub. This stub was brazed to the 1.6-mm-diam, 1.4-m-long, 304 stainless steel sensor rod. The rod had its first notch cut 29 cm from the magnetostrictive stub to rod joint and was notched again every 7.5 cm out to 1.2 m. These 13 notches gave 12 temperature zones. The rod was sheathed by a 6-mm-diam, 1.4-m-long 304SS tube. The Remendur and part of the rod fit inside the transducer housing, leaving the tube 1 cm longer than the rod at the far end. The tube was open

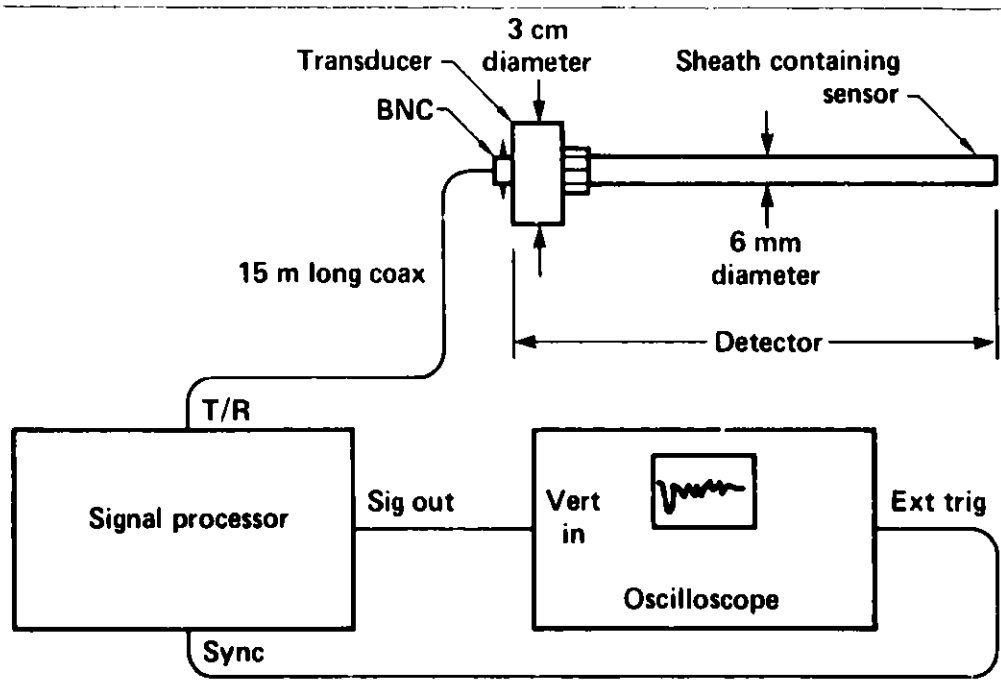

Fig. 2. Experimental setup for the ultrasonic temperature-measuring apparatus.

at that end but could be closed, if desired, to keep out contaminants that might affect the rod's characteristics.

The second detector (KANTHAL) that we employed was constructed at LLNL using the transducer housing from the first detector. The Remendur stub was removed from the first sensor rod and was brazed to a 1.6-mm-diam, 2-m-long rod of KANTHAL A-1* (an Fe, Cr, Al, Co alloy), which has a melting temperature of 1510°C and is typically used as heater element material in high temperature furnaces. The rod was notched at 38 cm and again every 15 cm out to 1.9 m. These 11 not hes gave 10 temperature zones. The rod was sheathed by a 6-mm-diam, 2-m-long tube of 304SS, which was 2 cm longer than the rod. The tube was capped at the far end.

The Signal Processor

The signal processor was a Panametrics Model 5055PR Pulser/Receiver, which was actually designed to operate with piezoelectric transducers, but worked quite well with the electromagnetic type we were using. The initial pulse, generated by the pulser and applied to the transducer was a negative-going 300 V, 20-ns-wide pulse. The reflected pulses from the discontinuities of the zone boundaries had amplitudes of 1 mV at the transducer. (The reflected pulses from the end of the sensor had a first-time reflection amplitude of 20 mV.) The pulses were filtered and amplified by the receiver. The reflected pulses from the zone boundaries were about 50 mV at the output. These pulses were then displayed on an oscilloscope and the time interval between them could be determined to within 100 ns.

CALIBRATION OF DETECTORS

The detectors were calibrated in a high temperature furnace. The furnace size allowed 14 cm of probe to be inside the furnace at any time. The zones of the 304SS detector, being 7.5 cm in length, were centered in the furnace, giving a 3-cm buffer on each end of the zone to the thermal gradient at the furnace wall.

Figure 3 shows the calibration curve for zone six of this detector, which is typical of the other zones. The black dots were obtained from the first temperature cycle. The triangles, diamonds, and squares were from subsequent cycles. Notice the hysteresis-like effect that occurred when the sensor was heated the first time. Also note that with this sensor rod, the sound transit time decreased after the initial heat-up.

---

*The Kanthal Corporation, Bethel, CT.

Since the temperature zones for the KANTHAL detector were longer than our furnace could handle (15 cm), we constructed a duplicate sensor rod using the same material but with zones only half the length (7.5 cm). This duplicate sensor rod was then calibrated using the furnace, and a polynomial fit was made to the curve obtained from its sixth zone. The calibration of the KANTHAL detector was accomplished using this polynomial and the actual length of the zones (15 cm) in the KANTHAL detector. The calibration curve for zone 6 of the duplicate sensor rod is shown in Fig. 4. The values represented by the circles were obtained during the temperature rise and by the squares during temperature fall. Notice that in this case, the sound transit time increased after the initial heat up. The reason for this directional difference between the first and second detector is not understood.

EXPERIMENTS

The Lawrence Livermore National Laboratory has two different-size oil shale retorts that are used to experimentally simulate the in situ retorting of shale.[6] The retorts are actually cylindrical vessels, vertically oriented. The larger retort is 0.9 m in diameter and 6.1 m in length (6-Mg capacity). The smaller retort is 0.3 m in diameter and 1.5 m in length (125-kg capacity). Shale is first rubbled and graded, and then placed within

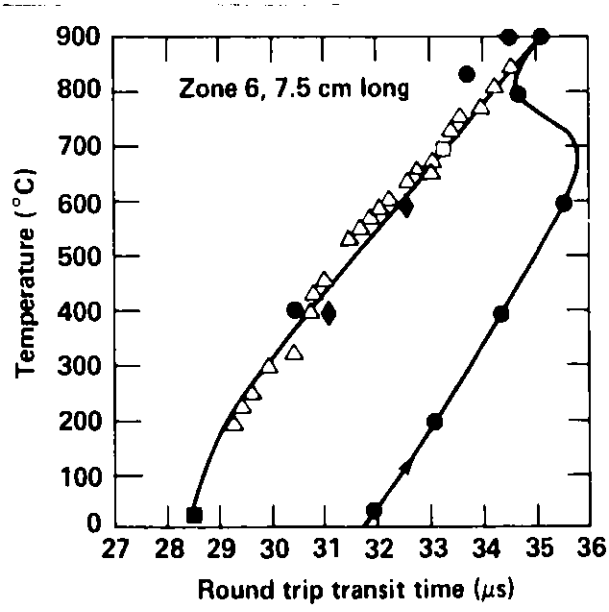

Fig. 3. Calibration curve for zone 6 of detector. Sensor material is 304 stainless steel with zone lengths of 7.5 cm.

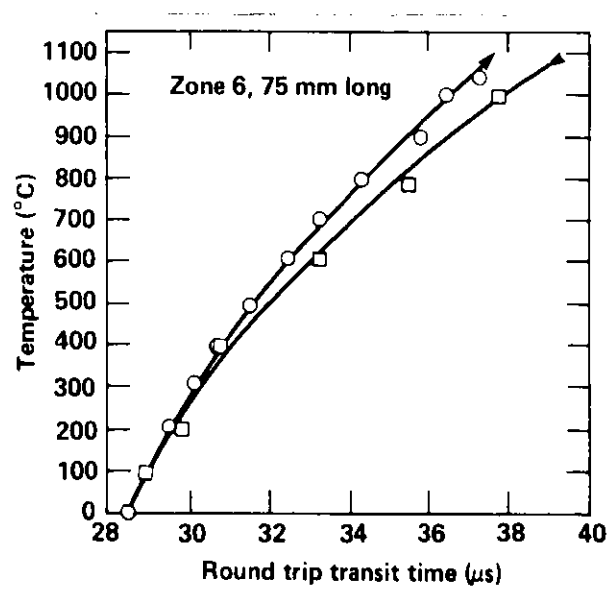

Fig. 4. Calibration curve for zone 6 of the duplicate sensor. Sensor material is KANTHAL A-1 with zone lengths of 7.5 cm.

t.e retort. Gas is forced through the rubble bed from top to bottom. The shale is ignited and the kerogen is pyrolyzed along this direction. The entire process resembles a burning, vertical cigarette.

here are four instrumentation ports or levels around the sides of these retorts spaced every 15 cm along their length. The levels are numbered sequentially along the length, starting with level 0 at the top. There are 11 levels along the small retort and 39 along the large. Instrumentation, typically type-K thermocouples, is installed through these ports into the oil-shale rubble bed as the shale rubble is placed within the retort.

The first detector (304SS) was installed in the large retort for run L-4 (Fig. 5a). This detector was installed radially through the center of the bed

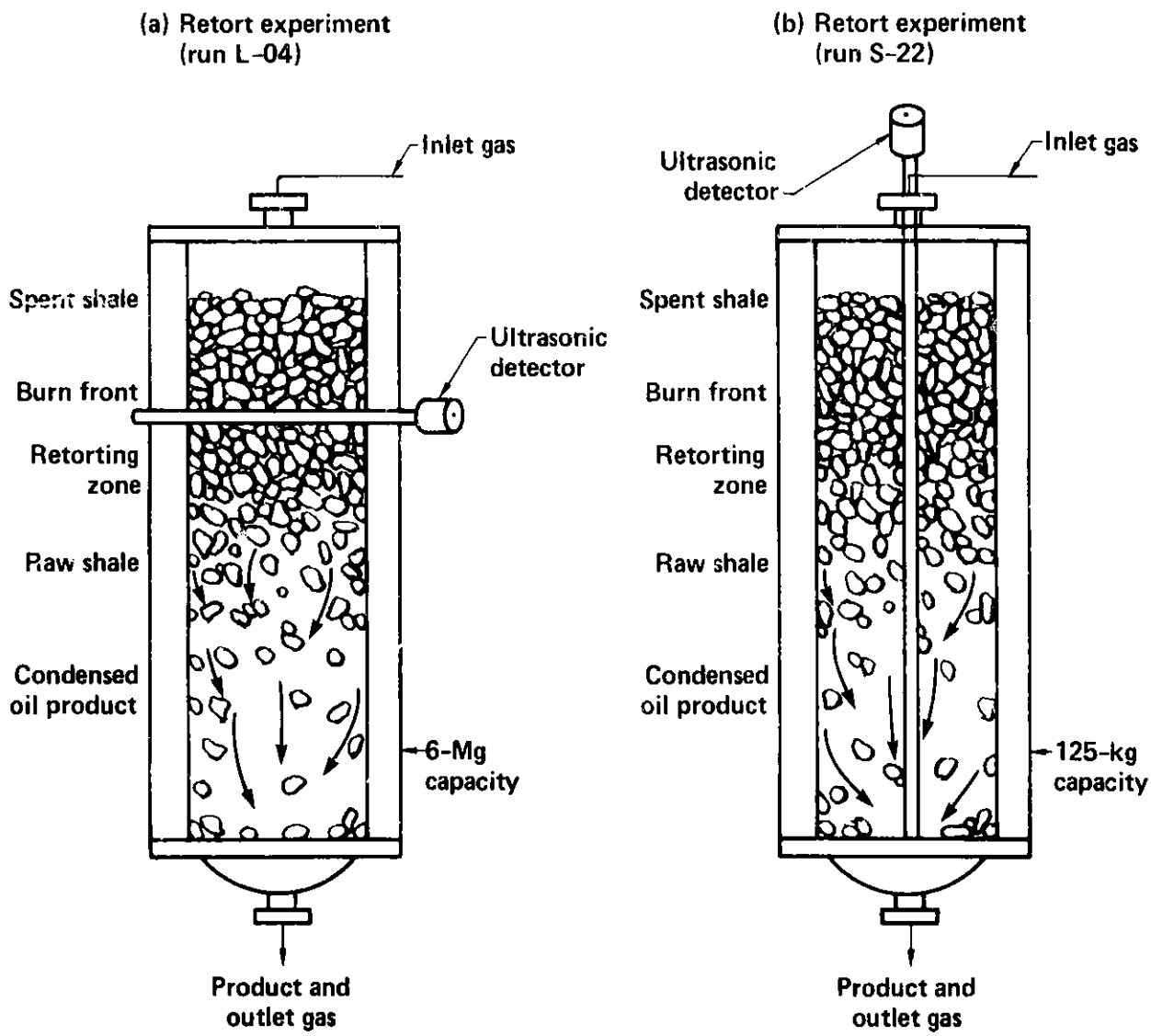

Fig. 5. Details of ultrasonic detector installation in oil shale retorts for tests during (a) large retort run L-04 and (b) small retort run S-22.

at level 8. We chose the detector length to give us 12 each, 7.5-cm temperature zones across the bed.

Zone 1 had thermocouples placed in the bed at one level above and one level below it (levels 7 and 9, respectively). Figure 6 compares the temperature readings of these three detectors versus time. As can be seen, the profiles of the detectors from the thermal pulse match quite well except at the higher temperatures. The largest error occurs at the peak temperature where the ultrasonic thermometer indicates a temperature 150°C higher than was measured by the thermocouples.

Some of the other zones had thermocouples in similar positions. They show this same tendency toward a 100 to 200°C error in the peak temperature. This seems to be a common problem with 304 stainless steel at these high temperatures and is probably the reason for the wide scatter at the higher temperature (>800°C) on the calibration curve (Fig. 3).

The second detector (KANTHAL) was installed in the small retort for run S-22 (Fig. 5b). The detector was installed axially through the center of the bed. The detector's zones were chosen to give us one temperature zone for each retort level. This gave ten, 15-cm zones along the length of the retort with the top end of zone 1 at level 0 and the bottom end of zone 1 at level 1. Therefore, zone 1 was effectively the average temperature at level 1/2, and zone 10 the average temperature at level 9-1/2.

Figure 7 compares a typical ultrasonic thermometer zone (zone 6, level 5-1/2) with bed thermocouples at the two extremities of that zone (level 5 and

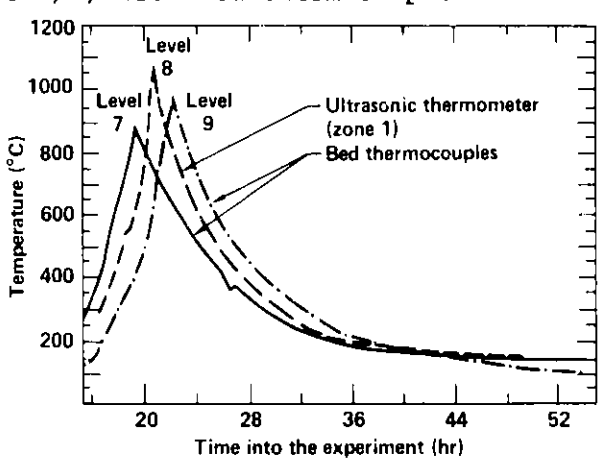

Fig. 6. Temperatures from bed thermocouples at retort levels 7 and 9 together with zone 1 of the ultrasonic thermometer at level 8. The data are from a retorting experiment (L-04) in our 6-Mg retort.

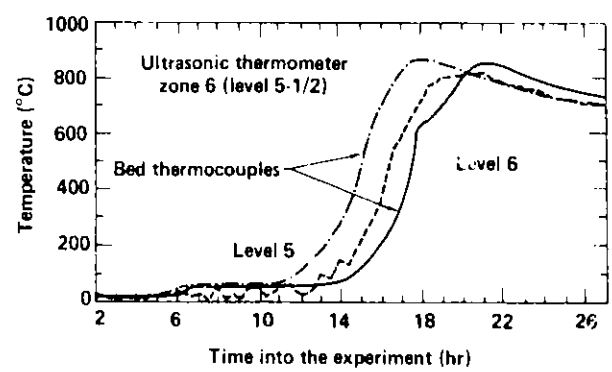

Fig. 7. Temperatures from bed thermocouples at retort levels 5 and 6 along with zone 6 (level 5-1/2) of the ultrasonic thermometer. The data are from a retorting experiment (S-22) in our 125-kg retort.

level 6). The three time profiles in this case match very well, with the ultrasonic thermometer possibly 50°C low at the peak temperature.

The most important thermal data for in situ retort operation is the shape and position (within the retort) of the retorting front. This is the temperature where practically all of the hydrocarbons are released from the shale. The temperature at which this occurs is approximately 400°C. The arrival times of this front along the central axis of the retort for run S-22, as measured by thermocouples and the ultrasonic thermometer, is shown in Fig. 8. The match, that is measurement accuracy, is extremely good.

SUMMARY

Temperature profiling of oil shale retorts provides information that allows one to control the operating parameters of the process to increase efficiency and the product yield. The thermal instrumentation requires only moderate precision, but must be able to perform cost effectively in hostile environments at long distances.

We have tested an ultrasonic temperature transducer in an environment simulating an in situ oil shale retort. We have obtained good agreement in temperature comparisons with thermocouples in the rubbled shale bed. These results have been encouraging. The need is indicated for further studies of the sensing element material and construction techniques.

We are currently attempting to interface the detector with a computer system that will permit automatic data acquisition, manipulation, and storage.

Before the end of the year we plan to evaluate a pair of ultrasonic transducers and the automatic data-gathering system at an in situ coal site in

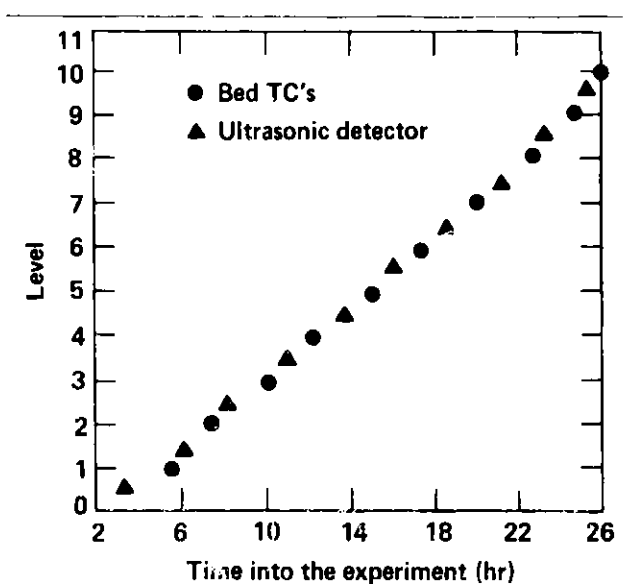

Fig. 8. The arrival times of the retorting temperature (400°C) as measured by bed thermocouples and ultrasonic thermometer. The data are from a retorting experiment (S-22) in our 125-kg retort.

Centralia, Washington. The sensor rods will be approximately 30 m in length and will contain 12 to 16 temperature zones.

ACKNOWLEDGMENTS

The author wishes to thank W. A. Sandholtz for bringing this technique to his attention; L. C. Lynnworth of Panametrics, Inc. for many helpful discussions; S. J. Spataro, and A. E. Lewis and J. H. Campbell for their encouragement and support of this effort; E. J. Frohwein, J. J. Scarafiotti and G. P. Berry for their invaluable assistance during construction and data acquisition.

REFERENCES

1. Papadakis, E. P., et al., "Ultrasonic Measurements of Young's Modulus and Extensional Wave Attenuation in Refractory Metal Wires at Elevated Temperatures with Application to Ultrasonic Thermometry," Journal of Applied Physics, Vol. 45, No. 6, June 1974, pp. 2409-2420.
2. Bell, J. F. W., "The Velocity of Sound in Metals at High Temperature," The Philosophical Magazine, Vol. 2, No. 21, 1957, pp. 1113-1120.
3. Lynnworth, L. C., "Ultrasonic Temperature Measurement Average and Profile," Measurement and Control, December 1979, pp. 106-108.
4. Lynnworth, L. C., "Attenuation Measurements Using the Pulse-Echo AB Method, Without Multiple Echo Reverberations in Specimen," Materials Evaluation, January 1973, pp. 6-16.
5. Lynnworth, L. C., and E. H. Carnevale, "Ultrasonic Thermometry Using Pulse Techniques," in: Plumb, H. H. (editor), Temperature - Its Measurement and Control in Science and Industry, ISA, Vol. 4, Part 1, 1972, pp. 715-732.
6. Sandholtz, W. A., et al., The Lawrence Livermore Laboratory Oil Shale Retorts, Lawrence Livermore National Laboratory, Livermore, CA, UCRL-52551 (1978).

APPLICATION OF SODIUM D-LINE REVERSAL TO SIMULATED COAL-FIRED MHD FACILITIES

Charles R. Campbell*, Thomas B. Malloy, Jr.** and Leslie E. Bauman***
MHD Energy Center
Mississippi State University
Mississippi State, MS 39762

ABSTRACT

A microprocessor-based, sodium D-line reversal, temperature measurement system has been developed at the MHD Energy Center at Mississippi State University. This system was designed to be used on the particle-laden environment of coal-fired facilities. Temperatures are derived by solving the radiative transfer equation applied to either the particle-free of the particle-laden condition. Measurements are made on the wings of the sodium D-lines in order to avoid the self-absorption due to cooler boundary layers in the flow. A description of the instrument and the temperature solutions are presented. This system has been successfully used at the Mississippi State University MHD test facility and at the Argonne National Laboratory AMPEL facility at Argonne, Ill. Results of the measurements on the AMPEL facility are presented.

INTRODUCTION

A temperature measurement system utilizing the technique of sodium D-line reversal has been developed for measurements on simulated coal-fired MHD flows. This widely used technique uses the absorption and emission of light at a strong resonance line, typically that of sodium, to determine temperature. Because of the need for remote, automatic operation, microprocessor control has been incorporated into the system. The particle-laden, coal-fired flow presents a difficult environment in which to apply the technique because of absorption, emission, and scattering of light by the particles. A temperature solution including the effects of particles has been programmed into the microprocessor system. The system has been tested and refined on the benchtop and on the Mississippi State University MHD facility. Joint experiments were performed with the system at the Argonne MHD Process Engineering Facility (AMPEL). Results of the measurements on the AMPEL facility are reported.

Supported by U. S. Department of Energy Contract No. DE-AC02-80ET-1560
*M. S. student, Physics
**Now at Shell Development Co., Westhollow Research Center, Houston,TX
***Assistant Professor, Physics and Chemistry

TEMPERATURE MEASUREMENTS

In a classical application of sodium line reversal, the brightness temperature of a calibrated lamp is adjusted such that the lamp appears neither bright nor dark when viewed through a flame at the sodium D-lines. Many variations and refinements of this technique have been used.[1,2,3] In order to achieve automatic operation and to have the capability to correct for the effects of particles on the temperature calculation, the Mississippi State University system does not seek the reversal point, but rather solves the radiative transfer equations for the temperature.

For clean combustion, i.e. where only sodium atoms contribute to the absorption and emission of light, the monochromatic radiative transfer equation is

$$dI = \alpha[B(T_g) - I]dx.$$

I is the light intensity, α is the absorption coefficient of the sodium atoms, $B(T_g)$ is Planck's blackbody radiant emittance at the gas temperature and x is a position coordinate. Most flames have temperature and sodium number density profiles across the line-of-sight and α and $B(T_g)$ are functions of position, so that this equation cannot be solved exactly. If constant properties across the flame are assumed, then the equation may be integrated to obtain the intensity across the flame

$$I(L) = B(T_g)[1 - e^{-\alpha L}] + I(0)e^{-\alpha L},$$

where L is the line-of-sight path length across the flame and I(0) is the lamp intensity. With this equation, four intensity measurements are sufficient to solve for temperature. Two measurements are made on the sodium line with and without the lamp intensity, and are referred to as M1 and M2, respectively. Two measurements are made off the line with and without the lamp intensity, and are referred to as M3 and M4, respectively. If a zero absorption coefficient off the line is assumed, the temperature is given by

$$\frac{1}{T_g} = \frac{1}{T_L} - \frac{\lambda}{C_2} \ln\left(\frac{M2 - M4}{M1-M2-M3+M4}\right),$$

where T_L is the lamp brightness temperature, C_2 is Planck's second radiation constant and λ is the average wavelength position of the measurements. $B(T_g)$ is assumed to be independent of wavelength over the region of the measurements. The optical depth of the flame at the wavelength of the on-line measurements can be calculated as

$$\alpha L = \ln\left(\frac{M3 - M4}{M1 - M2}\right).$$

Work by Daily and Kruger and others suggests that for a nonisothermal flame the line reversal temperature will be intermediate to the different flame temperatures.[4,5] For flows with a high temperature core and cooler boundary layers, a monochromatic line reversal measurement will approach the core temperature if the measurement in made on the wings of the line. They suggest measurements should be made at optical depths of 1.0 or less. For signal-to-noise considerations they suggest a region between 0.2 and 1.0.

Errors involved in line reversal temperature measurements have been reviewed by others.[6-9]

The above solution, referred to later as the clean solution, is not adequate when particles are present in the gas. If E is defined to be the extinction absorption ratio for the particles and η to be the particle absorption coefficient then the monochromatic radiative transfer equation can be written as

$$dI = [B(T_g)(\alpha + \eta) - I(\alpha + \eta E)]dx.$$

If constant properties are assumed, the integrated intensity across the flame can be written as

$$I(L) = \gamma B(T_g)[1 - e^{-(\alpha+\eta E)L}] + I(0)e^{-(\alpha+\eta E)L},$$

where

$$\gamma = \frac{\alpha + \eta}{\alpha + \eta E} .$$

If the particle constants are assumed to be independent of wavelength, then again multiple measurements can be used to solve for the gas temperature. Four additional measurements to those mentioned earlier are required. These are lamp-on and lamp-off measurements at a second wavelength on the line with a significantly different optical depth and lamp-on and lamp-off measurements before the flame is present. The resulting eight equations allow the gas temperature to be calculated. Optical depths and total extinction due to the particles can be calculated also.

The effect of particles on a reversal temperature is minimized at line center where the optical depth is large. However, as has been previously stated, the boundary layer effects are most severe at line center. The particle solution presented here and done by making measurements on the wings of the lines minimizes both errors.

SYSTEM DESCRIPTION

The Mississippi State University sodium line reversal system is packaged for relatively portable operation. Sophisticated control functions and calculations needed for the particle solution are possible in a portable package because of the use of a CMOS microprocessor.[10] A block diagram of the system hardware is shown in Figure 1.

Source-side components consist of a calibrated lamp with a regulated power supply, an optical chopper, a filter wheel, an iris diaphragm, a focusing lens and an alignment laser. The ribbon filament tungsten lamp is maintained at a constant temperature while the effective temperature is varied by inserting optical density filters in the light path. Three filters are mounted on a stepper motor controlled wheel. The chopper operating at 60 Hz provides alternate lamp-on and lamp-off signals.

The detector-side optical components consist of an iris diaphragm, a focusing lens, a monochromator and a photon counting system. The 0.6 m monochromator has adequate resolution to fully resolve the lines. The

wavelength position is scanned at 16 A/s. The slits are controlled with stepper motors.

The microprocessor performs photon counting operations with the lamp-on and lamp-off signals collected alternately in 4.5 ms intervals. All operator input to the microprocessor is through a keypad. The temperature and numerical entries are shown on a liquid crystal display. Permanent copy of the system operations and temperatures are printed on a 20-column printer.

The software consists primarily of three initialization routines and two temperature routines. The first initialization routine obtains slit settings for the different filters and measures the pre-flame lamp and background intensities needed for the particle solution. The second initialization routine, performed with the flame on, locates the position of the line maximum and selects the filter and slit settings. This routine on the current system requires two minutes. The third initialization routine selects the wavelength positions for off-line and on-line measurements. Criteria for the on-line positions are optical densities of 0.4 and 0.2. This routine requires 20 seconds. When changes in particle loading or stoichiometry occur which change the linewidths, the routine can be repeated. After the initialization routines are finished, temperature measurements can be done. Routines for the clean and particle solutions are programmed. A typical temperature temperature measurement requires about three seconds.

In addition, the software includes routines for calculating the corrections to the measured lamp brightness temperature, calculating the signal-to-noise ratio, plotting the lineshapes, and printing the temperature and optical density versus wavelength. The system operation is simplified for lengthy tests by a routine that permits pre-programming sequences of keystrokes which can be executed with a single key. The software was developed and refined during extensive benchtop and test stand experiments

AMPEL TESTS

The line reversal system was operated on the oil-fired test leg of Argonne National Laboratory's AMPEL facility during the period of May 14 to May 21, 1980.[11] Coal-fired MHD flow downstream of the channel and diffuser was simulated by burning a slurry of #2 fuel oil, coal fly ash and K_2SO_4 with preheated air. The system was positioned 3.0 m downstream of the combustor through transverse viewports. The inner diameter of the facility at this point was 0.56 m. The tests were run at fly ash mass loadings of 0%, 0.1% and 0.2% and at stoichiometric ratios between 0.75 and 1.23. The fly ash provided ample sodium for measurements. During clean combustion tests sodium carbonate was added to the fuel oil.

Example temperature data from two of the test days are shown on Figures 2 and 3. Plotted versus stoichiometric ratio are the line reversal temperatures, calculated calorimetry temperatures and thermocouple temperatures uncorrected for radiative heat losses. The thermocouple was positioned just above the optical axis of the line reversal system. Figure 2 shows data from clean fuel tests of May 14, 1980 and Figure 3 shows data from tests of May 16, 1980 with 0.2% fly ash loading.

During the tests, the measured temperatures peaked at a stoichiometric ratio of 1.05 as expected. The temperatures were highest with fly ash and seed loading, presumably due to reduced radiative heat transfer upstream from the measurement point.

Figure 4 is an example lineshape from the testing with 0.2% fly ash loading. The lower curve shows flame emission only and the upper curve shows the lamp through the flame. Both sodium lines have pronounced regions of self-absorption at line center due to the cooler boundary layers. The upper lineshape shows a condition close to reversal since the lamp temperature was 1956 K and the particle temperature solution gave 2010 K. It has been observed consistently at Mississippi State and at these tests that for particle-laden flows the clean solution yields a higher temperature than the particle solution. The difference between the two on the AMPEL facility was on the order of 40 to 60 K for the 0.2% fly ash loading and less for the 0.1% loading.

Figure 5 is a plot of calculated clean temperatures and optical densities versus wavelength across the first line of the lineshape shown in Figure 4. The plot shows the effects of the cooler boundary layers in that as the optical density increases toward line center, the temperature decreases. This is most pronounced at line center where the calculated temperature was 1930 K compared to 2057 K on the wings. The AMPEL data showed consistently that the optimum optical density for measurements is between 0.1 and 0.4. Calculated temperatures showed the effects of noise below an optical density of 0.1. Errors due to the boundary layer began above an optical density of 0.4. This in agreement with data from Mississippi State but differs from theoretical calculations done by Daily and Kruger, that suggested making measurements below an optical density of 1.0.[4]

SUMMARY

The sodium line reversal system has been demonstrated to be a reliable, automated instrument capable of remote operation. Its capability to account for the effects of particles in the temperature calculation makes it well suited for particle-laden flows. The AMPEL tests agree with the Mississippi State University tests that show optimum core temperature calculations should be performed at optical densities of less than 0.4.

ACKNOWLEDGEMENTS

The authors would like to thank Robert L. Cook of the MHD Energy Center for his work on the particle solution method and Claude Reed and Patrick Dunn of Argonne Mational Laboratory for their help with the testing.

REFERENCES

1. D. Lyddon Thomas, Combustion and Flame, 12, 569(1968).

2. H. M. Strong and F. P. Bundy, J. Appl. Phys., 25, 1527(1954).

3. I. A. Vasileva, B. Ya Shumyatskii, and D. N. Yundev, Opt. Spektrosk., 36, 267(1974).

4. J. W. Dailey and C. H. Kruger, J. Quant. Spectrosc. and Radiat. Transfer, 17, 127(1977).

5. H. M. Strong and F. P. Bundy, J. Appl. Phys., 25, 1521(1954).

6. D. Lyddon Thomas, Combustion and Flame, 12, 541(1968).

7. Y. Sasaki, Jap. J. Appl. Phys., 5, 439(1966).

8. W. Snelleman, Combustion and Flame, 11, 453(1966).

9. R. M. Kowalik and C. H. Kruger, J. Quant. Spectrosc. Radiat. Transfer, 18, 627(1977).

10. R. D. Benton and Leslie E. Bauman, Proc. 1980 IEEE Region 3 Conf., 114, Nashville, TN.

11. Patrick R. Dunn, Terry R. Johnson, and Claude B. Reed, ANL/MHD-80-13, Dec. 1980.

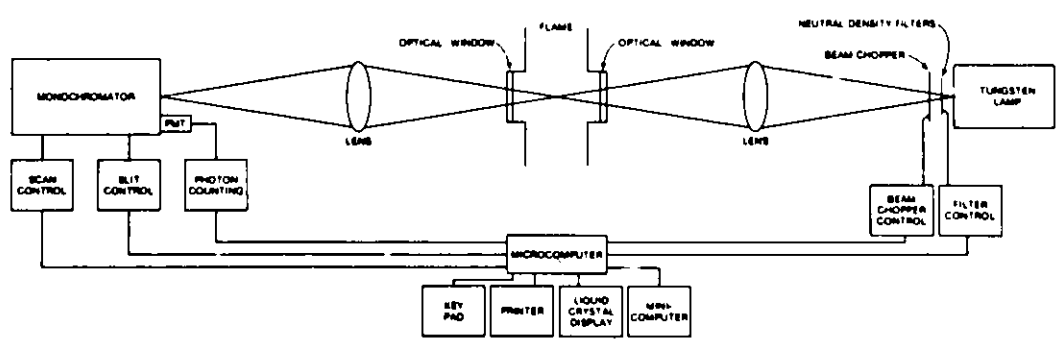

Figure 1. Block diagram of the line reversal system.

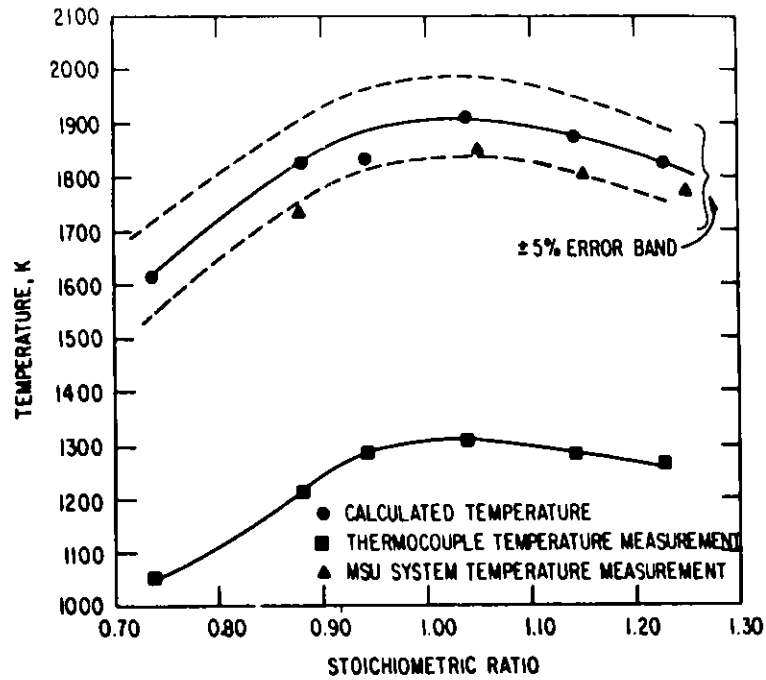

Figure 2. Gas temperatures for ANL/MSU 5/14/80 clean fuel tests.

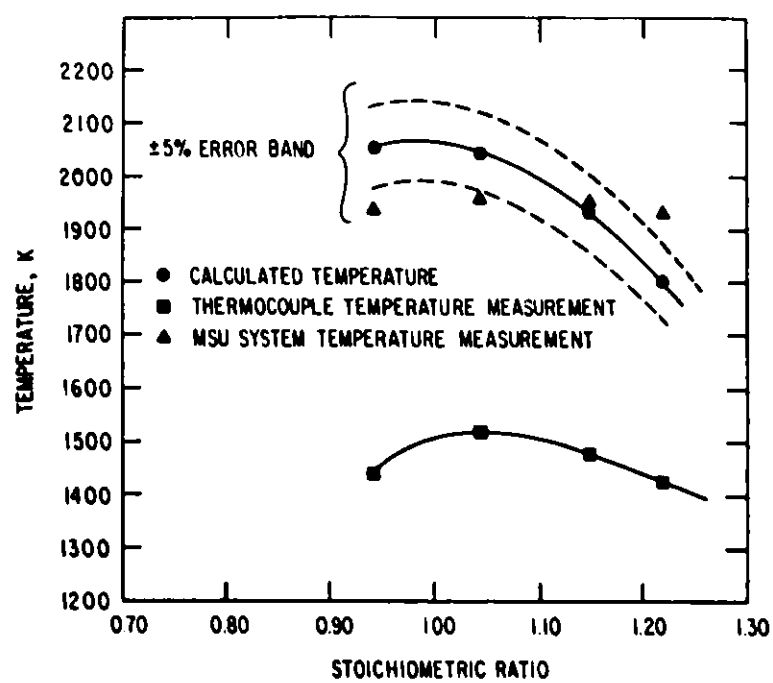

Figure 3. Gas temperatures for ANL/MSU 5/16/80 0.2% fly ash tests.

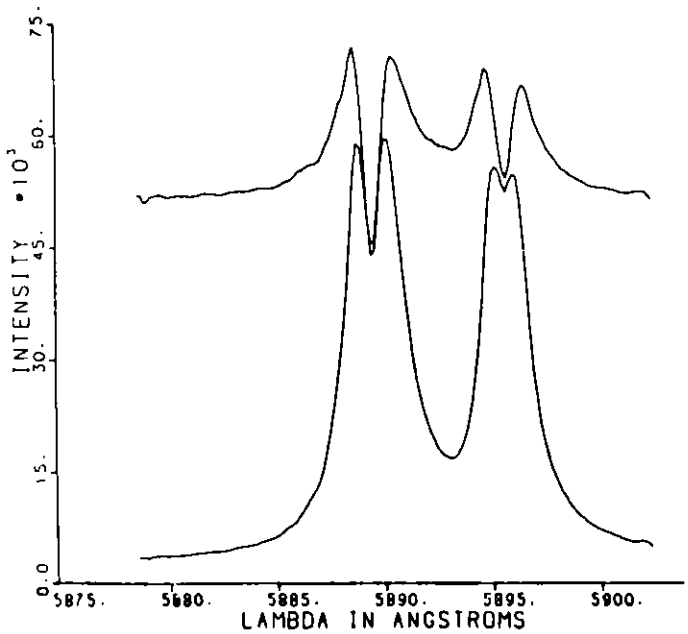

Figure 4. Lineshapes for ANL/MSU 5/16,1980 test with 0.2% fly ash and 1.05 stoichiometric ratio.

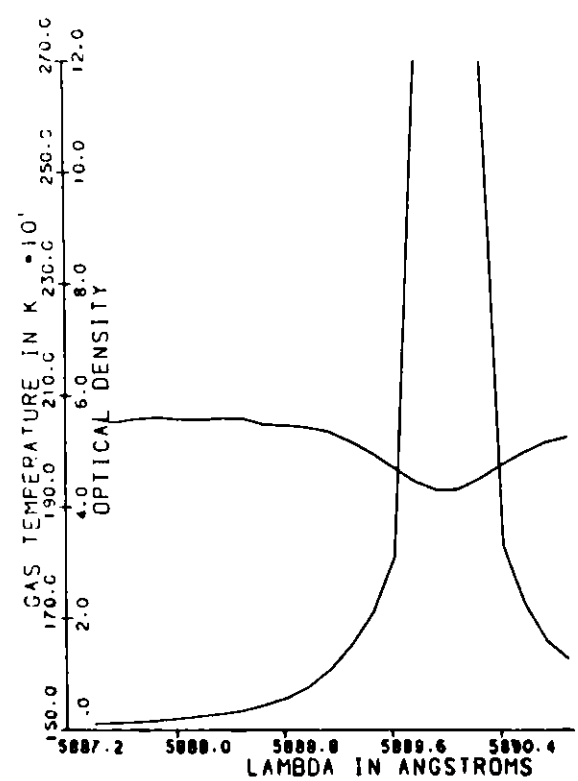

Figure 5. Clean solution temperatures and optical densities versus wavelength for ANL/MSU 5/16/1980 test with 0.2% fly ash and 1.05 stoichiometric ratio.

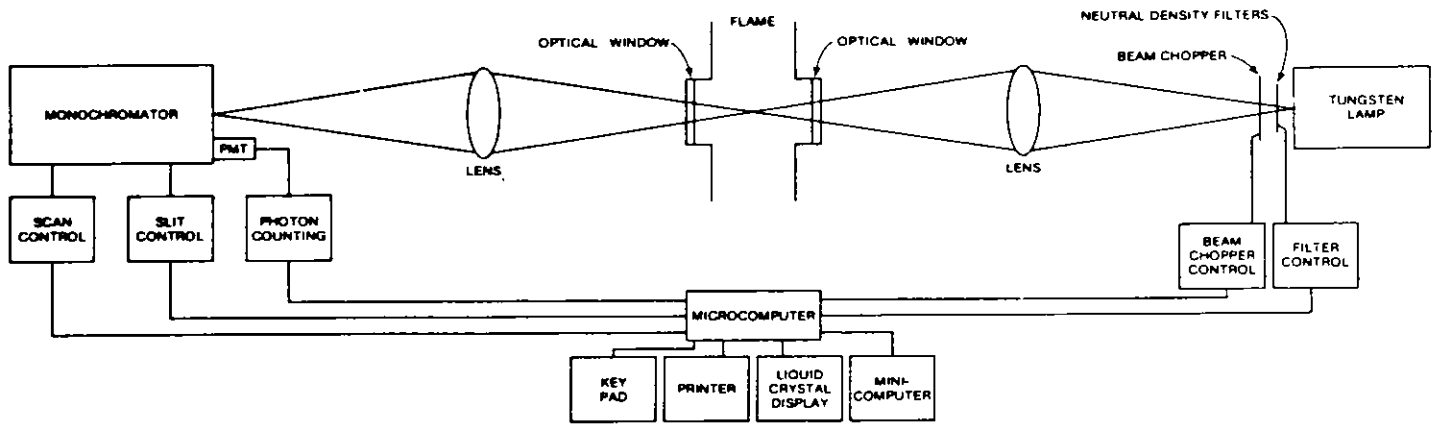

Figure 1. Block diagram of the line reversal system.

RAMAN-SCATTERING GAS TEMPERATURE MEASUREMENTS IN PARTICLE-LADEN FLOWS

W. L. Flower
Combustion Sciences Department
Sandia National Laboratories
Livermore, CA 94550

I. INTRODUCTION

The presence of particles in combustion gases introduces severe problems for the use of Raman-scattering techniques for making temperature and species concentration measurements. Incandescence from particles at the ambient gas temperature provides a radiative background which can exceed the weak Raman-scattering signal. Background-subtraction techniques (perhaps combined with high-powered pulsed lasers and gated detection) may be used to overcome the interference of this continuous background. A more serious problem arises when the energy of the individual laser pulses is sufficient to heat particles above the ambient gas temperature, causing the particle radiation to be modulated at the laser pulse repetition frequency. Discrimination against background radiation then becomes a more difficult task, since a portion of the background occurs only in coincidence with the Raman-scattered signal and is not eliminated by the standard gated-detection and background-subtraction technique.

The fundamental problem encountered when attempting Raman-scattering measurements in particle-laden flows is whether the probe laser power can be increased sufficiently to overcome the continuous background interference without causing significant laser-heating of the particles. This paper summarizes the results of an analysis for estimating perturbations in particle temperature induced by pulsed laser sources. One diagnostic system which is well suited for making time-averaged Raman-scattering measurements in flows containing micron-sized particles (e.g., fly ash) is identified. The remainder of the paper describes this system and its use in detail and describes experiments evaluating the feasibility of making Raman-scattering temperature measurements in various particle-laden environments.

II. DIAGNOSTIC SYSTEM SELECTION

If the uncertainties of making Raman-scattering measurements in luminous flows were determined only by the Poisson distribution describing the statistics of photon counting, data could always be acquired over a sufficiently long interval to yield an acceptably accurate difference between measurements of

signal-plus-background and background. The time t required to achieve accuracy $\epsilon = \Delta S/S$ in the signal is given by

$$t = \frac{1+2\frac{B}{S}}{\epsilon^2 S} \qquad (1)$$

where B and S are the average background and signal counting rates respectively, assuming that background and signal-plus-background are counted for equal times. This expression implies that enhancement of signal-to-background ratio, S/B, can lead to shorter data acquisition times, but that enhancement of S/B accompanied by a reduction in the signal counting rate can in some cases result in longer measurement times. In practice, measurement errors or temporal variations in the background can make it impossible to separate signal from background for small S/B no matter how long the integration time. Equation (1) does not account for such sources of error and is no longer appropriate when the dominant uncertainty is not that resulting from the statistics of photon counting. That is, S/B enhancement may be required to make accurate measurements even in some cases where Eq. (1) would indicate S/B enhancement is not profitable for reducing measurement time.

Reference 1 describes a simple theoretical model developed to predict the thermal behavior of a single particle irradiated by a pulsed laser source. Particles with radius greater than $\sqrt{\kappa\tau}$ (where κ is the thermal diffusivity in the particle and τ is the laser pulse length) are sufficiently large so that laser-heating of the particle surface is not affected by the finite particle size. Hence, it is reasonable to perform particle-heating calculations based on analysis of heat conduction in a semi-infinite slab. Such an analysis shows that the surface temperature perturbation induced by a laser pulse is proportional to the incident laser power flux and the square root of the pulse length but (by definition) independent of the particle size. For the case of small temperature perturbations of a dilute dispersion of particles, the total increase in the background interference from the dispersion of particles is proportional to the single-particle temperature perturbation (1). For particles much smaller than $\sqrt{\kappa\tau}$, it is reasonable to assume that the energy contained in the laser pulse has been uniformly distributed throughout the particle. The amount by which the particle has been heated may then be determined from simple energy conservation considerations to be proportional to the energy of the laser pulse and inversely proportional to the particle radius and the square of the laser beam diameter.

The system selected for the present experiments uses a cavity-dumped argon-ion laser (Spectra-Physics 166) laser of intermediate peak power (50-100W) and short pulse length (20 ns) combined with a high repetition rate (10^6/s) to obtain moderate average power (0.5-1.0W). The detection sampling gate width used with this system is 25 ns. This system improves the average signal-to-background ratio by a factor of about 10 relative to a

similar system using a 5-W continuous-wave laser, but the average signal count rate is reduced a factor of 5 relative to the 5-W system. The system hence improves the ultimate signal detection limit by a factor of 10 in cases where the statistical uncertainty of photon counting is not the dominant uncertainty. If photon-counting uncertainties are dominant, Eq. (1) indicates that in the limit of small S/B the pulsed Raman system reduces the time required to achieve a specified uncertainty by a factor of 2, relative to the 5-W cw system.

The predicted fractional change in particle surface temperature induced by the pulsed laser used here is $\delta T/T$ 7×10^{-3} for large particles. The slab model for large particles is a reasonable approximation for particles larger than 0.16 μm diameter. Figure 1 shows the value of $\delta T/T$ predicted by the model for particles irradiated by 20-ns, 100-W laser pulses in a 1-mm beam.

III. EVALUATION EXPERIMENTS

Experiments have been conducted to evaluate the performance of the Raman diagnostic system in four different environments which are similar to those found in different types of combustion systems: (A) a premixed methane/air flame which was moderately luminous but contained no particles was used for the initial checkout of the diagnostic system and data analysis procedure (2,3); (B) tests on a high-temperature arc-heated flow seeded with large ($\approx$100 μm) non-light- absorbing particles provided a more severe test of the ability to discriminate against high levels of background luminosity and particle-scattered light (4); (C) experiments on a highly sooting methane diffusion flame indicated the limitations of the diagnostic system in the presence of very small particles; and (D) temperature measurements made in a simulated process stream seeded with 5 μm fly ash particles are believed to be the first reported Raman-scattering temperature measurements in a highly particle-laden flow. The results of these tests provide insight into the suitability of the Raman diagnostic described above for different types of combustion environments. Some major observations from tests A, B, and C will be summarized here. The tests in the simulated process stream (D) are the primary emphasis of this paper and will be discussed in greater detail.

A. Premixed Methane/Air Flame Measurements

The basic diagnostic system used in tests on all of the different environments is similar to that used for the premixed methane/air flame measurements, shown in Fig. 2. A reference pulse generator triggers an RF pulse generator which dumps the laser energy by means of an intracavity Bragg cell. Delayed pulses from two other pulse generators trigger two electronic gates: a signal gate timed to pass the Raman-scattered signal

plus a portion of the background signal and a background gate which passes only background. Separate counters for signal-plus-background and background alone register the signals passed by these gates. Detection gate widths were 25 ns for each channel. For the premixed methane/air flame tests, a retro-reflecting multipass cell was used (5), increasing the effective laser power in the scattering volume by a factor of about 20.

Raman-scattered light was collected at an angle of 90 degrees from the probe laser beam and was focused on the entrance slit of a monochromator used for wavelength selection. In tests on the premixed methane/air flame, a 3/4-meter single monochromator was used; a double monochromator was used in all other tests. A cooled RCA31034A photomultiplier tube at the monochromator exit was the detector. The amplifier-discriminator was a PAR 1121. The spectrometer grating was sequentially set at predetermined wavelengths in the N_2 Q-branch spectrum, and photon counts were accumulated in individual pass-bands determined by the slit configuration. At each wavelength setting, a pair of digital counters registered the number of photons counted during the signal-plus-background and background-only gates, the difference of which is the Raman-scattering signal. The pass-band data analysis technique described by Hill, et al. (3) was used to determine gas temperature from the measured N_2 Q-branch Raman spectra.

The luminous region of the premixed methane/air flame extended approximately 5 mm above the 4-cm-diameter Meker-burner surface; there was no visible yellow/orange emission due to soot. In the luminous region of the flame the ratio of Raman signal to background radiation ranged from 0.2 to 1.0 in the portion of the spectrum used for temperature fitting. Excellent fits of calculated Raman intensities to the measured spectra were obtained (2).

B. Arc-Heated Flow Measurements

In the second series of diagnostic tests, a D.C. arc heater was used for generating high-temperature, high-pressure flows of nitrogen (4). Tests were performed in both "clean" and particle-seeded flows of arc-heated nitrogen at a nominal temperature and pressure of 2000K and 5 atm. In the seeded-flow experiments, monodispersed glass beads (either 50 or 100 μm diam in different tests) were added to the flow in a mixing section immediately downstream of the arc. Even the clean flow was highly luminous ($S/B \approx 0.1$), but Raman-scattering temperature measurements were possible. The radiant background was larger still in the particle-seeded flow ($S/B \approx 0.04$) but the Raman-scattered signal could be measured; however, due to problems with the flow facility, steady flow conditions could not be maintained for the time required for a temperature measurement ($\approx$5 min). The experiments did demonstrate, however, that some of

the major obstacles to making spontaneous Raman-scattering temperature measurements in particle-laden flows could be overcome: the ratio of Raman signal to background was improved sufficiently to permit temperature measurements in this highly luminous flow, and scattering of the probe laser light by particles was adequately discriminated against.

C. Methane Diffusion Flame Tests

More recently, tests have been made on a sooting methane diffusion flame to investigate the limitations of the measurement technique in the presence of submicron particles (e.g., 0.05-0.1 μm soot particles). In tests in which a single pass of the probe laser was focused to a diameter of 50 μm in the luminous region of the flame, the detection system measured modulation of background radiation synchronous with the laser pulses equal to about 1/3 of the steady unperturbed background. When the laser beam was defocused to approximately 1 mm diameter, the laser-modulated component of the background was no longer evident. However, the steady background was about an order of magnitude larger than in the focused-beam case (because of the larger collection volume required), and it was not possible to resolve the Raman signal. We conclude from these tests that while particle-heating presents no fundamental obstacle to the use of this system in sooting environments when 1 mm spatial resolution is adequate, the very high concentration of soot particles ($>10^9/cm^3$) in the flame studied here presents too large a source of background radiation to permit a Raman-scattering temperature measurement.

D. Measurements in a Simulated Process Stream

In the tests described in the remainder of this paper the Sandia Atmospheric Combustor Exhaust Simulator (ACES) facility (6) was used to provide a well-characterized particulate-laden environment for testing the Raman-scattering diagnostic system at conditions simulating those found in the exhaust stream from a coal-fired combustor. In these tests methane was burned in the combustor and additional air was added immediately downstream to control the temperature. Size-classified fly ash ($\approx$5 μm mean diameter) from the Exxon miniplant pressurized bed facility was added to the gas flow using a fluidized blown-bed particle feeder capable of delivering micron-size-range particles at rates up to 10 g/min. The weight loss of the feeder was monitored using an electronic scale to provide a record of particle feed rates as a function of time. The optical diagnostics test section has uncooled walls and contains four optical ports with 50-mm diameter quartz windows arranged at 90° intervals around the circumference of the flow channel. Purge air is supplied to each window to keep the window surfaces clean. The optical-diagnostics test section is followed by a physical-sampling section into which an isokinetic sampling probe may be inserted to provide information on the particle size

distribution. Mean flow velocity in the diagnostic section was approximately 40 m/s.

Nine basic test states spanning the temperature and particle-loading ranges of the facility were selected for the experiments. Tests were run with low (0-3 g/min), medium (3-6 g/min) and high (6-12 g/min) seed rates at nominal temperatures of 925K, 1175K, and 1425K. These test conditions result in particle loadings up to 6000 particles/cm^3 (dust loading up to 0.3 grain/scf). For comparison, the dust loading at the exit of a coal-burning pressurized fluidized bed combustor would be approximately 1-2 grain/scf. One stage of cyclone cleanup would reduce the dust-loading about an order of magnitude. Hence, the conditions of the diagnostic tests were not quite so severe as would be found at the combustor exit of a coal-burning fluidized bed power system, but were "dirtier" than would be found after cleanup at the turbine inlet.

The argon-ion laser beam (488.0 nm line) was focused in the flow channel by a lens just outside the beam-entry window and was reflected back upon itself a single time using a concave mirror located outside the opposite channel window to provide two focussed passes ($\approx$250 μm beam diameter) of the beam through the scattering volume. Scattered light was collected at 90 degrees. A 2.5-mm-long segment of the beam was focused at a magnification of 2 on the entrance slit of a double spectrometer which provided wavelength selection. For these probe-volume dimensions, the probability that a particle will be located in the probe volume was 0.8 at the highest particle-seeding rate used; hence, it would not be practical to use a "smart" detection system which measured Raman-scattered light only when no particle was present in the probe volume.

A PDP 11/34 computer was used in these tests to control the spectrometer grating position, to time the integration period spent at each wavelength setting, and to record in memory the accumulated photon counts in each data channel.

In the normal test sequence the combustor facility was operated for at least 15 min before starting data collection to permit the system to reach steady operating conditions. Because of the limited capacity of the particle-seeder reservoir, the seeding of particles into the flow was not started until immediately before beginning the data collection sequence. The seeder was refilled between temperature measurements when necessary.

Data were typically collected at 8-10 different grating positions spanning a 2.5 nm interval in the Stokes vibrational Q-branch of nitrogen. The spectrometer passband at each setting was approximately 0.23 nm full width at half maximum (500 μm entrance and exit slit widths). The integration times at the different wavelengths were independently selected so that signal

would be integrated for a longer period in those portions of the Raman band where the scattering signal was lower and hence more difficult to accurately determine in the presence of high background luminosity. Typically, the integration time per grating position ranged from 20 to 150 s and the total time required to scan the Raman spectrum to obtain a temperature measurement was 7-15 min. If simultaneous multi-channel detection were used, the time required per temperature measurement could be reduced to 30-150 s (the range of maximum integration times for the various test conditions).

Accurate temperature measurement in the present experiments hence requires that the flow temperature remain constant for 7-15 minutes, the time required to scan the Raman spectrum. In some of these earliest tests on the new ACES facility, the mean temperature varied by as much as 30 K over the measurement period, as indicated by a thermocouple located within 2 cm of the Raman-scattering probe volume. The effect of these temperature variations on the accuracy of the Raman-scattering measurement of mean temperature cannot be evaluated without knowing the exact temperature history.

Some difficulty was also encountered in maintaining a steady particle-seeding rate. Seed rates cited in this report are averages over the measurement period. There was good agreement between probe measurements of particle loading in the flow and the particle loading calculated from the seed delivery rate and mean flow properties. Hence, in spite of the difficulty in achieving steady particle delivery, the measured particle seeding rate provided a good measure of the instantaneous particle loading in the flow.

Considerable difficulty was found in operating the laser at the rated 1-W average power (0.5 W was the typical actual average), and in maintaining constant power during a test (a 10% decrease in average power during a test was common). Laser power was continuously monitored during each test, and measured Raman-scattering intensities were normalized by the average laser power during the measurement period to correct for laser-power variations The fact that slight fly ash deposits accumulated on the flow-tube windows during a test also reduced the effective laser power in the scattering volume, however no correction was made for this effect (<5% loss of transmission).

No significant difference was observed between measured intensities in the signal-plus-background and background-only data channels when the spectrometer was tuned off the Raman band. Hence, there was no apparent laser-induced interference (i.e., fluorescence or laser-induced incandescence) with the Raman-scattered signal at any of the test conditions. The lack of laser-induced incandescence is consistent with the analytical model for the heating of irradiated particles which predicts a surface temperature perturbation less than 0.5% for these test

conditions.

The average measured radiation background increased linearly with the particle seeding rate for tests at a fixed temperature. In the tests at a nominal temperature of 1425 K, the background with no particles added to the flow was approximately 220 counts/s, increasing by about 60 counts/s for each additional gram per minute of particle seeding. Of the background with no particle addition, about 70 counts/s came from the ambient light in the test bay, and the remaining 150 counts/s came from the hot flow-tube walls. Hence, the walls contributed the same background interference as a moderate particle seed rate, ≈ 2.5 g/min (about 1500 particles/cm^3 for these test conditions). For the 1175 K tests, each additional gram per minute of seed delivery contributed only about 8 counts/s to the measured background, and the walls added about 10-20 counts/s. At 925 K, most of the background interference resulted from ambient test bay light at all particle loadings; i.e., particle or wall radiation was not a problem at 925 K.

In tests at 1425 K and at the highest particle seeding rate, the ratio of Raman-scattered signal to background radiation ranged from 0.01 to 0.1 in the portion of the spectrum used for temperature fitting. The corresponding S/B range was 0.07 to 1.0 for the highly seeded 1175 K tests. If the pulsed laser were operating at the rated 1-W average power, the pulsed Raman-scattering diagnostic would have a clear advantage at both of these test conditions over a 5-W cw system in measurement time required to achieve a specified photon-counting statistical accuracy (Eq. (1)). Since the pulsed laser typically ran at half the rated power, however, the time required to achieve a specified accuracy would be equal for the pulsed and 5-W cw systems if photon-counting statistics provided the major uncertainty. However, the 5-W system would provide values of S/B from 0.002 to 0.02 at 1425 K and from 0.014 to 0.2 at 1175 K. It is doubtful if photon-counting statistics are limiting in these cases, and it is believed the pulsed laser system still has an advantage, even at its reduced operating power.

S/B was between 0.15 and 2.0 for the 925 K tests at the highest seed rate; however, these numbers have little physical meaning since most of the background was from ambient test-bay light. If this light were eliminated, the 925 K S/B would be large enough so that it would be advantageous to use a 5-W cw laser rather than the pulsed laser.

Table I lists the Raman-scattering temperature measurements at the various test conditions. Temperature limits shown here are the uncertainties in the fit of the calculated spectra to the measured intensities. These values should be considered only as relative indicators of the quality of the fits to the data rather than as absolute uncertainty limits. They provide no direct measure of experimental sources of error such as changes in flow

conditions during the measurement period. As noted previously, the gas temperature varied by up to 20-30 K during some runs. The radiation-corrected thermocouple measurements listed here reflect the temperature set at the start of each run. The radiation corrections ranged from +20 K for the lowest temperature runs to +150 K for the tests at 1425 K. The tests have been grouped into "low," "moderate," and "high" seed rate experiments; however, this distinction is in fact insignificant for the tests at 925 K since particle radiation was not the major contributor to the background in the tests at 925 K. Figure 3 shows a comparison of measured N_2 Stokes Q-branch Raman spectra with the calculated best-fit spectra for tests at the three different temperatures at which tests were run. The average seed rate was greater than 7 g/min in all three tests shown in Fig. 3. Agreement between measured and calculated spectra is very good in all three cases.

TABLE I -- RAMAN TEMPERATURE MEASUREMENTS

	925 K SET OPERATING TEMPERATURE		1175 K SET OPERATING TEMPERATURE		1425 K SET OPERATING TEMPERATURE	
	SEED RATE G/MIN	RAMAN MEAS. T K	SEED RATE G/MIN	RAMAN MEAS. T K	SEED RATE G/MIN	RAMAN MEAS. T K
0-3 G/MIN SEEDING RATE	0.6	952 ± 7	0.0	1182 ± 5	1.1	1436 ± 14
			1.3	1179 ± 9	1.5	1436 ± 23
			3.0	1171 ± 11	2.7	1352 ± 26
3-6.5 G/MIN SEEDING RATE	6.3	1136 ± 23	5.5	1204 ± 13	5.0	1351 ± 20
	6.4	1054 ± 26				
>6.5 G/MIN SEEDING RATE	7.0	1250 ± 30	6.9	1179 ± 13	7.5	1516 ± 33
	8.3	942 ± 27	8.8	1212 ± 24	7.6	1542 ± 37
	11.6	1062 ± 34	10.0	1246 ± 19		

The major sources of error in the Raman-scattering temperature determination arise from uncertainties in the measurement of the Raman-scattered intensities, uncertainties in the fit of calculated intensities to the measurements, and variations in mean gas temperature during the tests. Uncertainty in the thermocouple measurements results primarily from the approximations involved in the radiation correction of the thermocouple measurement. For nearly all of the tests at 1175 K and 1425 K, agreement between Raman-scattering and thermocouple gas temperature measurements is good. However, for several of the low-temperature tests the agreement between Raman-scattering and thermocouple measurements is relatively poor. Since the

thermocouple measurements should be accurate here (the radiation correction is small), this discrepancy is attributed to inaccuracies in the Raman-scattering technique in this particular application, as discussed below.

Raman-scattering measurements should be relatively easy to make at the lowest temperatures since the gas density is highest here and the interfering background radiation is lowest. However, the v = 1 excited vibrational level of nitrogen has a lower population at these lower temperatures, and hence the v = 1→2 peak of the Raman spectrum (at about 549.7 nm in Fig. 3) is smallest in these tests. As shown by Setchell (7), the accuracy of the Raman-scattering temperature measurement is most sensitive to the ratio of the v = 1→2 intensity to the v = 0→1 intensity at lower temperatures. In addition to the difficulty of measuring a small signal in the presence of background interference, the fact that the flow tube windows were losing up to 5% in transmission during a test caused the measured ratio of the v = 1→2 intensity to the v = 0→1 intensity to be in error on the high side (since the scan was performed in the direction of increasing wavelength). This would cause the measured temperature to be higher than the actual temperature, which is indeed the trend for the low-temperature tests as may be seen in Table I. Accurate temperature measurements should be possible at these lower temperatures if longer integration periods were used and corrections were made for loss of window transmission.

IV. CONCLUSIONS

The most important conclusion to be drawn from the present study is that Raman-scattering measurements of the average gas temperature in particle-laden flows are indeed possible. Determining temperature from Raman-scattering measurements using a moderate-power pulsed laser and a gated detection system has been demonstrated to be feasible at temperatures and particle loadings similar to those found in some practical systems of current interest. The probability of finding a particle in the Raman-scattering probe volume was 0.8 in the tests at the highest particle-seeding rate used here. Minimizing the interference from particle incandescence by measuring Raman-scattered light only when no particle is present in the probe volume is therefore not a practical alternative in such highly particle-laden flows.

No significant laser-induced particle incandescence was detected for the diagnostic system used in this study, an observation which is consistent with a simple analytical model for the effect of laser irradiation on particle temperature. The model does show, however, that for some ranges of particle size and laser power, the probe laser will significantly perturb particle temperature and prevent Raman-scattering measurements. Particles in the soot size range ($\approx$50 nm diameter) will be perturbed by even the moderate-power pulsed laser used in this

study. Micron-sized particles will be perturbed by the high-power pulsed lasers required for "instantaneous" (i.e., single-pulse) temperature measurements.

The fundamental limitation on the application of Raman-scattering measurement techniques is the ability to resolve the small Raman-scattered signal in the presence of a large source of background radiation. This restricts the quantity of particles which may be present and still permit a Raman-scattering measurement, but even more importantly restricts the temperatures at which measurements may be made, since background radiation increases much more strongly with particle temperature than with particle number density. The net effect of increased particle radiation is to increase the measurement time required to accurately distinguish the Raman-scattered signal from the background. Application of the technique is in turn restricted to environments which are steady over the time period reuired for the measurement (≈10 min for these tests). The measurement time could be reduced to approximately 1 min if simultaneous multiple channel detection were used, which requires only a modest increase in the extent and cost of detection instrumentation.

This work was supported by the Office of Fossil Energy, U. S. Department of Energy.

REFERENCES

1. Flower, W. L. and Miller, J. A., "An Analysis of Particle-Temperature Modulations Induced by Pulsed-Laser Sources," Western States Section/The Combustion Institute Paper 79-18, April 1979.

2. Mulac, A. J., Flower, W. L., Hill, R. A., and Aeschliman, D. P., "A Pulsed Spontaneous Raman Scattering Technique for Luminous Environments," Applied Optics 17, p. 2695 (1978).

3. Hill, R. A., Mulac, A. J., Aeschliman, D. P., and Flower, W. L., "Temperatures from Rotational-Vibrational Raman Q-Branches," JQSRT 21, p. 213 (1979).

4. Flower, W. L. and Aeschliman, D. P., "Pulsed Spontaneous Raman-Scattering Measurements in a Highly Luminous Flow," SAND78-8263, August 1978, Sandia Laboratories, Livermore, CA.

5. Hill, R. A., Mulac, A. J., and Hackett, C. E., "Retroreflecting Multipass Cell for Raman Scattering," Appl. Optics 16, p. 2004, (1977).

6. Wang, J. C. F., Flower, W. L., and Hardesty, D. R., "Diagnostic Development for Advanced Power Systems," ASME Paper

80-GT-128, March 1980.

7. Setchell, R. E., "Analysis of Flame Emissions by Laser Raman Spectroscopy," Western States Section/The Combustion Institute Paper 74-6, May 1974.

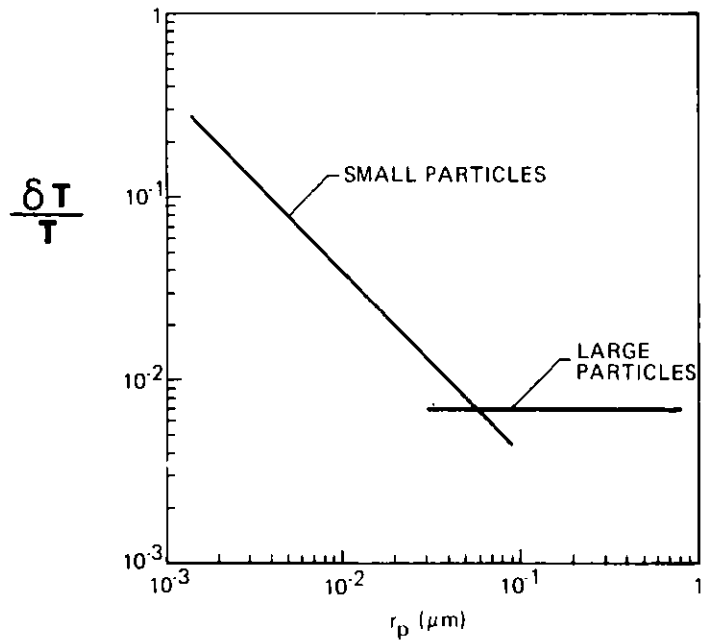

Figure 1 - Fractional change in particle surface temperature as a function of particle radius. Laser power = 100 W, pulse length = 200 ns, beam diameter = 1 mm.

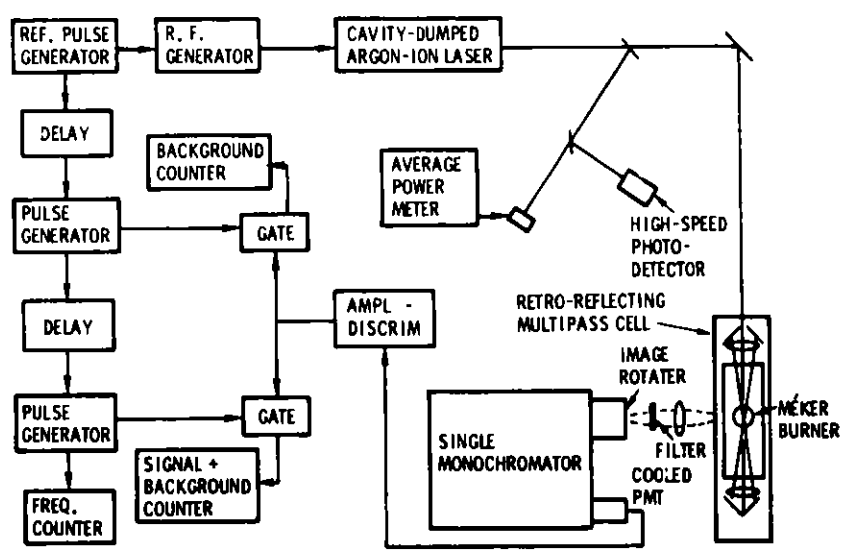

Figure 2 - Schematic of the pulsed Raman-scattering diagnostic for temperature measurement.

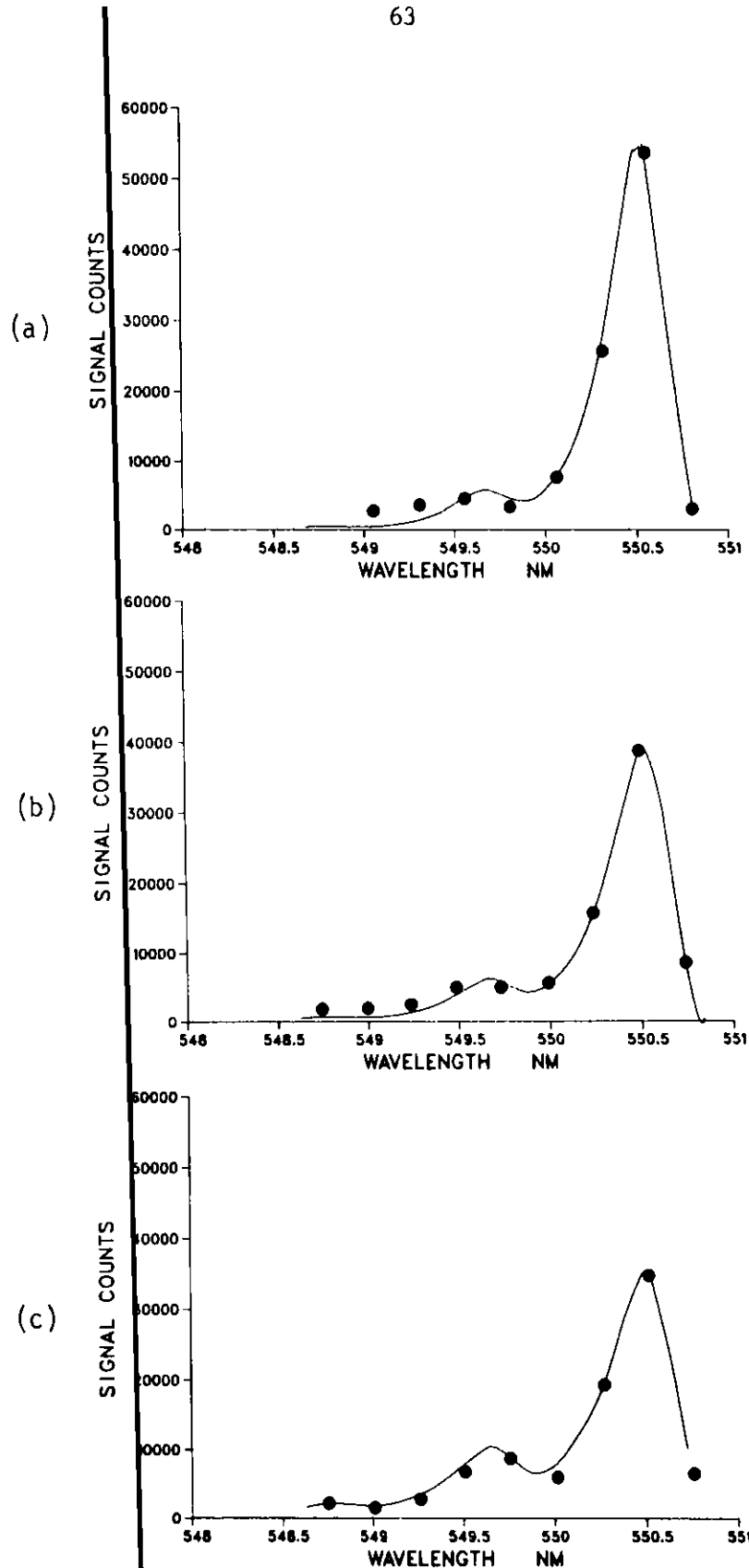

Figure 3 - Comparison of measured (•) Raman-scattered signal with the calculated spectra (-) which best fit the data for tests at (a) 925 K, (b) 1175 K, and (c) 1425 K nominal set operating temperature.

Monday Afternoon, June 8, 1981

Session A - Temperature

HIGH FREQUENCY ELECTROMAGNETIC BURN MONITORING UNDERGROUND COAL GASIFICATION

Frederick J. Deadrick*, Richard W. Hill and Edwin F. Laine
Lawrence Livermore National Laboratory
Livermore, California 94550
Mail Station: L-156
Phone: (415)422-8511
FTS: 532-8511

ABSTRACT A079

We have developed a high frequency electromagnetic (HFEM) remote sensing technique for the monitoring of in-situ burn fronts during underground coal gasification. The technique employs underground electromagnetic transmissions between boreholes to monitor changes in the radiowave propagation path as a function of burn activity.

By using several boreholes which span the burn path, and by raising and lowering electrically short antennas in the boreholes, multiple transmission paths may be traced to map the burn activity both vertically and horizontally. Changes in electrical conductivity of the coal occurs during the gasification, and by monitoring the signal paths as a function of time, we can map the location of the burn front.

In this paper we will describe our HFEM system and present some of the results obtained during the Hoe Creek-3 coal gasification experiment conducted near Gillette, Wyoming. The electromagnetic measurements will be compared with other test data including thermocouples and post-burn core sample results.

+This work was supported by the U. S. Department of Energy under Contract No. W-7405-ENG-48.

* Presenting Author

COAL ANALYTICAL REQUIREMENTS FOR OPEN CYCLE MHD POWER GENERATION SYSTEMS

F. E. Diebold, D. Dobb, & B. Christaens

Montana College of Mineral Science and Technology

The magnetohydrodynamics (MHD) power generation system coupled with a steam bottoming plant has a predicted efficiency of energy extraction that surpasses the conventional coal fired electric power generating plant. Due to the uniqueness of the MHD coal fired power system, there are some unique problems associated with the chemical composition of the fuel. It is the purpose of this paper to review some of these problems and to discuss the constraints the MHD system places upon the analysis of the solid fuel, coal.

In general the MHD coal fired system consists of burning pre-dryed coal ($\approx$ 2% moisture) with preheated air or oxygen enriched air (0.85 stoichiometry) to reach a plasma temperature of approximately 3000°K. In order to achieve the appropriate electrical conductivity of the plasma, K_2CO_3 is added to the combustor (1% K). The ionized gas is passed through a high magnetic field with the subsequent generation of a D.C. current. The temperature in the second and final stage of the combustor is higher than the ash vaporization temperature. Thus, that slag not rejected ($\approx$ 30%) in the first stage of the combustor is carried over into the channel in the vapor phase. Due to heat losses and power extractions, the plasma cools below the saturation pressure of the vaporized ash. The average radius of the slag droplets is typically 0.1 micrometer and the number density can be as high as $10^8/cm^3$. The volume of the plasma is increased in the diffuser so that the gas passes into a radiant boiler at $\approx$ 2200°K and $\approx$ 1 atm. The radiant boiler acts as an enthalpy extractor and condensed slag rejector. The gaseous ash and K_2CO_3 seed and nonoxidized volatiles exit at $\approx$ 1400°K into an after burner, in which this reducing gas is oxidized with preheated air or O_2-enriched air. Water that has been used to cool the walls of the combustor and channel are flashed to steam in the walls of the radiant boiler and after burner. Energy is extracted from this steam via a turbine, which in turn generates electricity. The cooled water is recycled to the combustor walls via some downstream heat extractors, through which the volatile coal components and seed are

passed. The sulfur is oxidized to sulfate in the after burner and as the temperature of the plasma is reduced in the air pre-heater, K_2SO_4 condenses and is removed by an electrostatic precipitator (ESP). This seed is converted to KCOOH and is recycled to the combustor. Environmental control is accomplished by NO_x reduction in the radiant furnace, sulfur capture by the K seed and particulate removal by the ESP.

The properties of the coal used as the fuel for this system do have a multitude of effects upon the performance of each component of the complete MHD system. The qualitative and quantitative effects of the coal properties are principally determined by thermodynamic data based computer calculations of equilibrium systems and limited simplified laboratory experimentation. The two coals selected as reference coals for these deliberations are Illinois #6 and Rosebud. There are two effects in the combustor, namely, the flame temperature and slag removed. The principal coal properties effecting the flame temperature is the Btu, moisture, and ash content. Computer calculations indicate that complete ash removal from Rosebud coal (8.7% ash) results in a 14% increase in the Btu and a 5% increase in the combustor flame temperature. The efficiency of slag removal in the first stage of the combustor is influenced by varying concentrations of the major metals (Na, K, Ca, Mg, Si, Al, Fe and Ti) in the ash. The prediction of the quantitative effect of these ash constituents upon the viscosity of the slag is difficult due to the interdependence of each component. There are four effects in the channel/diffuser, namely, the thickness of the slag layer, corrosion, and plasma and slag electrical conductivity. The thickness of the slag layer is influenced by the same major metals that effect the viscosity of the slag. A decrease in the FeO content of the ash is predicted to result in a decrease in the electrochemical corrosion of the cathode, less anode cavitation/erosion by O_2 and a diminution of dissolution corrosion. The conductivity of the plasma is significantly effected by the coal inherent moisture, heating value, amount of slag rejection, nonmetal concentration (H, F, P, C, S, & O) and major metal concentrations (Na, K, Ca, Al, Si, Fe, and Ti). The two effects in the radiant boiler are the rate of heat transfer and corrosion. A decrease in FeO and increase in SiO_2 contents in the coal ash have been observed to increase the slag fluidity and the increase of slag coating

does have a moderating effect of the refractory thickness on heat transfer. There appears to be insufficient data on the interaction between slag/seed and boiler materials in order to quantify the problems of corrosion. A decrease in FeO content of the ash has been suggested to result in a decrease in corrosion in the radiant boiler. The corrosion effects in the after burner are directly related to the reducing gases entering and the oxidizing gases exiting the burner. The reduction of FeO to Fe at the water cooled walls and the conversion of protective metal oxide films to sulfides by a high partial pressure of S in the reducing gases results in pitting and grain boundary penetration. K_2SO_4 is the principal condensate in the oxidizing gases and this sulfate acts as a flux and forms low melting mixtures with the protective metal oxide films. The function of the downstream components are heat and seed recovery. The combustor and radiant boiler can result in up to 90% slag rejection. Thus, K_2SO_4 constitutes most of the condensate in these downstream components and variations in coal ash components are of minor significance. Corrosion at the high temperature end is caused by K_2SO_4 and at the low temperature end by H_2, H_2O and trace amounts of chlorine in the coal. The efficiency of the seed recovery is significantly decreased by an increase of SiO_2 in the slag within the power train.

Although the quantitative effects of the coal properties upon the performance of the MHD system are not precisely known at this time, a list of the critical parameters has been established. Those coal properties that have been involved in corrosion, seed recovery and slag thickness have a relatively delayed effect. The implication is that these properties need not be determined in the coal within a short time frame, i.e., not continuously or in "real-time." Those coal parameters that effect the performance of the burner and the plasma electrical conductivity must be determined on a "real-time" basis. These are the Btu, moisture, ash, C, H, F, P, S, O, Al, Ca, Fe, K, Si, Na and Ti.

The time constraints imposed on the "real-time" coal analysis system can be determined by examination of the coal preparation system and coal feed rate into the combustor. The coal preparation system consists of a primary crusher, coal predryer and secondary pulverizer that are designed to reduce the coal to 100% -20 mesh and 80% -200 mesh and the moisture

from 35% to 2%. This coal is eventually fed under N_2 pressure (344 psia) to the combustor at a maximum flow of 13,800 lb/hr. Due to the cyclical operation of the flows into the coal injector hopper (3450 lb. in 3 min.) and the capacity of the coal injector hopper, the sequential analysis must be completed within 27 minutes and consist of gaining a representative sample from 3450 lb. of coal being fed into the coal injector within 3 minutes. Analysis of the coal stream into the next vessel, the lock hopper vessel, allows for an analysis of 32 minutes and 10 minutes to gain a representative sample of 3450 lb. of coal. The next analysis point that allows for a gain in analysis time is further back in the coal preparation system, i.e., of the coal fed into the 58 ton capacity storage bin. The continuous analysis of 3450 lb. of coal need not be completed for $\approx$ 9 hours. A further gain in analysis time ($\approx$ 20 hours) is at the point where coal (3/4" by 0 particle size and variable moisture content) from the primary crusher is fed into the 80 ton capacity storage bin. The major problem associated with analysis of coal at either of these two points further back in the coal preparation system is the uncertainty of the data representing that coal being fed into the combustor. This problem is due to the return of larger particles from a scalping screen. A similar problem associated with the coal analysis at points removed from combustor is the effect of the coal preparation components upon the variation of the coal properties.

In order to access the effect of a coal feeding system upon the variation in coal properties, a system in a conventional coal fired power plant was investigated. Coal was sampled prior to the distribution bin which distributes coal to the five silos in each power unit. Each silo feeds coal, via a paddle wheel dispenser into a bowl mill. Preheated air delivers coal (70% -200 mesh) from the bowl mill (20 tons/hr.) to the burner. Coal was sampled prior to the bowl mill, between the bowl mill and the burner and in the heavy particle rejection hopper. The analysis of these samples revealed that the range of the Si, Fe and total S concentrations and of the ash, moisture and Btu contents did not change significantly in coal fed into the plant compared to the coal fed to the burners. The range of Ca and K concentrations significantly decreased and that of Al and P significantly increased. Thus, the variability of the coal chemistry was changed

for some elements. Additionally, the efficiency of this organic-inorganic separation system by air classification was specific for pyritic sulfur, Fe and Ca (as calcite). None of the other elements were perferentially rejected with the heavy particles. The organic sulfur was significantly increased in the heavy particle rejected coal. Thus, it is apparent that segregation of inorganics and organics can take place within a coal preparation system and sampling and analysis of the coal streams as close to the combustor is advisable.

Another important consideration for the design of an appropriate "real-time" analysis system is the range of elemental concentrations and other coal properties to be expected. Since the Rosebud coal seam has been selected as the Western U. S. standard MHD coal, tipple samples collected at a conventional power plant have been analyzed over an approximate 2-year period. Each tipple sample represents a day's supply of coal to the two power generation units (400 tons/hr.) and the average concentrations represent 6.7×10^6 tons of Rosebud coal. Selected data are presented here as the average, daily variation expressed as % relative standard deviation and the analytical precision in parenthesis. Btu: 8733 $\pm$ 2.56 ($\pm$ 0.22), Ash: 8.67% $\pm$ 10.31 ($\pm$ 0.73), Moisture: 24.75 $\pm$ 6.61 ($\pm$ 0.76), S_{total}: 0.72% $\pm$ 19.89 ($\pm$ 4.2), C: 48.30% $\pm$ 11.99 ($\pm$ 2.06), H: 3.55% $\pm$ 5.16 ($\pm$ 2.73), N: 0.75% $\pm$ 15.34 ($\pm$ 4.32), Na: 0.026% $\pm$ 59.38 ($\pm$ 4.06), K: 0.033% $\pm$ 41.02 ($\pm$ 2.40), Ca: 0.82% $\pm$ 21.90 ($\pm$ 2.26), Mg: 0.18% $\pm$ 17.81 ($\pm$ 1.53), Si: 1.16% $\pm$ 13.53 ($\pm$ 1.52), Al: 0.68% $\pm$ 13.76 ($\pm$ 1.05), Fe: 0.37% $\pm$ 32.16 ($\pm$ 1.41), Ti: 0.031% $\pm$ 11.31 ($\pm$ 1.07), P: 0.0084% $\pm$ 37.10 ($\pm$ 10.17). The variation of each group of 27 day samples was also calculated. Additionally, the cumulative distribution plots were generated for each of the elements. The range of concentration that must be assimilated by a "real-time" analysis system were taken to be the values for the 95% and 5% cumulative probability. These values of the critical elements are expressed as mass/100g of coal. Moisture (0.5g-5.0g), C (46g-69g), H (4.1g-4.8g), N (0.75g-1.2g), S (0.55g-1.7g), P (0.005g-0.017g), Na (0.011g-0.06g), K (0.020g-0.067g), Ca (0.8g-1.5g), Mg (0.17g-0.29g), Si (1.5g-2.3g), Al (0.7g-1.1g), Fe (0.25g-0.75g), Ti (0.039g-0.056g).

Thus, the analysis system must be capable of the reaching above detection limits, of analyzing the range of concentrations, of obtaining

a representative sample of 3450 lb. of coal delivered within 10 mins., and reporting concentrations within approximately 30 minutes.

THE APPLICATION OF INFRARED-REFLECTANCE TECHNIQUES TO THE MONITORING OF MOISTURE IN COAL PREPARATION PLANTS

Günter Fauth
Bergbau-Forschung GmbH
4300 Essen 13
Federal Republic of Germany

ABSTRACT

Laboratory investigations have shown that in spite of the high absorptance of the black coal, moisture content of coal can be measured using the characteristic absorption bands at 1.94 µm and 2.94 µm. Using a commercial infrared moisture meter equipped with a monochromator, infrared reflectance spectra of moist coal samples of different top size, ash content, and type of coal can be obtained. Though the infrared reflectance technique suffers from a considerable influence of particle size, requiring calibration curves for each coal product in a preparation plant, it involves the important advantage that no special sampling is required and no influence of bulk density is exhibited. Several infrared reflectance meters have been tested on conveyor belts for metallurgical and steam coal and on filters for dewatering flotation sludges. Results and experiences of both the laboratory and the on-plant investigations are presented.

INTRODUCTION

The necessity of process control for hard coal preparation plants was stated repeatedly and in detail throughout the last Symposia on Instrumentation and Control for Fossil Energy Processes (1,2). One of the important prerequisites for process control is the availability of rapid-measuring devices for on-stream determination of moisture content. Moisture content needs to be measured and monitored on a variety of partial products as e.g. dust, centrifuged coal, dewatered sludges, middlings, and also final products like metallurgical or steam coal, for controlling individual equipments or process steps as e.g. screening, froth flotation, dewatering, blending and proportioning. Besides the quality criteria which read ash content, water content, and rank of coal, also particle size is a distinctive feature of the products. Said products are supposed to be measured and assessed either on conveyor belts at a transport rate of more than 1000 t/h or directly in preparation units as e.g. drum filters, belt-filter presses, or vacuum-belt filters.

For on-stream moisture determination of hard coal various physical measuring methods are available. Among these are the conductivity method, the capacitance method, various microwave techniques, and the infrared-reflectance (IRR) method (3-6). Since the required accuracy depends on the measuring and control task in question, and since the disturbance factors conditioned by changing bulk density, ash content, salt content, rank of coal, and temperature, vary considerably for the individual measuring methods, the best-suited method needs to be determined according to each individual task and for each individual product. The IRR-method seems to be suited for many tasks since it does not imply mechanical contact to the coal stream and consequently can be integrated directly into the process line without any separate sampling becoming necessary.

PRINCIPLES OF THE INFRARED-REFLECTANCE METHOD

This method implies intensity measurement of diffused reflected radiation of monochromatic light beams directed on the product stream. A part of this radiation hitting the surface of an absorbing substance is reflected, and another part penetrates the matter by refraction. Within the irradiated matter another portion is absorbed and the rest leaves the material and is refracted again. In case of pulverized matter these three processes viz. reflection, refraction, and absorption on and within the individual particles happen several times successively. In this case, additional scattering effects are likely to occur. Since the reflecting surfaces of all individual particles are oriented irregularly, no regular reflection is obtained but a diffused one which frequently is referred to as remission.

In case of mere mirror reflection on a plane surface, reflectivity increases, according to the Fresnel formulae, with increasing absorption coefficient. In contrast to this, reflectivity decreases with absorption in case of diffused reflection. These relations have been extensively discussed by KUBELKA and MUNK (7). Accordingly, reflectivity R is expressed as follows:

$$(1) \qquad F(R) \equiv \frac{(1-R)^2}{2R} = \frac{k}{s} \sim \frac{\varepsilon \cdot c}{s}$$

where k and s stand for absorption and scattering coefficient respectively. F(R) is defined as KUBELKA-MUNK function. A graph of this function is shown on Fig.1.

By reflectance measurement, therefore, concentration of absorbing components can be determined. This applies in particular if use is made of the selective absorption properties of the matter which, in the infrared range, are marked by characteristic absorption spectra. In case of moisture determination, the absorption bands of water in the near infrared range are relevant. They result from fundamental vibrations of the oxygen and hydrogen atoms in the water molecule as well as from their combination- and harmonic-vibrations. Fig.2 shows the logarithmic dependence of the absorption coefficient on wavelength. For moisture determination, the absorption bands at 1.45 µm, 1.94 µm, and 2.94 µm are particularly suited. In case of high water content and low basic absorptance of the material to be measured, measuring should be done at 1.45 µm or 1.94 µm, while in case of low moisture content or high basic absorptance, better results are obtained with the 2.94 µm absorption band.

As shown by equation (1), besides absorption also scattering will affect the reflectivity R. In order to reduce the influence of inconsistent and varying scattering as well as for avoiding measuring errors by ageing of the light source, dirt in the optic path, changing detector sensitivity, and amplification variations of the electronics, one or several reference wavelengths are used in industrial measuring instruments. These wavelengths are selected in a way that reflectance is not affected by moisture content.

In case of IRR measurements the water content is only recorded for the surface of the product. The penetration depth of the infrared radiation into water and the solid product itself is extremely low: the respective

value for water reads approximatly 0.3 mm at 1.94 µm. In industrial operation of this measuring method it is therefore absolutely necessary to have a constant correlation in time and space between the superficial moisture and total moisture.

Fig.3 shows the basic principle of the measuring technique used , with modifications, by almost all suppliers of commercial IRR instruments. The radiation generated by a light source is directed on the sample via focussing lenses and a mirror system. The wavelengths for the water absorption and reference measurement are generated by interference filters fitted to a rotating filter disk. The radiation reflected from the sample surface is bundled by a domed mirror and directed onto a photo-resistor.

The measuring device supplied by Pier-Electronic, Germany *, indicates the electronically generated difference A between the reference signal (I_R) and measuring signal (I_M). According to eq. (2) this corresponds to the ratio of both signals if the reference signal is maintained constant.

$$A = U(I_R) - U(I_M) = \text{const} \quad 1 - \frac{U(I_M)}{U(I_R)} \tag{2}$$

Since ageing of lamps and changing sensitivity by temperature effects may often be wavelength-dependent, two additional beams I'_M and I'_R is made use of in the Quadrabeam instruments supplied by Moisture Systems Corp., USA *, for better stability. These two reference beams are directed on the detector without passing by the sample, and evaluated as follows:

$$A = \frac{I_R}{I_M} \cdot \frac{I'_M}{I'_R} \tag{3}$$

The use of a second reference wavelength as practiced by an instrument supplied by Infrared Engineering, England *, is also intended to increase stability.

---

* Reference to a specific company is intended to facilitate understanding and does not imply endorsement by the Bergbau-Forschung GmbH.

FUNDAMENTALS OF WATER CONTENT DETERMINATION ON HARD COAL BY THE INFRARED-REFLECTANCE METHOD

In contrast to largely prevailing opinion, the initial tests already have shown that the IRR method for moisture determination can also be applied on the weakly reflecting hard coals. For a variety of types of coals well-founded calibration curves could be obtained. These initial measurements however, also have shown that the shape and the position of the calibration curves are largely affected by different interference filters. The spectral remittance received by the detector results from convolution of the spectral reflectivity of moist coal and the transmission function of the narrow-band interference filter. The determination of the transmission function and the characteristic properties derived therefrom as e.g. wavelength, transmittance, and half-width, is quite easily performed with conventional commercial infrared spectrometers. On the other hand, it was not yet possible to measure a reflectance spectrum of the water absorption bands in the coal by means of available reflection spectrometers due to the insufficient reflectance of the wet coal.

Therefore the sensor of an industrial IRR instrument was modified in such a way that one wavelength could be tuned continuously in the range between 1 and 3 µm by a separatly irradiated monochromator. The second wavelength was determined by an interference filter. The optic path of this modified sensor is shown on Fig.4. Since this measuring array is to be regarded as a single-beam spectrometer, comparative measurings with reference substances cannot be carried out synchronously but only consecutively. Correlation and evaluation of the consecutively measured spectra of wet coal and the reference substance was done by means of a desktop computer connected via an interface bus to the measuring array. This measuring array enabled determination of the spectral dependence of the water absorptance for a series of coal samples characterized not only by various moisture contents but also by varying particle size. As a typical example Fig.5 shows the indication of this reflectance measuring instrument for a metallurgical coal of different moisture content relative to dry coal as reference substance.

Fig.6 shows that the position of the maxima of the absorption bands evaluated for the above mentioned coal samples is dependent on the moisture content and the particle size and is situated within 1.93 µm to 1.955 µm. The half-width of these bands is about 80 to 120 nm. The position of the absorption band depends on the bond strength of the water to the coal surface. The bond type in turn depends on water content and the available surface resulting from the pore volume and the particle size. The half-widths of the transmittance function for the interference filters as used in commercial IRR instruments, however, are so great at 90 nm that a shifting of the water absorption band by approximately 20 nm resulting from various water bond types can be ignored generally.

Once the spectral dependence of water absorption is known for moist coal, the choice of the best-suited filter can be made. First of all, the filters should exhibit a highest-possible transmittance. The center-frequencies should be selected in a way that the transmission function of the reference wavelength filter and the water absorption band does not overlap and that a shifting of the water absorption band remains without effect.

Besides the 1.94 µm band discussed here in detail, also the 2.94 µm band is of interest for moisture determination on hard coal because of the high water absorptance and the resulting high sensitivity. This wavelength, however, implies use of more expensive quartz optics and more sensitive photo-detectors, which generally have to be cooled. Fig.7 shows a comparison of calibration curves for the measuring wavelengths 1.94 µm and 2.98 µm. As expected, due to the absorption constant which is higher by a factor of about 100, the sensitivity at 2.98 µm is by several times higher than at 1.94 µm. On the other hand, however, in case of moisture contents above 8 to 10 wt-%, saturation effects occur. With this type of coal the water-film thickness may be derived from the particle size distribution and the water content as to be about 3 µm. This implies that the radiation intensity is reduced to 2 % of the initial intensity within this water layer. In case of water contents exceeding 10 % the whole water-film thickness therefore is no longer measured. The high sensitivity in particular with small particle sizes makes appear the

2.94 µm absorption band particularly suited for investigations on coal-dust drying processes. Generally, for moisture determination of coal products found in coal preparation, the sensitivity given at 1.94 µm is completely sufficient so that further measurements for determination of interfering factors were consequently carried out only with this wavelength.

BASIC INVESTIGATIONS ON EFFECTS OF DISTURBANCE VARIABLES

Fig.8 shows the influence of particle size on the indication of an IRR instrument as a function of the water content. The measured values shown are those for a medium volatile coal with purposely prepared - and thus known - particle size distribution with top sizes of 1, 3, and 10 mm. The same results, qualitatively, are obtained if, by integration, calibration curves are constructed from the reflectance spectra obtained from the modified sensor system described above. It may be recognized that the sensitivity increases with particle size. Since the depth of penetration into the coal substance is negligibly low, absorption of the infrared radiation primarily takes place only in the water film around the coal particles. The thickness of the water film at a given water content decreases with larger surface i.e. with smaller particle size. The following table shows the decrease of the water film thickness at decreasing average particle size at a moisture content of 10 wt-% for the coal samples represented in Fig.8:

	Maximum Particle Size	Average Particle size	Idealized Surface	Water-Film Thickness
No.8	10 mm	5.3 mm	12 m^2/dm^3	10.7 µm
No.5	3 mm	1.6 mm	39 m^2/dm^3	3.3 µm
No.2	1 mm	0.16 mm	390 m^2/dm^3	0.3 µm

The direct measurements with an industrial instrument as well as the spectral investigations on the water absorption band show therefore that, when using IRR techniques for moisture determination of coal, basically the thickness of the water film around the coal particle is measured. This results in a strong dependence on particle size which requires a special calibration curve for each coal product obtained in preparation.

There are, however, fields of application in which basically not as much the water content is of interest but moreover a measure for the handleability and the flow behaviour of the coal. These properties are controlled more by the thickness of the water film around the coal particle than by the water content itself. Such tasks are involved e.g. in monitoring of screening and in pellets production.

In the lower part of the calibration curve, a deviation from linearity occurs which is conditioned by the evaluation process for the individual reflectance signals of the industrial IRR instruments. Only the direct indication of the KUBELKA-MUNK function F(R) is likely to yield a linear calibration curve. In operation practice, however, a limited moisture-measuring range only is required, so that this deviation from linearity is not too serious.

As almost every moisture measuring method also the IRR method determines the concentration of the water in the moist product by volume while, on the other hand, the water content is expressed generally in percent by weight. Disturbances therefore come up as soon as the density of the solid material changes. This happens in coal preparation in case of changing ash content. In contrast to this, changes in bulk density due to varied compression or particle size, cause no interference. As shown on Fig.9, the influence of ash content is based mainly on this volume effect. The dependence of the moisture indication for coal with different ash content but identical particle size distribution is shown. The moisture content is displayed once in percent by weight and once in percent by volume. In particular with high ash contents, the different background reflectance of the mineral components actually interferes. Furthermore, the rock components have no pore structure and are generally hydrophilic while coal is hydrophobic. This results in considerably different water binding phenomena and thus shifted water absorption bands.

Medium and high volatile coals do not show significant differences in IRR moisture determination. Anthrazite qualities, however, show greater deviations but they are mostly produced separately so that for each quality an own calibration curve can be used.

Using the conductivity method and the capacitance method, uncontrollably varying salt content interferes negatively in many cases. With the IRR method no influence of varying salt content could be stated.

ON-SITE INVESTIGATIONS IN COAL PREPARATION PLANTS

During measurements on laboratory scale, only relatively small surfaces of individual samples are inspected. In industrial operation, however, a continuous process stream is available for measurement so that statistical averaging methods can reduce the interference of disturbances, thus increasing accuracy. Published experiences and results of on-plant applications of the IRR method on moisture determination on coal are not known, except for coke (8). Therefore field investigations have been carried out over longer periods in three coal prep plants in the Ruhr District of West Germany.

The first site was a belt conveyor for the transport of the final product of the prep plant, in this case metallurgical coal, from the blending unit to the final product bunker. The IRR sensor was installed just downstream a transfer point on a bridge adjustable in height. By means of a ski-like device, the product stream was levelled over a width of approximately 100 mm. Two instruments supplied by different manufacturers were used over 6 months on a vacuum belt filter for dewatering of froth-flotation concentrate. The same instruments are now installed since approximately 6 months on the discharge of a standard ash monitor used for metallurgical and steam coal in alternating cycles.

Over the total testing period the instruments worked trouble-free. Outside, the optics of the sensors were fitted with a compressed-air flushing device which, as proven by repeated checks, was sufficient to keep dust and condensing humidity reliably off the optics. Light from outside the system did not affect measurements in any case.

Since with the IRR method only superficial water is detected, reference sampling from the process stream for checking calibration should be performed very carefully to be representative. Statistic evaluation of the

measuring results was made difficult by the fact that, under industrial conditions, the water content cannot be changed purposely over a wider range but varies only within narrow limits. Also additional moistening of the process stream cannot simulate live conditions satisfactorily. When stating accuracies, not only actual measuring errors of the instrument itself or errors induced by changing product properties is to be allowed for but also not completely representative sampling and errors in moisture determination by the oven-drying-method.

Fig.10 shows the results of investigations carried out on the metallurgical coal directly on the belt conveyor. For more than 200 samples a double standard deviation of the measured values of approximately 1 wt-% from a linear regression curve was recorded. This accuracy is sufficient for an acceptable moisture determination for simple control and monitoring tasks.

The measurements carried out on the vacuum belt filter yielded obviously less usable results. Both instruments installed yielded double standard deviations of about 2 to 3 wt-%. Investigations have shown that the fines content of the filter cake varied between 20 and 45 %. When eliminating this particle size influence by mathematical methods, a relative reduction of the standard deviation by 30 % was obtained. The changing fines content also results in a changing moisture gradient within the layer of the cake on the vacuum belt filter. A scraping of the layer for homogenisation and wiping off the fine froth layer yielded no improvement. The prerequisite for a constant correlation between superficial moisture and total water content can therefore not be met. Even though the measuring accuracy is not sufficient for controlling the operation of a vacuum belt filter, the IRR method is used successfully for monitoring the performance of the entire filter system operation.

The third field trial is still in progress. Here, a 3 t/h stream is sampled from the final product belt conveyor. This sample stream is conveyed by a screw conveyor through a plastic tube for determination of the ash content. At the discharge of said tube the coal sample exhibits a smooth surface which seemed to be very suited for IRR measurements.

It was found, however, that by the contact of the coal surface with the screw conveyor and the plastic tube as well as by changing compression of the sample, the correlation between superficial moisture and total water content is lost. Up to present no successful measuring therefore could be carried out on this site.

CONCLUSION

Measurements carried out on laboratory scale and in actual industrial operation have shown that moisture determination of hard coal may be possible by the infrared reflectance method. The method is suited for simple control and monitoring tasks within hard coal preparation. One of the advantages of the method is the fact that the respective instruments can be fitted to the process stream without causing any problems and that no particular sampling is required. A strong influence of particle size, however, makes the use of special calibration curves for each product to be measured compulsory. When selecting the installation site, care should be taken that a correlation, which is constant in time and space, between superficial moisture and total water content prevails. More challenging measuring and controlling problems may be met by microwave techniques. Investigations with very promising interim results on a phase-measuring method are in progress.

Research sponsored by the Arbeitsgemeinschaft Industrieller Forschungsvereinigungen e.V. under contract 3507 and 4350 and by the Energy R&D Program of the Government of the Federal Republic of Germany.

REFERENCES

1. K.R.Carr: Coal preparation plant automation: worldwide state-of-the-art and future directions. Proc. 1980 Symp. Instrumentation and Control for Fossil Energy Processes, Virginia Beach, Va, June 1980, pp. 104-122

2. G.Fauth: On-stream determination of ash and moisture content in West German coal preparation plants. Proc. 1980 Symp. Instrumentation and Control for Fossil Energy Processes, Virginia Beach, Va, June 1980, pp. 428-445

3. K.Hoffmann: Feuchtemessung durch Infrarotreflexion (moisture determination by infrared reflectance), Chemie-Ing.-Techn. 35(1963), pp. 55-62

4. F.C.Harbert, B.Sjoberg, J.Bak: Measuring moisture content on-line by infra-red method. Control & Instrumentation, January 1974, pp. 36-37

5. M.Goldstein: Near-infrared diffuse reflectance analysis - are we sure we know what we are measuring? SPIE Vol.197 Modern Utilization of Infrared Technology V (1979), pp. 256-264

6. B.Paul: A novel technique for infrared moisture measurement in paper mills. Siemens Forsch.-u. Entwickl.-Ber. 9(1980) No.2, pp. 105-110

7. P.Kubelka and F.Munk: Ein Beitrag zur Optik der Farbanstriche (a contribution to the optics of color paints). Zeitschrift Techn. Phys. 12(1931), pp. 593-601

8. Y.F.Bilimoria and J.L.Blattner: The infrared coke moisture analyzer at Inland,s No. 5 blast furnace. Ironmaking Proc., Metall. Soc. AIME 38(1979), pp. 216-223

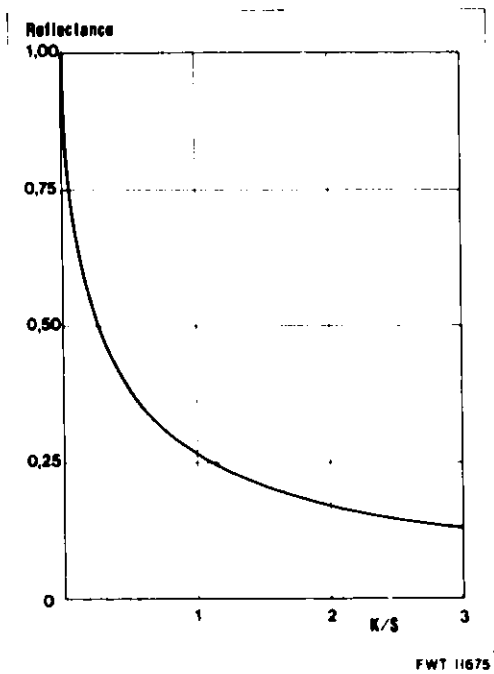

Fig.1:Dependence of reflectance on the ratio of absorption (k) and scattering (s) coefficient

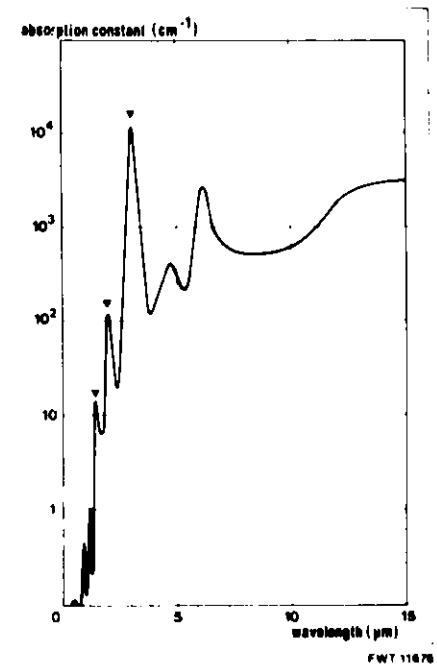

Fig.2: Absorption spectrum of water in the near infrared range

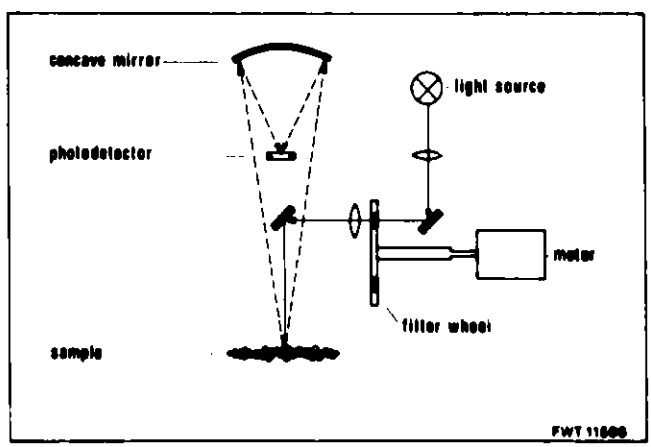

Fig.3: Measuring principle of infrared reflectance technique

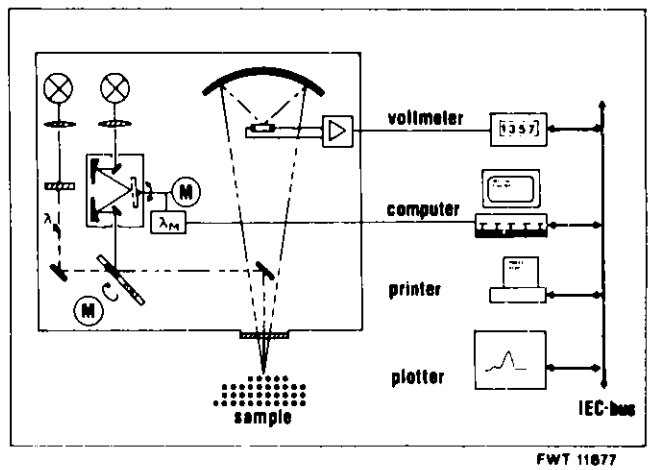

Fig.4: Diagram of the modified sensor instrument

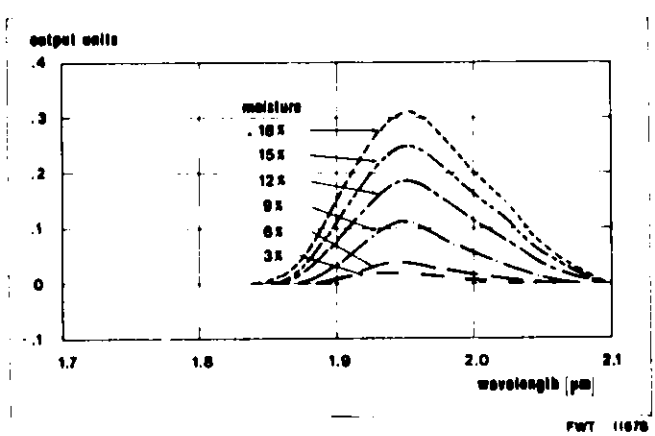

Fig.5: Reflectance spectrum of the water absorption band of a wet metallurgical coal of different moisture content

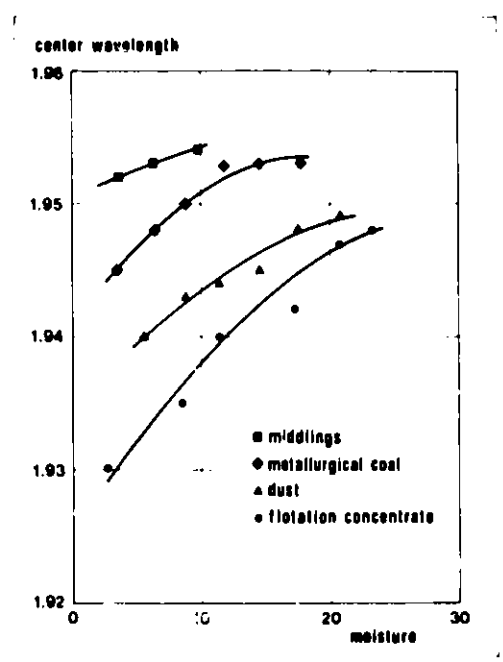

Fig.6: Dependence of the center wavelength of the water absorption band on moisture and particle size.
Top sizes:
Middlings 20 mm
Metallurg. coal 12 mm
Dust 1 mm
Flot. concentrate 0.75 mm

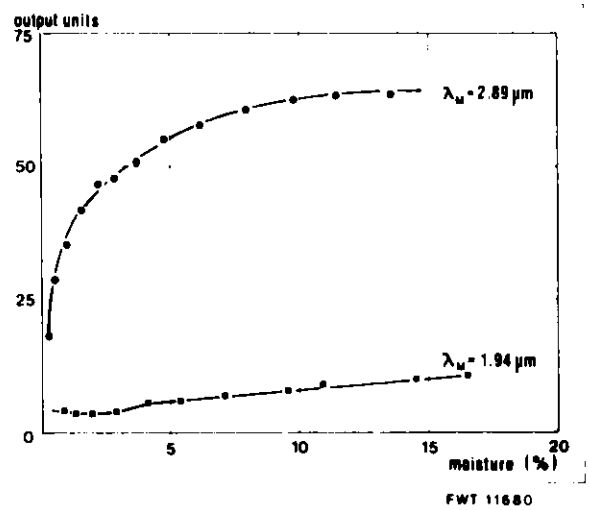

Fig. 7: Comparison of the IRR sensitivity at 1.94 µm and 2.94 µm of a top size 3 mm coal

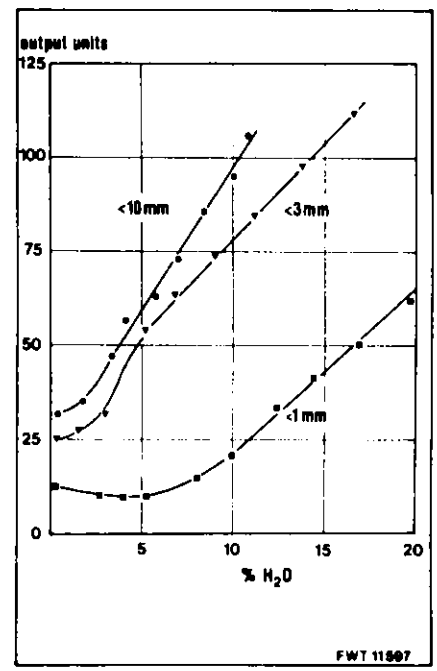

Fig.8: Influence of particle size

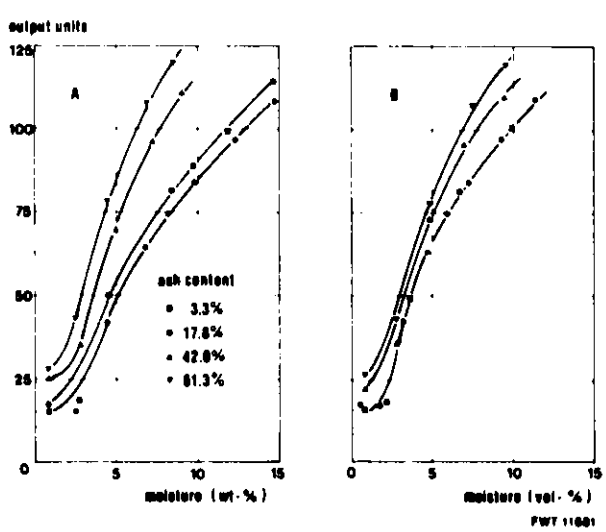

Fig.9: Influence of ash content

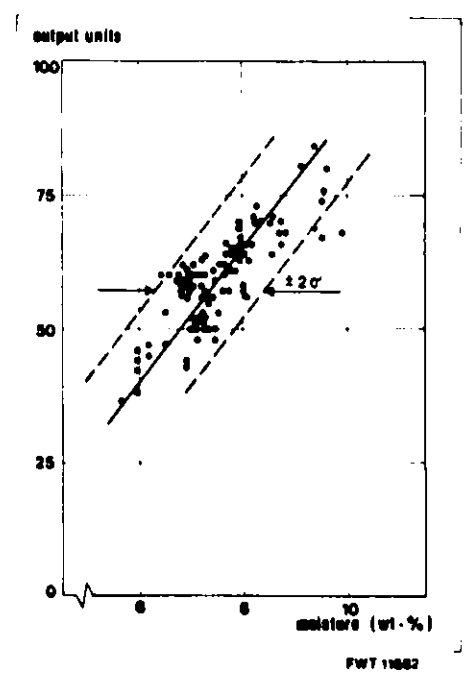

Fig.10: IRR results of a met. coal on a conveyor belt

Monday Afternoon, June 8, 1981

Session B - Analysis and Control

RESULTS OF ON-LINE NUCLEAR ANALYSIS OF COAL FOR PROCESS CONTROL

D. R. Brown*, T. Gozani, H. Bozorgmanesh,
C. Spencer, and H. Bernatowicz
Science Applications, Inc.
5 Palo Alto Square, Suite 200
Palo Alto, California 94304
Phone: (415)493-4326

ABSTRACT A075

On-line nuclear analysis of coal represents a significant advance in coal process technology. Real-time analysis of coal composition, ash content, and BTU value allow effective control of coal beneficiation and blending along with parameter control in synthetic fuel production. In coal fire plant, effective control of fouling and slagging of boilers can be achieved using on-line ash composition analysis.

In January, 1980, the first of these nuclear coal analyzers went on-line in a major U. S. utility to control the blending of high and low sulfur coals to meet stringent SO_2 emission requirements. The principles of operation of the analyzers are discussed. Data from on-line blending control will be presented showing the how composition analysis feedback can be used to maintain an optimum coal blending ratio.

Another new instrument, going on-line in summer of 1981, is a batch analyzer to control the scrubbing of coal in a coal washing plant. The specifications and uses of this instrument are discussed.

*Presenting Author

ON-LINE ANALYSIS OF COAL BY NEUTRON INDUCED GAMMA SPECTROMETRY ⁎

H.R. Wilde and W. Herzog
Staatliches Materialprüfungsamt NW, D-4600 Dortmund 41
Fed. Rep. of Germany

INTRODUCTION

Due to the increasing importance of coal for electric power generation as well as for gazification and liquefaction there is a growing need for on-line analysis of coal composition and quality in large process streams, since the efficiency of these combustion or conversion processes may be affected seriously by even small changes in coal composition [1].

Several methods for monitoring gross coal composition or special elements in the coal have been reported [2,3,4]. Among these the PNAA-method (prompt neutron activation analysis) has proven to be the most promising tool for the multi-element analysis of coal. This method is based upon the fact that the capture of a neutron by a nucleus leads to the formation of a highly excited compound nucleus which decays by the emission of γ-rays. The energy spectrum of these prompt γ-rays ($\tau < 10^{-10}$s) is characteristic of the emitting nucleus, and their production rate depends on the number of target nuclei, the bombarding neutron flux and the neutron capture cross section. So the number of γ-rays with a particular energy is directly proportional to the abundance of the emitting element. The use of isotopic sources such as Cf-252 allows the construction of relatively small irradiation facilities for the rapid analysis of large volume samples. For process control applications the analysis time must be less than the transportation time of the coal; this means, that an upper limit of 10 - 15 min. should be achieved.

⁎)Supported by Bundesministerium für Forschung und Technologie
D-5300 Bonn 1, Fed. Rep. of Germany

Possible applications include BTU-determination, ash analysis, sulfur determination or even complete elemental analysis for coal blending facilities or electric power plants. This paper presents the results of the laboratory experiments done at the Materialprüfungsamt Dortmund to study the effect of several parameters for optimal performance of an on-line coal analysis system.

EXPERIMENTAL

As a first step to an on-line analysis system for process control a testing facility has been built up using a Cf-252 neutron source with an actual strength of 1 mg. There were four main considerations in the planning of the experiments:

a) the 1 mg neutron source, installed for conventional activation analysis, had to be used,

b) the sample size should be variable in the range 50 - 150 kg,

c) the detector should have good energy resolution and low sensitivity against neutron irradiation,

d) the arrangement and the shields of neutron source, sample and detector should be designed flexibly to allow easy modification in order to optimize the system.

Following these design rules it will be possible to extrapolate from the data of the laboratory experiment to the parameters of a prototype system. A schematic graph of the experimental setup ist shown in Fig. 1. The sample and the detector have been installed on top of the screening container for conventional INAA analyses, separated by layers of borated polyethylene and lead to avoid activation of the iron in the container walls. The 1 mg Cf-252 source is moved up and down inside a zircaloy-tube by a step motor drive. Shielded by two cups of high purity lead and paraffin it can be moved out of the screening container to the center of the cylindrical sample holders containing up to 150 kg of coal. The source strength can be regulated within a

limited range by lowering the source position. To avoid background radiation the sample holders are made of polyethylene. They may be removed or installed with a small crane boom within a few minutes. The samples are surrounded by 10 cm of borated polyethylene - not shown in this figure - to reduce neutron induced background from the concrete walls of our laboratory.

The prompt gamma rays emitted from the sample are measured with a 22 % high purity germanium detector housed in a special horizontally extended cryostate assembly. The main advantages of high purity detectors compared with Ge(Li) detectors are the need of liquid nitrogen cooling only during operation and the apparently lower sensitivity to neutron damage. The use of NaJ detectors instead of germanium types has not been taken into account because of their poor resolution. The detector is positioned above the sample as shown in Fig. 1; it is surrounded by a multilayer decreasing-Z absorber to reduce low energy gamma background.

Paraffin loaded with 95 % enriched lithium-6-carbonate is used between sample and detector as a neutron absorber with good transmission for high energy gamma rays. From the backside the detector is shielded against thermal neutrons by a thicker layer of paraffin with natural lithium carbonate. Whereas the neutron absorption coefficients of natural boron and enriched lithium are about the same, the use of lithium is advantageous because it produces no gamma rays when capturing a neutron. In this way the total countrate is lowered by about 10 %.

The data processing system consists of fast linear amplifiers and a computer aided data acquisition system. Since the countrate amounts to 30 - 40 kcs due to the high strength of the Cf-252 source, the analogue electronics must be selected carefully; e.g. a combination of main amplifier and pileup rejector - though showing good performance in the test - caused uncontrollable loss of countrate in the experiment. So it was useless for a quantitative element determination. A 4096 channel pulse

height analyzer connected to a minicomputer collects the spectral data and allows an on-line analysis. A graphic plotter enables the immediate representation of the results.

Fig. 2 shows a spectrum of the background radiation measured with a pure polystyrene sample. For this measurement and for all further experimental data presented in this paper the collect time is 4000 s. Only a few photo peaks together with their escape peaks are to be seen: carbon and hydrogen are components of the sample material; lead and boron peaks are resulting from the shielding of the source and the detector, respectively;only small contributions to iron and silicon (in the low energy tail of the carbon peak, not shown here) come from the close concrete ceiling and must be subtracted from the analysis results. Moreover this spectrum shows that due to the compton background the first 1000 channels contain far more than half of the total countrate. Since the statistical error of peaks in this region is high and the sensitivity is low due to the high background, the first quarter of the spectrum is suppressed in all measurements. In this way the dead time of the analyzer is reduced by a factor of two; at countrates less than 10 kcs it amounts to 10 - 15 %.

OPTIMIZATION OF THE SETUP - TEST MEASUREMENTS

The sensitivity of this device is a complicated function of many parameters: it is not simply determined by the yield in a certain peak of the spectrum, because the background under the peak influences the experimental error, too. Both peak net area and background show a different energy dependence. So optimization of such a system must involve the arrangement of source, sample and detector, material and shape of the various shields and the source strength, simulated by variation of the source position. These test measurements have been done with a polystyrene coal matrix containing a few percent of sulfur or iron oxide. In order to save time and recycle material the added elements were filled into polyethylene bottles of 100 g

each and then distributed equally among the matrix. The result of optimizing the experimental arrangement is demonstrated in Fig. 3. It shows the high energy region of two spectra with 3400 keV$<$E$<$8000 keV. Whereas the background peaks of Si, Fe and Al (from the detector) are clearly suppressed, the spectral contrast of the elements in the sample, sulfur and carbon, could be increased appreciably.

Fig. 4 demonstrates the effect of changing the source position relative to the sample. Here the net area of the iron doublet 7632 + 7846 keV and the background under these not completely resolved peaks are plotted against the source position. In the scale of this figure zero means the highest possible position. Whereas the peak area does not change very much with the source position, the related background area increases steeply for positions $>$ -16 cm, thus giving rise to a quickly growing experimental error. The peaks of other elements show the same behaviour; however the starting point of the background rise depends slightly on the peak energy. A source position of -14 cm has proven to be the best value for this experimental setup.

Optimizing the performance the sample thickness is another important parameter. This test has been done with a high ash natural coal. Fig. 5 shows the behaviour of three different peak areas from all regions of the spectrum and the average trend of their related background when the sample thickness between the source housing and the detector is varied (c.f. Fig. 1). Within a few percent the peak areas may be regarded as independent from the sample thickness, whereas the background decreases clearly with rising sample thickness. This means that the accuracy of the measurement depends only slightly on the sample thickness, whereas the experimental error is affected appreciably by this parameter.

RESULTS AND DISCUSSION

Analysis of several samples of simulated coal as well as Western Germany coals shows a good spectral response of our system for the elements H, C, Al, Si, S,Cl, Ca, Ti and Fe, whereas the sensitivity for N, K and Na is lower. Fig 6 presents a spectrum of a coal sample from the Ruhr district with about 20 % ash content. The collect time is 4000 s. All elements mentioned above are to be seen clearly in this spectrum. Their absolute concentrations are not yet known - except sulfur and iron - because conventional chemical analysis is still under way. A preliminary calibration for sulfur and iron has been done by stepwise adding these elements to the coal sample. The added material was divided into portions of 100 g and packed in polyethylene bottles. The results of these measurements are shown in Fig. 7. Here the peak net areas are plotted against the added element content. In the upper part of the figure the peak area of the most prominent iron doublet and its single escape peaks is shown with different amounts of iron added. Obviously the yield is a linear function of the total element content, and thus extrapolating the two lines back leads to a basic iron content of about 3 %. Applying the same procedure to the three most prominent sulfur peaks shows good agreement for the 2379 keV and the 3221 keV lines. Extrapolating their yields leads to a sulfur content of about 1.1 %. The results of this calibration are compared with the wet chemical analysis results in Tab. 1.

Table 1: Comparison between chemical analysis and PNAA analysis results for sulfur and iron.

Element	yield per % in 1000 s ⁎)	chemical analysis	PNAA analysis
S	12.200 counts	1,35 %	1,1 %
Fe	9.100 counts	3,4 %	3,0 %

⁎) Only main peaks incl. escapes

The deviating behaviour of the 5220 keV yield shown by the dashed line is due to an interference of this sulfur peak with an iron escape peak. By this effect a much too high sulfur content is simulated. This deviation is an example what kind of errors may occur due to undetected interferences, if detectors with poor resolution are used; it demonstrates the necessity to use high resolution detectors in this type of experiments.

Calibration of the device will be continued by using the method described above as well as by analyzing samples with chemically determined elemental composition. As to be seen from the yields in Fig. 7 and Tab. 1 the quantitative determination of elements with good spectral response is now possible within 10 - 15 minutes time. Optimization of the system is continued with a stress on analysis time and detection sensitivity.

References

1) K. Hein, J. Engineering Power 99 (1977) 679

2) B.D. Sowerby, Nucl. Instr. Meth. 160 (1979) 173

3) A.W. Hall, I.W. Martin, R.F. Stewart and A.M. Poston, Precision Tests of Neutron Sulphur Meter in Coal Preparation Plant, Bureau of Mines Report No. 8038 (1975) 1

4) T. Gozani, The Development of Continous Nuclear Analyzer of Coal, ANS Trans. 28 (1978) 97

5) C.L. Herzenberg, N.M. O'Fallon, B.S. Yarlagadda, R.W.Doering, C.E. Cohn and K.G. Porges, Neutron-Induced Gamma Spectrometry for On-line Compositional Analysis in Coal Conversion and Fluidized-Bed Combustion Plants, Proceedings of the Third International Conference on Nuclear Methods in Environmental and Energy Research, Columbia, MO 1977

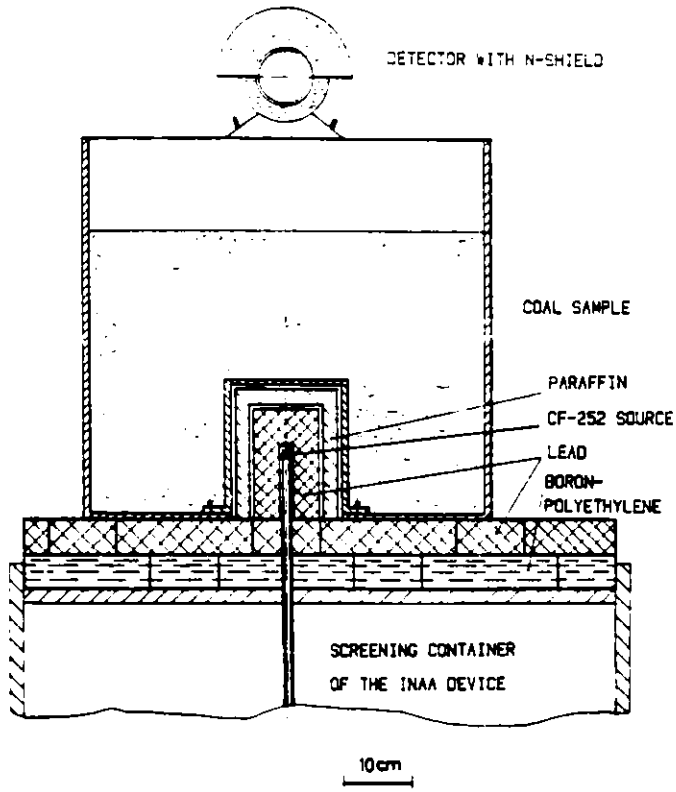

Fig. 1: Schematic graph of the experimental setup.

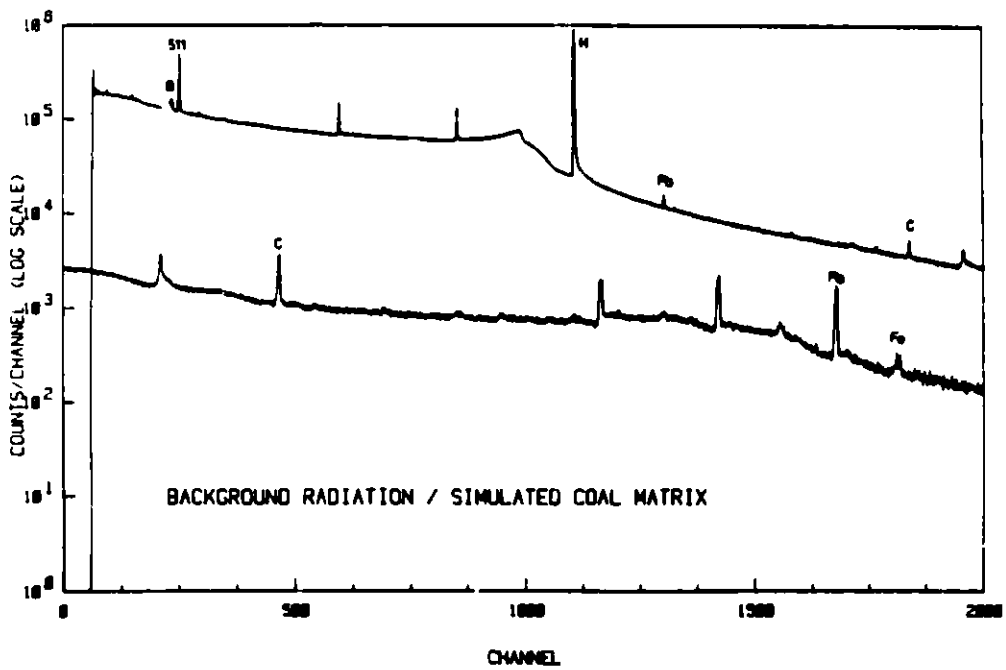

Fig. 2: Spectrum of the background radiation measured with a pure polystyrene sample to simulate the coal matrix.

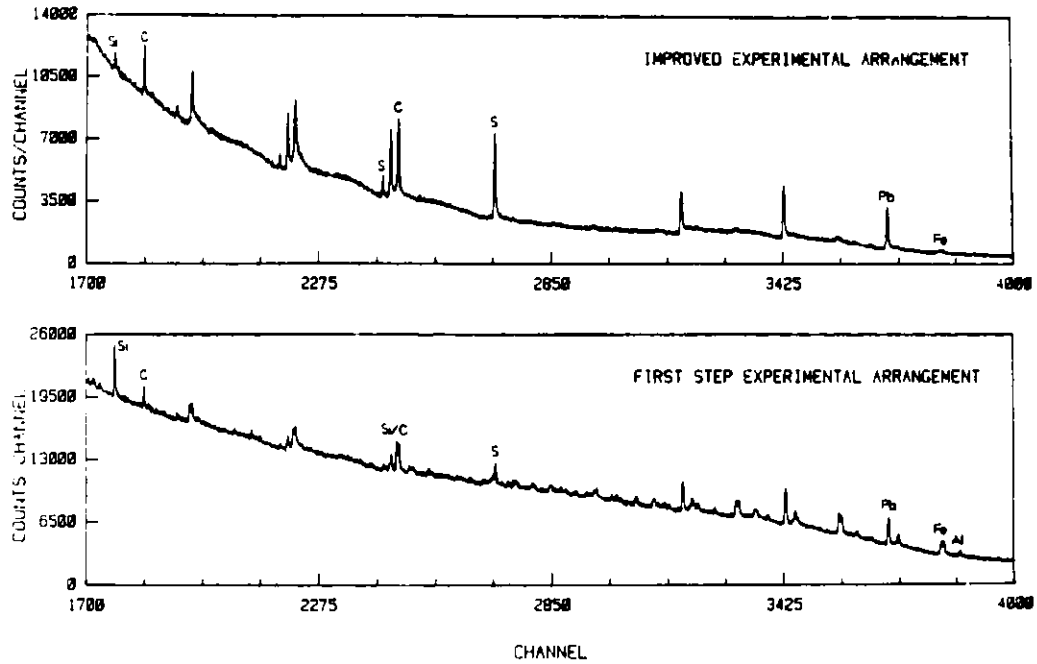

Fig. 3: Result of optimizing the experimental arrangement.

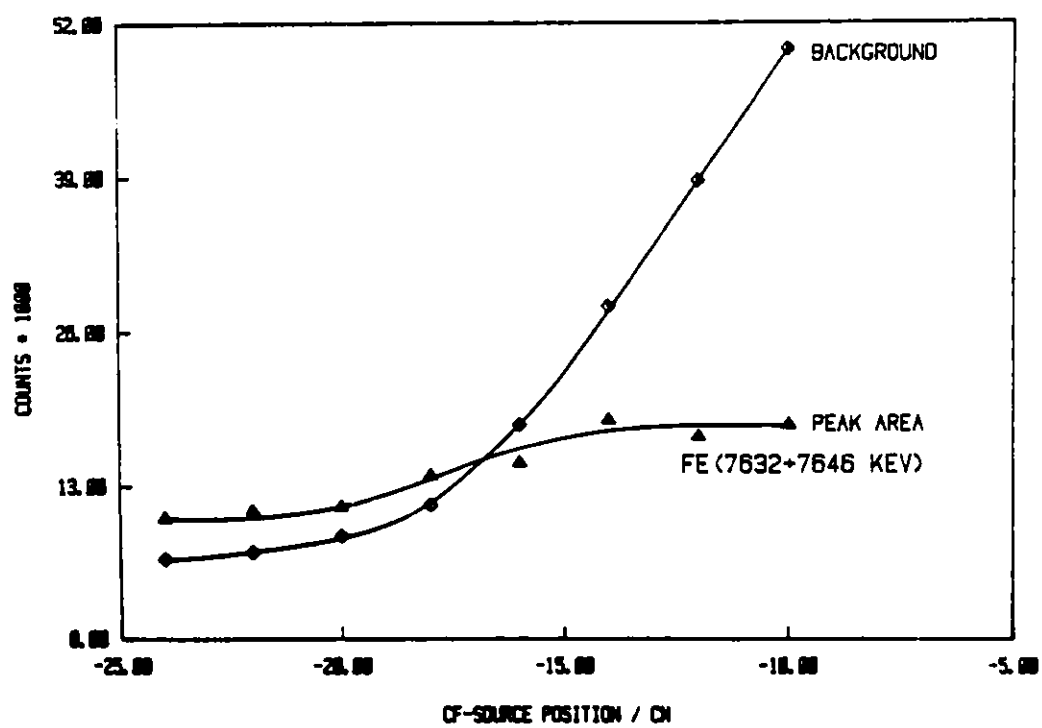

Fig. 4: Net peak area and related background as a function of the source position (∿ source strength).

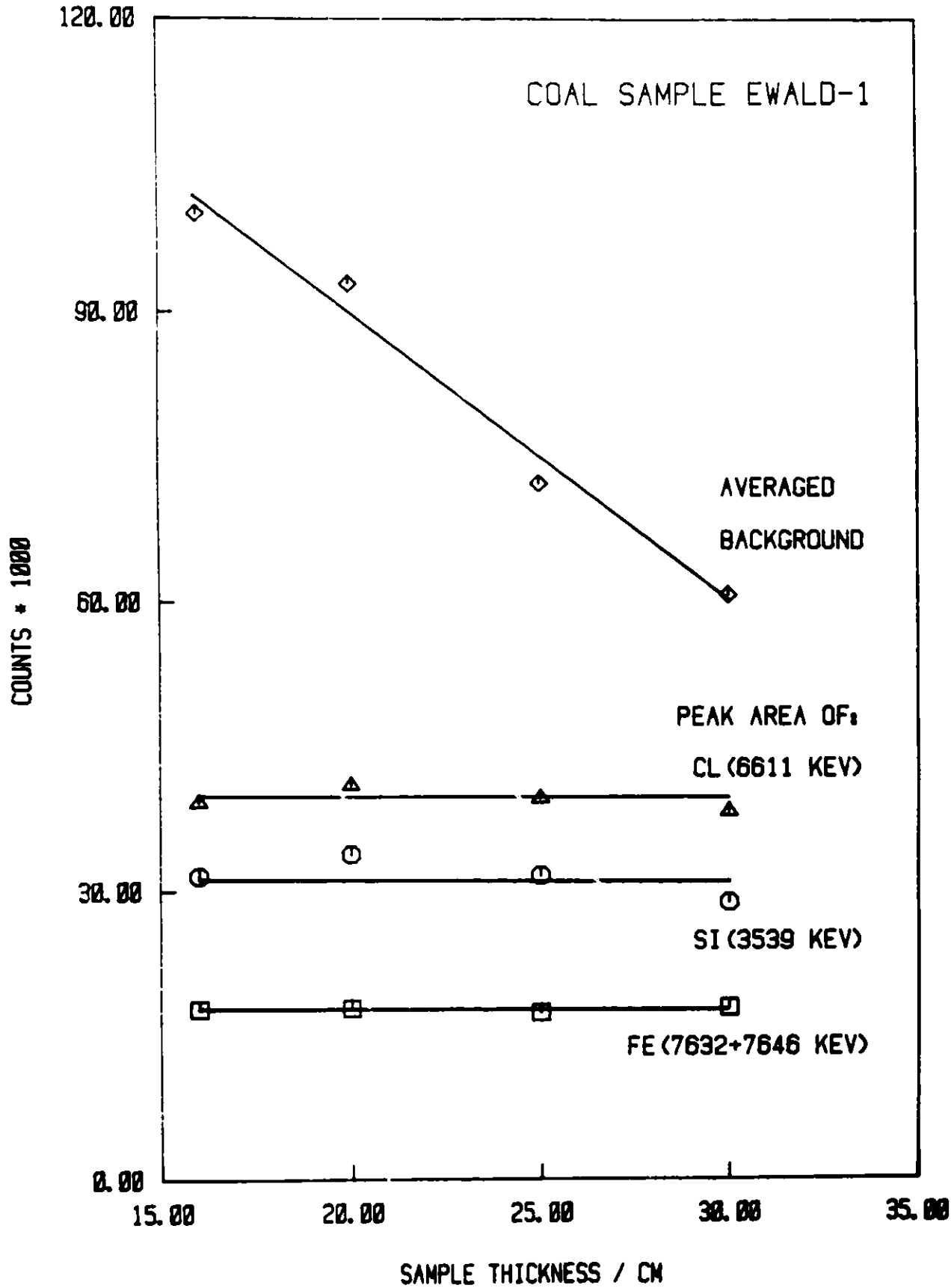

Fig. 5: Net area of three different peaks and average trend of their background as a function of sample thickness.

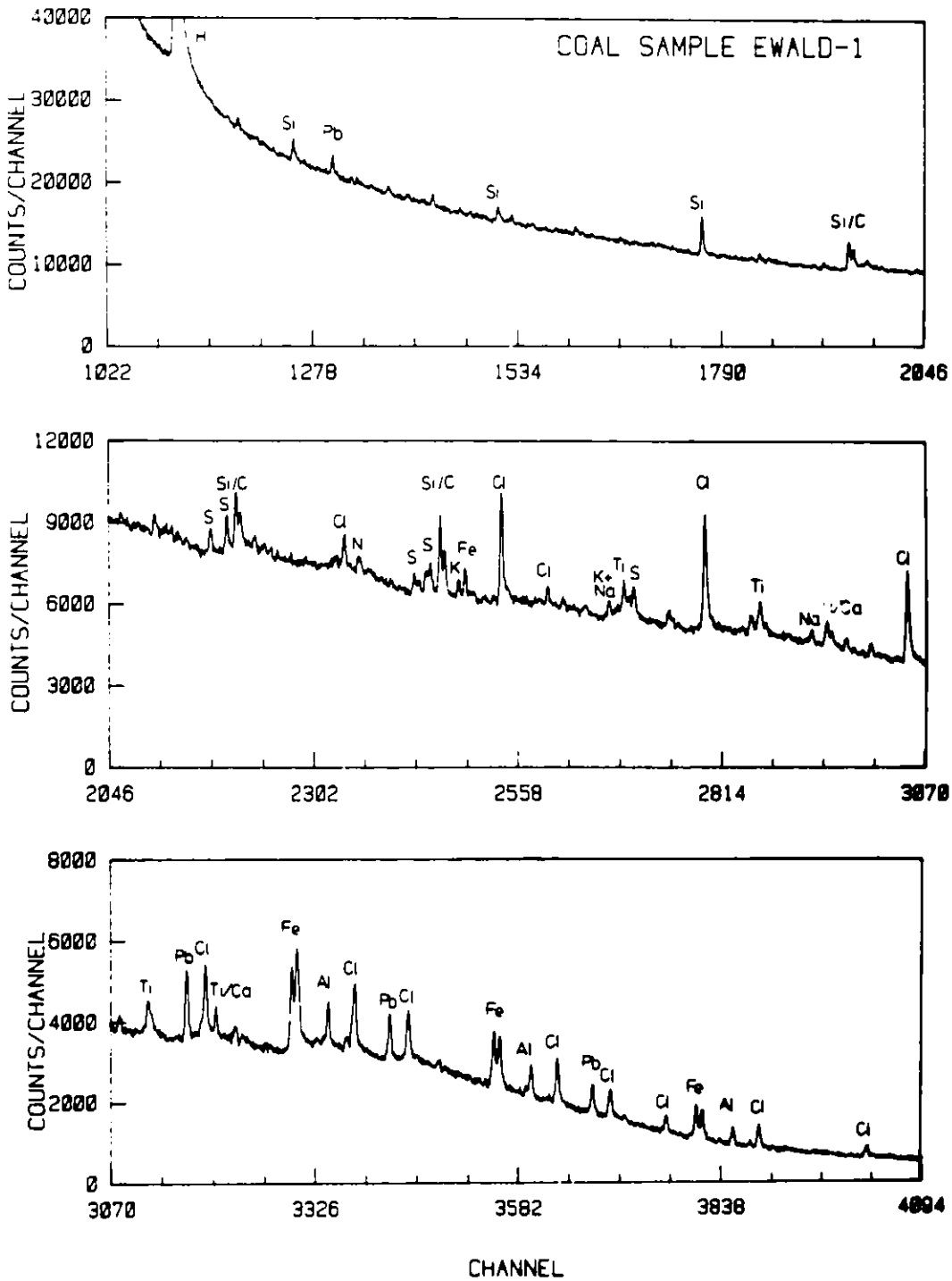

Fig. 6: Energy spectrum of a coal sample from the Ruhr district with about 20 % ash content. The collect time is 4000 s.

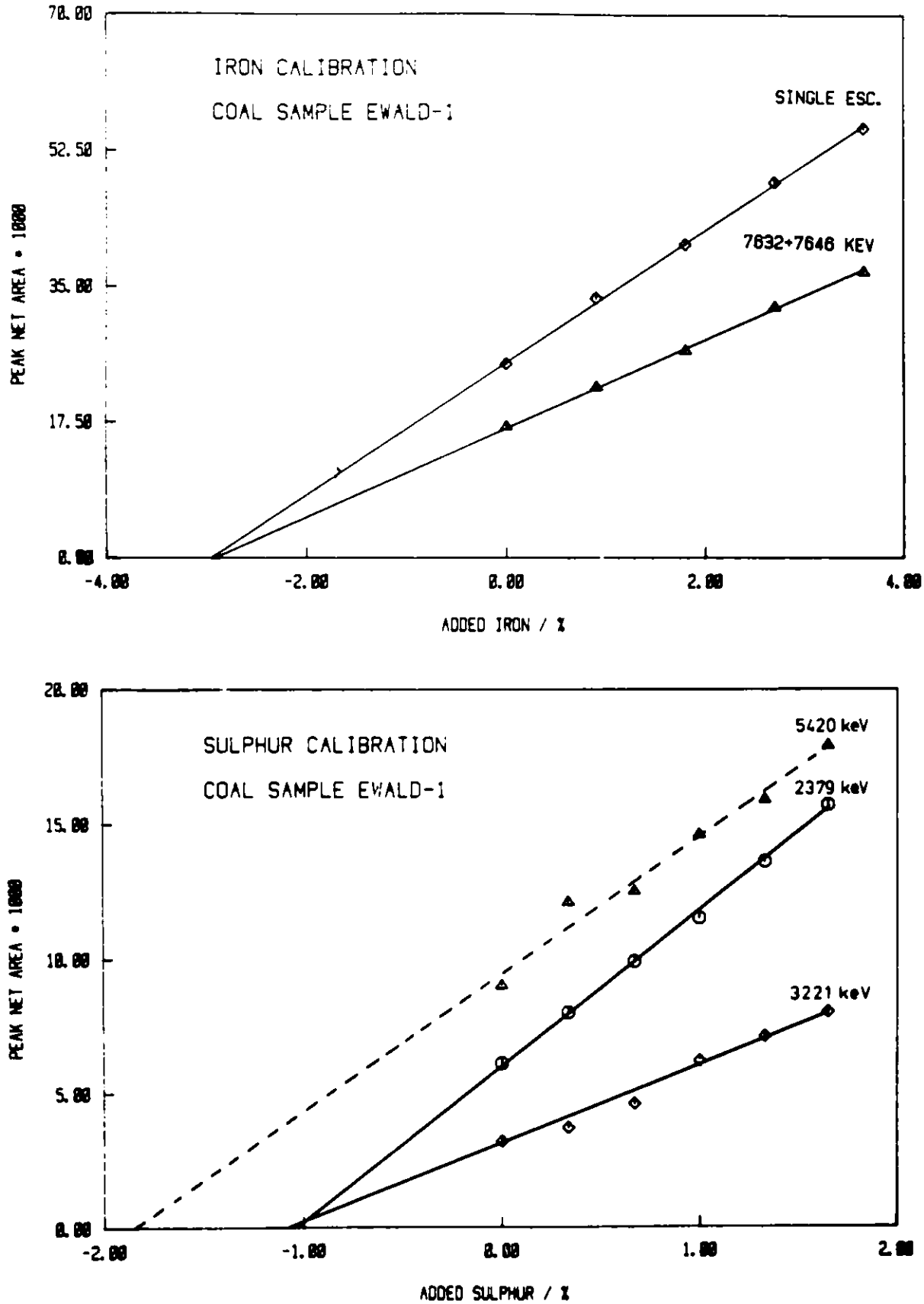

Fig. 7: Calibration curves for the elements iron and sulfur, measured by stepwise adding these elements to a natural coal sample.

NOVEL DESIGN OF PRESSURE VESSELS AND THERMAL SHIELDS IN COAL GASIFIERS*

Billy W. Loo
Lawrence Berkeley Laboratory
University of California
Berkeley, CA 94720 U.S.A.

ABSTRACT

This report describes a proposed solution to two outstanding problems in commercial-sized coal gasifiers, namely, detecting and locating any deterioration in the refractory thermal barrier and the construction of a safe pressure vessel utilizing advanced carbon fiber composite technology.

Design considerations are given for a typical gasifier some 30 feet in diameter by 150 feet tall with a maximum internal temperature and pressure of 2500°F and 1500 psi respectively.

A system of computer controlled cooling circuits is deployed between the refractory barrier and the external lightweight pressure vessel. Multiple levels of redundancy are built in to guard against any component failure. Through the sensing of coolant temperature and the modulation of coolant flow, a map of heat flux distribution over the gasifier wall may be generated with a spatial resolution of about 5 feet. It seems possible to maintain the coolant temperature rise by no more than 90°F with only a modest amount of coolant flow.

INTRODUCTION

In the coming decades, the U.S. is expected to rely increasingly on coal for a substantial fraction of its energy needs. Coal is one of nature's most important sources of energy and organic chemicals. The prudent and efficient use of this non-renewable resource is mandatory.

*This work was supported in part by the U.S. Department of Energy under Contract No. W-7405-ENG-48.

Modern processes of coal conversion and combustion share a common (although to varying degrees) set of operating conditions, namely, high temperture, high pressure and a very corrosive and errosive environment. The combination of these conditions is particularly severe where very large commercial-sized coal gasifiers are to be contemplated. The question of how large these gasifiers may be scaled depends not only on process efficiency and total economy but also on the limits of material and fabrication technology. Moreover, since these giant pressure vessels are the critical components of a multi-billion-dollar operation, the questions of long term reliability and safety are of paramount importance.

Consider a coal gasifier some 30 ft. (9.1 m) in diameter by 150 ft. (46 m) tall with a maximum internal temperature and pressure of 2500°F (1371°C) and 1500 psi (10.2 MPa) respectively. These typical figures are taken as an example to illustrate the generic nature of the problems and solutions. A refractory thermal barrier is generally required to insulate the wall of the pressure vessel from the internal heat and to increase the thermal efficiency of the process by reducing heat loss. Under the full infuence of a very errosive and corrosive environment together with thermal stresses which may develop due to temperature excursions, fault conditions may eventually develop in the refractory barrier. There is, therefore, a need for continuous monitoring the heat flux over the entire refractory wall in order to detect any onset of wall deterioration. Accessibility and the capacity to withstand the hostile environment again pose difficult problems for traditional methods of areal temperature measurement using thermal couple or infrared techniques. Other methods such as temperature sensitive paints, amoung other drawbacks, lack the necessary time responsiveness[1].

A second outstanding problem relates to the difficulties faced by the conventional thick wall steel vessel technology. For a given vessel of diameter D and internal pressure P, the minimum required wall thickness X can be computed as[2]:

$$X = \frac{0.5PD}{(S/F) - 0.6P}$$

where S and F are the material tensile strength and the safety factor required respectively. With typical values of S = 80 ksi (544 MPa) and F = 4 (e.g. steel SAE-980), the 30 ft. diameter vessel under consideration

will require a steel wall of 14 in. (36 cm) thick. Such a 150 ft. long cylinder would weigh 4278 tons (specific gravity 8.01 for steel) and obviously needs to be field assembled. The required plate fabrication, welding, and postweld heat treatment would clearly tax, if not exceed, the current limit of thick wall steel vessel technology. Moreover, an appropriate method for the safety inspection of such a vessel is yet to be found.

We shall attempt to take an integral approach to these two outstanding problems of continuous areal temperature monitoring and the fabrication of very large pressure vessels by considering the concept of an active thermal shield and the exploitation of high performance composite material technology[3].

"MEGACOON" DESIGN CONCEPTS

The "Megacoon" is a conceptual compound reactor construction designed as a substitute or extension of the conventional steel vessel technology. It consists of essentially two separate components which serve three functions: a lightweight fiber-wound outer cocoon which holds the pressure and a computer controlled active thermal shield which safeguards the cocoon from excess heat exposure as well as monitoring and localizing any development of hot spots from the possible degradation of the inner refractory wall.

Over the past decade, high performance carbon fiber composite materials are finding increasing applications in the military, aerospace and sporting goods industries[4]. The composite material consists of high strength carbon fibers of about 8 μm in diameter usually bonded in a matrix of thermal setting resin. The resulting composite possesses a unique combination of desirable properties which include very high tensile strength and stiffness, light weight, chemically inert, dimensionally stable, fatigue and creep resistant and ease of fabrication and shaping into required structural forms with a minimum of waste.

For example, the tensile strength and specific gravity of the Magnamite graphite AS/epoxy composite (Hercules Inc., Salt Lake City, Utah*) are

*Reference to a company or product name does not imply approval or recommendation of the product by the University of California or the U.S. Department of Energy to the exclusion of others that may be suitable.

225 ksi (1.53 GPa) and 1.55 respectively. Compared with the 14 in. steel pressure vessel considered above, the equivalent wall thickness would only be 5.0 in. (12.7 cm). Combining the factor of 2.8 advantage in strength with the factor of 5.2 in density, a carbon fiber cocoon may realize a weight saving of up to a factor of 14.5 over its steel counterpart. It should be pointed out that the strength of carbon fiber is highest along the fiber axis. However, crossplied techniques may be used to achieve near isotropic properties with a tradeoff in strength by up to a factor of 2.7. Since the lines of force in a long cylindrical wall are along the circumference, maximum advantage of the fiber strength may be realized. A stress field analysis of an actual vessel of a given shape will help to optimize the manner in which fibers may be applied for maximum reinforcement with minimum additional material. The significant point is that filament winding is a cumulative and flexible process that can be readily performed in the field. Thus very large and very strong pressure vessels may be fabricated without the limitations and drawbacks of the conventional steel vessel technology.

The main disadvantage of the carbon fiber composite structure is its working temperature limit (e.g. < 260°F or 127°C for graphite AS/epoxy). The question of adequate thermal shielding is therefore crucial.

One way of incorporating a system of active heat shields to assure the protection of the composite pressure vessel from the internal heat of a generic coal gasifier is depicted schematically in Fig. 1. As conceived, a primary and a secondary active heat shield are to be deployed between the refractory heat barrier and the composite pressure vessel. Each shield consists of an array of cooling pipes which are subjected to the same maximum pressure in the reactor but any convective contact with the hot gases is minimized. The water being circulated in the pipes will only be slightly above atmospheric pressure. There are, of course, many mixtures of optimum pipe sizes and configurations that may be chosen to suit a given set of reactor detail and temperature distribution. However, a simplistic example of uniformly spaced pipes will be given here to illustrate the principle.

Consider the cooling pipes to be, say, 6 in. (15.2 cm) in diameter. Each pipe constitutes a horizontal circle around the refractory barrier and

is fed by pipes entering vertically from the end of the vessel. Each set of, for example, three pipes (labeled A1, A2 and A3 in Fig. 1) could be connected in parallel to form an individual circuit with temperature sensors and flow controllers. Thus a wall of 150 ft. high will have an array of 300 pipes forming 100 separate circuits. The neighboring sets of pipes (the A's, B's and C's) are interleaved or stacked in alternation such that if any of them fails, two thirds of cooling power will still remain at a given section of the wall. A complete system of secondary active heat shield is deployed outside of the primary system as an additional measure of redundancy and safety.

In operation, a servo system will adjust the flow velocity in each pipe such that the temperature increase $\Delta T = T_{out} - T_{in}$ between the outgoing and incoming water is no more than, say, 50°C. Therefore, if T_{in} is 20°C, the entire primary active heat shield will be maintained at under 70°C. Since convection in the heat shield area is restricted by design, the primary mode of heat transfer will be by radiation. When the refractory heat barrier is intact, the amount of heat transfer to the wall will be quite limited. For example, take the case of a maximum temperature drop of 1300°C across a 10 cm thick refractory wall that has a thermal conductivity of 120 w/cm°C, the heat loss towards the outside will be 1.56×10^4 w/m^2. The required flow velocity in the horizontal pipes to maintain a ΔT of 50°C is only 1.95 cm/sec. In the event of a failure in a certain section of the refractory barrier, the maximum radiative heat load at 2500°F (1644°K) on the primary active heat shield will be 4.14×10^5 w/m^2 and the flow velocity required to maintain the same ΔT will be 51.8 cm/sec. This corresponds to a maximum flow rate of 9.45 l/sec (150 gal/min or 20 cfm) in each of the horizontal pipes. Since the radiative heat transfer depends on the fourth power of the absolute temperature of the source, the temperature rise in a circuit of constant flow or alternatively, the increase in flow velocity in a circuit kept at constant ΔT can be a very sensitive measure of any abnormality that may develop in the refractory barrier. The location of a circuit of abnormal flow requirement will indicate the vertical height of the hot spot. The spatial resolution of course will depend on the circuit configuration. In the example considered, a resolution of about 5 ft. (1.5 m) can be achieved.

In order to locate the position of the hot spot along the circuit (its

azimuthal coordinates), the computer may routinely scan each circuit by momentarily modulating the flow velocity V as idealized in Fig. 2. For example, V in circuit A is increased by a factor of two (or other appropriate factor) at time t_0 and returned to its normal flow at time t_3 as shown in Fig. 2a. For a normal circuit, ΔT will decrease linearly with time until it reaches a new equilibrium level "a" at time t_2. When the coolant is modulated from its normal flow rate, the rate of temperature change in approaching a new equilibrium is proportional to the rate of heat input per unit length along the conduit. Thus, a hot spot would give rise to an abrupt change in the ΔT vs. t plot as indicated by "c" at time t_1 in Fig. 2c. The time it takes the coolant to complete the flow circuit from the inlet temperature sensor to the outlet one is $t_2 - t_0$; therefore the determination of t_1 is the same as locating the hot spot along the flow circuit. If the hot spot is closer to the water inlet, t_1 will be proportionally closer to t_2. Similar arguments apply to the situation when the flow returns to normal level at t_3 and the location of t_4 with respect to t_3 and t_5 will be used as a check for the hot spot's circumferential position as determined during the high flow period.

It should be noted that the exact location of the hot spot can be even more readily identified by differentiating the change in temperature with time as is shown in Fig. 2d. The spikes "c'" and "d'" in Fig. 2d correspond to the signatures "c" and "d" in Fig. 2c. As a regular course of operation, the central location of these spikes may be pinpointed by additional mathematical techniques such as further differentiating Fig. 2d and locating the "zero crossing" points. With the aid of the on-line computer, a map of heat flux distribution over the entire reactor surface may be generated.

A noteworthy variation of the active heat shield described above is to devise an array of cooling pipes threaded by smaller pipes at appropriate intervals. The larger pipes are designed primarily for cooling, while the smaller ones are optimized for mapping heat flux distributions.

CONCLUSION

The preceding illustration of the generic Megacoon concept has shown that by exploiting the unique combination of desirable properties of carbon

fiber composites, one may foresee a potential jump in the ultimate size at which large pressure vessels may be fabricated as compared with that achievable by conventional steel vessel technology.

We have also shown that computer controlled active heat shields may serve the dual purpose of protecting the pressure vessel and locating any onset of deterioration in the refractory barrier. The method is sensitive and provides adequately fast time response and spatial resolution. The flexibility in the mode of operation and circuit deployment strategy should provide any desired level of redundancy for safety considerations. It is noted that in the illustrating example, only a modest amount of coolant flow is required to cope with extremely high temperature exposures. This means that it is even possible to operate the gasifier with a defective refractory barrier until it is convenient to implement repair. The maintenance of the heat shields at low temperatures should make pipes and components able to better survive the corrosive service environment for long times. This is an important consideration for example, if a thin metallic barrier lines the inside of the composite pressure cocoon.

ACKNOWLEDGEMENTS

The author wishes to express his appreciation to Yasuo G. Tokita of Hercules Incorporated for information and advice on carbon fiber composite technology. Helpful discussions with F.S. Goulding, F. A. Kirsten and other members of the staff of the Lawrence Berkeley Laboratory are also acknowledged.

REFERENCES

1. N.M. O'Fallon, R.A. Beyerlin, W.W. Managin, H.B. Karplus and T.P. Mulcahey, "A Study of the State-of-the-Art of Instrumentation for Process Control and Safety in Large-Scale Coal Gasification, Liquefaction and Fluidized-Bed Combustion System" ANL-76-4, January 1976.

2. D.A. Canonico, "Structural Integrity of Vessels for Coal Conversion Systems" ORNL/TM-6969, September 1979.

3. B.W. Loo, "Coal Gasification Vessel" Patent pending, D.O.E. Patent Case No. S-55127, RL-8124, IB-398, February 1981.

4. "Carbon Fiber Study" NASA Technical Memorandum 78718, May 1978.

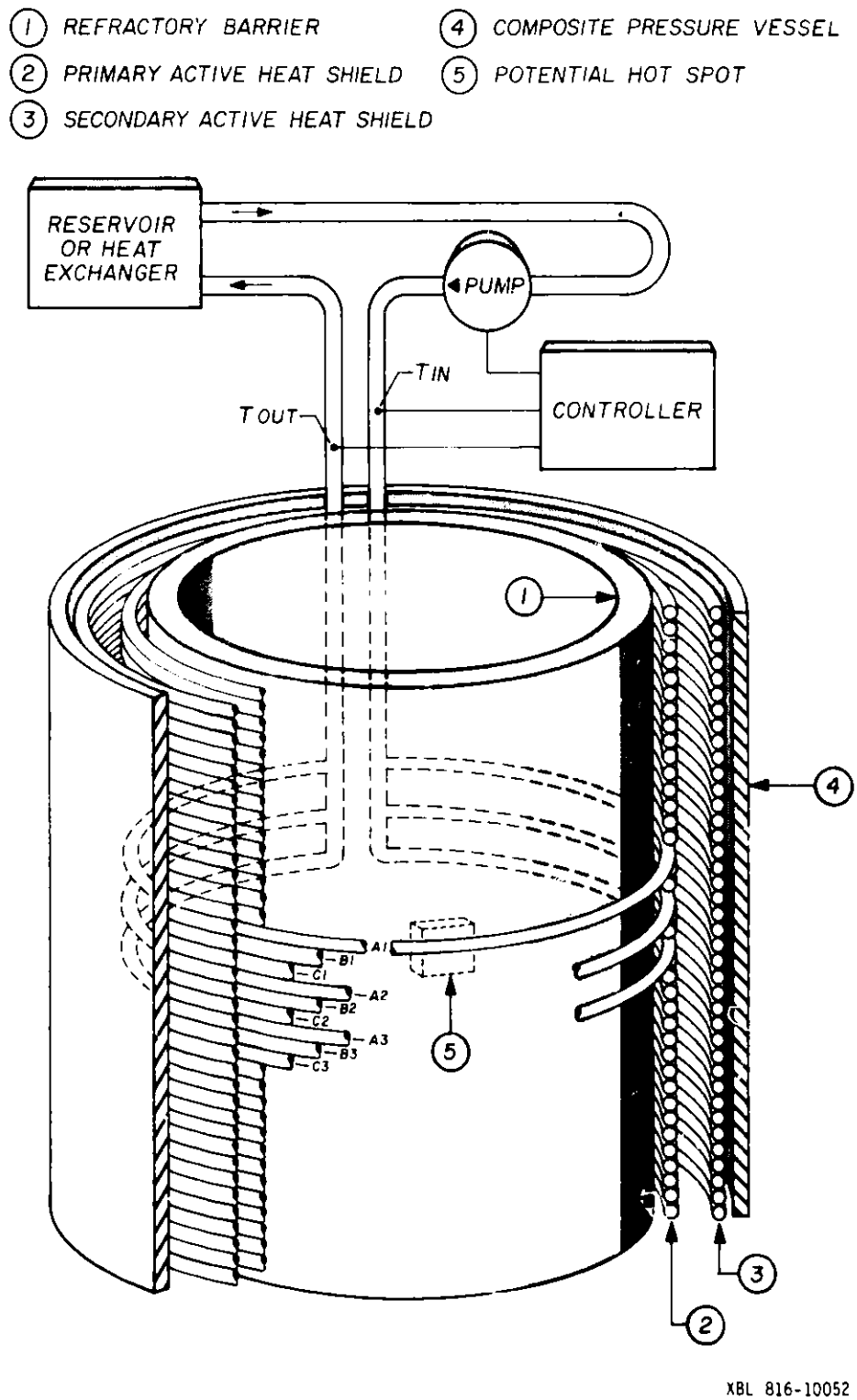

Figure 1. A schematic illustration of a composite pressure vessel with computer controlled active heat shields.

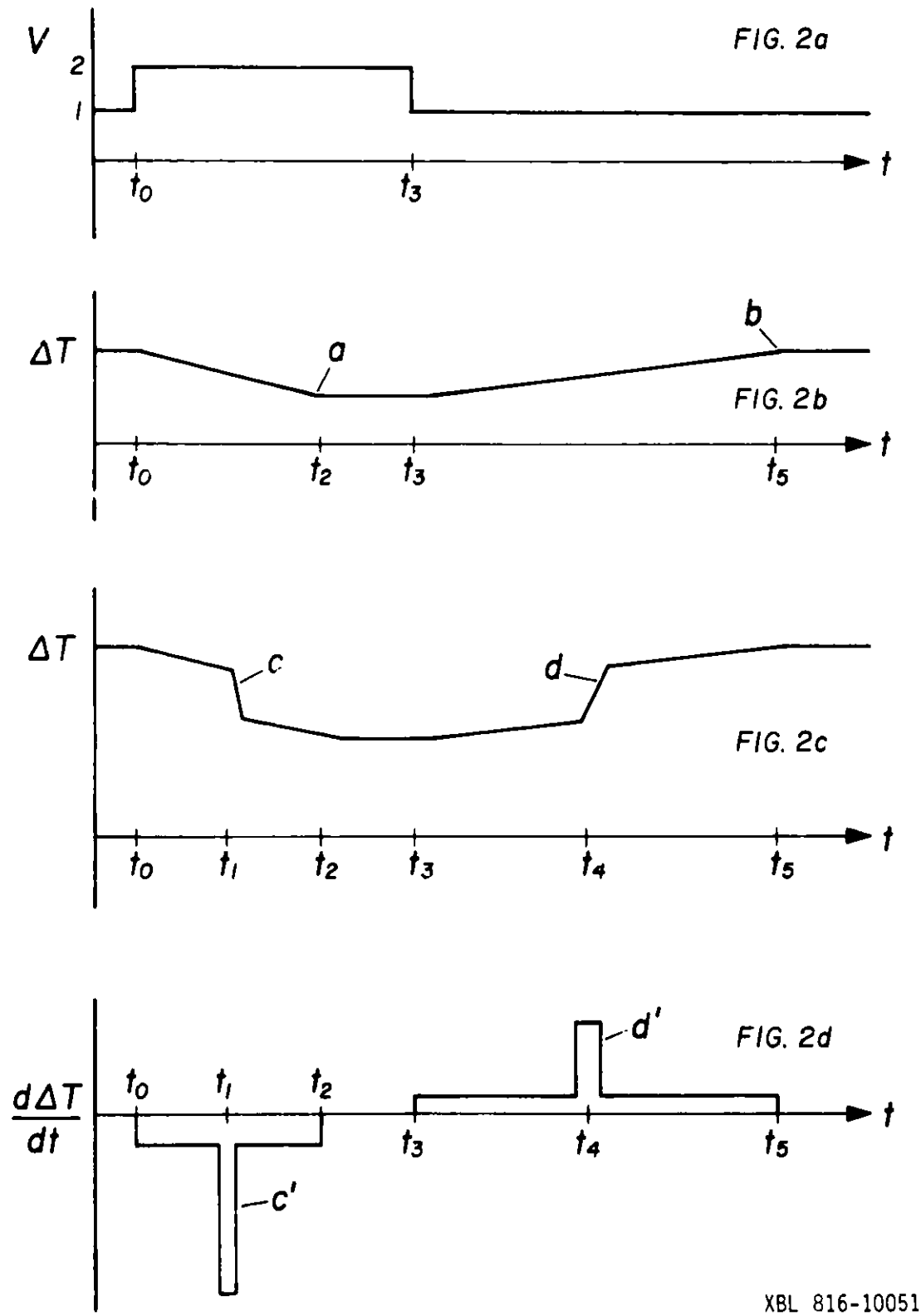

Figure 2. Idealized time responses of coolant flow velocity and temperature differentials.

AN ASSESSMENT OF COMMERCIALLY AVAILABLE INSTRUMENTS FOR ON-LINE MONITORING OF WORKPLACE AIR

J. H. Bochinski and S. L. Bergh
Enviro Control, Inc., Rockville, Maryland

J. P. Smith
National Institute for Occupational Safety and Health

INTRODUCTION

An "Assessment of Engineering Control Monitoring Equipment" was recently completed under contract with the National Institute for Occupational Safety and Health (NIOSH). This study will be useful for identifying on-line instrument systems that may be suitable for continuously monitoring the workplace air and engineering controls used in industry, including fossil energy processes. This paper covers the following:

- Background information for the NIOSH study
- How availability of monitoring systems was determined
- Criteria for determining suitability
- Some monitoring requirements in fossil energy processes
- Monitoring systems for fossil energy processes

BACKGROUND INFORMATION

It is recognized that simply implementing control technology will not ensure that workers are protected from hazardous chemical agents for the following reasons:

- Controls may malfunction or deteriorate in performance
- Work practices may not necessarily be followed correctly

Both instances present opportunities for worker exposure. Better protection can often be provided if the performance of the engineering control system is monitored frequently or continuously. A monitoring system to perform this function consists of several components:

- Sample delivery and conditioning system -- brings sample from monitoring location to analyzer and prepares it for analysis
- Detector or anlyzer and related electronics -- apparatus to determine concentration of substance of interest
- Display or alarm system -- informs workers of concentration present and indicates alarm or hazardous condition if appropriate

More complex systems can also include a component for data storage to enable estimation of worker exposure or location of problem exposure areas in the workplace.

This type of on-line system is being used effectively for monitoring the performance of control technology implemented in many industrial plants. Performance is determined through frequent or continuous sampling and analysis of air around a selected piece of equipment, from selected areas of a workplace, or from the discharge of a filtration/ventilation system. Monitoring systems can detect a control system failure to indicate immediate corrective action or detect trends toward failure for preventitive action. Also, monitoring systems can be used in the development and comparisons of control techniques. However, uninitiated users frequently underestimate the scope of the problem and the many pitfalls involved, with the result that:

- Instruments installed in given control monitoring applications can turn out to be unsuitable
- Cost overruns and time delays occur in remedying the technical and operational problems encountered

Some reasons for the above difficulties are that monitoring systems are selected on the basis of inadequate information and an incomplete definition of the monitoring application.

In view of the above concerns, NIOSH awarded a contract to Enviro Control, Inc., (Enviro) to compile information on monitoring systems from technical, trade, and manufacturing sources; recommmend monitoring techniques and equipment for single and multiple chemical agents, and for engineering control and recirculation systems; suppliment the literature information by survey of representative plants; identify gaps in monitoring technology and recommend R & D; and compile this information in a comprehensive report. A Final Report presenting the results of the study was recently submitted to NIOSH.

The conduct of the assessment and the writing of this report were organized with some realization of the vast complexity and wide range of monitoring devices available. Because of this, the problems encountered are manifold and complex. They include:

- Properly defining the application - (e.g., where to locate sensors, are all potential interferences identified, will the monitor function satisfactorily in the industrial environment, etc.).

- Knowing what a monitor can do - The full potential and limitations of most monitors are not adequately understood by the user or fully identified by the manufacturer.

- Transporting sample air - The difficulty of bringing the air sample to be analyzed to the monitor is often woefully underestimated by the user and/or not fully defined by the instrument manufacturer

- Presenting monitoring information - Information on the potential or actual failure of controls should be communicated in a manner to get the worker's attention and advise him of the probable location of the problem

- Realizing personnel needs - In many cases, there is a lack of appreciation of the need for properly trained and motivated personnel to operate and maintain the monitors.

Many manufacturers of monitoring devices attempt to meet the above user needs. However, not all the manufacturers have an appreciation of the difficulties and problems encountered by the users. Also, the lack of a common standard for specification of engineering control monitoring devices further compounds the confusion in the marketplace.

The report is organized so that the reader can conveniently locate and obtain the information pertinent to any particular area of interest.

The report is intended for use in both private and public sectors in the following ways:

- By NIOSH in promoting research and development of engineering control monitoring equipmert
- By potential users of monitoring equipment in selecting and specifying monitors
- By instrument manufacturers in designing and manufacturing monitoring devices to meet users' needs
- By OSHA in providing field personnel with a better understanding of how instrumentation can be used to reduce exposure

HOW AVAILABILITY OF MONITORING SYSTEMS WAS DETERMINED

The information on comercially available monitors supplied by manufacturers was compiled into a standardized format and reviewed by the technical staff. The sequence of steps that were involved are listed below:

a. A letter along with a copy of OSHA's list of hazardous chemical agents and permissible exposure (29 CFR 1910) was sent to

several hundred manufacturers of instrument requesting copies of published performance specifications for each model of their commercially available instruments they consider suitable for monitoring the chemical agents listed.

b. Initial returns indicated two serious problem areas facing potential users when communicating with instrument manufacturing firms, namely:

- Lack of standard terminology used to describe and discuss instrument performance specifications
- Lack of appropriate information supplied on instrument systems. Many instrument manufacturers did not address the monitoring system requirements (e.g., sample transport, interface with external visual or audible alarms) encountered by the user.

The first problem area was resolved by adopting portions of Environmental Protection Agency's terminology used in specifying air quality monitoring instruments. The proposed terminology was found acceptable by major firms in the industry and was subsequently approved by the NIOSH Project Officer.

The second problem area was addressed by structuring the Information Summary format to address the monitoring system requirements encountered by the users selecting engineering control monitoring equipment.

c. Information on each commercially available model deemed suitable by the manufacturer for monitoring engineering controls was tabulated in Information Summaries (using a format as shown in Figure 1).

Figure 1. Format for Information Summary

Reference No.

System Model No.	Name	Reference No.	Manfacturer
xxxx	Monitoring System	000-1	
System Component Model No.			
xxxx	Sample System	000-2	
xxxx	Sensor Assembly	000-3	
xxxx	Programmer	000-4	
xxxx	Readout	000-5	

CHEMICAL AGENTS MEASURED & PERFORMANCE SPECIFICATIONS
(For definition of specifications, see Section 6.0, Glossary of Terms)

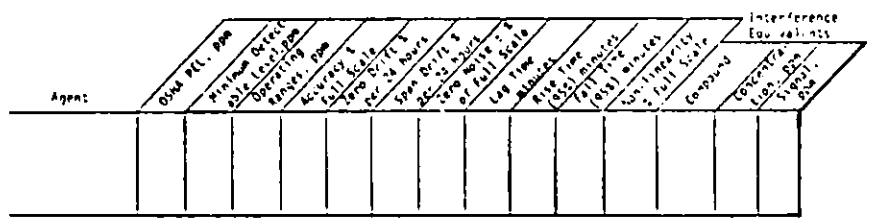

SYSTEM DESCRIPTION

Sample System

Sensor Assembly

Programmer

Readout

Figure 1.
(Continued)

SYSTEM SPECIFICATIONS

Operating Temperature

Operating Humidity

Hazardous Area Classification (Classification according to NE code)

Percent Up Time ("Percent up time" as defined in glossary)

Size and weight

Utility Requirements

Supplies and Reagents Required

OTHER SYSTEM CONSIDERATIONS

Operator Interaction

- Operator skill level required for operation and maintenance
- Operator time required for calibration and maintenance

Instrument Service Area & Support Facilities Required

Ruggedness and System Packaging

Any particular design standards or environmental testing standards complied with

Adequacy of Operating Manuals

A list of information concerning operation and maintenance supplied to the user.

Current Areas of Application

COST OF INSTRUMENT SYSTEM

Basis for estimate

Cost summary

d. The Information Summary compiled for each model was evaluated by the technical staff and information gaps were identified. The performance specifications published by instrument manufacturers were adapted to the standardized format.

e. A copy of the first draft of each Information Summary for each commercially available mode, along with a glossary of terminology for performance specification, was sent to the corresponding manufacturers requesting their comments and the additional information needed to complete the Information Summary for each model that appeared suitable.

f. The information returned by the manufacturer was evaluated and the Information Summary for each model was updated as appropriate. Users of some of the instruments were contacted at this time about their experiences with the instrument.

CRITERIA FOR DETERMINING SUITABILITY

Commercially available instruments that met the following requirements were considered technically suitable for monitoring engineering controls and work practices:

- Instrument is designed for continuous on-line operation (or can be readily adapted for continuous on-line operation)
- Instrument has a minimum detectable limit of less than 1/10 of the PEL for one or more chemical agents listed by OSHA in 29 CFR 1910 in the absence of interfering chemicals. Some exceptions were made where only one alternative was available for chemicals with a low PEL.

The above initial screening of instruments does not imply that an instrument would necessarily meet the users' requirements. These could involve one or more of the following considerations:

- Presence of interfering substances
- Cost of instrument installation and operation
- Skill levels required to operate and maintain the instrument
- Hazardous location classification.

Enough data were presented in the Information Summaries to provide the potential instrument users with information sufficient for assisting in:

- Preparing a definition of the application requirements for use in communications with instrument suppliers
- Evaluating additional information that may be supplied by instrument manufacturers
- Preparing preliminary cost analyses of instrument options
- Preliminary ranking of options
- Preparing instrument procurement specifications that address the system requirements of the monitoring application.

SOME MONITORING REQUIREMENTS IN FOSSIL ENERGY PROCESSES

The substances released to the workplace from fossil energy processes will depend to some extent on the fossil fuel and processes involved. Some of chemical agents to which workers could be potentially exposed while operating fossil energy processes are listed in Table 1.

MONITORING SYSTEMS FOR FOSSIL ENERGY PROCESSES

The commercially available monitoring systems that may meet the needs for monitoring volatile chemical agents in workplace air in fossil energy processes are listed in Table 2. No monitoring systems

TABLE 1. CHEMICAL AGENTS ENCOUNTERED IN FOSSIL ENERGY PROCESSES

Chemical Agent	Permissible Exposure 8-hr TWA ppm	Permissible Exposure 8-hr TWA mg/m^3
Ammonia	50	35
Benzene	10	-
Coal tar pitch volatiles (benzene soluble fraction) anthracene, BaP, phenanthrene, acridine, chrysene, pyrene	-	0.2
Coal dust (respirable fraction less than 5% Si O_2	-	2.4
Carbon black	-	3.5
Carbon dioxide	5000	9000
Carbon monoxide	50	55
Hydrogen sulfide	20	-
Nuisance dust	-	-
Respirable fraction	-	5
Total dust	-	15
Methyl mercaptan	100	410
Metals (1)	-	-
Naphtha (coal tar)	100	400
Sulfur dioxide	5	13
Toluene	200	-
Xylene	100	435

(1) Refer to The Federal Register (29 CFR 1910) for permissible exposure levels for specific metals.

are available for measuring the composition of particulates. Table 3 lists monitoring systems that may be suitable for measuring the total concentration of air-born particulates. The instruments listed in Table 3 do not discriminate between compositions of particulates.

The monitoring methods listed in Tables 2 and 3 fall into the categories listed in Tables 4, 5 and 6. These tables present the basic information on types of compounds detected, operating principles, and advantages and disadvantages of each category of monitor.

TABLE 2. COMPANIES SELLING MONITORS FOR MONITORING HAZARDOUS SUBSTANCES IN FOSSIL ENERGY PROCESS

Manufacturer/Model Name and No.	Ammonia	Benzene	Coal Tar Pitch Volatiles	Coal Dust	Carbon Black	Carbon Dioxide	Carbon Monoxide	Hydrogen Sulfide	Nuisance Dust	Methyl Mercaptan	Metals	Naphtha	Sulfur Dioxide	Toluene	Xylene
Anacon, Inc.															
Photometric process Analyzer/ Model #207	-	-	-	-	-	-	-	-	-	-	-	-	X	X	-
Beckman Instruments															
Fluorescent Ambient SO_2 Analyzer/ Model #953	-	-	-	-	-	-	-	-	-	-	-	-	X	-	-
Process Chromatograph System/ Model #6710	-	X	-	-	-	X	X	-	-	X	-	X	-	X	X
Ambient CO Monitoring System/ Model #866	-	-	-	-	-	X	-	-	-	-	-	X	-	-	-
Bendix Corporation															
Gas Chromatographic Monitoring System/Model #7000/007 & #9000/001	-	X	-	-	-	X	X	X	-	X	-	X	-	X	X
Carbon Monoxide Infrared Gas System/Model #8051-5CA	-	-	-	-	-	X	-	-	-	-	-	-	-	-	-
Byron Instruments, Inc.															
Total Hydrocarbons, Methane, and Carbon Monoxide Analyzer/Model #233	-	-	-	-	-	-	X	-	-	-	-	-	-	-	-

TABLE 2 (Cont'd.)

Manufacturer/Model Name and No.	Ammonia	Benzene	Coal Tar Pitch Volatiles	Coal Dust	Carbon Black	Carbon Dioxide	Carbon Monoxide	Hydrogen Sulfide	Nuisance Dust	Methyl Mercaptan	Metals	Naphtha	Sulfur Dioxide	Toluene	Xylene
CEA Instruments, Inc.															
Air Monitor/Model #CEA 555	X	-	-	-	-	-	-	X	-	-	-	-	X	-	-
Control Instruments Corporation															
Toxic Gas Detection System/Model #TGD	-	-	-	-	-	-	-	X	-	-	-	-	-	-	-
CVC Products, Inc.															
CVC Superspec 600 Mass Spectrometer	X	-	-	-	-	X	-	-	-	-	-	X	-	X	X
Delmar Scientific															
Micro-Rate™ Hydrogen Sulfide Sulfide Monitor/Model #DM-WMR	-	-	-	-	-	-	-	X	-	-	-	-	-	-	-
Dynamation, Inc.															
Area Monitors/Models for CO: #300, #2300/2500;	-	-	-	-	-	-	X	-	-	-	-	-	-	-	-
Model for H_2S: #110	-	-	-	-	-	-	-	X	-	-	-	-	-	-	-
ECOLYZER															
Monitoring Systems/Models #3000 & #8000	-	-	-	-	-	-	X	X	-	-	-	-	-	-	-

TABLE 2 (Cont'd.)

Manufacturer/Model Name and No.	Ammonia	Benzene	Coal Tar Pitch Volatiles	Coal Dust	Carbon Black	Carbon Dioxide	Carbon Monoxide	Hydrogen Sulfide	Nuisance Dust	Methyl Mercaptan	Metals	Naphtha	Sulfur Dioxide	Toluene	Xylene
EOCOM Corporation															
Fourier Multiplex Spectrometer System/Series #7000	X	X	-	-	-	X	X	X	-	X	-	-	X	X	X
Foxboro Analytical															
Multi-station, Multi-component Ambient Air Monitoring System/ Model #MIRAN-801	X	-	-	-	-	X	X	-	-	X	-	-	-	-	X
General Monitors, Inc.															
H_2S Gas Monitors/Models #2170 & #2250	-	-	-	-	-	-	-	X	-	-	-	-	-	-	-
Horiba Instruments, Inc.															
Gas Analyzers/Models #AIA 23/24 & #AIA 23/24 (AS)	-	-	-	-	-	X	X	-	-	-	-	-	-	-	-
Houston Atlas, Inc.															
Sulfur Gas Analyzers/Series #722 & #825	-	-	-	-	-	-	-	X	-	-	-	-	-	-	-
Infrared Industries, Inc.															
Gas Analyzers/Series #700	-	-	-	-	-	X	X	-	-	-	-	-	-	-	-

TABLE 2 (Cont'd.)

Manufacturer/Model Name and No.	Ammonia	Benzene	Coal Tar Pitch Volatiles	Coal Dust	Carbon Black	Carbon Dioxide	Carbon Monoxide	Hydrogen Sulfide	Nuisance Dust	Methyl Mercaptan	Metals	Naphtha	Sulfur Dioxide	Toluene	Xylene
International Sensor Technology															
Solid-State Sensor Gas Monitor	X	X	-	-	-	-	X	X	-	X	-	-	X	X	-
Interscan Corporation															
Gas Analyzers/LD Series	-	-	-	-	-	-	X	X	-	-	-	-	X	-	-
ITT Barton															
Area Safety Monitor/Models #409 & #412	-	-	-	-	-	-	-	X	-	X	-	-	X	-	-
Lear Siegler, Inc.															
Air Monitoring System/Model #SM1000	\	X	-	-	-	-	-	-	-	-	-	-	X	X	X
Gas Analyzer (NDIR)/Model #EM 202	X	-	-	-	-	X	X	-	-	-	-	-	-	-	-
Macurco, Inc.															
Carbon Monoxide Detector/Model #SS102	-	-	-	-	-	-	X	-	-	-	-	-	-	-	-
MDA Scientific, Inc.															
Continuous Monitors/Series 7000	X	-	-	-	-	-	-	X	-	-	-	-	X	-	-

TABLE 2 (Cont'd.)

Manufacturer/Model Name and No.	Ammonia	Benzene	Coal Tar Pitch Volatiles	Coal Dust	Carbon Black	Carbon Dioxide	Carbon Monoxide	Hydrogen Sulfide	Nuisance Dust	Methyl Mercaptan	Metals	Naphtha	Sulfur Dioxide	Toluene	Xylene
Mine Safety Appliance, Co.															
Luft-Type Infrared Analyzer/Lira Models #202 & 303	X	-	-	-	-	X	X	-	-	-	-	X	-	-	X
Carbon Monoxide Alarm/Model #704	-	-	-	-	-	-	X	-	-	-	-	-	-	-	-
Remote Sensing Hydrogen Sulfide Detector/Model #580	-	-	-	-	-	-	-	X	-	-	-	-	-	-	-
Remote Sensing Carbon Monoxide Detector/Model #570	-	-	-	-	-	-	X	-	-	-	-	-	-	-	-
Monitor Labs, Inc.															
Carbon Monoxide Analyzer/Model #8310	-	-	-	-	-	-	X	-	-	-	-	-	-	-	-
Process Analyzers, Inc.															
Process Chromatograph System/ Model #26-226-4P	X	X	-	-	-	X	X	X	-	X	-	X	X	X	X
Titrilog III/Model #26-105	-	-	-	-	-	-	-	X	-	X	-	-	X	-	-
Rexnord Gas Detection Products															
H_2S Detection System/Models #710 & #740	-	-	-	-	-	-	-	X	-	-	-	-	-	-	-

TABLE 3. COMPANIES SELLING MONITORS FOR MEASURING PARTICULATES

The manufacturers listed below indicate their instruments are capable of measuring all particulates. The instruments will not descriminate between chemical agents.

Manufacturers and Model Numbers

ATI
Powdered Material Detection System/Model ATI-722

Climet Instrument Co.
Remote-Location Multipoint Airborn Particle Sensor/Model #CI 225/210

GCA Corporation
Real Time Aerosol Monitor/Model #RAM-1
Ambient Particulate Mass Monitor/Model #APM
Fibrous Aerosol Monitor/Model #FAM-1

Gubelin Industries, Inc.
SIGRIST Continuous Operation Dust Monitor/Model #UP92TN

PPM, Inc.
Aerosol Monitoring System/CAM system

TSI, Inc.
Automatic Respirable Aerosol Mass Monitor/Model #5000
Respirable Aerosol Photometer/Model #5150

Chemical Agents Measured as Particulates

Certain coal tar pitch volatiles that form aerosols
Coal dust
Carbon black
Nuisance dust
Metals

TABLE 4. SUMMARY OF MONITORING METHODS - COMPOUND SPECIFIC MONITORS

MONITORING METHOD	SUBSTANCES MONITORED	BASIC PRINCIPLES INVOLVED	ADVANTAGES	DISADVANTAGES
• Gas Chromotography (With one of the following detectors)	• Volatile compounds	• Volatile compounds are absorbed onto a suitable column and then eluted with a carrier gas so that different compounds elute at different times and their concentrations are sensed by one of the following detectors:	• Well developed technology • Versatile instrument • Can be very sensitive to low concentrations when used with ionization detectors	• Slow response time • Column deterioration requires replacements • Mechanical complexity
- Flame Ionization	• Volatile organic compounds	• Measures electron current flow generated between electrodes when an eluted organic compound is burned in a hydrogen-air flame	• Very low detectable levels • Very little maintenance • Signal approximately a function of number of carbon atoms in compound	• Hydrogen and clean air supplies required
- Photoionization	• Volatile compounds	• Measures electron current flow generated between electrodes when volatile compound is irradiated with ultraviolet light	• Very low detectable levels possible • Very little maintenance	• Detector response depends on ionization potential of compound
- Flame Photometric	• Compounds containing sulfur	• Detects ultraviolet radiation resulting from burning sulfur compounds in a hydrogen flame	• Very specific for sulfur compounds • Very low detectable levels	• Hydrogen and clean air supplies required
- Thermal Conductivity	• Volatile compounds	• Sample and carrier gas flow over a heated resistance wire. Changes in thermal conductivity of gas cause changes of wire resistance which is measured	• Simple and inexpensive	• Minimum detectable levels not low enough for many applications

TABLE 4. SUMMARY OF MONITORING METHODS - COMPOUND SPECIFIC MONITORS (Cont'd.)

MONITORING METHOD	SUBSTANCES MONITORED	BASIC PRINCIPLES INVOLVED	ADVANTAGES	DISADVANTAGES
• Infrared Absorbance	• Most volatile compounds that absorb infrared radiation			
- Fourier Transform Infrared (FTIR)	• Most volatile compounds that absorb infrared radiation	• Radiation from an infrared source is split into two beams travelling separate paths by means of a beam splitter and mirrors and the two beams are then recombined into one. • An interferogram is generated at the detector by varying one of the paths (based on Michelson's work in 1880) • Operational and computational algorithms (Fourier Method) are used to automatically and simultaneously measure the concentration of several molecular species • Microprocessors are used to implement the algorithms in seconds	• Very short time (seconds) required for analysis • Extremely high resolution makes possible the elimination of interferences • Signal to noise (minimum detectable level) can be improved by extending the analysis time • Handles multicomponent mixtures without separation steps	• Current analyzer designs require air conditioned room • Highly trained technician required for maintenance
- Non-dispersive Infrared	• Most volatile compounds that absorb infrared radiation	• Chopped IR light beams are passed through a reference cell and a sample cell. Detectors sense differences in radiant energy in each path due to absorption • The difference in IR absorption is a measure of the component being measured.	• Simple mechanical design	• Interferences from other chemical compounds

TABLE 4. SUMMARY OF MONITORING METHODS - COMPOUND SPECIFIC MONITORS (Cont'd.)

MONITORING METHOD	SUBSTANCES MONITORED	BASIC PRINCIPLES INVOLVED	ADVANTAGES	DISADVANTAGES
- Variable Wavelength IR (Interference Filters)	• Most compounds that absorb IR	• Infrared radiation entering a sample chamber is filtered sequentia'ly by two or more interference filters in a cyclic manner • The interference filters are selected to pass desired wavelength bands of IR spectra of compounds being measured or interferirg with the analysis • A microprocessor is used to synchronize the IR detector readings with the interference filters and compute the concentrations of compounds after correcting for the overlapping of IR absorption spectra	• Simple mechanical design	• Interferences from other chemical substances present serious application problems • Not suitable for monitoring compounds with PEL's in low ppm range
• Colorimetry (Sensitized tape)	• Gaseous compounds that react with chemical reagents to produce a chemical substance with strong absorption spectra	• The air sample is impinged on a moving tape sensitized to develop a chemical compound that absorbs infrared radiation • A photometer is used to measure the quantity of the IR absorbing compound produced. The quantity of IR absorbing compound produced is a measure of the concentration of chemical compound of interest in the incoming air sample	• Simplicity and low cost • Can be very sensitive and selective	• Slow response (3 to 20 minutes) • Reagents required

TABLE 4. SUMMARY OF MONITORING METHODS - COMPOUND SPECIFIC MONITORS (Cont'd.)

MONITORING METHOD	SUBSTANCES MONITORED	BASIC PRINCIPLES INVOLVED	ADVANTAGES	DISADVANTAGES
• Colorimetry (Aqueous Media)	• Gaseous compounds that react with chemical reagents to produce a chemical substance with a strong absorption spectra	• The air sample is drawn through an aliquot of aqueous reagent solution and the chemical compound reacts to produce a chemical substance with a strong absorption spectra • A colorimeter is used to measure the quantity of the light absorbing compound produced. The quantity of light absorbing compound produced is a measure of the concentration of the chemical compound of interest in the incoming air sample	• Can be very sensitive and selective	• Slow response, 3-6 min. • Reagents required • Usually high maintenance required
• Luminescence	• A limited number of compounds	• The incoming air sample is reacted with a gaseous reagent to produce excited molecules which emit radiation in the UV range • The measured UV radiation is proportional to the concentration of the chemical being measured.	• Sensitive to selected compounds • Simple concept	• Limited range of compounds
• Electrochemistry	• Any gaseous compound that undergoes oxidation or reduction in an electrochemical cell.	• Measurement of electrical potential differences or current flow created by reaction of the compound within an electrochemical cell electrolyte or on electrode surfaces • Chemical scavengers are often employed to remove interfering compounds from the incoming air sample	• Low cost instrument	• Interfering compounds need to be removed from air samples • Slow response time

TABLE 5. SUMMARY OF MONITORING METHODS - MISCELLANEOUS COMPOUND SPECIFIC MONITORS

MONITORING METHOD	SUBSTANCES MONITORED	BASIC PRINCIPLES INVOLVED	ADVANTAGES	DISADVANTAGES
• Second Derivative Spectroscopy	• Volatile compounds that absorb light in the UV range	• A UV monochrometer is used to provide essentially monochromatic light to the sample cell. The radiation entering the sample cell is modulated with respect to time • The second derivative of the absorption spectra is determined electronically. The second derivative of the absorption spectra is linear with concentration	• Reduces the effect of interfering substances that show background absorption at the measuring wavelength	• Slow response time
• UV Absorption	• Certain compounds absorbing in the UV region	• Chopped UV light at a specified narrow wavelength range is passed through the sample chamber and a reference cell • The difference in absorption between the two light beams is a function of concentration of the compound being measured	• Low minimum detectable levels and high selectivity may be possible	• Only useful for measuring a limited number of compounds
• Semiconductor Matrix	• Gases that diffuse into and ionize within the matrix and cause a change in conductivity • Gases that adsorb and desorb and cause a change in electrical conductivity	• The sensor consists of a semiconductor matrix surrounding a constant temperature heating element. The matrix is sensitized to specific compounds of interest • When the chemical in the air sample interacts with the matrix and ionizes, a change in electrical conductivity takes place • The change in electrical conductivity is a measure of the concentration of the chemical being monitored	• Simple mechanical design	• Problems with interfering substances • Minimum detectable level acceptable in a limited number of applications • Zero drift may not be acceptable for certain applications
• Mass Spectrometry (time of flight) (other types possible)	• Volatile compounds	• The sample gas is ionized by a pulsed electron beam. The species of different mass numbers are separated by subjecting the ionized fragments to a negative polarity accelerating field, and allowing the ionized particles to pass through a drift region. The lighter ionized particles travel faster than the larger particles. Each compound generates a characteristic spectrum.	• Simple to operate	• Not useful for monitoring substances below 50 ppm concentration levels.

TABLE 6. SUMMARY OF MONITORING METHODS - MISCELLANEOUS COMPOUND NON-SPECIFIC MONITORS

MONITORING METHOD	SUBSTANCES MONITORED	BASIC PRINCIPLES INVOLVED	ADVANTAGES	DISADVANTAGES
• Flame Ionization	• Volatile Organic Chemicals	• Measures electron current flow generated between electrodes when an organic compound in the air sample is burned in a hydrogen-air flame. The electron current is proportional to the number of carbon atoms for certain families of organic compounds	• Very sensitive to organic chemicals	• Non-specific
• Photoionization	• Volatile Chemicals	• Measures electron current flow generated between electrodes when volatile compound is irradiated with ultraviolet light. The electron current is proportional to the concentration of the chemical	• Very sensitive • Simple mechanical design	• Non-specific
• Scattered Light	• All Aerosols and Particulates	• Aerosols or particles in an air sample stream passing through a beam of light will scatter impinging light • The scattered light intensity is a non-linear function of the particle concentration and particle size distribution • In some instances, a manufacturer claims, the signal from a scattered light detector can be analyzed in order to determine the amount of light scattered by particles within a given size range. This information can then be processed with a microprocessor to produce a signal linear with particle concentration	• Very sensitive for small particle sizes	• Non-specific • Needs to be calibrated for each application - Very sensitive to particle size distribution
• Electrostatic Precipitator/ Quartz Transducer	• Solids and Aerosols	• An electrostatic precipitator forces particles to land on a quartz crystal. As the dust collects on the crystal, the operating frequency of the crystal varies proportionally	• Simple to operate	• Non-specific
• Beta Gage	• Solids and Aerosols	• Particles are collected on a tape. The collected particles absorb Beta rays proportional to the total mass of particles collected	• Simple to operate	• Non-specific

AIR QUALITY AND THE ENVIRONMENTAL EFFECTS FROM AN UNDERGROUND COAL GASIFICATION TEST

P. W. Seabaugh, R. E. Zielinski and A. K. Agarwal
Monsanto Research Corporation
Mound Facility*
Miamisburg, Ohio 45342

J. W. Martin and A. J. Liberatore
U. S. Department of Energy
Morgantown Energy Technology Center
Morgantown, West Virginia 26505

ABSTRACT

In-situ coal gasification is a new technology currently under development by the United States Department of Energy (DOE). The Pricetown I field test is part of this continuing effort and was performed by DOE's Morgantown Energy Technology Center with Mound Facility providing the major instrumental and field crew support. The use of eastern bituminous coal resources with high sulfur content could be limited because of environmental regulations. Consequently an examination of the impact of sulfur containing and other possible gaseous components from the in-situ gasification on air quality is desirable from both an environmental and economical viewpoint. Using fast response analytical systems and real-time data acquisition a high density data base was acquired for 17 gaseous components of the product gas stream, including SO_2, H_2S, COS and HCN. The data show that almost all gaseous sulfur from the bituminous coal was emitted as H_2S. The SO_2 and COS values rarely exceeded the background of the instruments although the COS values did rise to about 100 ppm during the gasification phase. Except for one short period when values rose to 60 ppm, the HCN similarly stayed at the instrument background level of about 1 ppm. Because proven technology to clean H_2S from gas streams is available, the Pricetown test indicates that in-situ gasification of high sulfur bituminous coal on a commercial scale should not contribute to deterioration in air quality.

*Mound Facility is operated by the Monsanto Research Corporation for the U.S. Department of Energy under Contract No. DE-AC04-76-DP00053.

INTRODUCTION

As an alternative to oil and gas, the accelerated development of vast coal reserves invite an assessment of the realities of coal usage, including environmental considerations. Numerous coal reserves are not economically recoverable using conventional mining techniques. Underground coal gasification (UCG) offers a means of recovering energy in the form of heat and gas from coal without mining. It is a technology currently under development by the United States Department of Energy (DOE) with the Pricetown I field test[1] being a part of this continuing effort.

Because the use of eastern bituminous coal resources with high sulfur content could be limited by environmental regulations, an examination of the impact of sulfur containing and other possible gaseous components in the produced gas on air quality is desirable. Potential air pollutants[2] from coal include sulfur in the form of hydrogen sulfide (H_2S), sulfur dioxide (SO_2), carbonyl sulfide (COS), and carbon disulfide (CS_2), and nitrogen in the form of nitrogen oxides. Coal is known to be a heterogeneous material containing pyrite, sulfate, and organic sulfur. Conversion of the inorganic and organic forms of sulfur to their end products is not precisely understood but most likely involves different mechanisms. Similarly the conditions and factors controlling the conversion of coal bounded nitrogen to oxides and molecular nitrogen are not well understood[3]. Careful monitoring and high data density of produced gas compositions and process conditions will provide a data base from which insights can be gained for the development of controls for these potential pollutants. To evaluate the impact of potential air pollutants during the Pricetown I test, a high density data base was acquired for 17 gaseous components[4] of the produced gas using fast response analytical systems and real-time data acquisition.

DISCUSSION AND RESULTS

For discussion purposes coal combustion can be characterized by two distinct processes, decolatilization and gasification. To structure the analysis, the Pricetown I test is partitioned into six distinct phases which reflect a varying mix between these processes. Table 1 provides the identification and

dates for phase. During each phase high density data on gaseous sulfur and nitrogen species as well as process parameters were acquired for process and environmental evaluation purposes.

Analysis of the produced gas stream before entry to the incinerator shows that almost all gaseous sulfur from the bituminous coal was emitted as H_2S. Therefore the emitted SO_2 resulted from conversion of H_2S within the incinerator to SO_2. The amount of SO_2 emitted was computed by considering the stoichiometic conversion of H_2S to SO_2 as indicated by the equation

$$H_2S + 3/2\ O_2 \longrightarrow SO_2 + H_2O$$

In accordance with the stoichiometric equation, Figures 1-2 present the production of sulfur in lb/hr for the two phases of the test. As shown the hourly data depicts the overall change in sulfur production with most of the larger variations being associated with surface process changes. Trends and changes in trends are suggested in the cumulative plots shown in Figures 3 and 4. In Figure 3 the onset of a higher production rate during LE-1 is indicated by the break in the cumulative line on about August 16, 1979. By contrast, steady sulfur production rate during LE-2 can be deduced by the essentially constant slope shown in Figure 4. Table 2 summarizes the amount of SO_2 and sulfur produced for each phase of the test. As shown there the test generated less than 50 tons of SO_2 which is about one-half the amount permitted for a research and development operation.

A criterion[5] for the selection of a sulfur removal process is the CO_2/H_2S ratio. Normally high ratios favor processes that selectively remove H_2S whereas low ratios allow nonselective processes. Typical CO_2/H_2S ratios for the phases of the Pricetown I test are presented in Table 3. The ratios exhibit a range from 5-10 which would allow the selection of several candidate processes, depending on rates, compositions, and actual operating conditions[6]. For some processes, the exact amount of removal will depend on whether the process is used for selective or bulk removal of H_2S or CO_2 and on operating conditions. The hot carbonate (Benfield) and Stretford processes[5,6] probably warrant consideration. For CO_2/H_2S ratios greater than 8, reasonable estimate[6] of capital cost can be made by considering only CO_2 removal with the hot

carbonate process. In contrast, the Stretford process is highly selective to H_2S removal in the presence of CO_2.

In addition to their potential impact on the environment the gaseous sulfur and nitrogen components can mirror coal processes. The chemical transformation[7,8] of sulfur is affected by the relative rates of the competing devolatilization and gasification mechanisms and reactions and from devolatilization studies[9] it can be inferred that inorganic sulfur decomposes to mostly H_2S in the gas phase. Most of the organic sulfur bounded as sulfides and mercaptans will decompose to H_2S and CS_2, thus becoming another source for H_2S. Sample depths and relative amounts[10] of inorganic and organic sulfur are given in Table 3. The absence of SO_2 during both linkage and gasification phases could suggest that sulfur primarily is converted to the gaseous form through devolatilization reactions. Evaluation of the parallel tracking of ethane and H_2S as documented by the gas composition data further supports a conclusion for efficient thermo- and hydro-cracking of oils and tars during the predominantly devolatilization phases. From this aspect it is clear that the Pricetown I instrumentation approach can provide an opportunity for choosing an acceptable mix among competing criteria. Creating a response surface from which to set parameters to maximize the BTU content of the produced gas would at the same time tend to maximize the H_2S production. Similarly data acquired for other environmentally related species such as COS, HCN, NO and NO_2 could be used to generate multiple response surfaces for decision making on the maintenance of a desired balance via a feedback-control mechanism among competing environmental and economical criteria.

As previously indicated, the most important sulfur and nitrogen species of environmental significance was H_2S. Other species rarely exceeded their background levels although COS did rise to about 100 ppm during the gasification phase. Occasionally HCN would reach the 50 ppm level but generally stayed at the instrument background level of about 1 ppm. Nitrogen oxides reached levels ranging from 200-500 ppm with NO_x being zero for most of the test.

EXTRAPOLATION OF PRICETOWN I TEST RESULTS TO COMMERCIALIZATION VALUES

From Table 2 the average sulfur production rate in lb/day for the gasification phase can be approximated as 2100. The value is based on an average flow of about 2.8 MMSCFD and an average H_2S value of 0.9 mole%. Scaling to a 30 MMSCFD commercial size plant would forecast a production of about 11 tons/day.

With the CO_2/H_2S ratios provided in Table 3, it can be observed that the values ranged from 5-10 during the test. Because the flows varied from 0.06 to 2.8 MMSCFD for the same period, it can be inferred the same range of ratios could be expected for a 30 MMSCFD commercial size operation. Thus proven technology to clean H_2S from the produced gas should be available. For the gasification phase a HCN level of 1 ppm likewise suggests that HCN generated from a 30 MMSCFD plant would not degrade air quality.

SUMMARY

With the incentive to increase the use of high sulfur coal, methods and techniques for the detection, assessment, and control of nitrogen and sulfur pollutants have a prime emphasis. The Pricetown analytical and acquisition system was designed to acquire a high density data base for such detection, assessment, and control. The data indicate that the instrumention works exceedingly well, that near real-time control is feasible, and that commercial scale in-situ gasification of high sulfur bituminous coal should not degrade air quality.

REFERENCES

1. Zielinski, R. E., Seabaugh, P. W., Martin J. W., and Liberatore, A. J., "Eastern Underground Coal Gasification Process Instrumentation and Data Analysis," Proceedings of the 4th Underground Coal Conversion Symposium, Steamboat Springs, CO, July 17-20, 1978.

2. Phillips, W. R., "Purification of Gas from an In-Situ Coal Gasification Process," Proceedings of the 3rd Underground Coal Conversion Symposium, Fallen Leaf Lake, CA, June 6-9, 1978.

3. Wendt, J. O. L., Pershing, D. W., Lee, J. W., and Glass, J. W., 17th Symposium (International) on Combustion, The Combustion Institute, 77-87, 1978.

4. Zielinski, R. E., Seabaugh, P. W., Agarwal, A. K., Liberatore, A. J., and Martin, J. W., "Instrumentation Used for the Monitoring and Controlling of the Pricetown I Underground Coal Gasification Field Test," 1980 Symposium on Instrumentation and Control for Fossil Energy Processes, Virginia Beach, VA, June 1980.

5. Lovell, R. J., Dylewski, S. W., and Thurnau, R. C., "Control of Sulfur Emissions from Oil-Shale Retorts," 1980 Symposium on Instrumentation and Control for Fossil Energy Processes, Virginia Beach, VA, June 1980.

6. DRAVO Corporation, "Handbook of Gasifiers and Gas Treatment Systems," FE-1772-11, 1976.

7. Anthony, D. B., and Howard, J. B., AICHE J., 22 625 (1976).

8. Solomon, P. R., "The Evolution of Pollutants During the Rapid Devolatilization of Coal," Report NSF/RA-770422, NTIS No. PB 278496/AS.

9. Attar, A., Fuel, 1978, 57, 201-212.

10. Zielinski, R. E., and Larson, R. J., "A Physicochemical Evaluation of the HQ-1 Core from the Pricetown I, Underground Coal Gasification Test Site," MLM-MU-78-69-0005 (September 20, 1978).

TABLE 1. THE PRICETOWN I FIELD TEST IS CHARACTERIZED BY SIX PHASES.

PHASE	DATE
REVERSE COMBUSTION LINKAGE 1 (RCL-1)	JUNE 09 (13 HR)-JUNE 15 (11 HR)
REVERSE COMBUSTION LINKAGE 2 (RCL-2)	JUNE 15 (11 HR)-JULY 09 (15 HR)
REVERSE COMBUSTION LINKAGE 3 (RCL-3)	JULY 09 (15 HR)-JULY 23 (18 HR)
LINK ENHANCEMENT 1 (LE-1)	JULY 23 (18 HR)-AUG 19 (08 HR)
LINK ENHANCEMENT 2 (LE-2)	AUG 19 (08 HR)-SEPT 23 (16 HR)
GASIFICATION (GAS)	SEPT 23 (16 HR)-OCT 05 (12 HR)

TABLE 2. SULFUR DIOXIDE (SO_2) AND SULFUR SUBTOTALS AND GRAND TOTALS FOR THE SIX PHASES OF THE PRICETOWN I FIELD TEST, 1979

PHASE	DATE	LBS OF SO_2	LBS OF SULFUR
RCL-1	JUNE 09 (13 HR)-JUNE 15 (11 HR)	734	367
RCL-2	JUNE 15 (11 HR)-JULY 09 (15 HR)	3186	1593
RCL-3	JULY 09 (15 HR)-JULY 23 (18 HR)	1219	610
LE-1	JULY 23 (18 HR)-AUG 19 (08 HR)	3918	1959
LE-2	AUG 19 (08 HR)-SEPT 23 (16 HR)	38765	19383
GAS	SEPT 23 (16 HR)-OCT 05 (12 HR)	44455	22227
	GRAND TOTAL	92276	46139

TABLE 3. THE PRICETOWN UCG TEST PRODUCED A CO_2/H_2S RATIO TYPICALLY IN THE RANGE 5 TO 10, WHICH MAY ALLOW A NONSELECTIVE CLEANUP PROCESS

DATE	PHASE	CO_2/H_2S	RATIO
JUNE 13	RCL-1	11.1/1.6	6.9
JULY 04	RCL-2	10.5/2.0	5.3
JULY 21	RCL-3	11.3/2.0	5.7
AUG 10	LE-1	12.9/1.5	8.6
SEPT 14	LE-2	12.6/1.5	8.4
SEPT 29	GAS	9.0/1.1	8.2

TABLE 4. SULFUR FORMS AND DEPTHS FOR THE PRICETOWN HQ COAL CORE: DRY BASIS

SAMPLES	PR-1-22	PR-1-25	PR-1-26	PR-1-27	PR-1-28	PR-1-29
% PYRITIC SULFUR	9.60	4.58	2.19	0.86	0.74	0.64
% SULFATE SULFUR	0.04	0.00	0.00	0.00	0.00	0.00
% ORGANIC SULFUR	0.83	1.47	1.77	2.38	1.57	0.76
% TOTAL SULFUR	10.47	6.05	3.96	3.24	2.33	1.40

FIGURE 1

PRICETOWN I FIELD TEST RESULTS
REVERSE COMBUSTION LINKAGE - 2 PHASE
SULFUR PRODUCED DURING TEST PHASE

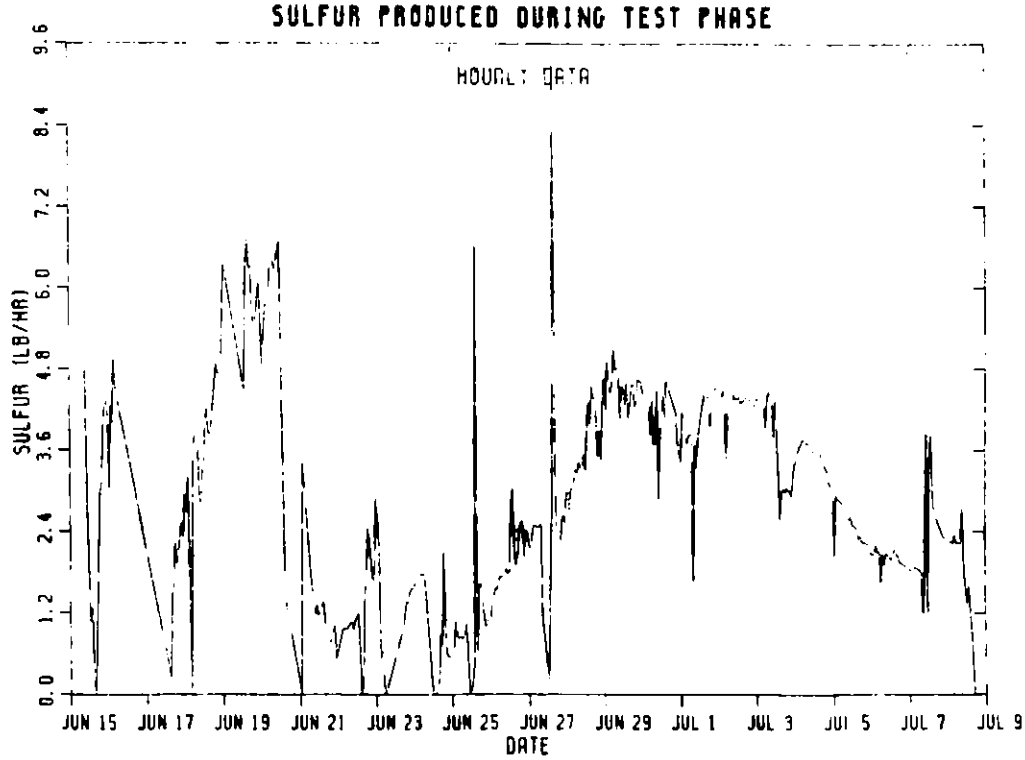

FIGURE 2

PRICETOWN I FIELD TEST RESULTS
ENHANCED LINKAGE - 2 PHASE
SULFUR PRODUCED DURING TEST PHASE

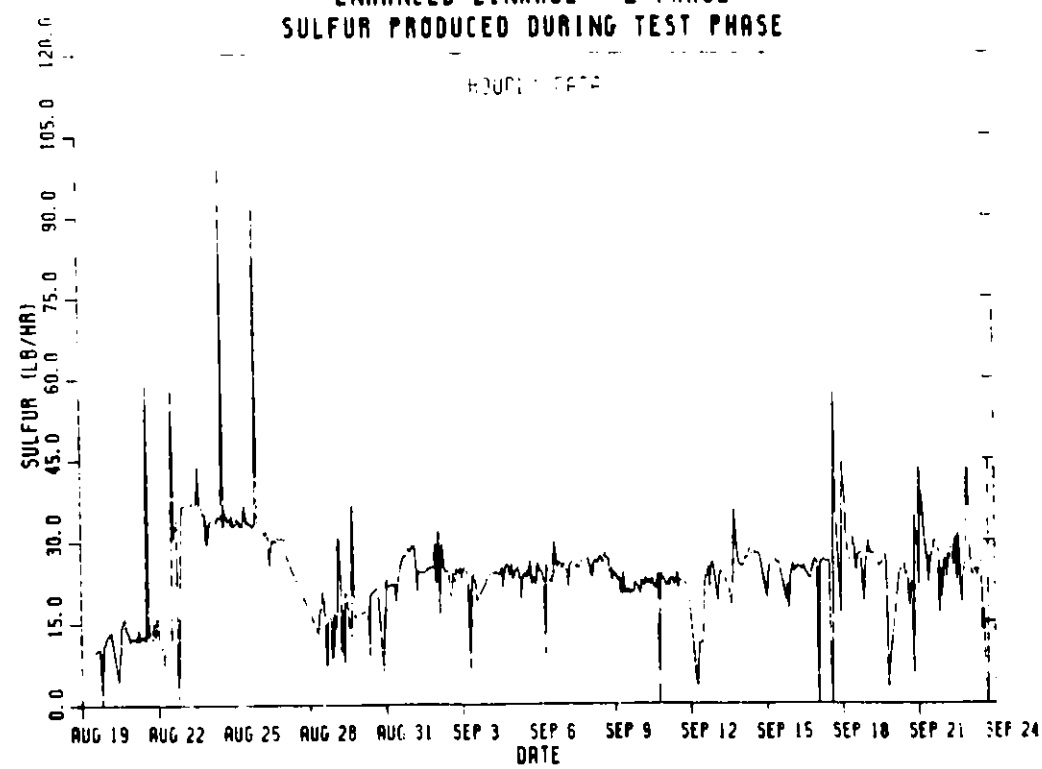

FIGURE 3

CUMULATIVE SULFUR FOR LE-1 PHASE

JULY 23 - AUG 19, 1979

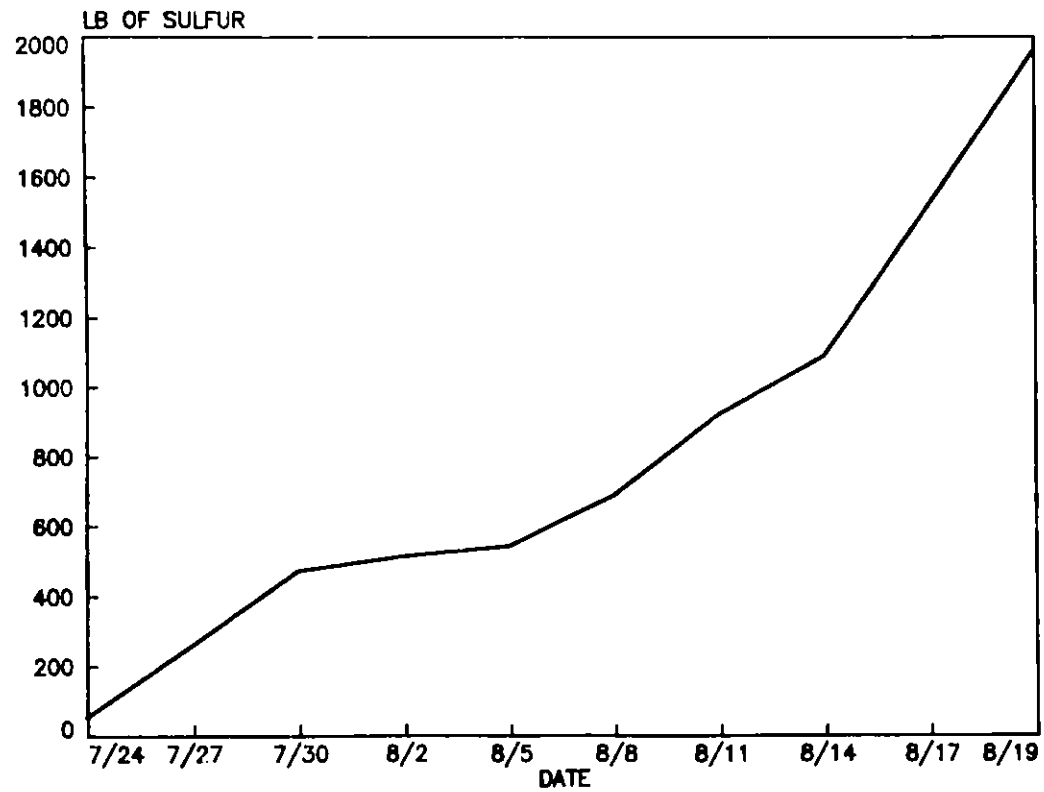

FIGURE 4

CUMULATIVE SULFUR FOR LE-2 PHASE

AUG 19 - SEPT 23, 1979

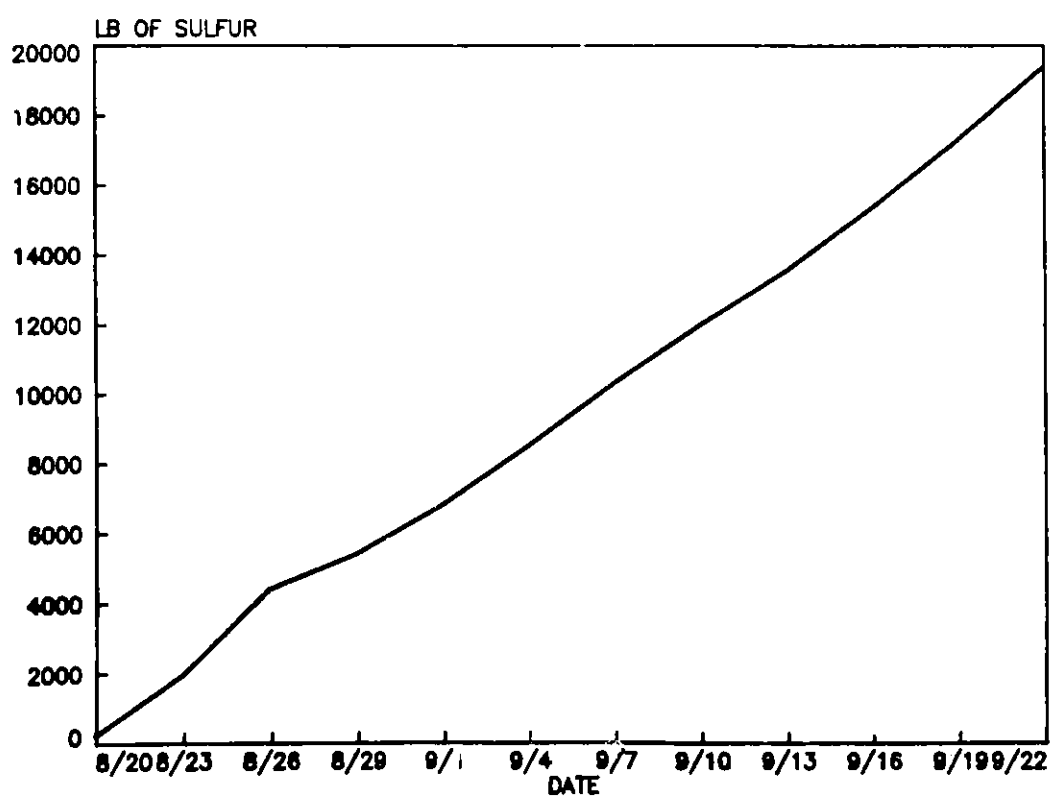

CONSIDERATIONS FOR THE DEVELOPMENT OF A LABORATORY FIELD SIMULATION PROGRAM FOR LANDFILL DISPOSAL OF COAL CONVERSION WASTES

By

William P. Gulledge [1/] and William A. Sack [2/]

INTRODUCTION

Technical requirements associated with the implementation of RCRA have promoted increased attention to landfill characteristics and attenuation mechanisms associated with solid waste disposal. Draft regulations for solid waste management identify specific quantitative technology for waste characterization and standards for disposal (1, 2). Compliance with the standards and cost-effective fill design will require a field simulation program which develops background information on waste characteristics and which is based on actual site information. This paper discusses some of the fundamental elements of such a program. A field simulation program for a proposed SRC II demonstration plant (3) is then developed to serve as a possible example.

The main purpose of a field simulation program is to develop, evaluate, and verify a methodology to simulate landfill leaching behavior with a minimum of field monitoring. The entire program must be cost effective such that it allows significant savings in dollar cost, yet provides results equivalent to a full scale field program. Confidence in the entire program is best obtained by understanding the individual program elements. The judicious use of sampling methods, laboratory testing, predictive models, and field monitoring practices provide the framework for a comprehensive field simulation program. At the outset, it must also be recognized that there are significant limitations on any laboratory-based program that is designed to approximate natural conditions and predict field conditions. Complicating factors include complex waste matrices, uncertainties regarding soil/leachate interaction over long time periods, actual performance of covers, liners and drainage systems, and uncertainties regarding actual site conditions including field placement of the waste, groundwater movement, and geological and climatic considerations. Field simulation programs should be relatively simply designed until these significant factors can be reliably estimated on the specific project level.

It is imperative to be aware of the physical and chemical characteristics of the proposed disposal site in order to properly simulate behavior in the laboratory. Table 1 lists some of the important waste and site characteristics which offset leachate generation and migration and which serve as input to the simulation program (4).

FIELD SIMULATION PROGRAM COMPONENTS

A number of approaches have been taken to simulate and predict field behavior. An adequate program should be systematically developed through

[1/] Environmental Engineer, Tennessee Valley Authority, Chattanooga, TN
[2/] Professor, Department of Civil Engineering, West Virginia University, Morgantown, WV

TABLE 1

CHARACTERISTICS AFFECTING LEACHATE MIGRATION

WASTE MATRIX	NATURAL CONDITIONS	POLLUTION MIGRATION
Waste Type	Groundwater Flow Rate	Rate of Migration
Buffering/Sorption Capacity of Waste	Groundwater Quality	Concentration of Gradients from Source Point
Rate of Leaching	Rate of Water Movement vs. Hydraulic Head	Plasticity and Liquid Limits of Soil
Controlled Leaching	Water Table	Vertical and Horizontal Migration
Linear or Asympotic Leaching Rate	Site Location	Oxidation vs. Reduction Conditions
	Relief Features	Gas Pocket Formation (Pore Space Geometry)
	Rainfall Characteristics	Disposal Site Age
	Freezing and Thawing	Liners/Covers Characteristics
	Evaporation Rates	Structural Integrity of Natural and Artificial Linders
		Soil pH
		Organic Matter Content of Soil

Source: Ref. 4

a series of specific tasks. Most programs involve some combination of sampling guidelines, laboratory testing, predictive modeling, and verification activity. Each of these components is discussed.

General Considerations and Sampling

A well designed sampling plan is fundamental to the success of the entire field simulation program, and yet sampling is usually given relatively little attention. The following considerations should be addressed.

1. Background information about the waste or soils;
2. Wastes or soils to be sampled;
3. Site presurvey to determine proper sampling points;
4. Sampling plan design to include choice of the proper sampler(s), sample containers, number, and volume of samples;
5. Sample handling procedures;
6. Sample shipping procedures;
7. Field and laboratory recordkeeping procedures;
8. Process information of the waste which has been produced.

Obtaining representative samples often requires considerable planning and effort. The physical characteristics of the waste will often dictate the method of sample collection and transport. The U.S. EPA in SW846(5) has identified six types of wastes based on the uniformity of the process generating the waste and the homogeneity of the contaminant distribution within the waste. The six types of waste are:

1. Uniformly homogeneous.
2. Non-uniformly homogeneous.
3. Uniformly, randomly heterogeneous.
4. Non-uniformly, randomly heterogeneous.
5. Uniformly, non-randomly heterogeneous.
6. Non-uniformly, non-randomly heterogeneous.

There are various suggested approaches for sampling the above waste types, and many methods are currently under review and revision. Obtaining a representative sample of a selected waste or statistically valid sample is a continuous concern, and if precision is an important element of the test program, it should be kept in mind that the standard error is inversely proportional to the square root of the number of samples tested. The best approach for designing a sample program is to incorporate as many site-specific, waste-specific variables as is possible.

Laboratory Testing Program

The laboratory testing program is a key element in the field simulation program linking the predictive modeling and field assessment elements. Conceptually, the laboratory program may be viewed both as a data generation link to supply information for use in predictive models and as a calibration or verification link to test assumptions used in predictive models.

In order to simulate field conditions, the laboratory program must consider characteristics of the waste and the site as well as other planned

features such as liners and covers. Table 2 lists a variety of tests which may be carried out on the waste and/or surrounding soils. In some cases, testing is done to determine if the waste is amenable to chemical stabilization/encapsulation procedures. Leachate extraction and subsequent contaminant attenuation on soil are widely used simulation procedures. Two basic types of leachate extraction procedures have been developed: batch and column extraction. A 24-hour batch extraction procedure (EP) using acetic acid has been prescribed by the EPA (6). Research conducted by Houle and Long (7) established a basis for the use of serial batch extraction testing as a foundation for predictive modeling. In a more complete approach, one combination of batch and column studies has been successfully used to simulate leaching action.

> "Batch experiments (as compared to column experiments)...eliminate the effect of convection and diffusion from the leaching process and provide information solely on the adsorption and/or precipitation phenomena. On completion of the batch experiments, the batch-column experiments 'are' performed to include the convection effects in the leaching process. The findings of the column studies...indicate that relative importance of diffusion with respect to convection and adsorption/precipitation." (8)

The above effort underway at the University of Miami is evaluating heavy metals attenuation using three different soil types. An initial batch extraction is conducted to determine the equilibrium attenuation time for shaking a given weight of waste material with a known volume of extractant. A second batch extraction is then conducted whereby varied weights of soil are shaken at the equilibrium time to determine adsorption isotherms for subsequent predictive modeling (8). The resulting field simulation activity is the determination of the maximum amount of cations absorbed by the soil for a specific environment.

Another component of the University of Miami program is the use of batch-column studies to simulate column tests.

> "Correlation between the two experiments essentially consists of interrelating the weight of the soil and volume of leachate used in the batch column experiment with the location of the ports and time interval between each sample collection of the continuous column experiment." (9)

This correlation of port volumes stems from work completed for EPA at the U.S. Army Dugway Proving Grounds. In summary, "the graded serial batch extraction procedure provides the flexibility, reliability, speed, and ease of interpretation needed to provide data for the derivation of empirical equations which contain a minimum of pitfalls for predicting the movement of...substances through soil." (7)

Gasifier slag similar to the waste which will be produced by the SRC II plant, has been subjected to both batch and column studies. Five types of batch leaching were conducted using a range of extractants ranging from distilled water to 0.1N HNO_3. The resulting leachates were analyzed for Be, SO_4, Cu, Ni, Fe, and all the elements of the EPA Interim Primary Drinking

Table 2 - Laboratory Tests Used In Field Simulation Studies

Test	Test Media	
	Waste	Site Soils
Leachate Extraction	X	X
Attenuation of leachate		X
Stabilization/Encapsulation	X	
Optimum Density	X	
Bearing Capacity	X	
Permeability	X	X
Particles Size Distribution	X	X
Gas Generation	X	
Compatability With Liner	X	X
Chemical Composition	X	X
Minerological	X	X
Runoff/Infiltration	X	

Water Standards. Column studies were also performed whereby twelve inches of slag were dosed daily with one liter of deionized water. Results indicate column leachate concentrations were less than batch leachates, and that the slag material is relatively inert. The leaching of trace metals does not appear to be a problem (3).

As indicated in Table 2 a variety of physical tests are often quite valuable for field simulation studies. In a study sponsored by EPRI on FGD sludge (10), samples were taken using a Shelby tube from an actual landfill for physical characterization of the waste and underlying soils. Tests were also conducted to measure saturated permeability and partially saturated hydraulic conductivity as a function of moisture content and pressure. Other tests carried out included particle density, bulk density, particle size, and water retention. Runoff testing maybe desirable to estimate potential loss of contaminants during construction. A runoff simulation box was used (11) to estimate washoff rates of trace metals from fly ash and to determine gross rates of infiltration of water into the ash. Further consideration is needed toward applying results from the testing procedures into predictive models and field verification efforts.

Predictive Modeling

Extraction and subsequent inorganic and/or organic analysis data can provide input into various predictive modeling uses such as equilibrium concentrations of selected trace elements or steady state soil attenuation. Models which are designed to predict saturated flow equilibrium are well developed. These leachate migration models have been developed in one, two, and three dimensions with the one-dimensional models experiencing wide spread use. A two-dimensional hydrologic model is being used (10) to predict contaminant distribution, arrival time (assumes no attenuation), and groundwater flow rates in FGD sludge. The model, which uses a finite difference formulation to represent the partial differential flow equation with numerical expressions, was calibrated using actual groundwater elevation data. The Waterways Experiment Station (12) recently developed an interactive computer program to simulate runoff, deep percolation, temperature, soil-water, and evapotranspiration of a waste disposal site. The model which can be used to take into account the influence of a cover and liner, is a modification of an SCS runoff method and the hydrologic portion of the USDA-SEA hydrologic model (CREAMS).

Research underway at the University of Notre Dame on fly ash pond leachates is designed to "develop a series of mathematical models for soil-water systems which couple the features of a finite element approach for describing the hydrodynamic flow regime and conservative solute transport with an equilibrium description of the sorption, ion exchange, precipitation, and complex formation reactions" (13). Plans are also underway to utilize this model on one-dimensional laboratory soil columns and to develop two-dimensional inorganic and organic transport models.

Previously mentioned research at the University of Miami has included one-, two-, and three-dimensional modeling. This activity involves the use of volume average transport equations formulated by Langmuir coefficients (8). The resulting leachate production and migration information will be field

verified. This approach to using Langmuir isotherms is based on the use of distribution coefficients or measurement of the retention of the solute by the soil matrix, a very important consideration in disposal site design.

An excellent review of simulation models as applied to landfill disposal siting was done by van Genuchten (14). He concludes that while tremendous progress in simulation technology has been achieved, no model yet exists which can simulate all of the physical, chemical, and biological processes that are operative in landfills.

Field Assessments

Verification of mathematical models is an important step in a field simulation program. This may be accomplished on either a small or large scale, although a smaller program enables greater control. Mixtures of sludge and fly ash have been recently monitored on both scales for permeability and leachate analysis. Small scale impoundments were constructed using above ground, vinyl-lined swimming pools with a capacity of 25 cubic yards of waste. Provision was made for collection of run-off, and primary and secondary leachates (15).

Five larger scale impoundments were also constructed, each with a capacity of 50 cubic yards. Soil moisture was monitored by suction lysimeters placed 6", 24", and 72" beneath the disposal site. Periodic analysis of groundwater and leachate indicated no contamination of surrounding groundwater by the sludge/fly ash mixture (15).

An experimental landfill (approximately 60' x 100') was constructed by the Tennessee Valley Authority for assessing the physical and chemical properties of scrubber sludge treated with forced oxidation. Runoff leachate and groundwater were sampled and analyzed for major and trace element species. Preliminary results from the early stage of this study determined that the landfill substratum is relatively impermeable and that the leachate and runoff are having no immediate effect on groundwater (16).

Very important to any field assessment program is the instrumentation used for leachate and groundwater monitoring. Piezometers are commonly used to determine pressure distribution within various geological and groundwater situations. Water sampling can also be undertaken if appropriate sealing materials are used in the drill hole. To determine any complex hydrogeological situation, the use of multiple piezometers and samplers should be used. An innovative approach to obtaining these multiple determinations is through the use of multiple valved piezometers within a single drill hole. By using inflatable packers between sampling locations, a single sample tube apparatus can be used. This approach offers a considerable advantage over trying to place several piezometer installations within a single drill hole (17), and the use of multiple piezometers on small landfills may provide an added degree of confidence in field assessments.

COMPREHENSIVE PROGRAM DEVELOPMENT

A field simulation program designed to interrelate laboratory and modeling activities and which is based on actual field data, is outlined below for the

proposed SRC II plant. The SRC II demonstration plant is to be located near Morgantown, West Virginia, and is to process approximately 6,000 tons of coal per stream day. As noted in Figure 1, many program components are interrelated. Major outputs and inputs of the program components are noted in Table 3.

Field Simulation Program for SRC II Wastes

It is estimated (3) that almost 800 dry tons per day (tpd) of solid waste residuals could be produced by SRC II in four major streams. Gasifier slag (720 tpd) makes up the bulk of the waste with lesser amounts of process sludges (43 tpd), spend catalysts and adsorbents (1 tpd) and salt brine (22 tpd) produced from an intermittantly operated zero discharge wastewater treatment system. Separate secure disposal landfills are planned for the gasifier slag and process sludges; hence they should be considered separately in the field simulation program. Preliminary investigation indicates that soils in the area of the proposed secure landfills are generally deep and of variable permeability and high silt and clay content. The following major steps are outlined for undertaking a program for the disposal of SRC II solid wastes:

- Verify and complete information for the proposed disposal sites. Existing data on hydrology, soils, geology and other site specific considerations should be compiled to be used as input to model variables and to field investigation plans. Variables of importance include depth to groundwater table, direction of groundwater flow, and soil permeability. Representative soil samples should be acquired for testing.

- Characterize solid wastes and soils. Analyze all solid waste materials quantitatively for inorganic trace metals and qualitatively for identified toxic organics. Quantitative analysis of toxic organics should be undertaken if the qualitative results indicate a significant presence of a specific class or compound. Characterization of slag produced from a Texaco Gasifier has been undertaken by ORNL (3). Data on the composition of process sludges, spent catalysts and salt brine are needed to identify potential hazardous components, water soluble compounds and elements which may be incompatible with liner material. Physical and chemical testing should also be performed on site soils as indicated in Table 2.

- Conduct batch extractions of all soild wastes and selected soil samples. At least two extractants should be used for each solid waste to cover both a worst case and the anticipated actual fill condition. For example, the EPA-EP which uses an acetic acid extractant is often considered to give worst case conditions for extraction of inorganic waste while a deionized water extraction may be more representative of actual conditions. Since it is proposed to use a common landfill for a number of the process wastes which are both organic and inorganic in nature, careful consideration must be given to evaluate multiple waste and leachate interactions. Extraction tests can be designed to provide data on leaching rate, degree of hazard, and worst case environmental impact. Extracts should be analyzed for inorganic (trace

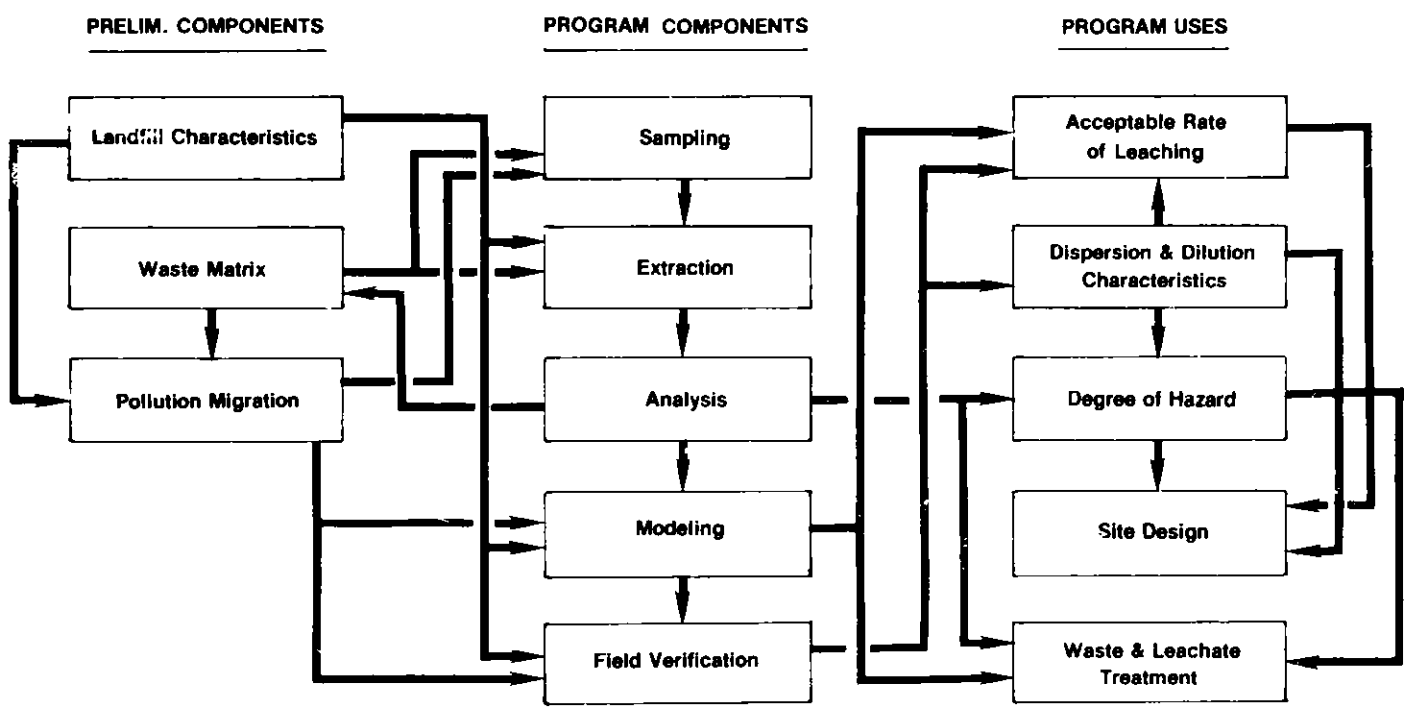

FIELD SIMULATION PROGRAM

FIGURE 1

TABLE 3

DESCRIPTION OF PROGRAM COMPONENTS

COMPONENT	INPUT	OUTPUT
1. Landfill Characteristics	A. Groundwater Flow and Quality B. Water Table C. Site Location and Characteristics D. Climatology	A. Site Specific Modeling Parameters B. Input to Design of Field Program
2. Waste Matrix	A. Waste Type and Composition B. Buffering/Sorption Capacity C. Leaching Characteristics	A. Selection of Sampler and Development of Sampling Plan B. Use/Selection of Extraction Procedures
3. Pollution Migration	A. Leachate Concentration B. Soil Characteristics C. Ionic Activity D. Disposal Site Age	A. Development of Predictive Models B. Selection of Monitoring Wells and Development of Field Program
4. Sampling	A. Waste Composition B. Waste Concentration	A. Sample for Subsequent Extraction
5. Extraction	A. Waste Sample B. Leaching Medium	A. Simulated Leachate
6. Analysis of Extract	A. Simulated Leachate B. Selection of Parameters for Analysis	A. Equilibrium Constants for Modeling B. Concentration of Selected Parameters
7. Modeling	A. Equilibrium Coefficients (Langmuir) B. Site Specific Considerations (Possible Adjustment to Equations) C. Extract Concentrations	A. Leachate Dispersion and Dilution Characteristics B. Leaching Rate C. Design of Field Monitoring Program
8. Field Verification	A. Groundwater Movement, Location, and Quantity B. Soil Composition C. Landfill Location (Near Surface Water?)	A. Leachate Dispersion and Dilution Characteristics B. Model Verification
9. Determine Acceptable Rate of Leaching	A. Leachate Movement Models B. Field Analysis Results from Monitoring	A. Design of Appropriate Disposal Site (Liners, Leachate Collection, etc.) B. Design Leachate Treatment System
10. Dispersion and Dilution Characteristics	A. Leachate Migration/Attenuation Models B. Field Monitoring/Leachate Concentration Results	A. Disposal Site Design Information B. Establish Hazard Degree of Waste in Landfill
11. Degree of Hazard Assessment	A. Analysis of Waste Material and Leachate B. Dispersion and Dilution of Leachate	A. Design of Disposal Site Information B. Assess Treatment Alternatives for Waste C. Pretreatment Options for Waste Material
12. Design of Disposal Site	A. Hazard Degree of Waste B. Predicted Dispersion and Dilution	A. Design of Disposal Site with Proper Degree of Control B. Selection of Appropriate Liner Material
13. Waste and Leachate Treatment	A. Analysis of Waste Material and Leachate B. Predictive Modeling of Leachate Concentration and Dispersion C. Degree of Hazard of Waste and Leachate	A. Design of Adequate Treatment System

metals, sulfur species, calcium) and toxic organics identified from the analysis of the waste sample (if modeling of organics attenuation is desired). Trace metals analysis can provide data on degree of hazard while parameters of higher concentration such as sulfate, chloride and calcium compounds (water extraction) can be useful for modeling efforts.

Extracts from the leaching of gasifier slag have already been analyzed for trace metals using five types of batch leaching (3). This information should be supplemented as needed with additional leachate tests and used for modeling input. Extraction of samples of process sludges, spend catalysts, and salt brine should be undertaken to provide similar information. It is recognized that obtaining representative samples of the later types of waste materials may be difficult, but simulated wastes or samples from similar industrial processes should be used in a limited manner for extraction testing. Soil samples from the planned disposal sites should be subjected to batch and batch-column tests to determine adsorption and equilibrium attenuation coefficients for leachate modeling of the disposal sites. Appropriate leachate from the solid waste extraction testing will be used as feed to the soil samples.

- Perform one-, two-, or three-dimensional leachate dispersion and dilution models of disposal sites. Langmuir coefficient models in one-, two-, or three-dimension can be used to estimate linear equilibrium adsorption conditions and account for maximum solubility values however, because of the soil characteristics and geology of the planned disposal sites (mine spoil overburden) a steady state equilibrium model may not be appropriate. A model or series of models are needed to predict contaminant transport in fractured and cavernous areas and to handle chemical attenuation processes for these geological conditions. A particle-tracking simulation model rather than a transport model may be appropriate for this situation.

- Establish column studies to correlate one-dimensional model results with column leaching behavior. Column extraction tests using the solid waste materials should be undertaken to compare leachate concentrations from these tests with batch extraction results and predicted concentrations from modeling. While the column tests will not provide a completely accurate picture of vertical leachate migration, they will furnish an approximation of major element leaching which can be correlated with models. Potential environmental impact from trace metal leaching can also be partly assessed from column studies.

- Correlate batch and column test results and predictions from two- and three-dimensional models with field monitoring program. Separate test landfill cells could be established for: 1) gasifier slag and 2) process sludges and other solid wastes for which common disposal is planned. The cells should be watered to simulate average annual precipitation and representative liner and leachate collection systems should be used to help determine compatability between liner and waste material and to assess extent of leachate production, migration, and

waste/soil attenuation. Test cells constructed with an adequate depth and designed to represent actual disposal conditions can be used to verify leachate concentrations predicted from modeling.

- Reevaluate disposal sites designs based on the field simulation effort and determine modifications needed or leachate treatment needs. Preliminary designs for the slag disposal area are shown in Figure 2. Results from the leachate extraction tests, modeling, and field monitoring can be used to prepare detailed designs of the liner, leachate collection and treatment system, and plans for the placement of the slag. Field simulation results on the other SRC II solid wastes can be similarly used in the preliminary design effort for the landfill designated to receive these wastes.

The last five components of Table 3 summarized potential use of a field simulation program. Each component is discussed in light of the SRC II project:

- Dispersion and dilution characteristics - Predictive modeling provides information on the rate, pattern, and potential toxics associated with leachate migration. Three-dimensional modeling has been utilized on existing fossil energy solid waste disposal sites; however, more tested one- and two-dimension models are recommended for use on the SRC II disposal sites.

- Degree of hazard assessment - Leachate extraction methods, analysis of solid wastes and extracts, and dispersion modeling can provide quantitative information on potential toxicity associated with the disposal of SRC II solid wastes. In turn, this information can be used to classify the waste by degree of hazard, with subsequent environmental control technology based on degree of hazard (18, 19). Specifically, pretreatment needs of the process sludges or salt brine, or treatment of the leachates produced from disposal can be assessed from the degree of hazard information.

- Disposal site design and monitoring - Information on degree of hazard model outputs, and environmental control technology can provide input into the necessary design requirements for a disposal site. The placement of leachate and groundwater monitoring instrumentation can also be aided by determining leachate movement rate and attenuation through extraction tests and modeling, and through characterization of site specific conditions.

CONCLUSIONS

1. A laboratory-based field simulation program for coal conversion solid waste disposal can provide valuable predictive information on the potential health and environmental effects that may result from landfill disposal of solid, semi-solid, and liquid waste materials.

2. The most reliable information on leachate migration can be obtained from field monitoring; however, large scale monitoring programs are cost

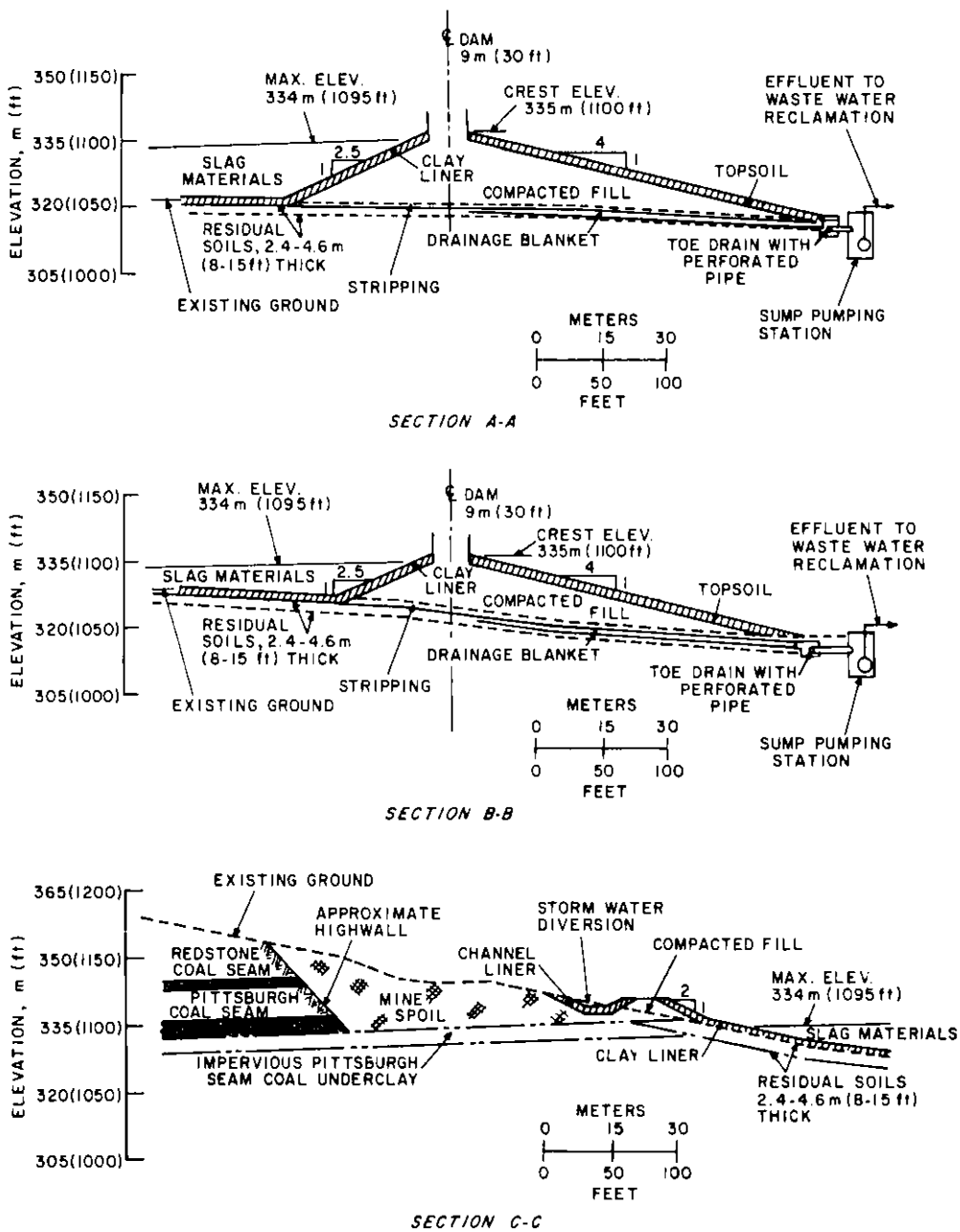

FIGURE 2. CROSS SECTIONS OF THE PROPOSED SLAG DISPOSAL AREA

prohibitive, and the simulation program seeks equivalent information at considerable cost savings.

3. A framework for a field simulation program has been given in this paper. Implementation of the program at the SRC II Demonstration Plant can aid in the development of the solid waste management system. References provided in this paper can be used to obtain specific information on program components with which the reader can use site-specific factors to design a site-specific/waste-specific simulation study.

4. Instrumentation and monitoring needs for the field simulation program center primarily on groundwater and leachate monitoring. Applicable equipment includes groundwater monitoring wells, well casings, packers, piezometers, automated samplers, and other site-specific items which may be required. Samplers required to collect surface run-off should also be included.

REFERENCES

1. Environmental Protection Agency, "Landfill Disposal of Solid Waste," Proposed Guidelines, Federal Register, March 26, 1979.

2. Environmental Protection Agency, "Hazardous Waste Guidelines and Regulations," Proposed Rules, Federal Register, December 18, 1978.

3. Department of Energy, Final Environmental Impact Statement, Solvent Refined Coal-II Demonstration Project, Volumes 1 and 2, January 1981.

4. Marshall Siting, Noyes Data Corporation. Landfill Disposal of Hazardous Wastes and Sludges, 1979.

5. Environmental Protection Agency, Test Methods for Evaluating Solid Waste - Physical Chemical Methods, SW846, 1980.

6. Environmental Protection Agency, "Hazardous Waste Management System," Rules and Regulations, Federal Register, May 19, 1980.

7. Martin J. Houle and Duane E. Long, "Interpreting Results from Serial Batch Extraction Tests of Wastes and Soils," in Disposal of Hazardous Waste, Proceedings of the Sixth Annual Research Symposium, EPA-600/9-80-010, March 1980.

8. Subrata Sengupta et al, University of Miami, Semi-Annual Report: Characterization and Environmental Studies of Pompano Beach Anaerobic Digestion Facility, Department of Energy, February 1980.

9. Subrata Sengupta et al, Annual Report: Characterization and Environmental Studies of Pompano Beach Anaerobic Digestion Facility, University of Miami, August 1979.

10. Electric Power Research Institute, Modeling the Fixed FGD Sludge Landfill - Conesville, Ohio (Phase I), Interim Report, CS-1355, March 1980.

11. TRC Environmental Consultants, "Pennsylvania Power and Light Fly Ash Study," Project No. 1077-N60-00, March 1980.

12. Environmental Protection Agency, Hydrologic Simulation on Solid Waste Disposal Sites, SW868, September 1980.

13. Thomas L. Theis et al, University of Notre Dame, "Hydrodynamic and Chemical Modeling of Heavy Metals in Ash Pond Leachates," Progress Report 7/79-7/80, Department of Energy, March 1980.

14. M. van Genuchten, "Simulation Models and Their Application to Landfill Disposal Siting; A Review of Current Technology," in Land Disposal of Hazardous Wastes, Environmental Protection Agency, EPA 600/9-78-016, August 1978.

15. N. C. Mohn et al, "Environmental Effects of Flue Gas Desulfurization Waste Disposal: A Laboratory/Field Landfill Demonstration," Combustion Engineering, Inc., and Louisville Gas and Electric Company, March 1979.

16. Radian Corporation, Field and Laboratory Study of Gypsum Landfilling at TVA's Widows Creek Station, Draft Final Report, August 1980.

17. Franklin D. Patton, "Groundwater Instrumentation for Mining Projects," Westbay Instruments, Ltd., May 1979.

18. Stacey L. Daniels, "A Critique of Hazardous Waste Characteristics and Listing and Presentation of an Alternative Classification System by Degree of Hazard," Dow Chemical U.S.A., March 13, 1979.

19. Stacey L. Daniels, "Addendum to a Classification by Degree of Hazard," Dow Chemical U.S.A., July 16, 1979.

"Capacitive Transducer For Measuring Dust Deposit on a Fabric Filter"

O.J. Tassicker
Electric Power Research Institute
Palo Alto, California 94034

ABSTRACT

Fabric filters are being developed for high-temperature (800-900°C), high-pressure gases (5-15 Bar) in combined cycle PFBC, as well as at more conventional temperatures (150°C). In order to optimize cleaning cycles of fabric filters, a capacitance gauge is under development to measure dust deposit on the fabric during operation. Laboratory tests are described for a ceramic woven bag, 1.5 m long by 0.14 m diameter. Using resuspended ash from a PFBC combustor, ash deposit was measured to a sensitivity of about ±0.1 kg/m^2. The capacitance dust gauge is providng useful information about the mechanism of cleaning.

INTRODUCTION

Fabric filters constructed of fine ceramic fibers are being developed[1,2,3] for the protection of gas turbines from erosion by suspended ash particles carried in the flue-gas from pressurized fluidized bed combustors. These filters must operate in flue gases at 8-900°C and at pressures from 5-15 bar. This calls for special materials, such as 10 μm dia. ceramic fibers to be used in the filter. A key issue in the development of a satisfactory filter is to find a cleaning method and cleaning cycle which removes the dust cake without overstressing the ceramic fiber.

The ceramic filters under development by Acurex and by Westinghouse/Buell employ felted and woven ceramic bags, respectively. These, being mounted on a perforated metal mandrel as shown in Figure 1, are mechanically centered. This enables closer center distances to be accommodated with savings in the overall volume of the filter module. Cleaning is accomplished by pulses of air admitted from the clean side of the bag, which, by flexing the bag, causes dust to shear-off in agglomerates and drop down into the hopper.

The magnitude, duration, and frequency of the cleaning pulses are the major development issues[4,5,6]. Penetration of particles through the bags occurs at times of cleaning. Frequent or vigorous cleaning, stresses the bags mechanically and shortens the life. A significant quantity of energy is expended during cleaning. Misdirected pulses clean some regions of a bag and others not at all. While such issues concerning effective bag cleaning apply equally to conventional fabric filters operating at 150 to 250°C, as well as to filters operating at 900°C, the situation is more difficult both analytically and experimentally, at high temperature and pressure.

At room temperature, bags have been illuminated internally by lamps; dust deposits are then visible as dark patches. In this way, qualitative indication of bag cleanliness is obtained.

The pressure drop across a bag as a function of gas velocity is a most important parameter. Many investigations[6,7] have been conducted to determine the specific resistance coefficient for the dust, K_2 defined by:

$$\Delta p = K_2 VW$$

Where Δp = pressure drop across dust cake and bag
V = gas velocity
W = dust thickness

Pressure drop has an obscure relation to the mass of deposit since the porosity of the dust cake is uncertain. Further, if a patch of dust should

fall from a bag, the pressure fall might fall by 50%, even though the remainder of the bag is thoroughly encrusted.

As an aid to designing and operating effective fabric filter cleaning, a capacitive transducer is under development to determine the total amount of dust distributed over a bag under operating conditons up to 900°C and high pressure.

LABORATORY SCALE FABRIC FILTER AND CAPACITIVE TRANSDUCER

The apparatus illustrated in Figure 1 has a single woven ceramic bag of 3M manufacture supported on a perforated metal cylinder, 14.89 cm diameter. The effective bag length is 130 cm. Cleaning is by pulse air jet of 3 to 6 bar. Surrounding the bag is a metal container 31.9 cm diameter. This device is designed for temperatures to 200°C.

The metal parts are insulated from each other by mica or silicone rubber to form a classic three-terminal cylindrical capacitor as illustrated in Figure 2. The inner perforated former (H), and the outer metal container (L) are the two principle electrodes. The upper and lower guards (N) eliminate end effects and define the capacitance C to exactly 130 cm of filter. Not shown in the figure, is an outer screen of wire mesh which, enclosing the apparatus, eliminates outside interference.

By means of existing commercial transformer ratio-arm AC impedance bridges, such as the Wayne-Kerr type illustrated in Figure 3, the capacitance C may be easily measured to four or five significant figures[8,9]. The unknown Cu connected to terminals H, L and N is the fabric filter module. The standard conductance Gs and capacitor Cs are contained within the bridge. At balance when the detector reads zero, then:

$$Cu = Cs \frac{Ns\ ns}{Nu\ nu}$$

The G term accounts for any losses in the unknown capacitor.

The three-terminal configuration of the capacitor and the three-terminal capability of the bridge entirely eliminate all lead effects from the measurement.

When a dusty gas is admitted to the chamber, a dust layer is deposited on the fabric and the capacitance increases steadily by a small value ΔC. The increment of capacitance ΔC is shown to be proportional to the mass of dust deposit.

A key to understanding the increment of capacitance ΔC is to appreciate that ash from coal combustion has definite and measurable dielectric properties.

DIELECTRIC PROPERTIES OF FLY-ASH

Tassicker[10] carried out in 1971 what is believed to be the first systematic measurements of the dielectric constant ε' of power station fly-ash. Conditions extended over a range of temperatures 20-220°C and frequencies 50 to

50,000 Hz. Typical results are shown in Figure 4 for dry fly-ash collected from the hopper of an electrostatic precipitator following the firing of pulverized coal. The trend of the dielectric constant ε' is to 3-3.5, as frequencies increase above 10 kHz. This behaviour is typical of glassy, or ceramic materials. The writer concluded that such ash behaves much as one would expect of a medium grade insulating material.

This leads to the hypothesis that a small deposit of similar ash in a fabric filter with three-terminal electrode geometry, ought to lead to measurable and predictable increments of capacitance.

FABRIC FILTER MODULE TEST CONDITIONS

Dry PFBC dust from the Exxon #3 cyclone hopper catch (test 78) was elutriated from a flask into a controlled dry air gas flow at atmospheric pressure. Gas flow into the test module of Figure 1 was equivalent to 0.6 m/min face velocity into the filter.

The filter was of 3M manufacture, comprising woven fibers 10 μm diameter with an analysis 62% alumina, 14% boria and 24% silica. Such a ceramic has a demonstrated 1100°C durability[2]. Total active cloth area in this experiment was 0.62 m^2.

Rate of dust admission during this test varied from 1.7 to 6.2 gram/min.

MEASUREMENT OF DUST DEPOSITION

Typical capacitance readings (obtained at a convenient audio-frequency), are listed in Table 1 below:

Table 1
Capacitance Readings
at $2\pi f = 10,000$

Clean electrodes	98.54 pF
With clean fibre bag	98.58 pF
With 'seasoned' fibre bag	98.83 pF
After 30 minute dusty gas	99.30 pF

A plot of capacitance for this test, as a function of nominal dust deposit on the bag expressed in kg/m^2, is shown in Figure 5. This plot is surprisingly straight. The abberant point at 1, is when a patch visibly detached from the bag.

The reasons for the small drop in capacitance when gas is flowing are still being investigated. It is surmized that as the fabric is pressed into the interstices of the perforated metal mandrel, it is in a region of lower electric field strength, and so contributes less to stored electric energy.

A mass balance performed, inlet to outlet, showed that of the dust elutriated from the measuring flask into the filter chamber, 7% deposited on areas

outside the capacitance measurement zone, or else penetrated the filter. This leads to the important observation that the sensitivity of measurement is 1.17 pF/kg/m^2, the dust load being averaged over the 130 cm of active bag.

The key to the success of this technique then, clearly depends upon having excellent capacitance measurement accuracy, which in this case is ±0.01%.

PULSE CLEANING OF FIBER

By means of pulses of air at pressures from 3.4 bar (50 psig) to 5.5 (80 psig) applied to the axial nozzle shown in Figure 1, the bag was cleaned several times during the test series.

One cleaning sequence is illustrated in Figure 6. The dust had already been deposited one month earlier, with the apparatus equilibrating at laboratory conditions meanwhile. The dust layer appeared to be flaky, probably due to adsorbed moisture.

Beginning with the dusty bag at an initial electrode capacitance of 99.20 pF, 19 pulses at 3.4 bar reduced the equivalent dust load to 98.77 pF. Another 100 pulses reduced the dust load to 98.56 pF. Then 15 pulses of 5.5 bar further cleaned the bag to 98.48 pF, visual inspection showing that the dust sheared off in large flakes. By now, the bag was virtually clean to the base capacitance of 98.48 pF.

Successive changes in capacitance thus accurately monitored the cleaning procedure.

In the projected application, to PFBC dust under very hot conditions, it now became essential to document the dielectric constant ε' for such ash.

DIELECTRIC CONSTANT OF PFBC ASH

By using using a small dielectric dust cell of the kind used earlier by Tassicker[10] in 1971 to examine pulverized coal-fired power station fly-ash, preliminary information has been obtained on PFBC ash.

Using such a three-terminal, cylindrical electrode test cell with dimensions:

ID = 5 cm; OD = 7 cm; length 6.1 cm

Together with the same transformer ratio-arm AC bridge as described in Figure 3, the data of Table 2 was obtained:

Table 2
Dielectric Test Cell
at $2\pi f = 10,000$

	c pF	G n
Clean electrodes	10.21	000.4
With alumina beads	35.30	6.4
With damp PFBC dust	46.20	331
With dry PFBC dust	19.90	3.6

The alumina beads were used as a control sample.

Preliminary results are shown in Figure 7 which demonstrates that when PFBC ash is thoroughly dried at 100°C, it has a relatively fixed dielectric constant over the audio frequency range. Ash at 20°C in the laboratory is obviously very moisture dependent.

Preliminary results up to 815°C are shown in Figure 8. Above 500°C at audio frequencies, the dielectric constant becomes very large indeed. The trend of results to 1 MHz suggests that ε' would tend to about 3 for all temperatures.

The preliminary findings are that PFBC ash has indeed reasonable and measurable dielectric properties which can be used with capacitance transducer for measuring dust loading on a fabric filter.

CONCLUSION

A capacitive transducer is under development, which can measure the amount of dust deposit on a fabric filter under operating conditions. Up to 200°C, the transducer is already developed sufficiently to provide a measure of dust deposit to about ±10%.

Dielectric properties of PFBC ash from the Exxon mini-combustor have been measured, and found to be adequate to support the capacitive technique up to 815°C. More work is in progress to document the relation between dielectric constant and mass; this will be reported elsewhere.

The technique promises to be a valuable tool for designing and optimizing cleaning cycles for some types of fabric-filters. Detailed information is provided about the rate of dust deposition, and mechanism of dislodgement. It shows promise of being an important adjunct to pressure-drop measurements.

Commercial precision electronic equipment is available for the capacitance determination.

ACKNOWLEDGEMENTS

The writer's colleagues, Dr. Tom Lippert and Dr. David Ciliberti of Westinghouse constructed the Fabric Filter Module with the capacitive features, and assisted with the measurements. Special thanks are due to them, and to the technician who skilfully assembled the equipment, John Meyer, for their dedication and support.

To Dr. Mike Shackelton and John Sawyer, colleagues from Acurex, the writer owes special thanks for constructing the dielectric test cell and for spending many supportive hours during the measurements.

The writer's colleague, Steve Drenker of EPRI, provided much encouragement and resources support.

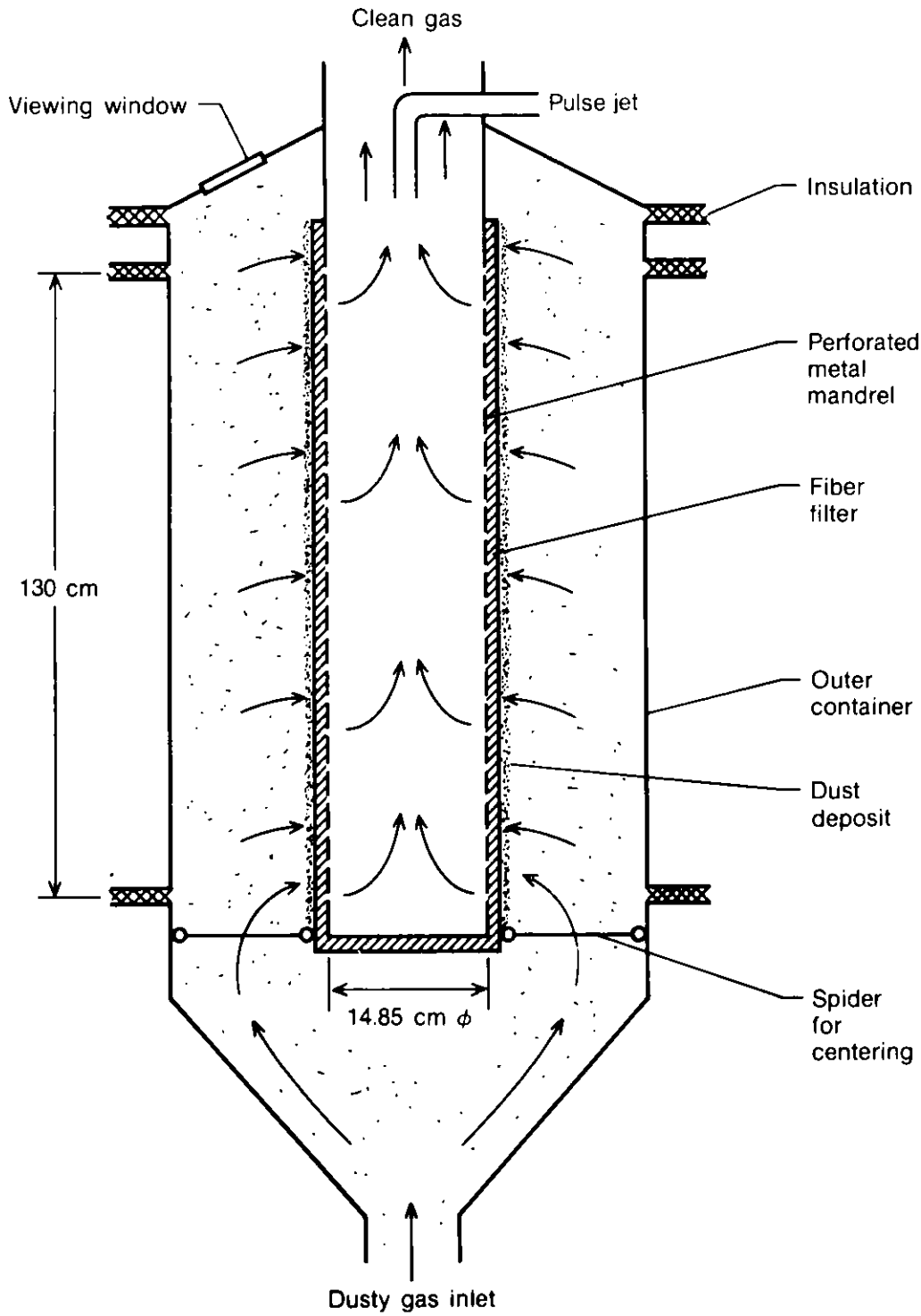

Figure 1. Fabric filter test module capacitive filter cake determination.

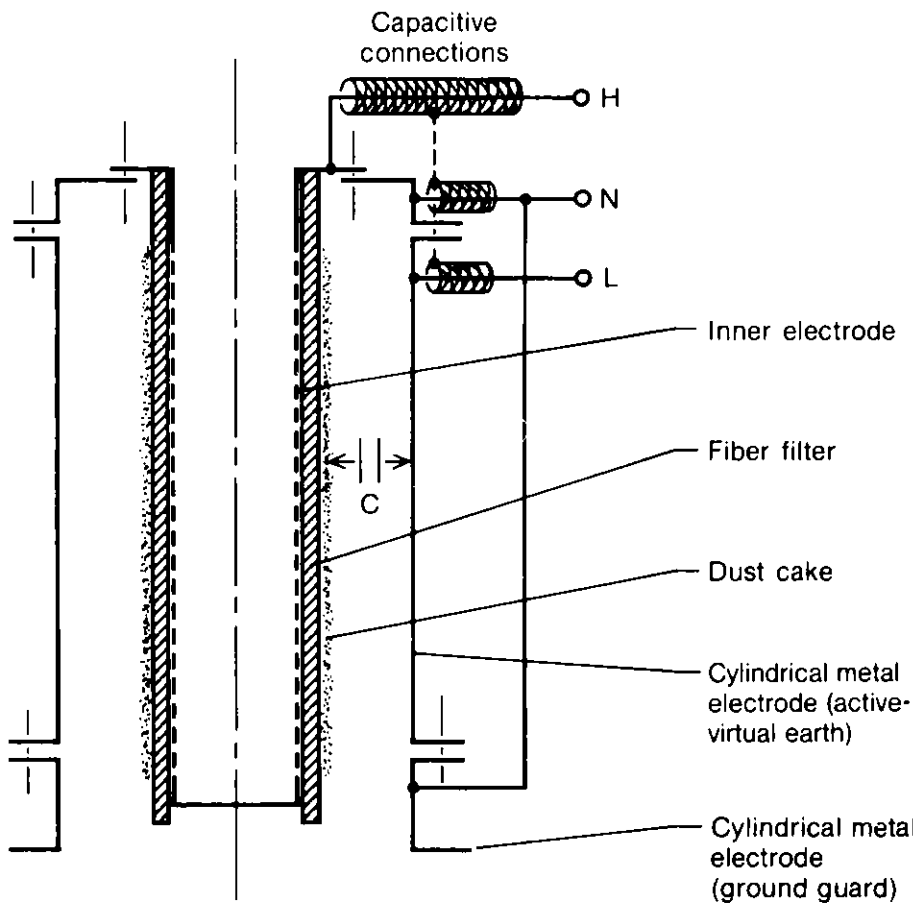

Figure 2. Determination of dust deposit by capacitance.

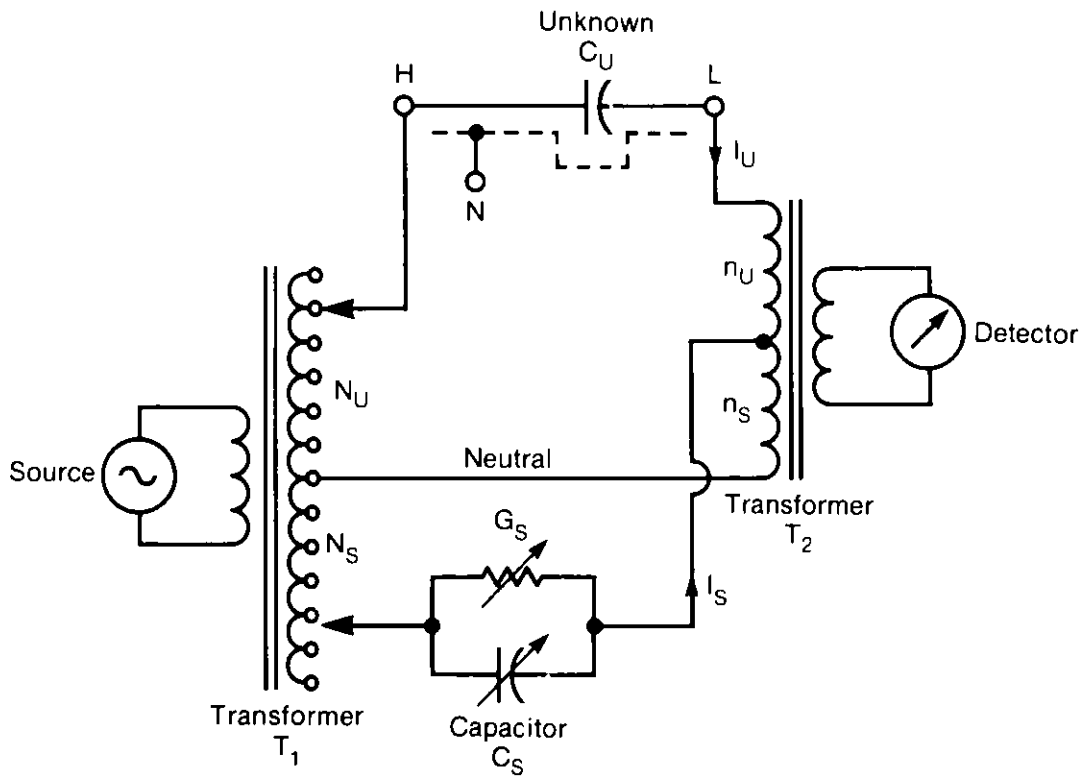

Figure 3. Three terminal capacitance determination by transformer ratio-arm bridge.

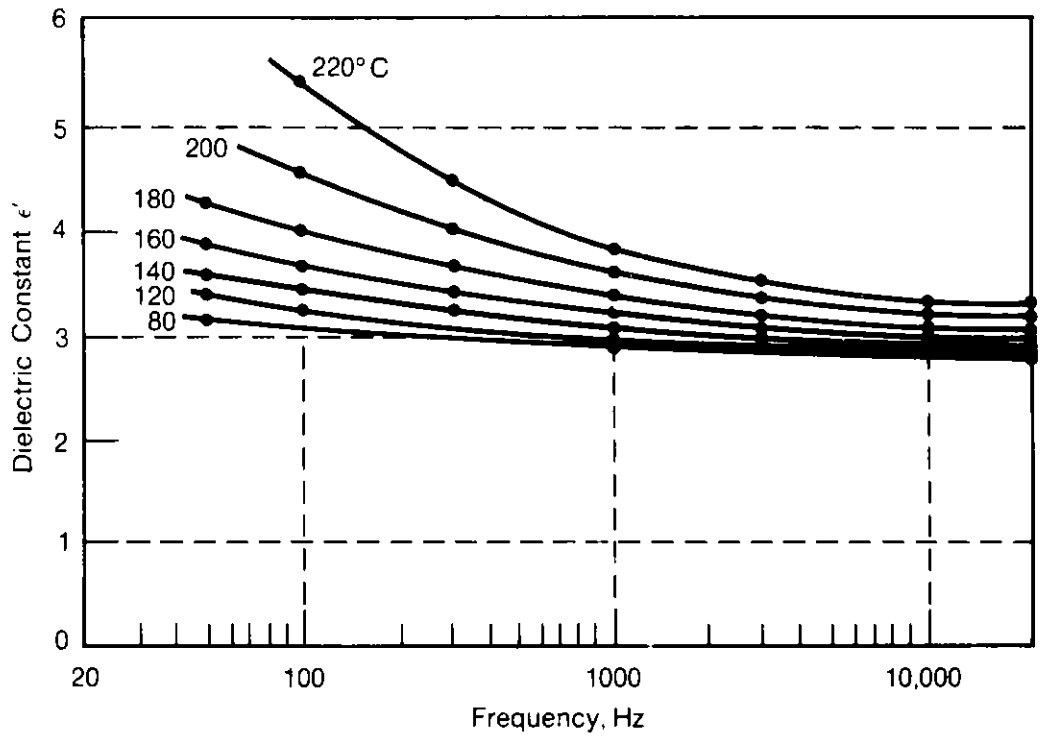

Figure 4. Dielectric constant, ϵ' of fly-ash.

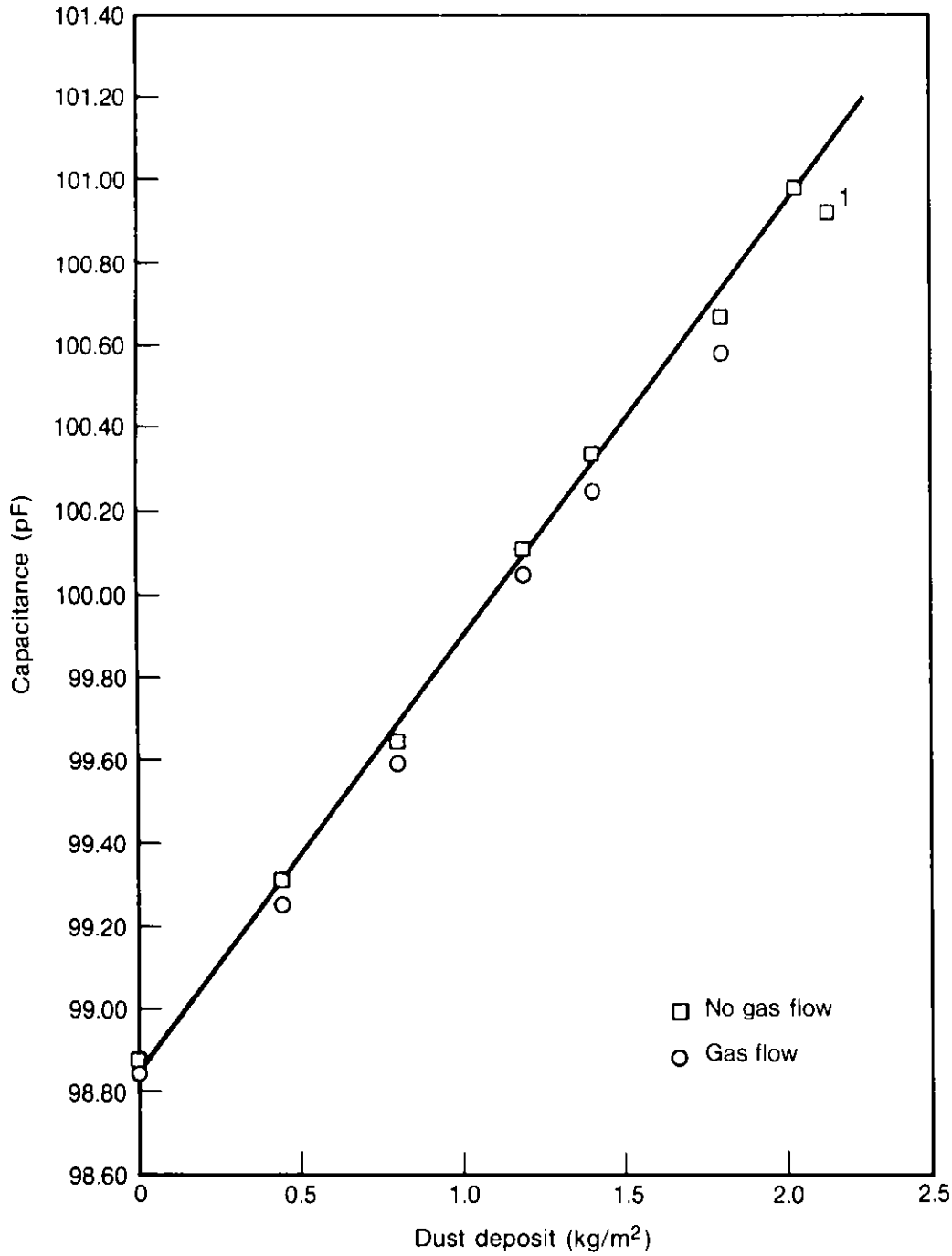

Figure 5. Dust cake deposit.

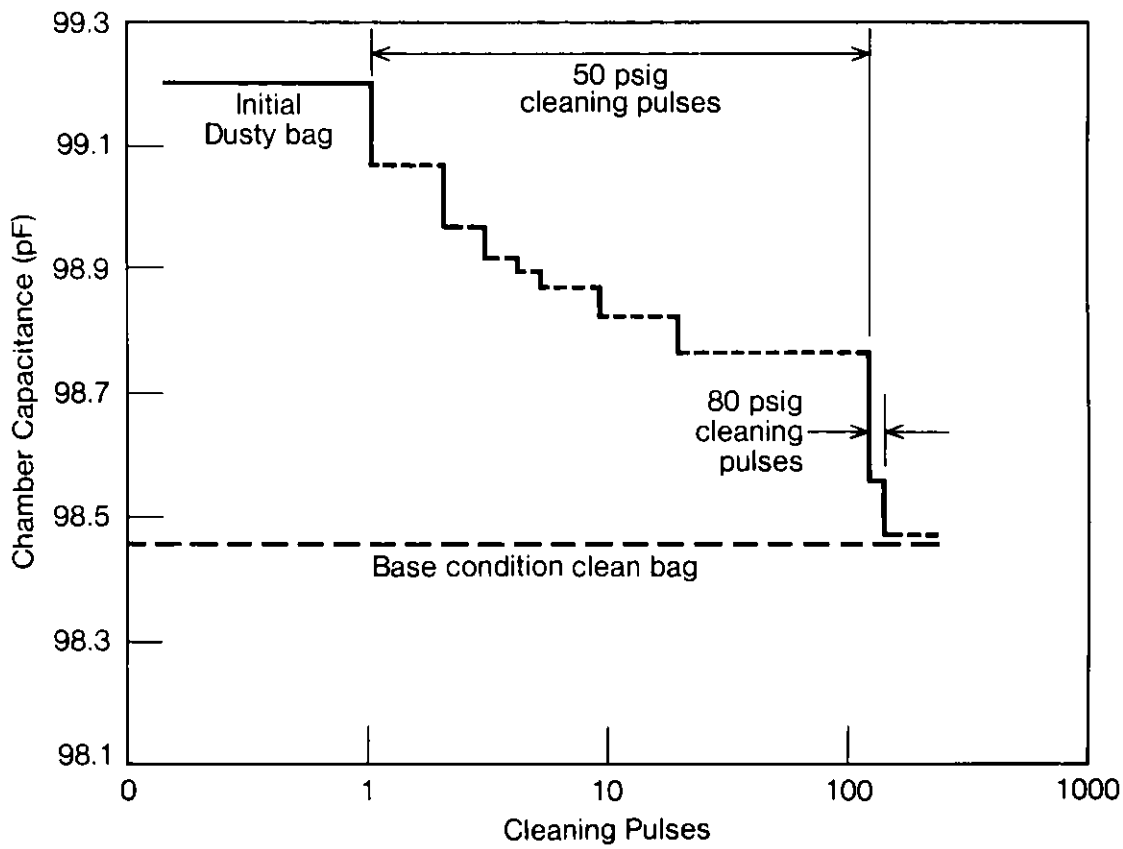

Figure 6. Pulse air cleaning of woven ceramic fiber filter.

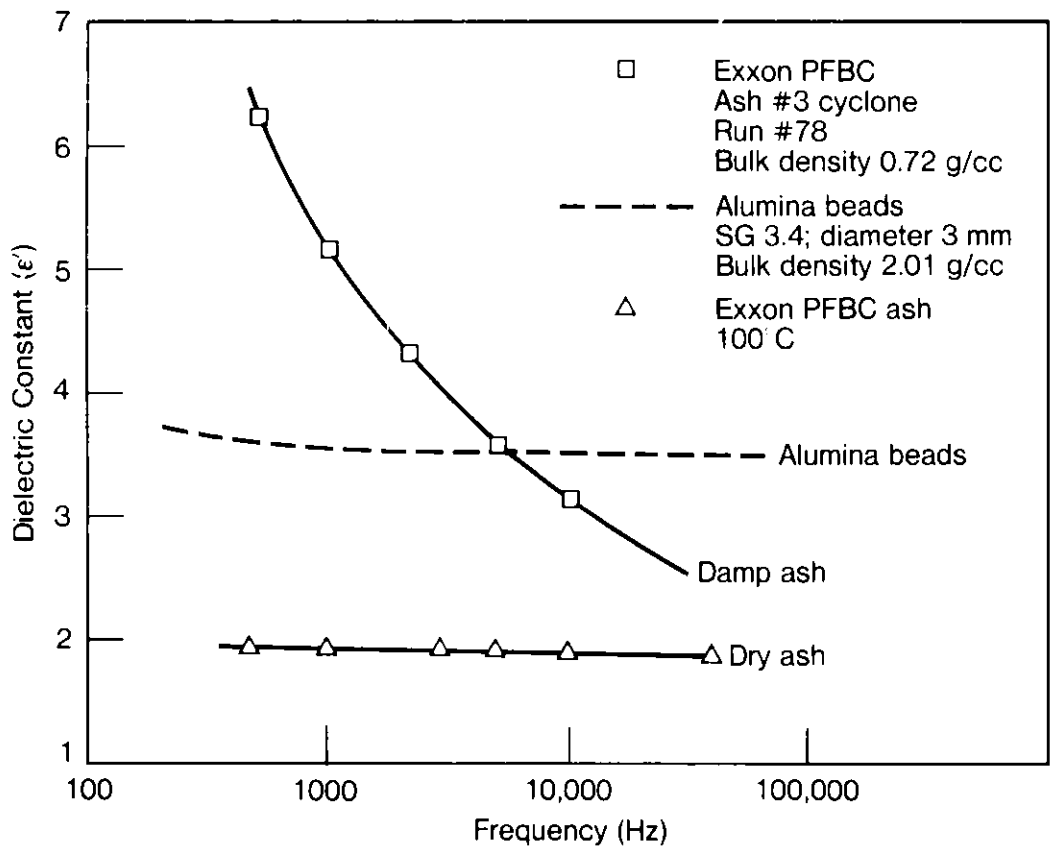

Figure 7. Dielectric constant, ε' alumina and PFBC ash.

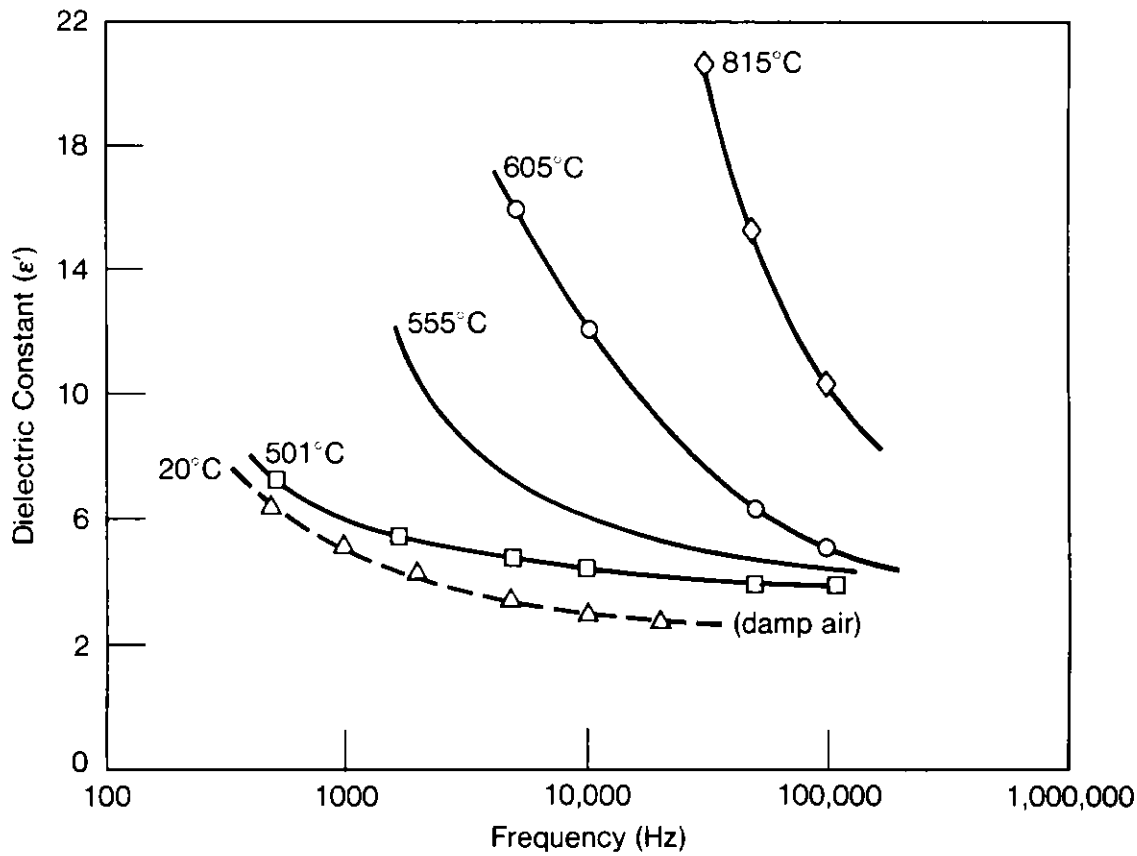

Figure 8. Exxon PFBC ash dielectric constant, ϵ'.

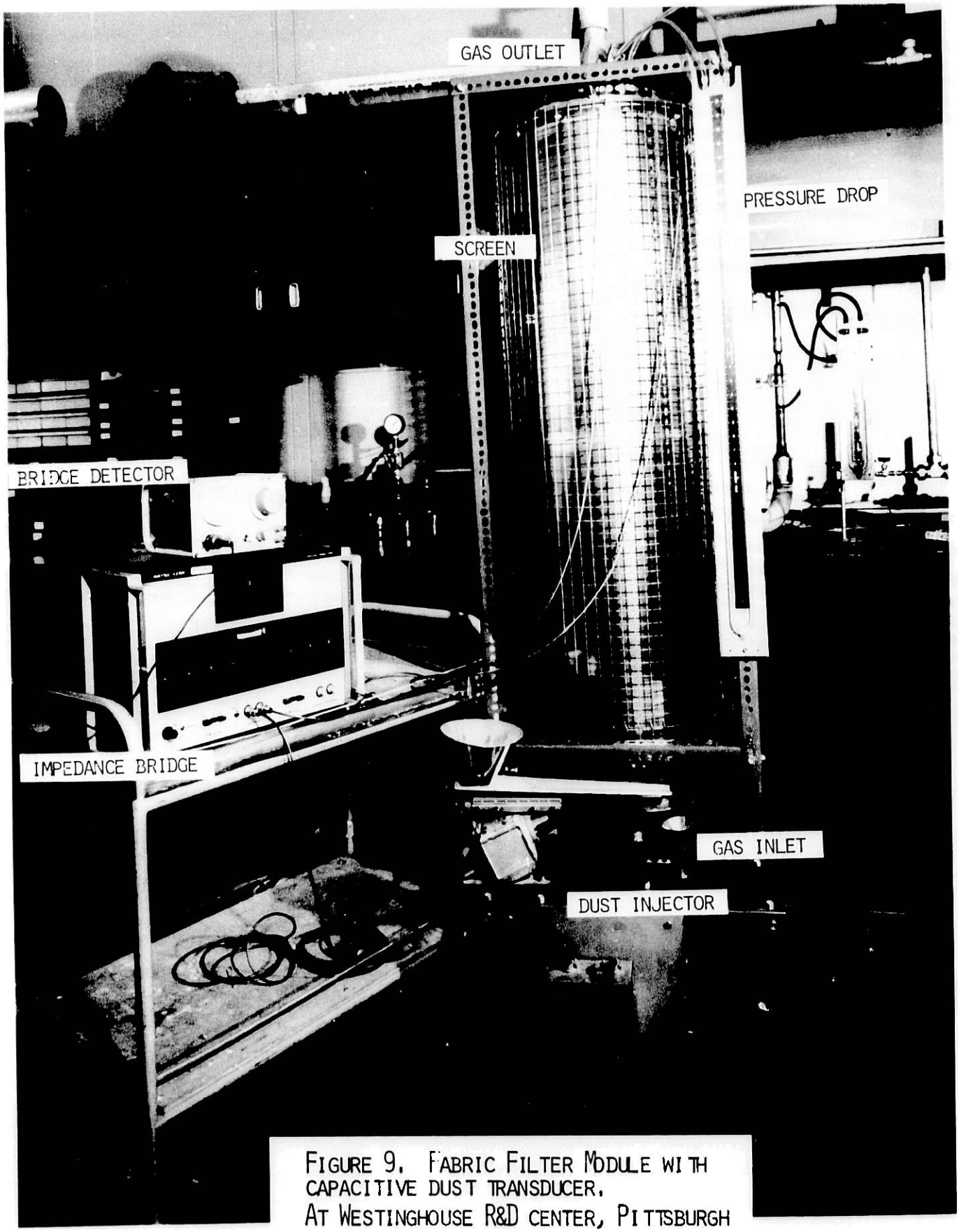

FIGURE 9. FABRIC FILTER MODULE WITH CAPACITIVE DUST TRANSDUCER, AT WESTINGHOUSE R&D CENTER, PITTSBURGH

REFERENCES

1. Ciliberti, D. F., and Lippert, T. E.; "Evaluation of Ceramic Fiber Filters for Hot Gas Cleanup in Pressurized Fluidized--Bed Combustion Power Plants", EPRI Report CS-1846, RP1336-1, May 1981.

2. Furlong, D. A., and Shevlin, T. S.; "Fabric Filtration at High Temperature"; Chem. Eng. Proc., January 1981, p89-91.

3. Shackelton, M., "Hot Gas Cleaning with Ceramic Filters", Porceedings of High Temperature, High Pressure Particulate Control in Coal Combustion Process Streams DOE Contractors Meeting, Morgantown, West Virginia, February 3-5, 1981, ed. by Science Applications, Inc.

4. Leith, D., Dwight D., Gibson, and Melvin W. First; "Performance of Top and Bottom Inlet Pulse--Jet Fibers", J. of Air Pollution Control Assoc., 28:696, 1978.

5. Iinoya, K., "Industrial Gas Filtration", p309-359, in 'Filtration Part 1, Principles and Practice', Marcel Dekker Publishing Co., Ed. by C. Orr, 1977.

6. Dennis, R., and Klemm, H. A., Fabric Filter Model Format Change, Volume I, Detailed Technical Report; Volume II, User's Guide, Industrial Environmental Research Laboratory, U.S Environmental Protection Agency, Research Triangle Park, N.C. Report No. EPA-600/7-79-043a, 600/7-79-043b, February 1979.

7. Ensor, D. S. et al; "Kramer Station Fabric Filter Evaluation", EPRI Report CS-1669, RP1130-1, October 1980, p6-1.

8. Rogal, B., "Recent Advances in Three-Terminal Bridge Techniques", Proc. Inst. of Electronics (GB), Vol. 4., No. 2, 1961.

9. Thompson, A.M., "The Precise Measurement of Small Capacitances", IRE Transactions on Instrumentation, Vol. 1-7, No. 3 and 4, December 1958, p245-253.

10. Tassicker, O. J., "The Temperature and Frequency Dependence of the Dielectric Constant of Power Station Fly-Ash", Staub-Reinhalt, Luft , Vol. 31, No. 8, August, 1971, p23-28 (German original, translation by EPA available in English).

A PAPER TAPE MONITOR FOR VAPORS OF POLYNUCLEAR AROMATIC COMPOUNDS FROM COAL-DERIVED PRODUCTS*

T. Vo-Dinh
Health and Safety Research Division
Oak Ridge National Laboratory
Oak Ridge, Tennessee 37830

ABTRACT

Recently, the existence of organic contaminants such as the polynuclear aromatic (PNA) compounds in the vapor phase have received special interest. Vapors from these high-boiling organic compounds, however, are difficult to detect because of their low vapor pressure. Traditional monitoring methods require elaborate sampling procedures over long periods of time using solid adsorbents such as charcoal or Tenax-GC (a porous polymer of 2,5-diphenyl paraphenylene oxide). The vapors collected into these absorbents must be subsequently extracted in the laboratory by thermal or chemical methods prior to analysis by gas chromatography. Sample loss due to desorption, sublimation, and photodecomposition during sample shipping time are common sources of errors in these conventional methods.

This work describes the development of a new method for detecting PNA vapors collected on filter paper. The technique can be employed in two devices, an active paper tape sampler or a passive dosimeter. In the active sampler, air is passed through the paper tape using a personnel pump. In the passive dosimeter, PNA vapors are collected according to diffusion and surface adsorption processes. The PNA compounds were detected directly on the paper by the room temperature phosphorescence technique (1,2). The active sampler can detect several vapors of PNA compounds such as fluorene, pyrene, or fluoranthene from coal products after sampling periods of one minute. The passive dosimeter can identify these PNA compounds and give the time weighted average exposure measurement compounds (after one-hour exposure). Preliminary results indicate that these techniques have a great potential as personnel and area monitors of organic vapors from high molecular PNAS compounds (3,4).

*Research sponsored by the Office of Health and Environmental Research, U. S. Department of Energy, under contract W-7405-eng-26 with the Union Carbide Corporation.

REFERENCES

1. T. Vo-Dinh and R. Hooyman, "Selective Heavy-Atom Perturbation for Analysis of Complex Mixtures by Room Temperature Phosphorimetry," Anal. Chem. 51: 1915–21 (1979).

2. T. Vo-Dinh and J. D. winefordner, "Room Temperature Phosphorimetry as a New Spectrochemical Method of Analysis," Appl. Spectrosc. Rev. 13(2): 261–94 (1977).

3. T. Vo-Dinh, "New Luminescence Techniques Simplify Air Analysis," Intech, pp. 45–48, May 1981.

4. T. Vo-Dinh, "Development of a New Passive Dosimeter for Polynuclear Aromatic Vapors," Proc. of EPA National Symp. on Monitoring Hazardous Organic Pollutants in Air, Raleigh, NC, 1981.

ACTIVITIES OF THE S.C.I.E.P. SUBCOMMITTEE ON FLOW MEASUREMENTS

Peter Alexander
TRW, Energy Engineering Division

The Flow Measurement subcommittee of the Society for Control and Instrumentation of Energy Processes was formed in July 1980. Four subcommittee meetings have been held. A list of subcommittee members and their affiliations is appended at the end of this text.

The goals of this subcommittee as defined by its members are to:

- Optimize the exchange of flow measurement information,
- Perform a continuing analysis of synfuels flow measurement and control requirements versus available instrumentation,
- Identify gaps in flow measurement and control technology and focus development efforts thereon.

The biggest benefit of all to members of the subcommittee does not appear above. This benefit is the animated and cordial communication which takes place between subcommittee members representing the synfuel industry, instrument manufacturers, DOE funded laboratories, and other interested parties.

The flow measurements being addressed by the subcommittee include multicomponent flows of solids and/or liquids and/or gases. Measurement of these flow rates is important for:

- Process control,
- Process optimization,
- Process economic analysis,
- Operating safety,
- Development of an understanding of process dynamics needed for scale up to commercial size operations.

The specific surface synfuel processes being addressed include SRC I and II, Hi-Gas, Co-Gas, U-Gas, H-Coal, and Donor Solvent. These processes are employed to produce liquid fuels and synthetic natural gas from coal.

Figure 1 shows a greatly simplified schematic of a generic surface coal processing operation. It is desirable to make accurate flow measurements at all the points marked by the letter "M". Measurements of input and output flow rates to all the key process steps are important to operation and optimization of the process. In order to follow and understand the dynamics of what is happening inside the hot preheater, reactor, and gasifier, it is desirable to have available a real time three dimensional picture of the flow distribution within each of these vessels. It must be remembered that the flows inside these vessels may be quite hot (> 800°F), have varying viscosity and turbulence, contain solids/liquids/gases in varying ratios, and have time varying elemental compositions.

Figure 1. Generalized Coal Processing Schematic

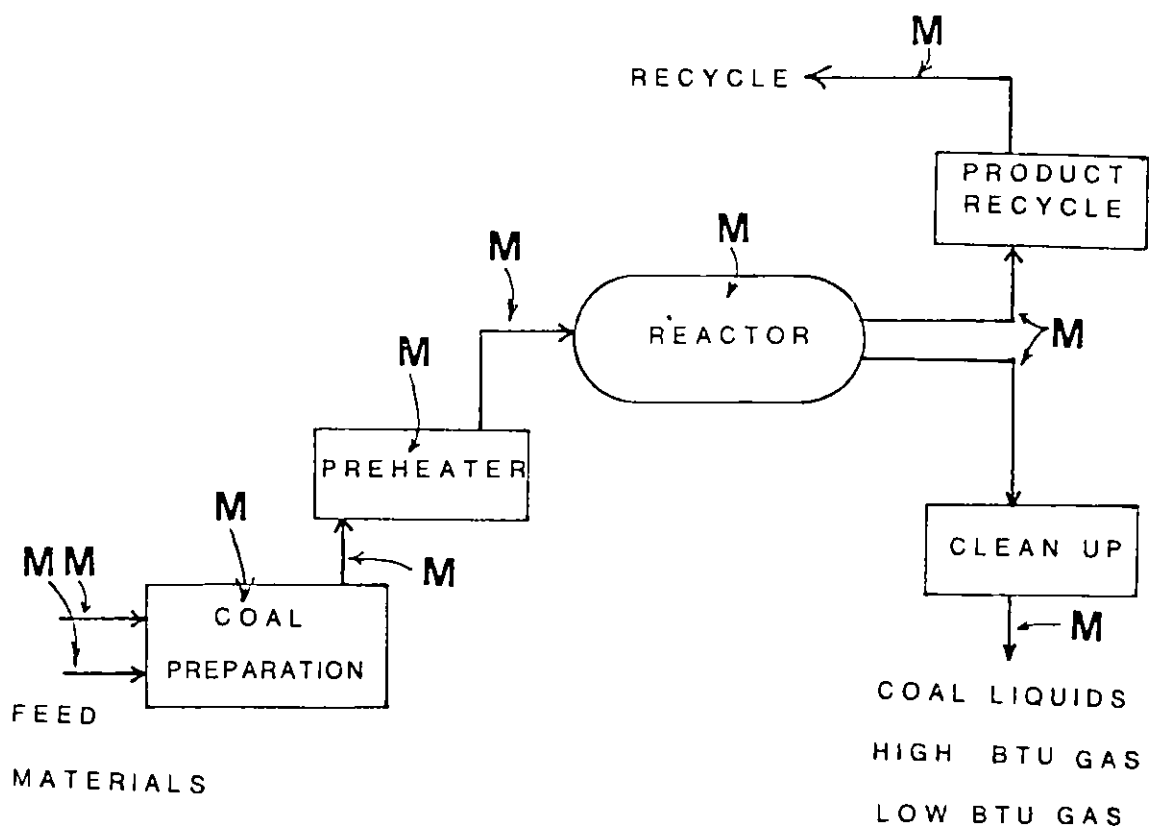

M-FLOW MEASUREMENT

In order to select the correct flow measurement instrument for a particular process application, or to determine if such an instrument needs to be developed, it is necessary to specify a number of parameters associated with the measurement to be made. Some of these parameters are listed below.

- Viscosity of flowing material
- Density of flow
- Ratio of solids to liquids to gases
- Particulate and gas concentrations in flow
- Composition of flow
- Accuracy necessary in measurement
- Required measurement sensitivity
- Range of flow values to be measured
- Pressure range over which measurement will be made
- Temperature range over which measurement will be made
- Reliability required of measurement instrument

A task force of the Flow Measurement subcommittee has been examining flow measurement requirements for several different synfuel processes. A second task force has been evaluating the ability of existing instrumentation to meet these requirements. These analyses will be made available for review and critique. Based on the above analyses a preliminary list of needs in the flow measurement area was developed by the subcommittee at its last meeting. These needs are listed below.

- Develop a three dimensional, real time, in situ flow monitor for use inside the preheater, reactor, gasifier.
- Develop a flow monitor for hot (> 800°F) feed and exhaust lines carrying flows with changing viscosity and varying ratios of solids, liquids, and gases.
- Develop a mass flow monitor to measure the flow rate of one phase in a two phase flow where the ratio of the phases is variable.
- Provide a high temperature flow test facility.
- Other measurement parameters are needed in addition to the flow measurement. These include: viscosity, particle size and distribution, composition, density, % solids, resistivity.

The purpose of developing a list of flow measurement needs is to focus the attention of the instrument manufacturers, the synfuel industry, and the government on this area. As a result some mechanism may be found to support the technology development necessary in this area.

The subcommittee also feels strongly that better coordination of activities with other similar groups in the Instrument Society of America, the Scientific Instrument Manufacturers Association, the American Society of Mechanical Engineers, the Department of Energy, etc. is extremely important.

Members of Flow Measurement Subcommittee

Name	Affiliation	Name	Affiliation
Peter Alexander	TRW	Donald Malone	Ashland Syn. Fuels
Joseph Basak	Dietrich Standard	Al Mark	JPL
George Borst	Barton Instr.	Harrison McDonald	Haake, Inc.
John Boynton	Foxboro Co.	Nowell Nelson	American Flow Syst.
Bill Bushnell	SRC International	Ray Owen	Taylor Instrument
B. J. Garcia	B & W	Kurt Placke	Micro Motion
Ira Goldberg	Rockwell Inter.	Paul Raptis	ANL
T. R. Heidrick	Alberta Research Council	Baldwin Robertson	NBS
Peter Herzl	Fischer Porter	Dough Simmers	Kamman Sciences
John Holtgrefe	Badger America	Maurice Turgeon	Catalytic Inc.
John Janssen	Honeywell	Vic Verbinski	SAI
Ray Kim	Babcock & Wilcox	Alfred Watson	Westinghouse
Chester Krcil	Conoco Coal	Stan Wohadlo	IGT
Dick Kwiatkowski	MSA		

FLOW MEASUREMENT FOR OPTIMISING THE FEEDRATE OF PULVERISED FUEL TO COAL-FIRED BOILERS

R. G. Green and S. H. Foo
Department of Instrumentation and Analytical Science,
The University of Manchester Institute of Science and Technology,
Manchester, U. K.

J. G. Phillips
Central Electricity Generating Board
Eggborough Power Station
Goole, North Humberside, U. K.

SUMMARY

A system is described which measures the velocity and also provides an output which is a function of the mass flow rate of airborne particles. Capacitance transducers are formed into the 14½ inch (370 mm) diameter pipes feeding the injectors of a 500 mw(e) coal fired boiler. These transducers sense the instantaneous changes in concentration of dielectric material within their sensing fields. The outputs of two transducers are used to obtain the average velocity of the powdered fuel by cross-correlation. The concentration is related to the mean value of the transducer output signal. The velocity and concentration signals are fed into a microcomputer which calculates and displays the instantaneous mass flow rate, it will also produce warning signals when the measured feedrates deviate significantly from their desired set point values. Outputs suitable for controlling the feedrate are available.

1. INTRODUCTION

An on-line microcomputer system has been developed for data analysis to optimise fuel efficiency in a coal fired power station boiler. It enables the flow into each of the 24 burners of a large boiler to be balanced and also gives warning of incipient blockage of an injector.

The instrument consists of two capacitance transducers, a cross-correlator, and interface unit, a PET microcomputer and its peripherals (Figure 1). The system is designed to counter the numerous problems involved in the measurement of solids flow rate in a coal fired boiler. Apart from the problem of the varying solids feedrate and conveying air velocity, there is the 'roping'

effect. A 'rope' is a band of fuel formed by the segregation of pulverised fuel (pf) and air. This travels as a helix along the pipelines resulting in a very irregular distribution and the fact that the shape and position of the helix depends upon the flow conditions suggests that the electrode used should be equally sensitive over the whole cross-section of the conveyor.

Another problem which may arise due to the roping effect is that of pipe blockage. On the horizontal section, the rope travels along the bottom of the pipe and hence slows down under the influence of the frictional forces with the pipe wall. This may result in a blockage which is very dangerous because a blocked pipe may ignite back causing an explosion. Detection of incipient blockage in the feed pipes, however, may be done by studying the shape of correlograms.

Figure 2. shows a schematic diagram of a milling and pf transport system showing the distribution of flow in the sections indicated.

2. THE CAPACITANCE TRANSDUCER

The capacitance transducer consists of two main sections namely the electrode and the sensing electronics (see Figure 3.).

The electrode shape and size depends upon the specific application, but basically it consists of a capacitor formed flush with the walls of the conveyor, so that there is no obstruction to restrict the flow. This capacitor is connected in parallel with an inductance to form a tuned circuit for a transistor oscillator. The frequency of oscillation varies with changes in electrode capacitance. An integrated f.m. demodulator circuit converts these changes in frequency to voltage changes; which contain components due to the average flow, fluctuations due to turbulence, etc., (flow noise), changes due to deposits on the electrode or electrode wear and drift in the working parts of the electrical components. Of these only the flow noise is required in the final electrical signal. Since the other voltage changes occur relatively slowly, they are filtered out by the a.c. amplifier which feeds the a.c. voltmeter, giving a d.c. current output of between 4-20 MA. The output of the a.c. amplifier is also available for cross-correlation. A refinement of the instrument is made by feeding the slow voltage changes into a voltage to capacitance converter; which in turn regulates the oscillator frequency so that the optimum electronic working points are maintained (Figure 3.) (Green 1974).

2.1. The Electrode

The original measurements of pf flow were made using 4 inch diameter electrodes which were held in position using standard 4 inch diameter inspection bosses (Figure 4.). These are localised detectors in the conveyor. It was noticed that the indicated flow could deviate even though the flow from the mill was constant. This was explained by the roping effect which not only causes an irregularity in the distribution of the flow, but the rope also changes its shape and/or position with minor air velocity or solids concentration variations. A second disadvantage of this electrode appears when cross-correlation measurements are made to determine the transit time and hence the velocity of the pf (section 3). The large width of the electrode in relation to the separation of the electrode produces in effect three correlation peaks. The resultant correlogram formed from the combination of the three peaks is very broad making it difficult to obtain an accurate transit time (Figure 4.).

These disadvantages may be eliminated by using a 'ring' electrode as described below.

2.1.1. The Ring Electrode

In this electrode a complete section of the conveyor is isolated from both up and down stream sections. The central section is 15 mm wide and is spaced using materials with low dielectric coefficients (e.g. PTFE), so that the physical gap between the two pieces of metal is 4 mm (Figure 5.).

The sensing electrode is hence a ring all round the circumference of the pipe wall which means that it will detect all round the conveyor and has a good penetration to the centre, whereas the 4 inch boss electrode described above could unfortunately be positioned diametrically opposite to the rope under certain flow conditions, or even having the rope precess near it periodically under other flow conditions. So, by using the ring electrode, flow signals will be detected irrespective of the shape and position of the rope or the regularities of the flow distribution (Green 1981). The correlogram obtained from the ring electrode is narrow and has a distinct peak hence accurate measurement of transit time can be obtained (Shackleton 1981).

3. THE CROSS CORRELATOR

The cross-correlator compares the a.c. signals from the two transducers and computes the transit time. Basically, this meant that the correlator follows

the passage of some disturbance in the flow and measures how long it takes that disturbance to travel to a downstream point (Beck 1981). The cross-correlation function is defined by:

$$Rxy\ (\tau) = \frac{1}{T} \int_{o}^{T} x(t-\tau)y(t)dt$$

It can be shown that this function has a maxmimum value when the cross-correlation lag, τ, is equal to the transit time, τ^*, of the tagging signals. Hence, if l is the transducers spacing then the flow velocity, $\mu = l/\tau^*$.

The shapes of the correlograms may be used to detect incipient blockage (Anderson-Bryan 1978). A set of curves made under laboratory conditions are shown in Figure 6. Curve (i) shows a sharp peak indicating that all the particles are travelling at approximately the same velocity. As particles start to separate out from the flow the width of the peak widens and the height falls due to the increasing spread in the particle velocities. Curve (ii) shows the pipe when separation is just commencing and curve (iii) represents a virtually blocked pipe condition. So, by studying the shapes of the correlograms a warning signal can be generated from any predetermined set of flow conditions.

4. THE PET MICROCOMPUTER AND ITS INTERFACE

The PET microcomputer gathers the necessary data from the transducers, the cross-correlation and the keyboard. The concentration and transit time signals are input into the PET via an interface box, whilst constant data such as transducer spacings is requested by the computer and is input via the keyboard.

The interface unit, the PETSET 1, connects the measuring system to the PET. It consists of a 16 channel, 8 bit analogue to digital converters (AIM16) and the PETMOD which connects the AIM16 to the IEEE and the user ports of the PET. The user port bits (Dϕ-D7) are used as signals from the AIM16 to the PET whilst the IEEE port bits (DIϕ1-DIϕ8) are used as signals from the PET to the AIM16. A POKE instruction will enable the AIM16 and start the conversion of the selected channel from analogue to digital form and a PEEK instruction will read the data into the computer.

For warning and controlling purposes, output signals can be sent via the IEEE or the User Port from the PET through digital to analogue converters to the device such as a valve or directly to alarms.

From the data it collected, the PET calculates the instantaneous mass flow rate continuously and displays it on the vdu. The calculated parameter will be compared with the set points and signals can then be sent to the appropriate control valves so that the required set points can be maintained.

The shape of the correlograms can also be closely monitored so that any incipient blockage is detected and appropriate action taken.

4.1. The Computer Algorithms

In many pneumatic conveying systems the transporting fluid velocity may have to be increased to prevent saltation at high solids flow rates. This increase in velocity decreases the instantaneous concentration of the particles within the electrode field resulting in a reduced output from the transducers even though the mass flow rate has actually increased (Figure 7.). It is essential that solid velocities be measured so that a relationship between mass flow rates and velocities may be determined, i.e.

$M = KCV^a$ where M = Mass flow rate, C = Meter reading α concentration,
V = solids velocity, a and K = system constants

This equation can be stored in a computer and the mass flow rate calculated.

CONCLUSION

By measuring the mass flow rate into each injector the distribution of pf into the boiler can be accurately controlled, which should increase the boiler balance and efficiency. It is estimated that for a boiler of 500 mw(e) capacity, a 0.5% increase in boiler efficiency will enable fuel costing in the order of £250,000 per boiler per annum to be saved. Furthermore the system described is capable of detecting incipient blockages which will reduce considerably the danger of explosion and hence improve the safety of the working environment. Other improvements in efficiency created by a more even distribution of pulverised fuel across the furnace, leading to a more uniform heat release within the furnace, are less quantifiable but nevertheless of real economic significance. These are:

Reduction of rate of metal loss on boiler tubes and less fire-side corrosion.
Reduction in boiler surface erosion.
Reduction in the rate of furnace slagging.
Reduction in the quantity of oil required for pf support.

REFERENCES

GREEN, R.G., 1974 'Frequency modulated transducers for gas/solids flow measurement', MSc Thesis, University of Bradford.

BECK, M.S., 'Correlation in instruments: Cross-correlation flowmeters', J.Phys.E: Sci. Instrum., Vol. 14, pp 7-19.

GREEN, R.G., 1981 'Capacitance flow transducers for multiphase system', PhD Thesis pending, University of Bradford.

SHACKLETON, M.E., 1981 MSc Thesis pending, University of Bradford.

ANDERSON-BRYAN, N.A., 1978 'Moisture and mass flow measurement of powdered and granular materials', MSc Dissertation, University of Bradford.

PETSET Instruction Manual 1980, CMC Connecticut Microcomputer.

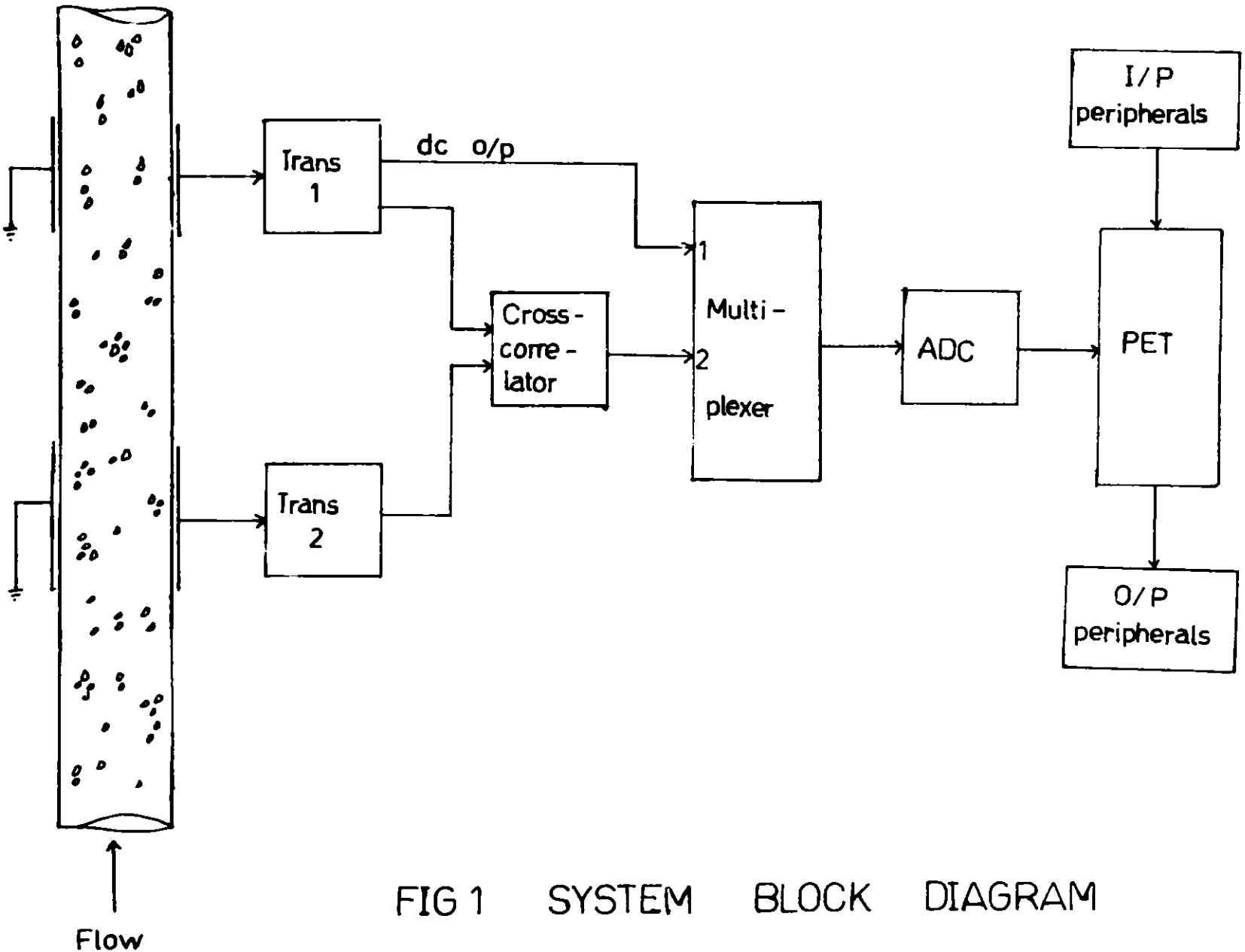

FIG 1 SYSTEM BLOCK DIAGRAM

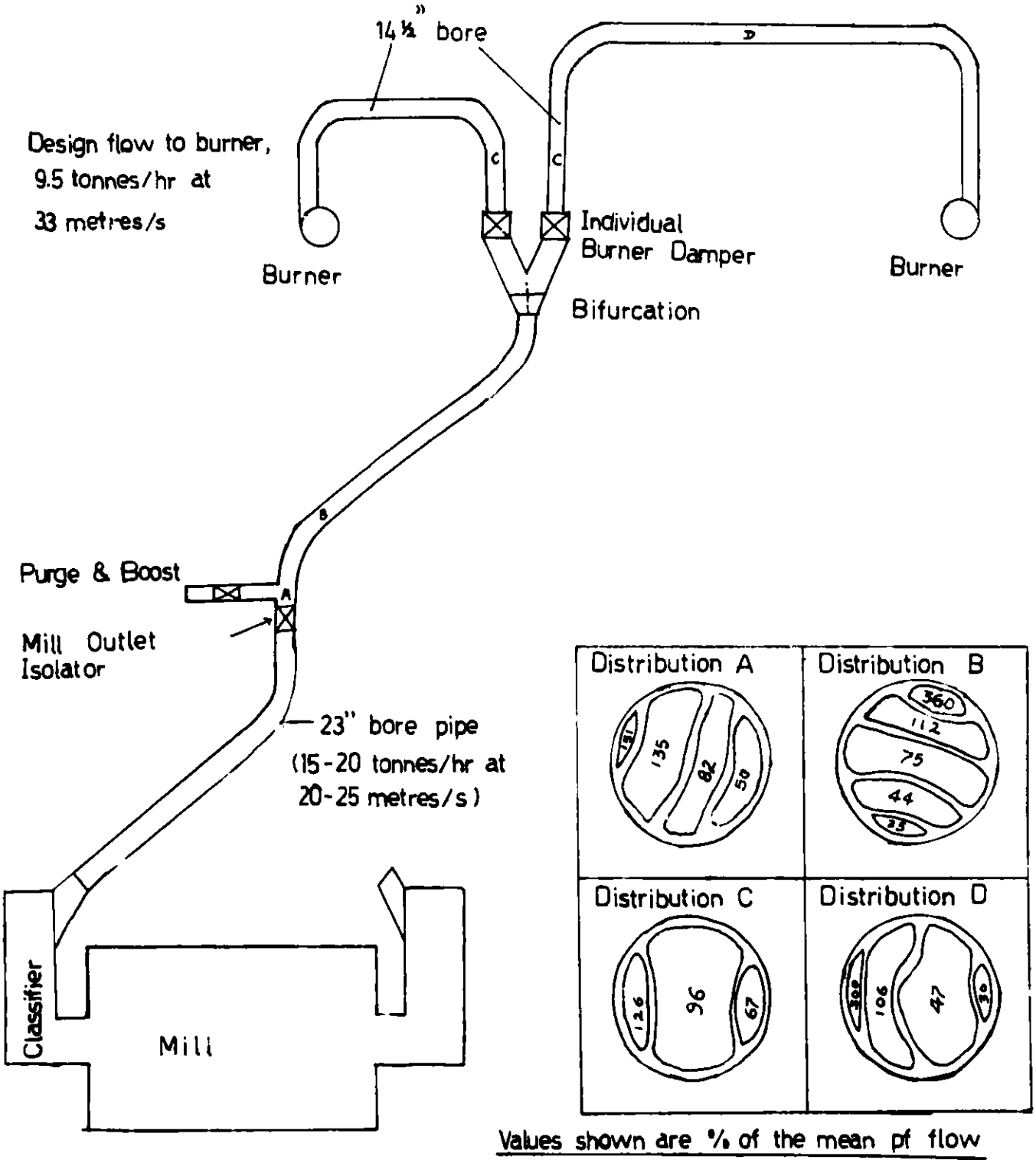

FIG 2 TYPICAL MILLING & PF TRANSPORT SYSTEM

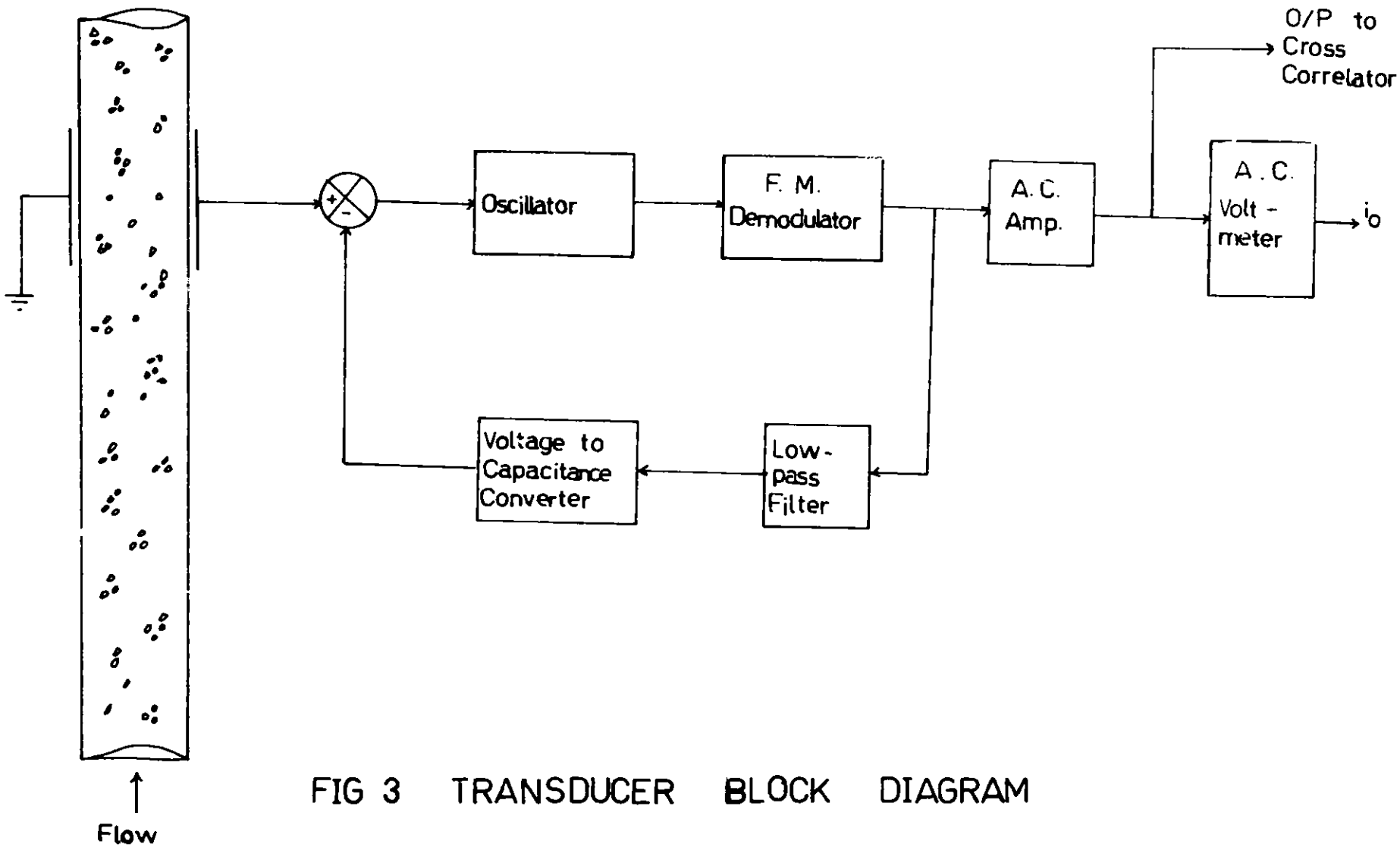

FIG 3 TRANSDUCER BLOCK DIAGRAM

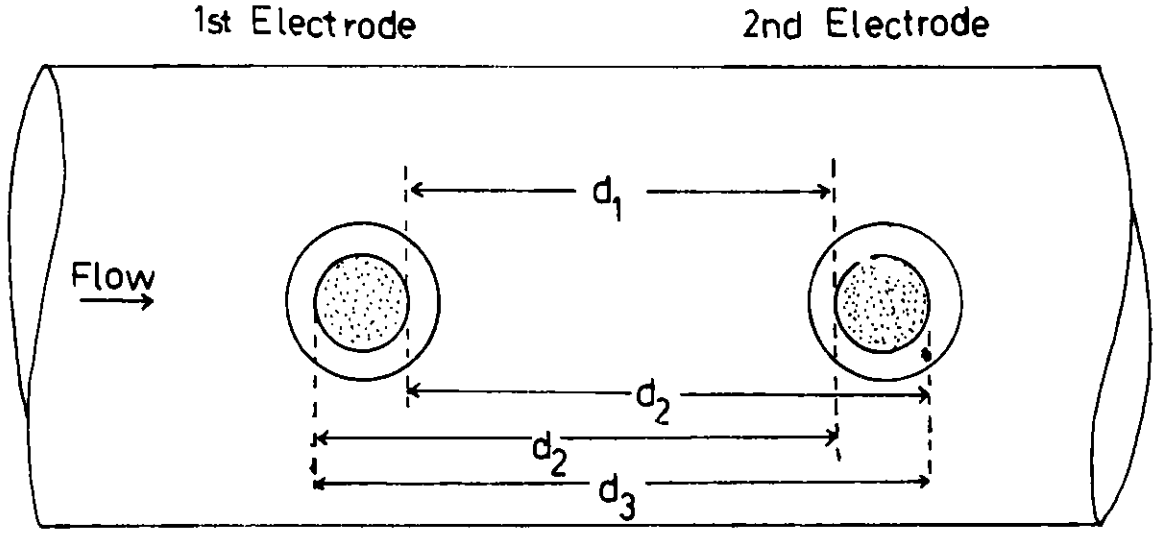

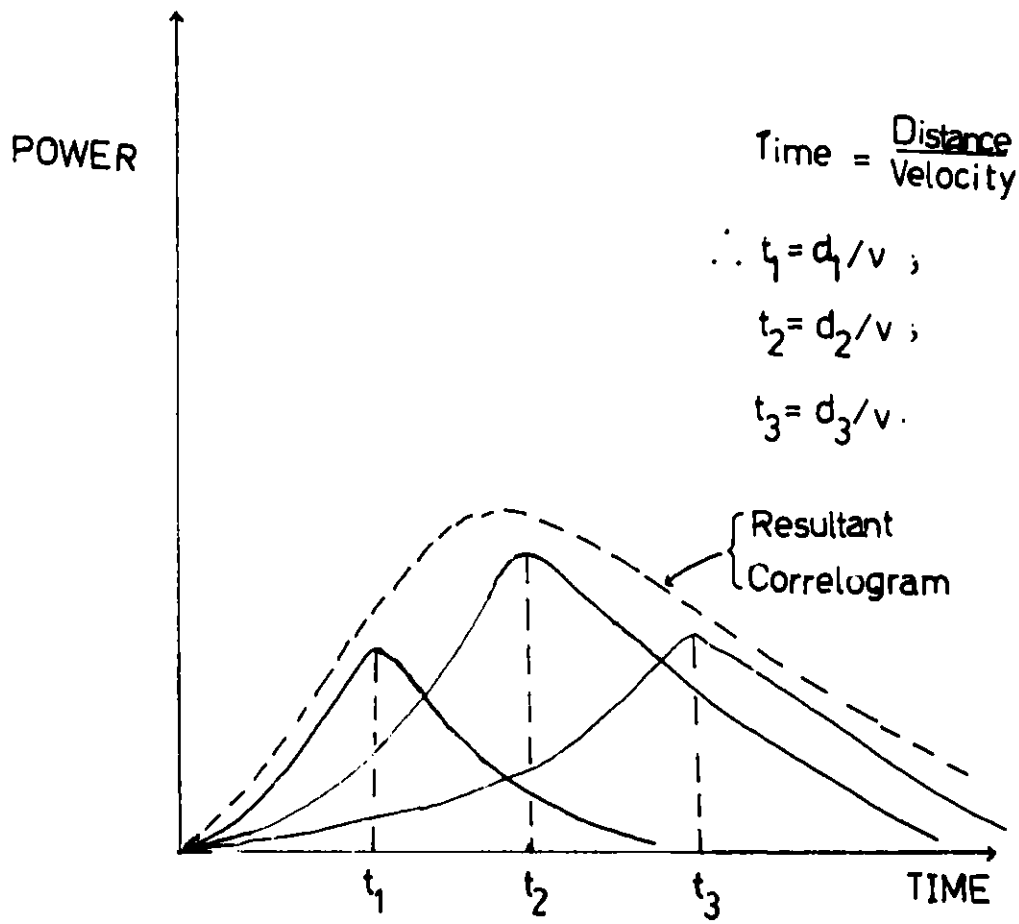

FIG 4 BOSS TYPE LOCALISED ELECTRODES & RESULTING CORRELOGRAMS

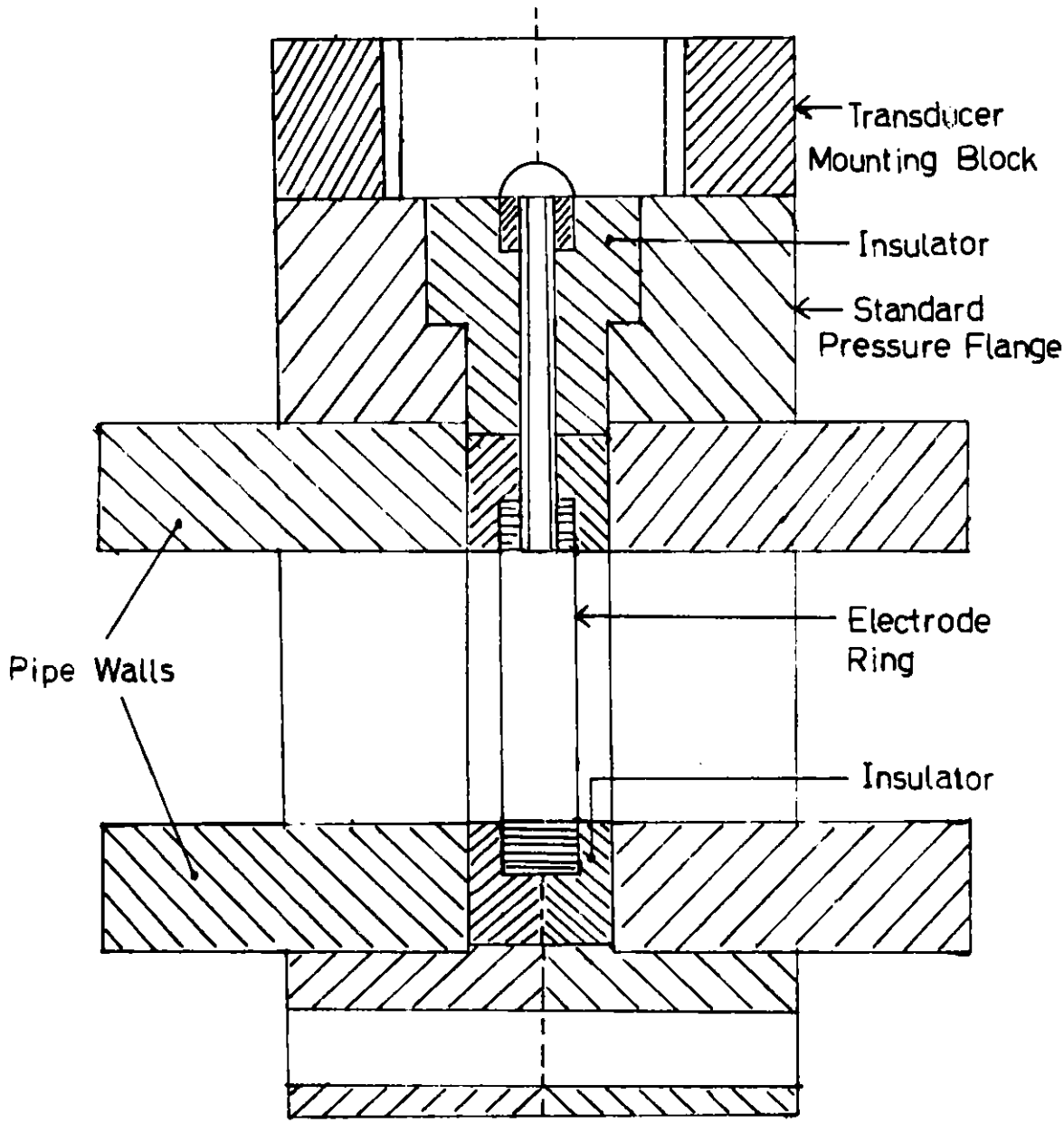

FIG 5 SECTION THROUGH A TYPICAL RING ELECTRODE

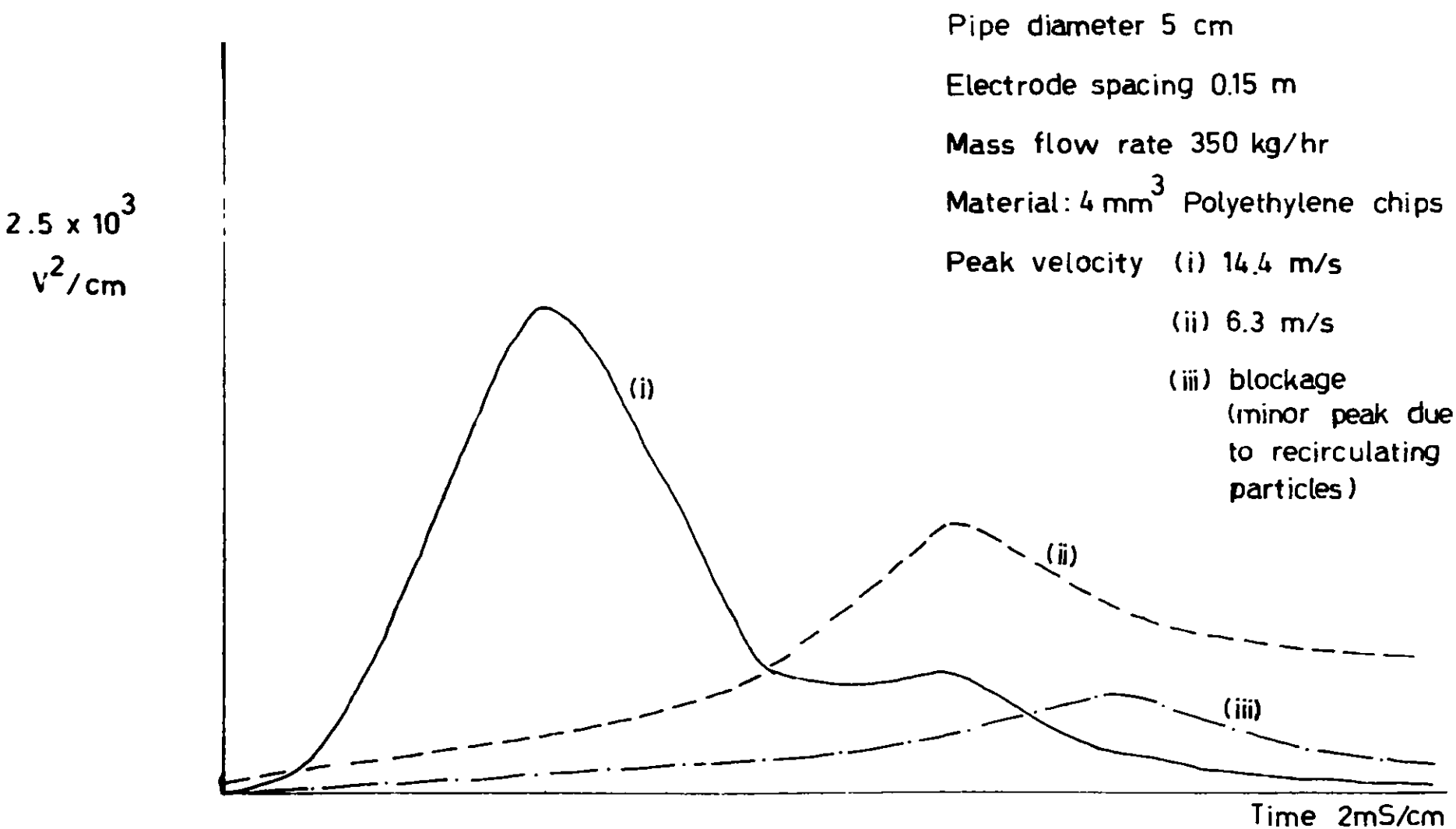

FIG 6 TYPICAL CORRELOGRAMS

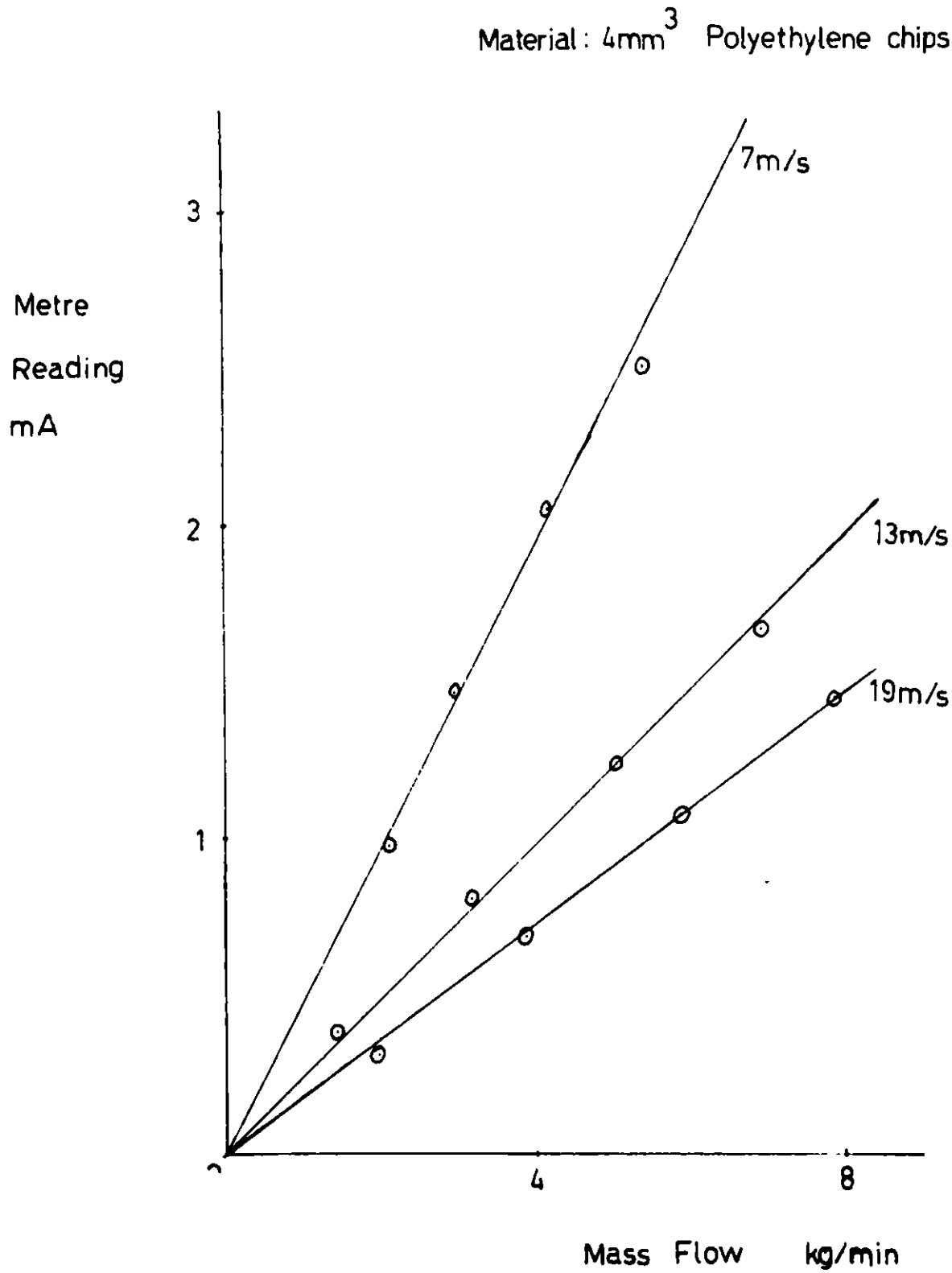

FIG 7 EXPERIMENTAL RESULTS

MEASUREMENT OF PNEUMATIC TRANSPORT OF PULVERIZED COAL*

M. P. Mathur
U. S. Department of Energy, Pittsburgh Energy Technology Center
P. O. Box 10940, Pittsburgh

G. E. Klinzing
Department of Chemical/Petroleum Engineering
University of Pittsburgh, Pittsburgh

Introduction

The means to transport solids of various sizes and shapes has always been a problem that required consideration of alternative methods and procedures. Much work has taken place over the years on the movement of solids by gases. However, the measurement of the two-phase flow of solid/gas is a very challenging problem.

Many techniques have been employed in an attempt to develop reliable flow monitoring devices. Nevertheless, at present there is a dearth of information regarding the suitability of such devices for various applications, including the pneumatic transport of coal in connection with gasification and power generation processes. After a careful survey of commercially available devices, an Auburn Monitor[1] and a Micro Motion flowmeter[2] were chosen for detailed testing and evaluation at PETC. The Auburn Monitor relates the dielectric properties of solid/gas mixtures to mass flow rate, while the operation of the Micro-Motion flowmeter is based on coriolis force exerted by the solid/gas mixture flowing through a U-tube. The mass flow rate of solid/gas in pipes is a function of many system parameters, such as conveying gas velocity, injector tank pressure, pipe radius, and pressure drop; and of particle parameters, such as particle size consist and moisture content. The present study encompasses detailed evaluations of the aforementioned devices over broad ranges of these parameters. The capabilities and limitations of these devices, and their useful operating ranges are discussed.

Facility Description

A test facility for the measurement and correlation of parameters affecting the pneumatic transport of coal has been constructed at PETC. The coal flow loop is shown in Figure 1, including the locations of the flow monitoring devices under study. The receiving hopper and the feed hopper were installed above the screw feeder. Four load cells were installed to monitor the coal in the receiving hopper. To prevent the transmission of the feed hopper weight to the receiving hopper, a flexible expansion joint was installed between the two hoppers. A second expansion joint was installed between the feed hopper and the screw feeder to isolate the screw feeder. By pressurizing the feed hopper with nitrogen, coal can be forced through either a 0.375-inch-diameter or a 1-inch-diameter test loop. A maximum of 25 psig can be safely applied to the hopper, which limits the current range of operating conditions. Pressure gauges were also installed on each hopper; and a transducer, which transmits

---

*The monitoring devices mentioned here were chosen because of their special features not found in other devices. Reference in this report to any specific commercial product, process, or service is to facilitate understanding and does not necessarily imply its endorsement or favoring by the United States Department of Energy.

signals to a digital meter, was installed on the feed hopper to monitor its pressure fluctuations. The flow of the transport gas (N_2) was monitored by an ITT-Barton turbine flowmeter that was calibrated against a rotameter.

Shakedown and Screw Feeder Calibration Tests

A number of shakedown and screw feeder calibration tests were conducted on the Coal Flow Test Loop (CFTL) system. The calibration of the screw feeder was accomplished by either transporting the coal from the lower injection tank through the complete loop into the upper receiving tank or transporting the coal to a preweighed drum placed on a weighing scale. For the 0.375-inch-diameter loop, the primary nitrogen transport gas flow was maintained at 2.5, 5.0 and 10.0 scfm (corresponding conveying gas velocities were 54.3, 108.5, and 217 ft/sec, respectively), and the tank pressure was varied between 0 and 16 psig.

In Figure 2, the actual mass flow rate is plotted as a function of tank pressure for a nitrogen gas flow rate of 2.5. The mass flow rate is a linear function of tank pressure, up to 16 psig, for each of the nitrogen flow rates. However, at higher tank pressures the relationship is non-linear. It should be pointed out that the screw feeder and the flow system were calibrated without any devices in the line. Since the Auburn Monitor device does not hinder the flow, the present calibration will still be good. However, when the Micro Motion device was installed, the mass flow rate changed, as is also shown in Figure 2. This will be discussed later.

Installation and Calibration of Monitoring Devices

Installation of Monitoring Devices

The candidate flow monitoring devices, an Auburn Monitor (A/M) and a Micro Motion monitor (M/M), were installed in the test loop. Pressure transducers were also installed at various critical points of the loop. The signals generated from the monitoring devices, pressure transducers, and the turbine flowmeter were fed into the computer.

Calibration of Monitoring Devices

The calibration of the A/M device in the 0.375-inch loop was accomplished by transferring pulverized coal from the feed hopper to a drum. The Auburn Monitor device had no effect on the flow rates observed earlier without monitors installed in the test loop.

The M/M device was first tested using water. It was then inserted into the 0.375-inch test loop for calibration with pulverized coal. It was noticed that at low tank pressures (<10 psig), the coal flow was of a slugging type and erratic when the M/M device was in line. The mass flow as well as the mass loadings (lb coal/lb N_2) through the test loop decreased when the M/M device was installed in the test loop, even though the system's input parameters (tank pressure and primary N_2 flow) were kept constant. The pressure differential across the M/M U-tube was substantial, which resulted in lower flows. To achieve higher flows and higher mass loadings, the M/M device was tested separately from the A/M device.

Results of Coal Flow Tests

In this study, coal flow tests were conducted with ten Montana Rosebud coals with different particle parameters, viz., particle size consist and moisture content. Particle

size consists and moisture contents of all the coals are listed in Table 1. These tests were done in two sets. In the first set the Auburn Monitor (A/M) alone was tested, while in the second set both the A/M and the Micro Motion (M/M) monitor were tested in the 3/8-inch coal flow test loop. The injection tank pressure was varied between 6 and 20 psig, and the primary nitrogen flow was maintained at 2.5, 5.0, 7.5, and 10.0 scfm during tests in the first set. For tests in the second set, the injection tank pressure was varied between 12 and 22 psig while maintaining the primary nitrogen flow at 2.5, 5.0, and 7.5 scfm. Each test condition was maintained for 30 minutes, and the data were averaged over this time interval. The nitrogen gas flows of 2.5, 5.0, 7.5, and 10.0 scfm correspond to superficial gas velocities of 54.3, 108.5, 163.0 and 217.0 ft/sec, respectively, for the 0.375-inch-diameter test loop.

In Figure 3, the mass flow measured by the Auburn Monitor is plotted against the actual flow given by tared weights from a receiving drum for the CFTL #1 coal at various N_2 flow rates. These tests were performed without the Micro Motion monitor in the test line. The agreement between mass flows monitored by A/M and the actual flows was quite good.

In Figure 4, the mass flow measured by the Auburn Monitor is plotted against the actual mass flow measured by the load cells for the CFTL #2 coal. The data points in Figure 4 represent N_2 flows of 2.5, 5.0, and 7.5 scfm and tank pressures ranging between 2 and 20 psig. The agreement between the actual flow and the A/M flow for all conditions measured was excellent. These tests were also performed without M/M in line.

Figure 5 compares the typical cumulative mass flows determined by the A/M device to those based on the actual tared weight. The data are displayed for various tank pressures and various nitrogen carrier gas flows. Since the tared weight data were taken at two-minute intervals, it is easier to compare cumulative weights registered by the A/M device to the tared weights. As can be seen in the figure, the tared weight data sometimes lag or lead the A/M data during the test. The A/M device measures the instantaneous flow of coal passing through the device, while the load cell data represents the average coal flow to the receiving tank over some discrete interval of time.

The data also indicated, as expected, that the higher mass loadings were obtained for the higher tank pressures and the lower superficial gas velocities. Also, for the same tank pressure, the mass loading decreased as the superficial velocity was increased.

The mass flow and the mass loadings (lb coal/lb N_2) through the test loop decreased when the Micro Motion monitor was installed in the loop even though the input parameters of the system (tank pressure and primary N_2 flow) were kept constant. In Table 2, the change in mass flow and mass loadings for the same system parameters are given. The pressure differential across the U-tube of the M/M was quite large. Installation of the M/M device in the test loop did not affect the performance of the A/M device, as is shown in Figure 6. In Table 3, the pressure differential across the M/M U-tube is given along with the pressure differential in the straight section (without M/M). The large pressure differential presumably results in the lower mass flow observed with the A/M device.

Next, the averaged voltage signal from the A/M was plotted against the averaged actual mass flow rate for all samples. In Figure 7, typical data showing the effect of coal moisture content on the performance of the A/M device are given. The coal

samples tested had roughly the same particle size distribution (~ 70% minus 200 mesh), but moisture contents were 1.0, 4.6, and 7.1 percent. The data points for the 1% and 4.6% moisture content coal samples fall on one straight line, while data points for the 7.1% moisture content coal fall on another straight line (high voltages). All data points in Figure 7 were averaged over 30-minute intervals in tests at the same primary nitrogen gas flow of 7.5 scfm. Similar data were obtained for all nitrogen gas flow rates for all samples studied.

The data indicate that a coal moisture content of up to 4.6% has no apparent effect on the A/M performance, while a 7.1%-moisture-content sample generates an enhanced voltage signal, presumably attributable to the large dielectric constant of water.

In Figure 8, the average voltage signal, $\bar{V}AM$, from A/M is plotted against the actual average mass flow rate for three samples having size consists of 34.3%, 55.2%, and 68.5% minus 200 mesh and nominal moisture content of about 7.4%. As before, each point on the graph represents an average over 30-minutes while the primary nitrogen gas flow was maintained at 7.5 scfm. Similar data for nitrogen flows of 2.5, 5.0, and 10.0 scfm were also obtained. The data indicate that although points from the high moisture content (~7.4%) samples are distinct from the 1% and the 4.6% moisture samples, they all fall on the same straight line irrespective of their particle size consists. Moreover, the voltage signal from the A/M can be related to the mass flow rate by $M = k_1 V + k_2$, where M is the mass flow rate, V is the voltage signal from the A/M, and k_1 and k_2 are constants to be determined experimentally.

Figure 9 shows the plots of the average voltage, $\bar{V}MM$, from M/M against the average mass flow rate from load cells for three samples with nominal size consists of about 70% minus 200 mesh (75.4, 75.0, and 68.5%) and moisture content of 1.0, 4.6, and 7.1, respectively. The data include all nitrogen flows examined. All data fall on one straight line irrespective of moisture content, unlike the data for the A/M. All the data points from samples of different particle size consists are clustered around a straight line, indicating little effect of particle size consists on measured mass flow rate.

The data from the second set indicate that the mass loading (lb coal/lb nitrogen) as well as the mass flow rate (lb/min) were considerably reduced with the M/M monitor inserted in the test loop due to a large pressure drop across the M/M monitor. Moreover, installation of the M/M monitor in the test loop did not affect the performance of the A/M device. Furthermore, as for the A/M, the M/M data can be related to the mass flow rate by $M = C_1 V + C_2$, where M is mass flow rate, V is the voltage, and C_1 and C_2 are constants to be determined experimentally.

Determination of Fluid Dynamic Parameters

In a two-phase flow, the particle velocity, V_p, is related to the voidage, ϵ, and solids mass flow rate, W_s, as

$$V_p = \frac{4W_s}{(\rho_p - \rho_f)\pi D^2 (1-\epsilon)} \qquad 1$$

where D is the diameter of the pipe through which the solid/gas mixture is flowing, ρ_p is the true density of the powdered coal, and ρ_f is the density of the fluid. By definition, the voidage fraction, ϵ, is the volume fraction of gas in the mixture. If ρ_f

and ρ_p are the gas and powdered coal densities, respectively, then voidage $\epsilon = (1 + L \rho_f/\rho_p)^{-1}$, where L is the solids loading defined as the pounds of coal per pound of nitrogen. For the 0.375-inch test loop, and for ρ_p = 85.5 lb/ft^3[3] and ρ_f = 0.0763 lb/ft^3, the particle velocity equation (1) becomes

$$V_p = 2.6 \times 10^2 \times W_s (1 + 9.78 \times 10^{-4} L)^2/L \qquad 2$$

For a given mass flow, W_s (lb/min), and solid loading, L, the particle velocity, V_p (ft/sec), can be calculated from equation 2.

The relationship between the superficial gas velocity, V_s, and the actual fluid velocity, V_f, is given by $V_f = V_s/\epsilon$.

The voidage fraction, ϵ, for each test run was calculated from the loadings, L; and the particle velocity, $\bar{V}_p$, was calculated using equation 2. The superficial gas velocity, V_s, was calculated using the nitrogen gas flow measured by the ITT Barton turbine flowmeter and the i.d. of the test loop pipe. From the superficial gas velocity and the voidage fraction, ϵ, the actual fluid velocity was calculated. Table 4 lists typical values of these parameters for two coals, viz., CFTL #7 and CFTL #8. Set 1 refers to tests with A/M alone, and Set 2 refers to tests with both A/M and M/M in the test loop.

For all superficial gas velocities, V_s, the actual fluid velocity, V_f, is greater than the corresponding particle velocity, V_p, as expected. The difference $(V_f - V_p)$ decreases as the tank pressure is increased. As expected, the voidage fraction decreases with the increased solid-mass flow. It should also be noted that at a constant tank pressure and constant superficial gas velocity, both the fluid velocity and the particle velocity are reduced when the M/M is inserted in the test circuit.

Conclusions

1. The Auburn Monitor can be used for monitoring coal/nitrogen mass flow. Variations in particle size distribution of coal between 30% and 70% minus 200 mesh and in coal moisture content up to 4.6% have no apparent effect on its performance. A coal moisture content of 7.4% enhances the voltage signal from the Auburn Monitor, presumably due to the large dielectric constant of water.

2. Insertion of the Micro Motion monitor into the test loop reduces the mass flow rate as well as the solid/gas loadings. Preliminary data so far indicate that the voltage signal from the Micro Motion monitor can be used to monitor the coal flow.

3. Fluid dynamic parameters such as voidage fraction, particle velocity, actual fluid velocity, and superficial gas velocity have been evaluated. Particle velocity is lower than the corresponding actual fluid velocity by no more than 8%.

References

(1) Auburn International Incorporated, One Southside Road, Danvers, MA
(2) Micro-Motion, Incorporated, Denver, CO
(3) Private Communication from J.M. Ekmann and Amy C. Ekmann.

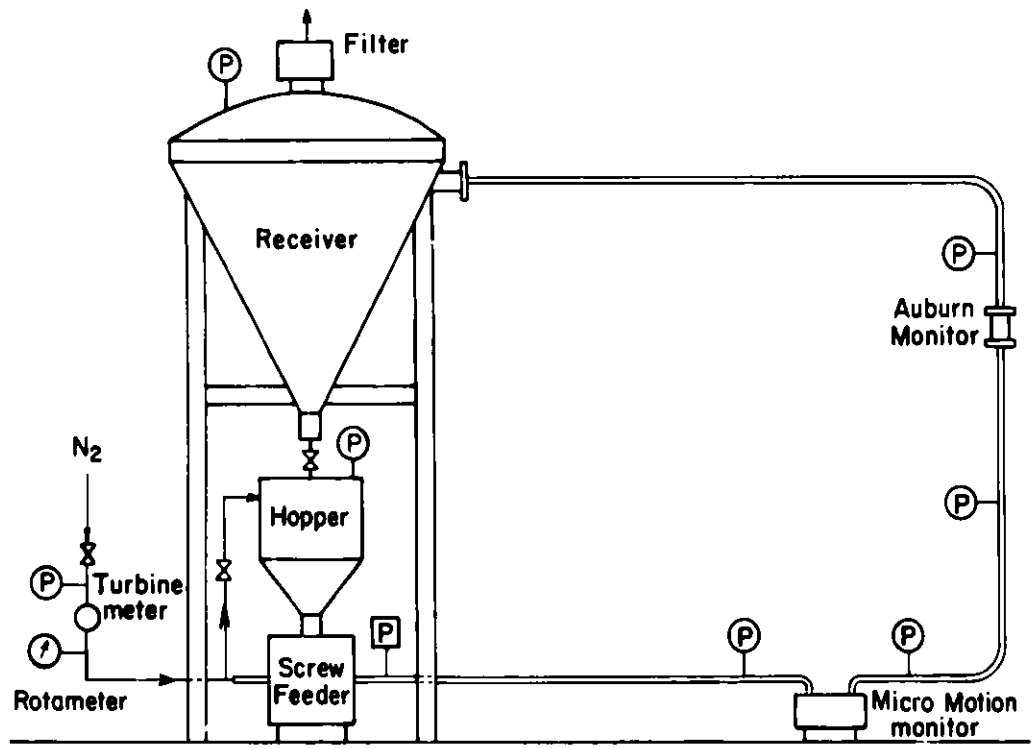

Figure 1.- Schematic of the Coal Flow Test Loop Facility.

Table 1. Particle Parameters of Montana Rosebud Coals

Mesh Size	CFTL #1 WT (%)	CFTL #2 WT (%)	CFTL #3 WT (%)	CFTL #4 WT (%)	CFTL #5 WT (%)	CFTL #6 WT (%)	CFTL #7 WT (%)	CFTL #8 WT (%)	CFTL #9 WT (%)	CFTL #10 WT (%)
+20	3.0	3.0	1.7	0	0.5	2.0	2.0	0.5	1.2	-
-20 +40	12.0	21.0	19.0	0	1.5	1.0	15.5	0.0	15.0	-
-40 +80	30.0	10.0	32.2	2.5	15.0	2.0	31.0	4.5	30.8	-
-80 +100	8.0	15.0	7.8	1.2	5.1	3.0	7.0	4.5	3.5	5.4
-100 +140	11.0	8.0	7.1	5.1	15.0	7.3	8.0	9.0	10.5	39.4
-140 +200	7.0		4.8	16.2	15.0	9.4	5.5	13.0	4.7	
PAN	29.0	43.0	27.5	75.0	47.8	75.4	31.0	68.5	34.3	55.2
MOISTURE (%)	4.0	4.0	1.0	4.6	1.5	1.0	1.5	7.1	7.4	7.4

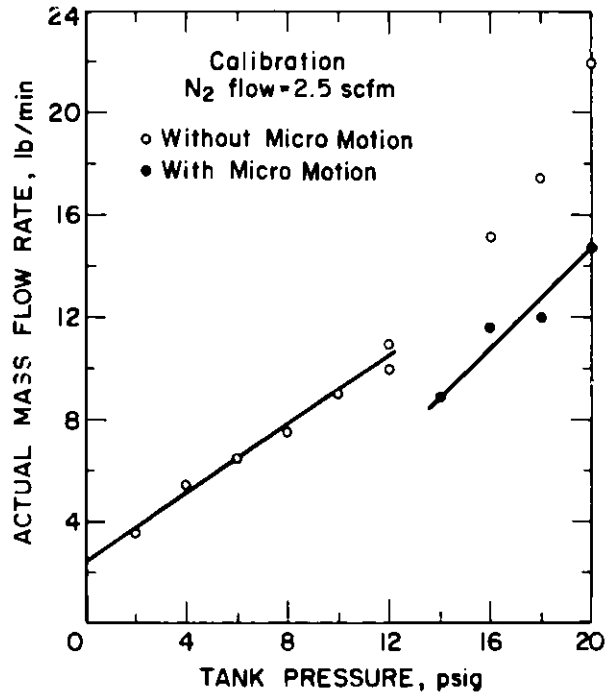

Figure 2.-Calibration of the injection system with and without Micro Motion monitor in the Loop Transport gas flow was maintained at 2.5 scfm.

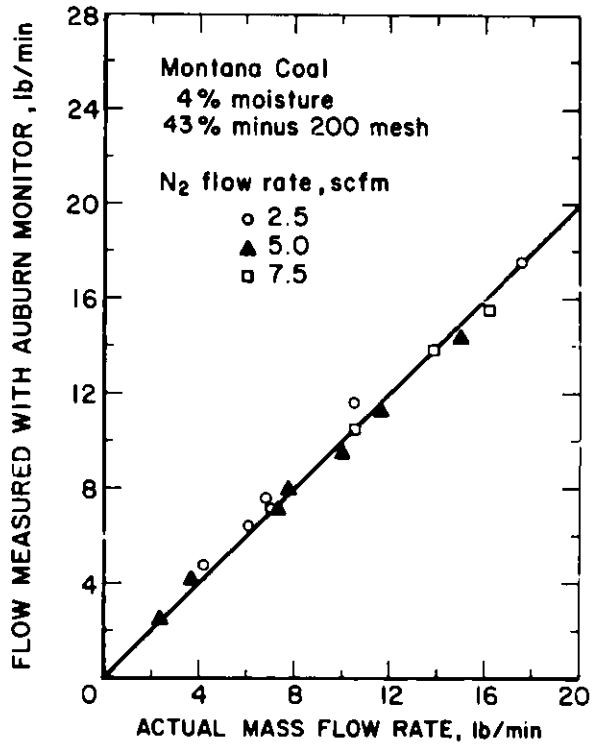

Figure 4.-Flow measured with Auburn Monitor versus actual flow (Micro Motion monitor not in line).

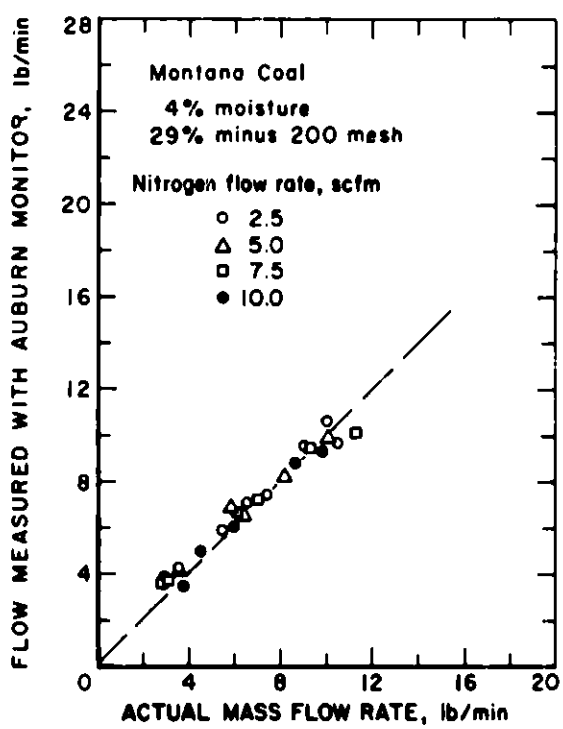

Figure 3.-Flow measured with Auburn Monitor versus actual flow (Micro Motion monitor not in line)

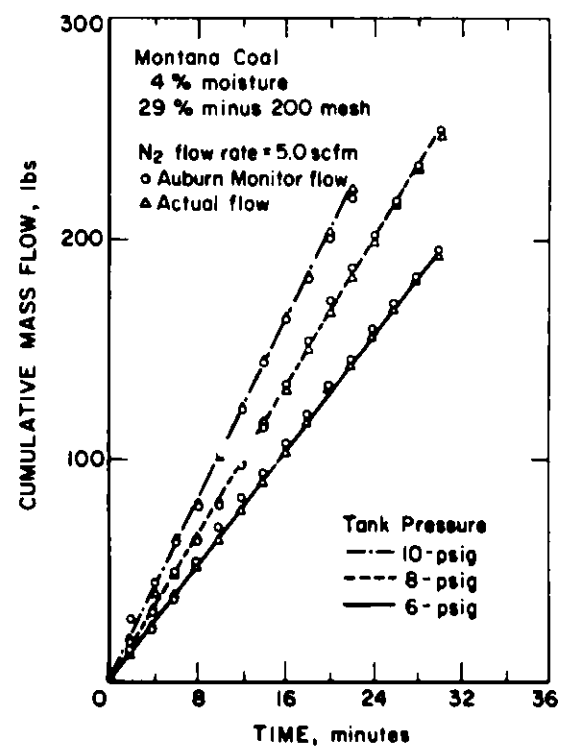

Figure 5.-Comparison of Cumulative flow measured with Auburn Monitor with actual flow (Tared weight).

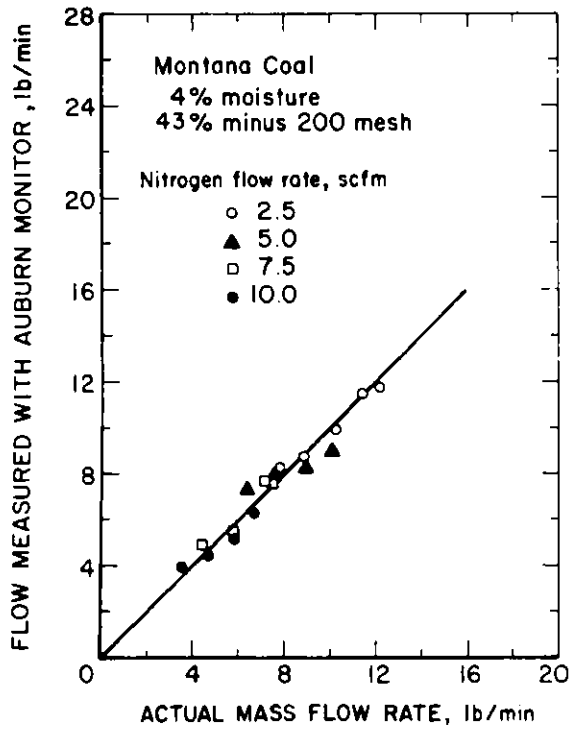

Figure 6.-Flow measured with Auburn Monitor versus actual flow (Micro Motion monitor in line).

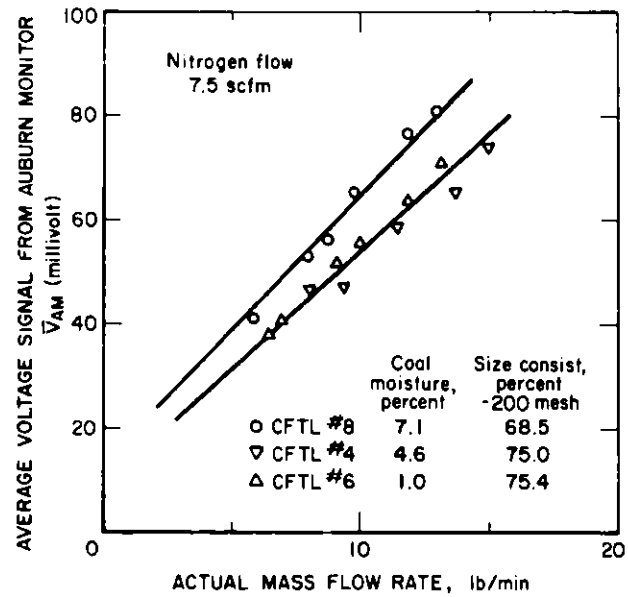

Figure 7.-Voltage signal from Auburn Monitor averaged over 30 minutes as a function of actual mass flow (Load cell) averaged over 30 minutes.

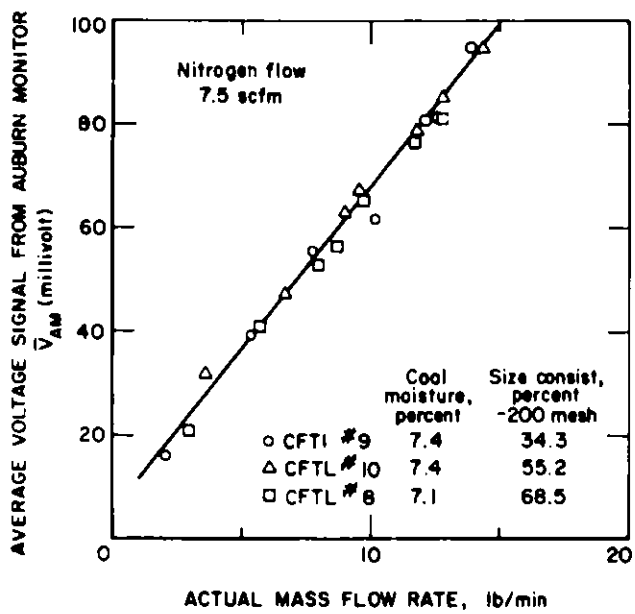

Figure 8.-Voltage signal from Auburn Monitor averaged over 30 minutes as a function of actual mass flow (Load cell) averaged over 30 minutes.

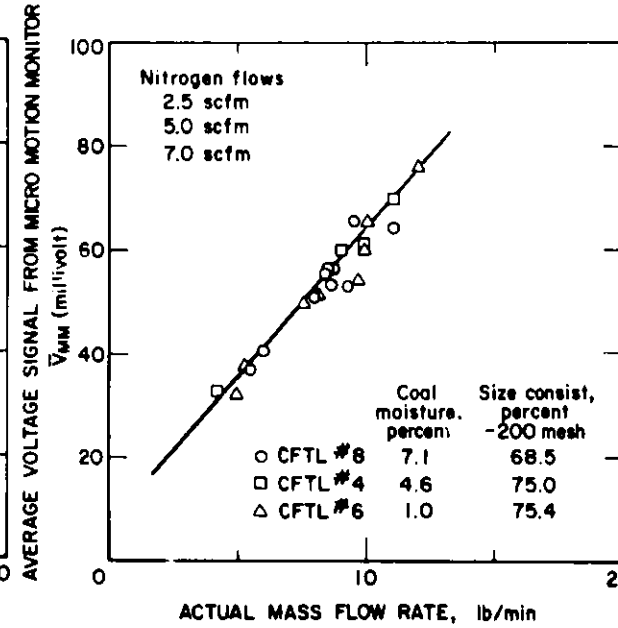

Figure 9.-Voltage signal from Micro Motion Monitor averaged over 30 minutes as a function of actual mass flow (Load cell) averaged over 30 minutes.

TABLE 2

EFFECT ON MASS FLOW WHEN MICRO MOTION DEVICE (M/M) IS INSERTED IN THE LOOP.[1]

N_2-Flow (scfm)	V_s^2 (ft/sec)	Tank Pressure (psig)	L^3 (lb coal/lb N_2)	Actual Flow (lb/min)	M/M
2.5	54.3	16	106	20.19	OUT
2.5	54.3	16	83	11.67	IN
2.5	54.3	20	141	26.83	OUT
2.5	54.3	20	77	14.71	IN
5.0	108.5	12	26	12.17	OUT
5.0	108.5	12	15	5.69	IN
5.0	108.5	4	18	5.82	OUT
5.0	108.5	4	9	2.91	IN
5.0	108.5	2	11	3.51	OUT
5.0	108.5	2	7	1.97	IN
10.0	217.0	12	12	9.79	OUT
10.0	217.0	14	8	6.29	IN
10.0	217.0	16	11	8.21	IN
10.0	217.0	18	14	10.95	IN

1. Montana Coal, 29% minus 200 mesh, 4% moisture
2. Superficial Gas Velocity
3. Coal to Nitrogen Mixture Loadings

TABLE 3

EFFECT OF PRESSURE DIFFERENTIAL ACROSS MICRO MOTION MONITOR ON MASS FLOW.[1]

N_2 Flow (scfm)	Tank Pressure (psig)	ΔP^2 (psig)	A/M[3] (lb/min)	M/M[4]
5.0	14	0.5	11.26	OUT
	14	3.5	7.00	IN
	16	0.7	14.09	OUT
	16	4.0	7.67	IN
	18	1.0	14.37	OUT
	18	5.5	8.13	IN
	20	1.5	15.06	OUT
	20	5.5	8.89	IN
	22	7.0	9.43	IN
7.5	14	0.4	10.55	OUT
	14	3.5	5.51	IN
	16	0.5	11.75	OUT
	16	5.0	7.72	IN
	18	0.7	13.81	OUT
	18	4.3	7.61	IN

1. Montana Coal, nominal 43% minus 200 mesh, 4% moisture.
2. Pressure differential across Micro Motion device.
3. Auburn Monitor data.
4. Micro Motion monitor.

TABLE 4

TYPICAL FLUID DYNAMIC PARAMETERS

Sample Number	Tank Pressure (psig)	V_s (ft/sec)	W_s (lb/min)	L (lb/lb)	E	V_f (ft/sec)	V_p (ft/sec)
CFTL #7							
SET 1	10	108.5	7.42	19.4	0.9813	110.6	102.9
	16	108.5	11.53	30.2	0.9713	111.7	105.2
	20	108.5	15.92	41.7	0.9608	112.9	107.5
SET 2	16	108.5	6.35	16.6	0.9840	110.3	102.4
	20	108.5	8.25	21.6	0.9792	110.8	103.5
CFTL #8							
SET 1	10	108.5	5.87	15.4	0.9852	110.1	100.7
	16	108.5	11.09	29.0	0.9724	111.6	105.0
	20	108.5	14.34	37.6	0.9645	112.5	106.6
SET 2	16	108.5	6.92	18.1	0.9826	110.4	102.8
	20	108.5	8.55	22.4	0.9786	110.9	103.6

V_s Superficial gas velocity (ft/sec)

W_s Mass flow rate (lb/min)

L Solid-gas loading (# of coal/ # of nitrogen)

E Voidage (Volume fraction of nitrogen)

V_f Fluid or Actual gas velocity (ft/sec)

V_p Coal particle velocity (ft/sec)

CFTL #7 Montana Rosebud Coal
Size Consist = 31.0% minus 200 mesh
Coal Moisture = 1.5%

CFTL #8 Montana Rosebud Coal
Size Consist = 68.5% minus 200 mesh
Coal Moisture = 7.1%

Set 1: With Auburn Monitor only

Set 2: With Auburn Monitor and Micro Motion in line

OPTIMIZATION OF THE INLET AND OUTLET GEOMETRY FOR METERING MASS FLOW OF GAS-SOLIDS MIXTURES IN A VENTURI

A.L. Payne and C.T. Crowe
Washington State University
Pullman, Washington

ABSTRACT

An experimental study was conducted to determine the effect of inlet geometry on pressure sensitivity and exit geometry on pressure recovery for a suspended gas-solids flow in a venturi. Past research work at Washington State University has indicated that the performance of the venturi is dependent upon Stokes number and particle-gas loading. The results presented here show that decreasing the inlet angle enhances the ability of the venturi to measure feed rates and that pressure recovery is a function of exit angle and particle-gas loading. Further results presented indicate that particle-gas loading can also be determined by laser light attenuation.

INTRODUCTION

The increased use of fossil fuel energy has developed the need for accurate and reliable methods to monitor the flow rates of solids in the flow of gas-solids mixtures. Applications include monitoring the feed rate of pulverized coal in feeder lines to furnaces, measuring the flow rate of solids conveyed pneumatically to fluidized beds and metering the flow rate of char in steam in coal gasification systems. These meters should be able to operate reliably at pressures as high as 1500 psi and 200°F. Their accuracy should be ±2% and operate with total pressure drops not exceeding 5 psi.

The capability of the venturi-meter to monitor the flow rate of gas-solids suspensions has been under study at Washington State University (WSU) for over three years. The advantages of the venturi as a solids flow meter are its simplicity, reliability and inexpensiveness. It is well suited to industrial environments and operable under a wide range of conditions. The studies at WSU have demonstrated that pressure drop across the throat of the venturi is sensitive to the solids loading in the conveying gas; in fact, the pressure drop varies linearly with loading at a fixed Stokes number. Loading is defined as the ratio of mass flow rate of the particles to mass flow rate of the gas. Stokes number is defined as the ratio of the particle relaxation time to gas residence time and is expressed as

$$ST = \frac{\rho_p d_p^2 U}{18\mu D_t}$$

where ρ_p is material density of the particles, d_p is the particle diameter, U is the gas velocity in the pipe, μ is the dynamic viscosity of the gas and D_t is the venturi throat diameter. The linear variation of the pressure drop ratio with solids loading for a fixed Stokes number is illustrated in Figure 1. On this figure ΔP_{TP} is the pressure drop due to the flowing particle-gas mixture, ΔP_g is the pressure drop due to the gas alone and Z is the loading.

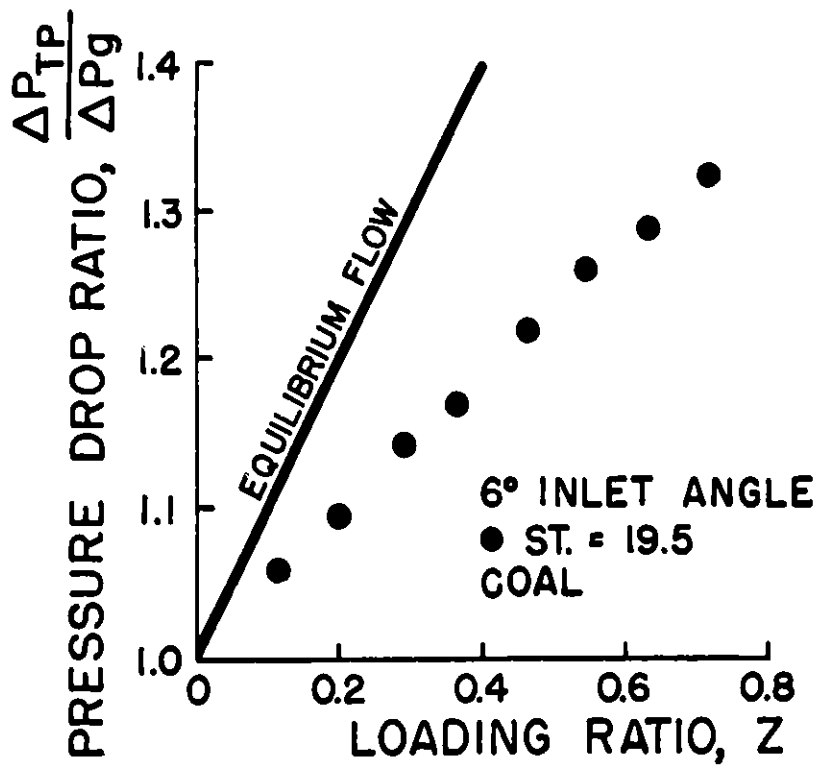

Figure 1. Pressure drop ratio versus loading ratio

Past research at WSU (1) has shown that a decrease in Stokes number corresponds to an increase in pressure drop for a given loading. This trend can be explained as follows. If the Stokes number is small, the particles respond quickly to gas and flow changes. As the Stokes number approaches zero, the particles and gas act as a homogeneous mixture which can be regarded as single phase fluid with a modified density. Acceleration of the particles by the gas requires a larger pressure drop in the flow. If the Stokes number is large the particles do not respond to gas phase changes causing the flow to act as a particle-free gas with a corresponding smaller pressure drop.

Recognizing the linearity of the pressure drop ratio with loading leads to the definition of the pressure ratio parameter.

$$P_r = (\Delta P_{TP}/\Delta P_G - 1)/Z$$

This pressure ratio parameter is the slope of the line for pressure drop ratio vs loading and is a function of Stokes number. The magnitude of the pressure ratio parameter is a measure of the sensitivity to loading. The dependence of the pressure ratio parameter on Stokes number for spherical particles in a standard ASME venturi and results for a non-standard venturi with inlets angle of 8° and 4° (2) are shown in Figure 2. The improved sensitivity of the venturi with decreased inlet angle is apparent in this illustration.

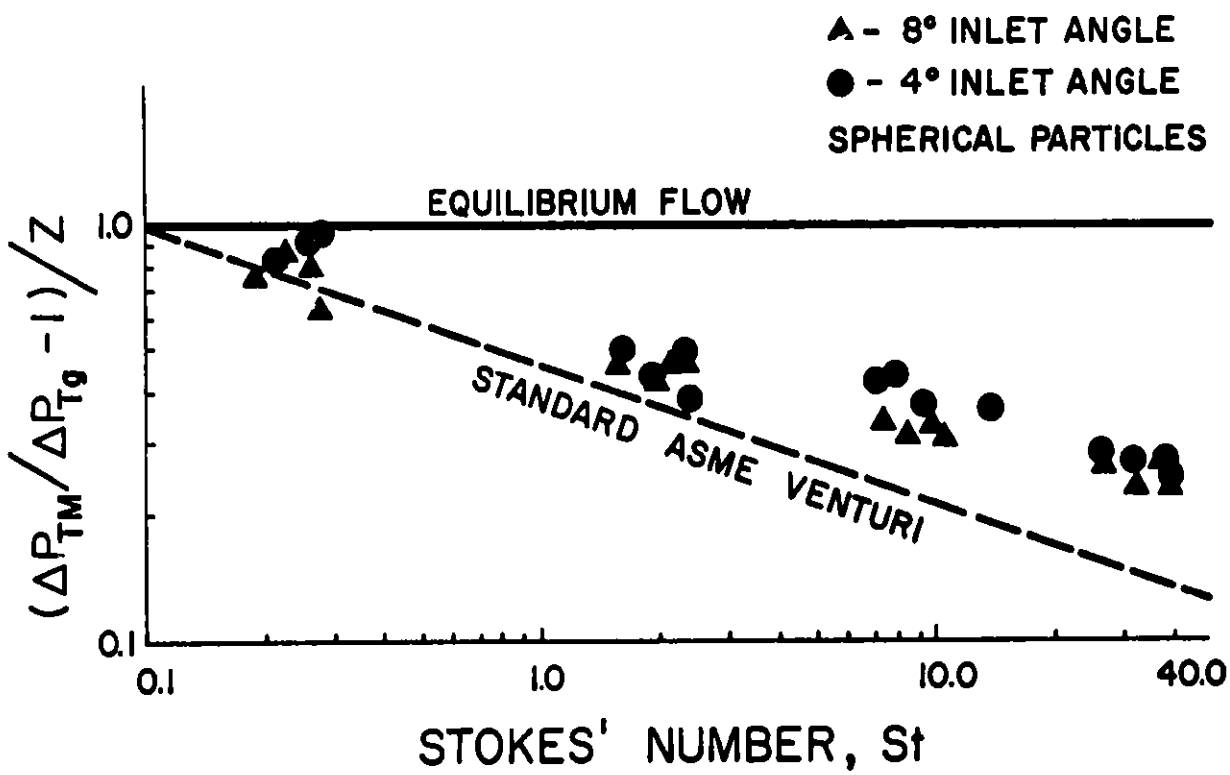

Figure 2. Pressure ratio parameter versus Stokes number.

The experimental set-up used in this study is shown in Figure 3. The flow of compressed air, entering the experimental system, is controlled by a flow regulator and is metered by a square edge orifice. Particles are introduced into the air stream by a mechanical auger powder feeder. This air-particle mixture then passes through a venturi where measurements of pressure drop and laser light attenuation are made. Finally, the particles and air are separated by a series of cyclone separators. A micro computer processor collects pressure drop data and loading information. The pressure drops are measured through pressure transducers connected to the micro computer by an analog to digital board.

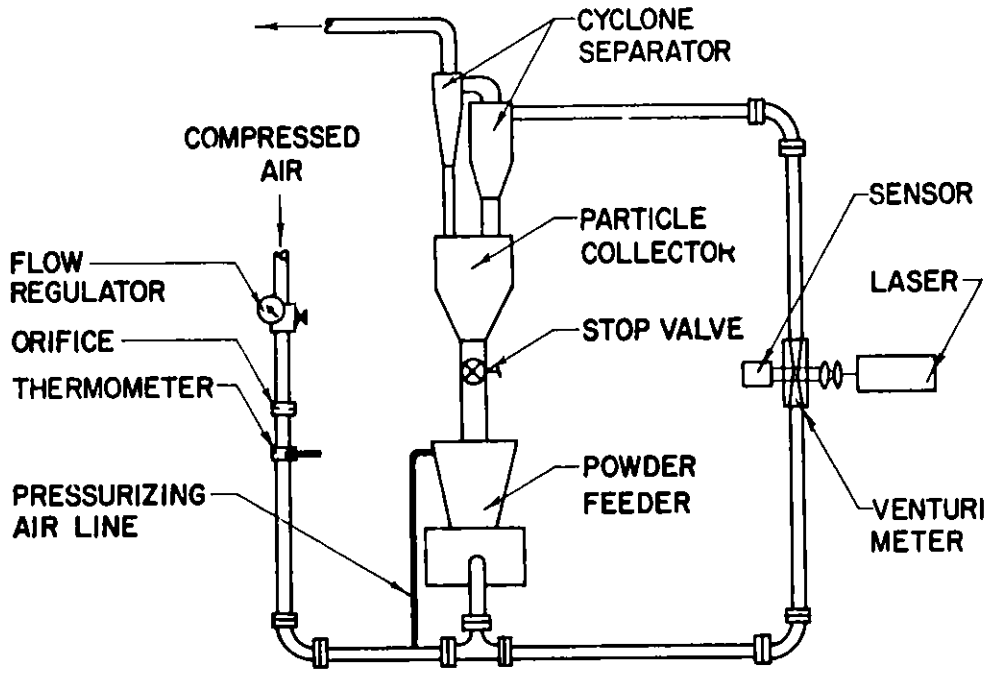

Figure 3. Experimental set-up.

A laser and photodetection system are mounted at the venturi throat section to measure the attenuation of a laser beam with loading. This approach has been studied by Fenton and Stokel (3) utilizing Beer's law which states that attenuation of radiation intensity by particle blockage per unit depth is proportional to intensity,

$$\ell n(I_L/I_0) = CL$$

where I_o is the reference intensity, I_L is the beam intensity after passing through the particle cloud, L is the path length, and C is a function of particle concentration.

The objectives of this experiment were to correlate the effect of Stokes number and loading with inlet and exit geometry and to correlate loading with laser-light attenuaton. Venturis with inlet angles of 12° and 6° and exit angles of 6° and 4° with a β-ratio of 0.5 were selected for this comparison. The different venturi configurations used for this study are illustrated in Figure 4.

The experiment was carried out with two different samples of pulverized coal. The mass median diameters of the two samples were 64 μm and 120 μm. A constant air mass flow rate was maintained while randomly picking particle feed rates to vary loading. The pressure drops between the venturi inlet and throat and between the venturi inlet and exit were measured at given air flow rates for different loading ratios. This approach gave data for a particular Stokes number. Other Stokes numbers were obtained by using different particle sizes and air flow rates.

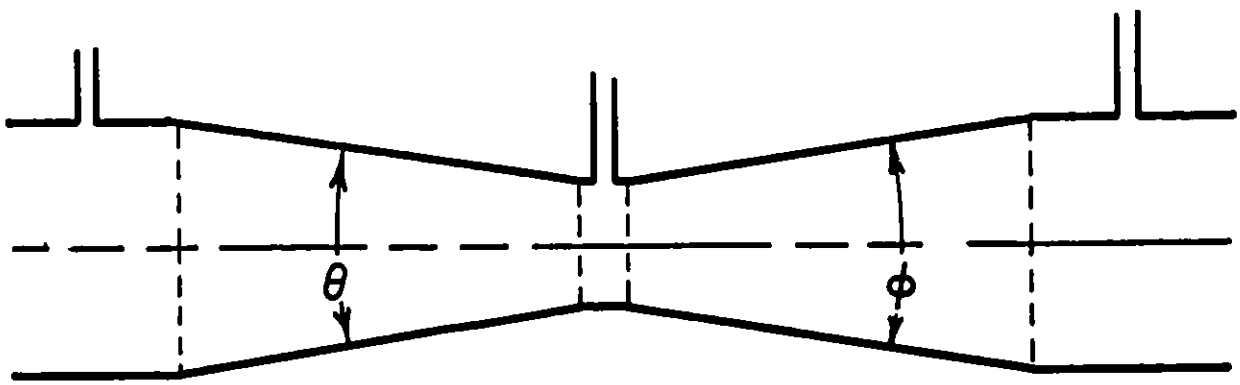

Figure 4. Venturi configurations

RESULTS

The effect of Stokes number on the pressure ratio parameter for inlet angles of 12° and 6° is shown in figure 5. Lines representing previous data obtained using spherical glass beads in a standard ASME venturi, inlet angle 21°, and a non-standard venturi, inlet angle 8°, are shown on the same figure. Note the apparent improvement in pressure sensitivity with the coal particles compared with glass beads. This improved sensitivity is due to increased particle drag of nonspherical coal particles.

The dependence of pressure recovery factor on loading for an exit angle of 6° and Stokes number of 6.64 is shown in figure 6. A line representing pressure recovery predictions from a numerical program (CONVAS 4) is also shown for a comparison. The pressure recovery factor is defined as

$$\frac{(\Delta P_{TTP} - \Delta P_{TG})}{\frac{1}{2} \rho_G (1 + Z) U^2}$$

where ΔP_{TTP} is the pressure loss across the venturi for gas particle flow, ΔP_{TG} is the loss for gas alone and ρ_G is the gas density. It is apparent from figure 6 that pressure recovery is a function of loading. The difference between the experimental observations and the numerical model is attributed to particle channeling. The numerical model, CONVAS, does not take two dimensional effects into account.

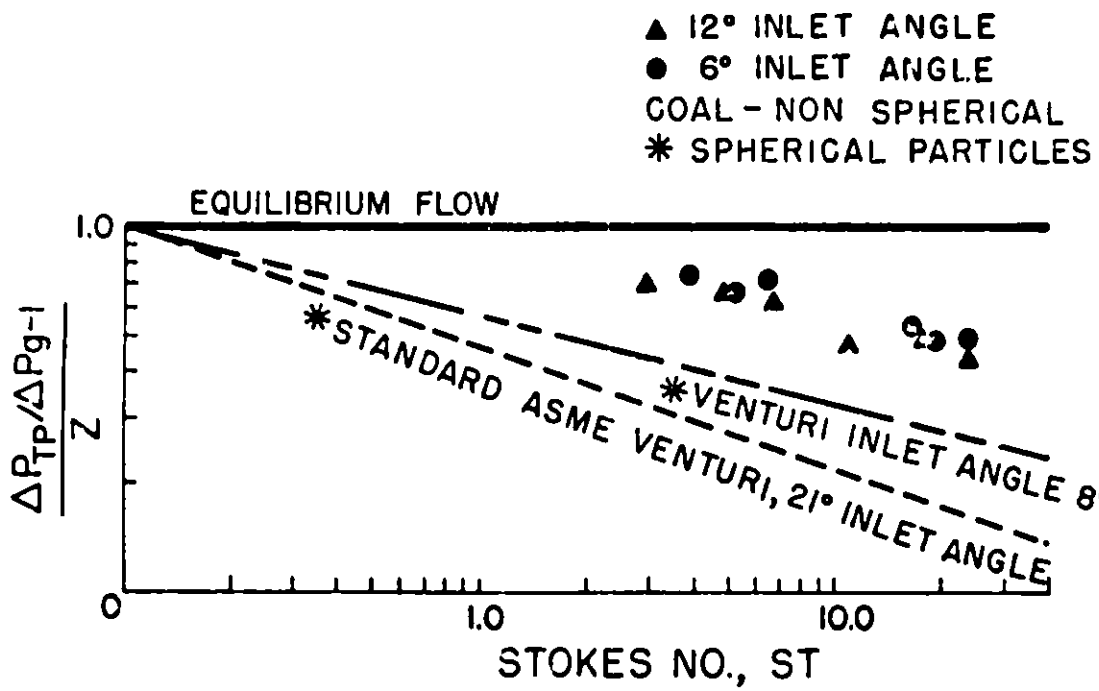

Figure 5. Pressure ratio parameter versus Stokes number.

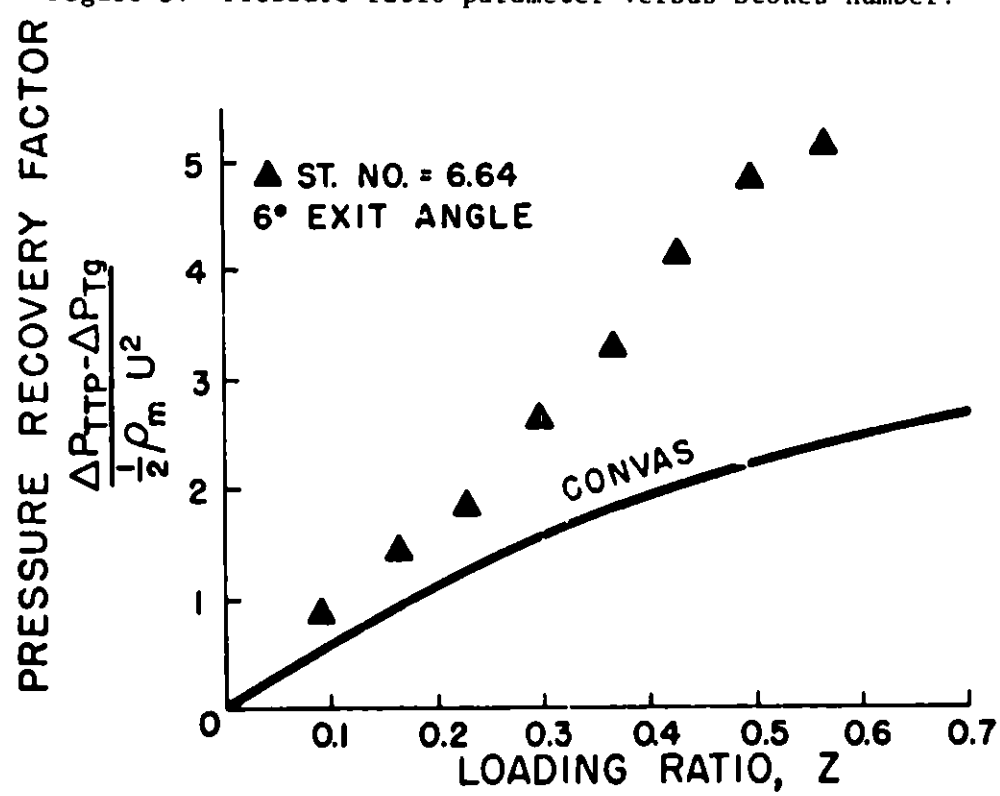

Figure 6. Pressure recovery factor versus loading ratio.

The effect of exit angle on the total pressure drop ratio is shown in Figure 7. Total pressure drop ratio is defined as the total pressure drop due to both phases divided by the pressure drop at the throat due to both phases. Note as the exit angle increases the total pressure drop ratio increases.

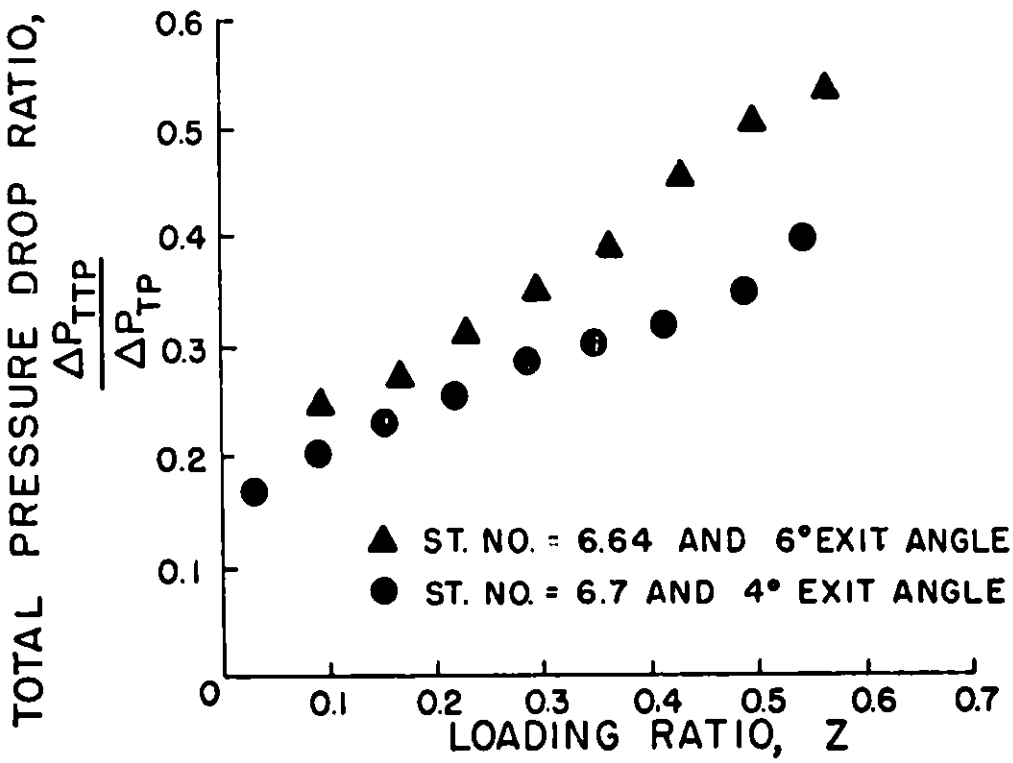

Figure 7. Total pressure drop ratio versus loading ratio

The effect of loading on laser light attenuation for coal particles of mass median diameter of 120 μm is shown in Figure 8. There is an apparent strong correlation between loading and laser attenuation. The simultaneous measurement of laser attenuation and two-phase pressure drop, ΔP_{TP}, allows one to determine the flow of both phases as illustrated in Figure 9. Measurements of the laser attenuation yields loading (from Fig. 8) which gives the ratio $\Delta P_{TP}/\Delta P_G$ on Figure 9. This ratio together with the measured ΔP_{TP} allows one to calculate ΔP_G. This value yields the gas flow rate from the conventional venturi equations. The solids flow rate is obtained by multiplying the gas flow rate by the loading.

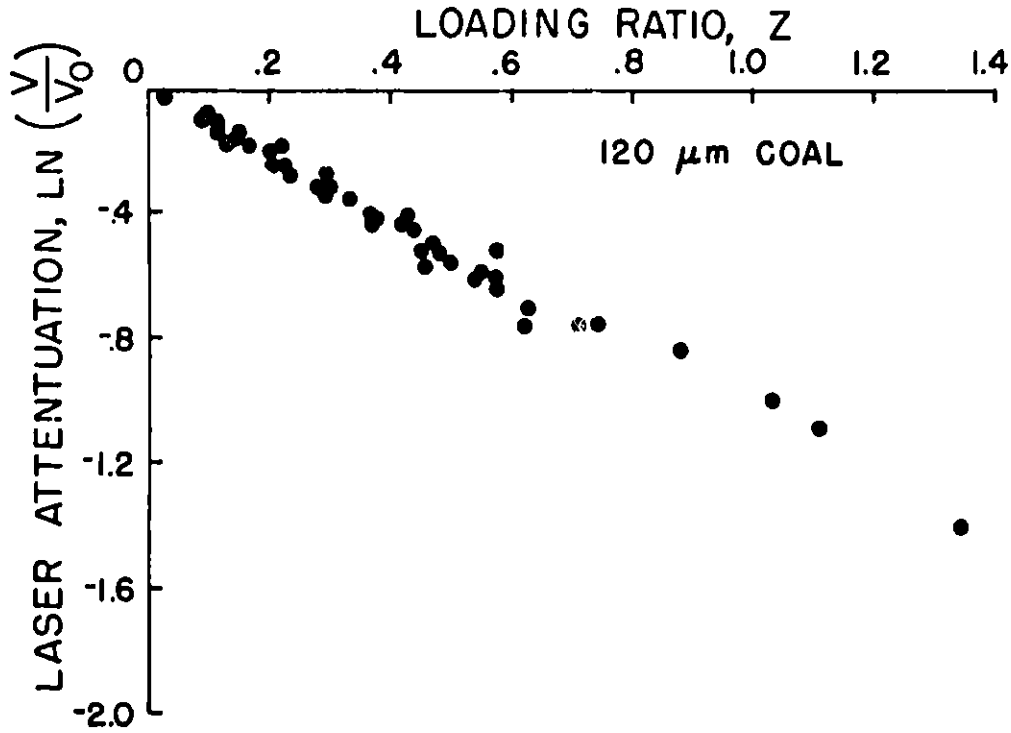

Figure 8. Laser attenuation versus loading ratio

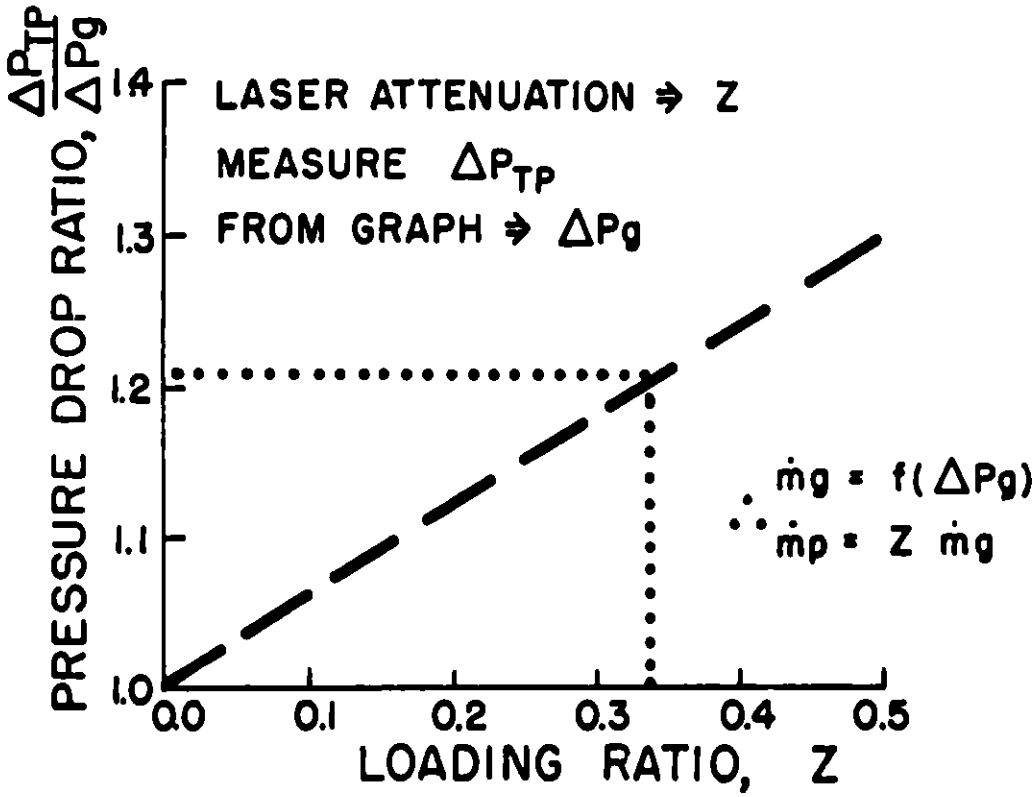

Figure 9. Pressure drop ratio versus loading

CONCLUSIONS

This experimental study has yielded the following conclusions:

1) Decreasing inlet angle on a venturi increases sensitivity at large Stokes number.

2) Non spherical particles increase sensitivity.

3) Pressure recovery is a function of loading.

4) Light attenuation can be used to determine loading.

ACKNOWLEDGEMENT

The authors acknowledge the support of DOE Grant DE-FG22-BDPC30212 and NSF Grant CPE-7925077. The authors also acknowledge the assistance of Professor D.E. Stock and Tommy Hellesto of the Mechanical Engineering Shops.

REFERENCES

1. Lee, J., "Scaling Laws for Metering the Flows of Gas-Particles Suspensions Through Venturis," Ph.D. thesis, Washington State University, 1980.

2. Payne, A.L., and Crowe, C.T., "Metering the Mass Flow of Gas-Solids Mixtures in Non-Standard Venturi Configurations," The Proceedings of the 1980 Symposium on Instrumentation and Control for Fossil Energy Processing, June 9-11, 1980, pp. 557-564.

3. Fenton, D.L. and Stokel, J.J., "Measurement of the Local Particle Concentration in Fully Turbulent Duct Flow," Int. J. Multiphase Flow, 1976, Vol. 3, pp. 141-145.

4. Sharma, M.P., "Numerical and Experimental Study of Gas-Particle Flows in Orifices and Venturis: Application to Flow Meter Design," Ph.D. thesis, Washington State University, 1977.

THE SONIC DOPPLER FLOWMETER

H. B. Karplus and A. C. Raptis
Argonne National Laboratory

D. Canfield
Pittsburg and Midway Coal Mining Company

ABSTRACT

An ultrasonic Doppler flowmeter has been successfully operated in a slurry feed line of the Solvent Refined Coal Pilot Plant at Fort Lewis, WA. The device is constructed such that all temperature-sensitive components are separated from a hot erosive environment by 1-ft long waveguides with only ultrasonic energy penetrating the pipe wall. The flowmeter was designed to indicate flow under turbulent and laminar flow conditions. Laminar flow conditions prevail in the SRC slurry feed lines. To measure both types of flow, a novel signal processor was needed because the Doppler spectrum in the laminar flow is flat with a sharp high-frequency cutoff. This cutoff is related to flow. It is measured automatically with a servo-controlled variable filter. Work is continuing on application of this technique to other coal slurry lines as needed for process definition and control. The information obtained in these applications will also be used to develop flowmeter designs suited to the larger lines on demo plants.

INTRODUCTION

Coal-processing pilot plants require a measurement of coal-slurry flow for control purposes and for accurate process development information for demo-plant design. Difficulties with available flow measuring schemes led to consideration of ultrasonic Doppler flowmeters. The most attractive feature of this technique is the placement of flowmeter transducers and other components entirely outside the pipe carrying the slurry, with only ultrasonic energy penetrating the pipe wall. This paper details the development and preliminary tests of such a Doppler flowmeter.

The Doppler technique is based on the measurement of the change of frequency of ultrasonic radiation scattered from the moving particles. The frequency shift, Δf, is proportional to the operating frequency, f, and the ratio of the vector component of motion velocity, $v \cos \theta$, in the direction of the ultrasound propagation velocity, c:

$$\Delta f = 2 f_o (v/c) \cos \theta.$$

The use of ultrasonic waves is attractive because of the relatively low propagation velocity and the ability to penetrate solid pipes and opaque slurries. To measure flow, ultrasonic waves are transmitted into the fluid, and scattered sonic radiation from the coal particles is detected and the frequency shift measured.

Commercial Doppler flowmeters have not been successful for measuring

flow velocity in hot coal slurries. This failure is due to the fact that transducers cannot accommodate the high temperatures encountered, and the flow of the fluid is laminar, which leads to a very broad Doppler spectrum instead of the narrow spectrum encountered with turbulent flow. Special techniques to overcome both these barriers will be described and illustrated by results obtained on the high-pressure slurry feed line[1,2] at the SRC-II Pilot Plant, Fort Lewis, WA.

HIGH TEMPERATURES

In the flowmeter at the SRC-II pilot plant, the ultrasonic energy was injected into the hot slurry through standoff waveguides[2], 300-mm (1-ft) long to keep the transducers cool. Conversion to shear waves in the waveguides,[3] using conventional plastic wedges, yields more favorable sound intensity and propagation direction in the fluid. In the configuration of Fig. 1a, the direction of propagation is determined in the pipe wall by the free surface reflector shown. This has the advantage of eliminating the uncertainty of refraction of sound waves in a temperature gradient as in Fig. 1b or 1c. Waveguides of the configuration 1a were brazed to the pipe and conventional transducers sold for nondestructive testing purposes were bolted to the remote end with their standard commercial mode conversion plastic wedges.

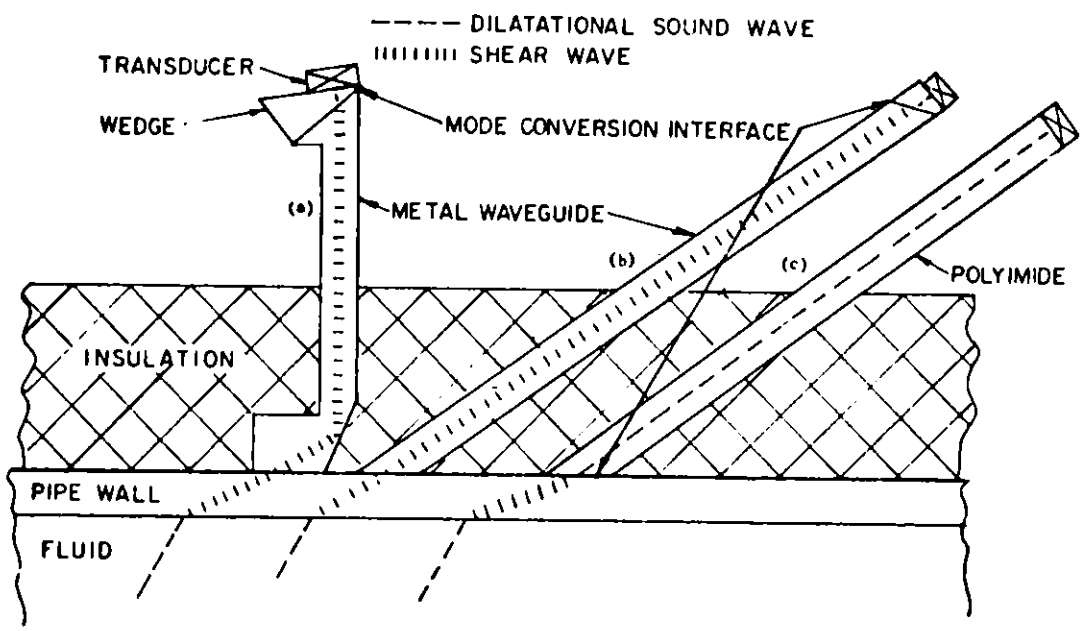

Fig. 1 Three forms of thermally isolating waveguides.

FLOW PROFILE EFFECTS

Fluid does not flow in a pipe at a uniform velocity, but rather the fluid near the wall flows slower than in the middle. In slowly flowing viscous fluids-- Reynolds number < 2300-- the fluid travels in lines parallel to the pipe axis. Flow velocity vs distance from the center is parabolic. The quantity of fluid in any velocity interval is the same as in any other velocity interval including the maximum velocity in the center; the average velocity of the fluid is one-half the maximum velocity.

High flow velocity (R_e > 3500) leads to turbulence with a much steeper velocity gradient near the wall and a more uniform velocity over the central region of the pipe. The resulting time-averaged velocity distributions for turbulent and laminar flow are shown schematically in Fig. 2. Turbulent flow yields a narrower range of fluid velocities, even though each point in the flow stream undergoes wider fluctuations.

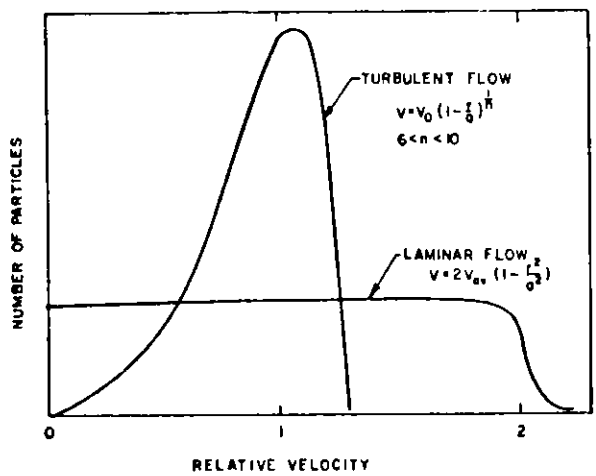

Fig. 2 Velocity of particles normalized to mean velocity vs number of particles.

The Doppler spectrum observed in the laboratory on an experimental water-coal slurry showed characteristics very similar to turbulent flow conditions (Fig. 3). A signal with such a narrow spectrum looks in the time domain like a tone of varying amplitude. Simple counting, as though it were a pure tone, yielded repeatable results consistent with the predicted Doppler shift of an idealized fluid of uniform particles flow rate.

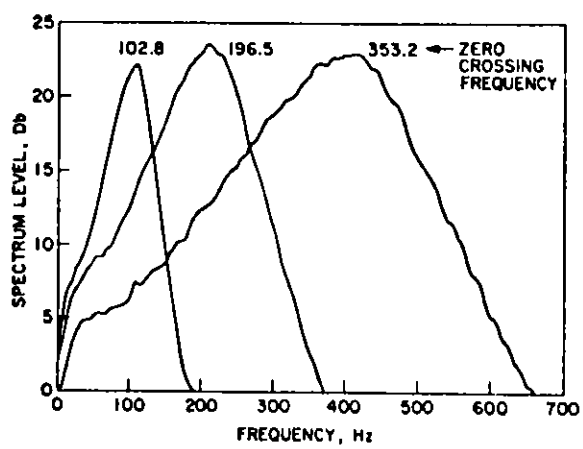

Fig. 3 Doppler-shift signal spectrum for turbulent flow and various velocities at the Laboratory loop.

This flowmeter was subsequently installed on the slurry pressure feed. The flowmeter behaved erratically. To explain the difficulty the spectrum of the Doppler signal was analyzed. These spectra show the flat characteristics of the laminar flow condition (Fig. 4). In addition, an intense low-frequency component was noted occasionally. Limited independent data on viscosity yielded a Reynolds number of about 100 corroborating the laminar flow hypothesized from spectrum observations.

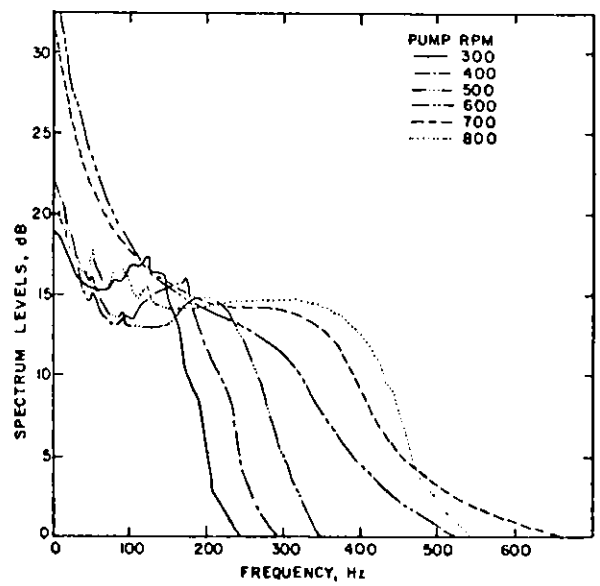

Fig. 4 Doppler-shift signal spectrum for laminar flow and various pump speeds at SRC-II.

THE MEASURING CIRCUIT

In subsequent tests, the simple counting technique was replaced by a measurement of the corner frequency of the spectrum. This corner frequency is theoretically twice the Doppler frequency produced by the average velocity. A servo-mechanism was designed to measure this corner frequency. A description of the resultant circuit is as follows: the occasional intense low-frequncy component of the spectrum is first removed with a high-pass filter, cutoff frequency, f_e. The output is then examined with a low-pass filter with a servo-adjusted cutoff frequency, f_f. The power (or voltage squared) content of a broad-band spectrum signal is proportional to its bandwidth. The output Doppler spectrum, $f_e - f_s$, is compared (Fig. 5) with the low-pass filtered portion of it, $f_e - f_f$. The low-pass filter is adjusted automatically to keep the ratio f_s/f_f constant. Thus, knowing the cutoff, f_f, the spectrum corner, f_s, and hence flow rate, can be evaluated. The circuit to accomplish this is shown in Fig. 6.

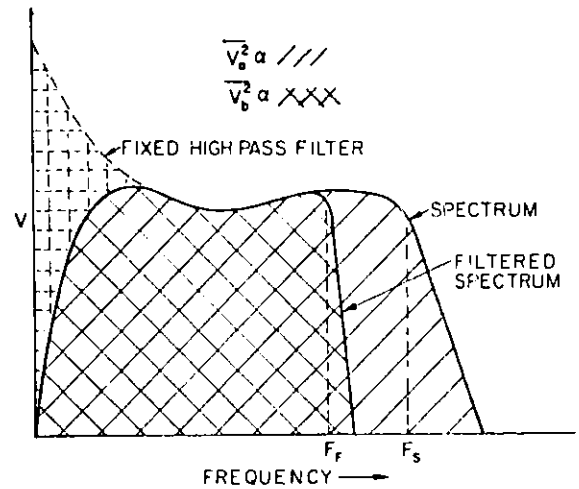

Fig. 5 To determine f_s vary f_f to keep V_b/V_a constant.

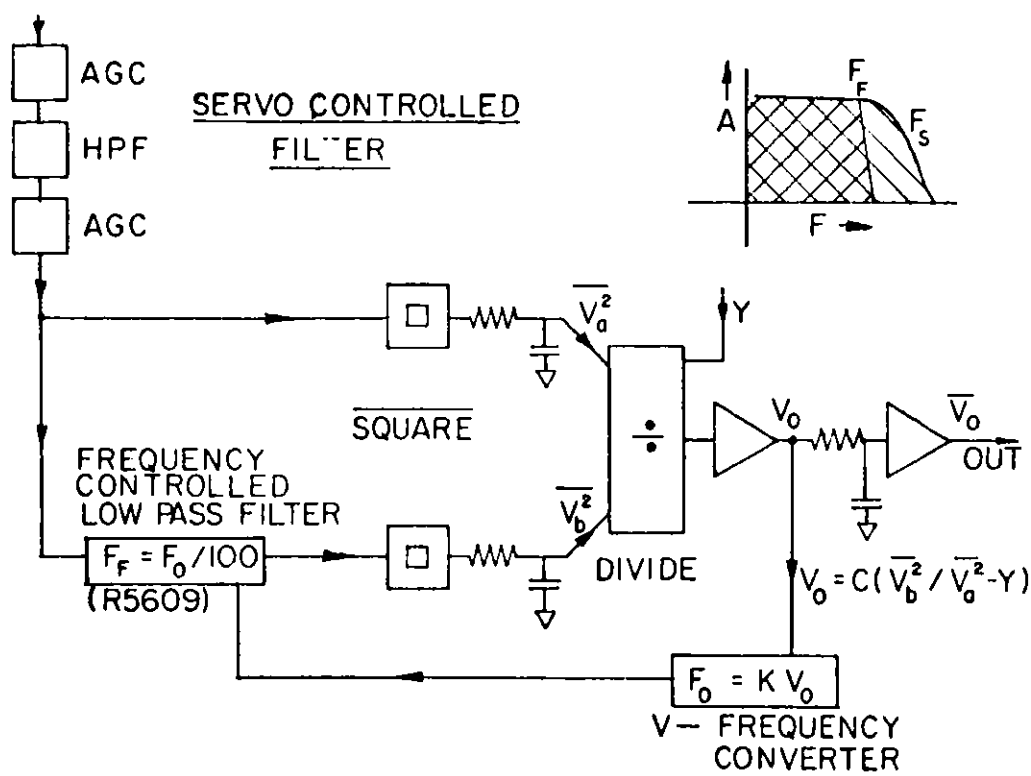

Fig. 6 Servo-controlled filter.

The averaged squared output voltage $\overline{V_a^2}$, and the averaged squared filtered output voltage $\overline{V_b^2}$, are fed to an analog divider, Model AD535. A fixed constant, K, is then subtracted from the ratio of the two voltages and the small difference is amplified to yield the voltage V_o. This voltage is converted by using a precision voltage-to-frequency converter, UAF32, to an oscillatory signal with frequency f_o, which is precisely proportional to V_o. This signal is used to operate the variable low-pass filter R5609 which has a sharp cutoff $f_f = f_o/100$.

Hence flow rate q:

$$= k_1 v_s = k_2 f_s = K k_2 f_f = K k_2 f_o/100 = K k_2 k_3 V_o = k V_o.$$

A residual nonlinearity is introduced by the finite feedback amplifier gain, but this can be kept to a fraction of 1% of full scale without violating stability requirements. This scheme of determining the high-frequency cutoff of the spectrum works equally well for any other spectrum shape, and has been demonstrated on the laboratory turbulent system. The calibration factor was different, because the ratio of the highest particle velocity to the mean flow velocity was not the same for turbulent and laminar conditions. However, by changing the fraction of the spectrum filtered by the adjustable filter, we could eliminate this difference if desired.

EXPERIMENTAL RESULTS

The described technique worked very well after solving another problem, which produced intermittent erratic behavior. It was found that the injection of minute quantities of hydrogen from a snubber, located in the line after the slurry charge pump produced very intense scattered signals about 100 times as intense as the signals from the slurry particles. The signal observed with this presence of high gas concentration showed a simple down-sloping spectrum, which was independent of flow rate. The scrubber was supplied with gas intermittently. During the brief periods when gas spilled into the line the Doppler meter readings were ignored. Automatic snubber level controls, eliminating gas spills may be designed.

The final calibration curve is shown in Fig. 7. Subsequent data from later runs exhibited more scatter, possibly related to changes in fluid properties. In particular, the variation of viscosity with shear rate may lead to changes in flow profile with resultant changes in the ratio of peak to mean velocity. This question is subject to future investigations.

CONCLUSIONS and RECOMMENDATIONS

After initially mysterious differences between laboratory and field observations were understood and overcome, a flowmeter was constructed, demonstrated, calibrated, and tested on the pressure-feed slurry line of the SRC-II Pilot Plant, Fort Lewis, WA. The chief feature of the flowmeter is the ability to measure hot erosive slurry flow with potentially excellent service life. Work is continuing to adapt the laboratory circuits and transducers to the processing plant environment using long-lived industrial components. High-temperature transducers obviating waveguides should also be investigated to permit the study of alternate pulsed operation.

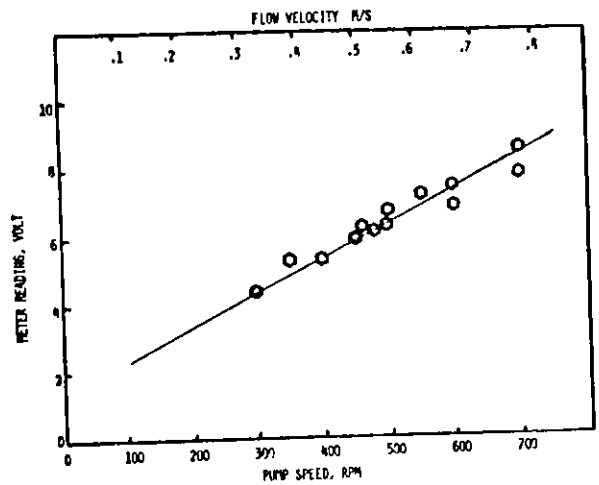

Fig. 7 Calibration of the flowmeter output vs pump speed for the test shown.

Additional investigations are needed to determine the ultrasonic scattering and attenuation in the slurry as a function of particle size, particle concentration,[5] and carrier fluid properties. This information is needed to scale-up designs of Doppler flowmeters for larger pipes as projected for demonstration plants.

ACKNOWLEDGMENTS

We would like to thank T. K. Lau, S. Lee and T. Simpson of DOE, R. S. Zeno, G. S. Rosenberg, T. P. Mulcahey, J. P. Bobis, G. A. Forster, and N. M. O'Fallon, all from ANL, for their support and encouragement in this work. We would also like to thank SRC-II personnel, especially Andy Danhoff and Ed King of P&M for their help and cooperation. And special thanks are due to Marty Miskevics and Tim Bernovich for their work on the electronics package, Howard Eisenbrandt for preparation of drawings and Nancy Heeg for the typing of this manuscript.

REFERENCES

1. A. C. Raptis, H. B. Karplus, and W. W. Managan, "Acoustic Doppler Flowmeter for Dense Slurry Flow Measurement, Part I-Design," Fossil Energy I&C Briefs, Vol. 1, No. 1 (Mar 1980).

2. H. B. Karplus and A. C. Raptis, "Slurry Flow Measurements Using An Acoustic Doppler Flowmeter," The Proceedings of the 1979 Symposium on Instrumentation and Control for Fossil Energy Processes, pp. 195-209, CONF-790855 (1979).

3. L. C. Lynnworth, "Fluid Flowmeter," U.S. Patent 3,575,050 (Apr 1971).

4. H. B. Karplus, A. C. Raptis, and D. R. Canfield, "Development and Testing of High-Temperature Acoustic Doppler Flowmeter," Argonne National Laboratory, ANL-FE-49609-TM01 (Feb 1981).

5. A. C. Raptis et al., "Measurements of Noise Background and Attenuation in Coal-Toluene Slurries," 1978 Ultrasonics Symposium Proceedings, IEEE Cat. #78CH1344-1SU.

MICROWAVE COAL-WATER SLURRY MONITOR

Ira B. Goldberg, William W. Ho and Kwang E. Chung
Rockwell International Science Center
Thousand Oaks, California 91360

Lowell R. McCoy
Energy Systems Group, Rockwell International Corp.
Canoga Park, California 91304

Ross I. Wagner
Rocketdyne Division, Rockwell International Corp.
Canoga Park, California 91304

INTRODUCTION

Advanced processes for the conversion of fossil fuels have created a need for new measurement and control methods which are beyond the present state-of-the-art. One specific need is the development of a practical method for the measurement of coal slurry flow rate and composition of solid-gas and solid-liquid systems (1). Because of the specific nature of slurry mixtures, most conventional measurement techniques are not applicable (2).

Microwave techniques offer an attractive method for flow velocity and composition measurement by using the cylindrical slurry pipe as a circular waveguide section. Microwaves fill the pipe section and thus provide an average composition over the instrumented volume. Although the microwaves cannot penetrate the metal pipe, antennae for transmission and reception can be recessed such that they are out of the flow stream. The minimum frequency for microwave propagation is related to the dielectric constant of the medium filling the pipe; this dielectric constant is in turn related to the composition of the aqueous slurry.

A microwave apparatus was constructed in order to measure concentration and flow velocity of coal-water slurries in 3/4 in. and 1-1/2 in. pipes with slurries of 40% to 65% coal. The results show that microwave techniques have the following advantages for measuring composition:

Precision to ±0.2% is obtainable.
Results are independent of flow rate and flow direction.
Temperature dependence is predictable.
Results are negligibly dependent on coal type.
Apparatus is non-intrusive.
Continuous measurement (< 0.1 s response time) is practical.

Cross correlation of two independent signals was used to determine flow velocities. Precision of better than ±2% could be obtained.

THEORY

Microwaves are able to propagate in cylindrical waveguide (pipes) in a variety of different modes. The lowest frequency is the TE_{11} mode, followed by the TM_{01}, TE_{21}, and TE_{01}. This mode designation is related to the magnetic and electric vectors of the microwaves in the pipe (3) and need not be discussed in detail here. Associated with each mode of propagation, is a cut-off wavelength, λ_c, given by

$$\lambda_c = 2\pi R/k(M) \qquad (1)$$

where R is the tube radius, and k(M) is 1.841, 2.405, 3.054, 3.832, respectively for the TE_{11}, TM_{01}, TE_{21}, and TE_{01} microwave modes. The cut-off frequency, ν_c, is related to λ_c by $\nu_c = c/\lambda_c$, where c is the speed of light.

The apparent wavelength of the microwaves in the waveguide, λ_g, is given by

$$\lambda_g^2 = \frac{\lambda_o^2 \lambda_c^2}{\lambda_c^2 \varepsilon - \lambda_o^2} \quad , \qquad (2)$$

where λ_o is the free space wavelength, and ε is the dielectric constant of the slurry. For standing waves, the significance of λ_g is that this determines positions along the waveguide where there is maximum or minimum magnetic field. For example, maxima occur at distances of 0, $\lambda_g/2$, λ_g, ... from the transmitter. When $\lambda_o = \sqrt{\varepsilon}\ \lambda_c$, $\lambda_g \to \infty$, so that there is no propagation in the pipe.

The separation between detector and receiver in the pipe was determined from the attenuation, which is given by

$$\frac{P}{P_o} = \exp(-\alpha x) \quad . \qquad (3)$$

The attenuation coefficient, α, is given by (3)

$$\alpha = 15.33\ (\tan \delta)/\lambda_g \quad . \qquad (4)$$

A value of $\tan \delta$ (loss tangent) = 0.24 which corresponds to 0.5 M salt solution at 1.43 GHz and 25 C (4) was used to represent the maximum power loss of the slurry. At a distance of 0.5 λ_g, the power in the pipe, P, is reduced to 16% of the incident power, P_o, while at 1.5 λ_g it is reduced to 0.4%.

Measurements of the dielectric constants of coal-water slurries gave values of 21 for 65% and 44 for 40% coal water slurries (5). Based on the estimated values of α and ε, receiver transmitter antenna separations, x, of 3.57 cm and 7.14 cm were selected respectively for the 3/4 in. and 1-1/2 in. pipe. The frequency at the maximum power into the receiver can be determined from Eq. (2) by substituting $\nu_o = c/\lambda_o$, and realizing that $x = \lambda_g/2$, to give

$$\nu_o = \frac{c}{\lambda_g \lambda_c \sqrt{\varepsilon}} (\lambda_c^2 + \lambda_g^2)^{1/2} = \frac{c}{2x\lambda_c \sqrt{\varepsilon}} (\lambda_c^2 + 4x^2)^{1/2} \qquad (5)$$

Since the frequency is determined by ε, and ε is dependent on the slurry composition, ν_o provides a measure of the coal contant.

EXPERIMENTAL APPARATUS

A schematic drawing of a pipe section containing microwave antenna and the associated detector electronics is shown in Fig. 1. For velocity measurements, two independent microwave systems separated by 3 times the receiver-transmitter distances were used.

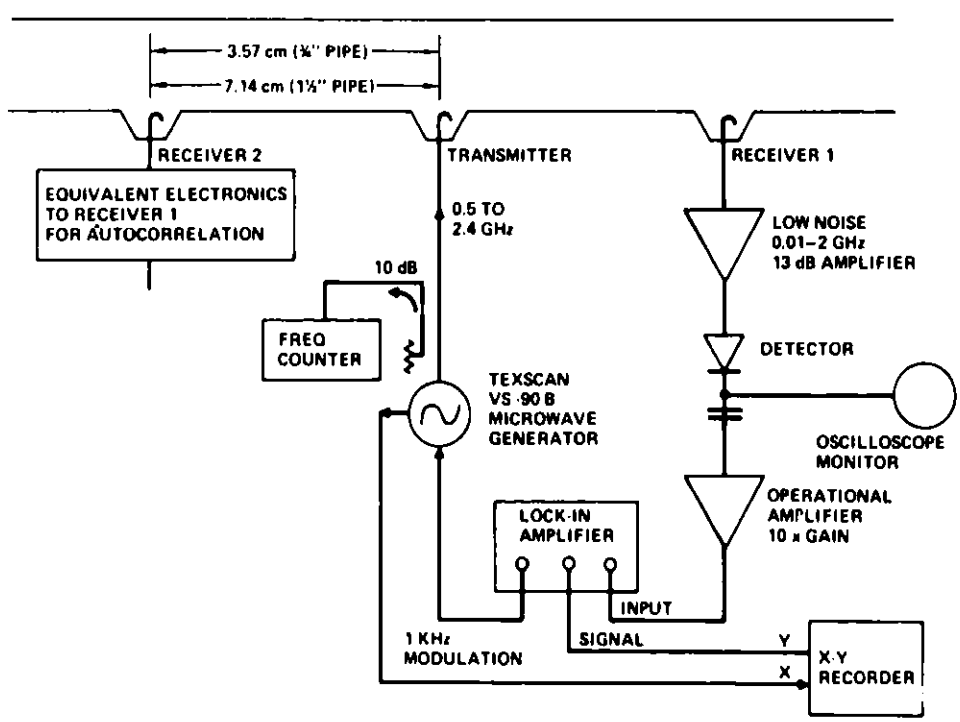

Fig. 1 Microwave coal slurry monitor and the associated electronics.

The microwave power was transmitted and received from the slurry via a coupling loop recessed into a fitting placed on the pipe. Microwave sweep generators which provide constant 20 mW power up to 2.45 GHz were modified to permit up to 1 kHz amplitude or frequency modulation of the source either

while set to a constant frequency or being swept by its internal controls. A variety of antenna which coupled the transmitter or detector to the waveguide were tested. While we found that coupling loops gave the best results, optimization is a matter of trial-and-error. Microwave amplifiers were used to increase the signal from the receiver antenna. The signals after the detector, were fed into a lock-in amplifier so that a low noise DC signal can be obtained.

In order to test the microwave apparatus, the recirculating flow system shown in Fig. 2 was constructed. The pump used was a progressing cavity pump. Tests were carried out using a flow rate of 1.5 l/s which permits linear flow velocities up to 385 cm/s through the 3/4 in. pipe and up to 96.3 cm/s through the 1-1/2 in. pipe, and 5.1 l/s which permits linear flow velocities up to 330 cm/s through the 1-1/2 in. pipe. The pipe in the flow system was made of copper for optimal microwave properties.

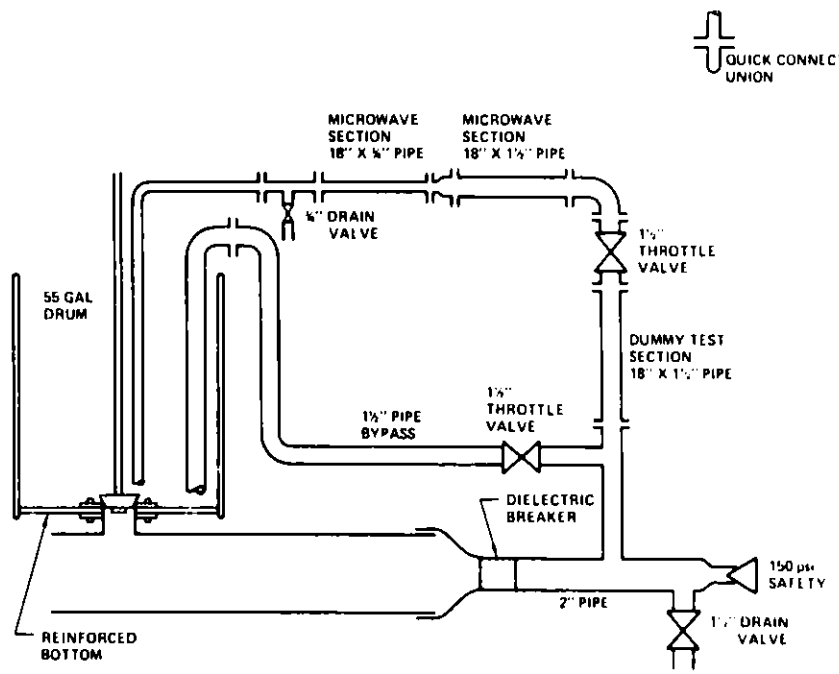

Fig. 2 Recirculating flow system for coal-water slurries.

COAL WATER SLURRIES

Composition Measurements - Preliminary measurements of the microwave performance of the instrumented 45 cm long pipe sections were carried out using static, homogeneous solutions of acetone and water. Typical signals that were obtained are shown in Fig. 3. The power from the receiver, shown in the lower curve, was obtained by using amplitude modulation. The derivative of the power with respect to frequency, shown in the upper curve, was obtained by using frequency modulation. Of the two points, A and B shown, the frequency of B is closer to the value predicted by Eq. (5). The actual value for the frequency is slightly smaller due to the volume of the antenna housings.

A series of measurements was carried out in order to determine the dependence of this characteristic frequency on the composition of the coal-water slurry. The frequency at the zero crossing of the derivative curve (Fig. 3) was used. The data for both 3/4 in. and 1-1/2 in. pipe, shown in Fig. 4, gave extremely good correlation with the coal composition. The scatter of data about the best line through the experimental points is within ±0.2% (absolute) of the composition. The factor which limits the accuracy of these measurements was our inability to more accurately measure the water in the coal.

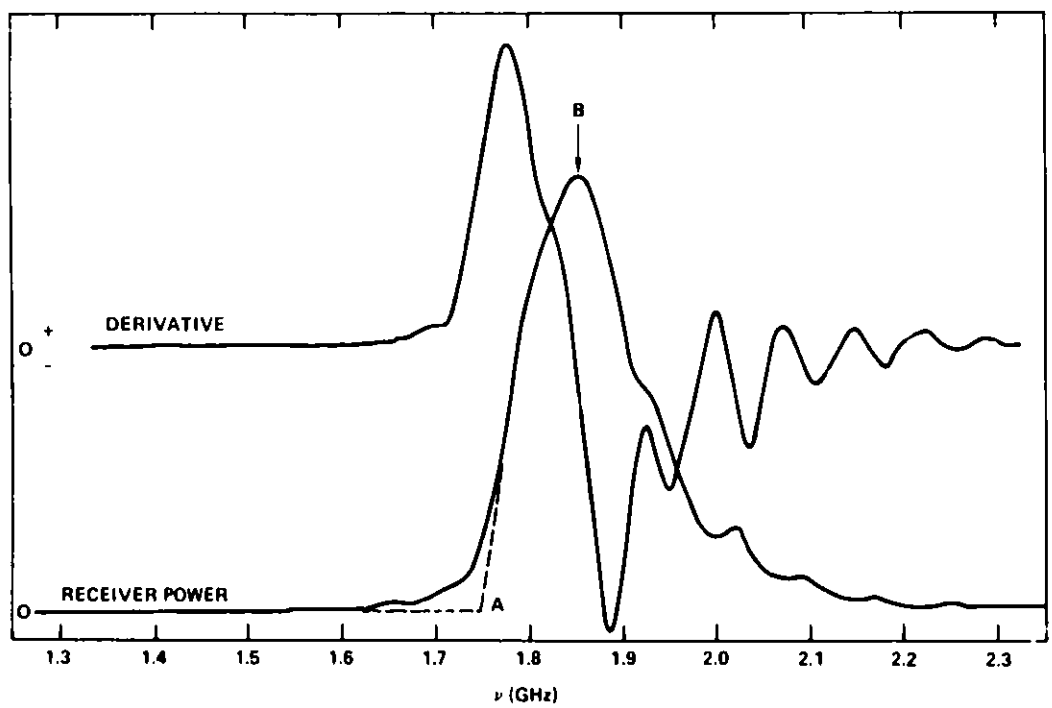

Fig. 3 Signal from the receiver antenna and the derivative of the signal with respect to frequency as a function of frequency for the 3/4 in. pipe test section containing 99.5% acetone.

The data show that the TE_{11} mode of propagation in the 1-1/2 in. waveguide gives a very weak signal. Based on the frequencies, it appears that the TE_{11} mode is detected in the 3/4 in. pipe, whereas more power is received in the TE_{21} mode for the 1-1/2 in. pipe.

The principal effect of temperature in this system is that it will influence the dielectric constant of the liquid portion since the dielectric constant of water exhibits a large temperature dependence. Measurements have

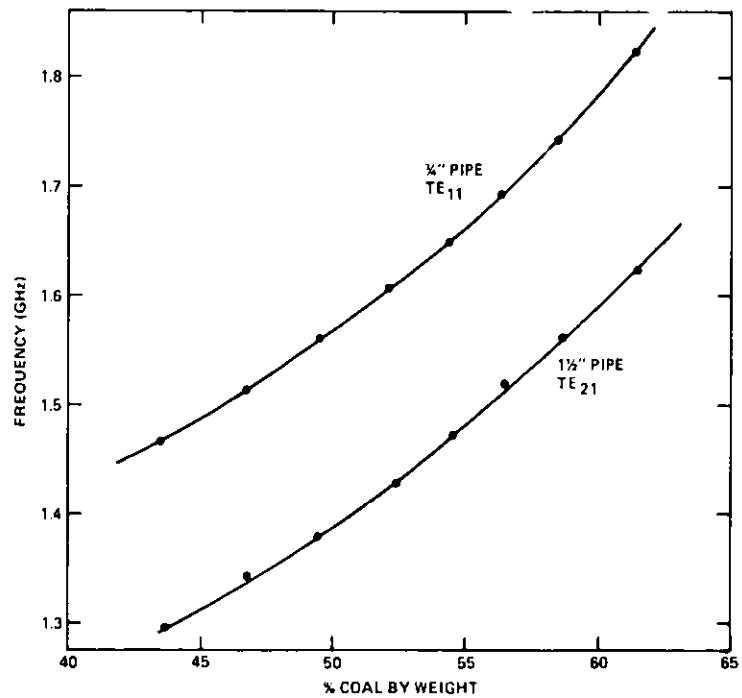

Fig. 4 Measured frequency of the slurry monitor on the weight percent of coal in the slurry for 3/4 in. and 1-1/2 in. pipes.

shown that the dielectric constant of dry coal is only slightly temperature dependent (6). Thus we expect that as the slurry becomes more dilute in coal, the effect of temperature would be more significant. The temperature dependence of the characteristic frequency was measured between 25° and 52°C, as shown in Fig. 5. The static (low frequency) dielectric constant of water decreases by about 12% between 25° and 50°C. This would be expected to cause an increase in the frequency of less than 6% (note that $\nu \propto \varepsilon^{-1/2}$). However, we observe a change of only 1-2% over this region. This small value may be due in part to the fact that a significant fraction of the water may be associated with the coal, as well as the fact that the coal contributes to the average dielectric constant. These results indicate that the temperature dependence is a small, but significant parameter in the measurement of the slurry composition. It would present no problem to compensate for this temperature dependence.

In principle, the flow rate of the slurry should not affect the results of the microwave measurements. Tests were carried out using slurry concentrations from 46 to 62% at flow rates from 23 cm/s to 370 cm/s in the 3/4 in. pipe, and from 6 cm/s to 330 cm/s in the 1-1/2 in. pipe. In the

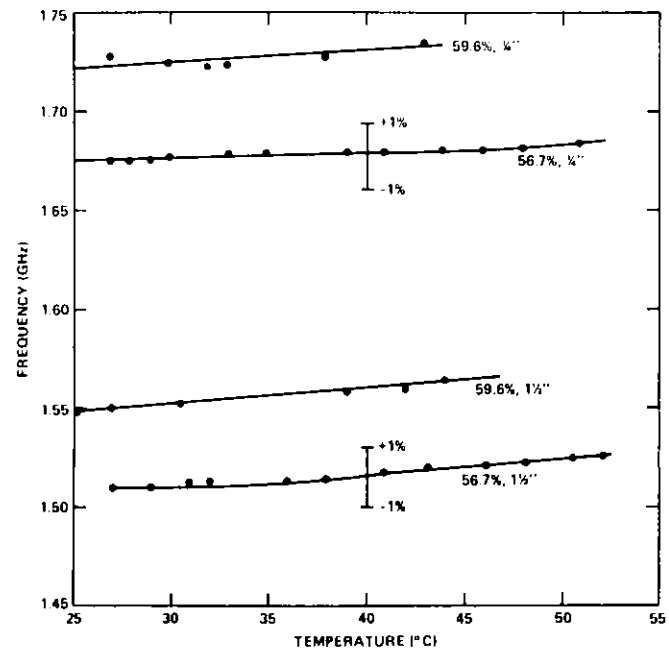

Fig. 5 Temperature dependence of the measured frequency of the coal water slurry. Bars on the graph indicate the expected frequency change for a +1% or -1% change of coal composition at 40°C.

worst cases, the scatter of data points is within 0.2% in terms of the concentration. However, the largest source of scatter of the data appeared to be due to temperature fluctuations, particularly when very high flow rates were used. One set of data was recorded with the microwave test section in vertical and horizontal positions. No difference was observed in either position. We do not expect significant differences between the vertical and horizontal positions as long as the flow is fast enough to maintain a uniform slurry. If the flow is stopped, the frequency measured in the vertical pipe drifts slowly due to settling of the suspended particles.

Flow Velocity Measurements by Cross Correlation - Cross correlation of signals from two detectors has been used to determine the linear flow rate of multi-phase systems (7). Conceptually, the method is as follows: In heterogeneous flowing systems, there are local variations of the composition. This results in fluctuations of the characteristic microwave frequency. A lock-in amplifier was used to follow the frequency changes in which the frequency variations are converted to a voltage. By using two detectors, it is possible to monitor the fluctuations at two different points along the pipe. This permits a maximum signal at the upstream detector to be related to

the same signal at a downstream detector at a later time, τ, and this time difference is directly related to the velocity of the slurry.

The cross correlation function, $C_{1,2}(\tau)$ for upstream signal $S_1(t)$ and downstream signal $S_2(t)$, is given by

$$C_{1,2}(\tau) = \int_0^t S_1(t)S_2(t \pm \tau)dt \quad . \tag{6}$$

This represents shifting signal S_2 forward or backward by time τ, so that the maximum overlap of the two signals can be determined. Measurements were carried out by recording the time dependence of both signals on a data acquisition system. These two signals were then cross-correlated by the digitized form of the correlation function,

$$C_{1,2}(m) = \sum_{n=0}^{N/2} S_1(n)S_2(n + m) \tag{7}$$

where N is the number of points in the array, and $m \leq N/2$. In this case, the appropriate correlation time, τ, corresponds to the maximum of $C_{1,2}(m)$, where τ is equal to $m\delta t$, in which δt is the time between data points. Oscilloscope measurements of the time dependent signal show a correspondence between the signal and flow rate. At slow flows, the root-mean-square amplitude appears directly related to the flow rate. When the flow is stopped, the signal drops to a constant value. This permits an indication of the no-flow condition such as that in a plugged line.

The signal from two slurry monitoring channels is shown in Fig. 6. By comparison of the upstream and downstream monitors, features of the upstream channel can be related to features that appear at a slightly later time on the downstream channel. The linear flow velocity determined from cross correlation data, v_c, was calculated by dividing the distance between zones of detection, z, by the correlation time,

$$v_c = z/\tau \tag{8}$$

The linear flow velocity based on mass flow, v_m, was calculated by Eq. (9),

$$v_m = m/\pi r^2\bar{\rho} \tag{9}$$

where m is the mass flow, r is the pipe radius, and $\bar{\rho}$'s the slurry density.

Results of the measurements on 53% coal slurry are shown in Fig. 7. The linear mass flow velocity, v_m, of the slurry is shown on the horizontal axes, and the correlation velocity, v_c, is shown on the vertical axes. Since the cross-sectional area of the 1-1/2 in. pipe is exactly four times that of the 3/4 in. pipe, the scale for the 1-1/2 in. pipe is expanded by a factor of four, so that a point on the plot corresponds to the same volumetric flow through either pipe. In nearly all cases $v_c \sim 1.4\ v_m$ for both 1-1/2 in. and 3/4 in. for all coal compositions tested. It appears that this is a manifestation of the fundamental properties of the two-phase flow (8).

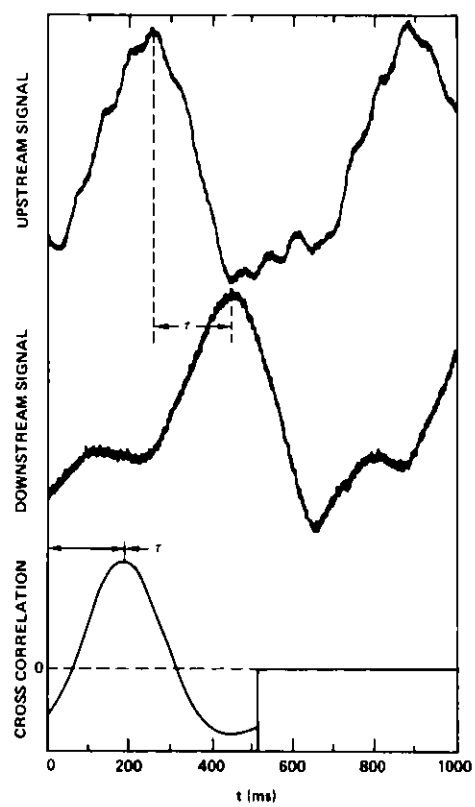

Fig. 6 Signals from upstream and downstream concentration detectors in 3/4 in. pipe, and the cross correlation of the first half of the upstream signal with the downstream signal.

CONCLUSIONS

Preliminary results indicate that microwaves can be used to accurately monitor coal concentration and flow velocity in slurry pipes. Details of this work can be found in Ref. 9.

ACKNOWLEDGMENTS

This work was partially supported by the Electric Power Research Institute under contract RP1654-2. We acknowledge the helpful discussions with Neal Richter of the Texaco Montebello Research Laboratory.

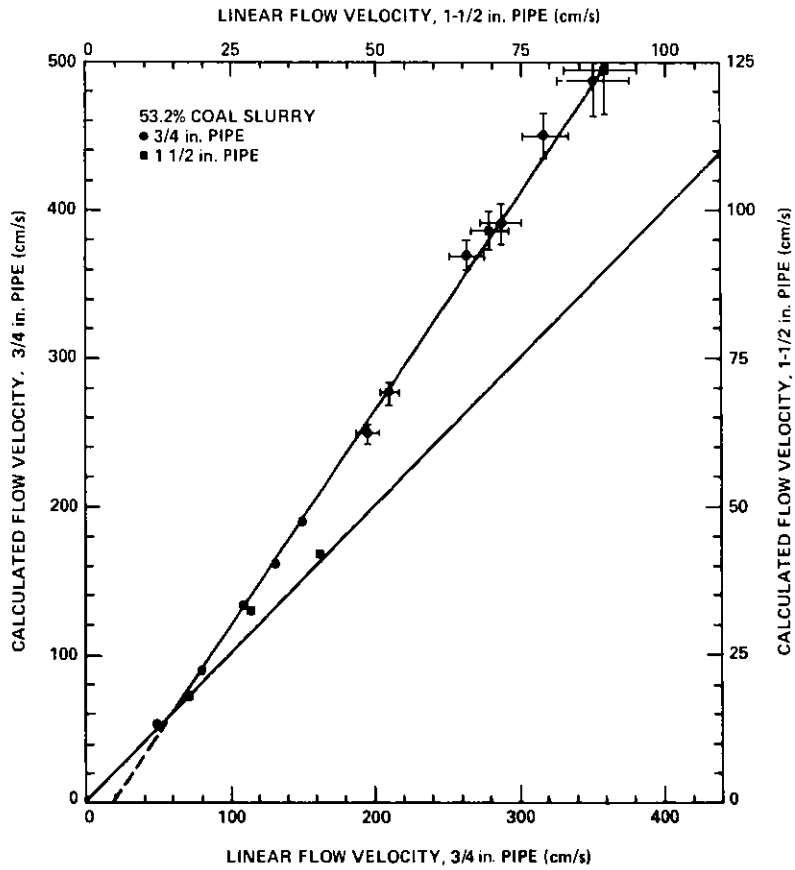

Fig. 7 Measured linear flow velocity for 53.2% coal slurry based on mass flow vs linear flow velocity calculated from correlation time. Ideal agreement shown by dark solid line.

REFERENCES

1. A. Mark, "Instrumentation and Controls for Fossil Energy Processes, Requirements," I and II, Jet Propulsion Laboratory, report 5030-437; Rev. A, December 15, 1980.
2. N.M. O'Fallon and R.W. Doering, "Review of Instrumentation Needs for Process Control and Safety in Advanced Fossil Energy Processes," Argonne National Laboratory report ANL-FE-49628-TM02.
3. S. Ramo, J.R. Whinnery and T. van Duzer, Fields and Waves in Communications, John Wiley, N.Y. Chapter 8, 1967.
4. W.W. Ho, A.W. Love and M.H. Van Melle, "Measurements of the Dielectric Properties of Sea Water at 1.43 GHz," NASA Reprt CR-2458, Dec. 1974.
5. I.B. Goldberg and K.E. Chung, Manuscript in preparation.
6. C.A. Balanis, J.L. Jeffrey and Y.K. Yoon, IEEE Trans. Geosci. Electronics. GE16, 316 (1978).
7. M.S. Beck, J. Phys. E. 14, 7 (1981) and references cited therein.
8. G.W. Govier and K. Aziz, The Flow of Complex Mixtures in Pipes, Van Nostrand Reinhold Co., New York, N.Y., 1972, Chapter 4.42.
9. I.B. Goldberg, W.W. Ho, K.E. Chung, L.R. McCoy and R.I. Wagner, Electric Power Research Institute Report, in press.

CHARACTERIZING MHD COAL COMBUSTOR PARTICLE FLUX WITH LASER VELOCIMETERS AND PARTICLE SIZING INTERFEROMETERS*

W. M. Farmer, J. O. Hornkohl, F. A. Schwartz,
D. Gonzalez, and T. V. Giel

The University of Tennessee Space Institute
Tullahoma, Tennessee 37388

ABSTRACT

The measurement of particle flux in high temperature coal combustors is of prime importance in combustor design improvements and in controlling combustion processes. Parameters affecting particle flux (mass concentration, size distribution, particle velocity, and the spatial distribution of the particle flux) are being characterized at the University of Tennessee Space Institute with a laser velocimeter and particle sizing interferometer. The laser velocimeter is capable of measuring two orthogonal components of velocity and utilizes microprocessor technology for instrumentation control and for producing near real time outputs of a wide variety including velocity distributions, flow angles, and power spectral densities. The particle sizing interferometer, which uses a similar optical system but processes the scattered light signals differently, measures a single component of velocity, particle size distribution, and the particle number density. These measurements are also available in near real time through the use of microprocessor technology. The purpose of this paper is to describe these instruments and their capabilities and discuss application examples where data appropriate to the characterization of fossil fuel combustion has been measured. The particle sizing interferometer application example results are compared to those obtained by mechanical means such as sieve analysis and found to be reasonably consistent.

TWO-COMPONENT LASER VELOCIMETER

The Gas Diagnostics and Energy Conversion Research Divisions at the University of Tennessee Space Institute (UTSI) have designed and constructed a laser velocimeter (LV) system which is based on the use of a two-component Bragg cell beam-splitter type laser velocimeter optical system. The laser velocimeter signal processor system was designed around a Z-80 microprocessor which is capable of near real time on-line data acquisition and reduction. The microprocessor controls the laser velocimeter signal processor and is equipped with software programs which allow the recording of various system parameters in addition to the measured data.

The optical configuration for the velocimeter is shown in Figure 1 and a photograph is shown in Figure 2. In this optical system, a TEM_{00} beam from a 2-watt Argon laser is passed through a double Bragg cell whose function is to simultaneously diffract and frequency shift 75% of the laser beam into three beams which are angularly separated from each other and the remaining 25% of the original beam.[1,2] This Bragg cell is a small water tank in which two quartz crystal transducers are mounted at right angles with respect to each other. Phase-locked-loop oscillators drive power amplifiers, which, in turn, drive the quartz transducers. The frequency of each phase locked loop is tunable in order that the transducers may be operated at maximum efficiency. The power of each power amplifier is variable and by controlling the power into the Bragg cell, and the cell orientation, four beams of equal

* Instrument fabrication was sponsored by the United States Department of Energy under Contract No. DE-AC02-79ET10815

intensity initiating at a common origin can be obtained. As shown in Figure 1, a lens set causes the four beams (only two of which are shown since the second pair are diffracted out of the plane of the paper) to focus at a common region in space (called the probe volume) which produces two orthogonal sets of moving planar interference fringes. Light scattered from these fringes by a moving particle is collected either in backscatter by Lens L1 or forward scatter by Lens L2 and directed to the photomultiplier tube (PMT). Noteworthy features of this approach are 1) both components of velocity can be detected with a single photomultiplier tube, and 2) the laser can be run in all colors for increased power density. Optical simplicity is thus obtained at the cost of increased electronic complexity. However, this trade off is desirable in most applications because it is easier to protect remote electronic components than adjacent optical components from the harsh environments encountered around MHD combustion systems.

Figure 3 shows the main components of the laser velocimeter system signal electronics including the Bragg cell electronics, burst counter signal processors, and the data acquisition electronics. As it is presently operated, one of the Bragg cell transducers is operated at a frequency near 15 MHz while the other one is operated near 45 MHz. The power spectrum of the photomultiplier tube signal produced by a particle at rest would show two strong spectral bands centered near 15 MHz and 45 MHz, and two weaker bands, centered near 30 MHz and 60 MHz. Motion of the particle will shift these spectral components of the signal away from their center frequencies. As long as the particle's velocity is not so large that two spectral components of the signal overlap, the signal frequencies can be electronically separated and the two strong signals processed individually.

Figure 3 shows how the two strong signal frequencies are separated, processed and recorded. The signal splitter divides the total signal amplitude into two equal parts, each of which is passed to a signal processing channel consisting of a doubly balanced mixer, phase-locked-loop local oscillator, low-pass filter, and burst-counter laser velocimeter signal processor. The signal channel responsible for processing signals produced by the 15 MHz Bragg transducer is called the 15 MHz channel while the other channel is called the 45 MHz channel. The local oscillator (LO) port of each mixer is driven by a phase-locked-loop (PLL) whose frequency is adjustable for each signal frequency which appears in the mixer's input (its radio frequency, or RF, port). The mixer's output (its intermediate frequency, or IF, port) contains both a sum and a difference of the IF and the LO frequencies but the mixer output is low-pass filtered to pass only the difference frequencies. In this way, the signal processors are not required to measure small deviations about the very high RF carrier frequencies thereby relaxing the burden on the precision and accuracy with which the signal frequencies have to be measured. This also greatly improves the signal/noise ratio of the input signal.

The signal frequency produced by a particle at rest, f_0, is the difference between the frequency of the local oscillator, f_{LO}, and the Bragg excitation frequency, f_B.

$$f_0 = f_{LO} - f_B \tag{1}$$

A component of velocity for a moving particle is determined from the difference of f_0 and the output frequency of the low-pass filter, f, as measured by the burst-counter laser velocimeter signal processor. (Actually, the burst processor measures 1/f, the signal period averaged over some integer number of periods). Component velocities are computed from the equation:

$$\underset{\sim}{V} = \delta(f_0 - f) \tag{2}$$

in which δ is the fringe period in the component direction (i.e. the distance between interference fringes). The magnitude of the velocity component is determined from the absolute value of $f_0 - f$ and the sign of the velocity component is determined from the sign of $f_0 - f$. A simultaneity checker rejects signal bursts that do not, at any point in time, simultaneously appear in both signal channels. Thus, the magnitudes and signs can be determined for two components of velocity, allowing determination of means, turbulence intensities, and velocity cross-correlation.[3]

An S-100 bus Z-80 computer controls essentially all system operating parameters. Notable exceptions are the photomultiplier tube high voltage, the laser power, frequencies of the four phase locked loop oscillators (two of which drive the double Bragg cell while the other two serve as local oscillators for the mixers), and the spatial position of the laser velocimeter probe volume.

Once the data has been acquired by the computer system, a number of data reduction algorithms are available for computing mean velocity and turbulent intensity either for a single velocity component or for a two-dimensional velocity vector. Additionally, to compute the power spectral density of the flow fluctuations an algorithm has been developed which is particularly suited to this type velocity system in that it takes velocity data which is acquired randomly in time and at an average data rate significantly less than required by the Nyquist sampling criteria. Under experimental conditions with controlled sources it has been determined that this algorithm is at least as good as those which have been used by much larger computer systems.[4]

PARTICLE SIZING INTERFEROMETER

The particle sizing interferometer (PSI) developed at UTSI utilizes a stationary beam-splitter rather than the Bragg cell type beam-splitter and measures only one component of velocity. In principle, the optical system functions in the same way that the standard fringe type laser velocimeter systems function. The theory necessary for understanding the particle size analyzer is described in numerous references available in the literature (see, for example, references 5-8). For instrument description purposes it is only necessary to understand that the signal processor measures the ratio of the sinusoidal amplitude of the signal generated by a particle passing through a fringe pattern and the mean amplitude of the signal. The ratio of these two amplitudes is called the signal visibility, V, and this ratio can be related to particle size when the shape of the particle can be assumed. For spherical particles, the visibility is related to the particle diameter (D) by the equation

$$V = \frac{2J_1(\pi D/\delta)}{\pi D/\delta} \qquad (3)$$

where J_1 is a first order Bessel function of the first kind. The visibility function in this case is monotonic when the particle diameter is roughly less than 1 fringe period and the minimum particle size which can be measured with the instrument is approximately 1/10 to 1/20 of the fringe period depending on the acceptable error or uncertainty in the measurements. For example, when the particle diameter is 0.1 δ then the measurement error in particle diameter, for 1% uncertainty in visibility, is approximately $\pm$ 30%. Figure 4 shows a schematic of a particle sizing interferometer typically used at UTSI. It can be adjusted to size particles from 0.3 to greater than 100 μm. Data reduction algorithms which are presently available for use with this instrument evaluate size distributions and the first four moments of that distribution from which other algorithms compute the arithmetic mean, the geometric

mean and geometric standard deviation, the volumetric mean diameter, the Sauter mean diameter, and the mass mean diameter. The mass extinction coefficient for the size distribution is computed when the variation of extinction efficiency as a function of particle diameter can be determined from Mie scattering theory. Additionally, number density is also estimated, and from these data mass concentration of the particle in terms of grams of particulate mass per unit volume of fluid is computed.

PSI APPLICATION EXAMPLES

To illustrate use of the PSI two examples are provided. These are, first, the measurement of coal dust being aerosolized by a fluidized bed, and second, the measurement of particles in a 2800°K combustor, flowing at 6 to 12 m/sec. at atmospheric pressure. In the first case, the coal dust to be measured was blown through the PSI sample volume after it had first been measured by a set of sieves. The sieving showed that the mass mean diameter of this dust was approximately 45 microns. The PSI measured distribution also showed that the coal dust had a mass mean diameter of approximately 45 microns. An example of one such distribution is shown in Figure 5. However, the PSI measurements also indicated very large numbers of small particles with diameters less than 5 microns but which contributed little to the mass distribution. Microscopic examination of these particles revealed that the coal dust did indeed have such particles and that they tended to agglomerate, presumably by electrostatic attraction. In the second example, which is discussed in detail elsewhere[9], the PSI was focused inside a 1 ft. diameter combustion chamber into which powdered coke was introduced. In this case, as the combustor was slowly brought up to temperature, the PSI showed that the particles underwent a very pronounced change in size distribution. Figure 6 illustrates how the distribution changes with combustor heat up. The measurements indicate that at a 2800°K temperature, the only measurable particles in the combustor were apparently slag falling off the walls. This was indicated by the absence of small particles, comparable sizes in the slag collected from the exhaust section and by the relatively low number density. In these measurements a half meter spectrometer was used to reject light radiated from particles. Background light could be adequately rejected with the slits of the spectrometer set such that a 1.5 angstrom pass band was available to the photodetector. In these measurements the particulate mass obtained under cold conditions was consistent with feed rates produced by the coke feed mechanism. Also under cold conditions, the PSI measurements were consistent with microscope measurements and sieve analysis. Under hot conditions the absence of PSI measurable small particles was verified by analysis of Mie scattering data and the particle sizes measured by the PSI were consistent with those which were obtained by analysis of the input coke and slag particles collected at the cooling coils of the combustor exhaust section.

SUMMARY

Electro-optical devices such as the laser velocimeter and particle sizing interferometer offer capabilities which were previously unobtainable with mechanical probes. These devices have been shown to yield results which are consistent with those obtained by mechanical devices when the mechanical devices can be used. The laser velocimeter which has been described does not require large computing facilities such as might have been called for only 4 or 5 years ago. It has been fully implemented using microprocessor technology. The PSI has demonstrated its capability in a high temperature flow, and background light rejection seems sufficient with a 1.5 angstrom background light filter. The PSI measurements have also been found to yield reasonable estimates of mass mean particle sizes when the particles are irregularly shaped.

REFERENCES

1. Farmer, W. M. and Hornkohl, J. O., "Two Component, Self-Aligning Laser Vector Velocimeter" Applied Optics, Vol. 12, pp 2636-2640, Nov. 1973.
2. Crosswy, F. L. and Hornkohl, J. O., "Signal Conditioning Electronics for a Laser Vector Velocimeter," Review of Scientific Instruments, 44, pp 1324-1332, Sept. 1973.
3. Barnett, D. O. and Giel, T. V. "Application of a Two-Component Bragg-Diffracted Laser Velocimeter to Turbulence Measurements in a Subsonic Jet," AEDC-TR-76-36 (ADA025355), May 1976.
4. Kar, M. L., "A Simplified Approach to Spectrum Estimation of Stochastic Processes," Ph.D. Dissertation, University of Tennessee, June 1981.
5. Farmer, W. M., "The Interferometric Observation of Dynamic Particle Size, Velocity, and Number Density," Ph.D. Dissertation, University of Tennessee, March, 1973.
6. Farmer, W. M. "Measurement of Particle Size, Number Density, and Velocity Using a Laser Interferometer," Applied Optics 11, p 2603, 1972.
7. Farmer, W. M. "Measurement of Particle Size and Concentrations Using LDV Techniques", Proceedings of the Dynamic Flow Conference, Disa Electronics and John Hopkins Univ., Sept. 1978.
8. Farmer, W. M., Harwell, K. E., Hornkohl, J.O. and Schwartz, F. A., "Particle Sizing Interferometer Measurements in Rocket Exhausts", Laser Velocimetry and Particle Sizing, Hemisphere Publishing Corp., New York, p. 518, 1979.
9. Farmer, W. M., Schwartz, F. A., Stallings, E. S. and Belz, R. A., "Particle Size, Number Density, and Velocity Measurements in a 2800°K Combustion System," AIAA Paper Number 81-1121, AIAA 16th Thermophysics Conference, Palo Alto, CA, June, 1981.

FIGURES

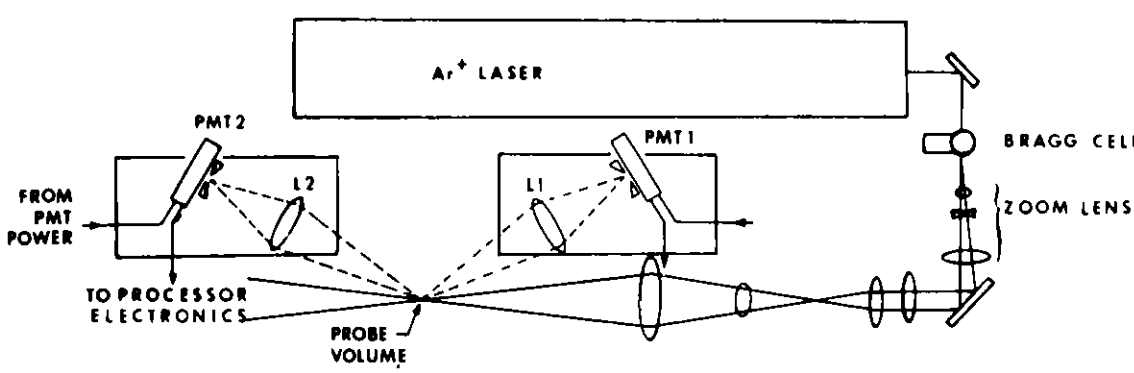

Figure 1. Schematic Diagram of Bragg Cell, Dual Scatter Laser Velocimeter Optical System.

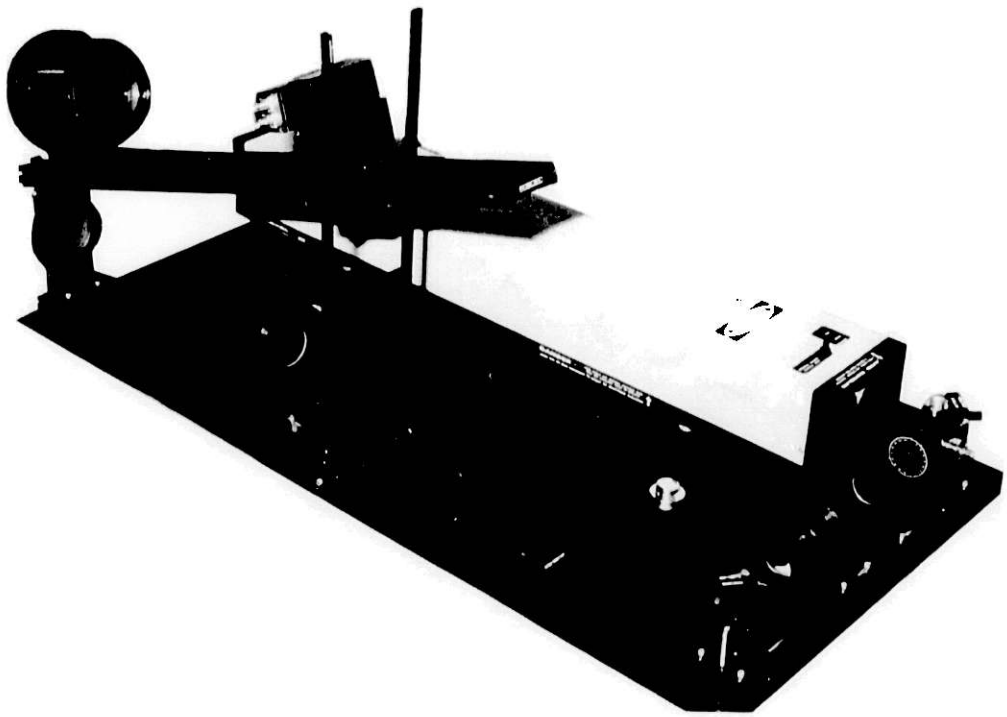

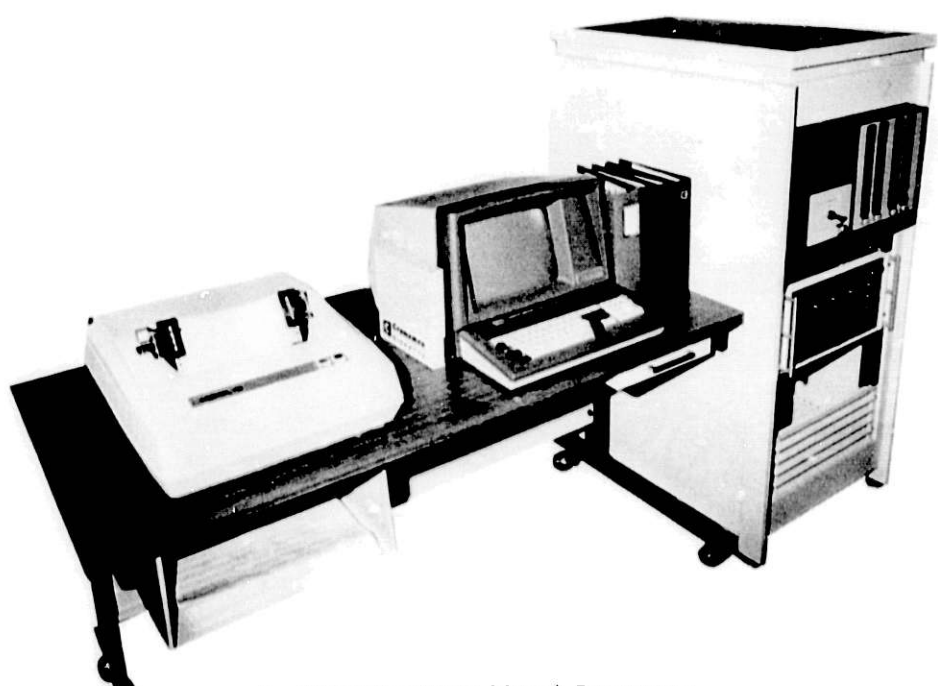

b. Computer-Based Signal Processor

Figure 2. Photograph of the Laser Velocimeter System

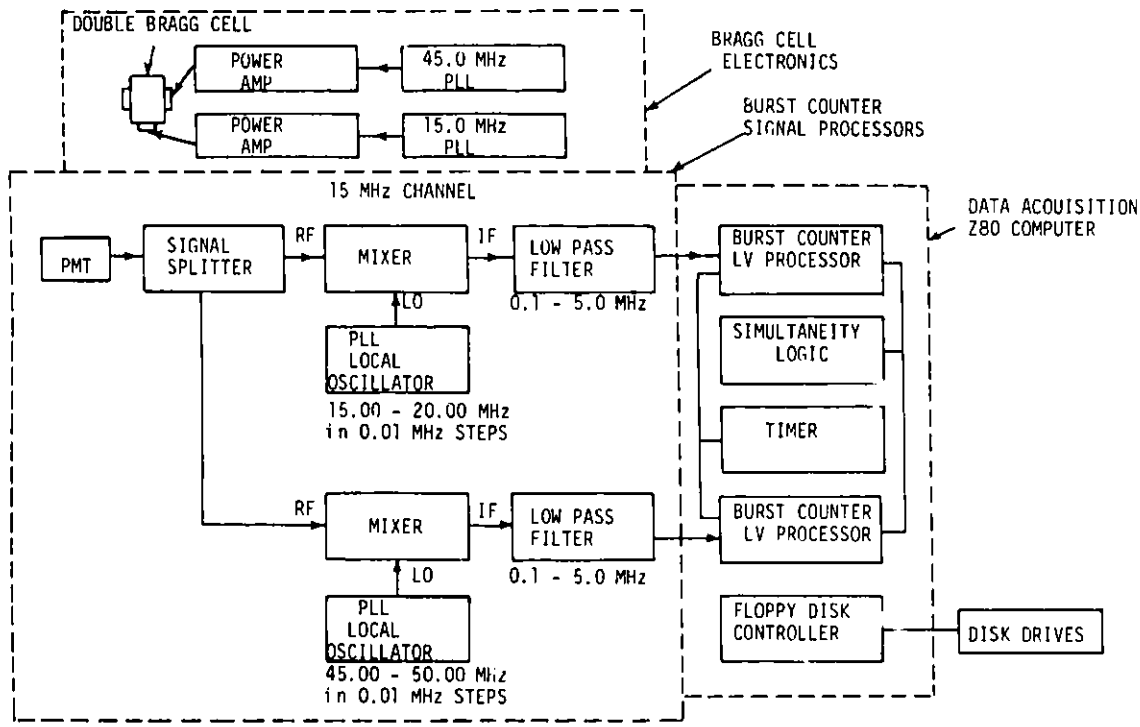

Figure 3. Block Diagram of LV Processor Electronics

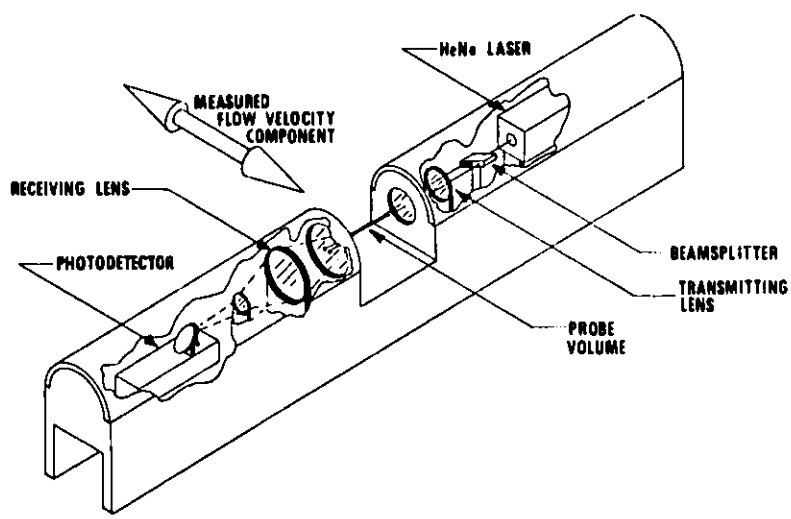

Figure 4. Schematic of PSI Optical System

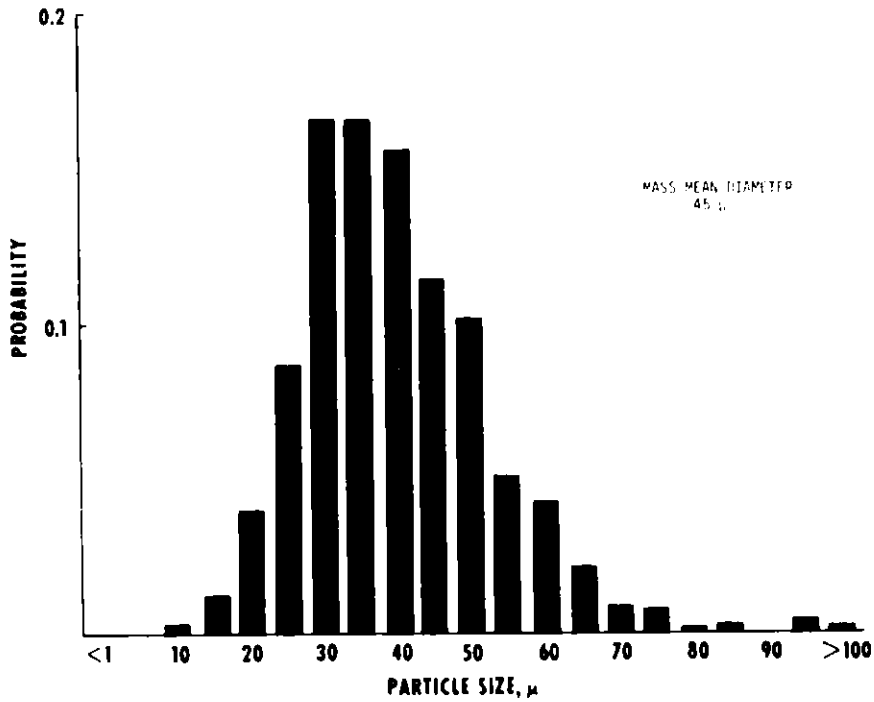

Figure 5. Example of PSI Measured Distribution for Coal Dust

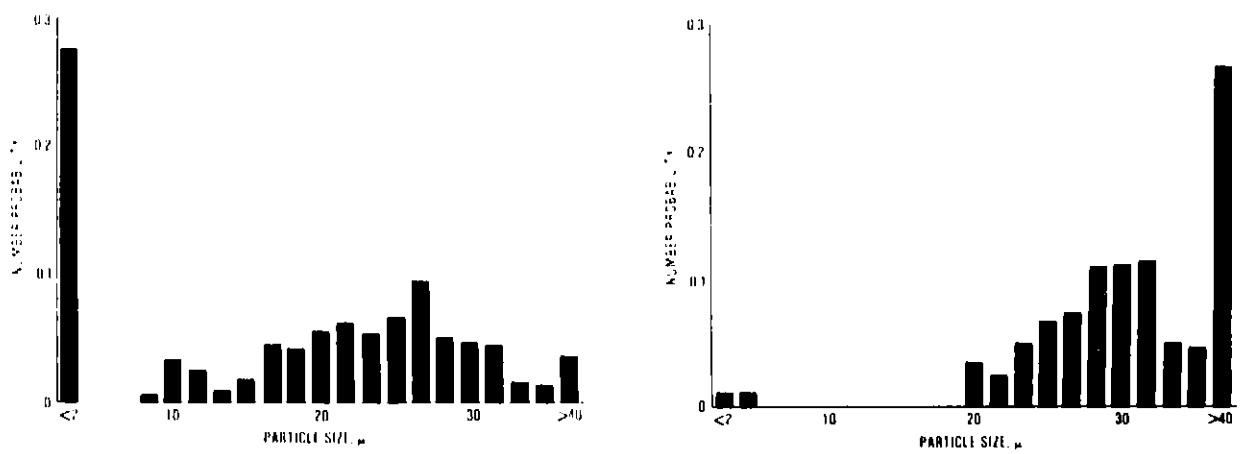

a. Initiation of Combustion

b. Full Combustion

Figure 6. PSI Measured Particle Size Distributions in 2800°K Combustor

APPLICATIONS OF ELECTRO-OPTICAL INSTRUMENTATION TO COMBUSTION PROCESSES

Frederic M. Zweibaum
Joseph Lamontagne
Barnes Engineering Company
Stamford, Connecticut 06904

ABSTRACT

The paper reviews the applications of electro-optical instrumentation in fossil energy processes. The paper considers four major aspects of the application of electro-optical instrumentation to coal gasification processes. First, is a study of capabilities in determining process characteristics. Second, is consideration of monitoring thoses physical characteristics significant to real-time quantitative measurement or process constituents. Third, is an analysis of capabilities in accomplishing quantitative analysis at a rate fast enough to detect significant deviations and in displaying the data in a form suitable for immediate process evaluation and control. Fourth, is a review of methods of storing the data in a form suitable for subsequent analysis and system design development. Reviews of typical data, analyses and interpretation are included.

ELECTO-OPTICAL PROCESS CONTROL

Previous Studies

Previous studies in electro-optical process control have been important in that they established that temperatures of so called "difficult" combustion processes can be measured with success. Such studies also indicated that important process control capabilities could be made available if real-time spectral analyses could be made of the process. This paper will proceed to indicate the capabilities that are required and go on to indicate current successes in achieving them.

Required Capabilities

To accomplish real-time process control of coal gasification requires that the electro-optical system have the capabilities:

1. To monitor those physical characteristics significant to the real-time quantitative measurement and process control.

2. To accomplish this data-monitoring at a rate fast enough to detect any significant deviations.

3. To display this data in a form suitable for immediate process evaluation.

4. To store this data in a form suitable for subsequent analysis.

5. To provide sufficient data for system design development and enlargement.

Providing the first of the above capablities requires an understanding of the physical nature of the process. To investigate the nature of the process within the reactor requires a recognition that the contents are, at various times and locations in solid, liquid and gaseous states. The investigation can be accomplished by measuring the contents' radiation emission, re-emission, transmission, absorption and scattering. Adequate measurements of these will provide for the determination of temperature, temperature/location profile, temperature/time profile, pressure, particle size, constituents, the magnitudes of the various phases that exist in the reactor, and also how these change with time and operating conditions.

To make non-contact process control measurements one requires one or more windows into the reactor and such a window must be capable of resisting the heat and pressure of the reaction within and must be kept clean of dirt and slag. Safety for the operators and the measuring equipment requires a remote control station for operating personnel and suitable pressure/temperature/contaminant isolation for the instrumentation.

Basis of Process Control

Real-time process control by radiation analysis is based upon a few basic principles. When infrared radiation is directed through a material, part of the energy is transmitted, part absorbed, and part reflected. The percentages of transmission absorption and reflection vary with wavelength in a manner that is unique to the specific material. Consequently, the spectral response curve of a material serves as a "signature" that identifies a material even when it is intermixed with other materials. Extensive collections of such spectral response curves have been made for a wide variety of materials and techniques have been devised for determining the concentrations of different materials in a mixture by spectral analysis.

It is characteristic of materials that in those spectral intervals in which they are good absorbers, they are also emmiters. Thus, the spectral distribution curve of self-emitted radiation also serves as a unique signature for identifying a material. By techniques that will be described, the spectral characteristics of both absorption and self emission can be determined simultaneously.

When a process is being conducted or a material is being produced, its spectral absorption or emission characteristics can be examined. If the process or product is such that a spectral analysis can be made, and if these are significant spectral variations as changes in the processing takes place, it may be possible to use this as a basis for real-time process control. The basic procedure is first to observe the nature of the spectral changes that take place. Then, spectral intervals, sequences and dwell times are selected to accentuate measurements of the changes that do take place. Computer analysis is then employed to determine from these spectral analyses the nature and degree of the process or product change away from the "ideal". This result is used with closed-loop servo control techniques to "zero in" the system back to its ideal form of operation.

While the process is being examined, each variation away from the initial "normal" is restored to ideal by examining the details of the spectral change and then determining (by computer techniques, if necessary) what adjustment in the input/output environment is necessary to restore the ideal condition. During the restoration process, spectral changes take place to indicate the trend and rate of trend back toward the ideal, and further control is exercized to prevent "overshoot" past the ideal. Thus, the complete system operates as a closed loop servo system in which the radiometric system operates as the error sensor and initial data processor, and the computer analyzes the error signals and determines the corrective signals that will most efficiently restore ideal conditions.

EXAMPLE OF COMBUSTION PROCESS SPECTRAL ANALYSIS

To be described here is the use of a Model 12-550 Mark II Spectral Scanning Radiometer for making analyses of spectral flame radiance from a tubular-can combustor. R. W. Claus in a 1981 NASA Technical Paper (1) reports the details of his investigation. The JT8D combustor used in the survey is representative of those widely used in commercial service. Measurements were made with the combustor installed in a test facility in which pressures and flowrate were controlled and measured. Internal temperature was monitored at a number of locations and three optical viewing parts were located at increasing distance downstream from the fuel input nozzle.

The radiometer was equipped with an indium antimonide detector and a two-element circular variable filter that permitted detailed spectral analysis between 1.55 and 5.5 micrometers. A mirror and translation, shown in Figure 1, system permitted the radiometer to view the flame process within the combustor through any selected viewing port.

Spectral measurements were made of flame radiance with Jet-A and ERBS fuels and over a wide range of operating conditions.

Spectral scans were produced, as shown in Figure 2, to show distinctly-different spectral radiance levels for each of the fuels as viewed through each of the ports and for different operating conditions. In addition, when the spectral curves were integrated with wavelength, it was possible to evaluate the contribution of the liner, soot, water vapor and carbon dioxide to the total radiation.

Different variations in spectral radiance for the two fuels was observed through each of the ports as the fuel-air ratios were varied (see Figure 3) and considerable differences were observed in flame temperature as well as in soot concentration. Similarly, similar distinct differences were observed as inlet air pressure was varied.

The concluding remarks indicated that the non-intrusive measurement technique employed in this investigation can provide insight as to the effect of combustor operating variables on flame temperature and soot concentration levels within the combustor.

SPECTRAL ANALYSIS OF FURNACE COMBUSTION

Spectral analyses were recently made of a furnace used for steam generation and employing either gas or oil as fuel. Also monitored were the percentage of oxygen and CO_2 employed in the combustion. Figure 4 shows a spectral radiance curve produced by the Mark II system with its data processing option when the fuel is gas with 0% oxygen and 12% CO_2 while generating 16,000 pounds of steam per hour. Very specific dips in the curve identify the mentioned combustion ingredients.

Figure 5 shows the same furnace using gas fuel with 2.4% oxygen in the combustion. Other differences in operating conditions are shown in the illustration. Note that there are major differences in the spectral radiance curve produced by these operating changes.

Other spectral radiance curves produced for oil fuel with a variety of operating conditions also show distinct differences from the gas fuel curves and from each other.

SPECTRAL ANALYSIS OF FLAME PROCESSES

In an investigation conducted by the authors a Mark II system was used to make spectral transmission curves of a propane flame contained in a chamber that restricted the escape of exhaust gases. The spectral curves reveal the constituents that were present during various control conditions and also can be used for automatic computation of the concentrations of individual compounds present.

Figure 6 shows the spectral transmission curve of the flame

under one set of operating conditions. The associated data processing system made the analysis shown inset into the curve area. The analysis shows the transmission and computed concentrations of H2O, CO and CO2. Figure 7 shows a similar curve for a slightly different set of operating conditions. Note that the inset data indicates that the system is capable of extracting significant differences in concentration from undramatic differences in the spectral curves.

CONCLUSION

It has been demonstrated that it is practical to produce moderate-resolution spectral radiance curves of combustion processes. It has also been demonstrated that these curves reflect a wide variety of changes in the combustion environment. It is estimated that appropriate spectral analysis techniques can be produced to define an extensive range of combustion process operating conditions, and that such spectral analysis is the basis for real-time process control.

REFERENCES

(1) R. W. Claus, Spectral Flame Radiance from a Tubular-Can Combustor, NASA Technical Paper 172, Feb 1981, Lewis Research Center, Cleveland, Ohio.

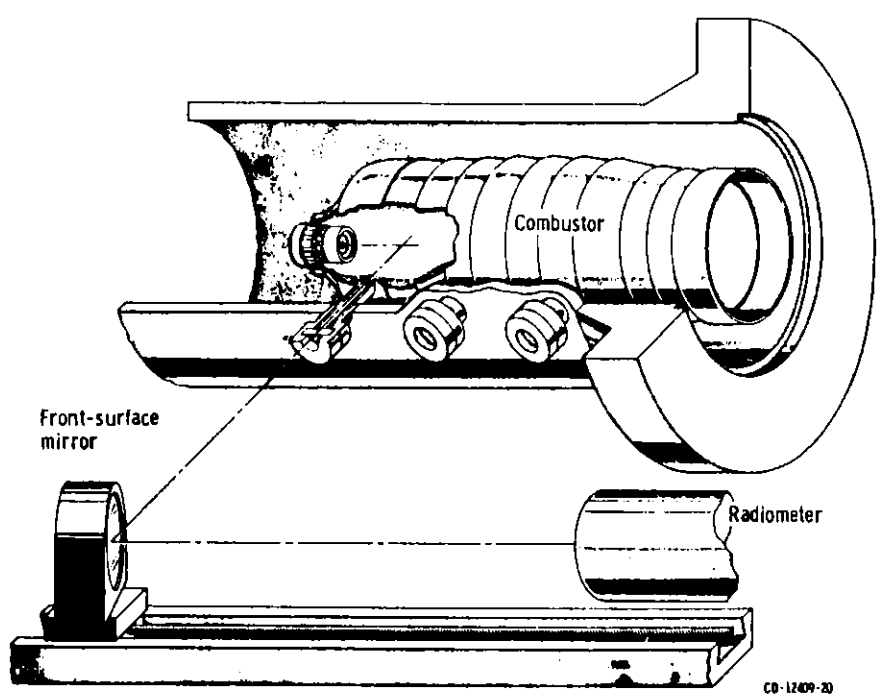

Figure 1. Schematic drawing of spectral radiometer optical path. Courtesy R. W. Claus, Ref (1)

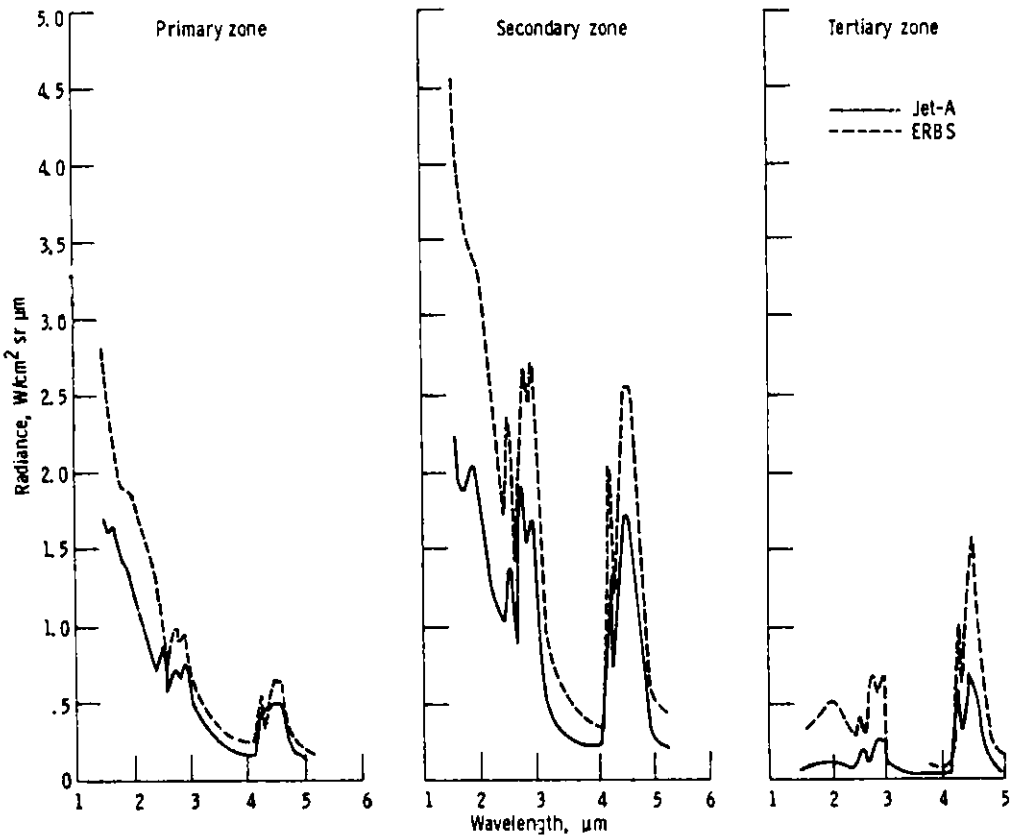

Figure 2. Spectral flame radiance as a function of fuel type for inlet-air pressure of 0.34 MPa, inlet-air temperature of 533K, and fuel-air ratio of 0.0155. Courtesy R. W. Claus, Ref. (1).

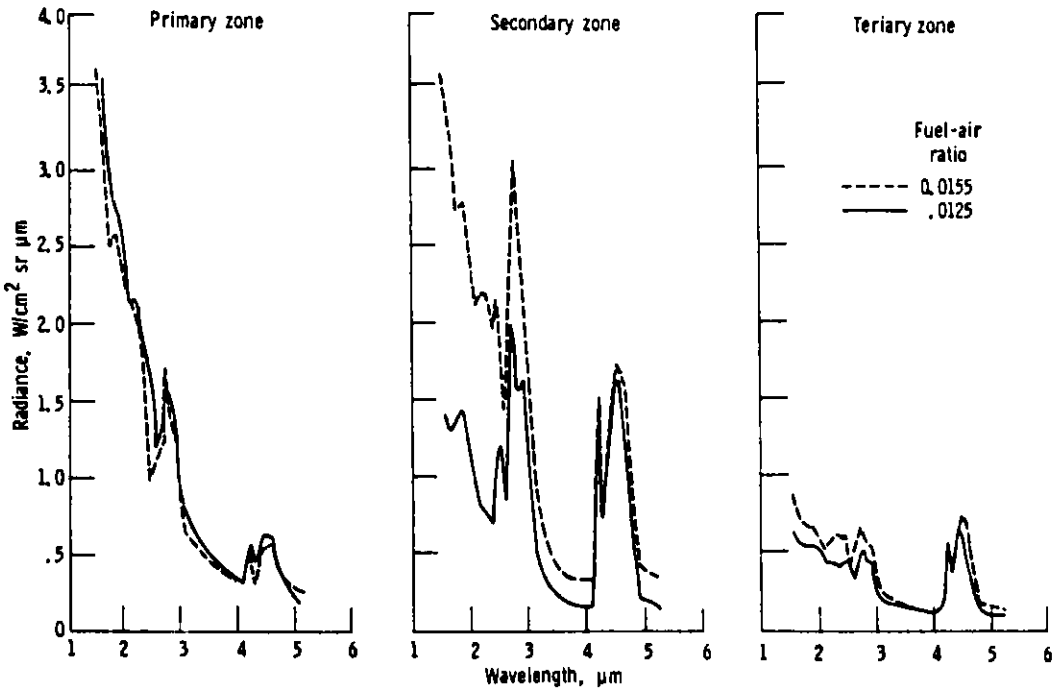

Figure 3. Spectral flame radiance as a function of fuel-air ratio and wavelength for Jet-A fuel at inlet-air pressure of 0.34 MPa and inlet-air temperature of 700K. Courtesy R. W. Claus, Ref (1).

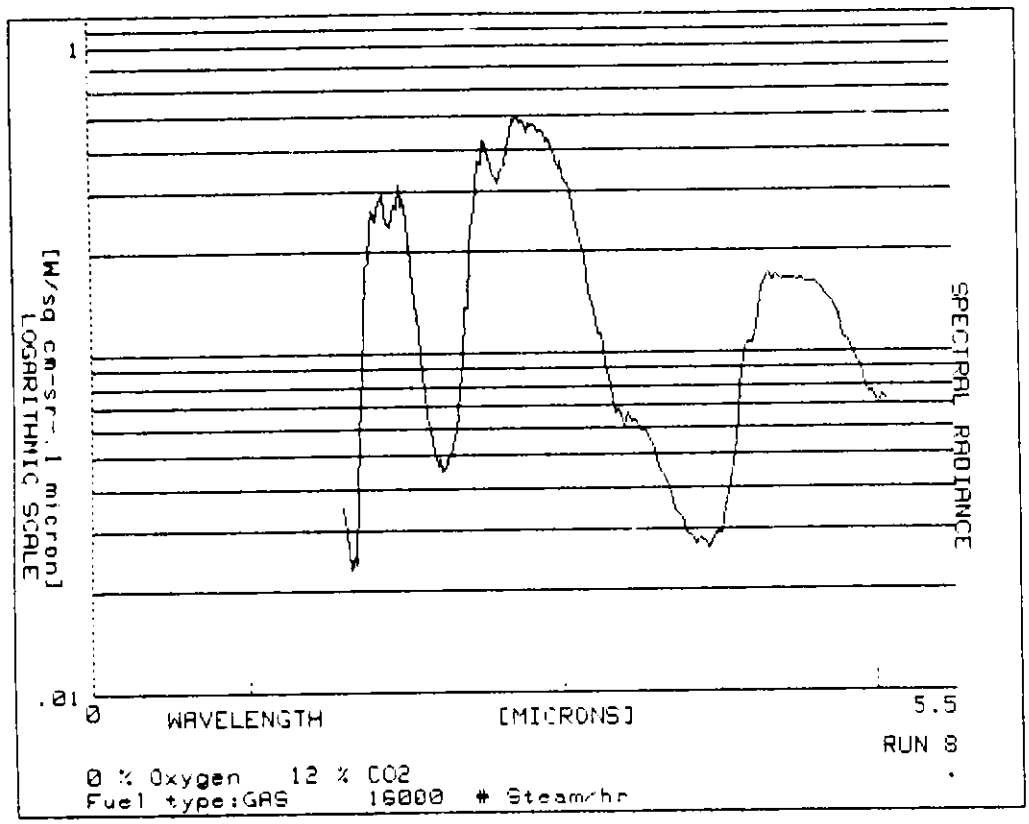

Figure 4. Spectral radiance curve of furnace combustion, Run 8, with indicated conditions.

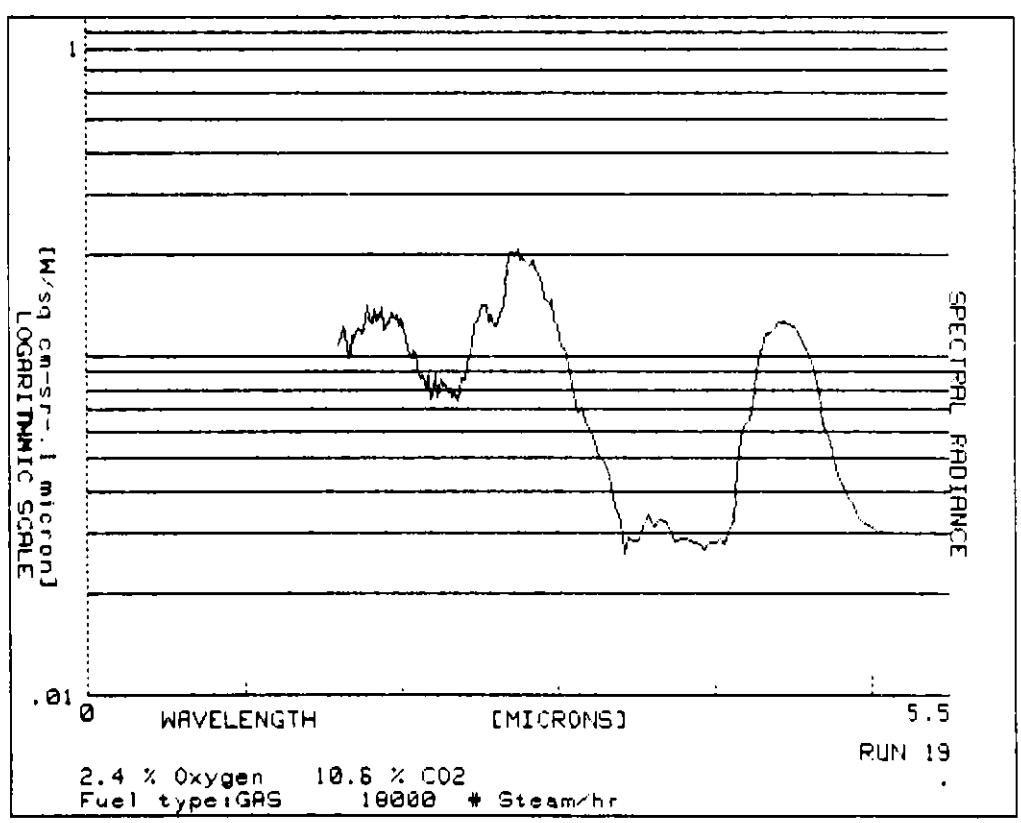

Figure 5. Spectral radiance curve of furnace combustion, Run 19, with indicated conditions.

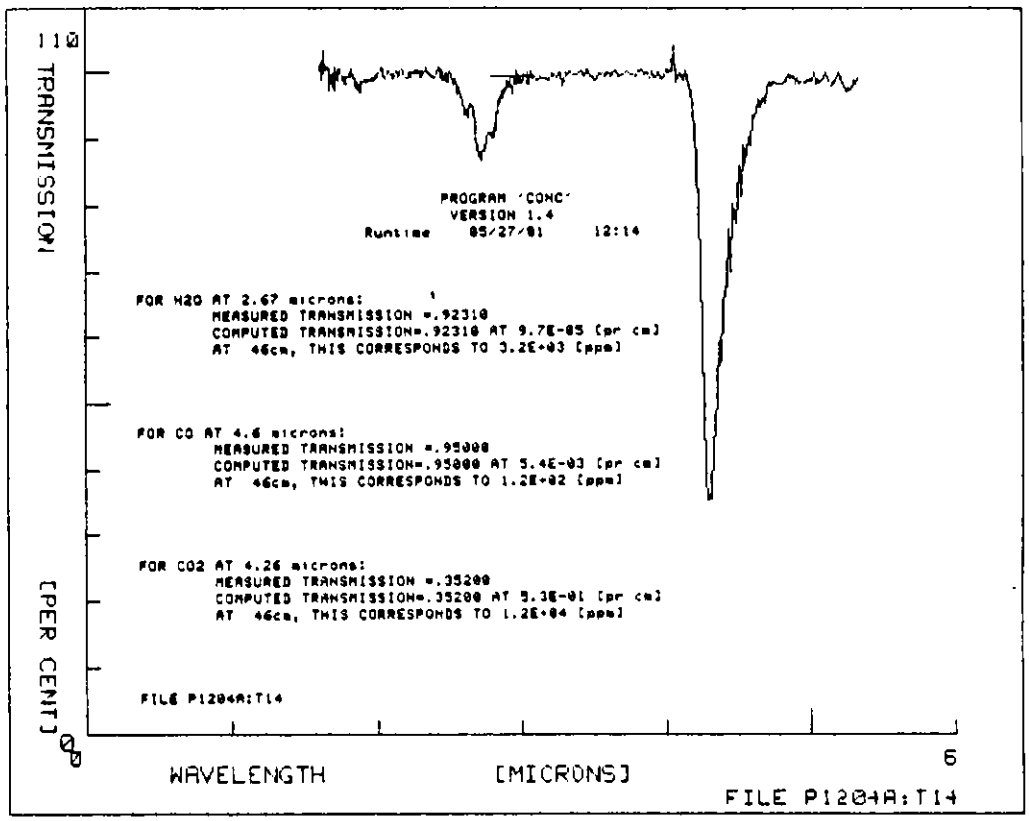

Figure 6. Spectral transmission of propane flame indicating constituent concentrations, Run 12:14.

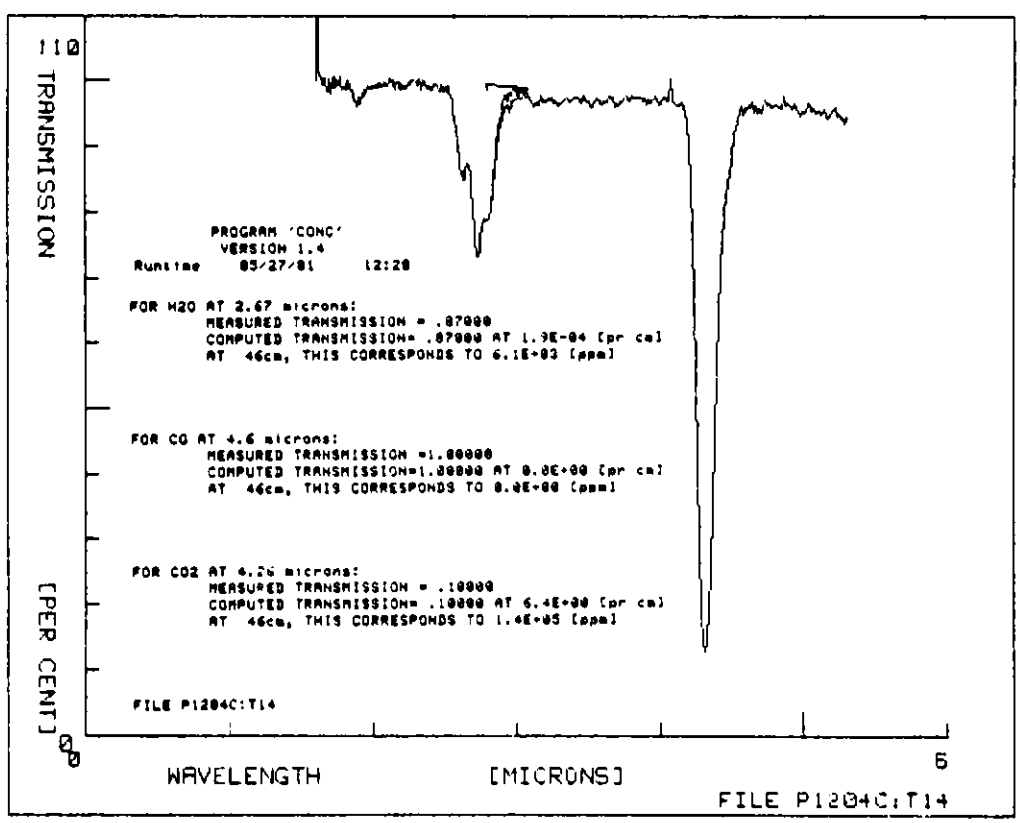

Figure 7. Spectral transmission of propane flame indicating constituent concentrations, Run 12:28

INSTRUMENTATION & CONTROL REQUIREMENTS FOR A MODULAR ATMOSPHERIC FLUIDIZED BED BOILER

August H. Zoll, A. Gregory Diamond
Curtiss-Wright Corporation

INTRODUCTION

During 150 years of coal mining in eastern Pennsylvania, over one billion tons of culm, a low-Btu mining waste, has been deposited above ground, accumulating in huge banks. These culm banks are not only eyesores but also environmental hazards due to the noxious fumes given off by spontaneous combustion and acid runoff. Because of its low energy content, approximately 4000 Btu/lb, and its poor fuel qualities, culm has had little economic value in the past. However, with rapidly rising energy costs and the feasibility of burning low heating-value fuels in a fluidized bed combustor, culm can be a viable low-cost energy source.

A department of Energy contract to develop a culm-burning Atmospheric Fluidized Bed Boiler (AFBB) was awarded to the Shamokin Area Industrial Corporation of Shamokin, Pa. as the prime contractor with a design, engineering, and construction team headed by Curtiss-Wright.

The Shamokin AFBB (Figure 1), scheduled for initial startup in mid-1981, will use culm as the sole fuel to produce 23,000 pounds per hour of 200 psig saturated steam which will be used by a nearby paper pulp processing plant.

The boiler is equipped with a digital control system which will provide safe and efficient automated operation. The control system includes load-following capability since the customer's steam demand will vary considerably.

PROCESS

In the Shamokin AFBB process (Figure 2), culm and limestone feed bins are periodically filled from materials preparation and storage systems. From the feed bins, culm and limestone are fed to the fluidized bed combustor by variable-speed screw feeders.

The culm is burned in a modular three-zone fluidized bed of ash and limestone in which the limestone is a sulfur sorbent. The three zones are not physically separated but are fluidized separately from three adjacent windboxes. Combustion conditions in the bed are controlled by adjusting four operating parameters: bed temperature, space rate, bed height, and effective fluidized area. Bed temperature is controlled between 1450°F and 1550°F for optimum sulfur capture and NO_x emission; space rate is varied between 3.5 fps and 5.5 fps for optimum fluidization, bed height is varied between 3 ft and 5 ft, and effective fluidized area is selected to be 64%, 82%, or 100% of the total fluidized bed area.

The energy released from the combustion in the bed produces steam in vertical water tubes located within the bed, in waterwalls surrounding the bed, and in a convective bank in the freeboard above the bed. Half of the steam is produced by the water tubes and waterwalls in contact with the bed where the heat transfer rate is high. The remainder is produced by the convective section where energy is reclaimedfrom the exhaust gases.

Fly ash in the exhaust gas is separated in a system consisting of one recycle cyclone and two cleanup cyclones. Particulate removed by the first cyclone is recycled into the fluidized bed to reclaim energy in unburned carbon and to recirculate unreacted limestone. At reduced load, optimum separation efficiency in the system is achieved by the shutdown of one cleanup cyclone to maintain a high gas velocity in the remaining one. Downstream of the cyclone system, additional energy is reclaimed from the exhaust gases by a fluidizing air preheater. A baghouse provides the final cleanup before releasing exhaust gas to the atmosphere.

Bottom ash removal rate from the fluidized bed is controlled using the ash Fluoseal®, a fluidized column. Energy is reclaimed from both bottom ash and fly ash in a feedwater-cooled fluidized ash cooler. Ash from the cooler is stored in a bin from which it is finally loaded on to a pneumatic truck for removal.

CONTROL SYSTEM

To achieve safe, efficient, and reliable operation, the control system was designed as a hierarchy of three distinct systems: The digital control system, the analog control system, and the safety interlock system (Figure 3).

Control for efficient operation and minimum exhaust emissions is provided by the digital control system. If the digital system fails, this control refinement will be lost; the analog system will assume control as a backup system to maintain safe operating conditions. The safety interlock system provides safety backup to the analog system and the failsafe design of the controls and instrumentation provides the final safety backup.

For a minimum plant startup and debugging period in a development program such as this, flexibility is required to refine the control strategy based on operating experience. Using the digital control system, control software can be easily modified with no plant downtime. The need for hardware modifications is minimized since only those functions necessary for safe backup control are hardwired in the analog control system.

The control system, shown in Figure 4, includes a color graphics CRT and a data logging printer to provide the operator with extensive monitoring capability.

CONTROL STRATEGY

The Shamokin AFB Boiler control strategy utilizes conventional boiler control techniques where possible, but, as shown in Figure 5, it differs in several important respects due to the unique characteristics of the fluidized bed and the culm fuel. Whereas, in a conventional boiler, the excess air is fairly constant, in the AFBB, excess air varies between 10% and 60% as space rate varies. Overfuel constraints during normal operation are not as critical as those in a conventional boiler because the excess air at the minimum fluidization space rate provides a large margin of safety. Because of the variable heating value of the culm, fuel feed rate does not accurately reflect Btu input and therefore cannot be used in the combustion control.

Figure 6 illustrates the Shamokin AFBB control strategy. The steam drum pressure control varies culm feed rate to meet steam demand by maintaining a steam drum pressure setpoint. As the culm feed is varied, the combustion control varies bed temperature, space rate, and bed height and maintains each within its limits as shown in Figure 5 for a single fluidized bed. In a three-zone fluidized bed with shutdown capability for two zones, on-off control of effective fluidized area provides further turndown. Figure 7 illustrates the effect of the load-following combustion control on the four operating variables. In a decreasing load situation, bed temperature is decreased until it reaches its lower limit. Then, space rate is decreased until it also reaches its lower limit. At this point, the combustion control reduces the effective fluidized area by defluidizing one zone. The resulting decrease in heat transfer area causes bed temperature and space rate to increase, allowing further turndown by repeating this cycle until only one zone is fluidized. The final variable affected by the combustion control is bed level, which is decreased from 5 ft to 3 ft. Using this control sequence in the digital combustion control, a fully automated load-following turndown of 2.5:1 is achieved.

In the SO_2 emission control, the limestone feed rate is varied to maintain SO_2 concentration in the exhaust gas at an environmentally acceptable level. The limestone feed rate is coarsely preset at a fixed ratio to culm feed rate. This ratio is based upon the average sulfur content of the culm and the sulfur capture rate at an average bed temperature. To adjust the feed rate to correspond to actual conditions, it is fine-tuned by SO_2 feedback from the exhaust gas analysis system.

Fluidized bed height control is accomplished by varying ash removal rate, and balancing the rate of culm and limestone feed, to achieve the bed height setpoint established by the combustion control.

INSTRUMENTATION

To implement the control strategy described, special applications of instrumentation and measurement are used. In-bed thermocouples measure bed temperature in eight locations, four of which (in Zone 1) are averaged for control purposes. The averaging can be modified as needed to obtain optimum control stability.

Annubars are used in air ducts to measure fluidizing airflow with a minimum pressure loss. This fluidizing airflow is corrected with bed temperature and pressure and divided by the effective fluidized area to calculate space rate.

Differential pressure transmitters measure the pressure drop across the fluidized bed in several locations and are also used to calculate bed height. Pressure taps in the fluidized bed and ductwork are continuously purged with clean air. Measurement fluctuations due to bubbling and slugging can be damped by calculation in the digital system software. The resulting stable signals can be used for bed height control.

Weigh cells are used to measure culm and limestone feed bin weight. The digital system will calculate feed rates (to be used in material and energy balances) by calculating the rate of decrease of feed bin weights. During a bin fill cycle the digital system will calculate feed rate by extrapolating data measured between fill cycles.

The exhaust gas analysis system continuously extracts exhaust gas through a shielded probe and heated sample line. Analyzers located in a control room cabinet continuously measure SO_2, NO_x, CO, CO_2, and O_2 concentration for recording and control.

SUMMARY

A control strategy has been developed to safely and efficiently control a modular atmospheric fluidized bed boiler system. Using this strategy, the AFBB, an inherently complex system, can be effectively controlled with no more operator effort than that required to control a conventional boiler. The strategy is independent of hardware and can be implemented in various configurations, including those involving integration with distributed control and energy management systems.

The system described herein provides control flexibility and comprehensive data measurement and display capabilities. A commercial application would not necessarily require all of these features and could employ the same strategy implemented on any one of several commercially available programmable controllers with direct digital control capability.

ACKNOWLEDGMENT

The Authors wish to acknowledge the efforts of the Dorr-Oliver Company, the Stone & Webster Engineering Company, and the E. Keeler Company who were members of the design, engineering, and construction team.

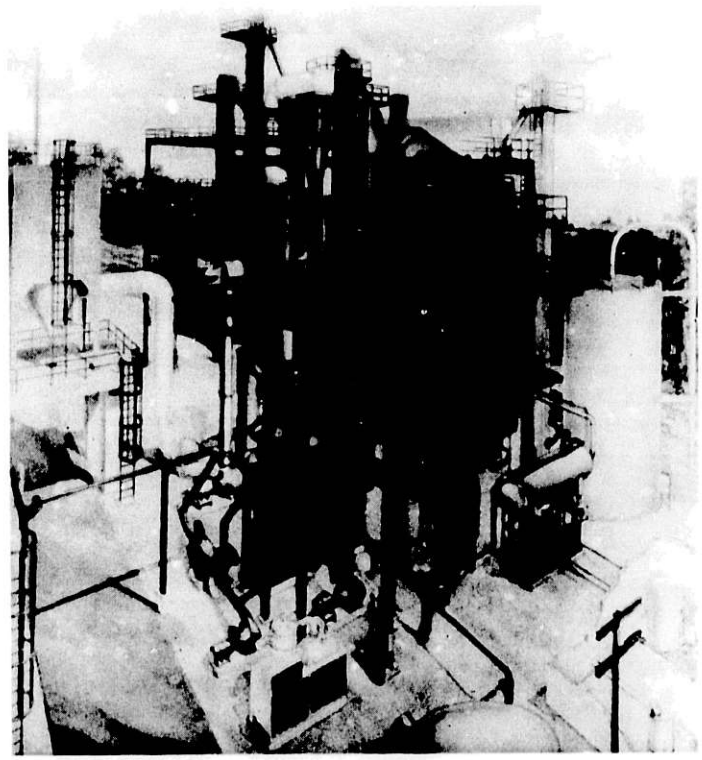

Figure 1 - Shamokin Atmospheric Fluidized Bed Boiler Plant

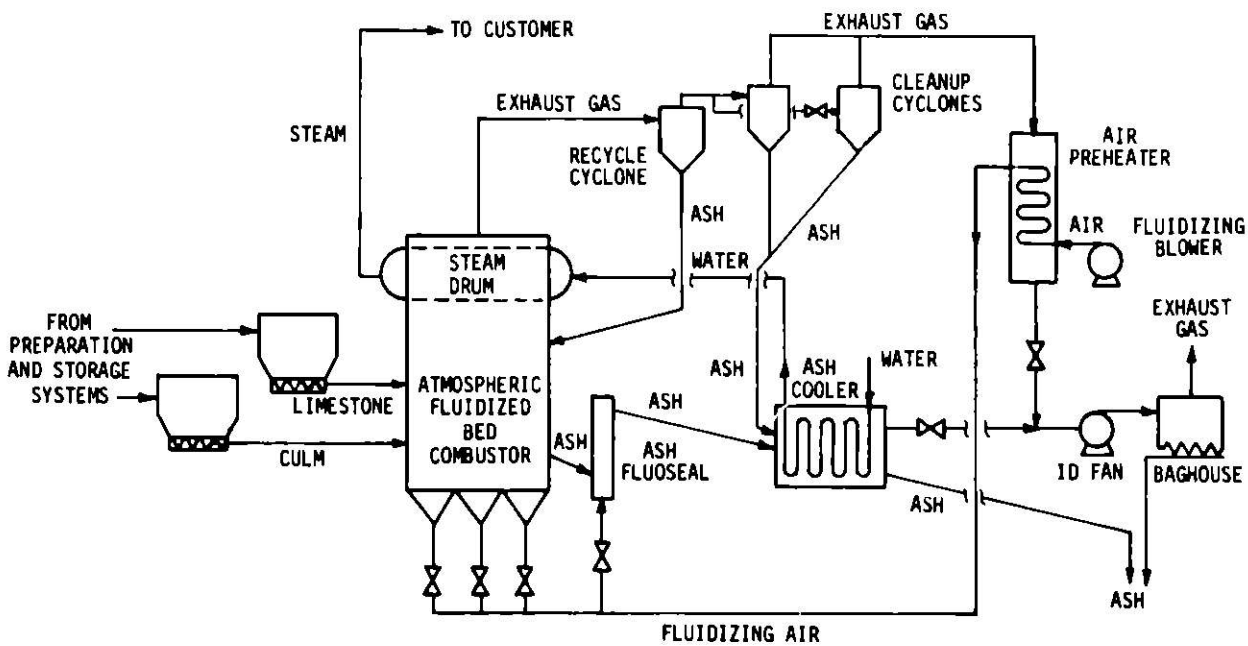

Figure 2 - Shamokin AFBB Process

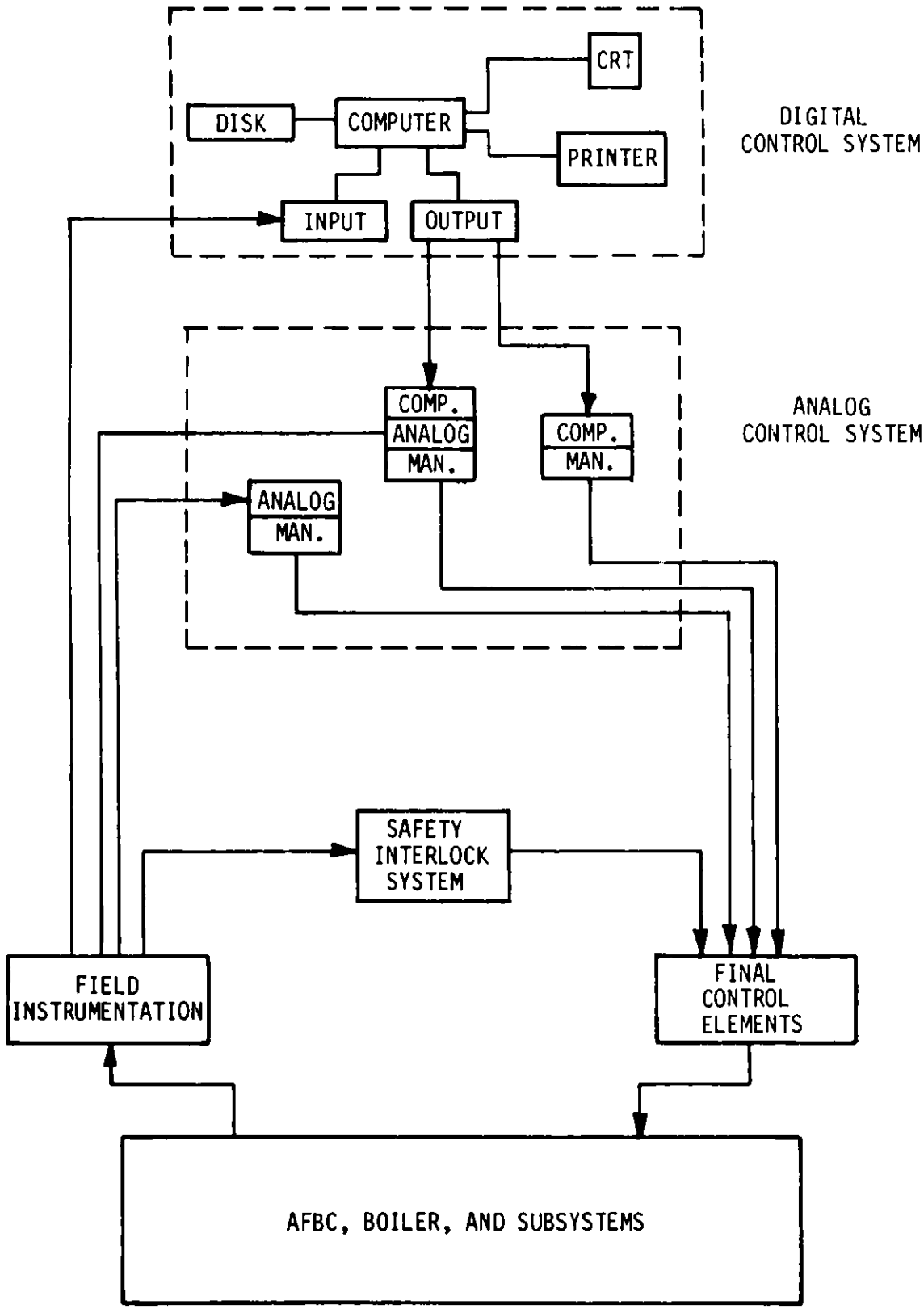

Figure 3 - Shamokin AFBB Process Control System

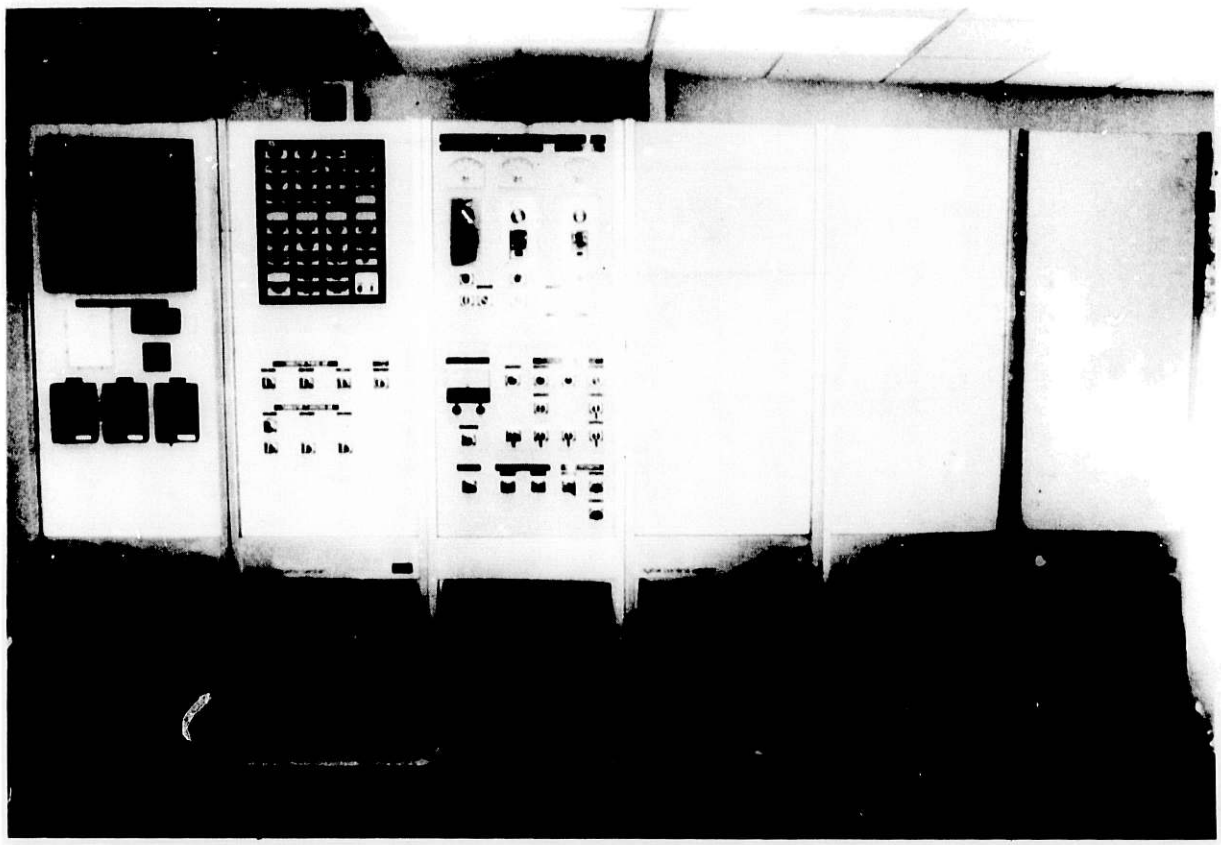

Figure 4 - Shamokin AFBB Control Room

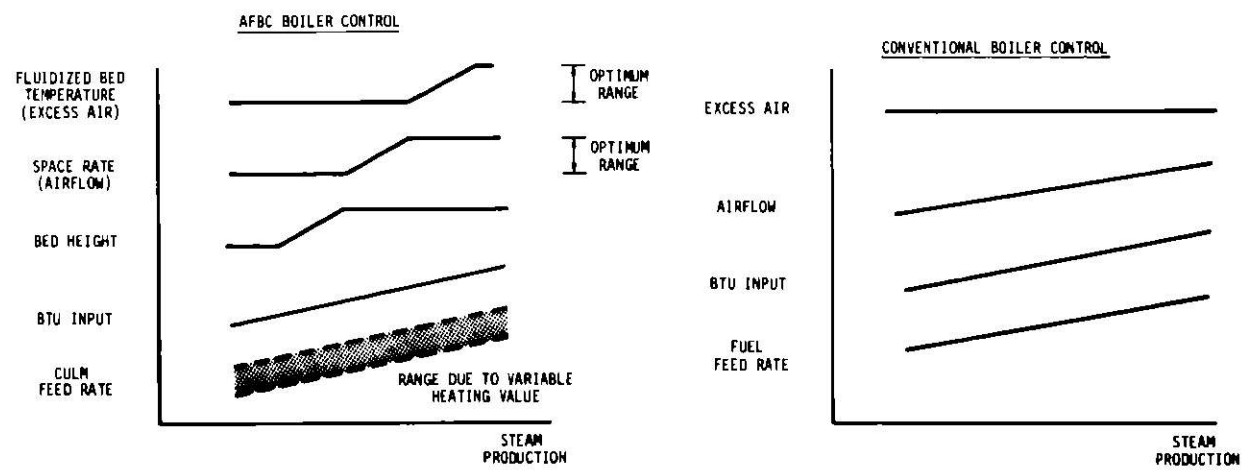

Figure 5 - Comparison Between AFBB Control and Conventional Boiler Control

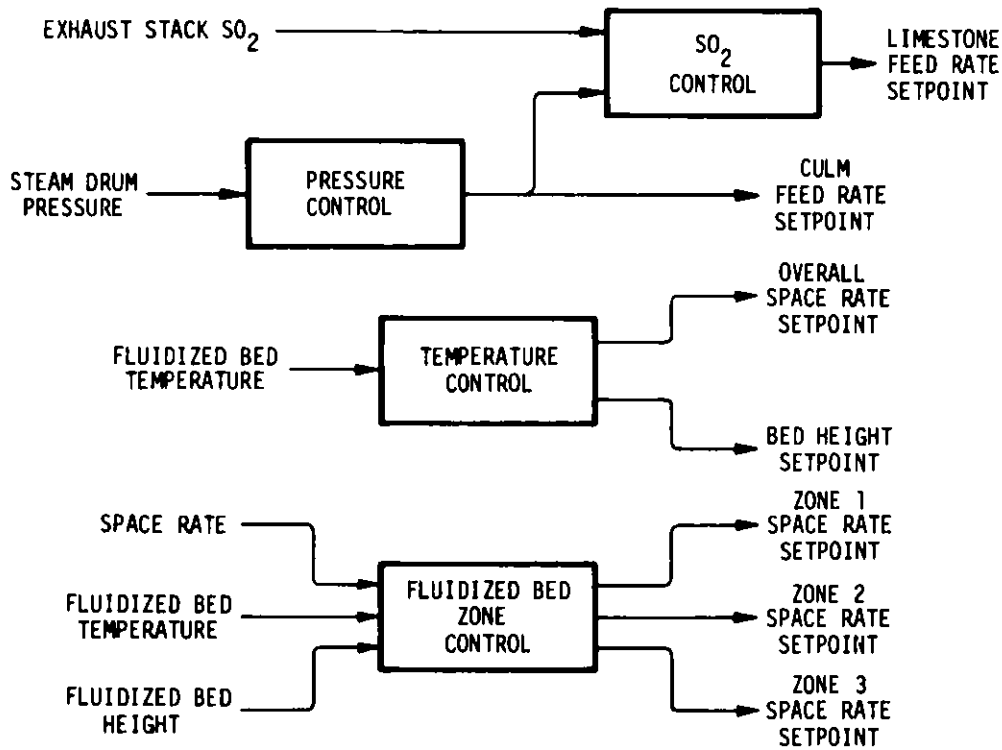

Figure 6 - Shamokin AFBB Control Strategy

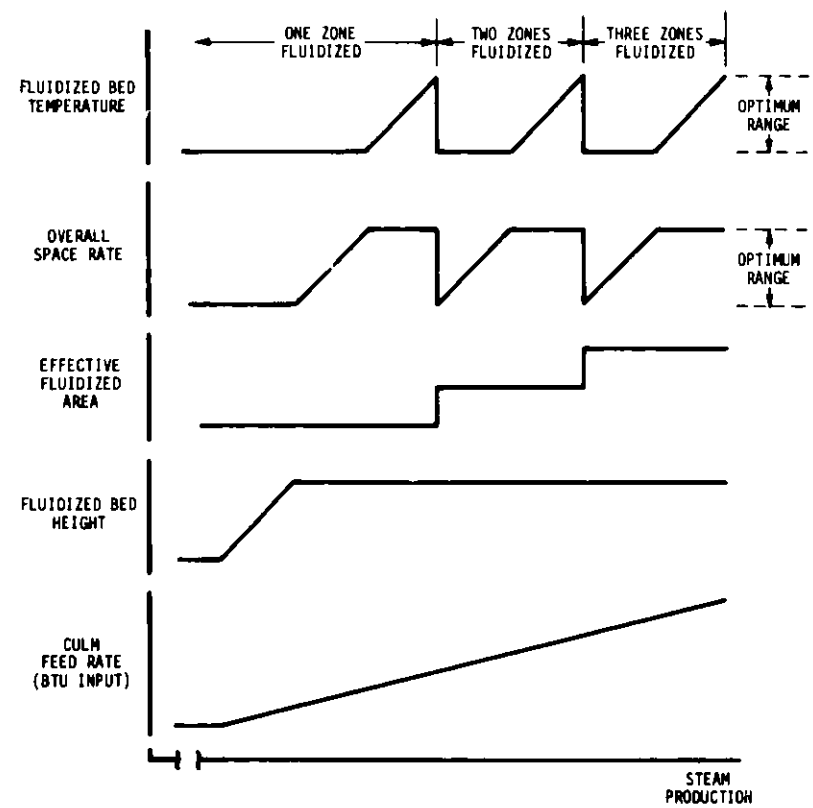

Figure 7 - Operating Variables During Load-Following Turndown

INSTRUMENTATION AND CONTROL FOR MHD POWER DEVELOPMENT - DESIGN AND PERFORMANCE

Michael L. Miller
Mountain States Energy, Inc.
DOE MHD Component Development and Integration Facility
Butte, Montana

INTRODUCTION

Magnetohydrodynamics (MHD) is currently being evaluated as an economical and environmentally acceptable process for generation of electric power from coal. Combined with a steam boiler bottoming cycle, it could, by allowing higher combustion temperatures, increase busbar efficiency by as much as 50 percent.

The MHD process involves passing an electron-rich plasma through a powerful magnetic field at high velocity. Direct current is thus generated and drawn off through the electrodes in the walls of the MHD channel generator. This DC power is inverted to AC to feed the power grid. The exiting plasma's residual heat drives a boiler-turbine-generator unit.

As part of the national MHD research program, the U. S. Department of Energy has established the MHD Component Development and Integration Facility (CDIF) in Butte, Montana. The CDIF provides a place to assemble MHD components into complete generation systems (test trains). These components may be provided by DOE contractors or by others, like the Electric Power Research Institute. They include combustor, channel (generator), magnet, inverter and any other components of a developmental nature for use in MHD electric power generation.

The CDIF has been activated and power generation testing accomplished during the past two years. This paper discusses some of the challenges of (and in some cases solutions to) instrumentation and control problems encountered during this initial phase of facility operation.

Hopefully this discussion will prove of use to those engaged in the development of MHD and other new energy processes. It may also encourage those with possible solutions to these problems to come forth with their ideas.

These challenges and special applications are presented as cases, with a brief description of the facility or component subsystems involved. Accompanying each case is a discussion of the subsystem involved and its role in the function of MHD development.

TWO-PHASE FLOW

To support accelerated realistic testing of 50 MW_{th} scale MHD channels in parallel with coal combustor development, an ash injected combustor (AIC) is used. The AIC, fueled by oil, produces a plasma similar to that of a coal fired combustor. This is accomplished by pneumatically injecting fly ash into the combustion chamber. The presence of the ash constituents in the plasma permits realistic slag formation on the channel walls. Slag formation affects electrode erosion, conductivity, and heat transfer.

It is necessary to control the rate of ash injection in order to accurately simulate coal-fired slagging. The present measurement system involves the use of weight measuring (load) cells on the ash hopper supports. While satisfactory for monitoring ash inventory, the repeatability and hysteresis characteristics of this approach do not lend themselves to feedback control. It is hoped that the approach developed for ash flow control could be adopted later for pulverized coal flow control. Two approaches are undergoing experiments presently at CDIF.

The first experiment combines a capacitive averaging densitometer and an ultrasonic Doppler velocimeter to compute mass transfer. This approach, originally suggested by Dr. Ralph G. Lightner, Facility Operations Director, Office of Coal-Fired MHD Power Systems, U. S. Department of Energy, has the advantage that no bends in or protrusion into the pipe

are required. This is important because pipe I.D. is small (1/4") and the line tends to plug easily. The densitometer is an Auburn Model 1090, with six capacitor plates. The velocimeter which was used is a Columbia Controls Ultrasonic Doppler Model 120. The small line size seems to pose significant difficulties in signal strength for this unit. Evaluation of other velocimeters is presently in progress.

The second approach will be to install a Micro-Motion Model C25AF Coriolis Effect Flowmeter. This approach, already used for coal flow at Argonne National Laboratory and at the Coal Fired Flow Facility, requires only a single commercial product. There is some concern about the use of this meter, which contains two 90° bends, with the erosive, easily plugging ash flow.

Presently the ash system is undergoing an engineering review to reduce plugging susceptability. After the completion of this review, flow meter testing will continue, probably around August 1981.

PLASMA LEAK DETECTION

The MHD channel generator is composed of about 300 alternating electrodes and insulation layers. Because of the large number of seams and mating surfaces, and also the very large temperature gradients and small wall thickness, leaks do occur in test channels. The layered construction allows economical repair of small holes; however, the highly erosive plasma causes small undetected holes to grow rapidly. Also, a large plasma leak could result in significant magnet damage if allowed to persist. Since this could mean large costs and test program delays, it is useful to detect leaks as soon as possible, and terminate firing upon detection.

The primary plasma leak detector at CDIF senses plasma leaks by an elevated carbon monoxide level in the magnet bore which surrounds the channel. This is a convenient parameter because, while normal atmospheric concentration of CO is low (<1 ppm), the plasma is typically about 9%

CO. Thus even a small leak will raise the CO concentration in the confinement of the magnet bore substantially. This method was successfully applied to the USSR U-25B experiment by ANL.

The CO sensing is accomplished by drawing a continuous sample through capillary tubes strategically located on the exterior of the generator. Vacuum pumps deliver this sample to the CO analyzers. The initial system used Ecolyzer Series 3000 Analyzers. A system presently being installed will use Beckman Model 865 Analyzers.

The system has proven itself to be quite sensitive to even very small leaks. In fact, acceptably small flange leaks at the quencher produced an elevation in CO level of 10-40 ppm. Better gasketing and ventilation have since reduced this level. However, this situation did call attention to the fact that CO may originate from sources other than channel leaks. The system was subsequently modified to monitor area CO level as well as magnet bore CO level. This allows observation of the offset between the two, which is the true indicator of a CO source in the bore.

Future developments on this system will include rate-of-change monitoring and automatic test train shutdown. These will be implemented using programmable logic control. Also, monitoring of water vapor and other compounds which might indicate a broken or burned hose is under consideration.

ARC DETECTION

As was noted in the previous section, the MHD generator is hidden from view during operation. Surrounded by thousands of power leads and cooling water hoses, it is enclosed in the magnet bore. Within this hidden maze of hoses and wires, electrical arcing can occur. The cause may be voltage transients, moisture-created conductive paths, or loose or damaged wiring. The arcing is destructive and disruptive to testing. It should not be confused with inter-electrode arcing inside the generator, which is also destructive but has other causes.

To detect external generator arcing, a system designed at CDIF is now being installed in the magnet bore. It consists of many fiber optic bundles connected to photo diodes mounted remote from the channel. This preserves the electrical isolation of the generator, which may have as much as 10KV potential below earth ground. By splitting the ends of each of the 12 fiber bundles into five branches, a total of 60 sensing ends are placed in the bore, allowing complete coverage in the confined space. Each bundle has its own photo-cell, a Clairex model CL-703 cadmium selenide cell.

Custom electronics allow a wide range of adjustment for the cell threshold. Because some ambient light level will persist in the bore, and because some arcs may be sensed only by reflection, good control of threshold is important. In addition, a Y-fitting near the cell end of the bundle allows light from a General Instruments Sub-Miniature Lens-End Light, Type TL 1-3/4, to be introduced into the bundle and emitted from the fiber ends. When this is done, the ends become light sources, and bundles opposite them may be tested in place. In operation, the programmable logic controller (PLC) monitoring the photo-cell outputs will automatically and periodically test all bundles. Failures are annunciated on the control console. For troubleshooting, local manual control of this feature is also available.

The detection of an arc is annunciated by a latched indicator on the console display. The location of the active bundle is indicated and an audible annunciator is activated. If the auto shutdown feature has been selected by the operator, detection of arcs by two or more bundles will automatically initiate the emergency shutdown sequence.

A secondary benefit of the system is that it could sense the presence of a luminous plasma or breach of the channel. It thus provides a backup to the CO leak detector discussed previously.

Problems encountered during the development of this system included attenuation beyond the specification in the custom-fabricated fiber

optic bundles. The extremely confined space in the magnet bore also made installation of the fibers a challenge. They are mounted in non-conductive Garolite (TM) pipe, which is attached by adhesive to the magnet bore liner.

This system has been bench tested and is presently being installed at the CDIF. It is expected to be operational by August 1981.

SURGE SUPPRESSION

In order to evaluate the electrical performance of the MHD generator, the voltage and current for the hundreds of electrodes must be monitored and recorded. For the 1A1 generator, some 1500 measurements are transduced via Hall effect devices to 1-5 VDC signals. These signals are inputs to the Data Acquisition System (DAS) computer. The DAS records each signal once per second, and can at the same time accelerate the scan and record on a limited number of inputs to 100 times per second.

Because electrode potential may be as much as 10 KV below earth ground, the Hall devices have a critical function as isolators. At some facilities, isolation breakdown has resulted in extensive damage to the DAS. Because of this, it was decided to add a second level of protection to the loop. This is the surge suppression module, located in the circuit between the Hall transducer and the DAS. The modules are mounted in racks which comprise the surge suppression assembly. The surge suppression assembly is composed of 1728 separate modules. There are 72 modules to a frame, three frames to a rack, with a total of eight racks.

Each module contains two circuits, one each for the high and low sides of the loop. Each circuit functions autonomously. The circuit is totally passive, imposing no degrading influence on the data so long as the voltage is less than or equal to 30 volts. If the voltage on the data lines rises above this threshold voltage, the circuit becomes a constant voltage device, and the current rises as a function of the applied voltage. If the voltage is above the threshold level in either

the energy or voltage regime, it forces the dual chamber gas tube to conduct, which limits the line-to-ground voltage to between ± 30 and ± 50 volts peak.

If the voltage anomaly is the result of the full 10,000 volts being applied to any circuit, either between the wire pairs or between any one and ground, the series fuse blows and the series resistor quenches any remaining arcing.

The circuits are designed to fail-safe if subjected to an overstress voltage. Fail-safe is defined as protecting the computer against an overvoltage under any circumstances possible in the system. Upon failure, the entire module must be replaced.

Prototype tests of this design were quite impressive. A 15 KV charge applied to the input side of a module caused a peak at the output of less than 100 volts amplitude and less than 1 nanosecond duration. After the peak, the voltage was held to about 40 volts. This was deemed quite satisfactory.

The surge suppression equipment was built for MSE by Lightning Eliminator Associates.

PLASMA TEMPERATURE SENSOR

Although it was not developed at CDIF, a discussion of special instruments would not be complete without mention of the plasma temperature sensor. Developed, installed, and operated by the staff of the MHD Energy Center at Mississippi State University, it is a Sodium D-Line Reversal Spectrometer. This microprocessor-controlled system has been used to monitor average plasma temperature in the combustor nozzle and diffuser sections of the test train. It has provided valuable reference data for the process modeling work of the MSE Project and Test Engineering Division.

This system is reported in detail in Session A, Temperature. We here express our gratitude to the Center for their continuing contribution to the CDIF. We hope this joint effort may become a model for other ventures with the many outstanding instrumentation and control groups working with fossil energy processes.

COMPUTER PROCESSING OF EXPERIMENTAL DATA FROM THE COAL GASIFICATION PDU

E.Tyrkiel, J.Dul, R.Cudnok

Institute of Nuclear Research
Department of Plasma Technology /18/
05-400 Otwock / POLAND

INTRODUCTION

The paper is composed of two parts, both dealing with the utilization of a computer in the investigations of a coal gasification process. The first part covers the introductory phase of a computer processing of the experimental data obtained from the coal gasification Process Development Unit /PDU/. The unit has been operated at the Institute of Nuclear Research in Świerk since 1978. In the second part the theoretical computer model of an entrained flow gasification process is shortly presented. The model is being developed to assist in the evaluation of the design and to optimize the operation of the PDU.

PDU RESEARCH PROGRAM

The unit was erected and put in operation to investigate the conversion process of pulverized coal with preheated air in an entrained flow system into low BTU gas /~1000 kcal/scm/. It was designed to convert 20 kg of Polish bituminous coal per hour at the near atmospheric pressure.

The general objective of the current program is a larger scale development of the process utilizing the method of an entrained flow gasification. The evolved process is to be used as a part of a system for producing gas for the combined cycle power plants operating on coal derived fuels. There is also a possibility of gasifying the coal by the combustion gases laden with seed and slag exhausted from the combustion chamber of the installation. It will simulate the conditions prevailing at the outlet of the MHD generator /method of combining MHD generator with chemical regeneration/.

Pursuant to this general objectives the PDU is being operated to examine the most important aspects of the process, i.e.:

- calorific value of the gas produced;
- carbon conversion ratio;
- thermal balance in order to estimate the efficiency of the scaled-up installation;
- the factors influencing the long-term operability of the process /the data of all key process variables and their effects on the characteristics of the process/.

Therefore, at the present stage of the investigations the great activity is intended to assure the direct and rapid collection, processing and recording of the experimental data obtained from the individual gasification runs of the PDU. In the near future the PDU will be equipped with a system of automatic on-line data handling with the

HP-1000 computer. The Data Aquisition System will be able to accept about 120 input signals from the test train and facility instrumentation. The on-line calculations will be performed, the data displayed on call, and recording using plotter or printer, as required.

COMPUTER PROCESSING OF THE EXPERIMENTAL DATA

During the period covered by this report a computer program in FORTRAN EXTENDED for determining the main parameters of the gasification process has been developed, and off-line calculations for a series of the PDU experimental runs have been performed by means of the CYBER 70 as well as of the HP-1000 computer. A BASIC version of the program has been also worked out. It will serve as a basis for later use in the system of automatic on-line data handling.

The algorithm of calculations has been formulated in compliance with the design and measuring equipment of the PDU. The program input data involve:

- physical constants and PDU design parameters;
- proximate analysis of the coal powder;
- flow, pressure and temperature distributions in the system for the chosen moments of operation time;
- ambient parameters;
- chromatographic analysis of the outlet gas composition /also for the chosen moments of operation time/.

The exact number of indispensable input data depends on the way in which the PDU is operated. The following basic possibilities of operation are provided for the PDU stand:

- one-stage process /gasification/ with a single coal feeding;
- two-stage process /combustion + gasification/ with primary and secondary coal feeding;
- one- or two-stage process with enrichment of the preheated air with oxygen and/or steam.

An example of the input data set is shown in Table I. It corresponds to two-stage process with preheated air without enrichment. In Table I the method of measurement of the individual input parameters is also shown. The reference marks in the last column indicate the corresponding points of measurements on a scheme of the PDU stand /Fig.1/.

As a result of the program execution the cumulative quantitative characteristics of the gasification process is obtained. In Table II the examplary printout from the HP-1000 computer is presented.

The algorithm is being developed to calculate material and heat balances of the stand.

Table I. Program input data

O.n.	Kind of data	Unit	Method of measurem.	Place of meas.
1	Experiment number	-		
2	Date	d,m,y		
3	Number of measurements	-		
4	Time of individual measurements	h,min	clock	lab.
5	Normal densities of gas components	kg/scm	from tables	
6	Gross heating values of gas comp.	kcal/scm	"	
7	Net heating values of gas comp.	kcal/scm	"	
8	Table of Reynolds number values	-	"	
9	Table of flow-number values for orifices	-	"	
10	Diameters of orifices	mm	PDU design	K_v,K_p
11	Atmospheric pressure	mm Hg	barometer	lab.
12	Rate of primary coal feed	kg/h	feed.marking	lab.
13	Rate of secondary coal feed	kg/h	"	"
14	Moisture of coal	w%	phys.analysis	phys.lab.
15	Gross calorific value of coal	kcal/kg	bomb calorim.	phys.lab.
16	Flow rate of main air	cu.m/h	rotameter	1
17	Static pressure of main air	atm	pressure gauge	2
18	Δp on the air orifice meter	mm H_2O	U - tube	3
19	Air orifice gauge pressure	atm	pressure gauge	4
20	Flow rate of primary auxiliary air	cu.m/h	rotameter	5
21	Static pressure of primary aux. air	atm	pressure gauge	8
22	Flow rate of secondary auxil. air	cu.m/h	rotameters	6,7
23	Static pressure of second. aux. air	atm	pressure gauges	9,10
24	Inlet air temperature	C	thermometer	11
25	Preheated air temperature	C	thermocouple	12
26	Δp on the gas orifice meter	mm H_2O	U - tube	13
27	Gas orifice gauge pressure	mm H_2O	U - tube	14
28	Outlet gas temperature	C	thermocouple	15
29	Outlet gas composition /by volume/	%	chromatographic analysis	16-lab.

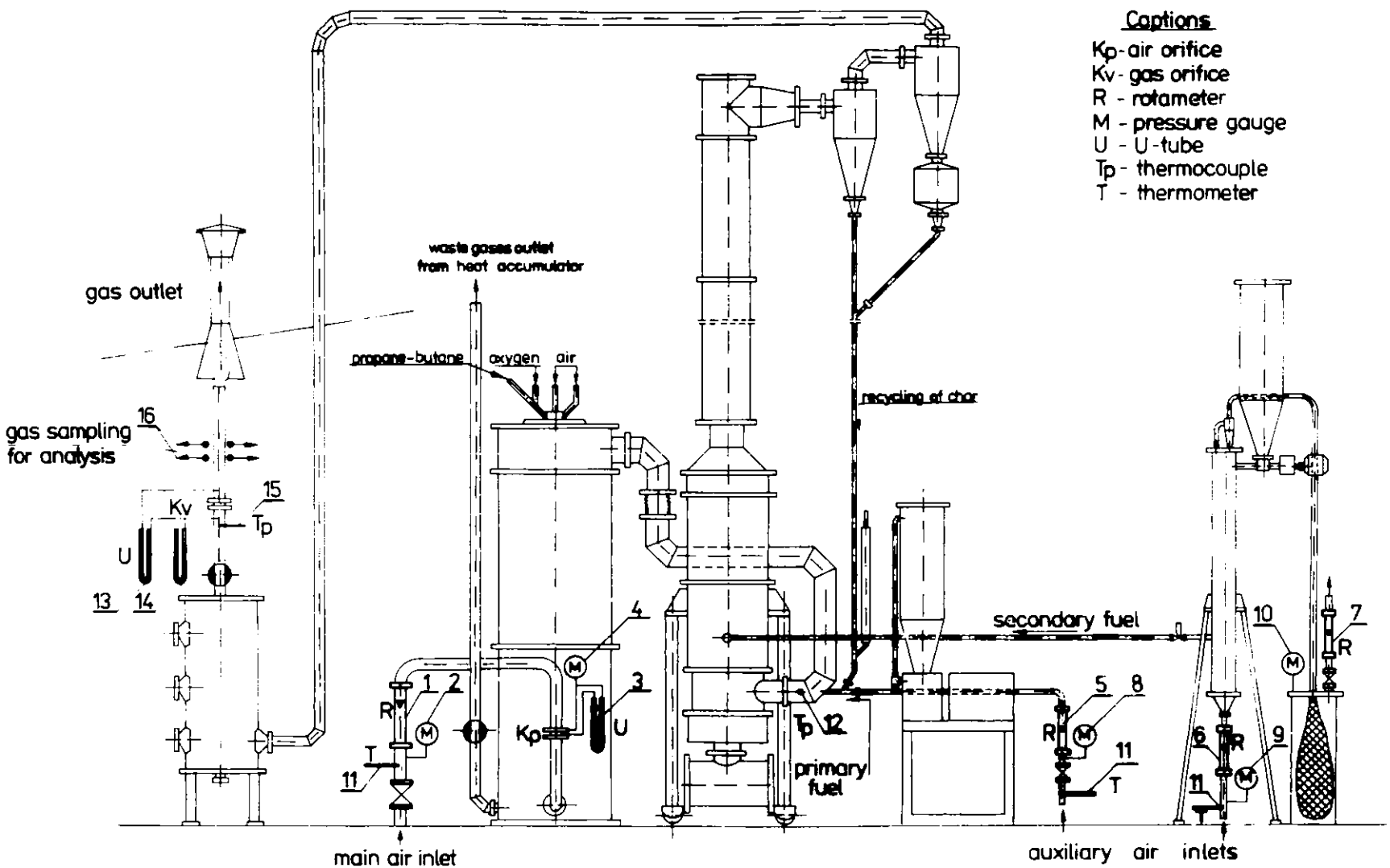

Fig.1. Scheme of measurements of flow and pressure distributions in the PDU system

Table II. Characteristics of the experiment

RESULTS OF THE EXPERIMENT OF COAL GASIFICATION
No 20 OF 19.11.1980

MOISTURE OF COAL WR = 3.90 %
GROSS CALORIFIC VALUE OF COAL QSCR = 4355.3 kcal/kg

P A R A M E T E R S		Time:	13.20	13.30	13.40	13.50	14.00	14.10	14.12	14.15
RATE OF PRIMARY COAL FEED	CR1	kg/h	11.40	11.40	11.40	11.40	11.40	11.40	11.40	11.40
RATE OF SECOND. COAL FEED	CR2	kg/h	9.00	9.00	16.80	19.50	20.80	20.80	20.80	20.80
RATE OF MAIN AIR - FLOW M.	GR	kg/h	72.78	64.05	64.05	71.22	71.22	53.59	46.41	39.36
RATE OF MAIN AIR - ORIFICE M.	GK	kg/h	72.72	64.15	65.11	70.50	70.50	53.48	41.89	37.12
RATE OF PRIMARY AUXIL. AIR	GS	kg/h	6.86	6.86	6.86	6.78	6.78	6.78	6.78	6.78
RATE OF SECOND. AUXIL. AIR	GF	kg/h	.20	.20	.20	.20	.20	.20	.20	.20
TOTAL RATE OF AIR	GP	kg/h	79.84	71.11	71.11	78.20	78.20	60.57	53.39	46.34
AIR:COAL RATIO	Ai	kg/kg	3.91	3.49	2.52	2.53	2.43	1.88	1.66	1.44
DRY GAS COMPOSITION /BY VOL./	UI									
CO2		%	11.50	11.00	11.00	12.50	9.50	9.00	9.50	8.50
CO		%	15.00	14.50	20.00	17.50	17.50	20.50	20.00	21.00
H2		%	4.50	4.00	7.00	6.50	7.00	8.00	9.00	10.00
CH4		%	0.00	.70	.50	.40	.90	1.50	1.00	1.60
O2		%	0.00	0.00	0.00	0.00	0.00	0.00	0.00	0.00
N2		%	68.00	70.00	63.00	62.00	64.00	62.00	61.00	60.00
T O T A L :		%	99.00	100.20	101.50	98.90	98.90	101.00	100.50	101.10
GAS OUTPUT RATE	VGN	Scm/kg	69.07	61.17	66.36	72.42	75.35	61.03	55.73	53.58
GAS OUTPUT DENSITY	RN	kg/Scm	1.27	1.28	1.27	1.25	1.22	1.23	1.22	1.20
GAS PRODUCTION BY VOLUME	VG	Scm/kg	3.39	3.00	2.35	2.34	2.34	1.90	1.73	1.66
GAS PRODUCTION BY MASS	GG	kg/kg	4.30	3.85	2.98	2.93	2.85	2.33	2.10	2.00
GAS:AIR RATIO	A2	kg/kg	1.10	1.10	1.10	1.16	1.10	1.24	1.27	1.39
YIELD OF COMBUSTIBLE GAS	VGC	Scm/kg	.66	.58	.65	.57	.59	.57	.52	.54
GAS HEATING VALUE, NET	QG	kcal/Scm	568.65	600.55	826.65	729.75	785.35	952.95	920.80	1028.0
GAS HEATING VALUE, GROSS	QSG	kcal/Scm	590.25	626.54	865.10	764.83	827.60	1005.9	973.70	1091.5
EFFICIENCY OF COAL GASIFIC.	ETA	%	45.89	43.14	46.74	41.16	44.47	43.77	38.69	41.70
TEMPERATURE OF PREHEATED AIR	TP	C	931.	907.	889.	889.	846.	825.	845.	868.

COMPUTER MODELLING OF THE PROCESS

To assist in the evaluation of the design of the PDU and also to serve as a tool in optimizing the operating phases of the program a computer model for predicting the performances of the system is being developed.
The model, while not completed yet, was formulated /Ref.1/ as a one--dimensional, steady-state model of an entrained flow combustion or gasification of pulverized coal. It includes the following basic phenomena which take place in the gasifier:

- one-dimensional fluid mechanics /movement of polydispersed coal particles and the gas/;
- coal reaction processes with the emphasis placed on the pyrolysis and heterogenous char oxidation by multiple oxidizers;
- gas-particle interactions with appropriate diffusion and kinetic rates;
- gas-phase reactions assumed to be in local chemical equilibrium;
- heat exchange within the reactor with the assumption that the process is adiabatic /it includes heat of reaction processes, heat transfer between gas and particles, particle-wall radiation and gas-wall thermal conduction/;
- recirculation within the reactor for a specified input /free jet/.

The resulting model predicts thermal, physical and chemical histories for both the gaseous and polydispersed particle phases. The solution technique uses step-by-step method /zone method/ with an iterative approach for the solution of non-linear gas-phase chemical equations coupled with a number of linear equations.

The modelling program has been developed in FORTRAN EXTENDED and designed for use with the CDC-CYBER 70 computer. Recently a great effort has been made to adapt the program for being used with the HP-1000 computer. The plotting routines, which are used for convenience in interpreting the output, have been also included.

The model assumes 10 coal particle sizes covering the diameter range 5 ÷ 150μ, with a Rosin-Rammler fractional distribution. The formulation of a two-step coal pyrolysis is based on the model of Gannon, Stickler, Kobayashi /Ref.2/; the heterogenous char oxidation controlled by diffusion is modelled according to Spalding /Ref.3/, and the recirculation process - upon the theory of Thring and Newby /Ref.4/.
Most of the data indispensable for calculations of physical, kinetic and thermodynamic parameters relating to coal, slag and gas mixture are taken from the literature and included in the algorithm of the program.

The program input data define the chemical composition and inlet proportions of coal and gasifying medium as well as the physical conditions of the process /inlet temperatures and overall pressure/. An example of the input data set is shown in Table III. It corresponds to one-stage gasification of a Polish bituminous coal[x/] by the preheated air enriched with 30% steam. The composition of the recirculating gas is an estimated one. An iterative approach for calculation of the composition of gas in the recirculation zone is being developed.

In the Fig.2 some of the results are presented. The following parameters: gas temperature TG, coal particle temperature TP /for the 3 chosen fractions: 10μ, 75μ, 150μ/, weight fraction of ash free coal MAF /for the same fractions/ and the gas composition /by volume/ are shown as functions of the axial location in the gasifier. The plot-diagram

---

x/ at the present stage of calculations sulphur content in the coal is included in ash content

is obtained from the HP-1000 computer.

The generalized nature of the model allows for calculations of both coal combustion and coal gasification characteristics. The refinements which have been introduced recently include two stages of the process /combustion + gasification/.

Table III. Input Data for Computer Modelling Program

********** I N P U T D A T A **********		
1. total pressure [atm]		1.00
2. rate of coal feed [kg/s]		0.00277778
3. ash content in coal [weight fr.]		0.186
4. ultimate analysis of ash free coal [weight fr.]		
	C	0.741
	H	0.052
	O	0.110
	N	0.009
	S	0.000
	Moisture	0.088
5. inlet weight ratios		
	CO/coal	0.000
	CO2/coal	0.000
	H2/coal	0.000
	H2O/coal	0.300
	CH4/coal	0.000
	O2/coal	0.680
	N2/coal	2.153
6. inlet coal particles temperature [K]		300.0
7. inlet temperature of gasifying medium [K]		1100.0
8. temperature of slag fusion [K]		1703.0
9. composition of recirculating gas [weight fr.]		
	CO	0.100
	CO2	0.100
	H2	0.002
	H2O	0.110
	CH4	0.001
	O2	0.000
	N2	0.688

References

1. J.Lesiński,B.Kruszewska,E.Tyrkiel: Theoretical calculations of the gasification process of pulverized coal with the preheated air in an entrained flow reactor /in Polish/. Int.elab. of INR-Swierk, N° 0-284/XVIII/77, Nov.1977
2. R.E.Gannon,D.B.Stickler,H.Kobayashi: Coal processing employing rapid devolatilization reactions in an MHD power cycle. 14-th Symposium on Engineering Aspects of MHD, Tennessee, 1974
3. D.B.Spalding, Proc.Inst.Mech.Engin., 168 /19/, 545-570, 1954
4. M.W.Thring,M.P.Newby, IV-th Int. Symposium on Combustion, 789-796, 1953

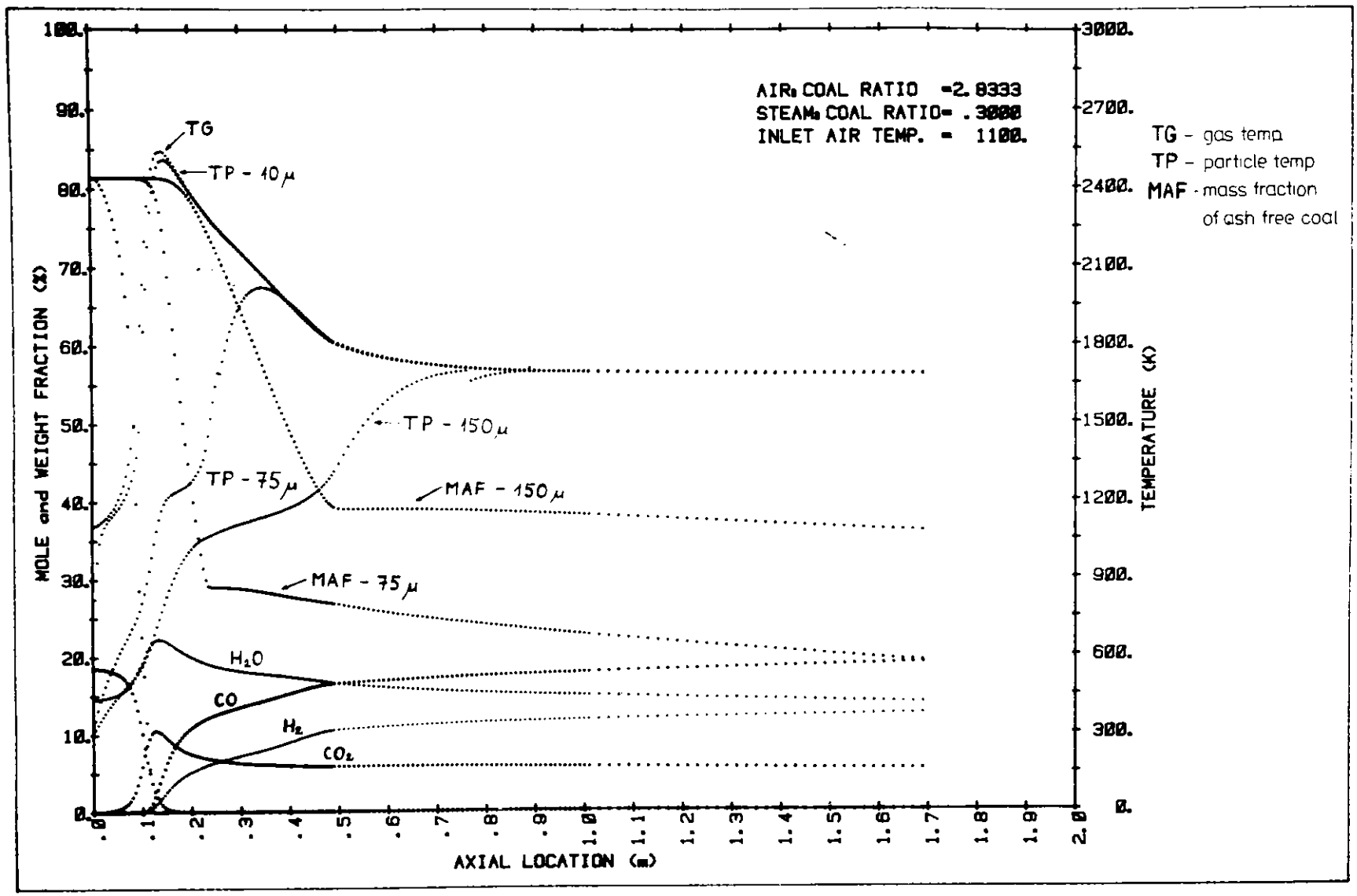

Fig.2. Some of the results of the computer modelling program

SOME ASPECTS OF THE DYNAMIC BEHAVIOUR AND CONTROL OF THE LURGI MOVING BED COAL GASIFIER

J. J. Albrecht and R. Reimert
Lurgi Kohle und Mineralöltechnik GmbH
Federal Republic of Germany

I General remarks to the process principle of moving bed gasification

Lurgi moving bed coal gasification is a well established process to convert coal into gas for a variety of applications such as production of synthesis gas or fuel gas.

Figure 1 shows a schematic diagram of a Lurgi gasifier applied in a combined power cycle demonstration plant; figure 2 shows British Gas Corporation/Lurgi slagging which has recently been developed by British Gas Corporation in cooperation with the Lurgi Company.

Common process principle of all varieties of moving bed coal gasification is the countercurrent movement of coal and gasification agent in the reactor. Coal is fed via automatically operated coal locks and a rotating coal distributor on to the moving bed. The coal bed moves continuously downward due to the consumption of solids by the reaction in the lower part of the reactor and the removal of ash. In the case of "dry ash" gasifier mentioned above, all ash is removed as a solid, slightly cinkert material; in the slagging gasifier ash is removed as liquid slag which is subsequently quenched into solid glassy frit.

From a process point of view particular features of the Lurgi moving bed gasifier are

- large residence time of the solid reactant. Under normal operating conditions solid residence time is $t_s > 2000$ s as compared to the gas residence time = $t_g > 10$ s.

- The control of coal feed to the reactor is not directly coupled to the steam-oxygen feed to the reactor. Due to the construction principle of the reactor, a constant bed height is maintained automatically at all times. This particular feature removes one of the more difficult control problems in gas-solid reactors.

Speaking about dynamics and control of these reactors, it is evident that in commercial applications the demands on the performance of the gasification reactors are to a great extent dictated by subsequent process steps such as e.g., synthesis reactors.

As an example, figure 3 presents schematically very simplified main control of gasification section of the Sasol II plant, which converts coal via gasification and Fischer Tropsch synthesis into liquid fuel. In this case the synthesis reactor controls the overall product gas flow and indirectly via pressure control the input of gasification agent to individual gasification reactors. Here we see clearly the requirement of good load following capabilities for commercially applied coal gasification.

This statement applies in particular to highly interconnected systems such as e.g. coal gasification integrated in a combined power cycle plant.

II Experimental results of dynamic tests at the air blown gasifier

Figure 4 shows the schematic process flow sheet of the steag combined power plant which had demonstrated the applicability of the air blown Lurgi gasifier for production of a low BTU-gas, which is suitable as a gas turbine feed stock.

A more detailed description of the working principle of this plant is given e.g., in a publication by Wien and Heyn (1).

According to demands on power output the gasifier output is required to follow set point changes in an minimum of time without impairing operational safety. In order to investigate the gasifier load following capabilities several experiments have been carried out. Figure 5 shows an example in which the steam/air feed to the reactor is changed continuously along a ramp by app. 3% change per minute. We notice, that the level of fluctuations of process variables increases slightly, however, no lasting effect could be observed.

Figure 6 represents a case in which the gasifier is started up almost instantaneously from a "hot stand by" of some hours duration. "Hot stand by" is defined here by gasifier operation with a gas production of less than 5% of nominal value. In both examples -- this and the previous picture -- the air-steam input into the gasifier had been manipulated manually. Gasifier pressure is still controlled automatically. Although not shown in figure 5 and 6 pressure control is not much affected by load manipulations. In general, the composition of the feed of steam and air is controlled using a ratio controller with steam as driver.

III Experimental results of dynamic tests at the British Gas/Lurgi slagging gasifier at Westfield

The capability of large load changes has recently also been demonstraced on the British Gas/Lurgi slagging gasifier at Westfield. Figure 7 shows an example for a step change of app. 30% in the feed of gasifications agent -- in this case steam and oxygen. As in the previous example of the air blown gasifier steam and oxygen are coupled using simple 3-term ratio control. Due to the low residence time the gas production follows almost instantaneously the steam/oxygen input. Again there is no noticeable effect on pressure control.

As expected continuous load changes lead to similar result (figure 8). All dynamic tests so far proved, that load upsets are easily tolerated. Results of a selection of representative experiments at the dry ash and the British Gas Corporation/Lurgi slagging gasifier are presented in figure 9. Further data from dynamic tests at the slagging gasifier are given in a recent paper by Sharman and Scott (2).

Based on load following requirements for combined power cycles Sharman and Scott presented a graph which shows that the moving bed gasifier responds faster than necessary over the full range of required load changes.

Up to now exclusively conventional 3-term feedback control has been applied to commercial or demonstration scale gasifier. Despite the relatively high level of statistical fluctuations, which are characteristic for some dependent variables of moving bed gasification, conventional controller proved to be capable of fulfilling all operational requirements.

Recent tests on the slagging British Gas Corporation/ Lurgi gasifier have shown, that there is scope to still improve conventional feedback control of gasifier operation. Tests so far had been carried out using completely separated feedback control loops for gasifier pressure and steam oxygen flow control (figure 10). In this case the flow of product gas fluctuates slightly according to momentaneous statistical variations of gas and coal movement in the reactor. Alternatively, a control set up has been tried, which eliminates product gas flow variations by manipulating the set point of the steam-oxygen control. Figure 10 presents the gasifier response to the switch over from one control mode to the other during normal operation. This example shows, that even small fluctuation of the gasifier output are effectively eliminated at the expense of steam oxygen flow variations. It should be noted, that step-and ramp changes can be just as accurately performed in this control mode as reported earlier.

In recent years advanced control configurations such as optimum feed forward control or adaptive control have been developed for applications in chemical engineering. These advanced techniques have not yet been applied to the Lurgi coal gasification process. In view of the favorable results from tests using conventional feedback control it appears still undecided if advanced computer control will make as much impact as in other fields.

IV Safety aspects

With increasing use of commercial scale coal gasification plants aspects of safety and easy operability become increasingly important.

Obviously, for any given chemical plant it is impossible to predict and simulate all conceivable, process upsets; as a rule it can be stated, that processes, which allow sufficient time for failure identification and corrective action by the operator, are more easily handled than processes with extremely fast responses. This may contradict our statements made earlier about fast response requirements. As we see our last example, however, a fast gasifier response in combination with a large time constant for the solid reactant in a moving bed gasifier assists in stabilizing operation in a minimum of time after a process upset.

Picture 11 shows a case in which the coal feed to the reactor is momentarily stopped. As a consequence the product gas temperature rises and the operator, realizing the irregularity lowers for a short period steam/oxygen feed to the reactor. Apart from the almost instantaneous response of the product gas flow normal gasifier reactions proceed nearly undisturbed as expressed by a representative product gas concentration; this is in close agreement with results presented earlier of step- and ramp changes.

Conclusions

We have presented here some experimental results regarding the dynamics of the Lurgi moving bed coal gasification reactor. On the evidence of our experiments we see, that this type of reactor lends itself to easy manipulation.

There is obviously large scope to complement our experimental results by mathematical modelling. Given the physical and chemical nature of the process mechanistic models are necessarily extremely complex. Apart from valuable theoretical insight, which mathematical modelling may provide, applicability for plant operation appears still to be limited especailly in view of the favorable result of our simple experiments.

(1) Wien, H Heyn, K
Stand der KDV-Kraftwerkstechnik
VDI-Berichte Nr. 363, 1980, S.21-27

(2) The British Gas/Lurgi slagging gasifier
What it can do
R.B. Sharman J.E. Scott

Proceedings of
Coal Technology 80
3rd Exhibition Coal Utilization
Houston, 1980

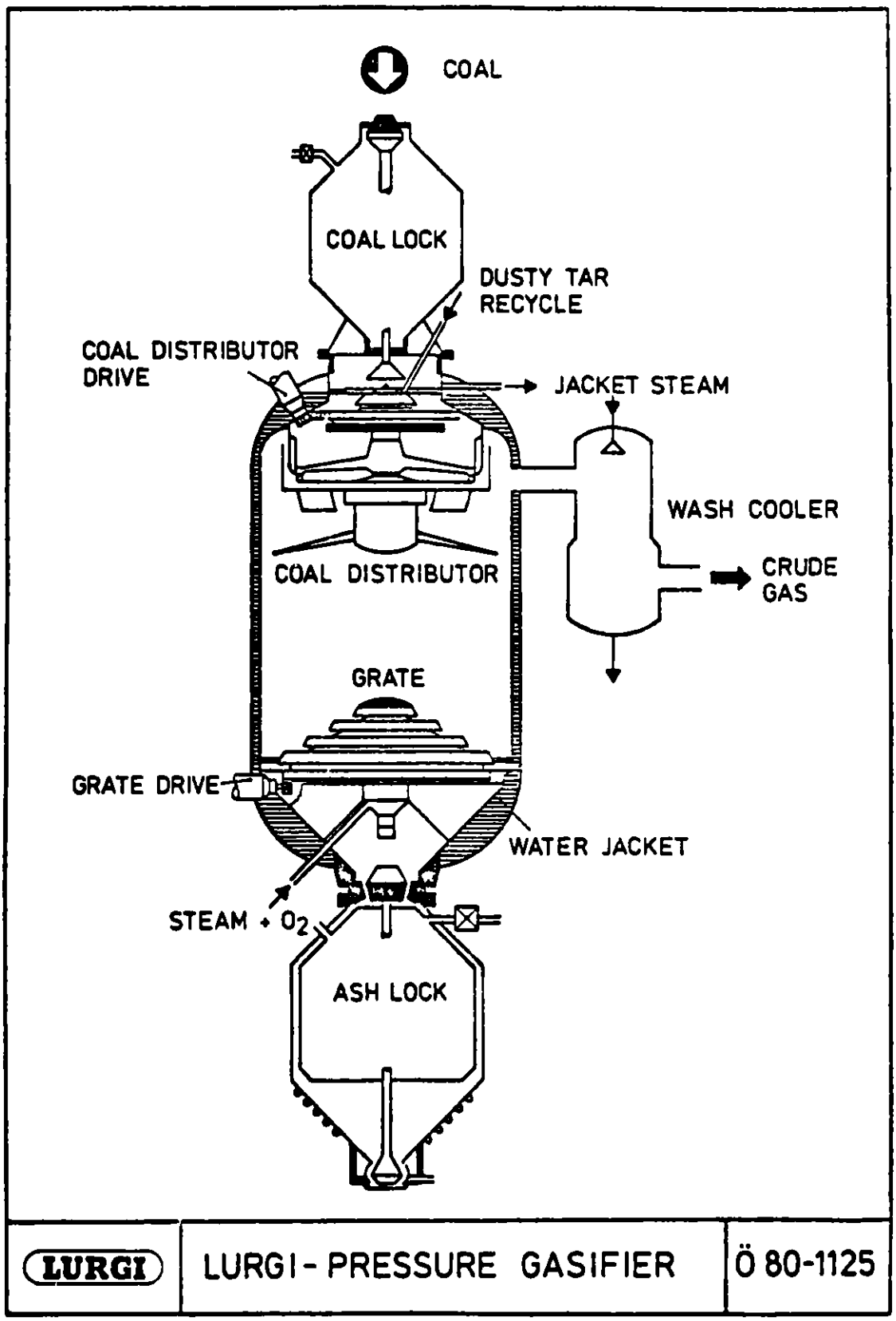
COAL
COAL LOCK
DUSTY TAR RECYCLE
COAL DISTRIBUTOR DRIVE
JACKET STEAM
WASH COOLER
COAL DISTRIBUTOR
CRUDE GAS
GRATE
GRATE DRIVE
WATER JACKET
STEAM + O_2
ASH LOCK
LURGI
LURGI - PRESSURE GASIFIER
Ö 80-1125

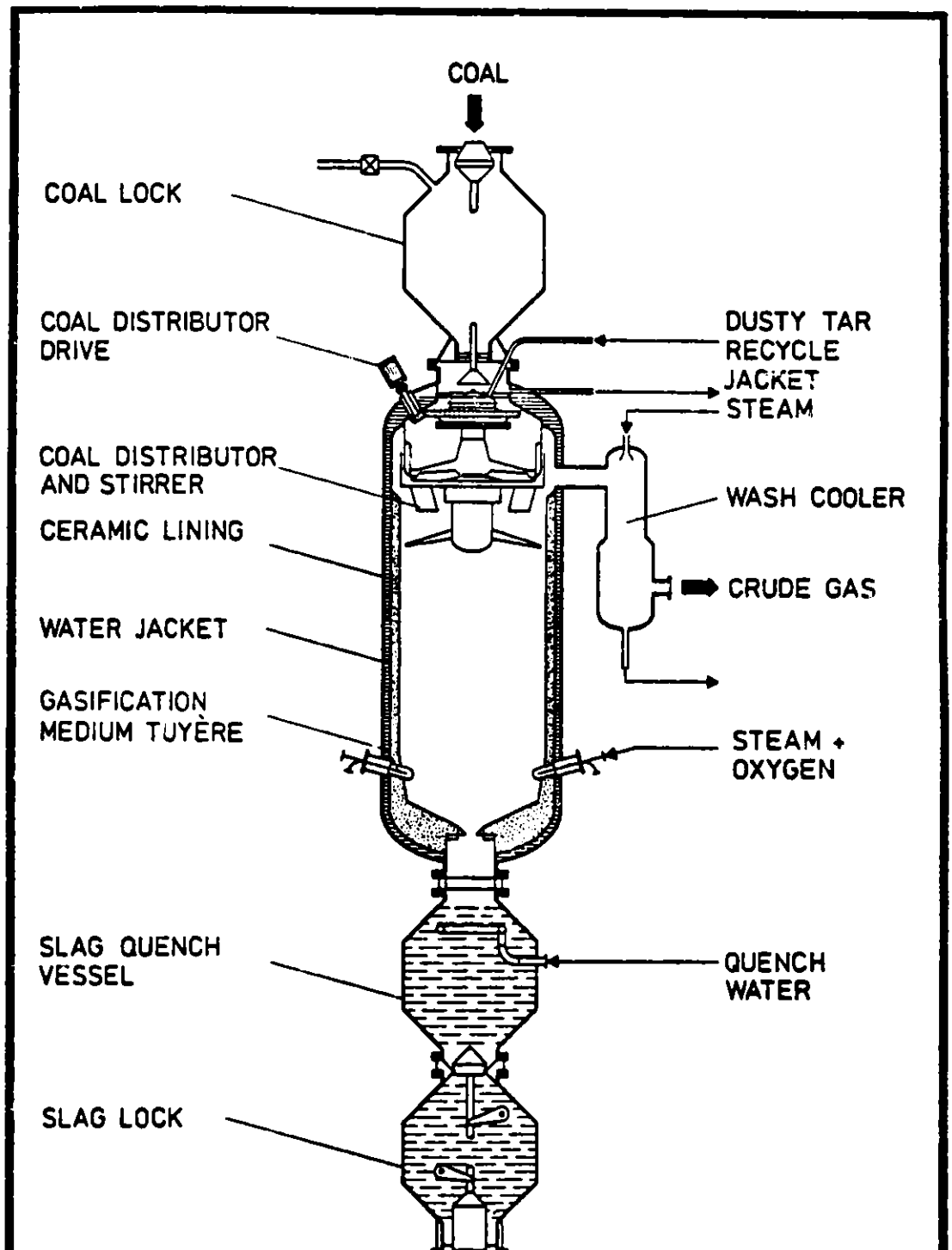
COAL
COAL LOCK
COAL DISTRIBUTOR DRIVE
COAL DISTRIBUTOR AND STIRRER
CERAMIC LINING
WATER JACKET
GASIFICATION MEDIUM TUYÈRE
SLAG QUENCH VESSEL
SLAG LOCK
DUSTY TAR RECYCLE
JACKET STEAM
WASH COOLER
CRUDE GAS
STEAM + OXYGEN
QUENCH WATER
LURGI
SLAGGING GASIFIER IN WESTFIELD
Ö 80-1124

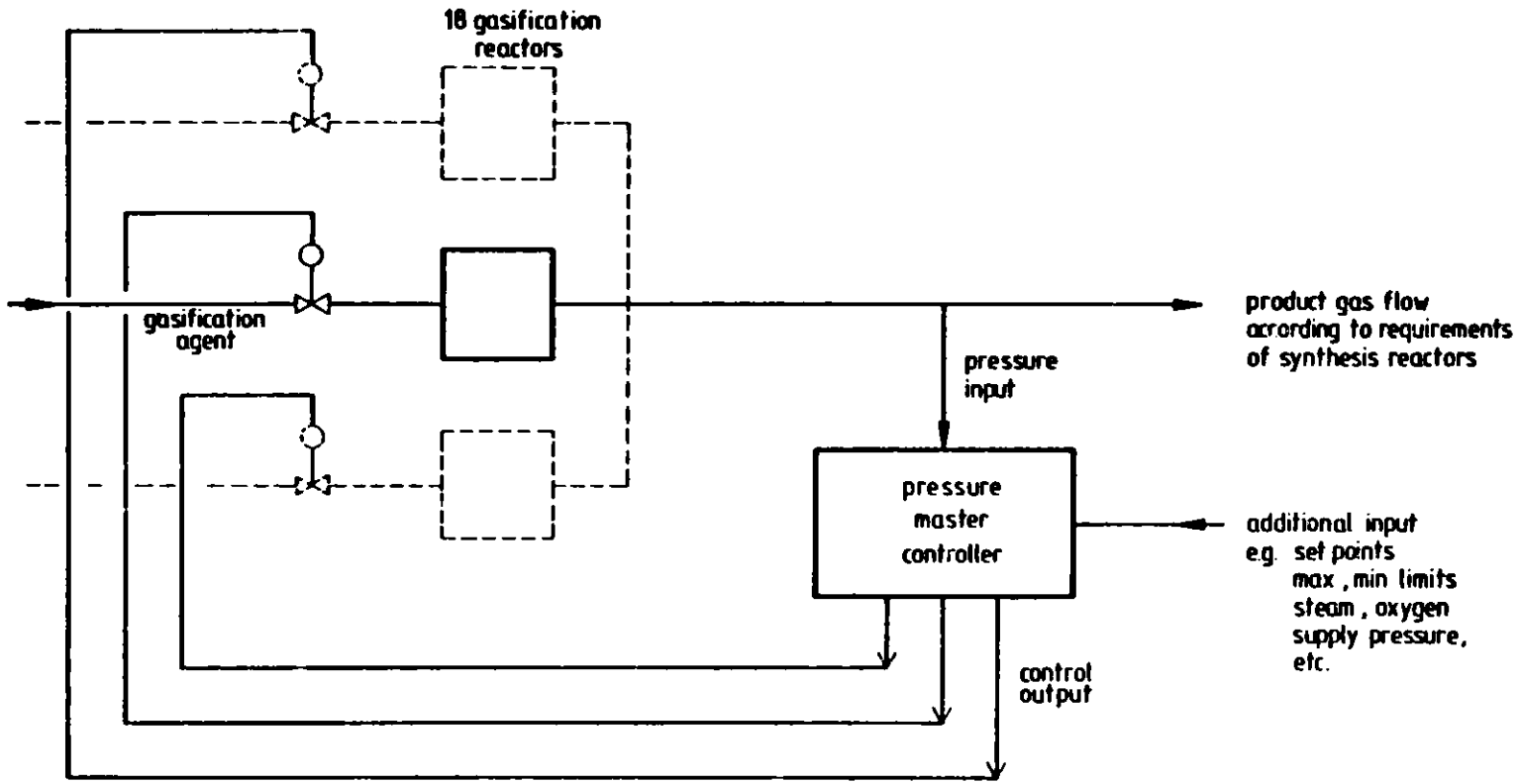

LURGI

simplified scheme of main controls for gasification section SASOL II plant

Ö81-1099

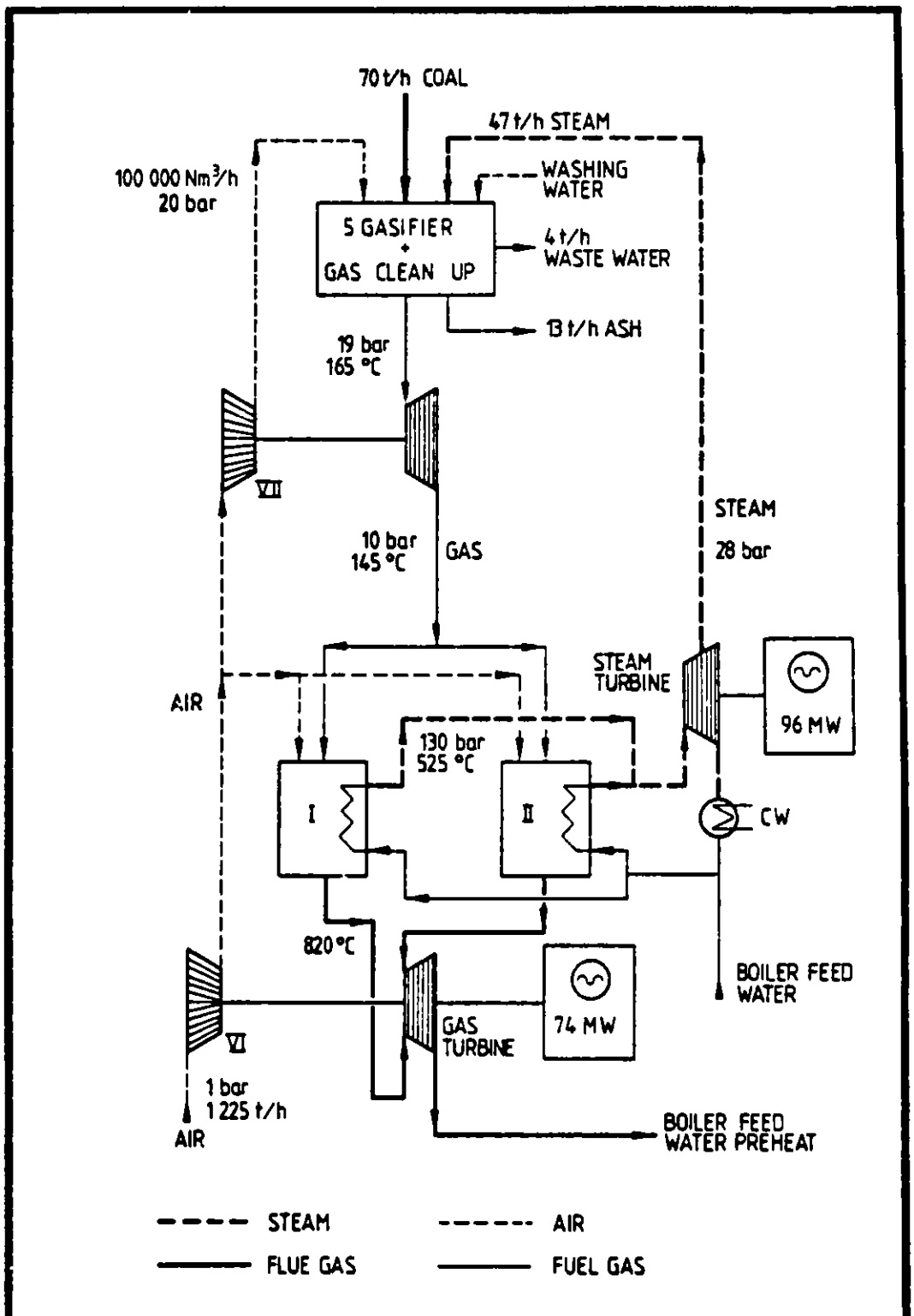
70 t/h COAL
47 t/h STEAM
100 000 Nm³/h
20 bar
WASHING WATER
5 GASIFIER + GAS CLEAN UP
4 t/h WASTE WATER
13 t/h ASH
19 bar
165 °C
VII
10 bar
145 °C
GAS
STEAM
28 bar
AIR
STEAM TURBINE
96 MW
130 bar
525 °C
I
II
CW
820 °C
BOILER FEED WATER
VI
GAS TURBINE
74 MW
1 bar
1 225 t/h
AIR
BOILER FEED WATER PREHEAT
STEAM
AIR
FLUE GAS
FUEL GAS
LURGI
combined cycle power plant
Ö81-1100

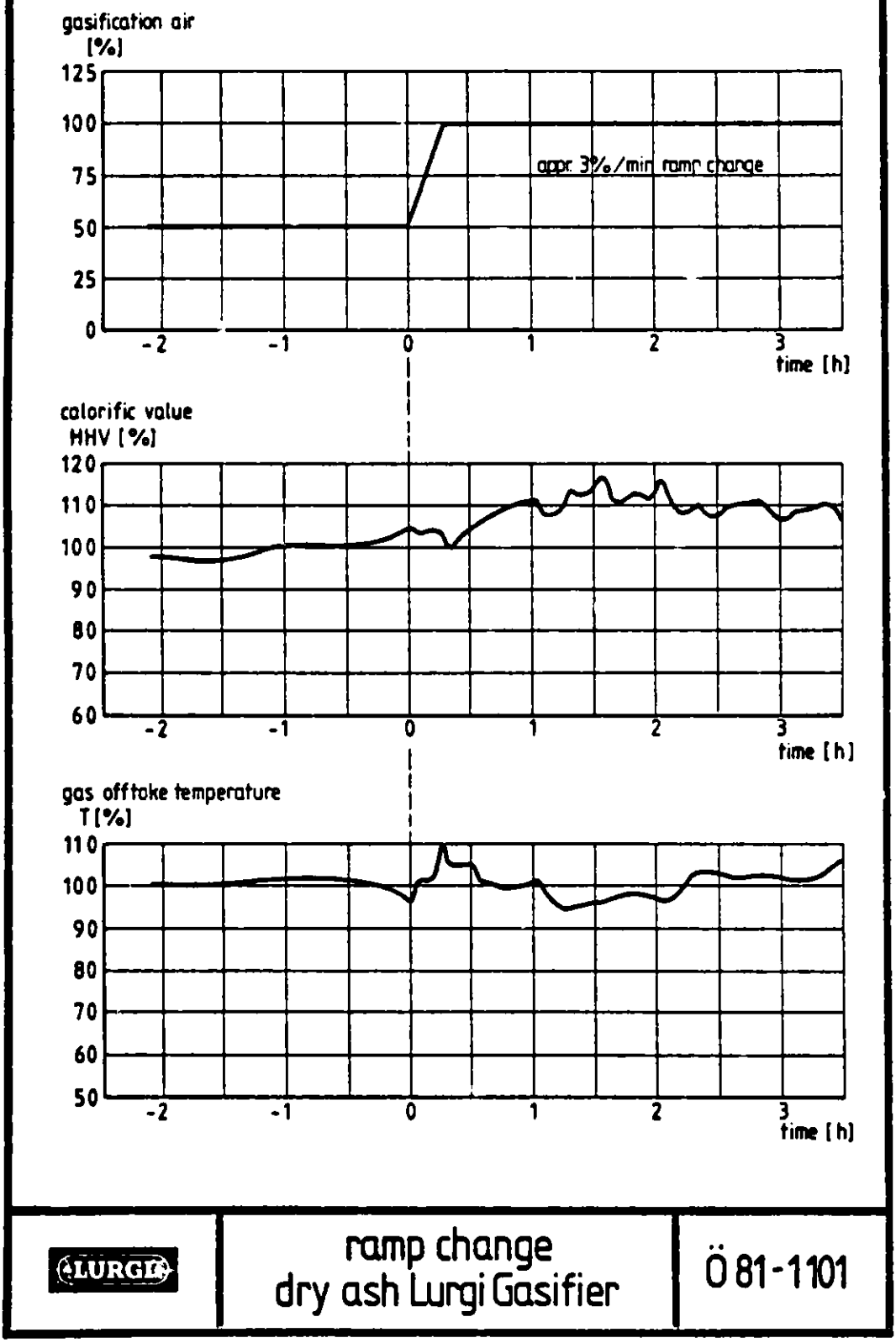

LURGI	ramp change dry ash Lurgi Gasifier	Ö 81-1101

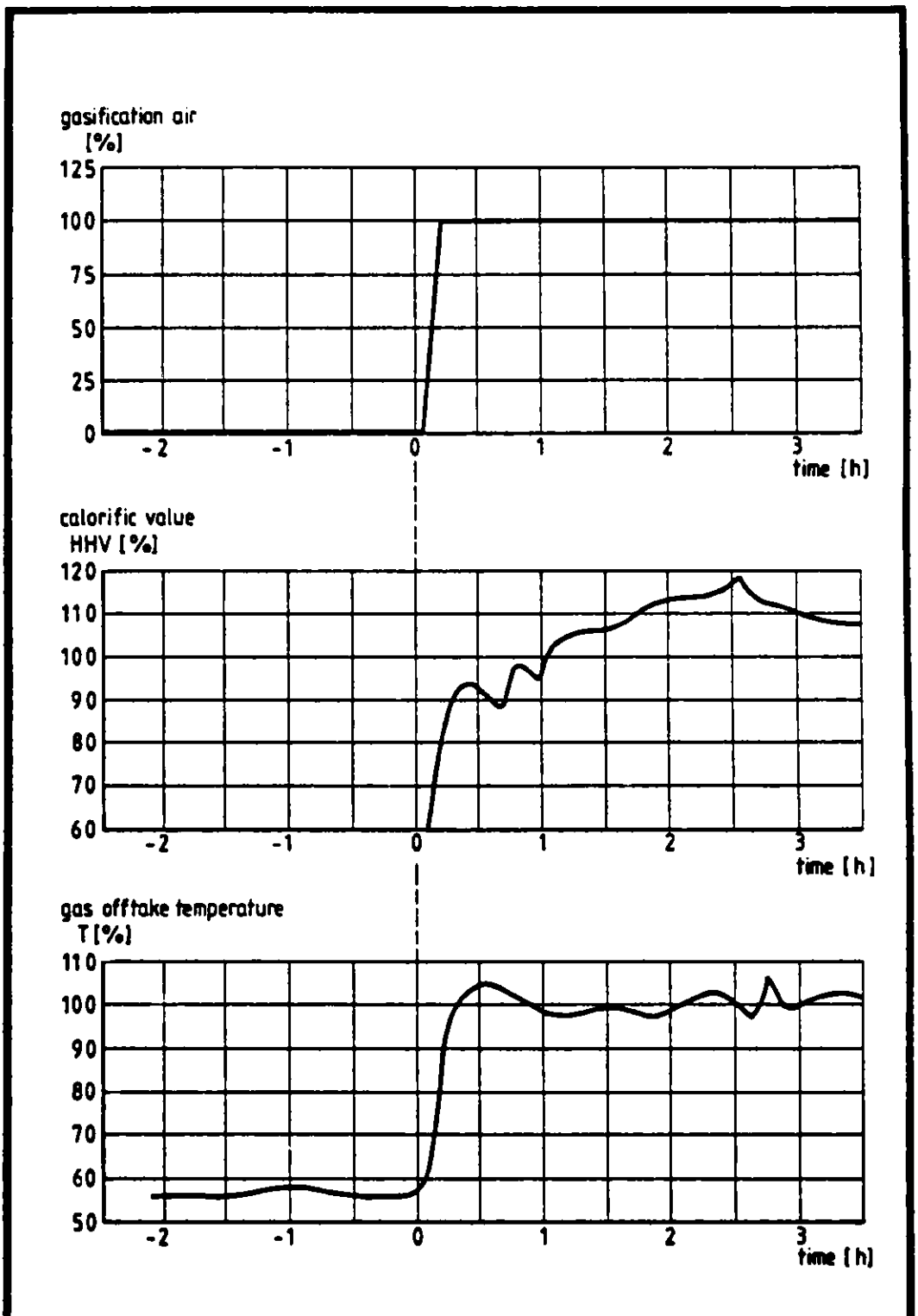

LURGI	start up from hot stand by dry ash Lurgi Gasifier	Ö 81-1102

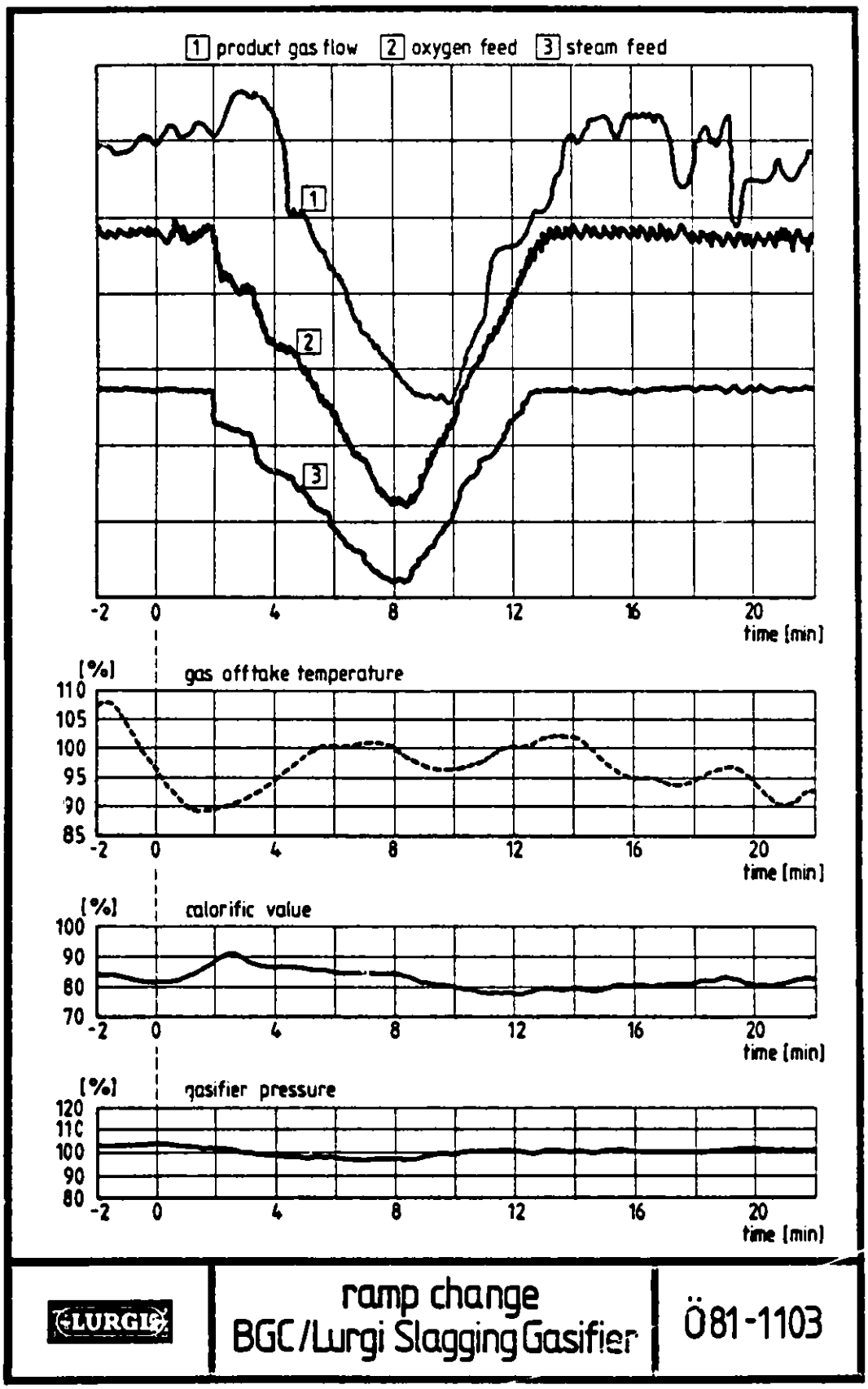
1 product gas flow
2 oxygen feed
3 steam feed
-2
0
4
8
12
16
20
time (min)
[%]
gas offtake temperature
110
105
100
95
90
85
calorific value
100
90
80
70
gasifier pressure
120
110
100
90
80
LURGI
ramp change
BGC/Lurgi Slagging Gasifier
Ö81-1103

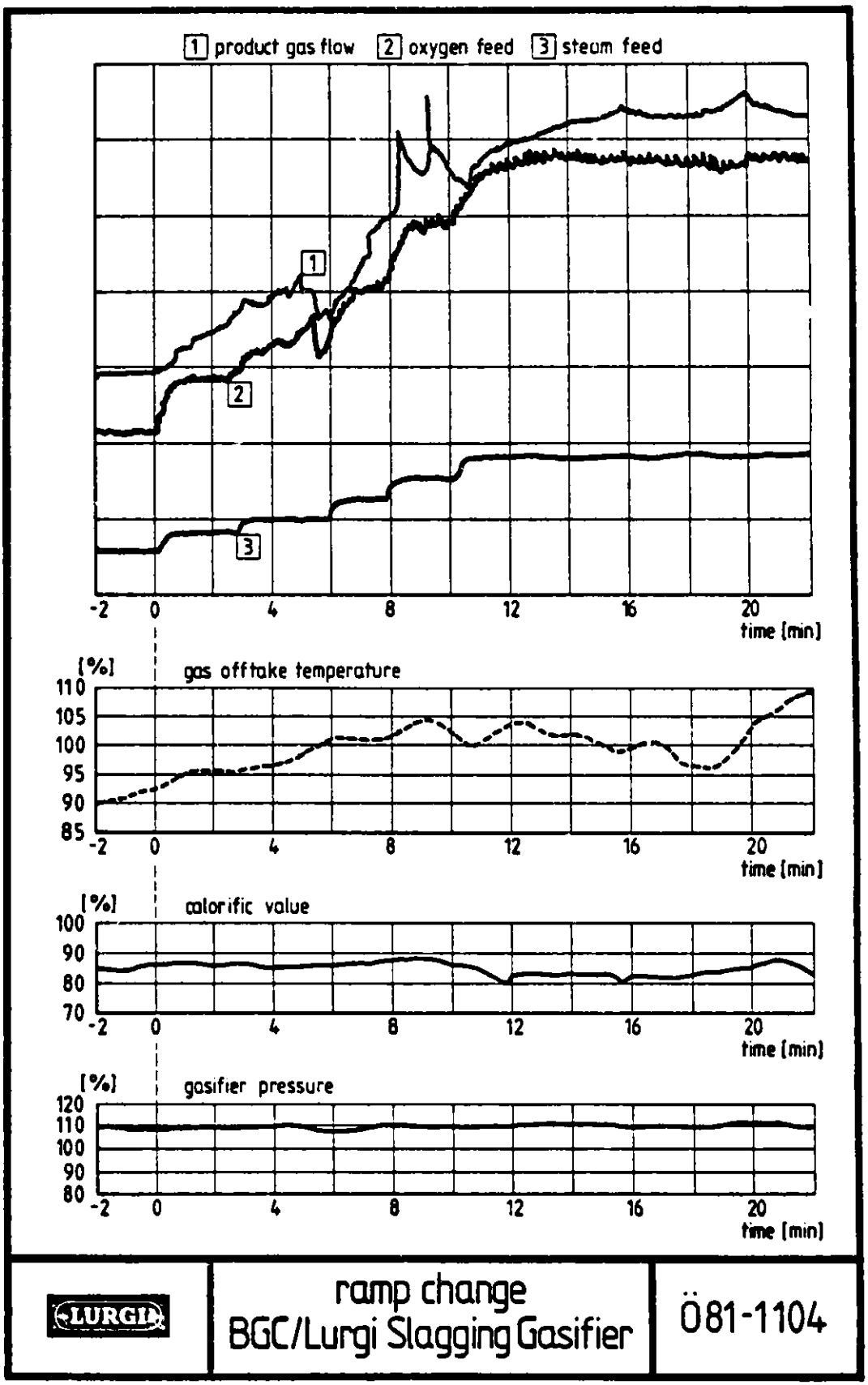

LURGI

ramp change
BGC/Lurgi Slagging Gasifier

Ö81-1104

Range	Air blown Lurgi Gasifier	Britisch Gas/Lurgi Slagging Gasifier
76 - 96 %	± 20 % in less than 0,5 min	app. 8 % /min
48 - 96 %	0,5 % /min 3 % /min	app. 10 - 20 % /min
30 - 100%		app. 3 - 14 % /min
	rapid start up 0-96 % in less than 10 min (20 % - 96 % in less than 4 min) ≙ 19 % /min	

LURGI

selection of dynamic tests
Lurgi dry ash Gasifier - BGC/Lurgi Gasifier

Ö81-1105

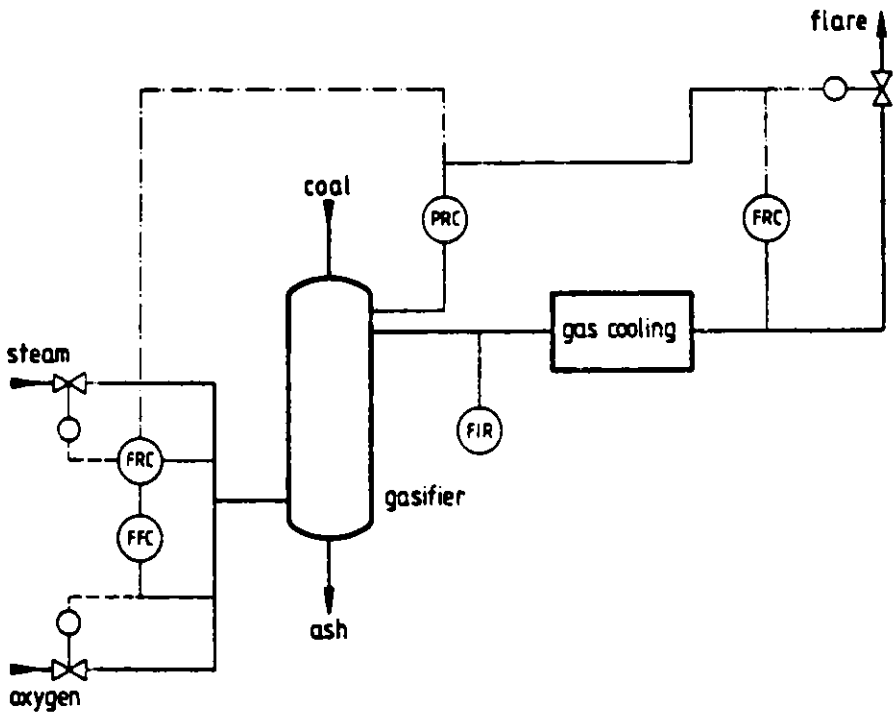

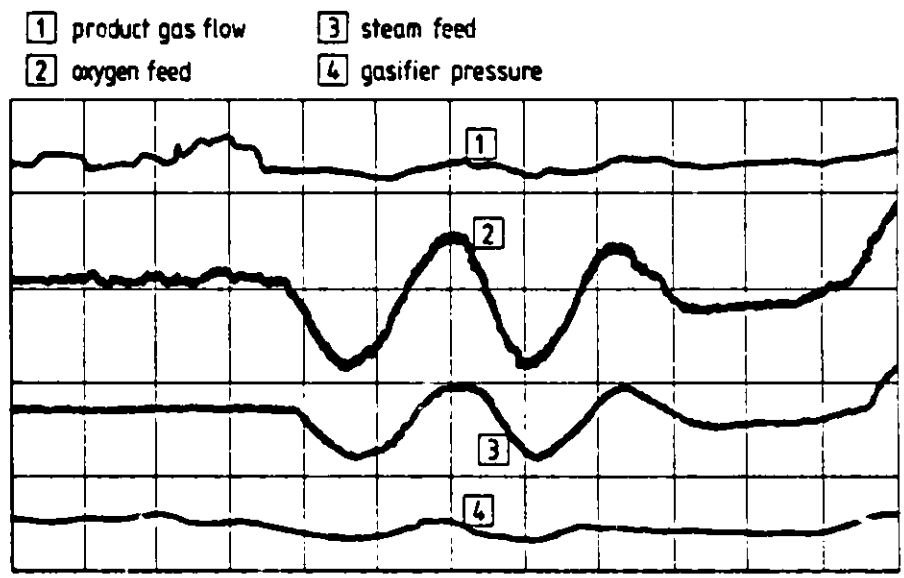

LURGI	switch of control modes BGC/Lurgi Slagging Gasifier	Ö81-1106

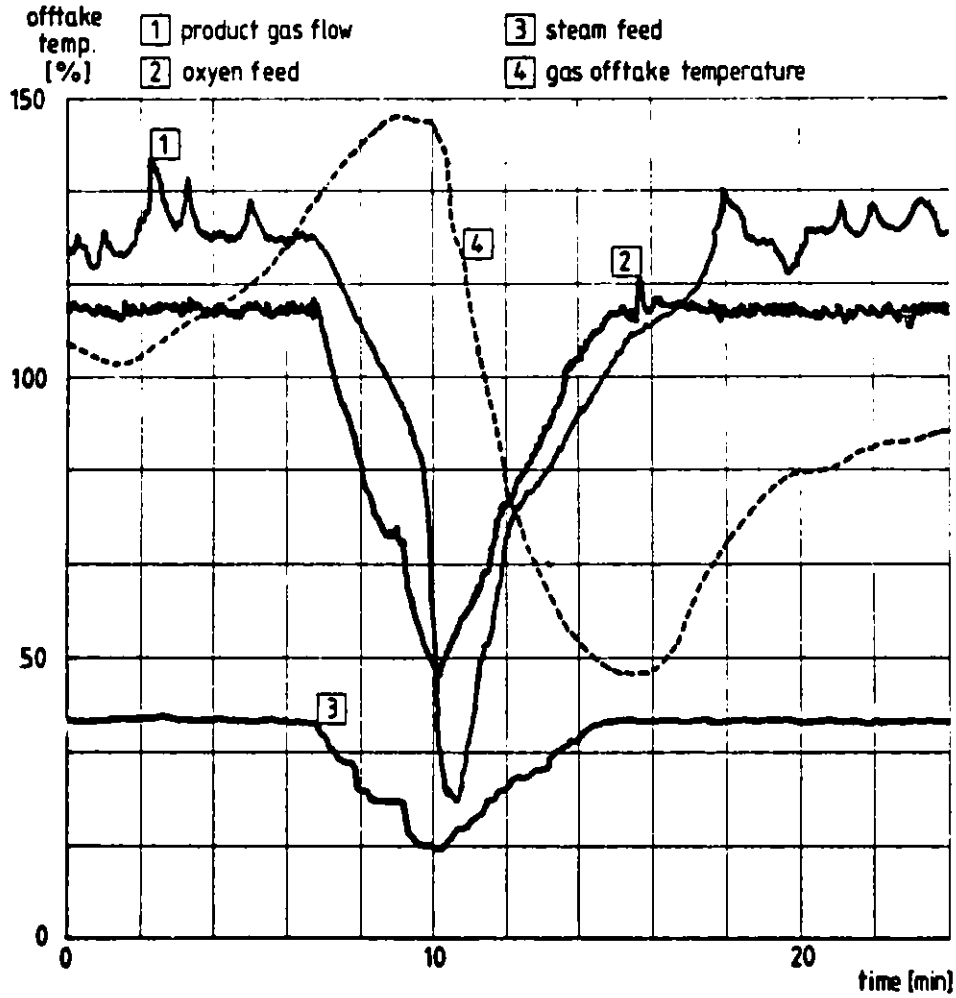

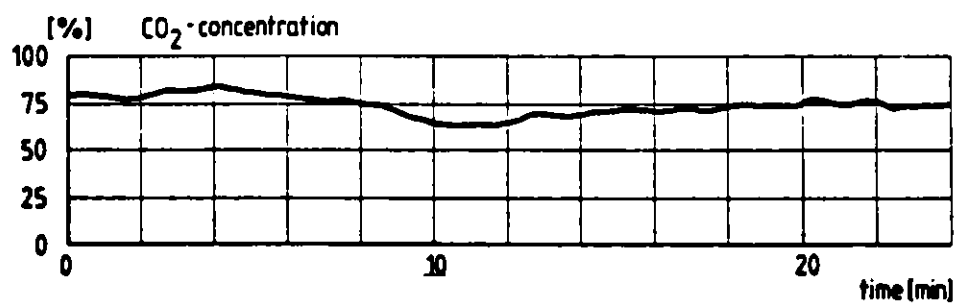

LURGI

process disturbance
BGC/Lurgi Slagging Gasifier

Ö81-1107

COMPUTER-BASED PROCESS CONTROL AND INSTRUMENTATION OF RHEINBRAUN'S HYDROGASIFICATION OF BROWN COAL

Gerd W. Felgener, Hans-Peter Gerigk and Lothar Schrader

Rheinische Braunkohlenwerke AG
Federal Republic of Germany

SUMMARY

Coal gasification plants require highly developed process control and instrumentation. In the main, these requirements might be met by using advanced electronics. It remains to be investigated in the course of the plant's daily operation to what extent modern technology will replace or practically complement established principles.

Rheinbraun has been engaged in developing and improving coal gasification processes such as the High Temperature Winkler Process and the Hydrogasification Process. Both processes are sponsored by the Ministry of Research and Technologie of the Federal Republic of Germany. The computer-based process control system is demonstrated by the example of the hydrogasification pilot plant in general; whereas lock hopper system, gas analytics as well as feed-back controlling are explained by a more detailed description.

1. INTRODUCTION

Since the 70's research in the field of coal gasification plant development has been ranking high again due to economic and political reasons. In the field of coal gasification it was possible to improve and further develop various principles which now in the 80's allow to design and construct greater plants being more efficient.

As to pressure coal gasification plants of the new generation high requirements are in particular to be met by the continous control and instrumentation techniques in order to ensure safe and reliable operation. It is shown on the one hand that various individual operational units or components of such plants have been used in industrial process engineering for some time, such as raw gas scrubbing or cryogenic gas separation, but in view of the overall management it is on the other hand of importance to ensure optimum coordination of all different operational units

within the major system taking into account the various possible interrelations and the different behaviour as to partial load. Computer-based process control and instrumentation takes a valuable share in solving these problems.

This paper outlines the process control and instrumentation system as it is currently used by Rheinische Braunkohlenwerke AG (Rheinbraun) in connection with the planning and construction of coal gasification plants. The pilot plant for hydrogasification of coal being under construction is to serve as an example.

2. RHEINBRAUN'S COAL GASIFICATION PROCESSES

Rheinbraun is engaged in mining brown coal from efficient opencast mines. The main part of the run-of-mine coal is supplied to power stations for the generation of electricity. In recent years, however, supplies for coal conversion purposes have again an increasing share in the overall production.
The 1979 data show that about 19 million metric tons of the total annual coal production of 116 million metric tons were used in coal conversion plants; primarily for the production of briquettes, meanwhile it has been increasingly used for the production of brown coal powder and brown coal fine coke. For the time being gaseous and liquid products have been produced in semi-technical pilot plants.

Rheinbraun's special center of interest as to its activities in the fields of research and development is the conversion of brown coal into gaseous and liquid products. The objective is to develop conversion technologies in pilot plants up to production maturity for further running on commercial scale.

2.1 HIGH-TEMPERATURE WINKLER (HTW)-PROCESS

The High Temperature Winkler Process has been developed for generating synthesis gas, reducing gas and hydrogen. This pressure gasification process is environmentally acceptabel; coal is converted at a pressure of about 10 bars and temperatures up to 1 100 °C with oxygen and steam being the gasification agents.
Plannings for a commercial scale demonstration plant are based on the results obtained from a pilot plant which has been operating since 1978. The design of the first construction phase includes one gasification and gas

treatment line generating gas with a capacity of about 40 000 cubic meters (STP) per hour; it is to be completed by 1984.

Three further gasification lines are to be added in the second construction phase which is to be completed in 1987; the total annual output will then be 1 billion cubic meters of synthesis gas. Our company's subsidiary, Union Rheinische Braunkohlen Kraftstoff AG (Union Kraftstoff) will use this synthesis gas for the production of methanol; synthesis gas by gasification of residual oil will thus be replaced by synthesis gas from brown coal.

2.2 HYDROGASIFICATION (HKV)-PROCESS

Hydrogasification of coal is a key process for generating methane, a substitute for natural gas (SNG).
This pressure gasification process with coal being converted in the fluidized bed with hydrogen at pressures up to 120 bars and temperatures up to 920 °C is also in accordance with environmental requirements. Development of this gasification technology started in 1973 by planning a semi-technical pilot plant having a throughput of about 500 kg run-of-mine coal per hour. This plant was started in 1975 providing the basic condition for the pilot plant (throughput 25 metric tons of run-of-mine coal per hour) how being under construction. In addition to an extension in the plant's scale (by a factor of 50) the process design too was complemented by a raw gas scrubbing line (acid gas scrubbing) with subsequent cryogenic gas separation. Lining up these individual process steps allows to test the coal conversion process from the beginning to the final specified product (methane).

Operation of the pilot plant is the last intermediate step before comissioning of a demonstration plant. In this demonstration plant scheduled for 1990 hydrogen, required for hydrogasification of coal, will be produced by HTW gasification of the residual char received in the hydrogasification plant. It is further possible to combine both hydrogasification of coal and operation of a high temperature nuclear gas cooled reactor; this allows to save about 40 per cent of the feed coal. These activities are carried out within the scope of the project "Prototype Plant Nuclear Process Heat" (Prototypanlage Nukleare Prozesswärme), in which several coal mining and reactor engineering companies are engaged.

Figure 1 shows process combinations for the gasification of brown coal. Detailed descriptions of these coal gasification plants and their inclusion in a superordinate energy conception are referred under (1), (2), (3), (4) and (5).

3. COMPUTER-BASED PROCESS CONTROL AND INSTRUMENTATION

3.1 SHORT DESCRIPTION OF THE PILOT PLANT FOR HYDROGASIFICATION OF COAL

As to process engineering the pilot plant under construction (Fig. 2) consists of 4 operational units: coal feeding, gasification, Amisol scrubbing and cryogenic gas separation. Brown coal, predried to 12 weight percent is supplied in silo trucks for intermediate storage. According to the process design the coal is subsequently dried in a spiral tube pneumatic drier; after separation from the transporting gas in a cyclone the coal is fed through two weighing hoppers and two double-locks into hoppers from where it is continuously fed into the gasifier through rotary screw feeders.

Gas required for hydrogenation is preheated to 600 °C in the H_2-heat exchanger. Further heating of the gas is carried out in the combustion chamber by partial burning of hydrogen with oxygen; subsequently the gas is fed into the gasifier where it reacts with coal in the fluidized bed.

The coal is gasified at pressures of up to 120 bars and temperatures of up to 900 °C in the gasifier lined with bricks (inside diameter 1 m, height about 8 m).

The residual char obtained is water cooled, either directly or indirectly, and discharged via lock hopper system at the lower part of the fluidized bed. The char is fed via weighing bunker into the residual char bunker for intermediate storage. Transport is carried out in silo trucks.

From top of the gasifier the raw gas (maximum throughput 15 000 m^3/h STP) is fed into the dust cyclone where about 90 per cent of the coal fines are separated; after cooling the fines are discontinually discharged via looks, and supplied into the residual char bunker.

The raw gas which is freed from dust to a large extent flows through a heat exchanger where the hydrogenation gas is preheated. After further utilization of waste heat in a waste heat boiler the gas is subject to water scrubbing in order to remove those solid particles remaining from separation in the dust cyclone.

Hydrogen sulfide, organic sulfides and carbon dioxyde are separated from the raw gas by subsequent Amisol washing.

The purified raw gas is separated by cryogenic separation into the following three fractions: methane, hydrogen and carbon monoxide plus nitrogen. Methane is given to the Methan piping network, Hydrogen is recycled into the gasifier via the above mentioned heat exchanger as hydrogenation gas. The remaining small corbon monoxid + nitrogen fraction is supplied to Union Kraftstoff.

If the gas purity does not meet the requirements of the subsequent process units, as it could be the case with starting or breakdowns, the gas will be used as fuel or flared.

The lock hopper system is supplied by nitrogen which is stored in a gasometer and recompressed. Union Kraftstoff supplies hydrogen as well as all other agents required such as oxygen, nitrogen and steam.

3.2 PRINCIPLES OF MODERN CONTROL TECHNIQUE

"Control technique" is a general term lacking precise differentiation as to all other superordinate terms. In the following the term "control technique" covers the overall range of superordinate monitoring, control and control feedback of complete systems.

On the basis of the present state-of-art as for today's established compact control technique with parallel recording, new control systems mainly including serial information on color display units are being introduced. A third kind of control techniques, combining new methods with those which have been well tested for many years, might turn out to be appropriate.

From today's point of view the compact control panel technique, based on the method of decentralised task distribution, has shown good results in the past.

These control panels show, however, certain disadvantages and sometimes even fail to be sufficient in flow shut display, information processing and lack of electronic intelligence for special fields of application as to measuring and control techniques. But these disadvantages can successfully be eliminated by process computers and color display units so that mosaic diagrams and switchboards, such as recorders were unnecessary to a large extent what would be a further advantage. The operator in the control room will in particular benefit from the combined operation of process computer and color display system being an "opening" for the process.
Today's multipurpose color display systems are equipped for versatile fields of application even with simple input devices such as light pens or key boards. Thus the "opening" will even become a "gateway" to the process reviving the operational relationship between man and machine to be controlled.

Discussions on the plant's degree of automation are to take into account that even the most foresighted planning connot prevent all possible kinds of breakdown. In the case of complex breakdowns it is therefore necessary that the control room personnel has the possibility of taking action.

On the basis of these considerations table 3 represents the basic model of a control technique for coal gasification process with information processing and display being performed by process computers and color picture screens. This basic model coordinates both the operator's work and the above mentioned method of decentralised task distribution. (Ref. 6,7,8,9).

3.3 PROCESS CONTROL SYSTEM: PURPOSE AND CONCEPTION

Though control and instrumentation systems show many differences as to technical purpose and design. There are, however, certain similarities regarding the basic problems and their possible solution.

The purpose of the control and instrumentation system is:
- to improve the plant's technical safety
- to increase the efficiency and availability of the process.

For the solution of such problems preference is given to process computers.

Therefore it is no exaggeration that the electronic process control system is given the central position as shown on figure 4.

Prior to the solution of these basic problems a lot of partial problems have to be solved by the process computer system. The first step of using the process computer in connection with the plant's operation (on line-open loop) includes data logging (analog and binary), flow sheet display with superimposition of current operational values and curve tracing and bar charts on color display units, log data documentation, filing of operational data on data carriers, computation as to balances, characteristics and efficiency as well as short-term and long-term monitoring of important components of the plant such as the lock hopper systems of a pressure coal gasification plant.

According to Rheinbraun's planning the pilot plant is to be equipped with a decentralised control system with the individual control loops and the instrumentation system having access to the overall process computer system.

The computer system design (fig. 5) includes a process computer for the control loops and a central development computer for further computation.

The process computer circuit is accessabel to important analog and binary signals. In addition the process computer is equipped with two color monitors displaying bar charts of the desired values, measured values and place values of the control circuits as well as graphical alarm indications. Furthermore, the computer is equipped with process periphals and keyboards for operating controller modules and the computer, an alpha-display, a type-writer, a matrix printer, two cartridge disk drives and a magnetic tape. The magnetic tape is the off-line interface to Rheinbraun's computer center where the stored process data are evaluated in detail.

The central development computer is accessable to a limited number of analog and binary signals. The periphal unit of the central computer includes the necessary process signal output devices a color video system with four monitors for the display of graphical plant sheets including actual values, curve tracing and bar charts, two alpha-displays, a high-speed and a low-speed printer, two cartridge disk-drives and one hard-copy device. Both computers are connected for the purpose of data exchange.

This computer system implies a certain degree of redundancy and decentralisation of the overall system. In the case of breakdown of one computer its tasks can at least partially be carried out by the other one.

The process computer system is to be adapted into the pilot plant progressively. The plant's operation will change from on line - open loop to on line - closed loop with advancing experience.

In the following some of the general problems are described in detail on the basis of three examples as to measuring technique, control engineering and feed-back controlling (Literature reference 10, 11, 12).

3.3.1 MEASURING TECHNIQUE - GAS ANALYTICS

The pilot plant requires data acquisition and evaluation of a number of gas flows (about 12 gas flow lines with 8 components) for reasons of safety, process control and plant balancing. Four multi-flow process gas chromatographs equipped with micro-computers are used to solve this problem. This allows to abtain analysis data already evaluated and relatively up-to-date. The process computer can fetch the processed data from external data storage. These values are further processed in the process computer according to superordinate algorithms. Figure 6 shows the control and data processing block diagram for a process gas chromatograph. Data control, logging and evaluation is performed centrally by the micro-computer. Even with problematic chromatograms this electronic intelligence allows to obtain a relatively perfect data evaluation. Examples are given by figures a), b) and c) of the figure 6.
(Ref. 13, 14).

3.3.2 CONTROL ENGINEERING - COAL LOCK HOPPER SYSTEM

In general process computers are used for process monitoring and process control.
But even during the plant's planning phase process computers can be efficiently used for process engineering. The objective is to examine (to simulate) complex technical processes as early as possible in order to ensure perfect construction of the plant. These examinations turn out to be very advantageous as to the plant's safe and reliable operation; the critical phase of commissioning will be shortened considerably. The results obtained will give proof the safe operation of the plant components.

Against this background Rheinbraun carried out analytic tests in cooperation with Krupp-Atlas-Elektronik referring to the logical pattern and operation of the coal lock hopper control system on the basis of undisturbed operation on the one hand and operation disturbed by the breakdown of signal devices on the other hand. These tests were to determine whether raw gas escapes from the gasifier via the lock hopper system. (Fig.7).

According to the present state-of-art these tests were carried out by a combination of process computers and color display units (Fig. 8), allowing simulation of the lock hopper system control, definite change of signals and detailed representation of the whole lock hopper system control pattern on display screens.

The test was carried out in two steps using a process computer. The first step included examination of a given logic diagram as to its correct logical pattern with subsequent correction. The following second step included disturbance of this error-free logical diagram by simulation of 54 breakdowns as to instruments and 22 breakdowns as to actuators with subsequently analysing the results. Analysis of the breakdown effects showed that as far as the tests are concerned operation of the lock hopper system is considered to be safe, i.e. no raw gas escapes from the gasifier via the lock hopper system.

In addition to the examinations carried out in connection with planning tasks, the process computer is to solve problems occuring during the plant's operation. As to the lock hopper system the main task of the computer is to maintain a continuous check on the process control; this includes timing control of all operations of the lock hopper system as well as error control. These processes can be graphically displayed on color display units showing the flow sheet of the lock system with actual valve positions, and data on pressure, temperature and filling level being superimposed (Fig.7a). In addition the lock hopper cycle diagram (Fig.7b) and the sequence diagram (Fig.9a) can be displayed as to the present situation. Input and output data on present combinations are displayed on another color picture. If one of the combinations required is not established the pertinent input pulse is to be displayed by color change or flash symbol (Fig.9b). Such a strict order of control and information display should allow to optimize the lock system control without delay (Ref. 15).

3.3.3 FEED-BACK CONTROL - SET-POINT CONTROL

The process computer controlling plants for process engineering is connected with a large number of control loops. Dependent on the plant's design, the philosophy of the systems, the safety requirements and the degree of automation either a direct digital control (DDC) or a set point control (SPC) is used.

The pilot plant for hydrogasification of coal uses the SPC control. This results in an order of analog controllers with superordinated process computer which is connected to the controller only for the purpose of set point preset.
For the rest the computer capacity is fully available for process monitoring, control tasks, program control, and for computing process variables which are not directly measurable.

Such a circuit maintains the decentralized system for the distribution of tasks since each control loop is controlled by a single analog controller of its own while the process computer is to solve superordinary problems.

Figure 10 shows the schematic circuit diagram for controller with remote set point via process computer, representing that prior to any process variable preset by the computer, information exchange between process computer and controller is required. As for example the sign-on messages (status signals) have to be exchanged in order that computer and controller are able to identify each others mode of operation.

Special notice is to be taken of the computer-controller shift, or shifting from controller mode to computer mode. Bumpless transition is to be ensured in both cases.
In the case of shifting from computer mode to controller mode bumpless transition can be obtained by internal tailing of the desired value at the controller side. In the case of shifting from controller mode to computer mode the problem can be solved at the computer side by pertinent software. As to our system the latest desired value is requested from the set point memory of the controllers by the process computer, comparing this value with the recomputed desired value; as for the controller this new designd value is approached by the appropiate algorithm.

As to operational safety and efficiency this too is an example for the advantages which can be attributed to decentralized task distribution.
(Ref. 17, 18).

/ 1 / Speich, P. — Braunkohlenveredlung - ein Beitrag zur Energie und Rohstoffversorgung, Brennst.-Wärme-Kraft 28 (1976) Nr. 5, S. 183 - 189

/ 2 / Speich, P. — Technische und wirtschaftliche Gesichtspunkte der Braunkohlenveredlung, Brennst.-Wärme-Kraft 32 (1980) Nr. 8, S. 307 - 312

/ 3 / Teggers, H.
Falkenhein, G. — Hydrogasification of brown coal using process heat from high temperature gas-cooled nuclear reactors, Lignite Symposium, Grand Forks, May 18 - 19, 1977

/ 4 / Schrader, L.
Teggers, H.
Theis, K.-A. — Hydrierende Vergasung von Kohle, Chem.-Ing.-Techn. 52 (1980) Nr. 10, S. 794 - 802

/ 5 / Felgener, G.
Hüttner, R.
Schrader, L. — Forschungs- und Entwicklungsarbeiten zur hydrierenden Vergasung von Kohle mit nuklearer Prozeßwärme, BMFT-FB-T 80-007, Forschungsbericht, Juni 1980

/ 6 / Unbehauen, H. — Aufgaben der Leittechnik im Wärmekraftwerk, Brennst.-Wärme-Kraft 30 (1978) Nr. 6, S. 243 - 245

/ 7 / Urbach, W. — Systemgedanke in der Automatisierung, Erdöl und Kohle-Erdgas-Petrochemie vereinigt mit Brennstoff-Chemie, Heft 3 (1975), S. 126 - 131

/ 8 / Worch, C.
Zscherpe, J.
Prozeßrechner - ein Mittel zur Intensivierung der Inbetriebnahme von neuen Chemieanlagen, Chem.-Techn., Heft 5 (1977), S. 248 - 251

/ 9 / Höppner, U.
Einsatz von Farbsichtsystemen in der Prozeß- und Leitstandtechnik, Industrie-Elektrik + Elektronik, Heft 17, (1980) S. 457 - 460

/ 10 / Whitehead, B.
Fuge, C.
Computerüberwachung und Steuerung von Olefinanlagen, Technik und Wissenschaft, 45 (1979), S. 55 - 66

/ 11 / Kuhlmann, A.
Sicherheit in Konventionellen Kraftwerken, Brennst.-Wärme-Kraft 32 (1980), S. 241 - 247

/ 12 / Joschek, H-J.
Helmstädter, G.
Dehler, J.
Langensiepen, H-W.
Quantitative Risikoanalysen in der chemishen Industrie, Chem.-Ing.-Techn. 52 (1980), S. 123 - 132

/ 13 / Fa. Siemens
Prozeßchromatograph P 101 mit Mikroprozessor, E 699/1000

/ 14 / Fa. Applied Automotion, Inc.
Optichrom 2100
Process Chromatograph System, DWO 5237 1/78

/ 15 / Stockburger, D.
Kühner, H.
Sicherheit-integrierter Bestandteil bei der Planung von Chemieanlagen, Chem. Ind. XXXI/Februar 1979, S. 92 - 96

/ 17 / Welfonder, E.
Alt, M.
Oellig, W.
Lampert, A.
Regelungstechnik und Prozeßdatenverarbeitung, Brenn.-Wärme-Kraft 31 (1979) S. 182 - 187

/ 18 / Schäfer, M.
Elektrische Regler für Anlagen mit Prozeßrechner, Echardt ICE-Bericht VI, S. 16 - 23.

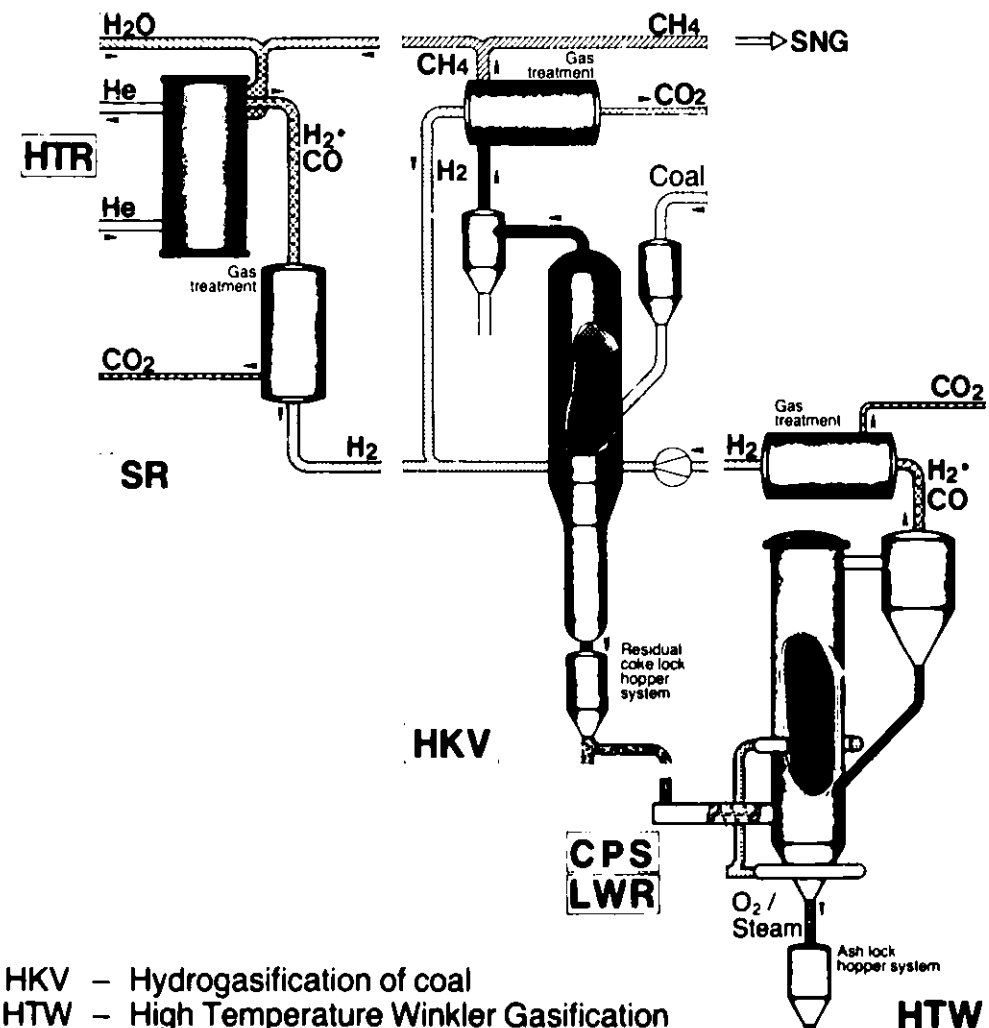

HKV – Hydrogasification of coal
HTW – High Temperature Winkler Gasification
CPS – Coal Power Station
LWR – Light Water Reactor
HTR – High Temperature Reactor
SR – Steam Reformer

Figure 1

Process Combination for Gasification of Brown Coal: Hydrogasification of Coal – Steam Reformer or Hydrogasification of Coal – High Temperature Winkler Process	RHEINBRAUN

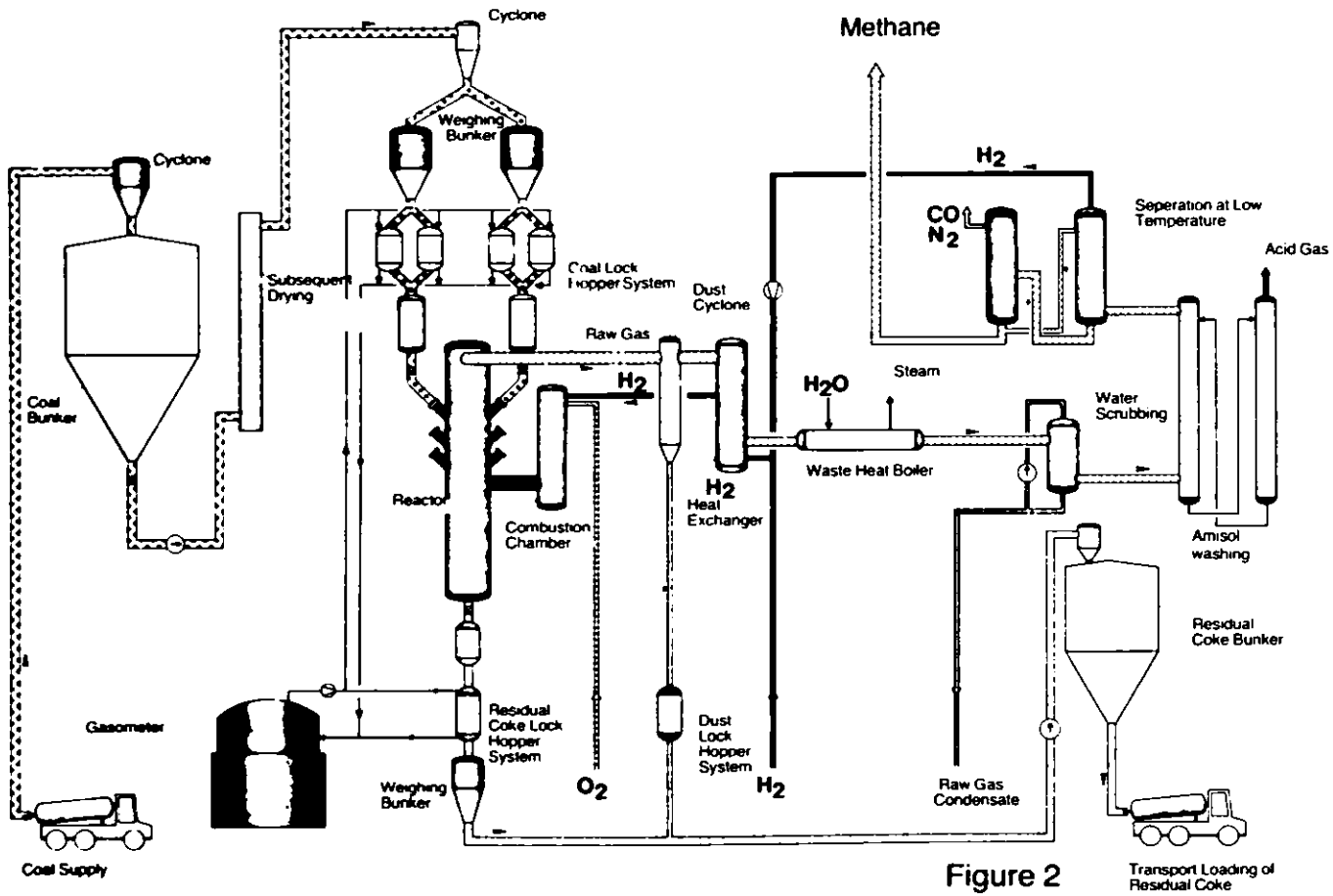

Figure 2

Pilot Plant for Hydrogasification of Coal

RHEINBRAUN

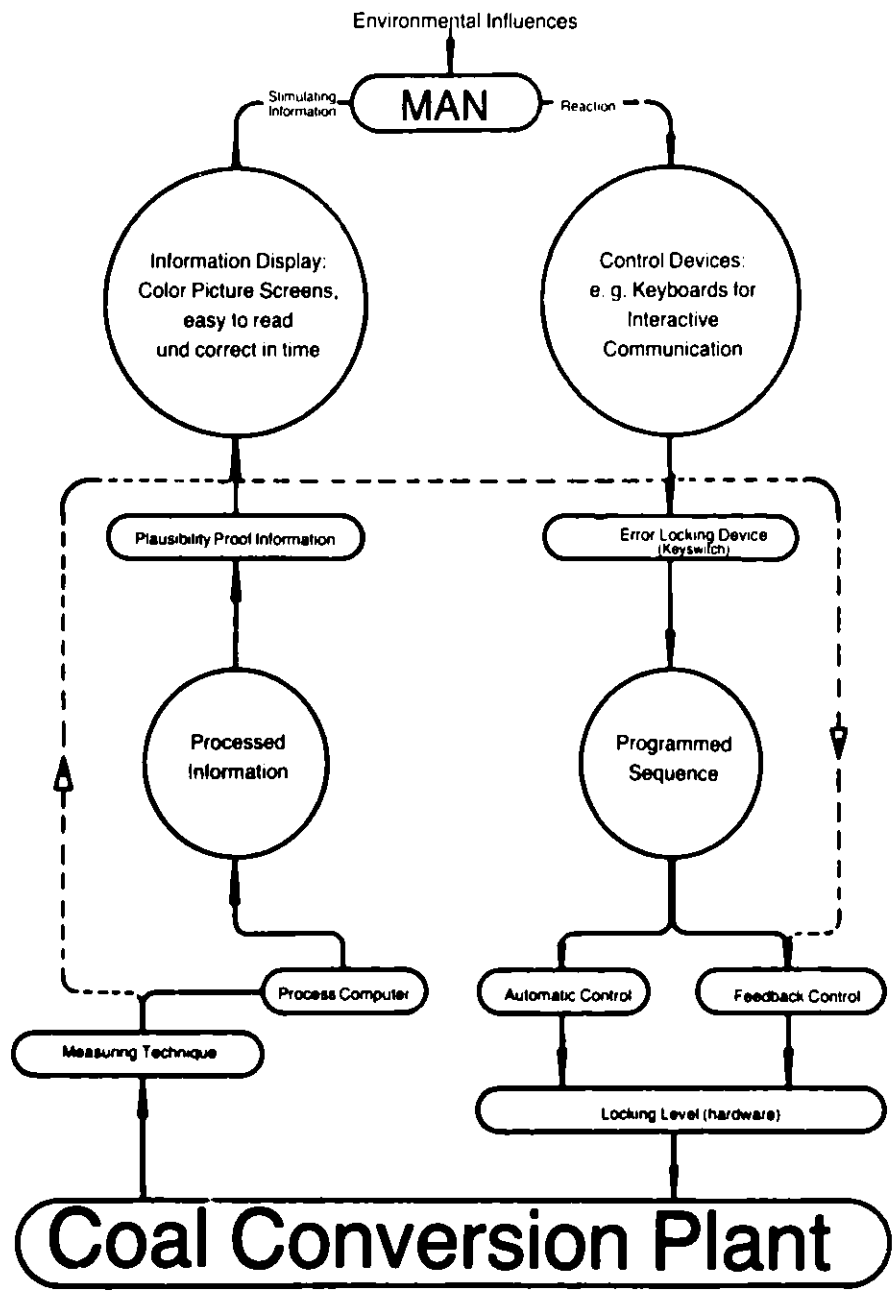

Figure 3

Pilot Plant for Hydrogasification of Coal
Control Technique – Basic Model

RHEINBRAUN

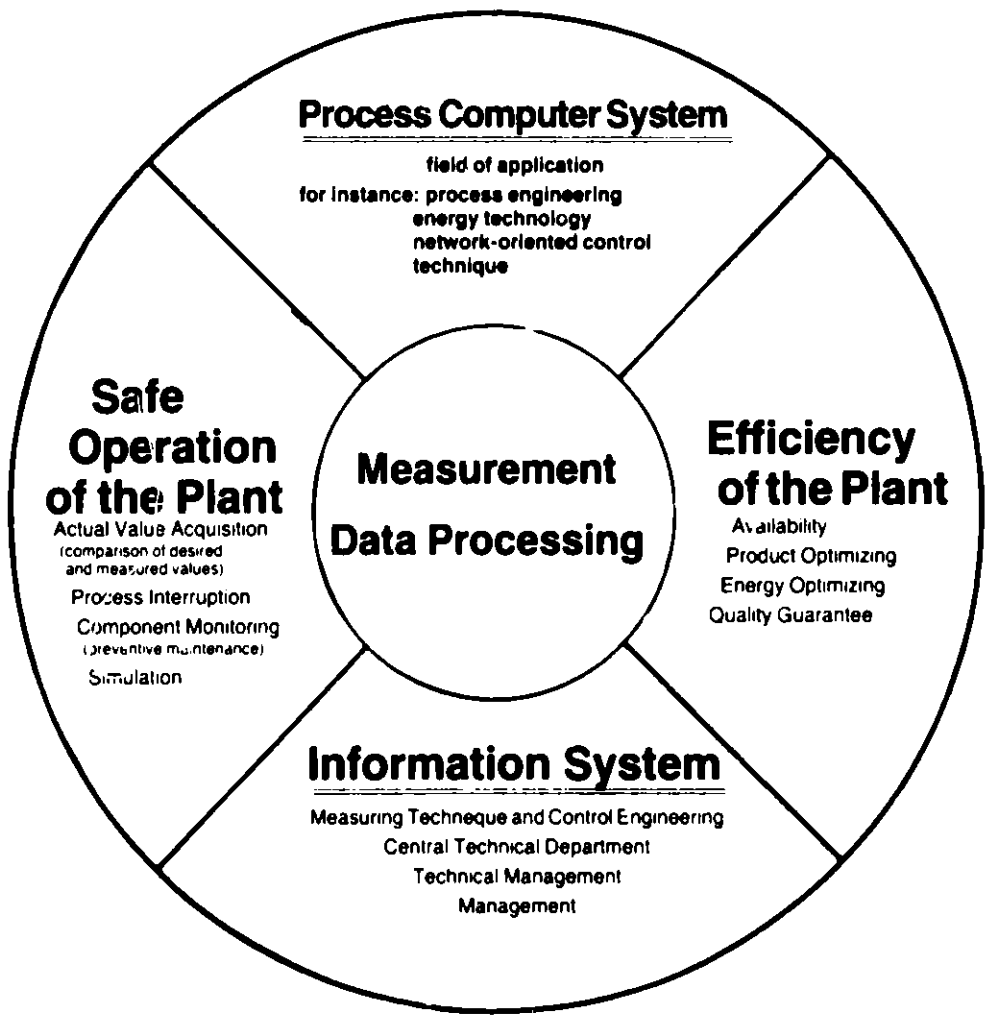

Figure 4

Tasks of a Process Computer System

RHEINBRAUN

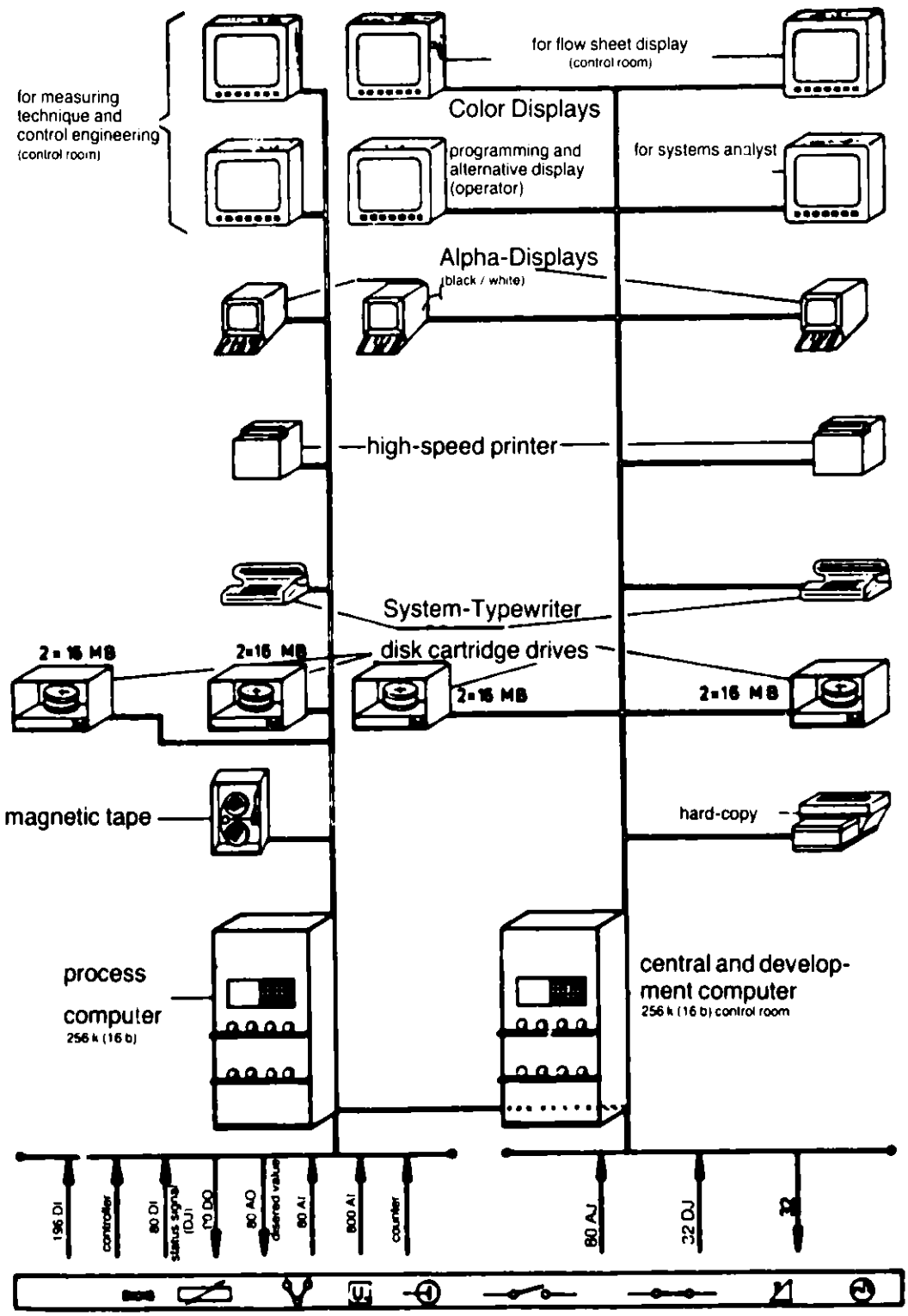

Figure 5
Quantitive Structure of the Process Computer System
Pilot Plant for Hydrogasification of Coal

RHEINBRAUN

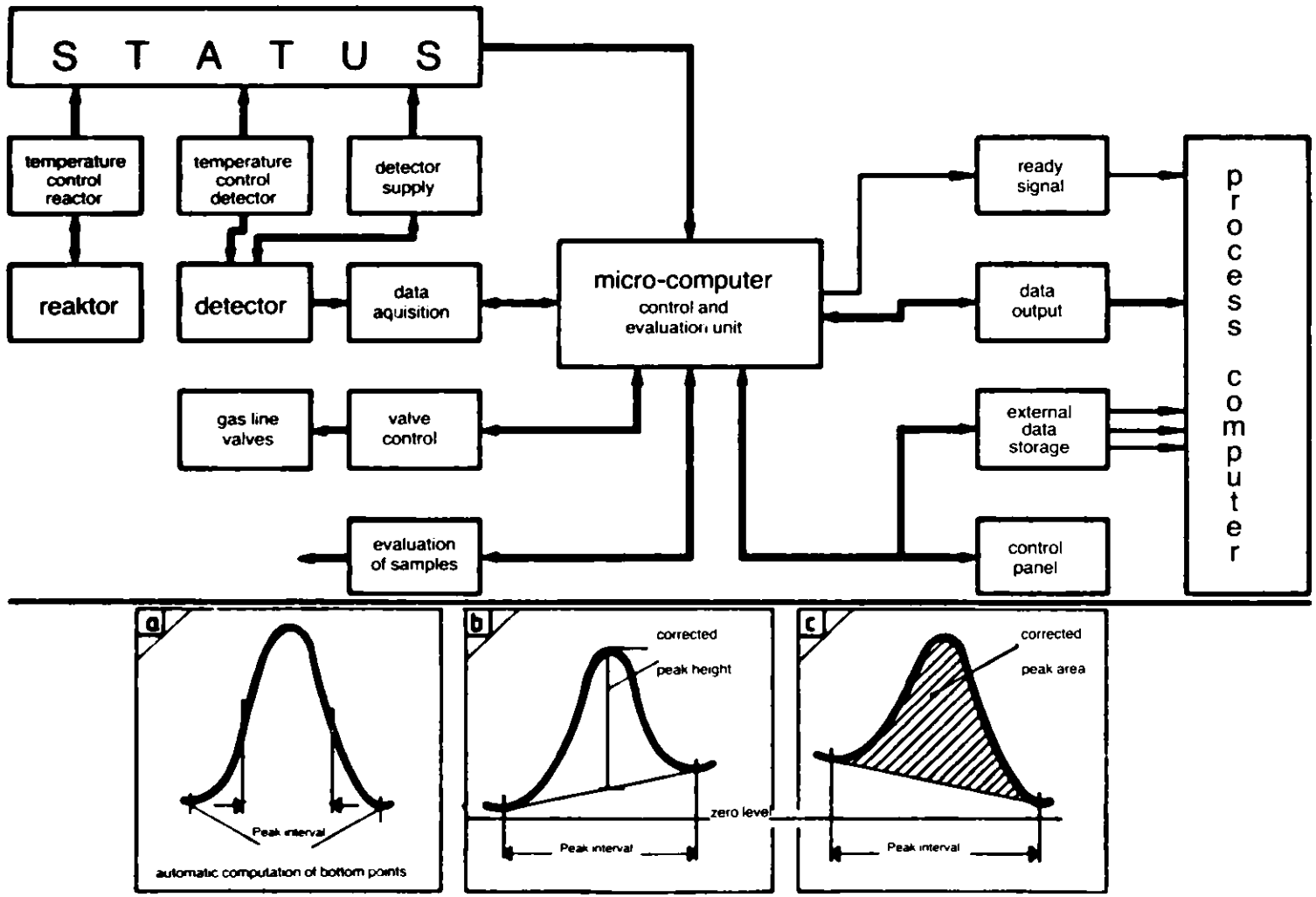

Figure 6

Control and Data Processing – Process Gas Chromatgraph – Pilot Plant Hydrogasification of Coal

RHEINBRAUN

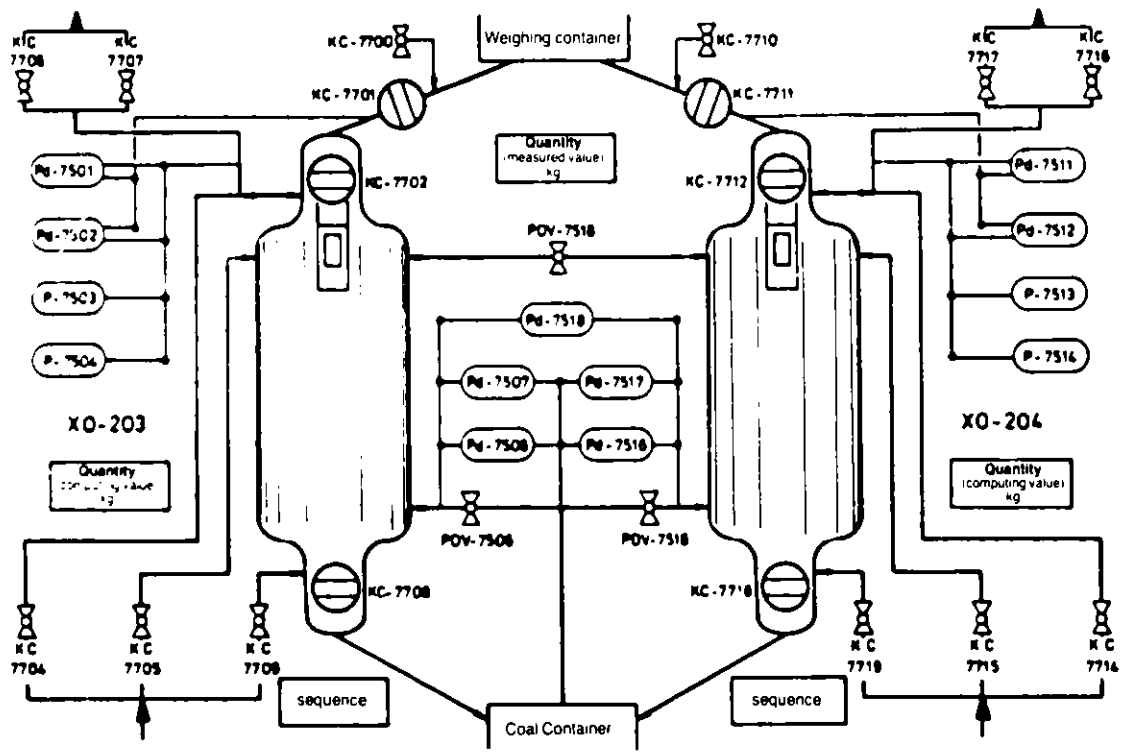

a) plant components of a double-lock hopper system

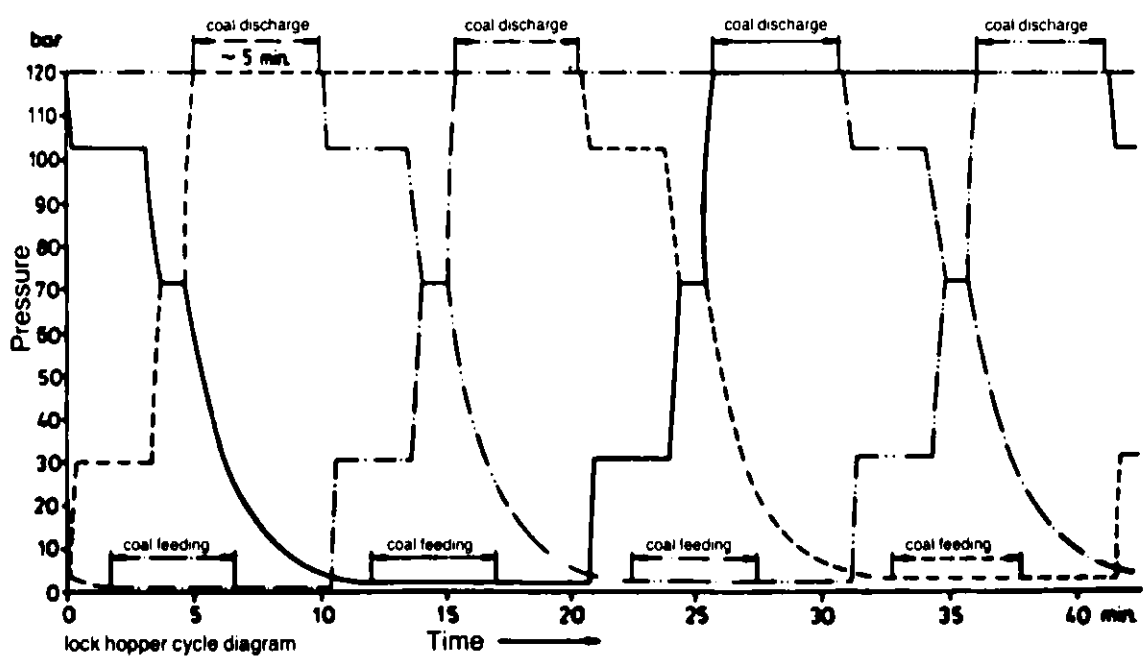

lock hopper cycle diagram

Figure 7

Coal Lock Hopper System – Pilot Plant
Hydrogasification of Coal

RHEINBRAUN

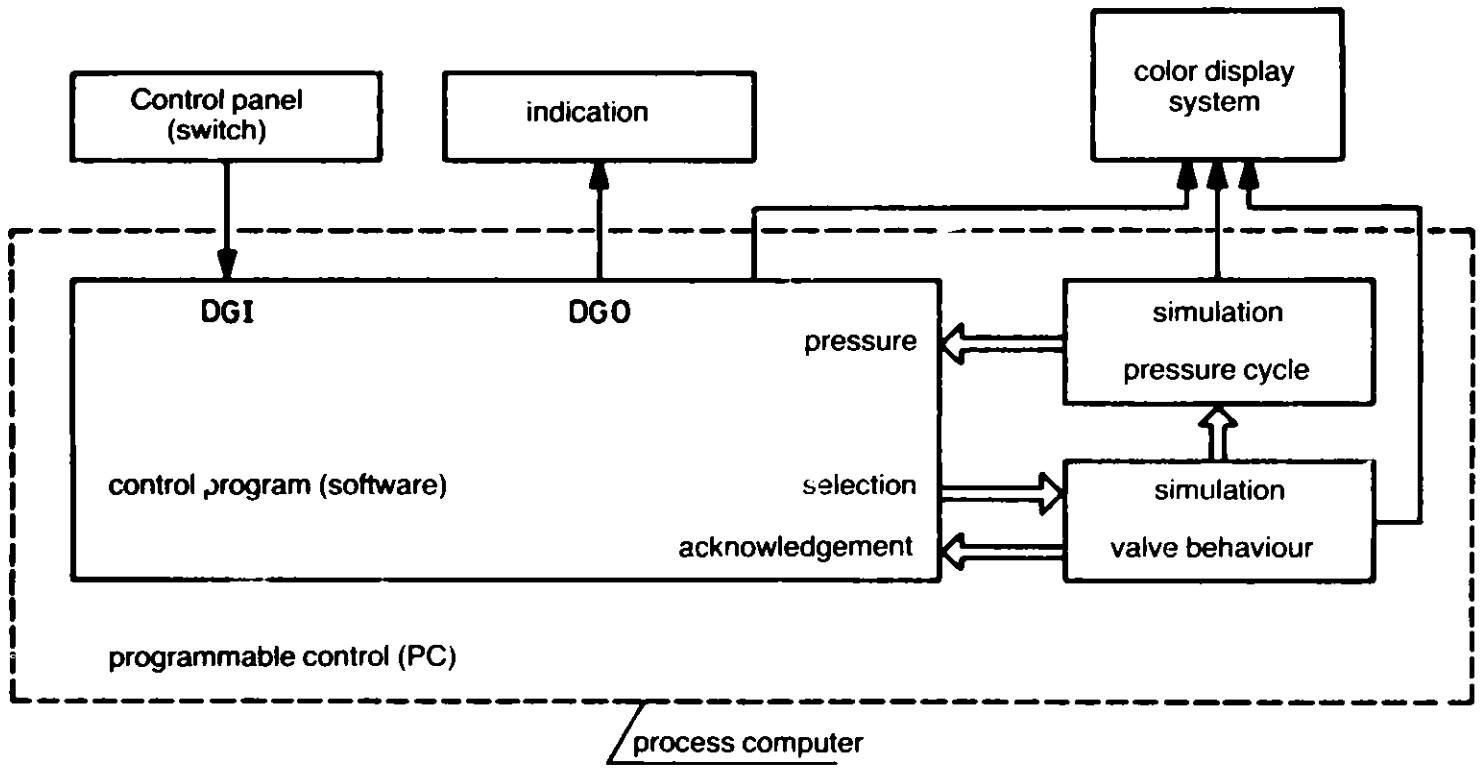

Figure 8

Structure of the programmable control for Lock Hopper System Simulation
– Pilot Plant Hydrogasification of Coal

RHEINBRAUN

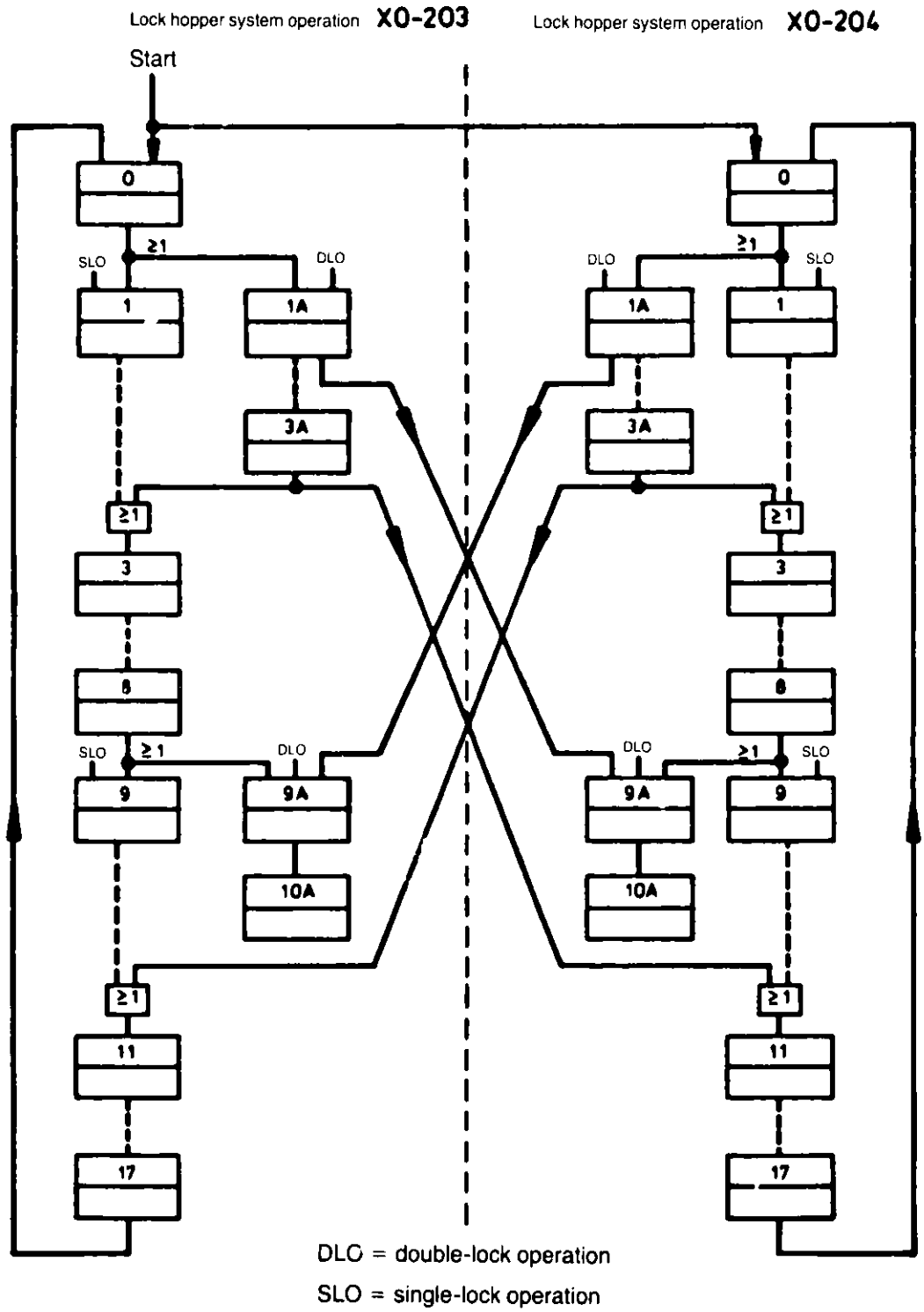

Figure 9 a

Sequence of Lock Hopper System Operation for single-lock and double-lock operation – Pilot Plant Hydrogasification of Coal

RHEINBRAUN

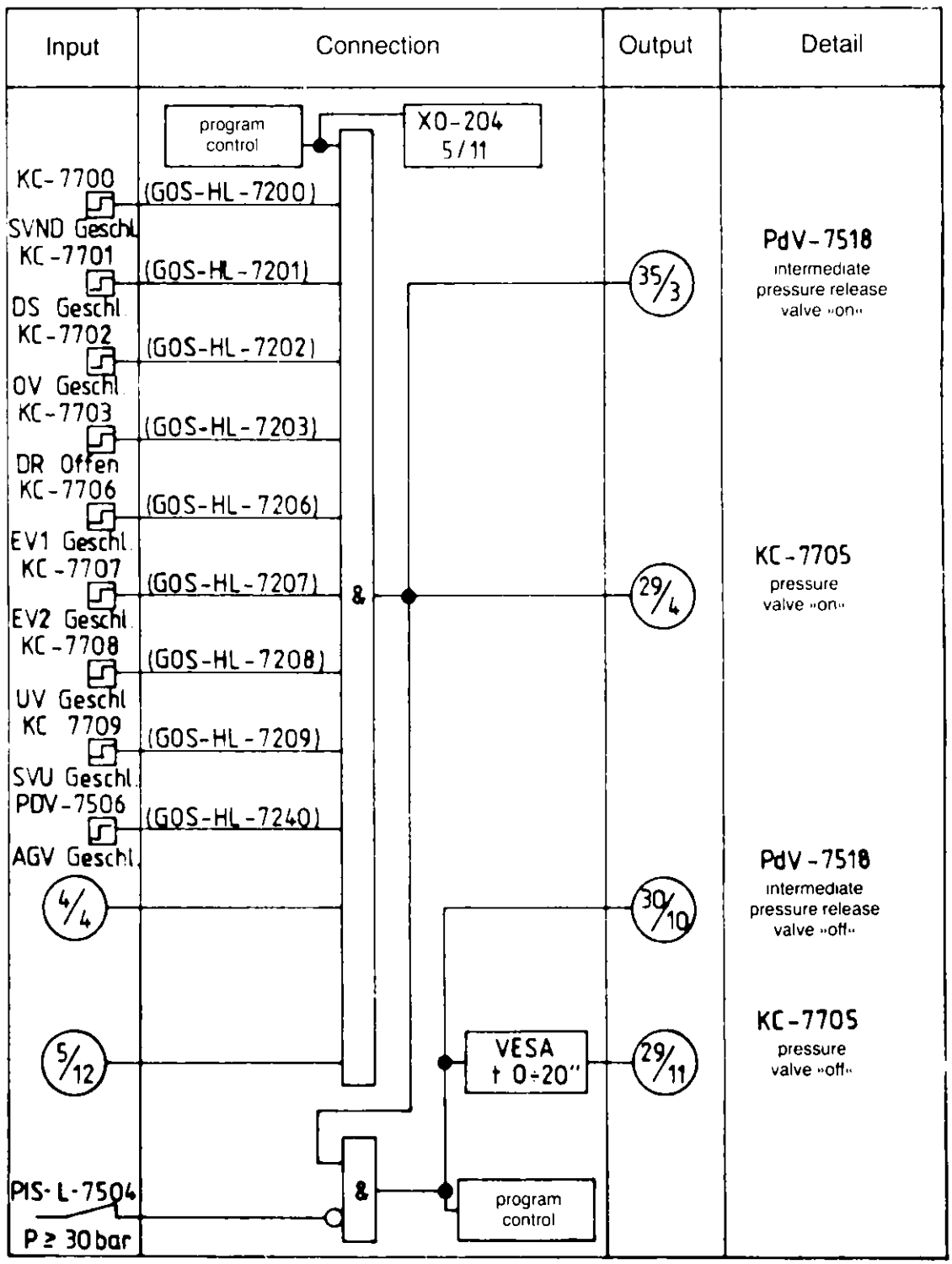

Example for a Lock Hopper Control Sequence

Figure 9b

RHEINBRAUN

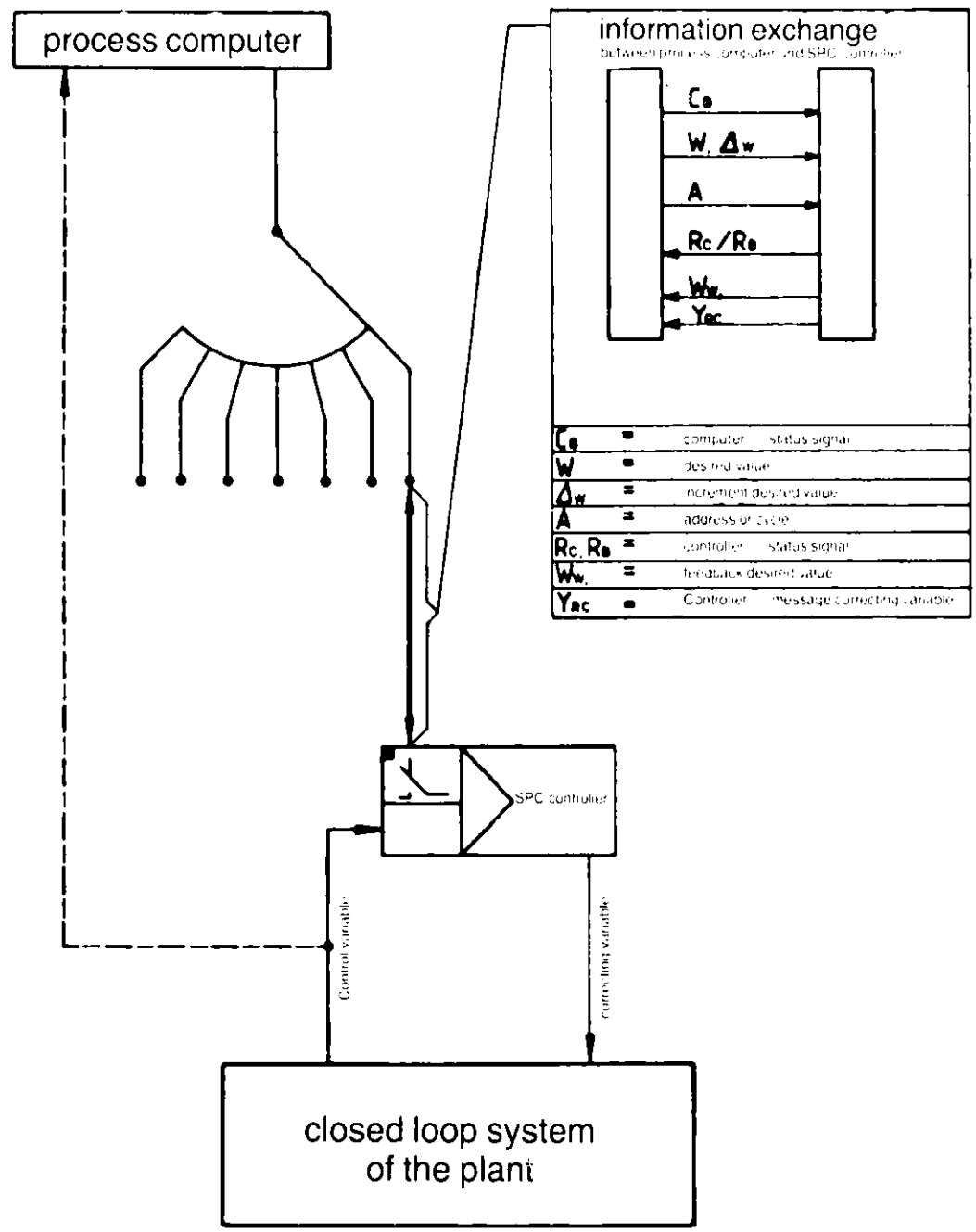

Figure 10

Process Computer and SPC-Controller
combined circuit-Pilot Plant
Hydrogasification of Coal

RHEINBRAUN

ON-LINE ANALYSIS AND SAMPLING OF PROCESS AND PRODUCT VARIABLES FOR THE PRICETOWN I UNDERGROUND COAL GASIFICATION FIELD TEST

A. K. Agarwal, R. E. Zielinski and P. W. Seabaugh
Monsanto Research Corporation
Mound Facility*
Miamisburg, Ohio 45342

ABSTRACT

Instrumentation and a sample handling system designed for real-time analysis and control of an Underground Coal Gasification Field Test worked well in capturing all the data to accurately analyze the process and adequately identify necessary process changes in spite of the wide variations in the process conditions and product composition. The real-time measurement of water was successfully made by the CG analysis. The key to the reliable continuous on-line gas analysis was a well designed sample conditioning system. This instrumentation can be easily modified for application to other coal conversion processes.

INTRODUCTION

Emerging synthetic fuel technologies have several goals. These include: The economic production of a synthetic fuel that is environmentally suitable for use at other locations; the maintenance of a safe and environmentally acceptable production plant; and the achievement of optimum production with greater than 90 percent "on-stream" operating time.

To accomplish these goals, real-time process control and analytical sampling are necessary. Instrumentation and techniques to meet these demands have not yet been fully developed. Process sampling and control is a critical issue for continuous process optimization and also for the minimization of environmental impacts. As the flowstream proceeds through the process steps, its chemistry is changed. It is desirable to know the altered composition of the material instantly for the following reasons:

- To decrease the time required for assessing operational problems and returning to optimized operating parameters.
- To achieve a level of process control sufficient to guarantee environmental compliance while maintaining optimum product quality and volume.
- To develop early predictions of process changes and related product quality.

One of the most difficult coal conversion processes to monitor or control is underground coal conversion (UCC), which is the recovery of energy from coal

*Mound Facility is operated by the Monsanto Research Corporation for the U.S. Department of Energy under Contract No. DE-AC04-76-DP00053.

through an in-situ conversion process. In this process, the unexpected is the usual occurrence and real-time data analysis and process control is a must in order to not only optimize the process but also to maintain it under the influence of severe external variables, i.e. change in reactor size, flow pattern changes in the reactor, restricted flow due to tar coalescence and larger influxes of unanticipated water.

For the deepest and most difficult UCC test performed to date in the United States an instrumentation system was designed that was both unique and versatile. This system functioned well and can be readily modified to monitor other coal conversion processes in real-time.

In the following sections, the system will be described and its performance during the actual field test will be evaluated and proposed next generation modifications for universal application will be presented.

PRICETOWN I

Pricetown I was a relatively small scale field test designed to provide information concerning the feasibility of in-situ coal gasification in a deep (900 feet), thin (~8 feet), high volatile A, Pittsburgh coal.

The Pricetown I Field Site consisted of three Product/Injection (P/I) Wells spaced 60 and 40 feet apart. These wells were completed into the coal seam and were capable of functioning as either injection or production wells because of the versatile arrangement of the piping (Figure 1). Four monitoring (M) wells were located randomly in the field area. These wells were instrumented with downhole thermocouples and gas samplers.

The test was divided into eight phases: Preignition flow testing; RCL-1 (P/I-2 to P/I-3); RCL-2 (P/I-3 to P/I-2); RCL-3 (P/I-2 to P/I-1); LE-1 (P/I-1 to P/I-2); LE-2 (P/I-1 to P/I-2); Gasification (P/I-1 to P/I-2); and Post Test Monitoring. The Preignition Phase was designed to establish gas flow characteristics and instrument response times. The RCL (Reverse Combustion Linkage) Phases were designed to establish a devolatilized permeable path between the wells. The LE (Link Enhancement) Phases were utilized to enhance the conductivity of the linkage path. The Gasification Phase was a high flow period in which a major portion of the coal seam was gasified. The Post Test Monitoring Phase was conducted to verify that the coal seam returned to its ambient temperature.

During the entire test, approximately 800 tons of coal were affected and approximately 54 MMSCF of gas were produced with an average heating rate of 161 BTU/SCF. Additional information regarding the specific details of the test can be found elsewhere[1,2,3].

INSTRUMENTATION

The specific details of the instrumentation system were presented previously[4], and only a brief overview will be presented here.

1. Analytical System

Two Bendix Model 7000 Gas Chromatographs (labeled GC1 and GC2) provided the most extensive analysis of the product gas. The two chromatographs were linked together so that their 15 minute cycles started together; therefore the gas was sampled by the two chromatographs at the same time. GC1 was used to measure the major components of the product gas and GC2 the minor components (Table 1). A Perkin Elmer Model MGA 1200 Process Mass Spectrometer also provided a measurement of the major components in the gas (Table 2). The mass spectrometer not only provided a redundant system for the analysis of the major components, but was also used to accurately control and characterize the process since several hundred updates for each component were possible in the time required for one complete chromatographic analysis. A Thermo Electron Model 10AR Chemoluminescent NO/NO_x Analyzer measured the nitric oxide and nitrogen dioxide content of the gas.

Product gas from the process piping was heavily contaminated with fly ash and organics during the test. Extensive cleanup of samples of product gas was required before it was suitable for analysis. Monsanto Flowtran was used to design a three stage cleanup system for the product well gas. Figure 2 presents a schematic diagram of the gas analysis system. The first two stages were housed in ovens and were similar in design. Gas entered the oven and passed through a condenser coil where it was cooled; liquid was collected in a catch pot. The gas next entered an electrostatic precipitator (ESP) which removed particulates and mists from the gas stream. A micron sized filter removed any remaining particulates in the gas stream before the gas exited the oven. The first stage (oven), operated at 350°F and removed flyash and the heavier organic compounds from the gas. Electrically traced tubing (Samuel Moore - 375°F) carried the gas from the first stage, located on the process piping, to the second stage, housed in the instrumentation building. The second stage oven was set at 200°F and removed the lighter organic compounds from the gas. Flowtran was especially helpful in setting the temperatures of these ovens in order to balance the contaminant loading between them. Parallel lines were used up to this point to insure the availability of samples for analysis. A manual 3-way valve inside the sample handling system was used to select either one of the two sample conditioning systems. Product gas was presented to the gas chromatographs after the first two stages of cleanup. This gas included condensibles, principally H_2O, with dewpoints lower than 200°F. The third stage of the product gas cleanup system was a series of two cold finger type condensers. These condensers lowered the dewpoint of the gas to approximately 43°F to protect the mass spectrometer and NO_x analyzer from liquids.

Monitor Well gas remained relatively clean while the wells functioned due to the low flow rate (approximately 25 liters/minute) at which gas was extracted from these wells and the intimate contact of the gas with the well walls (which acted as a 900 foot condenser at 54°F). Condensibles carried out of these wells by the gas were vaporized in electrically traced sample lines (Samuel Moore - 250°F) that carried the gas from the Monitor Wells to the instrument building. This gas was passed through a series of micron sized filters before presentation to the gas chromatographs. Two cold finger type condensers lowered the dewpoint of the gas to 43°F before analysis by the mass spectrometer. Early

in the test the samplers in the wells became contaminated with fly ash and condensibles. This contamination plugged the samplers and they could not be reopened using either high pressure air or high pressure solvent wash.

Monitor well gas was introduced for analysis via a ring manifold. The analytical instruments were time shared between the various gas sources by having control valves V_1 through V_4 and V_{10} under the direction of the computer. Additionally, the mass spectrometer instrument was directed by the computer through valving internal to the instrument to analyze either the product gas or the gas from the ring manifold (one of the test wells). Both of these gas streams flowed continuously through the mass spectrometer, although only one was being analyzed at a time. In the event of a computer failure, all valves were manually controlled; data was collected on bar graph recorders associated with the gas chromatographs and by a datalogger associated with the mass spectrometer and NO_x analyzer.

The arrangement of the automatic valving was such that any gas source (M_1 through M_4, or the product gas) could be connected to either the two GCs or the mass spectrometer. The NO_x analyzer was not time-shared but was dedicated to the product gas stream.

Time sharing logic was built around operation of the mass spectrometer. Thus, in operation, the mass spectrometer alternately analyzed the product gas and whichever of the monitor wells was connected to the ring manifold (through one of V_1-V_4). The mass spectrometer stream switching occurred at the rate of about once every two minutes, toggling alternatively between monitor well gas and product gas.

Automatic valves V_1 to V_4 opened in sequence. However, one of the four was always open to supply monitor well gas to the monitor well channel of the mass spectrometer.

Maximum utility was derived from the two GCs, which had approximately a fifteen minute analysis cycle time, by basing the selection of the source gas on the relatively high-speed mass spectrometer analysis. In other words, the GCs were directed to analyze the particular gas source of most interest as determined by the computer from the mass spectrometer analysis. Valve V_{10} was the selector valve for the GCs and was either in a position to flow product gas or monitor well gas to the GCs.

Summarizing the overall logic, the mass spectrometer alternatively analyzed the monitor well gas and the product gas on approximately a four minute cycle. Both streams flowed continuously through the instrument. As the product gas was being analyzed for a two minute period, the selected monitor well gas continued to flow. At the end of the product gas analysis period (2 minutes) the mass spectrometer began analysis of the monitor well gas for a two minute period. The mass spectrometer then switched back to the product gas, and after a very brief delay, the next monitor well valve (V_1 - V_4) was opened in sequence. Thus the mass spectrometer analyzed the product gas alternatively with one of the monitor wells. This allowed maximum time (4 minutes) for monitor well line purge, and devoted most of the overall analysis time to the product gas. The overall cycle time, assuming four monitor wells, was fifteen minutes.

A computer program allowed the mass spectrometer to dwell for more than one cycle on any monitor well having a gas composition of particular interest. However, the product gas continued to be analyzed alternatively.

2. Analog System

The analog instrumentation provided flow, pressure, and temperature monitoring as well as process controls and alarms for the high and low pressure air systems, the product gas, and incinerator systems. The instruments were monitored and controlled on a modular designed control panel with a 16 point anunciator, 4 indicating controllers, 12 signal indicators, and 2-3 pen recorders. The measurements of importance were integrated into the automatic data acquisition system to provide real-time data for process control, trend analysis, and system alarms.

3. Automatic Data Acquisition and Control System

To ensure reliability and to minimize the likelihood of total system failure the data acquisition and control system was distributed among four microprocessor primary satellite systems. The design of the system is shown in Figure 3. As indicated, the two gas chromatographs, the mass spectrometer and the two Doric temperature and gas train instrumentation data loggers were each controlled by individual microprocessors. The main function of the system was to acquire data and to present it in a form for decision purposes. In accordance with this need, the host module provided 16 types of graphs of variables or combinations of variables. The logic for real-time control and switching of the gas chromatographs and mass spectrometer among four monitoring well sample streams and the produced gas stream was located within the mass spectrometer microprocessor.

4. Event Driven Algorithms

Event driven algorithms were used to avoid collecting data under conditions where the value of a variable was constant to within a predetermined statistical limit. Such data contain no new information. Controls were, however, incorporated to detect the onset of a slowly evolving trend so that such trends could be mapped with sufficient detail. Likewise, by considering a balance between false alarm and the non-detection of an event, the algorithms ensured sufficient data density to map rapidly occurring events. For the data loggers, a full scan was taken every 22 seconds but unless a particular channel was active, data was actually acquired and stored at some preselected interval. Screening the process data in this fashion resulted in an estimated 96 percent decrease in the number of readings processed by the host computer over the course of the test (about 7 million readings, as opposed to 190 million)[5].

REAL-TIME DATA AND PROCESS CORRELATIONS

An UCG process is a quasi steady state process. The reactor of an UCG system is quite different compared to the reactors used in the chemical industry. In an UCG process, the reactor changes its geometry with respect to time and

this requires a very close monitoring of the process. The steady state production of the product gas requires process changes to take into account the changing reactor geometry and the influence of external variables, such as water influx. During the Pricetown I test, data were acquired in an efficient and accurate manner and correlated very well with the process. Some of these data are presented below.

1. Normal Data Presentations

Normal data presentations in real-time included plots of acquired data, processed data and ratios. These could be presented as actual data, hourly, shift or daily averages. Typical examples of these presentations are shown in Figures 4 through 6. As can be seen from the figures, the process could transist rapidly or be quite stable, however, the control algorithms were effective in capturing all transient data so process effects and interactions could be identified.

In addition to the plots and tabulated readings, BTU values were calculated as well as real-time mass balances.

2. Back Pressure Change and Its Effect on Gas Composition

Back pressure changes in the production line led to significant changes in the gas composition and there were correlated with the process chemistry. For an example, back pressure in the production well was changed from 250 psig to 100 psig on August 29, at 0500 hrs. This led to a reduction in the BTU value of the gas as can be seen in Figure 7. Methane and hydrogen sulfide also declined in a similar trend as depicted in Figure 8. The decline trends for the BTU value, CH_4 and H_2S followed each other very closely. These declines can be attributed to the less cracking of tars and light oils. This is the reason that the methane and hydrogen sulfide followed each other. Reducing the back pressure led to less residence time and hence less cracking. A timely analysis of the gas was helpful in controlling the process by identifying the changes that had to be made in the process parameters.

3. Real-time Water Analysis

The real-time water analysis was very important and the instrumentation employed for that task during the Pricetown I test performed very well. Figure 9 shows the water analysis for the day of September 13, 1979. This figure indicates that the mole percent water in the product gas declined from 5.5% to 3.0% at 1300 hrs. This was followed by product gas temperature decline. The mole percent water and the temperature curves tracked very well. Actually, the product gas was saturated with water and a decline in the temperature led to the condensation of water in the piping system. This was not related to the underground process.

There were other instances where the water in the product gas was related to the underground process. For instance, on September 27, 1979, there were changes in the mole percent water in the product gas and the heating value of the gas followed these changes (Figure 10). This was due to underground process chemistry. An influx of the water in the reactor led to less cracking

of tars and light oils and in turn led to a lower heating value of the gas produced. This correlation at the 1300 hr was very striking when the mole percent water increased from 2.7% to 5.6% and this resulted in a decline in the heating value from 132 BTU/SCF to 123 BTU/SCF.

Real-5ime water analysis is a critical element of a control system for synfuel applications since accurate mass balances are required to key process optimization changes.

4. Comparison of Gas Chromatograph and Mass Spectrometer Values

For backup and comparative reasons, a capability to measure several gaseous components common to both a gas chromatograph and the mass spectrometer was possible. As noted, the mass spectrometer served as the prime composition monitoring instrument and provided the input to the logic system for controlling and selecting the particular gas stream to be serviced by the gas chromatographs and the mass spectrometer. Figure 11 presents the cross plot for H_2S and indicates good agreement between the instruments over both composition range and time. A similar degree of correlation is realized for CO and the other common components.

The explanation of the complex Pricetown I data were possible due to the accurate analytical system and the data acquisition system which was event driven. Due to the event driven nature of the data acquisition system, important data were never missed.

PROPOSED MODIFICATIONS

The instrumentation designed for the Pricetown test functioned above design expectations. To further modify the system several design changes are being considered to provide fully automated process control and automatic process optimization.

The two important control parameters for UCG processes (only for air injection) are flow and pressure. In the case of steam/oxygen injection, the steam to oxygen ratio will be the most effective control parameter. In order to optimize gas quality, the injection flow and process back pressure must be controlled. Because if is possible to automatically control these parameters, logic will be included in the data acquisition system not only to analyze for the occurrence of external events that perturb the process but also to reconcile and subsequently initiate corrective actions using computer actuated valving. Since the analytical system is acquiring and processing data in real-time, gas composition, gas quality and mass balances are available data for decision control. This same logic can be utilized for process optimization during steady state operations.

For steady state operation of an air injection UCG process, flow and pressure values are initially selected to provide optimum gas quality and composition. Once these values and their appropriate operational ranges are established,

Note: The identification of the instrumentation by manufacturer and model number is provided for complete data presentation. It is in no way meant to be an endorsement for that specific instrument.

TABLE I

GAS CHROMATOGRAPHIC ANALYSIS

GC1		GC2	
COMPONENT	RANGE	COMPONENT	RANGE
NITROGEN	0-100%	ETHANE	0-2%
OXYGEN + ARGON	0-25%	PROPANE	0-2%
CARBON MONOXIDE	0-20%	BUTANE	0-2%
CARBON DIOXIDE	0-20%	CARBONYL SULFIDE	0-.1%
HYDROGEN	0-25%	SULFUR DIOXIDE	0-3%
METHANE	0-50%	HYDROGEN SULFIDE	0-3%
WATER	0-20%	HYDROGEN CYANIDE	0-.2%

TABLE 2

MASS SPECTROMETER ANALYSIS

COMPONENT	RANGE
HYDROGEN	0-100%
NITROGEN	0-100%
METHANE	0-100%
CARBON MONOXIDE	0-20%
OXYGEN	0-100%
HYDROGEN SULFIDE	0-10%
ARGON	0-2%
CARBON DIOXIDE	0-20%

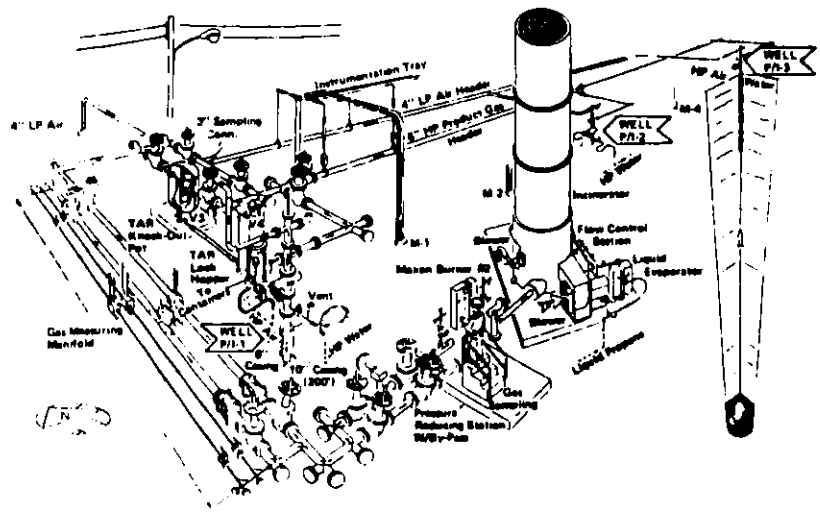

FIGURE 1

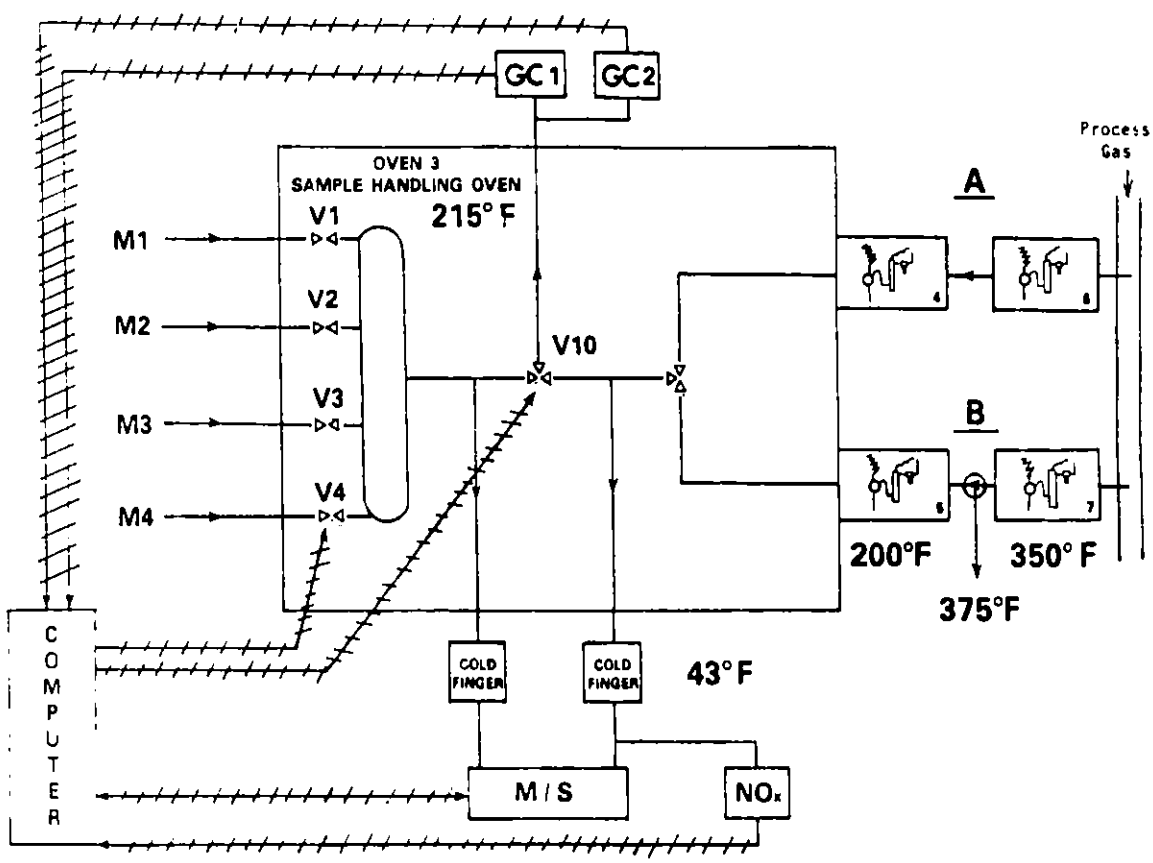

GAS ANALYSIS SYSTEM

FIGURE 2

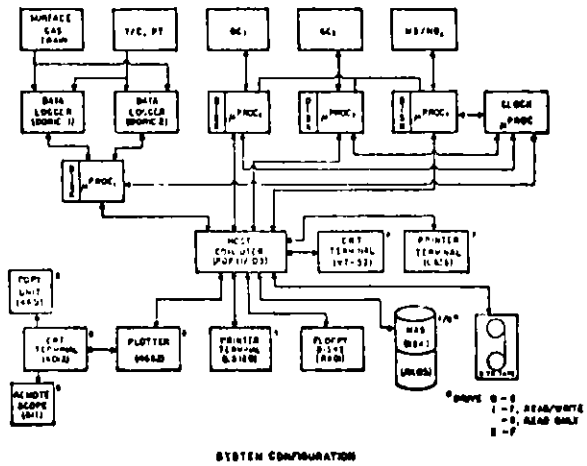

FIGURE 3

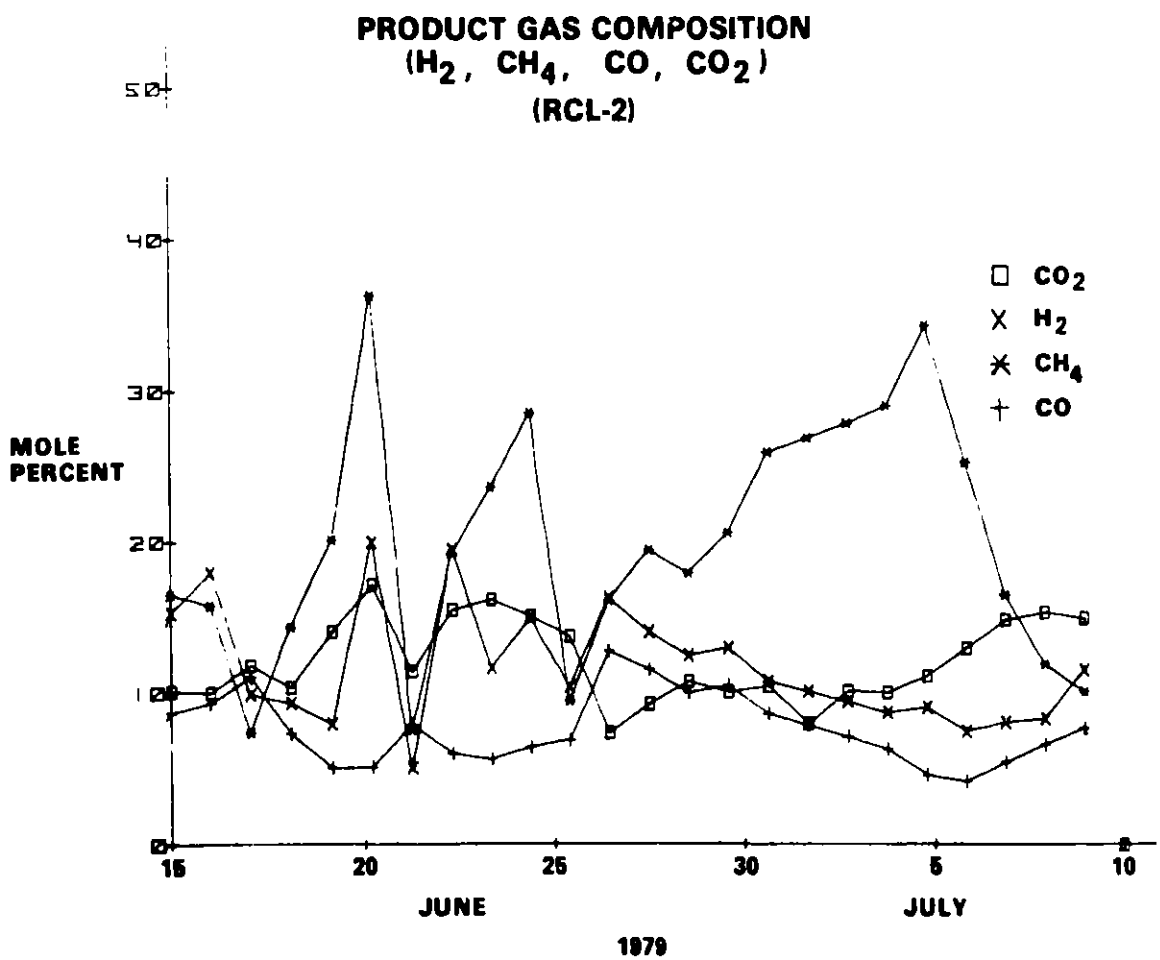

FIGURE 4

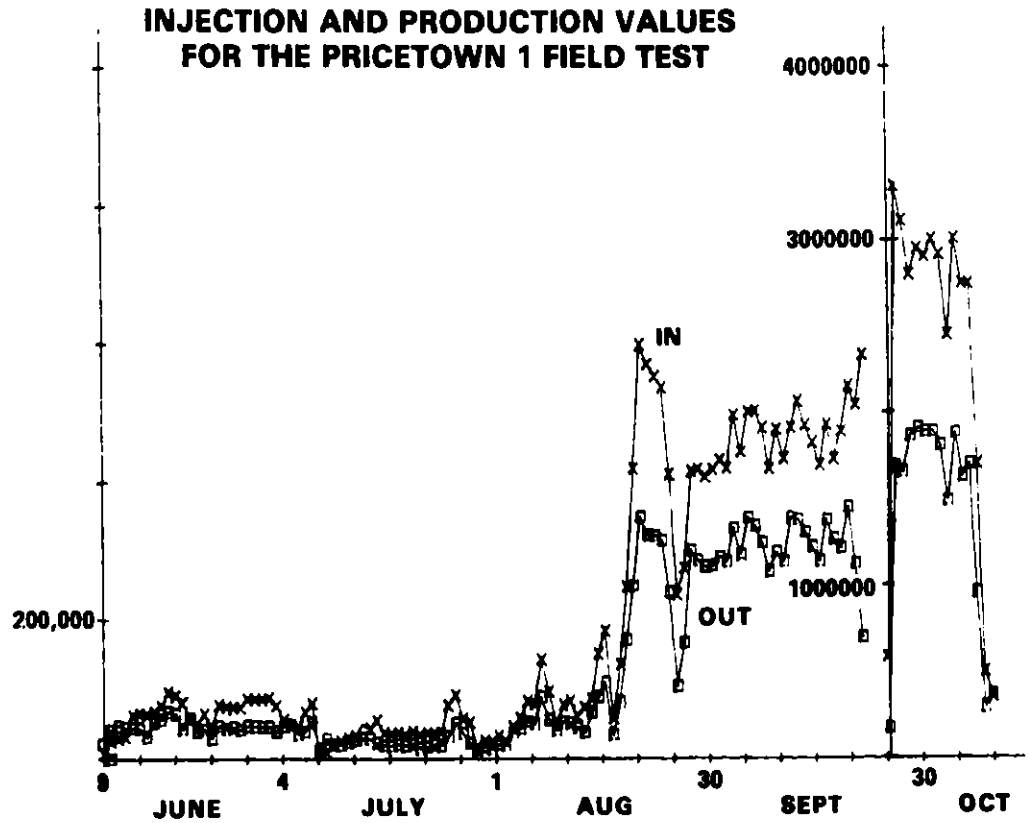

FIGURE 5

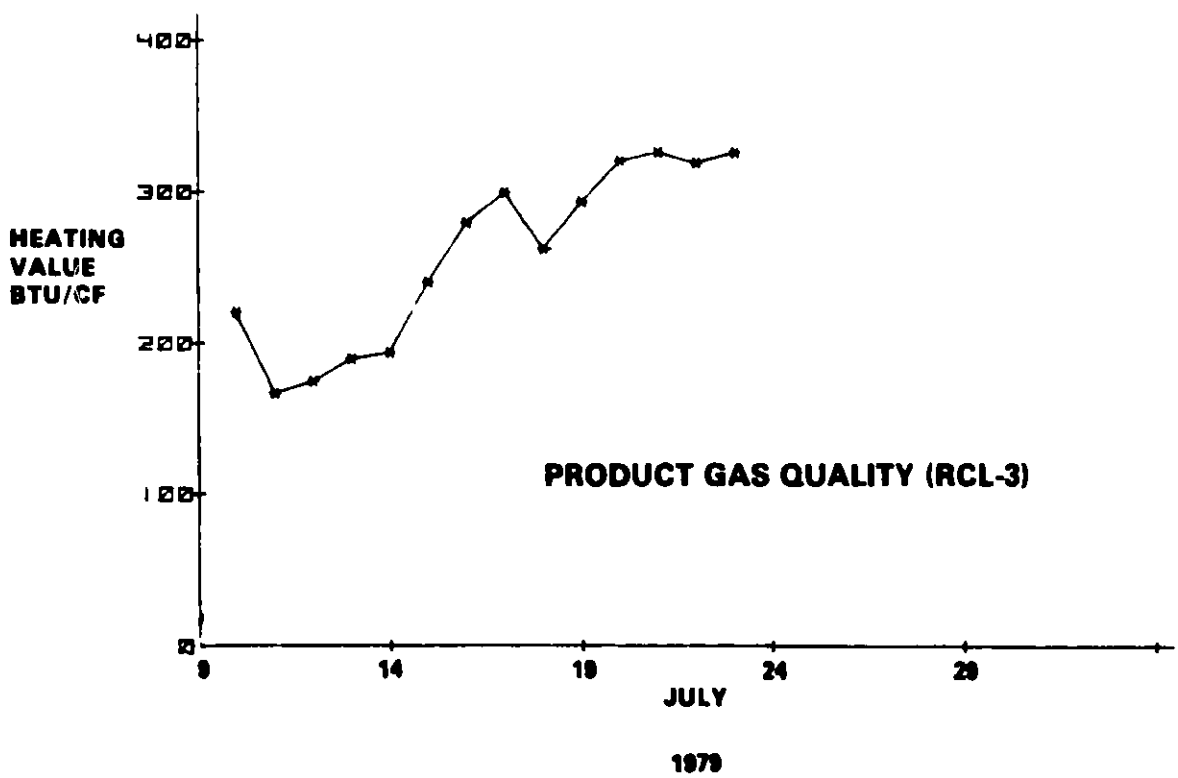

FIGURE 6

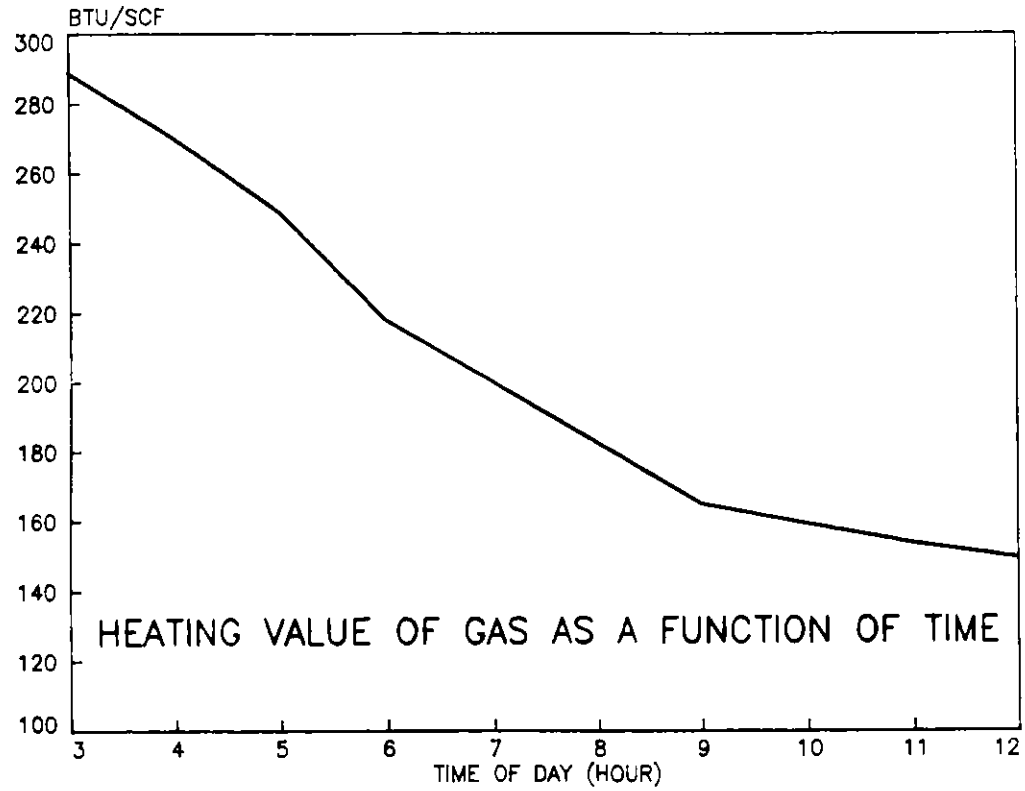

FIGURE 7

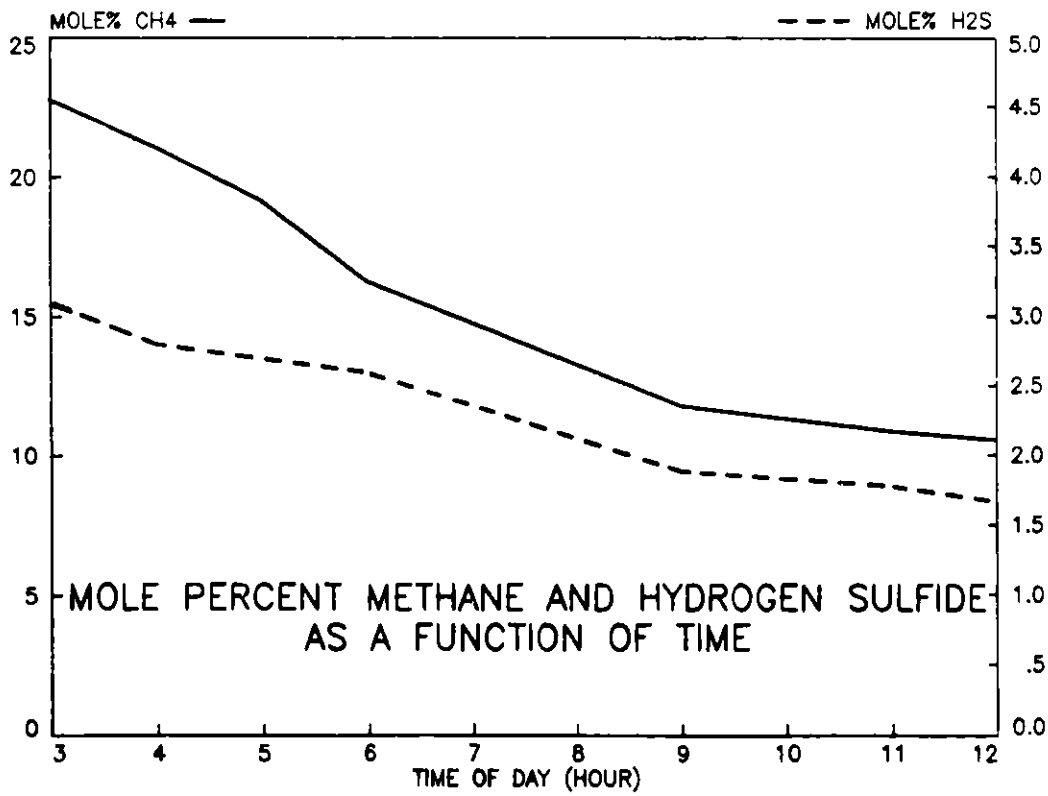

FIGURE 8

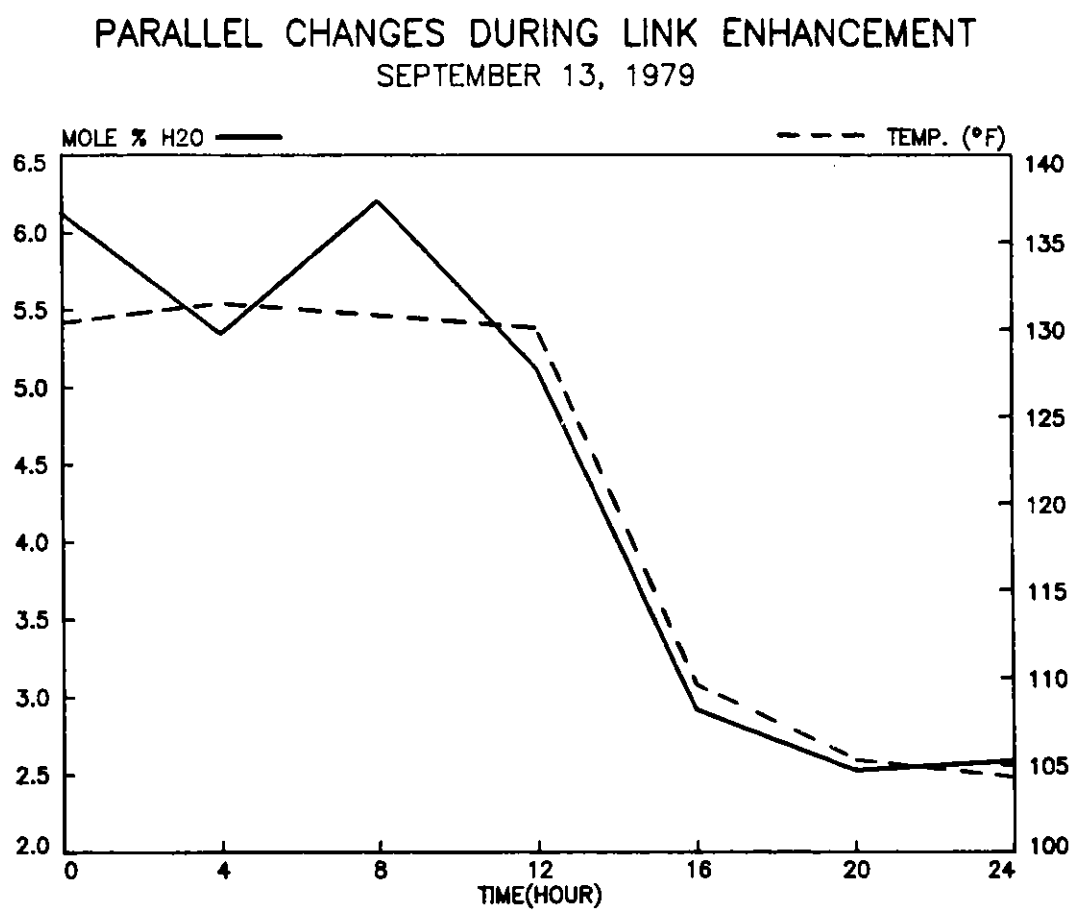
PARALLEL CHANGES DURING LINK ENHANCEMENT
SEPTEMBER 13, 1979
MOLE % H2O
TEMP. (°F)
6.5
6.0
5.5
5.0
4.5
4.0
3.5
3.0
2.5
2.0
140
135
130
125
120
115
110
105
100
0
4
8
12
16
20
24
TIME(HOUR)

FIGURE 9

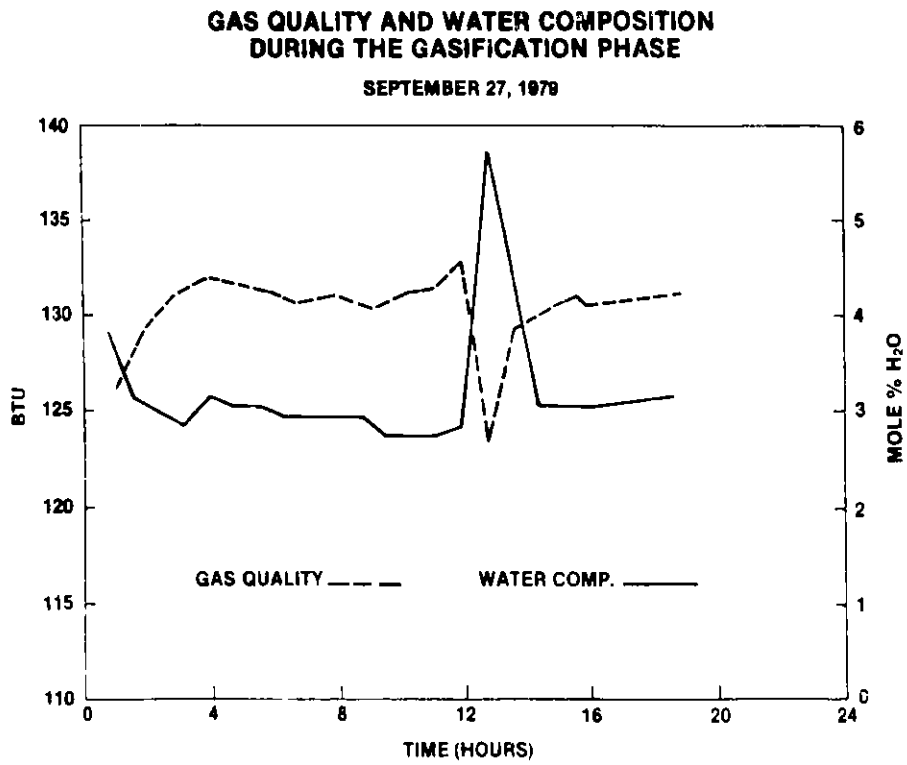

FIGURE 10

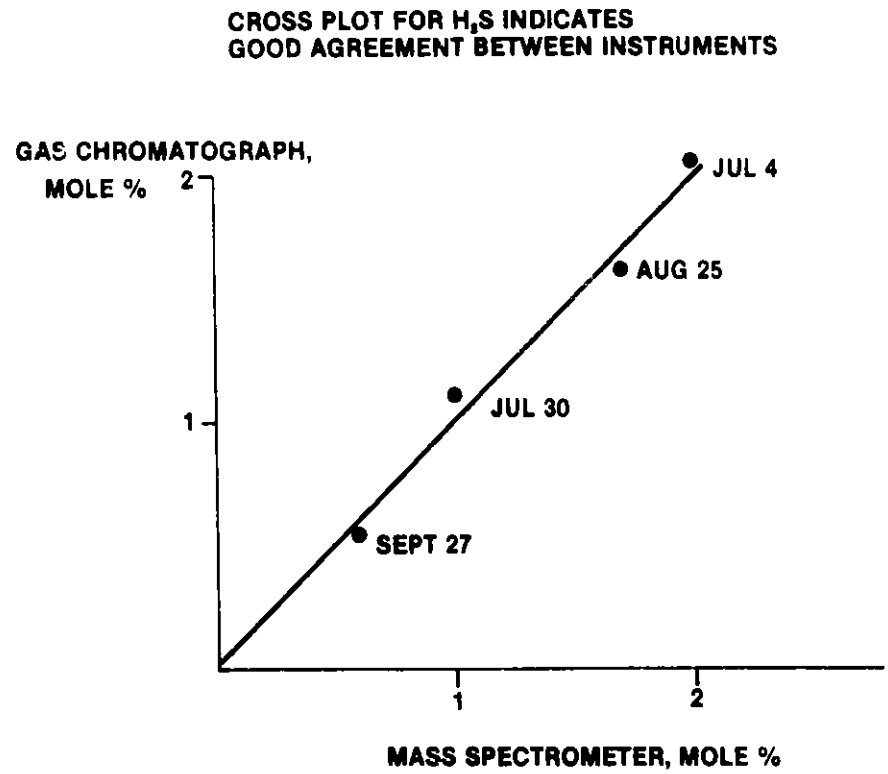

FIGURE 11

control algorithms at two levels can be imposed on the system.

These algorithms will establish process limits for normal automatic operation and control and alarm limits that will alert to operator that a more direct and immediate course of process changes is required.

This type of control is required not only for underground coal gasification processes but also for all synfuel operations and can be made possible only because of the unique analytical system which can provide complete real-time data, including accurate water analyses, for decision quality mass balances.

CONCLUSIONS

The Instrumentation System designed for the analysis and control of the Pricetown I Field Test worked beyond expectations. Because it analyzed the process in real-time, it allowed the operators to make effective changes and to maintain the process. With the modification of the sampling system for specific applications, this system can be used for application in most synfuel processes.

The logic modifications that can be incorporated into the system will allow it to optimize the process by automatically controlling the process variables for optimum product composition, quality or environmental control.

REFERENCES

1. "Pricetown I Data Analysis," Agarwal, A. K., Zielinski, R. E. and Seabaugh, P. W., in the Proceedings of the Sixth Underground Coal Conversion Symposium, July 13-17, 1980, Shangri-La, Oklahoma, CONF-800716, U.S. DOE.

2. "A Successful Underground Coal Gasification Field Test in a Thim Seam, Swelling Eastern Bituminous Coal," Martin, J. W. and Liberatore, A. J., in the Proceedings of the Sixth Underground Coal Conversion Symposium, July 13-17, 1980, Shangri-La, Oklahoma, CONF-800716, U.S. DOE.

3. "A Successful In-Situ Coal Gasification Test in the USA," Agarwal, A. K. and Zielinski, R. E., to be presented at the Second World Congress of Chemical Engineering, Montreal, Canada, October 4-9, 1981.

4. "Instrumentation Used for the Monitoring and Controlling of the Pricetown I Underground Coal Gasification Field Test," Zielinski, R. E., Seabaugh, P. W. and Agarwal, A. K., in The Proceedings of the 1980 Symposium on Instrumentation and Control for Fossil Energy Processes, June 9-11, 1980, Virginia Beach, Virginia, CONF-800602, Argonne National Laboratory, Argonne, Illinois.

5. "Pricetown I Data Acquisition System," Walker, W. K., Ciramella, A. F., Kessling, W. E., Proceedings of the Digital Equipment Computer Users Society, Vol. 6, No. 4, U.S.A. Spring, 1980.

PROCESS GAS CHROMATOGRAPHY MONITORING OF COAL GASIFICATION PRODUCT GAS

ABSTRACT

Michael R. Fuchs, Gordon C. Page

Radian Corporation is under contract to the Environmental Protection Agency - Industrial Environmental Research Laboratory to conduct an environmental assessment of low-BTU gasification. As part of this program, source test and evaluations are performed at viable gasification processes to gather environmental and process data. Included in the source test evaluations of two gasification processes, Radian has used process gas chromatographs to monitor the product gas for environmental and process parameters. Process gas chromatographs provide semi-continuous data of sulfur species (H_2S, COS, CS_2, SO_2) and ammonia (NH_3) which indicate minimum and maximum concentrations of the potential pollutants and also allows the determination of the average concentration of the parameter. Continuous sulfur species and ammonia data allow pollution control systems to be designed to limit emissions during periods of maximum pollutant concentrations as well as during average or normal conditions. Process gas chromatographs analytical results of H_2, CO, CO_2, and O_2 allow recognition of less than optimum performance of the gasification process.

PROCESS GAS CHROMATOGRAPHS MONITORING OF COAL GASIFICATION PRODUCT GAS

Michael R. Fuchs, Gordon C. Page

Radian Corporation

INTRODUCTION

Radian Corporation is under contract to the Environmental Protection Agency - Industrial Environmental Research Laboratory (EPA-IERL) to conduct an environmental assessment of low-Btu gasification. As part of this program, source test and evaluations are performed at viable gasification processes to gather environmental and process data. Included in the source test evaluations of two gasification processes, Radian has used process gas chromatographs to monitor the product gas for environmental and process parameters.

The results of process gas chromatograph analyses of gasification product gas are most useful

- to provide data for design criteria of pollution control systems, and
- to provide data for process performance monitoring and evaluation.

The most common practice in monitoring low-Btu gasification product gas for environmental parameters is the collection of gaseous grab samples for bench gas chromatograph analysis or impinger techniques. However, data determined by these techniques may be misleading if the sampling time frame of the grab or impinger sample is during a period of abnormally low or high concentration of the parameter(s) being tested. Process gas chromatographs provide data which show fluctuations in parameter concentrations.

Minimum and maximum concentrations of the test parameters are available as well as the data necessary for determination of the average concentration of the parameter. The design of pollution control systems must consider fluctuations in concentrations to provide a process capable of removing sufficient quantities of the pollutant to comply with emission regulations during periods of above typical concentration levels.

Process gas chromatographs also prove to be useful in monitoring process performance by providing analyses of major gases. Of the major gases for which analyses can be performed, CO, H_2, CO_2 and O_2 are the most pertinent. CO and H_2 are the two major energy sources produced by low-Btu gasification and an increase of CO_2 and O_2 concentration in the product gas is an indication of a reduction in process efficiency.

The two gasification processes tested were a Wellman-Galusha at the Glen-Gery Brick Company in York, Pa., and the Riley Gas Producer at the Riley Stoker Research Center in Worcester, Ma. The Wellman-Galusha is a single-stage, thick fixed-bed, atmospheric pressure gasifier and the Riley Gas Producer is a single-stage, thin fixed-bed, atmospheric pressure gasifier.

The feedstock of the Wellman-Galusha was anthracite, and lignite was the feedstock at the Riley Gas Producer facility. The Glen-Gery facility was partially funded by DOE's Gasifiers in Industry program. Riley-Stoker Corporation is the licensor of the Riley Gas Producer. Monitoring was performed during a test commissioned by American Natural Service Company.

SYSTEM DESIGN

Process gas chromatographs comprise an automated analytical system using gas chromatographs. Instrument operations including sample injection, column back flush, column switching, etc., are controlled by electronic units. Analytical results are semi-continuous; a set of data is produced with each sample injection which occur at 5 to 15 minute intervals depending upon instrument operating conditions. Instrument results have been logged on strip chart recorders.

Radian Corporation, through its EPA funding, has purchased process gas chromatograph systems from two suppliers: Applied Automation, Inc., and Bendix Corp. The two systems provide identical analytical capabilities. The findings presented in this paper are the results of analyses performed using the Applied Automation system.

Each system consists of three gas chromatographs containing either a flame ionization detector, a flame photometric detector, or a thermal conductivity detector. The instruments are capable of the following analyses:

- FID - hydrocarbons (CH_4, C_2H_6, C_2H_4, C_3H_8, C_3H_6, C_4+),
- FPD - sulfur species (H_2S, COS, CS_2, SO_2), and
- TCD - ammonia (NH_3), major gases (CO, CO_2, O_2/Ar, H_2, CH_4, N_2).

Both process gas chromatograph systems are housed in a portable building which is air conditioned. The instrumentation is susceptible to temperature fluctuations and dirty environments which have required enclosing the systems in the portable building.

Sample gas supplied to the instrumentation must be free of particulate and moisture. Additionally, many low-Btu product gas streams have significant concentrations of oils, both as mist and vapors, which must be reduced in concentration prior to analysis of the product gas. Product gas streams which do not contain oils, such as the Glen-Gery facility which had anthracite feedstock, are filtered using glass fiber medium and dried using a Perma-Pure® drier. The filter and drier are both heated. The Perma-Pure® drier utilizes an osmotic membrane through which gaseous moisture migrates into a dry purge gas passed along the exterior walls of the membrane. The sample gas is transferred to the instrumentation in electrically heat-traced stainless steel tubing. Sample gas treatment of product gas streams which do contain oils such as the Riley Gas Producer with lignite feedstock includes an electrostatic precipitator (ESP). The ESP is placed prior to the filter and Perma-Pure® drier, and removes aerosol material including oils and, along with the filter, is housed in a heated oven and maintained at a temperature below the minimum instrument temperature. The temperature controlled ESP reduces the oil dewpoint of the product sample gas to below 225°F.

The Applied Automation instrumentation has been used to analyze product gas streams at Wellman-Galusha (Glen-Gery) and Riley Gas Producer low Btu gasifiers. The compounds for which analytical results are available at each site are:

	FID	FPD	TCD
Glen-Gery	CH_4	H_2S, COS CS_2, SO_2	NH_3
Riley Gas Producer	CH_4, C_2H_6, C_2H_4, C_3H_8, C_4+	H_2S, COS	CO, H_2, CO_2, O_2/Ar, N_2

Tables 1 and 2 present the instrument operating specifications and column materials used at each low-Btu process.

TABLE 1. APPLIED AUTOMATION PROCESS GAS CHROMATOGRAPHS

Chromatograph Detector Unit	Compound Detected	Temperature (°C)	Cycle Time (Minutes)	Column
FPD	COS, H_2S, CS_2, SO_2	141	4.0	0.30 m x 3.2 mm Teflon with 40% Carbowax on Chromosorb P (80/100 Mesh) and 3.7 m x 3.2 mm Teflon with 1% TCEP on Porasil B (80/100 Mesh)
FID	CH_4, C_2H_6, C_2H_4, C_3H_8, C_3H_6, C_4^+	141	7.5	0.60 m x 3.2 mm Stainless Steel with Porapak T (80/100 Mesh). 4.3 m x 3.2 mm Stainless Steel with Porasil A (80/100 Mesh). 0.30 m x 3.2 mm Stainless Steel with Chromosorb G (80/100 Mesh)
TCD	NH_3	141	8.25	1.5 m x 3.2 mm Stainless Steel with 1% Polyethylene Imine on Porapak T (80/100 Mesh) and 4.6 m x 3.2 mm Stainless Steel with 1% Polyethylene Imine on Porapak T (80/100 Mesh)
TCD	H_2, CO, CO_2 O_2/Ar, N_2	2.85	10.25	4.0 m x 3.2 mm Stainless Steel with Porapak Q; 3.0 m x 3.2 mm Stainless Steel with Molecular Sieve 5A

FPD = Flame Photometric Detector
FID = Flame Ionization Detector
TCD = Thermal Conductivity Detector

TABLE 2. OPERATING SPECIFICATIONS FOR BENDIX PROCESS GAS CHROMATOGRAPH

Chromatograph Detector Unit	Compound Detected	Temperature (°C)	Cycle Time (seconds)	Column
FPD	Sulfur Species	81	480	0.9 m x 3.2 mm Stainless Steel with BSG (Bendix Sulfur Gas Packing); 1.8 m x 3.2 mm Stainless Steel with Porapak Q; 0.6 m x 3.2 mm Stainless Steel with BSG
FID	Hydrocarbons	70	300	0.9 m x 3.2 mm Stainless Steel with Porapak Q; 1.8 m x 3.2 mm Stainless Steel with OPN on Porasil C 0.6 m x 3.2 mm Stainless Steel with OPN on Porasil C
TCD	Major Gases	60	310	2.4 m x 3.2 mm Stainless Steel with Porapak Q; 1.5 m x 3.2 mm Stainless Steel with Porapak Q; 2.4 m x 3.2 mm Stainless Steel with Molecular Sieve SA

ENVIRONMENTAL DATA

Of the analyses performed by process gas chromatographs, results of sulfur species and ammonia are most useful as aids in the design of control technology. The vast majority of gaseous sulfur emissions of low-Btu gasification processes is as hydrogen sulfide with lower concentrations of carbonyl sulfide, carbon disulfide, and sulfur dioxide. Combustion of the product gas converts the reduced sulfur species to oxides of sulfur. 104 percent and 53 percent of the sulfur fed to the process with the coal feedstocks was emitted in the product gas of the two processes sampled, Wellman-Galusha, anthracite feedstock; and Riley Gas Producer, lignite feedstock, respectively. Assuming that all sulfur species in the product gas are converted to sulfur dioxide during product gas combustion, resulting emission rates of the Wellman-Galusha and Riley Gas Producer facilities would be 0.94 lb $SO_2/10^6$ BTU and 1.10 lb $SO_2/10^6$ BTU, respectively, based upon average concentrations of sulfur in the product gas using process gas chromatograph analytical results and BTU ratings of the coal feedstocks. Figures 1 through 4 graphically present the process gas chromatograph analytical results for sulfur species at the Wellman-Galush (Glen-Gery) facility. Figure 5 presents the sulfur species results determined by process gas chromatograph at the Riley Gas Producer.

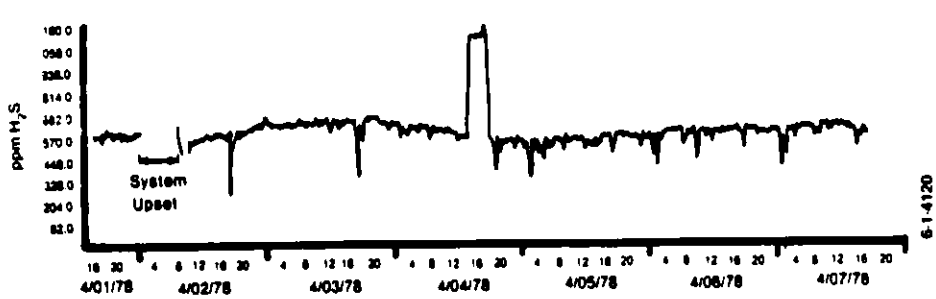

Figure 1: Process Gas Chromatograph Results-Hydrogen Sulfide Concentration in Product Gas

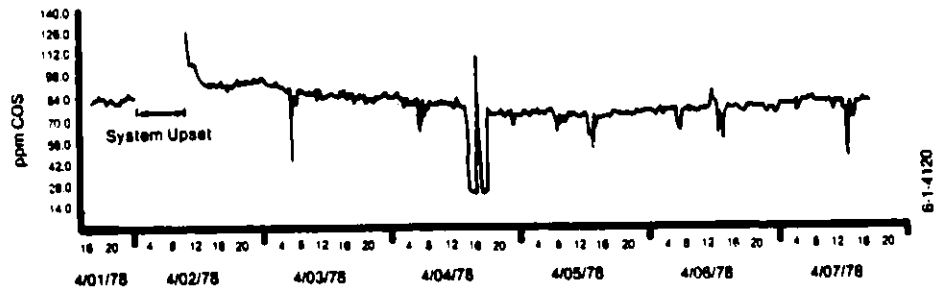

Figure 2: Process Gas Chromatograph Results-Carbonyl Sulfide Concentration in Product Gas

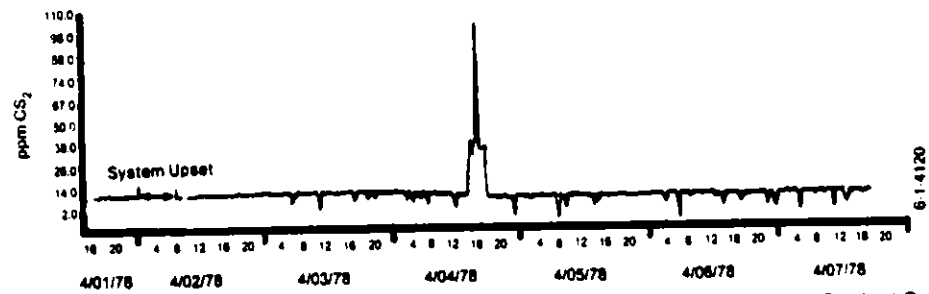

Figure 3: Process Gas Chromatograph Results-Carbon Disulfide Concentration in Product Gas

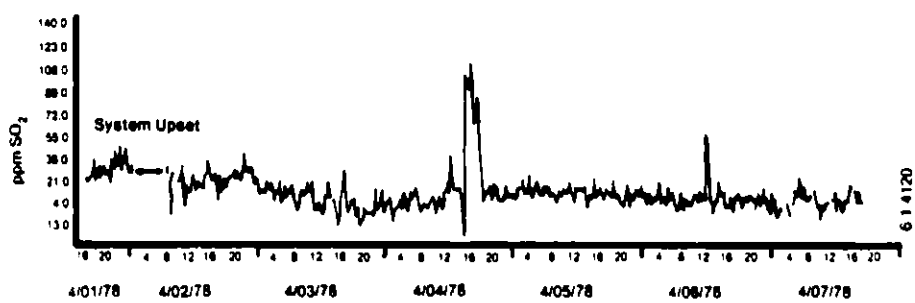

Figure 4: Gas Chromatograph Results Sulfur Dioxide Concentration in Product Gas

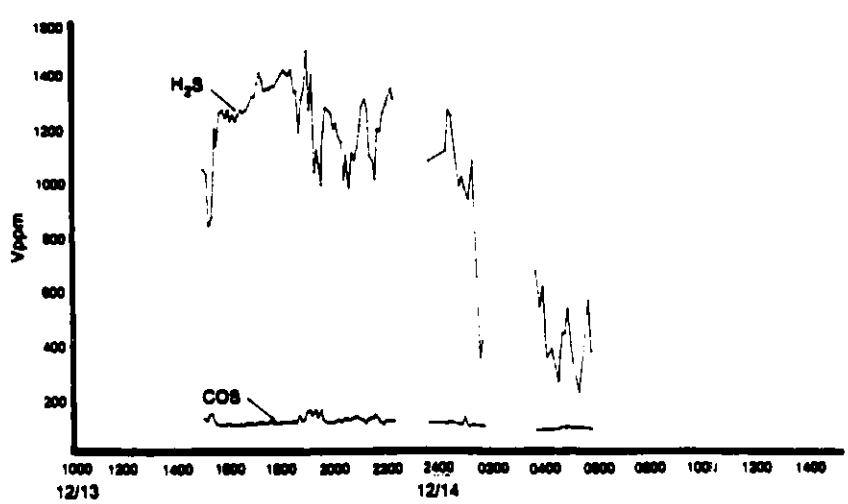

Figure 5: Process Gas Chromatographs Results-Sulfer Species Concentration in Product Gas

Data resulting from grab sample analyses, either by gas chromatographs or impinger techniques, may inaccurately represent sulfur concentrations if the samples are collected during periods of inordinately high or low concentrations of sulfur in the product gas. To present this point, the sulfur emission rate of the combustion effluents of the Wellman-Galusha product gas could range from 0.74 lb $SO_2/10^6$ BTU to 0.98 lb $SO_2/10^6$ BTU and the Riley Gas Producer emission rate could range from 0.29 lb $SO_2/10^6$ BTU to 1.47 lb $SO_2/10^6$ BTU based upon minimum and maximum concentrations of sulfur in the product gas streams at a given time. The New Source Performance Standard for sulfur emissions of coal-fired boilers is 1.20 lb $SO_2/10^6$ BTU. The average sulfur concentrations of the respective anthractive and lignite feedstocks of the Wellman-Galusha and the Riley Gas Producer were 0.61 percent and 1.10 percent on a dry weight basis. The variance of oxides of sulfur emission rates resulting from sulfur species in gasification product gas indicates the value of product gas monitoring of sulfur species using a process gas chromatograph.

Ammonia and other reduced gaseous nitrogen species including hydrogen cyanide are produced during the gasification process. During combustion of product gases, reduced gaseous nitrogen species are converted to oxides of nitrogen. Generally, the ratio of nitrogen as ammonia to nitrogen as hydrogen cyanide in low-Btu product gas is in the range of 4 to 8. Therefore, continuous monitoring results of ammonia in product gas is a valuable aid in the design of control devices for eventual oxides of nitrogen of combustion effluents. Analytical results for ammonia in the product gas of the Wellman-Galusha facility are presented in Figure 6.

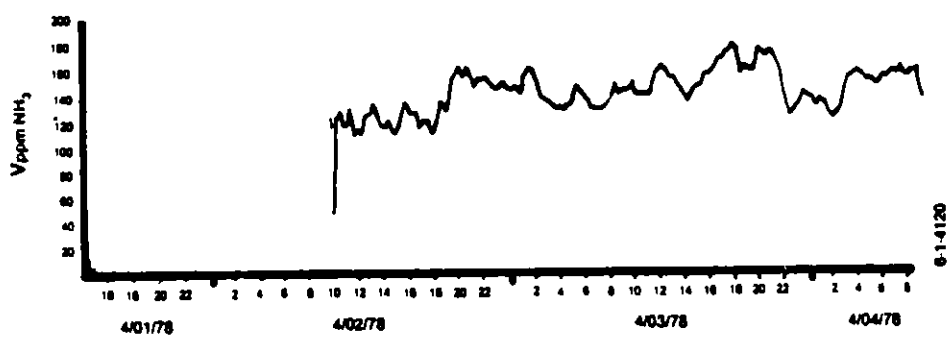

Figure 6:Process Gas Chromatograph Results-Ammonia Concentration in Product Gas

The NSPS for oxides of nitrogen is 0.60 lb $NO_2/10^6$ BTU. Based upon minimum and maximum ammonia concentrations as determined by process gas chromatographs and assuming complete oxidation of ammonia, oxides of nitrogen emissions resulting from the combustion of Wellman-Galusha product gas would range from 0.085 lb $NO_2/10^6$ BTU to 0.17 lb $NO_2/10^6$ BTU. The oxides of nitrogen concentration of the combustion effluent would be 0.15 lb $NO_2/10^6$ BTU based upon the average ammonia concentrations. This data does not include the NO_x contribution of hydrogen cyanide or the formation of oxides of nitrogen by thermal oxidation of nitrogen.

The ammonia concentration of the product gas at another Wellman-Galusha facility having a lignite feedstock was a factor of 4.7 higher than the product gas ammonia concentration at the Glen-Gery plant and the ammonia concentration of the Riley Gas Producer was a factor of 6.1 higher than at the Glen-Gery plant. Coupling the data that ammonia concentrations of other gasification facilities have been considerably higher than at the Glen-Gery plant, and that on the order of 10 to 30 percent additional nitrogen as hydrogen cyanide is present in the product gas, continuous monitoring of product gas streams for ammonia can supply valuable data for the design of control technologies.

PROCESS DATA

The energy source products of low-Btu gasification are hydrogen (H_2), carbon monoxide (CO), and hydrocarbons (HC). H_2 and CO are primarily produced by the steam-carbon reaction:

$$C + H_2O \rightarrow H_2 + CO$$

HC's are produced by pyrolysis of the coal and hydrogasification. Carbon dioxide is formed in the oxidation zone of the process and CO is also formed by the Boudard reaction:

$$C + CO_2 \rightarrow 2\ CO$$

During periods of inefficient operation of a gasifier, CO_2 concentrations increase. This is most often due to air flow problems through the bed created by ash agglomeration or uneven coal distribution.

To evaluate the variability of performance of a gasifier, continuous monitoring of H_2, CO, CO_2, and HC's provide the most useful data.

Figure 7 presents continuous monitoring data for major gases at the Riley Gas Producer. There are four discernable periods during which the concentrations of H_2 and CO decrease while the concentration for CO_2 increases. The relationship of the shifts in concentration is indicative of less than optimum performance of the gasifier as predicted by the reactions presented above. For each period, the time at which the shift in concentrations began coincides with gasifier ash removal which may have caused poor air distribution through the bed.

To support this proposition, the monitoring system was evaluated to determine if the analytical response time was short enough to identify fluctuations in gas composition due to ash removal. The residence time of the sample gas treatment and acquisition system was a maximum of one minute. The operation cycle of the Applied Automation TCD instrument is 10.25 minutes. Therefore, the shift of product gas concentrations of H_2, CO, and CO_2 could be detected within 12 minutes which is sufficient time to detect gas composition shifts due to ash removal which normally requires a minimum of 30 minutes to complete.

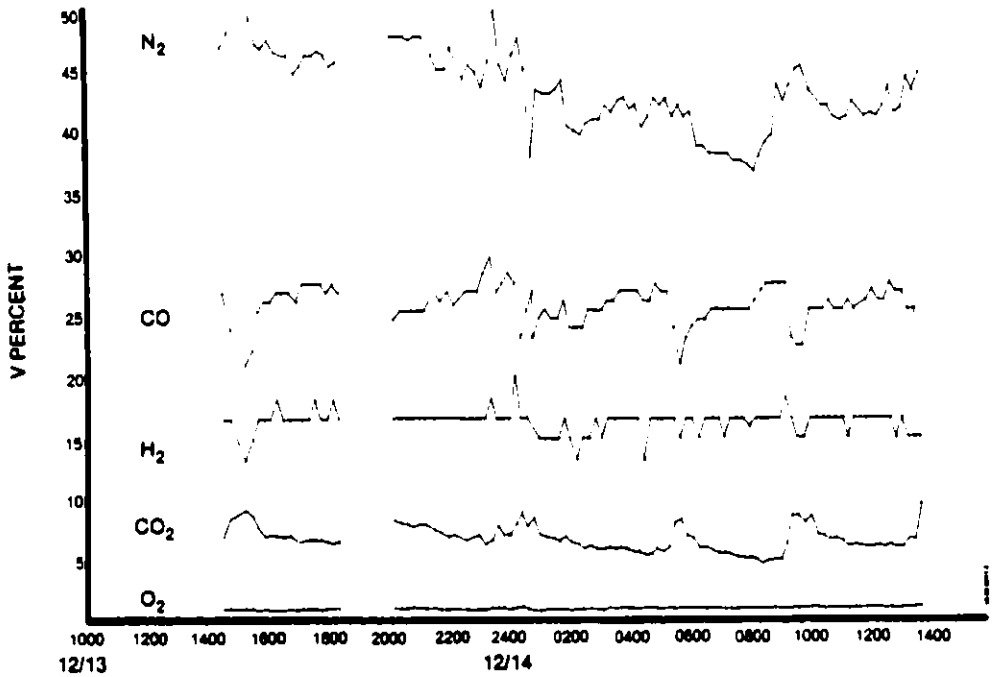

Figure 7: Process Gas Chromatograph Results-Major Gases Concentrations in Product Gas

The data verify the advantages of gasification process performance monitoring by process gas chromatography.

Hydrocarbon analyses at the Wellman-Galusha and Riley Gas Producer facilities did not fluctuate in a manner which could be directly viewed as operational deviations. This may be due to the formation of hydrocarbons in the upper regions of the gasifier as the coal is fed or as the coal lies on top of the coal bed and thereby somewhat removed from possible oxidative areas of the system. The hydrocarbon data generated at the Wellman-Galusha's is presented in Figure 8 and Riley Gas Producer hydrocarbon data is presented in Figures 9 through 11.

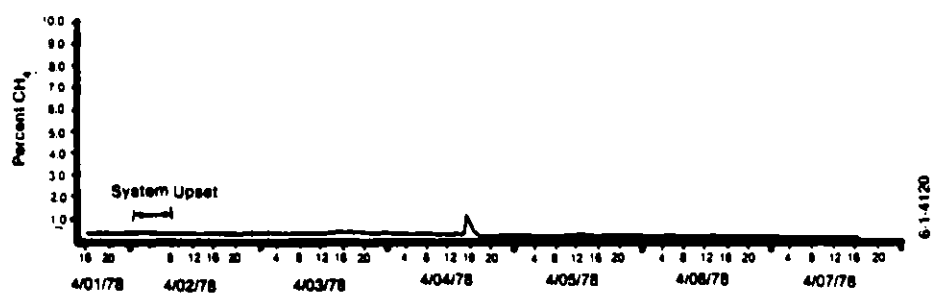

Figure 8: Process Gas Chromatograph Results-Methane Concetration in Product Gas

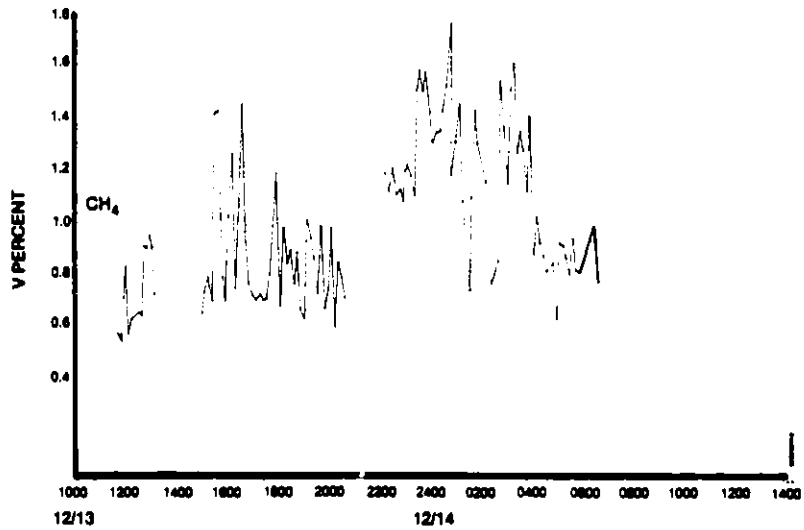

Figure 9: Process Gas Chromatographs Analytical Results
Methane Concentrations in Product Gas

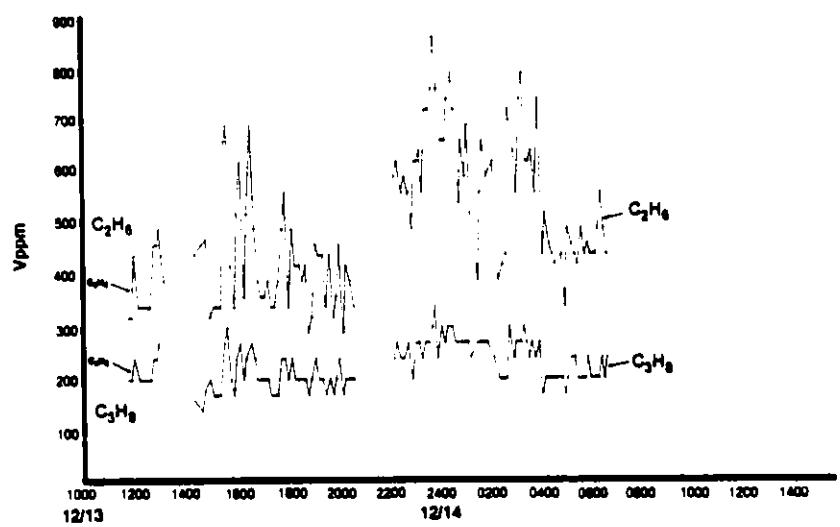

Figure 10: Process Gas Chromatograph Analytical Results
Ethane and Propane Concentrations in Product Gas

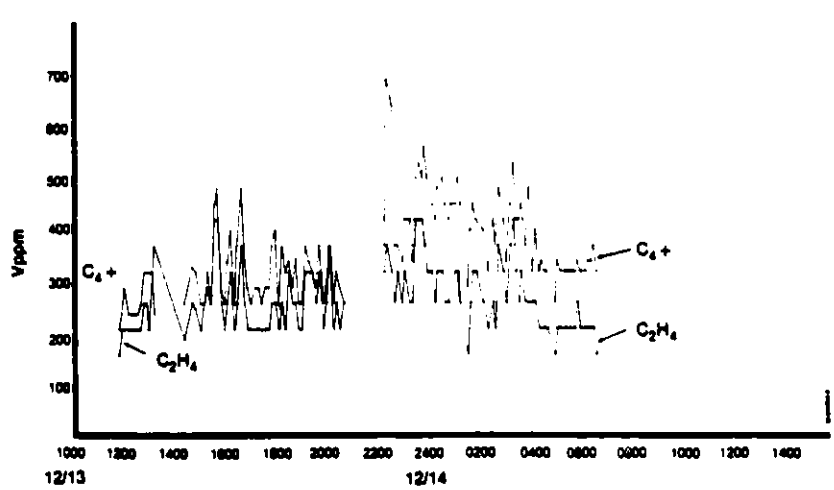

Figure 11: Process Gas Chromatograph Analytical Results
C_4 + Isomer and Ethylene Concentrations in Product Gas

DATA VERIFICATION

During testing at the Wellman-Galusha facility analyses of the product gas for hydrocarbons and sulfur species were also performed by bench gas chromatographs on grab samples. The samples were pressurized into bombs following filtration and moisture removal of the sample gas and were injected directly into the instruments utilizing sample loops. Instrument conditions of the bench gas chromatographs were:

FID	
Column:	6 ft. x 3.2 mm stainless steel with Porapak Q (100/ 120 mesh)
Carrier Gas:	N_2
Carrier Flow:	40 cc/min.
Detector Temperature:	200°C.
Oven Program:	40°C for 8 minutes; 8°C/minute to 220°C; 220°C for 4 minutes.

FPD	
Column:	10 f5 x 3.2 mm Teflon with 1 percent TCEP [1,2,3-tris (2-cyanoethyoxy propane)] and 0.5% H_2PO_4 on Carbopak B (60/80 mesh).
Carrier Gas:	N_2
Carrier Flow:	20 cc/min.
Detector Temperature	190°C
Oven Program:	40°C for 5 minutes; 20°C/minute to 90°C; 90°C for 10 minutes.

The results of the process and bench gas chromatographs for hydrocarbons and sulfur species were compared. The hydrocarbon results, methane, produced by the process and bench gas chromatographs are essentially identical. Instrument sensitivity of the process gas chromatograph precludes correlation of results.

Table 3 presents the comparison of the sulfur species data determined by the two instruments. The percent differences of the analyses by the two methods based upon bench gas chromatograph analysis is: H_2S - 9%, COS - 13%, CS_2 - 1600%, SO_2 - 85%. The standard deviation of the variance of the analyses is also presented. Variance standard deviations of H_2S and COS are below 15% while CS_2 and SO_2 analytical variance standard deviations are two and one orders of magnitude higher. However, concentrations of CS_2 and SO_2 were quite low which most probably accounts for the large analytical variance standard deviations of the two parameters.

TABLE 3. COMPARISON OF SULFUR SPECIES ANALYTICAL RESULTS DETERMINED BY PROCESS AND BENCH GAS CHROMATOGRAPH

Parameter	Process Gas Chromatograph (ppm)	Bench Gas Chromatograph (ppm)	Variance Standard Deviation (α)
H_2S	620	842	
	590	658	
	580	576	
	670	712	
	670	652	
	660	669	
			13%
COS	82	100	
	92	99	
	91	107	
	88	95	
	84	87	
	85	87	
			12%
CS_2	11	0.92	
	11	<0.5	
	11	0.89	
	11	<0.5	
			1900%
SO_2	23	77	
	23	8.8	
	13	7.2	
	11	10	
	6	4.6	
			130%

In addition to continuous monitoring of the Wellman-Galusha product gas for ammonia using a process gas chromatograph, samples of the product gas were also collected in a series of two Greenburg-Smith impingers containing five percent sulfuric acid for quantitation of ammonia. The samples were analyzed using a distillation/titration method. The analytical results for ammonia as determined by the two techniques and also the standard deviation of the analytical variance are presented in Table 4. The average difference of the two techniques based upon the impinger technique analytical results is 14% and the standard deviation of the analytical variance is 19%.

TABLE 4. COMPARISON OF AMMONIA ANALYTICAL RESULTS DETERMINED BY PROCESS GAS CHROMATOGRAPH AND IMPINGER TECHNIQUE

Parameter	Process Gas Chromatograph (ppm)	Impinger Technique (ppm)	Standard Deviation (α)
NH_3	140	160	
	150	204	
	130	127	
			19%

REFERENCES

1. Environmental Protection Agency. New Stationary Source Performance Standards: Electric Utility Steam Generating Units. Federal Register, 44, (113): 33580-33624, June 11, 1979.

2. Thomas, W.C., K.N. Trede and G.C. Page. Environmental Assessment: Source Test and Evaluation Report -- Wellman-Galusha (Glen-Gery) Low-Btu Gasification. EPA-600/7-79-185. Radian Corporation, Austin, Texas, August 1979.

3. Fuchs, M.R., R.A. Magee, and P.M. Jeans. Environmental Assessment: Source Test and Evaluation Report -- Riley Gas Producer Low-Btu Gasification, Radian Corporation, Austin, Texas (DRAFT). Contract No. 68-02-3137.

Tuesday Morning, June 9, 1981

Session C - Sampling and Analysis

AN AUTOMATED MASS SPECTROMETER FOR ON-LINE GAS ANALYSIS[+]

R. G. Bedford* and R. W. Crawford
Lawrence Livermore National Laboratory
Livermore, CA 94550
Phone: (415)422-6065, 422-6309
FTS 532-6065, 532-6309

ABSTRACT A077

A Time of Flight (TOF) mass spectrometer has been adapted for on-line gas analysis under computer control. This report describes the instrument and its application to coal gasification experiments in the field and in the laboratory.

The mass spectrometer system can be considered in three parts: the inlet, the mass spectrometer, and the computer. The inlet was designed and built at our Laboratory. It has a manifold of ports for gas standards and samples which can be connected to a reservoir where both temperature and pressure are controlled to ensure quantitative results. Gas flows from this reservoir into the mass spectrometer ion source through an atmospheric inlet device. The mass spectrometer is a standard CVC MA-3B time of flight instrument with a turbomolecular vacuum pump.

The spectrometer is interfaced to a remote, time-shared computer with a commercially available modular unit using an IEEE-488 bus. Computer programs are available to calibrate the mass scale, record the background spectrum, and maintain a library of standard gas cracking patterns. All of these programs presently require operator interaction. Refinements are being made to implement automatic updating of the background spectrum. After calibration and initialization procedures are completed, analyses can be scheduled at intervals as short as one every thirty seconds. These analyses can continue for periods of 24 hours or longer without operator intervention. The analysis routine scans the sample spectrum, strips the background, and computes the mixture composition using a stepwise linear regression algorithm. Precision of concentration measurements are about $\pm$2% of the amount present and typical limits of detection are about 0.1%, barring interference. The data acquisition system is being modifed to increase the dynamic range.

The mass spectrometer system has proven to be extremely stable and reliable. The mass scale has not changed since the original calibration. Standard gas cracking patterns and relative sensitivities have been reproducible to within the $\pm$3%.

[+]Work performed under the auspices of the U.S. Department of Energy by the Lawrence Livermore Laboratory under contract #W-7405-Eng-48.

*Presenting Author

THE APPLICATION OF CRYOGENIC SPECTROSCOPY TO THE DETERMINATION OF IMPURITY CONCENTRATION IN COAL GASIFIERS

R. F. Holland and G. P. Quigley
University of California
Los Alamos National Laboratory
P. O. Box 1663
Los Alamos, NM 87545

INTRODUCTION

The use of infrared absorption spectroscopy for determining the molecular composition of gas mixtures depends on identifying absorbing gas species from their spectral pattern and determining species concentrations from the magnitude of their absorbance in the spectrum of the mixture. Analysis for species having low concentrations in a gas may require long optical paths. In the analysis of complex mixtures, overlapping of spectral features can confuse identification, and strong absorption by major constituents of the mixture can mask absorption bands of species present at lower concentrations.

A method which earlier work at Los Alamos[1,2] has shown can effectively improve both the specificity and sensitivity of the ir technique involves condensing and dissolving a sample gas in a cryogenic liquid and observing the infrared absorbance of the cold solution.

We will describe preliminary experiments aimed at testing the applicability of this method to analysis for minority species in coal gasifier product gases.

The appeal of cryogenic solution spectroscopy for the minority species analysis rests on the following facts:[1,2]

(1) A number of small molecules have been shown to be soluble at low-to-moderate concentrations in the liquefied rare gases and a few other cold liquids that are optically clear for all or parts of the middle-ir spectral region.

(2) In the cold (100-200 K) solutions, ir absorption bands of the solute tend to be narrow, with full widths at half-maximum absorbance typically 1-10 cm^{-1}, as compared with 30-100 cm^{-1} typically observed in gas-phase bands at room temperature. The band-narrowing reduces band overlap for easier analysis of

complex mixtures. Also, since the absorbance per molecule is approximately the same in the liquid and gas phases, the narrowing increases the peak absorption and lowers the density required for detection.

(3) Condensation of the gaseous species reduces the volume, permitting greater absorption for a given optical path length. Furthermore, differences in volatility permit the concentration and infrared absorption by some minority species to be enhanced relative to some of the absorbing majority species.

(4) Finally, infrared absorption bands of materials in the solutions, while narrower overall than in the gas phase, have no fine structure and are broad enough that the spectral resolution required for accurate absorbance measurements (1-2 cm^{-1}) is well within the capability of common infrared spectrometers.

The effective increase in sensitivity is demonstrated in Fig. 1 (Ref. 1) where a spectrum of the ν_3 band of warm CO_2 gas is compared with the same band of CO_2 in cold liquid xenon. The CO_2 molecular density in the solution is one-hundredth that of the gas. The ν_3 band of $^{13}CO_2$ is perceptible near 2270 cm^{-1}. The concentration of this isotopic species in the solution is ~0.02 molar ppm.

The spectral simplification in the cold solutions is demonstrated in Fig. 2 (Ref. 1) which shows bands of two halocarbons which overlap in the gas-phase spectra (II, III), but are clearly distinguished in the spectrum (I) of the solution in liquid air.

For the solutions of Figs. 1 and 2, the absorbing species were easily condensed as minor impurities in the clear solvents. In an analysis of a gasifier product, one must sample a mixture containing, in addition to the minor species of interest, quantities of both strong absorbers such as CO_2 and less readily condensible gases such as H_2. To simulate the minority species analysis, we cryogenically sampled gas mixtures with NO, NO_2, N_2O, NH_3, SO_2, and COS representing minority species, and with CO, CO_2, CH_4, and H_2 present as majority species. The samples were dissolved in liquid xenon for the spectral observations.

EXPERIMENTAL PROCEDURE

To simulate a gasifier product gas, a gas mixtures was prepared by combining 1-psi partial pressure each of minority species NO, NO_2, N_2O, NH_3, SO_2, and COS, in that order. To the mixture, we added 83 psi of CH_4, 200 psi of CO_2, 498 psi of CO, and 213 psi of H_2, for a total pressure of 1000 psi. It is understood that combination of the NO_2 with itself and with NO to produce N_2O_4 and N_2O_3 and possible other reaction products may occur. However, if this is ignored the mixture would consist of 0.1% of each minority species, and of 8.3% CH_4, 20% CO_2, 49.8% CO, and 21.3% H_2.

The gas mixture was admitted to a spectral cell (Fig. 3) at room temperature and 10,000 torr (193 psi) pressure. The cell was valved off just above the gas inlet and cooled to -186°C. Most of the H_2, CO, and CH_4 was then pumped out, reducing the pressure to 135 torr. The cell was then valved off again, warmed to -110°C, and Xe gas admitted to fill the cell with liquid xenon (LXe) to an overpressure of 1688 torr. The liquid was stirred and the cell was vented to reduce the overpressure to 876 torr (near the vapor pressure of the LXe). The infrared transmittance of the solution in the middle infrared (4000-500 cm^{-1}) was then scanned with a Perkin-Elmer Model 180 grating spectrometer operating with a spectral resolution of ~2 cm^{-1}.

RESULTS

Spectra of the LXe solution for two interesting regions are shown in Figs. 4 and 5. Figure 4 shows the ν_3 bands of N_2O and COS, which are easily distinguished from the strong CO_2 absorption and the absorption by residual CO remaining in solution. Absorption in the two minor-species bands is about that expected for the N_2O and COS present in the dissolved gas mixture. Judging from these spectra, each species could probably be detected with one-hundredth of the absorbance observed, which would correspond to concentrations of about 10 ppm in the simulated gasifier product gas.

It should be pointed out that while the CO_2 present in the gas mixture has been retained and is dissolved in the xenon solvent, the CO, which was half the gas sample, has been reduced to a concentration not

very much greater than the minority species. In the gas-phase spectrum, both the N_2O and COS ν_3 bands are strongly overlapped by the CO (0-1) band.

The spectrum of Fig. 5 shows the strong ν_3 band of SO_2 and the N_2O and N_2O_4 bands in the vicinity of the ν_4 band of CH_4. Like the CO, the CH_4 concentration has been substantially reduced. This fact, and the band-narrowing in solution, permits easy resolution of the minority-species features; whereas in the spectrum of the sample gas mixture, all would be strongly overlapped by the CH_4 ν_4 band. Absorbances of the SO_2 and N_2O bands are about as expected for the concentrations present in the gas sample.

The N_2O_4 band appears in Fig. 3, because essentially all the NO_2 is converted to the dimer in the solution.

No NH_3 bands nor NO bands were observed in the solution spectra, and the N_2O_4 concentrations appeared substantially lower than expected for the NO_2 present initially in the gas sample. NO is sufficiently volatile that part of it may have been removed with the pumpout of H_2, CO, and CH_4. A possible reason for the reduction of NO_2 and the absence of NH_3 and NO is that a small amount of H_2O may have been introduced in the gas handling. This would permit reaction of NO_2, NO, H_2O, and NH_3 to make NH_4NO_2. No special precautions were taken to minimize H_2O, since it will be present in the gasifier product.

NO is a relatively weak absorber; however, in the cold solutions it combines with NO_2 to form N_2O_3 which is a strong absorber. Also, NO is readily oxidized by O_2 to NO_2 which (as N_2O_4) is a strong absorber in solution. It may be possible to treat the sample gas with O_2 and analyze for NO as NO_2.

The results described above demonstrate some of the advantages of cryogenic solution spectroscopy noted in earlier work[1,2] and described in the Introduction. The spectra of a synthetic mixture of gases dissolved in liquid Xe indicate that this approach may be useful in analysis of gasifier product gases for at least some minority species.

A number of questions and possible problems should be mentioned. Among the most crucial problems is the elimination of water and particulate matter which, when present in substantial quantities, will tend to plug lines into a cooled cell. The solubility of minority species in cryogenic solvents has been measured for only a very few solvents

and solute materials. Most transparent (or partially transparent) cryogenic liquids are poorer solvents than xenon. Xenon is moderately expensive (about $17 per charge in our one-half-in. cell); however, this expense probably can be reduced by cleaning and recycling the xenon. Our experiment suggests that, with the half-inch cell and the procedure used here, N_2O, COS, SO_2, and possibly NO_2 can be detected at ~10 ppm in the sample gas. It has not been demonstrated that these materials will remain in the condensate at low concentrations; however, if they do, the sensitivity may possibly be increased by condensing more of the sample gas.

REFERENCES

1. S. M. Freund, W. B. Maier II, R. F. Holland, and W. H. Beattie, Anal. Chem. 50, 1261 (1978).

2. W. H. Beattie, W. B. Maier II, R. F. Holland, S. M. Freund, and B. Stewart, SPIE Vol. 158 Laser Spectroscopy, p. 113 (1978).

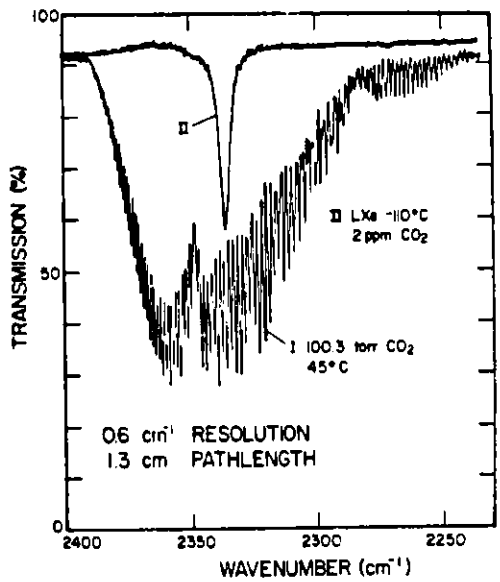

Fig. 1. Infrared absorption spectrum of 100.3 torr of CO_2 vapor at 45°C (curve I) and that of 2 ppm (in mole ratio) of CO_2 dissolved in liquid Xe at -110°C (curve II). Note that the CO_2 molecular density in the liquid solution is one-hundredth that of the gas.

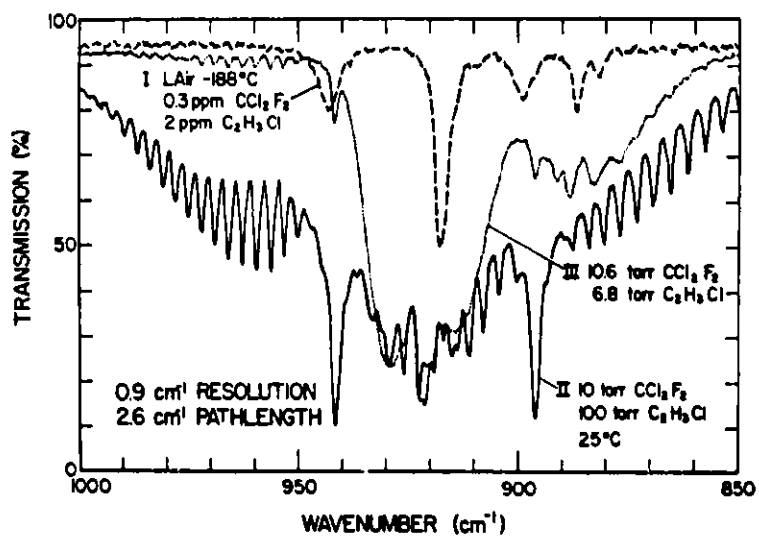

Fig. 2. Infrared spectrum (curve I) of a mixture of CCl_2F_2 (0.3 ppm; features at 917.5 and 886.5 cm^{-1}) and C_2H_3Cl (2 ppm; features at 943.0 and 899.0 cm^{-1}) dissolved in liquid air at -188°C, and spectra of 25°C mixtures of 10 torr of CCl_2F_2 and 6.8 torr of C_2H_3Cl (curve III). Notice the relative ease with which the solute bands are distinguished in the solution spectrum.

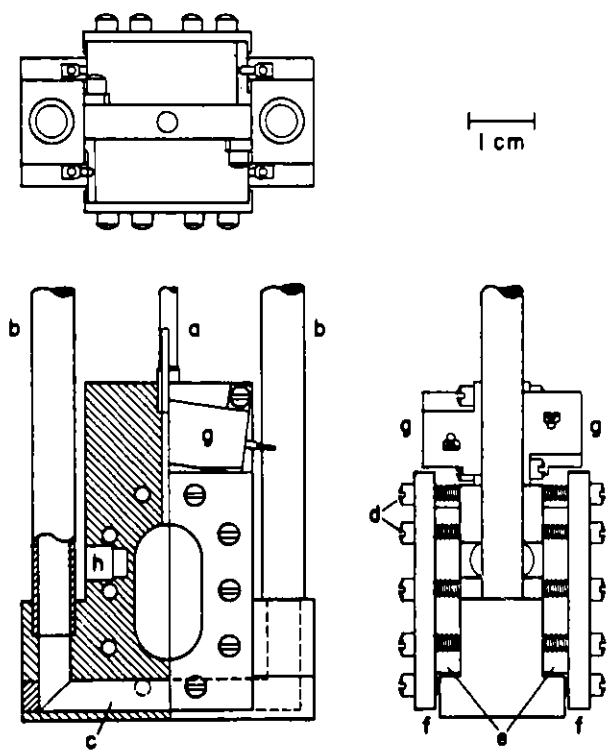

Fig. 3. Cryogenic spectral cell. The cell body is copper. The interior of the cell is connected to a gas-handling manifold through the fill tube, a; liquid nitrogen coolant is forced through tubes, b, and channel, c, in pulses whose length is determined by a temperature controller. Spring washers and screws, d, hold the windows, e, (here AgCl) and window clamps, f, in place. Resistors, g, are used for rapid cell warmup with coolant off or with coolant on, to warm the upper part of the cell when filling to help keep inlet lines free of solid condensate. Copper has been removed at h to decrease thermal conduction. Thermocouples are attached near top and bottom of the cell for temperature measurement and control. A maximum temperature differential of ~ 20°C can be maintained between the top and bottom at -100°C. With temperature regulated and heaters off, the cell temperature at the top is within 1-2°C of that at the bottom. The cell is suspended from an appropriate flange, which fits into a vacuum jacket with KCl windows. The optical path length through the cell is 1.37 cm, and the cell volume is 2.5 cm^3.

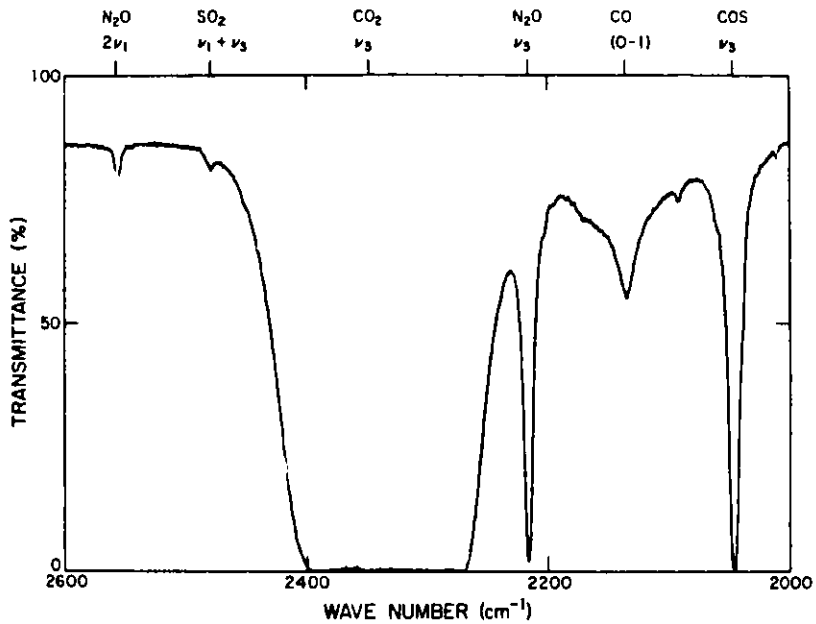

Fig. 4. Infrared transmittance of a solution prepared by dissolving a mixture simulating coal gasifier product gases in liquid xenon. The solute gas mixture originally included 0.1% each of NO, NO_2, N_2O, NH_3, COS, and SO_2 in 8.3% CH_4, 20% CO_2, 49.8% CO, and 21.3% H_2. Treatment of the mixture to remove most of the CO, H_2, and CH_4, and possible accidental removal of most of the NH_3, NO_2, and NO is discussed in the text. Densities of N_2O, COS, SO_2, N_2O_4, and CO_2 in solution correspond approximately to 10, 10, 10, 2, and 2000 torr, respectively, of these gases at room temperature. Temperature of the solution is -110°C. The spectrometer cell used is that shown in Fig. 3. Absorption bands of solute species are marked.

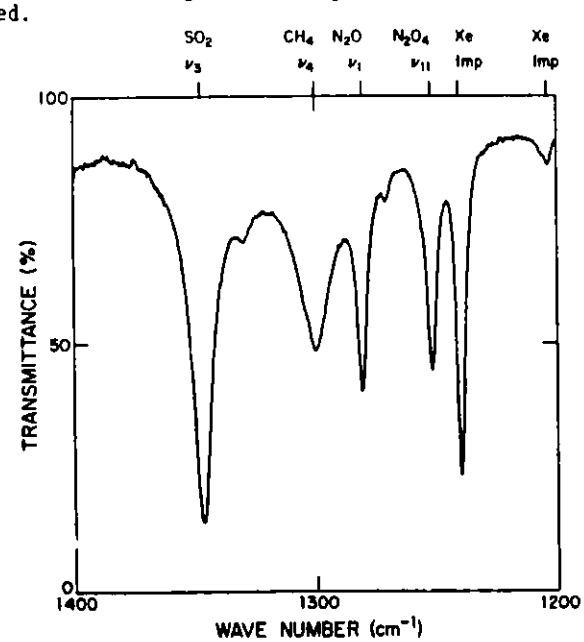

Fig. 5. Infrared transmittance of the same sample used for Fig. 4. Absorption bands of known solute species are marked, as are two bands due to unidentified impurities in our xenon solvent.

AUTOMATIC SAMPLING AND ANALYSIS FOR A COAL CONVERSION REACTOR

Harrison R. Cooper

Harrison R. Cooper Systems, Inc.

Composition analysis of coal and other bituminous materials associated with synfuel conversion implies requirements for determining impurities which can influence process efficiency. In addition to proportions of solids to liquids (unconverted to converted material), information on impurity constituents such as heavy metals sulfur, and ash components, are needed. Various techniques for continuous process stream analysis are conceptually possible, but the X-ray fluorescence process stands out as commercially proven technique with a successful application history. This discussion will focus on methods of automatic sampling and analysis with potential to enhance efficiency of synfuel production from coal and related materials.

Automatic Sampling and Analysis of Nonhomogeneous Materials

The specific problem associated with composition analysis in two phase solid-liquid materials lies in the need to supply a representative sample stream to the analyzing device. This problem is keyed to assuring that a small stream taken from the bulk flow is identical (within a statistical limit of error) in all parameters to the large flow. The definition demands the percent solids in the

---

Presented at the 1981 Symposium on Instrumentation and Control for Fossil Energy Processes, San Francisco, California, June 8-10, 1981

sample be representative in the sample stream, and further that the particle size distribution be the same in both. Also, the proportion of each component (pyrite, ash and so forth) be equivalent in the sample and bulk streams.

Automatic sampling procedures developed in mineral processing for automatic control can be offered as initial technique for solid-liquid mixtures. The classical technique, applicable to flow out of pipes or troughs in open atmospheric sampling, is the traversing method. The principle is to take a complete systematic "cut" of the stream at frequent short time intervals. Depending on the size of the particles in the stream, the speed of traverse can be relatively high. A rugged design for such needs is shown in Fig. 1. These types of sampling machines can be controlled to provide a steady flow of material to the analyzer. Sampling in a closed system, and under pressure, leads to greater complications. The best approach to assuring a representative sample will be taken is a "thief" at the vertical discharge of a pump. In any event, experience drawn from mineral industry practices is generally employable in developing an effective scheme for reliable automatic sampling of slurries.

The automatic sampling system is then coupled to an automatic analyzer, of which on-stream analyzers employing X-ray fluorescence are the well known proven devices. An example of such equipment is illustrated in Fig. 2. The analyzer is typically provided in a complete integral system with controlled slurry feed for sample presentation. Internal operating functions are usually microprocessor controlled for continuous stand-alone use.

X-ray Fluorescence Analysis Technique

X-ray fluorescence analysis is a technique of determining elemental content of materials by the interaction of high energy photons with the atoms in the material to be analyzed. The X-ray source provides the high energy photons. These are absorbed by the atoms and, consequently, a secondary photon is released by each atom that absorbs a source photon. The released photon has a characteristic energy. The process of absorption and release is called fluorescence.

Each element in the periodic table can be recognized by the energy of the released photons generated by the X-ray fluorescence process. Photons are also scattered in the interaction of the source radiation and matter. When translated to a systematic process of beaming radiation energy on the sample and measuring response radiation from resulting excitation, a reliable and efficient non-destructive measurement procedure can be constructed for elemental analysis of materials.

Historical Background

X-ray fluorescence analysis (XRF) equipment made its first appearance in the mid 1950's, and became quickly established as an industrial testing method. Applications to industrial quality control and continuous process stream analysis began in the early 1960's in the cement industry, mineral processing industry, and in primary production of steel and alloy metals. Reviews of applications in extractive metallurgy, and to analysis of allow metals, are cited (1), (2).

Improved electronics technology and equipment refinements brought XRF to an accepted status for industrial use in the 1970's. XRF techniques may be adapted to acquiring data important for process control in coal and synfuel production, by providing key composition variable data as sulfur, ash, iron and measurements of trace element content. Analyses can be performed on slurries of coal and other solids in oil or water media, as well as liquid phase hydrocarbons.

Description of Method

X-ray fluorescence analysis requires a source of energetic photons in the 0.5 to 3 angstrom range, and a detector for photons applicable to this range. Electronic analysis of the photon energy is required, which can be in combination with a diffraction system to separate photons into an energy level representing an element of interest. A simplified description of this scheme is presented in Fig. 3.

XRF analysis in essence requires a finite time to take a measurement, perhaps 10 seconds at a minimum, but extending to as long as five minutes. The process is therefore not instantaneous or continuous, but periodic.

Methodology of XRF analysis has evolved to the point where a number of practical variants can be examined in specifying optimal procedures. An example is choice in the source of exciting radiation. A high energy X-ray tube will emit intense radiation, and the tube can employ a variety of internal target metals allowing the user to select from a range of energy distributions. Photon energy on the low end of the range are best for light element analysis, and vice versa. A requirement for XRF excitation is that radiation must

exceed a specific energy level for the process to take place. High intensity X-ray tubes are expensive and there are complexities in their use. An alternative is to use a low energy tube, but cost savings may be overruled by the slower cycle of measurement. For some applications, a long measurement time is impractical. Another alternative is use of a radioactive isotope for source radiation. Although this approach has many positive features, there are also disadvantages. The primary concern is obtaining a radioisotope with the proper energy for efficient excitation, and a second concern is the strength of the source in practical application. With regard to the latter, health and safety considerations preclude use of sources with significant energy and the result is frequently overly long time requirements for efficient measurement. This discussion of source radiation highlights certain practical problems in selecting an approach to XRF analysis which best suits the application. Questions with the same focus are necessary in determining how best to carry out detection, photon energy analysis, and other practical matters relating to XRF analysis, as pertinent to the application.

Comparison to Other Analytical Techniques

Process stream analysis for coal and synfuel materials can be accomplished as well by other methods competing with XRF. It is necessary to consider such alternates in conjunction with evaluating whether XRF procedures are optimum for an application. Most alternates are not as far along in performing the service duty in routine day-to-day operation. The alternates include neutron activation, atomic absorption, and mass spectrometry. Neutron activation analysis is available in two forms -- prompt gamma

emission (PGE) and thermal neutron absorption (TNA). The TNA approach is widely employed in iron ore slurry analysis, primarily for Si determination. The method depends on measuring the radioactivity induced by exposure of the sample to several minutes in a neutron field. PGE analysis has more recently reached a state of practicality, using higher energy neutrons to generate characteristic radiation from absorption. The PGE approach is being applied to bulk coal analysis in solid phase, and could be applied to liquid phase hydrocarbons as well. The method is less likely to be practical for water slurries, because the neutron field is moderated by hydrogen in water.

Accuracy In The Application of XRF

The analytical capability of XRF diminishes as the atomic numbers decrease. Analysis of elements below atomic number 13 (aluminum) in slurries becomes infeasible, because the measurement path of helium gas will attenuate the fluorescent photons. Vacuum XRF (not feasible for slurry applications) remains effective to as low as atomic number 8. Conversely, the sensitivity of XRF generally increases with rising atomic number of the element. The influence of back scatter radiation can be a problem for some elements when measuring low concentrations, but resolution can be reached through mathematical treatment of the measurement data.

Fortunately, the significant composition characteristics of coal materials processed in synfuel conversion reactors can be derived from XRF analysis. Heavy elements are typically determined to a level

of a few parts per million, particularly in the liquid phase. Even lower concentrations can be handled by polarized radiation.

Many analytical requirements may call for use of additional sophistication to resolve questions of composition. For example, the determination of percent solids in a coal-oil slurry or coal-water slurry will require resolution of differential scatter radiation detected as the outcome of the liquid and solid phases being different in average composition and density. However, the differences are not great. Conventional absorption of gamma radiation source does not make an accurate distinction, for example. X-ray scattering can be detected in the coherent and incoherent forms (also termed respectively Rayleigh and Compton). The line separation can be made quite accurately with wavelength energy dispersion, and by pulse energy discrimination on the respective peaks. Figure 4 illustrates the degree of resolution attainable with coal-water slurry scattering, an application very similar to coal-hydrocarbon. The key factor is the differential is created by the primary (coherent) scattering being a function of the scatter cross section to the first degree, while incoherent is to the third. Influence of ash components, sulfur and other composition variables may be taken into account in the percent solids determination by mathematical treatment of the data.

Calibration

Measurements with an analyzer provides only indirect data, but the XRF process can be modeled mathematically by describing absorption of the primary X-ray source in the sample, and simultaneous emission of fluorescent radiation. This signal radiation is also absorbed and scattered.

Scatter is also accountable through mathematical interpretation. The parameters of X-ray absorption, scatter, and yield are documented for all the elements, as well as the energy of emission lines and so forth. Multi-element slurries consisting of varying levels of elements ranging from heavy to light give rise to complex interactions as interelemental absorption and scattering effects take place. By compiling pertinent data, an accurate description of the XRF process can be computed, and a reliable means of calibrating an analyzer for multielement analysis, using laboratory analysis as primary standards. In many cases, greatly simplified procedures using multiple linear regression can be employed with adequate results.

Typical results with XRF for sulfur and silicon, two elements of primary interest in synfuel processing, are given in Fig. 5. The readout is linear in this case, but the linearity of pulse counts is generally valid over limited ranges of concentration, depending on the elements in the matrix. Expectations of accuracy range from relative values of one percent at best to ten percent for low concentrations.

REFERENCES

1. Cooper, H. R., "On-Stream X-ray Analysis," A. M. Gaudin Memorial Volume 2, M. C. Furestenau, editor, American Institute of Mining, Metallurgical. and Petroleum Engineers, Inc., New York, New York, 1976, pp 865-894.

2. Birks, L. S., "X-ray Spectrochemical Analysis," Interscience Publishers, New York, 1959.

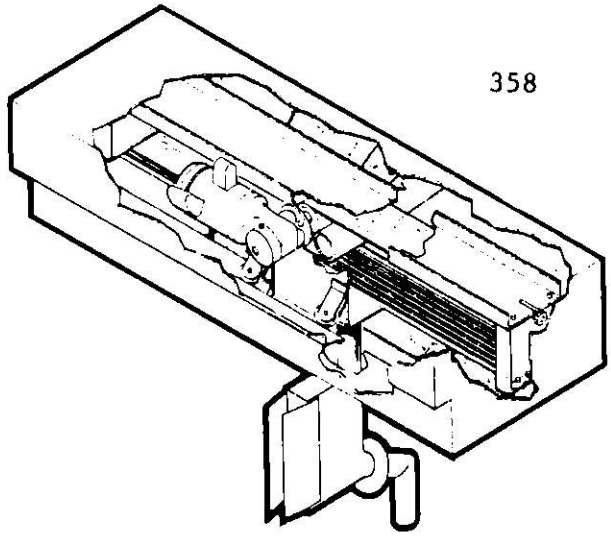

FIG. 1 - POWEROLL™ TRAVERSING SAMPLER

FIG. 2 - SCHEMATIC DIAGRAM OF X-RAY FLUORESCENCE ANALYZER

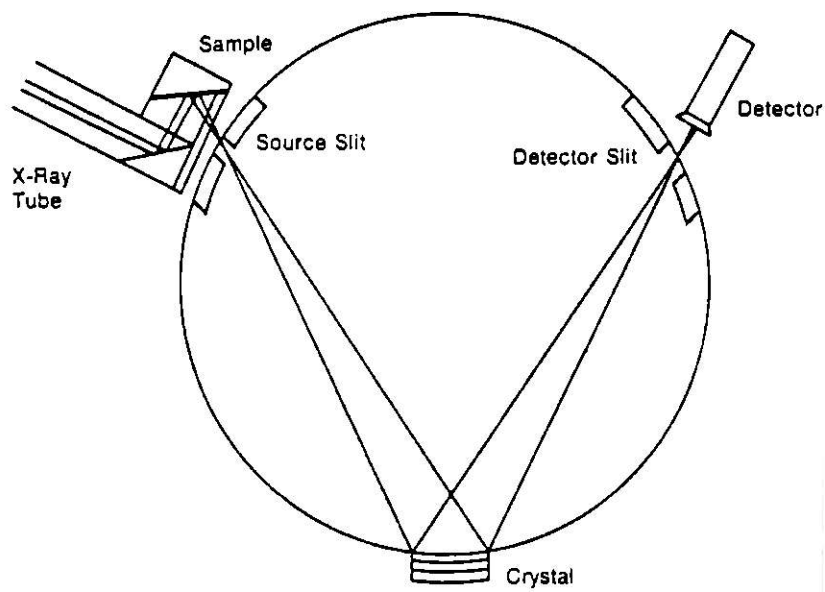

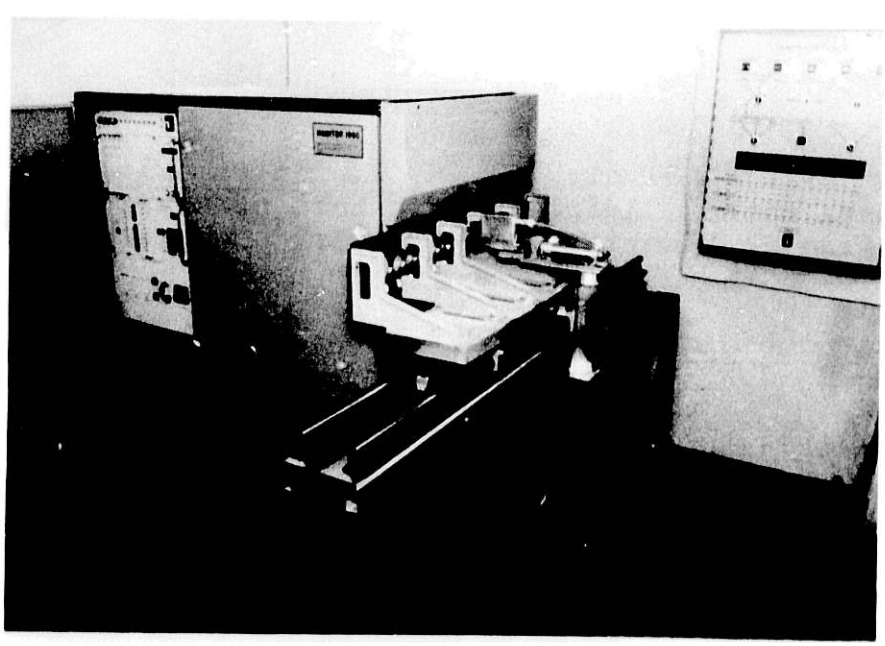

Figure 3
MONITOR 1000
On-Stream X-Ray
Fluorescence Analyzer

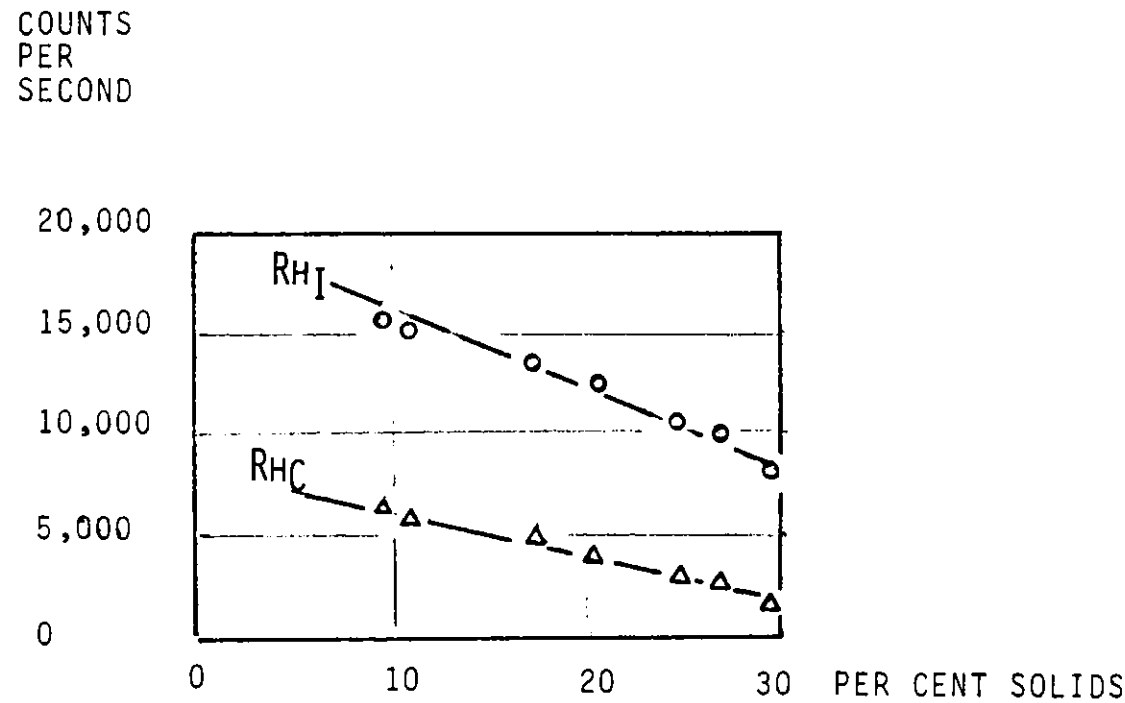

FIG. 4 - SCATTER RADIATION IN COAL-WATER SLURRY

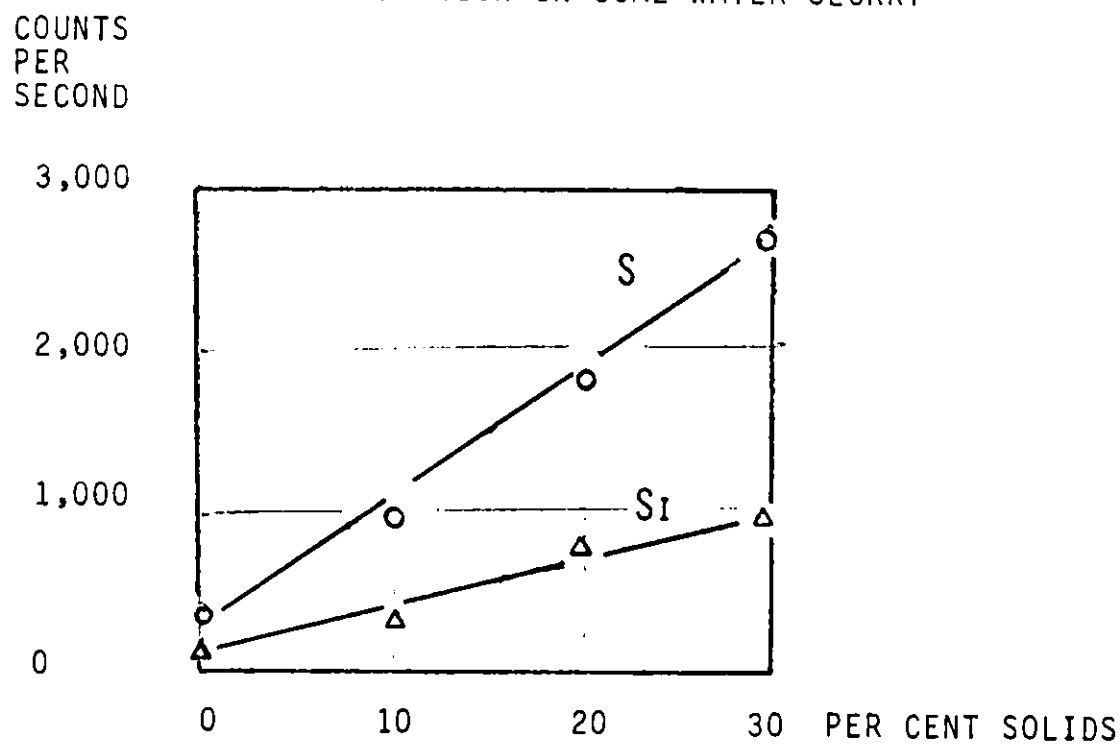

FIG. 5 - SENSITIVITY TO SILICON AND SULFUR FLUORESCENT RADIATION

A PORTABLE AUTOMATIC MONITOR FOR CONTINUOUSLY MEASURING SULPHURIC ACID VAPOUR IN COMBUSTION GASES

R.C. Hotchkiss
P.J. Jackson
CEGB.Marchwood Engineering Laboratories, Marchwood, Southampton.

Dr.D.A. Hilton
Severn Science Ltd, Thornbury, Bristol.

SUMMARY

The concentration of sulphuric acid in combustion gases is a dominant factor in determining the thermal efficiency, maintenance requirements and the impact on the environment of many fossil energy processes.

A portable automatic continuous analysis and sampling system has been developed for measuring sulphuric acid vapour ("SO_3") in gas at concentrations between 0.5 and 100 v.p.m. A gas sample is withdrawn via a heated probe through a silica wood filter and any sulphuric acid is dissolved in 4:1 propan-2-ol: water solution; the ratio of flow rates of gas and solution is kept constant at a chosen value. Sulphate in the solution is determined by passing it through a static porous bed of barium chloranilate which yields an equivalent concentration of acid chloranilate ion. This is measured photometrically at its absorption peak at 535 nm.

The sampling probe and analyser are linked by a flexible umbilical; probe and umbilical can each be up to 5 m long. The instrument is compact and suitable for measurements on industrial plant or in laboratories over a wide range of ambient temperatures; there is easy access to components for maintenance.

The construction and performance of the instrument are described. The monitor has been in commercial production since July 1978, and has been applied extensively in research on conventional and fluid bed (atmospheric and pressurised) combustion plant.

INTRODUCTION

The principal constituents of flue gas from the combustion of fossil fuels are nitrogen, carbon dioxide, water vapour and excess oxygen but sulphur dioxide is also present, at typically 100 to 2500 volume parts per million (v.p.m). A small proportion of the SO_2 is oxidised to SO_3 which can have deleterious effects on plant surfaces and on the external environment since it combines with water vapour below about 300°C to form sulphuric acid. At the usual concentrations of sulphuric acid present (1 to 100 v.p.m.) the dewpoint is between 110 and 160°C, varying slightly with water vapour concentration.[1] Condensing acid forms a sticky film which collects solid products of combustion. These deposits may eventually

become re-entrained in the gas stream resulting in the release of "acid smuts" from the chimney to the environment. When the flue gases cool on discharge to the atmosphere, the sulphuric acid condenses imparting significant opacity to the plume.

There is an incentive to burn fuel in the most efficient way commensurate with minimising corrosion of the plant and the discharge of solid material and opaque gases to the environment. It is therefore desirable to measure SO_3 in the flue gas of conventional combustion systems and to be able to determine the SO_3 production characteristics of alternative coal conversion technologies such as fluid bed combustion. Several methods are available. Most involve batch-sampling techniques which are time - and labour-consuming and produce only an integrated value over the sampling period of many minutes: at best, four or five observations per hour are possible. Continuously recording instruments have been described previously [2,3,4] but these monitors were not sufficiently portable to be available for use at all relevant locations. Much of the experience gained in the use of the earlier automatic monitors has been used to produce the first portable, continuously recording instrument for measuring sulphur trioxide in flue gases. It was designed to be sufficiently rugged and compact for intermittent plant testing, capable of unattended operation for periods up to 2 days and of continuous use for at least several weeks over a wide range of ambient temperatures.

DESCRIPTION

Principle

In common with its predecessors, the monitor described here operates on the basis that SO_3 or H_2SO_4 in the gas sample is converted to sulphate ions in an aqueous solution of propan-2-ol (isopropanol). Isopropanol inhibits the oxidation of SO_2 which is invariably present in much larger quantities than SO_3. The solution is passed through a porous bed of barium chloranilate crystals[5] in which the following reaction occurs:-

$$SO_4^{2-} + BaC_6O_4Cl_2 + H^+ \rightarrow BaSO_4 + HC_6O_4Cl_2^-$$

The acid chloranilate ions released absorb light preferentially at 535 nm and their concentration is measured using a continuous flow photometer. By maintaining a constant ratio of flow rates of the gas sample and absorbing solution, the concentration of acid chloranilate ions is directly proportional to the sulphate ion concentration in the isopropanol solution and hence to the SO_3 concentration in the gas.

The monitor consists of three units [6](Figure 1): a sample probe in which the initial contacting of gas with isopropanol solution occurs, an analyser unit in which the solution/gas mixture is treated and the chemical processing undertaken, and a recorder.

Standard Probe Unit

For most industrial steam-raising plant where it is necessary to

limit cold end corrosion, a suitable sampling point for measuring SO_3 is at the boiler outlet; for larger boilers, between the economiser outlet and the air heater inlet. Using the standard probe, gas can be sampled up to 350°C but, at high temperatures, there is a possibility of catalytic oxidation of SO_2 on the surface of the sampling tube. In these circumstances the probe should be surrounded by a water cooled jacket. It is also necessary to prevent the duct wall and any support provided for the probe tube from acting as heat sinks and producing potential condensation sites within the probe. Air leaking past the probe at high velocity, due to large pressure differentials between the duct and atmosphere, can also cause local over-cooling. Adequate sealing and external insulation of the relevant part of the probe will avoid problems.

The flue gas is removed at a measured rate (typically 0.5 Nl/min) through a heated tube (normally silica). It then passes through a heated silica wool filter to remove particulates and into it is injected the 4:1 isopropanol-water solution inside a graphite-filled PTFE block. The silica tube is supported inside a steel tube electrically heated to about 250°C, i.e. well above the acid dewpoint. The filter and contacting end of the graphite-filled block are enclosed in an oven maintained at 200°C. Precautions which must be taken to avoid sampling errors are discussed in reference 6.

Analyser Unit

The analyser is connected to the probe by an umbilical consisting of silicone rubber tubes for solution supply and return lines and a power cable. In the analyser unit the isopropanol/water/flue gas mixture passes to the reaction bed via a No.4. porosity sintered glass filter in which any acid aerosol is coalesced with the bulk of the solution which continuously rinses it through the unit. The solution and gas flows are then separated. The gas is extracted and discharged to atmosphere via flood traps, a flow control valve and a flow meter. The solution is drawn through the barium chloranilate reaction bed with an approximately equal volume of gas to preclude flooding. The liquid containing acid chloranilate ions in proportion to the sulphate reacted is then degassed and passed to the photometer for measurement. Reference 6 describes this equipment in more detail.

The monitor is calibrated by passing solutions of sulphuric acid in 4:1 isopropanol:water mixture through the analyser, temporary connections being made to pump the solution directly to the top of the reaction bed.

There are a number of options available for changing the standard scale range. Gas and liquid flow rates can each be varied by factors of at least two, the length of the cuvette can be reduced, and an optical filter of different density can be used in the photometer; for higher sensitivity, such as would be required for atmospheric measurements, a longer cuvette could be provided.

Performance characteristics of the monitor are described in

reference 6 where the effects of SO_2 and HCl are also quantified.

Comparison with the Selective Condensation Method

Many investigators have used the manual method based on selective condensation of sulphuric acid at surface temperatures above 60°C [7] because of its simplicity and low initial cost. This method has been favoured recently in the U.S.A., due to poor experience with the EPA method involving passage of a large volume of gas through a small volume of static isopropanol solution. [8] A comparison of the manual co-current isopropanol/gas flow method, [7,9], which employs the same method of collecting the SO_3 from the gas as does the monitor, and the selective condensation method by a major British oil supplier [10] yielded results with no significant difference. More recently, comparisons between the instrument described here and the selective condensation method have been made in an Italian power station. [11] Tests have also been undertaken in the present study [12] in which synthetic gas mixtures containing 11% v/v water vapour and sulphuric acid in the range 10-40 ppm were sampled concurrently and analysed by the monitor and by the British Standard condensation method. In some of these tests sulphur dioxide was added to yield concentrations of about 2000 v.p.m.

The British Standard 3 porosity sinter gave results more variable, and significantly lower by a mean of 7 v.p.m. SO_3, than did the monitor. With the British Standard 4 porosity sinter, the condensation method yielded results similar to those of the monitor but somewhat more variable. A statistical comparison of these two sets of results showed that the mean difference (British Standard minus monitor) was + 0.13 v.p.m. SO_3, statistically non-significant. The standard deviation between pairs of results by the two methods was 3 v.p.m. SO_3.

OPERATIONAL EXPERIENCE

Conventional Combustion

Monitors of this design have been used extensively in a number of power plants in the U.K., U.S.A. and western Europe. Early in the development of the instrument, a prototype operated successfully at a CEGB power station for several weeks, with interruptions only for servicing and the replacement of expendable components. It is now the normal method of analysis for SO_3 in flue gas within the CEGB, and some of the research data obtained has been quoted in published papers.[13,14,15,16,17]. Some of these measurements were used to demonstrate the efficacy of additives in reducing the SO_3 concentration in the gas. As an example, figure 2 shows the dramatic variation in SO_3 concentration during trials at a large oil-fired power station, with and without the addition of fine magnesium hydroxide. In addition, the instrument has been used for environmental monitoring in iron-ore sinter plants, sulphuric acid plants and large incinerators. [18]

Application to Fluid Bed Combustion

SO_3 measurements have been made on a small laboratory bed [19] and on both atmospheric and pressurised pilot scale coal-fired fluidised combustors. [14,20]. Some of these measurements were carried out under conditions where solids loadings in the sampled gases were orders of magnitude greater than those normally encountered in 'back-end' flue gas on conventional oil or coal fired power plant. The situation is further exacerbated because of the high pressure in PFBs for which the standard probe design is unsuitable. Figure 3 shows the technique used to sample flue gas from a PFB duct where the gas temperature after reheat was about 800°C. The design aims to fulfill the SO_3 sampling criteria which in this instance were:

(a) The length of the probe through which the gas was drawn was minimised.

(b) In order to minimise particulate sampling, the gas was withdrawn from the combustor in a direction of 180° to the main flow.

(c) To ensure that as little steel surface was exposed to the gas flow as possible, the probe was lined with quartz and borosilicate glass tubing. The external surfaces of the sampling system were all wound with tape heaters and maintained at a temperature of >200°C.

(d) It was necessary to instal two valves in the gas line. The second was used to control the gas flow rate. The time for which the gas was in contact with metal surfaces in these valves was minimised by passing a high flow (>20 litre min^{-1}) of gas through them, expanding it to atmospheric pressure and withdrawing about 500 ml min^{-1} into the SO_3 monitor.

(e) Variations in the total gas flow through the valves as well as that through the monitor were found not to influence the SO_3 concentrations in the gas. As a result, it was concluded that little or no perturbation was occurring in the sampling system by absorption/desorption/catalysis on metal surfaces.

(f) Periodic cleaning and replacement of the filter within the SO_3 monitor probe was necessary because of the large quantity of ash and partially sulphated dolomite carried through the system. However, there was never any indication that acid vapour was reacting with the material collected in the filter, the only detectable effect being a reduction in sample gas flow-rate with time.

(g) The sampling contactor was maintained at 180°C - i.e. above the acid dewpoint but below the temperature at which significant dissociation of H_2SO_4 to SO_3 and H_2O occurs.

Plots of the SO_3 concentration against time for one of the 200-hour tests are shown in Figure 4 as an example of the data obtained. The significance of the data is discussed in reference 20.

A gas sampling system incorporating a thermostatted self cleaning cyclone has been developed for use on particularly "dirty" gas streams, e.g. in the freeboard of a pressurised fluidised combustor.

REFERENCES

(1) HALSTEAD, W.D. & TALBOT, J.R.W., (1980). J.Inst.Energy, 53, 142.
(2) LAXTON, J.W. & JACKSON, P.J. (1964). J.Inst.Fuel, 37, 12.
(3) JACKSON, P.J., LANGDON, W.E. & REYNOLDS, P.J. (1969). Paper to ASME Winter Annual Meeting Nov.16-20, 1969. L.A., U.S.A.
(4) JACKSON, P.J., LANGDON, W.E. & REYNOLDS, P.J. (1970). J.Inst.Fuel, 1970. 43, 10.
(5) BRITISH PATENT NO. 1030541, 2 January 1964.
(6) JACKSON, P.J., HILTON, D.A. & BUDDERY, J.H. (1981), to be published in J.Inst.Energy.
(7) BRITISH STANDARD 1756: Part 4: 1977.
(8) U.S. ENVIRONMENTAL PROTECTION AGENCY. Standard of Performance for Stationary Sources. Federal Register 41 (111),June 1976. 23083-5.
(9) FIELDER, R.S., JACKSON, P.J. & RAASK, E.R. (1980). J.Inst.Fuel, 33, 84.
(10) BRITISH PETROLEUM RESEARCH CENTRE,Technical Memorandum No.120366(1966).
(11) ENTE NAZIONALE PER L'ENERGIA ELETTRICA (ENEL) DCO. Relaz No.50.
(12) JACKSON, P.J., WEIGHT, R.P. & HOTCHKISS, R.C. (1980). Unclassified CEGB Note RM/M/N116. Available from the Librarian, Marchwood Engineering Laboratories.
(13) CUNNINGHAM, A.T.S. & JACKSON, P.J. (1978). J.Inst.Fuel, 51, 20.
(14) HOTCHKISS, R.C., BURDETT, N.A. & LANGDON, W.E. (1979). Paper to Conference "Future Energy Concepts". Inst.Elect.Engrs., London, 30 Jan - 1 Feb. 1979.
(15) BURDETT, N.A., HOTCHKISS, R.C. & FIELDES, R.B. (1979). Paper to 3rd Int.Symp. on Control of Sulphur and Other Gaseous Emissions. Inst. of Chem.Engrs. Salford, April, 1979.
(16) BURDETT, N,A., HOTCHKISS, R.C., SQUIRES, R.T., HORSLEY, M.E., & McCULLOUGH, J.B., (1979). Paper to 2nd Int.Conf. on Energy Use Management, Los Angeles. 22-26 Oct. 1979.
(17) BURDETT, N.A., GLIDDON, B.J. & HOTCHKISS, R.C. (1980). Combust. Science and Technology, 23, 103, June 1980.
(18) HILTON, D.A., (1979). Severn Science Ltd. Report 206.
(19) FIELDES, R.B., BURDETT, N.A. & DAVIDSON, J.F., 1979. Trans.I.Chem.E., 57, 276-80.
(20) PILLAI, K.K. & WOOD, P., 1980. J.Inst.Energy. December. 159-75.

ACKNOWLEDGEMENT

The authors wish to thank many of their colleagues at MEL and SSL for their contributions to the work reported here. This paper is published by permission of the CEGB.

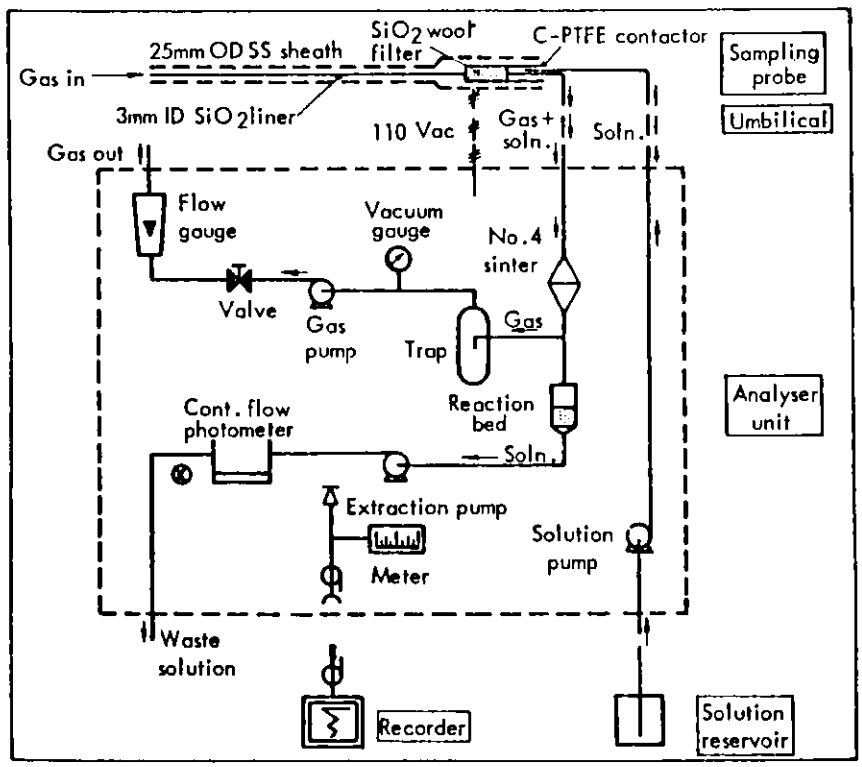

FIGURE 1. FLOW DIAGRAM OF SO_3 SAMPLING PROBE AND ANALYSER

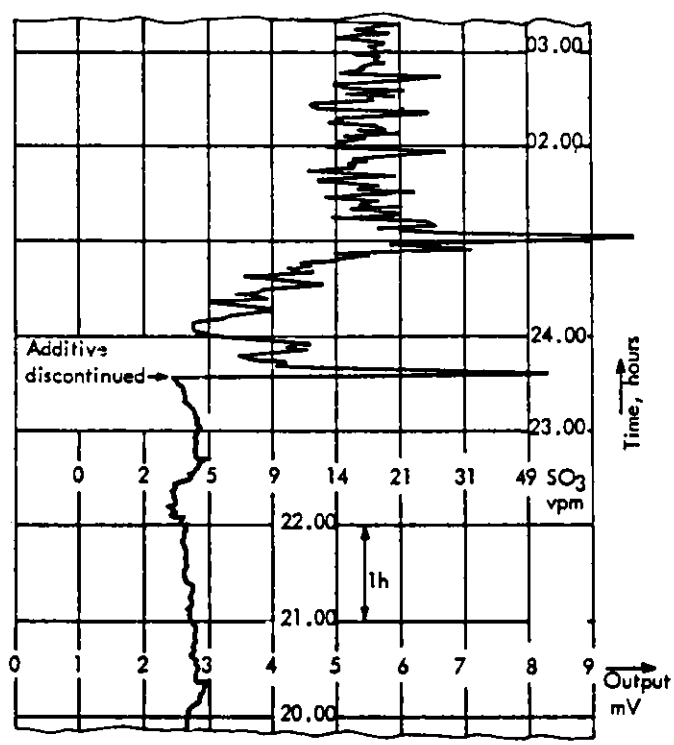

FIGURE 2. RECORDER CHART: LARGE POWER STATION BOILER WITH AND WITHOUT ADDITIVE

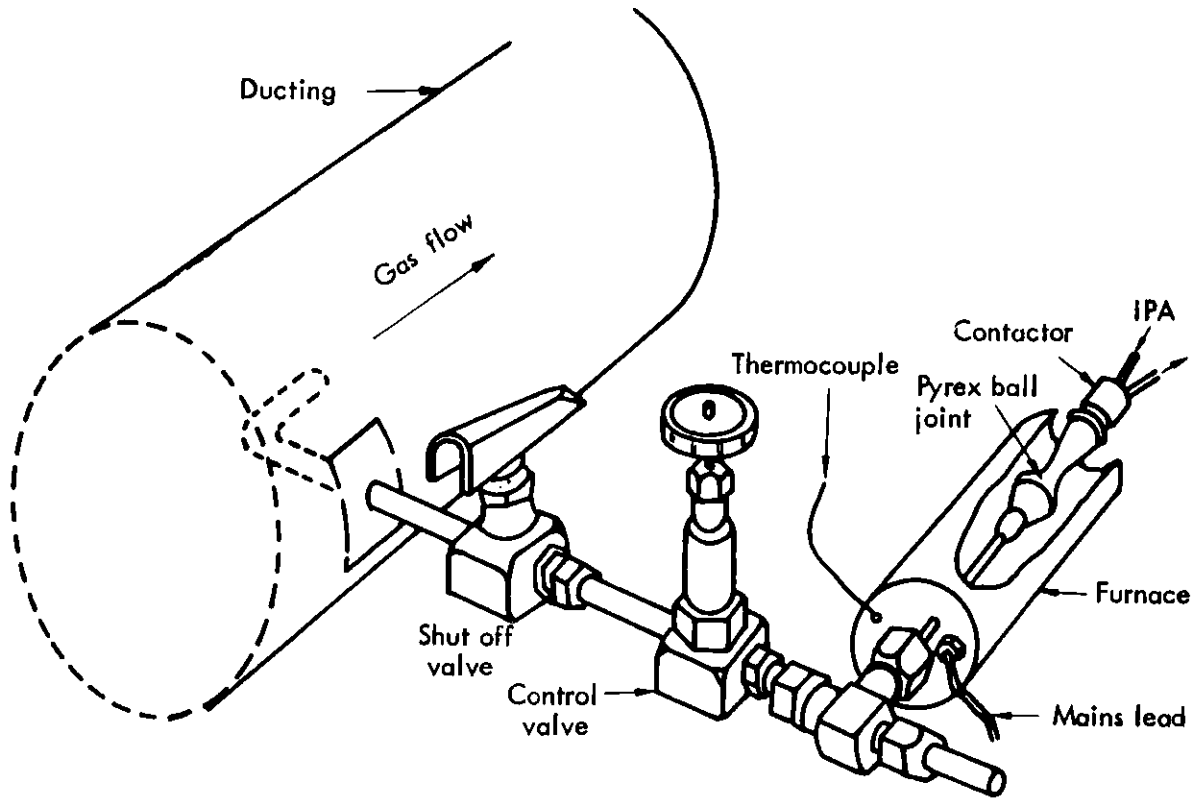

FIGURE 3. PRESSURISED FLUIDISED BED GAS SAMPLING SYSTEM

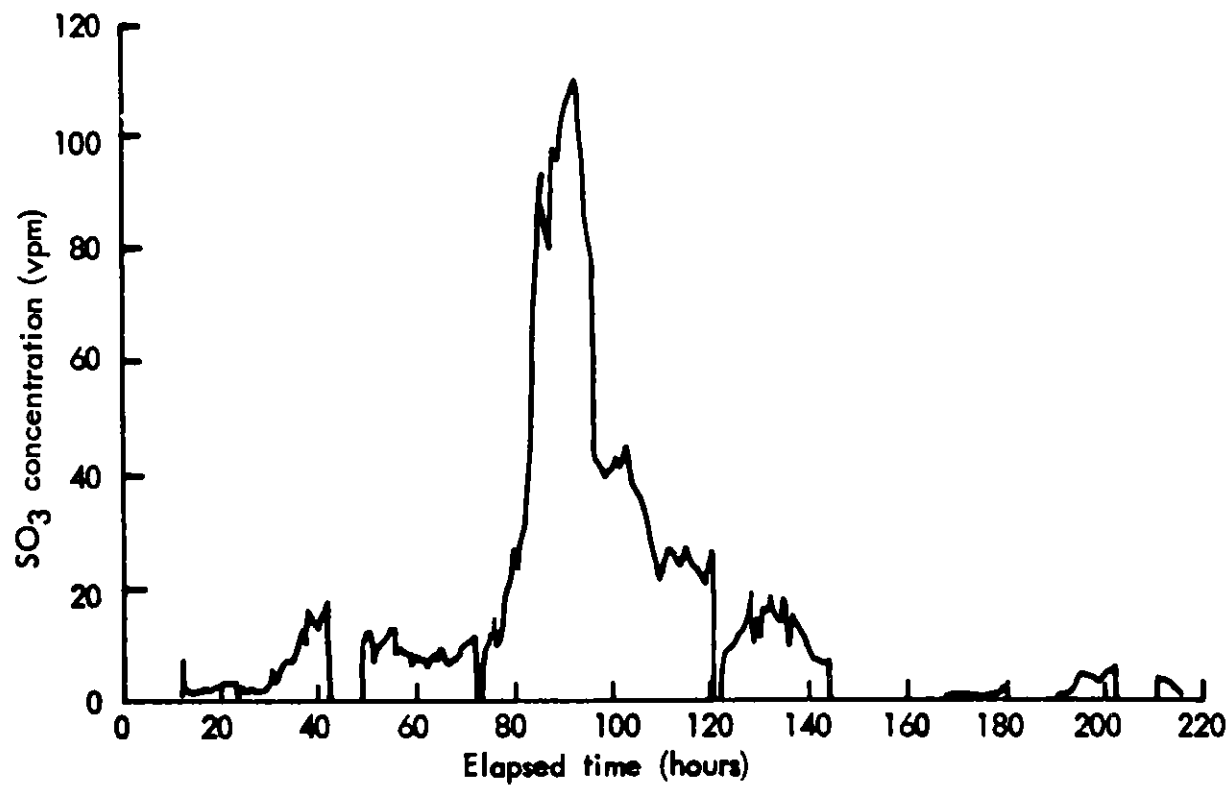

FIGURE 4. SO_3 MEASUREMENTS ON A PFB COMBUSTER

THE APPLICATION OF NEUTRON BACKSCATTER TECHNIQUES TO LEVEL MEASUREMENT PROBLEMS

A. M. Leonardi-Cattolica, D. H. McMillan,
A. Telfer, L. H. Griffin and R. H. Hunt

Shell Development Company

INTRODUCTION

The principles involved in the use of neutrons to detect the presence of hydrogen are well known.[1,2] Hydrogen measurement devices based on these principles are used extensively for well logging.[2] And moisture gauges which employ neutrons[3] are widely used. However, comparatively little attention has been paid to the value of these principles for solving level measurement problems.* In an industry like the petrochemical industry, where the raw and processed materials nearly always contain substantial amounts of hydrogen, level measurement instruments employing neutrons have wide application.

We have designed and built portable level detectors and fixed level monitors based on neutron scattering and detection principles. The main components of these devices, which we call neutron backscatter gauges, are a neutron emitting radioisotope, a neutron detector, and a ratemeter. The gauge is a good detector for hydrogen but is much less sensitive to most other materials. This allows level measurements of hydrogen bearing materials, such as hydrocarbons, to be made through the walls of metal vessels. Measurements can be made conveniently through steel walls which are a few inches thick.

We have used neutron backscatter gauges in a wide variety of level measurement applications encountered in the petrochemical industry. In a number of cases, the neutron techniques have proven to be superior to conventional level measurement methods, including gamma ray methods.

A portable neutron backscatter gauge which is very useful for making level measurements will soon be commercially available. And we expect that fixed level monitors based on the same principles will follow.

THE NEUTRON BACKSCATTER GAUGE

The principal components of a neutron backscatter gauge, the neutron source, the neutron detector and the ratemeter are arranged as shown in

---

* The utility of neutron techniques for making level measurements was brought to the authors' attention by a report, internal to Shell Companies, from the Koninklijke/Shell-Laboratorium, Amsterdam (Shell Research B. V.) in The Netherlands. The results of work on this subject were given therein.

Figure 1 in a typical level measurement application. The source is mounted next to the neutron detector and together they are placed near the exterior of the vessel wall.

The source must emit energetic neutrons. ^{252}Cf (californium) sources have been used exclusively in this work but other sources such as $^{241}Am/Be$ (americium/beryllium) are also suitable. The average neutron energies for the ^{252}Cf and $^{241}Am/Be$ sources are on the order of a few million electron volts (MeV)[4]. Data on ^{252}Cf and $^{241}Am/Be$ sources are listed in Table 1. Neutron emission rates in the range 10^4-10^6 neutrons/sec are adequate for most applications. These rates are so low that the sources are very easily handled in a safe manner. Approximate exposure rates at a distance of one foot are given in Table 1.

^3He detectors are used because of their high thermal neutron detection efficiency. The detector consists of a sealed tube filled with gas, ^3He being the main component. The tube also contains a central electrode. A voltage is applied between the central electrode and the tube wall. When an energetic, charged nuclear particle passes through the gas in the tube, some of the gas molecules are ionized. The ions and electrons are accelerated by the applied electric field producing a current pulse. Charged nuclear particles are generated inside the detector by the neutrons which enter the detector and react with ^3He. The nuclear reaction is

$$^3He + n \longrightarrow {}^3H + p + .765 \text{ MeV} \qquad (1)$$

The energy released by the reaction is shared between the tritium nucleus and the proton. It is the energetic charged particles produced by this reaction that ionize gas molecules in the detector. The number of current pulses generated per unit time (pulse rate) is therefore related to the number of neutrons entering the detector per unit time. The current pulses are counted by the ratemeter. The output of the ratemeter is a signal which is proportional to the pulse rate.

The cross section for reaction (1) is a strong function (approximately $E^{-\frac{1}{2}}$)of the kinetic energy (E) of the neutron. The cross section is less than 1 barn for neutron energies above a few tenths of an MeV[5]. The detector is insensitive to neutrons coming directly from the source because the reaction cross section for these energetic neutrons is so small (recall that the average energy of the neutrons emitted from the ^{252}Cf and $^{241}Am/Be$ sources is greater than 1 MeV). This allows the source to be placed next to the detector in a backscatter gauge. On the other hand, ^3He detectors have very high detection efficiencies for low energy neutrons because the reaction cross section is very large. The thermal neutron cross section (neutron energy equal to 0.025 eV) is 5330 barns[5]. ^3He detectors are available which have efficiencies approaching 100 percent for thermal neutrons. The strong dependence of detector

sensitivity on neutron energy makes the backscatter gauges very sensitive to the presence of materials which are good moderators, i.e., those that are efficient in reducing the energies of neutrons to the range where the detectors are efficient. When the backscatter gauge is placed in the immediate vicinity of a good moderator, the number of low energy neutrons reaching the detector will increase substantially. And the change in the number of current pulses produced per unit time will be easily measurable.

Hydrogen is the most effective moderator and materials which contain substantial amounts of hydrogen are also effective moderators. Hydrogen is effective for two reasons:

1. The elastic scattering cross section for hydrogen is relatively large and

2. In most collisions between a neutron and a hydrogen nucleus, a substantial fraction (on the average one-half) of the energy of the neutron is transferred to the hydrogen nucleus. Roughly 20 collisions with hydrogen are required to reduce the energy of a 1 MeV neutron to the thermal range. A much larger number of collisions is required to achieve this result with all but the very lightest of the other elements.

A neutron backscatter gauge is very sensitive to the presence of hydrogen bearing materials but relatively insensitive to the presence of non-hydrogen bearing materials commonly encountered in petrochemical plants. Therefore, a neutron backscatter gauge can be viewed as a "hydrogen detector" in many level measurement applications. In a typical application, a vessel wall made of a non-hydrogen bearing material like steel separates the neutron backscatter gauge from a hydrogen bearing material whose level is to be measured. If the separation is not too great, the presence of the vessel wall does not prevent level measurements from being made. This is illustrated by the data in Table 2. The water level can be determined through the one inch steel plate to an accuracy of approximately an inch in 2 or 3 minutes without using calibration procedures. Count rate vs. water level are plotted in Figure 2. The data were obtained using a ^{252}Cf source with a neutron emission rate of 1.5×10^5 neutrons/sec and a 4 atmosphere ^3He detector. The diameter of the detector was 1 inch and the active length 6 inches.

In most cases, level measurements can be made from the exterior of a vessel. However, if material which contains a substantial amount of hydrogen surrounds the vessel, it may be difficult or impossible to make the desired measurement externally. A vessel with a water or oil jacket, for example, might require that the neutron backscatter gauge be mounted in a well in the vessel.

A neutron backscatter gauge is only sensitive to material located within inches of the source and detector. Therefore, the geometry shown in Figure 1, which results in the detection of low energy "backscattered"

neutrons is generally employed in level measurement applications. However, transmission measurements, in which the source and detector are separated allowing a moderator to be interposed, are useful for some applications.

The neutron backscatter gauge can be used to determine the level of any type of interface not just liquid-gas interfaces like the water-air interface of Figure 2. In the next section an example of the detection of a foam-gas interface is discussed.

FIXED LEVEL MONITORS

Description

In fixed level monitoring applications, the source and detector can be mounted on the exterior of a vessel as shown in Figure 1 or in a well mounted in the vessel. In the former case, a "reflector" of the type shown in Figure 3 can be used to advantage. The source and detectors are shown mounted in a reflector made of carbon but other materials such as aluminum are also suitable. Some of the neutrons emitted from the source in directions away from the target, in this case the vessel, will reach the target because their initial trajectories are altered by collisions with the atoms in the reflector. The result is a modest gain in signal to noise ratio and reduced radiation levels in areas other than the target area.

The sides of the carbon block in Figure 3, with the exception of the side between the source and target, are covered with cadmium sheet. Cadmium has a very large capture cross section for neutrons with energies of a few tenths of an electron volt and less. Most of the low energy neutrons which enter the cadmium are captured by it. This reduces the sensitivity of the backscatter gauge to moderators which are in the vicinity of the gauge but not in the target area.

Applications

Neutron backscatter gauges are being used as fixed level monitors in several applications in Shell Companies. In the near future, we expect to install neutron backscatter gauges on coke drums for the purpose of monitoring coke levels. In coking operations, a high molecular weight hydrocarbon liquid is heated to temperatures on the order of 900°F and pumped into a large insulated vessel (coke drum) like the one shown in Figure 4. The pumping rate is such that it takes many hours to fill the drum. The liquid hydrocarbon is converted to coke and materials of lower molecular weight than the starting material in the coke drum. The materials which are gaseous at the operating temperature of the drum are taken off overhead as the drum fills with coke.

A means of determining when a drum has been filled with coke is required in coking operations. Feed rates and times can only be used to obtain approximate coke levels. It has been demonstrated that a neutron backscatter gauge can be used for this purpose.

The source/detector assembly shown in Figure 3 was used in the demonstration tests. The neutron source was 0.6 micrograms of ^{252}Cf (emission rate: 1.4×10^6 neutrons/sec). Two ^3He detectors (4 atmosphere pressure, 6 inch active length, 1 inch diameter) were employed. The source/detector assembly was mounted against the sheet metal which covers the insulating brick lining on the exterior of the drum as shown in Figure 5. In this arrangement, neutrons must penetrate an inch of steel and two inches of ceramic brick and return to the detector.

The results of one of the tests are shown in Figure 6. At the beginning of the test the material in the interior of the drum near the source/detector assembly was low density gas phase material. The change in signal level which occurred just after 14:00 indicates the presence of material (a foam) opposite the source/detector assembly which more effectively moderates the neutrons than the gas. Shortly thereafter, the continuous injection into the drum of a defoaming agent was begun. This suppressed the foam and the level dropped to a point below the backscatter gauge as indicated by the return of the signal to the baseline value. The second rise in the signal occurred at 14:30 when material with a hydrogen density greater than that of the gas again reached the level of the source/detector assembly.

There are a number of other features of the neutron backscatter gauge signal vs. time record that can be accounted for in terms of the operation of the coker. For example, the decline in signal level between 18:00 and 19:30 indicates that the coke level in the drum declined to a point just below the backscatter gauge. This was later confirmed by direct measurement when the cover plate on top of the coke drum was removed. A sharp increase in signal occurred near the end of the water quench phase of the operation at 23:50. It indicates that the temperature of the coke near the neutron backscatter gauge had decreased to a value below the boiling point of water. (Water in the liquid phase would produce a strong signal). The sharp decline in the signal at 0:45 indicates that the liquid water had been drained from or had evaporated from the coke in the immediate vicinity of the gauge. The signal increase at 2:15 occurred when water was again introduced into the coke drum at the start of the coke cutting operation. The return of the neutron signal to its baseline value at 5:25 occurred when coke was removed from the vicinity of the neutron backscatter gauge.

Comparison of Neutron Backscatter and Gamma Ray Results

The conventional means of monitoring coke levels is with gamma ray instrumentation. A gamma ray source is placed inside the coke drum at a distance on the order of a foot from the vessel wall. A gamma ray detector

is placed outside the coke drum. As the density of the material between the source and detector increases, the number of gamma rays reaching the detector per unit time decreases. The arrival of the foam front and the presence of coke are readily observed with this instrumentation, as indicated by the results in Figure 7. The neutron backscatter results shown in Figure 8 were obtained with the backscatter gauge mounted beside the gamma ray instrument. (Figure 8 is the 13:00 - 16:40 section of Figure 6). The two sets of data were obtained simultaneously. Note that the general shapes of the two curves are very similar and that the arrival times of the foam front determined with the two instruments are the same.

The information obtained from the gamma ray instrumentation is entirely satisfactory for the purposes of operating the coker. However, coke is removed from the drum by drilling with a water jet. During this operation there is a risk of damaging the instrumentation. For this reason, existing gamma ray equipment will be removed from the coke drums in one of our refineries in favor of neutron backscatter gauges.

PORTABLE NEUTRON BACKSCATTER GAUGE

Description

Very low intensity neutron sources can be used in most level measurement applications. Since heavy shielding for personnel protection is not required, it is possible to build a portable backscatter gauge weighing only a few pounds. The principles which apply to measurements made with the portable backscatter gauge are the same as those which apply to fixed level monitors.

One version of the portable backscatter gauge is shown in Figure 9. The gauge consists of a ^{252}Cf source, a ^{3}He detector (4 atmosphere pressure, 1 inch diameter, 6 inch active length), a wand to which the source and detector are attached and a battery powered combination ratemeter/scaler. The relative positions of the source, detector and wand are shown in Figure 10. The gauge weighs 12 pounds. A much lighter gauge could be made by using a lighter ratemeter/scaler.

The 36 inch wand provides a means of keeping the source away from the operator when the instrument is in use. For a ^{252}Cf source with an emission rate of 2.3×10^{5} neutrons/sec (0.1 micrograms of ^{252}Cf), the combined gamma ray/neutron exposure rate measured at the end of the wand away from the source is less than 0.25 mrem/hr. That is more than a factor of ten below the maximum permissible occupational exposure level of 2.5 mrem/hr for a 40 hour work week. The exposure rate at a distance of 1 foot from the source is approximately 2 mrem/hr. An 8 inch diameter, boron impregnated polyethylene bioshield, provides personnel protection when the instrument is being transported or stored. The wand is shown

engaged in the bioshield in Figure 11. The exposure rate measured at the surface of the bioshield is less than 9 mrem/hr for the 0.1 microgram ^{252}Cf source. It is less than 2 mrem/hr 6 inches from the surface bioshield.

Applications

The portable neutron backscatter gauge has proven to be a valuable tool for measuring levels. The data in Table 2 and Figure 2 are examples of results obtained with the portable gauge. It is easy to use and is often the most convenient means of 1) measuring levels in vessels which have no level sensing devices and 2) checking or calibrating level sensors such as differential pressure cells and gamma ray level gauges after instal-lation. The gauge has also been used to detect two phase flow in pipes and to determine if pipes were empty before cutting into them.

Not all of the problems addressed with the portable backscatter gauge are straightforward. For example, insight has been gained into the design and operation of distillation columns as a result of studies on foaming and tray flooding which were carried out with a portable backscatter gauge.

SUMMARY

The use of neutrons as a probe to detect the presence of hydrogen is a very useful means of solving level measurement problems. Neutron backscatter gauges are particularly valuable tools for measuring the levels of hydrogen bearing materials where:

1. conventional methods are difficult to apply
2. a non-intrusive method is required or
3. a portable instrument capable of making rapid measurements is needed.

The use of neutron backscatter gauges within the Shell Companies is growing steadily. And in a number of applications, of which the monitoring of coke levels is an example, the neutron backscatter technique is preferred over gamma ray methods.

REFERENCES

1. Knoll, G. F., Radiation Detection and Measurement, Chapter 15, John Wiley and Sons, New York (1979).
2. Tittman, J., "Radiation Logging", Petroleum Engineering Conference, University of Kansas, Lawrence (1956).
3. "Neutron Moisture Gauges", International Atomic Energy Agency Technical Report Series No. 112, Vienna (1970).

4. Lorch, E. A., "Neutron Spectra of ^{241}Am/B, ^{241}Am/Be, ^{241}Am/F, ^{242}Cm/Be, ^{238}Pu/^{13}C and ^{252}Cf Isotopic Neutron Sources", International Journal of Applied Radiation Isotopes, 24, 585-591 (1973).

5. Stehn, J. R., Goldberg, M. D., Magurno, B. A. and Wiener-Chasman, R., Neutron Cross Sections, Vol. 1 Brookhaven National Laboratory - 325 Edition 2 Supplement 2.

TABLE 1

^{252}Cf AND $^{241}Am/Be$ NEUTRON SOURCES

	^{252}Cf	$^{241}Am/Be$
Half Life	2.65 years	433 years
Neutron dose rate at a distance of 1 foot for an emission rate of 10^5 neutrons/sec.	~ 1 mrem/hr	~ 1 mrem/hr
Gamma ray exposure rate at a distance of 1 foot for an emission rate of 10^5 neutron/sec.	~ 0.1 mR/hr	~ 1 mR/hr
Activity of a source with an emission rate of 10^5 neutrons/sec.	23 μCi	45 mCi

TABLE 2

DETECTION OF THE PRESENCE OF WATER THROUGH A
1 INCH THICK STEEL PLATE WITH A NEUTRON BACKSCATTER GAUGE

	Count Rate (counts/second)
Detector and source in air	13
Dectector and source mounted against a 1 inch thick steel plate with	
a) air on the other side of the plate	14
b) water on the other side of the plate	51
c) air-water interface at the same level as the source and detector	23

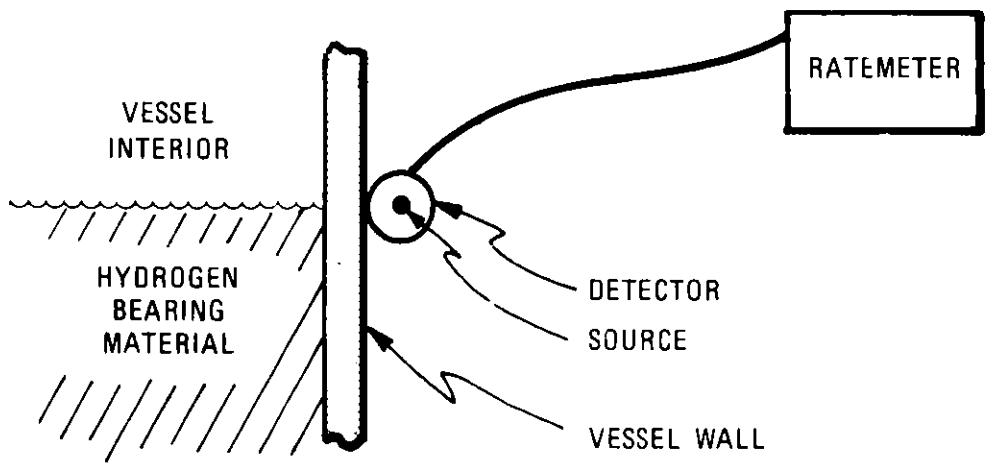

Figure 1. Typical Neutron Backscatter Gauge Component Configuration for Level Measurement Applications

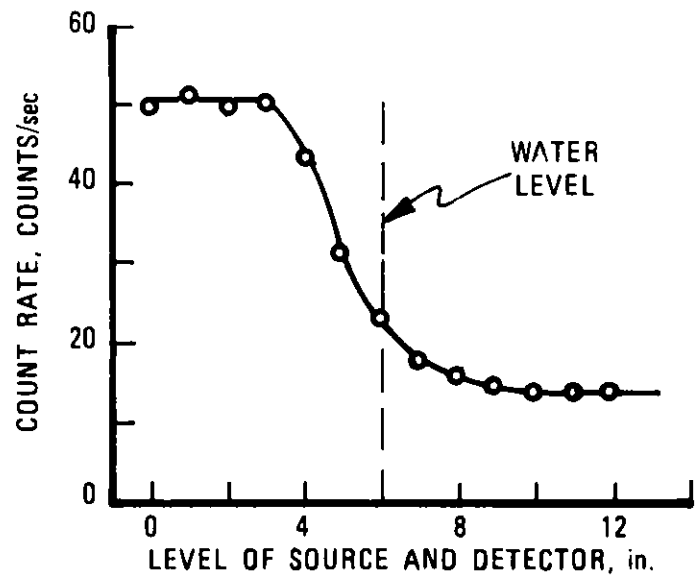

Figure 2. Water Level Determination Through a 1 Inch Thick Steel Plate

04506

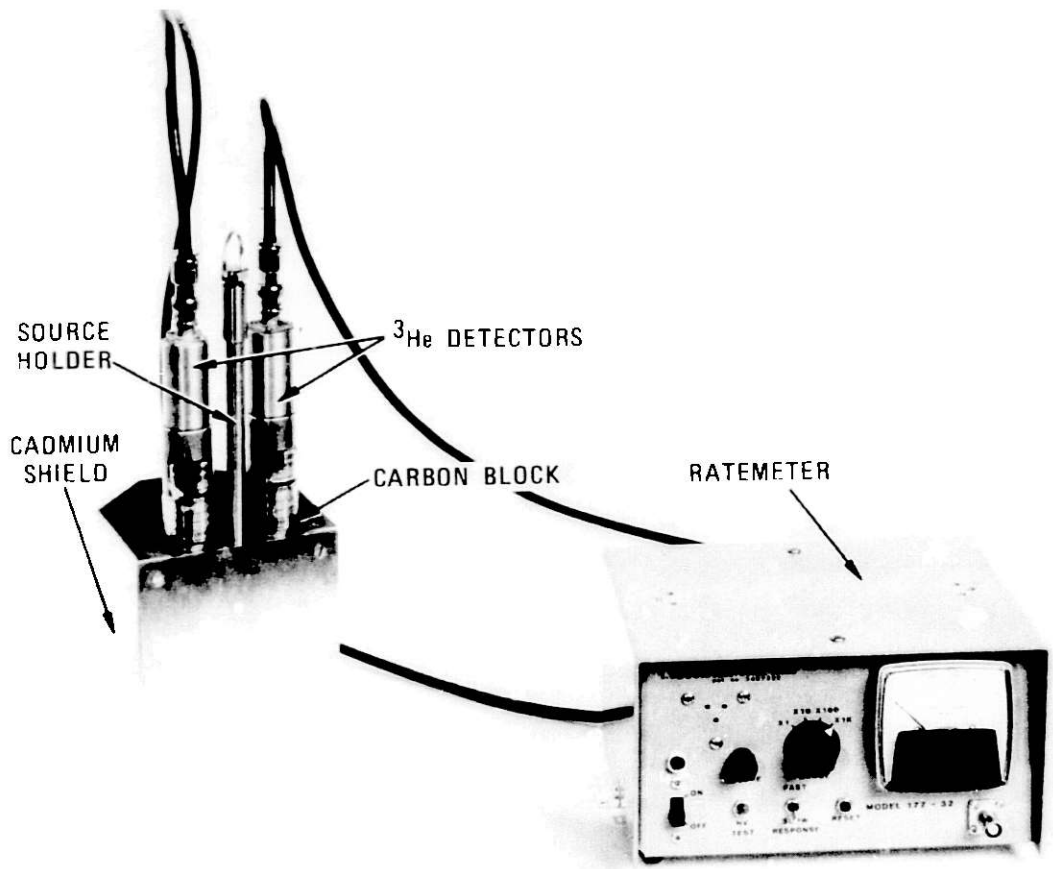

Figure 3. Neutron Backscatter Gauge

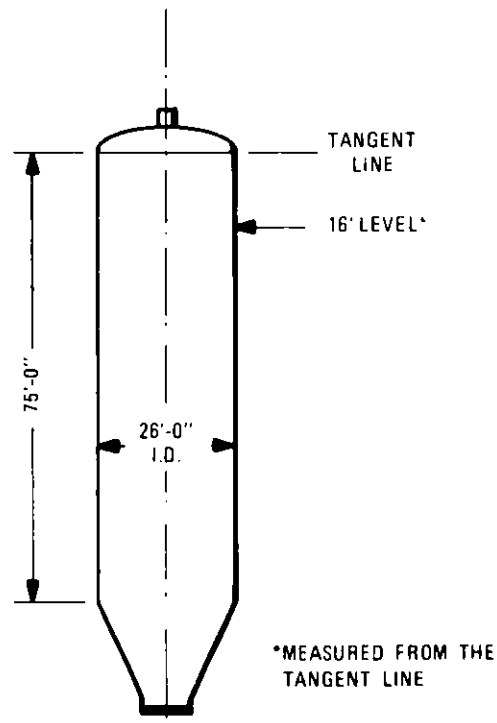

Figure 4. Coke Drum.Neutron Backscatter and Gamma Ray Measurements Made at the 16 ft Level

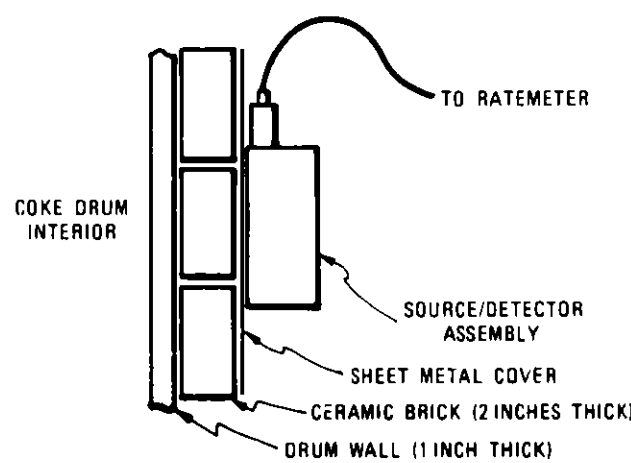

Figure 5. Source/Detector Assembly on the Exterior of the Coke Drum

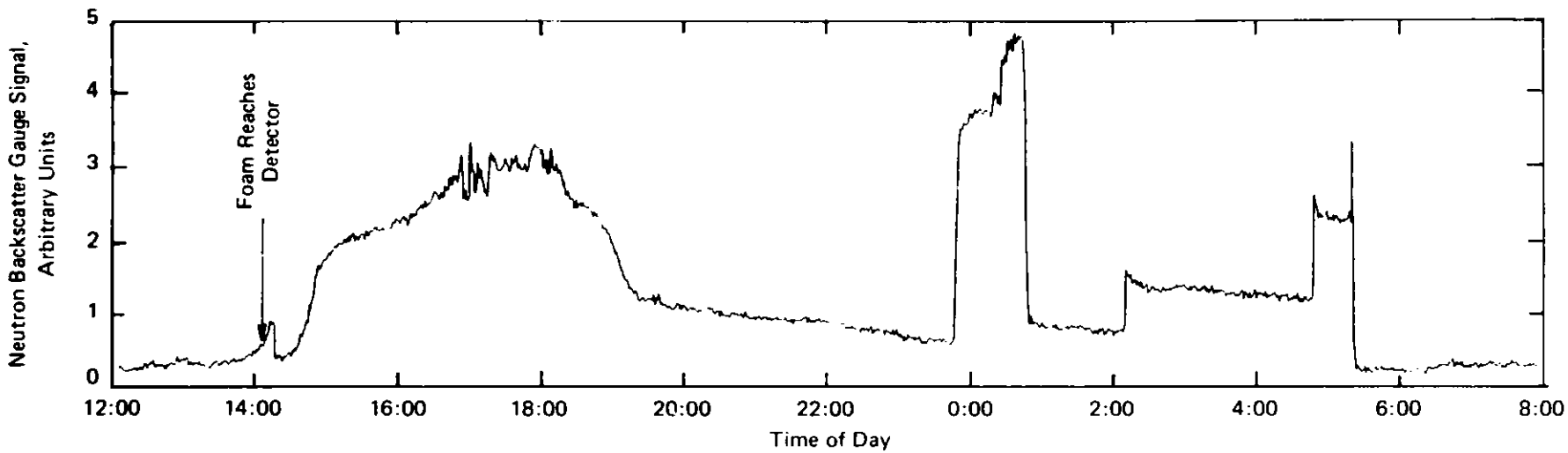

Figure 6. Neutron Backscatter Gauge Signal vs. Time
Gauge Mounted on the Coke Drum at the 16 ft Level as Shown in Figures 5 and 6

04506

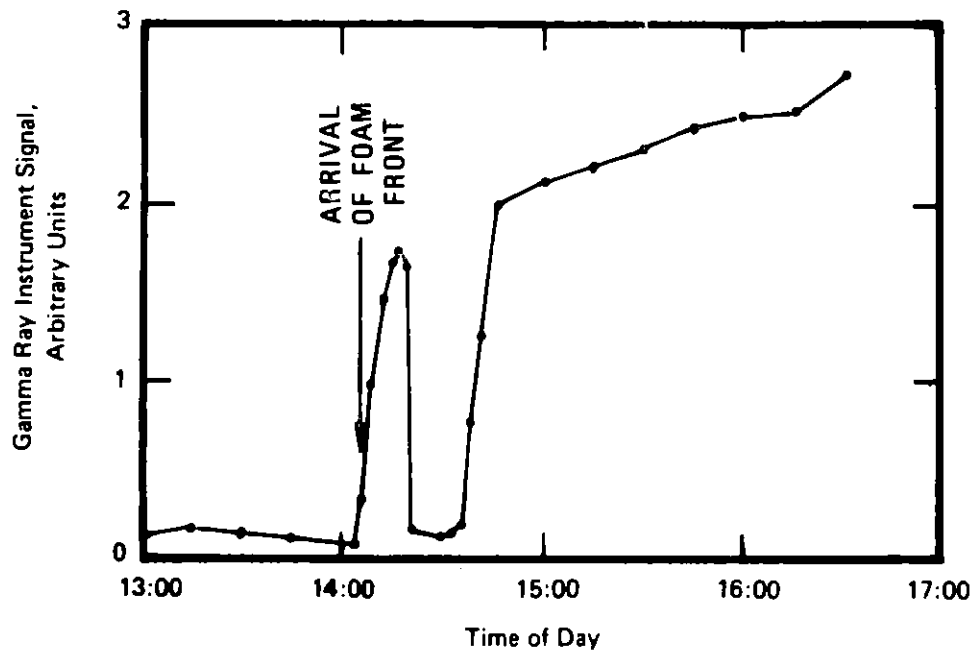

Figure 7. Gamma Ray Signal vs. Time

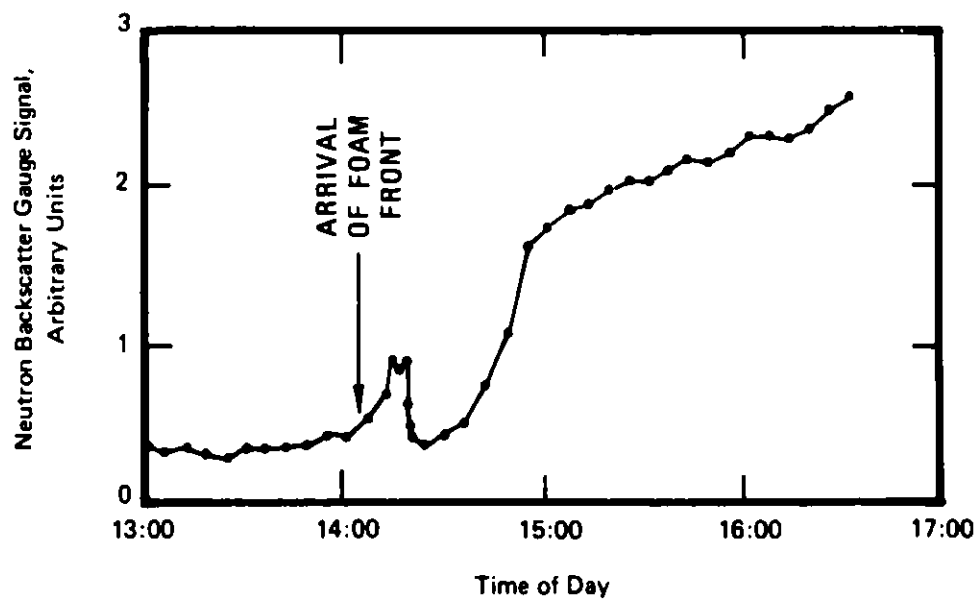

Figure 8. Neutron Backscatter Gauge Signal vs. Time

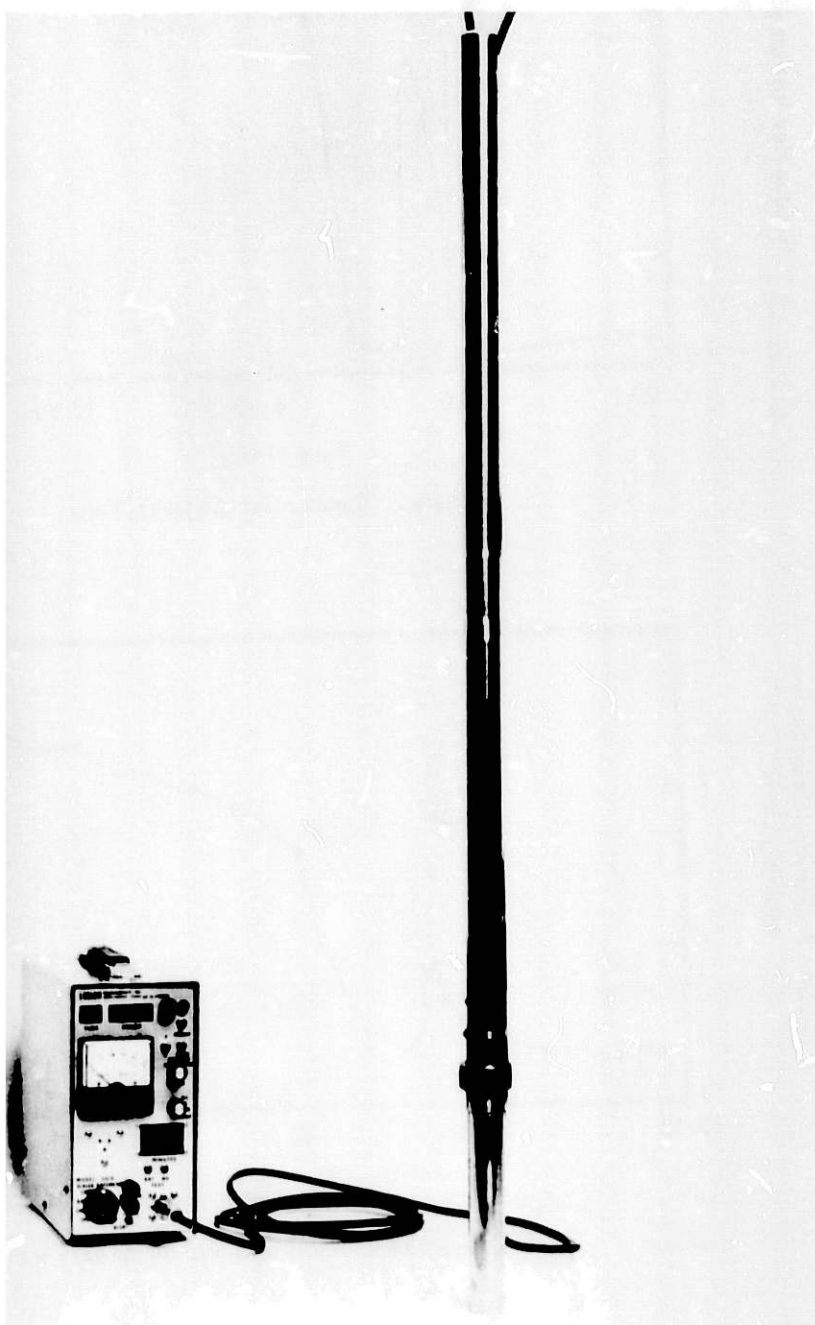

Figure 9. Portable Neutron Backscatter Gauge

CUTAWAY VIEW OF DETECTOR PROBE

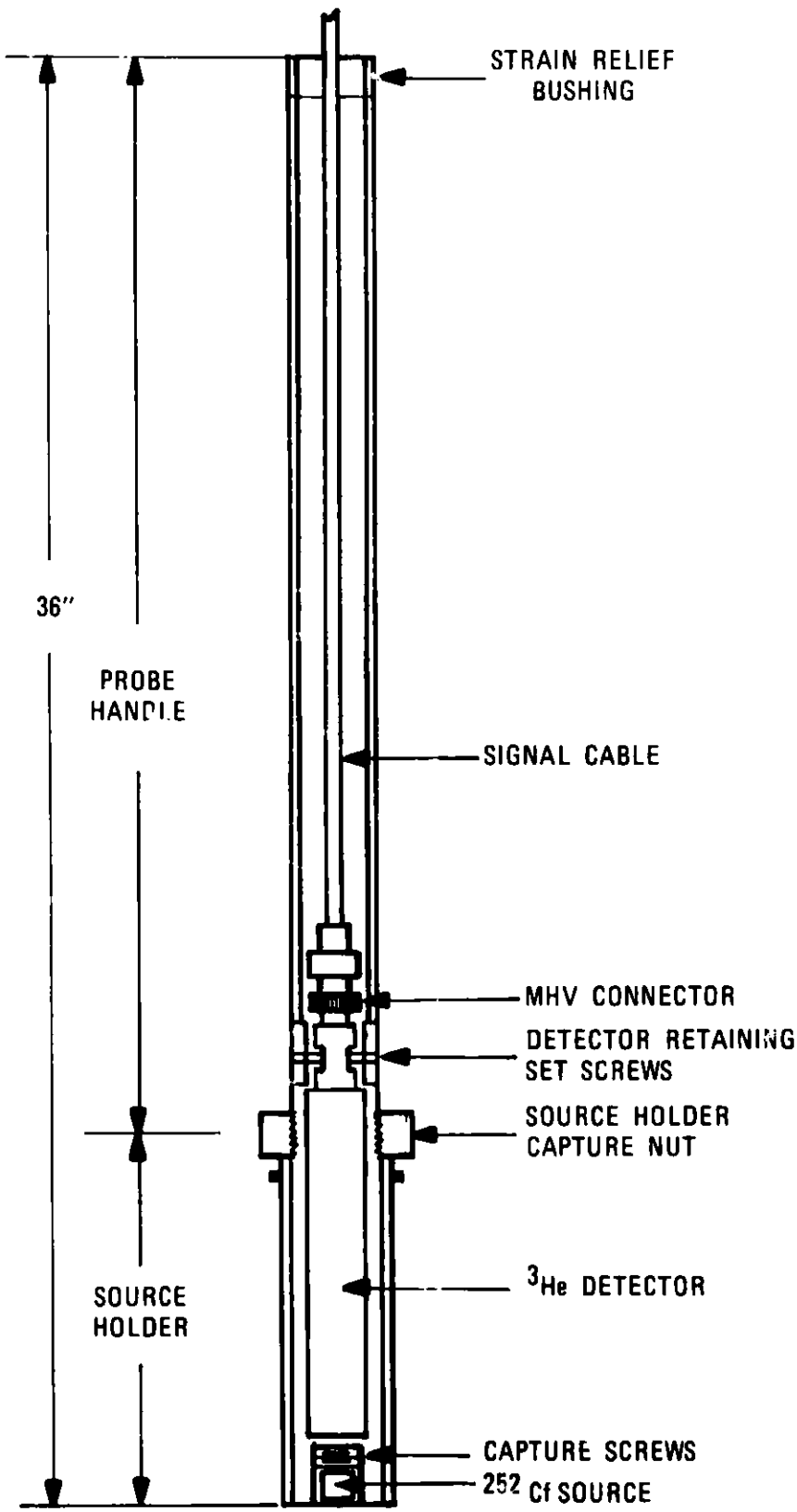

Figure 10. Cutaway View of Detector Probe

04506

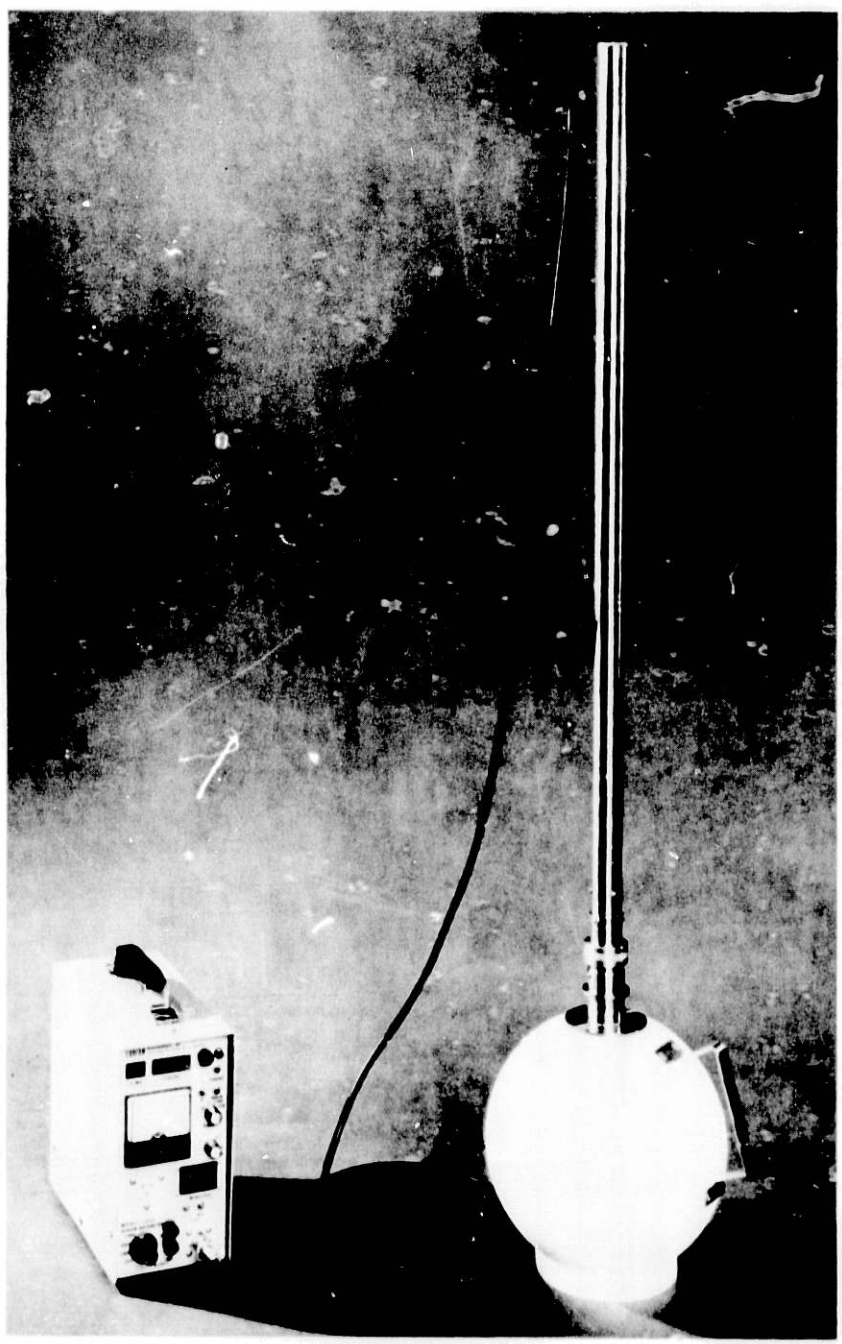

Figure 11. Portable Neutron Backscatter Gauge with Wand Engaged in Bioshield

02815

THE DESIGN AND USE OF DENSITY GAUGES FOR FOSSIL ENERGY PROCESSES*

D. G. Sample, M. G. Thomas, and J. K. Linn
Sandia National Laboratories, Albuquerque, New Mexico 87185

INTRODUCTION

Many of the proposed processes for alternate energy sources are being developed with little or no real data detailing mass flow rates, flow regimes, solids settling, plugging, etc.[1] Process upsets resulting from such deficiencies require time-losses for major turn-arounds, and limit processing flexibility (necessary for these processes to provide a range of products). Although progress is being made in some areas by in-stream measurements, many times intrusive measures contribute problems necessitating process-redesign and system changes, which can be avoided by non-intrusive measurements.

Over the past years, we have been directly involved in advanced research for the processing of coal, particularly with regard to direct liquefaction. Two years ago, we suggested and provided examples for the use of radiometric techniques for analyzing ash in coal, monitoring gas/liquid and liquid/solid interfaces, solids accumulation in pipes, and flow characteristics.[2] Last year we described in detail an experiment, utilizing the neutron activation of catalysts, that showed the mixing characteristics of the H-Coal reactor and which subsequently led to the determination of catalyst deactivation.[3]

SPECIFIC APPLICATION

The current research and application involves distinguishing a subtle solid-liquid/liquid interface. The specific application is the development of a catalyst level detector for the H-Coal 1" Bench Reactor, which is a 1" ID, 3/16" wall reactor, as depicted in Figure 1. The reactor contains catalyst (slumped configuration) which is expanded to roughly twice its

* This work supported by the U.S. Department of Energy.

H - COAL BENCH REACTOR

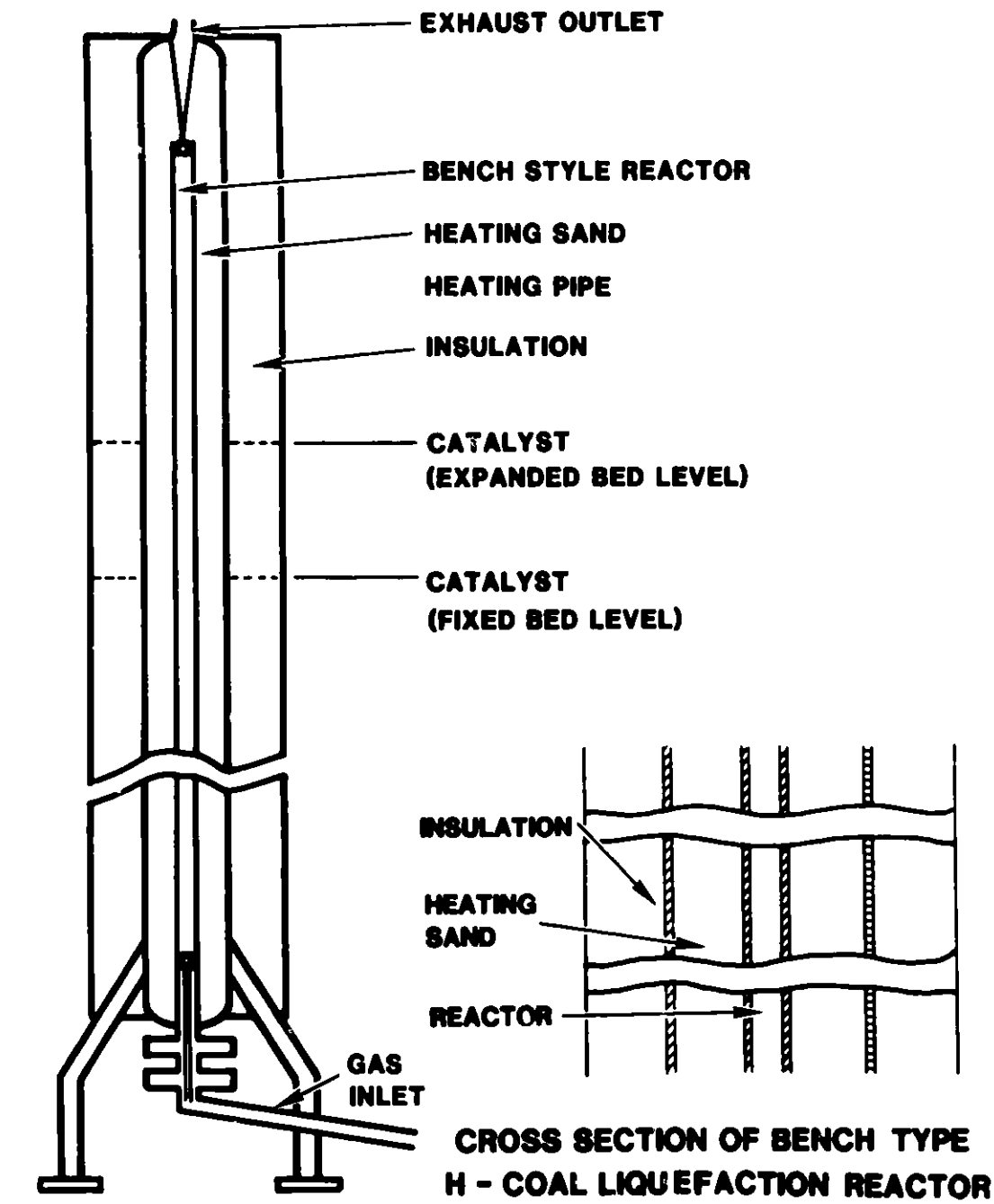

FIGURE 1

volume during runs. The level the catalyst reaches in the reactor is currently an estimated parameter. Thus, there is no control nor any empirical information regarding the fluid dynamics of the system which affects the rates of reaction. In order to provide necessary process control, an isotope/detector system has been designed to continuously measure the density of the material at any specified height in the bed. From the density variations, the height of catalyst and the uniformity of distribution can be determined during runs.

A difficulty associated with measuring the density variations is the amount of material involved, see Figure 1. There is approximately 1/2" steel in the walls of the reactor, 4" of heating sand, 1/4" steel in the walls of the pipe containing the sand, 4" of insulation, and a 1/32" metal retainer sleeve.

The isotope/detector systems are shown in pictorial form in Figure 2. The source system utilizes a Cs^{137} isotope as the gamma radiation source located in an adjustable collimator. The Cs^{137} is a highly monoenergetic gamma emitter with energies of approximately 600 keV. It also has an attractive half-life of 25 years, which reduces the need for frequent re-calibrations. The density of the cesium material is high enough to allow a high specific activity within a small source size. This small source size, in conjunction with a collimator, can provide greater resolution due to less scattered radiation.

The detector system utilizes a BiGe scintillator which is compatible with the Cs^{137} isotope and is more temperature insensitive than other commonly used materials. This BiGe scintillator also has a fast response time and low dark current. A block diagram of the detector is shown in Figure 3. Analogous to the source, the detector is placed in an adjustable collimator. The yoke assembly holds both the source and detector and is mounted on lead screws. The lead screws have encoders at both ends and a variable speed motor that allows for scan speeds up to 6 inches per second. This yoke assembly is also depicted in Figure 2. The scan speed will affect signal-to-

PICTORIAL DIAGRAM CATALYST LEVEL DETECTOR

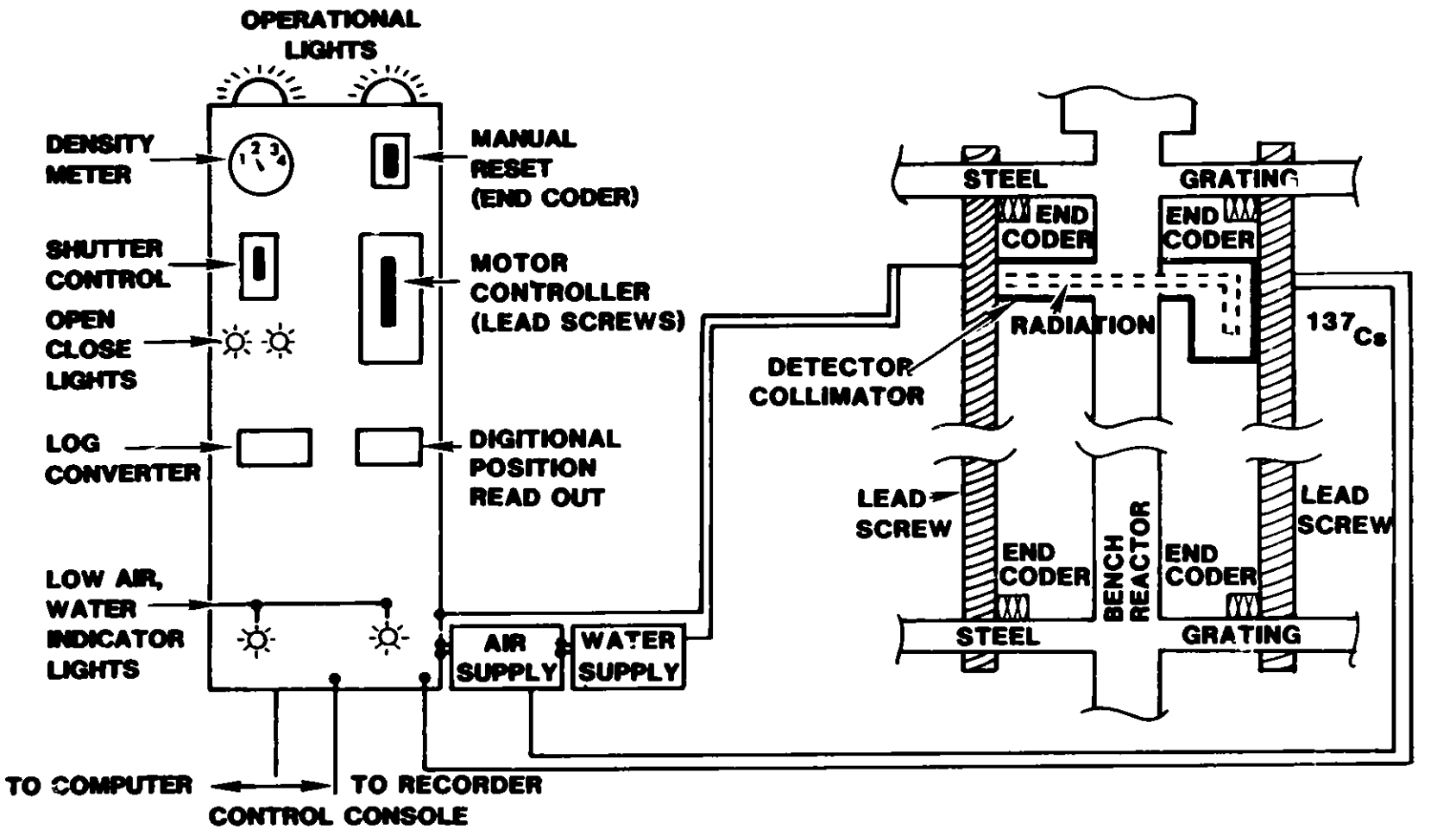

Sandia National Laboratories

FIGURE 2

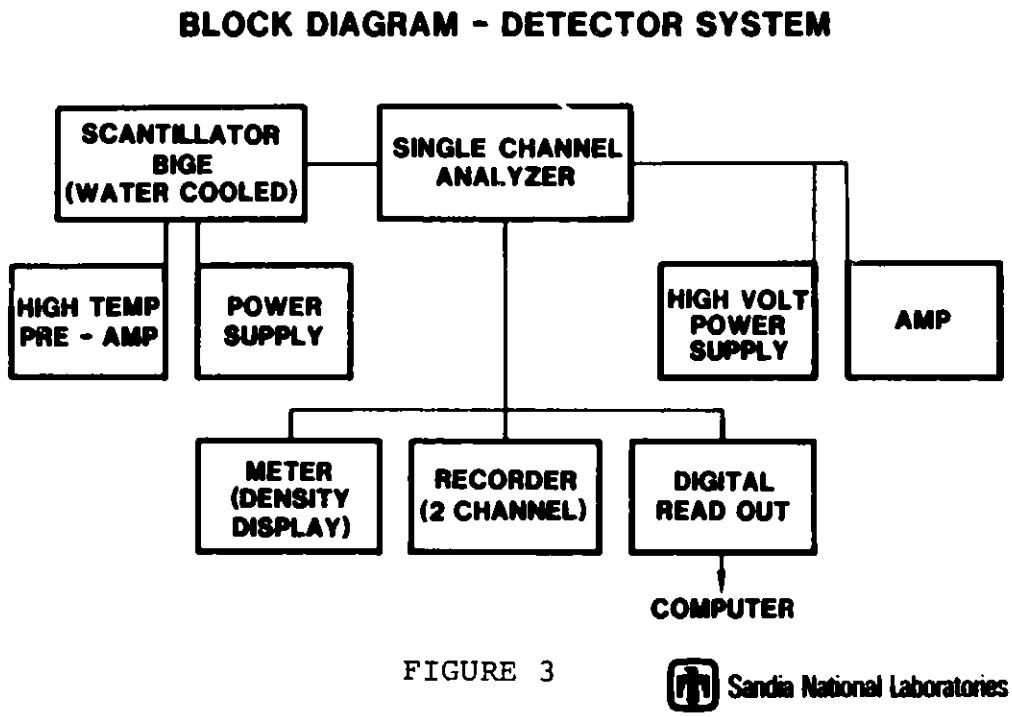

FIGURE 3

noise ratios; that is, the time constant of the filter circuit will be directly affected (as the scan speed increases the time to interrogate the signal decreases). There is, however, a stop-and-stare mode that will allow for indefinite interrogation periods.

SYSTEM CAPABILITIES

The system described has been designed to operate as a high-resolution density gauge. The variation in density that we are attempting to distinguish is small--the density difference between a coal slurry ($\rho \approx 1.1$) and a coal slurry containing $\sim$ 25% by volume catalyst ($\rho \approx 1.5$) is about 1% of the total system (remembering that retainer, insulation, sand, and reactor walls are included in the total density).

Experimental data have been collected on a static system as depicted in Figure 1, cross-section, with the density gauge in place. These data are presented in Table 1 for the three

Table 1. Counting Data for Reactor Configuration

Configuration	Counts*	Noise %	Signal (% change)
Oil only	163, 672	0.3	0
Slumped bed	158, 483	0.4	3.2
Expanded bed	161, 423	0.3	1.4

* Plus background.

configurations of interest. The signal difference between the two cases of interest--distinguishing between no catalyst and ∿ 25% by volume is ∿ 1.8% with a signal/noise ratio of 5/1. The time constant use for these experiments was 20 seconds, but this can be reduced, if necessary, by the use of a larger source. Likewise, the signal/noise ratio can be improved, as required, by increased size of the source. These trade-offs can be optimized only with the system in place with the H-Coal Bench Unit in operation.

SUMMARY

A density gauge has been designed to function as a catalyst level detector in the H-Coal 1" Bench Reactor. The system utilizes a Cs^{137} source and a BiGe scintillator as a detector. The source/detector systems are encompassed in a yoke which can be maneuvered over ∿ 1/3 of the reactor height. Both catalyst level and bed uniformity can be measured. The system, as tested, can distinguish coal slurry and roughly 5% catalyst by volume.

REFERENCES

1. "Overview of Coal Conversion Process Instrumentation", B. G. Liptak, C. P. Leiter, Technical Memorandum No. 1, ANL-FE-49628-TM01, May (1980).

2. "X-Ray Imaging of Coal Derived Products", D. G. Sample, M. G. Thomas, Proc. of the 1979 Symposium on Instrumentation and Control for Fossil Energy Processes, ANL-79-62, Conf-790855, p. 475, Denver, CO, August (1979).
3. "The Tagging of an H-Coal PDU Run", D. G. Sample, M. G. Thomas, Proc. of the 1980 Symposium on Instrumentation and Control for Fossil Energy Processes, ANL-80-62, Conf-800602, p. 123, Virginia Beach, VA, June (1980).

HOMOGENEOUS MULTIPHASE NON-NEWTONIAN FLOW IN A COAL SLURRY PREHEATER

J. Hsu and R. Jungerhans
Kinetics Technology International Corporation
Pasadena, California

ABSTRACT:

In this study, the coal slurry preheater of the SRC-I coal liquefaction process has been investigated. A mathematical model for a homogeneous three-phase non-Newtonian flow, with first order reaction is proposed.

A computer program has been developed for the simultaneous solution of the governing equations. Heat transfer coefficients, pressure drop and heat of reaction are calculated along the heater coil and compared with a set of the Wilsonville pilot plant data (run 159 of March, 1979). (ref. 1 and 2)

I. INTRODUCTION

Solvent refined coal is a very low ash, low sulfur, and high BTU content material. One of the major steps of the SRC-I process is the slurry preheater. In the preheater, coal is dissolved in a hydrogen donor solvent under pressure. At the same time, liquid and gas are generated by means of hydrogenation and/or hydrocracking of the dissolved coal. The coal slurry flow is a three phase non-Newtonian fluid flow with heat and mass transfer occuring simultaneously. There are only few publications dealing with this problem. (ref. 3 through 11)

The purpose of this study is to set up and analyze a flow model which represents the true mechanism of the coal slurry process in the preheater. The model is tested against existing pilot plant data. (ref. 1 and 2)

II. THEORY AND MODEL

A. The Fluid Mechanics

The coal liquefaction process in the preheater is a three phase

fluid flow process. Solid coal particles are well mixed with hydrogen gas and solvent in the mixing tank and are transported into the preheater. However, the coal particles are small compared to the preheater coil diameter. The particle size is about 200 mesh for the pilot unit. Therefore, the three phase fluid, or slurry, can be treated as a normal two phase flow. In the simulation, the solid particles and the liquid solvent are combined as a single liquid phase. Based upon this assumption, the slurry flow regime can be calculated. When the fluid temperature reaches 400° F or above, the flow is in the range of homogeneous two phase flow regime.

(B) Viscosity Calculation Method

The detailed mechanisms of the coal conversion are discussed as follows: One of the major steps is that the coal will swell, disintegrate and become a high viscosity non-Newtonian fluid. (ref. 11) The fluid no longer follows the Newtonian fluid behavior, i. e., the response shear rate of the fluid will not be directly in proportion to the acting shear stress. A team at the Oak Ridge Lab. (ref. 12) developed a pseudo-plastic non-Newtonian fluid model to analyze this phenomena. In this model, the shear stress is assumed to vary with the shear rate to power n, i. e.,

$$\tau_s \text{ (shear stress)} = \frac{K}{g_c} \left(-\frac{dU}{dr}\right)^n \qquad (1)$$

Where n is the viscosity index ≤ 1 ; K is a function of temperature. The viscosity μ, of the fluid is defined as:

$$\mu_1 = \frac{K}{g_c} \left(-\frac{dU}{dr}\right)^{n-1}$$

The constant K and the index n of the fluid viscosity are determined as follows:

first, the shear stress duty of the slurry (or liquid phase) is separated from the main two phase fluid flow. The Bankoff's method (13) is employed to analyze the flow pattern. The vapor void fraction α_v and velocity U_v distribution are in the form of:

$$\frac{\alpha_v}{\alpha_{v,cl}} = \left(\frac{r}{R_o}\right)^m \qquad m \text{ is a constant} \tag{2}$$

$$\frac{U_v}{U_{v,cl}} = 1 - \left(\frac{r}{R_o}\right)^2 \tag{3}$$

The two phase flow velocity, density, and viscosity are calculated using the weighting factor α_v and the properties of each phase. Second, by considering the slurry flow as a single liquid flow in the pipe, the local liquid viscosity is determined. Therefore, the shear stress of the slurry can be correlated to the bulk liquid velocity through the same type of power rule:

$$\tau_s = \frac{K^{**}}{g_c}\left(\frac{8U_b}{D_i}\right)^{n^*} \tag{4}$$

here, $n = n^* \qquad K = K^{**}\left(\frac{3n+1}{4n}\right)^{-n}$

The effective viscosity of the slurry becomes:

$$\mu_{eff} = \frac{K^{**}}{\frac{3n+1}{4n}}\left(\frac{8\,U_b}{D_i}\right)^{n^*-1} \tag{5}$$

The viscosity index "n" can be calculated for a given pressure drop gradient from:

$$n = \frac{\ln\left[\frac{D_i}{4}\left(\frac{\Delta P}{\Delta L}\right)_{tp}\right]}{\ln\left[8\,U_b/D_i\right]} \tag{6}$$

(C) The Kinetic Model

The overall coal conversion is calculated according to a first order reaction. (ref. 14)

$$XA = XM \quad (1-e^{-K_p \tau_p}) \tag{7}$$

$$\text{where } K_p = K'_o \, T^m e^{-E/RT_{out}} \tag{8}$$

$$\text{and} \quad \tau_p = V_e/F \tag{9}$$

(D) The Heat Balance

(i) The unbalanced heat calculation.

The unbalanced heat is defined as the energy difference between the heat input and the sensible heat. Consider an element of the heater coil as shown in Figure (1). The total heat input to this element is the heat flux from the coil wall times the coil surface area. The sensible heat will be the product of the total flow and the inlet and outlet temperature difference times the mean heat capacity. That is:

$$\text{unbalanced heat} = q_w A_s - C_p \, W_t \, \Delta T \tag{10}$$

(ii) The over-all heat balance equation.

For the same element shown in Figure (1), we can make the two dimensional energy balance around the element. The energy convected to and from the element will be balanced by the heat conduction, the viscosity dissipation, and the heat source or sink generated by the chemical reactions.

$$\rho \, U \, C_p \frac{\partial T}{\partial Z} = \frac{\partial}{\partial r} \left(k \frac{\partial T}{\partial r} \right) + \mu \left(\frac{\partial u}{\partial r} \right)^2 + Q_v \tag{11}$$

$$\text{Where:} \quad Q_v = H(T) \frac{W_s}{A_1} \frac{\partial (XA)}{\partial Z}$$

The corresponding boundary conditions are:

$$Z = L \quad T = T_{out} \quad XA = XA_{out} \quad \frac{\partial T}{\partial Z} = o \qquad (12)$$

$$Z = o \quad T = T_{out} \quad XA = XA_{in} \quad \frac{\partial T}{\partial Z} = o \qquad (13)$$

$$r = o \quad \frac{\partial T}{\partial r} = o \qquad r = R_o \quad -k \frac{\partial T}{\partial r} = q_w \qquad (14)$$

(E) The Solution of the Governing Equations

There is no analytic solution to the governing equations. (eq. 1 through 14) The momentum, heat and mass balance equations have to be solved simultaneously. A computer program, based upon a finite element method, has been set up to solve these equations.

III RESULTS AND DISCUSSION:

The following data from the pilot plant have been used as input to the model.

- process temperature profile
- pressure drop
- absorbed duty
- coil throughput

The calculated results are as follows:

1. Viscosity

   The calculated viscosity for the coal slurry is between 10 and 34 c p.

   The viscosity is calculated from the measured pressure drop. It should be kept in mind that the pilot plant operates in a laminar flow regime. For a commercial size installation, operating in turbulent flow, higher pressure drop and viscosity can be expected.

2. The tubeskin temperature has been calculated, while assuming a steadily increasing flux profile up to 70% of the total coil length.

These temperatures are compared with the measured skin temperatures in figure 2. (flux I)
The inside film coefficients are in the order of 50 BTU/hr feet^2 ^{o}F, the average heat of reaction (unbalanced heat) per poung converted coal is in the order of 200 BTU/lb.

3. In order to obtain a closer agreement between the calculated tubeskin temperature profile and the measured data, a slightly modified flux has been assumed. (see figure 2, flux II)
The average heat of reaction for the modified flux is in the order of 600 BTU/lb.

IV. FUTURE WORK

1. More runs of the pilot plant data should be analyzed to improve the kinetic model of coal conversion.
2. A modified turbulent flow model or a model of transition from laminar to turbulent flow should be developed to simulate a commercial size unit.

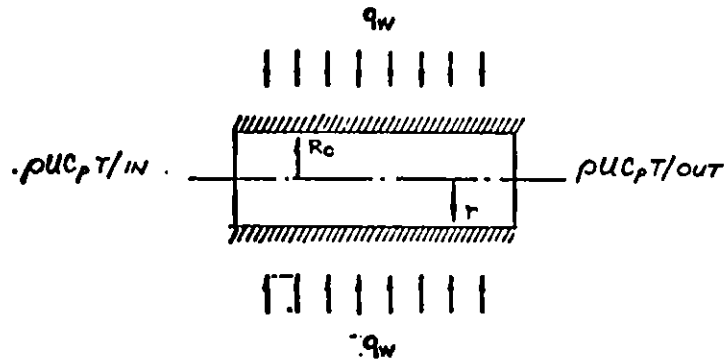

$$\text{UNBALANCED HEAT} = q_w A_s - C_p W_t \Delta T$$

$$\Delta T = T_{OUT} - T_{IN}$$

$$\therefore A_s = 2\pi R_o$$

FIGURE (1) : UNBALANCED HEAT ELEMENT CALCULATION

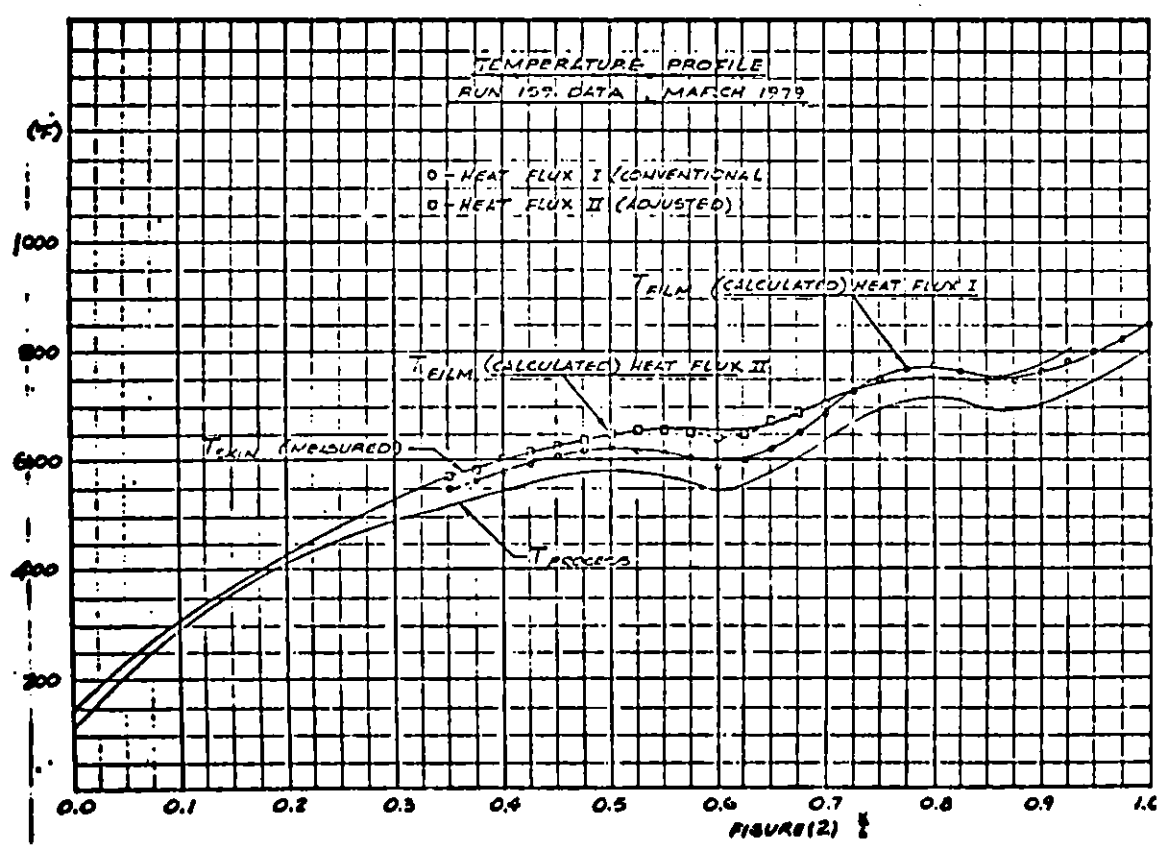

FIGURE(2)

NOMENCLATURE

A_l	Cross section area of the pipe (ft^2)
C	Coal concentration (mol/ft^3)
D_i	Inside coil diameter (ft)
E	Activation energy of the reaction (Btu/lb-mole)
F	Volumetric flow rate of slurry (ft^3/hr)
h_T	Heat transfer coefficient of Traeger model (lb/hr ft^2 ^oF)
ΔH	Heat of reaction (Btu/lb-mole)
H(T)	Heat of reaction (Btu/lb. coal converted)
K	Non-Newtonian viscosity constant (lb/sec-ft)
K'_o	Constant (hr^{-1})
K*	Rate constant (hr^{-1})
K**	Non-Newtonian viscosity constant when shear stress applied at the wall (lb/sec-ft^{-1})
K_p	Rate constant, (hr^{-1})
n	Non-Newtonian index
n*	Non-Newtonian index when shear stress applied at the wall
p	Pressure (psia)
$\left(\frac{\Delta P}{\Delta L}\right)_{tp}$	Two phase pressure gradient (psi/ft)
q_w	Heat flux at pipe wall (Btu/hr ft^2)
r	Radial distance in cylindrical coordinates (ft)
R	Gas constant (ft-lb_f/lb-mole ^oF)
R_o	Radius of the pipe (ft)
T_s	Tube skin temperature (^oF)
T	Fluid temperature (^oF)
U	Velocity (ft/sec)
V_e	Effective reaction volume (ft^3)
W_s	Solid flow rate (lb/hr)
p	Density (lb/ft^3)
W_t	Total flow rate (lb/hr)
XA	Total coal conversion (lb of coal converted/lb coal)

XM	Local coal conversion (lb coal converter/lb coal per element)
t_s	Shear stress of slurry (lb_f/in^2)
t_p	Residence time (hr)
α_v	Vapor void fraction
μ	Viscosity (centipoise)
μ_l	Slurry local viscosity (centipoise)
μ_{eff}	Effective viscosity of slurry(centipoise)

REFERENCES

1. "Solvent Refined Coal (SCR) Promise". Annual Report, January - December 1978, Wilsonville Pilot Plant Data, Catalytic, Inc.

2. "Solvent Refined Coal Pilot Plant". Quarterly Technical Progress Report for the period January - March, 1979. Wilsonville Pilot Plant Data, Catalytic, Inc .

3. Johnathan Tutleman "SRC II Research Project" Report of KTI, February, 1978.

4. Jadvani, K., Schwalbe, S., Fischer, J. "Multi-phase Flow of Gas and Liquid and Gas and Coal-Slurry Mixtures in Vertical Pipes". Argonne National Laboratory, Argonne, Illinois for ERDA (ANL-76-116).

5. Gee, R. E. and Lyon, J. B. "Non-Isothermal Flow of Viscous Non-Newtonian Fluids". Ind. Eng. Chem. 1957, Vol. 47, pp. 956.

6. Oliver, D. R. and Young Hoon, A., "Two-phase Non-Newtonian Flow" Trans. Inst. Chem. Eng., London, England, 1968 Vol. 46, Part I to Part II.

7. Weller, Sol, Pelipetz, M. G. and Friedman, Sam. "Kinetics of Coal Hydrogenation", Industrial Eng. Chem. July 1951, pp. 1575.

8. Suhas Gun, J. Sama, etc. "A Mechanical Study of Hydrogenation of Coal 1 and 2". Fuel. 1979, Vol. 58, March, 171-182.

9. Lee, M. H., Guim, J. A. and Tarrer, A. R., "A Dispersion Model for the Solvent Refined Coal Process". Am. Chem. Soc. Div. Fuel Chem. Prepr. V. 22, pp. 150-160, 1977.

10. Irving Schwager and Teh Fu Yen. "Coal-liquefaction Products from Major Demonstration, Processes 1 Separation and Analysis". Fuel 1978, Vol. 57, February pp. 100 - 104.

11. Richard K. Traeger, "Engineering Kinetics of Short Residence Time Coal Liquefaction Processes". SAND 78-2154 Sandia Laboratories, Albuquerque, N. M.

12. Oswald, G. E., and Thurgood, J. R. "Physical Properties of Coal Liquids and Slurry Preheater Projects". The Department of Energy Project Review Meeting, March 1979. DOE

13. Hsu, Y. and Graham, R., "Transport Processes in Boiling and Two-phase Systems". McGraw-Hill.

14. W. H. Weber and A. Basu, Catalytic, Inc. "Coal Dissolution Studies Utilizing the Slurry Preheater at the Wilsonville SRC Pilot Plant". Coal liquefaction Preheater studies, the Department of Energy project review meeting, March 21, 1979.

ACKNOWLEDGEMENT

The permission to present this paper, as given by Catalytic, Inc., Philadelphia, is kindly acknowledged.

OPERATION OF A BENCH-SCALE, COAL-SOLVENT SLURRY HYDROLIQUEFACTION SYSTEM*

G. E. Oswald, E. L. Youngblood, D. D. Lee, and J. R. Hightower
Chemical Technology Division
Oak Ridge National Laboratory
P.O. Box X
Oak Ridge, Tennessee 37830

ABSTRACT

A bench-scale, continuous-flow, coal-solvent slurry hydroliquefaction system [Coal Liquids Flow System (CLFS)] has been operated at Oak Ridge National Laboratory to make rheological and density measurements on slurry under processing conditions encountered during the preheating operation in the Solvent-Refined Coal (SRC-I) and H-Coal direct liquefaction processes. Successful measurements have been made at up to 730 K and 20.8 MPa (3000 psig) hydrogen pressure. The system consisted of high-pressure delivery systems for both slurry and hydrogen, slurry preheater, reactor/dissolver, vapor-liquid separator, gas back-pressure control system, and slurry pressure letdown system. Maximum slurry throughput was 4 kg/h. A capillary or pipeline viscometer (PLV) was used for rheological characterization measurements, and density measurements were made using a gamma radiation absorption density instrument. Both instruments were located at the preheater discharge; so the slurry passed through them, at temperature and pressure, immediately after being heated to the temperature of interest. Design of the system required the solution of several unusual instrument and control problems such as liquid level detection at high temperature and pressure, slurry mass feed rate measurement, and slurry pressure letdown. Rheological characterization measurements at 13.9 MPa (2000 psig) on slurry prepared from 35 wt % Illinois No. 6 coal (-170 mesh)/65 wt % Wilsonville SRC-I recycle solvent showed that the slurry was Newtonian at temperatures below 400 K and became increasingly pseudoplastic as temperature was increased. Also, the slurry exhibited an unusual increase in viscosity with increasing temperature between 500 and 650 K as the heated coal became plastic. As temperature was increased beyond 650 K, slurry viscosity rapidly decreased to the level observed at temperatures below the onset of the increased viscosity behavior. System design and solutions to operational problems are discussed. The results of rheological characterization measurements and density measurements are presented.

INTRODUCTION

Knowledge of the physical properties of coal liquids under process conditions is essential for the proper design of processing equipment (i.e., heat exchangers, reactor vessels, vapor/liquid separators, and process piping

*Research sponsored by the Fossil Energy Office, U.S. Department of Energy under contract W-7405-eng-26 with the Union Carbide Corporation.

systems) for large-scale direct liquefaction processes. Physical property measurements are also important in the operation and control of such processes. A bench-scale, continuous-flow, coal-solvent slurry hydroliquefaction system was designed, constructed, and operated to make rheological and density measurements on slurry under the processing conditions encountered during the preheating operation.

During the preheating operation the temperature of the coal-solvent slurry is typically increased from about 360 to 725 K at pressures from 13.9 to 20.8 MPa (2000 to 3000 psig). Over this temperature span, the slurry undergoes rapid physical and chemical changes as the coal depolymerizes and interacts with solvent; these transformations have profound effects on slurry rheology and density. Specialized instruments were developed for the measurements. Both the capillary viscometer and gamma radiation absorption density instrument could operate at up to the CLFS design limits of 811 K (1000°F) and 31 MPa (4500 psig).

SYSTEM DESCRIPTION

A simplified flow sheet for the Coal Liquids Flow System (CLFS) is presented in Fig. 1. The CLFS is a small-scale, coal-solvent slurry hydroliquefaction facility consisting of high-pressure slurry and hydrogen delivery systems, slurry preheater, reactor/dissolver, vapor-liquid separator, gas-back pressure control system, and slurry pressure letdown system. The two physical property instruments were located sequentially at the preheater discharge, and measurements were made on the total flow through the system at temperature and pressure.

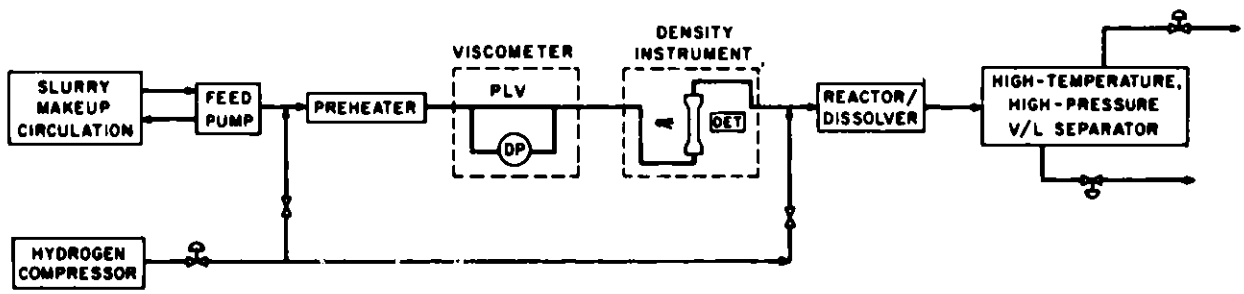

Fig. 1. Coal Liquids Flow System.

Slurry feed rate was determined by monitoring a continuous readout electronic load cell (National Controls, Inc. 3220-100-0.01 with DORIC 420 Digital Indicator) upon which the 14-L capacity stirred feed tank rested. Piping connections to the feed tank were by dip tube or flexible hose so that the weight measurement of the load cell would not be impaired. The output of the

load cell indicator was computer monitored, and feed rate was calculated by weight difference over every 5-min period. A progressive cavity pump (Moyno 3L2 with Viton stator) circulated slurry from the feed tank, by the suction ports of the positive displacement feed pumps (Milton-Roy A-1-33-49-SM and Bran-Lubbe N-K51), and back to the feed tank. The positive displacement pumps were equipped with tungsten carbide check valves for slurry service. Two feed pumps were required because of periodic fouling of the check valves on the pump heads; only one pump was operated at a time. The adjustable stroke length of these pumps permitted variation of feed rate. Maximum pump capacity was 1.1×10^{-6} m^3/s (1 gpm) per pump.

The preheater consisted of 12.2 m of 2.77-mm-ID x 6.35-mm-OD tubing with surface electrical heaters capable of supplying 2.2×10^4 $J/s \cdot m^2$ heat flux based on inside surface area. The preheater was arranged in a serpentine configuration with each horizontal run measuring ~1.8 m long. Surface thermocouples were spaced at 30-cm increments. Heat input was divided into two zones; the first 7.3 m of the preheater comprised the first zone and the next 4.9 m comprised the second. Triac controllers (LFE 230) manipulated heat input based on skin temperature measurement near the end of each heating zone. Slurry residence time in the preheater was nominally 60 to 100 s depending on slurry flow rate.

The preheated slurry passed directly into the viscometer and then to the density instrument at temperature and pressure. Depending on operational mode, hydrogen was metered to the system and combined with the liquid stream either upstream from the preheater or downstream from the physical property instruments at the reactor/dissolver inlet. The reactor/dissolver (31.75 mm ID x 0.762 m long, Autoclave Engineers 78-03198-1) provided residence time at high temperature and pressure for additional conversion of the slurry to liquid products. Typical residence time ranged from 10 to 30 min depending on slurry flow rate; temperature was maintained at ~715 K by a clamshell furnace. Thus, it was assured that the slurry entering the vapor-liquid separator would be processed beyond the increased viscosity stage and would possess increased fluidity. The vapor stream exiting the separator (typical operating temperature was 600 K) was cooled to condense and to trap light liquids and then throttled to control system pressure. The liquid phase was cooled to 360 K and discharged through a pressure letdown valve with tungsten carbide trim (Badger Meter 3445) to control the liquid level in the separator. Liquid holdup in the separator was ~100 cm^3.

A special dual electrode capacitance-type point level detection system was used to control the liquid level in the separator. The electronics package was Drexelbrook Engineering 406-1000, and the probe was an in-house design for the extreme temperature and pressure based on Drexelbrook designs for less severe conditions. This system could operate on liquid media which behave as either electrical conductors or dielectrics. (This was necessitated because coal liquids tend to behave as dielectrics at low temperature and as conductors at higher temperatures.) When process liquid reached the level probe, a three-way solenoid valve was energized, allowing a slow bleed of air to the slurry pressure letdown valve actuator, which opened the valve slowly. When the liquid level dropped below the end of the probe, the solenoid valve was de-energized,

rapidly venting air from the valve actuator and causing the valve to close quickly. Thus the valve opened and closed cyclically in a sawtooth pattern, which prevented solids buildup at the valve seat.

All piping in the system was Autoclave Engineers "medium pressure" coned and threaded connections. The vapor-liquid separator was constructed from 25.4-mm-OD x 14.2-mm-ID tubing and fittings of the same type. An air-driven booster compressor (Haskel Engineering A-1700) supplied hydrogen to the system at up to 34.7 MPa (5000 psig).

An on-line digital computer data acquisition and analysis system (Digital Equipment Corporation PDP-11/34) was used to monitor

1. preheater electrical heat input,
2. 18 key preheater temperatures,
3. inlet and outlet temperatures of the pipeline viscometer,
4. mass feed rate of slurry to the system,
5. differential pressure of the pipeline viscometer,
6. detector amplifier output of the gamma radiation absorption density instrument, and
7. internal and external temperatures of the pressure vessel for the gamma radiation absorption density instrument.

Rheological and density calculations were made on-line.

The capillary viscometer system consisted of a straight, horizontal length of tubing (2.77 mm ID x 0.61 m long) with differential pressure taps and a solvent purge system to clear the taps of accumulated solids during experimental operations (Fig. 2). The pump for this purge system was similar to the feed pumps; it could also be used to feed solvent to the preheater inlet. An electrical trace heater (with independent control system) maintained isothermal conditions along the tube; internal thermocouples monitored inlet and outlet temperatures. A Foxboro model 13H transmitter with liquid-filled pressure taps was used to monitor differential pressure. The output from the transmitter was filtered to attenuate noise in the differential pressure signal caused by the discrete strokes of the feed pump, and then it was converted to an electrical signal for transmission to the on-line digital computer for rheological calculations.

Figure 3 is a diagram of the gamma radiation absorption density instrument. The unit consisted of a commercially available gamma radiation absorption instrument (Kay-Ray 3600F) used with a 30-mm-ID x 42-mm-OD pressure vessel constructed at ORNL. An independently controlled electrical trace heat system maintained isothermal conditions. Density was determined by measuring the attenuation of 662-keV gamma rays from the ^{137}Cs source as they passed through the process fluid. An ionization chamber detected the radiation after it passed through the pressure vessel walls and the process liquid. The detector output was amplified and transmitted to the on-line computer for density calculations. A correction was made for the variation in pressure vessel wall density with temperature.

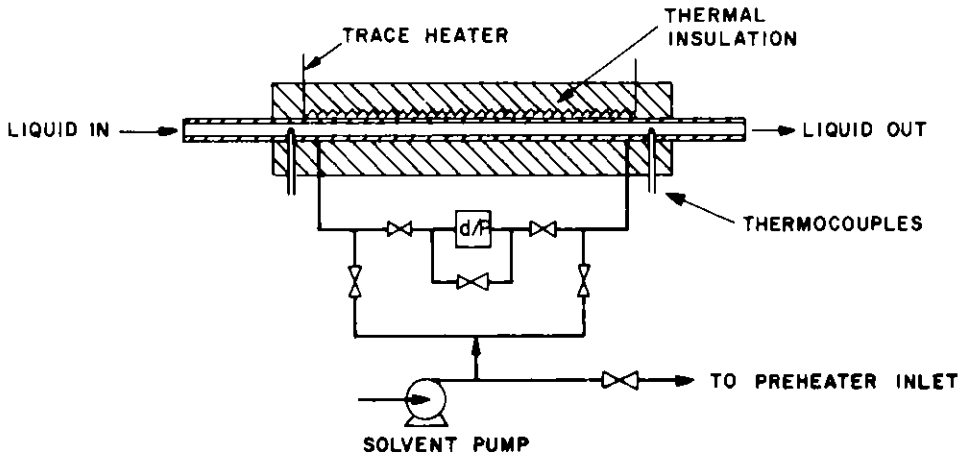

Fig. 2. Pipeline viscometer (PLV).

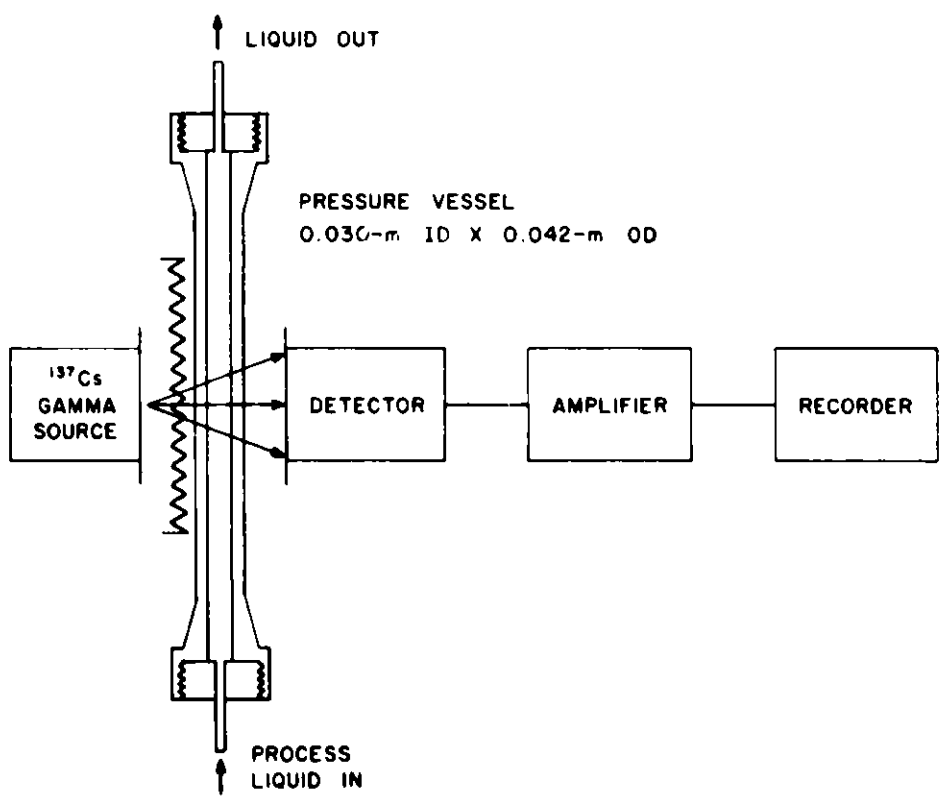

Fig. 3. Gamma radiation absorption density instrument.

OPERATIONS

Start-up involved clearing oxygen from the system by taking it through pressure purge cycles with high-pressure helium delivered from cylinders and heating the system to the designated temperature. Once the system reached the desired temperature and pressure, process (coal-derived) solvent was fed to the system to check overall operation. When it was confirmed that all components were operating properly, hydrogen and slurry feed were initiated, and the experimental plan was executed. When the experimental measurements had been completed, shutdown was accomplished by first flushing residual slurry out of the system with process solvent and then purging hydrogen from the system by means of helium pressure purge cycles.

The capillary viscometer was used to make two different types of rheological measurements. First, to produce a rheogram (plot of shear stress vs shear rate) for slurry, a data set of pipeline viscometer differential pressure at various slurry flow rates was generated at constant temperatures and pressure. Slurry feed rate was varied incrementally from ~1 kg/h up to the feed pump maximum of ~4 kg/h. Preheater discharge temperature and viscometer temperature were automatically controlled at the temperature selected for investigation. These measurements could be interpreted for liquid phase only flow, so hydrogen was introduced into the slurry flow at the reactor/dissolver inlet, located downstream from the physical property measurement instruments. Second, to produce a record of viscometer differential pressure as a function of temperature at constant slurry mass flow rate, slurry was fed to the system at a constant rate, and the preheater discharge temperature and viscometer temperature were incrementally increased together from ~400 to ~725 K. During both types of measurements, the viscometer differential pressure taps were purged periodically with solvent to remove any accumulated solids. The viscometer was calibrated with process solvent against Brookfield and Cannon-Fenske viscometers before each run.

The gamma radiation absorption density instrument, located downstream from the viscometer, was operated continuously during the rheological measurement runs. The slurry passed through the pressure vessel in upflow. An internal thermocouple within the pressure vessel monitored slurry temperature; other thermocouples on the surface of the pressure vessel were used for temperature control. Slurry temperature within the pressure vessel was controlled to match viscometer temperature.

RESULTS

The constant temperature-variable slurry mass flow rate data from the capillary viscometer were analyzed to determine the shear stress vs shear rate relationship (rheogram) through use of the Rabinowitsch-Mooney analysis.[1] First, the raw data were converted into a flow curve — a logarithmic plot of wall shear stress (τ_w) vs the flow parameter 8V/D, where V is the liquid

superficial velocity and D is the viscometer internal diameter. The wall shear stress is defined by force balance over the length (L) of the viscometer:

$$\tau_w = \frac{D\Delta P}{4L} , \tag{1}$$

where ΔP is the pressure drop across the viscometer. Figure 4 is a representative flow curve for a slurry of 35 wt % Illinois No. 6 coal (-170 mesh)/ 65 wt % Wilsonville SRC-I recycle solvent at 550 K and 13.9 MPa. A rheogram is constructed from a flow curve by converting 8V/D values to wall shear rate ($\dot{S}_w$) using the following equation:

$$\dot{S}_w = \frac{8V}{D}\left(\frac{3n + 1}{4n}\right) , \tag{2}$$

where n is the slope of the flow curve at the corresponding value of 8V/D. Since the flow curves generated for the Illinois No. 6 coal slurry were well described by straight-line fits, the slope n is constant for all values of 8V/D for a particular data set. This simplifies the application of equation 2. The rheograms produced for 35 wt % Illinois No. 6 slurry at 13.9 MPa are presented in Fig. 5. Inspection of these rheograms indicates that the slurry was essentially Newtonian at 400 K and became increasingly pseudoplastic (shear thinning) as temperature was increased to 700 K.

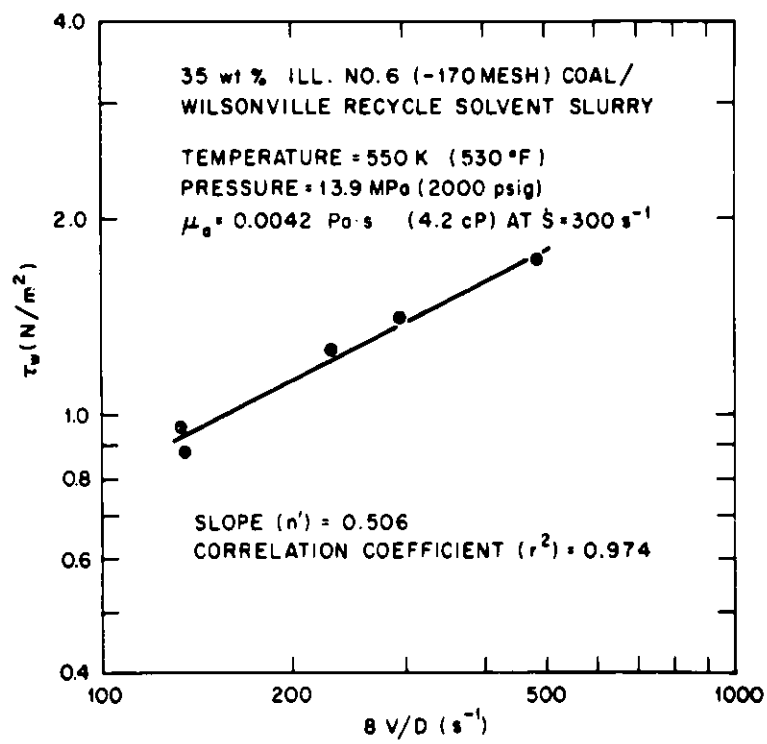

Fig. 4. Flow curve for 35 wt % slurry at 550 K and 13.9 MPa.

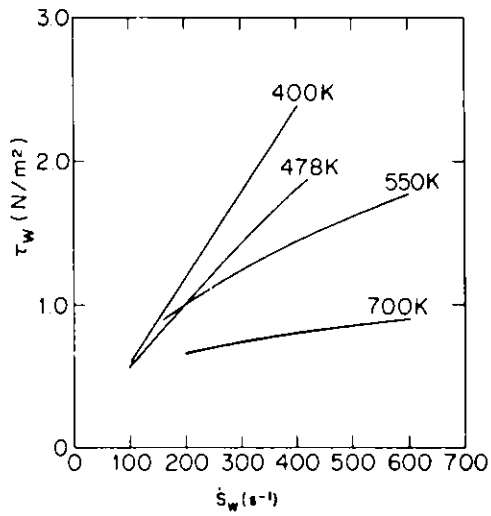

Fig. 5. Rheograms for 35 wt % Illinois No. 6 coal slurry at 13.9 MPa (2000 psig).

Slurry behavior is metastable at temperatures from ~570 to ~700 K because of rapid depolymerization reactions and coal-solvent interaction. This situation prevented acquisition of meaningful flow curve data over this range of temperatures. In order to get information on slurry flow behavior over this temperature range, constant slurry feed rate-variable temperature viscometer runs were conducted.

A typical plot of viscometer differential pressure vs slurry temperature is presented in Fig. 6 for a slurry mass flow rate of 0.665 g/s at 13.9 MPa. The unusual increase in viscosity between 500 and 650 K probably resulted from the plastic swelling behavior of the bituminous coal as it depolymerized over this temperature range. The rapid decrease in viscosity between 650 and 700 K occurred as the rate of depolymerization decreased and the liquified material was stabilized by the hydrogen donor capacity of the solvent. Peak viscosity was about 17 mPa·s (17 cP) and occurred at 650 K; viscosity at the 500 K minimum was 3.6 mPa·s at 300 s^{-1} shear rate.

The results of density measurements on coal slurry and process solvent from 300 to 700 K at 13.9 MPa are presented in Fig. 7. The slurry density measurements deviated from the straight-line relationship established at lower temperatures in the temperature range 500 to 700 K. This sharp drop in density is believed to result from swelling of the coal particles during depolymerization. The drop in density occurred over the same temperature range as the increased viscosity behavior, so both phenomena are probably related to the same physical/chemical changes occurring in the slurry. Both the slurry density minimum and viscosity maximum occurred at ~650 K.

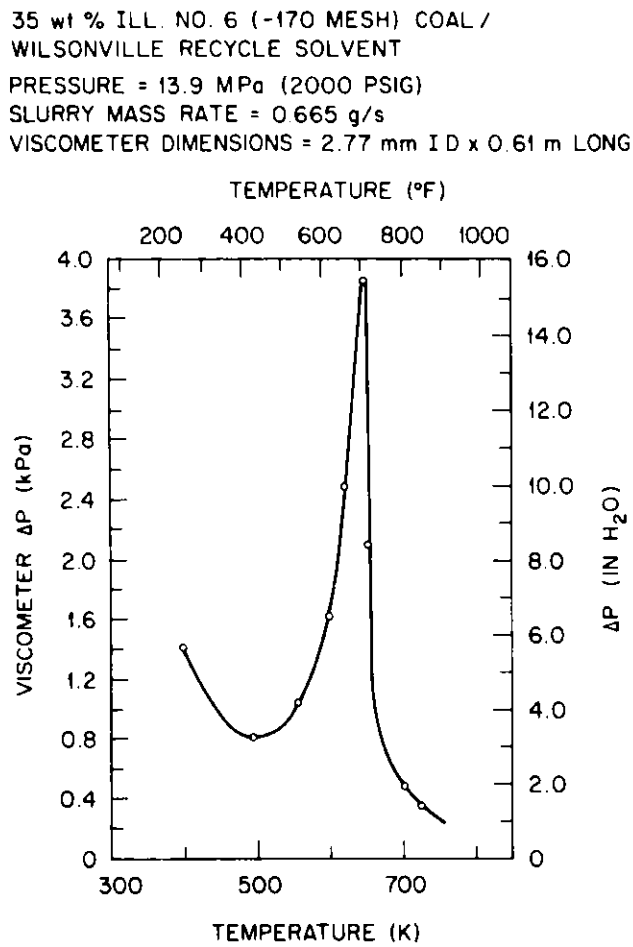

Fig. 6. Pipeline viscometer differential pressure vs slurry temperature.

The attenuation of gamma rays passing through matter is expressed by Lambert's Law:

$$I = I_0 e^{-\mu\rho x} , \qquad (3)$$

where I_0 is the radiation at the detector with no process fluid in the vessel, I is the radiation at the detector when the vessel contains process fluid, μ is the mass absorption coefficient, ρ is the density of the process fluid, and x is the path length. The mass absorption coefficient is the summation of the product of the mass absorption coefficient for each element times the mass fraction of each element in the fluid.

The mass absorption coefficients for the main elements, except hydrogen, found in coal and coal liquids are very close to the same value. The coefficient for hydrogen is about double this value. Since the variation in

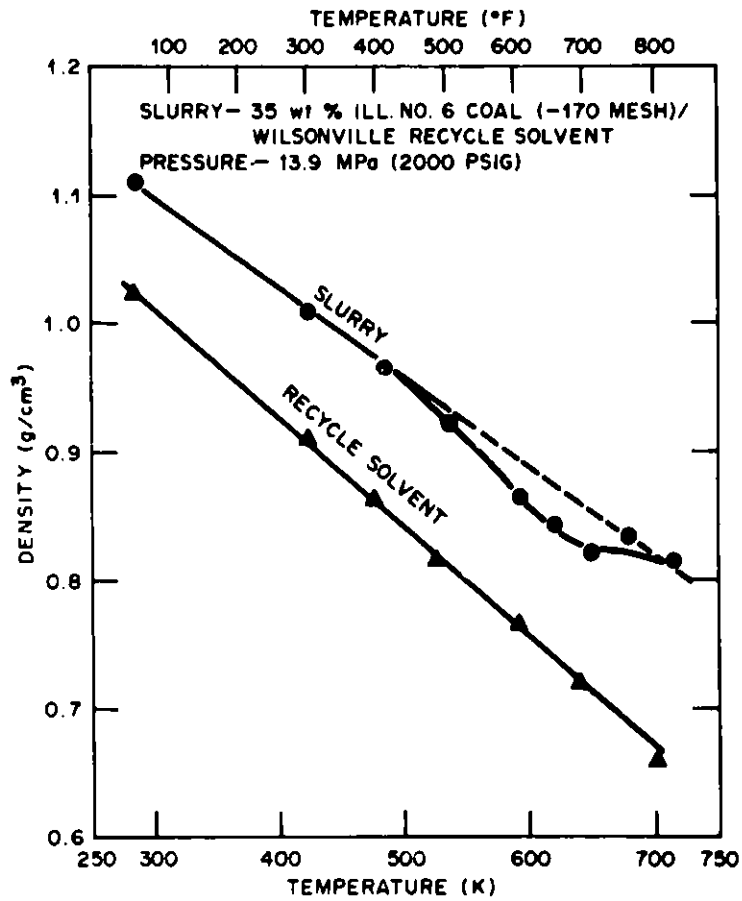

Fig. 7. Density of SRC-I slurry and recycle solvent.

slurry hydrogen content from run to run was small (typically <1.5 wt %), the total mass absorption coefficient was assumed constant, and with a fixed value of the path length the radiation reaching the detector was only a function of liquid density.

The instrument was calibrated using liquids and slurries of known density. The output of the detector amplifier was linearized and transmitted to the on-line computer. Correction was made for the decrease in vessel wall density with increasing temperature before density was calculated.

REFERENCES

1. A. H. P. Skelland, Non-Newtonian Flow and Heat Transfer, Wiley, New York, 1967, pp. 28-32.

LEVEL MEASUREMENT AND CONTROL SOLVENT REFINED COAL (SRC-I) PILOT PLANT

M. J. Barroody
Catalytic, Inc.

INTRODUCTION

In the solvent refined coal (SRC) process, where viscous liquids of varying specific gravity are treated at elevated temperatures and pressures, the detection of vessel liquid levels for measurement and control is a very challenging undertaking. It is also an essential factor in process control and, as such, must be given special consideration.

There are a number of systems currently available that can be used to measure and control process vessel levels. Most of these conventional systems provide adequate level detection and in some cases they have been applied at the SRC pilot plant. This paper describes specialized instrumentation that is used to monitor critical SRC process vessels that operate at higher pressures and temperatures.

The solvent refined coal pilot plant at Wilsonville, Alabama, is a 6 tpd facility that was designed, constructed, and is being operated by Catalytic, Inc. Operation with coal began in January 1974. Southern Company Services directs the project under contract with the sponsors, the United States Department of Energy and the Electric Power Research Institute.

The SRC process, in general terms, starts with the mixing of fine coal and process solvent in a slurry blend tank. After agitation, the mixture is pumped through a slurry preheater where it is heated and hydrogen is injected at high pressure. The hydrogenated coal slurry then passes to a reaction vessel. After a specified residence time, the slurry is passed through a cooler to a high pressure separator. At this vessel, entrained gases

and slurry are separated and the slurry is flashed through letdown valves to an intermediate pressure Flash Tank. After flashing, the mixture is passed to a vacuum column where additional separation of the components occurs.

Accurate level measurement and control in the two-stage vapor-liquid high pressure separators are vital to sustained process operations and can significantly effect product quality. This paper will describe the level measurement and control systems that have been developed for these two particular vessels, and also describes other level detection systems at the SRC facility.

HIGH PRESSURE SEPARATOR

Controlling the slurry level in the high pressure separator is vital to the process because this vessel is fed by a reaction dissolver where residence time is a critical factor and because of the high operating temperatures and pressures. The operating pressure is generally maintained at about 2,100 psig and the temperature varies from 730 to 815°F, depending on the operating mode.

The level in the separator is monitored by two differential pressure transmitters, each equipped with two purged dip tubes. The dip tubes are 316 stainless steel cut to a specified length. Each transmitter is connected to a two-mode controller which, in turn, is tied into a set of letdown valves. Continuous level controlling is done through the letdown valves.

The purging system for the vessel pressure transmitters consists of a main hydrogen feed line to a purging station. Hydrogen pressure is set at 2,500 psig, 400 psig higher than the vessel operating pressure. Hydrogen flow is controlled by restriction orifices (ROs). The ROs are constructed of capillary-type

tubing installed in a union and soldered in place. These ROs are tested for the required consumption prior to installation to determine the capacity of each RO. This is necessary because the capillary tubing size varies. High pressure needle valves are used to shut off the hydrogen flow when maintenance is required.

Figure 1 shows the high pressure separator, its level transmitters and the two dip tubes that are immersed inside the vessel (one high and one low). The transmitters are located approximately 10 feet above the vessel. The purge station is about 5 feet from the transmitters and is also above the vessel.

Protection against transmitter impulse line plugging and backflow into the transmitters' sensing capsules is afforded by locating the purging system and transmitters above the vessel. Also, operating the purging system at a higher pressure than the vessel prevents orifice plugging and in turn prevents the transmitter indicator from showing wide fluctuations and false readings. Plugging can also occur when oil from the hydrogen compressor reaches the ROs.

To zero the transmitters, it is necessary to equalize the pressure and volume of gas that the ROs allow into each of the transmitter's impulse lines. An imbalance will effect calibration. The flow of hydrogen from the ROs must be minimal so it does not effect the transmitters level monitoring activity.

There are two impluse lines connected to each transmitter. One enters on the low pressure side of the transmitter and one enters at the high pressure side. The low pressure impulse line is connected to the top of the vessel and, importantly, it is a dry line. Because it's dry, errors that could occour due to vapor pressure changes above the coal slurry in the vessel are prevented. The high pressure impulse line from the transmitter is

connected to the bottom of the vessel's tangent line.

The transmitter range is set for the approximate levels at which the vessel will operate. At this point, it is imperative to know the specific gravity of the vessel's contents. This helps set the transmitter fo the proper range. The specific gravity of coal slurry varies from 0.9 to 1.2, or higher, depending on the percentage of solids.

When the level in the high pressure separator reaches a predetermined point, the transmitters send a quantified level increase signal to the level controllers. The controllers, in turn, open the valves to discharge only the amount of slurry that is necessary to maintain the required level. The flow is monitored by Venturi-type flow meters in the bottom of the vessel. The slurry passes through the letdown control valves to the flash tank.

FLASH TANK

After entering the Flash Tank, the pressure is dropped from 2,100 psig to 150 psig through the letdown valves. The level in this vessel is monitored by a system similar to that used in the high pressure separator. It's a purged system with the transmitters located above the vessel and connected by a dry impulse line entering the low side of the transmitter which attaches to the top of the vessel, and a line connecting the transmitter's high pressure side and the vessel bottom. Restriction orifices (ROs) are, as with the separator, important components. See Figure 2.

Monitoring the flash tank level can be problematic, mainly because of the continuous operation of the letdown valves. The level readings will often swing, even with purged impluse lines, and extra care should be taken in interpreting readings.

NUCLEAR SYSTEMS

Nuclear level detectors have been installed at the Wilsonville pilot plant during the last six months to back up the conventional pneumatic systems at the high pressure separator. The nuclear continuous level system consists of a small radiation source, a detector, and the corresponding electronics plus an I/P convertor and a pneumatic receiver indicator. The strength of the nuclear radiation source is determined by the vessel wall thickness and inside diameter, and the level range. The detector length is determined by the level range, and the mounting angle of the source.

When the radiation source shutter is opened, a beam of radiation passes through the vessel toward the detector. The strength of the signal when it hits the detector is the factor used to determine the vessel level, because the radiation is absorbed to varying degrees as it passes through more or less of the vessel's contents. The strength of the signal received at the detector is inversely proportional to the level in the vessel.

An amplifier is used to enhance the signal after it is received by the detector. The amplified signal is then fed to the I/P convertor where a 3 to 15 psi output is produced when 4 to 20 ma is induced. The output pneumatic signal is then deliverd to an indicator where it is calibrated in inches of water.

The nuclear continuous level system has no contact with the slurry and is therefore independent of temperature and pressure. It transmits level changes faster than a pneumatic system but the electronic equipment has malfunctioned due to moisture, cable noise signals, and fluctuations in the plant power supply.

OTHER LEVEL DETECTION SYSTEMS

The previously discussed systems for level detection, measurement and control are not the only means available to monitor level changes. At the SRC pilot plant, the nature of the system and instrumentation is determined by the conditions under which it will operate. Some conventional systems that are used in Wilsonville, under appropriate conditions, are the following:

- Floats are used when the specific gravity of the liquid is constant and the service is not severe. They give reliable indications under the proper conditions.

- Displacement systems are used when interface measurements are required. Displacers will move with interface and specific gravity changes and work only in low temperature and pressure environments.

- Capacitance probes are used in oil/water separation vessels of minimum vibration, varying pressures, and low temperatures. They are specially suited to high and low level point indication where a pump operation is controlled.

- Conductance systems are used for a high/low level detection. They are inexpensive and make excellent pump controls where conductivity exists. (Note that probes for capacitance and conductance will lose their sensitivity as buildup accumulates on the probes.)

- Level control by vessel weight works well in situations where the liquids are well mixed.

Gas bubblers, and sonic and ultra-sonic level detectors and monitors are not being used at Wilsonville.

There are advantages and disadvantages of using conventional instrumentation for level monitoring and control in processes like solvent refining. One significant advantage is that conventional instrumentation is not as expensive; another is that, in most cases, a reliable level signal can be obtained even at high pressure and temperature conditions with a corrosive material. But, there are disadvantages as well. Among the disadvantages are plugging in the ROs and impulse lines (that can be real maintenance headaches), inaccurate level sensing due to specific gravity changes as process conditions shift, the difficulty of providing a tap connection on a high pressure vessel, and the need to replace dip tubes periodically due to corrosion and errosion.

CONCLUSION

Level measurement and control in the solvent refined coal process, much like other petro-chemical processes, must be sensitive to varying process and plant condiions. Conventional systems have been suitable for many applications, but special consideration must be accorded when larger, commercial-size facilities are equipped. The time and care expended in the design phase can save much time and trouble later.

The applicability of nuclear level detection systems in a commercial-size plant is also questionable. It would demand a powerful nuclear source to penetrate the heavy vessel walls and viscous liquids, and that may pose safety problems.

It is imperative that manufacturers and designers work together to assure safe reliable instrumentation solutions to process control problems in larger scale solvent refined coal facilities.

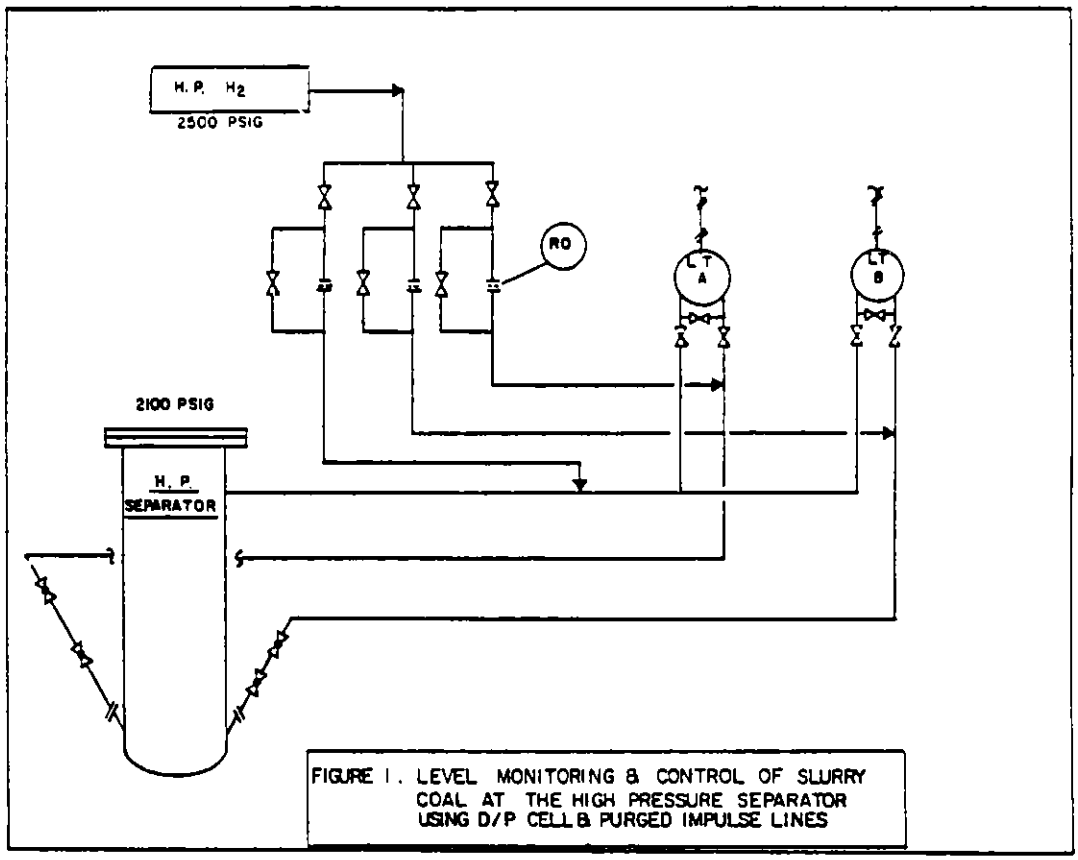

FIGURE 1. LEVEL MONITORING & CONTROL OF SLURRY COAL AT THE HIGH PRESSURE SEPARATOR USING D/P CELL & PURGED IMPULSE LINES

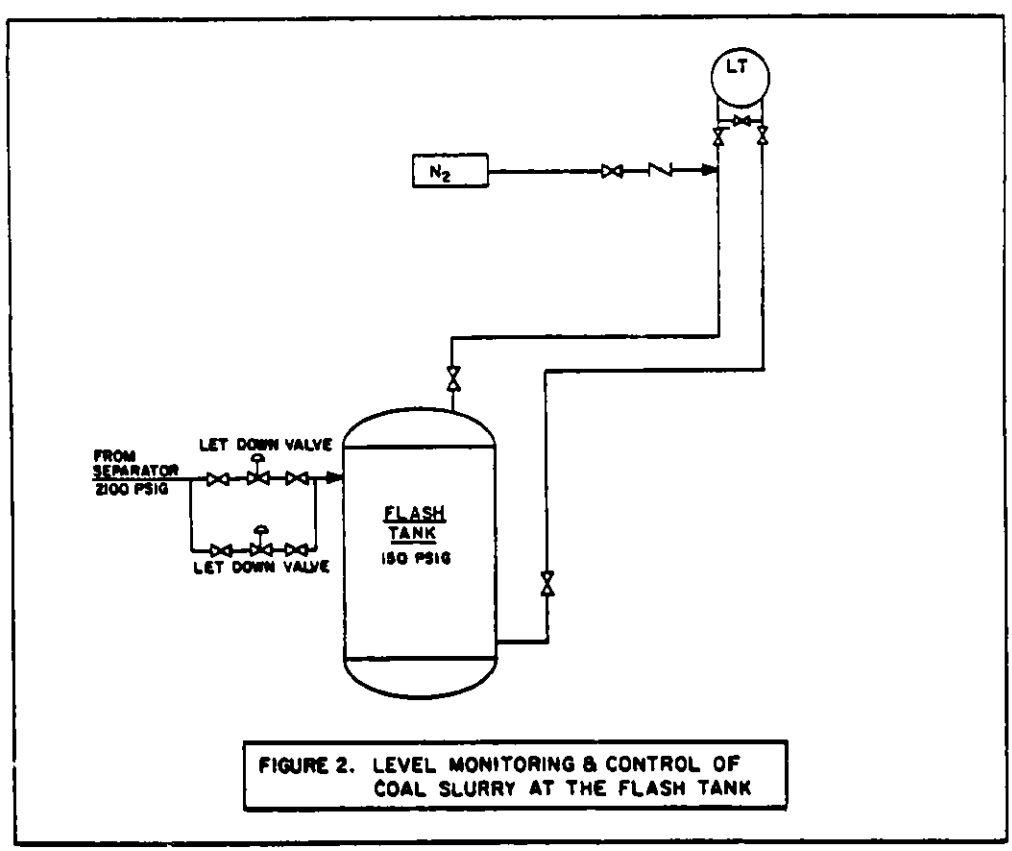

FIGURE 2. LEVEL MONITORING & CONTROL OF COAL SLURRY AT THE FLASH TANK

LUNCHEON ADDRESS: PRIVATE INDUSTRY AND SYNFUELS, THE INSTRUMENTATION AND CONTROL ROLE

E. A. Lloyd
Hydrocarbon Research, Inc.
McLean, Virginia

I am happy to have this opportunity to be with you once again. It is obvious that interest in synthetic fuel process instrumentation and control is vigorous and growing from what I have seen so far. All of you who participate in this symposium are to be commended. I am glad to have had the opportunity to support this organization in my previous role; certainly it has had and will continue to have a full measure of my moral support.

Since this symposium is for those involved in I&C activities, I would like to spend a few minutes bringing into focus the potential magnitude and challenges of the gestating synfuels industry for which we in private industry must provide the means to instrument and control. As some of you may know, 15 days ago I joined you in private industry as the Director, Energy Resources Development of Hydrocarbon Research Incorporated (a subsidiary of Dynalectron Corporation) in McLean Virginia. Thus, I am now in the base of the tetrahedral pyramid I described several years ago which had I&C firms, A&E constructors and process developers in the base or foundation, with DOE and the government at the point, out

of the real action. HRI can qualify principally as a process developer but I dare say we could also qualify as an I&C firm.

Where does private industry stand today in its ability to support the live birth and nurture of a synthetic fuels industry?

A series of studies* were completed last year which addressed the capability of the industrial base required to achieve a daily synfuels production of one million barrels per day by 1990 and three million barrels per day by the year 2000. We set those parameters before President Carter established his goals of 500,000 bbls/day by 1987 and 2 million by 1992, but we bracketed the problem.

These studies were sponsored by DOE and were conducted by four contractors representing a breadth of interest. These were Bechtel National, Mechanical Technologies Inc., UOP/SDC, and Monsanto Research Corporation. These organizations examined many aspects of bringing a synfuels industry into being.

*"Achieving a Production Goal of One Million B/D of Coal Liquids by 1990" March 1980, DOE/FE/10490-01. Available from National Technical Information Service (NTIS) U.S. Department of Commerce, 5285 Port Royal Road, Springfield, Virginia, 22161. Printed Copy $29.00; Microfiche $4.00.

Since it is not possible to completely examine the interdependence of all of the factors which potentially influence the start of a new industry, the results cannot be considered definitive. However, these studies do present a valuable insight into the technical needs and potential barriers to achieve a signficant level of production.

The analyses were based on an implementation schedule required to produce the target quantities using a nominal 60,000 barrels/day plant size and using a population mix of production processes. The first plants used indirect liquefaction processes with plant startup commencing in 1985. Plants using direct liquefaction processes were to be on-line by 1987. Regional siting considerations were included in the studies.

The overall conclusion is that either the one or three million barrel per day scenario could be implemented without major dislocation to the U.S. economy as a whole. But to do so without major problems, action must be planned and taken to overcome potential labor, material and equipment impediments.

The study found that almost 39 million manhours would be needed in construction labor for the indirect coal liquids plants, but only 22 million for the direct liquefaction

plants. The difference is because the indirect plants and essentially two plants in one--a gasification plant at the front end connected to a liquefaction plant at the back.

Likewise, almost 4.5 million manhours of engineering would be required for the indirect liquefaction plants but only 2.3 million for the direct liquefaction plants.
Assuming that one wants to achieve a million barrels per day production by 1990 and then 3 million barrels per day by the turn of the century--which would require 20 plants in ten years and 60 within the next 20 years--an on-site labor peak of 85,000 persons will be required around 1985 as design and construction of these plants moves into full swing. That is about two percent of the total projected U.S. construction work force.

Add operation and maintenance, and on site labor requirements are projected to be about 160,000 persons by 1990. Compared to the total workforce, these requirements are significant, but as a whole, they do not appear to present an insurmountable obstacle to achieving the production goals.

Yet overall employment statistics can be deceiving in analyzing where labor might be constrained. Shortages may occur for particular technical or craft skills or in certain regions, so the analysts were asked to look at specific labor issues in particular.

Here are just a few.

The most serious challenge to engineering manpower would occur between now and 1985, the early years of the commercial synfuels program. Many of the new engineers will come from our colleges and universities. As many as 8500 of the Country's expected additions to the engineering workforce could be required by the new coal liquids industry. That's about four percent of the total number of new engineers expected to join the labor force in that time frame.

But the picture changes somewhat when you look at chemical engineers now working in process design and project work. Design and engineering firms in the U.S. (like HRI) probably have no more than 3600 chemical engineers in these areas at present. Although the formation of engineering teams for these coal liquefaction projects does not appear to be an insurmountable challenge, to achieve 1 million barrels of oil per day by 1990 and 3 million barrels per day by the year 2000, we are going to have to increase the process engineering workforce in this Country in the next five years by 1300 chemical engineers--a 35 percent increase.

Part of the increase will be met by experienced engineers transferring from other industries However, the major

portion of the supply should come from new chemical engineering graduates. Unless we can stimulate students in our colleges and universities today to see opportunities in this field or find some way to make the use of qualified engineers more effective, we face the possibility of either increasing severely the competition for competent engineers in other fields or running short. I believe we should begin very quickly to train engineering assistants so that the limits of supply of process engineers can concentrate on engineering rather than subprofessional tasks.

On the other hand, the supply of civil, electrical, industrial and mechanical engineers will not present as challenging a staffing problem.

Looking at construction labor requirements--and keeping the same one million per day target of synthetic liquids by 1990 and three million by the year 2000--we find that the peak periods will occur around the mid 1980's when almost 73,000 persons will be required, some 17,000 of them pipefitters, over 7000 electricians, almost 6000 welders, roughly 6400 carpenters, some 4000 ironworkers, and over 30,000 other related jobs.

Here it becomes important to look at regions and the availability of building tradesmen in various locales. Up

to 27 percent of the current union craftsmen in some crafts will be needed in some part of the Country, primarily in the Great Lakes and Appalachian states. But in some regions, like the Great Plains and Northern Rocky Mountain states, up to 81 percent of the current union craftsmen in individual crafts may be required.
To meet the labor requirements in these regions, we must expand the use of non-journeymen, expand apprenticeship and training programs, and coordinate better with vocational schools.

Perhaps most importantly, we need a concerted effort by labor, private industry and government working together.

I've dealt primarily to this point with on-site labor requirements. But it is obvious that a national undertaking of this scale will also have a significant ripple effect in the employment profiles of the equipment and manufacturing industries.

For example, the synthetic fuels industry in our scenario will require industry to produce in the year when the requirement peaks--probably around 1985--almost 37 million square feet of heat exchangers. That's almost three-fourths of the Nations production capacity.

Annual production of pressure vessels with walls 1.5 inches to 4 inches thick must top 80,000 tons in the mid 1980s. Almost 2.5 million total horsepower of centrifugal compressors wil have to be produced annually in the peak production periods--again in the mid 1980s. And the list could go on.

It is clear that tasks of this magnitude with its widespread impact on this nation is an undertaking appropriate to the private sector. There is no way the government will be able to do more than encourage the construction of the first few plants; the thought of the Congress appropriating 3 billion dollars for each of 60 plants, 180 billion dollars or more, is mind boggling.

When we focus on instrumentation and control you can see the problems with much better resolution. One need only scan through the topics contained in the program for this symposium to grasp the breadth of the technology requirements essential to the successful operation of a synfuels industry. We must also recognize that success is measured from both the engineering and profitability points of view.

It will be essential that the I&C industry be able to meet the needs of the process and plant designers effectively. The primary responsibility for doing this must rest with those who supply the measuring devices and control

systems. It has already been noted that this nation's I&C equipment manufacturers are a unique resource capable of responding to the endless challenges presented by our ever changing process industries.

This does not imply that there is no potential contribution to be made by government. Clearly there are some undertakings which are appropriate for government support. It is in the best interest of this Nation that our instrumentation industry be kept as strong and effective as is possible. It is appropriate that government observe its traditional role of undertaking those high risks, long time efforts which contribute to but do not compete with the private sector. This is being accomplished by supporting research at our universities, national laboratories, and energy technology centers. A vital part of this program is technology transfer which includes the continued cultivation of the government/industry dialogue. Both industry and government can take justifiable pride in the steps already taken in the development of a working partnership. Congress is taking a leading role in removing traditional barriers. We will all benefit from supporting this partnership to the best of our abilities. Many of us have sensed this developing partnership at meetings such as this, our workshops and our informal gatherings.

Our deliberations during this symposium can and hopefully will continue to be an important contribution to this emerging industry to you individually and to our respective company interests. I am rapidly learning what HRI is and can do. I would be pleased to discuss these issues and how we might get together; the only question is the classic "your place or mine?"

A SLURRY TEST LOOP FOR FLOWMETER EVALUATION AND CALIBRATION

K. G. Porges, S. A. Cox, C. J. Kampschoer, C. E. Cohn, E. F. Groh,
E. F. Lewandowski, R. W. Doering
Argonne National Laboratory
Argonne, Illinois 60439

D. S. Hacker
University of Illinois, Circle Campus
Chicago, Illinois 60680

Almost all flowmeters -- of conventional or novel type -- require calibration, i.e., a comparison of instrument readout(s) to standard devices or systems deployed on the same stream. This service is readily provided for homogeneous flow: some details, to be sure, regarding calibration equipment and procedures continue to receive much attention, but questions of a fundamental nature have long been settled.

Calibration schemes developed for strictly homogeneous fluids can be reasonably extended also to quasi-homogeneous emulsions and suspensions. Even when such media are non-Newtonian and their motion thus cannot be classified according to a Reynolds' Number, it can be quantitatively described by medium-average parameters (velocity, density and component fraction). As a practical consequence, mass flowrate, volumetric flowrate, and mean medium velocity all are mutually proportional -- just as for homogeneous fluids except that the constants of proportionality vary with component fraction.

Now suspensions are, unarguably, slurries; however, there also exist slurries of a rather different type in which the solid and liquid phases are more loosely coupled. In general terms, slurry type depends on particle size and size distribution, particle surface smoothness and tendency to agglomerate, liquid-solid density difference and liquid viscosity -- to mention just the most obvious influences. In the absence of a comprehensive theoretical description, it can only be suggested that agglomeration, large particle size range, low-viscosity liquid phase and large density differences tend to promote radial as well as vertical concentration of the solid phase as well as solid drag or slip, i.e., a difference in phase average velocities, superposed on radial velocity distributions.

In such a slurry, exemplified by coal gasifier feedstock, mass and volumetric flowrates and mean medium velocity are no longer directly proportional to each other. Consequently, conventional flow measurement schemes, which rely on proportionality, do not work, in that their readout cannot be calibrated. What is needed in this situation is a combination of two or more concurrent measurements of different variables, and that kind of combination instrument in turn requires a test system of rather special design for complete calibration. To make the argument somewhat more quantitative, some straightforward relations between mass and volumetric flowrates Q and F, solid and liquid mean phase velocities v_s and v_ℓ, intrinsic densities ρ_s and ρ_ℓ, volume fractions f_s and f_ℓ, and duct cross sectional area S can be readily established:

The mass flowrate

$$Q = S[v_s f_s \rho_s + v_\ell f_\ell \rho_\ell] \tag{1}$$

and volumetric flowrate

$$F = S[v_s f_s + v_\ell f_\ell] \tag{2}$$

yield the density of a sample withdrawn from the flowing medium by diversion,

$$\rho_m^* = Q/F \tag{3}$$

which differs from the mean density within the duct

$$\rho_m = f_s \rho_s + f_\ell \rho_\ell \tag{4}$$

by

$$(\rho_m - \rho_m^*)/\rho_m^* = f_s f_\ell (v_\ell - v_s)\ (\rho_s - \rho_\ell)(S/Q) - [1-(f_s + f_\ell)]\ ; \tag{5}$$

the second term of that expression vanishes for $f_s + f_\ell = 1$, i.e., the ideal case of phases completely filling the duct, while the first term vanishes for the case, discussed earlier, of quasi-homogeneous slurries. We note now further that

$$f_s v_s = (Q - \rho_\ell F)/(\rho_s - \rho_\ell) \tag{6}$$

hence, the solid feedrate

$$Q_s = S\rho_s (f_s v_s) \tag{7}$$

can be determined through online measurements of the mass and volumetric flowrates, e.g. by timed diversion into a volume-calibrated tank and subsequent weighing; Equation (5) is not affected by the presence of a third phase (gas) in the duct.

However, for calibration purposes one would wish to measure the flow parameters v_s, v_ℓ, f_s, f_ℓ independently, and this evidently calls for some additional measurement device(s).

In principle, one can determine the solid volume fraction f_s from a gamma transmission "densitometer":

$$\ln(I_\ell / I_m) = K f_s, \tag{8}$$

where I_ℓ = radiation intensity observed when the duct is filled with pure liquid and I_m = intensity transmitted through the slurry; it is further assumed that $f_s + f_\ell = 1$. In practice, this measurement turns out to be marginal: the constant K involves the C/H ratio and intrinsic density difference between liquid and solid components; when these are very similar (as for a coal slurry in a coal-derived hydrocarbon liquid), K becomes extremely small and very long measurements, with highly stable equipment, are required to make a determination at barely acceptable statistical precision. Liquid-solid contrast is somewhat better for X-rays and low-energy gamma radiation, which, however, cannot penetrate through heavy casing and thus can be applied only to ducts allowing the insertion of a thin radiation window (hence, to slurry lines running at low pressure). Other means of determining medium average density ρ_m or solid volume fraction f_s also have certain drawbacks; for example, the dielectric constant of the medium can be readily determined in an insulated duct section on which capacitor plates have been applied, but that measurement is highly sensitive to the presence of water or other polar molecules and also varies strongly with temperature (and somewhat less with solid distribution through the duct).

Now, rather than a direct measurement of f_s, a direct measurement of v_s, Q and F can yield both parameters, according to Eq (6). As it happens, such a measurement can be done with high accuracy by PNA tagging[3], provided that a specific tag be accepted by the solid, but not the liquid, component. The ash fraction of coal offers such a tag, N^{16}, with suitable halflife and emission spectrum. With that measurement, as well as the timed dump, all flow parameters are determined for the case of a slurry completely filling the duct; in the presence of a third phase, an X-ray transmission scheme can be deployed in addition.

These various considerations guided the design of the Slurry Loop Test Facility (SLTF) at our Laboratory, a 2" Sch 40 pipe loop specifically intended for coal slurry flowmeter testing and calibration. Mass and volumetric flow measurements are provided through sample diversion with precision timing and load cell-supported, volume calibrated dump tanks. The main dump tank drains back into the system through a check valve; the diverter, shown in Fig. 1, obtains 2-millisecond timing precision through optical sensors attached to the air-driven piston diversion mechanism. The articulated snout in the picture was mounted outside its container, for illustrative purposes. Outflow from the diverter normally passes into a large holdup tank, whose purpose is both to provide a reservoir for the pump and to allow induced activities in the medium to decay before reentering the loop. For the former purpose, which is essentially a matter of keeping the pump inlet pressure constant during the diversion and thus prevent diversion from lowering the pumping speed, the holdup is divided amongst two tanks of about 85 gal. capacity each, interconnected by a Gooseneck which effectively decouples the upper and lower holdup tanks.

The pump, driven by compressed air and thus explosionproof, is a 2-chamber diaphragm type producing a strong pulsed-flow component. The pump outlet is connected to a selective Depulsing manifold featuring a standpipe, commercial bladder snubber and large surge tank; these various components are readily

identified in Fig. 2. This part of the system was designed to simulate conditions often obtaining at slurry feedline measurements sites, where positive-displacement pumps are used to bring the medium up to the reactor pressure (2-3-kpsi). Flowmeter error resulting from pulsed flow is still a matter of dispute[1-2] while there seems to be agreement on the possibility that such errors could be quite large; it is thus clear that flowmeter calibration for a slurry feedline must include a determination of pulsing effect. As for the design of the Depulsing manifold, hydrodynamics fails here: such equations as can be written down defy integration. A customary analogy with electrical filtering, in which surge tanks are represented by capacitors and elements causing a pressure drop by resistances, is depicted in Fig. 3. Fig. 4 shows the readout from a downstream strain gauge pressure sensor at various pulsing levels, for illustration.

The loop itself, attached to the Depulser outflow, consists of a 6-meter straight run, turnaround and 10-meter straight run, whence a short vertical leg returns to the Diverter. Test equipment can be installed at the downstream end of each straight run; the 10-meter section also is the permanent site of the PNA velocity meter, described previously[3]. Figure 5 shows the various components of the system, in diagrammatic form.

The PNA installation calls for heavy gamma and neutron shielding for both instruments and personnel. Personnel protection is provided in the STLF by a 6' shielding-concrete vault enclosing the entire facility; detector shielding has been subject to considerable redesign and gradual improvement. Electronics also is being revised and improved. At present, data acquisition with a Multi-scaler controlled by a sequencer is followed by storage on magnetic tape and subsequent computer processing; direct acquisition by computer and immediate data processing is in preparation. The software program for that scheme can be readily incorporated in an online microcomputer/processor, allowing the entire system to be deployed as a temporary installation for purposes of calibrating installed flowmetering equipment, in the field.[3-4]

In closing, we would like to add some remarks regarding the kind of results the STLF can achieve. With the 3-fold (or 4-fold) parameter measurement scheme described, slurry flow parameters can be measured with an error margin of less than 1%, and flowmeters of various design can thus be thoroughly tested and calibrated. However, the system is limited to low pressures and temperatures, as well as biologically benign liquids, which prohibits an entirely realistic simulation of typical coal gasifier feedline conditions. A high-pressure test loop would have to provide the following features:

(a) Fully automated Diverter and Dump Tank, enclosed in a pressure vessel
(b) Thermally insulated and heatable holdup pressure vessels
(c) A suitable compressor and charging line
(d) Circulating pump
(e) Automated Pulsed-Flow system, incl. Surge tank
(f) High-bay shed, with adequate ventilation and crane.

In addition, special provisions are needed for the installation of ancillary sensing equipment (pressure, level etc.). The cost of such an installation would thus be considerable, even when advantage can be taken of the availability of certain components and/or a suitable building. However, there seems to be no fundamental limitation of a technical nature to the construction of this facility, whose cost would be amortized through savings in design and operating schedules of coal gasifier plants.

A discussion of preliminary slurry flow measurements, announced in the Abstract of this paper, would lengthen it beyond reasonable bounds and is therefore planned for future publication. Some samples of PNA runs are presented in Figs. 6-8, just to illustrate the rather different "signatures" one obtains for different media.

REFERENCES

1. D. R. Keyser, "Unsteady Orifice Flow Measurement, Its Theory and Observation," Proc. 2nd. Int'l. Symp. on Flow Meas. & Control, W. Durgin, ed., ISA (1981)

2. R. C. Mottram, "Measuring Pulsating Flow with a Differential Pressure Meter," ibid.

3. K. Porges, S. Cox, R. Doering, C. Kampschoer, and C. Herzenberg, "Calibration of Flow and Feedrate Meters in Situ by Means of Pulsed Neutron Activation," Proc. 1980 Symp. on Instr. & Control for Fossil Fuel Processes, ANL-80-62, Argonne National Laboratory (1980).

4. P. Kehler, "Two-Phase Flow Measurement by Pulsed Neutron Activation Techniques," ANL-NUREG-CT 78-17, Argonne National Laboratory (1978).

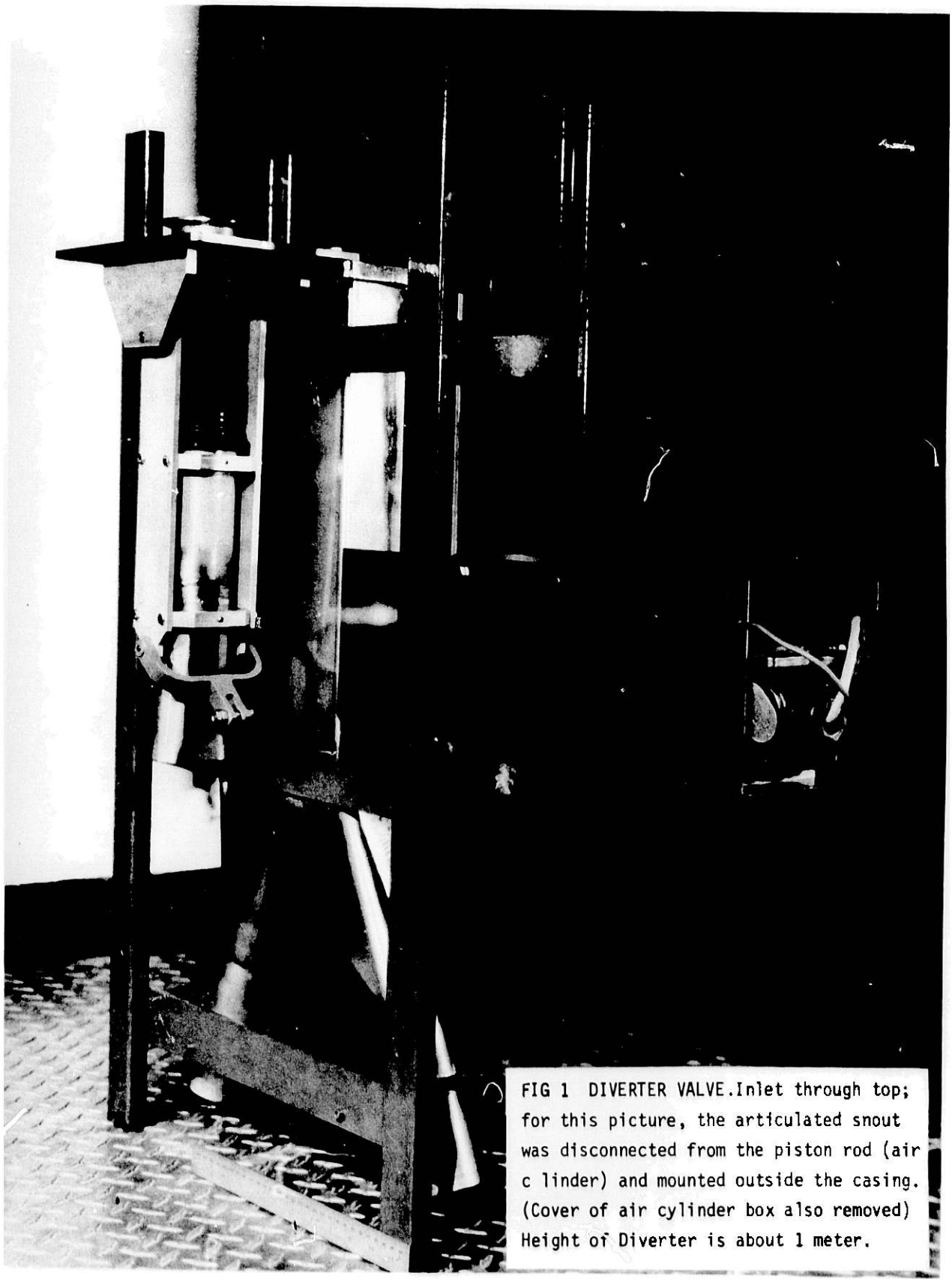

FIG 1 DIVERTER VALVE. Inlet through top; for this picture, the articulated snout was disconnected from the piston rod (air c linder) and mounted outside the casing. (Cover of air cylinder box also removed) Height of Diverter is about 1 meter.

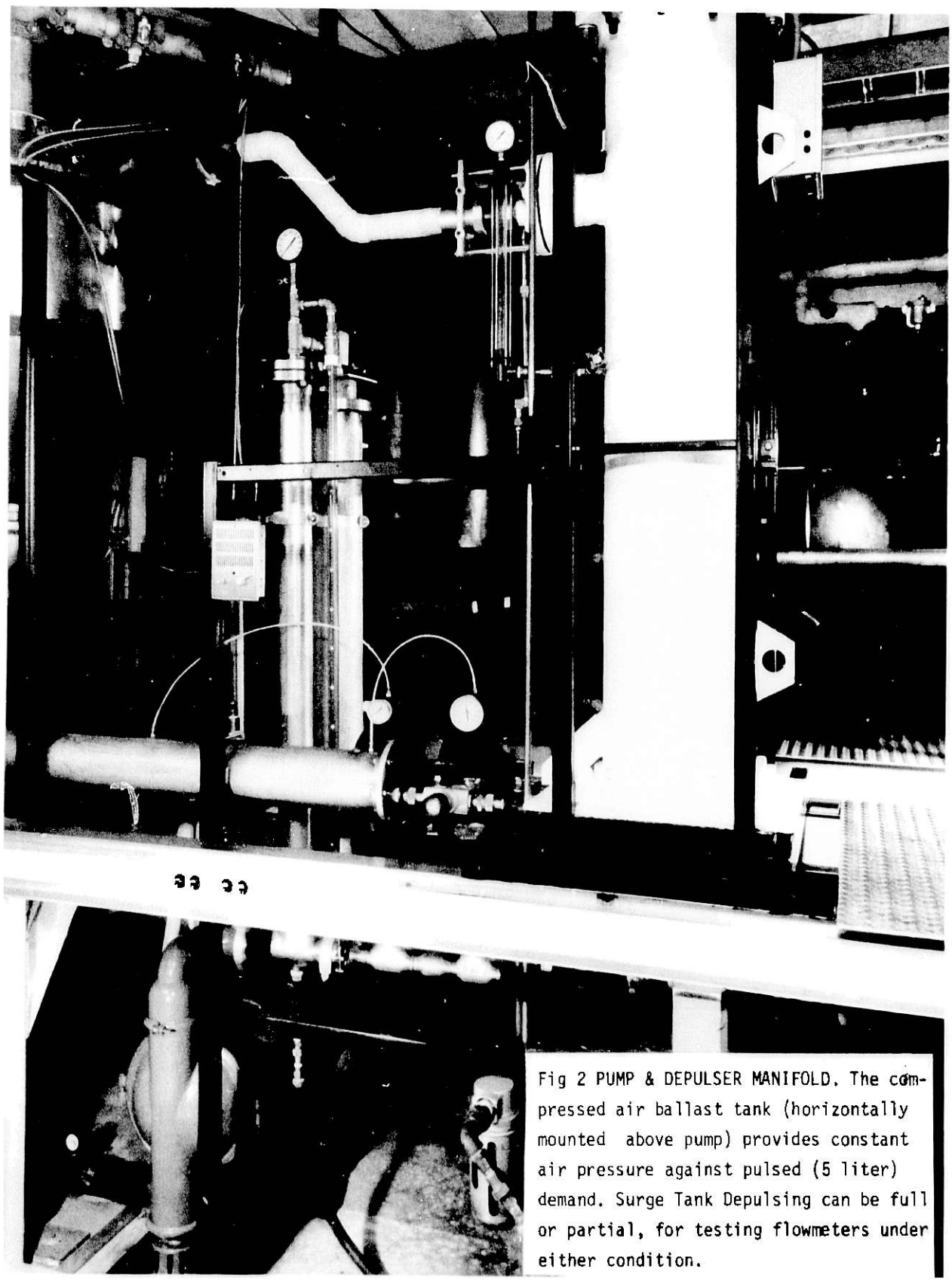

Fig 2 PUMP & DEPULSER MANIFOLD. The compressed air ballast tank (horizontally mounted above pump) provides constant air pressure against pulsed (5 liter) demand. Surge Tank Depulsing can be full or partial, for testing flowmeters under either condition.

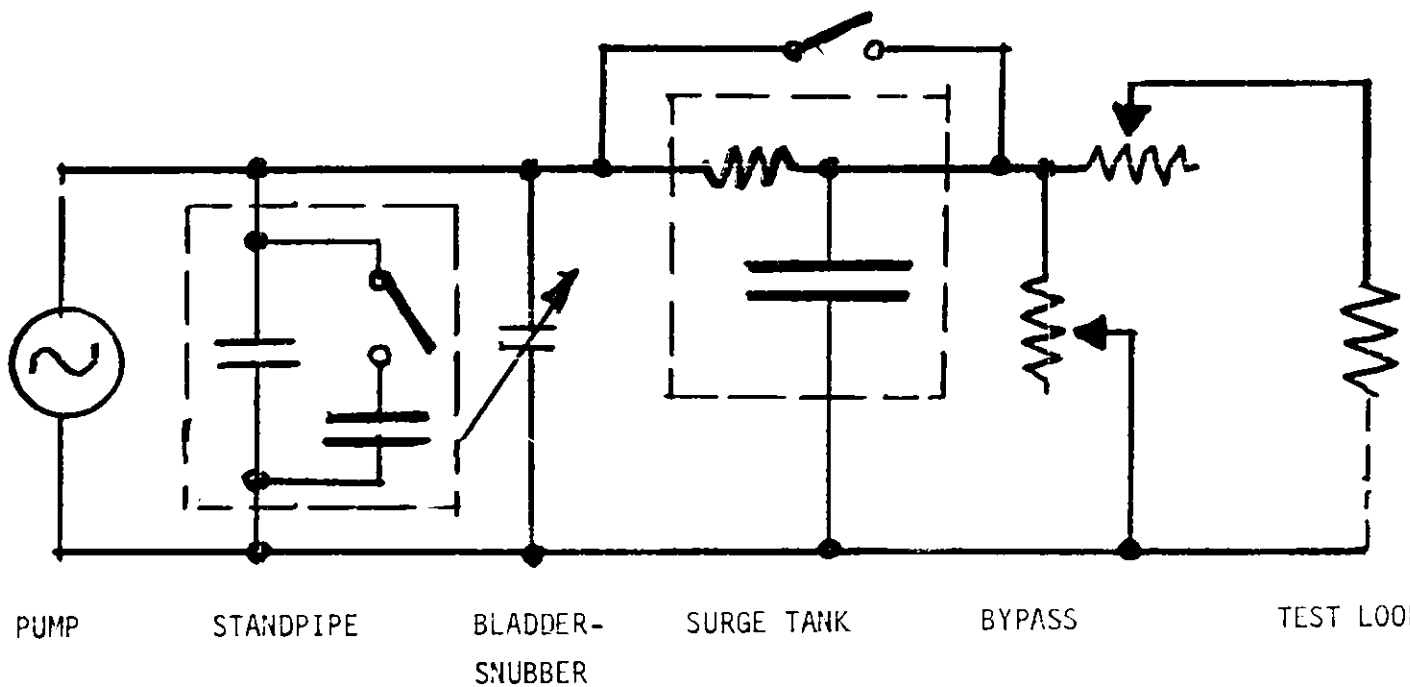

Fig 3 ELECTRIC CIRCUIT ANALOGON OF SELECTIVELY DEPULSED LOOP

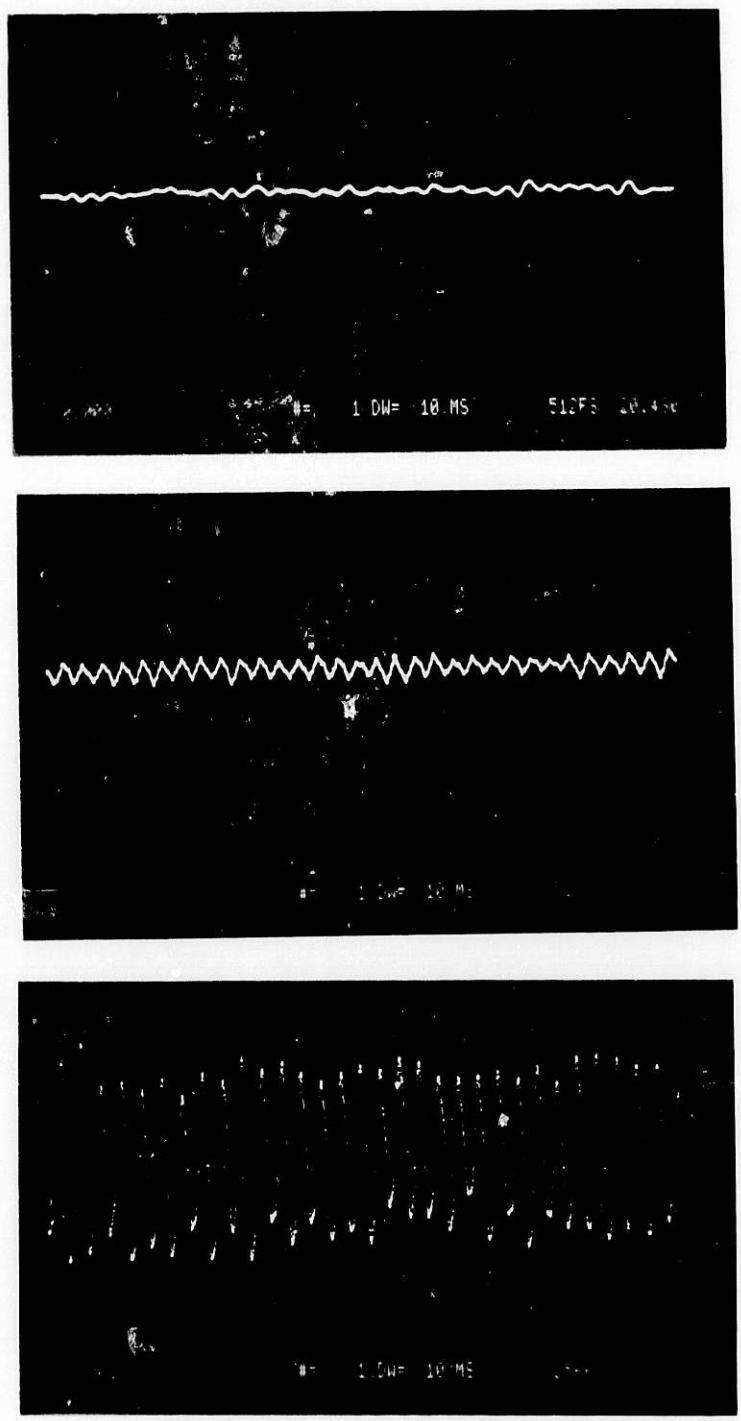

Fig 4 PRESSURE GAUGE READOUT AT DIFFERENT DE ULSING LEVELS

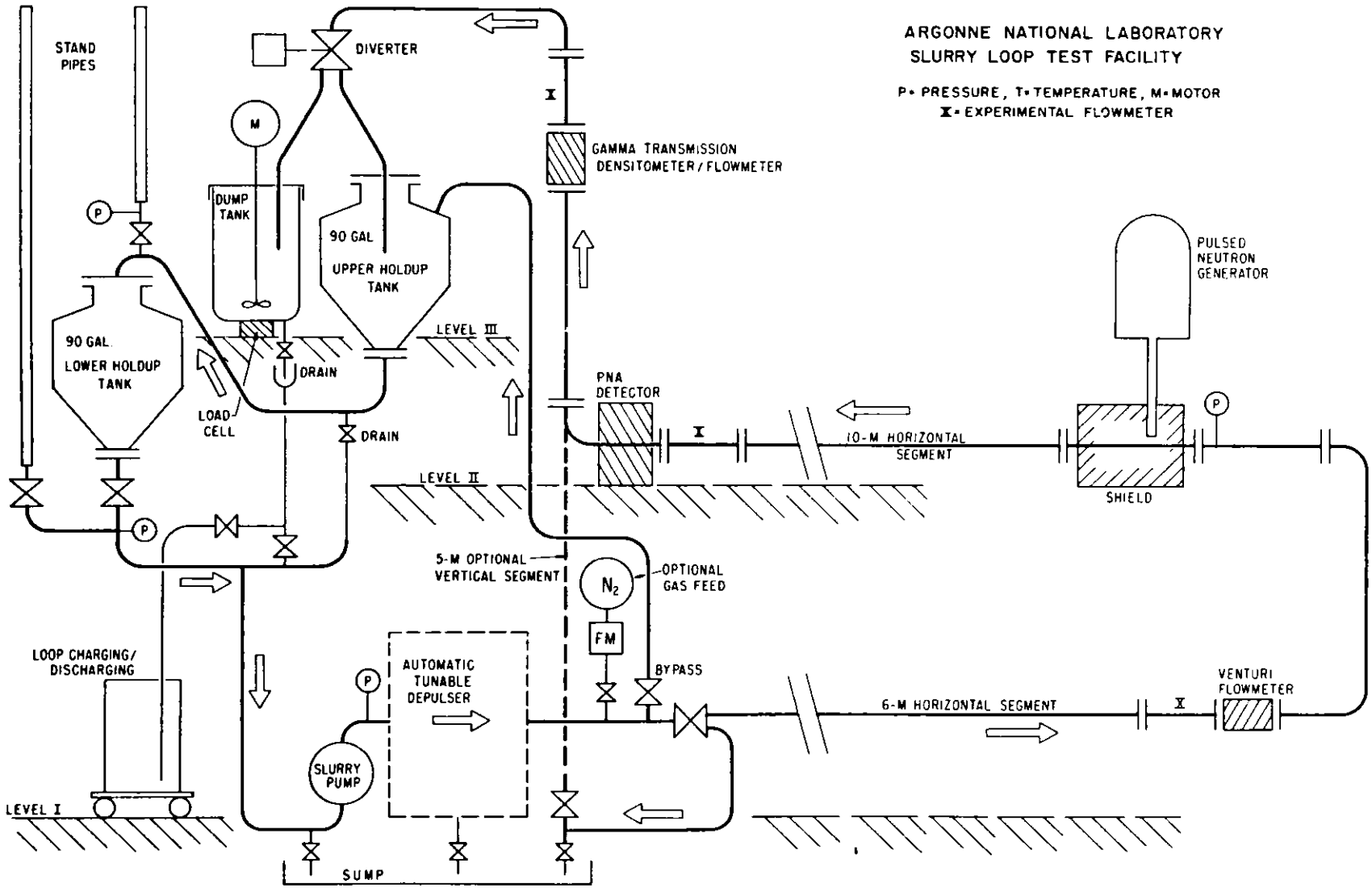

Fig 5 STLF SCHEMATIC, 3/81.

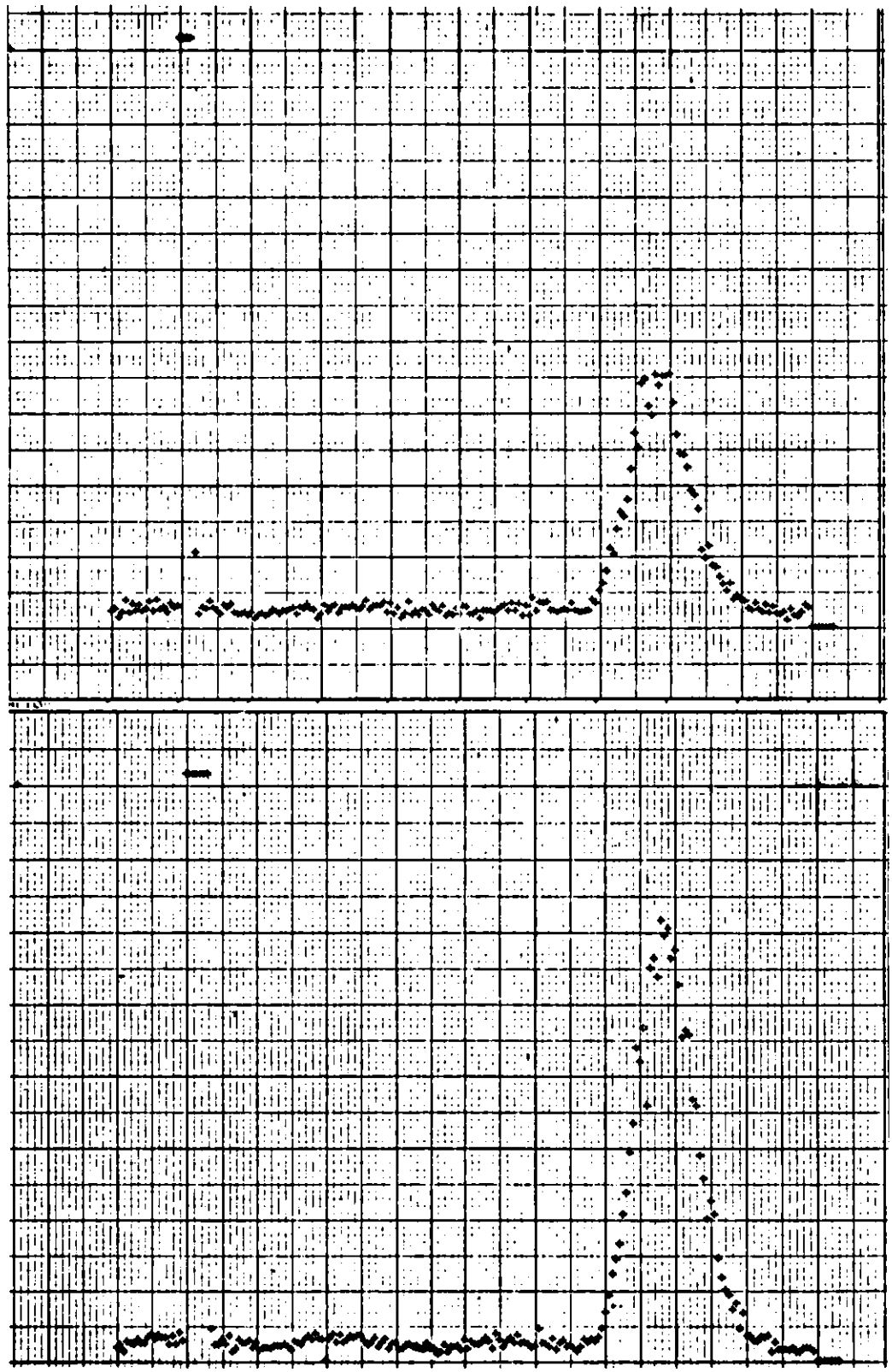

Fig. 6. PNA DATA RUN, SAMPLE. Medium: H_2O; ordinate = count rate, abscissa = time. Gamma "flash" accompanying neutron burst causes flat-topped peak just beyond start of acquisition, the other peak results from transit of activity through the gamma detector. TOP: low flowrate; BOTTOM: fast flow (at shorter time scale). Note peaks are almost symmetric, indicating large Reynolds' numbers (quasi-slug flow).

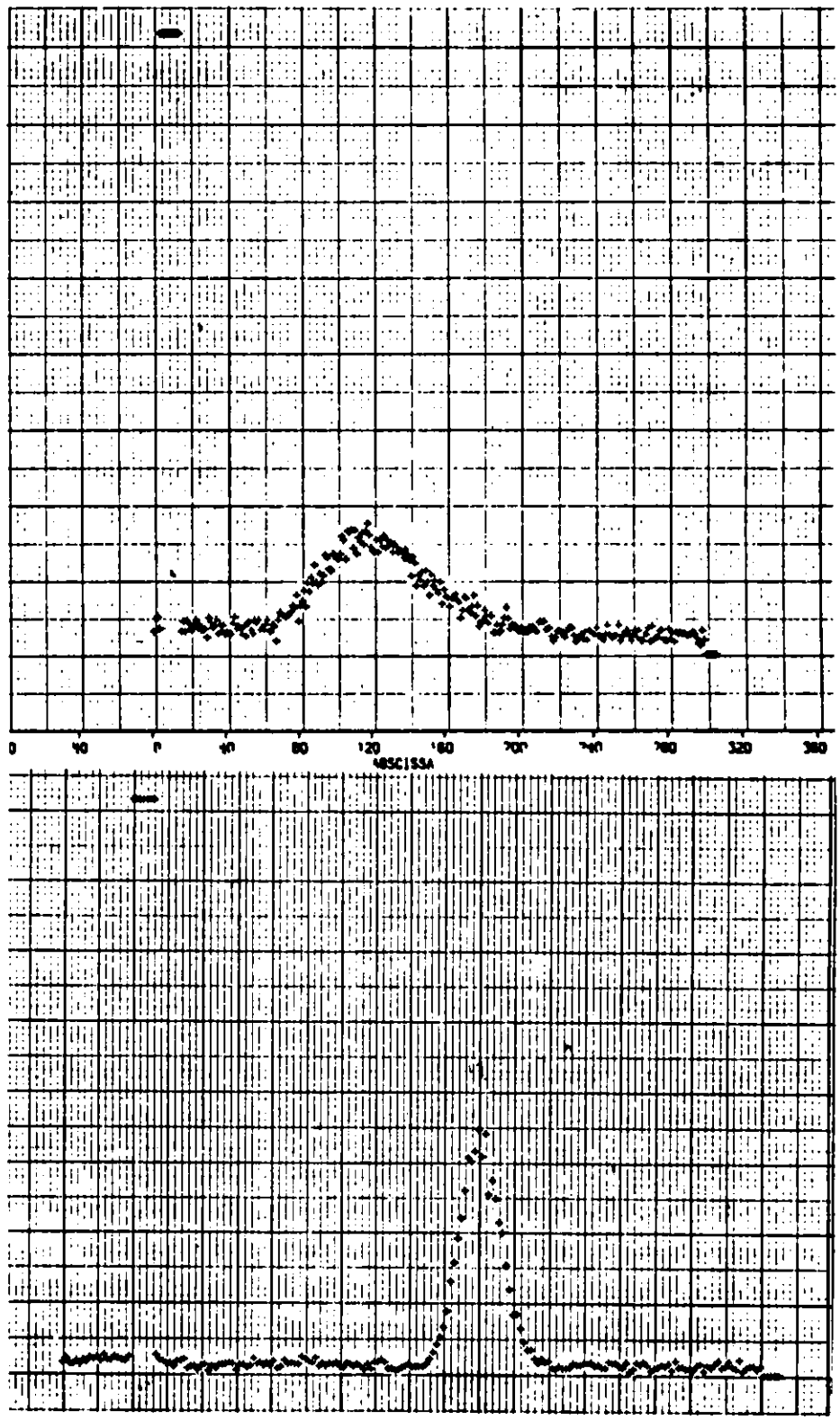

Fig. 7. PNA DATA RUN SAMPLE II. Bottom: dilute slurry (60 cp viscosity); fast flow. Shape of peak indicates large Reynolds' number. Top: heavier slurry (150 cp viscosity), slow flow, compressed time scale. Shape of peak is characteristic of Reynolds' numbers below 2000, strongly asymmetric.

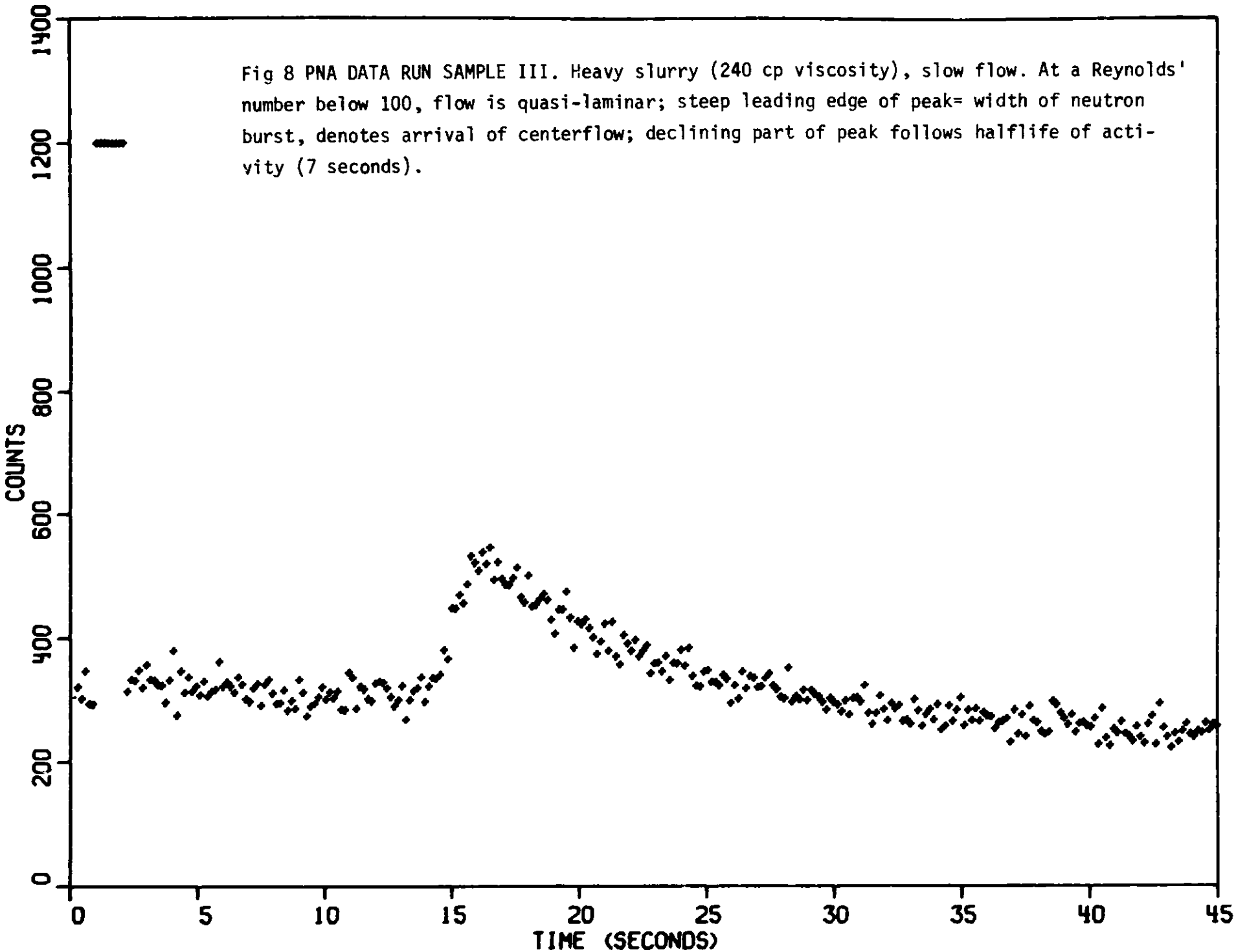

Fig 8 PNA DATA RUN SAMPLE III. Heavy slurry (240 cp viscosity), slow flow. At a Reynolds' number below 100, flow is quasi-laminar; steep leading edge of peak= width of neutron burst, denotes arrival of centerflow; declining part of peak follows halflife of activity (7 seconds).

SOLIDS CONCENTRATION MEASUREMENT AND FLOW MEASUREMENT OF SLURRIES AND SLUDGES USING ULTRASONIC SENSORS WITH RANDOM DATA ANALYSIS

W Balachandran, Research Fellow, Department of Electronics, University of Southampton, and M S Beck, Professor of Instrumentation, University of Manchester Institute of Science and Technology, Manchester, England

ABSTRACT

A range of instruments based on random data analysis has been developed for measuring solids concentration and fluid flow in gas/solid and liquid/solid systems; they are of particular value in fossil fuel processes because they offer no obstruction to flow and the sensors require virtually no maintenance. This paper will concentrate on the application of ultrasonic sensors to liquid/solid systems.

For solids concentration measurement, an ultrasonic beam is projected across the pipe diameter and interacts with the flowing sample. The inhomogeneities present in the sample scatter the ultrasound, resulting in amplitude modulation of the transmitted beam. The average modulation index of the received ultrasound signal is shown to be a function of suspended solids concentration, flow velocity and mean particle size. In a constant velocity system, if the mean particle size remains sensibly constant, then the received signal will be proportional to suspended solids concentration. This instrument could also be used for on-line monitoring of suspended solids concentration in a variable velocity system by compensating for the velocity changes using the cross correlation technique described below.

The flow velocity is measured by cross correlating the output signals from two axially spaced ultrasonic sensors, similar to those used for solids concentration measurement. In tests using sand/water slurries, a meter factor of 0.84 ± 0.02 was observed to calibrate the measured cross correlation velocity against actual mean flow velocity for flow of Renolds Number from 3×10^3 up to 75×10^3. The flowmeter performance was not affected by changes in particle size and concentration.

1. INTRODUCTION

Flow measurement is essential for the efficient operation of any process and for example the high efficiency and low labour requirements of modern petrochemical plants is based on the ready availability of a wide range of instruments, including flowmeters. Processes using solid fossil fuels as raw materials will be no less dependent on adequate instrumentation and this paper describes ultrasonic instrumentation which does not obstruct the flow and should require very little maintenance for solids concentration and velocity of two-phase slurries and sludges.

For reliable measurement of slurry flow it is essential to use a flowmeter which offers no obstruction. The electromagnetic flowmeter can be used with slurries, but it suffers from the disadvantages of having a lining which can wear out, being expensive particularly for large line sizes, and it has to be removed from the pipeline for calibration. The cross correlation flowmeter which will be described uses a normal pipe without any lining, the cost does not increase significantly with line size increase, and the calibration is based on the absolute measurement of pipe diameter, sensor spacing and a time delay measured by a cross correlator with a crystal clock as a reference standard.

The same primary sensor which is used for cross correlation flow measurement can also be used to indicate the concentration of the solids in the pipe. For this application the instrument requires calibration against an independent standard, but has the advantage of being very cheap and is inherently free from zero drift, so it can be used to measure the small concentrations of solid materials.

The instruments described in this paper have been evaluated using slurries ranging from sand/water mixtures to sewage works sludges. It is thought that these extremes encompass a reasonably wide spectrum of the rheological properties likely to be encountered in fossil fuel processing plants.

2. ULTRASONIC SENSOR DESIGN

The arrangements for measuring suspended solids concentration and flow velocity are illustrated in Figures 1 and 2 respectively. It will be seen that identical transmitter receiver systems are used for both these measurements and therefore the instrumentation of either channel A or channel B of the cross correlation flowmeter can be used as the major part of the solids concentration measurement system illustrated in Figure 1.

When acoustic signals are transmitted through a solid/liquid suspension the pressure amplitude of the received signal fluctuates in a random manner about its mean value. The main cause of these fluctuations is due to scattering of ultrasound by the discontinuities present in the propagating medium. In this system longitudinal ultrasonic waves are propagated across the conduit. The beam can be either parallel or divergent; with a divergent beam, the weighting due to the velocity profile will not be uniform. Furthermore, a

receiver located in a divergent beam would only receive part of the transmitted acoustic energy resulting in a lower electrical output from the receiving sensor. Therefore to achieve regular weighting of the flow profile and to receive maximum energy, a narrow and parallel beam is desirable.

For a circular disc sensor, vibrating in its fundamental mode, the range of the Near-field (X) in the propagating medium is given by

$$X = \frac{D^2}{C} \cdot f$$

where D is the diameter of the sensor
C is the velocity of sound in the medium
f is the operating frequency.

From the above expression it is clear that for a fixed Near-field, at higher operating frequencies, a narrow and parallel beam can be obtained with small diameter (<10 mm) sensors. Attenuation of ultrasound in solid/liquid suspension is mainly due to the scattering effect of the suspended particles[1]; therefore the attenutation coefficient is directly proportional to the fourth power of the frequency, so high operating frequencies are undesirable for this application. At lower frequencies, the sensor diameter would be large and unsuitable for practical applications. Based on the above considerations a frequency of 1 MHz was chosen for the 28 mm diameter pipe used in this work.

2.1 CONSTRUCTION OF SENSOR

A piezoelectric ceramic crystal (PZT - 5A) of flat disc shape and diameter 10 mm operating in the thickness mode at a frequency of 1 MHz is used as the basic sensing element. For many practical applications, the sensor should be robust in all prevailing environmental conditions, and the sensing element be well protected so that the flowing sample does not come in contact with the element. This can be achieved by using a protective case for the sensing element. In this the crystal is coupled to the case in such a way that the composite assembly operates in the fundamental mode.
In practice, therefore, an internal diameter of 15 mm was chosen for the case, and when operated at 1 MHz with a 10 mm crystal, the sensor would transmit 37.5 mm of Near-field. Other critical parameter in the design of the case is the thickness and material of the front face (transmission plate).

For this application stainless steel of front face thickness $\frac{\lambda}{2}$ (= 2.90 mm) is chosen in order to achieve good acoustic matching between the crystal and the case, and to avoid corrosion which could be easily brought about by the flowing sample. The crystal selected for this work has silver coated electrodes on the flat faces. An electrical connection is made to the positive face by soldering a piece of wire, and the opposite face is bonded to the inside of the front face of the case, with a silver loaded epoxy, of minimal thickness to ensure electrical contact between the crystal and the case, taking care that the crystal face is bonded parallel to the front face. The open end of the sensor case is fitted with a lid, incorporating a BNC socket, which provides external electrical connection to the sensor.

2.2 BANDWIDTH OF SENSOR

The most important characteristics of an acoustic sensor are to achieve wide bandwidth and low transmission loss, which give good sensitivity. In practice it is difficult to accomplish both criteria simultaneously. In most applications a compromise is inevitable, so that the bandwidth can be increased without too much loss in sensitivity. The bandwidth of flow noise signal is normally less than 500 Hz, therefore it is required that the sensor bandwidth is higher than this value, so that there will be no significant attenuation of the higher spectral components. Although air backed sensors are widely used, because of the large impedance mismatch between the sensors and the load, the bandwidth is narrow. This may, however, be increased by the use of the backing material. For this work backing material having a characteristic impedance higher than that of the crystal is used to achieve good acoustic coupling and a sufficiently wide bandwidth.

3. MEASUREMENT SYSTEM

3.1 SOLIDS CONCENTRATION MEASUREMENT

The sensors described above were incorporated in an instrument which has been developed for on-line monitoring of suspended solids concentration and flow velocity of solid/liquid suspensions. A narrow and parallel ultrasonic beam is projected across the pipe diameter and by using a phase locked loop (see Figure 1), the acoustic path length between the transmitter

and the receiver is maintained constant. In this the phase of the transmitted signal is 90^{o} phase shifted and compared with the phase of the received signal using a phase comparator. The output from the phase comparator is fed back to the voltage controlled oscillator (VCO), which drives the transmitter. In a conventional phase locked loop, the loop goes into lock when the transmitted and the received signals are 90^{o} out of phase. The additional 90^{o} phase shift network incorporated extends the locking capability of the loop such that it goes into lock when the transmitted and received signals are 0^{o} or 180^{o} out of phase. If the phase of the received signal changes with respect to the transmitted signal, then the output voltage (error signal) will be in the appropriate direction to drive the VCO to correct for the error. Thus the feedback nature of the PLL causes the VCO to synchronise (or lock) with the incoming signal. Once in lock, the VCO frequency is identical to the input signal except for the finite phase difference. Hence, any phase variation due to slow changes in path length can be corrected.

The transmitted ultrasonic beam in the form of a carrier wave is scattered by the turbulent motion of the suspended solids in the medium. The random fluctuations of the scattered signal modulate the carrier wave in amplitude, phase and frequency. The amplitude modulated received signal is demodulated to recover the scattered signal. The analysis of the amplitude of the demodulated signal by either an averaging voltmeter or auto-correlation techniques, results in an output which is related to the suspended solids concentration as shown in Figure 1.

3.2 FLOW VELOCITY MEASUREMENT BY CROSS CORRELATION

A schematic diagram of the cross-correlation flowmeter is shown in Figure 2. In this the electrical output from the two ultrasonic beams, which are axially spaced (axial separation = L) along the direction of the flow are cross-correlated and resultant correlation peak indicates the time of travel τ (between the two beams) of the inhomogeneties present in the sample[1]. The flow velocity (Vc) is then derived from the transit time

$$\text{i.e. } V_m = L/\tau$$

4. MEASUREMENT RESULTS AND DISCUSSION

Experimental results shown in Figures 3, 4 and 5 suggest that the meter reading (averaging voltmeter) is a function of suspended solids concentration, mean particle size and mean flow velocity of the flowing sample. The instrument can be made to respond only to suspended solids concentration by installing it in a constant velocity system in which the mean particle size remains reasonably constant (see Figure 6). This can be achieved by fitting the instrument on a sample line where the test sample is drawn off the main pipe line or open channels using a suitable pump. For the instrument to operate, turbulent flow is essential, but with this sampling arrangement, the sample delivered to the test section is turbulent, therefore it can be used to monitor the suspended solids concentration even when the main pipe line flow is laminar. Since the sampling is continuous, and the response time of the instrument is thirty seconds, it is felt that the meter output would depict reasonably well the true suspended solids concentration of the solid/liquid suspension in the main pipe line. In the cases where the mean particle size is variable, compensation has to be done. There are no suitable on-line instruments available to monitor continuously any change in the particle size of the flowing solid/liquid suspension. For this reason sample have to be withdrawn at intervals and subject to off-line measurements, the calibration can then be corrected for the variation in particle size. The instrument could also be used in a variable velocity system by incorporating a velocity compensation function. For constant particle size this depends on the turbulence of the flowing sample. At a fixed concentration, it should be possible to calibrate the instrument against various velocities and determine the compensation function (see Figure 4). The flow velocity can be continuously monitored using cross-correlation techniques and then as shown in Figure 7 the meter reading can be compensated against velocity changes. Hence, this system could be used in turbulent full pipe flows for continuous monitoring of suspended solids concentration of solid/liquid suspensions.

Practical tests were carried out using the cross-correlation flowmeter and a typical calibration curve is shown in Figure 8. A meter factor of 0.84 ± 0.02 was established to relate the measured cross-correlation velocity against actual mean flow velocity, for Reynolds numbers in the range 3×10^3

to 75 x 10^3. A repeatability of ± 1% was obtained using an integration time of approximately five seconds.

The flowmeter accuracy is unaffected due to changes in suspended solids concentration (0.2 → 2.5 w/w), particle size (90 μm → 1000 μm) and gas bubbles (<5/1).

Previous researchers who worked on ultrasonic cross-correlation flowmeters using clip-on transducers reported that although cross-correlation peaks were obtainable, they tended to be unstable. Negative peaks as well as skewed peaks were observed from time to time. These problems have been entirely eliminated in the system described in this paper by using identical transducers of the flush mounting type and the closed loop control system. The absence of pipe walls eliminated the unknown phase changes which may occur within the walls, as such, both channels were found to behave almost identically to each other. With this arrangement, when both channels are locked, not only is the phase relationship satisfied but also the difference in operating frequencies is found to be less than 20 kHz (minimum change in frequency required to change the acoustic pathlength between transmitter and receiver). Under these conditions the phase difference between the two received signals is found to be almost 0^o, thus satisfying the required condition to maintain the sign integrity of the correlation peak. Once the system is initially locked with a positive cross-correlation peak, it is then unforeseeable that the environmental changes which may occur, could shift the difference in operating frequency more than 20 kHz[2]. Therefore the phase difference between the two received signals will always remain at or near 0^o. Hence the cross-correlation peak will remain positive.

An ideal cross-correlation flowmeter should have unity meter factor at all flow rates. However, for the flowmeter described in this paper, the meter factor is found to deviate from unity i.e. the measured cross-correlation flow velocity is faster than the mean flow velocity. The mean flow velocity is an equally weighted integral of all the velocity components in the flow profile. If the correlation flowmeter derives its signals in any way other than by an equally weighted contribution from every point on the profile, it cannot register the mean flow velocity. The ultrasonic correlation flowmeter sensing volume is a cylinder equal to the diameter of the transducer and height equal to the diameter of the pipe. We will now

show that the flowmeter transducers are not equally sensitive to all points within this sensing volume. In a fully developed turbulent flow, the frequency distribution of the turbulent components is characterised by the suspended solids present in the flowing sample. Different frequency components travel with the different convection velocities[3]. The lower frequency components (larger particles), by virtue of the fact that they are large, occupy the majority of the space within the sensing volume. They assume velocities comparable with those near the centre of the pipe. The higher frequency components (small particles) migrate to the laminar sub-layer where the fluid moves more slowly, and as such the lower frequency components are only moderately influenced by the small particles. The finite size of the transducers and their axial separation, produces an effect of a low-pass filter[4], the cut-off frequency being about 300 Hz. Therefore the flow noise signal is heavily weighted by the lower frequency components. Hence the cross-correlation flowmeter tends to read high.

The lower flow range limit of the ultrasonic cross-correlation flowmeter depends on the settling properties of the suspended solids. Only turbulent flows can keep the suspended solids in suspension. For a 28 mm diameter pipe, Figure 8, shows that the lower limit is 0.2 ms^{-1}. At lower velocities (< 0.2 ms^{-1}) there is insufficient turbulence to give correlatable signals. The instrument worked well and the normalised cross-correlation ($\simeq$ 0.3) was high up to the maximum available pumping velocity of 3 ms^{-1}. There is no reason to suppose that the instrument would not continue to work at higher velocities.

5. CONCLUSIONS

This paper has described instrumentation for solids concentration and flow velocity measurement of slurries which does not obstruct the flow and should require very little maintenance. The sensors and associated electronics use standard components in a simple and inexpensive configuration. Modern developments in microcomputers have led to the design of simple cross correlators which should become available at realistic market prices[4].

REFERENCES

1. Balachandran, W, and Beck, MS, 'Solids Concentration Measurement and Flow Measurement of Slurries and Sludges using Ultrasonic Sensors with Random Data Analysis, Part I and Part II'. Accepted for publication, Trans. of IMC 1981.

2. Balachandran, W, and Page, H R S, 'Closed-loop Control System for Ultrasonic Flow Measurement'. Submitted for publication, J.Phys.D.

3. Heidrick, T, Azad, R S, and Bamerjee, S, 'Phase Velocities and Angle of Inclination for Frequency Components in fully developed turbulent flow through pipes'. Proc. Symp. on Turbulence in Liquids, Missouri-Rolla Univ. pp 149-157 (1971).

4. Beck, M S, 'Correlation in instruments: cross correlation flowmeters'. J.Phys.E: Sci.Instrum., Vol. 14, pp 7-19, January 1981.

5. Taylor, G, 'The transport of vorticity and heat through fluids in turbulent motion'. Proc. Royal Society of London, Series 4, Vol. 135, p 658 (1935).

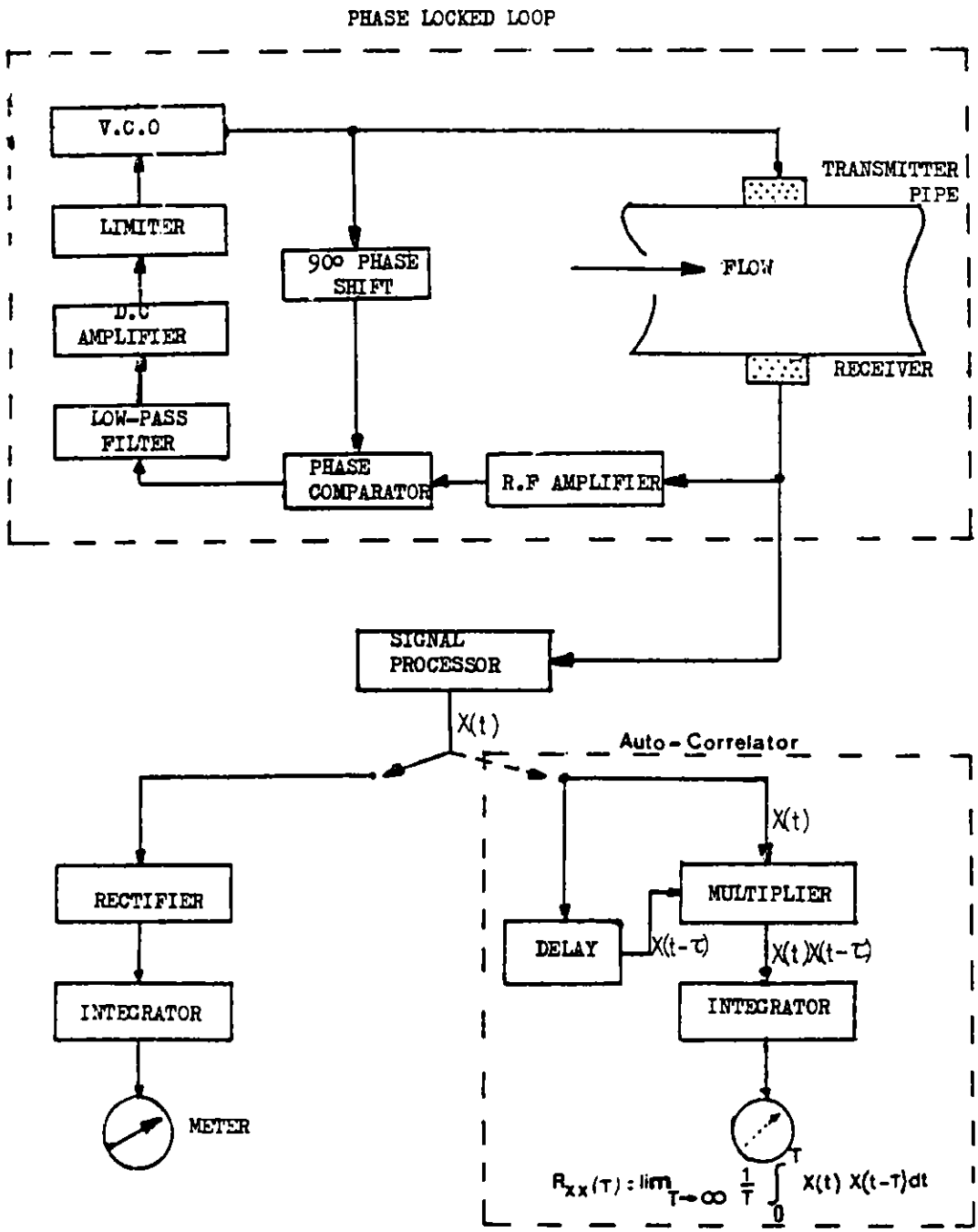

Fig 1 Experimental arrangement for suspended-solids-concentration measurement

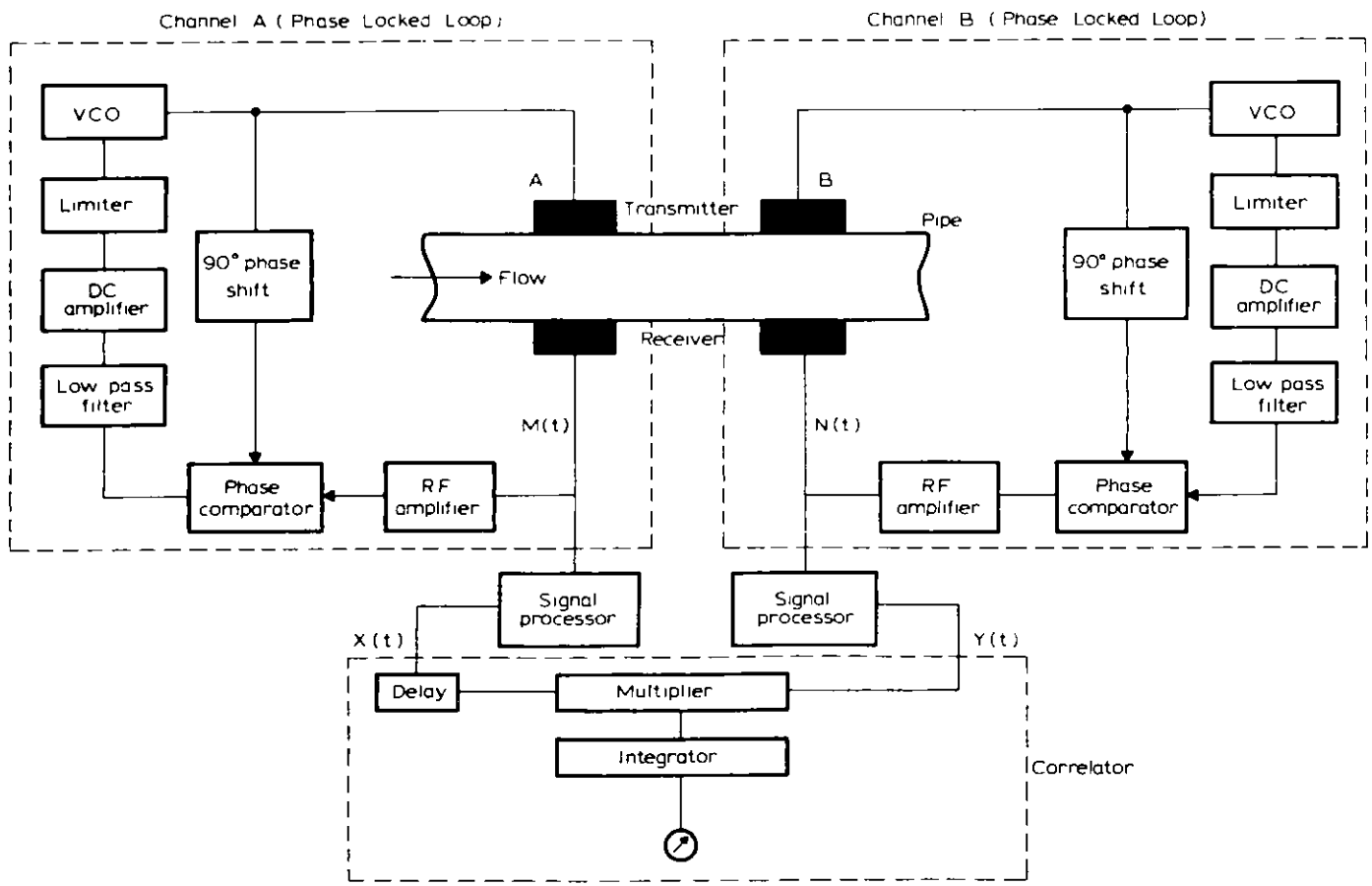

Fig 2 Block schematic of cross-correlation flowmeter

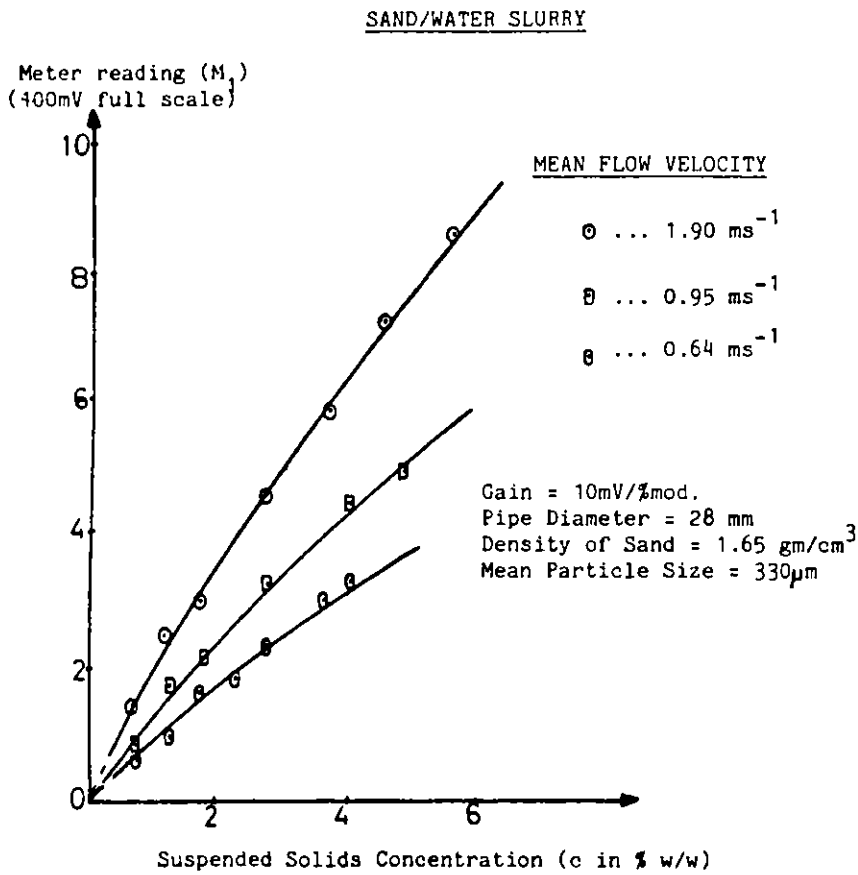

Fig 3 Sand/water slurry: solids-concentration measurement at various mean-flow velocities (linear scale)

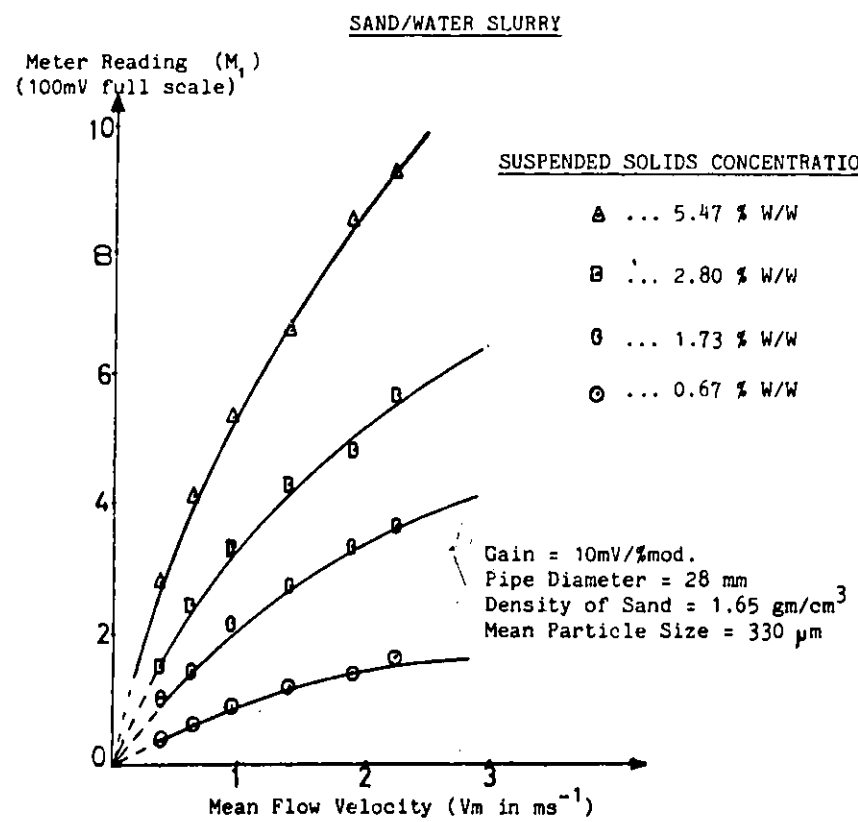

Fig 4 Sand/water slurry: solids-concentration-measurement calibration curves (linear scale)

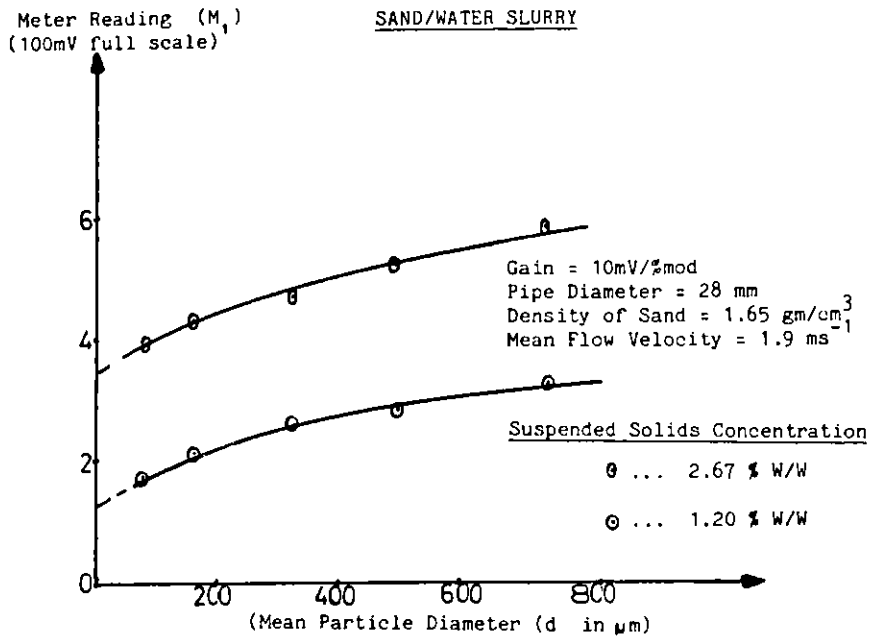

Fig 5 Sand/water slurry: Variation of meter reading with different particle sizes (linear scale)

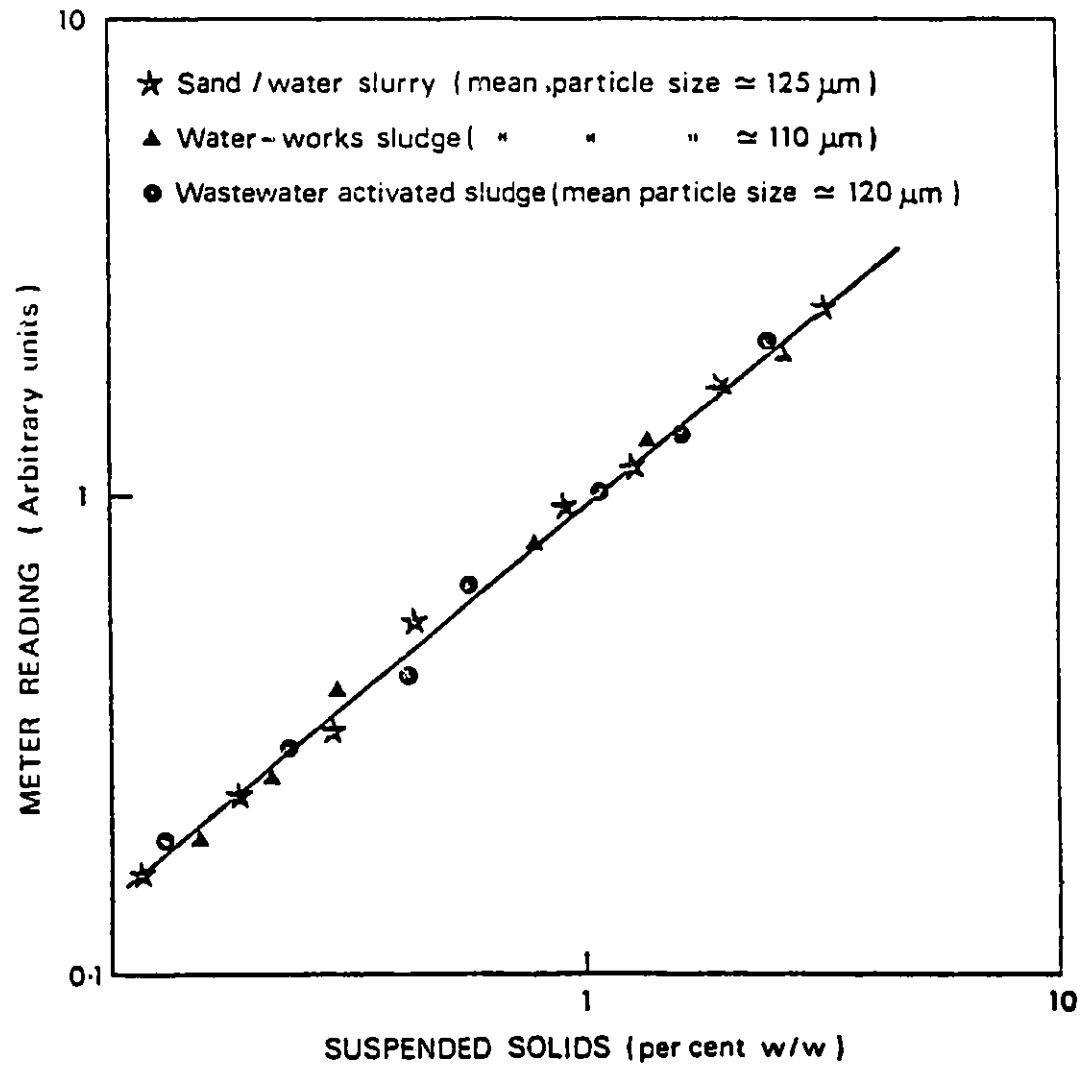

Fig. 6 Suspended-solids concentration meter calibration curve for mean flow velocity of 1 ms^{-1}

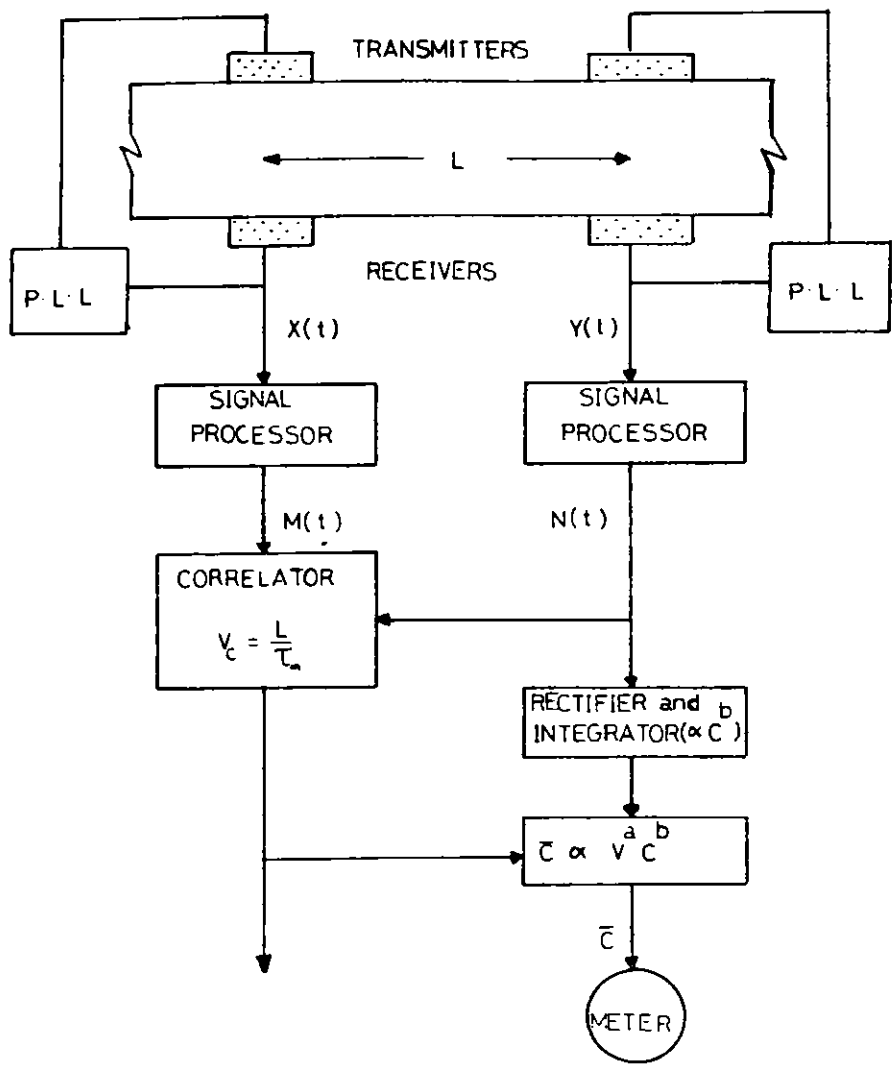

Fig 7 Measurement of suspended-solids concentration in a variable-velocity system

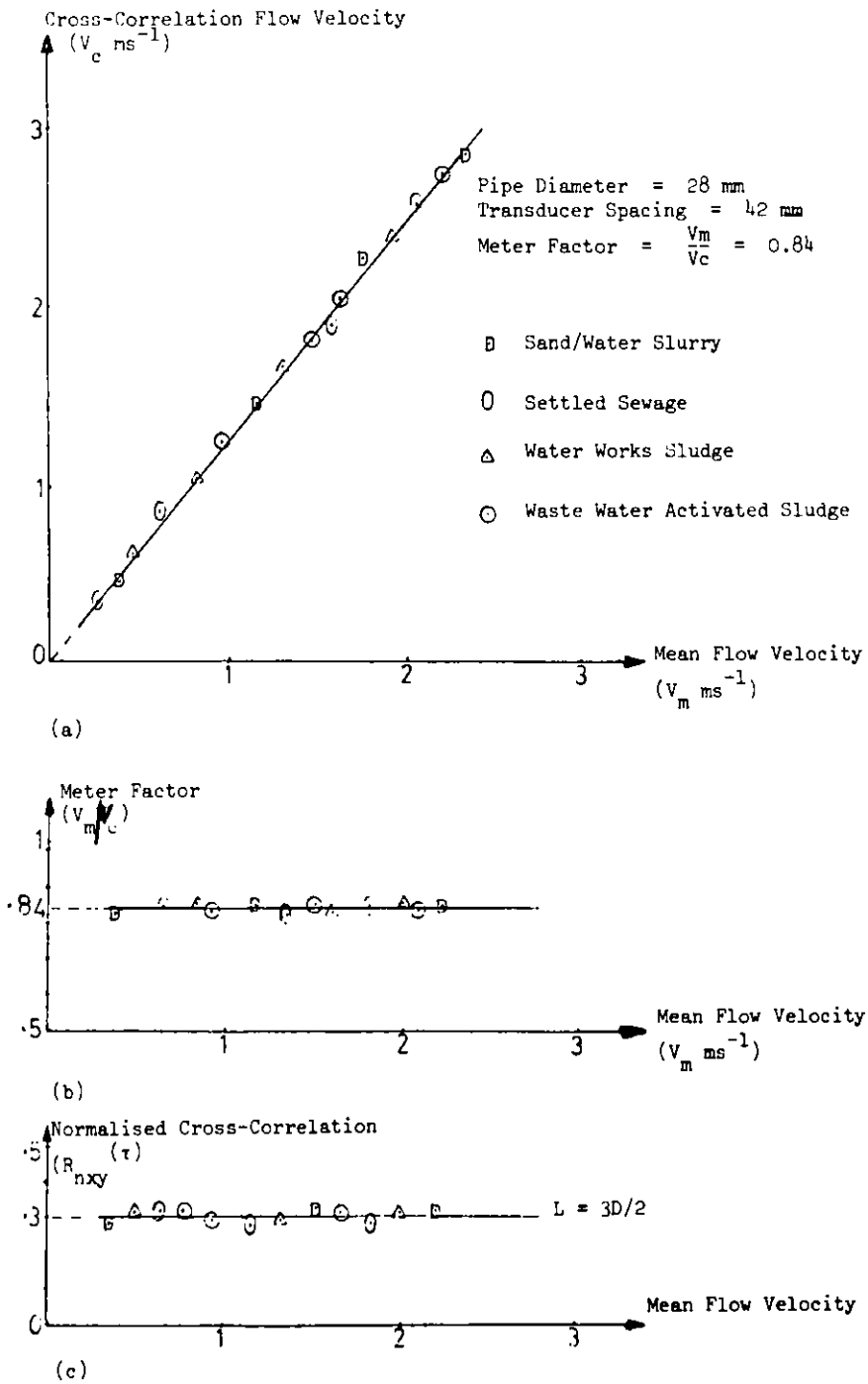

Fig 8 Ultrasonic cross-correlation flowmeter calibration: (a) Transport-velocity calibration curve; (b) Linearity error; (c) Normalised cross-correlation calibration curve

LIGNITE-WATER SLURRY FLOW MEASUREMENT USING A VENTURIMETER

R. Hasan, D.N. Baria, N.M. Chowdhury
University of North Dakota

ABSTRACT

This paper presents the results of an investigation into the use of venturimeter as a flow metering device for slurries. The flow rates of lignite-water slurries through a two inch black iron pipe containing known weight percent lignite have been measured by direct weighing. The concentration of lignite has been varied from 0 to 40 percent and the flow velocity has ranged from 2.4 ft/sec to 6.0 ft/sec. The pressure drop measured across three venturies with 0.75 inch, 1.0 inch, and 1.5 inch throat diameters have been correlated with these flow rates.

The single-phase venturi equation is found to hold true for slurry flow as well, so long as the density for the slurry is used. The discharge coefficient is found to be a weak function of the Reynolds Number; first increasing and then decreasing with Reynolds Number. The average value for the discharge coefficient for the slurry flow is about the same as that for single phase water flow. The discharge coefficient is also found to depend on slurry concentration. The venturi throat to pipe diameter ratio did not appear to affect the results.

INTRODUCTION

Transportation of solids - such as coal and other minerals - as slurries, may be economically advantageous over long distances. A summary of various slurry pipelines, presently in operation or in the planning stage, has been presented by Price (1980). For certain coals, water as a suspension agent eliminates the necessity of prior drying and facilitates the use of wet "run-off-mine" coal. The Texaco Coal Gasification Process is primarily based on coal-water feed-stocks. As a result, the use of a gasifier system at the end of a coal slurry pipeline has some clear advantages (Child, 1979). The use of coal-water slurry feedstock in gasifiers offers a number of advantages over dry dust feed or use of lock hoppers. Slurry flow metering is therefore important.

LITERATURE SURVEY

Various devices have been developed for measuring slurry flow rates. Thus, flow meters have been devised which measure the slurry velocity from the magnitude of the EMF produced when a magnetic field is placed diametrically across the slurry flow path (Kao and Mathias, 1978). For intermittent flow velocity measurement, tracer technique was found to be quite accurate by Shurin and Yopfin (1960). Use of ultrasonic sound wave has also been found to be a satisfactory technique for slurry velocity measurement (Sheen and Raptis, 1979; Karoplus and Raptis, 1978; McShane, 1974). Kao and Kazanskij (1979) and Liptak and Leiter (1979) present an excellent survey of the various methods used for slurry flow metering.

The use of a venturimeter for slurry flow rate measurement, however, would be simpler and cheaper than the other devices mentioned above. If the slurry is assumed to behave like a homogeneous fluid, the single-phase venturi

equation (for horizontal flow)

$$V = C \left[\frac{1}{1 - (D_t/D_p)^4}\right]^{1/2} \quad [2g_c \, \Delta p/\rho]^{1/2} \tag{1}$$

may be used for flow measurement. In place of the liquid density ρ, however, the density for the slurry should be used. Thus

$$\begin{aligned} V_m &= C \left(\frac{1}{1-\beta^4}\right)^{1/2} \quad [2 \, g_c \, \Delta p/\rho_m]^{1/2} \\ &= C \, (1/1-\beta^4)^{1/2} \quad [2g \, \Delta h_m]^{1/2} \end{aligned} \tag{2}$$

Venturimeters have been used for flow rate measurement of mixtures of air and pulverized coal (Carlson et al., 1948), air and fine solids (Barth, 1957), and air and glass beads (Payne and Crow, 1979). Brook (1962) has obtained excelled agreement between theoretical predictions (equations 2) and experimental results for the flow of bakelite-water mixtures and basalt-water mixtures. Brook found the values of C (in equation 2) for the mixture to be about the same as that for single-phase water flow ($0.95 \leq C \leq 0.97$). Similar results were obtained by Dementyew (1954) with sand-water and coal-water slurry.

The present study was undertaken to investigate the suitability of a venturimeter as a flow metering device for lignite-water slurry over a wide range of concentration and velocity.

EXPERIMENTAL SET-UP

To investigate the flow characteristic of lignite-water slurry, a closed loop was designed and fabricated. Figure 1 schematically shows the system. The slurry from the mixing tank is pumped through the horizontal test section made of two inch sch. 40 black iron. The slurry is then returned to the mixing tank through a return leg. One venturi is placed just before the test section. The other two venturies are placed on the return leg. All the venturies are sufficiently away from any fittings to avoid any end effect. The return leg is also fitted with a transparent section for flow visualization. A three-way valve diverts the flow to a weighing tank for direct flow measurement.

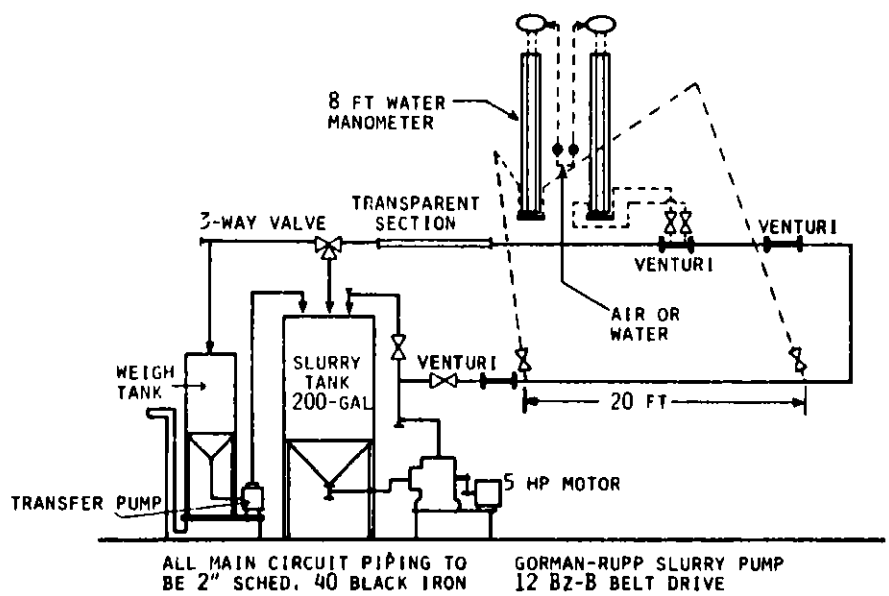

FIGURE 1 - SKETCH OF THE SLURRY PUMPING - PRESSURE DROP TEST APPARATUS

Differential manometer, with mercury as the fluid, was used for measuring pressure drop across the venturi for high flow rates. At low flow rates, the absolute pressure at the venturi inlet and throat were measured in feet of water. The water columns were maintained at a readable level by a common air bias to both the legs of the manometer. Slurry was prevented from entering the manometer by projecting the connecting tubing upwards before entering the manometer.

RESULTS

The data obtained for pressure drops across the three venturimeters at corresponding flow rates are used to obtain discharge coefficients C and Reynolds Number. As expected, the coefficient for single-phase water flow rises with Reynolds Number until the flow is fully turbulent ($>6 \times 10^4$). Thereafter, C is a constant (See Figure 2). This fully developed value for C varies somewhat among the three meters being 0.906 (for $\beta = 0.375$), 0.932 (for $\beta = 0.75$), and 0.961 (for $\beta = 0.50$).

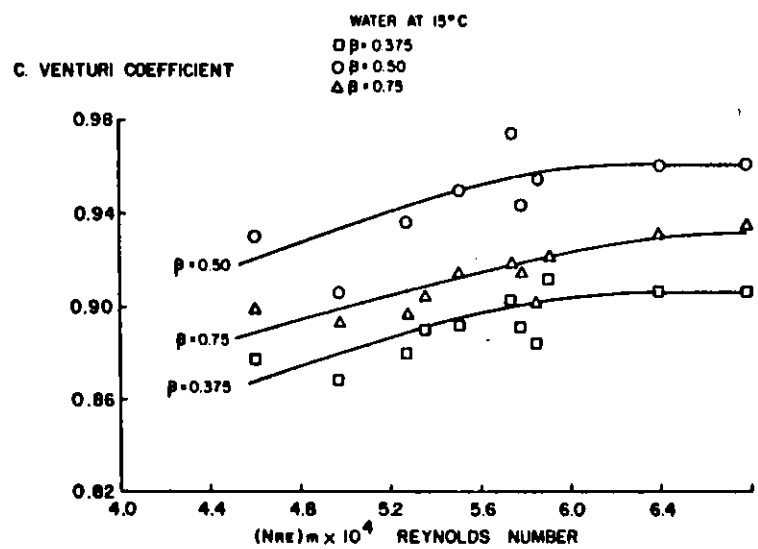

FIGURE 2 - VENTURI COEFFICIENT VERSUS REYNOLDS NUMBER FOR WATER USING THREE DIFFERENT VENTURI METERS.

For slurry flow, the Reynolds Number was defined in terms of pipe diameter slurry velocity (assuming homogeneous flow), slurry density and carrier medium (water) viscosity. Thus

$$(N_{R_e})_m = D_p V_m \rho_m / \mu_w \qquad (3)$$

Values of discharge coefficients obtained at various flow rates and concentrations for the three meters (using equation 2) are plotted in Figures 3, 4, and 5. As can be seen from these plots, the discharge coefficient at high Reynolds Number (>60,000) for all slurry concentrations and venturies is about the same as that for single phase flow. Thus, at high Reynolds Number, the discharge coefficient is independent of Reynolds Number, slurry concentration, or throat diameter and is the same for single-phase fluids and slurries. Data at lower Reynolds Number is difficult to take since critical velocity is soon reached causing the slurry to begin to settle.

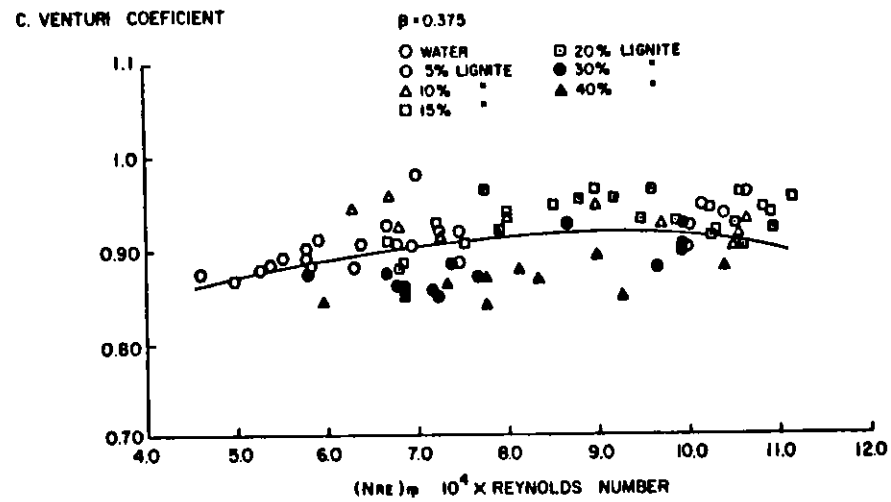

FIGURE 3 - VENTURI COEFFICIENT VERSUS SLURRY RENOLDS NUMBER FOR DIFFERENT SLURRY CONCENTRATION USING A 0.75 INCH VENTURI METER.

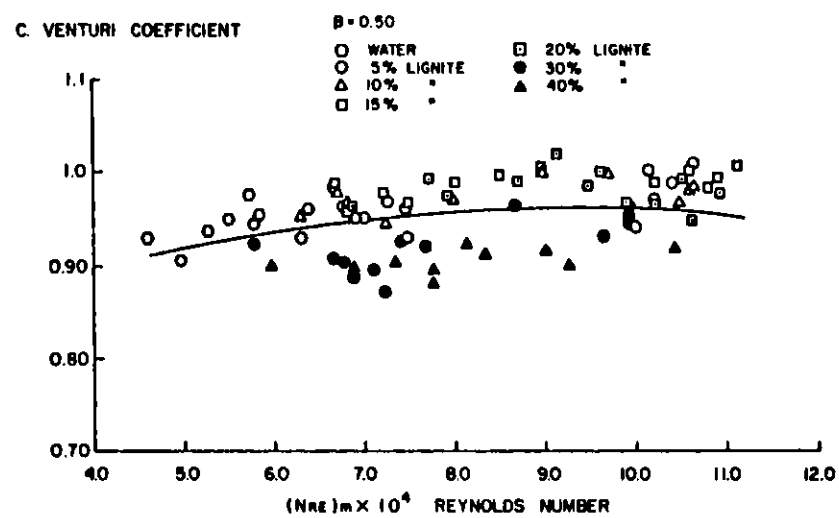

FIGURE 4 - VENTURI COEFFICIENT VERSUS SLURRY RENOLDS NUMBER FOR DIFFERENT SLURRY CONCENTRATION USING A 1.0 INCH THROAT VENTURI METER.

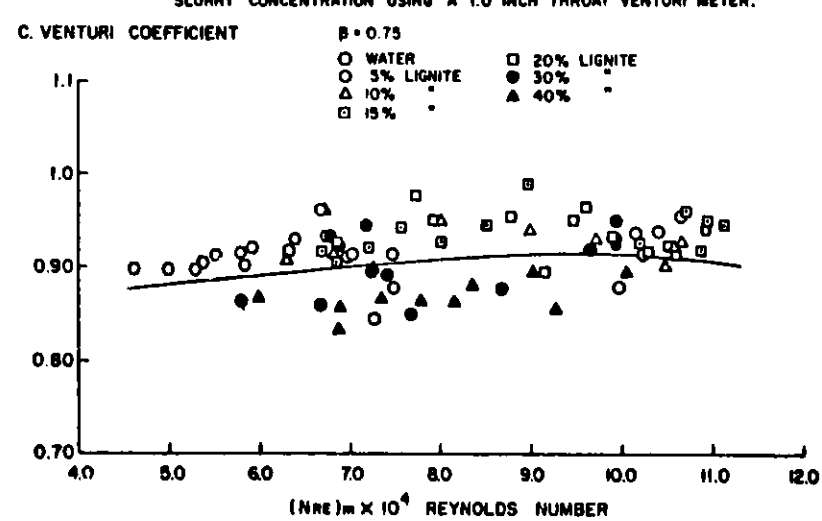

FIGURE 5 - VENTURI COEFFICIENT VERSUS SLURRY REYNOLDS NUMBER FOR VARIOUS CONCENTRATIONS USING A 1.5 INCH THOAT VENTURI METER.

Figures 3, 4, and 5 also indicate that the discharge coefficient is a weak function of Reynolds Number even at high Reynolds Number. This becomes more evident when the discharge coefficient for any particular concentration is plotted against Reynolds Number as shown in Figures 6 and 7. The discharge coefficient is first found to increase and then decrease with Reynolds Number. However, the variation is small. Figure 8 shows a plot of discharge coefficient against slurry concentration and indicates that the discharge coefficient first increases and then decreases with slurry concentration. Further data at higher slurry concentration are needed to confirm this trend.

Particle size distribution was obtained before the experiment as well as after about 100 hours of operation. No degradation in size was observed. Furthermore, there did not appear to be any erosion of the venturies or the pipes.

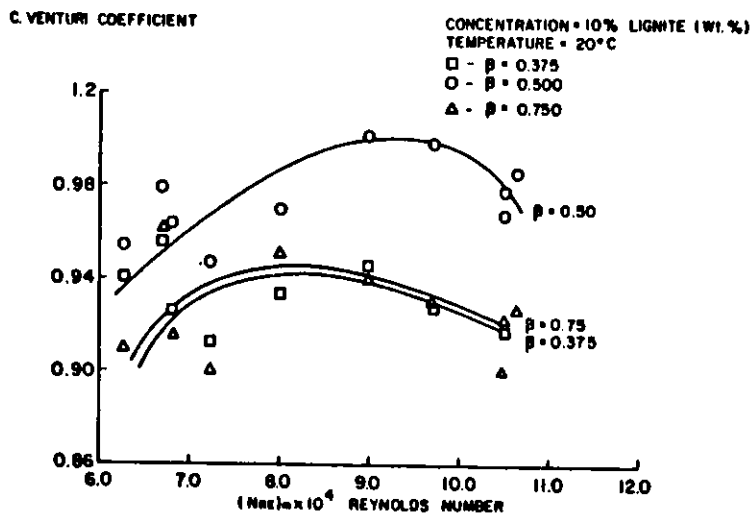

FIGURE 6 - VENTURI COEFFICIENT VERSUS SLURRY REYNOLDS NUMBER FOR A 10% (WT.) LIGNITE WATER SLURRY USING THREE DIFFERENT VENTURI METERS.

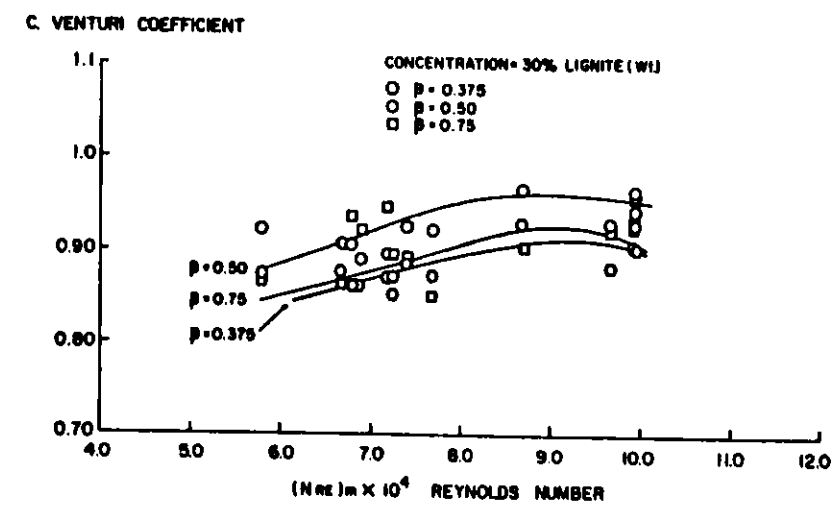

FIGURE 7 - VENTURI COEFFICIENT VERSUS SLURRY REYNOLDS NUMBER FOR A 30% (WT.) LIGNITE-WATER SLURRY USING THREE DIFFERENT VENTURI METERS.

DISCUSSION

As indicated earlier, our data shows that the discharge coefficient of the slurry and the carrying medium is approximately the same. This agrees with the work of Brook (1962) and Dementyew (1954). Brook's work (but not Dementyew's) also agrees with our finding that the discharge coefficient is a weak function of Reynolds Number. Neither Brooks nor Dementyew found the discharge coefficient to be dependent upon slurry concentration. However, it should be noted that Brook only investigated slurries with a maximum concentration of 20 percent.

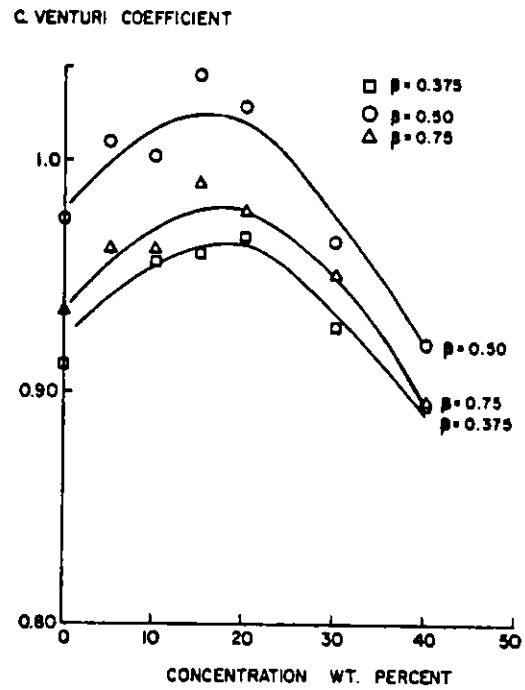

FIGURE 8 - VENTURI COEFFICIENT (PEAK VALUE) VERSUS SLURRY CONCENTRATION.

CONCLUSIONS

1. For measurement of slurry flow rates, a venturimeter can be used. However, the slurry density must be used in the flow equation.

2. The discharge coefficient for single phase flow may also be used for slurry flow with little loss of accuracy.

3. For greater accuracy, the meter should be calibrated. This is because of the fact that the discharge coefficient appears to be a weak function of the Reynolds Number. At high slurry concentration, the coefficient may also be dependent on concentration.

NOMENCLATURE

C	Venturi discharge coefficient
D	Pipe diameter
g	Acceleration due to gravity
g_c	Conversion factor, 32.174 (ft.) (lb.)/(sec^2) (lb_f)
h	Height of liquid (to express pressure)
Δh	Difference in pressure expressed in liquid column height.
N_{R_e}	Reynolds Number, $DV\rho/\mu$
P	Pressure
ΔP	Pressure difference
V	Velocity of flow

Greek Letters

β	Ratio of venturi throat diameter to pipe diameter D_p/D_t
ρ	Density

Subscripts

m	Mixture (slurry)
p	Pipe
t	Throat (venturi)
w	Water (carrying medium)

REFERENCES

Barth, W., "Neues Verfahren Zur Bestimung der augenblicklich gefoerderten Gutmengen im Luftstrom bei pneumatischer Foederung," Chem. Tech., Vol. 29, (1957), as reported by Brook, N. (1962).

Brook, N., "Flow Measurement of Solid-Liquid Mixtures Using Venturi and Other Meters," Proc. Inst. Mech. Engrs., V. 176, No. 6, pp. 127-140, (1962).

Bruhl, H., Doctoral Dissertation, Franzius-Inst. TU, Hannover, (1976), as reported by Kao, et al. (1979).

Carlson, H.M., Frazier, P.M., and Engdahl, R.B., "Meter for Flowing Mixtures of Air and Pulverized Coal," Trans. ASME, V. 70, p. 65, (1948).

Dementyew, M.A., Proc. WNIG, V. 52, (1954), as reported by Kao, et al. (1979).

Kao, D.T., Kazansikij, I., "On Slurry Flow Velocity and Solid Concentration Measuring Techniques," Proceedings of the 4th Int. Tech. Conf. on Slurry Transportation, March 28-30, (1979), pp. 102-120.

Kao, D.T., and Mathias, J.J., Internal Rep., Franzins Inst. TN Hannover, (1978), as reported by Kao, et al. (1979).

Karplus, H.B., and A.C. Raptis, Proc. Ultrasonics Symposium, ICC, (1978).

Kazaniskij, I., and Mathias, H.J., Hydrotransport 5, BHRA, (1978).

Liptak, B.G., and Leiter, C.P., "Overview of Coal Conversion Process Instrumentation," Govt. Publication No. ANL-FE-49628-TM01.

McShane, J.L., Flow, V. 1, Part 2, (1974).

Payne, A.L., and Crowe, C.T., "Metering the Mass Flow of Gas-Solids Mixtures in Non-Standard Venturi Configuration," Proc. Symp. Inst. and Control for Fossil Energy Processes, June 9 - 11, 1980, New Cavalier, Virginia, pp. 557-564.

Price, W., "Slurry Pipeline Projects Inch Along to Completion," Chemical Engineering, pp. 75-77, June 16, 1980.

Sheen, S.H., and Raptis, A.C., "HYGAS Coal-Slurry Mass-Flow Measurements Using Ultrasonic Cross-Correlation Technique," Govt. Publication No. ANL-FE-4922-TM07, September, 1979.

Shurin, W.D., and Yupfin, A.P., Grosstroyisdat, (1960), as reported by Kao, et al., (1979).

METERING GAS - PARTICLE FLOW IN ANNULAR VENTURIMETERS

M.L. Werner and C.T. Crowe
Washington State University
Pullman, WA 99164

ABSTRACT

The use of annular venturimeters for metering single-phase flows allows one to shorten upstream calming lengths. An experimental study is being conducted at Washington State University to determine if comparable reductions in calming length are achievable with annular venturimeters for metering gas-solids flows. The results presented in this paper show that the calming length for annular venturimeters can be markedly reduced without loss of meter sensitivity. The results also indicate that the added pressure loss due to increased surface area does not appreciably degrade the sensitivity of the annular venturimeter.

INTRODUCTION

The use of coal as an energy source in the United States is growing and will continue to grow as the supply of oil dwindles and its cost continues to climb. This trend has lead to the further development of power plants fired by pulverized coal, fluidized bed combustors and coal gasification systems which have created the need for improved methods to meter the solids flow rate in gas-solids mixtures. This need is apparent in balancing pneumatic feed lines to furnaces, in the transport of solids to fluidized beds and in the transport of char by steam in coal gasification systems. The conditions under which the metering device must operate vary from near atmospheric conditions in pneumatic lines feeding furnaces to high pressure (1500 psig), high temperature (1200°F) conditions in coal gasification units. The metering device must also have an accuracy of $\pm$2% and operate reliably for one year(1).

A metering concept which appears attractive because of its ruggedness (reliability) and simplicity (inexpensiveness) is the venturimeter. These devices have been used with confidence for many years to meter the flow rate of single phase fluids. Studies at Washington State University have shown

that the verturimeter also shows promise as a meter for gas-particle flows. These studies have shown that the pressure drop across the venturi varies linearly with loading (particle flow rate/gas flow rate). The slope of the linear variation depends on the Stokes number which is the ratio of particle response time to the gas residence time in the venturimeter and given by

$$St = \frac{\rho_p d_p^2 U}{18 \mu D_t}$$

where ρ_p is the particle density, d_p is the particle diameter, U is the gas velocity, μ is the dynamic gas viscosity and D_t is the venturi throat diameter. This parameter is the primary scaling parameter in system design.

One shortcoming of the venturimeter is the upstream calming length necessary to obtain consistent results. The ASME Code requires that pipe fittings responsible for flow disturbances be at least 20 pipe diameters upstream of the venturi. In many applications this necessary calming length may be unachievable. A venturi configuration which appears to be less influenced by upstream flow disturbances is the annular venturi shown in Fig.1.

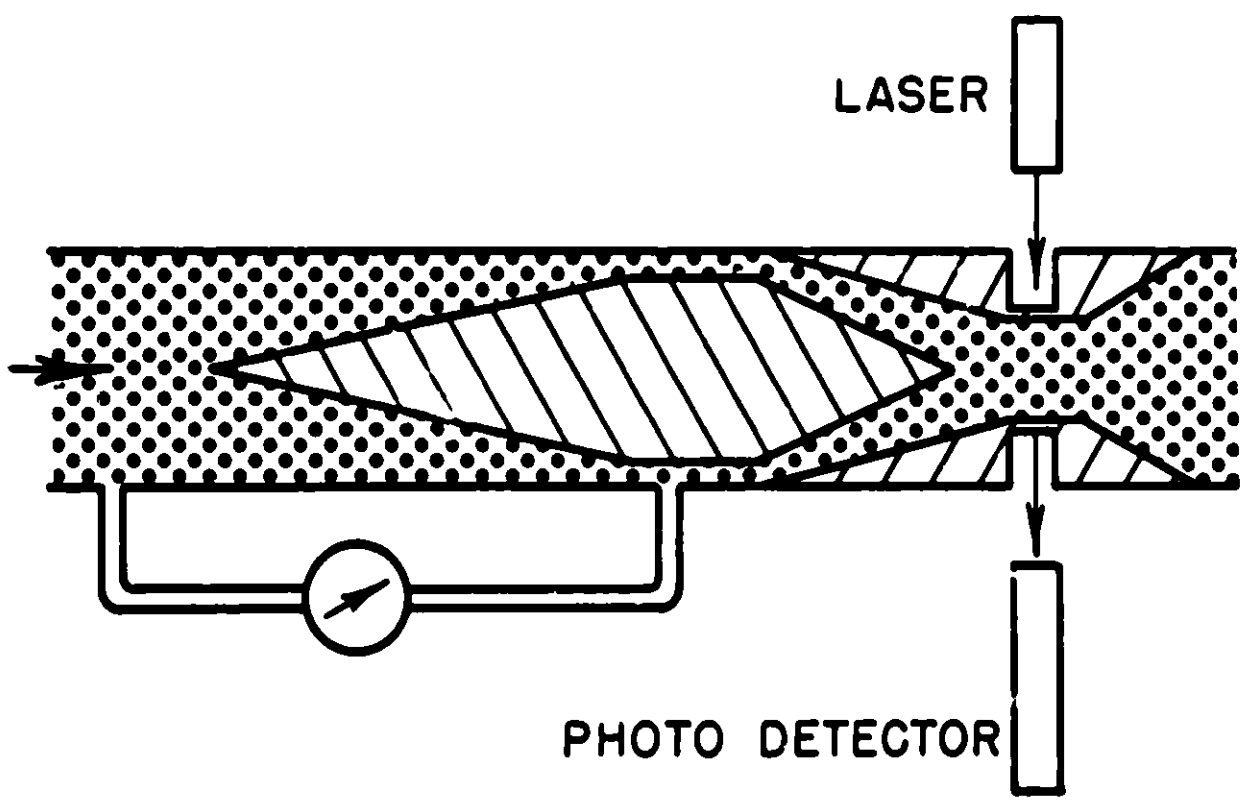

Figure 1. Schematic diagram of annular venturimeter

This configuration will tend to attenuate axial vortex motion by moving the flow farther from the pipe axis. One disadvantage of the annular venturi is the increased surface area compared with that for the conventional venturi and the potentially larger pressure loss. Numerical studies performed at WSU have shown this loss is comparable with that of a conventional venturi and, thus, should not be a serious consideration.

SYSTEM DESCRIPTION

The experimental apparatus used for this investigation is shown in Fig.2. Compressed air was supplied at 90-95 psig to aflow regulator and throttled down to working pres ures. The air velocity and mass flow rate were measured by pressure readings across a square-edged orifice. Coal was fed into the system by an auger powder feeder. The two-phase mixture then flowed through the test loop and the annular venturimeter. Recovery of the coal was accomplished by two cyclone separators. Pressure drops were measured between the entrance and throat of the venturimeter.

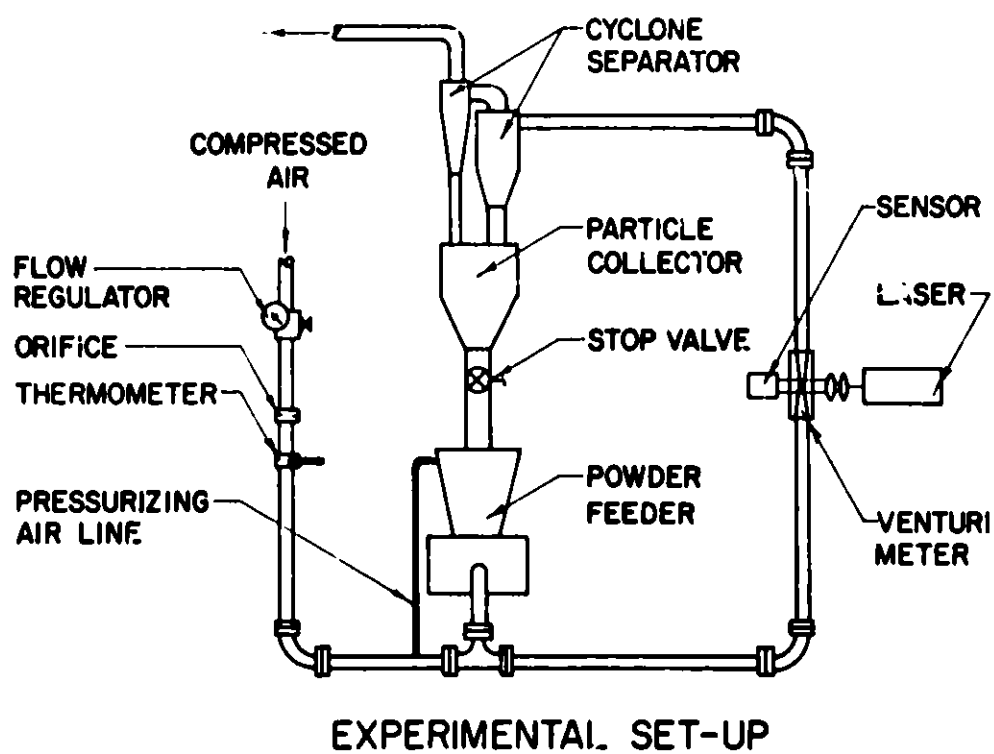

Figure 2. Experimental Set-up

Pulverized coal with mass median particle diameters of 64 microns and 120 microns were used in this study. These diameters, as well as the distribution of particle diameters, were obtained using a Coulter counter. The density of coal was measured to be 1390 kg/m^3 (87 lbm/ft^3).

A photograph of the annular venturimeter used on this study is shown in Fig.3. The meter was fabricated from Lucite to facilitate visual observations. The centerbody was made from aluminum. The pressure taps were located in the pipe at the entrance to the venturimeter and at 1/4 pipe diameter from the corner of the centerbody. The pressure taps were continuously purged to prevent clogging. The conventional venturi shape at the exit of the venturimeter was used for laser attenuation measurements.

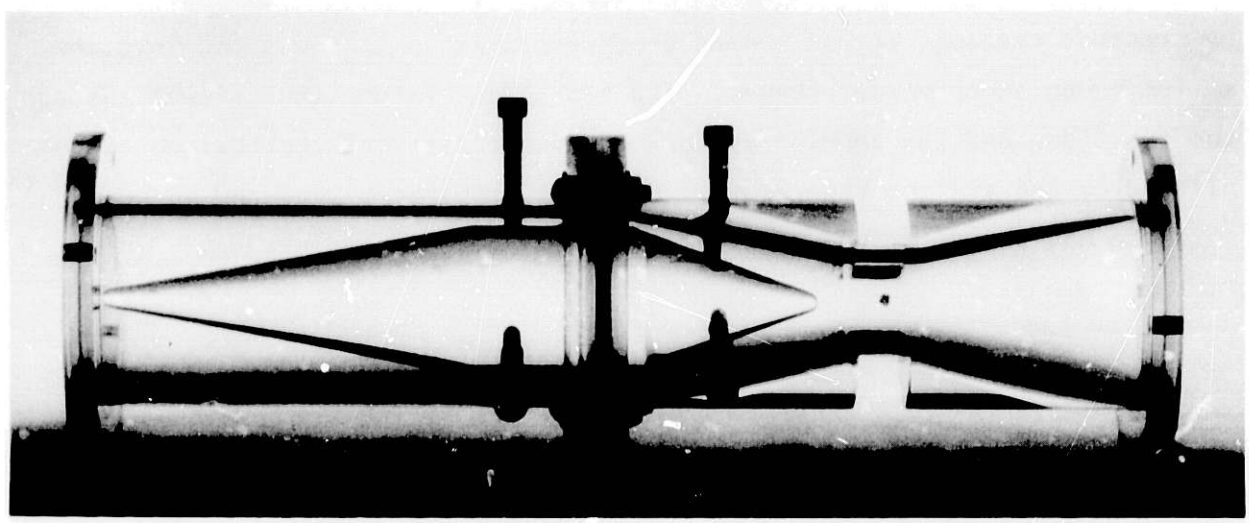

Figure 3. Photograph of Annular Venturimeter

The tests were carried out by first setting the air flow rate and recording the pressure drop, then introducing pulverized coal to achieve a desired loading and measuring the "two-phase" pressure drop. The venturimeter was oriented vertically and located 20 and 5 pipe diameters from the upstream elbow.

RESULTS

The experimental results obtained for the annular venturimeter were evaluated by making comparisons of the measured performance with a conventional venturi, with a numerical model and at the two locations with respect to the upstream elbow.

Pressure ratio data for a conventional venturimeter and annular venturimeter at a Stokes number of seven are shown in Fig.4. Both meters had the same throat area/pipe area ratio and inlet half angles that differed by only one degree.

One notes that the performance of the annular venturimeter is nearly indistinguishable from that for the conventional venturimeter. The increased surface area, and pressure drop due to friction, for the annular venturimeter appears to be unimportant.

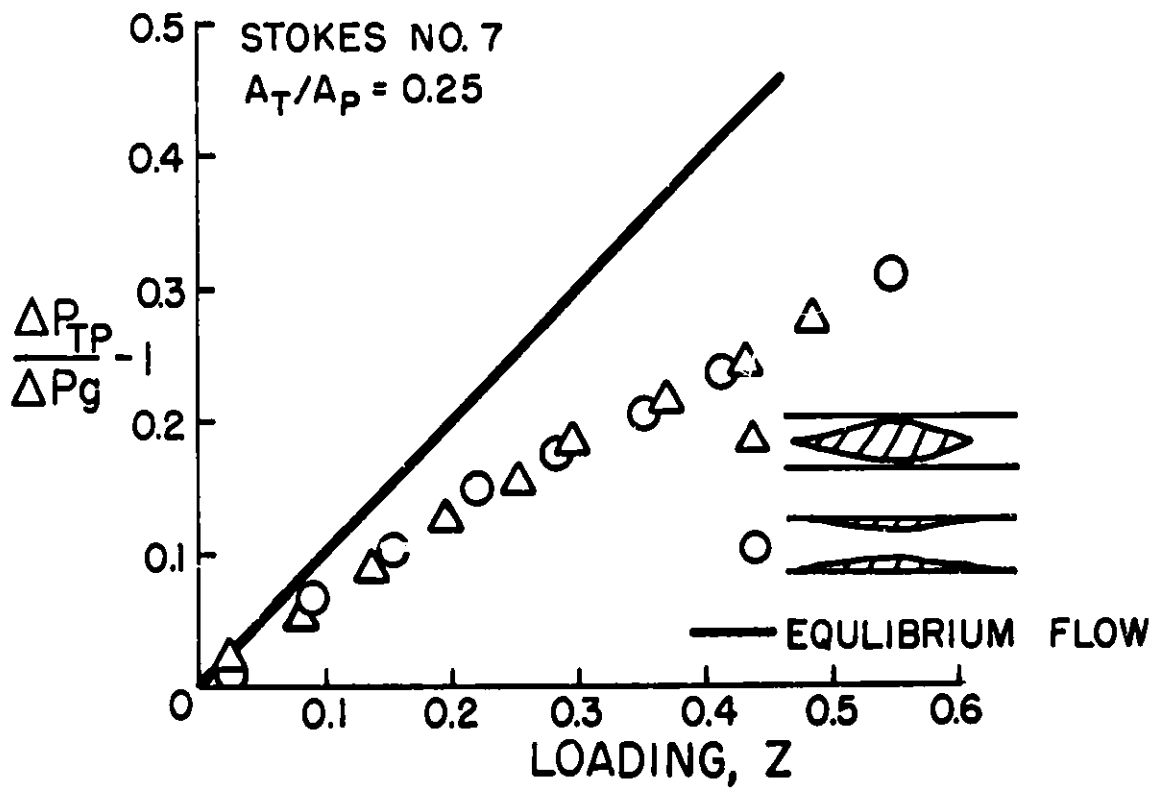

Figure 4. Comparison of performance of conventional and annular venturimeter

A comparison of the experimental results for the annular venturimeter with a quasi one-dimensional numerical model developed at Washington State University (2) is shown in Fig.5. The numerical model predicts a pressure drop somewhat higher than measured which is probably due to two dimensional effects, especially adjacent to the corner on the plug. Also, the numerical model does not include the increase in frictional force due to the presence of the particulate phase.

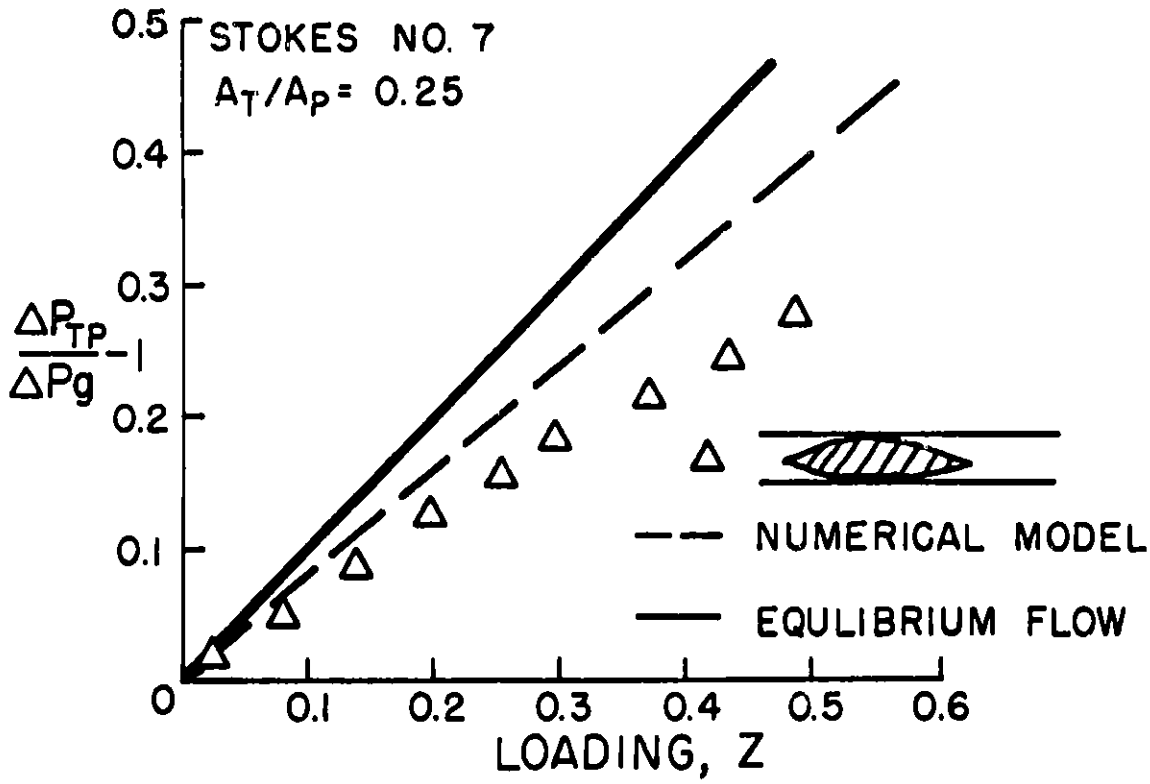

Figure 5. Comparison of predicted and measured performance of annular venturimeter

The effect of upstream calming length was measured at two Stokes numbers. The results are shown in Figs. 6 and 7. One notes that the meter performance at both Stokes numbers appears, within experimental error, to be unaffected by reducing the calming length to 5 diameters from the usual 20 diameters. This obervation lends support to the proposition that the annular venturimeter may be better suited to systems with limited space. These results have been obtained for low (St=7) and moderate (St=27) Stokes numbers. Performance at high Stokes numbers has not yet been measured.

Reducing the calming length from 20 to 5 diameters effects an approximate 3% reduction in flow coefficient for the annular venturimeter.

CONCLUSION

Experimental results have shown that the performance at the annular venturimeter for gas-solids flows is essentially the same as that for conventional venturimeters. The performance of the annular venturimeter is

unaffected by upstream calming length to lengths as short as 5 pipe diameters from an elbow.

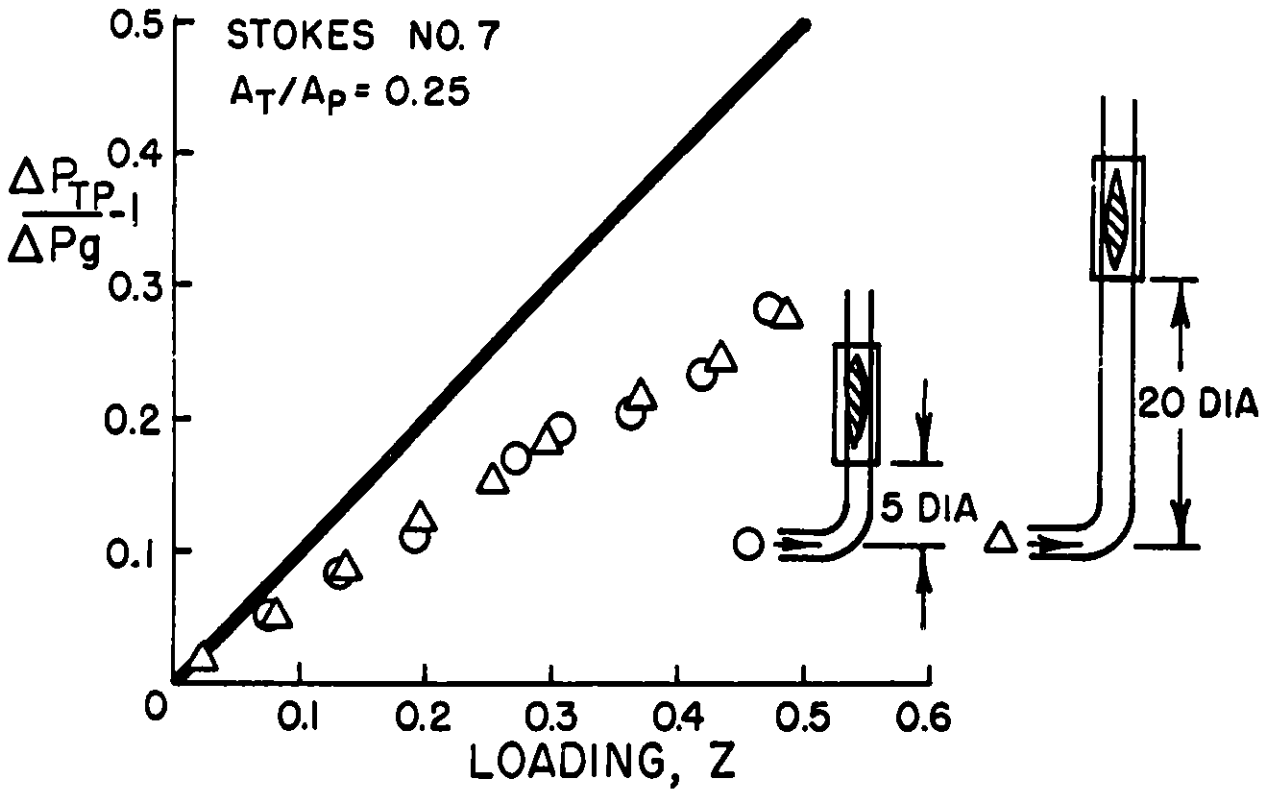

Figure 6. Effect of calming length on performance of annular venturimeter with St = 7.

ACKNOWLEDGEMENTS

The support of DOE Grant DE-FG22-80PC30212, and the partial support of NSF Grant CPE-7925077 is appreciatively acknowledged. The excellent workmanship of the Mechanical Engineering Shops under the direction of Mr. Tommy Hellesto is also acknowledged.

REFERENCES

1. "Instrumentation and Control for Fossil Energy Processes," Vols. 1 & 2, U.S. Department of Energy, Report 5030-437, Revision A, Dec. 15, 1980.

2. Sharma, M.P. and Crowe, C.T., "A Novel Computational Model for Quasi One-Dimensional Gas-Particle Flows," Jnl. of Fluids Engr., 100, 3, pp. 343-349, 1978.

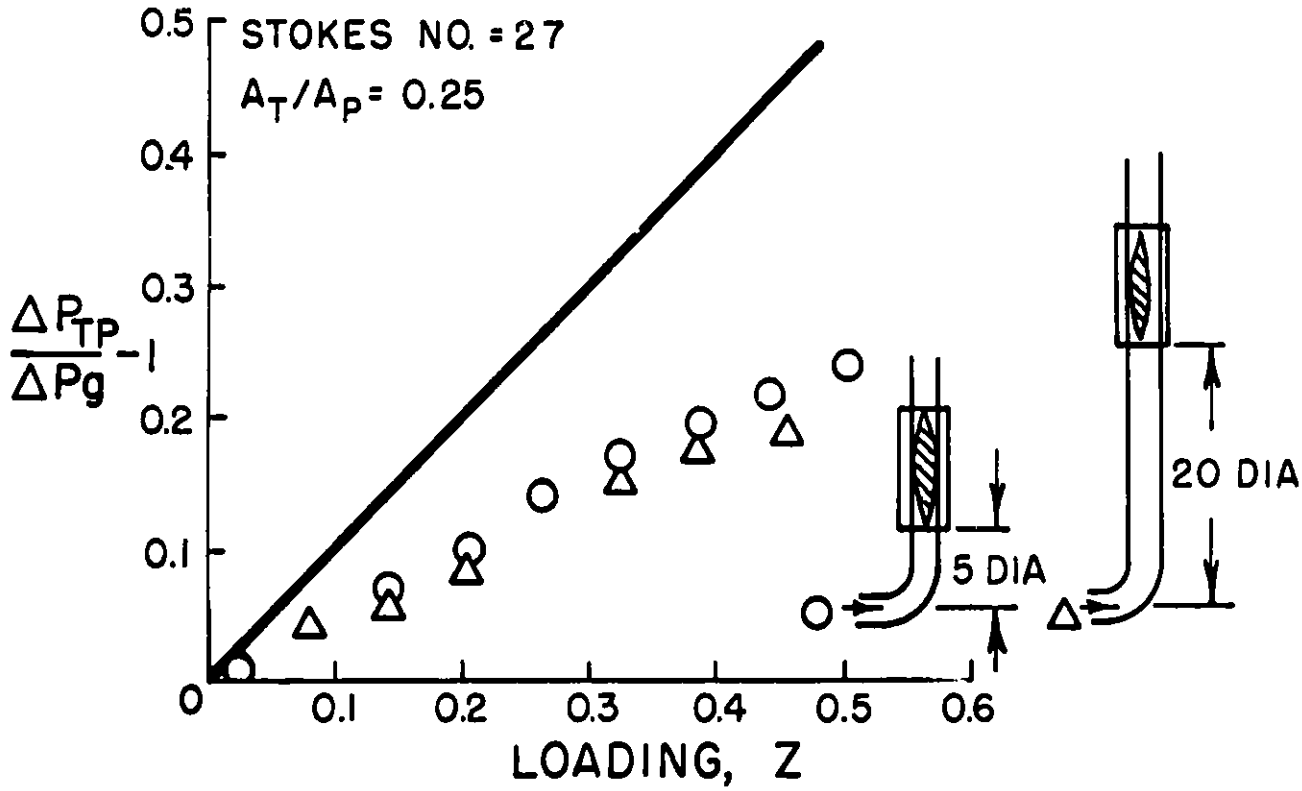

Figure 7. Effect of calming length on performance of annular venturimeter with St = 27.

A PERFORMANCE COMPARISON BETWEEN A CORIOLIS COAL FLOWMETER AND A MICROPROCESSOR-BASED TANK WEIGHING SYSTEM

Claude B. Reed, Thomas E. Zinneman, and Robert J. Blaskovitz, Jr.
Argonne National Laboratory, Argonne, IL

ABSTRACT

Data are presented comparing two independent methods, a Coriolis mass flow meter and tank weigh system, of measuring pulverized coal flow rate. Both methods are employed simultaneously in a dense-phase coal transport system. The Coriolis meter is located immediately upstream of a coal combustor and provides a continuous analog signal from which not only the average coal flow rate, but also the stability of the coal flow may be determined. The tank weigh system utilizes three load cells which are monitored by a microprocessor-based force computer. Both the weight of coal in the tank and the flow rate, based on the time rate-of-change of the coal weight, are computed continuously. Data presented includes a comparison of both systems using water and coal as the fluid mediums. In both cases, a third method which consisted of weighing the discharged medium in a barrel, was used as the reference system. Flow rates were varied over a range of 0 to 30 lbs/min.

INTRODUCTION

A pulverized coal combustion system has been installed at the Argonne MHD Process Engineering Laboratory (AMPEL). This coal combustion system provides high temperature combustion gases to MHD Heat and Seed Recovery (HSR) components and is part of the National MHD Program.

The integrated facility is capable of supporting a variety of tests and experiments related to the development of the combined system downstream of an MHD channel-diffuser. These experiments include measurements of basic physical processes such as heat and mass transfer, particle behavior in the hot exhaust gas streams, tests of small prototype components, and materials investigations. Recent experimental work at AMPEL in support of the National HSR Program has been designed to:

1. Investigate the heat and mass transfer characteristics of a seed and slag laden combustion gas in the range of conditions typical of an open-cycle MHD steam bottoming plant,

2. Investigate the reaction kinetics of NO_x in an MHD combustion gas,

3. Demonstrate feasibility of general design concepts for key MHD downstream components,

4. Test ceramic and metallic materials for use in the MHD downstream system, and

5. Test process instrumentation.

Work in this last area is reported here.

FACILITY DESCRIPTION

Coal Flow System

The coal flow system used in this work is shown in Fig. 1 and schematically in Fig. 2. The system consists of a coal tank into which coal is loaded through a lock hopper. The lock hopper and a bag filter are located above the coal tank as shown in Fig. 1. The bag filter prevents the escape of fines to the atmosphere. The coal tank is equipped with a double convex pressure breaker cone and a nitrogen fed fluidizer near the base. The cone partially supports the weight of the coal in the coal tank and the fluidizer provides a lubricating film of gas between the wall of the coal tank and the coal itself. At the base of the coal tank is a ball valve followed by a mixer assembly. The mixer assembly serves a dual purpose; first, in mixing the coal with incoming transport gas (air or nitrogen) and second, in throttling the coal flow rate from the coal tank. In the mixer valve assembly, coal and transport gas are combined and converted to a dense-phase mixture for transport to a combustion system. The base area of the coal tank is shown in Fig. 3.

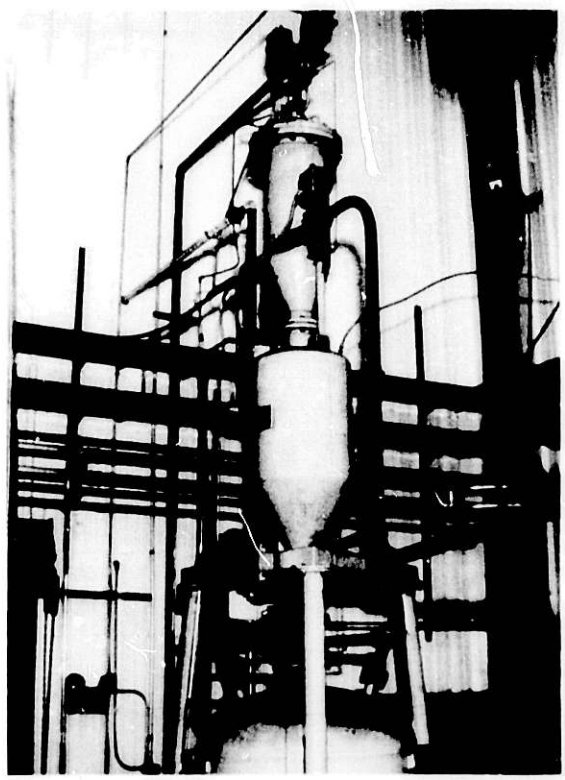

Figure 1. Coal Tank System

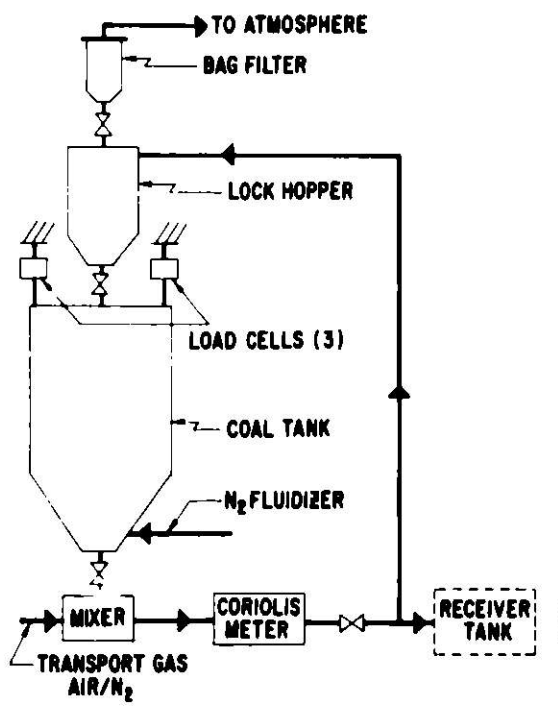

Figure 2. System Schematic

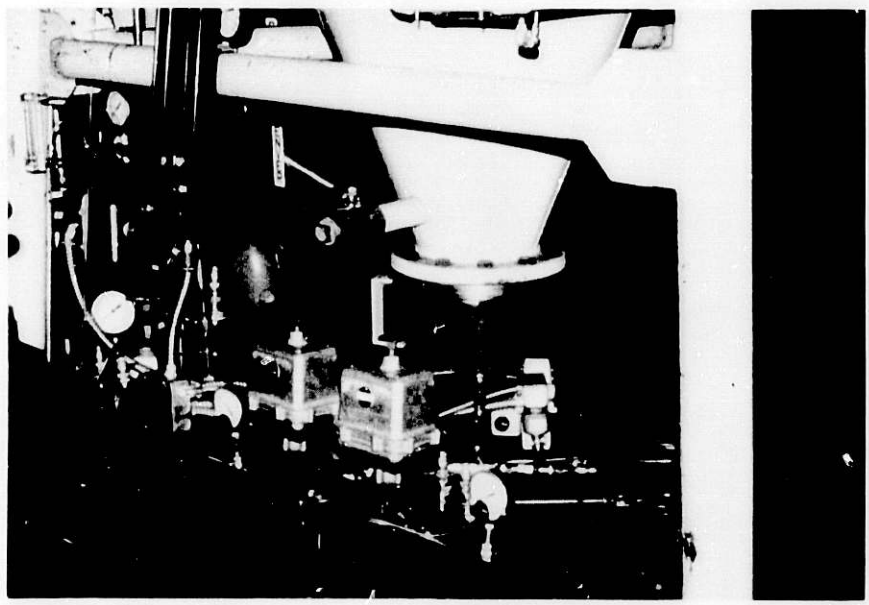

Figure 3. Base Area of Coal Tank

During the testing reported here, the dense-phase mixture of coal and transport gas were passed through a Coriolis flow meter, then into either a receiver tank or into the lock hopper for temporary holding, as shown in Fig. 2. The capacity of the coal tank is approximately 4,000 pounds and a tank or "ullage" pressure of 30 psig max. was maintained during testing. The most stable coal flow rates were produced at quite low ullage pressures of 5-10 psig. The coal feed system was designed to operate at coal flow rates of 7.2 to 21 lb/min with coal to transport gas mass ratios of 10:1 to 100:1.

Coal Tank Weigh System

A model 1011 force computer was purchased from the Orbitran Co. of Lakeside, California. The unit is essentially a microprocessor-based system for weighing-orientated digital processing and control applications. The inputs to the system are the outputs of three load cells, each of 2,000 pound capacity, from which the coal tank is suspended. One of the load cells is shown in Fig. 4. Linearity calibration and correction adjustments are provided internally. The microprocessor monitors the output of each load cell, computes, and displays the gross weight of the system. The tare weight of the coal tank can be entered into the system, via thumbwheel switches. In this case, the microprocessor then displays the net weight of the system. An analog signal, linearly proportional to the displayed weight, is also available for remote monitoring.

To provide an indication of the mass flow rate, the microprocessor automatically determines the difference in weight over 10 second intervals and calculates the flow rate which is displayed as the INCREMENTAL WEIGHT. This display is updated every 10 seconds. In addition, 10 consecutive INCREMENTAL

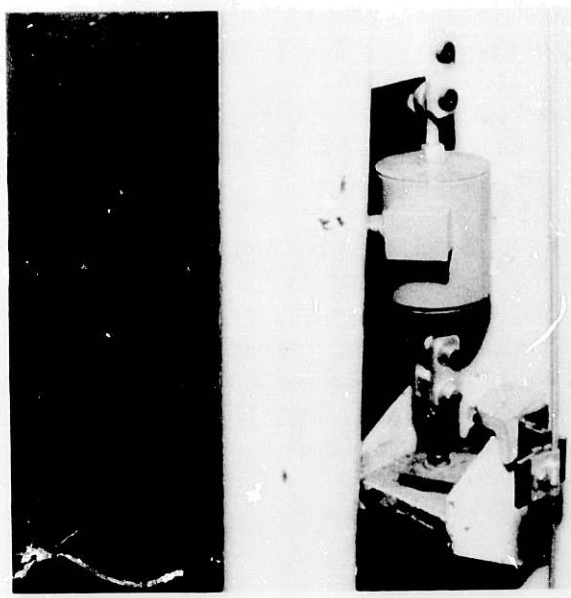

Figure 4. Load Cell

RATE numbers are averaged to determine an average flow rate over a 100 second interval. This number is displayed as the AVERAGE RATE and is also updated every 10 seconds. Analog signals representing both rates are available for remote monitoring.

Coriolis Mass Flow Meter

A model B50 mass flow meter was purchased from Micro Motion Inc. of Boulder, Colorado. This flow meter measures the mass flow rate of the material passing through the flow tube by detecting the Coriolis or gyroscopic force associated with the moving fluid particles. The flow meter essentially consists of a U-shaped flow tube and a leaf-spring which act as opposite legs of a tuning fork. An electromagnetic oscillator excites the tuning fork, thereby subjecting each moving particle within the pipe to a Coriolis-type acceleration. The resulting forces angularly deflect the U-shaped tube an amount that is proportional to the mass flow rate within the pipe.

The angular deflection of the tube is optically measured twice during each cycle of the tuning-fork oscillation. The output of the optical detector is a pulse that is width-modulated proportional to the mass flow rate. This signal is then conditioned to provide a square-wave output whose frequency is linearly proportional to the mass flow rate or an analog output whose amplitude is linearly proportional to the mass flow rate.

A remote flow indicator is provided which converts the frequency of the square-wave output to a flow rate indication. The indicator also includes a resettable digital integrator which displays the total mass flow.

Instrumentation and Data Acquisition

A mini-computer based data acquisition system (DAS), which consists of a Plessey Micro-1 minicomputer, a Lear Siegler ADM-3A interactive display terminal, a Wangco F2221 magnetic disc drive, and Computer Products RTP7480 Wide Range Analog Input system was used to sample and record data. The DAS provides the capability to randomly access and digitize 512 analog signals in thirteen software selectable full scale input ranges from ± 2.5 mV to ± 10.24 V at a scanning rate of 40 samples per second.

The three analog output voltages from the microprocessor-based tank weighing system, indicating net coal weight, incremental flow rate, and average flow weight, were recorded. The analog output voltage from the Coriolis mass flow meter, which provides an indication of the instantaneous flow rate, was also recorded. To obtain an analog signal representing the integrated flow from the mass flow meter, the frequency output from the meter was fed to a pulse counter. The output of the counter was then converted to an analog signal by a digital-to-analog converter. A block diagram of the tank weigh system and mass flow meter instrumentation is shown in Fig. 5.

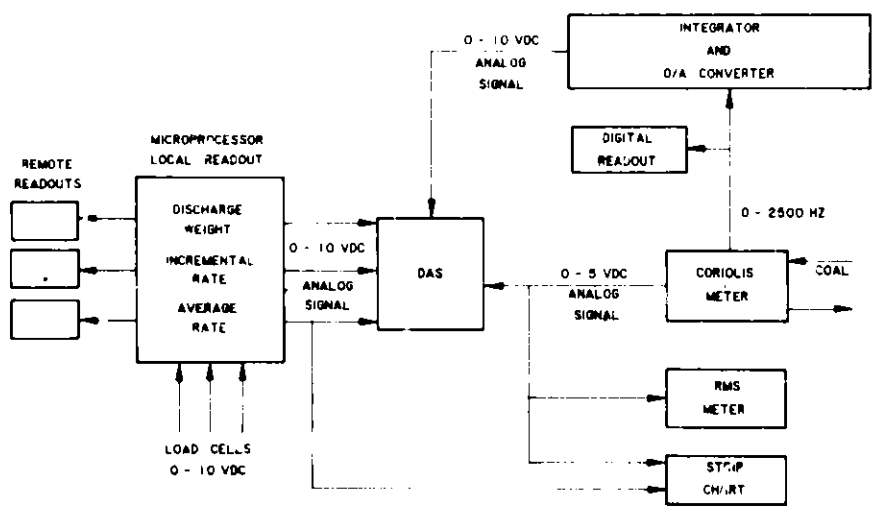

Figure 5. Instrumentation Schematic

In addition, the following analog signals were recorded on the DAS: coal hopper pressure; ΔP between coal hopper and lock hopper; lock hopper pressure; venturi inlet and outlet pressures for fluidizer and mixer lines; mixer valve position; and temperatures of the fluidizer and transport gases.

TEST RESULTS

Coal Hopper Weigh System Calibration

The coal hopper weigh system was calibrated for a weight range of 0 to 5,000 pounds. The accuracy is specified as ± 0.01% of full scale or ± 0.1% of applied load, whichever is greater. The resolution of the system is .2 pound.

During the installation of the system, a static calibration was performed by applying known weight increments, in the form of carbon steel bricks, to the coal hopper. Internal gain and linearity adjustments were made to achieve the desired calibration.

Coriolis Mass Flow Meter Calibration

Calibration of the mass flow meter was accomplished using water as the test fluid. The test setup consisted of monitoring the flow of the water through the mass flow meter, which was then discharged into a barrel. Data was recorded at nominal flow rates of 5, 10, 15, 20, and 25 lbs/min. The reference flow rate was established by weighing the amount of water discharged into the barrel over a time interval, typically between 15 and 30 minutes.

The total integrated flow as displayed by the Coriolis meter totalizer and the integrator/D-A converter was recorded. In addition, the analog output signal representing the total counts recorded by the integrator/D-A converter unit was recorded by the data acquisition system. In all cases, these three readings agreed to better than .1%.

The analog signal from the mass flow meter, which represents the instantaneous flow rate, was also recorded by the data acquisition system. This signal usually indicated several percent higher than the average mass flow rates as determined from the total integrated flow. This behavior was accounted for in subsequent use of the analog signal.

In comparing the average mass flow rate, as determined from the total integrated count, with the reference flow rate, the reference rate was found to be approximately two percent higher. However, rather than try to recalibrate the meter (frequency and analog adjustment controls are provided), a correction factor was applied to all recorded data.

Water Flow Rate Comparison

To provide a "head-to-head" comparison of the two systems under more favorable conditions than possible with coal, the following tests were performed. All coal was emptied from the coal tank and the tank filled with water. Several flow conditions similar to previous coal flow conditions were run with water as the medium. The coal tank was pressurized, forcing the water out of the coal tank, through the Coriolis meter and into the receiver tank. The fluidizer flow rate was set to a value typically used in coal operations. A typical strip chart recording of the Coriolis meter analog output and the tank weigh system output obtained during these runs is shown in Fig. 6.

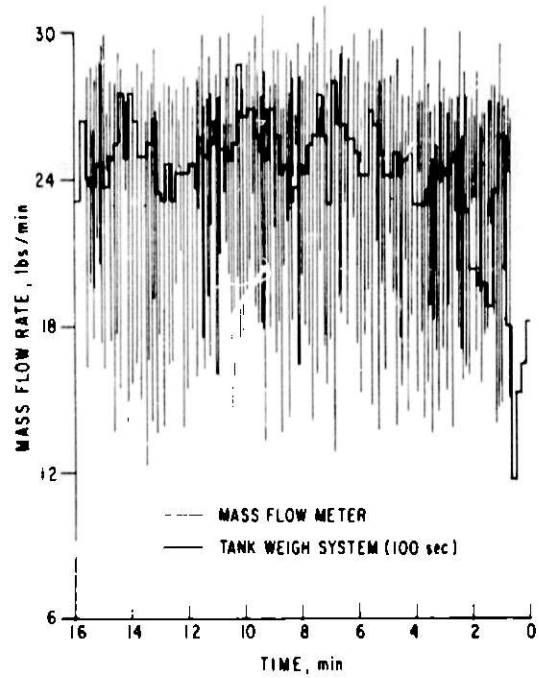

Figure 6. Water Flow Strip Chart, Unsteady Flow

The analog signal from the Coriolis meter exhibited an extremely erratic behavior as seen in the figure. The tank weigh system flow rate output, also shown in this figure, is the step-like signal. The step-wise nature of the weigh system signal stems from its being a digital signal which is updated only every 10 seconds. In these water comparison tests, which we term unsteady flow, the Coriolis meter indicated a lower average mass flow than did the tank weigh system or the reference barrel weight. Fig. 7 is a plot of the average mass flow measured by each of the three methods versus the tank pressure. This figure shows the poor agreement of the Coriolis meter with either the barrel weight or the tank weigh system during unsteady flow. The agreement between the barrel weight and the tank weigh system, as can be seen from Fig. 7, is much better than that of the Coriolis meter and the tank weigh system.

The unsteady flow was caused by vigorous mixing of the fluidizer gas with the water as the water left the tank. A two-phase flow was created which, by the time it reached the Coriolis meter, became inhomogeneous. This inhomogeneous flow could have disrupted the frequency of the Coriolis meter U-tube vibration and hence rendered its readings inaccurate.

To remedy this difficulty and permit the water flow comparison to proceed, the fluidizer flow rate was reduced. This eliminated the generation of a two-phase gas-water flow leaving the coal tank and rendered the water flow single-phase and steady. Fig. 8 is a typical strip chart recording of the Coriolis meter output and the tank weigh system output during one of the steady water flow comparison tests. For this particular flow rate, the agreement between the Coriolis meter and the tank weigh system was quite good. Fig. 9 shows the relative agreement between the two systems for several different average flow rates.

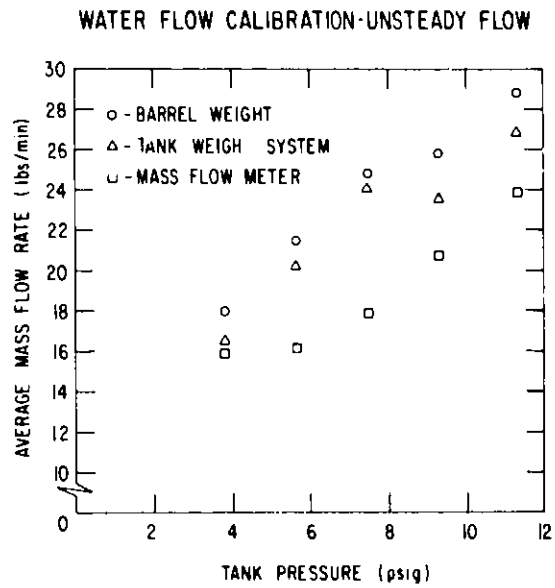

Figure 7. Water Flow Calibration, Unsteady Flow

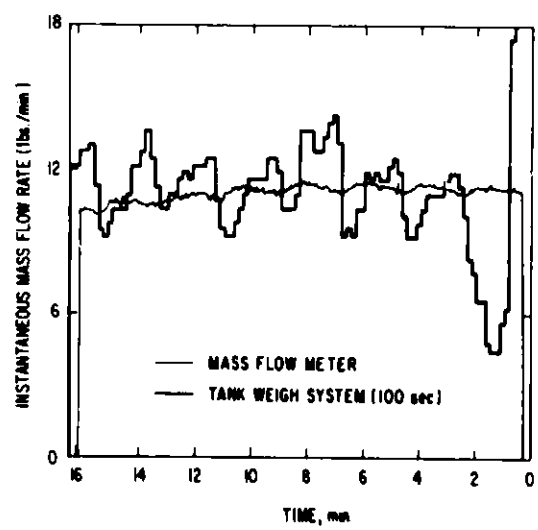

Figure 8. Water Flow Strip Chart, Steady Flow

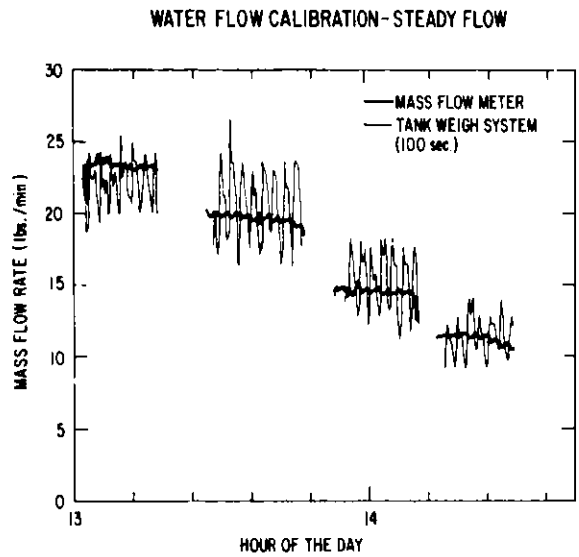

Figure 9. Water Flow Calibration, Steady Flow

In this comparison, the Coriolis meter also agreed very well with the barrel weight, Fig. 10.

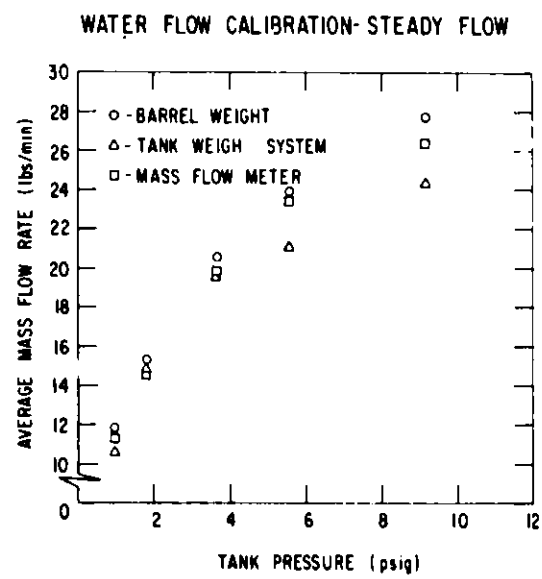

Figure 10. Water Flow Calibration, Steady Flow

Coal Flow Rate Comparison

Coal flow rate comparison tests were conducted by filling the tank with coal, and transporting the coal out of the tank, through the Coriolis meter and into a receiver tank. These tests were performed at five tank pressures. The results are shown in Fig. 11. A divergence among the three methods of measuring mass flow rate can be seen as the mass flow rate increases. A greater unsteadiness in the Coriolis meter signal was seen to qualitatively correlate with higher mass flow rate. Apparently, the unsteadiness in the coal flow interferes with the vibration of the U-tube at its natural frequency, leading to inaccurate results. This behavior has been noted previously by Baucum[2].

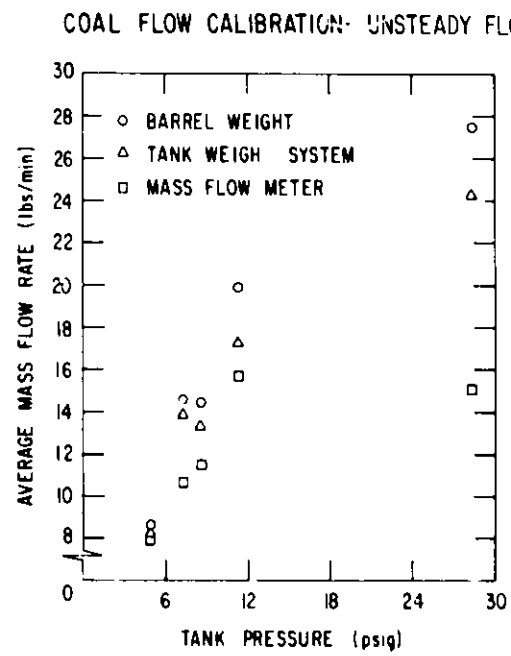

Figure 11. Coal Flow Calibration, Unsteady Flow

Coal Transport Data

Fig. 12 is a plot which compares the outputs of the Coriolis meter and the tank weigh system during combustion testing conditions (i.e., the coal was discharged into the combustor and burned). The coal flow was quite dense in this case, about 50:1 and moderately stable (∿.9 #/sec RMS). The flow rates of the two systems exhibit moderate agreement. It should be kept in mind that the tank weigh system has a 100 second time constant.

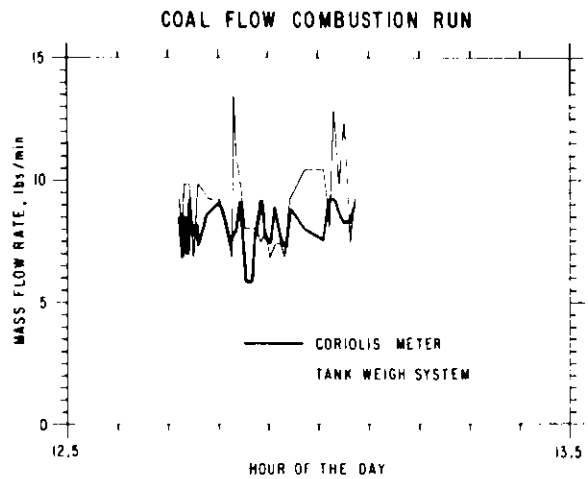

Figure 12. Coal Flow Combustion Run

Conclusion

The results of the tests using both water and coal as the flow medium indicate that the Coriolis meter used in this system provides accurate flow rate measurements under conditions of steady and uniform flow. However, if the flow medium becomes unsteady or non-uniform, the output signal from the Coriolis meter becomes erratic. This behavior could possibly be associated with a disruption in the oscillation of the U-tube of the Coriolis meter, which could be caused by the random forcing function provided by the unsteady or non-uniform flow. This behavior was reported previously by Baucum.[2] However, even under these conditions, the Coriolis meter can serve as a valuable diagnostic tool by indicating whether the flowing medium is stable or not.

As to the data provided by the tank weigh system, the average mass flow rate (calculated using the change in total weight over a period of 15 to 30 minutes) was consistently on the order of 10-15 per cent lower than the reference rate, under conditions of both steady and unsteady flow. This behavior could be the result of a slight misalignment of the load cells or possibly mechanical interference with the vertical motion of the tank, preventing full transfer of the load to the load cells.

The instantaneous flow rate (100 seconds) exhibits an oscillatory nature, as can be seen on Figures 8 and 9. However, the average value of the signal agrees quite well with the Coriolis meter signal (steady flow). The source of this oscillation has been traced to a variation of the tank ullage pressure caused by the dead band of the pressure regulating system. Steps will be taken to reduce these pressure variations.

Acknowledgements

The authors wish to thank Mr. J. K. Basco for his outstanding and dedicated assistance in assembling the equipment and conducting the tests. The authors also wish to acknowledge the efforts of Messrs. D. D. Pushis, W. B. Leniek, M. L. Romine, V. R. Fletcher, and R. A. Molson in completing the work reported here on time.

References

1. Plache, K. O., "Coriolis/Gyroscopic Flow Meter," Mechanical Engineering, March 1979.

2. Baucum, W. E., "Evaluation of a Coriolis Mass Flow Meter for Pulverized Coal Flows," UTSI Report FE-10815-45, Energy Conversion Division, Univ. of Tenn. Space Inst., December 1979.

EFFECTS OF TEMPERATURE TRANSIENTS ON VOLUMETRIC GAS FLOW MEASURING SYSTEM

Dr. Joel M. Siegel
The BDM Corporation
1746 Cole Blvd.
Golden, Colorado 80401

The accuracy of a volumetric gas flow measuring system can be reduced by temperature transients occuring during the measurement process. Since such systems are often used as a primary standard, it is important to be able to account for these effects.

Phenomonologically, system gas temperature will be influenced by two effects. The first is the heat transfer caused by the communication of the system gas with the containment vessel; the second is the temperature change due to the adiabatic processes associated with pressure changes in the system.

The basic principles of operation of the volumetric gas flow measuring system are reviewed. An analytic method of developing first order temperature corrections is presented. Heat transfer by conduction, convection, and radiation is discussed and their relative effect under various circumstances is evaluated. The effects of conduction are determined analytically by a solution of Fourier's Law of Heat Conduction for cylindrical geometry. A fundamental mode solution is taken as a first order representation of this effect. Application to the response of the gas flow measuring system is presented. Temperature changes due to adiabatic processes are analyzed and their effect on the flow measuring system is evaluated. Fast and slow leakage criteria for heated vessels are developed.

Two other approaches to temperature corrections are discussed. The first involves the use of a computer simulation of the contributing processes to numerically determine the temperature profile and response. The second approach would entail the use of sufficient instrumentation to accurately map the temperature profile and response time of the system. Equations are developed to input the above results with the measuring system's operational analysis to input the above results with the measuring system's operational analysis to produce flow corrections. The advantages and disadvantages of these other approaches are discussed.

I. INTRODUCTION

Flow is determined in a volumetric gas flow measuring system by measuring the change in pressure for a known time in a fixed volume at constant temperature (ref. 1). The volume flow or leakage rate (L) from the test volume in standard volume per time for an ideal gas is given by

$$L = -\frac{\partial n}{\partial t} R \frac{T_S}{P_S} \qquad \text{I-1}$$

where n is the number density of gas molecules, R is the ideal gas constant and T_s and P_s are standard temperature and pressure, respectively.
Note that

$$\frac{\partial n}{\partial t} < 0 \text{ when } L > 0, \text{ and}$$

since $n = \frac{PV}{RT}$ (ideal gas approximation) and V is constant volume of cylinder,

$$L = \frac{T_S}{T}\left(\frac{PV}{P_S T}\frac{\partial T}{\partial t} - \frac{V}{P_S}\frac{\partial P}{\partial t}\right) \qquad \text{I-2}$$

This paper is based on a valve leakage error analysis (ref. 2) performed by the author for the Morgantown Energy Technology Center (METC).

The system under consideration (refs. 3, 4) consists of a heated metallic cylinder into which ambient gas (air or N_2) is injected under pressure. A Uson Model 310 Pressure Decay Leak Test Unit (Uson) is used to measure the leakage rate of gas out of the cylinder. The Uson indicated leakage rate (L_u) as given by the Uson manual (ref. 5) is

$$L_U = \frac{V\,(P(o) - P(t))}{P_S t}$$

I-3

where P(t) is pressure at time t. The effects of temperature transients occuring during the measuring process are analyzed analytically in the following sections.

II. CALCULATION OF TEMPERATURE OF GAS(r,t) AS A FUNCTION OF POSITION AND TIME IN A HEATED CYLINDER

An "idealized" calculation is performed to obtain an analytic expression for the spatial and temporal distribution of the temperature of the gas in the test region. The assumptions which go into the calculation are summarized in Figure II-1. A constant temperature T_o on the cylinder surface is assumed for simplicity. Also the change of the thermodynamical parameters of density (ρ), thermal conductivity (k), specific heat capacity (c), and thermal diffusivity (α) in space and time will be neglected. The goal of this analysis is to develop an approximate first order solution. The only heat transfer mechanism considered is conduction since convection and radiation can be shown to be negligible for the METC system.

Starting with Fourier's law for Heat Conduction,

$$\alpha \nabla^2 T(\vec{r},t) = \frac{\partial T(\vec{r},t)}{\partial t} \qquad \text{II-1}$$

and substituting $T(\vec{r},t) = T_x(\vec{r})\ T_t(t)$ in (II-1) and dividing both sides of the equation by $T(\vec{r},t)$ gives

	CONCEPT/SYSTEM	MODEL	ASSUMPTIONS
1.	TEST REGION	FINITE CYLINDER	SURFACE IRRUGULARITIES ARE NEGLIGIBLE.
2.	THERMODYNAMIC PARAMETERS (DENSITY, THERMAL CONDUCTIVITY, SPECIFIC HEAT CAPACITY, THERMAL DIFFUSIVITY)	CONSTANT	SPATIAL AND TEMPORAL VARIATIONS ARE SMALL.
3.	GEOMETRIC CONFIGURATION IS 3-DIMENSIONAL	MODEL IS 2-DIMENSIONAL	SYSTEM IS AZIMUTHALLY SYMMETRIC.
4.	THERMODYNAMIC PROCESSES	HEAT CONDUCTION	"LINEARIZED" ANALYSIS PERMITS CONSIDERATION OF HEAT CONDUCTION SEPARATELY.
5.	BOUNDARY CONDITIONS	CYLINDER WALL IS AT T_0; TOTAL VOLUME OF GAS IS AT T_A INITIALLY	UNIFORM TEMPERATURE DISTRIBUTION OF WALL AND NO HEATING OF GAS AS IT ENTERS TEST REGION.
6.	SOLUTION IS A SUM OF INFINITE SERIES	SELECT FUNDAMENTAL MODE (SEE EQUATION BELOW)	SUFFICIENT TIME HAS ELAPSED SO THAT THE CONTRIBUTION OF HIGHER MODES IS NEGLIGIBLE.

$$T(\vec{r},t) = T_o - (T_o - T_a)\, J_o\left(\frac{2.405}{a} r\right) \sin\left(\frac{\pi z}{\ell}\right) e^{-\alpha\left[\left(\frac{2.405}{a}\right)^2 + \left(\frac{\pi}{\ell}\right)^2\right]t}$$

Figure II-1. Models and Assumptions Required for the Temperature Distribution Calculation

$$\alpha \frac{1}{T_x(\vec{r})} \nabla^2 T_x(\vec{r}) = \frac{1}{T_t(t)} \frac{\partial T_t(t)}{\partial t} \qquad \text{II-2}$$

It is well known that the separation of $T_x(\vec{r})$ into r and z dependent functions $T_x(\vec{r}) = T_r(r)\, T_z(z)$ eliminating θ by assuming azimuthal symmetry, gives rise ultimately to the solutions:

$$\begin{aligned} T_r &= A_1 J_o(\beta r) + A_2 Y_o(\beta r) \\ T_z &= A_3 \sin(\gamma z) + A_4 \cos(\gamma z) \end{aligned} \qquad \text{II-3}$$

Note: (r, θ, z) are cylindrical coordinates.

In order to satisfy the boundary condition that the temperature on the surface of the cylinder remains at T_o at all times, it is convenient to express $T_{(\vec{r},t)}$ as

$$T_{(\vec{r},t)} = T_o + T_r(r)\, T_z(z)\, T_t(t) \qquad \text{II-4}$$

where $T_r = T_z = 0$ on the surface of the cylinder ($r = a$, $z = 0$, $z = \ell$). At $r = 0$, $Y_o(\beta r) \to \infty$ which implies $A_2 = 0$ in equation II-3). The A's are "scale constants"; β and γ are "separation constants". T_o is the surface temperature of the cylinder. Additional boundary conditions on the surface at the cylinder are

$$T_r(r = o, r = a) = 0 \text{ and } T_z(z = 0, z = \ell) = 0$$

Due to the periodicity of transcendental functions the surface boundary conditions lead to a series of solutions. For T_r one has

$$T_{r_n} = A_{1_n} J_o(\beta_n r) \qquad \text{II-5}$$

where β_n is given by $J_o(\beta_n a) = 0$. At z=0, $\cos(\gamma z)=1$ which implies $A_4=0$ in equation (II-3).

The solutions for T_z are

$$T_{z_n} = A_{3_n} \sin(\gamma_n z) \qquad \text{II-6}$$

where γ_n is given by $\sin(\gamma_n \ell)=0$.
Taking all linear combinations of the above solutions, one finds

$$T_{\vec{r}_{ij}} = \beta_{ij} J_o(\beta_i r) \sin(\gamma_j z) \qquad \beta_{ij} = A_{1j} A_{3j}; \qquad \text{II-7}$$

but for each spatial solution $T_{\vec{r}ij}$ there is a corresponding temporal dependence $T_{\vec{r}ij}$ in terms of the separation constants. Thus plugging back the product solution into equation (II-2) gives

$$\alpha \frac{\nabla^2 T_{\vec{r}_{ij}}}{T_{\vec{r}_{ij}}} = -\alpha(\beta_i^2 + \gamma_j^2) = \frac{\partial T_{t_{ij}}}{\partial t} \frac{1}{T_{t_{ij}}}, \qquad \text{II-8}$$

which solving for T_{rij} yields

$$T_{t_{ij}}(t) = T_{t_{ij}}(t=0)\, e^{-\alpha(\beta_i^2 + \gamma_j^2)t} \qquad \text{II-9}$$

Combining (II-9) with (II-7) and taking all linear combinations, equation (II-4) becomes

$$T(\vec{r},t) = T_o + \Sigma_{ij} \; T_{ij} \, J_o \, (\beta_i r) \sin (\gamma_j z) \, e^{-\alpha(\beta_i^2 + \gamma_j^2)t} \qquad \text{II-10}$$

where α is thermal diffusivity and β_i and γ_j are separation constants determined by geometry. The T_{ij}'s are constants determined by the initial temperative distribution.

Each term in equation (II-10) with a given i and j in the sum is called a mode and evolves in time with its own separate time dependence. The mode for $i = j = 1$ is called the fundamental mode. Since $\beta_i > \beta_1$, and $\gamma_i > \gamma_1$ for all $i > 1$, the fundamental mode decreases more slowly in time than any other mode. Thus, after a comparatively short amount of time all the other modes will decay away and the temperature behavior will be given solely by the fundamental mode. In doing a first order analysis to demonstrate how the T_{ij} can be determined, T_{11} for the fundamental mode will be calculated with all other T_{ij} given by $i \neq 1$, $j \neq 1$ set at zero. This would be the best one term approximation to the actual temperature distribution. Equation (II-10) for the fundamental mode solution becomes

$$T(\vec{r},t) = T_o + T_{11} \, J_o \, (\beta_1 r) \sin (\gamma_1 z) \, e^{-\alpha(\beta_1^2 + \gamma_1^2)\, t} \qquad \text{II-11}$$

with $$J_o \, (\beta_1 a) = 0 \Rightarrow \beta_1 = \frac{2.405}{a}$$

and $$\sin (\gamma_1 \ell) = 0 \Rightarrow \gamma_1 = \frac{\pi}{\ell}.$$

Also at $t = 0$, $T_{(r = 0,\ z = \frac{\ell}{2},\ t = 0)} = T_a$

where T_a is ambient temperature. This assumes no heating of the gas in the center of the cylinder has occured at t = 0. Thus,

$$T_{(\vec{r}=0,\ t=0)} = T_o + T_{11} = T_a \Rightarrow T_{11} = T_a - T_o. \qquad \text{II-12}$$

which substituted into (II-11) gives the first order solution

$$T(\vec{r},t) = T_o - (T_o - T_a)\, J_o\left(\frac{2.405}{a}\, r\right) \sin\left(\frac{\pi z}{\ell}\right) e^{-\alpha\left[\left(\frac{2.405}{a}\right)^2 + \left(\frac{\pi}{\ell}\right)^2\right]t} \qquad \text{II-13}$$

Figure II-2 graphically depicts the approximate solution, (a), and the actual solution, (b).

For small time intervals of measurement, equation (I-3) for Uson leakage (L_U) can be approximated by

$$L_U \simeq -\frac{V}{P_S}\frac{\partial P}{\partial t} \qquad \text{II-14}$$

which substituted into equation (I-2) yields

$$L = \frac{T_S}{T}\left(\frac{PV}{P_S T}\frac{\partial T}{\partial t} + L_U\right). \qquad \text{II-15}$$

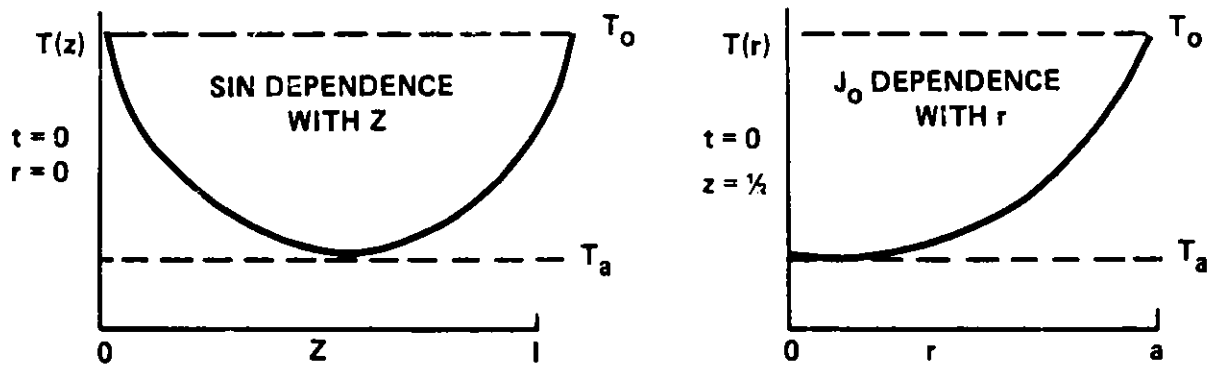

(a) GRAPH OF APPROXIMATE TEMPERATURE PROFILE AT t = 0

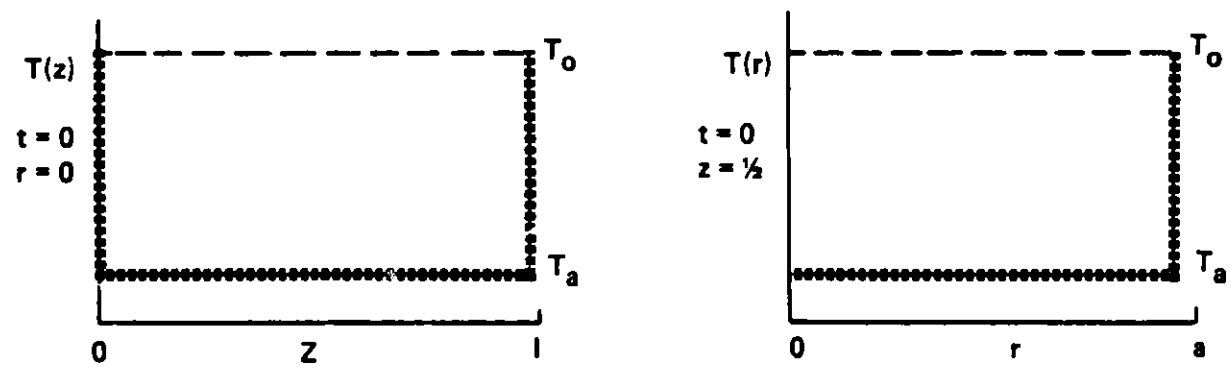

(b) GRAPH OF ACTUAL TEMPERATURE PROFILE AT t = 0

Figure II-2. Approximate (a) and Actual Solutions (b)

Taking the partial derivative of equation (II-13) with respect to time yields

$$\frac{\partial T(\vec{r},t)}{\partial t} = \chi\,(T_o - T_a)\,J_o\,(\beta r)\,\sin\,(\gamma z)\,e^{-\chi t} \qquad \text{II-16}$$

or simply

$$\frac{\partial T}{\partial t} = \chi\,(T_o - T) \qquad \text{II-17}$$

which substituted in (II-15) becomes

$$L = \frac{T_S}{T}\left[\frac{PV}{P_S T}\,\chi(T_o - T) + L_U\right] \qquad \text{II-18}$$

III. USON ERROR CORRECTION DUE TO ADIABATIC COOLING

The leakage rate (L) given by (I-2) is an instantaneous quantity whereas the Uson measures an average leakage rate ($\bar{L}$) over the measuring interval (t) which is given by

$$\bar{L} = \frac{\int_o^t L\,dt}{t} = -\frac{T_s V}{P_s t}\int_o^t\left(\frac{1}{T}\frac{\partial P}{\partial t} - \frac{P}{T^2}\frac{\partial T}{\partial t}\right)dt \qquad \text{III-1}$$

The equation of state for an adiabatic process of an ideal gas is

$$PV^{\gamma} = \text{constant} \qquad \text{III-2}$$

where γ is the ratio of specific heats (C_p/C_v). In the system under consideration the volume occupied by a given number (n) of molecules will vary as 1/n. Recalling n=PV/RT in equation (III-2) yields the condition

$$P^{1-\gamma}T^{\gamma} = \text{constant} = K = P_o^{1-\gamma}\, T_o^{\gamma} \qquad \text{III-3}$$

where P_o and T_o are any simultaneous temperature and pressure measurements usually taken as "initial conditions." Note the volume in (III-2) is the volume occupied by specified gas molecules (n) and should really be expressed V(n). V(n) is a variable which changes with n. However, V in PV=nRT is the volume of the test cylinder, which remains constant.

Solving for T in equation (III-3) yields

$$T = K^{1/\gamma}\; P^{1-1/\gamma} \qquad \text{III-4}$$

Substituting (III-4) in equation (III-2) gives

III-5

$$\tilde{L} = -\frac{T_s V}{P_s t}\int_o^t \left[K^{-\frac{1}{\gamma}}\, P^{\frac{1}{\gamma}-1} - K^{-\frac{2}{\gamma}}\, P^{\frac{2}{\gamma}-2+1}\, K^{\frac{1}{\gamma}}\,(1-\tfrac{1}{\gamma})\, P^{-\frac{1}{\gamma}}\right]\frac{\partial P}{\partial t}\,dt$$

$$= -\frac{T_s V}{P_s t}\, K^{-\frac{1}{\gamma}}\int_o^t \left[P^{\frac{1}{\gamma}-1} - 1 - \frac{1}{\gamma}\, P^{\frac{1}{\gamma}-1}\right] dp$$

$$= -\frac{T_s V}{P_s t}\, K^{-\frac{1}{\gamma}}\,\frac{1}{\gamma}\int_o^t P^{\frac{1}{\gamma}-1}\, dp$$

$$= -\frac{T_s V}{P_s t}\; K^{-\frac{1}{\gamma}}\left[P(t=0)^{\frac{1}{\gamma}} - P(t=t)^{\frac{1}{\gamma}}\right]$$

To correct the Uson, solve equation (I-3) for P(t) to get

$$L_U = \frac{V[P(o) - P(t)]}{P_s t}, \text{ solving for } P(t), \qquad \text{III-6}$$

$$P(t) = - \frac{L_U P_S t}{V} + P(o),$$

which replacing (III-6) in (III-5) yields the result

$$\bar{L} = \frac{T_S V}{P_S t} K^{-\frac{1}{\gamma}} \left[P(o)^{\frac{1}{\gamma}} - \left(P(o) - \frac{L_U P_S t}{V} \right)^{\frac{1}{\gamma}} \right] \qquad \text{III-7}$$

Thus, measuring temperature and pressure at the start of the Uson run (T_o, P_o) will provide the input for the correction.

To get a first order correction which more easily shows the effect of changing a parameter or operating regime on Uson error, consider using a binomial expansion on the brackets in equation (III-7) for two different operating conditions. First consider the case

$$\frac{L_U P_S t}{V P_o} << 1 \qquad \text{III-8}$$

which would apply to a low leakage rate, short time of measurement, or high operating pressure P_o. Recalling (III-7) one can write

$$\left[P(o)^{\frac{1}{\gamma}} - \left(P(o) - \frac{L_U P_S t}{V} \right)^{\frac{1}{\gamma}} \right] = P_o^{\frac{1}{\gamma}} \left[1 - \left(1 - \frac{L_U P_S t}{P_o V} \right)^{\frac{1}{\gamma}} \right]$$

and expanding $\left(1 - \frac{L_U P_S t}{P_o V} \right)^{\frac{1}{\gamma}}$ to first order in $\frac{L_U P_S t}{P_o V}$

gives $\left(1 - \frac{L_U P_S t}{P_o V} \right)^{\frac{1}{\gamma}} \simeq 1 - \frac{1}{\gamma} \frac{L_U P_S t}{P_o V}$ + higher order terms. $\qquad$ III-9

Replacing (III-9), and (III-7) yields:

$$\bar{L} \simeq \frac{T_S V}{P_S t} K^{-\frac{1}{\gamma}} P_o^{\frac{1}{\gamma}} \left[1 - \left(1 - \frac{1}{\gamma} \frac{L_U P_S t}{P_o V} \right) \right]$$

$$\bar{L} \simeq \frac{T_S V}{P_S t} K^{-\frac{1}{\gamma}} P^{\frac{1}{\gamma}} \frac{1}{\gamma} \frac{L_U P_S t}{P_o V} = T \frac{K^{-\frac{1}{\gamma}}}{\gamma} P^{\frac{1}{\gamma}-1} L_U \qquad \text{III-10}$$

which recalling III-3 becomes

$$\bar{L} \simeq \frac{T_S}{T_o} \frac{1}{\gamma} L_U \text{ for } \frac{L_U P_S t}{V P_o} << 1 \qquad \text{III-11}$$

Note: $\bar{L} < L_U$; i.e. the Uson reads high for this case. Next, the more likely condition that

$$\frac{L_U P_S t}{V P_o} >> 1 \qquad \text{III-12}$$

(easily reachable experimentally by letting t be large) is also explored. The large t would give an average leakage which might mask what the leakage at high pressure is before the pressure is reduced and the leakage rate itself by the prevailing leakage. A high leakage rate in L_U would be an interesting condition for inspection since that would bolster the need for doing the adiabatic temperature correction in the first place.

This time the bracket from (III-7) can be expressed as

$$\left[P_o^{\frac{1}{\gamma}} - \left(P_o - \frac{L_U P_S t}{V} \right)^{\frac{1}{\gamma}} \right] = \left[P_o^{\frac{1}{\gamma}} - \left(\frac{L_U P_S t}{V} \right)^{\frac{1}{\gamma}} \left(-1 + \frac{P_o V}{L_U P_S t} \right)^{\frac{1}{\gamma}} \right]$$

which using binomial expansion to first order $\frac{L_U P_S t}{V}$ gives

$$\left[P_o^{\frac{1}{\gamma}} - \left(\frac{L_U P_S t}{V}\right)^{\frac{1}{\gamma}}\left(-1 + \frac{P_o V}{L_U P_S t}\right)^{\frac{1}{\gamma}}\right] \approx P_o^{\frac{1}{\gamma}} - \left(\frac{L_U P_S t}{V}\right)^{\frac{1}{\gamma}}\left[-1 + \frac{P_o V}{\gamma L_U P_S t} + \ldots\right]$$

$$\approx P_o^{\frac{1}{\gamma}} + \left(\frac{L_U P_S t}{V}\right)^{\frac{1}{\gamma}} - \left(\frac{L_U P_S t}{V}\right)^{\frac{1}{\gamma}-1}\frac{P_o}{\gamma} = P_o^{\frac{1}{\gamma}}\left[1 + \left(\frac{L_U P_S t}{V P_o}\right)^{\frac{1}{\gamma}} - \left(\frac{L_U P_S t}{V P_o}\right)^{\frac{1}{\gamma}-1}\frac{1}{\gamma}\right] \qquad \text{III-13}$$

Combining equations (III-7), (III-12), and (III-13) yields

$$\bar{L} \approx \frac{T_S V}{P_S t} P_o^{-\frac{1}{\gamma}+1} T_o^{-1}\left(\frac{L_U P_S t}{V}\right)^{\frac{1}{\gamma}} \quad \text{or}$$

$$\bar{L} \approx \frac{T_S}{T_o}\left(\frac{V P_o}{P_S t}\right)^{1-\frac{1}{\gamma}} L_U^{\frac{1}{\gamma}} \qquad \text{III-14}$$

Since $\gamma > 1$, $1-\frac{1}{\gamma} > 0$ so that as $t \to \infty$, $\bar{L} \to 0$ as expected.

To determine the nature of the correction factor, construct

$$\frac{\bar{L}}{L_U} = \frac{T_S}{T_o}\left(\frac{V P_o}{P_S t}\right)^{1-\frac{1}{\gamma}} L_U^{1-\frac{1}{\gamma}} = \frac{T_S}{T_o}\left(\frac{V_o P}{L_U P_S t}\right)^{1-\frac{1}{\gamma}} \qquad \text{III-15}$$

which with (III-12) leads to the condition

$$\frac{\bar{L}}{L_U} < 1 \qquad \text{III-16}$$

which implies that the Uson reads high.

Equations (III-18) and (III-11) can be used to develop a fast-slow leakage rate criterion: Fast leakage will be differentiated from slow leakage by a particular value of L_U (not leakage rage, but measured leakage rate) which will be called critical Uson leakage rate (L_U). Using equation (III-11) to first correct for L_U appearing in (II-18) the requirement that $L_U \to L_{U_c}$, $L(\bar{L}\ (L_U)) \to L_{U_c}$ yields the condition

$$L_{U_c} = \frac{T_S}{T}\left[\frac{T_S}{T_o}\frac{1}{\gamma} L_{U_c} + \frac{PV}{P_S T} x(T_o - T)\right] \qquad \text{III-17}$$

$$L_{U_c} = \frac{\frac{T_S}{T}\left(\frac{PV}{P_S T} x(T_o - T)\right)}{1 - \frac{T_S^2}{T\, T_o \gamma}} = \frac{PV\, x(T_o - T)\, T_S T_o \gamma}{P_S T\,(T\, T_o \gamma - T_S^2)}$$

$$L_{U_c} = \frac{T_S\, PV\, x\, T_o \gamma\, (T_o - T)}{T\ P_S\, (T\, T_o \gamma - T_S^2)}$$

IV. CONCULUSIONS

Simple analytical methods for correcting volumetric gas flow measuring systems have been presented. Results of these analyses applied to the METC facility are summarized in Table IV-1. The analysis is described as linearized first order. "First order" refers to the restriction to fundamental model solution in equation (II-13). The linearization refers to the method of dealing with conduction heating and adiabatic cooling effects separately rather than concurrently as actually happens. This leads to an undetermined error in the analysis.

TABLE IV-1. TABLE OF RESULTS

$\chi = \alpha\,(\beta_1^2 + \gamma_1^2)$ units of hr^{-1}

$\alpha = \frac{k}{cp}\,\beta_1 = \frac{2.405}{a}\,\gamma_1 = \frac{\pi}{\ell}$

$a = .33'$ (radius of pipe)

$\ell = 2'$ (length of pipe)

χ =	$67hr^{-1}$	$11.2hr^{-1}$	$2.8hr^{-1}$	$1.0hr^{-1}$
T =	200°F	600°F	1000°F	1000°F
P =	20 psia	200 psia	600 psia	1600 psia
$60\,\frac{1}{\chi}$	0.9 min	5.4 min	21 min	56 min

[e-folding time]

$L = \frac{T_S}{T_o}\,\frac{1}{\gamma}\,L_U$ $\qquad \gamma = \frac{7}{5}$ (for diatomic gases)

$\frac{T_S}{T_o}\,\frac{1}{\gamma}$	
	$T_S = 68°F$, $P_S = 14.7$ psia
.44	$T_o = 200°F$
.36	$T_o = 600°F$
.26	$T_o = 1000°F$

$$L_{U_c} = \frac{T_S\,PV\,\chi(T_o - T)\,T_o\gamma}{T\,P_S(T\,T_o\gamma - T_S^2)}$$

L_{U_c}	T_o	T	P
.33 SCFM	2000°F	1000°F	1600 psia
.14 SCFM	1400°F	1000°F	600 psia
.37 SCFM	1000°F	600°F	200 psia
.38 SCFM	400°F	200°F	20 psia
.21 SCFM	300°F	200°F	20 psia
.32 SCFM	200°F	100°F	20 psia

Two general methods for determining the gas flow rate in which one can potentially maintain a known uncertainty are computer simulations and empirical determinations. Computer similation can be accomplished directly by means of several specific codes created to handle gas flow. These codes nominally include heat transfer and thermodynamic effects with a wide range of boundary conditions.

The empirical method involves a large number of thermocouples distributed inside the test volume to accurately map the temperature distribution. Rewriting equation (I-2) for n approximately isothermal volumes (V_i) in V as determined by the thermocouple L becomes

$$L = \sum_{i=1}^{n} L_i \qquad \text{IV-1}$$

where L_i the leakage rate in V_i is given by

$$L_i = - \frac{T_S}{P_S} \frac{V_i}{T_i} \left(\frac{\partial P}{\partial t} - \frac{P}{T_i} \frac{\partial T_i}{\partial t} \right) \qquad \text{IV-2}$$

Using n Uson's (one for each V_i) one can rewrite equation (II-15) as

$$L_i = \frac{T_S}{T_i} \left(\frac{PV_i}{P_S T_i} \frac{\partial T_i}{\partial t} + L_{u_i} \right) \qquad \text{IV-3}$$

where L_u is the reading of the Uson in Volume V_i. Substituting equation (IV-3) in (IV-1) gives the total leakage rate. The accuracy of this method will be extremely sensitive to the time response of the thermocouples used to map the temperature distribution.

Although potentially very accurate, the computer and empirical methodologies described are costly and time consuming. The analytic approach developed in sections II and III provides quick and easy results while sacrificing accuracy. Thus, it is recommended that the linearized first order analytical techniques be used as an initial indicator of system accuracy. Based on those results one can then evaluate whether or not to undertake a more sophisticated and costly approach.

APPENDIX
REFERENCES

1. R.E. Wendt, Jr., Flow Measuring Devices Part Two, Vol. 1.
2. Final Report Valve Leakage Error Analysis Valve Dynamic Test Unit.
3. Prototype Lockhopper Valve Test Plan - FE 2213-016-09R1-MERC
4. SOA Lockhopper Valve Test Plan METC 78/2.
5. Uson Model 300 Series Leak Detector Manual.
6. SOA Valve Testing and Development Program Test Procedures VDTU MERC 78/5.
7. METC Interim Report No. 192.
8. METC Interim Report No. 407.
9. H.S. Carslaw and J.C. Jaeger, CONDUCTION OF HEAT IN SOLIDS, Oxford University Press (1959).

A SYSTEMS-LEVEL DYNAMIC MODELING APPROACH FOR THE TVA 20,000-TPD COAL GASIFICATION FACILITY

D. Berkowitz, T. Greenlee, M. Ringham, and V. Sumaria

JAYCOR, 11011 Torreyana Road, San Diego, California 92122

ABSTRACT

A top-down, systems-level, lumped-parameter, state-variable modeling approach that has been applied to the TVA 20,000-TPD gasification plant is discussed. This approach, which is based on first principles, results in a model that is mathematically characterized by a system of first-order nonlinear ordinary differential equations. These equations, which represent the entire plant with a balanced level of detail in each subsystem, are suitable for developing digital and hybrid simulations. The resulting simulations can be used for systems engineering tasks such as (1) determination of plant operating profiles, (2) investigation of failure responses and propagation, (3) determination of measurement and control strategies, (4) analysis of performance margins, (5) simulation of overall facility operation, and (6) analysis of system interactions.

1. INTRODUCTION

The need to understand and moderate plant transients and component interactions induces the study of systems engineering issues. A model/simulation-based approach can be a cost-effective means for gaining the required understanding of such issues provided the model level of detail is balanced with respect to the issues to be resolved, the cost of model development, and the cost of simulation operation. This paper describes a top-down approach to model/simulation design and development that can achieve this balance. Major steps in this approach are:

- Specification definition and review
- Model/simulation-design
- Model/simulation development
- Verification/validation

These steps are detailed in Section 2.

2. DETAILS OF THE APPROACH

2.1 SPECIFICATION DEFINITION AND REVIEW

The initial step in any top-down model development approach is the development of a specification for the model. The main input to this specification is a listing of the intended uses of the model. Typical systems engineering issues pertinent to a gasification plant that end up defining uses of the model are:

- Determination of turndown/turnup capability of plant in response to variations in demand for product gas.
- Evaluation of plant operation with failed or partially failed components.
- Determinaton of optimal startup/shutdown and operating point transition strategy for plant.
- Examination of proposed measurement and control strategies.
- Examination of stability characteristics and transient operation at off-nominal design conditions.

Once model uses have been identified, specification development focuses on the baseline process design. Typically, gasification plant baseline design is described by process and control or process and instrumentation diagrams that define process components, component connections, tentative control strategy, and steady-state constituent energy/mass balances.

Using the list of uses, the process and control diagram, and an understanding of the function and operation of each subsystem, the model developer synthesizes a specification for model content and level of detail. Often this specification is written up to ensure agreement between the model requestor and the model developer.

2.2 DYNAMIC MODEL/SIMULATION DESIGN

In this step, the model specifications developed (Section 2.1) are converted into model design guidelines and further detailed prior to actual model/simulation development. The objectives (or function) and constraints of each system/component in the facility are reviewed. The relationship of systems/components to one another is also assessed in light of the intended model uses. Some systems/components may be dropped from further consideration at this time

if their function is secondary to main process objectives or usage plans. A refined process and control diagram is constructed that includes only those systems/components relevant to the intended usage of the model. A consistent and convenient nomenclature is selected and a causality diagram is constructed that reflects the flow of information in the model. System state variables, together with other variables and constraints, are identified throughout the facility. Segments of the facility that can be conveniently modeled (in light of causality relationships) are defined as partitions, which may be a single system/component or a group of the same.

State variable selection is a crucial part of model design since it relates intended model usage, required level of model detail, model development costs, and simulation running costs. The following statements motivate use of state-variable or lumped-parameter models and define their characteristics.

The most detailed and accurate simulation of a coal gasification facility could be based on distributed-parameter representations of the processes occurring in its systems/components. These representations are characterized mathematically by partial differential equations (PDEs). Unfortunately, a facility simulation consisting of coded PDEs is costly to run, and is typically much more detailed than is required for systems engineering tasks such as (1) determination of plant operating profiles, (2) investigation of failure responses and propagation, (3) determination of measurement and control strategies, (4) analysis of performance margins, (5) simulation of overall facility operation, and (6) analysis of system interactions. Such detailed simulations can serve as excellent links to experimental data for verification and validation.

A simulation having a reasoned and adjustable level of detail is required for systems engineering tasks. It must be based on the application of engineering judgment (appreciation of intended model usage, significant physical effects, and required solution time) and formal manipulation of distributed-parameter representations.

Appropriate models/simulations can be designed and developed by approximating the distributed-parameter representations with lumped-parameter state-variable representations, which are mathematically characterized by systems of first-order nonlinear ordinary differential equations (ODEs). The ODEs are developed by volume-averaging the PDEs over "control volumes" that are defined by considering (1) regions of the facility with significant mass, energy, and

momentum storage, (2) anticipated model usage, and (3) validity of assumptions required in the averaging process.

The approach described in this paper advocates development of lumped-parameter state-space models for gasification facilities. The facility model is developed by applying the concepts of this volume-averaging approach to all systems of the facility simultaneously. The resulting system of ODEs will be characterized by the vector forms

$$\dot{X} = f(X,U,P), \qquad Y = g(X,U,P) \ ,$$

where

X = a vector of state variables (usually analogs of mass, energy, or momentum such as density of the analog of mass storage in a tank, enthalpy as the analog of energy storage in a fluid, or temperature as the analog of energy storage in metal, flow as the analog of momentum storage in a pipeline; other choices of state variables are made as required).

U = a vector of process control inputs such as valve positions or gas flow rates.

P = a vector of parameters such as volumes, flow resistances, heat transfer coefficients, or chemical properties.

Y = a vector of process output variables such as gas pressure, process flow rates, etc.

Values of the state vector (X) vary with time, as indicated by the differential equation. At any instant of time, this vector is the minimal set of data (when taken together with the input vector U) that uniquely determines the future solutions of the system of equations. The state variables reflect the "history" or "memory" of the system, and as such represent a "starting point" for solution of the system of equations. When the input and parameter vectors are known, all other process variables are determined from the state variables.

The success of this approach to facility modeling has been previously demonstrated in several modeling efforts conducted by JAYCOR staff members. The approach yields overall facility simulations with the appropriate balance between usage requirements and system/component model detail.

2.3 MODEL/SIMULATION DEVELOPMENT

This step focuses on the development of state-variable equations and algebraic equations for the systems/components of the various partitions defined for the facility. These equations will arise from application of the volume-averaging results to various control volumes. The system/component partitions referred to in the first step (Section 2.1) are then formed by collecting appropriate equations, which will generally be systems of nonlinear ODEs and nonlinear algebraic equations requiring parameter values and initial conditions. These values and conditions will be determined by calibrating the model to a set of steady-state design conditions (e.g., full-load operation).

Simulation languages are typically used to implement the solution of the equations representing the facility. System/component partitions can be coded in a fashion that relates modular sections of the code directly to the process flow diagram. This makes the simulation easily readable and self-documenting. Once the simulation language statements are written, the coded system/component partitions are loaded and the simulation language translates the statements into sorted FORTRAN, which is executed to produce desired transient solutions.

After each system/component partition of coded equations has been debugged, analysis and verification can be performed. The inputs for each partition are subjected to step functions and solved. Linear models of the partition are produced by a Jacobian generating subroutine, which allows the user to bring a system of nonlinear ODEs to steady state (using a Newton-Raphson procedure) and compute matrices A, B, C, and D for the vector matrix forms

$$\dot{X} = AX + BU \ , \qquad Y = CX + DU \ .$$

The matrices A and B can be used to check controllability (coupling of inputs to states). The Jacobian generating routine also computes the eigenvalues of A, which can be used to analyze the step response of the partition with respect to a modal decomposition. These linear analysis tools can also be used to investigate the reasonableness of the partition and overall plant simulation models.

Finally, coded system/component partitions can be integrated into the facility model. Causality relationships for each partition are checked with respect to all other partitions with which it interfaces. Boundary conditions

of the partitions are matched with each other and the partitions sequentially assembled into the facility model. Stability checks and eigenvalue analyses are made at every stage of interconnection. This method is preferable to the alternate method of complete model assembly with subsequent stability checks, in which case it is more difficult to isolate errors or problem areas. Stepwise integration permits examination of system/component interactions and identification of potential stability or dynamic response problems as individual partition eigenvalues are compared with combined partition engenvalues.

Experience obtained in the design/development of similar large-scale lumped-parameter dynamic models/simulations has shown that the integration process can enhance understanding of the physical process being modeled. This enhanced understanding often suggests alternate causality or modeling strategies that increase model efficiency.

2.4 VERIFICATION/VALIDATION OF DYNAMIC MODELS AND SIMULATIONS

This step plays a major role in development of realistic and appropriately detailed models. It is the basis for determining the refinements required to change initial models (developed without the aid of an operating simulation) into final models (models accepted as adequately representing process behavior to the degree required for the intended usage). Verification/validation procedures are performed to develop confidence in a model or simulation's capability to predict the behavior of the process modeled.

Verification of the models/simulations developed in the previous step (Section 2.3) is accomplished by ensuring that model equations were properly developed, coded, and solved. Knowledge of baseline design steady-state mass and energy balances will allow verification of static model/simulation accuracy. Once this is accomplished, a partial verification of dynamic accuracy is produced by recognizing that dynamic response generally depends on physical quantities such as storage volumes and metal masses, which are readily determined static design parameters. If the design has not been finalized but these parameters are known to lie in some interval of values, a parameter sensitivity study using the dynamic model can reveal the probable variation in transient response characteristics.

Model/simulation validation refers to the process through which the model/simulation becomes accepted as a valid representation of plant performance by comparison with actual facility or component data. The validation process

involves small adjustments of model constants and parameters within the region of uncertainty associated with spatial averaging, and simplifying assumptions built into the model. Often, quantitative information may be limited to expected steady-state heat balances or performance data, and to data scaled or extrapolated from other facilities of the same size or type. This data can be used to partially validate component/system models. If data for several operational conditions is available, data for one load level can be used for calibration and the remaining data can be used for validation.

Validation of dynamic characteristics is less exact in a design project since transient data is normally unavailable. Yet state-space models once validated for steady-state response are usually accurate for dynamic response because dynamic response generally depends on physical quantities such as storage volumes and metal masses. If the model equations are functionally correct, transient validation gains credibility directly from steady-state validation.

3. CONCLUSIONS

A top-down approach to developing systems-level models for gasification plants has been described. The approach provides for developing a facility model with a balanced level of detail that is consistent with the intended usage. Model detail, simulation development costs, and simulation running costs are controlled by allowing the modeler to define the appropriate level of representation via a lumped-parameter modeling method based on the volume-averaging of distributed parameter relationships.

Tuesday Afternoon, June 9, 1981

Session B - Process Control - Part 2

DYNAMIC RESPONSE OF AN OXYGEN-ENRICHED MHD-STEAM POWER PLANT WITH CONVENTIONALLY-BASED CONTROL

D. A. Rudberg,* J. C. Shovic, D. A. Pierre and J. A. Evans
Montana State University
MHD & Energy Research
119 Roberts Hall
Bozeman, Montanta 59717
(406)994-2500

ABSTRACT AO78

A first-principle dynamic control system model has been developed for simulation of complete, typical MHD-steam plants, and for control system design and evaluation for such plants. The particular configuration modeled has features consistent with current trends in ETF concepts. The oxidant is atmospheric air blended with oxygen to 35 percent mole fraction oxygen, and it is delivered by a shell-and-tube recuperative air heater at nominal 1100-1200F (867-922K). The main electrical turbine-generator, the oxidant compressor turbine, and the oxygen separation plant turbine are all steam driven. The main turbine set is a reheat configuration operating at 1815 psi/1000F/100F (12.51 MPa/811K/811K). Steam for the oxidant compressor turbine and the oxygen separtion plant turbine is obtained from the hot reheat heater under normal operation. For start-up, shut-down, or abnormal conditions, oxidant compressor steam and oxygen separation plant steam are obtainable as throttled flow from the main steam header or from an auxiliary steam generator. Nominal thermal input is 300 MW. Electrical output is 108.0 MW with 51.5 MW MHD power and 56.5 MW main turbine-generator power at 100 percent of design.

Responses of the plant model to variations on two basic controls strategies are presented. One control is labeled "MHD-following" because of its relation to boiler-following control. With ramp demand inputs, such control is characterized by a wide range of load following ability (from poor to excellent, depending on oxidant compressor controller gains), relatively large internal plant perturbations, and a tendency toward instability when gains become high. The second strategy is related to turbine following control, and because of the prominence of the MHD topping cycle, has been labeled "MHD-leading". Response to ramp demand changes is characterized by moderate load following capability, moderate internal plant peturbations, and a generally stable nature.

Wide-range sweeps of main turbine and oxidant compressor turbine controller parameters under MHD-leading and MHD-following control strategies are made, yielding a family of responses for each of the control strategy variations. Typical responses from each family are selected for display and analysis. Points of high demand or stress under various control strategies are identified and implications for component design are discussed.

*Presenting Author

PERFORMANCE ANALYSIS OF THE MHD STEAM COMBINED CYCLE INCLUDING THE INFLUENCE OF COST

G. F. BERRY
C. B. DENNIS

ARGONNE NATIONAL LABORATORY
ARGONNE, ILLINOIS

Abstract

An important function of system analysis is to conduct parametric investigations of system-dependent variables in order to determine their influence on system efficiency and cost. To accomplish this task, a comprehensive computer code has been developed that can be used to analyze or simulate system behavior. The computer code is extremely flexible and robust. Many different systems have been evaluated, including open-cycle MHD power plants, closed-cycle liquid-metal MHD systems, fusion plants, community energy systems, optical lens problems, and coal-fired power plants. This paper presents the results of a parametric study of an open-cycle MHD power plant.

Changes in efficiency and cost of electricity with variations of combustor heat loss, magnetic field intensity, air preheat temperature, compressor pressure, diffuser efficiency, and plant size will be described and discussed. Comparisons of results from parametric studies and from multiple parameter optimization will also be presented.

Of particular interest will be a discussion of the features of the systems code that make it unique, and others that make it efficient and robust. Also, the principle of recursiveness in systems analysis will be discussed.

INTRODUCTION

One objective of the MHD System Analysis project at ANL has been the determination of the sensitivity of the system performance to variations in specific topping cycle parameters of the MHD-steam plant. This goal has been

achieved, at least at the level of first-order component models. To conduct these parametric investigations, a comprehensive computer code has been developed, which will analyze and simulate an MHD plant for any number of different configurations, automatically holding constraints so as to perform either sensitivity studies or optimizations on the particular configuration of interest. A summary of selected results that have been generated is presented here.

The focus of attention in ANL/MHD System code development has been the overall structure and philosophy of systems simulation. Because of the need for quick simulation of changing power plant configurations and designs, a method of system representation was sought that would allow easy changeover from one plant configuration to another. Careful planning and innovative programming led to the formulation of a network of codes [1,2,3], modularized to allow easy addition or replacement of specific component models, property libraries, or optimization techniques, as well as to provide a simple, user-oriented format for system set-up and solution. The executive code (or driver) contains no identifiers related to any particular physical system; it is used to control the solution of a system analysis problem and to perform optimization when required. To connect this control section and the specific power plant component models, an interface module is needed. Here, all information is passed by streams of data (i.e., steam, air, gas, coal, power, costs, etc.) between models, which data are selectively modified, as required, by each model. Property data (unique to the fuel being consumed) are not identified within the models of the MHD power plant components, but, instead, are provided in additional, interchangeable utility modules. This generalized, modular network, therefore, does not restrict the systems analyst to a single plant design, or even type of design.

During this initial phase of MHD System code development, in which the philosophy of system simulation has been formulated, some of the mathematical models used have been simple, although reasonably accurate. In order to develop and demonstrate the capabilities of the ANL/MHD System code concept--generalized recycle construction, parameter sweeps, optimization, graphics, free-form input and formatted output, file storage and recovery, user-tested diagnostics, component model checkout and debugging--less-detailed component

models have been employed. However, in conjunction with developing and programming the MHD System code, the development of sophisticated models that simulate the individual power plant components in greater detail is continuing. The first-stage models now used are, in general, simplified versions of the relationships promulgated in the more-detailed and complex component models, many of which have been or are being developed. In fact, this first phase of MHD System code development, which is to demonstrate that it is functioning and particularly useful as a systems analysis tool, will be followed by a second phase that will incorporate these more-detailed component models as much as possible into the MHD System package. For the present, however, it is advantageous to demonstrate certain capabilities of the ANL/MHD System code with the first-order models.

It was considered essential to extend the analysis beyond studying the sensitivity of system efficiency to component performance. One obvious alternate point of comparison is the system cost. However, if the results are to be meaningful, making the cost of electricity (COE) the desired objective function requires reasonably accurate estimates for the component costs, and the costs calculated by the ANL/MHD code are validated by positive agreement [4] with the results of other designs. Further, any cost algorithm included in such a systems analysis as that ongoing at ANL -- in which a very broad range of system parameters is under study -- must be so formulated as to be valid across a large number of parameters. With this concept in mind, relationships for estimating the installed costs of each major system component were developed. However, to coincide with the first-stage concept of component simulation used during development of the MHD System code and, also, for the present demonstration, first-order representations of power plant performance and economics have been programmed. One area of the second-stage model development mentioned earlier is more detailed representation of system objective functions that juxtapose more sophisticatedly the trade-off between system performance (efficiency) and cost, which is so vital to system optimization. The present study illustrates the need for the general form of the objective functions in determining system efficiency and COE for parameters varying over a wide range of interest, by examining the results of the parameter trade-off study presented herein. As will be shown, the optimum plant

may be different when based on minimum cost of electricity than when based on maximum thermodynamic efficiency.

DESCRIPTION OF THE MHD/STEAM POWER PLANT

The MHD/steam plant considered in this study is illustrated in Fig. 1. After proper preparation, Illinois #6 coal and compressed air preheated to 2500°F (1640 K) are supplied to the MHD combustor. The combustor is assumed to operate fuel-rich, so as to reduce nitrogen oxide production while yielding a higher flame temperature (to enhance electrical conductivity in the combustion gas). Alkali-metal seed, a potassium compound, is added to the combustion gas of nominal 4600°F (2810 K) temperature.

The flow is expanded at a high-subsonic Mach number through the MHD channel. Because the electrical output of the MHD generator is direct current, it is converted to alternating current in an inverter system, and can then be supplied to a power grid. Beyond the generator, the combustion gas is diffused, then it enters the radiant boiler section of the steam generator. The steam-cycle feedwater is used to cool the combustor, the MHD generator, and the diffuser.

In the radiant boiler, the combustion gas is further cooled, and secondary air is then added to complete the combustion of the coal. The gas must remain in the radiant boiler long enough for the concentration of nitrogen oxides to approach its acceptable equilibrium level. Typically, this residence time, above 3000°F (1920 K), is two seconds.

From the radiant boiler, the exhaust gas flow enters the regenerative, high-temperature air heater system, then continues downstream to the secondary furnace. This furnace incorporates the steam superheater, the steam reheater, and the low-temperature air heater that heats air to approximately 1400°F (1030 K).

The combustion products are routed through the economizer and the electrostatic precipitator before being exhausted through the stack. The alkali-seed compounds are recovered in the precipitator and the heat exchangers.

Several components that do not greatly influence the over-all system performance have been eliminated from consideration here (their costs are accounted for). The seed make-up and recovery units, as well as the coal handling system, fall into this category. A second significant simplification of the system model is the steam turbine/compressor arrangement; conceptually, the entire system has been replaced with a two-stage reheat system, the power needed to drive the compressor simply being subtracted from the gross power produced by the steam turbines. No regenerative feedwater heating is assumed. The design details of providing cooling towers for the condensers have also been neglected.

ANL/MHD SYSTEM PARAMETER STUDY

Having arranged the input to model the MHD-steam plant depicted in Fig.1, the system code was used to investigate the sensitivity of the plant thermodynamics and cost to several of the more important parameters.

The initial parametric study investigated two performance parameters: cycle thermodynamic efficiency and cost of electricity for change in air preheat temperture. The results of the investigation are represented in Fig. 2. As expected, the cycle efficiency improves with increase in combustor pressure and air preheat temperature. The optimum combustor pressure predicted for this system configuration with a 2500°F (1640 K) preheat temperature is more than 8 atm (0.8 MPa). As expected, increasing the preheat temperature yields maximum efficiency at higher combustor pressures. The results are different, however, if the optimization concerns minimizing the cost of electricity as computed by the cost algorithm. These results show that the cost of power reaches a minimum where the combustor pressure is less than 8 atm, with the lowest COE occurring at the highest air preheat temperature.

The system sensitivity investigation also studied the influence on power costs of system size, field strength, combustion heat loss, and diffuser pressure recovery coefficient. The directly-fired preheater system of Fig. 1 was again chosen as the configuration of a full-size plant. Parametric computations were run, with the combustor pressure as the principle indepen-

dent variable. The base plant was assumed to have a 2000-MW(t) input, a preheat temperature of 2500°F (1640 K), magnetic field strength of 5 T, combustion heat loss of 5%, diffuser pressure recovery coefficient of 0.6, and steam bottoming plant efficiency of 41%. Variations in performance were computed around this plant, and the results were plotted, normalized to the base plant performance.

Several important constraints were maintained automatically by the code. In particular, the current density was established at 1 A/m^2, and the diffuser exit pressure was set to 1.14 atm (115 kPa). The recycle mechanism of the executive code is the procedure used to maintain these constraints. The exit temperature of the radiant boiler was held to 1900 K, in accordance with present practice, to insure that the slag has condensed on the boiler walls and the seed remains in particulate or vapor form. The temperature of steam leaving the radiant boiler was held at 670 K (this establishes the size of the steam plant). A supercritical steam plant was used in all cases.

Figure 3 presents results for the base case, and indicates the sensitivity of the COE and thermal efficiency to variations in field strength and combustor pressure. The thermal efficiency of the base case is approximately 49.3%, and the cost of electricity is approximately 47.0 mill/(kW•h). The maximum efficiency occurs at combustor pressures greater than 8 atm; the minimum cost of electricity at less than 8 atm.

The following three figures are a graphic display of the sensitivity of MHD power plants to diffuser efficiency, combustor heat loss, and plant size for varying combustor pressures. The effect of diffuser efficiency on both cost of electricity and plant efficiency can be determined by comparing the appropriate members of this set. In particular, in Fig. 4, the maximum cycle efficiency for the full-size, 2000-MW(t) plant with 2500°F preheat air, is shown to increase one percentage point when diffuser efficiency is increased from 50% to 70%. Figure 6 indicates that the maximum cycle efficiency will increase approximately one percentage point if the field strength is held constant and the size of the plant is increased to 3000 MW(t) from 1000 MW(t). Comparable data can be abstracted from the other curves presented in these figures.

ANL/MHD SYSTEM OPTIMIZATION

One of the most valuable services that can be provided by a system modeling program is optimization, in which a given objective function can be minimized by varying chosen parameters. However, this capability is most difficult to provide. In recent years, much numerical analysis has been performed in regard to the theory of nonlinearly-constrained optimization and its application to specific algorithms, and has been followed by empirical studies of the implementation of those algorithms. Nevertheless, the optimization process has not been fully automated for all physically-reasonable, few-parameter problems, even where the objective function is smooth and its derivatives are given directly by the model. A general system optimization program is a more difficult problem to formulate, in that derivatives are not usually provided by the model, and must be obtained -- if they exist -- by difference approximations. Furthermore, the objective function may be discontinuous or excessively noisy because of truncation error. Nevertheless, a system optimizer should be capable of monitoring the degree of smoothness of the desired objective function and selecting the appropriate optimization algorithm, changing from one to another as it updates the information on the progress toward a solution. The ANL/MHD System optimization package is just that -- a large code with rudimentary intelligence, managing several sophisticated optimizers called as required, any one of which is capable of producing the required optimization for specific types of models and objective functions.

After the sensitivity analysis, which demonstrated the effectiveness of the ANL/MHD System code by investigating the effect of several key parameters on an OCMHD power plant performance, an optimization study was performed over primarily the same key variables [5]. Again, using the configuration depicted in Fig. 1, optimizations were performed to minimize the objective functions cost of electricity and system inefficiency, for a 2000-MW(t) plant. The independent parameters varied to determine the optimum were combustor pressure, combustion air preheat temperature, combustor heat loss, the B field of the MHD generator, channel load factor or resistance, and diffuser pressure recovery coefficient. The results in the table below demonstrate the usefulness of system analysis in general but, more particularly, demonstrate

the need for more sophisticated system objective functions. The difference between the two designs lies in the effect of the optimized parameters on size and efficiency of the MHD channel and, hence, on size and cost of the magnet. The similarity between the two designs is a direct result of the constraints imposed on the optimization: maximum combustion air preheat temperature of 2750°F, minimum combustor heat loss of 4%, maximum average B field of 6 T, and a maximum diffuser pressure recovery coefficient of 0.70.

Optimum Plants Based on
Cost of Electricity and System Efficiency
with Channel Constraints

	Optimized Objective Function		
	Reference Case	Efficiency	COE
Thermodynamic eff, %	48.2	52.2	51.8
COE, mill/(kW•h)	47.26	45.41	44.82
Preheat temp, °F	2500	2750 (max)	2750 (max)
Diff press. recovery coeff	0.60	0.70 (max)	0.70 (max)
Channel load factor	0.8	0.853	0.794
Avg B field, T	5.0	6.0 (max)	6.0 (max)
Comb heat loss, %	5.0	4.0 (min)	4.0 (min)
Comb pressure, atm (10^5 Pa)	7.0	8.1	8.1
Channel length, m	20.4	25 (max)	20
Channel Hall field, V/m	1881	2118	2472
Channel power, MW	568	713.6	702.0
Req'd. compressor power, MW	174	190.1	190.4
Net electrical power, MW	965	1043.6	1036.5

Although optimization is a valuable analytical tool for evaluating MHD power plants, it cannot be used indiscriminately without a thorough evaluation of the results. In the first-order level objective functions now used for plant efficiency and cost of electricity, few implicit constraints exist. They must be added explicitly as in the numerical constraints for the key variables mentioned. This is the difficulty in performing design optimization: it is not clear which parameter to constrain, nor what value to assign to that constraint. A plant designed for maximum efficiency alone places an inadequate limit on the length of the channel, for example, so that an ex-

tremely long, although very efficient channel would be formulated for the optimized design. The 25 m channel length found for the efficiency optimization was the maximum allowed in the optimization study. The limit of 25 m was set, in part, because a 1-D channel model was used with no provisions for boundary layer separation, a phenomenon that would, presumably, be represented in a more realistic model. Also, studies involving longer channels indicated only minor improvements in efficiency for a major increase in channel length. Clearly, as an objective function, cost of electricity which includes plant efficiency in its formulation, is a step in the right direction. (The most efficient, yet cost-effective channel was found yielding the minimum cost of electricity under the other constraints imposed.) However, an objective function should also include the effects of component reliability and maintainability, as well as efficiency and cost. These factors are among those considered in the second-stage objective function analysis now in progress.

CONCLUSIONS

The study supports the conclusion that, assuming channel conditions are unconstrained, a plant designed for maximum thermal efficiency will be operated at a different set of parameters than one designed to provide a minimum cost of electricity. It is clear that consideration of minimum COE may be more important than maximum efficiency in postulating designs of power plants.

Optimization is a valuable analytical tool for evaluating MHD power plants. However, it cannot be used indiscriminately without thorough evaluation of the results. An objective function based on cost is more meaningful than an objective function based on efficiency, although other factors, including component reliability and maintainability, must also be considered. To meet this demand, more emphasis must be directed toward developing superior cost algorithms and more elaborate economic models as one aspect of a developing system objective function analysis.

REFERENCES

[1] Cook, J. M., "User's Guide for GSMP - A General System Modeling Program," ANL/MHD-79-11, Argonne National Laboratory, Argonne, IL, November, 1979.

[2] Dennis, C. B. and Berry, G. F., "User's Guide for the GSMP/OCMHD System Code," ANL/MHD-80-7, Argonne National Laboratory, Argonne, IL, December, 1980.

[3] Geyer, H. K., "GPSAP/V2 with Applications to Open Cycle MHD Systems," ANL/MHD-80-15, Argonne National Laboratory, Argonne, IL, January, 1981.

[4] Berry, G. F. and Dennis, C. B., "Performance Analysis of the MHD-Steam Combined Cycle, Including the Influence of Cost," ANL/MHD-80-3, Argonne National Laboratory, Argonne, IL, August, 1980.

[5] Berry, G. F., Cook, J. M., and Dennis, C. B., "Application of Polyalgorithmic Optimization to MHD Power Plant Design," IASTED, SFE-81-85, San Francisco, CA, May 20-22, 1981.

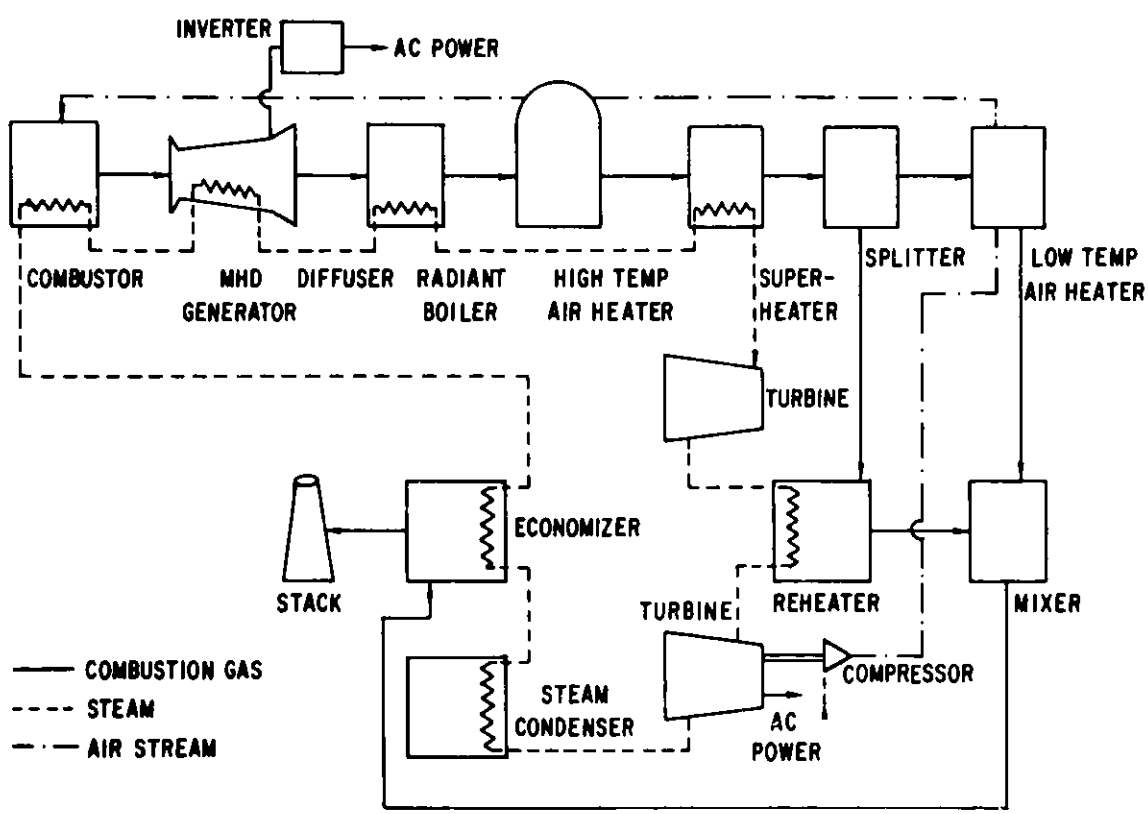

Fig. 1 MHD Power Plant Configuration

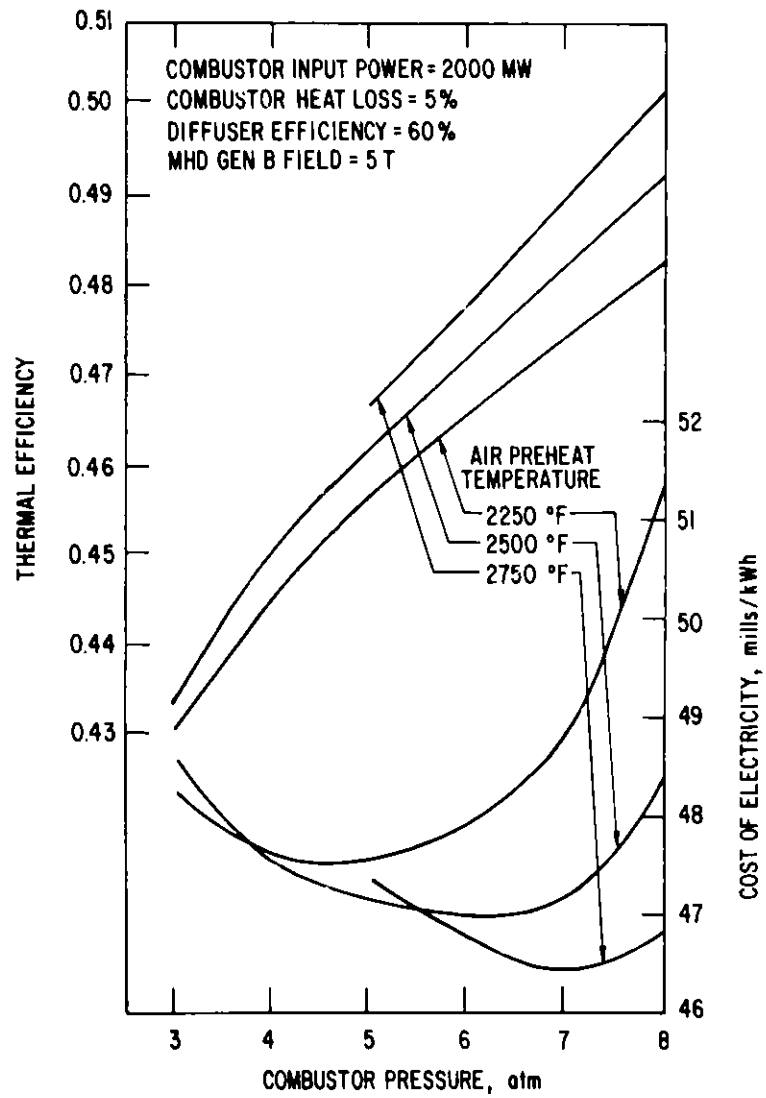

Fig. 2 Thermal efficiency and cost of electricity vs combustor pressure for combustion air preheat temperature

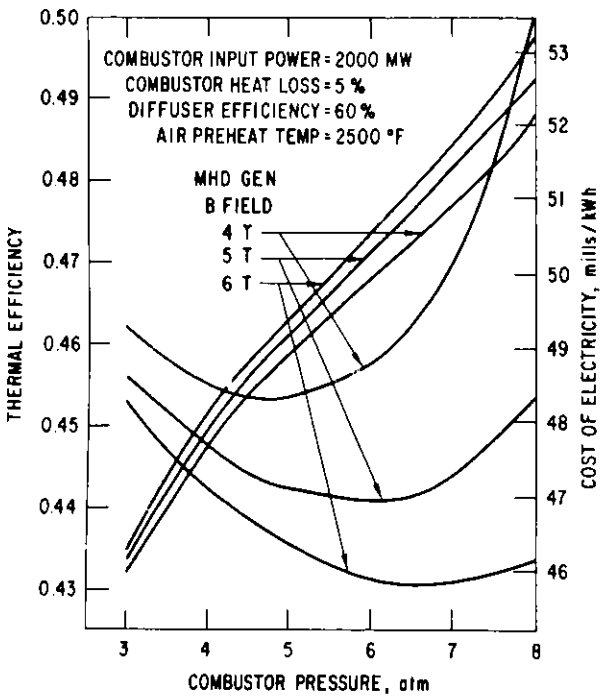

Fig. 3 Change in EFF and COE with Comb Pressure and Channel B Field

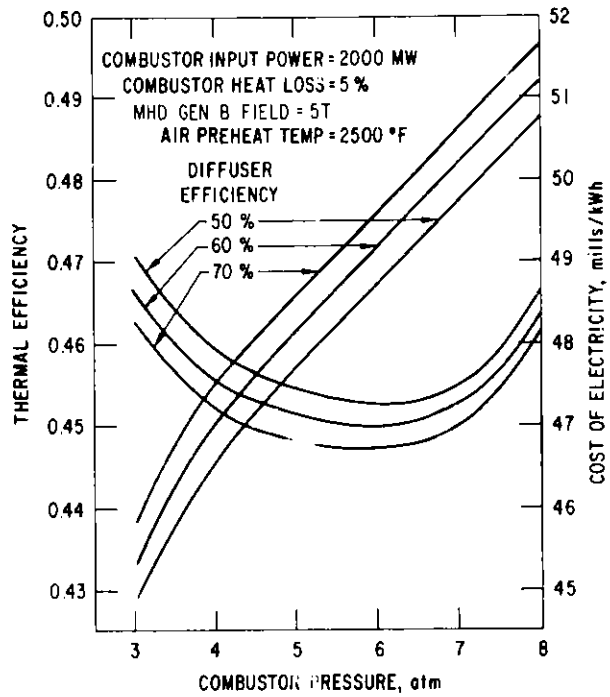

Fig. 4 Change in EFF and COE with Comb Pressure and Diffuser Efficiency

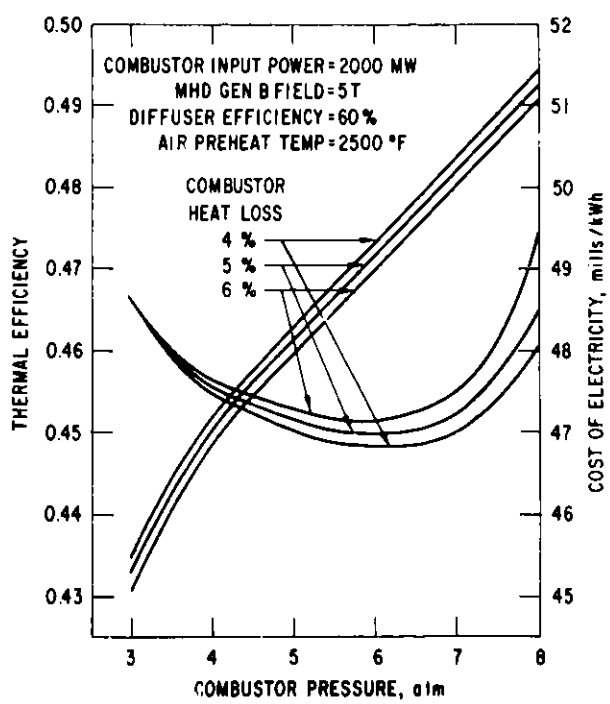

Fig. 5 Change in EFF and COE with Combustor Pressure and Heat Loss

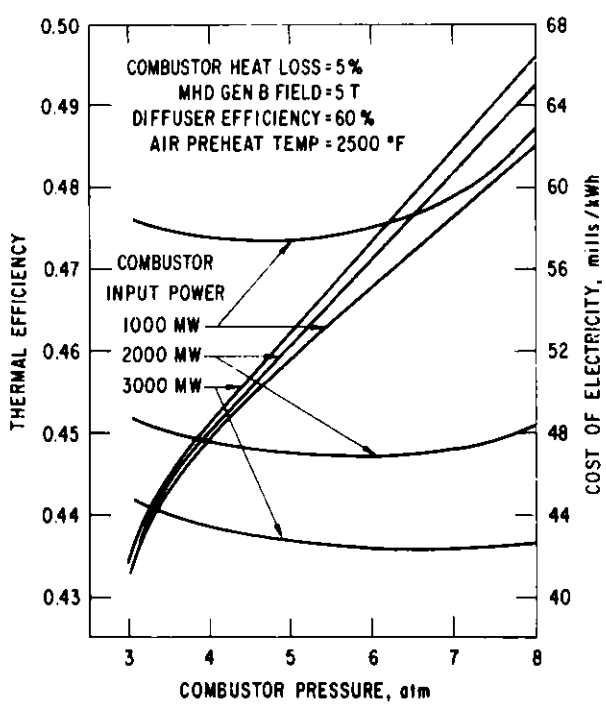

Fig. 6 Change in EFF and COE with Combustor Pressure and Input Power

TRANSIENT MODELING OF FROTH FLOTATION AND VACUUM FILTRATION PROCESSES*

C. H. Brown, Jr.
G. O. Allgood
G. S. Cauright
W. R. Hamel
Chemical Technology Division
Oak Ridge National Laboratory
Oak Ridge, Tennessee

ABSTRACT

Transient models of the froth flotation and vacuum filtration processes as applied to fine-coal beneficiation are presented. The models consist of sets of simultaneous ordinary differential and algebraic equations which were derived based on the principles of conservation of mass. The froth flotation process model was developed by drawing the analogy between a single flotation stage and a continuous stirred-tank reactor. Flotation kinetics were described by a model that is first order in displacement of solids concentration from equilibrium. The kinetic parameters were obtained by analysis of published experimental data. The vacuum disc filter model was developed by subdividing the filtration cycle into filtration, drying, and blowoff. The filtration and drying portions of the operating cycle were described by classical representations of these two unit processes. Equations that describe the filter vat dynamics are also presented, thus completing the mathematical representation of filtration.

INTRODUCTION

The application of modern process control technology in the coal preparation industry has become more important due to the projected increase in coal usage and costs, the stiffer environmental regulations, and the fact that available coal generally requires more stringent cleaning than in the past. Mathematical analysis of coal preparation processes facilitates detailed studies in the areas of process control and economics and evaluation of existing and potential instrumentation devices.

In a typical coal preparation plant, shown schematically in Fig. 1, run-of-mine coal is initially crushed to a maximum size of 10 cm (4 in.). This coarse material is subsequently split, using a combination of vibrating screens and cyclones, into a coarse fraction, 10 cm by 0.6 cm (4 in. by 1/4-in.); a medium size fraction, 0.6 cm by 0.06 cm (1/4-in. by 28 mesh); and fine coal that is less than 0.06 cm in diameter (28 mesh by 0). Cleaning operations used in the coarse coal circuit are jigs and heavy media washers.

---

*Research sponsored by the Pittsburgh Mining Operation, Coal Preparation Division, U.S. Department of Energy, under contract W-7405-eng-26 with the Union Carbide Corporation.

Typical separation steps used in the medium coal circuit are coal washing tables (e.g., Deister tables) and cyclones (either heavy media or water only). The fine coal circuit consists of froth flotation followed by filtration to effect drying of the floated coal. Plant water balance closure is provided by a gravitational thickener which removes suspended solids from the process water, thus enabling recycle of the cleaned water.

The remainder of this paper presents a summary of the development of dynamic models for the fine coal cleaning processes of froth flotation and clean coal drying via vacuum filtration. A more complete discussion of the dynamic model development, implementation, and results may be found in Ref. 1.

FINE COAL CIRCUIT

A schematic diagram of the fine coal circuit in a typical preparation plant is shown in Fig. 2. The feed slurry is treated with reagents to promote stable foaming and preferential attachment of coal particles to air bubbles. The froth flotation process partitions the incoming slurry into a clean coal (froth) stream and a tailings (mineral rich) stream. The clean coal stream is dried in a vacuum disc filter, producing dry coal and aqueous filtrate. The tailings from the froth cell are treated with caustic soda to adjust the pH and polyacrylamide to promote flocculation of the suspended solids in the gravitational thickener. Clarified water from the thickener is recycled to the front end of the process, and the thickened refuse is dried in a vacuum filter.

FROTH FLOTATION

Froth flotation is a unit operation involving the segregation of the solid component in a slurry into a valuable concentrate and a less valuable tailing through the selective attachment of air bubbles to the valuable component. The process requires the use of fine material, typically less than 250 μm, and the addition of chemicals to the feed slurry to promote frothing and attachment of the particles. A common terminology describing the groups of chemicals used has become well established.

A frother is a substance that dissolves in vigorously aerated water to produce a stable foam. An alcohol such as methyl isobutyl carbinol (4-methyl-2-pentanol) is commonly used as a frother in the coal industry.

A collector, also called a promoter or coater, is an agent added to the feed slurry to promote the preferential attachment of the coal particles to the air bubbles. Fuel oil is a commonly used collector in coal flotation.

The standard flotation machine is a large stirred vat (shown in Fig. 3). The feed slurry is introduced at one end of the cell, froth is removed at the sides by rotating paddles, and tailings exit at the opposite end. The impeller provides vigorous agitation of the slurry by drawing air into the cell and dispersing it from a submerged vortex chamber as minute bubbles.

Cell volumes vary according to the tonnage of material to be treated, but they generally range from 1.1 to 28 m^3 (40 to 1000 ft^3) with an average size of 6 to 14 m^3 (200 to 500 ft^3) in the coal industry. Froth flotation equipment is usually built and operated as multiple units, with a typical coal beneficiation plant utilizing 5 to 6 units.

The only process control instrumentation now utilized with froth flotation is for liquid-level control. The liquid level is sensed by a differential pressure cell installed at the tailings exit, with one half immersed in the liquid and the other half at atmospheric pressure. This level controller signals a pneumatic actuator that operates valves or an adjustable weir plate to maintain a fixed liquid level in the froth cells.

The overall control of the froth flotation operation in coal beneficiation plants depends entirely on the experience of the fine coal circuit operator. He visually checks the froth and tailings output of the cells and manually adjusts the reagent addition rates.

Dynamic Model

In developing the dynamic model of the flotation process, the following assumptions were made:

1. The operation of a series of froth cells is analogous to the operation of a series of stirred chemical reactors as shown in Fig. 4.

2. Within each stage, no solids concentration gradients exist (i.e., it is a continuous stirred tank reactor).

3. No intermixing occurs between stages.

4. Slurry level is assumed constant.

5. Flotation rate is governed by first order kinetics. Inherent in this assumption is that the kinetics of the process do not vary with particle size.

6. Slurry pH is assumed to be controlled at the optimal level for flotation.

7. Aeration rate is assumed constant at the optimal rate.

Basic equations are derived from mass balances on solids, water, and ash and on a volume balance for each stage. A complete set of equations for an arbitrary flotation stage is given in Table 1. Equations (1.1) through (1.3) define the state variables of the system and Eqs. (1.4) through (1.10) define the auxiliary variables and relationships necessary to complete the model.

Table 1. Summary of equations for the froth flotation dynamic model

Equation Number	Equation	Comments
(1.1)	$\frac{dC_{ST_i}}{dt} = \frac{\dot{V}_{UF_{i-1}}}{V_i} (C_{ST_{i-1}}) - \frac{\dot{V}_{UF_i}}{V_i} (C_{ST_i}) - k (C_{ST_i} - C_\infty)$	Solids mass balance
(1.2)	$\frac{dC_{LT_i}}{dt} = \frac{\dot{V}_{UF_{i-1}}}{V_i} (C_{LT_{i-1}}) - \frac{\dot{V}_{UF_i}}{V_i} (C_{LT_i}) - \frac{\beta_i}{V_i}$	Liquid mass balance
(1.3)	$\frac{dC_{AT_i}}{dt} = \frac{\dot{V}_{UF_{i-1}}}{V_i} (C_{AT_{i-1}}) - \frac{\dot{V}_{UF_i}}{V_i} (C_{AT_i}) - \frac{\dot{A}_i}{V_i}$	Ash mass balance
(1.4)	$\dot{V}_{UF_{i-1}} = \dot{V}_{UF_i} + \dot{V}_{OF_i}$	Volume balance
(1.5)	$\dot{V}_{OF_i} = (\beta/\rho_L) + (r V_i/\rho_c)$	Volume flowrate to overflow
(1.6)	$\dot{A}_i = X_{A_i} \left(\sum_{j=1}^{i} \dot{M}_{OF_i} \right) - \sum_{j=1}^{i-1} \dot{A}_j$	Ash flowrate to overflow
(1.7)	$R_i = \left[\frac{C_{SOF_i} \dot{V}_{OF_i}}{C_{SOF_i} V_{OF_i} + C_{ST_i} \dot{V}_{UF_i}} \right] (100 - R_{i-1}) + R_{i-1}$	Cumulative solids recovery
(1.8)	$X_{A_i} = f (R_i)$	Ash fraction in floated material[a]
(1.9)	$k = f (M, D, CT)$	Flotation rate constant
(1.10)	$C_\infty = f (M, D, CT)$	Limiting concentration

[a]This function was generated from data reported in the literature.

Recovery as defined in Eq. (1.7) is a cumulative quantity, which is necessary to utilize the batch data analyzed to produce ash versus recovery data mentioned previously. The stage recoveries in Eqs. (1.7) and (1.8) incorporate a time delay to reflect the slurry transport delay.

Equations (1.9) and (1.10) complete the description of the flotation system and represent the parameters in the first order kinetic model of flotation.

Equations (1.1) through (1.10) sufficiently characterize the dynamic behavior of one froth cell (ten equations in ten unknowns). An N stage froth flotation unit is simulated by cascading this set of equations N times.

Flotation Kinetics

Relationships are required to define ash concentration in the solid product as a function of recovery [see Eq. (1.8)], and flotation rate constant and limiting concentration as a function of reagent loadings and coal type [see Eqs. (1.9) and (1.10)]. Laboratory froth flotation data[2] were analyzed and found to be well represented by the relationship

$$r = k(C_{ST} - C_{\infty}) \ . \qquad (1)$$

The laboratory batch flotation tests involved parametric investigations of flotation rate as a function of coal type and initial loadings of frother (methyl isobutyl carbinol) and collector (kerosene).

The kinetic analysis consists of fitting a two-parameter rate equation to the experimental flotation rate data. Rewriting Eq. (1) yields:

$$dC_{ST}/dt = -k\ (C_{ST} - C_{\infty})$$

which upon solution by separation of variables becomes:

$$(C_{ST} - C_{\infty}) = \alpha e^{-kt} \ . \qquad (2)$$

From Eq. (2), it is inferred that the solids concentration in the batch tank should decay exponentially with time to a value of C_{∞}. The two parameters of interest in the model [Eq. (2)] are C_{∞} and k. Shown in Fig. 5 is an example of a typical fit of Eq. (2) to a set of experimental data. As predicted by the model, the solids concentration decays exponentially with time to a limiting value of 24.4 kg/m^3 (1.52 lb/ft^3) with an initial slope of 3.72 (1/min). Data from each of the twenty tests performed on six different coals were analyzed in the manner shown graphically in Fig. 5.

The results for limiting concentration and flotation rate constant indicate that the coals tested can be subdivided into two groups; similar behavior is encountered in each group. For the results obtained with Lower Freeport coal, the flotation rate constant varies insignificantly with both

kerosene and methyl isobutyl carbinol (MIBC) loadings, as shown in Fig. 6. The variation of C_∞ with reagent is shown in Fig. 7 for Lower Freeport coal. Little effect on C_∞ is noted with variations in kerosene, but there is an initial drop in C_∞ upon increasing the MIBC dosage from 0.05 to 0.1 g/kg; further additions have little noticeable effect.

The second group of coals consists of Sewickley, Waynesburg, Lower Kittaning, Pittsburgh, and Illinois No. 6 seam materials. With these coals there is a gradual increase in rate constant with increasing kerosene loading in the 0.0 to 0.25 g/kg range. Above 0.25 g/kg, the rate constant changes only slightly. There is an initial increase in rate constant upon increasing MIBC loading from 0.05 to 0.1 g/kg, and only slight effects with further additions. At the lowest MIBC loadings, the limiting concentration decreases slightly with increasing kerosene loadings; this trend tends to level out with increasing MIBC loading. With constant kerosene loading, C_∞ decreases significantly with increasing MIBC loading. The decrease in C_∞ is most significant at low MIBC loadings and tends to become much less important at higher loadings.

The ash content of the floated material is specified as a function of solids recovery in Eq. (1.8). Experimental data[2] are utilized to calculate the ash content of floated solids as a function of recovery, kerosene loading, and MIBC loading. An example of the type of data used to calculate ash content is shown in Fig. 8.

CLEAN COAL FILTER

A vacuum disc filter is employed in many coal preparation plants for the final dewatering of fine coal product. Overflow from the froth flotation unit is fed by gravity to the filter; hence the filter input stream consists of a thick slurry with some residual froth. Solids content may vary from 15 to 55 wt %.[3]

The operation of a vacuum disc filter unit can be conceptualized as shown in Fig. 9, where the complete filter cycle is described for one segment of one disc. Feed slurry to be filtered is contained in a large stirred vat. The cycle begins as the disc segment is immersed in the slurry; a vacuum is then applied and cake is formed on both sides of the segment as the disc rotates through the slurry. Clean filtrate passes through both the filter and cake, then is diverted and collected from the vacuum piping. With further rotation the segment leaves the slurry, cake formation ceases, and moisture trapped in the cake voids is removed by continued vacuum. Drying continues until, at a fixed angular position, the vacuum is removed, and a pressure slightly above atmospheric is applied to the segment. This dislodges the cake, which is further removed and guided by a scraper blade to fall onto a conveyor below. Cake removal occurs just prior to the reentry of the disc segment into the slurry.

Each segment follows the same sequence, with a 36° phase difference between adjacent segments. For a 10-disc filter, 10 segments (one on each disc) will work in unison for each of the 10 (per disc) phase sequences.

Slurry level in the tank is presently maintained by manual control. If the level falls below a minimum height, filter segments will not be fully submerged when vacuum is applied. This is the pneumatic equivalent of a short circuit; the pump cannot maintain the vacuum, and filtration effectively stops. The result is a shutdown of the clean coal filter, which is disruptive to the entire fine coal circuit. Slurry overflow at the weir is also undesirable, since the overflow stream is recycled to the head of the fines circuit. Flotation product slurry is difficult to pump due to its strong tendency to reform into froth. Weir overflow is, however, preferred over the possibility of the drive shaft becoming submerged.[4]

Given the above constraints, the operator must maintain the slurry level within a 15-cm (6-in.) "free board." This is accomplished, for a variable volumetric feed rate, by varying the disc rotational velocity, and, rarely, by signaling the froth operator for greater or lesser output from the flotation cells. Disc speed can be varied between 1.1 and 11 minutes per revolution (MPR).

Dynamic Model

In developing the dynamic model, certain simplifying assumptions were made.

1. The tank slurry is assumed to be a homogeneous mixture; that is, there are assumed to be no spatial concentration gradients.

2. Tank cross-sectional area is assumed constant over the operating height variation.

3. All effects of particle size distribution are neglected. For use in cake drying calculations, a median particle size (100 mesh) is assumed.

4. Cake void fraction is assumed to have a constant value.

5. Pressure drop across the filter and cake is assumed to be independent of flow rate.

6. Specific cake resistance is held constant.

7. The transition from cake formation to drying is assumed to take place instantaneously, as the centroid of the segment exits the slurry. This point was further fixed at a single angular position (i.e., slurry height variations have negligible effect). Thus, cake formation, drying, and cake removal all occur over fixed angular intervals.

8. Flow of filtrate through the cake is assumed to be laminar.

9. Cake moisture content during drying is assumed to approach a limiting value (residual saturation) which does not vary.

The equations that describe the operation of the filter can be viewed as three distinct groups: equations describing solids concentration and slurry level in the filter vat, the filter cake formation equations, and the filter cake drying equations. These three groups are discussed below.

The governing equations for dynamic modeling of the tank are given in Table 2 as Eqs. (2.1) through (2.7). As in the flotation model, mass balances for the filter tank can be written for both solid and liquid phases [Eqs. (2.1) and (2.2)]. In addition, an overall volume balance can be written [Eq. (2.3)]. Equations (2.1) through (2.3) define the state variables of the system; the supplementary relationships are given in Eqs. (2.4) through (2.7).

The model for filter cake formation is based on the basic cake formation equation, as given by Purchas.[5] A summary of the filter cake formation equations for an arbitrary filter segment "i" is given in Table 3. Equation (3.1) gives the volumetric flowrate of filtrate through segment "i" as a function of filter area, pressure drop, filtrate viscosity, and resistance to flow through the cake and the filter medium. Equation (3.2) relates the mass rate of solids accumulation on the filter cake to the volume rate of filtrate collected through the variable C. Equation (3.3) relates C to known quantities of tank solids and physical properties data. Finally, Eq. (3.4) defines the cake thickness as a function of solids accumulation rate and physical parameters.

The model for the drying portion of the filter cycle is patterned after that of Brown.[6] A summary listing of the equations in the drying model is given in Table 4. Drying is characterized by the gradual displacement of liquid from the cake voids by air.

A fraction of the liquid will be trapped, by capillarity and surface tension, between passages with air in flow. Since the liquid continues to flow in the smaller passageways until the larger, adjoining voids lose their liquid flow and begin to carry air, it is assumed that the fraction of voids containing trapped, nonflowing liquid is proportional to the fraction containing air in flow. Equation (4.1), based on this assumption, relates the cake saturation to the effective and residual saturation values. Equation (4.2) defines the variation in effective saturation with drying time. The constant represented in Eq. (4.3) is the result of linearization of a term in the solution to the Darcy equation for flow of fluid through a porous bed. Equations (4.4) through (4.9) are the necessary supplementary equations to complete the model. Equations (4.1) through (4.9) are sufficient to model the drying cycle, which continues until the cake is blown off the disc at a fixed angular position.

Table 2. Summary of filter tank equations

Equation Number	Equation	Comments
(2.1)	$Q_{is}C_{ss} - \dot{M}_c = A_T\dot{h}C_{st} + A_T h\dot{C}_{st}$	Solids mass balance
(2.2)	$Q_{is}C_{\ell s} - Q_{oc}C_{\ell c} - \dot{V}\rho_\ell = A_T\dot{h}C_{\ell t} + A_T h\dot{C}_{\ell t}$	Liquid mass balance
(2.3)	$A_T \frac{dh}{dt} = Q_{is} - Q_{oc} - \dot{V}$	Volume balance
(2.4)	$\dot{M}_c = \sum_{i=1}^{10} \dot{M}_{ci}$	Mass rate of solids to the cake
(2.5)	$\dot{V} = \sum_{i=1}^{10} \dot{V}_i$	Volume rate of filtrate through the filter
(2.6)	$Q_{oc} = \dot{M}_c/\rho_b$	Volume rate of "material" removal to the filter cake
(2.7)	$C_{\ell c} = \varepsilon\rho_\ell$	Concentration of liquid in the filter cake

Table 3. Summary of filtration equations

Equation Number	Equation	Comments
(3.1)	$\dot{V}_i = \frac{A_F^2 P}{\mu(r M_{ci} + A_F R)}$	Volumetric flowrate of filtrate through the filter
(3.2)	$\dot{M}_{ci} = C\dot{V}_i$	Mass rate of solids accumulating on the cake
(3.3)	$C = \frac{C_{ST}}{\frac{C_{ST}}{\rho_\ell} - (\frac{\varepsilon}{1-\varepsilon})\frac{C_{ST}}{\rho_c}}$	Mass of solids deposited to the cake per volume of filtrate removed
(3.4)	$L_i = M_{ci}/(\rho_c \cdot A_F)$	Cake thickness

Table 4. Summary of drying equations

Equation Number	Equation	Comments
(4.1)	$S = \frac{S_e - 2S_eS_r + S_r}{1 - S_eS_r}$	Filter cake saturation
(4.2)	$S_{ei} = \left[\frac{KPt_i(y-1)}{k\mu L_i^2\varepsilon} + 1\right]^{(\frac{1}{1-y})}$	Filter cake effective saturation
(4.3)	$k = \frac{(1 - S_r)^2 + 1}{2}$	Linearized term in the Darcy equation
(4.4)	$V_{ci} = M_{ci}/\rho_b$	Cake volume
(4.5)	$\rho_b = \rho_c(1 - \varepsilon)$	Cake bulk density
(4.6)	$V_{vi} = \varepsilon V_{ci}$	Volume of voids in the cake
(4.7)	$V_{\ell i} = S_i V_{vi}$	Volume of liquid in the cake
(4.8)	$M_{\ell i} = V_{\ell i}\ \rho_\ell$	Mass of liquid in the cake
(4.9)	$K = D_p^2 F_{Re}/F_f$	Cake permeability

SUMMARY

Dynamic process models of two unit operations that are commonly used in the coal preparation industry were developed. These models, when implemented on an appropriate dynamic simulator, can be used to perform systems analysis studies in the areas of process control and economics. With appropriate development and verification work, the models could also serve as the basis for froth flotation and vacuum filtration process controllers.

The froth flotation model incorporates a well known tanks-in-series concept with laboratory flotation kinetics data. The model is essentially a system of cascaded first order lags, which is easily solved using available digital simulation methods.

The filtration model combines concepts from the different unit processes of mixing, filtration, and drying into one dynamic model.

The next logical step in continuation of this work is model verification. Field data are necessary to prove the adequacy of these models for process control design.

REFERENCES

1. G. S. Canright, C. H. Brown, Jr., G. O. Allgood, and W. R. Hamel, *Dynamic Modeling and Control Analysis of Froth Flotation and Clean Coal Filtration as Applied to Coal Beneficiation*, ORNL/TM-7829, Oak Ridge National Laboratory (in preparation).

2. K. J. Miller, *Evaluation of Collector Addition in the Flotation of Various U.S. Coals*, PMTC-7(80), Pittsburgh Mining Technology Center, July 9, 1980.

3. J. W. Leonard (Ed.), *Coal Preparation*, 4th ed., American Institute of Mining, Metallurgical, and Petroleum Engineers, Inc., Baltimore, Maryland (1979), pp. 12-54–12-71.

4. L. C. Peterson, President, Peterson Filters Corporation, personal communication to G. S. Canright, June 1980.

5. D. B. Purchas, *Industrial Filtration of Liquids*, 2nd ed., CRC Press, Cleveland, Ohio (1971), p. 431.

6. G. G. Brown, *Unit Operations*, John Wiley and Sons, Inc., New York (1950), Ch. 17.

NOTATION FOR FROTH MODEL

$\dot{A}$	Mass flowrate of ash to overflow, kg/min
C	Concentration, kg/m^3
CT	Coal type
D	Collector loading, g/kg
k	First order rate constant, min^{-1}
M	Frother loading, g/kg
$\dot{M}$	Mass flowrate of solids, kg/min
R	Solids recovery, percent
r	Flotation rate, $kg/m^3 \cdot min$
t	Time, min
V	Volume, m^3
$\dot{V}$	Volumetric flowrate, m^3/min
X_A	Mass fraction of ash in the overflow

Greek letters

β	Mass flowrate of liquid to the overflow, kg/min
ρ	Density, kg/m^3

Subscripts

AT	Ash in the tank
LT	Liquid in the tank
SOF	Solids in the overflow
ST	Solids in the tank
∞	At infinite time
OF	Overflow
UF	Underflow

NOTATION FOR FILTER MODEL

A	Area, m^2
C	(No subscript), mass of solids deposited per volume of filtrate collected, kg/m^3
C	(Subscripted), concentration, kg/m^3
D	Diameter, m
F	Factor
h	Height, m
K	Cake permeability, m^3/min^2
k	Constant used in Eqs. (4.2) and (4.3)
L	Cake thickness, m
M	Mass, kg
P	Pressure drop, Pa
Q	Volumetric flowrate, m^3/min
R	Filter medium resistance, m^{-1}
r	Filter cake resistance, m/kg
S	Saturation
t	Time, min
V	Volume, m^3
y	Constant used in Eq. (4.2)

Greek letters

ε	Cake porosity
ρ	Density, kg/m^3
μ	Viscosity, Pa·s

Subscripts

b	Bulk phase
c	Coal
e	Effective
F	Filter
f	Friction factor
i	Segment number
is	To the tank
ℓ	Liquid
ℓc	Liquid in the cake
ℓs	Liquid in the slurry
ℓt	Liquid in the tank
oc	Overall to the cake
P	Particle
Re	Reynolds number
r	Residual
SS	Solids in the slurry
ST	Solids in the tank
T	Tank cross section
v	Voids in cake

Superscripts

	Time derivative

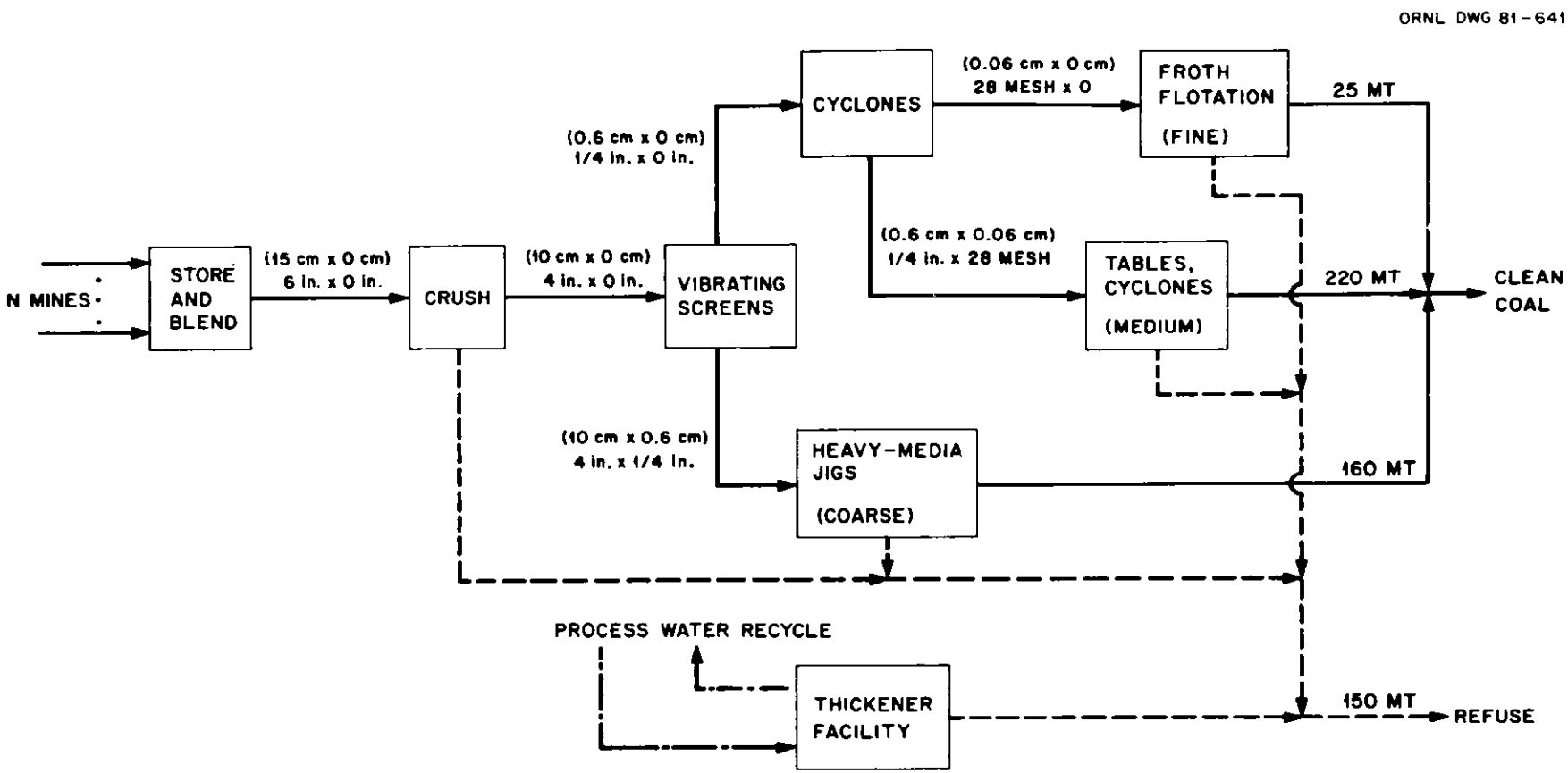

Fig. 1. Schematic diagram of coal preparation process.

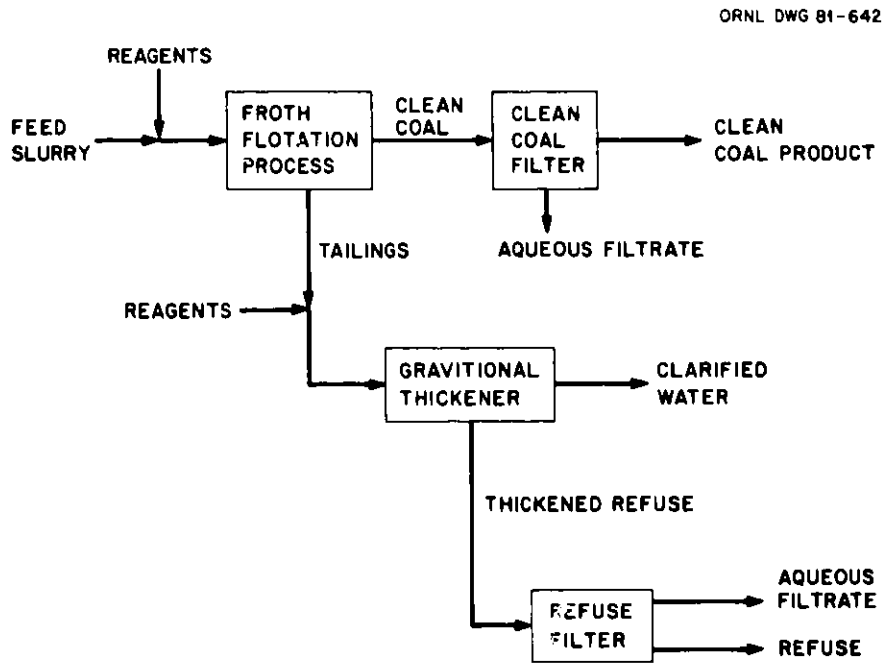

Fig. 2. Fine coal circuit process flowsheet.

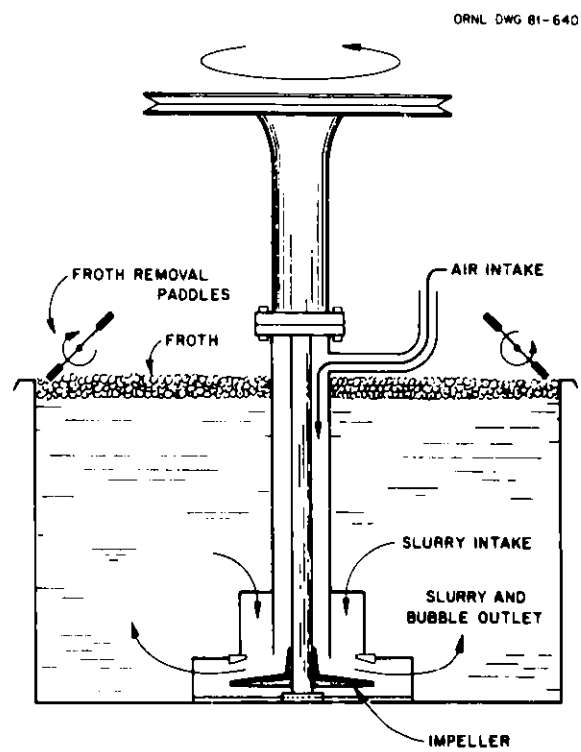

Fig. 3. Typical froth flotation cell cross-section.

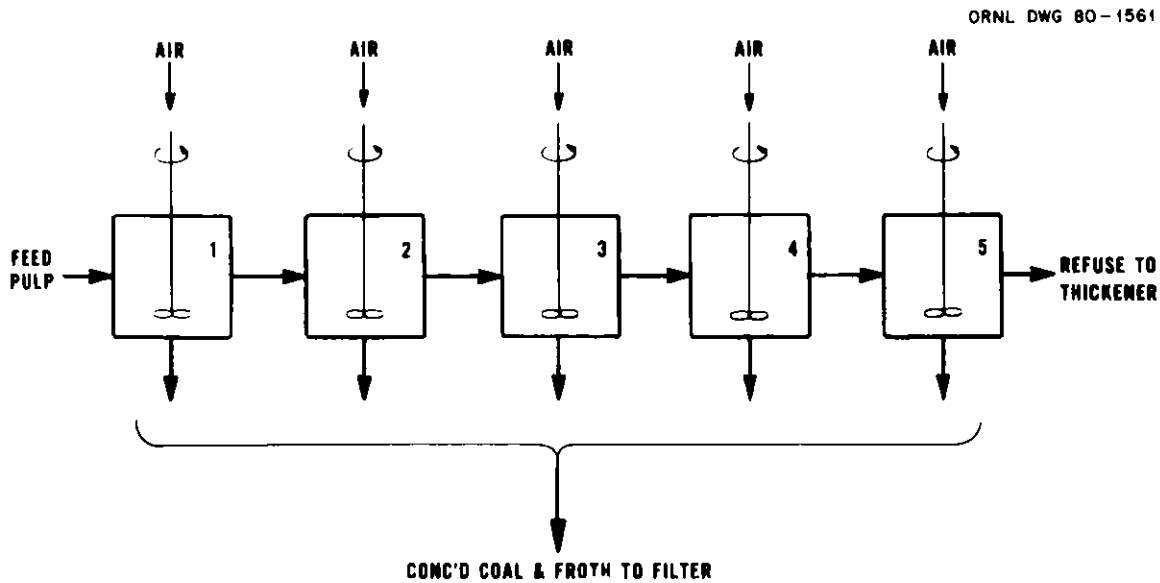

Fig. 4. Tanks-in-series model.

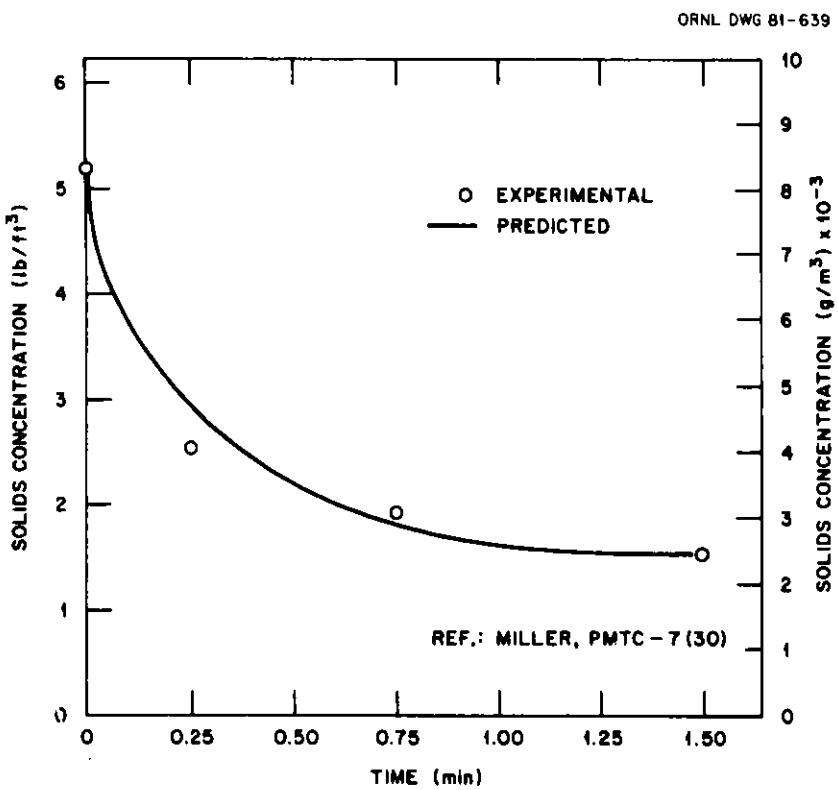

Fig. 5. Batch flotation results for Lower Freeport coal; frother loading 0.05 g/kg, collector loading 0.0 g/kg.

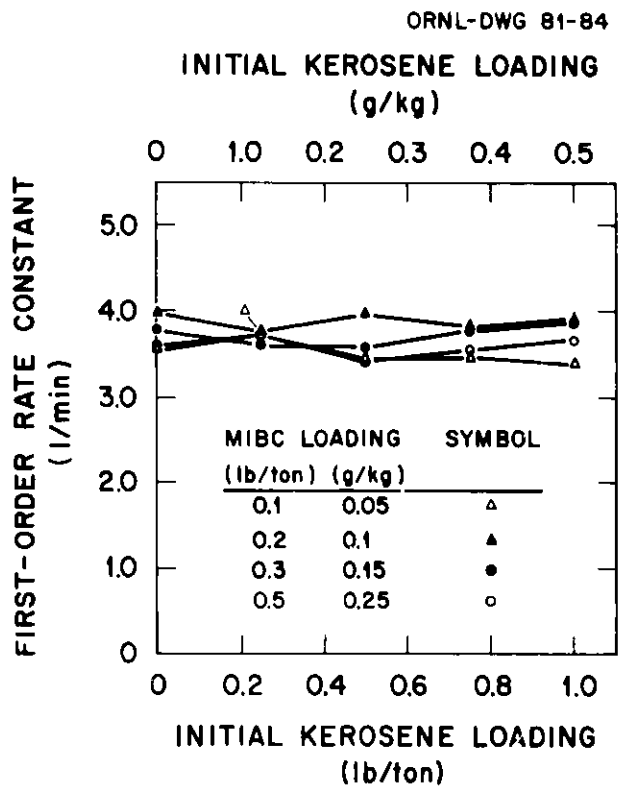

Fig. 6. Rate constant vs kerosene loading as a function of methyl isobutyl carbinol for Lower Freeport seam coal.

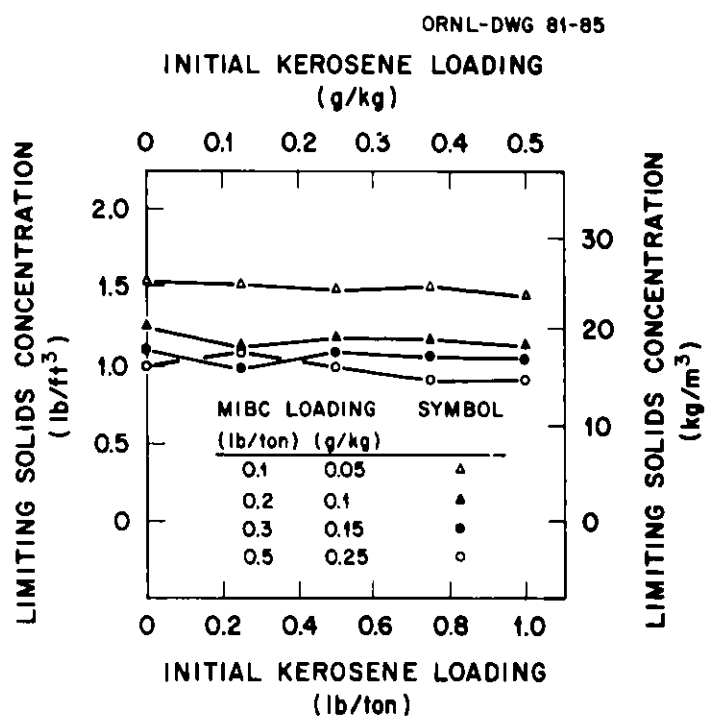

Fig. 7. Limiting solids concentration vs kerosene loading as a function of methyl isobutyl carbinol (MIBC) loading for Lower Freeport seam coal.

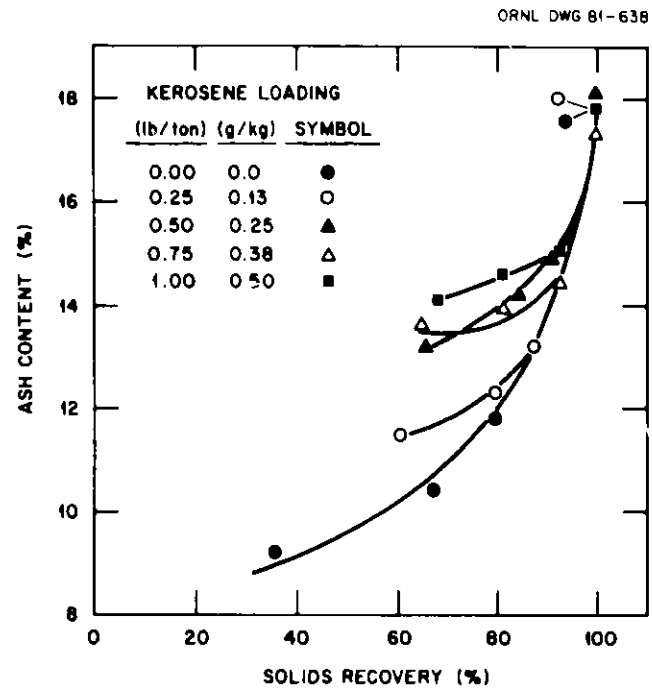

Fig. 8. Ash content vs solids recovery as a function of kerosene loading with initial loading of 0.15 g/kg methyl isobutyl carbinol (MIBC) for Waynesburg seam coal.

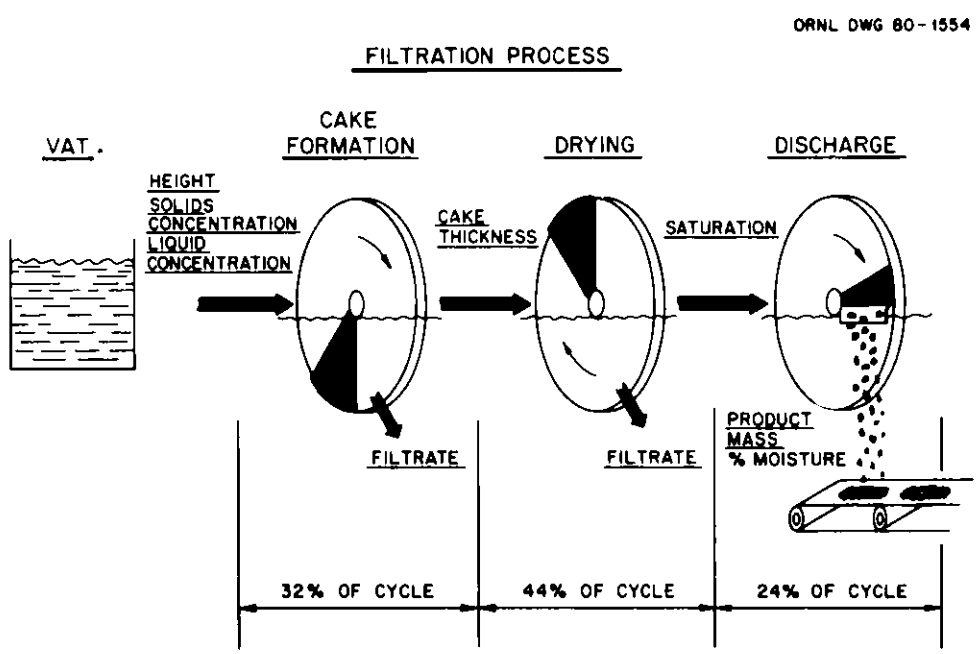

Fig. 9. Process diagram for a vacuum disc filter unit.

DYNAMIC SIMULATION OF THE COAL FROTH FLOTATION AND FILTRATION PROCESSES+

Geoffrey S. Canright,* G. O. Allgood,
C. H. Brown, Jr., and W. R. Hamel
Oak Ridge National Laboratory
P.O. Box X
Oak Ridge, Tennessee 37830
Telephone: (615) 574-5692

ABSTRACT

A digital computer simulation is presented for two unit operations from the fine-coal circuit of coal preparation plants. Transient mathematical models of the flotation process and the fine-coal filter were the basis for the simulation, which was carried out using the IBM Continuous System Modeling Program (CSMP). Control strategies representative of those currently in use, as well as a proposed automatic control, were modeled and applied to each unit. The fine-coal filter performance was expressed in terms of cake moisture content at discharge. Performance of the flotation unit was quantified in terms of overproduct ash content and salable coal lost to the tailings. A standard feed disturbance was input to the flotation process and carried through the overflow to the filter. Performance of the various control schemes was compared according to the above criteria. The two filtration controls showed no significant difference in performance; however, the flotation results gave a definite ranking of the three control strategies. A simple economic analysis (payout period) was performed for the two flotation control alternatives that yielded the best performance. The analysis indicated that substantial savings could be realized by the automatic control of froth flotation.

+Research sponsored by the Pittsburgh Mining Technology Center, Coal Preparation Divison, U.S. Department of Energy under contract W-7405- eng-26 with the Union Carbide Corporation.

INTRODUCTION

The preceding paper[1] describes the development of detailed transient models for two processes, froth flotation and vacuum filtration, which are central in the operation of the fines circuit of coal cleaning plants. One of the immediate uses for such models is the simulation and performance evaluation of prospective control strategies for these same processes. Simulation can be a cost-effective amd time-saving tool for the coal preparation industry, as it has proved to be for other process industries. The chief obstacle to be overcome is the lack of sound, reliable models for the various unit operations; the models reported in the accompanying paper represent one step towards the laying of a sound analytical base for process simulation and control design.

In this paper, some of the control techniques currently applied to coal froth flotation and clean coal filtration are modeled, and a proposed control scheme using available instruments is modeled for each operation. The process models are then run with a standard disturbance applied at the feed stream, under the control of each of the modeled control schemes. The results of the simulation suggest the relative effectiveness of the various controls in terms of quantitative performance criteria. These results are used, in the case of froth flotation, in a simple economic analysis to give rough indication of the cost-effectiveness of the proposed automation. The filter controls show negligible difference in performance; hence, economic analysis is not applied to them. The results in any case should be considered to be preliminary in nature, until field testing and subsequent refinement of the models have been carried out.

VACUUM FILTER CONTROL MODELS

Control, as presently applied to the clean coal vacuum filter, consists of maintaining the slurry level in the filter tank within the operating limits of the device. Too low a level is completely unacceptable since it causes loss of vacuum and shutdown of the unit -- and hence of the fines circuit. Slurry overflow is highly undesirable

since the excess must be returned to the head of the fines circuit, and the slurry is difficult to pump due to the presence of residual frothing agent.

The operator maintains slurry level within the limits by varying the speed of rotation of the filter disks, and hence the throughput rate of the process. Filter cycle time in turn affects the final moisture content of the filter cake, which is the real performance variable of the vacuum filter. Disk speed is determined, however, by the need for slurry level control.

Manual Control Model

A model of filter manual control requires examination of the dynamics of the motor, drive train, and load. The motor drives the disk shaft through a variable pulley which is adjusted by the operator. The electrical time constant of the motor is considered negligibly small. The mechanical time constant of the system is given by the ratio of load inertia (J) to load viscous friction (F), or

$$T_m = J/F \tag{1}$$

Approximate calculations for J and F indicate that the mechanical time constant is on the order of tenths of a second. Since this response is much faster than any of the remainder of the filter system, inertial effects are also neglected, and the drive train is modeled as if the operator can change disk speed instantaneously.

The strategy of a human operator is difficult to simulate. In the model implemented, the "operator" notes the height (H) and change in height (ΔH) of coal slurry in the tank, at one minute intervals. The model discriminates between five intervals for slurry height; and it is sensitive to the magnitude and direction of ΔH. Control is achieved by adjustment of the pulley ratio (and hence disk speed).

Automatic Control Model

Manual filter coal is satisfactory in that an operator can successfully keep the slurry level within the prescribed limits. Accuracy of control, within these limits, if of no real benefit, and

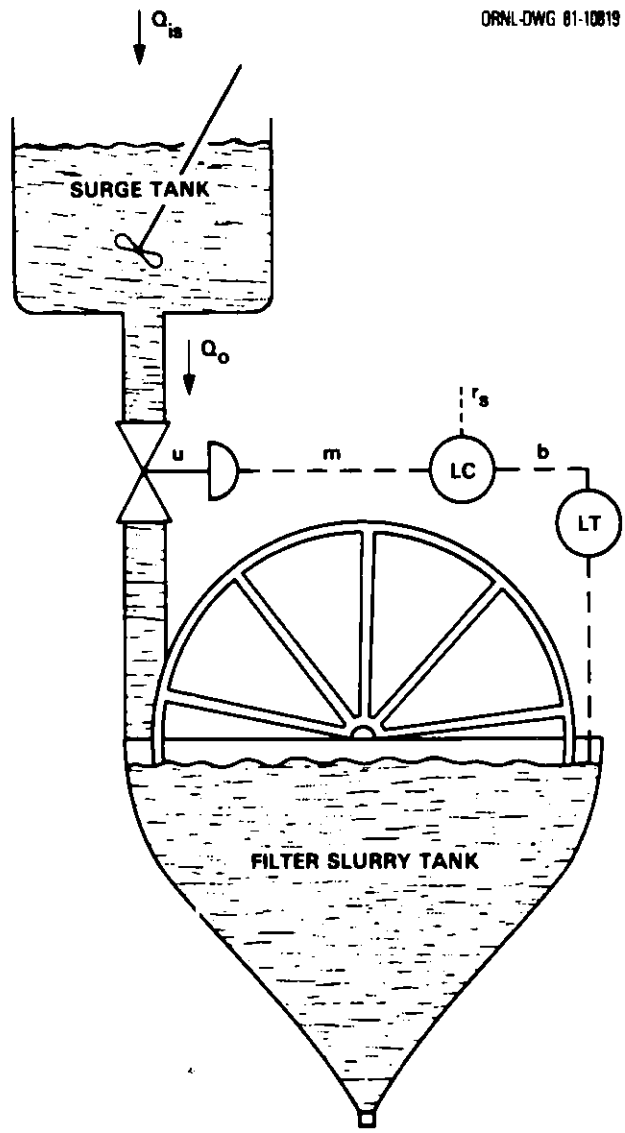

Figure 1.

hence could not justify the expense of automatic control. It is possible, however, that if the disk drive could be run at a fixed speed, some improvement in cake moisture content could be realized. A control scheme which allows for fixed disk speed is shown in Figure 1.

Normally, slurry is fed by gravity from the flotation cells to the filter tank. It is not feasible to pump froth overproduct due to a significant residue of frothing agent.[4] In the proposed scheme, a surge tank is fitted into the gravity feed line; flow from the surge

tank to filter tank is driven by gravity, and controlled by a valve. A level signal from a suitable sensor (e.g., a capacitance-type continuous level transmitter) is input to a P-I controller which drives the valve. The real question mark in this arrangement is the required size of surge tank, which depends on the expected maximum fluctuations in volumetric flow from the froth cells. The first step, however, is to determine whether or not driving the disks at a fixed speed gives a significant improvement in cake moisture content over the present variable-speed control.

The surge tank is treated as a well-stirred tank. The volume balance, solids balance, and liquid balance for the tank are; respectively,

$$\dot{h}_s = (Q_{is} - Q_o)/A_s, \tag{2}$$

$$C_{ss}\, Q_{is} = h_s\, A_s\, \dot{C}_{sst} + C_{sst}\, (Q_o + \dot{h}_s\, A_s), \tag{3}$$

$$C_{ls}\, Q_{is} = h_s\, A_s\, \dot{C}_{lst} + C_{lst}\, (Q_o + \dot{h}_s\, A_s), \tag{4}$$

where h_s = slurry height in surge tank,

A_s = tank cross-sectional area,

Q_o = volumetric flow exiting tank,

Q_{is} = volumetric feed rate,

C_{ss} = concentration of solids in feed slurry (mass/vol.),

C_{ls} = concentration of liquid in feed slurry,

C_{sst} = concentration of solids in surge tank,

C_{lst} = concentration of liquid in surge tank.

Flow from the surge tank is given by

$$Q_o = A_o \sqrt{2gh_s}, \tag{5}$$

where A_o = valve orifice area.

The valve is modeled as a linear gain with a time response given by a first-order lag. The level sensor is assumed to give instantaneous response with negligible error.

FILTER SIMULATION RESULTS

For the purpose of control comparison a feed disturbance to the filter is generated using the froth flotation model. A step change in feed percent solids at the flotation unit inlet is propagated through the unit, and appears at the overflow as a change in volumetric flow (Q_{is}) and overflow solids concentration (C_{ss}).

Figs. 2 and 3 give slurry level in the filter tank vs. time, for manual and automatic control, respectively. The limits of the vertical axis are equivalent to the operating limits.

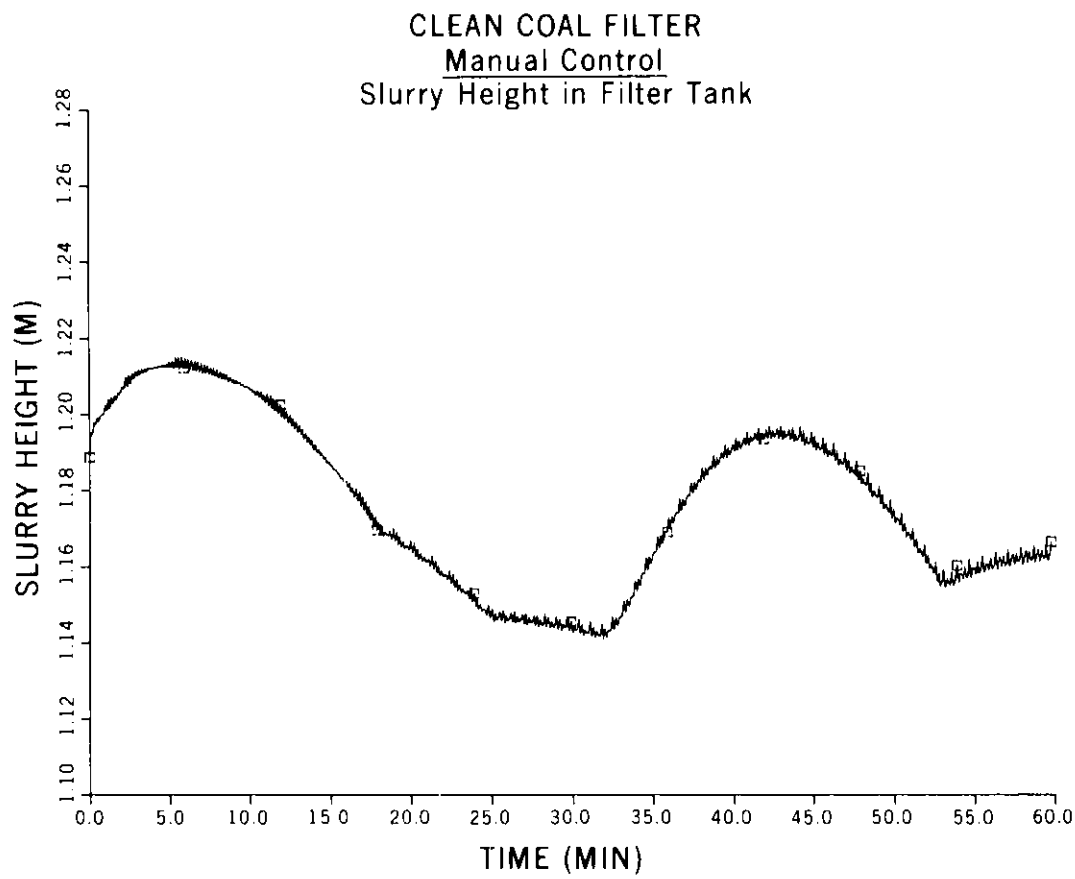

Figure 2.

Product moisture is calculated on a cumulative basis for each simulation run. Final values are: under manual control, 30.3% moisture; under automatic control, 29.7%. This difference is too small to be considered significant. The automatic control, while absorbing feed fluctuations at the surge tank and enabling operation at a fixed disk speed, shows no real improvement in product moisture.

FROTH FLOTATION CONTROL MODELS

The objective of flotation control is to float as much product as possible without letting the ash content of the product exceed a specified maximum. Unfortunately, there is no practical, inexpensive instrument currently available to monitor ash content in a coal stream.

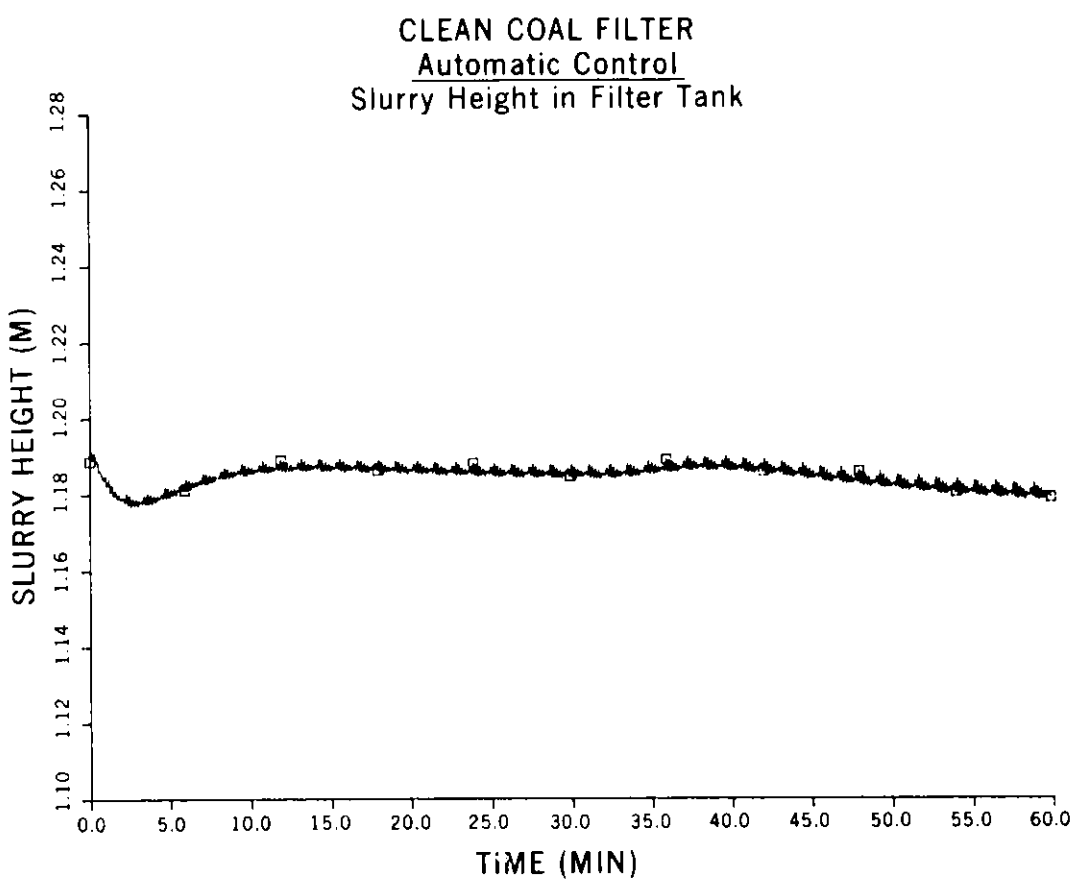

Figure 3.

Hence present controls rely on one of two methods: a predictive technique based on laboratory analysis of the feed coal, or a reactive technique based on human assessment of the overflow and underflow streams.

In the first method an optimum reagent loading (lbs. reagent per lb. feed solids) is chosen for each reagent from laboratory flotation tests. Each value for reagent loading (a mass ratio) is then translated into a reagent flow rate, by assuming an average or baseline value for solids flow in the feed. Reagent flows are set to the chosen value, and changed only when further lab tests call for a new value.

An alternative control method requires a human operator to periodically inspect the color or "feel" of the tailings stream and/or overproduct. Using his experience, the operator judges whether too much coal is being lost to refuse, or too much solids are being floated. He then adjusts reagent flow rates in order to change the flotation rate.

The hypothetical control method, to be compared to the above methods, is a variation on the first, or predictive technique. In the proposed method, shown in schematic form in Fig. 4, solids mass flow rate in the feed is calculated based on signals from bulk density and volumetric flow sensors in the feed stream. Reagent flow rates are adjusted, based on this calculated solids mass flow, to maintain a constant mass ratio (loading) of reagents to solids in the feed. The reagent loading is the set point, chosen again by laboratory analysis.

The model for manual control uses "color" of the refuse stream as the controlled variable, where "color" is a weighted sum of "pure" coal concentration and ash concentration. The (simulated) operator acts to keep tailings "color" close to a set point which is chosen to give typical values for solids recovery. The interval between adjustments and the magnitude of the adjustments, depends upon the degree of deviation of the refuse color from the set point.

ORNL -DWG 81-10820

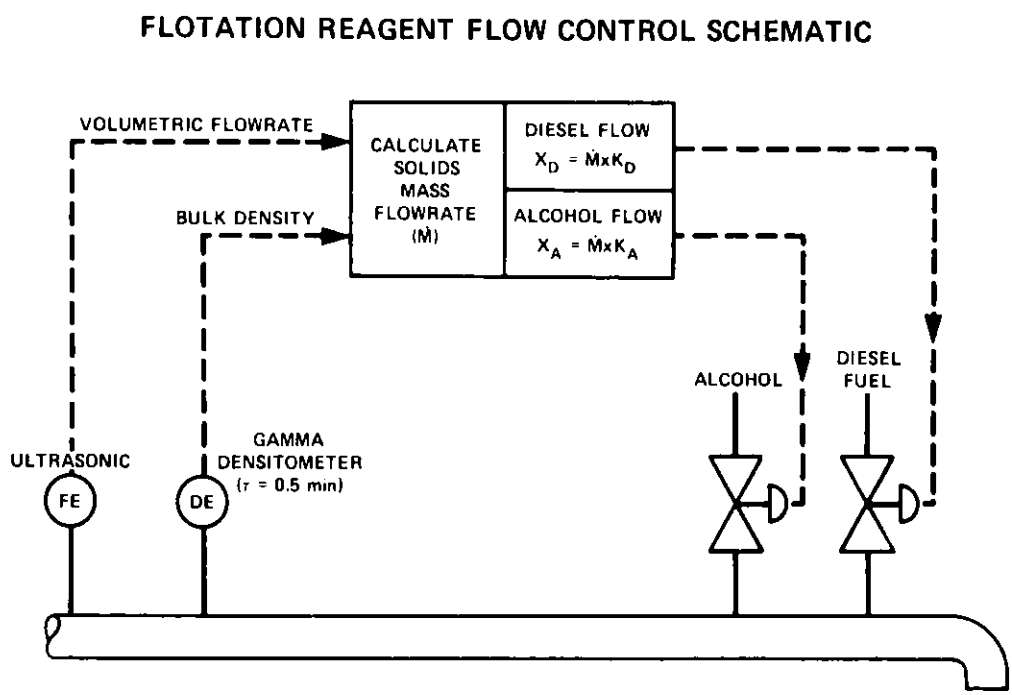

Figure 4.

For the predictive or fixed-flow technique, a reagent loading is chosen by using the model to find the maximum solids recovery possible within the ash specification. A baseline solids feed rate is also chosen which is the same for all three controls. This gives an optimum flow rate for frother and coater, which is not changed throughout the simulation run.

The same reagent loading is the set point for the automatic control. Here the densitometer response is characterized as a first-order lag (T = 0.5 min.), while the flow sensor, calculator, and reagent metering pumps are treated as having instantaneous response.

FROTH FLOTATION SIMULATION RESULTS

Each simulation run consists of two hours of simulation time. A set of four feed disturbances is generated in the following way: Feed solids content is held to 10% for the initial period of the run; between 20 and 35 minutes, the solids content is increased to between 12% and 15%; the solids content returns to baseline (10%) between 70 and 80 minutes, and is held there until 120 minutes. Each controller is run four times, for the same set of four disturbances.

Table 1 gives the results of the simulation runs in terms of solids recovery, product ash content, and salable product (i.e., the amount of solids at 7.8% ash) lost to refuse. These results of course must be considered suggestive rather than definitive. The model incorporates only a subset of the variables active in the real process. Hence the simulated performance of the controllers is very likely better than could be expected in a real application. However, it is interesting to compare the three schemes to one another in this context.

The figures for recovery show a definite ranking both in magnitude and in variability. The 'tightest' controller is able to operate close to the limit on ash (7.8%) without overshoot, giving the highest yield. The manual control yields a product with the lowest average ash and percent recovery; yet after one two-hour run (approximately one carload of product) the ash specification was exceeded. Hence the control whose performance shows the greatest fluctuation is forced to operate at a lower mean yield in order to avoid penalty.

The two controls which give the best performance may be compared on an economic basis. The simulation runs give the difference in product yield for a two-hour period, which may be translated into a dollar value by assuming a price for the product. Two-hour figures may be extrapolated to a yearly basis (4,160 hours) by making some

Table 1. Flotation Performance Comparison

	Recovery (%)		Ash (wt.%)		Product to Refuse (tph)	
	Range of Values	Avg. Value	Range of Values	Avg. Value	Range of Values	Avg. Value
F	69.1 - 69.54	69.33	7.69-7.71	7.70	5.80-6.57	6.16
M	67.35 - 68.87	68.16	7.25-7.89	7.63	6.55-6.82	6.68
A	70.12 - 70.21	70.16	7.74-7.77	7.75	5.55-6.02	5.77

(F) Fixed Reagent Flow (M) Manual Control (A) Automatic Control

assumption as to the overall frequency of the feed disturbances which give rise to the difference in performance. In Table 2, two cases are considered: (1) that the performance improvement of automatic control is representative for all operating time, or (2) that the improvement is realized on the average only one-quarter of the time. Differences in reagent usage are taken into account.

Table 2. Yearly Profit Increment -- Automatic Reagent Control Vs. Fixed Reagent Flow

		Product Value	
		$43/ton	$30/ton
Frequency of Disturbance	Continuous	$167,200	$115,100
	2X/day	$ 41,800	$ 28,800

Installation of the automatic control is estimated at a total installed capital cost of $77,000. Based on the simulation results, the payout period for the installation may range from less than six months to approximately 2 1/2 years.

CONCLUSION

Dynamic models have been written for coal froth flotation and vacuum filtration which incorporate the first-order effects of the two processes. The models have been implemented in a simulation language (CSMP), and have provided credible results.

The models have been used to predict the performance of various control schemes, some currently in use and some hypothetical. The results, which are preliminary but do have some qualitative validity, indicate a potential for significant yield improvement and dollar savings, realized by automatic reagent control in flotation. The filtration results indicate no significant improvement in product quality (moisture content).

REFERENCES

1. Brown, C. H., Jr., G. O. Allgood, G. S. Canright, and W. R. Hamel, "Transient Modeling of Froth Flotation and Vacuum Filtration Processes", Proceedings of the 1981 Symposium on Instrumentation and Control for Fossil Energy Processes, ANL-81-62, CONF 810607, National Technical Information Service, Springfield, VA.

2. Canright, G. S., C. H. Brown, Jr., G. O. Allgood, and W. R. Hamel, "Dynamic Modeling and Control Analysis of Froth Flotation and Clean Coal Filtration as Applied to Coal Beneficiation", ORNL/TM-7829, Oak Ridge National Laboratory, Oak Ridge, TN (1981).

3. Joseph W. Leonard (ed.), Coal Preparation, Fourth Edition, pp. 12-54 through 12-71, American Institute of Mining, Metallurgical, and Petroleum Engineers, Inc., Baltimore, MD (1979).

4. Lynn C. Peterson, President, Peterson Filters Corp., telephone conversation, June 1980.

OVERVIEW FROM SCIEP PARTICULATES SUBGROUP

J. C. F. Wang
Combustion Research Division
Sandia National Laboratories
Livermore, California

The SCIEP Particulate Subgroup held its first mini workshop at Sandia National Laboratories, Livermore, CA, on April 23-24, 1981. Over 30 people from industry, universities, and national laboratories participated. Twenty participants presented their experiences, background and questions related to particulate control and instrumentation during the first day meeting.

A group discussion session was held on the second day. Critical areas on particulate R&D needs were identified and discussed. Participants agreed to submit a few pages of white papers on the identified topics to J. Wang, the Subgroup Coordinator, after the meeting. A summary on the submitted papers is being prepared and will be released to public in the near future.

A Subgroup Steering Committee was formed at the end of the group discussion session. Committee members are W. Bergman (Lawrence Livermore National Laboratory), W. Farthing (Southern Research Institute), and M. Shackleton (Acurex Corporation).

The topics discussed during the workshop is listed in the Appendix. We welcome comments on these topics at anytime. If anyone is interested in participating in the Particulate Subgroup (SCIEP membership is not required), please contact the Subgroup Coordinator or members of the Steering Committee.

SUGGESTED TOPICS FOR SCIEP PARTICULATE WORKSHOP SUMMARY

I. Application Requirements
   - A. Gas Turbines
   - B. Boilers and Combustors
   - C. Safety
   - D. EPA
   - E. Other Processes

II. Instrument Calibration
   - A. What are needed?
   - B. Standard Sources
   - C. Instrument Specifications
   - D. Validation Standards

III. Parameters and Conditions
   - A. Mass
   - B. Size and Size Distribution
   - C. Number Density
   - D. Shape
   - E. Hardness
   - F. Electric Charge
   - G. Index of Refraction
   - H. Surface Area
   - I. Chemical Composition
   - J. Velocity
   - K. Time Response
   - L. Temperature and Pressure

IV. Interface Requirements

- A. Sampling
- B. Dilution
- C. Window

V. Available Instruments

- A. In-situ
- B. Off-line

VI. What's Next?

- A. Subgroup's Function
- B. Future Workshops

DUST SAMPLING AT HIGH TEMPERATURE AND PRESSURE

R. L. Markoja and M. A. Shackleton
Acurex Corporation
485 Clyde Avenue
Mountain View, California 94042

Dr. Richard Jack, Project Director
NCB (IEA Grimethorpe) Ltd.
Grimethorpe Nr. Barnsley
South Yorkshire, S72 7AB, England
Seconded from Central Electricity Generating Board

B. N. Gaglia
NCB (IEA Grimethorpe) Ltd.
Grimethorpe Nr. Barnsley
South Yorkshire, S72 7AB, England
Seconded from Sterns-Roger
Denver, Colorado

ABSTRACT

One critical problem requiring solution in developing fossil energy processes is particulate removal at high temperature and pressure. To evaluate performance of hot gas cleaning devices, it has been necessary to develop particle sampling equipment for use under the temperature and pressure extremes encountered. Acurex has developed particle sampling equipment for a number of difficult environments, including the experimental pressurized fluidized bed combustor (PFBC) operated by International Energy Agency (IEA) Grimethorpe in England. This paper is a description of the sampling needs and objectives at Grimethorpe, and a detailed description of these automated sampling devices.

Introduction

The high-temperature, high-pressure (HTHP) particle sampling systems are designed to collect flyash samples from the ducts of the PFBC located at Grimethorpe, England.

The Grimethorpe PFBC project was organized under the auspices of the IEA with the implementing agreement signed in Paris in November 1975. This project is equally funded by the governments of the United States of America, the Federal Republic of Germany, and the United Kingdom.

The PFBC has been built next to a British National Coal Board Power Station at Grimethorpe, England. The power station provides utilities, including steam for startup purposes. When operating, the PFBC will pass steam back to the power station turbines to produce electricity.

The facility has been designed to study the combustion, heat transfer, gas cleanup, corrosion, and energy recovery systems in a PFBC large enough for data to be used in the analytical modeling of a commercial unit. The facility is expected to demonstrate that PFBC can provide energy in an environmentally cleaner, more efficient, and less costly means than conventional combustion of coal.

The Acurex probe systems shown in figures 1 and 2 are to be used in the combustor off-gas system where dust loadings are nonuniform across the duct. The probes are designed to automatically traverse the off-gas ducts and collect a representative sample of the dust at an isokinetic rate.

The primary objectives of the dust collection systems are to provide data for:

- Construction of mass and elemental balances
- Determination of off-gas cyclone cleanup efficiencies
- Establish characteristics of the input stream for the tertiary cleanup, turbine blade cascade test loop
- Investigate the gas and dust distribution in parallel streams of the exhaust gas system
- Verify the accuracy of various fixed dust probes installed throughout the exhaust gas system

During a typical sampling operation, the probe is positioned at one or more points along a duct diameter and maintained in position for a given time interval while the sample is withdrawn. Large particles are collected by a cyclone while small particles are captured by a filter. After traversing the duct, the probe is retracted and the particulate matter is removed and weighed. On the basis of sample weight and measurements of total sample gas flow, the concentration of particulate matter in the duct can be determined. Coulter counter or other laboratory techniques can be used to determine particle size distribution. Typical sampling conditions are stream velocities of 2 to 36 m/s at 10 atmospheres and $870^{o}C$ and particle loadings ranging up to 1.7 g/m^{3}.

A computer is used to position the probe, maintain isokinetic sampling conditions, and retract the probe under certain alarm conditions. The computer printout provides a record of the data collected and gas stream characteristics.

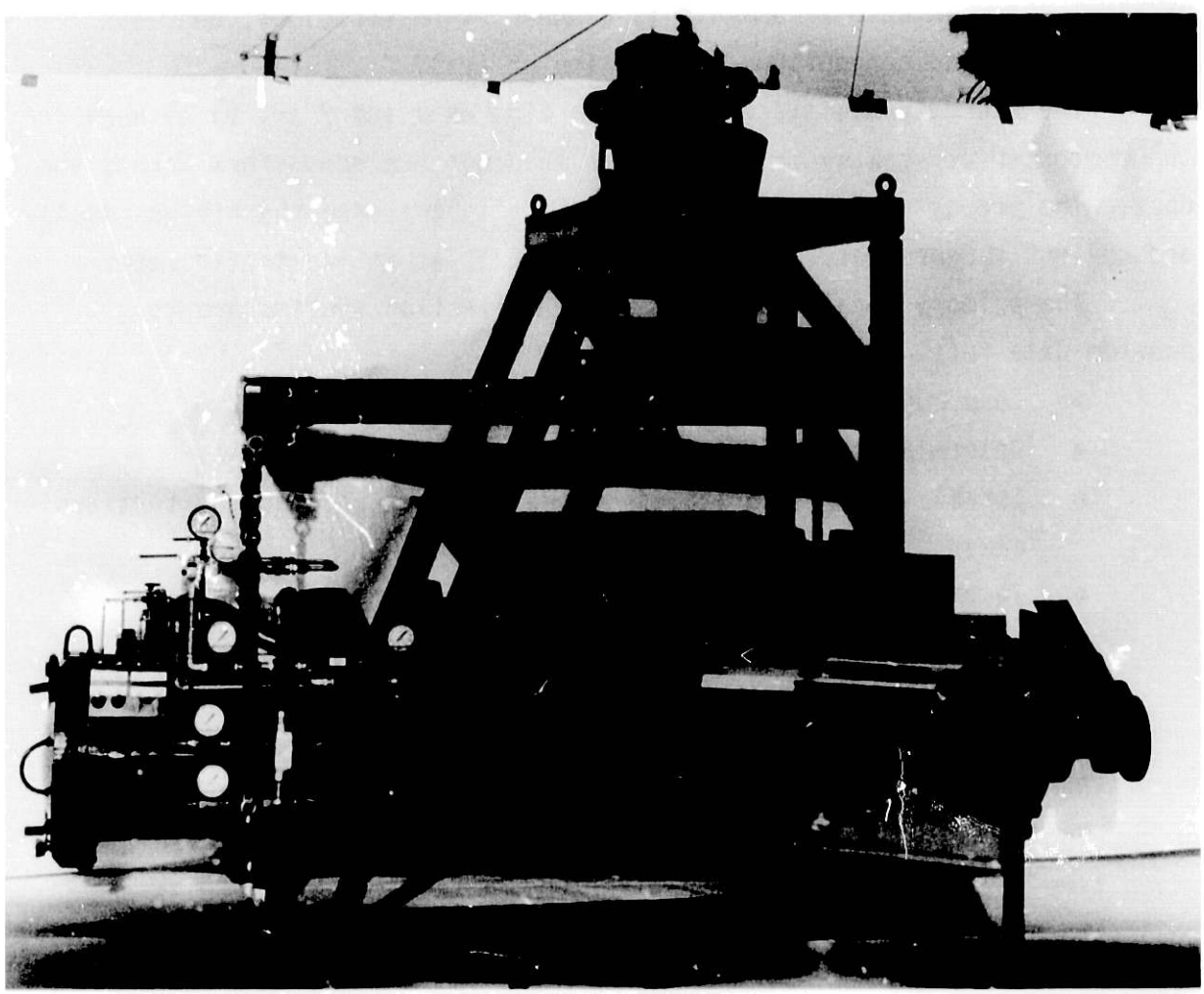

Figure 1. High-Temperature/High-Pressure Particle Sampling System

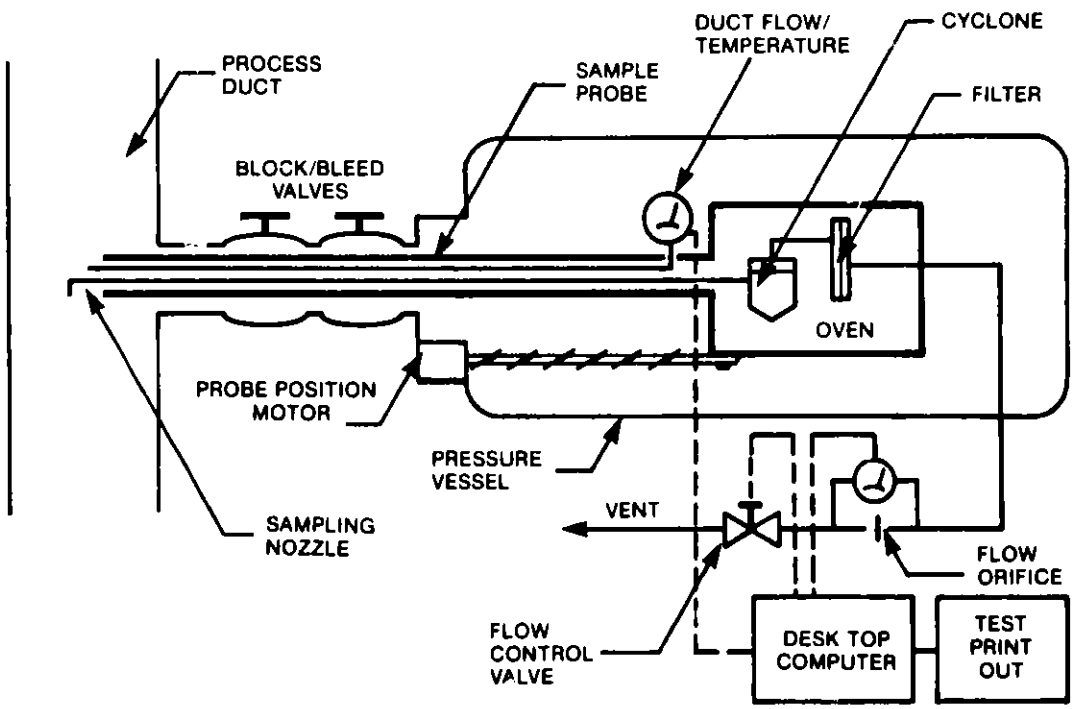

Figure 2. High-Temperature/High-Pressure Particulate Sampling System Schematic

Sampling will be performed at 12 different locations within the Grimethorpe facility. All ducts have two 4-inch bore block and bleed valves at each sample location through which the probe is inserted. A spool piece between the probe vessel and the block and bleed valves aids in alignment of the probe housing.

The sample probe system requires an envelope of 1.3 meters (plus personnel access) wide by 4 meters long, and 3 meters above the grating.

Sampling System Components

The HTHP sampling probe system consists of the following major components or subassemblies:

- Sample probe and cyclone/filter oven
- Traversing mechanism
- Pressure housing
- Sample flow control
- Coolant flow control
- Electrical instrumentation and controls
- Computer

Each of these are described in the following paragraphs.

Sample Probe and Cyclone/Filter Oven

The sample probe consists of a protective water-cooled exterior shell; internal sampling tube; end cap supporting the sample nozzle, pitot tube and thermocouple sensor; and an oven containing the sample collection cyclone and filter. The length of the probe allows it to pass through the two block and bleed valves, the duct insulation, and traverse up to a 1-meter diameter duct.

The probe exterior shell is water-cooled to maintain a surface temperature of less than 260^{o}C. The water flowrate is manually controlled to have an exit temperature of not more than 65^{o}C.

The sample tube within the probe shell has two electric resistance heating elements to preheat the tube to approximately 300^{o}C prior to acquiring a sample. After sample flow begins, the sample tube is cooled to 300^{o}C by a flow of nitrogen coolant over the outside of the sample tube. The electric heater temperature is sensed by a thermocouple mounted halfway along the heated length of sample tube and is controlled by the computer.

The sample probe end cap provides a mounting surface for the sample nozzle and the S-type pitot tube and thermocouple for measuring the gas velocity. In addition, an obstruction sensing rod that provides a stop-forward-motion signal to the computer to prevent probe damage protrudes through the end cap. The water used to cool the probe exterior shell also cools the end cap.

The oven containing the cyclone and filter is of double-wall-insulated construction. It contains an electric heating element to heat all internal components to 300°C. The heating element temperature is sensed by a thermocouple mounted inside the oven and controlled by the computer.

The cyclone is designed to have a particle cut size of 2.2 μm. The filter holder and cyclone are designed for continuous operation at 300°C and short term exposure to 540°C.

Traversing Mechanism

The sample probe and oven are supported by a carriage which rolls the length of the pressure vessel to provide the traverse motion for the probe. A ball screw drive moves the carriage to each sample point and has a positioning accuracy of ±6 mm. A potentiometer located on the drive gear box provides an electrical signal to the computer of the probe's position. Limit switches prevent the probe from being driven into the far wall of the duct or the rear access door.

The drive motor has a brake capable of stopping the probe within 0.1 second. The brake operates whenever power to the motor is removed. A manual brake release and crank attachment is provided so the probe may be manually retracted or positioned.

Pressure Housing

The pressure housing is built to ASME Pressure Vessel Code standards for operation at 1,825 kPa and 93°C. The vessel has a hinge-supported hatch for removal of the cyclone and filter and an interface flange for all instrumentation and control wires, coolant, and sample tubes. The pressure housing is pressurized with nitrogen during operation to minimize the inflow of dust from the duct. A pressure relief valve is used to prevent overpressuring of the vessel.

The entire probe system is supported by a constant load spring hanger to prevent overloading of the system ducts due to their thermal expansion.

Sample Flow Control

A flexible line is used to transport the sample gas from the cyclone and filter to the interface flange and out to a flow-measuring orifice and motor-driven flow control valve. Based on the flow measured at the metering orifice, the valve is automatically adjusted to maintain isokinetic sample rate. After passing through the flow control valve, the sample gas is piped to an exhaust vent. The nitrogen gas used to pressurize the vessel before sampling is initiated and also piped to the exhaust vent.

Coolant Flow Control

The sample probe is provided with two cooling means: water for the probe exterior shell, and nitrogen for the sample tube. In addition, the pressure vessel is continuously purged with nitrogen both for cooling and minimizing inflow of the duct gases.

Coolant flowrates are manually controlled by adjusting flow control valves on the probe vessel. Flowrates are measured by orifice meters. All flow streams contain flow switches that verify flow and transmit electrical signals to the computer. Should any flow fail, the computer and backup circuitry will retract the probe from the duct. The flow switches are interlocked to a timer which can allow for momentary flow interruptions.

Electrical Instrumentation and Controls

Electrical instrumentation and controls are contained in a dust-tight enclosure located on the probe. All power to the motors and heater elements is switched at this site. In addition, controls at this site include emergency probe retraction and manual probe advance or retract for servicing. All other control functions are handled by the computer located in the control room. Table 1 lists the instrumentation located at the probe site.

Computer

The computer system consists of the computer, disk drive, video display, and printer. It inputs all temperature, pressure, and flow

Table 1. Probe System Instrumentation

Measurement	Method	Transducer Signal
Gas velocity	Pitot tube	(Computed)
Duct temperature	Thermocouple	4 to 20 mA
Static pressure	Transducer	4 to 20 mA
Differential pressure	Transducer	4 to 20 mA
Probe position	Potentiometer	0 to 5 volts
Sample flowrate	Orifice	(Computed)
Orifice temperature	Thermocouple	4 to 20 mA
Orifice pressure	Transducer	4 to 20 mA
Orifice pressure differential	Transducer	4 to 20 mA
Waterflow	Flow switch/ orifice meter	0 volts "off" 5 volts "on"
N_2 coolant flow	Flow switch/ orifice meter	0 volts "off" 5 volts "on"
N_2 purge flow	Flow switch/ orifice meter	0 volts "off" 5 volts "on"
Filter pressure	Pressure switch	0 volts "off" 5 volts "on"
Sample probe temperature	Thermocouple	4 to 20 mA
Sample gas temperature	Thermocouple	4 to 20 mA
Oven temperature	Thermocouple	4 to 20 mA
Probe obstruction	Mechanical switch	0 volts "off" 5 volts "on"
Probe full extend	Mechanical switch	0 volts "off" 5 volts "on"
Probe full retract	Mechanical switch	0 volts "off" 5 volts "on"
Water temperature	Thermometer	Local indicator
Water pressure	Pressure gauge	Local indicator
N_2 pressure	Pressure gauge	Local indicator
Vessel pressure	Pressure gauge	Local indicator

indication data; calculates gas velocity and sample flowrate; and prints a record of this data. In addition, the computer positions the sample probe within the duct and maintains an isokinetic sampling rate, according to the programmed instructions of the operator. The computer will also automatically retract the probe during nitrogen or waterflow loss or if an obstruction is detected. Should any fault (loss of coolant, obstruction) occur, the computer will flash the fault on the video screen and describe the emergency procedures taken.

Conclusion

The automated extractive particle sampling equipment produced for the experimental PFBC at Grimethorpe will provide a number of benefits to the research effort:

- Reliability -- data will be collected from precise points within the duct as directed by the computer program rather than rely on operator skill
- Repeatability -- a programmed sampling traverse can be repeated avoiding operator error
- Versatility -- the particle collection components (cyclone and filter) are located in one oven. An inertial impactor train or optical sensor could be substituted providing a number of options for particle analysis. With an optional high-temperature filter located on the hot end of the probe, vapor phase alkali can be deduced from laboratory analysis of the collected samples.
- Safety -- operation of the probe is controlled from a remote location thus minimizing operator exposure to the hot, high-presssure ducts
- Economy -- since the computer directs most sampling, one operator could control several probes or could do other tasks while the samples are being obtained

The automated particle sampling technology pioneered for the IEA Grimethorpe PFBC could be extended to other industries and technologies and represents an example of the benefits derived from support of advanced fossil energy process research.

Tuesday Afternoon, June 9, 1981

Session C - Particulates

A DISCRETE PARTICLE SIZE ANALYZER USING A SMALL ANGLE FORWARD SCATTERING TECHNIQUE[+]

Ralph T. Bailey
Research and Development Division
Babcock and Wilcox Co., Alliance, OH

and

James C. F. Wang[*]
Daniel A. Tichenor
Combustion Science Department
Sandia National Laboratories, Livermore, CA 94550
Phone: (415) 422-2786
FTS 532-2786

ABSTRACT A029

A small-angle near-forward scattering (SANFS) technique[1] has been identified as a promising method to measure particle sizes of 1 to 50 μm diameter. A prototype optical system based on the SANFS technique has been built and tested at Sandia National Laboratories - Livermore. Response curves of particle sizes vs the scattered light intensity from this prototype system have been established using known-size apertures and particles. They agree closely with the calculated response curves based on the Mie scattering theory. A coincidence detector has been successfully implemented to reduce the measuring volume of the SANFS detector to about 10^{-4} cc. Preliminary test results of the particle size distribution from an oil atomizer have been obtained and found to depend on the amplitudes of the coincidence trigger signal. Detailed discussions of the measurement procedure and accuracy of the SANFS system are reported.

[+]This work supported by the U.S. Department of Energy, and Babcock and Wilcox Co.

[*]Presenting author.

[1]Wang, J.C.F., "Optical Particulate Size Measurements Using a Small-Angle Near-Forward Scattering Technique," presented at Second Symposium on Transfer and Utilization of Particulate Control Technology, Denver, CO, July 23-26, 1979; SAND79-8246, July 1979, Sandia Laboratories, Livermore, CA.

PARTICLE SIZE DETERMINATION OF COAL IN COAL OIL MIXTURES

T. E. Morris
Leeds & Northrup Co. - MICROTRAC Div.
(A Unit of General Signal)
Largo, Florida 33543

Ryan Nelson
Vetter Research
Costa Mesa, CA 92626

ABSTRACT

This paper describes techniques for determining the particle size distributions of dry pulverized coal powder and pulverized coal in coal oil mixtures (COM), utilizing the MICROTRAC particle size analyzer. The analysis of dry pulverized coal powder is accomplished using the standard four liter aqueous sampling system. The COM must be dispersed and suspended in an organic solvent, such as toluene, for analysis. This requires the conversion of the instrument from the standard four liter sampling system to a 250ml stainless steel sample cell with a self-contained stirring system.

The techniques used to prepare the coal and COM's for analysis will be presented along with methods used in representative sampling. A comparison of data will be made between the aqueous standard system and the non-aqueous small volume sample cell (SVSC) on the raw pulverized coal and the COM. The techniques employed can be extended for use on a number of SVSC applicati ns requiring special suspension and sample preparations.

INTRODUCTION

Particle size distribution analysis is one of a number of major concerns in the production of coal oil mixtures (COM) due largely to the relationship with the viscosity, stability, and rheology of the batch COM. Techniques for obtaining particle size distributions, in this application, are limited due to the complex nature of the COM. The measurement of a wide distribution particulate of dry coal powder in a relatively high viscosity media, as compared with aqueous systems used in most particle size measurement devices, presents a challenge to sampling techniques, dispersion techniques and instrument performance.

The stability and rheological properties of the final COM product are reported by Cherry[1] to be influenced by particle size and concentration, in addition to, oil viscosity, water concentration, chemical additives[1], and the surface properties of the coal[2]. The relationship of these parameters with viscosity are shown in Figure 1. The settling characteristics of the COM is related to the particle size distribution of the pulverized coal in the COM, therefore affecting the stability. Aikens and Ekman[3] report that as the mean size of the particles present in the COM increase, the rate of settling also increases. In addition, as the larger particles begin to settle, this initiates the settling of moderate size particles that might otherwise remain in suspension longer[3].

The rheological properties of a COM that effect the overall mixability result from a complex interaction of varying parameters such as viscosity, temperature, coal concentration and particle size. This interaction can be seen in Cherry's table on mixing parameters[1] (Figure 2).

This paper will concentrate on the measurement techniques of obtaining a particle size distribution of pulverized coal, both dry and in a COM, using the MICROTRAC Particle Analyzer. This instrument utilizes laser light scattering and Fraunhofer diffraction to obtain a particle distribution from 1.9 to 176 microns.

INSTRUMENT THEORY

The scattering of light by small particles produces information that allows determination of particle size. If the particle dimension is large compared to the wavelength of light, the resulting scattered light can be described by Fraunhofer diffraction theory. Illuminated particles produce diffraction patterns which are then summed optically to determine the total particle size distribution. The intensity distribution of the Fraunhofer diffraction pattern is given by the following equation[4].

$$I(\omega) = \varepsilon K^2 \alpha^4 \left[\frac{J_1(K\alpha\omega)}{K\alpha\omega}\right]^2$$

where

$I(\omega)$ = The light intensity as a function of angle with respect to the optical axis.

ε = Incident beam intensity.

α = Particle radius.

$K = \frac{2\pi}{\lambda}$

J_1 = First order bessel function of the first kind.

If the total diffracted light is measured, the resultant signal will be proportional to the area of the particles producing the diffracted light. In many industrial applications, it is more useful to measure the amount of volume of particulates in the process. A unique optical filter designed for MICROTRAC produces signals proportional to the total volume of particulates in the measurement region. If the material density if known, the measurement can be translated to sample mass[5]. The angular distribution of light diffracted by particles is inversely proportional to the size of a particle, while light intensity is directly proportional to the size of particles.

In the standard system, particulate samples inserted into the sampling system (Figure 3) disperse themselves homogeneously throughout the sampling system. A fraction of this dispersion circulates through the sample cell where is diffracts laser light. Particles at this point scatter light in accordance with Fraunhofer diffraction theory. The sample passes through the cell and is returned to the chamber where it will be continuously agitated and recirculated. After the laser beam interacts with the particles, a lens (Figure 4) collects the resultant scattered flux and the main beam, and focuses them onto the mask assembly. An opaque spot is used to block the main beam while allowing the transmission of the diffracted light. The summation of the

diffraction patterns from particles of various sizes in the sample material is carried out by the photodetector and the electronic computational system. The output is a thirteen channel histogram which displays cumulative percent passing or retained (Figure 5).

The instrument allows for the conversion of the standard 4 liter aqueous system to a 250ml round bottom stainless steel small volume sample cell (Figure 6). This system can be utilized for a particle analysis in various solvents. Particles are suspended by either a variable speed overhead stirring mechanism or a magnetic stirring bar driven by water through the sample pump. Particles randomly pass though the laser light, scattering the light the same way as in the standard system. An initial warm-up period of 15 to 30 minutes and a set Zero on a blank sample is required at the days start up for both systems.

PROCEDURES

Control points for all demonstrations were chosen from the data at 88 microns, 62 microns, 44 microns, mean volume diameter (MV), and the 50% percentile (PM). A 30 second low level ultrasonic agitation was employed for each sample to break up loosely occuring agglomerates and to assure uniform treatment of samples for each group of analyses. Five sequential 200 second analyses were made of each set of samples with mean and one standard deviation values calculated for each control point. The analyzer was interfaced with a MICROTRAC Data Module for data gathering and computational convenience. Specific individual procedures for each demonstration will be appendixed.

PARTICLE ANALYSIS OF DRY PULVERIZED COAL IN AN AQUEOUS SYSTEM

The particle analysis of the dry pulverized coal can be accomplished by using the standard 4 liter aqueous system. To demonstrate the instrument repeatability and the ability of an operator to sample the material from a batch process, one (3-gram) sample was extracted from a one quart container of dry pulverized coal (representing the batch process). The particles were then suspended and properly dispersed prior to analysis according to procedure A (Appendix). The degree at which the particle analyzer can repeat an analysis for one sample of dry coal powder can be shown in Table One.

The repeatability of an analysis is important in determining particulate stability in a fluid system. For example, if particles were introduced into the measurement system as agglomerates, the attrition associated with the circulating system would cause particle comminution, indicated by the systematic reductions in particle size with time. If the particulates were reacting with the suspension, then dissolution or agglomeration may be observed by smaller loading values and particle size, or larger loading values and particle size respectively.

Sampling bias can occur as a result of the way in which the operator extracts the sample from the bulk powder. One method in sampling bulk material is to take multiple samples from different locations within the bulk material and mix the samples into one container, analyze several samples, and average the results. An example of this method and the associating sampling variations can be seen in Table Two where five sample (3-gram each) were

MULTIPLE ANALYSES OF ONE SAMPLE OF DRY COAL POWDER
SHOWING INSTRUMENT REPEATABILITY

RUN #	1	2	3	4	5	$\bar{M}$	σ
%-88	74.7	75.1	75.0	75.5	73.9	74.8	.6
%-62	61.3	61.3	61.6	61.8	62.2	61.6	.38
%-44	49.0	48.5	48.2	47.6	48.3	48.3	.51
MEAN VOLUME	57.7	57.6	57.7	57.6	58.4	57.8	.34
50% TILE PM	45.2	45.9	45.9	46.6	45.9	45.9	.19

TABLE ONE

VARIATION IN SAMPLING DRY COAL (ANALYZED
IN STANDARD SYSTEM)

SAMPLE	1	2	3	4	5	M	STD.DEV.
%-88	74.8	75.0	74.4	75.5	76.5	75.2	.8
%-62	61.6	61.8	62.0	61.7	62.4	61.9	.3
%-44	48.3	48.2	49.4	47.6	49.6	48.6	.8
MEAN VOLUME	57.8	57.6	57.5	57.3	56.1	57.2	.7
50% TILE PM	45.9	46.1	44.8	46.8	44.5	45.6	1.0

TABLE TWO

extracted from various locations within the larger container of dry coal powder and analyzed according to procedure B (Appendix). Good sampling techniques resulted in a low degree of sampling variation as indicated in Table Two. Contributing as well to the low sampling variation was the high ratio of test sample to the total sample material. As the ratio is reduced, the probability of variation in sampling generally increases, stressing the importance of representative sampling.

SAMPLE ANALYSIS OF DRY COAL POWDER IN AN AQUEOUS SYSTEM USING A SMALL VOLUME SAMPLE CELL (SVSC)

Since the COM analysis will eventually be made in the SVSC as opposed to the standard 4-liter system, it will be necessary to evaluate the degree of variability caused by the difference in the two systems.

The standard aqueous system of the particle analyzer can be converted to a 250ml stainless steel sample container (Figure 6) that allows for a particle analysis to be performed in an aqueous or non-aqueous system. The sample container has a larger cell pathlength than is used in the standard 4-liter system. This requires that considerably less material be introduced into the cell, since more particles pass through the laser beam at any one time. This reduction in the sample loading ratio increases the inherent error present in operator sampling and sampling techniques. As seen in Table Three where four, 20-30 milligrams of dry pulverized coal were carefully extracted from a 3-gram sample with each sample analyzed according to procedure C (Appendix), using tap water as the carrier. Note that the variation between samples was significant and showed the coal, on the average, to be biased toward the fine end, due to the difficulty in sampling such a small quantity representatively.

VARIATION IN SAMPLING DRY COAL (ANALYZED IN SVSC) 20-30 MG

SAMPLE	1		2		3		4			
	M	STD.DEV.	M	STD.DEV.	M	STD.DEV.	M	STD.DEV.	M	STD.DEV.
%-88	82.2	1.3	79.6	2.6	88.5	4.2	89.5	2.5	85.0	4.8
%-62	70.0	.7	65.6	.5	69.7	1.8	73.9	1.0	69.8	3.4
%-44	56.0	.5	50.8	1.3	53.2	1.6	58.5	.9	54.6	3.3
MEAN VOLUME	50.2	.8	54.1	1.3	47.7	2.3	46.0	1.2	49.5	3.5
50% TILE PM	38.0	.2	42.9	1.3	39.7	1.8	35.5	.7	39.0	3.1

TABLE THREE

Suspending larger quantities of particulate in a highly viscous medium prior to sampling improves the sample-to-sample variation as well as the agreement of the two systems, while instrument repeatability for each sample remained relatively consistent. To test the above method a three gram sample of the dry pulverized coal was suspended in enough glycerin to make a viscous paste and analyzed according to procedure D (Appendix). The results in Table Four show good agreement between the low loading SVSC (20-30 mg) and the higher loading standard system (3 grams) with smaller deviations between sampling, than the 20-30 mg dry sample extraction method.

A comparison of all three methods, as summarized in Table Five, clearly shows agreement between the two systems in column one and three. Development of the correct sampling procedure, consisting of increasing the viscous of the mixture during the sampling process, allowed representative sampling of the 20-30 mg sample.

SAMPLE ANALYSIS OF DRY PULVERIZED COAL POWDER IN NON-AQUEOUS SYSTEM USING A SMALL VOLUME SAMPLE CELL (SVSC)

The particle analysis of COM that will require suspension and dispersion in a nonaqueous solvent, such as toluene, can utilize the SVSC provided the

VARIATION IN SAMPLING DRY COAL WITH GLYCERIN
(ANALYZED IN SVSC)

SAMPLE	1		2		3		4			
	M	STD.DEV.	M	STD.DEV.	M	STD.DEV.	M	STD.DEV.	M	STD.DEV.
%-88	78.1	3.9	75.4	2.9	76.3	1.6	72.8	2.6	75.7	2.2
%-62	65.3	1.8	62.6	1.1	63.8	1.2	61.4	.4	63.3	1.7
%-44	50.9	1.3	48.1	1.6	49.3	1.2	47.7	2.2	49.0	1.4
MEAN VOLUME	54.4	2.7	57.5	1.0	56.6	.86	57.2	1.4	56.4	1.4
50% TILE PM	42.7	1.4	45.8	1.6	44.4	1.2	46.2	2.6	44.8	1.6

TABLE FOUR

COMPARISON OF STANDARD SYSTEM AND SVSC SYSTEMS

	STANDARD WET		COAL DRY SAMPLING ONLY SVSC		GLYCERIN AND COAL SVSC	
	3-5 gr SAMPLE		20-30 mg SAMPLE		APPROX.20-30 mg SAMPLE	
SAMPLE	M	STD.DEV.	M	STD.DEV.	M	STD.DEV.
%-88	75.2	.8	85.0	4.8	75.7	2.2
%-62	61.9	.3	69.8	3.4	63.3	1.7
%-44	48.6	.8	54.6	3.3	49.0	1.4
MEAN VOLUME	57.2	.7	49.5	3.5	56.4	1.4
50% TILE PM	45.6	1.0	39.0	3.1	44.8	1.6

TABLE FIVE

chosen suspension does not bias the particle distribution by rapid, partial or total dissolution. Bias due to the type of suspension can be determined by analyzing the dry pulverized coal in the questioned solvent. Since increasing the viscosity clearly improves the agreement with the standard wet system and the sampling variability of dry COM, three grams of dry pulverized coal was slurried with #6 fuel oil to suspend the particulate and then analyzed in toluene using the SVSC in accordance with procedure E. The results obtained from the analysis in the standard system and the SVSC glycerine mixture are compared with the SVSC toluene analysis in Table Six. Results indicate that an analysis in toluene and the initial suspension in #6 fuel oil has little or no short term effects on the particle size distribution.

A COMPARISON OF A TOLUENE SUSPENSION AND A WATER SUSPENSION USING THE SVSC

	DRY COAL STANDARD WET 3-5 gm SAMPLE		GLYCERIN AND COAL SVSC Mix 20-30 mg		DRY COAL SVSC W/TOLUENE Approx. 20-30 mg Suspended in #6 oil	
SAMPLE	M	STD.DEV.	M	STD.DEV.	M	STD.DEV.
%-88	75.2	.8	75.7	2.2	76.7	1.7
%-62	61.9	.3	63.3	1.7	63.7	.5
%-44	48.6	.8	49.0	1.4	49.3	.5
MEAN VOLUME	57.2	.7	56.4	1.4	56.2	.6
50% TILE PM	45.6	1.0	44.8	1.6	44.7	.4

TABLE SIX

COM ANALYSIS IN A TOLUENE SUSPENSION

As mentioned previously, extending the particle analysis to COM requires considerable more awareness of sampling techniques than is necessary in the SVSC dry coal analysis. COMS typically drawn for analysis are from large batch process on the order of thousands of gallons of mixture. Arriving at a smaller representative workable quantity (500ml) is extremely difficult but important. As with the sampling of the dry coal powder, sampling representatively can be accomplished if the COM is sampled from various locations within the batch process and combined with several samples into one large composite. Heating and stirring of the COM must be applied to suspend particulates while removing small samples. Contents of the large container of the compiled COM should continually be split and sampled in the above procedure until a sample of less than 500ml COM is achieved.

A large batch of coal oil mixture, 30% concentration, was fabricated from the remaining coal sample and #6 fuel oil for demonstrating instrument performance and sampling reproducibility on COM. Results from the analysis using procedure F (Appendix) are listed in Table Seven. The degree of sampling variation in the analysis of COM using a toluene suspension are compared with prior analyses employing several different systems and carriers. The results, on the average, are showing the COM particle analysis to be slightly smaller than the standard wet system. Since the same pulverized coal powder was used in all of the experiments, the differences must be attributed to a small degree of sampling bias as well as the smaller ratio existing between the test sample to the total sample. Further experimentation involving large numbers of samples would verify this thesis.

ALTERNATIVE SUSPENSION IN SVSC

COM particle analysis utilizing the MICROTRAC particle analyzer is not limited only to a toluene suspension. Experiments on coal particle analysis

COMPARISON OF COM ANALYSIS WITH OTHER SYSTEMS AND SUSPENSIONS

	DRY COAL STANDARD WET		GLYCERIN AND COAL SVSC		DRY COAL SVSC W/TOLUENE		COM SVSC W/TOLUENE	
SAMPLE	M	STD.DEV.	M	STD.DEV.	M	STD.DEV.	M	STD.DEV.
%-88	75.2	.8	75.7	2.2	76.7	1.7	78.9	1.9
%-62	61.9	.3	63.3	1.7	63.7	.5	65.6	1.3
%-44	48.6	.8	49.0	1.4	49.3	.5	51.3	1.4
MEAN VOLUME	57.2	.7	56.4	1.4	56.2	.6	53.8	1.8
50% TILE PM	45.6	1.0	44.8	1.6	44.7	.4	42.5	1.5

TABLE SEVEN

in COM have involved various sampling processes and sample preparations as shown in procedure G (Appendix). Table Eight shows a partial list of alternate suspensions that are currently being used in the SVSC for COM particle analysis. The COM, in these applications, were first washed free of fuel oil using hot kerosene followed by multiple washes with methanol, or other suitable solvents. This is achieved through the utilization of a millipore manifold to contain the coal samples during washing. The coal forms a cake that must be redispersed with surfactant such as TRITON X-100 10% solution and minimal dispersion assistance such as ultrasonic agitation.

ALTERNATIVES TO TOLUENE SUSPENSION

DEGREE OF DISPERSION	COAL STATUS	SUSPENSION	METHOD
+	DRY POWDER	H_2O	FLOW CELL SVSC
++++	DRY POWDER	500ml TRITON X-100 750ml G.E. AF93 W_2O	FLOW CELL
++	DRY POWDER	KEROSENE	SVSC
+++	DRY POWDER	METHANOL	SVSC
++++	DRY POWDER	SEDISPERSE A-11	SVSC

ALTERNATIVES TO TOLUENE SUSPENSION (cont'd)

DEGREE OF DISPERSION	COAL STATUS	SUSPENSION	METHOD
++++	COAL/OIL	KEROSENE	SVSC
++	COAL/OIL	METHANOL	SVSC
+++	COAL/OIL	METHANOL SOME TRITON	SVSC
++++	COAL/OIL	SEDISPERSE A-11	SVSC

TABLE 8

SUMMARY AND CONCLUSION

The data presented in this paper shows a series of logical steps in the development of a method to analyze coal-oil mixtures (COM). Starting with the dry coal in the standard aqueous system, coal was subsequently run in a small volume system containing water and then a solvent (toluene). Finally, the COM was introduced directly into this small cell container, containing toluene, producing results that agree with those of the dry coal originally analyzed.

The large quantities of sample used in the standard 4-liter system make sampling a much easier task. The small samples necessary for the small cell analysis make representative sampling more difficult. Results of these comparisons show that the sampling problem can be overcome, and results of the COM are in good agreement with those of the dry coal analysis in the standard system.

The particle analysis of COM is not limited to the SVSC with a toluene suspension. As reported there are various combinations of suspensions and sampling procedures. The method described in this paper for determining the influences of systems, solvents, sampling and operators is one that can be extended to evaluate any procedure.

REFERENCES

1. N. N. Cherry, "The Application to Plant Operation of Laboratory Practices Used in the Characterization of Coal-Oil Mixtures," Third International Symposium on Coal-Oil Mixture Combustion, April 1961.

2. G. D. Botsaris, Y. M. Glazman, M. A. Viola, P. S. Goldsmith and R. J. Haber, "Characterization and Structural Studies of Various Types of COM," Dept. of Chemical Engineering, Tufts Univ.

3. A. C. Aikens and J. M. Ekmann, "The Effect of Coal Particle Size on Settling Behavior of Coal-Oil Mixtures," Third International Symposium on Coal-Oil Mixture Combustion, April 1981.

4. M. Born and E. Wolf, "Principles of Optics Pergamon Press, New York, 1959, pg. 385.

5. E. C. Muly and H. N. Frock, "Industrial Particle Size Measurement Using Light Scattering," Optical Engineering 19(6), 861-869 Nov/Dec 80.

APPENDIX

PROCEDURES

A. Five, three gram samples were extracted from the larger container. The coal was sampled after inverting the container twenty times with several inversions made during the sampling procedure. The five samples were then recombined and resplit in the above procedure. One five gram sample was then dispersed using two drops of *Triton X-100 (10% solution). Small amounts of water were added to the coal powder until a uniform paste was formed. Additional water was added until a 25ml slurry was achieved. To produce a uniform dispersion the water coal slurry was then treated ultrasonically for 30 seconds in a 125 watt ultrasonic bath, while providing manual stirring. The pretreated slurry was then added to the 4 liter basin of the MICROTRAC for measurement. The sample container was washed twice with water to remove residual particulates. (*ROHM and HAAS Co., Philadelphia, PA.)

B. The remaining four samples from procedure A were used for this demonstration. The samples were prepared in accordance with the above procedure.

C. A three gram sample of dry pulverized coal was extracted from various locations within the larger container. The three gram sample was inverted twenty times to uniformly mix the composite. Four, 20-30 milligram samples of dry pulverized coal were extracted from the three gram sample employing the inversion technique and each dispersed with two drops of 10% solution of TRITON X-100. Water was added to make a 20ml coal water slurry. Each slurry was then ultrasonically treated for 30 seconds in a 125 watt ultrasonic. The contents of one container was added to the SVSC containing approximately 200ml of filtered water. The sample container was washed twice, to remove all residual COM particulates, and added to the SVSC for analysis.

D. The remaining sample from procedure C was slurried with enough glycerin to form a thick viscous paste. Four, 2-3 drop samples were extracted from the paste with each placed in a beaker containing two drops of TRITON X-100 10% solution. 20ml of water was added and prepared for analysis according to procedure C.

E. Three grams of dry pulverized coal was slurried with #6 fuel oil. Four, 2-3 drop samples were extracted from various locations in the slurry. Each 2-3 drop sample was added to a glass beaker containing 25ml of filtered toluene. Each sample was ultrasonically treated for 30 seconds while providing mechanical stirring. The entire contents of one glass beaker per analysis was added to the SVSC containing 200ml of filtered toluene. The container was washed twice with 10ml of toluene to remove residual particulates and added to the SVSC.

F. Ten ml samples were extracted from the batch COM from various locations. The samples were then combined into one container. The sample was heated to 160°F and stirred by an overhead stirrer for 30 minutes. The sample was continuously split until a less than 300ml sample was achieved. The sample was heated and stirred for 15 minutes. Five, two drop samples were extracted from this sample and added to five glass beakers containing 25-30ml of toluene. The pipets used to extract the COM were washed clean of residual COM with the contents of the beaker. Each sample was manually stirred to dissolve the COM then ultrasonically treated for 30 seconds in a 125 watt ultrasonic bath. Manual stirring was provided during the ultrasonic treatment. The entire contents of one beaker was added to SVSC containing 200ml of filtered toluene. Two 20ml rinses were made to remove residual particulates from the container and added to the SVSC. The sample was allowed to disperse and stabilize in the SVSC for 1 minute prior to analysis.

G. SEDIMENTATION ANALYSIS PROCEDURE

Each COM is sampled at three points using pipets. Sample points = depth of penetration from COM surface = .5 cm, 4.5 cm, 9.0 cm. (Surface sample is taken first to avoid disruption of layers.) (Progression is top to bottom.)

Samples are spaced via triangular method to avoid above-mentioned disruptions, e.g.,

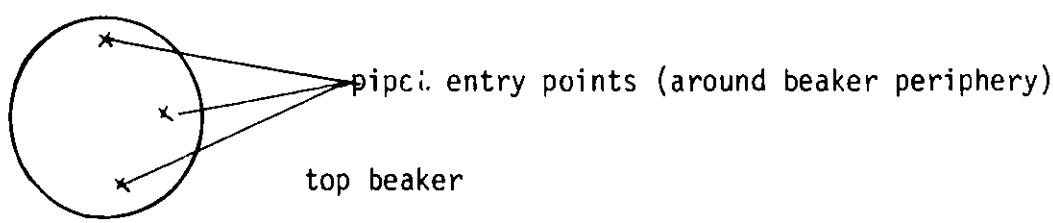

1. After entry, pipet disruption is minimized through maintenance of elevated temperature in beaker which lowers viscosity, increasing rate of layer stabilization.

2. Allow pipet to remain in mixture for 15 seconds. This will minimize penetration disruption of layers prior to vacuum filling of pipet to 0.65ml.

3. After removal, the outside of each pipet is wiped off and the inside is rinsed free of COM onto a 0.8µm filter using warm kerosene.

4. The filter paper can then be washed with methanol or left wet with kerosene, if analyzed in kerosene. Add directly to filtered blank SVSC.

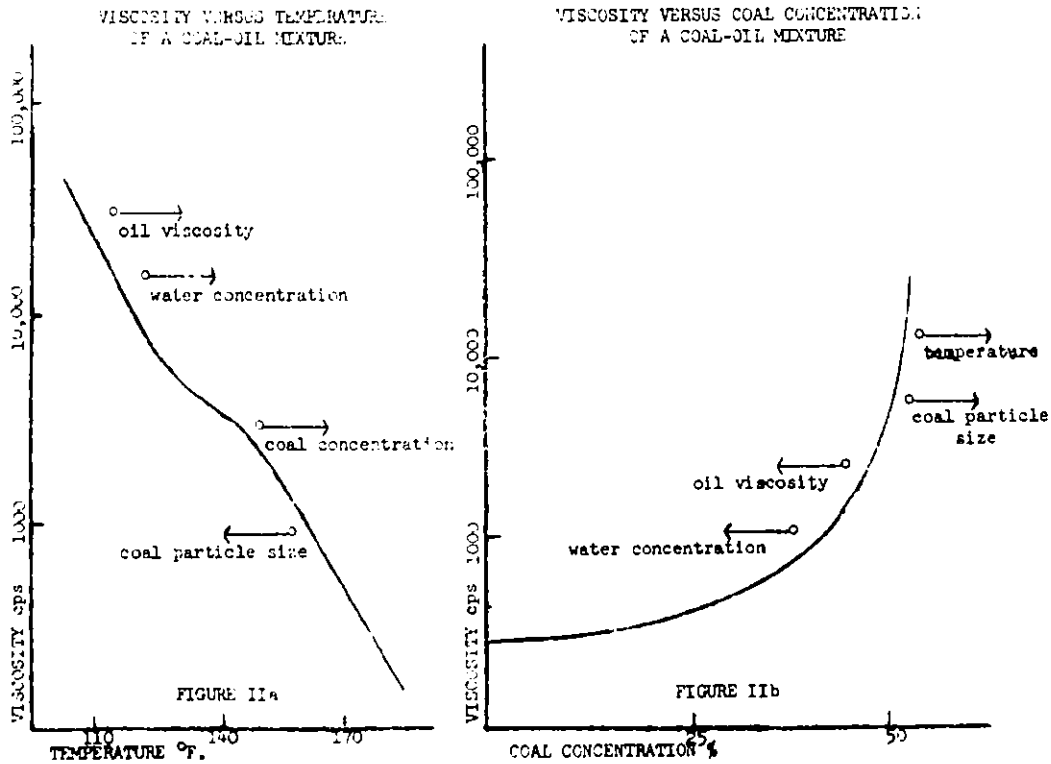

Figure 1 (from Ref. 1)

MIXING PARAMETER RANGES

COAL CONCENTRATION %	PARTICLE SIZE DISTRIBUTION % -200M	VISCOSITY cps	TEMPERATURE °F	RESIDENCE TIME Min.
50	90	7000	150	40
20	75	1000	120	20

Figure 2 (from Ref. 1)

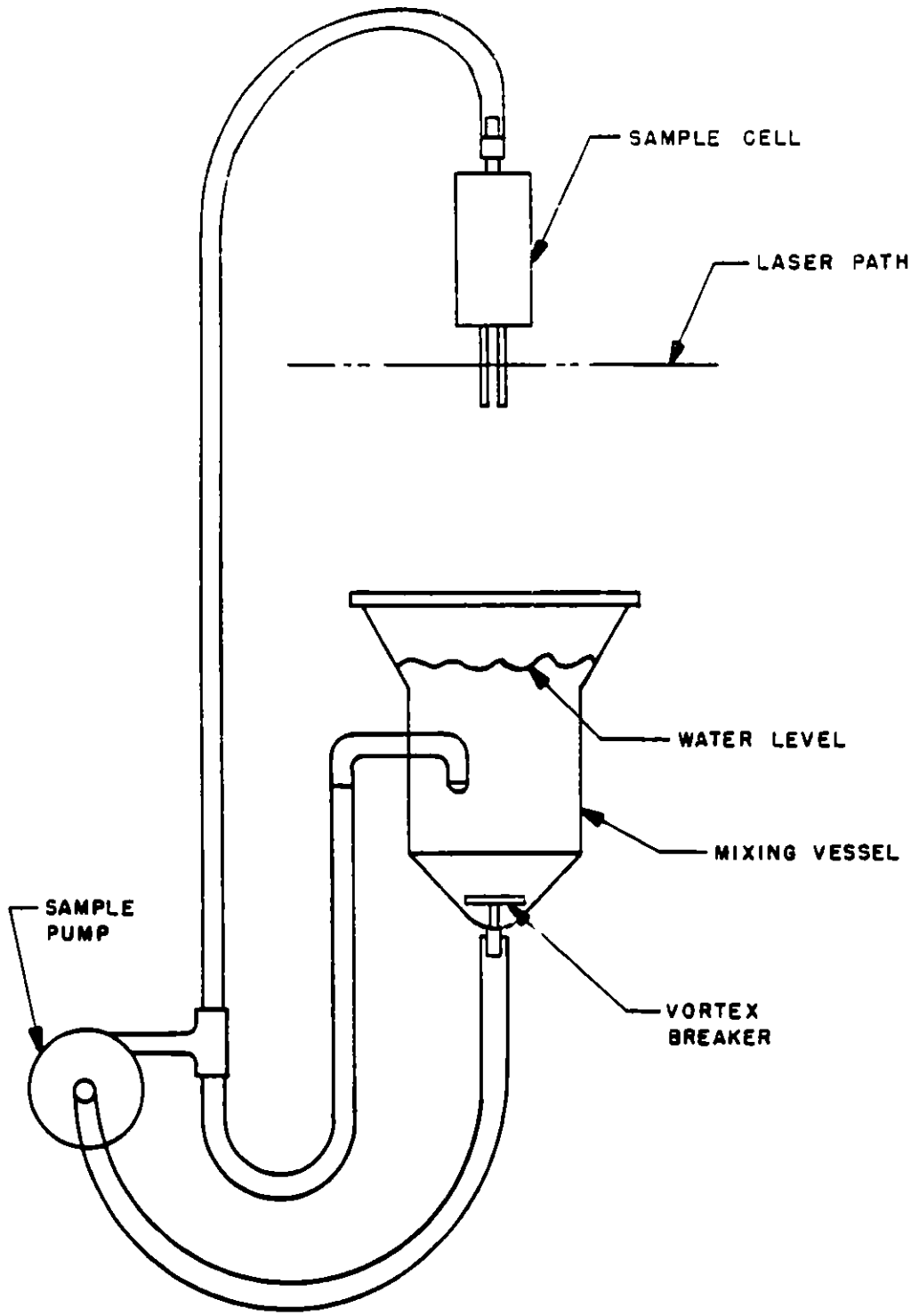

STANDARD RECIRCULATION SAMPLER SYSTEM

FIGURE 3

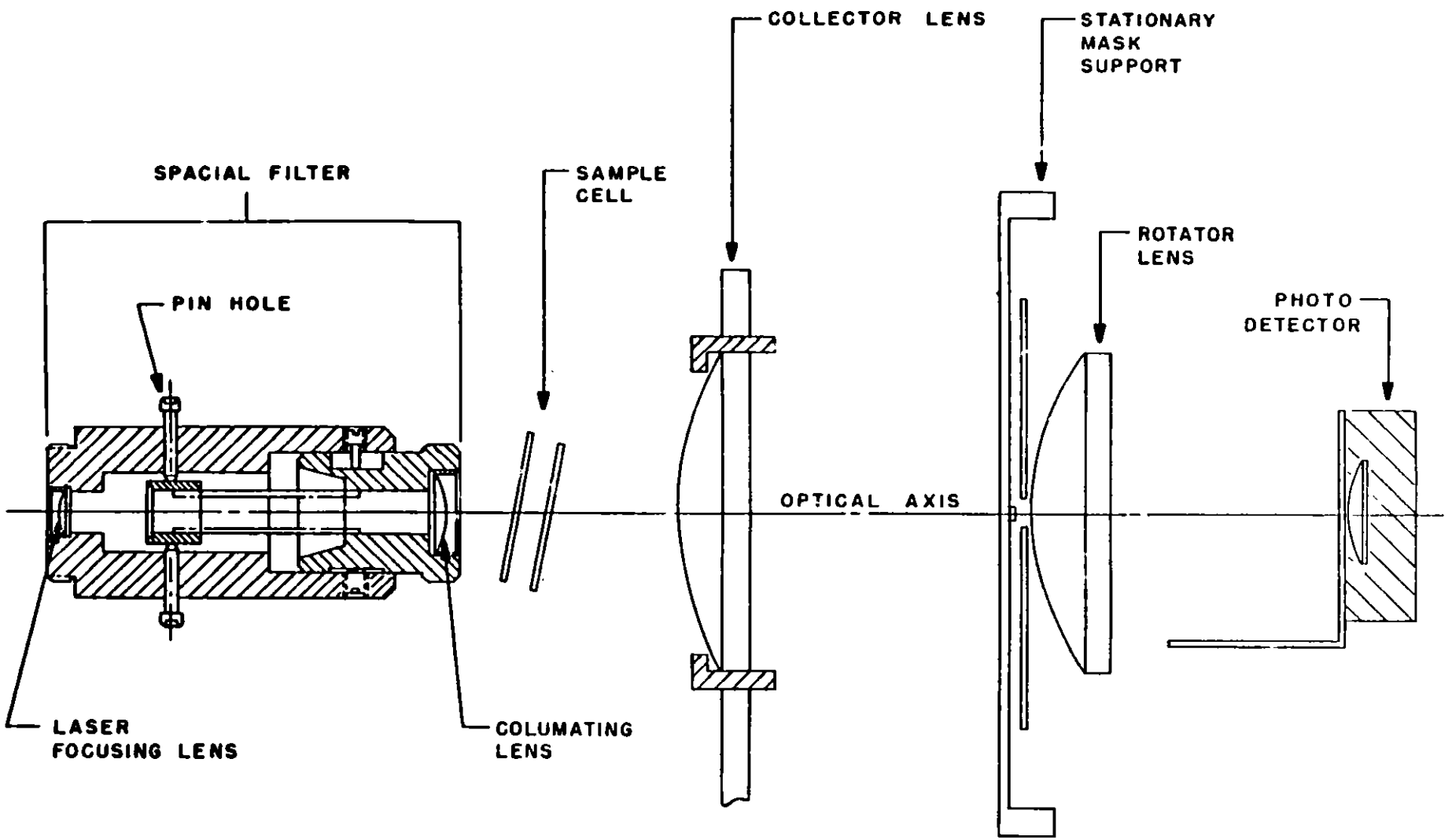

MICROTRAC OPTICAL COMPONENT POSITIONS

FIGURE 4

TYPICAL DATA PRINTOUT

Sample Number and Position ID

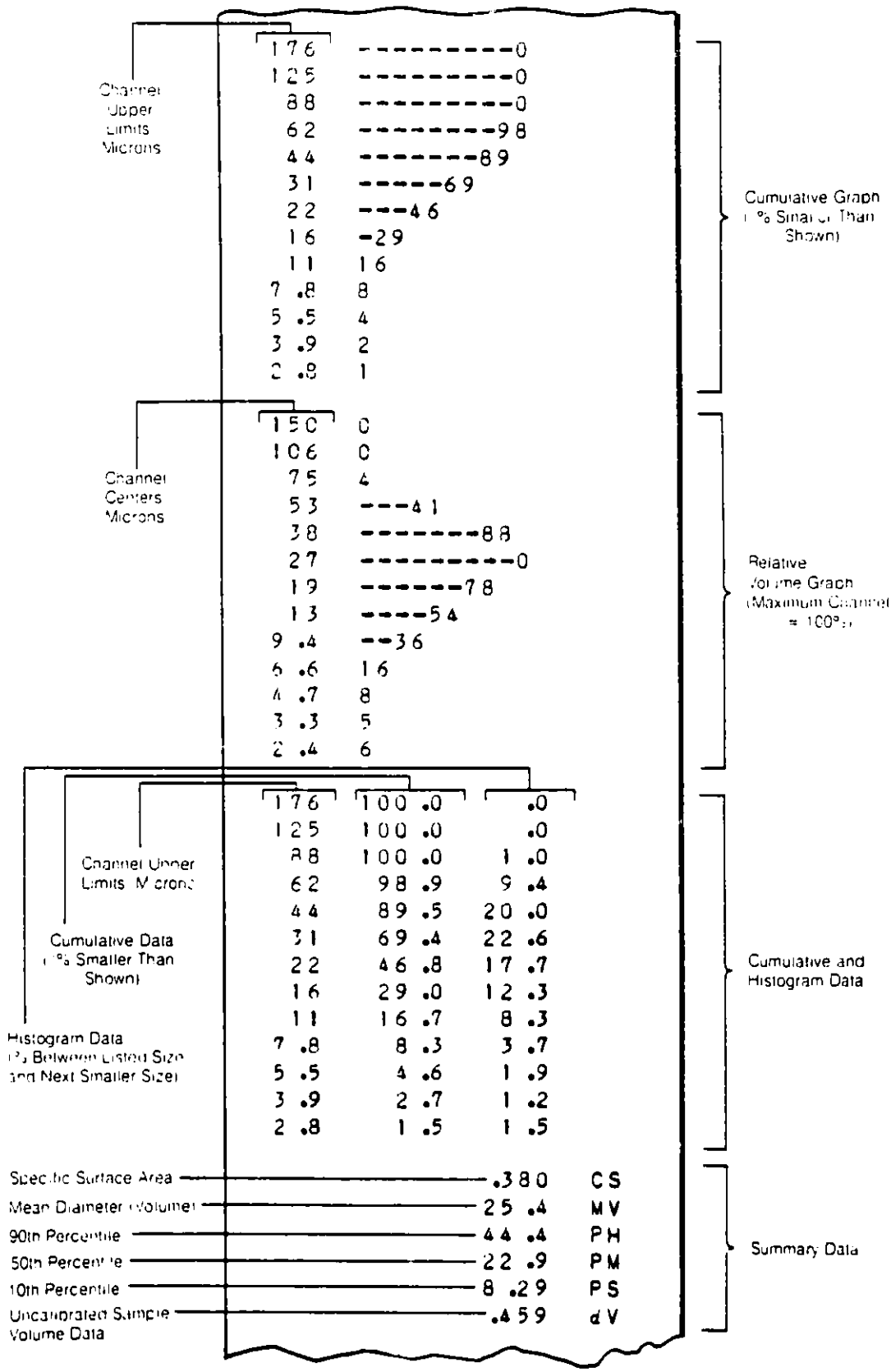

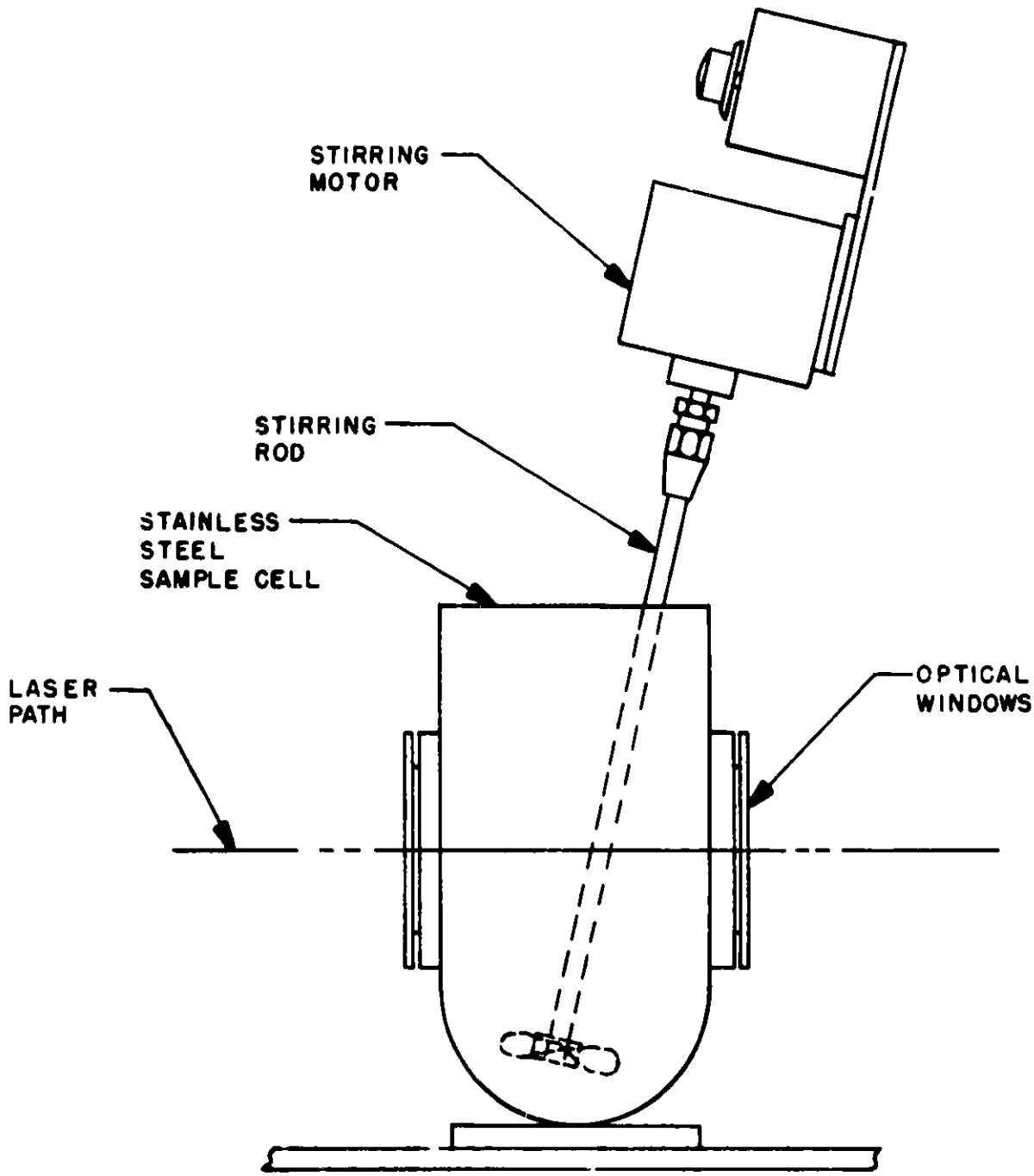

SMALL VOLUME SAMPLE CELL

FIGURE 6

"A Mobile In Situ Optical Particle Counter for 0.3-80 μm Particles at Number Densities up to $10^6/cm^3$."

Donald J. Holve

Sandia National Laboratories
Division 8521
Livermore, CA 94550
Ph. (415) 422-2688

An in situ optical technique described previously (Holve & Self 1979; Holve, 1980) is extended for measurements of submicron particles at number densities corresponding to typical flue gas conditions (10^5-10^6 particles/cm^3 at 0.4 m). The method is based on near forward light scattering which minimizes sensitivity both to particle shape and refractive index. The optical arrangement consists of a mobile optical bench with a 0.6m cutout for access to ambient or combustion flows (Figure 1). Two beams and two detectors are combined with a single light collection path to cover the size ranges 0.3-4μm and 4-80μm, respectively. The method uses an intrinsically stable deconvolution technique to account for intensity variations within the optical sample volume. The amplitude scattering spectrum is rapidly deconvolved on a small mini computer and results displayed in near real time (~10 sec.).

Results are presented for measurements of monodisperse polystyrene spheres in the size range 0.26-4 μm which agree with the Mie theory calculations of the response function (Figure 2). A frequency distribution for a commercial oil droplet atomizer (TSI Model #3076) is shown in Figure 3 and is in agreement with general vendor specifications. These results, in conjunction with the previous measurements, demonstrate the capability of this technique for in situ measurements in the size range 0.3-80μm at number densities up to $10^6/cm^3$.

SUBMICRON PARTICLE ANALYZER

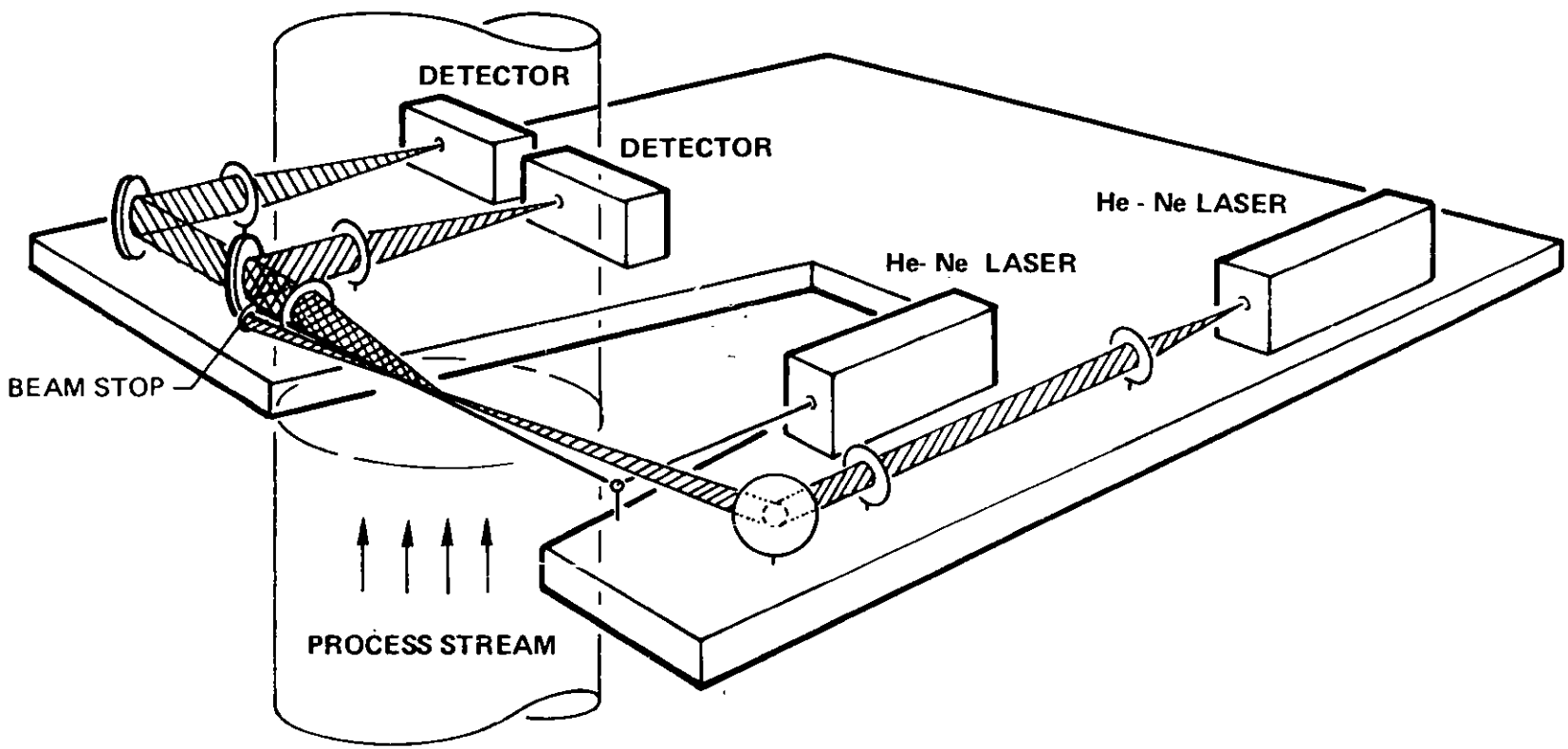

Figure 1

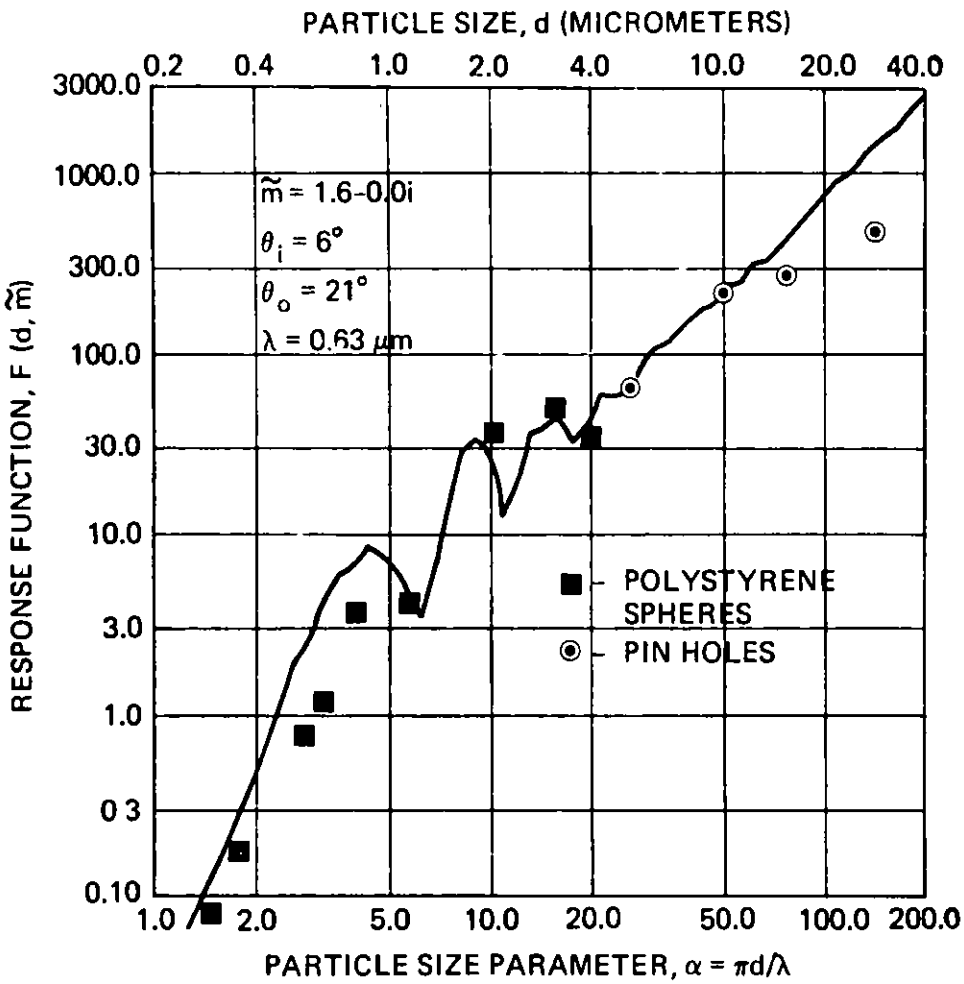
PARTICLE SIZE, d (MICROMETERS)
0.2
0.4
1.0
2.0
4.0
10.0
20.0
40.0
3000.0
1000.0
300.0
100.0
30.0
10.0
3.0
1.0
0 3
0.10
RESPONSE FUNCTION, F (d, m̃)
m̃ = 1.6-0.0i
θi = 6°
θo = 21°
λ = 0.63 μm
POLYSTYRENE SPHERES
PIN HOLES
1.0
2.0
5.0
10.0
20.0
50.0
100.0
200.0
PARTICLE SIZE PARAMETER, α = πd/λ

Figure 2

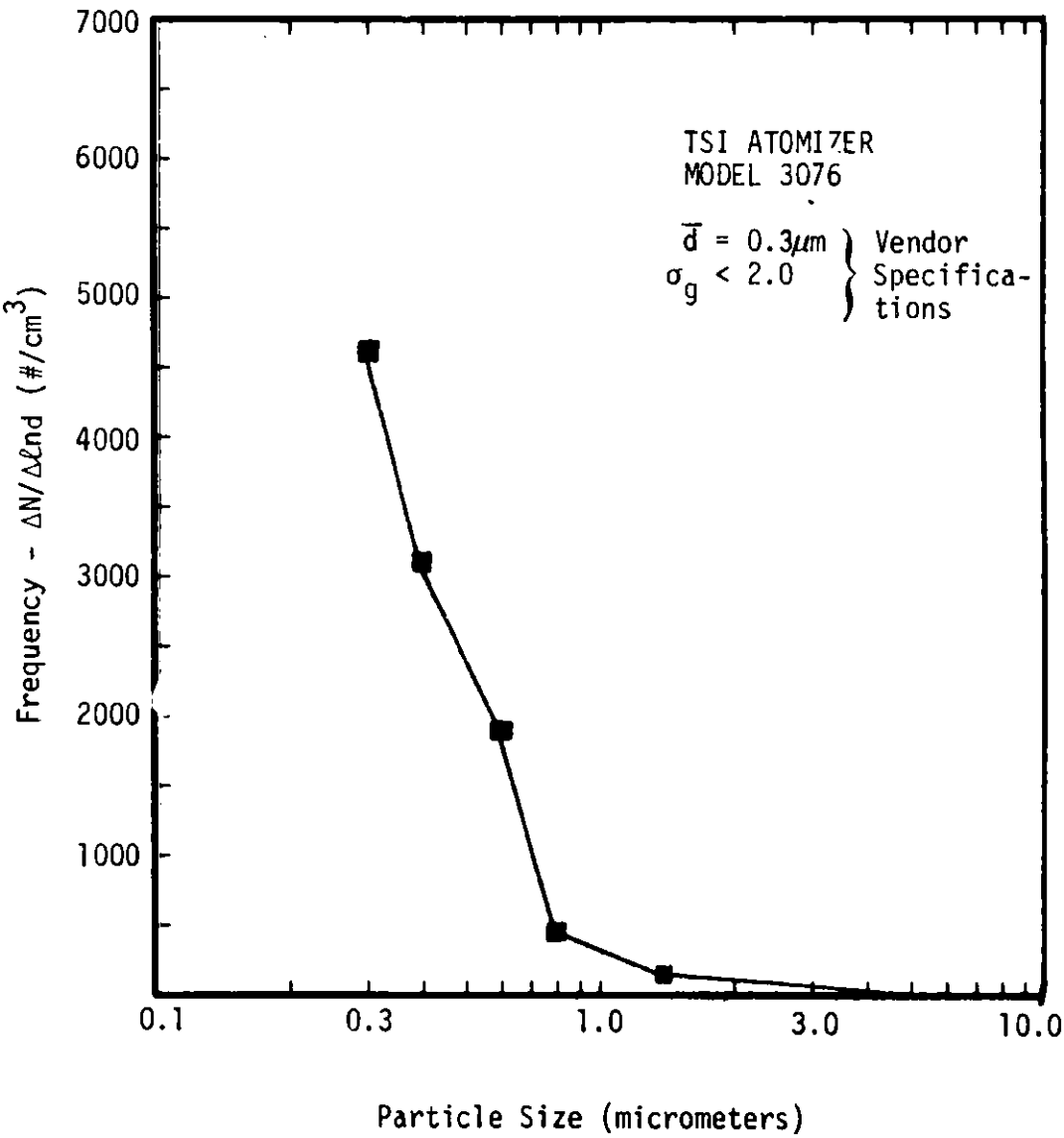
TSI ATOMIZER
MODEL 3076
$\bar{d}$ = 0.3μm
σ_g < 2.0
Vendor Specifications
Frequency - ΔN/Δℓnd (#/cm^3)
7000
6000
5000
4000
3000
2000
1000
0.1
0.3
1.0
3.0
10.0
Particle Size (micrometers)

Figure 3

IN-STACK OPTICAL PARTICLE SIZING - A CONTINUOUS MONITOR FOR FINE PARTICLES

A. L. Wertheimer
E. S. VanValkenburg
Leeds & Northrup Company

ABSTRACT

A prototype instrument has been developed for in-situ monitoring of fine particulates in stack emissions. The instrument employs a helium neon laser and two modes of optical scattering to provide continuous measure of particles in the size range 0.2 to 20 micrometers (microns) diameter. The work reported here was sponsored by the Environmental Protection Agency (EPA Contract No. 68-02-3253).

INTRODUCTION

Monitoring of particulate emissions from stationary stacks has been by measure of opacity or by extractive sampling. Opacity measurements, either across the stack or through the plume, yield little information on particle size, yet we know that particle size is a critical parameter in assessing health effects of particulate emissions.[1] Particle size data can be derived from small samples extracted from the flue gas stream or by inertial impactor, but such sampling may not be representative and, at best, is a very tedious and time-consuming procedure. What is needed is an in-stack monitor which will continuously measure particle emissions. Leeds & Northrup Company has developed such an instrument. This instrument measures the amount of total particulate and differentiates the fine particle emissions from the less-health-risk larger particles, as shown in Figure 1.

The size of particles emitted into the atmosphere affects both the air transport of the particles and the extent of inhalability. Fine particles, defined as those smaller than 2 to 3 microns, experience little gravitational settling and are carried long distances from the emitter. When suspended particles are inhaled, the larger particles enter only the upper bronchial

track and are quickly expelled, while the fine particles are deposited in the alveoli where they may be trapped for several days.[2]

The EPA, and others concerned with air pollution, are vitally interested in establishing a size-specific standard for particulate emissions. Such a standard would benefit those industries and utilities that are presently opacity limited but emit low levels of inhalable fine particles. Some facilities are unduly constrained in allowable emissions because the opacity measurements do not distinguish harmless particles and condensate from the more hazardous submicron particles.

The Leeds & Northrup instrumentation is designed for in-situ monitoring of solid and liquid particulates and provides continuous measurement of particle size distribution in the flue gas emission. The particles are optically sampled and measured by detecting the flux scattered by particles illuminated by a laser source, as shown in Figure 2. This method of measurement has no effect on either the physical particle distribution or the fluid stream being monitored. The results of field tests show good correlation with aerodynamic sizing, indicating that the particles from such stacks are largely spherical in shape and quite homogeneous. Thus, this type of instrumentation is especially well suited for on-line measurement of particles in stack emissions.

SYSTEM DESCRIPTION

The prototype instrument includes four separate portable units: an optical probe assembly, an electronics console, power supply and air purge blower.[3] Photographs of these units are shown in Figure 3. The optical probe is 60 inches long and can be inserted through a standard 4-inch i.d. port into the gas stream. This stainless steel probe is oriented in the stack or duct so that the gas flow is through the 14-inch long slot near the end of the probe.

A close-up view of the electronics console with cover open is shown in Figure 4. Processed data are printed at selected time intervals for permanent record. A printer tape take-up reel is provided to enable the instrument to be operated unattended with the console cover normally closed. The blower unit provides a continuous flow of air into the probe to prevent deposition of dirt and condensation on windows located at each end of the sampling slot.

The instrument specifications are presented in Table I.

TABLE I

IN-STACK PARTICLE MONITOR

Operational Specifications

Particle Size Range	0.2 to 20 μm diameter
Particle Size Discrimination	Five volume fractions: 0.3, 1.0, 3.5, 7.5, 15 μm
Particulate Loading Range	5 to 1000 mg/m^3 (2 to 400 ppb by volume)
Data Integration Time	5 seconds to 12 minutes
Stack Temperature	260°C maximum (500°F)
Instrument Temperature	0° to 43°C (32 to 110°F)
Power Requirements	20A, 115V, 60 Hz

Physical Dimensions

Probe Length	60 in. with sample slot 1 x 14 in.
Probe Assembly	80 x 10 x 10 in., 70 lbs.
Blower	29 x 19 x 17 in., 50 lbs.
Control Console	15 x 16 x 10 in., 20 lbs.

PRINCIPLES OF MEASUREMENT

Optical sizing has been previously restricted to measurement of individual (isolated) particles crossing a narrow beam of light. However, as a result of Leeds & Northrup's extensive research, it is now possible to automatically extract particle size distributions from composite diffraction patterns for large numbers of particles. Thus, there is no need to resolve

individual particles and a wide range of particle loadings can be accommodated.

The forward scatter flux is measured at four discrete angles between 1 and 10° of the laser beam axis (see Figure 2). These signals are combined to generate volumetric loadings for four contiguous size ranges from 1 to 20 microns. The submicron particles are measured by detecting polarized light scattered orthogonally from the laser beam. This principle is known as polarization-dependent 90° scattering.[4] The difference in intensities produced by scattering at 90° from the two polarizations yields data on particle size. Furthermore, this relationship is not dependent on refractive index.

MICROPROCESSOR FUNCTIONS

Scatter signals are transmitted from the probe to detectors located outside the stack via optical fibers. The outputs of the detectors are digitized and processed in the electronics console. The resultant data are combined to provide a five-channel histogram and a measure of total loading. The processed data are integrated and then printed in the format shown in Figure 5. The loading is designated "DV" in the printout and can be calibrated in mass loading units.

A block diagram of the microcomputer and associated electronics is shown in Figure 6. The microcomputer uses a Z-80 processor, and the memory has 8K of PROM and 2K of RAM. Signals from the preamplifiers and console panel switches are entered via the six input ports. Eleven output ports are used to operate the digital LED display and printer.

Before the instrument is installed in the stack, optical background signals are measured and automatically stored in memory. These background data are subsequently subtracted from the scatter measurements, data are averaged over the selected integration interval (5 seconds to 12 minutes), and the size distribution and loading are calibrated and printed out.

CALIBRATION

Calibration of this type of instrumentation involves setting the gains of the detector amplifiers and adjusting their individual contributions in the microprocessor algorithm. This algorithm consists of two parts: one for the forward scattering and one for the submicron range.

Calibration of the four forward detectors is accomplished by filling the sample volume with a characterized aerosol. The aerosol must have a well defined narrow size distribution of spherical particles and be uniformly distributed throughout the sample region in the probe. An air suspension of 3-10 micron glass beads is suitable for the large size range, while cigarette smoke was found convenient for calibrating the submicron range. The particles in filter cigarette smoke are smaller than one micron, with a peak at about 0.3 micron. Cigarette smoke was drawn into a mixing chamber where it was directed through the probe and exhausted into a laboratory hood. The forward channel gains and weighting constants were adjusted in accordance with the predicted scattering for such submicron particles.

The measured particle size distribution of cigarette smoke is shown in Figure 7A. To test the validity of the calibration, other materials with broader distributions were suspended and measured. Figure 7B shows data for Dioctyl Phthalate (DOP) aerosol, and Figure 7C shows the instrument response to a suspension of 3 to 10 micron glass beads. Data on the DOP agree well with the manufacturer's specifications. Microscopic examination of the glass beads revealed some clumping in the sample which accounts for the relatively large fraction of material in the 15 micron channel.

FIELD TEST RESULTS

The prototype instrument was tested at a coal-fired electric utility plant. These tests included parallel measurements with inertial impactor to enable the optical data to be compared with aerodynamic sizing methods. The optical instrument and inertial impactor were located in adjacent ports in the outlet duct of the electrostatic precipitator. The airflow was vertically downward, as shown in Figure 8. The duct is 32 feet wide and 7 feet deep and leads to the stack exhaust fan. The sampling ports are approximately 30 inches apart. EPA representatives installed a University of Washington Mark III cascade impactor and processed that data. We were responsible for the optical measurements. The stack conditions are listed in Table II.

TABLE II

STACK CONDITIONS DURING TEST

Stack gas velocity:	45 to 50 feet/second
Stack gas temperature:	230 to 300^{o}F
Flue gas pressure:	-2 inches of Hg

Preparation for impactor measurements were accomplished in accordance with standard procedures. This process consumed several hours and involved measurement of temperature, velocity and pressure to establish isokinetic sampling, and the impactors were preheated to the flue gas temperature to avoid condensation.

In contrast with this procedure, no special preparation was required for the optical instrument. The background was set, then the probe was inserted in the stack, final alignment was executed when its temperature stabilized and data on the particulate emission were immediately available. Data from the impactor measurements were not available until two weeks after these tests were completed.

Data from two of the tests are shown in Figur : 9. The comparative data for the optical instrument and the impactor are plotted here as cumulative particle size distributions.

The measured specific gravity of the particles was 2.5. This factor was used to convert the optical volumetric loadings to mass loadings. The mass loadings measured during the first day of the test varied from 20 to 23 $\mu g/m^3$. On the second day the loadings dropped to 7 $\mu g/m^3$.

The optical measurements tend to report slightly larger particle size than the impactor, but the general correlation is good. The optical measurements show bimodal distributions due to large numbers of particles in the 10 to 25 micron range. This bimodal characteristic could not be confirmed from the impactor data, although there is evidence of a second peak above 10 microns in one of the impactor runs.

The prototype in-stack instrument was delivered to the EPA upon completion of these tests, and further evaluations are now in process by EPA. Results of tests performed in the EPA simulated stack and at other industrial and utility plants indicate good agreement between optical and impactor measurements. Thus, the feasibility of in-stack continuous measurement of particle size and loading has been demonstrated. Now we are looking for suitable applications for this new instrument capability.

REFERENCES

1. Cowherd, C., "The Technical Basis for a Size-Specific Particulate Standard,"J.APCA, 30-9, 971-982,1980.

2. Miller, F. J., Gardner, D. E., Graham, J. A. and Lee, R.E.,Jr. "Size Consideration for Establishing a Standard for Inhalable Particles," J. APCA, 29-6, 611-615, 1979.

3. Wertheimer, A.L., "Modification of Optical Instrument for In-Stack Monitoring of Particle Size," EPA Final Report 68-02-3253, 1981.

4. Wertheimer, A. L., U.S. Patent 4,134,679.

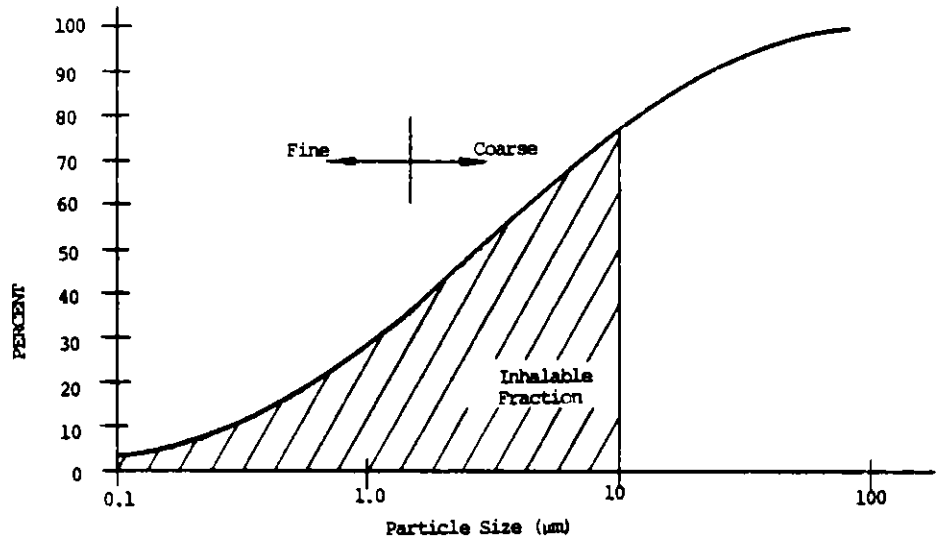

FIGURE 1

Particulate Classification

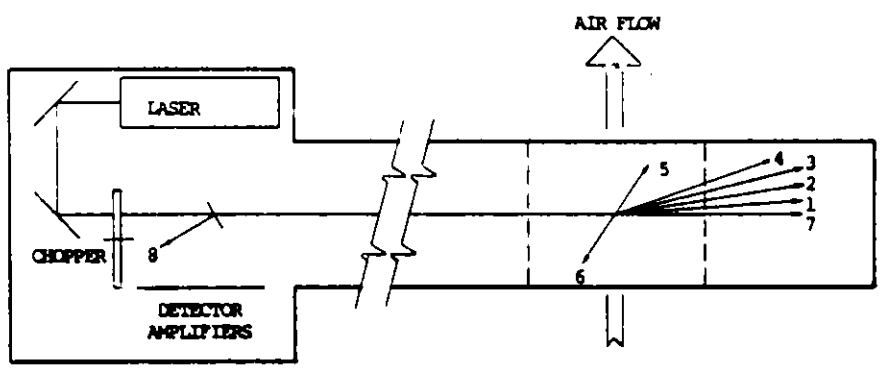

FIGURE 2

Optical Instrument Schematic

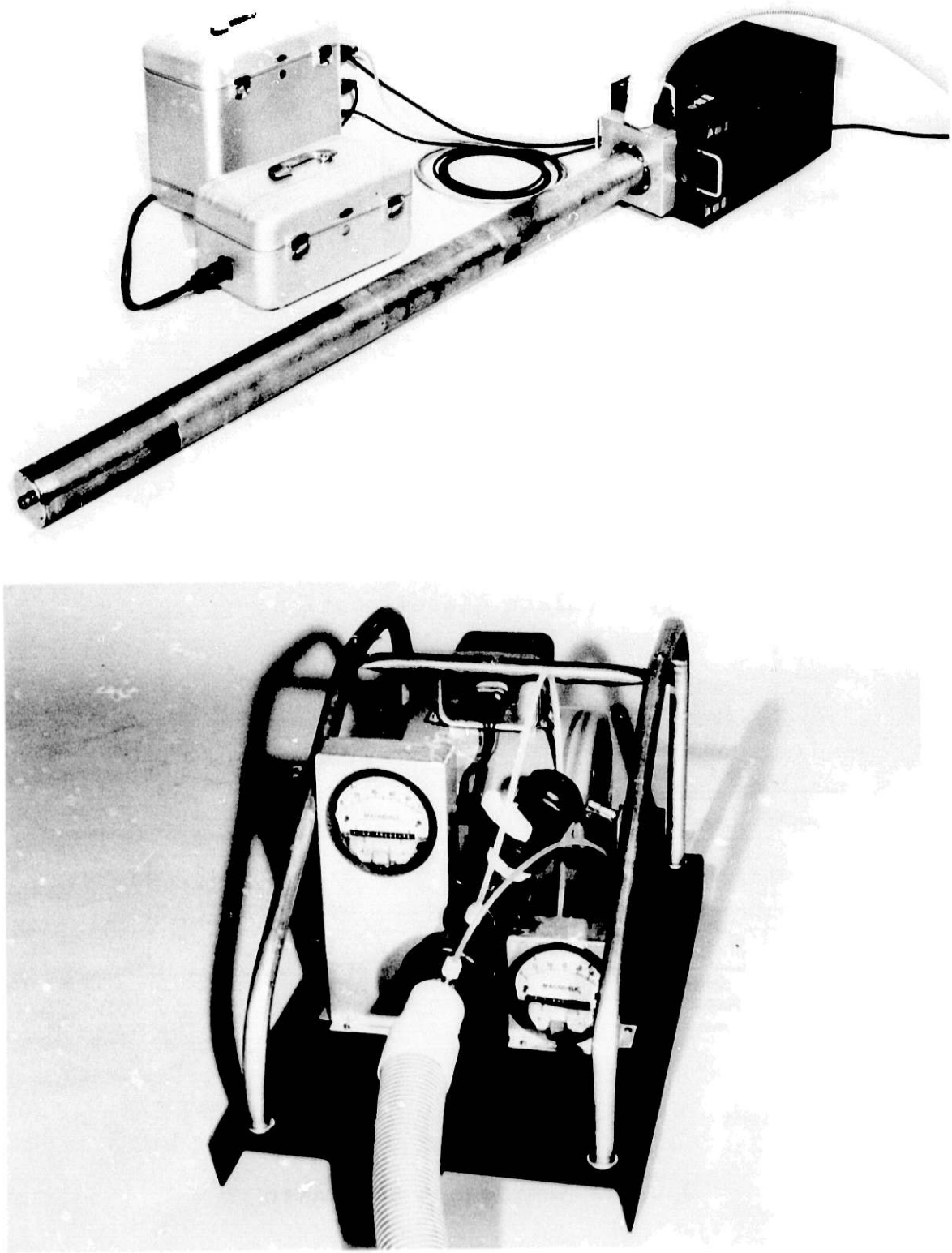

FIGURE 3

Photographs of Instrument

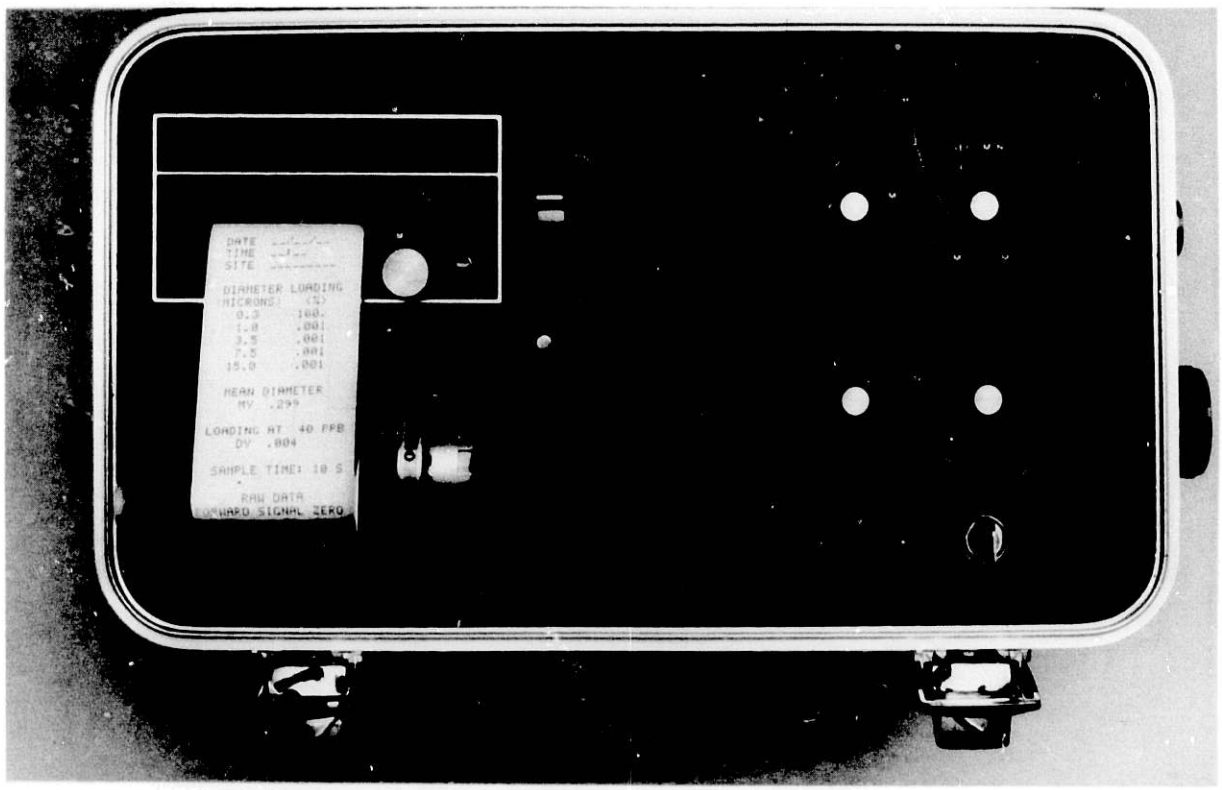

FIGURE 4
Close-Up View of Console

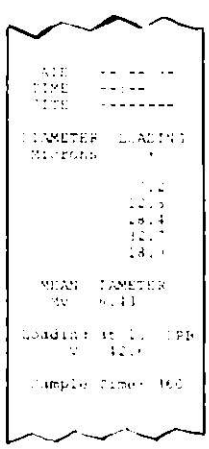

FIGURE 5
Data Format

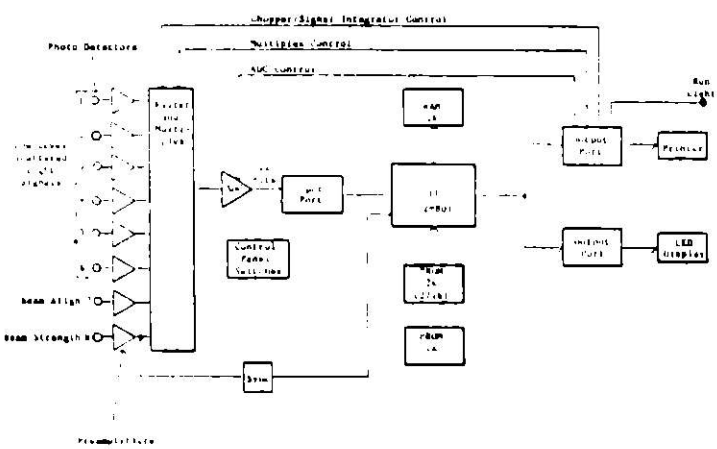

FIGURE 6
Electronics Block Diagram

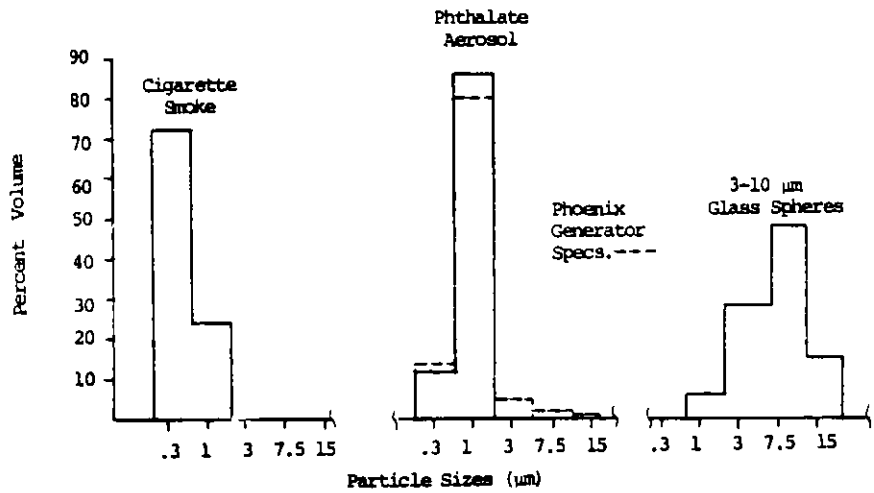

FIGURE

7A 7B 7C

Instrument Calibration

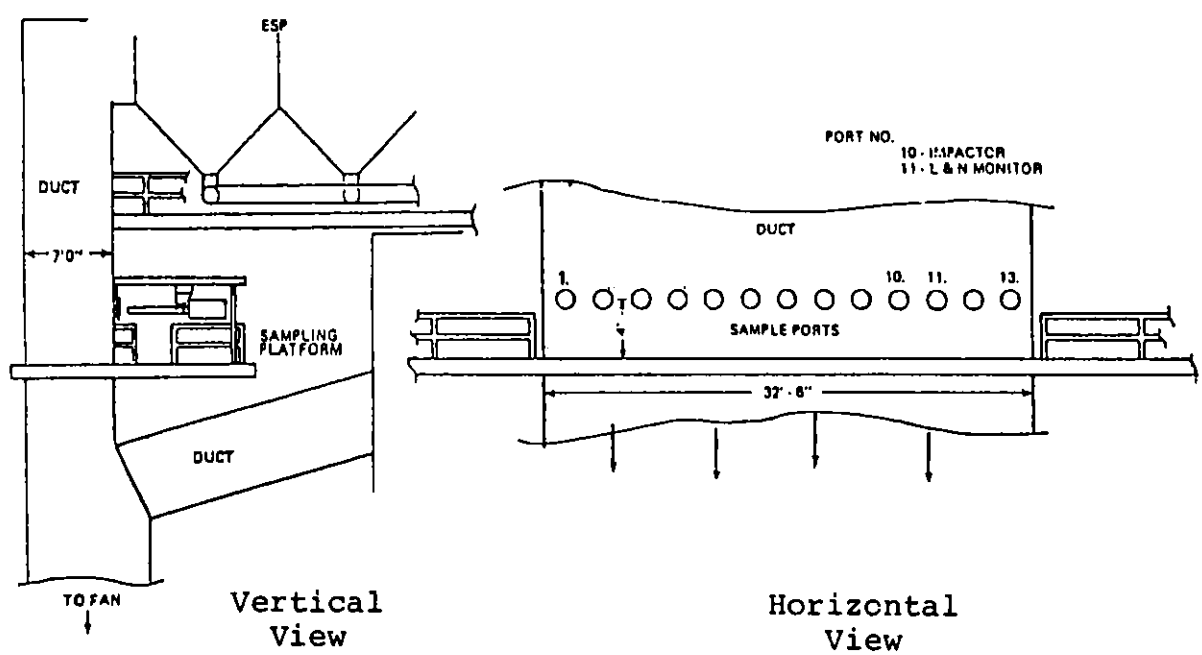

FIGURE 8

Field Test Diagram

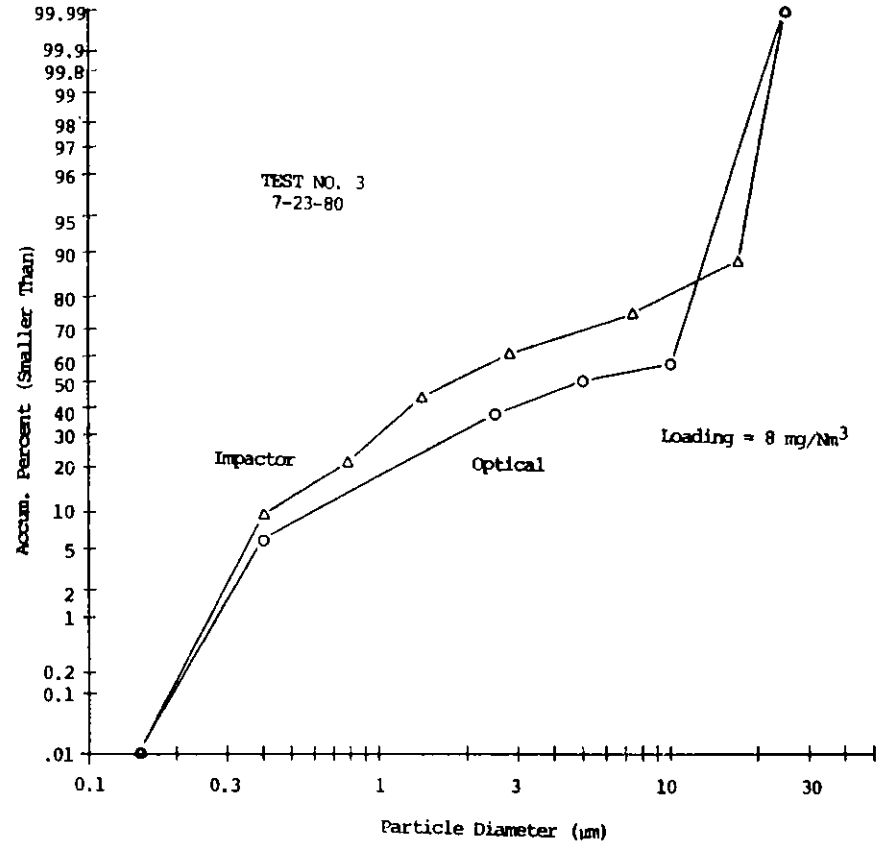

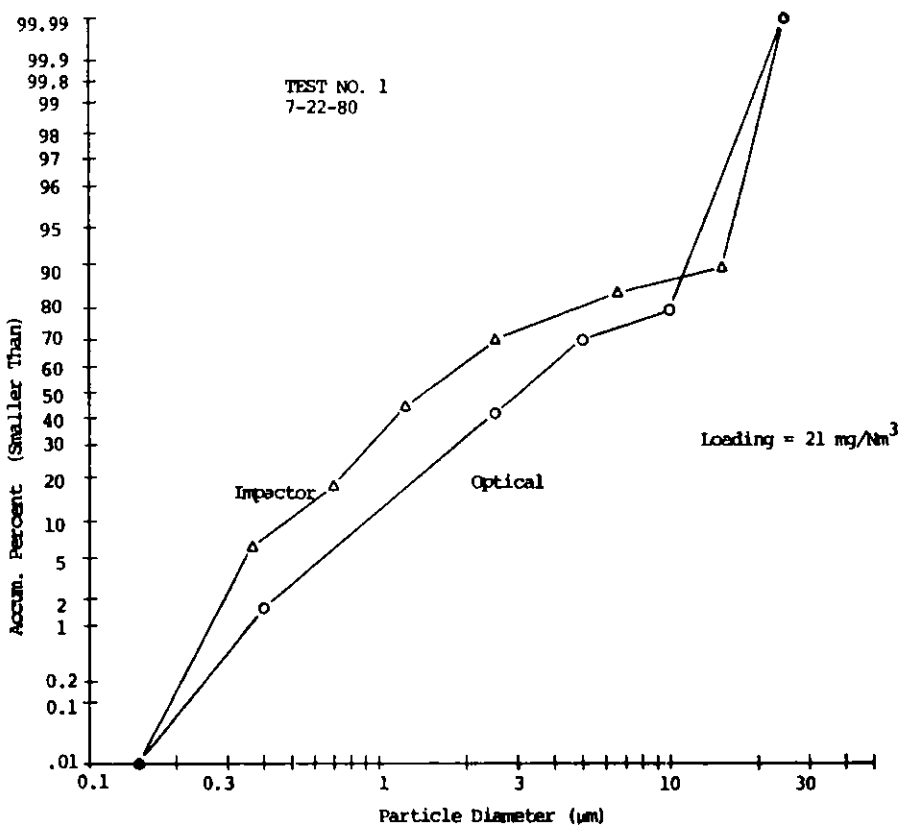

FIGURE 9

Optical and Impactor Measurements at Utility Plant

Tuesday Afternoon, June 9, 1981

Session D - Special Topics

POTENTIAL APPLICATIONS OF NUCLEAR REACTOR INSTRUMENTATION TO FOSSIL ENERGY FUEL PROCESSES

W. H. Roach
Instrumentation Development
EG&G Idaho, Inc.
P.O. Box 1625
Idaho Falls, Idaho 83415
Phone: (208) 526-2047
FTS 583-2047

ABSTRACT A089

The Instrumentation Development Branch of EG&G Idaho, Inc. designs and develops advanced instrumentation for use in water reactor safety programs sponsored by the United States Nuclear Regulatory Commission. Developed and tested for a severe pressurized water nuclear reactor environment, several of the instrument types could have application in fossil fuel plant measurements. A review of selected instrumentation and their potential application in fossil fuel energy processes will be given, concentrating on gamma ray densitometers.

A PILOT PLANT TO SIMULATE IN-SITU GASIFICATION

M. Mohtadi
F.H. Franke
W. Wenzel
H.W. Gudenau
M. Kurth

The Aachen University of Technology, Institut für Eisenhüttenkunde, Intzestr. 1, 5100 Aachen, West Germany

ABSTRACT

The pilot plant was constructed to simulate the underground gasification process at coal blocks of 4 m length and 0.32 m diameter at a constant pressure and under pressure-swing conditions.

By means of the pressure-swing operation the massflow which decisively influences the gasification rate, shall be improved.

The gasification experiment can be implemented at a maximum pressure of 60 bars with the gasification agents air, oxygen, hydrogen and steam as well as with their suitable mixtures.

The whole plant consists of 5 component groups: reactor with piping equipment, gasification agent equipment, product gas utilization, heat- and massflow measurement and control and safety equipments.

The gasification tests carried out up to now under stationary and pressure change conditions showed that the plant is well suited for the simulation of underground coal gasification. Some test results have been presented already.

INTRODUCTION

In the Federal Republic of Germany alone, the stocks of bituminous coal which could not be mined by conventional mining procedures, amounted to some hundred billion tons. Under this point of view underground gasification offers a sensible possibility

of application. For the utilization of these tremendous stocks the so-called borehole mining can be applied. Such a method is applied in the production of mineral oil and natural gas.

In contrast to the American Program the "Bundesministerium für Forschung und Technologie (BMFT = Federal Ministry of Research and Technology) and the "Projektleitung Energie" (PLE = Project Management Energy) attach great importance to a sound preparation of the field test by means of basic research in the laboratory[1,2]. This research is mainly carried out at the "Institut für Eisenhüttenkunde, Aachen" (Institute for metallurgy of iron). The In-situ research program at our Institute mainly has to carry out tests in laboratories for the simulation of the underground gasification process at compact coal samples which have been bored underground[3]

LARGE AUTOCLAVE PLANT

The large autoclave plant is a special equipment to simulate the underground coal gasification process in a coal block sample of 4 m length under static and under pressure swinging conditions. The tests can be carried out at a maximum pressure of 6o bars with the gasifications agents air, oxygen, hydrogen, and steam as well as with their mixtures.

Figure 1 shows the flow scheme of the plant. This plant consists of a steam generator, two gas heaters, the reactor, a dust filter and the burning furnace. The steam generator is in a position to produce 135 kg/h steam at a pressure of 8o bars and a temperature of 5oo ^{o}C.

The oxygen heater is conceived for a maximum of 11o kg/h oxygen and a temperature of 3oo ^{o}C.

The air or hydrogen heater heats a maximum of 85 kg/h air or 15 kg/h hydrogen up to 5oo ^{o}C.

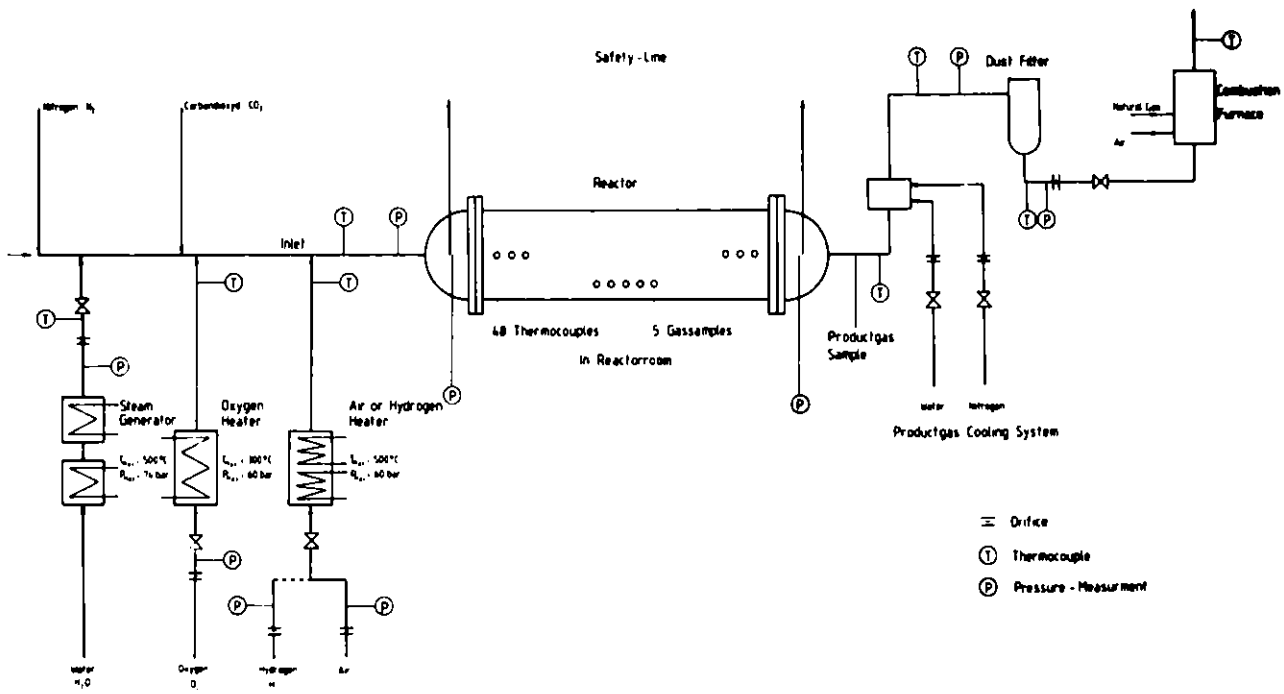

Figure 1

ARRANGEMENT OF THE REACTOR AND SAFETY EQUIPMENTS

The reactor consists of a cylindrical centrepiece and of two flanged covers. The reactor is composed of a gas-tight inside liner of Incoloy 8oo in corrugated tube form with sliding bar for the insertion of a coal sample, for a pressure- and heat-transmitting steel jacket of 15 mo 3, figure 2. For the installation of thermocouple elements, gas analysis lines, heatings, and ignition devices altogether 23 flanges are available.

This new system with gas-tight inside liner has been chosen to keep the voidage as small as possible for pressure-swing, to reduce the heat losses and to protect the brick lining

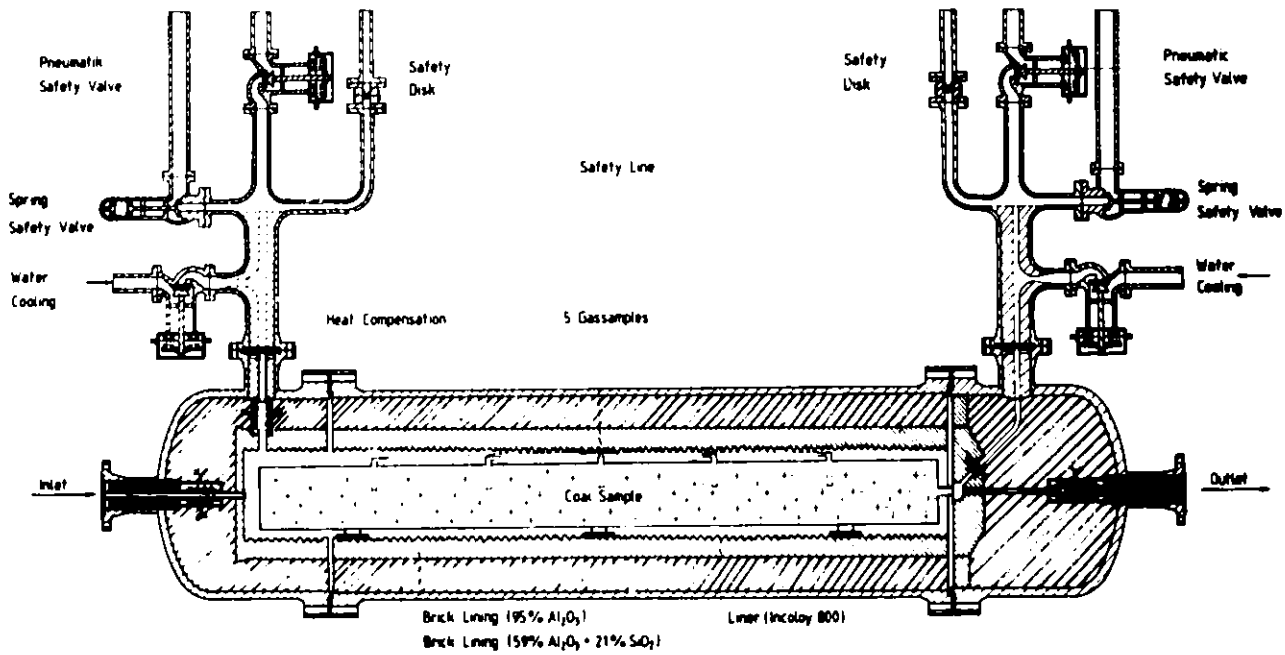

Figure 2

and the bearing outside jacket against the condensable components as well as against aggressive gases. In order to control the gas tightness of the inside liner, flow detectors are fixed at the outside jacket. Inlet- and outlet gas lines of the reactor are equipped with compensators due to the great thermal expansion.

For safety reasons the autoclave is equipped with a triple safety system respectively at the inlet and the outlet side. If the maximum operating pressure is exceeded (p = 6o bars), an on- and off-valve which is controllable opens at 62 bars. If this valve does not open and if a further pressure increase takes place, a spring safety valve depressures the reactor at an internal pressure of 64 bars. Further more if this equipment does not respond a rupture disk is destroyed at 66 bars and the reactor depressures.

The control of the jacket temperature of the reactor is done by a semi-conductor element being installed in screen-shape which can respond on its complete length and which switches off the process when the admissible maximum temperature is exceeded.

For the cooling of the reaction temperature in cases of emergency carbon dioxide can be used.

In order to avoid an overheating of the product gas line and of the fittings, nitrogen or water are admixed to cool the product gas at too high temperatures.

MEASURING AND CONTROLLER SYSTEM

For the measurement of the process parameter a special measuring- and controller system has been developed. In fig. 1 most important measuring points are represented. The massflows of the gasification agent are registered by means of orifices.
For the registration of the temperature and of the gas composition in the coal sample 48 thermocouple elements as well as 5 gas sampling points are provided. The temperature of the product gas and the composition are continuously registered. Since the plant had been conceived for hydrogenating as well as for oxidizing gasification an interlocking system for safe operation of the plant was necessary. Safety measures concerning this interlocking system are represented in table 1. If the inner pressure of the reactor is higher than 62 bars, or if the liner temperature is higher than 1ooo ^{o}C, or if the reactor jacket temperature is higher than 3oo ^{o}C, and if the inner pressure of the reactor gets higher than 2o bars an emergency depressuring takes place and the plant switches off. Besides the variation of the different gasification agent mixtures the process control can take place via the temperature of the gasification agent or by the proportions of the gasification agent, the temperature in the coal being the command variable (e.g. burning front temperature).

SAFETY MEASURES CONCERNING THE INTERLOCKING SYSTEM

ϴ internal pressure of the reactor	>	6o bars	opening of the product gas valve
ϴ internal pressure of the reactor	>	62 bars	emergency depressuring of the reactor
ϴ liner temperature	>	1ooo °C	
ϴ temperature of the reactor jacket	>	3oo °C	
and internal pressure of the reactor	>	2o bars	
ϴ Flow measurement at the outside jacket of the reactor at 1o l/h			
ϴ temperature of the product gas	>	1ooo °C	cooling of the product gas
ϴ measurement of the nitrogen pressure of the cooling nitrogen	>	65 bars	
ϴ H_2O-pressure measurement of the cooling water	>	65 bars	
ϴ inertization (before the test begins)			no release of the gasification agent

Table 1:

Moreover there is a possibility to keep the streams of the gasification agent and of their temperature constant. In this way the coal temperature as command variable is dropped.

The plant has been conceived for stationary as well as for pressure-swing. In fig. 3 the pressure- and massflows are represented depending on time at different kinds of operation. Case (a) shows the usual stationary operation. In the case of b and c the pressure is increased by a closing of the product gas valve. When the pressure is released in the reactor, the product gas valve is opened, the supply of the gasification agent being interrupted. Case b and c additionally differ from each other by a holding time, the reactor pressure remaining constant and the gasification- and product gas valve remaining closed. Case d is similar to case b, the gasification agent being supplied constantly and the pressure-swing being caused by an opening and closing of the product gas valve. All presented kinds of operations are controlled automatically by the plant.

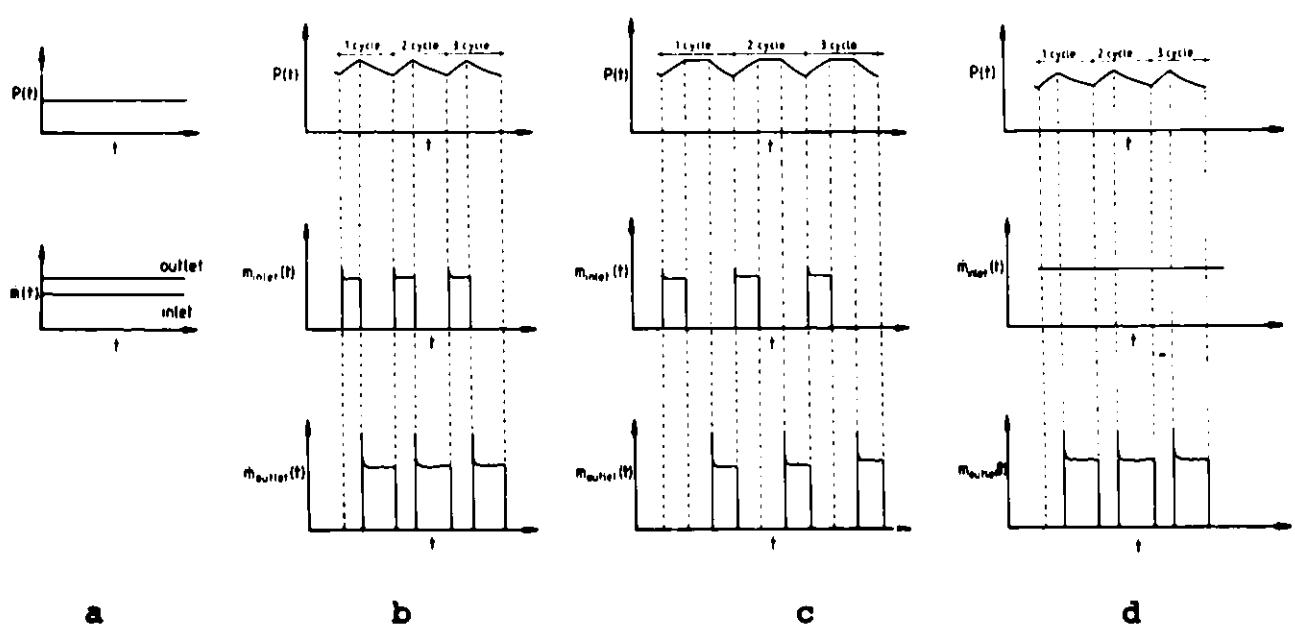

Figure 3

FUNCTIONING CAPACITY OF THE GASIFICATION PLANT

The plant has been operating since June 1980. Up to now 9 tests for the simulation of underground gasification with air/steam mixtures have been carried out successfully under stationary- and under pressure-swing conditions.

Some test results shall be presented here. In fig. 4 the temperature courses in the coal sample depending on the test period are represented for an air/steam gasification at 10 bars. The arrangement of the thermocouple elements can be seen from the lower part of the diagram. The massflows of the product gas and of the gasification agent as well as the heat value and the composition of the product gas are registered above the test period in figure 5. Moreover the gas profiles after a gasification of 30 hours as well as the sampling points along the coal sample are shown in fig. 6.

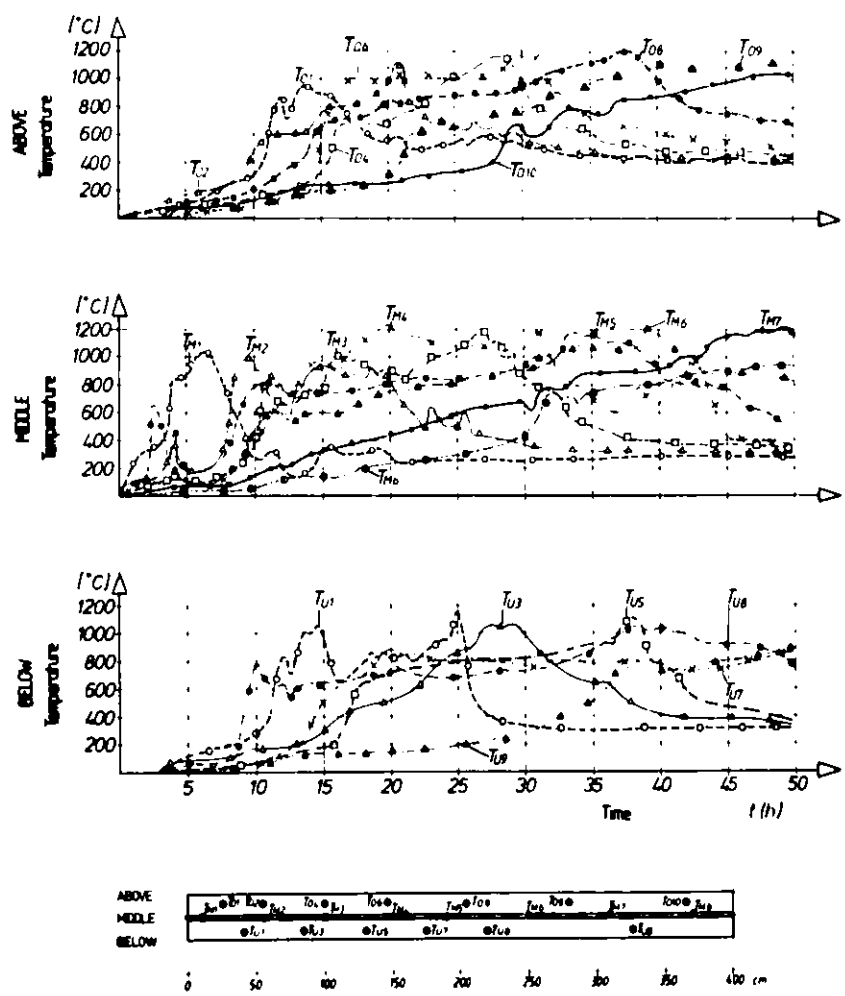

Figure 4

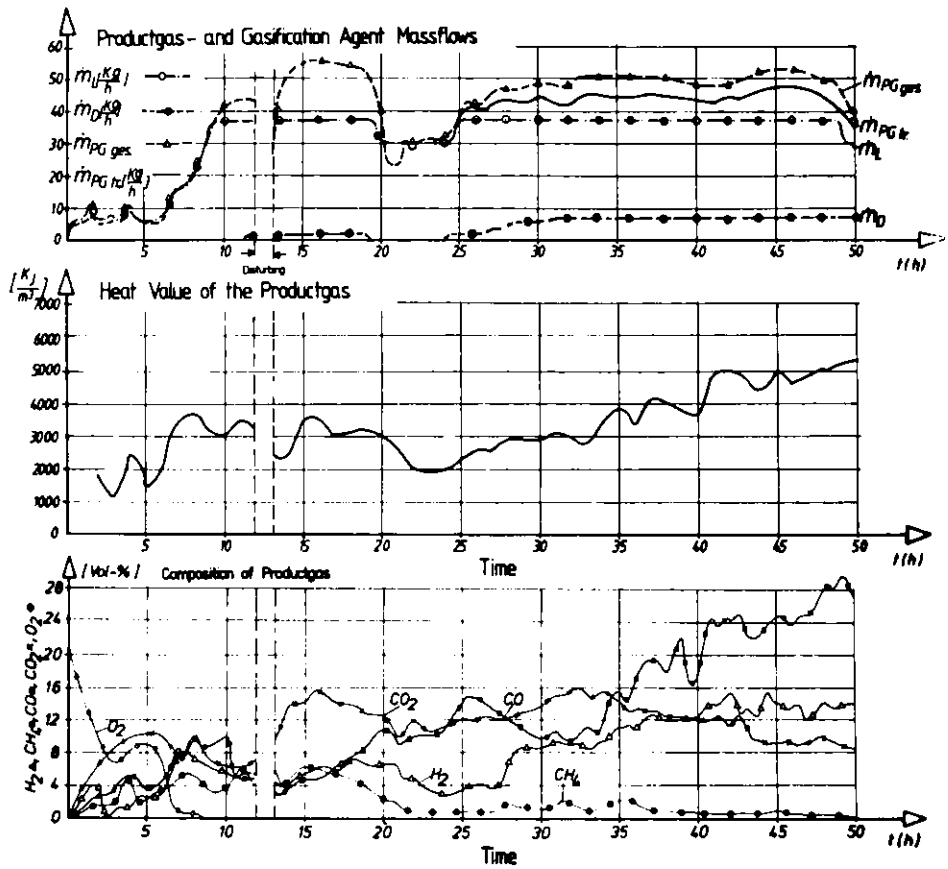

Figure 5

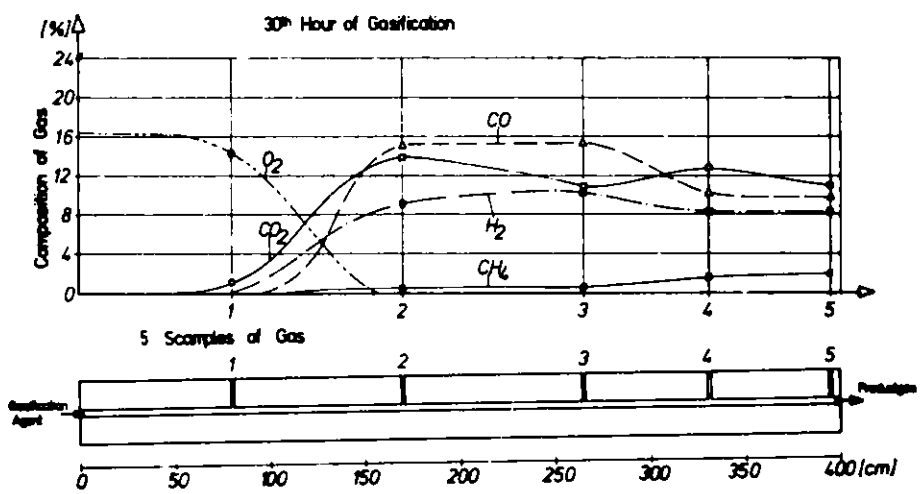

Figure 6

ACKNOWLEDGEMENT

The financial contributions of the "Bundesministerium für Forschung und Technologie" under Project Management of the Projektleitung nichtnukleare Energieforschung (PLE)" at the "Kernforschungsanlage Jülich (KFA)" made this project possible.

REFERENCES

1. Neumann, R.: Kohlevergasung unter Tage. VDI-Zeitung Nr. 34, 26. August 1977

2. Pusch, G.: Eine Zwischenbilanz nach dem ersten Quartal einer neuen Technologieentwicklung. Statusreport 198o Geotechnik und Lagerstätten, der Projektleitung Energieforschung (PLE) KFA Jülich, Band II, S. 553

3. Wenzel, W., H.W. Gudenau, M. Mohtadi: Untertagevergasung tiefliegender Steinkohle Arch. f.d. Eisenhüttenwesen, 51 (198o) Nr. 6, S. 249/56

REMOTE CONTROL OF TRACER GAS INJECTION USING VLF ELECTROMAGNETIC WAVES

Dennis F. Moore and Thomas F. Turner
Laramie Energy Technology Center
P. O. Box 3395, University Station
Laramie, WY 82071

ABSTRACT

The remote control system described makes it possible to install tracer gas canisters at selected locations in a modified in situ oil shale retort during rubbling. After rubbling, the tracer gas is released on command from the surface. These gas canisters are installed from the surface through existing retort access holes. Coded transmission is used so that the canisters can be triggered individually. The battery operated receiver with each canister can stand by for several months and then release the tracer gas when the appropriate signal is received. The proposed system would provide an economical method for obtaining tracer information.

PROBLEM DEFINITION

The Vertical Modified In Situ (VMIS) method of retorting oil shale is nearing commercial scale operation. This method requires mining a void, then blasting into the void to form a chimney of rubble. After blasting, the rubble is ignited at the top; air flow is established from top to bottom; and the burn front moves downward, retorting the oil shale in front of it. Shale oil is collected at the bottom of the retort and pumped to storage. A schematic of the process is shown in Figure 1.

Most of the experimental work on large retorts has been done by Occidental Oil Shale Incorporated (OOSI), however, Rio Blanco Oil Shale Company (RBOSC) has recently rubbled two retorts and retorted one of those. The

mining and blasting procedures used by the two companies differ substantially. Occidental prefers to mine the intended void and rubble the retort with one timed blast sequence. RBOSC mines a void at the bottom of the planned retort and then sequentially blasts layers of rock into this void (1).

One of the problems encountered during retorting is flame front channeling resulting in the burning, coking or by-passing of potential product. Channeling is caused by nonuniformities in flow which are in turn caused by local differences in the particle size distribution and void fraction. If the flow properties of the retort are known in advance, channeling often can be reduced or eliminated by modifying retorting strategy. The most common method used to measure airflow distribution is gas tracer testing. This entails injecting a small amount of easily detectable tracer gas into the air inlet or into the top of the rubble zone and monitoring its concentration at sampling points farther down the retort. Typically, the injection is a narrow concentration pulse and the data output at any sampling point is a significantly wider pulse. The time of arrival of a pulse is used to calculate air flow velocity and, in some cases, the active void of the retort. The pulse shape can indicate the amount of dispersion, dead volume, and mass flow depending on how much is already known about the rubble. In the past, intermediate level access drifts and sampling ports have been used to monitor tracer concentration during tracer tests (2,3). Intermediate level sampling provided detailed information on flow velocities in the mid region of a retort. Sampling only at the outlet of a retort severely limits the degree to which a rubble chimney can be characterized.

As VMIS technology approaches commercialization, economic constraints will limit the amount and type of instrumentation in each retort. The number of thermocouple and gas sampling ports at intermediate levels of the retorts probably will be reduced or eliminated. Since this intermediate level will no longer be available, insufficiently detailed data will be obtained to make major retorting strategy changes with confidence. New technology is needed that provides economical and simple methods of determining the gas flow characteristics of individual retorts.

The RBOSC sequential rubbling method offers advantages for development of a new type of instrumentation. One of the new items is a canister developed by Lawrence Livermore National Laboratory (LLNL) that releases a tracer gas when it reaches a predetermined temperature. The canister is placed into the retort between detonations of the blasting sequence through holes previously drilled for blasting. The location of each canister is determined by the rubbled shale level and the horizontal coordinates of the blast hole. Outlet gas flow from the retort is continuously monitored and the time of arrival of each tracer gas is recorded. The times of arrival of tracers from many canisters are then used to map the temperature front in the retort. This is a valuable technique, but it obviously cannot be used to interrogate a cold rubbled zone before ignition.

PROPOSED SOLUTION

In response to the need for more pre-retorting information Laramie Energy Technology Center (LETC) has designed, built, and tested components of a system which allows detailed pre-retorting tracer testing, but does not require mining instrument drifts or drilling gas sampling ports. The system uses multiple tracer release units in the same manner as the LLNL thermally released tracer canisters, but in this case tracer is released by remote control from the surface using a Very Low Frequency (VLF) transmitter. Figures 2-5 show the sequential blasting method and the location of the remotely activated tracer release units. The dotted lines in Figures 2-5 outline the planned completed retort and solid lines indicate the current void and rubble locations. For each blast, the blast holes, shown as verticle solid lines in Figures 2-5, are loaded with explosive and then all are detonated. The fractured rock falls and forms the rubble pile below. The tracer release units would be lowered into place just prior to loading the blast holes. Each unit on a level would contain a different tracer gas and each level would have a different activation code. A typical tracer test would be run by first injecting a different tracer gas in each blast hole and recording the concentrations of the different gases at the outlet with respect to time. Next, the first layer of release units would be activated

and again the outlet concentrations would be monitored. This procedure would be repeated until the entire retort was characterized. The first two injections in this sequence are shown in Figures 6 and 7. The first is a traditional top-of-rubble injection and the second is a remotely activated tracer release. The residence times for increments of the retort height would be found by subtraction; pulse shape would be used to calculate dispersion and dead volume.

This tracer release system would provide the same information as a system using gas sampling ports, but would have the advantage of not needing any additional mining for placement of instrumentation. The units could be placed during the survey of the top of the rubble after each blast. A down-hole TV system is normally used to survey, measure particle size, and inspect the walls of the blast holes. The addition of a latch mechanism to the bottom of the camera would allow placement and inspection of the remotely activated tracer release unit, and yet allow the normal surveying operation to proceed almost unchanged. It is believed that this design has great potential when used in retorts created by long delay sequential blasting methods.

SYSTEM DESIGN

Design Considerations

The design of the proposed system for remotely activated tracer release is based on the following requirements:

Survival - The subsurface unit must be packaged to survive rubbling of the shale and must have at least three months battery life.

Adequate range - Frequency selection, transmitter design and receiver design must provide reliable operation to a depth of at least 250 m in a lossy medium (overburden and oil shale) where the dominant interference is from power frequency harmonics.

Ease of installation and operation - The subsurface units must be small enough to be installed from the surface through existing access holes. The transmitter must be capable of operating with a portable power source and the set-up time for the transmitter and it's antenna should be kept to a minimum.

Cost - The total system cost must be comparable to the cost of installing sample taps by mining. Although the transmitter can be used at many locations, the subsurface units cannot be recovered. Therefore, their cost is a more critical factor in minimizing the total system cost than is the cost of the transmitter.

Design Decisions

Frequency and antenna selection - Electromagnetic noise in underground coal mines has been investigated and the results summarized in a report by Arthur D. Little Incorporated (4). Equations for electric and magnetic field strength in a lossy medium are given by Holmes and Balanis in (5) and a curve showing attenuation of the vertical magnetic field component as a function of distance is found in Figure 2-1 of (4). Based on these references it was decided that the signal spectrum should be centered near 3 KHz. A loop antenna was chosen for the transmitter because the surface space requirements are acceptable and a loop is easy to install. A loop antenna was chosen for the receiver because it provides good sensitivity in a small package.

Modulation and coding - The transmitted signal is modulated so that the subsurface units can be activated individually at selected times by using different modulation codes. All of the subsurface receivers can be tuned to the same frequency. Power frequency harmonics or interfering signals have a low probability of activating the units because these sources of interference are not appropriately coded.

Frequency shift keying (FSK) modulation was selected using the two frequencies 3030 Hz and 3150 Hz. The ability of the receiver to discriminate between the correct signal and interfering signals is greater for FSK than for amplitude shift keying (ASK). Furthermore, for FSK the same demodulation threshold is optimum for any input signal-to-noise ratio. Modulation techniques are discussed by Gregg (6) and others.

A standard binary code such as the American Standard Code for Information Interchange (ASCII) could be used. This would provide a relatively large number of possible codes. For the prototype system which uses a small number of codes, a simpler coding scheme has been implemented. A square wave having a different frequency for each code is used to FSK modulate the transmitter. The receiver in each of the subsurface units can be activated by only one of the frequency codes. This simplified code can be decoded at less cost than would be required to decode ASCII.

Packaging, battery selection and installation - With the aid of a structural engineer, a package for the subsurface unit is being designed that will be able to survive rubbling. For the present time, the package dimensions will be approximately 0.2 m x 0.8 m, but smaller packages could be developed in the future. Based on preliminary investigation, it is believed that the packaging problems can be solved.

The subsurface unit will be powered by Alkaline-Maganese Dioxide, size D flashlight cells. These are relatively inexpensive, have a larger capacity to size ratio than Carbon-Zinc cells and provide a more constant voltage as a function of time under load.

It is proposed that the subsurface units be lowered into place from the surface through the same holes that are used to install explosives. A down-hole camera would be used to observe the position of the unit. When the unit is in place it will be buried in gravel to help distribute the impact from later rubbling.

SYSTEM DESCRIPTION

Transmitting Unit

A diagram of the transmitting unit is shown in Figure 8. The unit is powered by an inverter connected to a 12 volt storage battery. The tone encoder generates a square wave having the selected frequency which the modulator uses to shift key the sine-wave carrier between 3030 Hz and 3150 Hz. The FSK signal from the modulator is amplified to produce a current (i(t)) of several amperes in the transmitting loop. For the field test (to be described later) the RMS current in the transmitting loop was 2.0 A. A long circular loop of wire is placed on the ground surface to form the transmitting loop antenna. The field test was conducted using a loop having a diameter of approximately 44 m. The capacitor (C) series resonates the loop. Resistor (R) is added to increase the bandwidth of the circuit to minimize frequency distortion of the transmitted signal. It also provides a convenient way to measure the loop current. The total cost of the transmitting unit is approximately $5000.

Remotely Activated Tracer Release Unit

A diagram of the subsurface unit is shown in Figure 9. The unit is powered by a battery pack consisting of Alkaline - Manganese Dioxide, size D, 1.5 volt cells. These are conventional size D alkaline flashlight batteries. The voltage (v(t)) induced in the loop is amplified and filtered by the preamplifier which has a gain of 72 dB and a 3 dB bandwidth of 166 Hz centered at 3090 Hz. The preamplifier output is hard-limited to provide a 0.5 volt squarewave that carries the FSK modulation. The demodulator output contains the frequency code that was selected for transmissions. If the tone decoder is tuned to the frequency code that was transmitted, the solenoid valve opens releasing the tracer from the canister. The solenoid valve is latched open to insure that the canister will be emptied. The system was designed for a 300 cc canister to be filled to a maximum pressure of 1.03×10^4 KPa (1500 psi). The total cost of the parts in the subsurface unit is less than $300.

EXPERIMENTAL RESULTS

Preliminary Laboratory Tests

Laboratory tests verified that the receiver had more than adequate sensitivity and interference rejection. The receiver did not respond to false signals such as power frequency harmonics or to a strong carrier or even to the presence of two strong carriers regardless of their frequency separation. This rejection of two false carriers is effected by using FSK and hard-limiting.

Field Test

The transmitter and receiver were field tested using the Occidental Oil Shale Inc. mine at Logan Wash which is approximately 56 km (35 miles) northeast of Grand Junction, Colorado. The configuration for this test is shown in Figure 10. The transmitting unit was located on the surface above the mine. The current in the transmitting loop was adjusted to 2.0 A RMS. The plane of the loop dipped approximately 6° with the up dip end to the north. For this field test a single turn of RG-59U coaxial cable was used. The shield of this cable was used as the conductor in order to minimize the resistance and inductance of the loop.

The receiver was taken into the upper level of the mine which is 221 meters below the surface. A light bulb was substituted for the tracer release solenoid to provide visual indication of signal detection and a true RMS meter was used to measure signal and noise levels. The receiver was hand carried throughout a section of the mine to determine the usable coverage area. The signal was reliably detected within at least a 100 m radius circle centered directly below the center of the transmitting loop. To the north and northeast the radius was at least 122 m. With the transmitter turned off, the electromagnetic noise level in the mine was low enough (approximately 3×10^{-8} A/m$\sqrt{\text{Hz}}$) that it is conservatively estimated that the receiver would have detected the signal to a depth of at least 300 m all else being constant.

CONCLUSION

Components were designed, built, and tested for a remotely activated tracer release system which addresses needs in VMIS technology. This system has many advantages, including: easy placement, small size, simple operation, and low cost. The flexibility of the system allows the number of subsurface units to vary depending on problems or successes in blasting. Extensive mining is not needed if it is decided to increase the number of tracer release levels.

Tests performed on the system have been successful. Preliminary survival studies are in progress and it is hoped that packaged subsurface units will be in operation on the next appropriately designed retort.

REFERENCES

1. Rio Blanco Oil Shale Company, Annual Progress Report, Tract C-a January 1979-December 1979 Gulf Oil Corp./Standard Oil Co. April 1980

2. Occidental Vertical Modified In Situ Process, Summary Report, November 1, 1976- October 31, 1977 TID-28053, November 1977

3. Occidental Vertical Modified In Situ Process, Annual Report for the Period November 1, 1977-October 31, 1978 SAN-1848-T2, March 1979

4. Survey of Electromagnetic and Seismic Noise Related to Mine Rescue Communications, Volume I, PB-235069, Arthur D. Little Inc., January 1974

5. Electromagnetic Wave Propagation Within A Subsurface Coal Seam for In Situ Gasification Application, Progress Report May 1, 1976-April 30, 1977, J. J. Holmes and C. A. Balanis, ORO-5081-12, ERDA, 1977

6. Analog and Digital Communication, W. D. Gregg, John Wiley and Sons, New York, 1977

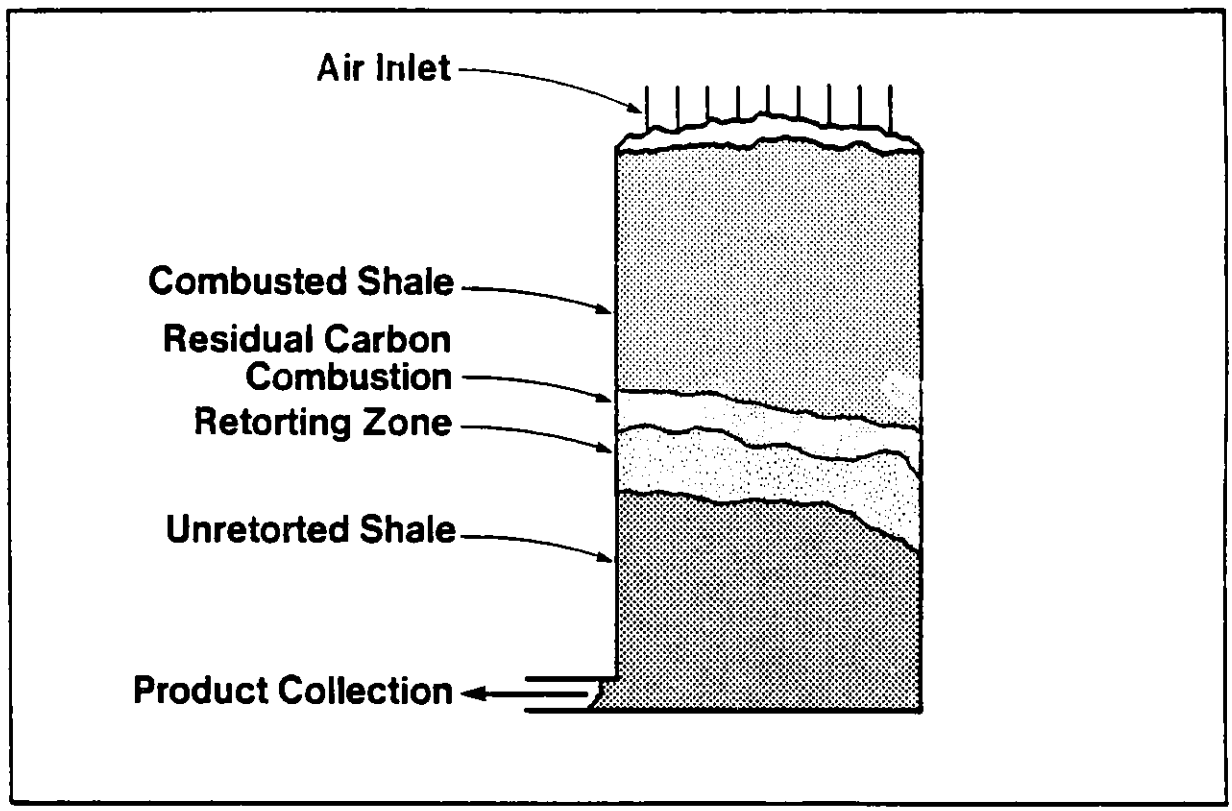

Figure 1. Retort in Operation

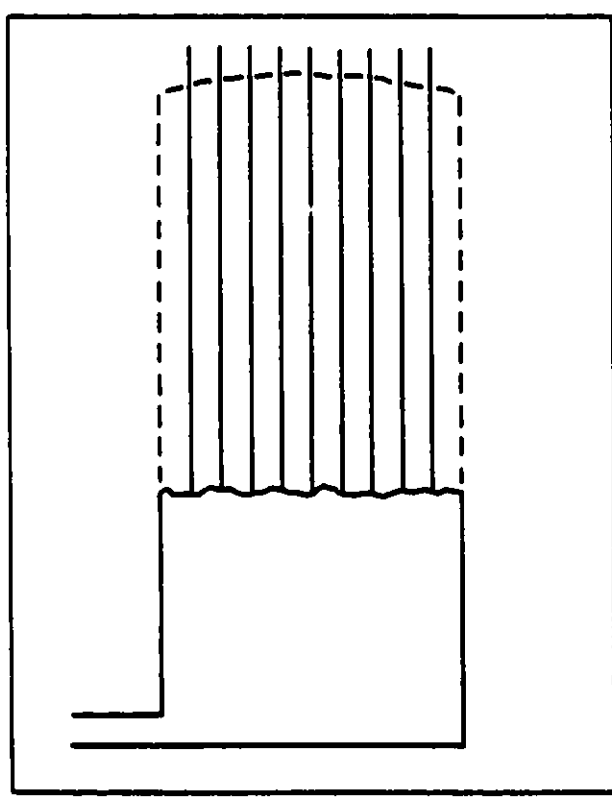

Figure 2. Retort Before Blasting

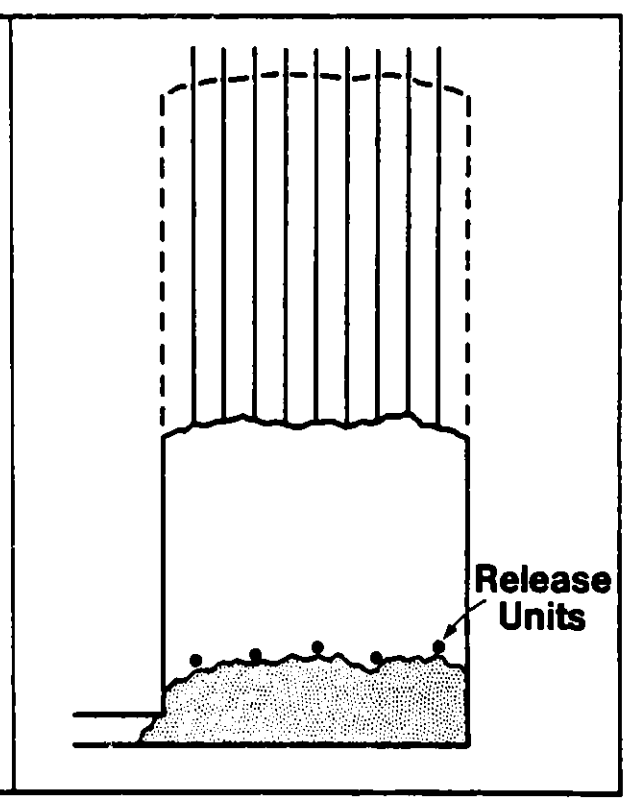

Figure 3. After First Blast

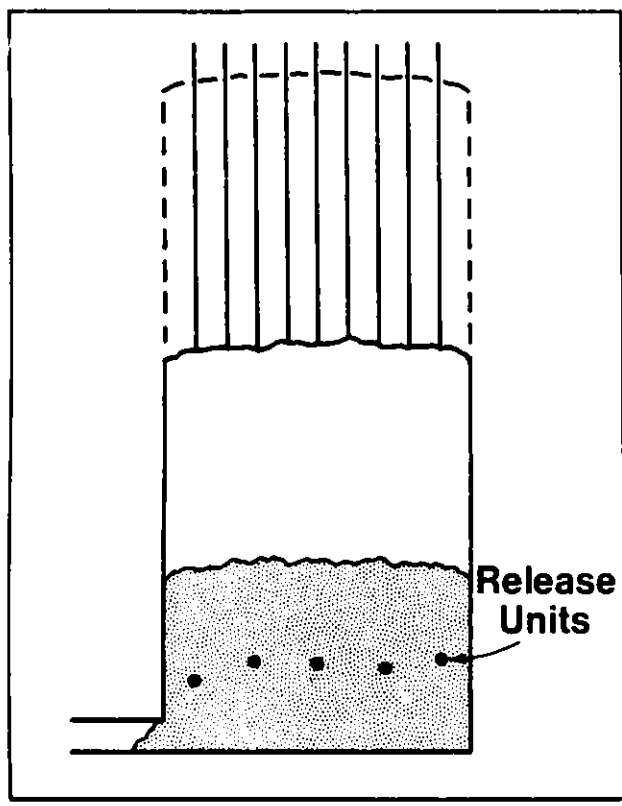

Figure 4. After Second Blast

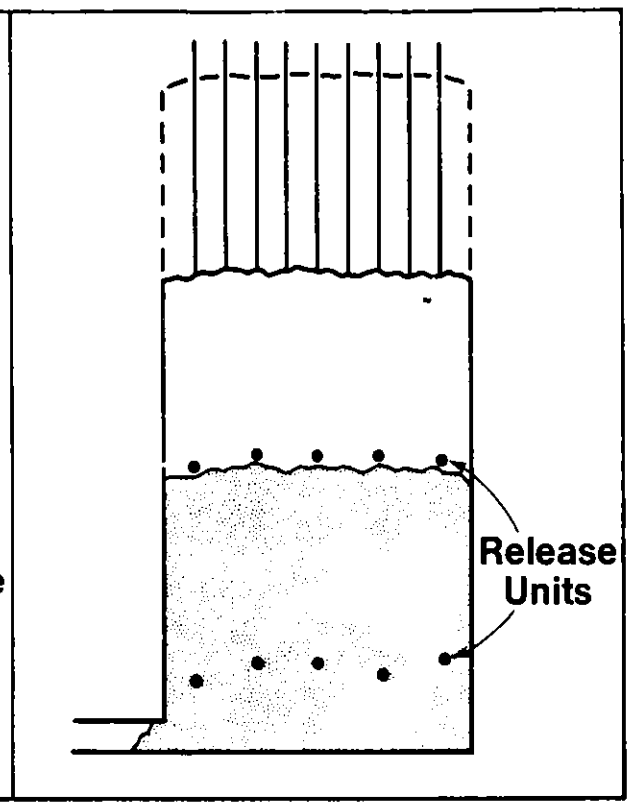

Figure 5. After Third Blast

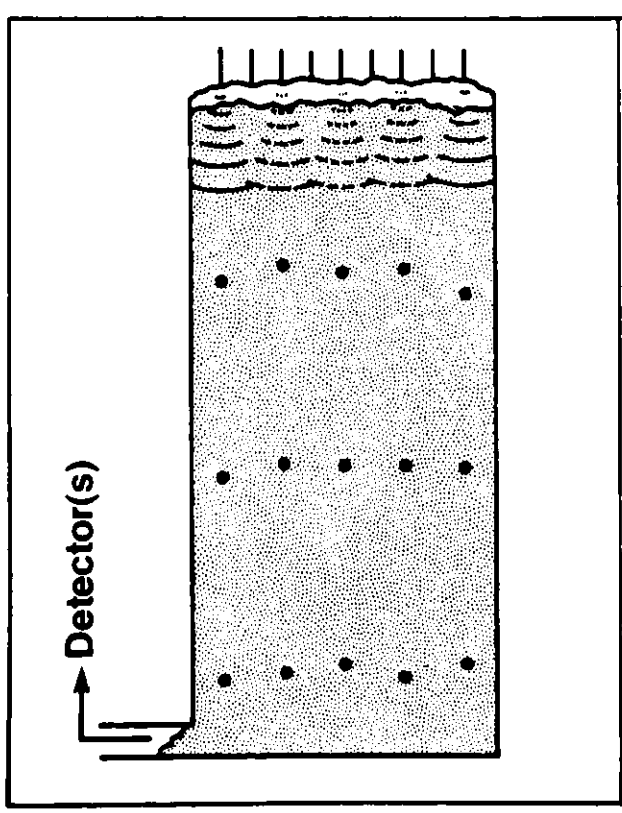

Figure 6. Traditional Injection in Completed Retort

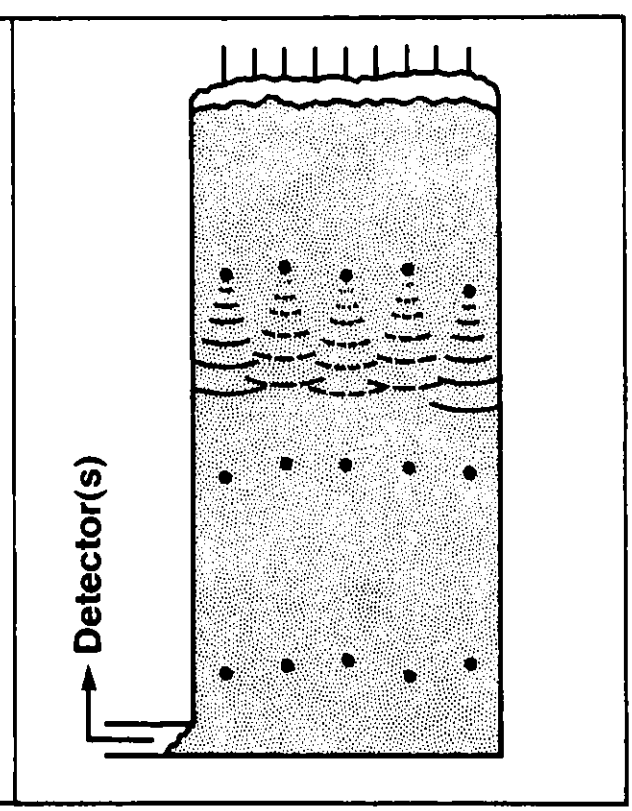

Figure 7. Remote Release

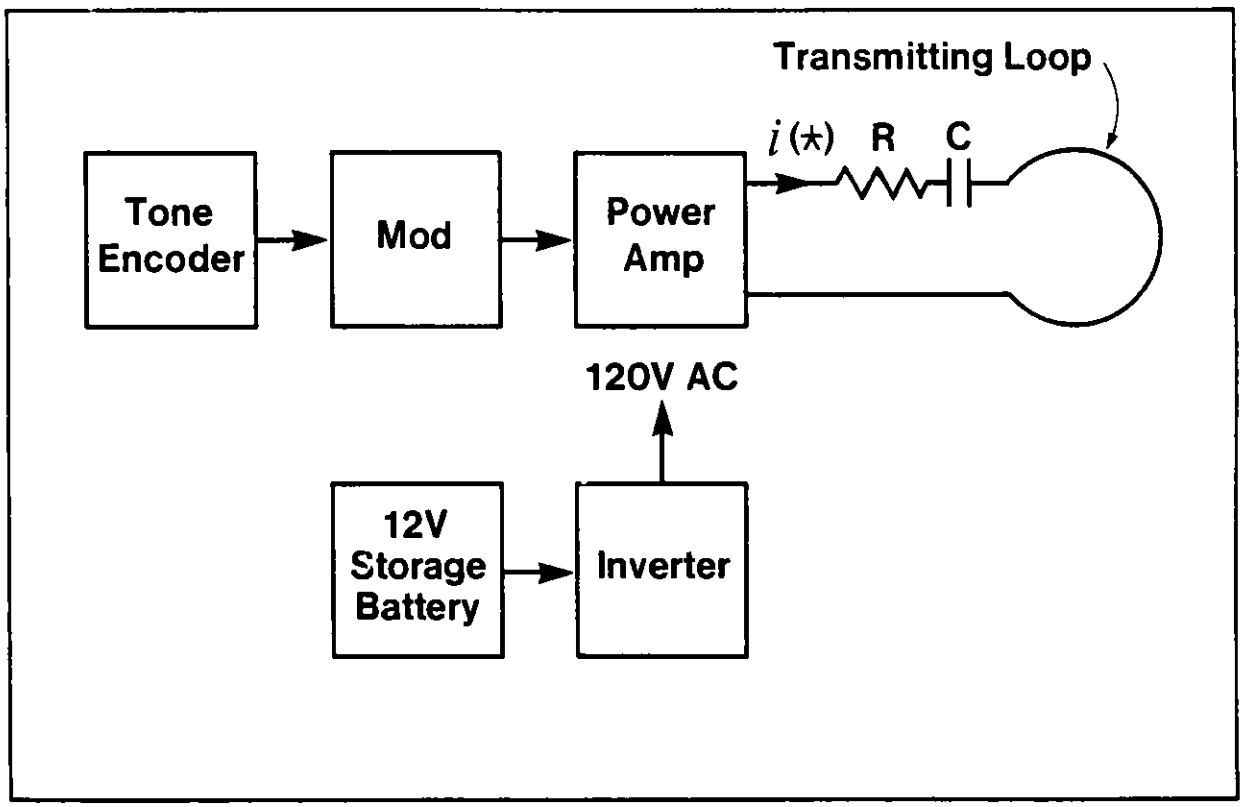

Figure 8. Transmitter Unit

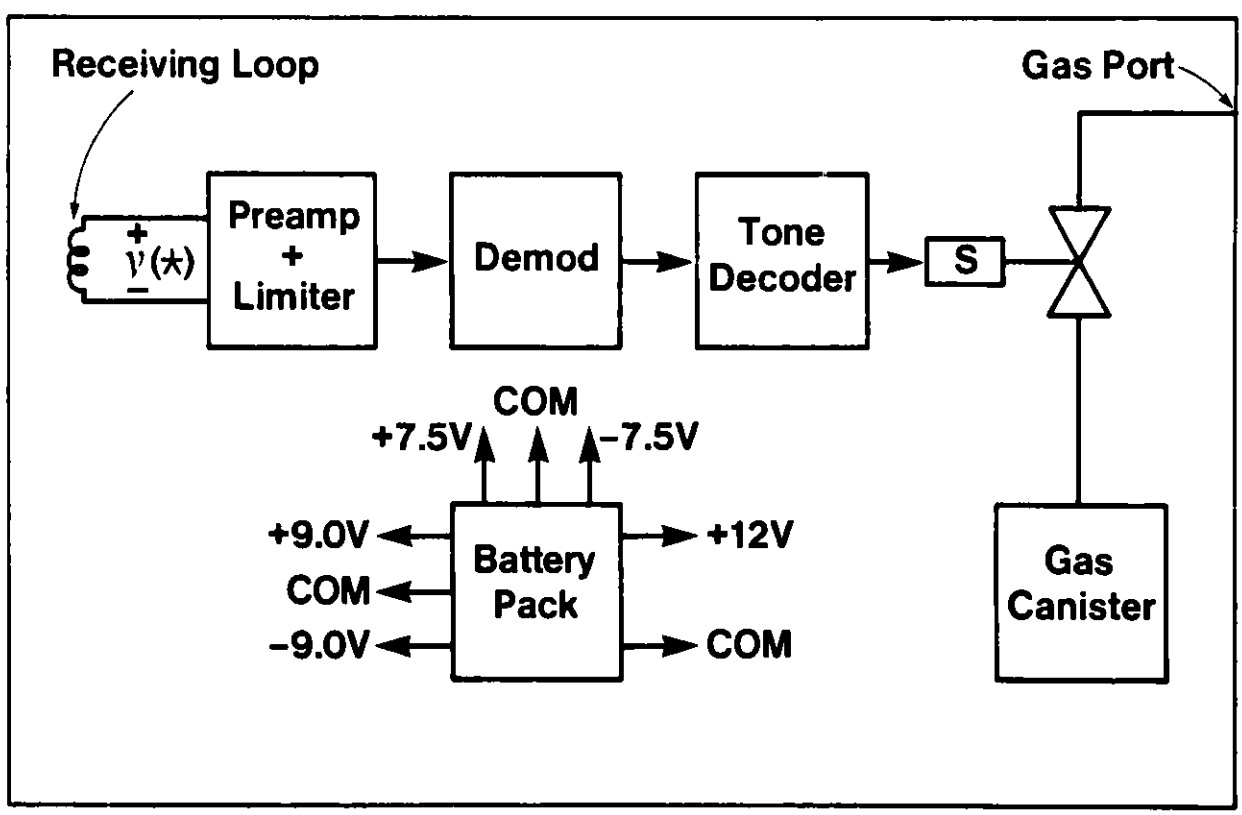

Figure 9. Remotely Activated Tracer Release Unit

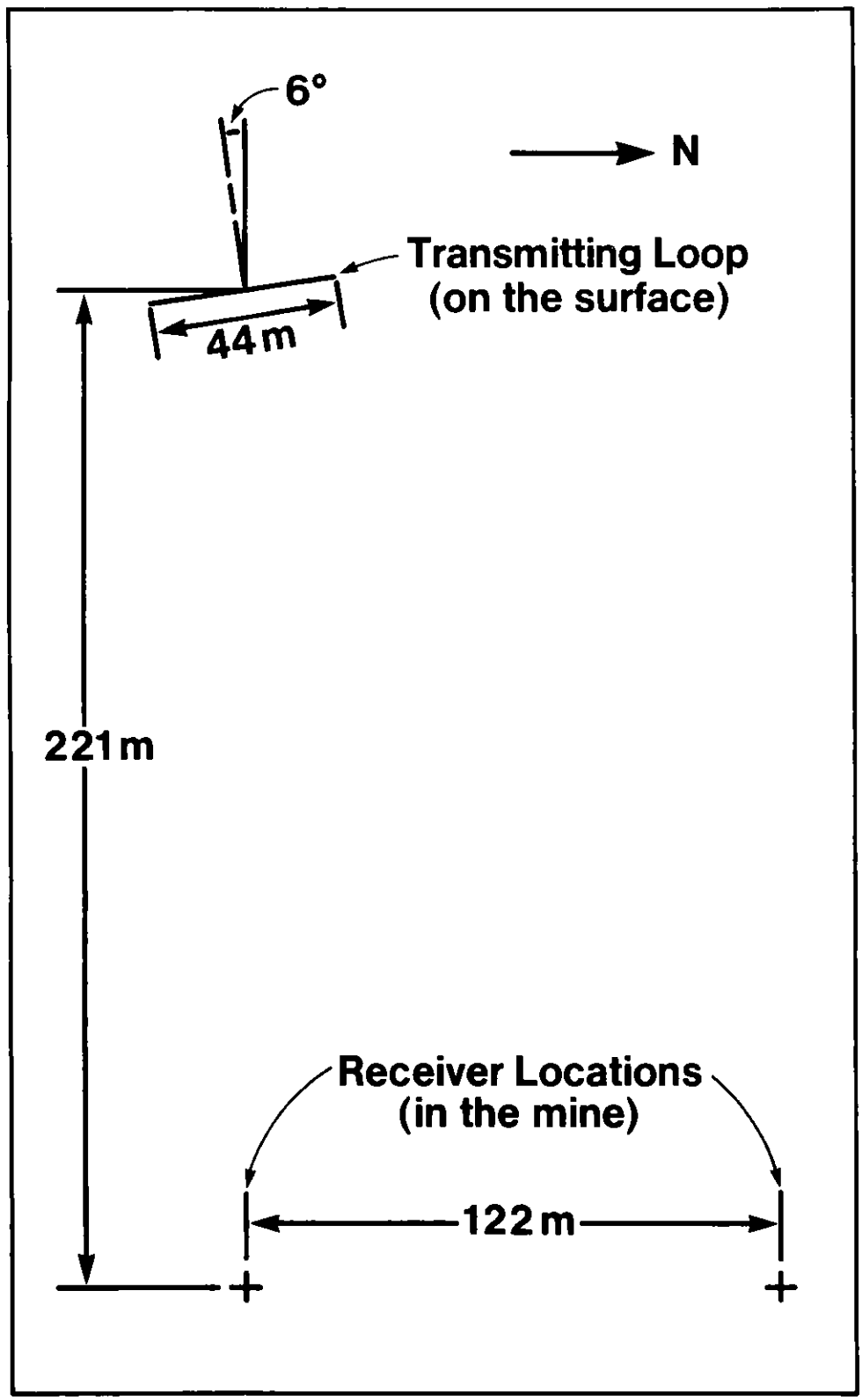

Figure 10. Field Test Configuration

PULVERIZED COAL COMBUSTION DETECTION USING CROSSCORRELATION TECHNIQUES

Paul Longrigg, Senior Member, IEEE.
Solar Energy Research Institute. Golden, Colorado.*

Abstract - Coal in its various forms is regaining popularity as a fuel because of the rapid depletion of other fossil fuels, such as oil and natural gas. This has occurred despite some of the environmental hazards associated with its use.

One of the most efficient methods of utilizing coal to raise steam for electrical power generation, is by pulverizing or crushing it into a fine powder. It is then entrained into a stream of primary combustion air for transporting to the steam generator or boiler. Upon arrival at a burner, the coal dust is mixed with secondary air, and burnt in suspension.

Coal flames of this type have traditionally been hard to detect in a burner management and fuel control system, yet such systems are vital to the safe and efficient operation of a pulverized coal-fired boiler.The detection difficulties are mainly due to flame sensor line-of-sight obscuration problems, inter-burner discrimination in multi-burner installations, and the general turbulence of the main fire ball within the furnace cavity.

This paper describes a pulverized coal combustion detection technique that employs the correlation between the acoustic energy radiated by coal particles undergoing combustion, and the electro-magnetic emissions in the infra-red, given off by short lived chemiluminescent carbon radicals, residing in the combustion zone of the flame.

INTRODUCTION

On pulverized coal-fired boilers or steam generators, the problems associated with flame detection are many and varied, partly due to the equipment involved in supplying fuel to the burners; to the difficulty in igniting coal as compared to gas or liquid fuel, and to the characteristics of the flame itself. Variations in primary air flow and temperature, air register position, and coal characteristics, such as moisture and particularly volatile matter, can significantly affect the flame that is produced. The time delay involved in proving main flame after feeder start adds complications to the detection system. The detector location and sighting angle presents a problem with the added interference of coal pipes, and partial masking of the primary combustion zone by a thick fan of pulverized coal particles. There also exists a greater risk of losing ignition on coal due to a fuel interruption, which places even more emphasis on obtaining a reliable system despite the increased number of problems. Finally, the choice of the flame sensing device is important, for it must be capable of sensitive discrimination from background interference, such as hot furnace refractory and other nearby operating burners.

FUEL SAFETY SYSTEM

A fuel safety system must have highly reliable components; must be *fail-safe*, and must be able to discriminate between adjacent burners. The flame detector must see the flame which it is designed to protect, and it should see *absolutely* no other flame.

To set the stage for a fuel explosion in a furnace there must be an accumulation of unburned combustibles mixed with the correct concentration of air, and an ignition source.

The philosophy that sensing the presence or absence of flame is sufficient to prevent a furnace explosion is not realistic when applied to a large multi-burner modern utility boiler. In these large boilers, stratification may occur which could result in pockets of an explosive mixture. Also, when all burners are contributing to a common flame envelope, the failure of several burners to ignite may result in a fuel rich mixture which could cause a total flame extinction. Discrimination may be defined as the scanner's ability to see the flame from one burner only, and to exclude all other burners, including the main fire ball.

Some traditional coal flame detection techniques have involved either the use of ultra-violet radiation or the so called 'flicker' effect in the visible red.

Ultra-violet radiation levels are relatively high in the combustion zone, and as a consequence the use of U.V. overcomes the adjacent burner discrimination problem. However, this method suffers severely from coal dust obscuration, due to the wavelength-to-coal dust particle size ratio. Coal dust particle size varies between 5 and 500 micron diameter with 60% being in 30-50μ range. The U.V. method can on occasion be made to work satisfactorily, but it is very problematic, and cannot be made generally applicable to all coal flame detection situations.

Pulverized coal flame detection in the visible red using flame flicker has proven more successful than the U.V. method. The 'flicker' is caused by refractive index changes (Schlieren effects) in furnace gases due to temperature gradients. Vortex shedding off air registers is also thought to have some effect on gas movement in front of sensors. Frequency selective circuitry is employed after the 'flicker' sensor.

While this method has met with more success than most others, it still suffers from two distinct disadvantages. One is that it can be confused by shimmer caused by hot gas movement over the refractory liner. Boiler walls and refractory radiate strongly in both the long visible and near infra-red. It also suffers from a considerable burner discrimination problem in most multi-burner installations, for the near I.R. envelope around the flame can be quite extensive.

The monitoring of two inter-related parameters, and measuring their correlation coefficient or degree of similarity in real-time, obviates the burner discrimination and refractory shimmer problem. It also mitigates the coal dust obscuration problem, for long I.R. wavelengths are employed.

Causes of Coal-Fired Furnace Explosions (Ref 1)

1. Loss of flame on load reduction.
2. Loss of flame on decreasing load.
3. Reducing load - a flameout, then re-ignition by ignitors.
4. Loss of flame, then re-ignition from slag.
5. Flameout on decreasing load - trip blocked.
6. Steady pressure; flameout.
7. Increasing load. Failure of steam flow transmitter; air on manual, and fuel on automatic.
8. Steady load; lost fire; mill not tripped.
9. Loss of supporting energy - coming on-line.
10. Unstable fires due to wet coal.
11. Coal gas unstable after loss of supporting fuel.
12. Unstable flames under steady high load.
13. Flameout.

* Current employment affillation. Initial work outlined in this paper was done while author was employed with Forney Engineering Company.

14. Steady load; flameout.
15. Increasing load. Manual - increase fuel, inadequate increase in air.
16. Wet coal. Loss of feeder. Coal gas unstable resulting in flameout and re-ignition.
17. Wet coal. Lost mill; igniters in service to stabilize situation.

The list might easily include as many as 30 boilers which have experienced an explosion due to one of the above situations. As a result of investigations of coal fired boiler explosions the following insight has emerged:

1. The majority of furnace explosions occur in coal fired units as a result of a furnace 'flameout' condition with subsequent re-ignition.
2. A furnace is most vulnerable to a 'flameout' condition during load changing.
3. Unstable flames can occur at all boiler loads.
4. Furnace fire instability is a major contributing factor in boiler explosions.
5. Some factors contributing to furnace fire instability are:
   (a) Wet coal
   (b) Loss of a part of the 'in-service' equipment
   (c) Loss of supporting ignition energy.
6. Certain automatic control failure modes can cause hazardous furnace conditions.
7. Operating combustion controls in a manual mode, is questionable under changing load conditions.
8. The by-passing or disconnection of inputs that would otherwise trip the boiler, could result in a hazardous furnace situation.

COAL BURNERS

Circular burners use tangentially disposed vanes built into the air register to mix the fuel and air, and to produce the necessary scrubbing action on the coal particles.

Thus, while the fuel is introduced to the burner in a fairly dense mixture at the center, its dispersal by an impeller is such that it penetrates the secondary air stream introduced independantly of the primary air and coal.

The primary objective of a pulverized-fuel burner is to combine air and fuel, ideally without an excess of either. Burner tip velocities range from 45 to 65 meters per minute. (Figure 1 shows a typical dual feel coal burner of medium capacity.)

These velocities are critical, for flashback into feed tubes can easily occur at low velocity. Deposition of fuel in feed pipes can occur unless the velocity exceeds 20 m/s, and the air/coal ratio exceeds 1.5:1 by weight. Table 1 below shows some typica' values of primary and secondary air temperatures and velocities:

TABLE 1

	Water-tube Boiler	Shell Boiler
Primary Air:		
% of total flow	20	25
temperature, °K	375	375
velocity, m/s	35	15
Secondary Air:		
% of total flow	80	75
temperature, °K	500	300
velocity, m/s	40	25

These quantities are not only vitally important in the design of a boiler as a heat exchange device, but the burner management system design must also take them into account.

SPECIAL FEATURES OF PULVERIZED-COAL-FLAME RADIATION

The spectral radiances of a pulverized-coal flame indicate that a coal flame radiates mostly as a continuum source due primarily to radiation by the burning of pulverized coal particles. Measurements with hot and cold targets permit determination of the flame spectral emissivity as a function of wavelength. Thereby we can determine whether the coal flame radiates as a graybody, i.e. *whether its emissivity is independent of wavelength.*

The following relationships were used to determine the flame spectral emissivity:

$N_1(\lambda)$ = flame spectral radiance measured with cold target background

$N_2(\lambda)$ = flame spectral radiance measured against hot furnace wall background

$$N_2(\lambda) = N_1(\lambda) + \tau_\lambda \cdot N_3(\lambda) \qquad (1)$$

where τ_λ is the spectral transmittance of the flame, and $N_3(\lambda)$, is the spectral radiance of a blackbody at the furnace wall temperature. (Previous measurements had confirmed the validity of assuming that the furnace wall is a blackbody radiator.) Solving Eq.(1) for τ_λ, we get

$$\tau_\lambda = \frac{N_2(\lambda) - N_1(\lambda)}{N_3(\lambda)} \qquad (2)$$

Applying Kirchhoff's law to obtain the flame spectral emissivity, we get

$$\epsilon_\lambda = 1 - \frac{N_2(\lambda) - N_1(\lambda)}{N_3(\lambda)} \qquad (3)$$

Kirchhoff's law applies only to true absorption i.e. does not include scattering effects. The pulverized coal flames contain solid particles which cause scattering. As it is not possible to separate scattering from the true absorption, the emissivities determined from the flame spectral measurements with hot and cold background can be considered effective spectral emissivities combining both absorption and scattering effects. A typical example of effective spectral emissivities, from 1 μm to 5 μm at 450 mm along a flame axis, is shown in Fig. 2. *These data show that, although the emissivity is high, the flame does not radiate as a graybody.*

In measuring the spectral radiance of pulverized coal flames, the spectral absorption band due to methane at 3.5 μm is observed. Methane that appears in absorption (i.e. spectral lines below the flame background), indicates that some unburned methane is present in the cooler portions of the flame and in the recirculating gases. Methane absorption was observed for all flames and at all positions along the flame. However, the amount of absorption, i.e. the depth of the absorption lines, varied with flame position. In general, the absorption was highest in the first part of the flame near the burner. Although the methane absorption appears to be strong, the concentration of methane may be quite small.

In addition to the methane absorption spectrum there were also indications of re-absorption by CO at 4.67 μm. The absorption was quite low, however, and it was not possible to obtain an indication of any trend of CO absorption with flame position. Neither the CO absorption nor the methane absorption affects the measurements in the 1.4 μm to 2.2 μm region. (Ref. 2.) For large intense coal flames, temperatures in excess of 1925°c have been measured. These fall to 1650°c or lower at flame boundaries depending on furnace cavity design, and fall to at least 1400°c and as low as 900°c at the furnace exit.

These high temperatures allow the formation of ions and short-lived chemi-luminescent radicals, which are mainly concentrated in the combustion zone.

COMBUSTION SOURCE NOISE

If a small element of fuel, of mass M, burns at constant pressure with α times its mass of air, and if the heat evolved expands the products to K times their original volume, a mass $(K-1)\alpha M$ of the surrounding gases will be displaced. Such a displacement is affected by the radiation of a pressure wave which starts a movement away from the element as soon as burning starts. It is eventually followed by a reverse expansion wave which brings the surroundings to rest again

when burning is finished. If the rate of heat release is constant during the burning time, the pressure between the waves will be flat topped as they spread away from the particle.

A pressure pulse would be sensed by an observer as the front of the pressure wave reaches his position, and another when the rear of the wave passes. The magnitude of the pressure rise and thus the effect on the observer, would depend on the value at which the *rate* of burning suddenly rose. Between the pressure pulses, however, the observer would perceive nothing if the burning rate was steady since the pressure, although above atmospheric, is constant. (Ref. 3.)

TURBULENT HYDROCARBON FLAMES AND FREE RADICALS

A model commonly employed to describe turbulent premixed diffusion flames, is that of considering such flames to be composed of an assembly of burning elements that vary continually in size and position, each element evolving into an increased volume of heated gas. Acoustically, this model of a turbulent flame is equivalent to an assembly of monopole sound sources of different strengths and frequencies distributed throughout the reaction zone of the flame, and thus giving rise to a broadband spectrum of flame noise. Using this model, an acoustic theory given by Thomas et al Ref. 4 predicts that the far field pressure in the radiated sound waves will be *proportional to the rate of change of the rate of volume increase of gases during combustion, this quantity is then proportional to the rate of combustion.* This may be described in mathematical notation thus:

$$\frac{d}{dt}\left[\frac{dV}{dt}\right] \quad \text{where V = gaseous volume}$$

The technique described here measures the rate of change of the rate of combustion in coal flames, and as such will detect whether fuel is undergoing combustion. Burning coal gives luminous (carbon) flames, and the base or flame front of such flames show emissions from chemi-luminescent free radical species such as C_2,CH, and OH (hydroxyl radical). Normal radiation from such flames is more or less a continuum with the burning of carbon monoxide into carbon dioxide being responsible for the main heat release. The extent to which free radical radiation lines show from the continuum radiation,is dependant upon flame turbulence, with C_2 and CH radicals merging in the U.V. and phototopic range of wavelengths, while the OH radical still maintains singularity at high Reynolds number, as does the C_2 radical in the infra-red. Emission from free radicals, such as C_2 and CH are known to be confined almost exclusively to the reaction zone in hydrocarbon-air flames. These radicals are present in sufficiently small quantities to assure that their intensities of emission are not affected by self-absorption, so that intensities of the blue CH or green and infra-red C_2 bands are proportional to the volume of the reaction zone, which in itself is a measure of the rate of consumption of constituent combustible gas, derived from the fuel. Furthermore, fluctuations in Q (see Appendix One) should be reflected in fluctuations of the intensity of the emission. Thus, the time derivative of the emission intensity from a chemi-luminescent free radical should be proportional to dQ/dt, the rate of change of heat release in the high temperature region of the flame front.

There is also a sharp increase in temperature across the reaction zone (the gas composition also changes from reactant to product molecules and this may cause a change in volume, depending on the stoicheiometry of the initial fuel/air mixture). The rate of change of the volume is proportional to the reaction zone area. Again, fluctuations in the area of the reaction zone will cause fluctuations in the rate of volume increase. Since the radiated sound pressure is proportional to the rate of change of the rate of increase of volume of the evolving gases, it too will be correlated with fluctuations in the area of the reaction zone. (Ref. 5.)

Sound pressure is proportional to the rate of change of the rate of combustion, because the volume of the luminous reaction zone is a measure of the rate of combustion. Free radical chemi-luminescent combustion species are used because of their general confinement within the combustion zone, and because of the self-absorption of other combustion products.

Due to the high chemical reactivity of radical concentrations, they decay rapidly to very low equilibrium values and in general no C_2, CH, or OH radiation is observed downstream of the combustion zone.

C_2 radicals emit in more than one wavelength region of the complete spectrum from the ultraviolet into the infra-red. Characteristic bands appear in the ultraviolet region with band heads at 2149.2 Å, and 2312.6 Å, in the regions 2378-3000 Å and 3580-3860 Å, and in the Swan bands in the visible region at 4350-6800 Å. In the infra-red, emission appears at 12,091 and 17,657 Å; (1.2 and 1.766 um).

The 1.76 um line is the one that is utilised in this work, because of the previously noted obscuration problems at shorter wave-lengths, and the null in continuum radiation shown in Fig. 3.

This paper describes a method of *combustion detection* based on the proposition, that the rate of combustion is proportional to the intensity of emission given off by free radicals such as C_2 or CH, that are generally confined to the reaction zone of hydrocarbon flames. The first derivative of a free radical luminescent intensity corresponds to the rate of change of combustion, because it has been *experimentally* demonstrated that the modulation of the radical emission is directly related to the sound generation in a pulverized coal flame front. (Ref. 6.)

The correlation between these two parameters is shown in Figures 4A and B. The first Fig. 4A shows a differentiated signal from the C_2 radical, and that due to combustion noise.

A degree of similarity is detectable by eye in these two waveforms. On the other hand, Fig. 4B from an extinguished burner, shows marked dissimilarity.

Instrumentation techniques are now available which correlate such parameters in real time, and this will be discussed in the latter half of this paper.

INSTRUMENTATION

Correlation

Correlation is the process of relating one object, phenomenon, or quantity with another. In other words, it is a process of establishing similarity. In some activities, it might be sufficient to say that two quantities appear similar; alternatively, it may be possible to derive a single number, a correlation coefficient, which expresses any similarity quantitatively. However, to express the similarity between two waveforms, a single coefficient is not a sufficiently precise description for the degree of correlation must depend upon the relative timing of the two waveforms. For example, two sinusoids of the same period will have maximum correlation when coincident in phase and zero correlation when the phase shift between them is a half period. Correlation is a particularly valuable technique in establishing coherence between seemingly random signals (see Appendix 2). This aspect of correlation is used in this application.

Mathematically, correlation is well covered in existing literature, and the use of correlation for research purposes has been established for over a decade or more. The micro-processor now lends this powerful statistical technique to such mundane procedures as coal combustion detection.

Fig's 5A and B show the analog of both infra-red C_2 and combustion noise signals. The first derivative of the I.R. radical signal is input to the A/D converter, thereafter it is delayed appropriately by the cross correlation programme in the micro-processor. This is shown in Fig. 6, 'Crosscorrelation Implementation'.

Multiplexing

As coal fired boilers are multi-burner installations, solid state multiplexing for both the acoustic and I.R. sensors, is required. This takes the standard form of a junction field-effect transistor multiplexer, followed by sample-and-hold circuitry, together with analog to digital conversion, as shown in Fig. 6. JFET multiplexing is used in this application in preference to CMOS, because of its 'blow-out' immunity to high transient voltages, which in power station installations is a serious consideration. At the start of the implementation program outlined in Fig.6. two parameters are input, sampling rate and then the number of sampling points required between processing periods. The program then sets up a clock to take analog samples at a specified rate, allocates an area of memory as a single precision buffer to hold delayed (photo-cell) samples. Sampling rate is adjusted, such that aliasing errors are eliminated by utilizing the Nyquist criterion $\Delta t \geq \frac{1}{2B}$, where B is the highest frequency present, and Δt is the sampling interval. It will also set up a double precision buffer to hold processed data. After these short housekeeping routines, the data collection part of the program starts.

The memory updating process can be visualized as continually storing data in a closed loop. After each revolution of the loop, the old data in the shift register is replaced by a new sample. As each data sample is converted into an equivalent digital value by the analog-to-digital converter, it is deposited into the single precision store. This buffer acts in a manner similar to a shift register. For each new sample entered, the oldest sample is lost off the end.

As the data is being shifted along in the single precision store, calculations are performed to update the program. Each data point is multiplied by the most recent complementary sample, and the product is added to the corresponding cell in the double precision store area. Appendix 2 gives the calculations formed by this real time crosscorrelation algorithm.

In order to conserve core in the micro-processor, analog differentiation is done on the signal output from the photo-cell, before it is digitized.

Digital micro-processors can be used for signal correlation purposes, but being serial in operation do it on a sampling basis. The advantages over the parallel crosscorrelator are that there is flexibility with the number of correlation points, as this is related to the number of memory locations, which can be increased by the addition of more random access memory (RAM), and that a small number of standard elements are used, greatly reducing costs.

The basic elements are drawn in Figure 6. The flow diagram for a micro-processor-based correlator is shown in Figure 7. An interrupt signal begins the operation, and at the required rate, which also determines the delay interval, samples of 'x' and 'y' are pushed into the stack. A convenient number is 256. After the samples have been stored the first 'x' sample is multiplied with each of the 'y' samples in turn; the product being stored in a corresponding register. As the 'x' and 'y' inputs are represented digitally by their signs, the multiplication is accomplished with an exclusive OR Instruction, the result of which is used to decrement or increment a register corresponding to the appropriate delay. When the 256 multiplications have been completed, the process is repeated with a new sample of 256 points of 'x' and 'y' until a counter overload is detected.

SENSORS

Electro-magnetic

A multilayer three cavity interference filter, mounted in front of an indium sulphide ($I_n S_b$) photo-conductive cell with a germanium lens, is used to isolate the narrow line C_2 radical signal at 1.76 microns. Such an interference filter, of fixed wavelength and bandwidth, can be considered either a monochromator or a Fabry-Perot interferometer, that will extract narrow line discrete signals in the presence of strong continuum background radiation.

The spectral response of both the interference filter and the $I_n S_b$ photo-cell is shown in Figure 8.

Because of the high temperature environment, the photo-conductive cell is kept at about 30°C by means of a small thermo-electric cooling pile. Clean aspirating air is run over the interference filter, for the cavities have a temperature/wavelength coefficient of between 0.1 to 0.2 Å/°C. Aspirating air also prevents the buildup of ash on lenses exposed to the furnace cavity.

The infra-red sighting tube is positioned such that the center line of tube and burner intersect each other at about 40 cms (16") from the burner tip, depicted in Figure 1.

Vertical separation between burner center lines is 140 cm (55") with a lateral separation of 250 cm (100").

Sonic

The monitoring of sonic energy given off by the pulverized coal particles, undergoing combustion, was effectively solved by using a line type of microphone.

As will be realised hanging a conventional microphone in near proximity to the flame front is a virtual impossibility, because of the extreme dust and heat conditions.

As a consequence it was decided to utilize the many sighting tubes which are normally placed around a burner, for conventional flame monitoring purposes. These sight pipes can often be up to 3 to 4 meters in length, and can therefore serve ideally as the pipe element in a line microphone; see Fig. 1. Line or shot-gun microphones employ a long slotted tubular structure in front of a conventional microphone; like a capacitor or electret type.

The primary reason for using this type of microphone was that sound from the flame front arrives at the burner-mouth with narrow angles of incidence. The line microphone accepts these narrow incidence sound fields relatively unattenuated, while those arriving at other angles reach the sensor through a multiplicity of paths, with resultant interference and therefore cancellation.

The directional sensitivity of the line microphone depends upon the total length, and a pipe of eight wavelengths long has a 3 dB. point of about 20° off center line.

While this method of sound detection avoided placing the microphone element in a severe heat environment, it was nevertheless necessary to provide aspirating air, to keep the sound pipe free of ash and clinker.

COMBUSTION CONTROL

The utilization of crosscorrelation techniques ensures detection specificity of any one coal burner in a multiple burner installation. If the correlator fails to continuously signify a suitable crosscorrelation identity between light and sound signals for 'X' seconds, fuel supplies to the affected burner are cut off. This avoids the build up of uncombusted material in the furnace cavity, and thereby ensures safe boiler operation; in this respect at least. In the event of a single burner failure which is surrounded by a group of similar, yet operating burners, the sonic energy picked up by the line microphone on the affected burner will not correlate with the signal from the C_2 radical photo-sensor. While sonic energy from other burners will certainly be picked up by the combustion detection instrumentation, light energy from the narrow segment of the I.R. spectrum monitored will be considerably diminished. This is because the radical signal is strictly confined to the high temperature region of the combustion zone.

Whatever the level of signals passed is not really important, as long as they are in excess of processing threshold. What is important is the fact that they are *uncorrelatable or correlatable*. It is on this premise, that this whole concept of pulverized coal combustion detection lies.

Whilst the primary function of this instrumentation is concerned with burner and fuel management, its proper operation can have an effect on combustion pollution control.

For instance, in fly ash collection control, of the many factors influencing electrostatic precipitator efficiency, one of the most important is loading. If the precipitator gets into an overload condition due to uncombusted coal particles entering it, then particulate effluent control is compromised, notwithstanding the explosion hazards. Also uniformity of the air/fuel ratio at each burner is a predominant factor in the generation of nitric oxide; a control pollutant. If uncombusted coal is allowed to be emitted from a burner not having an associated combustion zone, this can affect the air/fuel ratio of adjacent burners. In boilers with NO_x quenching ports, a single bad burner can control excess O_2 and thus the air and subsequent NO product of all other burners.

Figures 9A and B show typical crosscorrelogram signals for two pulverized coal burners on a multi-burner installation. As can be seen the transition between 'flame' and 'no-flame', is quite distinct, and is used to actuate burner management control circuits that are depicted in Figure 6.

CONCLUSIONS

With our ever diminishing fuel reserves, it has become apparent that we must burn coal in the most efficient manner possible, and with minimum impact upon our environment. To do this will require new and ever increasingly sophisticated instrumentation techniques.

The technique that has been described in this paper utilizes the relationship between the sound and light given off by coal particles undergoing combustion. By real-time crosscorrelation analysis, it can be established that coal entering a furnace cavity, is in fact undergoing combustion, thus avoiding waste, and the possible build up of explosive deposits.

Because of coal dust obscuration at short optical wavelengths, radical radiation at infra-red wavelengths is employed. The region of the spectrum in which the radical radiation is incident must be chosen carefully. Continuum radiation from the coal particles can obscure the radical line, if that area of the spectrum wherein the line lies is predominantly CO_2 radiation. Thus Fig. 3 shows a relatively low level of continuum radiation in the region 1.6 to 1.8 μm. Employment of a narrow band 5Å interference filter ensures that the energy incident upon the detector is primarily derived from the C_2 radical.

With the process of converting back to coal as a primary fuel for electrical power generation and other purposes, a great deal is being written about the generation of low B.T.U. gas from coal by various methanation processes.

But one thing must be kept in mind here. The most efficient way to use coal is by direct combustion. *Any process to convert coal or upgrade it for environmental purposes will inevitably require the additional expenditure of energy.* Thus, coal in pulverized form represents one of the most energy efficient forms of its utilization, and it therefore behooves us to perfect the technique.

The investigation has demonstrated that combustion detection rather than flame detection per se, is a preferable parameter to monitor for burner flame proving.

APPENDIX 1

Sound Generation by the Particulate Elements in a Pulverized Coal Flame

According to simple acoustic theory, the instantaneous sound pressure, P(t), measured at a distance, 'd', from a monopole sound source situated in a medium of density, ρ, is given by the equation:

$$P(t) = \frac{\rho}{4\pi d}\left\{\frac{d}{dt}\left(\frac{dV}{dt}\right)\right\}_{t-T} \qquad (1)$$

where dV/dt is the rate of volume generation at the source. The quantity d(dV/dt)/dt is termed the strength of the monopulse source, and is evaluated at the retarded time (t-T) where T corresponds to the time taken for the sound wave to propagate from the source to the point of detection. If a turbulent flame is regarded as being made up of a distribution of 'n' combustible elements, each evolving an increased volume of heated gas, and therefore, acting as a monopole sound source, we may write for the 'i'th element:

$$\frac{dVi}{dt} = (E-1)q_i \qquad (2)$$

where q_i is the volumetric rate of consumption of a combustible gas mixture in the element, and E is the volumetric expansion ratio of burnt to unburnt gases and is a constant for a given flame.

From equations 1 and 2, the far field pressure in the individual waves that emanate from the combustion element is given by:

$$P_i(t) = \rho/4\pi d\ \{d/dt(E-1)q_i\}_{t-T} \qquad (3)$$

When the acoustic properties of a turbulent flame are considered, it is important to remember that the frequency spectrum of the pressure in the radiated sound wave extends over two or three octaves, and that pressure waves radiated from different combustion elements (in this particular study - pulverized coal particles) will, in general, differ in phase. Only for an infinitesimal flame or region of noise generation will the total sound pressure in the far-field always be given by a simple summation over all burning elements of the component pressure, $P_i(t)$ - the dependent variable in eq. 3. With large flames of a size comparable or larger to component quarter wavelengths of the emitted sound wave, this simple summation will not be valid. For such flames, differences in the value of T (propagation time) for waves emitted by individual combustion elements then become comparable to the corresponding quarter-periods, so that the individual pressure waves no longer have the same relative phase differences at any point in the far-field as they originally had at their points of gaseous evolution in the combustion zone. However, for flames of practical size, certainly smaller than 27 m (i.e. $c/f \times 4$ where $c = 3 \times 10^8$ velocity of light in meters, and f is the main pressure wave component, determined experimentally to be between 25 to 30 Hz), the differences in T for the individual waves are small compared to their quarter periods, and as such retain approximately the same relative phase differences as they had at the flame in propagating to a point in the far field. Thus if the means of detecting the pressure variations is *restricted to a small frequency band* in the pressure spectrum, the total instantaneous sound pressure at the detection point is given by simple summation in the form:

$$P_{(t)} = \Sigma_n P_i(t) = P/4\cdot\pi\cdot d(E-1)\cdot\left\{\frac{dQ}{dt}\right\}_{t-1} \qquad (4)$$

where $Q = \Sigma q_i$ the total gaseous volumetric rate of combustion in the flames ignition zone.

APPENDIX 2

Autocorrelation

Mathematically, the autocorrelation function is defined as:

$$R_{x.x,(\tau)} = \lim_{T\to 0} \frac{1}{T} \int_0^T x(t)\cdot x(t-\tau)dt$$

where x(t), is the time function of interest, and is multiplied by a time delayed version of itself, i.e. x(t-τ), with the product of the two values averaged over the observation time, T. The resulting average approaches an exact correlation as T approaches infinity.

Autocorrelation Function

The top sinusoid is multiplied by the middle one. The middle waveform is identical to the top, but delayed by one time unit.

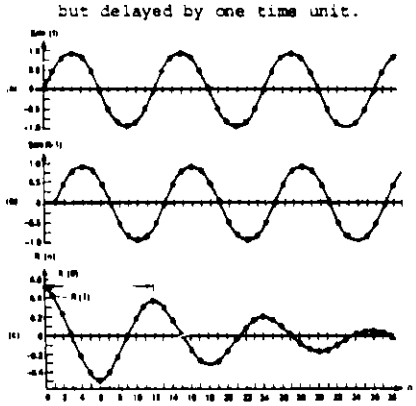

This product gives the R(0) coefficient shown in the bottom waveform.

Crosscorrelation

Crosscorrelation is very similar to autocorrelation, with the difference being that the first input is multiplied by a time delayed version of a second dependent or independent signal, rather than a time delayed version of itself.

The crosscorrelation function of a waveform having two, not necessarily independant waveforms is defined as:

$$R_{x.y,(\tau)} = \lim_{T\to\infty} \frac{1}{T} \int_0^T x(t)\cdot y(t-\tau)dt$$

To apply digital computing techniques to the above equation it is convenient to approximate the average by sampling the signals at regular intervals of say - t, and then summing a finite number k, of the sample products.

Rewritten in discrete form, the crosscorrelation equation becomes:

$$Rx\cdot y,(N\Delta\tau) = \frac{1}{K+1} \sum_{i=0}^{K} x(t)\cdot y(t-N\Delta\tau)$$

where n = 0,1,2,3,...,n.

The maximum time delay, τ max, is divided into N intervals of Δτ each, and the time between samples, Δt, is made equal to the time delay increment Δτ.

REFERENCES

[1] Raymond J. Murphy et al, "Boiler Operational Safety and Burner Management Systems for Coal Fired Boilers." Forney Engineering, Co, Dallas, Texas.

[2] Gunter J. Penzias, "Spectroscopic and Spatial Distribution of Radiation in Industrial Flames, with reference to Improved Measurements and Control of Steam Generators: Phase 3 - Spectral Radiation of Intermediate-Scale Coal Flames." Edison Electric Institute. Report E.E.I. RP 57. March 1968.

[3] Bragg S.L., "Combustion Noise." J. Inst. of Fuel. Jan. 1964.

[4] Thomas A. et al, "Flame Noise: Sound Emission from Spark-Ignited Bubbles of Combustible Gas." Proc. Roy. Soc. A294. p.449. 1966

[5] Rosenfeld J.L.J. Shell Research Ltd. Private Communication.

[6] Hurle I.R. et al, "Sound Emission from Open Turbulent Premixed Flames." Proc. Roy. Soc. A303. pp. 409-427. 1968.

ACKNOWLEDGEMENTS

The initial conceptual work outlined in this paper was funded by Forney Engineering Company of Dallas Texas to whom patent rights have been assigned.

Subsequent work was carried out after discussions with personnel of the New Zealand Electricity Department, at Wellington & New Plymouth. New Zealand.

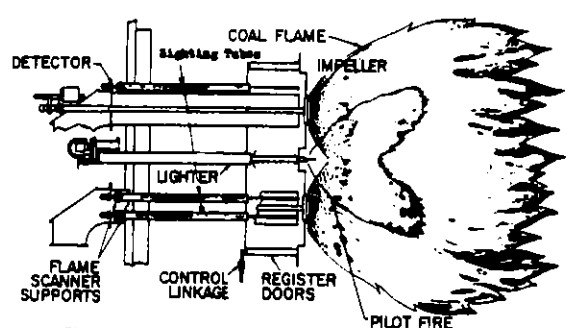

Figure 1. Typical Pulverised Coal Burner's

FIGURE 2

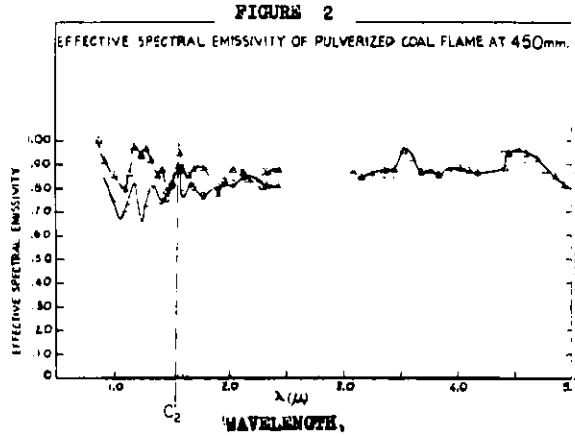

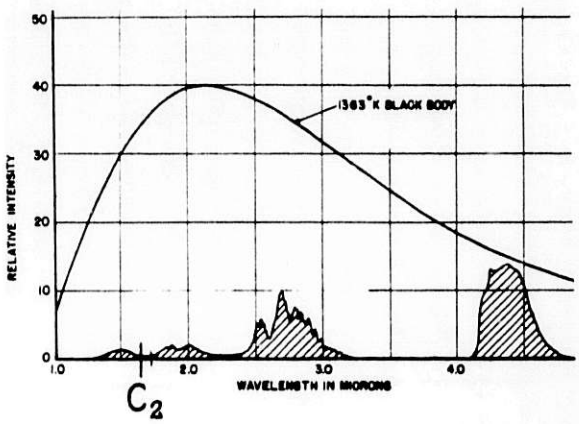

Figure 3. PULVERIZED COAL SPECTRAL DISTRIBUTION

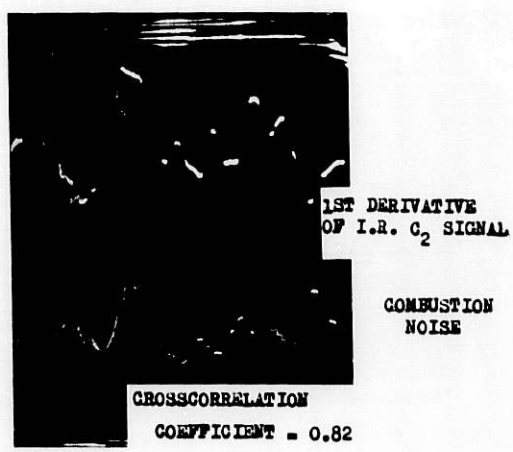

FIG. 4A. COAL PARTICLES UNDERGOING COMBUSTION.

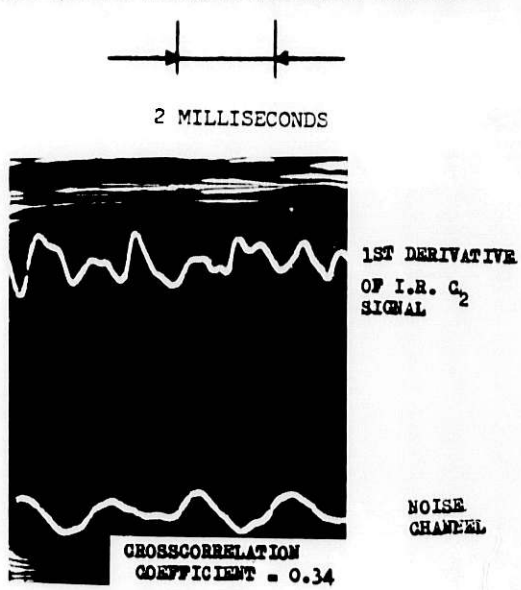

FIG. 4B. NON-COMBUSTION OF COAL PARTICLES

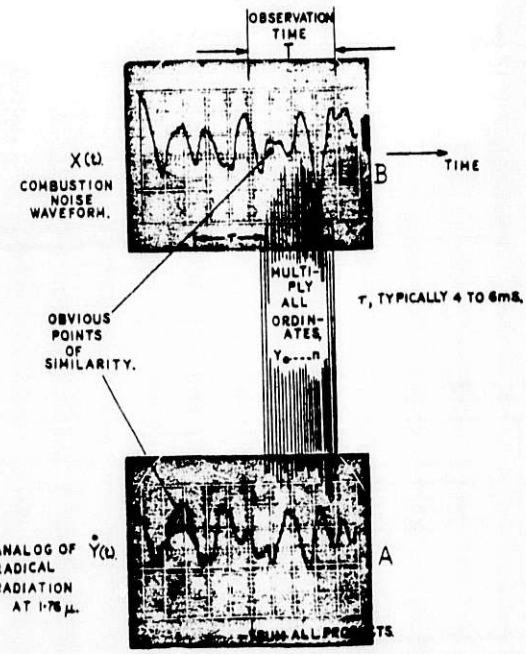

FIG.5. I.R. & SOUND WAVEFORMS CROSSCORRELATION

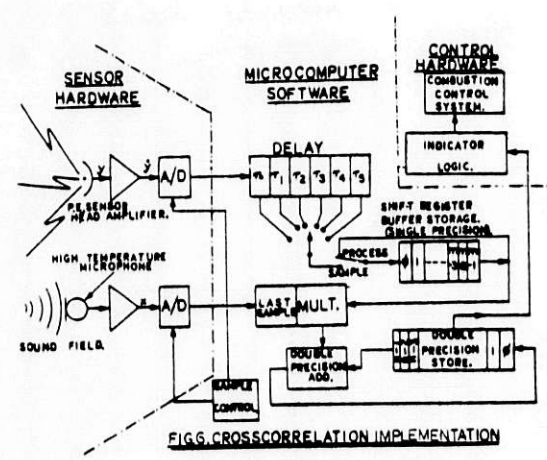

FIG.6. CROSSCORRELATION IMPLEMENTATION

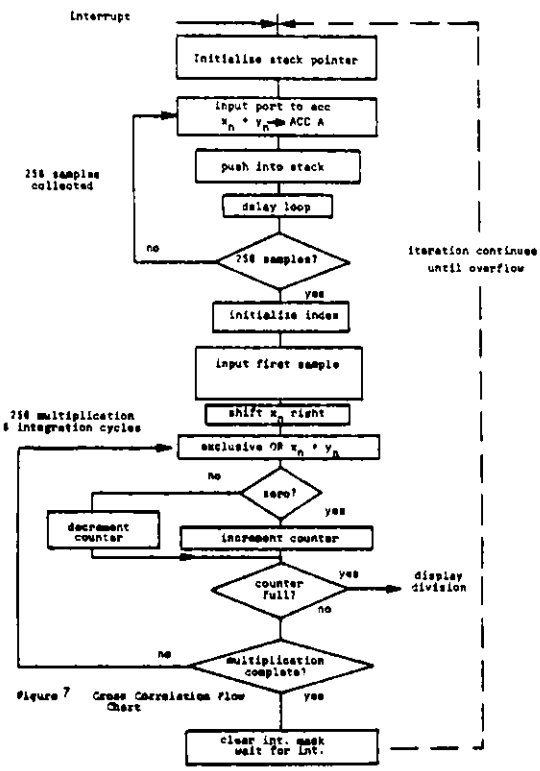

Figure 7 Cross Correlation Flow Chart

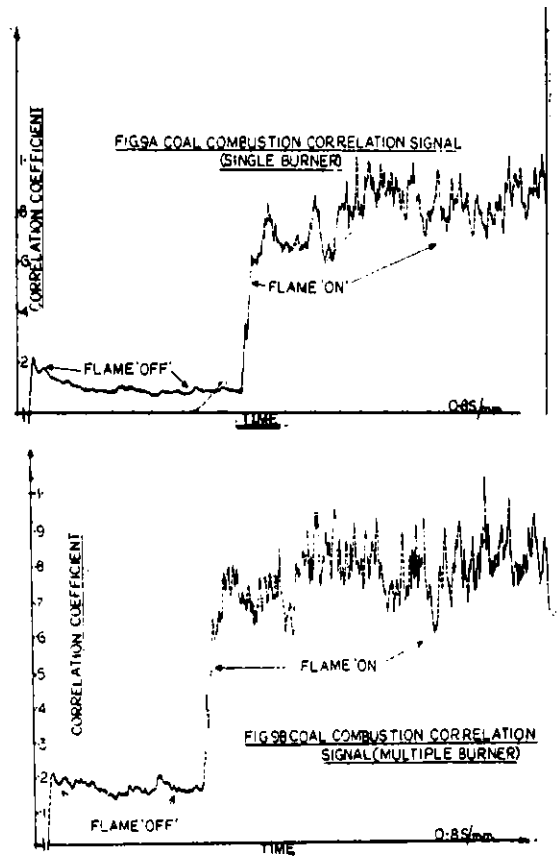

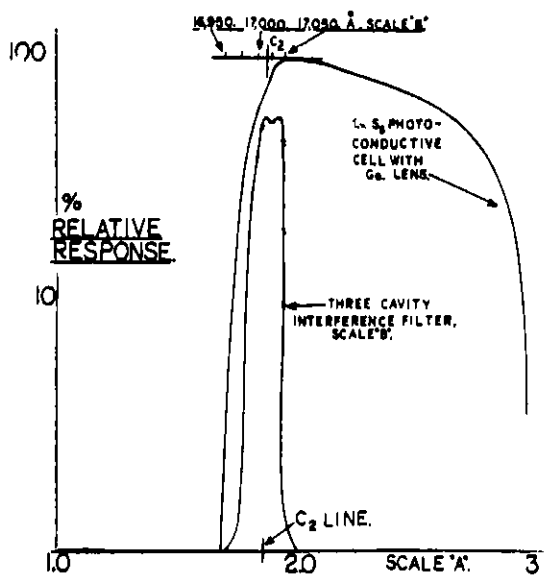

FIG. 8 WAVELENGTH IN MICRONS.

MOLTEN CARBONATE FUEL CELL INSTRUMENTATION ASSESSMENT†

P. Alexander, A. Apte, H. Fein, P. LaRosa, and P. Westcott
TRW Energy Engineering Division

ABSTRACT

The operation of a molten carbonate fuel cell, fed by the process gas stream from a surface coal gasifier, has been studied. Detrimental process gas contaminants have been identified and the concentration levels at which they must be maintained and controlled have been determined. It was found that As, Cl, F, S, and Se must be measured at concentrations as low as 3 ppb and as high as 100 ppm. Recommended monitoring techniques to accomplish this include gas chromatography, atomic absorption spectroscopy, ion chromatography, and pulsed fluorescence spectroscopy.

1. INTRODUCTION

In order for a fuel cell power plant to be a useful energy contributor, it must be able to use commercially available fuels and produce AC electrical power. A fuel cell generator system(1) has three components, which are shown schematically in Figure 1. The fuel processor converts a fossil hydrocarbon fuel to a hydrogen-rich gas that is fed to the fuel cell stacks to produce DC power. The power conditioner or inverter transforms the DC power to AC power compatible with user requirements.

This study focuses on a molten carbonate fuel cell (MCFC) power plant fueled by coal; specifically, the fuel processor section of the power plant, which converts coal to a gas suitable for MCFC. This study addresses the monitoring and controlling of contaminants, in the fuel gas stream, that are detrimental to the performance of the fuel cell power section. The study objectives are to:

- Identify the process gas contamination concentrations expected to be present in the gas stream from a surface coal gasifier and determine which of these contaminants will be deleterious to the operation of the fuel cell power section.
- Determine the concentration levels at which these deleterious contaminants must be monitored and controlled.
- Develop a process gas monitoring and contaminant control scheme and assess the ability of existing analytic instrumentation to meet the monitoring and control needs.
- Identify gaps and development needs in the monitoring instrumentation:

†This work was supported by Argonne National Laboratory under contract #31-109-38-6108.

2. CONTAMINANTS DETRIMENTAL TO MCFC POWER PRODUCTION

As a minimum, the power production section of the molten carbonate fuel cell (MCFC) power plant consists of: fuel cells, a catalytic combustor, a boiler for the bottoming cycle. Additionally, either a gas turbine or hot gas expanders may be used. A recently completed study(2) concludes that using gas turbines in a MCFC power plant is not an attractive option.

A conceptual design for a MCFC power production section using gas expanders was developed(3) to examine the effects of contaminants at various concentration levels. In this conceptual design it was assumed that the fuel processor section operated at a pressure of 450 to 1000 psi, while the power production section operated at 150 psi. The gas from the fuel processing section was let down in pressure across a fuel expander. After exchanging heat with anode exhaust, the fuel gas entered the anode of the fuel cell. At the anode, typically 80 to 90 percent of the CO and H_2 in the gas were oxidized to H_2O and CO_2 by electrolytic reactions. The typical components involved were:

- Ni anode on a stainless steel support.
- Li_2CO_3, K_2CO_3 electrolyte.

These components and the catalytic combustor are critically affected by the contaminants in the fuel cell feed gas. The major detrimental effects of sulfur, hydrogen chloride, hydrogen fluoride, arsenic and selenium are:

- Degradation of the fuel cells' performance has been experimentally observed at H_2S concentrations as low as 1 ppm. Degradation of nickel catalysts in methanation reactors has been observed at H_2S concentrations as low as 0.02 ppm. Without more extensive research data being available, this level has been selected as the lower limit of acceptable total sulfur concentrations. Controlling the total sulfur concentration passing through the fuel cells is required since SO_2 and possibly other sulfur bearing compounds can be reduced to H_2S at the cathode, and migrate to the anode through the electrolyte.

  Hydrogen chloride will attack the carbonate ion in the electrolyte at concentrations above 1 ppm, necessitating early replacement of the electrolyte. Hydrogen fluoride is less reactive to carbonate ions and may not interfere with performance below 100 ppm concentrations. The control and monitoring levels have been set at 0.2 and 1.0 ppm respectively to provide a conservative margin.

- Arsine and selenium hydrides are known to degrade catalytic combustors at levels of 3 to 5 ppm by weight or 0.003 and 0.005 ppm by volume. They are not expected to reach concentrations higher than 0.03 and 0.05 ppm due to decomposition.

The specifications for controlling these contaminants and the levels at which they should be monitored are summarized in Table 1.

Table 1. List of Detrimental Contaminants

Contaminant	Expected Chemical Form	To Be Monitored	To Be Monitored And Controlled	Expected Level (ppm by Volume)
As	AsH_3	X		0.003-0.05
Cl	HCl		X	0.2
F	HF	X		1.0-90
S	H_2S		X	0.02 or 0.5*
Se	H_2Se	X		0.005-0.03

*The two different contaminant levels were obtained using two independent analytic approaches.

3. GAS CLEAN-UP AND CONTAMINANT CONCENTRATION CONTROL

Figure 2 displays various processing options to convert coal to fuel cell feed gas. As seen there are two major chemical cleanup processes - Bulk Sulfur Removal and Trace Elements Removal irrespective of whether a high or low temperature cleanup system is utilized. Although the details of the trace element process will vary with the choice of cleanup system, trace element removal involves the passage of contaminated gas over a solid absorbent to remove trace gaseous components. Such a system can be designed to operate at a nearly steady contaminant level in the clean gas irrespective of the contaminant level in the dirty gas.

The fact that trace element removal processes are relatively insensitive to the contaminant level of the entering gas stream is the basis of the selected control strategy which is schematically shown in Figure 3. This strategy involves the real time control of the bulk sulfur removal process and monitoring of the contaminant levels downstream of the trace elements removal process. The purpose of the downstream monitoring is to prevent a break-through of contaminants from the solid absorbent bed. The trace element removal process shown in Figure 3 consists of two iron oxide beds. One bed is in a feed gas desulfurization mode while the other is being regenerated. After most of the iron oxide is spent that bed is taken out of service and the other is switched to operate in the desulfurization mode.

The purpose of the bulk sulfur removal process is to remove as much sulfur as economically feasible from the gaseous stream prior to the trace sulfur removal process. Control of the Bulk Sulfur removal process is required to minimize the amount of sulfur reaching the trace element and trace sulfur removal stages in the presence of upsets in gas flow rate and/or sulfur concentrations. There are many different processes to remove sulfur compounds from gases. Irrespective of the particular process they are all based on the use of a solvent to scrub sulfur compounds from the gas. As the concentration of sulfur compounds in the product gas increases, the solvent rate in the absorber should be increased to remove additional quantities of sulfur compounds. This means that the solvent regeneration rate must also be increased. Proper control of the clean-up process can be achieved by controlling the solvent rate to the absorber using two input signals, the gas flow rate and exit gas sulfur concentration. In the event of a failure of a critical component in the clean-up system a gaseous stream with too high a level of contaminants may reach the fuel cell. To cope with

such a situation a monitoring and emergency flare system is used to divert the fuel cell feed gas to the flare.

4. SAMPLE COLLECTION APPROACH

One of the surface gasifier cases considered during this study is shown schematically in Figure 4. Two points A and B are indicated on this figure as locations from which gas samples for contaminant analysis will be collected. Point A is located after the bulk sulfur removal system and will be used to monitor the effectiveness of that process. In the event that sulfur levels in the input stream to this removal process need monitoring, then an additional monitoring station could be set up just prior to the bulk sulfur removal stage.

Point B follows the trace contaminant removal operation and is used to monitor the effectiveness of this function. The location of B following the heater allows any contamination exchange between the primary and secondary elements of the heat exchanger to be monitored.

The mechanisms for obtaining the process gas samples at points A and B are shown in Figures 5 and 6. Control valves to regulate flow rates and permit components to be replaced or repaired are not shown. The process gas is filtered to remove particulates and then cooled to a temperature acceptable to the on-line monitoring instrumentation. The gas flow line is heat traced up to the heat exchanger to prevent collection of condensable liquids from the process gas stream. These liquids are collected in the knockout tank following the gas cooling operation. It is possible that the condensation process will remove so much analyte from the process gas stream that the composition of the condensate liquid will have to be monitored to correct the analyte levels monitored downstream in the on-line analyzer. A pressure regulator provides a controlled pressure input to the analytic instruments. Data from the on-line analysis is stored in the minicomputer or microprocessor. This device also contains the logic to generate a process control signal. This signal can be used to alter the flow rate of the sulfur removal solvent or to switch the process gas flow from the fuel cells to the flare. The microprocessor logic might also call for generation of a control signal which would switch in a new contaminant removal guard bed.

The requirements for contaminants to be monitored on a continuous basis for control purposes at points A and B are listed in Table 2 together with other parameters relating to the measurements.

5. INSTRUMENT PERFORMANCE CHARACTERISTICS

Available analytic instrumentation technology was surveyed in terms of its ability to perform the measurements listed in Table 2. This survey and review of the literature was controlled by the following set of instrument performance guidelines.

- Ability to analyze one or more of the analytes in Table 2 in the predicted concentration range,
- Commercial availability,

Table 2. Instrumentation Monitoring Requirements

	Requirements					
Analyte	Range of Measurement	Accuracy	Response Time	T	P	Process Gas Composition
Bulk S	0.5 to 10 ppm	± 20%	5 min.	1250°F	175 psia	
Trace S	0.02 to 0.10 ppm	± 20%	5 min.	1200°F	165 psia	H_2 32-52%
HCl	0.1 to 10 ppm	± 20%	5 min.	1200°F	165 psia	CO 26-42%
HF	0.1 to 90 ppm	± 20%	8 hr.	1200°F	165 psia	H_2O 2-24%
AsH_3	0.003 to 0.05 ppm	± 20%	5 min.	1200°F	165 psia	CO_2 0-16%
SeH_2	0.005 to 0.03 ppm	± 20%	8 hr.	1200°F	165 psia	CH_4 2-4%
						N_2 ~ 1%

- Reasonable measurement response time,
- Previous usage in a similar applications.

Table 3 lists the instrumentation concepts which were uncovered as candidates for fuel cell feed gas monitoring.

Table 3. Instrumentation Candidates

Broad Range	Narrow Range	Specific Purpose
Gas Chromatograph	Infrared Spectrophotometer	Pulsed Fluorescence Spectrophotometer
Mass Spectrometer	Atomic Absorption Spectrophotometer	
Plasma Emission Spectrophotometer	Ion Chromatograph	
Neutron Activation Analysis		

None of the instruments listed could be placed directly into service on a molten carbonate fuel cell gas stream and meet all of the desired performance characteristics. Some techniques could not reach the detection limit requirements, some require sample conditioning procedures which could not be bought as "off-the-shelf" accessories, and some require on-line process control monitoring. Table 4 summarizes the potential detection limits of each candidate instrument for each analyte. Directly under each analyte at the top of the table is listed the minimum concentration value which must be measured. Each of the reported detection limits in the table was acquired directly from instrumentation manufacturers or their performance brochures. It is encouraging that at least one instrumental technique can be found, for each analyte, which has the potential to measure that analyte at the required concentration. In most cases there is likely to be some difficulty

in using that instrument on the fuel cell gas stream.

Table 4. Detection Limits for Candidate Instruments

	ANALYTES AND SENSITIVITIES				
Candidate Technique	Total Sulfur 0.02 ppm	HCl 0.2 ppm	HF 1 ppm	AsH_3 0.003 ppm	SeH_3 0.005 ppm
Gas Chromatography	0.01 ppm As H_2S in Flame Photometric Detector	0.001 ppm Hall Detector	0.001 ppm Hall Detector	0.01 ppm with Photoionization Detector	0.01 ppm Estimated
Mass Spectroscopy	100 ppm	NA	NA	100 ppm	100 ppm
Atomic Absorption	NA	NA	NA	0.0001 ppm	0.0001 ppm
Infrared Spectrophotometry	No Instrumental Data	1000 ppm	1000 ppm	No Instrumental Data	No Instrumental Data
Plasma Emission	0.03 ppm in Water	NA	NA	0.05 ppm in Water	0.1 ppm in Water
Ion Chromatography	0.001 ppm As S^{-2} or SO_4^{-2} in H_2O	0.003 ppm in H_2O	0.001 ppm in H_2O	0.001 ppm As AsO_3^{-3} or AsO_4^{-3} in H_2O	0.01 Estimated
Neutron Activation	NA	0.10 ppm Off Line	0.8 ppm Off Line	0.001 ppm Off Line	0.020 ppm Off Line
Pulsed Fluorescence	0.005 ppm As SO_2	NA	NA	NA	NA

From Table 4 it becomes readily apparent that mass spectroscopy, infrared spectrophotometry and plasma emission instruments can not meet the detection limit requirements for any of the analytes as on-line monitors. Neutron activation could meet the detection limit requirements for HCl and AsH_3 but it could only perform these analyses off site at a nuclear reactor

Table 5. Summary of Conclusions Regarding Suitability of Candidate Analytical Techniques

Candidate Technique	Analyte	Suitability of Technique
Gas Chromatography	S HCl, HF AsH_3, SeH_2	Total sulfur analyses can be obtained by adding up the concentration of H_2S, COS, and each mercaptan in the gas stream. This need for several analyses will contribute to analytical error and slow response times. HCl and HF can be analyzed using a carbopak column with 20% perfluoroether and 20% benzophenone and a hall detector. This system has not been previously used for process control monitoring. AsH_3 and SeH_2 analysis by GC has not been demonstrated at the 3 to 5 ppb level. Detector development would be appropriate.
Atomic Absorption	AsH_3, SeH_2	AsH_3 and SeH_2 analyses by AA is expected to provide the best performance. Direct gas sampling is possible although there is a lack of experience in using AA as a full time process control monitor.
Ion Chromatography	S HCl, HF AsH_3, SeH_2	Since all samples must be converted to the aqueous phase, this technique has secondary preference for S, AsH_3, and SeH_2 monitoring. Removal of HCl and HF with water during gas sample cooling may be an advantage if IC is used to monitor these two analytes. S, AsH_3 and SeH_2 would require oxidation to anionic forms prior to analysis, adding to the complexity of the sample handling system. IC's have not been designed to meet the rigors of full time process control service.
Pulsed Fluorescence	S	This technique would be preferred for total sulfur analyses. Direct gas sampling is possible although some development of an enclosed flame SO_2 converter would be required.

facility. The recommended candidate analytic techniques are gas chromatography, atomic absorption, ion chromatography, and pulsed fluorescence. The suitability of these techniques is discussed in Table 5.

REFERENCES

1. Benjamin, T.G., Camara, E.H., and Marianowski, L.B., "Handbook of Fuel Cell Performance". Prepared by Institute of Gas Technology for U.S. Department of Energy. Contract #EC-77-C-03-1545, May 1980.

2. Healy, H.C. et al., "Development of Molten Carbonate Fuel Cell Power Plant Technology". Quarterly Technical Progress Report No. 2. Prepared by United Technologies Corporation for Department of Energy. Contract #DE-AC01-79ET15440. August 1980.

3. Alexander, P., Apte, A., Fain, H., LaRosa, P., and Westcott, P. "Assessment of Instrumentation for Monitoring and Controlling Contaminants in Fuel Streams for Molten Carbonate Fuel Cell Power Plants. Prepared by TRW for Argonne National Laboratory. Contract #31-109-38-6108. May 1981.

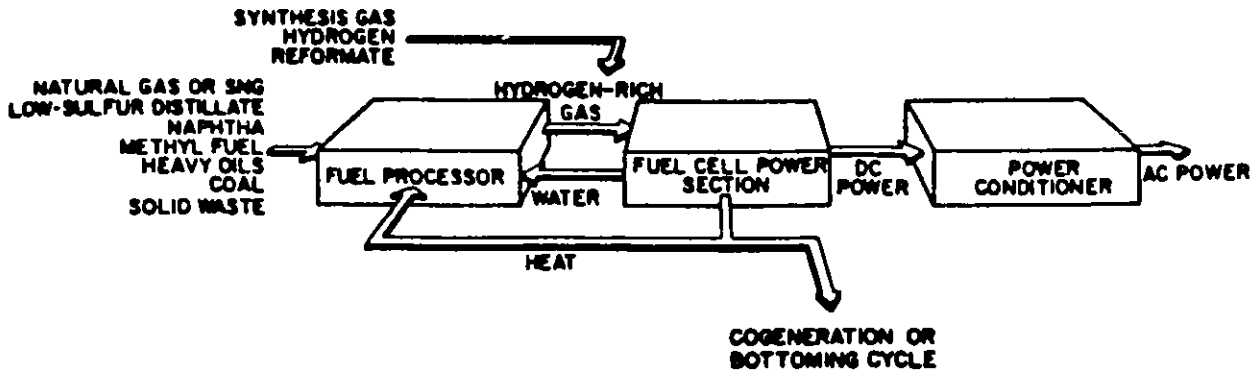

Figure 1. Complete Fuel Cell Power Plant

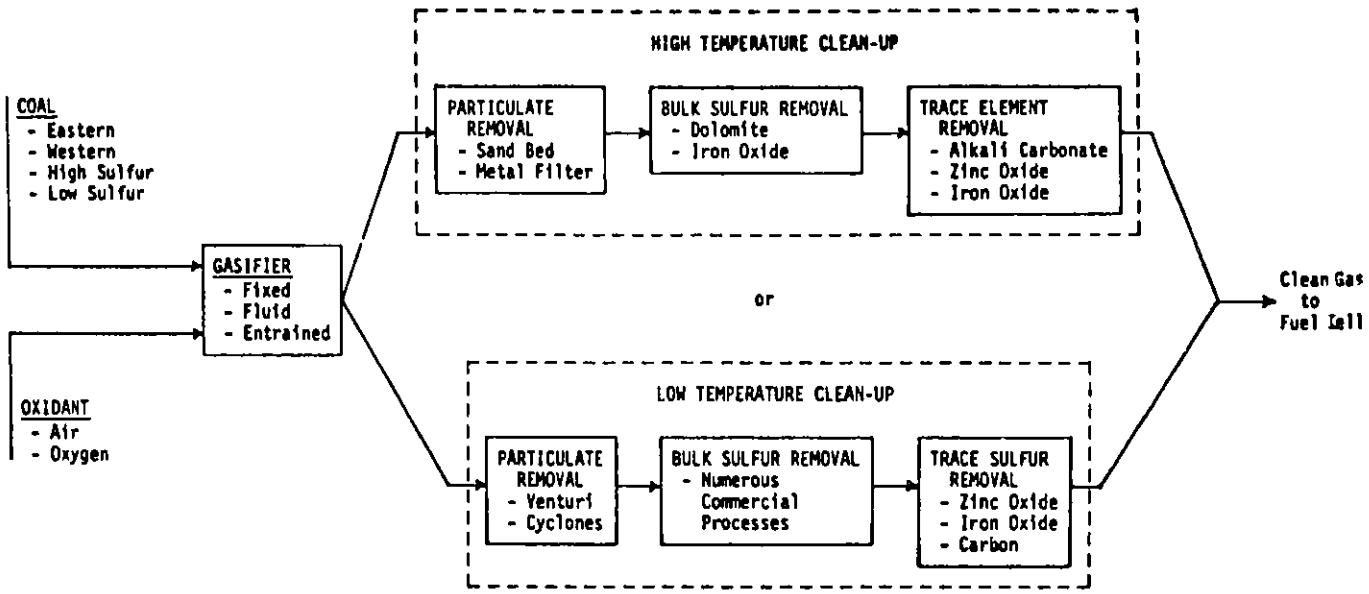

Figure 2. Options in Coal to Clean Fuel Cell Feed Gas

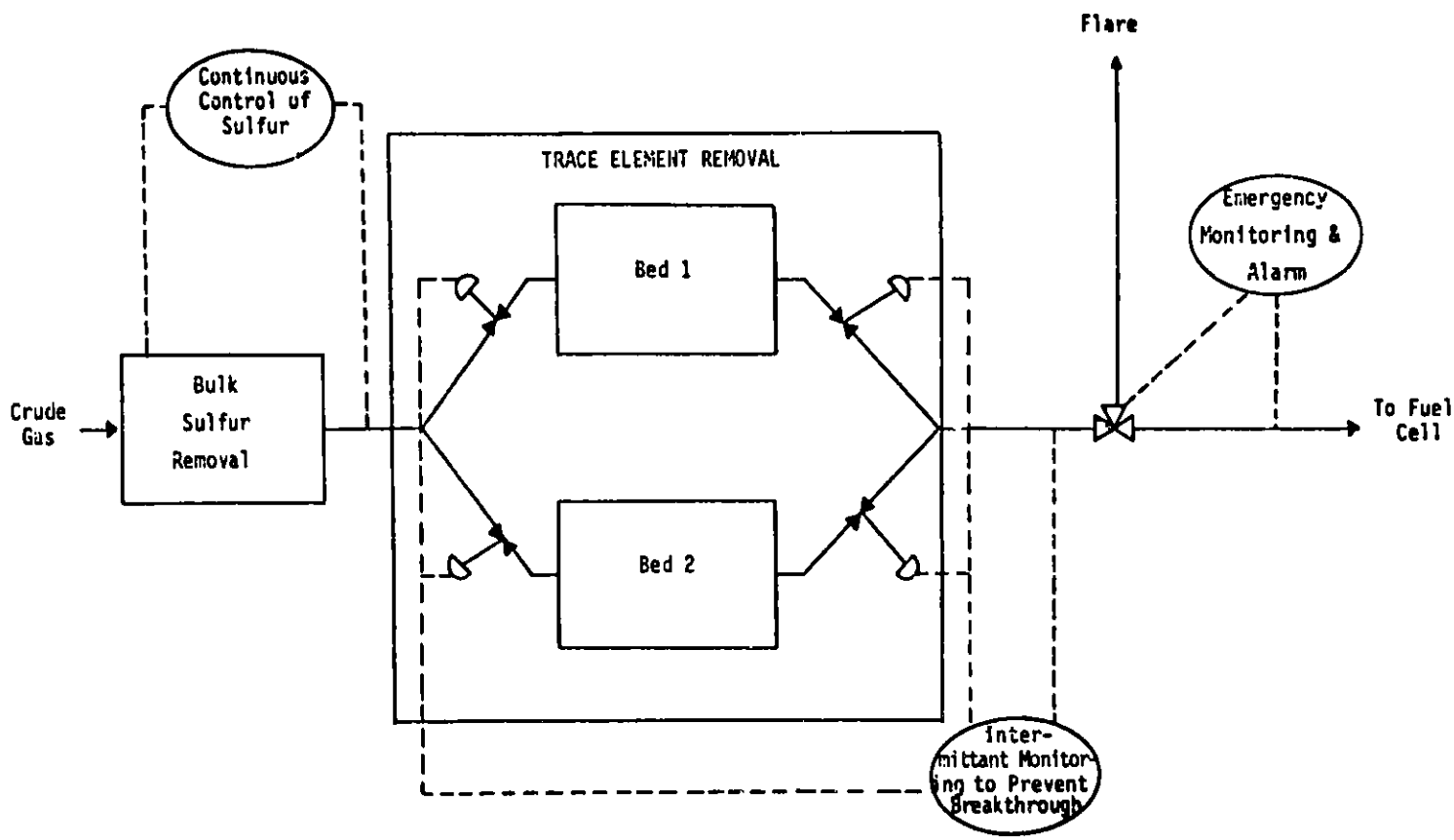

Figure 3. Schematic of Control Strategy

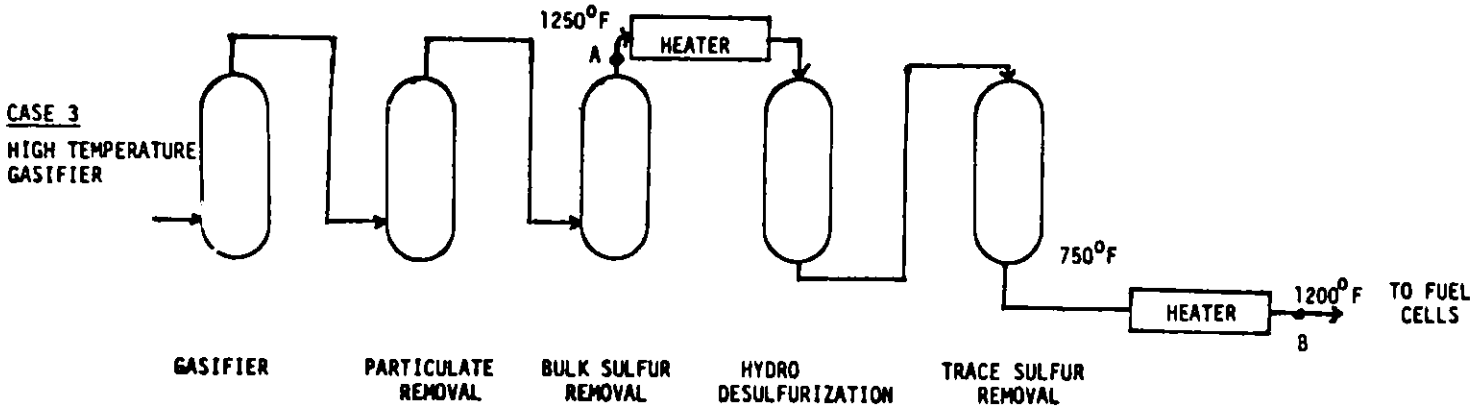

Figure 4. Location of Gas Analysis Points "A" and "B" with Respect to Three Gasifier Cases Considered

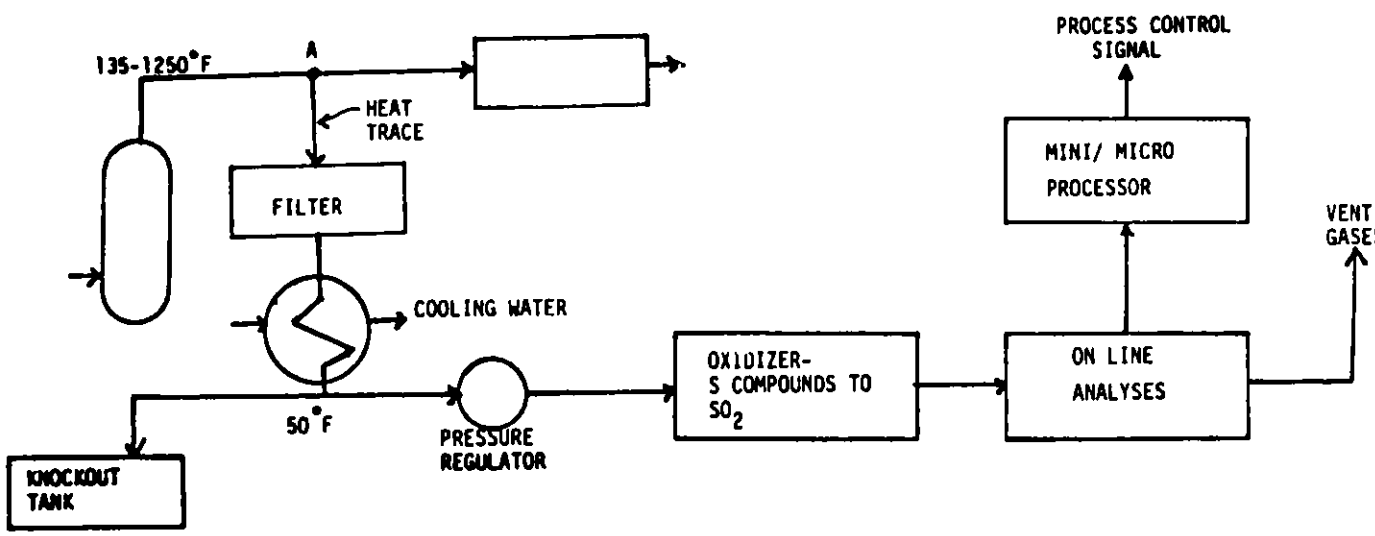

Figure 5. Monitoring Procedure at Point "A" Following Bulk Sulfur Removal

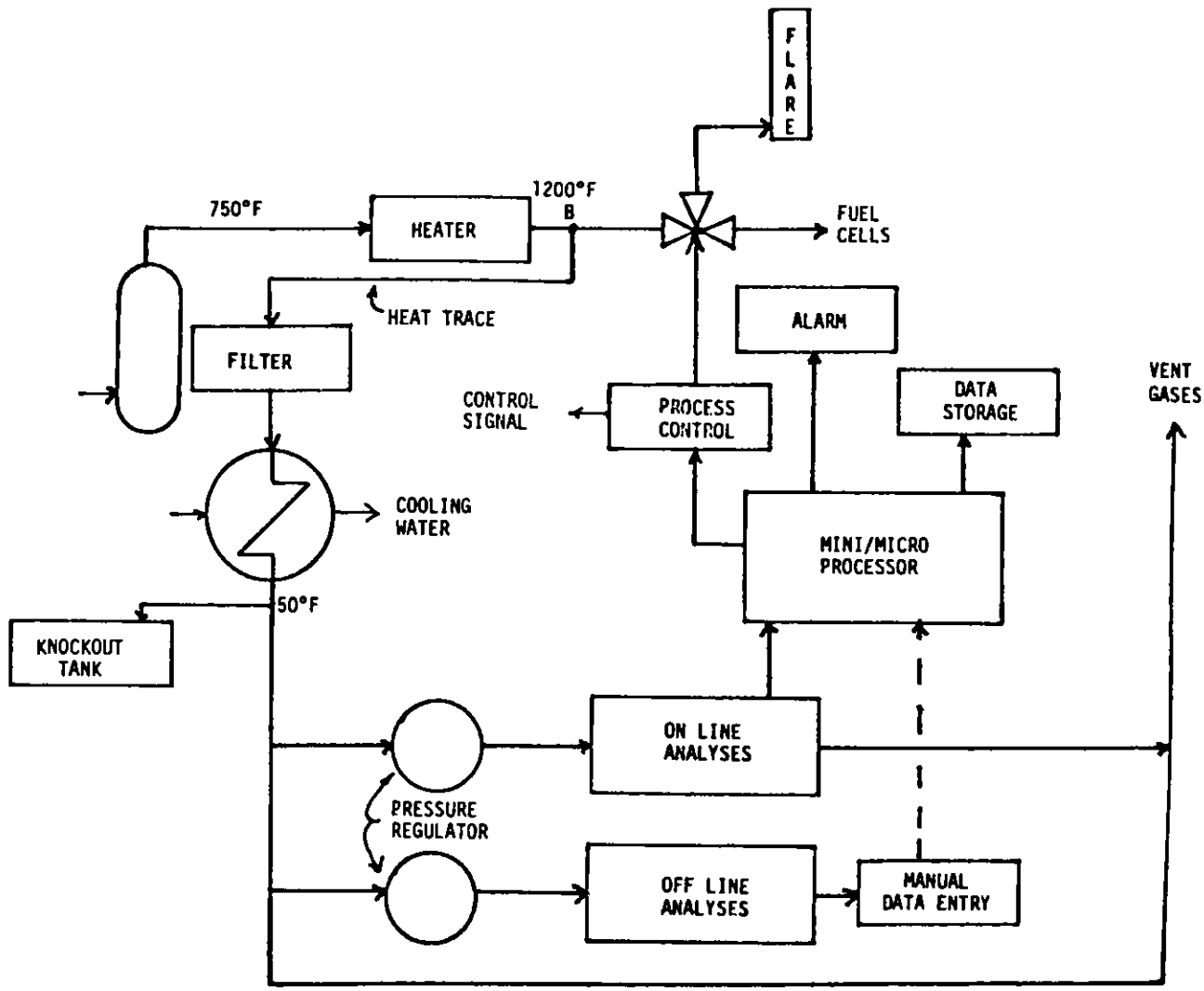

Figure 6. Monitoring Procedure at Point "B" at Inlet to Fuel Cells

THE USE OF ION CHROMATOGRAPHY IN THE ANALYSIS OF SOLVENT REFINED COAL PROCESS WASTEWATER

Marsha Wender Timmerman

Air Products and Chemicals, Inc.
Allentown, Pennsylvania 18105

Introduction

Air Products and Chemicals, Inc. is currently under contract to the Department of Energy (DOE) to characterize and then assess the biotreatability of the wastewater expected from the Solvent Refined Coal-I (SRC-I) demonstration plant to be constructed in Newman, Kentucky. Process recycle wastewater is effluent water from the SRC process area. Samples were obtained from the two DOE SRC pilot facilities - one at Fort Lewis, Washington (operated by The Pittsburg & Midway Coal Mining Company) and the other at Wilsonville, Alabama (operated by Catalytic, Inc. and Southern Company Services, Inc.). The Fort Lewis samples were obtained while that plant was operating in the SRC-I mode. (The Wilsonville plant only operates in the SRC-I mode.) The Fort Lewis samples will be referred to as process recycle wastewater (PRW) and the Wilsonville samples as V105.

Both wastewater samples were similar in composition and overall concentration. Concentrations of some of the ions varied with the composition of the feed coal. The samples were complex mixtures of organic and inorganic pollutants. The waters contained approximately 1.5% dissolved hydrogen sulfide (H_2S), 1.5% ammonium (NH_4^{+1}), 2.0% organics (mostly phenolics) and a host of smaller constituents that significantly contribute to the potential pollution problem.

Analysis of ions, such as NH_4^{+1}, NO_2^{-1}, NO_3^{-1} and PO_4^{-3}, is necessary to properly monitor the progress of a biotreatment system. Three techniques for anion and cation analyses were tried. These techniques were the Technicon Auto Analyzer(R) (an automated system for colorimetric analysis), various specific ion electrodes and the Dionex Ion Chromatograph (IC). Only IC was capable of easily separating the interfering organics from the inorganics.

Procedure

The Dionex Model 16 IC was used in these experiments. This system was outfitted with a WISP$^{(R)}$ (Waters Associates Intelligent Sample Processor) autosampler and a VISTA 401 (Varian computerized data system) data system. IC is a technique employing a combination of ion exchange, eluant suppression and conductimetric detection. The basic technique is described by Small, Stevens and Bauman (1975). Procedures for analysis of anions (F^{-1}, Cl^{-1}, NO_2^{-1}, PO_4^{-3}, Br^{-1}, NO_3^{-1}, and SO_4^{-2}) and cations (Na^{+1}, NH_4^{+1}, and K^{+1}) in water are fully described by Dionex (1978); however, when one analyzes samples as complex as the process waters, modifications are necessary.

Anion analysis for all 7 ions was possible using two different eluants. The column configuration (all columns were plastic, manufactured by Dionex) consisted of two 4 x 50 mm precolumns, a 4 x 250 mm separator column and a 9 x 100 mm suppressor column. An eluant consisting of .0015 M $NaHCO_3$ and .0012 M Na_2CO_3 was used to measure F^{-1}, Cl^{-1}, and NO_2^{-1}; the .003 M $NaHCO_3$ and .0024 M Na_2CO_3 eluant was used for the analysis of the other ions. The flow rate was set at 20% or 92 ml/hr for the weaker eluant and 30% or 138 ml/hr for the stronger eluant.

Cation analysis (Na^{+1}, NH_4^{+1}, and K^{+1}) was accomplished as recommended by Dionex Corporation (1978). The column configuration consisted of a 4 x 50 mm precolumn, a 4 x 200 mm separator column and a 9 x 100 mm suppressor column. The eluant was .005 N HCl; it was pumped at 15% or 69 ml/hr.

Weak organic acids (acetate, formate, and propionate) could be analyzed using the anion column configuration with a very weak eluant (.0015 M $NaHCO_3$) or by using the Dionex Ion Exclusion (ICE) columns. The ICE column configuration consisted of a 9 x 200 mm separator and a 6 x 150 mm suppressor. The eluant was .001 N HCl pumped at a flow rate of 42 ml/hr.

Results

Figure 1 shows the standard run of all 7 ions using the stronger eluant. Figure 2 shows a standard run with the half strength eluant; only F^{-1}, Cl^{-1} and NO_2^{-1} definitively separated. NO_3^{-1}, Br^{-1} and PO_4^{-3} would elute

from the column, but at the same retention time; SO_4^{-2} would not elute. Use of the weaker eluant reduced the water dip, thereby permitting better quantitation of Cl^{-1}. The weaker eluant also separated Cl^{-1} from weak organic acids such as acetate and propionate; these organics coelute with Cl^{-1} when strong eluant is used.

Figure 3 shows the PRW and V105 chromatograms using the stronger eluant. Both chromatograms are similar; the only measurable constituent was SO_4^{-2}. The peak at 6 minutes is a mixture of Cl^{-1} and weak organic acids. Figure 4 compares the chromatograms of PRW and V105 samples using the weaker eluant. Both samples are similar and both contain large quantities of Cl^{-1}. Note that the Cl^{-1} values in this chromatogram are significantly less than those in Figure 3. The unidentified peak before Cl^{-1} is probably a mixture of the weak organic acids; it was these weak organics that coeluted with Cl^{-1} when the strong eluant was used. Quantitative data for all ions is summarized in Table 1.

Figure 5 is the standard chromatogram for cations. Figure 6 presents the PRW and V105 chromatograms for cations. The important observation in these chromatograms is the broadness of the Na^{+1} peak. Preliminary evidence indicates that something coelutes with Na^{+1}.

Figure 7 shows the comparison of weak organic acids using the traditional anion columns and the ICE columns. Separation using the ICE columns was superior. More weak acids were separable using the ICE columns and the occurrence of interferences by other anions was decreased.

Figure 8 presents PRW and V105 chromatograms using the ICE columns. Significant amounts of acetate and propionate were evident. The peak at 23 minutes is probably unidentified organic material. When these samples were analyzed on the anion columns, only large quantities of acetate were identified; it was not possible to separate acetate from propionate under the specified conditions.

Discussion

IC has proved to be a very useful tool for cation and anion analyses of SRC process wastewaters, if one is careful to avoid the pitfalls caused by the complex nature of the samples. Addition of methanol (5%) to all eluants was very effective in preventing the organics from hanging up in the column and eventually poisoning it.

pH proved to be another critical factor. Due to the high buffering capacity of these waters, diluting with the weak acidic eluants was usually not sufficient to reduce the sample pH to below 5; only when the pH was properly adjusted did sharp, nicely separated peaks result. Also, having the same pH in the sample and the eluant helped in the reproducibility of retention times.

Peak identification and quantitation were accomplished using both retention times and spiked samples. Linearity of peak response was not extensively checked, as it has been previously reported by Hoover and Yager (1980) and Bogen and Nagourney (1979).

For anion analysis, it is mandatory that two separations be done. The Cl^{-1} levels may be critical to future plant operations; Cl^{-1} could be responsible for corrosion problems. The Cl^{-1} content of the water will vary depending on the coal shipments. The two proposed separations will also be suitable for detailed wastewater plant effluent analyses; more anions would be expected in the effluent due to nutrient addition and also potential nitrification.

The significant SO_4^{-2} levels measured are probably not representative of the actual process wastewater. Oxidation of the H_2S present in the sample is an ongoing process once the sample is exposed to the air. There is also some evidence indicating that the H_2S will be converted to SO_4^{-2} while in the presence of the eluant (Dionex, Personnel Communication).

Extensive checking with spiked samples and various weaker eluants led to the conclusion that there were no significant interferences occurring with the ammonia determination. If any simple amines were present, they should

separate after the NH_4^{+1} peak (Dionex, 1978a). Using the same techniques, the evidence indicates that there was an interference occurring with Na^{+1}. Atomic absorption analysis did not verify the Na^{+1} value generated on the IC. No identification of the interference is possible at this time.

The Dionex ICE columns were very successful in measuring simple organic acids. It was surprising to find such significant quantities of simple organics in a sample with such a complex matrix. It is anticipated that other organic acids can be identified after making appropriate system modifications.

Acknowledgement

Sincere thanks go to W. E. Daniels of Catalytic, Inc. and R. E. Perrussel of The Pittsburg & Midway Coal Mining Company, for their efforts in arranging for the respective samples.

Bibliography

1. Bogen, D. C. and S. J. Nagourney (1979) "Ion Chromatographic Analysis of Cations at Baseline Precipitation Stations". In: Ion Chromatographic Analysis of Environmental Pollutants, Vol. 2, ed. Mulik, J. D. and E. Sawich, Ann Arbor Sci., Ann Arbor, Michigan.

2. Dionex Corporation (1978) "Analytical Methods in Ion Chromatography".

3. Dionex Corporation (1978a) "Application Note #6".

4. Hoover, T. B. and G. D. Yager (1980), "Ion Chromatography of Anions", EPA-600/4-80-020.

5. Small, H., T. S. Stevens and W. C. Bauman (1975), Novel Ion Exchange Chromatographic Method Using Conductimetric Detection, Anal. Chem. 47, 1801.

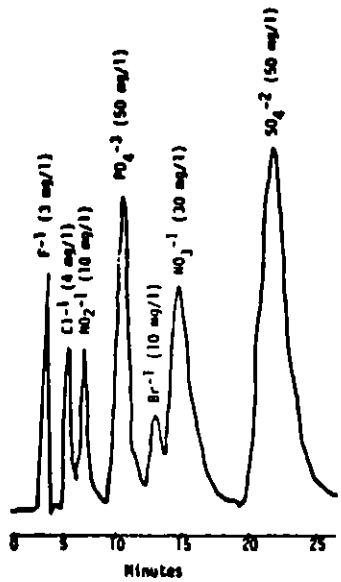

Figure 1: Strong Eluant Anion Standard

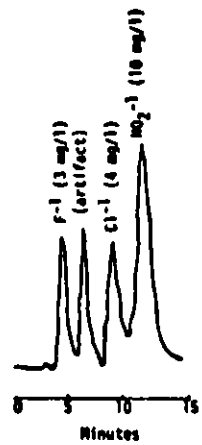

Figure 2: Weak Eluant Anion Standard

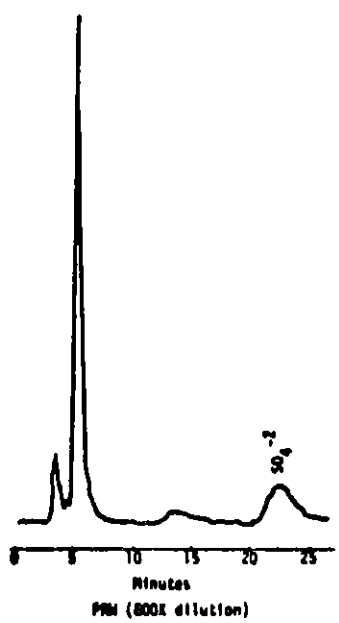

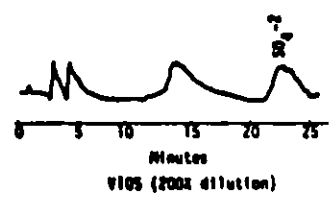

Figure 3: Strong Eluant Anion Runs

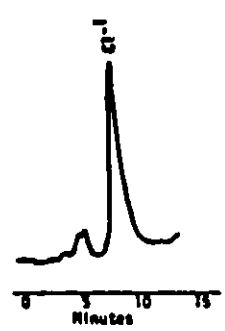

Figure 4: Weak Eluant Anion Runs

TABLE 1

QUANTITATIVE DATA[1]

	PRW (mg/l)	V105 (mg/l)
Anions		
Cl^{-1}	900	250
SO_4^{-2}	1000	900
Weak Anions		
Acetate	1700	700
Propionate	900	250
Cations		
Na^{+1}	*	*
NH_4^{+1}	20000	12400

*Not calculated due to interference

[1]Data represents the values for the samples in the chromatograms only

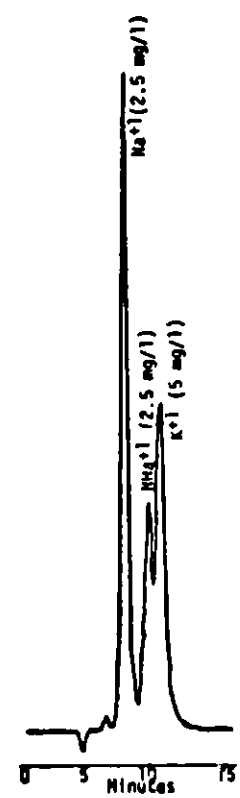

Figure 5: Standard Cations

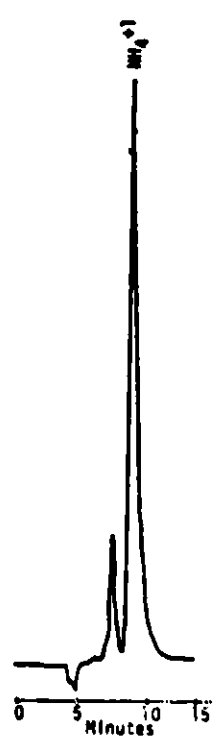

V105 (2000X dilution)

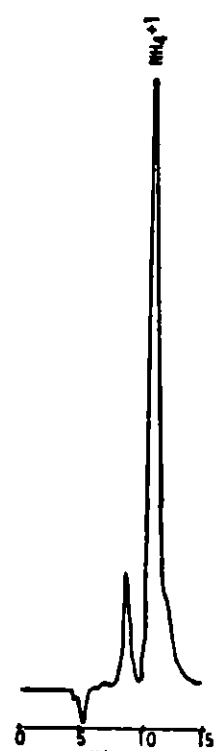

PRW (2000X dilution)

Figure 6: Cation Runs

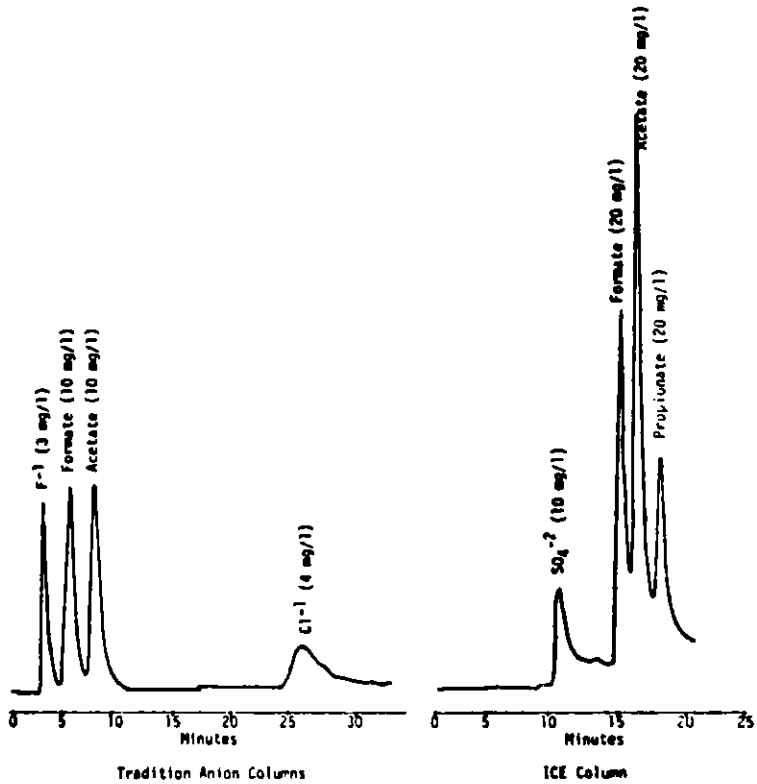

Figure 7: Weak Organic Acids

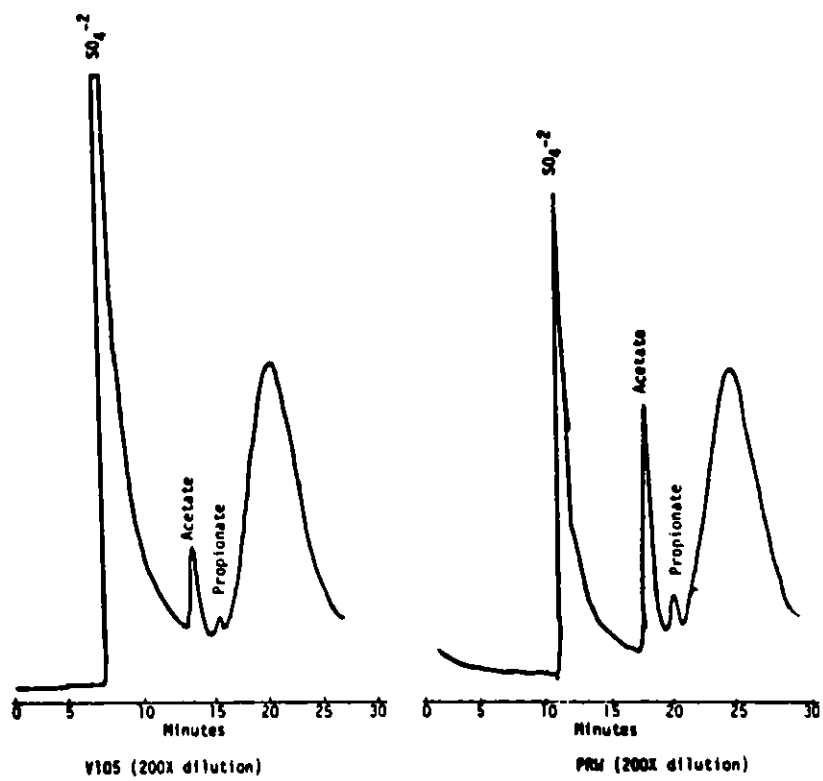

Figure 8: Weak Organic Acids Analysis with ICE Columns

H-COAL PILOT PLANT HIGH PRESSURE AND TEMPERATURE LETDOWN VALVE EXPERIENCE

N. D. Bond
Ashland Synthetic Fuels, Inc.
Ashland, Kentucky

The H-Coal Pilot Plant was designed to handle a maximum of 600 tons/day of coal and operate in three different coal liquefaction modes. Currently, the plant is running the syn-fuel mode which operates at a maximum of 225 tons/day of coal feed.

Plant System

The H-Coal Pilot Plant high pressure letdown train (Figure 1) consists of a two-stage letdown system. The coal slurry is piped from the reactor (K-201) @ 3000 psig and 850°F to a flash drum (Q-224) where reactor gases are separated out overhead. The slurry then moves to the first letdown valve LV-202 through a parallel piping train, designated as "A" and "B" trains. Each train is equipped with one letdown valve along with double block valves upstream and downstream of the letdown valve. Only one letdown valve is used at a time. The LV-202 valve drops the pressure from 3000 psig and 850°F to 1200 psig and 750°F. Next, this fluid enters a flash drum and the gases are separated out overhead. The coal slurry now flows through another parallel train to the second letdown valve called LV-204. Again, only one valve operates at one time, but this train has a double block valve system upstream only with a single block valve downstream. The LV-204 valve drops the pressure and temperature from 1200 psig and 750°F to 50 psig and 740°F.

After the second stage, the coal slurry enters a flash drum (Q-203) and is then ready for deashing and oil spearation.

LV-202 Valve versus LV-204 Valve

The LV-202 valve is designed for 3600 psig at 875°F. The inlet conditions of 850°F, 39,921 lbs. of liquid and 5,545 lbs. of solids are changed at the outlet to 750°F, 38,665 lbs. of liquid, 1256 lbs. of vapor and 5,545 lbs. of solids. The valve experiences more flashing than does the LV-204 valve, but under the extreme pressure the gas vapors occupy less volume. Generally, the valve can be sized fairly close by ISA CV equations with a correction factor of 10%.

The LV-204 valve is designed for 1400 psig at 875°F. The inlet conditions are 750°F, 47,634 lbs. of liquid, and 5,595 lbs. of solids. The outlet conditions are 47,082 lbs. of liquid, 552 lbs. of vapor, and 5,595 lbs. of solids. The LV-204 valve has less flashing than the LV-202 valve, but the flashing expands more causing a choke flow condition that would occur in gas service valves. This valve tends to be a cross between a gas and liquid flow and therefore sizing for the LV-204 valve must be done using the gas/liquid equations.

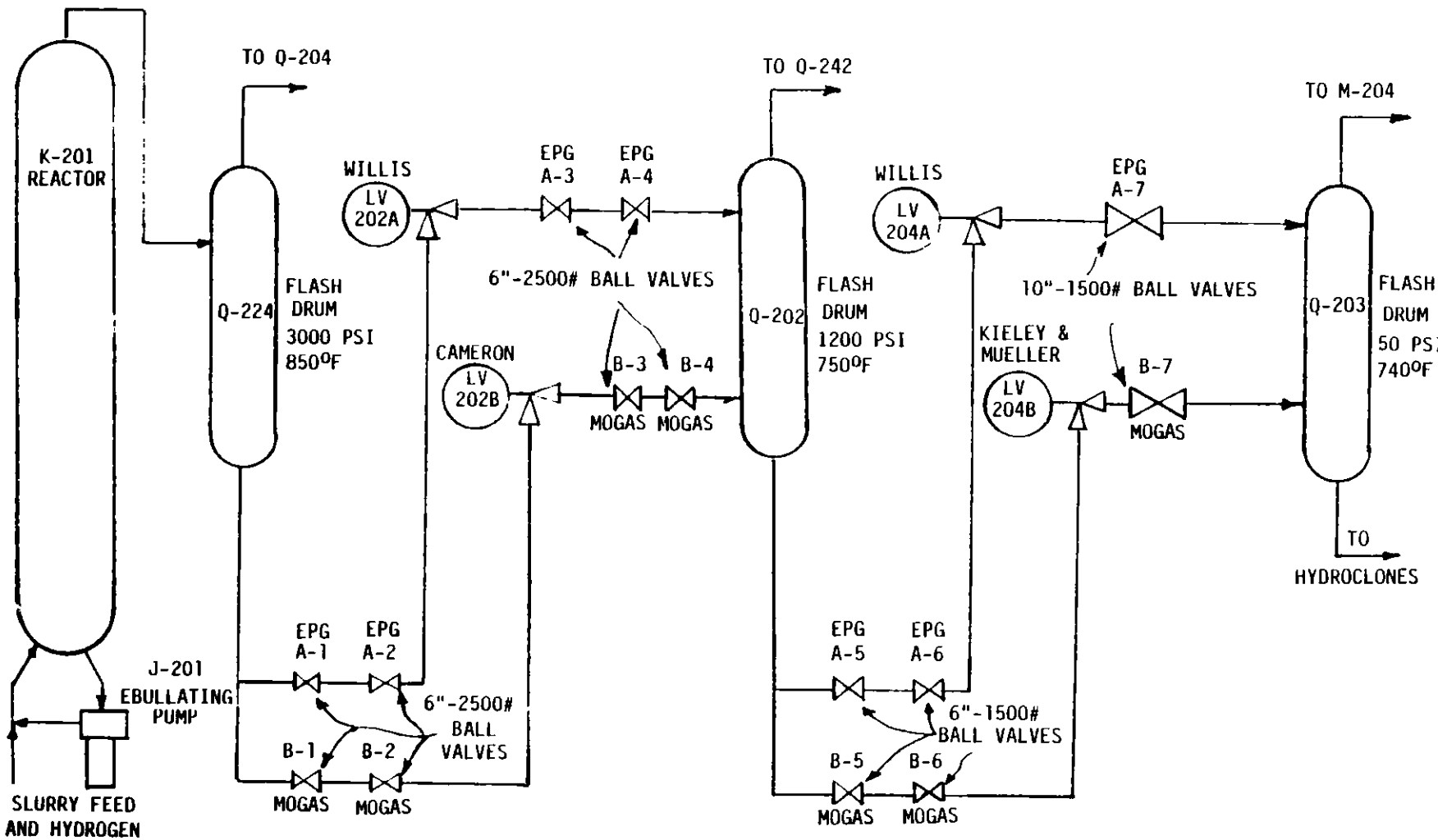

REACTOR AND LETDOWN SYSTEM

During normal operation, the LV-202 valve sees the more severe conditions of temperature and pressure drop, but also this valve operated in direct response to reactor conditions. If the reactor temperature or feed rates vary, the valve will have to adjust accordingly. The LV-204 sees more stable flow conditions after the gases are separated from the coal slurry for the second time. This valve does not vary much in level control as does the LV-202 valve, which helps reduce trim wear. Also the flashing under high pressure is lessened in the LV-204 case and reduces trim wear even though the solids content varies from 20-25% in the LV-204 valve versus 17-23% in the LV-202 valve.

The valves used in the H-Coal Pilot Plant for Coal Runs #1 through #5 were the Willis angle valves (see Figure 2). These valves used a rotating and stationary disc arrangement that had either one or two holes in them. The flow traveled through the body of the valve and was throttled by the rotating disc and stationary disc holes by the degree of alignment. A downstream fixed choke-orifice was installed with each valve to take a percentage of the pressure drop, which helped extend the valve trim life.

Coal Run #1

While circulating hot oil before Coal Run #1, five failures of the silver soldered tungsten carbide disc to the stainless steel holder occurred on the rotating disc of the Willis valve. These failures occurred in the LV-202 service which had the higher operating temperature of 850^{o}F. To eliminate this problem in the LV-202 valves, one solid 17-4PH SS heat treated rotating disc with one 1/2" diameter hole was installed in LV-202B and the other solid 17-4 PH SS rotating disc with two 3/8" diameter holes was installed into LV-202A. Each of these LV-202 valves had tungsten carbide silver soldered into stainless steel for the stationary discs and a 32/64" downstream choke made of tungsten carbide.

The LV-204 valves were each installed with two 1/2" diameter holed discs made of tungsten carbide silver soldered into a stainless steel holder for both rotating and stationary discs. The downstream orifice was a 40/32" hole size made of tungsten carbide.

In Coal Run #1, the LV-202B valve operated for 12 hours before level could not be maintained. Control was then switched to LV-202A which operated for three hours before level problems started. Since the LV-202B was not repaired yet, the coal run was aborted. To bring the plant down, level in the first flash drum, Q-224, was maintained by throttling the EPG block valves which severely eroded the block valve bodies.

When the LV-202B and LV-202A valves were examined, severe erosion of the 17-4 PH SS rotating disc was found to have caused the valve failure.

During Coal Run #1, 72.8 tons of coal passed through LV-202B and 18.2 tons through LV-202A. Only the LV-204B was used in the second letdown service and showed minor wear.

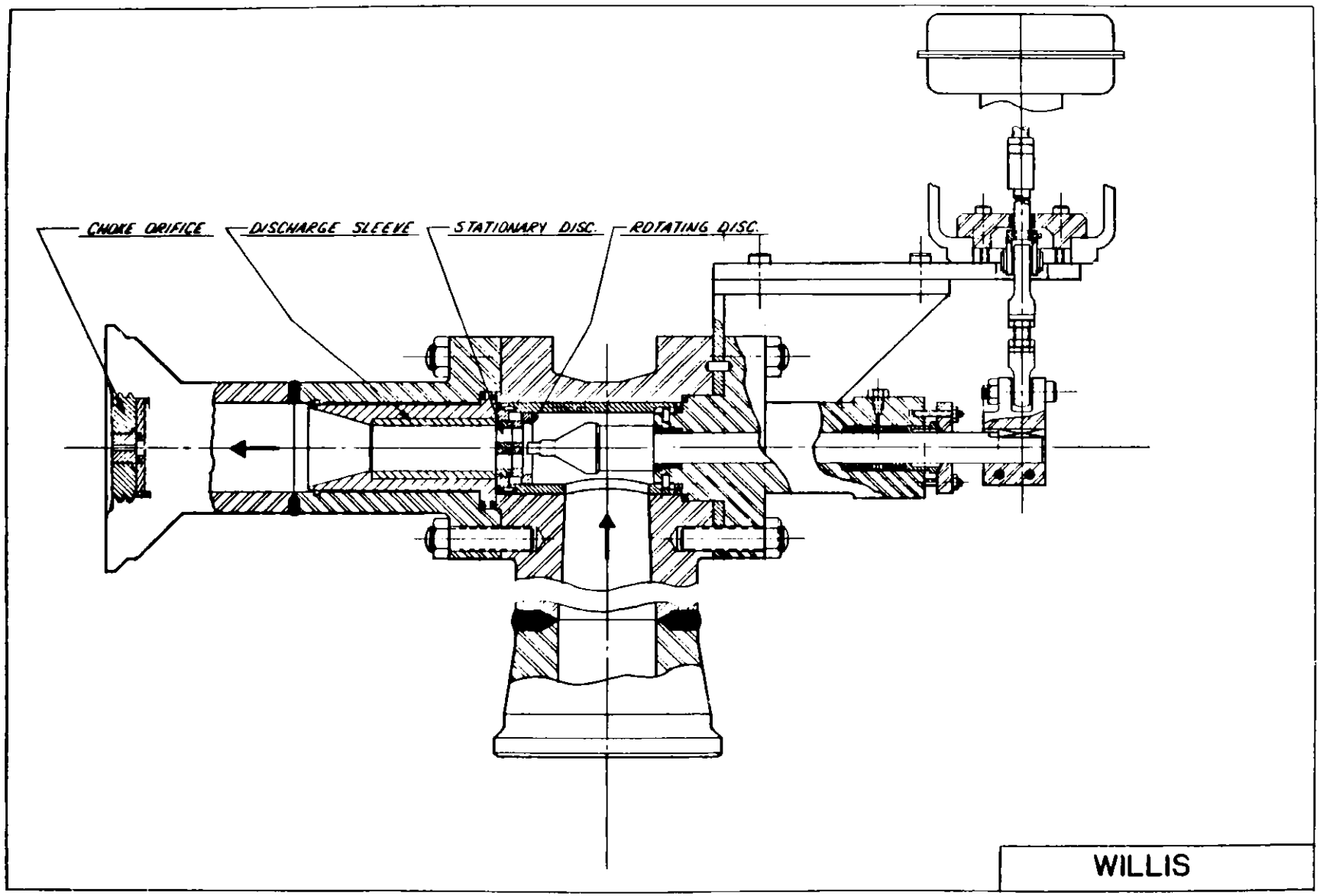
CHOKE ORIFICE
DISCHARGE SLEEVE
STATIONARY DISC.
ROTATING DISC.
WILLIS

WILLIS VALVE DEVELOPMENT COAL RUN #1 - #5

	LV-202 Service				LV-204 Service			
Coal Run	Hours of Coal	Tons of Coal	Tons Coal Hour	Valve Condition	Hrs. of Coal	Tons of Coal	Tons Coal Hour	Valve Condition
0	0	0	0	Five failures of silver soldered WC piece on rotating disc during hot oil Circulation	0	0	0	No Problems Experienced
1	12	72.8	6.07	Solid 17-4 PH-SS Heat treated rotating disc with one ⅛" hole severely eroded	15	91	6.07	Minor wear to trim only
2	9	51	5.67	Mechanical held WC piece work for rotating disc	9	51	5.67	Silver soldered rotatg. disc failed after Run 3
3	108	470.12	4.35	Mechanical holder held up well; WC trim severely eroded	119	518	4.35	Shrink-fitted WC disc work for rotating disc. New 25/64" orifice kept valve opened 40-60%
3	11	47.88	4.35	Shrink-fitted WC piece worked well for rotating disc, but trim severely eroded.				
4	8	17	2.13	Solid K-701 WC rotating disc was cracked through the disc	8	17	2.13	New TMT-5 stationary disc showed no wear
5	96.5	465.13	4.82	Silver solder failed on stationary disc; stellite orifice severely eroded; TMT-5 coat stationary disc worn less than rotating disc	118	568.76	4.82	TMT-5 coated rotating & stationary discs showed little wear. 25/64" stellite orifice showed little wear & kept vlv. open 40-80%
5	70	337.4	4.82	TMT-5 coated trim worn the stationary lock seal ring holder worked well but SS integral choke showed gas erosion in top hole & solids erosion in bottom hole	70	337.4	4.82	Minor wear to TMT-5 coated trim;orifice had no wear & kept val.open 40-80%;wear to SS integral choke in stationary lock seal rng.hold.worn like LV-202 valve.

Coal Run #2

Before Coal Run #2 was started the LV-202A had a rotating disc made of tungsten carbide shrink-fitted into a stainless steel holder and the LV-202B had a tungsten carbide disc held in a stainless steel mechanical holder installed into LV-202B. The LV-204 valves remained the same as was used in Coal Run #1. The downstream choke-orifices were 32/64" for LV-202 and 40/32" for LV-204.

During Coal Run #2, a total of 51 tons of coal were throttled by LV-202 and LV-204 valves.

The LV-202B and LV-204B valves were used during the run. The mechanical holder used in LV-202B held up well with minor wear due to the tungsten carbide. The LV-204B also had minor wear, but the silver soldered rotating disc was replaced with a shrink-fitted tungsten carbide rotating disc and silver soldered stationary disc with two 3/8" disc holes. Also, the choke orifice was changed to a 25/64" diameter hole made of 17-4 PH SS.

Coal Run #3

The LV-202A valve used a shrink-fitted tungsten carbide rotating disc and a tungsten carbide silver soldered stationary disc with two 3/8" diameter holes each. The LV-202B used a tungsten carbide disc held in a mechanical collar with one 1/2" for the rotating disc and a silver soldered tungsten carbide disc with two 1/2" diameter holes for the stationary disc. Both valves used a downstream orifice of 32/64" diameter size.

The LV-204A used a silver soldered rotating and stationary disc with two 1/2" diameter holes and a 40/32" choke orifice. The LV-204B used a shrink-fitted tungsten carbide disc for the rotating disc and a silver soldered tungsten carbide disc for the stationary disc with each disc having two 3/8" diameter holes. The downstream choke orifice was a 25/64" size made of 17-4 PH SS.

During Coal Run #3, a total of 518 tons of coal was throttled by the LV-202 and LV-204 valves.

The LV-202B was started up on and lasted 108 hours and throttled 470.12 tons of coal before severe erosion of the two discs caused level control problems.

The LV-202A was used for eleven hours and passed 47.88 tons of coal. It also showed severe wear. Both of these valves operated at 10-20% opened at all times during the run.

The LV-204B was the only valve used in the second stage of letdown during the run. The trim was eroded, but not as severe as the LV-202 valves. The 25/64" orifice made of 17-4 PH SS grew to a 27/64" hole size in the inlet, but eroded to a cone shape exiting the 3/4" thick orifice. This trim/choke arrangement allowed the valve to stay open 40-60%.

The results of the LV-204B valve indicated a need for a 20/64" orifice for LV-202 and a 25/64" orifice for LV-204 to allow the trim life to be extended.

Coal Run #4

During Coal Run #4, a total of 17 tons were processed. Only two valves, LV-202B and LV-204B, were used.

The LV-202B used a solid K-701 tungsten carbide rotating disc and a K-701 tungsten carbide disc silver soldered into a SS holder for the stationary disc. Each had two 3/8" holes. The choke orifice was a 20/64" made of stellite overlay. When the valve was examined, only minor surface wear was found on both discs, after 8 hours of coal service, but the rotating disc had a crack running through it and had to be scraped.

The LV-204B valve used a tungsten carbide disc with two 5/16" holes that were brazed and mechanically held in a SS holder. The stationary disc used a tungsten carbide disc coated with TMT-5* with two 3/8" holes silver soldered into a SS holder. The orifice was a 25/64" made of stellite overlay. The valve showed no wear on the stationary disc and polished wear on the rotating disc, also, after 8 hours of coal service.

Coal Run #5

During Coal Run #5, 1173 tons of coal were throttled by the LV-202 and LV-204 valves. During the run, the letdown valves were removed by pulling the coal feed and flushing the entire system with oil so that the EPG block valves would not be cycled on coal slurry which extended their life.

The following describes the LV-202 and 204 Willis Valve trims that were installed and run on coal slurry during coal run #5. The parts described will be the rotating disc, stationary disc, discharge cone, orifice, and the orifice discharge cone. (See Figure 4)

The LV-204B was removed from service after it could not maintain level control. The following describes the trim components:

The rotating disc had been in coal slurry service for 35.5 hours during Run #5, but a total of 435 hours were logged when earlier runs were included. The holder was a brazed and lock rung design that used a tungsten carbide disc with two 5/16" for trim material. Slight wear was observed only.

The stationary disc had the same coal slurry time as the rotating disc. The disc was made of tungsten carbide coated with TMT-5 and was silver soldered into a 316 SS holder. When this holder was removed, the tungsten carbide disc had rotated about 45^{0} and then locked itself into the holder. This was the first silver solder failure to occur to the stationary disc. This failure caused the holes to align incorrectly. Only slight wear was observed to the face of the disc. The downstream sleeves of the stationary disc, made of VC-19 tungsten carbide and coated with TMT-5, showed no apparent wear.

---

* TMT-5 - Proprietary packed difussed coating applied by Turbine Metal Technology located in Burbank, California.

The orifice was originally a 25/64" size and grew only an .001". This orifice was made of 17-4 PH SS with stellite weld overlay for hard facing and was used in coal slurry service for 35.5 hours.

The discharge cone downstream of the orifice was made of 17-4 PH SS with stellite weld overlay. This piece was used in coal slurry service for 35.5 hours. The original hole size was 25/64" and this was enlarged to about 52/64". The stellite welds were cracked from welding before the coal run and these welds separated through the 25/64" hole region only. The cone region showed no wear at all and the weld flash was still intact.

This valve was replaced with a lock ring rotating disc assembly and a silver soldered stationary disc. Both pieces had tungsten carbide coated with TMT-5.

Valve LV-202A was pulled after 96.5 hours of coal slurry service when it could not control level. This valve had identical trim to the LV-204B described above.

The rotating disc was a brazed lock ring design and used tungsten carbide for the disc material. This disc had severe erosion across both 5/16" holes. The grooves and pits were as deep as 1/8".

The stationary disc used a tungsten carbide disc coated with TMT-5 and was silver soldered into a 316 SS holder. The disc had rotated about 45^{o} when the silver solder failed. The disc itself had grooves that were 1/8" deep at the two 3/8" holes and tappered smoothly to the surface of the disc. There was no erosion across the face of the disc as had occurred on the rotating disc. The disc looked like it could have still been in operation had the braze not failed.

The discharge cone downstream of the stationary disc showed no apparent wear. This cone was made of 17-4 PH SS with a stellite weld overlay.

The orifice was originally a 20/64" hole size. This grew at about a 9/16" diameter. The backside was eroded irregularly. The orifice was made of 17-4 PH SS with a stellite weld overlay. The discharge cone downstream of the orifice could not be pulled.

This trim set clearly showed that the TMT-5 coating limited the erosion of the tungsten carbide disc. The silver solder failure was probably aggravated when an actuator controller problem allowed the trim to be opened/closed rapidly for about one minute. The trim was replaced with a lock ring rotating disc and a silver soldered stationary disc. A new lock-seal ring stationary disc was designed shortly after these two braze failures.

Valves LV-202B and LV-204B were pulled to change out the silver soldered stationary discs and replace them with the new lock seal ring style. These two valves were still in operating condition when removed. Below is a description of the two trim sets:

The LV-202B was pulled after 77 hours of coal slurry service. Most of this time, the trim was throttled in the 10-20% range. The rotating and stationary discs were tungsten carbide coated with Ti-Diborde and TMT-5. The rotating disc was worn very little. Two small grooves propagated from each hole of the disc which were about 1/16" deep.

The stationary disc had little surface wear, but inside the holes irregular erosion had occurred increasing the diameter from 3/8" to about 1/2". The silver solder had not shown any movement.

The downstream discharge cone made of 17-4 PH SS with stellite weld overlay showed no wear. The 25/64" diameter orifice was worn to about 9/16" and the downstream side showed considerable wear. This orifice was made of 17-4 PH SS with a stellite weld overlay. The discharge cone downstream of the orifice had severe erosion, 3/4" into the throat area, that had grown to about 1¼". The stellite was gone in this section, but further downstream little wear occurred.

The LV-204B was pulled after 118 hours of coal slurry service even though it was operating satisfactorily. Much of the valve's time was logged while throttling with 40-80% range. The rotating and stationary discs were tungsten carbide coated with TMT-5.

The rotating disc showed no appreciable wear! The stationary disc had some minor wear that propagated from the holes in a tappering fashion with the wear being about 1/8" deep at the disc holes.

The discharge cone downstream of the stationary disc was made of 17-4 PH SS coated with stellite weld overlay. No apparent wear could be detected.

The orifice was originally a 25/64" size and had grown to about 26/64". This was made of 17-4 PH SS with stellite weld overlay. The discharge cone downstream of the orifice made of 17-4 PH SS with a stellite weld overlay showed severe wear only about 3/4" inside the hole. The cone section showed little wear.

A construction flaw in the new lock-seal ring stationary disc holder was discovered in the LV-202B. This problem caused damage to the holder and to the valve body. The flaw was corrected in the spare valve, and this valve was reinstalled into LV-202B. Two other valves, the LV-202A and LV-204B had similar problems, but no damage occurred. These valves were then reinstalled with revised trim.

When the LV-202A was being inspected, minor wear had occurred on the molybedum disc coated with TMT-5 after running for a day on oil with 2-3% solids. This trim was replaced with tungsten carbide coated with TMT-5. Further testing of molybedum or metal-coated discs will be abondoned for the present. This poor showing of the molybedum coated disc was probably caused by the rapid thermal expansion of the metal versus the coating which allowed gaps that were attached by the solids. The wear on the disc was minor, but when compared to a tungsten carbide coated disc during the same time period, it was inferior.

After the plant was shut down the LV-202B and LV-204B were pulled for inspection after each had gone 70 hours on coal slurry.

The LV-202B used locking ring holders for both rotating and stationary discs. Both tungsten carbide discs were coated with TMT-5. The new lock-seal ring stationary disc had a small choke made of 17-4 PH SS immediately downstream of the two 3/8" holes of the tungsten carbide disc. The rotating disc showed signs that the valve spent most of the time throttled in the 10-20% range which allowed the discs' holes to be barely cracked opened, if any at all. The wear was about 1/8" deep in some areas with small grooves propagating from the holes of the disc.

The stationary disc was installed with the two holes aligned top and bottom in the horizontal plane of the valve. The bottom hole in the tungsten carbide disc was worn considerably more than the top hole. Looking down the 17-4 PH SS choke attached to the discharge of the tungsten carbide disc, the bottom hole was worn in a cone shape flowing away from the entrance and the top hole had a wear pattern much like the shape of a venna-contrata. The top hole tappered back to about a 3/8" hole size downstream before exiting the choke.

This separate wear pattern in this holder looks as though stratification of the coal slurry had occurred before the fluid enters the train of the Willis valve. Gases primarily flowed through the top hole and coal slurry through the bottom. The metal-c ring seal between the tungsten carbide disc and the holder was eroded severely, but no leakage occurred because the coal slurry had sealed the disc.

The orifice was originally a 22/64" size with stellite weld overlay for hardfacing. This was enlarged to about 9/16" in diameter. The discharge side of the orifice was rough and jagged with wear being irregular.

The discharge cone downstream of the orifice was made of 17-4 PH SS with stellite weld overlay for hardfacing. The entrance hole was originally 48/64" size and was enlarged to about 1". The stellite was worn away to about a depth downstream of 3/4" into the cone. The remainder cone section was worn slightly with the stellite coating still being intact. This valve, again, was severely throttled because of the orifice being enlarged. The valve was still in an operational condition.

The LV-204B was pulled after 70 hours of coal slurry service. The materials of construction for the trim were identical to the LV-202B just described.

The rotating disc showed little wear other than polishing of the surface.

The stationary disc showed signs of separate wear for each hole. The top hole was worn less than the bottom hole, and the downstream 17-4 PH SS choke showed a similar wear pattern as in the LV-202B valve but less severe. Again, stratification of the coal slurry was occurring before the Willis valve causing irregular wear patterns to erode the tungsten carbide discs.

The discharge sleeve downstream of the stationary disc made of VC-#134 tungsten carbide showed no apparent wear.

The orifice was originally a 25/64" hole size and was measured 25/64" after removal. Stellite weld overlay was used to hardface the orifice.

The discharge cone downstream of the orifice made of 17-4 PH SS with stellite weld overlay showed little wear.

Again, these two valves were in severe service, with much of the time being logged when being throttled in the 10-20% range. The orifice sizing for the LV-204 seems to point to a 25/64" diameter hole. The LV-202 is still in question with a 22/64" diameter hole size being tried currently. In each case, the orifice will take about 70% of the pressure drop once plant operating conditions are reached.

Out of the six valves that were used in coal slurry service, four of these valves were pulled before the trim had been run to extinction. The overall average run time for these six valves was 80 hours. This was about four times better than was averaged before.

The LV-202 valves in each case lost their orifice shortly after being put on coal slurry, so there was little difference in trim material as compared to previous runs. The TMT-5 coating alone can account for the improved run time of these valves.

The LV-204 trim appears to have less severe service than the LV-202 trim. In each case the trim looked like it could have run close to, if not more than, 200 hours.

To correct the problems of the LV-202 orifices, tungsten carbide coated with TMT-5 orifices will be used in both LV-202 and 204 valves. At this time, tungsten carbide coated with TMT-5 is the best combination to use in the Willis valves.

The lock seal ring stationary holder used successfully towards the end of the coal run was modified for Coal Run #6 by shrink-fitting tungsten carbide sleeves coated with TMT-5 into the integral choke downstream of the stationary disc.

Coal Run #6

Coal Run #6 used Illinois #6 coal. The plant processed 8,207.81 tons of coal in 1092 hours. The following report describes the valves that were used in LV-202 and 204 letdown valve service.

Before the #6 coal run began two new letdown valves were installed into the "B" train system along with the new Mogas block valves. (Figure 5) These new valves were the Cameron installed into LV-202B and the Kieley and Mueller installed into LV-204B. The "A" train remained the same as was used during coal run #5 with the Willis being used for letdown valve service and the EPGs for block valve service. This was advantageous for two reasons:

(1) The Willis could double as a block valve which meant the EPG valves would be left open reducing the chance of wear while opening under coal slurry service.

(2) The Willis valves could be brought into service very quickly with minimal chance of thermal shocking the the carbide trim, since only small pieces of tungsten carbide held in mechanical holders were used.

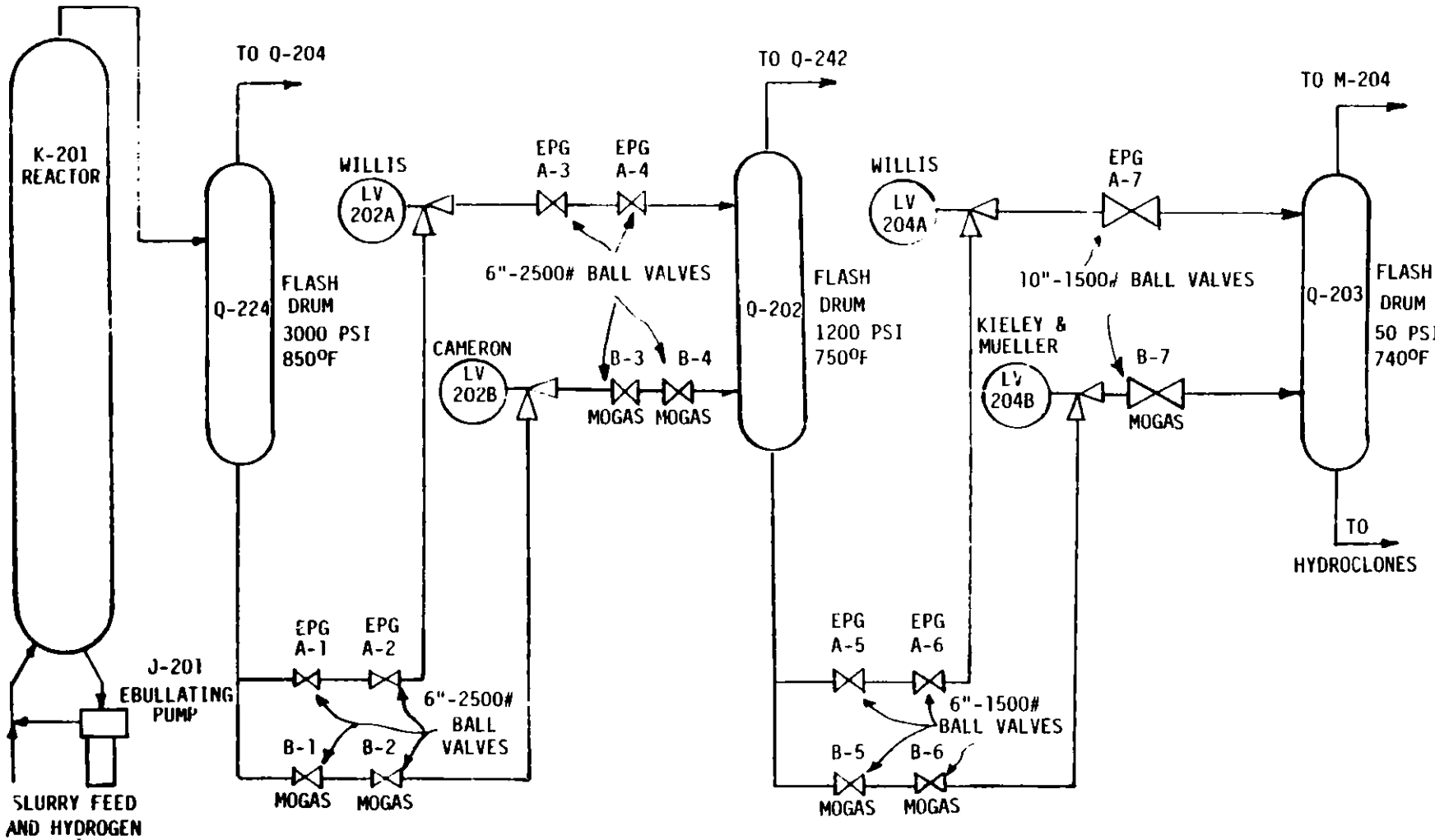

REACTOR AND LETDOWN SYSTEM
COAL RUN NO. 6

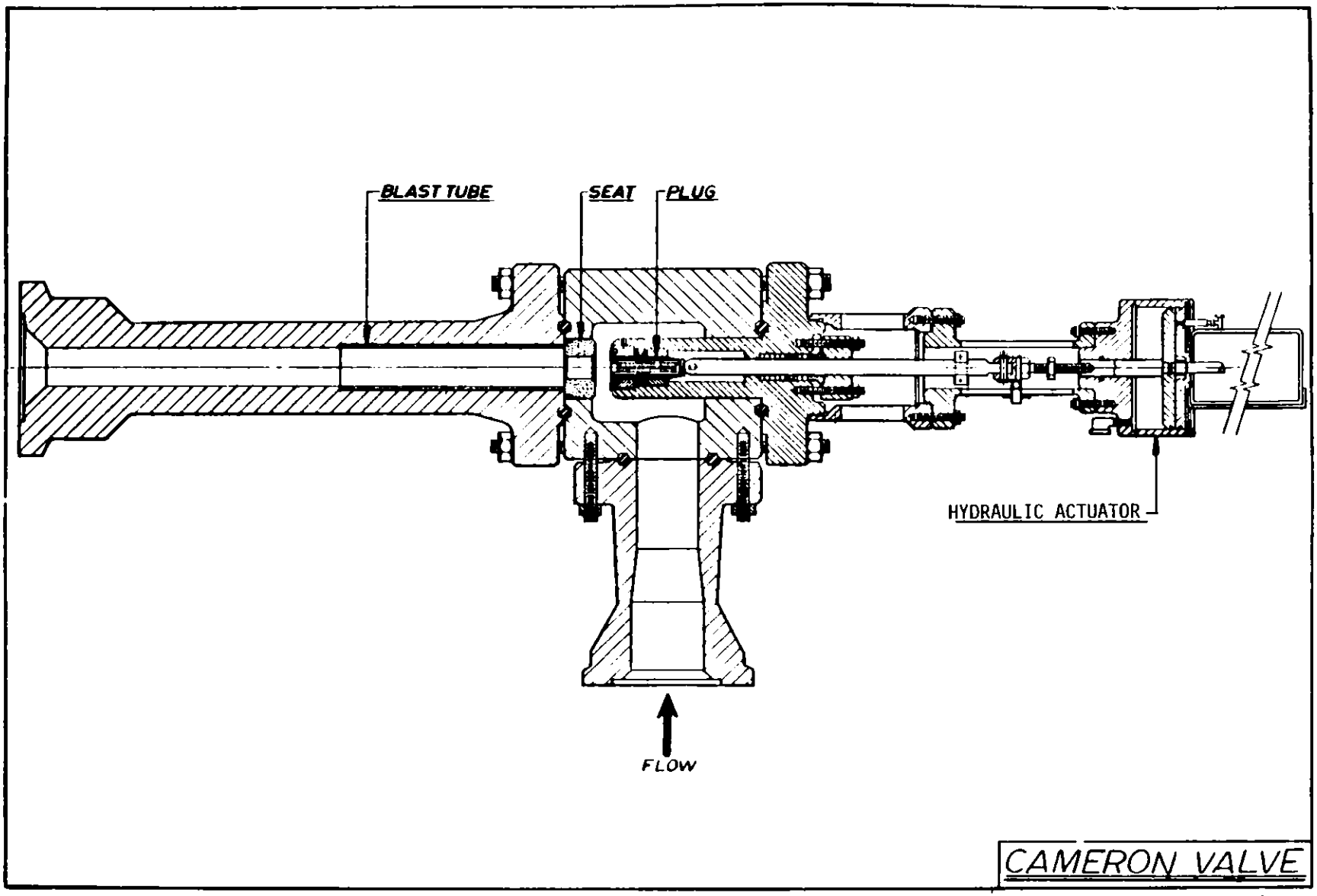
BLAST TUBE
SEAT
PLUG
HYDRAULIC ACTUATOR
FLOW
CAMERON VALVE

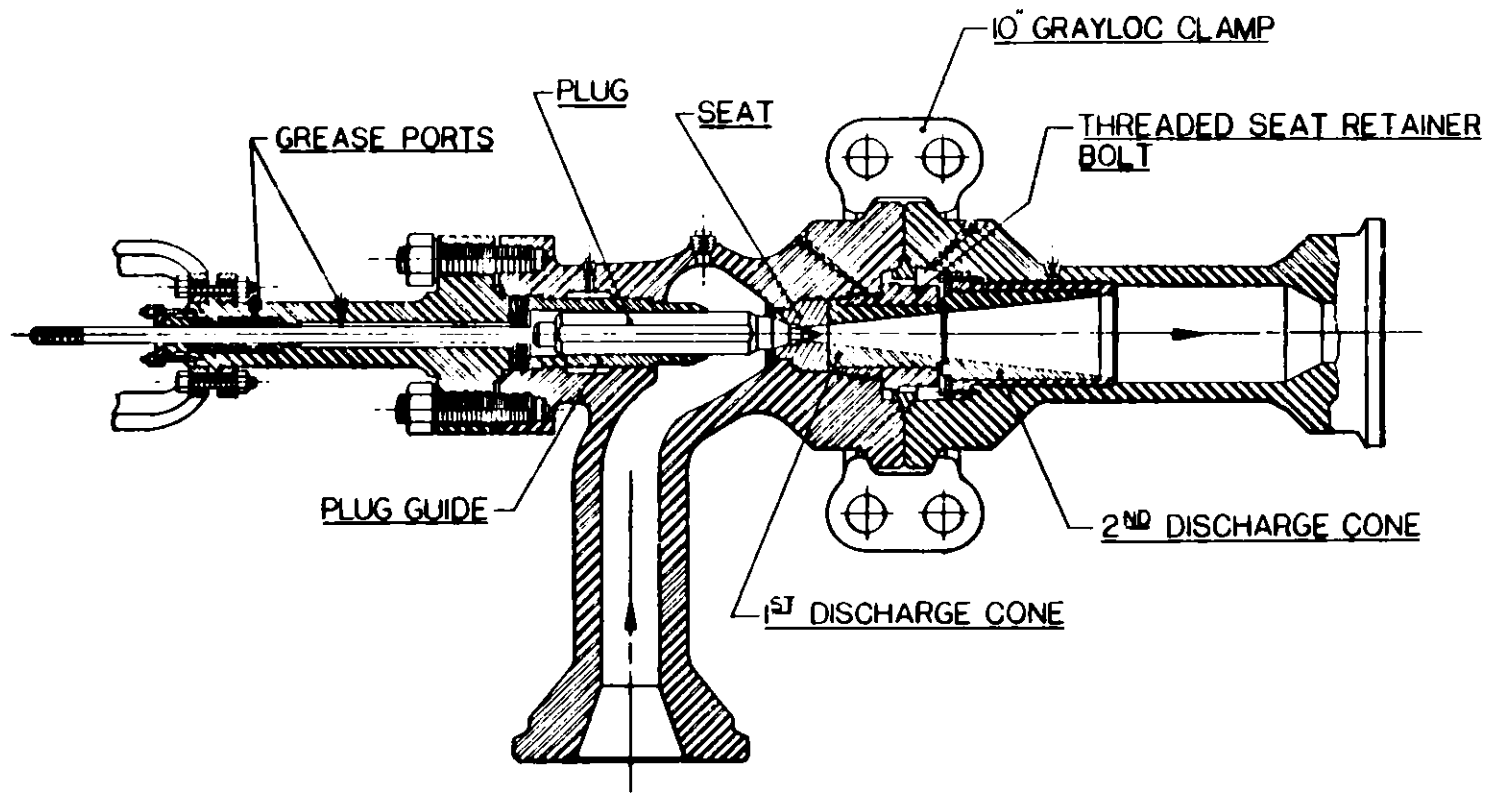

KIELEY - MUELLER

667

COAL RUN #6 VALVE DATA

Valve	LV-202 Service				LV-204 Service			
	Hours of Service	Tons of Coal	Tons Coal Hr.	Reason to pull valve out of service	Hours of Service	Tons of Coal	Tons Coal Hr.	Reason to pull valve Out of service
Willis	94.41	746.8	6.61	trim failure; choke O.K.	187.58	1283.9	6.84	Valve pulled to change trim; trim worn but in operating condition
	23.25	217.7	9.36	Valve body leaks, trim worn slightly				
Cameron	387.5	2772.7	7.16	Valve plugged; trim worn but still in operating condition	0	0	0	Trim Broke on start up
	199.92	1634.8	8.18	Valve trim badly worn				
Kieley &Mueller	216.17	1599.5	7.38	Valve was plugged; shrink fit holder cracked; trim slightly worn	554	4042.2	7.3	Valve shows no wear; choke retainer damaged
					340.4	2881.7	8.47	Valve shows no wear; choke retainer damaged valve pulled after shutdown
	8.5	67.5	7.94	Trim broken;valve trim was same as used during 554 HR LV-204 Run				
	161.25	1323.1	8.21	Plug tip broken, plug & tip worn but in good shape, valve pulled after shutdown choke retainer damaged				

Also, at this time, all the LV-202 and 204 valves were installed with a fixed downstream orifice made of tungsten carbide coated with TMT-5. This was done primarily to give operations time to make a valve switch should an actuator fail open causing the upstream flash drum to overpressure the downstream flash drum. Also, the downstream orifice would take a percentage of the pressure drop which would extend trim life in the valve.

The Cameron valve installed before Coal Run #6 into LV-202B was supplied to the H-Coal plant free for testing purposes by Cameron Iron Works located in Houston, Texas. (Figure 6) Along with the valve, Cameron brought an engineering staff on site to iron out any start-up problems with the valve. This valve was the smallest version designed and built of Cameron's oil choke letdown valve line. The trim used was a 1" balanced ported plug and seat made of GE-883 tungsten carbide and coated with TMT-5. The fluid passed through the body with throttling occurring at the plug and seat. The actuation of the valve was done by a hydraulic actuator and control system also supplied by Cameron. The downstream orifice used was a 22/64" hole.

The Kieley and Mueller valve installed into LV-204B was a larger version of a similar valve Exxon had been using successfully in their Baytown, Texas, coal liquefaction plant. (Figure 7) This valve was also a plug and seat design, but the fluid flowed through a sweep-flow body before being throttled by the trim. The plug, seat, and first discharge cone were made of shrink-fitted K-701 tungsten carbide. The plug guide and the second discharge cone were made of stellite #6. Grease ports were also added to help maintain the valve during operation and for disassembly, but these could not be utilized because isolation valves for the grease plugs had not been received at that time. The seat retainer bolt was gold-plated to reduce galling of the threaded portion during assembly and disassembly. A downstream orifice size of 25/64" was installed before Coal Run #6 began.

The LV-202A Willis valve was installed with the improved version of the trim used towards the end of Coal Run #5. A 22/64" orifice was fitted into the tail pipe before the start-up.

The LV-204A Willis valve used the same trim as LV-202A, but used a 25/64" orifice installed in a transition spool piece between the letdown valve and the block valve.

During the start-up of the coal run, the Cameron valve operated smoothly as did the Kieley and Mueller.

After 387.5 hours and 2772.7 tons of coal processed, the orifice in the Cameron valve became plugged and had to be removed from service. Operation was switched to the LV-202A Willis valve until the Cameron was replaced by the second Kieley and Mueller valve. The new Kieley and Mueller valve was put into LV-202B service as soon as possible with the Willis being returned to standby service. The Cameron was disassembled and was found to have worn 3/16" back on the plug and 1/8" deep in the seat area. The 22/64" orifice was worn only a few mils. A new 1" trim was installed, but design of a 3/4" solid trim was started by Cameron engineers.

After 554 hours and 4042.2 tons of coal were processed, the orifice retainer made of SS eroded out because of a gasket failure. The valve was pulled to examine this problem. Severe damage to the Grayloc hub of the valve discharge pipe and seal ring had occurred because of this, but no leakage occurred. The valve trim indicated no noticeable wear and was retained for future service. A Willis valve was temporarily installed into LV-204B until the Kieley and Mueller could be rebuilt.

The LV-202B Kieley and Mueller appeared to be plugged and was replaced by the original Kieley and Mueller valve that had run in LV-204B service. The second Kieley and Mueller valve lasted 8.5 hours before it plugged. During the interruption, the LV-202A Willis valve was used until the Cameron valve was put into LV-202B service.

The Kieley and Mueller valve was pulled from service and had a new tail piece installed with a different orifice design hours before the pluggage occurred because it had the same choke design that failed on the LV-204 Kieley and Mueller. Fortunately, no damage resulted, but the change allowed the coal slurry to build up a residual material in the upstream piping. When the LV-202B Kieley and Mueller valve was put back into service, this material immediately plugged the first Kieley and Mueller valve and later broke the plug of the second Kieley and Mueller valve installed into LV-202B service.

The first LV-202B Kieley and Mueller valve had 3/32" worn from the radius of the plug and very little from the seat. The 15-5 PH SS holder, for the shrink-fitted K-701 piece, was found cracked. These cracks were thought to be caused by either stress risers from a vibrational shock of the trim or by thermal shock. A mechanical plug holder called the "Tampa" plug was modified to fit the Kieley and Mueller valve after observing this.

The second LV-202B Kieley and Mueller valve showed no additional wear to the trim as observed when it was removed from LV-204B service. Both valves orifices showed no apparent wear.

After 94.91 hours and 746.21 tons of coal being throttled, the LV-202A Willis valve was pulled out of service.

The valve had been used off and on for three times with the valve taking 600 - 800 psig pressure drop and the choke 1000 - 1200 psig pressure drop. The valve was opened as much as 65%, but towards the end, it was opened between 10 and 20%.

When the valve was disassembled, severe erosion to both the rotating and stationary discs had occurred. The downstream orifice showed wear of one mil only and was retained for further service. The valve was rebuilt with more trim and used for an LV-202A spare.

The LV-204A Willis valve was pulled for examination after 187.58 hours and 1283.9 tons of coal being throttled. The valve was opened from 70 - 90% with the valve taking 150 psig pressure drop and the orifice 1000 psig pressure drop.

The trim was worn, but was in good shape and could have operated longer. The orifice showed no wear, but was too restrictive and was bored out to a 27/64" size. New trim was installed in the valve and used for an LV-204A spare.

After 199.92 hours on coal and 1634.82 tons were processed, the LV-202B Cameron valve failed to control level. The valve was pulled and disassembled for examination. The plug was severely worn and lost about 3/4" off the tip. The seat was worn 1/8" deep in a ring shape about a 1/4" inside the inlet of the seat. The orifice was worn about 2 mils.

The valve started off about 45% opened, but process conditions were changed that caused the valve to be throttled about 10% opened for the last 50 hours of valve operation. This position of the trim caused rapid deterioration of the plug and seat. The valve was refitted with the new 3/4" trim for Coal Run #7.

The LV-202A Willis valve was pulled after 23.25 hours of service and 217.66 tons of coal, because of a bad bonnet flange leak. The valve trim took 1200 psig pressure drop and the orifice 600 psig. The valve never opened more than 30% and averaged 10-20% opened.

The rotating and stationary disc showed minor wear only during this operation. This was the first use of TMT-745 in a Willis valve and it wore considerably less than a TMT-5 trim with similar hours. The valve was rebuilt for Coal Run #7.

After the end of Coal Run #6 of the LV-202B and LV-204B Kieley and Mueller valves were pulled for examination.

The LV-202B valve had operated 181.25 hours with 1323.1 tons of coal being processed. The valve was operated about 35% open and took 900 psi pressure drop with the orifice taking 900 psi. The 5/8" trim featured the "Tampa" plug design. This plug holder held up excellently, but the carbide plug tip had been thermal shocked off causing irregular erosion of the plug and seat. Both plug and seat could have operated much longer with the tip broken, but less wear would have occurred under normal circumstances. The orifice showed no wear; however, the retaining system was starting to erode because of a metal to metal seal failure.

The LV-204B valve had operated 340-342 hours on 2881.71 tons of coal before being disassembled. The valve had operated about 60% opened with the valve taking 550 psi pressure drop and the choke 600 psi.

The trim made of K-701 shrink-fitted into 15-5 SS holders was in excellent shape with little wear. The orifice also showed little wear, but the seal system had failed on the SS retainer which eroded the Grayloc hub and seal ring to a point where leakage could have occurred.

Both valves were repaired and rebuilt for Coal Run #7.

The new Cameron and Kieley and Mueller valves made Coal Run #6 possible for the letdown service, but none of these two valves could have been pulled without successful operation of the Mogas block valves. These block valves were cycled as much as 14 times under coal slurry conditions without slurry leakage.

The Willis valves used in LV-202 and 204 service both set records for Willis valves, but their trim life was a matter of hours compared to the days life of the Cameron and Kieley and Mueller valves. The Willis still will be used for backup service for Coal Run #7 because they can take thermal shock without failure and can be used as a block valve with quick open service.

As shown in Coal Run #5, the TMT coatings again helped reduce erosion on the tungsten carbide parts. The new TMT-745 (tungsten T_1 - B_2) far exceeded the previous TMT-5 coating and will be standardized in Coal Run #7.

The orifices made of tungsten carbide and TMT-5 were very effective with little or no wear being done in either LV-202 or 204 cases. The 25/64" hole sizing for the LV-202 valve allowed a 50% pressure drop with good valve control characteristics. The 27/64" size of the LV-204 valve appeared to be still too restrictive and will have to be resized in Coal Run #7.

Six valves were used in LV-202 with the Cameron setting the record of longest time and coal tonnage of 387.5 hours and 2772.7 tons.

Three valves were used in LV-204B with the Kieley and Mueller valves setting the longest overall time and coal tonnage of 554 hours and 4092.2 tons. Both valves averaged about 17-25% solids which equates to about 50 tons/day of solids at maximum conditions.

The LV-202 valve sizing of 1" for the Cameron or 5/8" for the Kieley and Mueller as used in Coal Run #6 was too large and will be reduced to 1/2" diameter in the Kieley and Mueller valve for Coal Run #7. LV-204B valve sizing of 5/8" diameter trim for the Kieley and Mueller valve appears to work very well and will be retained. The new Cameron trim of 3/4" diameter will be tried in LV-204 service for Coal Run #7.

CONCLUSION

To summarize the progress of the LV-202 and LV-204 valves, the Willis was developed to last about 100 hours, which is the expected life for this valve design in our coal liquefaction process, whereas the Cameron and Kieley and Mueller valves have lasted for days with good results. The Cameron and Kieley and Mueller valves still have not reached their full potential in plant operation and, along with the new Masoneilan, Paul and Hammel Dahl valves, future progress in the high pressure and temperature letdown valves is anticipated.

The people of the H-Coal Pilot Plant would like to thank the valve manufacturers for their extra efforts in providing us with technical support and, of course, these valves for our LV-202 and LV-204 service.

H-COAL PILOT PLANT LV-202 & LV 204 COAL SERVICE VALVE HISTORY

COAL RUNS #1 - #5

Coal Run	Valve Number	Valve	Trim Description	Orifice Size	Tons of Coal	Hrs. on Coal	Tons/Hr Coal	Valve Condition After Removal
0	LV-202 A/B	Willis	Rotating Disc -2-3/8" holes in WC disc silver soldered into a SS holder. Stationary disc - 2½" holes in WC disc silver soldered into a SS holder.	32/64" WC	0	0	0	Five failures of the silver soldered rotating disc.
1	LV-202B	Willis	Rotating Disc - Solid 17-4 PH SS heat treated with 1-½"holes. Stationary Disc - 2-½"holes in a WC disc silver soldered into a SS holder.	32/64" WC	72.8	12	6.07	Severe erosion of the 17-4 PH SS rotating disc.
1	LV-202A	Willis	Rotating disc - Solid 17-4 PH SS with 2-3/8" holes. Stationary disc -2-3/8"holes in a WC disc silver soldered into a SS holder.	32/64" WC	18.2	3	6.07	Severe erosion of the 17-4 PH SS rotating disc.
1	LV-204B	Willis	Rotating & Stationary discs - 2-3/8" holes in a WC disc silver soldered into a SS holder.	40/32" WC	91	15	6.07	Minor wear to trim.
2	LV-202B	Willis	Rotating disc - Mechanical held WC disc with 1-½"hole. Stationary disc - 2-½"holes in a WC disc silver soldered into a SS holder.	32/64" WC	51	9	5.67	Minor wear to trim.
2	LV-204B	Willis	Rotating & Stationary discs - 2-½"holes in a WC disc silver soldered into a SS holder.	40/32" WC	51	9	5.67	Minor wear to trim
3	LV-202B	Willis	Rotating disc - Mechanical held WC disc with 1-½" hole. Stationary disc - 2-½" holes in a WC disc silver soldered into a SS holder.	32/64" WC	470.12	108	4.35	Severe erosion of both Rotating & Stationary discs. Valve opened 10-20%.

COAL RUNS #1 - #5

Coal Run	Valve Number	Valve	Trim Description	Orifice Size	Tons of Coal	Hrs. on Coal	Tons/Hr Coal	Valve Condition After Removal
3	LV-202A	Willis	Rotating disc - Shrunk fitted WC disc into a SS holder - 2-3/8" holes. Stationary disc - WC disc silver soldered into a SS holder. 2-3/8" holes.	32/64" WC	47.88	11	4.35	Severe erosion of both the rotating & stationary disc valve opened 10-20%.
3	LV-204B	Willis	Rotating disc - Shrunk fitted WC disc into a SS holder - 2-3/8" holes. Stationary disc - WC disc silver soldered into a SS holder. 2-3/8" holes.	25/64" 17-4 PH SS	518	119	4.35	Worn trim but operational. 25/64" 17-4 PH SS worn to 27/64" size. Valve opened 40-60%.
4	LV-202B	Willis	Rotating disc - solid K-701 WC. 2-3/8" holes. Stationary disc - K-701 WC disc silver soldered into a SS holder.	32/64"	17	8	2.13	Rotating disc was removed when a crack was found running through it. Stationary disc was retained.
4	LV-204B	Willis	Rotating disc - Brazed & Mechanical held WC disc in a SS holder - 2-5/16" holes. Stationary disc - WC disc silver soldered into a SS holder - 2-3/8" holes TMT-5 coated WC disc.	40/32" WC	17	8	2.13	Trim showed no wear and was retained for Coal Run #5.
5	LV-204B	Willis	Rotating disc - Brazed and Mechanical held WC disc into a SS holder - 2-5/16" holes. Stationary disc - TMT-5 coated disc silver soldered into a SS holder - 2-3/8" holes.	25/64" Stellite Overlay	171.01	35.5	4.82	Valve failed to control level when silver solder Stationary disc WC piece moved. TMT-5 coated stationary disc shows less wear than rotating disc.
5	LV-202A	Willis	Rotating disc - Brazed and mechanical held WC disc into a SS holder - 2-5/16" holes. Stationary disc - TMT-5 coated WC disc silver soldered into a SS holder - 2-3/8" holes.	20/64" Stellite Overlay	465.13	96.5	4.82	Valve failed because silver solder broke on stationary disc. Rotating disc severely eroded while TMT-5 coated stationary disc could still be in operation. 20/64" stellite orifice eroded to 5'8" dia.

COAL RUNS #1 - #5

Coal Run	Valve Number	Valve	Trim Description	Orifice Size	Tons of Coal	Hrs. on Coal	Tons/Hr Coal	Valve Condition After Removal
5	LV-202B	Willis	Rotating disc - T_1B_2 & TMT-5 coated WC disc held in a lock ring SS holder. 2-3/8" holes. Stationary disc - T_1B_2 & TMT-5 coated WC disc silver soldered into a SS holder 2-3/8" holes.	25/64" Stellite Overlay	371.14	77	4.82	Valve pulled to avoid another silver solder failure. Both discs show heavy erosion, but still could be operated. The 25/64" choke eroded to 9/16" dia. Valve throttled in the 10-20% range.
5	LV-204B	Willis	Rotating disc - TMT-5 coated WC disc. held into lock SS holder 2-3/8" holes. Stationary disc - TMT-5 coated WC disc silver soldered into a SS holder - 2-3/8" holes.	25/64" Stellite Overlay	568.76	118	4.82	Rotating disc polished only. Stationary disc had some erosion. The 25/64" stellite orifice grew only 9 mils. Valve was throttled in the 40-80% range.
5	LV-202B	Willis	Rotating disc - TMT-5 coated WC disc held in a lock ring SS holder. 2-3/8" holes. Stationary disc - TMT-5 coated WC disc held in a lock seal ring SS holder. 2-3/8" holes	25/64" Stellite Overlay	337.40	70	4.82	Both discs show heavy erosion. Stationary disc holder made of SS had integral choke which eroded differently for each hole. Top hole showed gas wear & bottom hole showed solids wear. Valve experiencing stratafication of the fluid. Stellite choke was eroded.
5	LV-204B	Willis	Rotating disc - TMT-5 coated WC disc held in lock ring SS holder. 2-3/8" holes. Stationary disc - TMT-5 coated WC disc held in lock seal ring SS holder - 2-3/8" holes.	25/64" Stellite Overlay	337.4	70	4.82	Minor wear to both discs. Stellite 25/64" choke shows no apparent wear. The SS holder with integral choke for the stationary disc showed some stratification wear pattern as did the LV-202B.

Coal Run #6

Coal Run	Valve Number	Valve	Trim Description	Orifice Size	Tons of Coal	Hrs. on Coal	Tons/Hr Coal	Valve Condition After Removal
6	LV-202A	Cameron	1" dia. plug & seat made of GE-883 WC & TMT-5 coated.	22/64" WC & TMT-5 Coating	2772.7	387.5	7.16	Orifice plugged & valve removed. Plug worn 3/16" but still operational. Seat had circular wear 1/8" deep in inlet. Orifice worn only a few mils. Valve opened 25-38%.
6	LV-204B	Kieley Mueller	5/8" dia. plug & seat made of K-701 WC shrink fitted into a 15-5 PH SS holder.	25/64" WC & TMT-5 Coated	4092.2	554	7.3	Valve pulled when choke retainer failed causing erosion to Grayloc connectors. Valve trim shows no apparent wear. Valve opened 60%.
6	LV-202B	Kieley Mueller	5/8" dia. plug & seat made of K-701 WC shrink fitted into a 15-5 PH SS holder.	25/64" WC TMT-5 Coated	1599.5	216.67	7.38	Valve pulled because same style orifice installed as LV-204B K & M valve. Plug worn about 3/32" around tip evenly. Seat shows no apparent wear. Orifice did not wear & shows no wear. 15-5 PH SS plug holder had cracked where the K-701 WC piece was held. Valve opened 25-40%.
6	LV-202B	Kieley Mueller	5/8" dia. plug & seat made of K-701 WC shrunk fitted into a 15-5 PH SS holder. Trim used 554 hours in LV-204B service.	25/64" WC & TMT-5 Coated	67.51	8.5	7.94	Valve removed when it plugged. Plug tip broken & valve full of coke & coal resids. No further wear on trim was seen.

COAL RUNS #1 - #5

Coal Run	Valve Number	Valve	Trim Description	Orifice Size	Tons of Coal	Hrs. on Coal	Tons/Hr Coal	Valve Condition After Removal
5	LV-204A	Willis	Rotating disc - Brazed and mechanical held WC disc in SS holder. - 2-5/16" holes. Stationary Disc - K-701 WC disc silver soldered in SS holder. 2-3/8" holes.	25/64" Stellite Overlay	96.4	20	4.82	Minor wear on both discs Stellite orifice showed no wear.

Coal Run #6

Coal Run	Valve Number	Valve	Trim Description	Orifice Size	Tons of Coal	Hrs. on Coal	Tons/Hr Coal	Valve Condition After Removal
6	LV-202A	Willis	Rotating Disc - TMT-5 coated WC disc held in lock ring SS holder. 2-3/8" holes. Stationary disc - TMT-5 coated WC disc held in lock seal ring holder with integral WC choke sleeves. 2-3/8" holes.	22/64" WC & TMT-5 Coated	746.8	112.5	6.64	Trim severely eroded. Orifice showed no wear Valve trim took 600-800 psig pressure drop & choke 1000-1200. Valve opened from 20-80%.
6	LV-204A	Willis	Rotating Disc - TMT-5 coated WC disc held in lock-ring SS holder. 2-3/8" holes. Stationary disc - TMT-5 coated WC disc held in lock ring holder with integral WC choke sleeves. 2-3/8" holes	25/64" WC & TMT-5 Coated	1283.9	187.58	6.84	Valve pulled to examine trim. Rotating disc showed minor wear and stationary disc had 1/8" deep wear in holes. Choke showed no wear Valve took about 150 psig. Valve opened 70-90%.
6	LV-202B	Cameron	1" dia. plug & seat made of GE-883 WC & TMT-5 coated.	25/64" WC & TMT-5 Coated	1634.82	199.92	8.18	Valve pulled when it failed to control level. Plug severely eroded. Seat had 1/8" deep circular ring of erosion in inlet of seat. Valve had to maintain level at 10% open last 50 hours because of process demands.
6	LV-202A	Willis	Rotating disc - TMT-5 coated. WC disc held in lock-ring SS holder. 2-3/8" holes. Stationary disc - TMT-745 coated WC disc held in lock seal ring holder with integral WC choke sleeves. 2-3/8" holes.	25/64" WC & TMT-5 Coated	217.66	23.25	9.36	Valve pulled because of bonnet leaks. Trim showed minor wear. Valve trim took 1200 psig pressure drop and was opened 10-30%. Orifice took 600 psig pressure drop & showed no apparent wear.

Coal Run #6

Coal Run	Valve Number	Valve	Trim Description	Orifice Size	Tons of Coal	Hrs. on Coal	Tons/Hr Coal	Valve Condition After Removal
6	LV-2028	Kieley Mueller	5/8" dia. 3% Binder WC coated with TMT-745 plug & seat. Plug feature new mechanical holder "Tampa" design.	25/64" WC & TMT-5 Coated	1323.06	161.25	8.21	Valve pulled after shut-down. Plug tip broken off from possible thermal shock & caused irregular but minor wear to seat. Orifice retainer was slightly eroded.
6	LV-2048	Kieley Mueller	5/8" dia. plug & seat made of K-701 WC shrunk-fitted into a 15-5 PH SS holder.	25/64" WC & TMT-5 Coated	2881.71	340.42	8.47	Valve pulled after shut-down. Trim shows no apparent wear. Orifice retainer severely eroded and damaged Grayloc connectors.

CURRENT STATE-OF-THE-ART OF BLOCK VALVES FOR SYNTHETIC FUEL PLANTS

V. L. Mogas, *President*
M. E. Beasley, *Vice President, Engineering*
Mogas MW, Inc.

INTRODUCTION

Synthetic fuel plants operate under a variety of conditions depending on the type of process involved. The process descriptions are described in references (1), (2), and (3). No matter which process is selected, process control and isolation valves are necessary. In general, the block valves isolate process stages, control (let-down) valves and other equipment.

The most severe service is in the process control area (reference 4) where extremes in temperature and pressure are compounded by highly corrosive and erosive fluids. A combination of design features and material selection is necessary to achieve reliable block valve service.

PROBLEM DESCRIPTION

In synthetic fuel service, block valves must meet certain criteria related to service conditions. Due to the erosive nature of the coal slurry mixture under multi-phase flow conditions, a smooth, streamline bore must be presented when the valve is open. In addition, since the coal particles will settle into stagnant areas, the bore must be sanitary meaning there are no openings that will allow the coal particles to enter the valve cavity or operating mechanisms. As a corollary to this latter point, it is highly desirable that any moving parts move in such a manner as to not displace volume that could become packed with coal fines. Members that move within their own volume about an axis of rotation are preferred.

Only metal-to-metal seals should be considered. The abrasive nature of the process and the temperatures and pressures experienced dictate this requirement. Non-metallic materials and low hardness metals for seals will not endure the service conditions. This point is well documented in references (4) and (5).

The materials must be able to resist the process corrosion, erosion, temperature and pressure. In most cases a base material alone is not sufficient. Tungsten Carbide and other ceramics described in reference (5) are the obvious exception. To improve the performance properties of the base material, platings and coatings are employed. Proper coating selection must include corrosion resistance, high hardness, temperature stability and compatibility with the base material as regards thermal expansion, bonding, etc. An in-depth technical discussion is beyond the scope of this paper; however, specific application results are reported below.

From an operational viewpoint, block valve maintenance is of primary concern. This requires that the valve be easily serviced and repaired. Sealing members must be replaceable, stem seals must be capable of being tightened under operating conditions, and valve assembly must be uncomplicated and straight forward.

DESIGN FEATURES

With the above criteria in mind, a ball valve with the below details is considered to be one of the best solutions to the synthetic fuels block valve problem. The valve to be described is shown in Figure (1) along with its trim specifications.

All critical seals (Body-End Connection, Ball-Seat, and Stem-Body) are metal-to-metal. The pressure containing members are designed for rigid performance in piping systems normally found in the process control area. The valve is bi-directional so that flow orientation is not required.

PARTS LIST **TRIM SPECIFICATIONS**

Item	Quan	Description	55 - Full SS Valve -20°F to 1000°F
1	1	Assembly, Ball and Seat Ring	
1A	1	Ball	AISI 410 Stainless St Chrome Carbide Coating
1B	2	Dog	Stellite #6
1C	2	Clip, Dog	Inconel X-75
1D	2	Ring, Seat	Stellite #3
2	1	Body	ASTM A182 Gr F316 Stainless Steel
3	2	Connection, End	ASTM A182 Gr F316 Stainless Steel
5	2	Gasket, Body	18-8 Stainless St Asbestos Filled
6	1	Indicator, Position	AISI 1020 or Equal
7	AR	Nut	ASTM A194 Gr 2 Cad Plt
8	1	Nut, Operating Wrench	AISI C-1213 or equal
11A	2	Spring, Load	AISI 316 Stainless Steel
12	1	Gland, Packing	AISI 1020 or equal
13	1	Ring, Splined Stem Stop	AISI 4130 or equal
14	1	Ring, Lower Stem Packing	AISI 1020 Aerocoat 4 Coating or Impervious Graphite
15	1	Ring, Upper Stem Packing	Impervious Graphite
16	2	Screw, Load	SAE Grade 5
17	1	Stem	AISI 660 Stainless Steel
18	AR	Stud	ASTM A193 Gr B7 Cad Plt
19	AR	Stud	ASTM A193 Gr B7 Cad Plt
20	1	Washer, Load	AISI 1020 or equal
21	2	Washer, Lock	AISI 1020 or equal
25	1	Bushing	Impervious Graphite
26	1	Pin, Locating	AISI 316 Stainless Steel

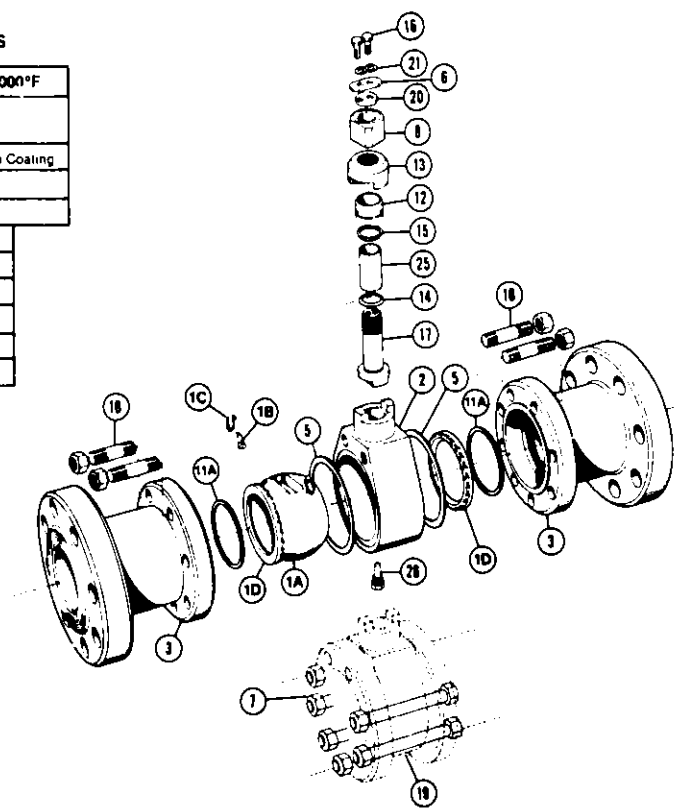

Figure 1. Exploded View of Synthetic Fuels Block Valve

The sealing member is a solid, spherical ball with a non-integral stem. This floating design offers several advantages over the trunnion mounted concept. As a result of the seat load springs, the clearance between components is kept to a minimum to prevent coal particles from entering the seal areas and the cavity. Also, sharp corners on the seat rings wipe the ball during rotation to prevent coal particles from scratching the sealing surfaces. The spherical ball also rotates completely within its own geometry so that displacement of solid particles is not necessary.

This valve has a rotating seat. Each time the valve is actuated into the full open position, the dogs located on the ball (see Figure 2) engage the notches in the seat rings and rotate the seat ring a few degrees. This ring rotation allows the wear caused by the venturi effect to be spread over the entire seat ring circumferential area instead of being concentrated at one point. This greatly reduces the erosion effects and increases the life of the valve in this service.

The ball has a double arcuate cut machined into opposite lips of the ball bore. Figure 3 shows this. This double arcuate cut in the ball matches the edge of the seat ring so that, as the valve is

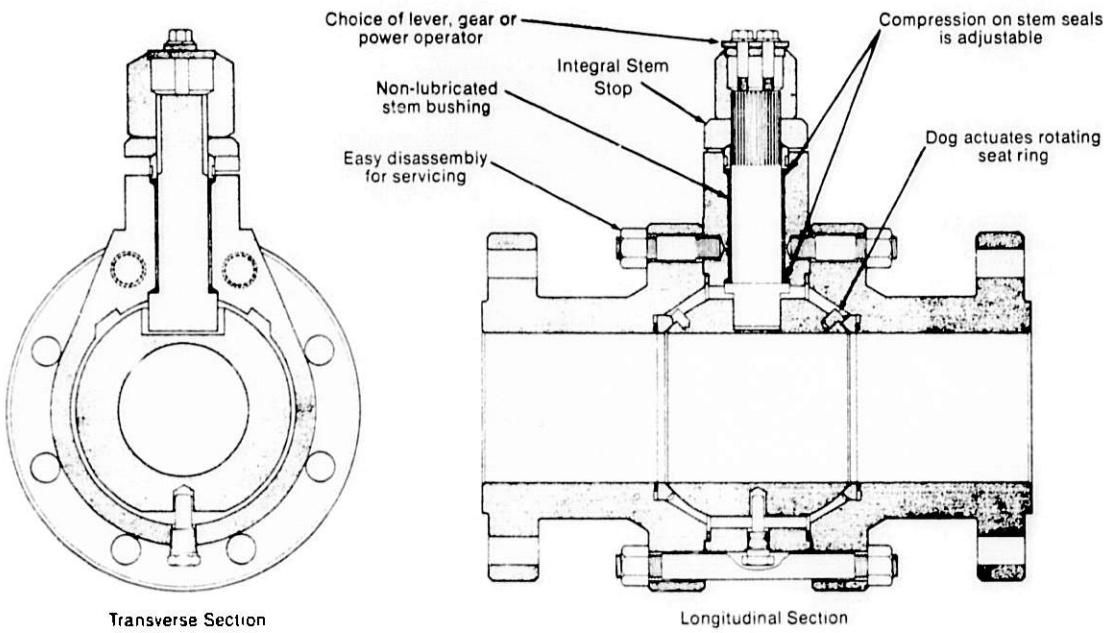

Figure 2. Ball Valve Cross Sectional View

opened and closed, the pinpoint opening of a normal ball is eliminated. The opening is now a line which drastically reduces the venturi erosion damage. Also any erosion is spread over a larger area of the seat ring and ball interface increasing the valve service life.

The other important area of any valve is the stem and associated packing. The stem is sized to handle normal operating torques at low stress levels. Also since the stem is not integral, it is not subjected to the loads imposed on a trunnion mounted design.

The stem-body have two important safety features incorporated into their design (see Figure 2). The first relates to the integral stem stops that prevents over-torquing of the stem and allows accurate positioning of the ball bore. The second feature is the shoulder on the stem that prevents it from being blownout due to operator error in removing the packing gland.

As related to the packing, it is pressure energized on the lower seal and packing gland and load screw energized on the upper seal. The lower seal is either metal or carbon graphite and the upper seal is carbon graphite. The load screws shown in Figure 2 allow the stem seals to be tightened under operating conditions should a minor leak develop. A combination of the lower seal and safety shoulder allows the upper seal to be replaced under operating conditions.

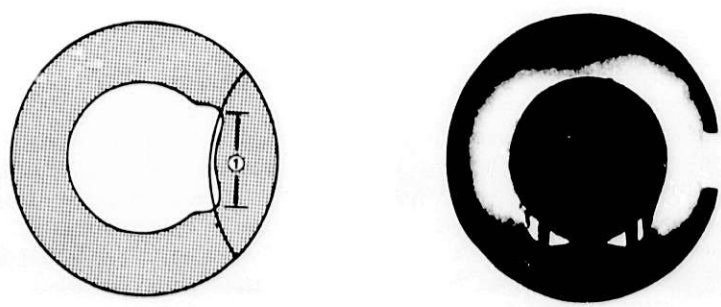

Figure 3. Double Arcuate Cut Ball

Some operators have developed elaborate purge systems to minimize the effects of particle settlement in the cavity. The construction of this valve and the geometry of the cavity lends itself for use with a purge system. Although field data is not conclusive at present, it is indicated that a purge system will extend the valve service life.

FIELD EXPERIENCE

To date, the major field experience has been at Ashland's Synthetic Fuel plant in Catlettsburg, Kentucky. The block valves described above are being used in the let-down train and consist of 6" and 10" sizes.

These valves have been operated an average 10 to 15 times under various pressure, flow, temperature and media concentration conditions. The majority of the cycles have been under normal operating conditions with no attempt to purge or cleanup prior to cycling. In at least one case, an emergency existed that required rapid closure.

The valves have operated with only minimal problems. They have sealed to original specified tightness every time, both hot and cold and during thermal heatup and cooldown. Initially, there was minor stem and seal leakage which was eliminated by tightening the stem load screws. Also on one occasion a minor body gasket leak was eliminated by tightening the body bolting.

After 45 days of service, two valves were pulled from the lines and inspected. All sealing surfaces (stem, body, ball, seat) were in like new condition. There was no evidence of erosion, corrosion, pitting, scoring or gaulling. In fact, the condition was so good that it was hard to tell that the valves had been subjected to the severe operating conditions.

The balls were 410 stainless steel with chrome carbide coating (LC-1 put on by the Union Carbide Linde d-gun). This combination withstood the conditions. The only problem noted was chipping of the coating in a noncritical area near the stem slot. This chipping was induced by the mechanical load from the stem and was not caused by the process erosion or corrosion. A design change is expected to eliminate this problem.

In reviewing this data, it is obvious that this valve will work in synthetic fuel block valve service. The key to this success is the design simplicity coupled with manufacturing quality. The minimum number of parts are precision made to exacting tolerances. This reduces the number of failure points and the number of possible failure modes giving acceptable service life for this application.

REFERENCES

1. "Coal Conversion: How To Deal With Valve Problems", D. J. Deutsch, *Chemical Engineering*, December 1, 1980, pp 41-43.

2. *Proceedings of the Second Symposium on Valves for Coal Conversion and Utilization*, October 15-17, 1980, DOE/METC/SP-81/1

3. *The Proceedings of the 1980 Symposium on Instrumentation and Control for Fossil Energy Processes*, June 9-11, 1980, ANL-80-62.

4. "Materials, Equipment for Conversion to Coal," D. J. Deutsch and P. M. Kohn, *Chemical Engineering*, June 2, 1980 pp 35-58.

5. *Application of Advanced Materials and Fabrication Technology to Let-Down Valves for Coal Liquefaction Systems*, January 1977, EPRI AF-305.

PACKED BED LETDOWN SYSTEM*

P. K. Carlson
Oak Ridge National Laboratory

INTRODUCTION

As large-scale commercial direct coal liquefaction plants are built, it will become important to maximize the reliability of operation and to minimize capital and maintenance costs. Pilot plant operations to date have revealed some serious shortcomings in using conventional components in direct liquefaction processes, even when designed for so-called severe service. The problem is exemplified by the high pressure dissolver (or reactor) slurry letdown valve (ΔP = 13 to 20 MPa, T = 400°C, about 10% by weight fine mineral solids in hydrocarbon slurry) where off-the-shelf and modified conventional control valve designs have given service of a few hours to, at best, a few thousand hours. Reliability improvements proposed or implemented thus far have included such approaches as generous sparing plans with multiple letdown stages (see Figure 1), the use of "exotic" erosion resistant materials, and a few

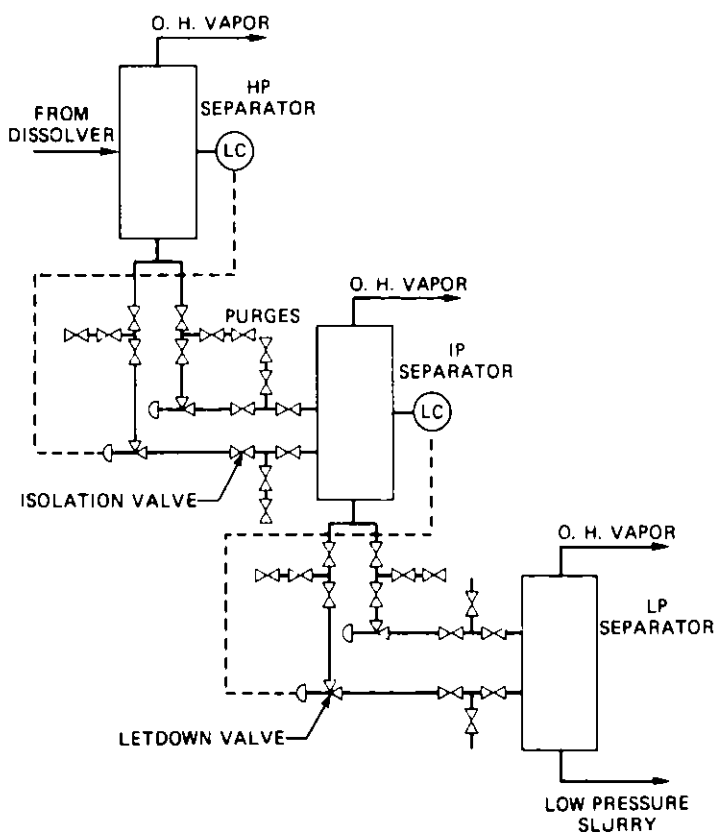

Fig. 1. Typical conventional letdown system.

*Research sponsored by the SRC Projects Office, Oak Ridge Operations Office, U.S. Department of Energy under contract W-7405-eng-26 with the Union Carbide Corporation.

unconventional or novel valve designs. In general, the proposed solutions either increase complexity and expense without guaranteeing improvement, or place too much emphasis on the use of materials which are more difficult to manufacture and use and which give unpredictable results. Following a brief background discussion of letdown valve failure causes, a completely different approach will be explored.

BACKGROUND

The two principal types of failure reported in letdown valves have been trim erosion and breakage or separation of trim. Better material selection and design practice, including the use of internally streamlined designs, the use of series fixed flow chokes to share pressure drop with the valve, and particularly a shift to such materials as low percentage binder cemented tungsten carbide (e.g., Kennametal K-701), have reduced erosion substantially over the earliest letdown valves. Erosion potential over a commercially required service life of, say, 10,000 h, however, remains considerable. Studies at Battelle Columbus Laboratories indicate that hot coal slurry impinging K-701 at 50 m/s and a 50° angle of incidence will erode at a rate exceeding 1 μm/h penetration, or 1 cm in 10,000 h. Moreover, velocities of this magnitude can result from relatively modest 1.38 MPa (200 psi) pressure drops.

The other major reported problem, breakage or separation of trim, has resulted primarily from the use of the extremely brittle, erosion resistant materials. Trim of these materials is more apt to fail by vibration and other mechanical stresses which tougher materials would tolerate, by thermally induced stresses resulting from their use in conjunction with other materials, or by separation of hard coatings from dissimilar substrates. Failure times from these types of occurrences are widely scattered, mechanisms are less well understood, and further improvement may be difficult to achieve. Some designs currently in use seem to be approaching the optimum.

THE PACKED BED LETDOWN SYSTEM

Rather than continuing to focus on modifying valves to enable them to withstand extreme conditions, the approach proposed here is to substantially reduce the erosive potential, allowing the use of more conventional materials. A given reduction in pressure can be obtained at low velocity if spread over a considerable distance or done in a series of small increments. The long flow "labyrinth" presented by a packed bed of spheres functions in this manner. Once dimensions are established, a bed can be easily constructed, consisting in its simplest form of one or more joined pipe sections, filled with spherical packing. The fluid velocity within the packed bed can be controlled by tailoring the column diameter to the volumetric throughput; then the length can be chosen to yield the desired pressure drop. The packing size is selected to enable included flow passages to accommodate the solid particles present in the slurry and to discourage coking and solids buildup within the bed by minimizing static holdup. Although the concept of using packed beds for pressure reduction is not new — in fact, such devices are currently being manufactured by at least one firm (Hitco, Inc., located in Gardena, California) — the hot, flashing slurry application of direct coal liquefaction would be new, requiring more complicated and untested design procedures.

Flow controllability presents a problem in using the packed bed since it operates as a fixed flow resistance. As slurry flow rate, composition, and physical properties vary during operation, a method of "throttling" the flow is necessary. In the Hitco system this function is provided by installing a valve in series with the packed bed, which drops some fraction of the total pressure depending on the flow rate. Though a system such as that offered by Hitco could be used in the direct liquefaction application, most of the disadvantages of current valve/choke arrangements would be retained. Other methods of configuring packed beds for flow control are possible (see Figure 2), including the following: (1) Multiple beds in series and/or parallel flow circuits, switching beds in or out by block valves to vary the flow resistance in a stepwise manner. This method would subject one or more block valves to a

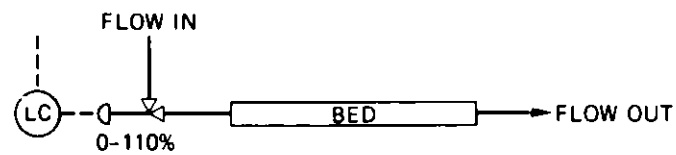

CONVENTIONAL VALVE CONTROL

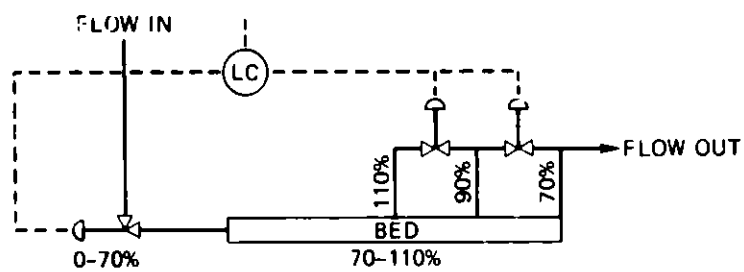

STEPWISE/CONTINUOUS CONTROL

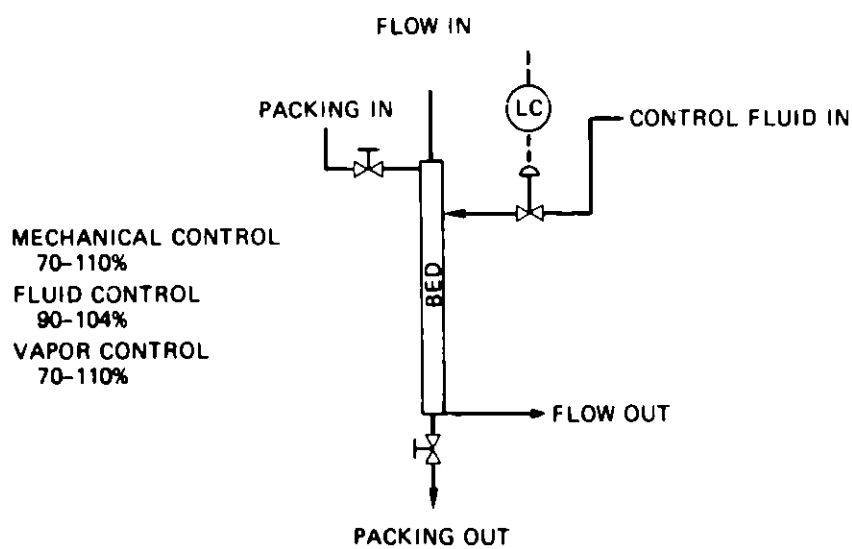

FLUID/MECHANICAL BALL LEVEL CONTROL

Fig. 2. Possible packed bed flow control configurations (percentages indicate range of flow control possible with particular configuration).

very severe cycling service. (2) Mechanical packing addition and removal systems to allow onstream variation of the packed length of the bed. The development of such capability would in itself be a major effort, comparable in cost and complexity to that of developing a new valve type. Since the responsiveness of this mode of control would be slow, it would best be utilized in conjunction with other means of flow control, where it would serve to "optimize" the bed to plant operating conditions. (3) The primary focus of our research at ORNL, involving the controlled addition of a second fluid stream into the bed, along with the slurry, to displace bed flow capacity away from the slurry. The control fluid would be either the hot, high pressure vapor exiting overhead at the high pressure separator vessel or the liquid condensate which results from the cooling of this vapor (see Figure 3). In either

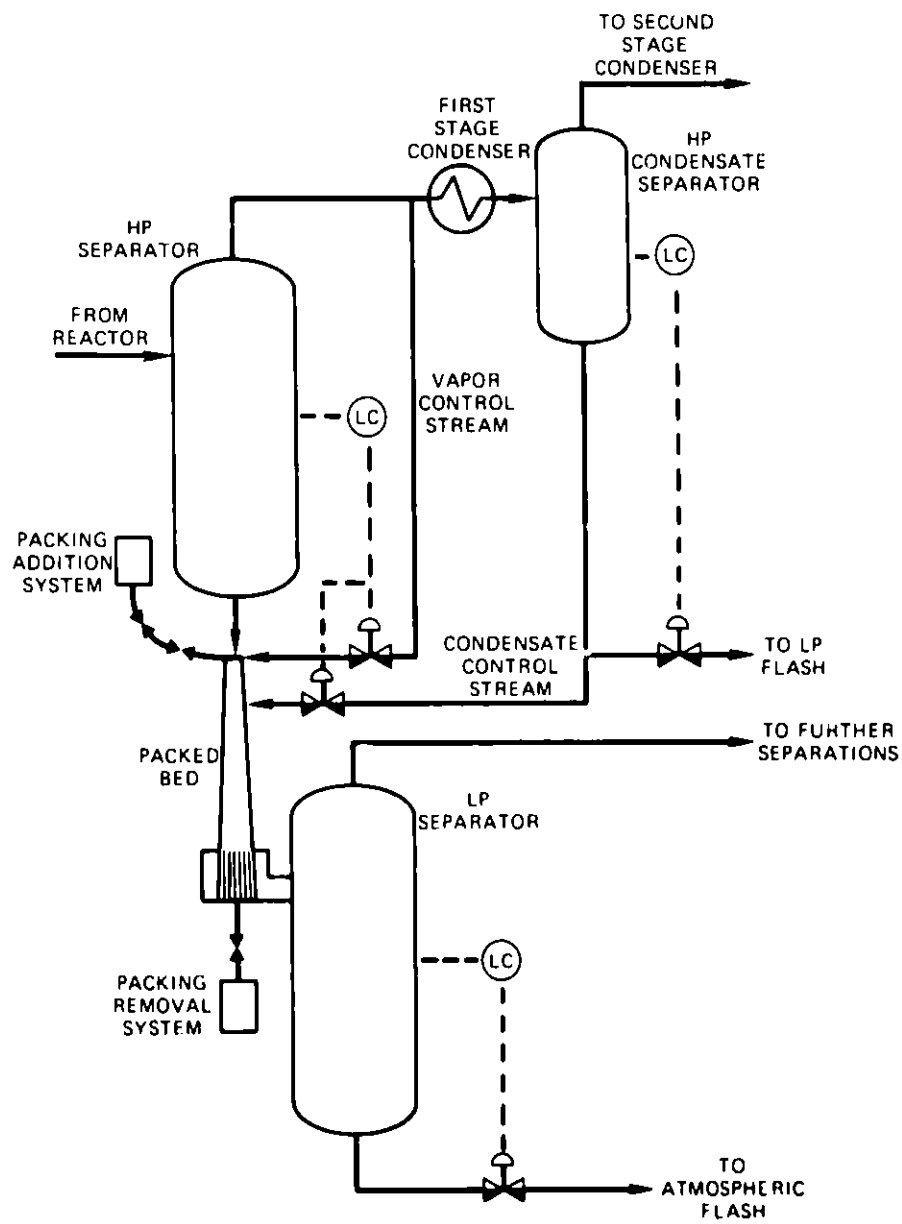

Fig. 3. Two possible process sources of control fluid for packed bed system.

case, controlled changes in the rate of addition of the clean material would effect opposite, differing magnitude changes in slurry flow through the bed. The use of "fluid" control would eliminate the need for control valves in contact with slurry, so would be preferable at least over a limited control range (a range practical for flow "trimming" during or near lined out operation). Supplemental control, by conventional valve or one of the other methods previously discussed, would be needed only for extended periods of low plant throughput, such as startup or as a result of major process equipment failures.

DEVELOPMENT WORK AT ORNL

Development of the packed bed system at ORNL has been under way since October 1979. The project consisted of inhouse exploratory studies until the fourth quarter of fiscal 1980, when DOE support was obtained. At that time, the project was to have culminated in the testing of a packed bed device at a pilot plant. However, DOE budget revisions have forced a suspension of this task. Inhouse work at ORNL has, meanwhile, included analytical feasibility studies and operation of a small-scale packed bed experiment. The following sections summarize the work done in these areas.

Computer Design Studies

Basically, a packed bed can be designed for a specific pressure drop/throughput condition by varying three geometric parameters, the effects of which are as follows:

Parameter	Effect of increase for a given throughput (others held constant)
1. Bed length	increases ΔP
2. Bed diameter	decreases ΔP
3. Ball diameter	decreases ΔP

For the case of direct liquefaction dissolver slurry letdown involving a fluid which progressively vaporizes as its pressure drops, $\Delta P/\Delta L$ (pressure drop per unit length) is a complicated function of pressure and other parameters, including those above, and must be integrated numerically over the required pressure range to get overall length. In handling erosive potentially coking slurries, it is necessary to impose constraints on bed diameter to control velocity and ball diameter to insure that flow voids will pass solid particles and minimize the static holdup of hot slurry.

A computer program has been written to design beds using available literature correlations for two-phase, co-current flow through packed beds for $\Delta P/\Delta L$ and liquid holdup (necessary to determine the separate phase velocities). The procedure for multicomponent flashing flow uses the computer to carry out iterative vapor/liquid composition calculations and to numerically integrate the function "$1/(\Delta P/\Delta L)$" vs P to get overall length. As pressure is lowered, the diameter of the column is varied in some specified fashion to keep velocity below a preset maximum. The procedure requires as input information, data on each coal liquefaction mixture component (i.e., its mass flow

rate, molecular weight, K-value (from V.L.E. data) as a function of pressure and temperature, latent heat of vaporization, and heat capacity.) Computer results are given in Figure 4 for two design cases, one sized for the SRC-II Demonstration Plant and the other for the H-Coal Pilot Plant.

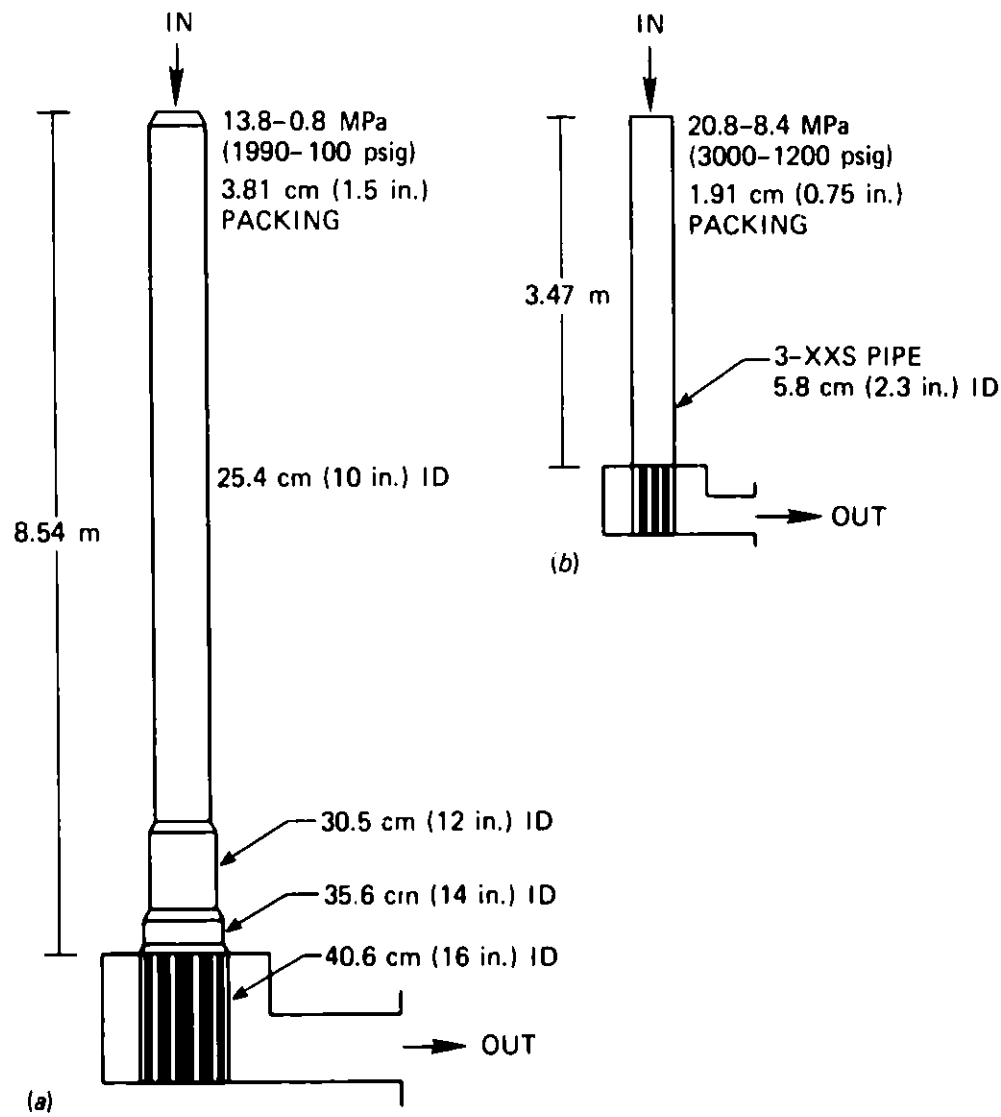

Fig. 4. Computer designed packed beds. (a) SRC II demonstration plant (50% plant throughput). (b) H-coal pilot plant.

Computer Fluid Control Studies

A second computer program has been written to accept bed dimensions calculated in the first program, and to compute the flow rate of control fluid (specified composition and temperature) which, when added at a specified axial location, results in a given percentage reduction in the flow of slurry. Other required input information is the same as that used in the bed design program. The quantity of control fluid which must be added for a given slurry

flow reduction is dependent on several factors, including the volumetric properties of the control fluid (vapor or liquid); if a liquid, then its volatility; temperature; point of injection; and so forth. Feasibility considerations include the rate of production of the fluid, the final temperature reduction which can be tolerated (as a result of adding a cooler fluid or increasing cooling by vaporization), and the diverting of unreacted hydrogen (potential recycle hydrogen) into the low pressure vapor handling system for the case of using high pressure separator vapor. The penalty for use of vapor would be a required increase in the capacity of the lower pressure vapor system to recover hydrogen for recycle, while the major disadvantage of using the liquid system would be its limited range of control. Table 1 indicates the

TABLE 1. FLUID CONTROL CALCULATIONS

SRC-II Demo Case

SLURRY FLOW VARIATION [%(WT.) OF DESIGN]	CONTROL FLUID REQUIRED [%(WT.) OF DESIGN RATE OF PRODUCTION]	UNREACTED H_2 TO LOW PRESSURE SYSTEM [%(WT.) OF COAL INPUT]	FINAL TEMPERATURE OF LETDOWN MIXTURE [°C(°F)]	SOURCE OF CONTROL STEAM
+10	0	0	411(771)	Dissolver
+ 5	.4	.03	410(770)	Effluent
0	.8	.06	409(769)	Separator
- 5	1.2	.09	409(768)	Vapor
-10	1.6	.12	408(766)	431°C (807°F)
-15	2.1	.15	407(765)	13.8 MPa (1990 PSI)
-20	2.6	.19	406(763)	
-25	3.2	.23	405(762)	
-30	3.8	.28	404(760)	
+ 4	0		411(771)	1st H.P.
+ 2	12		409(768)	Flash Drum
0	25		407(765)	Bottoms
- 2	37	NONE	405(762)	371°C (∿700°F)
- 4	49		404(759)	13.5 MPa (1950 PSI)
- 6	61		403(757)	
- 8	74		401(754)	
-10	86		400(752)	
-12	98		398(749)	
	H-Coal Pilot Plant Case (Syncrude Mode)			
+10	0	0	447(840)	High
+ 5	1.5	.2	448(838)	Pressure
0	3.0	.3	447(837)	Separator
- 5	4.8	.4	447(836)	Overhead
-10	6.8	.6	446(834)	Vapor
-15	8.8	.8	445(833)	454°C (850°F)
-20	10.8	1.0	444(831)	20.8 MPa (3000 PSI)
-25	13.2	1.2	443(829)	
-30	15.8	1.4	441(826)	
+ 4	0		449(840)	High
+ 2	4		447(837)	Pressure
0	12	NONE	444(831)	Condensate
- 2	22		440(824)	Separator
- 4	35		436(817)	Bottoms
- 6	49		431(808)	260°C (∿500°F)
- 8	67		425(797)	20.4 MPa (∿2950 PSI)
-10	94		417(783)	

turndown capabilities and shows the effects of using vapor vs liquid control as applied to the SRC-II and H-Coal designs given previously.

Experimental Work

In an attempt to study the behavior of packed beds of spheres flowing two- and three-phase mixtures at high throughputs, a small scale test loop is being operated at ORNL. Determining the applicability of two-phase pressure drop correlations from the literature to very high throughput (pressure drop) beds is the primary goal of the work; however, such issues as plugging and pulsation are also being studied. The loop uses a 186-cm long x 2.43-cm ID (one-inch Sch. 80) bed with spherical packing of either 0.635 cm (0.25 in.), 0.476 cm (3/16 in.), or 0.3 cm diameter. The device is fed by slurry pump and a supply of high-pressure N_2 gas at ambient temperatures. Pressure taps are located along the axis of the bed; instruments record the axial pressures, and the flows of gas and/or liquid (slurry).

A large amount of data, at various gas/liquid flow combinations with overall bed pressure drops as high as 8.37 MPa ($\Delta P/\Delta L$ ~200 psi/ft), have been obtained. The data have been compared to pressure drop per unit length predictions based on various literature correlations, especially that of Larkins et al. The form of Larkins correlation and the range of data from which it was formulated at first seemed to indicate its logical extension to this work, but our experiments show significant deviation and suggest a better correlation is possible. This is indicated in Figure 5. Any proposed correlation, however, must still be considered only a first attempt in its application to flashing coal derived slurries; pilot plant experiments will ultimately be necessary to insure the validity of the correlation.

REMAINING TECHNICAL ISSUES

At the time of writing, successful operation of a packed bed type of slurry letdown device has not yet been demonstrated in direct liquefaction service. Though pilot plants have tried a number of valve designs for the letdown application, they have all been more or less standard configurations supplied by industry. Since the packed bed concept represents a substantial departure from current design for direct liquefaction, successful completion of an inplant experimental program will be necessary to provide reasonable assurance as to the feasibility of packed beds for this application.

The simplest experiment is envisioned as simply a packed section spool piece in series with an existing letdown valve. This experiment could provide insight into the following technical issues: (1) plugging and coke deposition in packing; (2) erosion of packing and wall, abrasion of packing and wall by vibration of packing, etc.; (3) adequacy of ΔP sizing correlations for packed beds in multiphase, multicomponent, flashing flow at high throughput rates.

Further experiments to demonstrate such things as fluid, stepwise, or mechanical ball level means of control could be carried out following initial feasibility experiment.

TWO-PHASE FRICTIONAL PRESSURE DROP PER UNIT LENGTH FOR PACKED BEDS OF SPHERES IN COCURRENT FLOW AT HIGH THROUGHPUT RATES

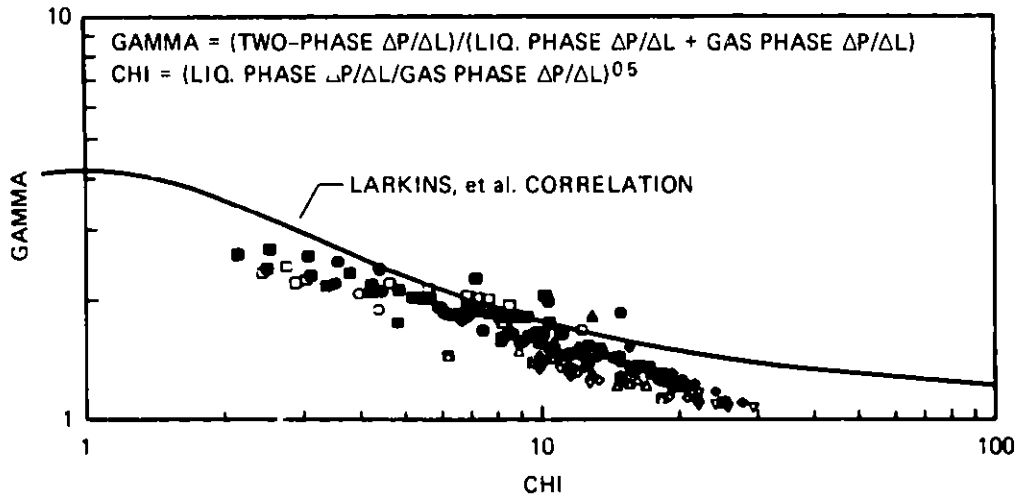

EXPLANATION OF POINTS

OPEN		SOLID		INSCRIBED	
WATER + N_2				WATER/ETH.GLYCOL + N_2	
μ_L=.91-.61 cp Packing=3 mm glass		μ_L=1.12-.72 cp Packing=4.76 mm steel		μ_L=6.4-4.1 cp Packing=3 mm glass	
Re_L	Re_G	Re_L	Re_G	Re_L	Re_G
□ 1350	1020 - 3220	■ 2800	1620 - 5400	⊠ 250	1100 - 3280
○ 2470		● 4100		⊗ 420	
△ 3360		▲ 5190		⧄ 650	
◇ 4430		◆ 6600		⊕ 990	
▽ 6400		▼ 8390		⧖ 1245	

Re_L = Liquid Phase Reynolds No. = $\dfrac{\dot{m}_L D_P}{A \mu_L (1-\epsilon)}$

Re_G = Gas Phase Reynolds No. = $\dfrac{\dot{m}_G D_P}{A \mu_G (1-\epsilon)}$

$\dot{m}_L$ = Liquid Mass Flow Rate

μ_L = Liquid Absolute Viscosity

D_P = Packing Diameter

$\dot{m}_G$ = Gas Mass Flow Rate

μ_G = Gas Absolute Viscosity

A = Flow Area (based on empty 2.43 cm I.D. pipe)

ϵ = Packing Void Fraction

Fig. 5. Two-phase frictional pressure drop per unit length for packed beds of spheres in cocurrent flow at high throughput rates.

REFERENCES

1. Clauer, A. H., I. G. Wright, D. N. Shetty, and J. H. Peterson, "Evaluation of Advanced Materials in Laboratory Tests and Pilot Plant Service for Use in Liquefaction Letdown Valves," Third Progress Report for March 11, 1980, to June 10, 1980, prepared by Battelle Columbus Laboratories for the Department of Energy.

2. Larkins, R. P., R. R. White, and D. W. Jeffrey, "Two-Phase Concurrent Flow in Packed Beds," AIChE J. 7(2), 231 (1961).

3. Leavenworth, H. W. Jr. and J. E. Kelley, "Development of Wear-Resistant Valve Materials," First Quarterly Progress Report, October 1978 to December 1979, Second Quarterly Progress Report, January 1979 to March 1979, Albany Metallurgy Research Center, Bureau of Mines, U.S. Department of the Interior.

4. Block, F. E., J. E. Kelley, and H. W. Leavenworth, Jr., "Wear-Resistant Materials for Coal Conversion and Utilization," First Progress Report, October 1979 to April 1980, Albany Research Center, Bureau of Mines, U.S. Department of the Interior.

5. Hatcher, D. W., T. M. Andress, and W. A. Bush, "Survey of Industrial Coal Conversion Capabilities: Letdown Valves," Oak Ridge National Laboratory/TM-6585, November 1979.

6. Sweeney, D. E., "A Correlation for Pressure Drop in Two-Phase Co-Current Flow in Packed Beds," AIChE J. 13(4), 666 (1967).

7. Midoux, N., M. Favier, and J. C. Chapentier, "Flow Pattern, Pressure Loss and Liquid Holdup Data in Gas-Liquid Downflow Packed Beds with Foaming and Non-Foaming Hydrocarbons," J. Ch. E. Jap. 9(5), 350 (1976).

THE ROLE OF TEST FACILITIES IN EVALUATING INSTRUMENTATION FOR LARGE SCALE FOSSIL ENERGY PROCESSES

D. J. L. Lin and R. H. Hickman
Forney Engineering Company, Addison, Texas

ABSTRACT

A calibratable flow test bench designed to accomodate various liquid/solid feedstock for the Syn-fuel projects, is an essential and practical tool for the evaluation of hydrodynamic characteristics of the selected liquid/solid test medium and the determination of instrument accuracies and service life in the liquid/solid feed environment.

1. INTRODUCTION:

Forney Engineering Company is a manufacturer of liquid and gaseous fuel burners and related boiler front piping, burner management, and fuel handling systems. Recent interest in coal-related alternative fuel utilization, has prompted the search for varifiable data on the combustion and flow characteristics of these alternative fuels. Similarly, much of the syn-fuel feedstocks are in the form of liquid/solid mixture, and are in need of test-verified flow and combustion data for the design of the liquification plants. During the past two years, a 25 t/h liquid/solid flow test loop and a 70 MKB (millions of BTU per hour) water cooled combustion furnace were constructed and put into operation at the Company's Carrollton, Texas Plant. In the interest of advancing syn-fuel production, our company has made the test facilities available to other companies that are engaged in the development of syn-fuel processes and equipment. Some of the tests conducted and/or contracted for this year's undertakings are:

a. Flow characteristics of coal/oil mixtures in 50/50 wt. ratios with both bituminus and sub/bituminus coal, and 60/40 coal/water mixtures.
b. Combustion tests of coal/oil mixtures, methanol/coal mixtures, and coal/water mixtures.
c. Metering device calibration for liquid/solid fuels.
d. Wear tests on pump components for solid/liquid flows.

2. DESCRIPTION OF TEST FACILITIES: - (Equipment list per Table 1)

a. FLOW TEST LOOP: - (Figure No. 1)
This flow test facility consists of two 1000 gallon storage and calibration tanks, each equipped with heating coils in the tank bottoms. One tank has a motorized agitator and dump chute for mixing and blending pulverized solid fuel with that of the liquid fuel. One 500 gallon liquid fuel tank complete with heating coil and transfer pump is available for the preparation of liquid fuel.

The two 1000 gallon storage/calibration tanks are intertied by 6" schedule 40 pipes that feed to a six inch pump suction manifold. The 6" X 4" pump manifold can accommodate various types of liquid and slurry feed pumps up to 200 GPM or 50 t/h capacities. The feed pump can take suction from either tank and discharge into any one tank.

The piping in the 25 t/h test loop consists of 6" schedule 40 pipe for the pump suction and 2" schedule 40 pipe in the discharge side. The test loop has a 30 foot straight run which has a removable 10 foot test section. The test section has parallel 2" and 1" lines complete with pressure taps for water or mercury manometer readings across each of the test lines. The 30 foot straight section also has flanged manifold for flow meter installation. At the end of the straight run a removable spool is provided for erosion tests on pipe, elbows and tees. The test section can be lengthened to fascilitate other measurement requirements. All lines are heat traced and insulated.

The 2" discharge piping can be increased to 4" size to form a 50 t/h test loop upon the corresponding increase of feed pump size.

A branch line connects the flow test loop to the 70 MKB test furnace via an in-line fuel heater.

b. TEST FURNACE: - (Figure No. 2)

The test furnace is a water jacketed combustor capable of short term testing at 70,000,000 BTU/HR and long term testing at 30,000,000 BTU/HR. The combustion air can be preheated to 600F and the flue gas monitoring consists of O_2, NO_x, SO_x, CO, CO_2 and particulates.

Both natural gas and No. 2 fuel oil are available for ignition fuel, or as warm-up fuel and fuel source for supporting flame.

The facility has a steam source of 700 PPH saturated steam at 200 PSIG and a compressed air source of 195 ACFM at 150 PSIG and temperature up to 400 F.

The test furnace has an Texas Air Control Board permit to test liquid and liquid/solid fuel under variance. The annual allowable particulate emission is limited to 2000 pounds per year. Our company has placed a single test particulate emission limit of 300 pounds for each contracted combustion test.

The test furnace is 8' in diameter and 27 feet long with observation ports through the full length of the furnace for flame observation and photographing. The furnace has no refractory for artificial flame stabilization.

The furnace is equipped with a roll-away windbox for easy burner changes. The fuel is supplied to the burner using the pump mentioned in the section on the test loop. A return line back to the storage tank from the burner is for line warm-up to atomizing temperature. The heater is unlike typical fuel oil heaters where the fuel is fed through the shell side, but is fed through the tube side to eliminate any solids drop-put when firing slurries.

The combustion air is provided by a forced draft fan with an inlet metering tube. The flow control is provided with an inlet damper with an electric operator or manual handwheel. The air flow is measured with a U-tube water monometer across an orifice in the metering tube. The discharge duct has an in-duct gas fired air heater for elevating the combustion air up to 600°F.

3. AVAILABILITY OF TEST FACILITIES:

Both the Flow Test Loop and the Test Furnace are available for tests by others. Company personnel are available for test assistance and certification of test results, if required. Some typical liquid/solid flow and combustion tests are listed as follows: -

a. Calibration of flow measurement devices.
b. Calibration of mixture level devices.
c. Determination of pipe friction factors, f'tting resistances, and control valve coefficients.
d. Determination of pump NPSH requirements.
e. Determination of erosion/corrosion rates on piping, fittings, throttling devices, thermal wells. instrument taps, and pump internals.
f. Determination of liquid/solid stability rate under throttling, pumping, and continuous recirculation.
g. Effect on liquid/solid mixture viscosity when subjected to throttling and pumping.
h. Optimization of fluid temperature and velocities for the flushing of settled liquid/solid mixture in a piping system.
i. Determination of atomization requirements for the combustion of a liquid/solid mixture.
j. Determination of ignition requirements of the liquid/solid.
k. Determination of liquid/solid fuel flame shape and length.
l. Determination of liquid/solid fuel flame stability with or without auxiliary flame support.
m. Establishment of flame emmissivity factors for the liquid/solid fuel.
n. Optimizing flame detection requirements of the solid/liquid fuel combustion.
o. Hot and cold light off of a liquid/solid fuel.
p. Steam purge requirements of the solid/liquid fuel burner.
q. Burner tip wear evaluation under liquid solid fuel erosion.

4. CONCLUSIONS:

The test facilities described above have provided Forney Engineering Company and our customers valuable information relating to the measurement, control, and combustion of liquid/solid mixtures. Proper utilization of the above test facilities in the testing of liquid/solid fuel or syn-fuel feedstocks, may lead to better instruments, control systems, piping and pumping systems of the future; as well as more reliable and efficient combustion of the coal related fuels of tomorrow.

TABLE I - EQUIPMENT LIST, LIQUID/SOLID TEST FACILITY

EQUIPMENT DESCRIPTION	SIZE OR CAPACITY
OIL HEATING AND STORAGE TANK	500 gallons
LIQUID/SOLID MIXING AND STORAGE TANK	1000 gallons
LIQUID/SOLID STORAGE AND CALIBRATION TANK	1000 gallons
FEED PUMP COMPLETE WITH 15 HP VARIABLE SPEED DC MOTOR DRIVE	100 GPM
OIL TRANSFER PUMP	5 GPM
DRUM UNLOADING PUMP	10 GPM
INLINE FUEL HEATER & TANK HEATING COILS	
70 MKB WATER COOLED TEST FURNACE	
ATOMIZING STEAM SUPPLY	700 PPH 200 psig saturated
COMPRESSED AIR SUPPLY FOR AIR ATOMIZATION	195 CFM @ 150 psig & UP TO 400 F
VARIOUS SIZES OF FD AND PA FANS	
ASSORTMENT OF INTERNAL MIXED, EXTERNAL MIXED, AXIAL FLOW, TRI-STAGED AIR ATOMIZED, STEAM ATOMIZED, HOT COMPRESSED AIR ATOMIZED BURNERS.	

ATOMIZER TEST STAND

The atomizer test stand consists of an eight (8) foot high, eight (8) foot wide and five (5) foot deep box where the atomizer sprays against a plate sitting five (5) feet from the tip. This allows visual, photographic and laser techniques to determine quality of atomization.

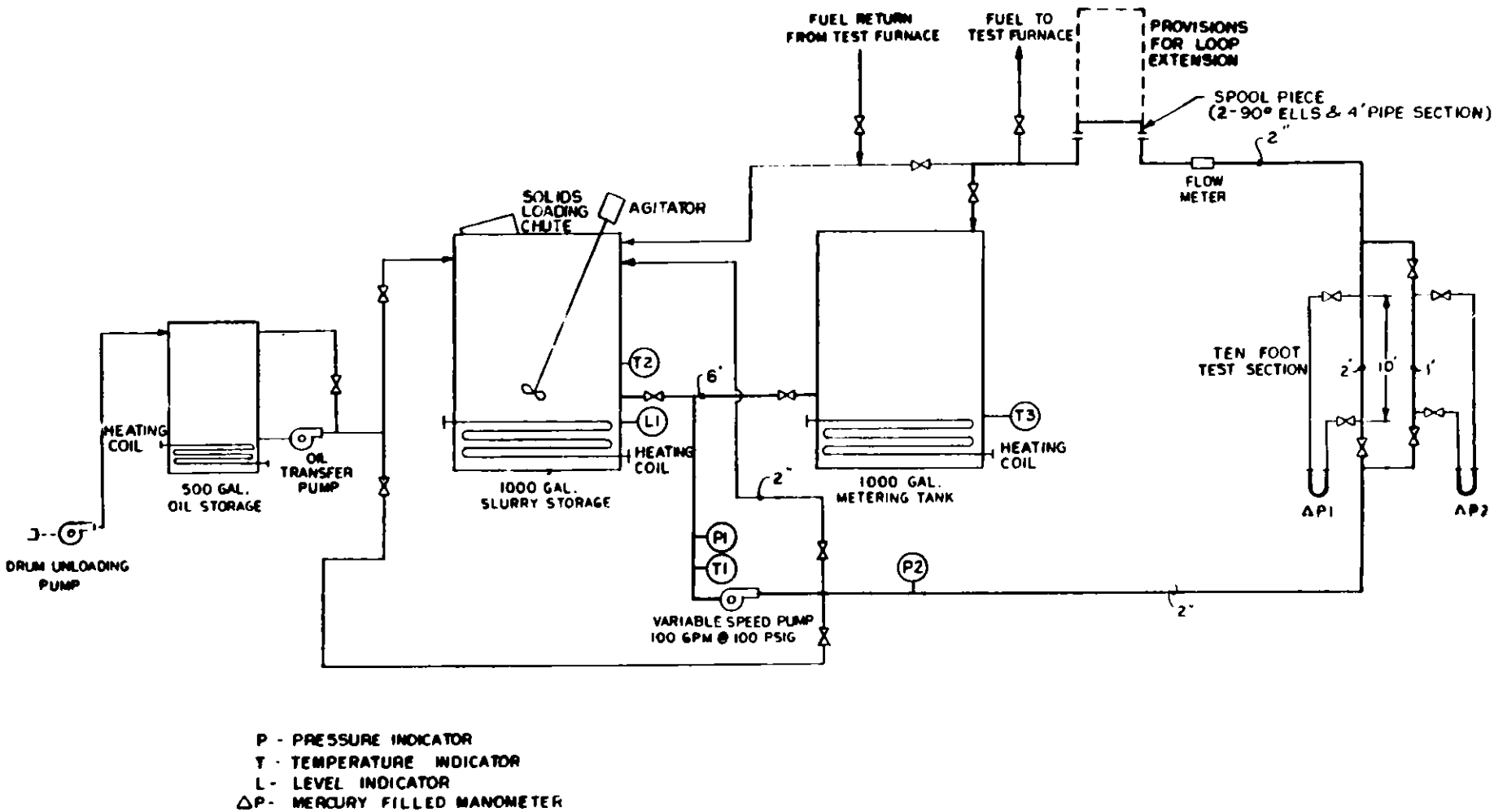

Fig. 1. Flow Test Loop

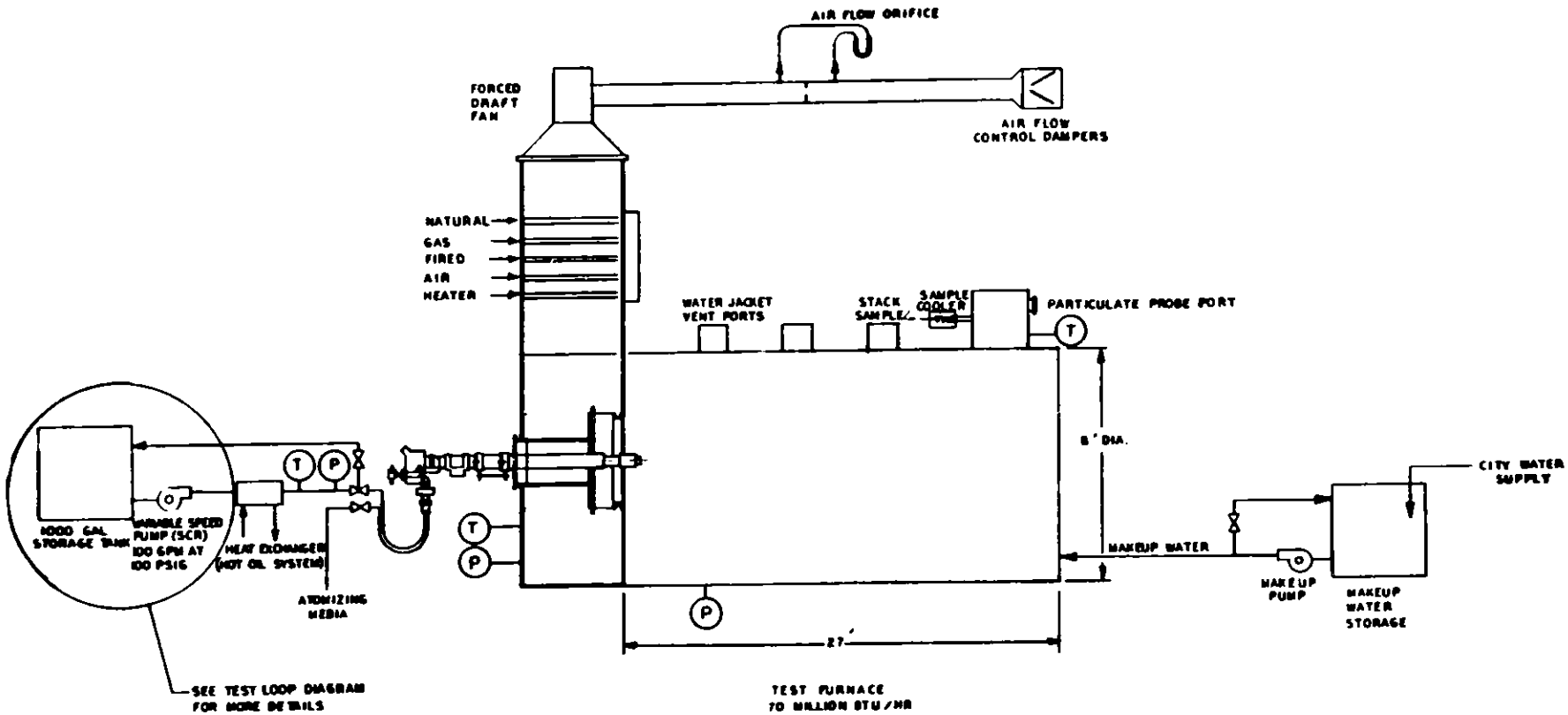

P - PRESSURE INDICATOR
T - TEMPERATURE INDICATOR

Fig. 2. Test Furnace

A MATHEMATICAL MODEL TO SIMULATE HORIZONTAL IN SITU OIL SHALE RETORTING

John H. George
Department of Mathematics
University of Wyoming

Robert Halcomb
Institute of Paper Chemistry

H. Gordon Harris
Department of Chemical Engineering
University of Wyoming

1. INTRODUCTION

A mathematical model was developed to simulate the in situ retorting of oil shale via a horizontal mode of operation. At one time, several experiments had been proposed; a trench test at the Laramie Energy Technology Center involving a 3m × 3m × 16m rectangular shape, and a project at Cowboy Canyon, Wyoming. Unfortunately, neither test reached completion due to funding priority rearrangements, but the mathematical model that was developed to support these projects was completed [5] and will be discussed here.

A typical proposed experiment involved rubblizing the bed by explosive fracturing, after a suitable overall void fraction had been obtained by mining out part of the oil shale bed (sometimes called modified in situ oil shale retorting [2,4] in contrast to "true" in situ retorting [9]). The rubblized bed of oil shale would then have been ignited at one end, and the combustion front propagated in the horizontal y-direction by injecting air into the ignited end at several different vertical levels. As the flame front propagated through the bed along the y-axis, the oil formed by retorting would have flowed downward to be recovered in a trough or sump in the bottom of the well.

From this brief description, it is apparent that horizontal retorting is similar to the more conventional vertical mode of operation, with one important difference: if the bed is sufficiently thick, the combustion at the top of the oil shale bed can "override" the combustion at the bottom of the bed. The override effect is assumed to be primarily a result of product oil moving downward through the bed due to gravitational forces. As the oil moves downward, volatile gases tend to move upward and forward through the porous bed, following the path of least resistance. As a result, some oil is burned at the bottom of the retort, slowing the advance of the combustion zone there,

while the volatile rising gases encourage a more rapid propagation of the flame front in the upper part of the bed.

As a result of the override effect, horizontal retorting cannot be satisfactorily approximated by the various one-dimensional models for vertical retorting which are currently in use [1,2,4,5,6,9], and a two-dimensional model must be employed. In the work described herein, a two-dimensional model, constructed in a relatively simple fashion from a one-dimensional model [5,6], is used to investigate flame front override, and its effect on the overall retorting process.

As a first approximation, we have assumed the primary cause giving rise to override is due to the downward flow of the product oil, and subsequent combustion of a fraction of this oil. The effects resulting from rising of the volatile gases are assumed to have a negligible influence on the material and energy balances, but a method of inclusion into the model will be discussed. If experimental data becomes available, the model will be modified accordingly.

The essential effects causing horizontal motion of a traveling temperature wave are produced by a layered one-dimensional model. Consequently, the main features of the one dimensional model will be outlined before proceeding to a description of the two-dimensional model.

2. ONE-DIMENSIONAL MODEL

The LETC basic one-dimensional model is shown schematically in Figure 1,

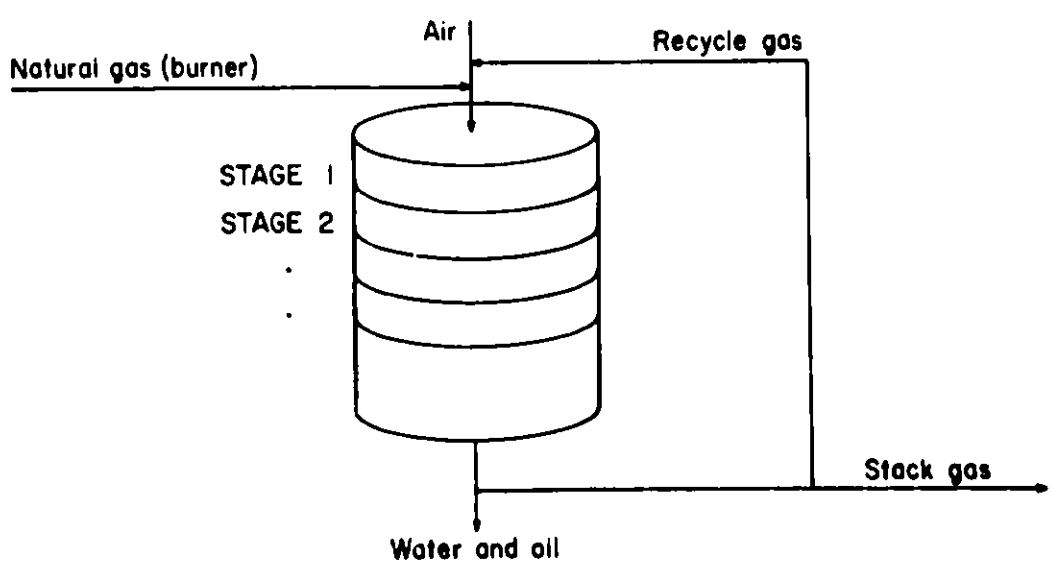

FIGURE 1

[1,4,5,6,7]. The one-dimensional model has been described elsewhere [1,4] and includes the following components [4,6].

1. Gas phase energy balance (steady state)
2. Liquid/solid energy balance
3. Material balances and reaction kinetics for formation and consumption of the following constituents:

(a) Oxygen	(g) Ethane (+ hydrogen + light hydrocarbons)
(b) Nitrogen	(h) Oil
(c) Carbon dioxide	(i) Water (liquid)
(d) Carbon monoxide	(j) Kerogen
(e) Water (vapor)	(k) Carbonates
(f) Methane	(l) Residual carbon

4. Spherical particle heat up and resulting kerogen decomposition (for up to five particle sizes)
5. Combustion of the following constituents:
   (a) Recycle gases
   (b) Retained oil
   (c) Residual carbon
6. Oil retention in the retort
7. Channeling effects: by assuming incomplete combustion it is assumed that fractional parts of the air arriving at stage i are channeled to stages $i + 1$ and $i + 2$
8. Heat loss to the surroundings

3. HORIZONTAL TWO-DIMENSIONAL MODEL

To obtain the horizontal two-dimensional model, the one-dimensional model was employed as follows:

(1) a single retort was constructed from four one-dimensional retorts to produce the desired physical size;

(2) these four smaller retorts (placed on their sides) were then referred to as different levels, level 1 being the top retort and level 4 being the bottom retort (see Figure 2);

(3) the oil was allowed to flow or drip down from level to level, and

(4) the oil dripping from the 4th level was added to the oil recovered from the end of the retort.

In this work the heat loss term was assumed to be negligible and the second-order, more complicated effects of gas rising from level to level were

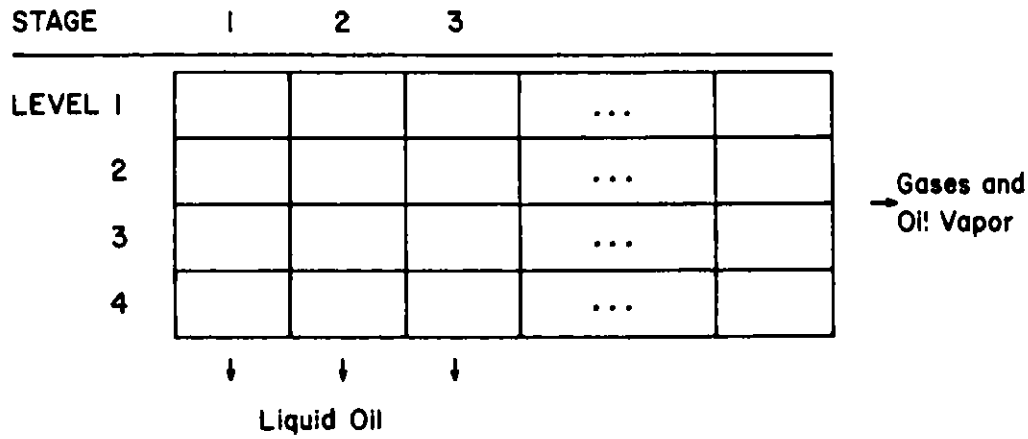

FIGURE 2

neglected. As a consequence the only link between the four levels was the oil dripping downward.

Figure 2 shows the directions of motion for the combustion front, the air flow and the oil flow.

Several different schemes were investigated for enabling oil to drip from level to level. In these schemes calculations proceed through the levels and stages in an inverted N fashion so that after each time incrementation the elements are processed in the sequence (1,1), (2,1), (3,1), (4,1), (1,2), (2,2), (3,2), (level, stage), etc. The processing at each of the elements in the two-dimensional model is carried out exactly like the processing in the one-dimensional model except for the additional process of dripping oil to lower levels.

4. A SCHEME FOR DRIPPING OIL

The most promising scheme introduced two variables to account for (1) oil retention on the shale (CWOR) and (2) residence time of the oil in a particular element (IDPT). For every element (i,j) CWOR pounds of oil (if present as a result of kerogen decomposition) are retained in the element to cover the surfaces of the shale particles. The remainder of the oil produced in the element is permitted to drip through the bed at a specified rate. The dripping is accomplished as follows. Each of the four levels is subdivided into three sublevels giving a total of twelve sublevels. Sublevels 1, 2 and 3

correspond to level 1, sublevels 4, 5 and 6 to level 2, sublevels 7, 8 and 9 correspond to level 3 and sublevels 10, 11 and 12 correspond to level 4. The oil produced in element (i,j) in excess of CWOR is stored in three equal portions in the appropriate sublevels for that (i,j) element. When a specified number of time increments has elapsed, corresponding to the residence time IDPT, the oil retained in the various sublevels is pushed down one sublevel. This is the oil that is excess of CWOR for each element. The oil continues to be stored in the appropriate sublevels and is pushed down one sublevel every IDPT time increment. For example, the oil that was originally stored in sublevel 1 will be found in sublevel 2 after one "push" or time step and in sublevel 6 after five time steps, and finally in oil recovered after twelve time steps. Oil that was originally stored in sublevel 7 will be in oil recovered after six time steps. For the purpose of burning the oil trapped in the retort, the model lumps the appropriate sublevels together into the four basic levels. Rough calculations [3] indicate CWOR = 20, see also [8].

5. RISING GASES

At each stage in the computation, the total gas produced includes oil vapor. In element (i,j) assume a fraction g_1 of the total gas produced in element (i,j) moves into element (i,j+1). Also assume a fraction $(1 - g_1)$ of the gas produced in element (i,j) is diverted upward to (i+1,j+1). The gas that collects at the top in level 1 is then diverted out as usual.

6. RESULTS

Figure 3 illustrates results obtained using data from the 150-ton retort [7]. The dotted lines indicate the 1000°F profiles and the solid lines indicate the 1200°F profiles while the peak temperatures are listed at each level in degrees F. By moving downward through the figures, the temperature wave can be visualized and the override observed.

In order to conserve computer time we reduced the model bed length from 43 feet to 19 feet and scaled the shale load proportionally.

7. CONCLUSIONS

The scheme used here can be explained more readily from first principles. However, other schemes can be devised which have the override effect and could be used in some situations [5]. In Figure 3, the oil retained in the layers

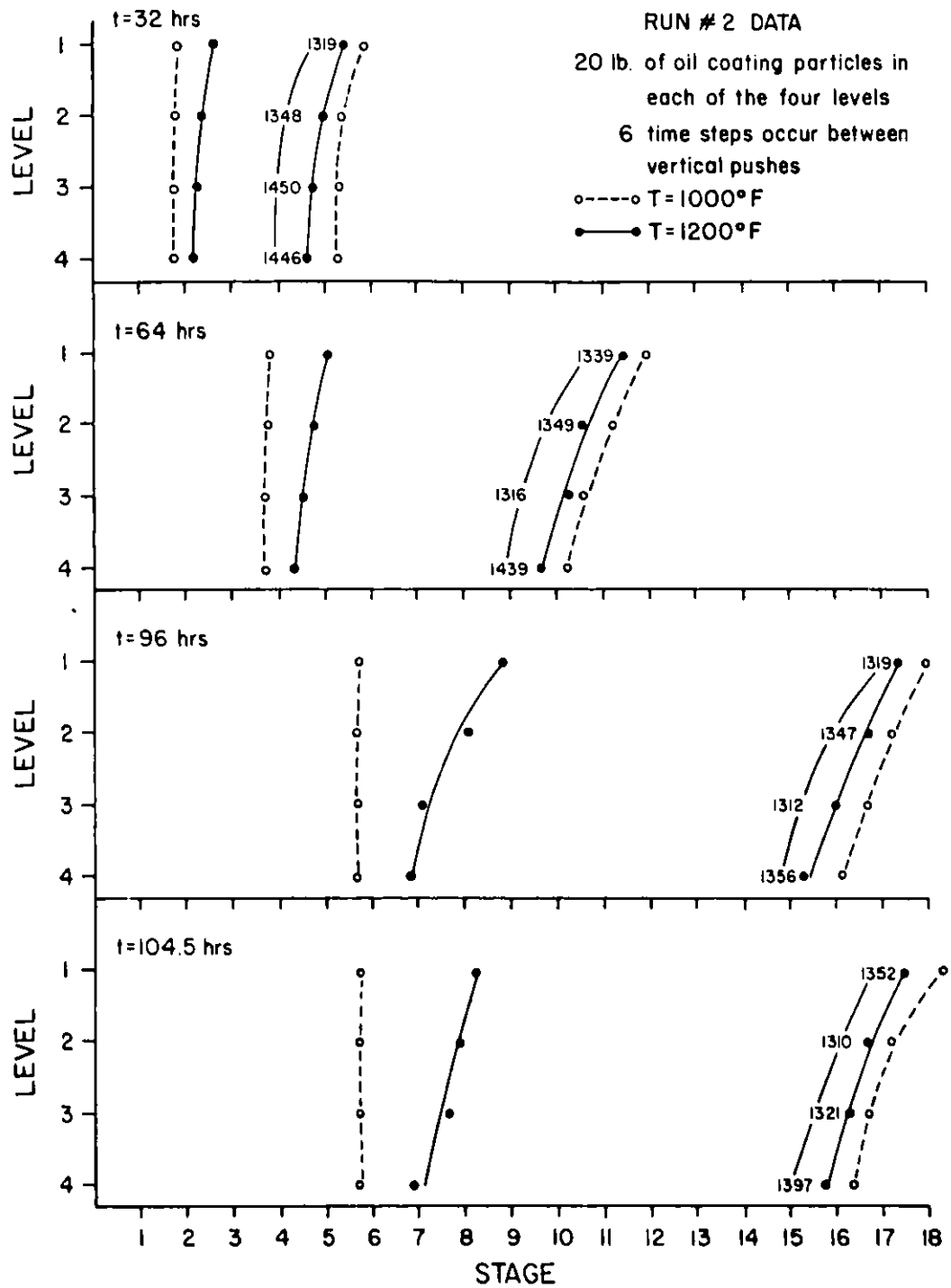

FIG. 3 TEMPERATURE PROFILES AT REPRESENTATIVE TIMES

spreads the combustion zone to about 3 meters at t = 104.5 hours. The latest Lawrence Livermore model [2] has included several chemical reactions we did not consider. Among these are the reaction of residual carbon with CO_2 and the water gas shift ($CO + H_2O \rightarrow CO_2 + H_2$). We hope to investigate the effects of these reactions on our model as well as improve the carbon combustion model, and include radiation heat transfer effects, as developed in unpublished work of Charles Mitchell.

8. ACKNOWLEDGEMENT

The authors would like to acknowledge the helpful discussions with L. Dockter, J. McKenna and D. Fausett.

9. REFERENCES

1. Ahmad, A., L. Dockter, J.H. George, and H.G. Harris, A mathematical model for in situ oil shale retorting, First Intl. Conf. on Math. Modeling IV, Rolla, Missouri, 1781-1789, 1977.

2. Braun, R.L., Mathematical modeling of modified in situ and above ground oil shale retorting, Lawrence Livermore National Laboratory Report UCRL-53119, January 1981.

3. Carley, J., private correspondence.

4. Dockter, L., and H.G. Harris, A mathematical model of forward combustion retorting of oil shale, LETC/TPR-78/1, July 1978.

5. George, J.H., and H.G. Harris, Mathematical modeling of oil shale retorting, LETC/1761-15/1, December 1979.

6. Halcomb, R.A., A mathematical model for a horizontal in situ oil shale retort, Ph.D. Thesis, Department of Mathematics, University of Wyoming, 1980.

7. Harak, A.E., L. Dockter, A. Long, and H.W. Sohns, Oil shale retorting in 150 ton batch-type pilot plant, Rept. of Inv. 7995, Bureau of Mines, 1974.

8. Minster, R.A., and D.W. Fausett, Fluid flow through packed columns of crushed oil shale, Laramie Energy Technology Center, LETC/RI-80/5.

9. Tyner, C.E., and P.J. Hommert, Numerical modeling of a true in situ oil shale retort, Sandia Laboratories Energy Rept., SAND-78-1306, January 1979.

THE ROLE OF SITE CHARACTERISTICS IN THE CONTROL OF UNDERGROUND COAL GASIFICATION

B. E. Bader and R. E. Glass
Sandia National Laboratories
Albuquerque, New Mexico 87185

ABSTRACT

Underground Coal Gasification (UCG) offers many potential economic and environmental advantages. Offsetting these advantages is the substantial lack of ability to control the UCG process. For example, only three elements of external process control have been utilized. These are: (1) injected gas composition, (2) injected gas flow rate, and (3) product gas pressure. Variation of these independent variables in UCG tests has resulted in mixed indications of their effectiveness.

This study indicates other possible elements of control based on the results of recent field tests and modeling efforts. These elements are associated with the selection of the specific site where the process is conducted and with the design of the test itself. The results of previous UCG field tests have indicated that the conditions that exist in the coal seam and overburden before the start of the combustion process may dominate all other factors. These conditions are the geotechnical characteristics, such as faulting and groundwater hydrology, as well as the details of the test layout, well completions, and linking method.

Evidence exists to support the thesis that these preignition conditions can be dominant factors in process control of in situ operations. The data from recent UCG tests have been analyzed with respect to the effect of the site geotechnical characteristics and the test design. The results of this analysis indicate that geologic faulting, coal seam permeability distributions, well completions, and coal strength are important elements of control in the process behavior. Attempts to influence Hanna IVB by varying external process parameters could not overcome these effects. Similar results have been observed in other UCG tests.

INTRODUCTION

The success of the underground coal gasification (UCG) process depends upon the efficient and economic utilization of the resource. To accomplish this a large percentage of the available coal must be converted to gas. The results of the UCG field experiments in meeting this goal have been mixed.

One method of gasifying coal underground, which has been extensively tested in both the U.S. and the Soviet Union, is the linked vertical well (LVW) process. In this technique, a vertical injection well and a vertical gas production well are completed into the coal seam and a high permeability path (link) is created between this process well pair. A successful LVW test needs to have the link established near the bottom of the coal seam with subsequent gasification progressing most rapidly along the link. If the link and subsequent gasification occur at the top of the seam, as in an

override situation, the results are high thermal losses to the overburden and poor resource utilization. Among the methods that have been used to establish this link are explosive fracturing, directionally drilled holes and reverse combustion.

To conduct an efficient UCG process an understanding of the process and its controlling parameters is required. The only three elements of process control that have been employed are (1) the injected gas composition, (2) the injected gas flow rate, and (3) the product gas pressure. Results of the Hanna and Hoe Creek series of UCG field tests indicate that the conditions that exist in the coal seam and overburden at the start of the linking and gasification process may dominate all other factors. These conditions involve site specific characteristics such as the geotechnical characteristics of faulting and groundwater hydrology, the coal properties of strength and permeability, and the parameters of test design including well completions and linking method.

This paper combines field test and analysis results to identify a number of these site specific parameters. The discussion centers on the flow and mechanical properties of the seam. There are other potentially critical parameters and processes such as the petrographic constituents of the coal, the chemistry of combustion, and the in situ stress distribution which also can affect the quality of the UCG process.

RESULTS FROM RECENT TESTS

The Laramie Energy Technology Center (LETC) conducted a series of four UCG tests at a site near Hanna, WY.[1] Hanna I, Hanna II, and Hanna IV were designed to demonstrate and improve the LVW technology. Hanna III was designed to study the impact of UCG on groundwater quality. Figure 1 is a map of the Hanna area showing the locations of the three technology development test sites and some of the known geotechnical characteristics.

Hanna I was the initial test of the LVW process using reverse combustion linking. Following the Hanna I test, Hanna II was designed in three phases. Phase 1 was to study the reverse combustion linking process with consideration of the effects of seam anisotropies. Phases 2 and 3 consisted of reverse combustion linking of two sets of process wells spaced approximately 20 m apart. Following the linking step, each set of wells (module) was gasified. The linking and subsequent gasification progressed along the bottom of the seam with consumption of the entire vertical extent of the seam in each module. Among the reported results[2,3] was the preference for flow up dip along a minor fracture trend. This direction also corresponded to one of the four clear sets identified in the Hanna basin.

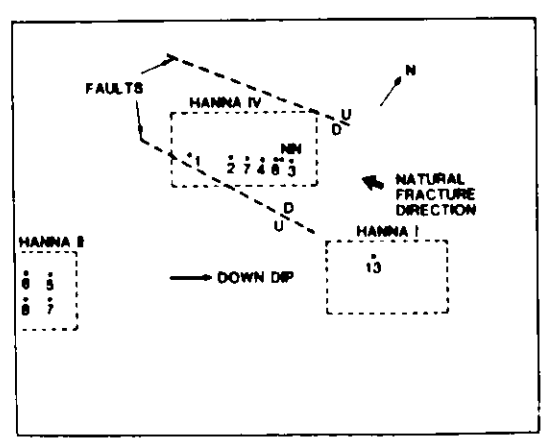

Figure 1. Hanna Test Site.

Following the successful Hanna II test, the Hanna IV[4] test was planned with the intention of increasing the process well spacing, thus improving economic prospects. The Hanna IV plan involved three steps. These were to (1) create a 30 m link between wells 1 and 2 by reverse combustion, (2) gasify along this link and concurrently create a 46 m link between wells 2 and 3, and (3) gasify between wells 2 and 3 to verify sweep width to well spacing relationships. The test encountered difficulties in the linking step with poor communication between wells 1 and 2 and with excessive water influx. Additional problems were caused by poor completion of well 2 allowing air flow along the outer wall of the well casing. The result was a link established between the process wells at the top of the seam. The subsequent gasification attempt then resulted in an override. This portion of the test was terminated and a revised plan for subsequent testing was developed. This next portion of testing was designated Hanna IVB.

In Hanna IVB, a link was established between wells 7 and 3 via a series of relayed links even though the test as designed had to propagate the combustion front across a fracture system.[5] In fact, preignition air acceptance tests for Hanna IVB showed a substantial pressure buildup in well 13 of the Hanna I test, southeast of the Hanna IVB test site. This pressure buildup presumably resulted from air communication along the fractures. Further effects of the fracture system were noted during reverse combustion when one of the links proceeded first in a direction perpendicular to, then parallel to the fracture system.

In addition to the air injection tests which determined lateral flow paths, spinner logs were used to determine the vertical permeability structure in the wells. Spinner log results[6] for well NN near process well 8, are shown in Figure 2. The figure shows high permeability zones at 4, 7 and 8 m above the bottom of the seam. Also shown in the figure are the thermal responses in well NN during reverse combustion. The figure clearly shows the correlation between the thermal front and the high permeability zone at 7 m. Other instrument wells also showed thermal activity corresponding to the other high permeability zones. Examination of the core from well 7 indicated layers of broken, shaley coal and massive coal, roughly corresponding to the high and low permeability zones shown in Figure 2.

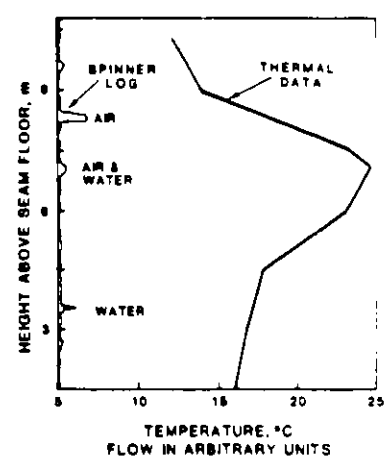

Figure 2. Preignition Spinner Log and Reverse Combustion Thermal Data in Well NN During Hanna IVB.

The Hanna IV test was not conducted in the ideal geologic setting. As indicated in Figure 1, a fracture system crossed the direction of desired linking between wells 3 and 7. Furthermore, the preignition flow logging had indicated three high permeability zones in the coal seam. The ability of two external process control parameters, flow rate and pressure, to control the process under adverse conditions was severely tested in this experiment.

Even though the linking was required to cross fractures, a link was established. However, the linking paths progressed along the high permeability zones established in the preignition flow logging. During linking each of these zones experienced thermal activity, clearly establishing the correlation between preignition permeability and the subsequent location of the reverse combustion link. Further, the gasification stage propagated along the established links. These results demonstrate the critical role the air flow patterns play in the successful operation of a reverse combustion linked UCG test.

The Hoe Creek series of tests run by Lawrence Livermore National Laboratories (LLNL) also was examined for the importance of site characteristics to the UCG process. These tests were designed to test the various linking methods. At Hoe Creek I the link was established by explosive fracturing, at Hoe Creek II reverse combustion linking was used, and at Hoe Creek III the drilled hole link was used. Of most interest are the results of the Hoe Creek III test.[7] This test used a directionally drilled hole (DDl) to establish a reliable link low in the coal seam. This was done to overcome override problems such as those experienced after using reverse combustion linking during the Hanna IV and Hoe Creek II tests.

A comparison of the results of the gasification stages of the Hoe Creek III test with the Hanna II test are of interest. Both of these tests had established links low in the coal seam, yet the results of the tests differed markedly. The Hanna II test had a combustion front that progressed most rapidly at the bottom of the seam, with subsequent consumption of the upper portion of the seam. During the Hoe Creek III test, although the drilled hole acted as desired to control the lateral direction of propagation of the combustion front, a vertical slot formed along the length of the drilled hole which resulted in a greater consumption of the coal at the top of the seam than at its base.

To investigate the phenomenon of this slot formation, LLNL performed supporting laboratory tests on cavity growth. These results[8] indicated that the preferred cavity growth direction in the Wyodak coals common to the Hoe Creek site is perpendicular to the bedding planes. This is shown in Figure 3. The mechanism responsible for these results is not understood, but is believed to be associated with the mechanical properties of the coal.

ANALYSIS

Analyses were conducted to examine the behavior of the Hanna IV and Hoe Creek III field experiments. Flow problems dominated the Hanna IV results while the most notable result from the Hoe Creek III test was the development of the slot along the directionally drilled hole. A series of calculations were performed to evaluate the effects of permeability and well spacing on air flow in a water saturated coal seam simulating some of the Hanna conditions. Another series of calculations investigated thermoelastic effects around a

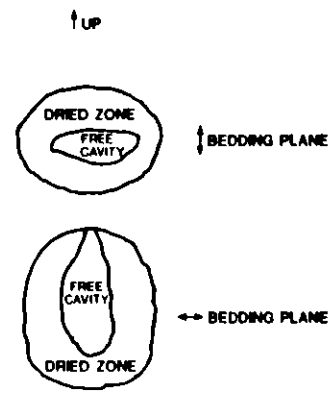

Figure 3. Cavity Growth in Wyodak Coal (After Shannon[9]).

horizontal hole in a coal seam to determine what conditions might lead to the development of a vertical slot.

The model[9] used to examine the effects of permeability and well spacing was based on the flow equations for two-phase, two-dimensional, immiscible Darcy flow. A water saturated coal seam, 230 m long by 10 m thick by 1 m wide, with impermeable boundaries was considered in the calculations. The normal permeability of the seam was assumed to be 100 md which approximates the permeability seen in flow tests on the Hanna coal.[11] High permeability zones were arbitrarily chosen to be either 250 md or 500 md. Results were calculated for air injections into the coal for the following four cases: (1) an isotropic, homogeneous seam with 100 md permeability, (2) a high permeability zone in the top meter of an otherwise homogeneous seam, (3) a high permeability zone between 5 and 7 meters, and (4) a high permeability zone in the bottom meter.

Figures 4 and 5 show the results for air injection into the seam for two of the cases. The injection and production points are indicated on the figures by the triangles along the abscissa with air being injected in the left triangle. The shaded areas represent the high permeability zones. The movement of the air front is represented by the 25% air saturation contour. This contour was selected as representative of the progress of the air front as it displaced water in the seam. In all the cases with a high permeability

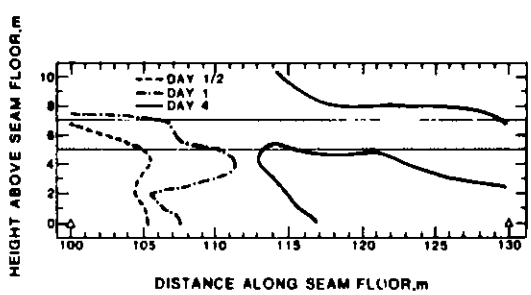

Figure 4. Air Front Movement with a High Permeability Zone, k = 250 md (Shaded) at Midseam.

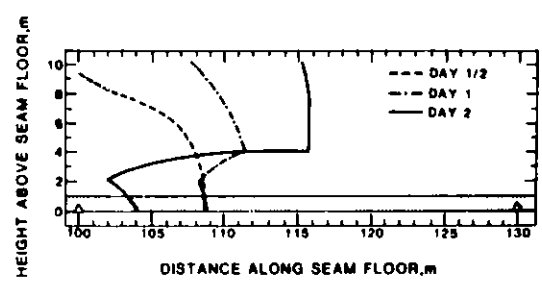

Figure 5. Air Front Movement with a High Permeability Zone, k = 500 md (Shaded) at the Bottom of the Seam.

zone, the dominant air flow was off the bottom of the seam due to bouyant forces separating the water and the air. This effect is most notable in Figure 5. In this case, even though the high permeability zone is at the bottom of the seam, it remains filled with water forcing the air to rise and flow in the less permeable region of the coal. The impermeable boundaries used in the model leave only the production well as a water outlet and this could cause the water/air flow separation to be greater than would actually be the case. However, the results of the calculations do give flow paths similar to the linkage paths seen during the Hanna IVB test in that the high permeability zones at midseam and above experienced most of the activity.

Other permeability structures also were considered. Tests on the Hanna basin coals indicated that it has orthotropic permeability characteristics.

To examine the effect this has on the flow paths, two cases were run: (1) K_x = 500 md and K_z = 100 md and (2) K_x = 100 md and K_z = 500 md, where the x-axis is coincident with the seam floor and the z-axis is vertical. Figure 6 shows that the case of high horizontal permeability led to the most favorable air flow paths.

On day 1, the air front was expanded in a roughly circular form with some bouyancy induced vertical elongation. By day 3, it has reached the roof of the seam and is moving as a vertical front, before the front has progressed even half way towards the production well. In contrast, at the end of the first day for a 10 m spacing, the front has already extended to the process well without reaching the roof of the seam. The air front subsequently reaches the roof of the seam. A thermal front following this pattern would yield the favorable results experienced during the Hanna II test.

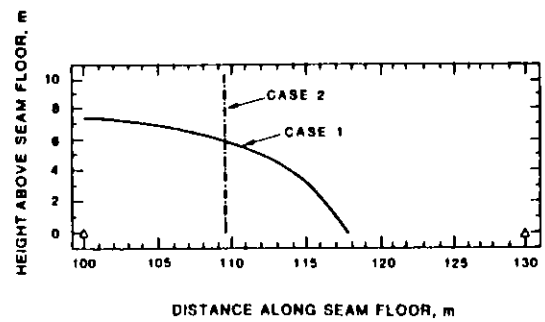

Figure 6. Air Front Through Orthotropic Coal. Case 1, k_x = 500 md, k_z = 100 md. Case 2, k_x = 100 md, k_z = 500 md.

To determine possible causes for the preferred growth direction behavior seen in the Hoe Creek III field test and the LLNL laboratory tests, thermoelastic effects were investigated. The anisotropic thermomechanical[12] effects were investigated using thermal[13] and structural[14] finite element programs. In particlar, the effect of orthotropic strength was investigated. It has been established for some coals that the ability to withstand stress is a function of loading direction. In particular, it has been shown that some coals will fail under a tensile loading perpendicular to the bedding plane at a lower stress level than if the load is parallel to the bedding plane.[15] To investigate the effect of this phenomenon in a UCG test, it is necessary to generate the stress distribution resulting from overburden and thermal loads. To determine the region where failure (cracking) will occur, a yield stress is assumed for each direction and only in that area where the directional stresses exceed the yield stresses will cracking occur.

The test case consisted of a 10 m thick by 100 m wide coal seam resting on an elastic rock bed. A horizontal hole, 0.15 m in diameter was centered 1.075 m off the seam floor. The thermal and mechanical properties for coal were $E = 3.792 \times 10^6$ Pa, $\nu = 0.44$, $\alpha = -1 \times 10^{-6}/°C$, $k = 0.2083$ w/mK, $\rho c = 1513$ J/Km^3; and for rock $E = 7.068 \times 10^6$ Pa, $\nu = 0.22$, $\alpha = 0./°C$, $k = 1.869$ w/mK, $\rho c = 1535$ J/Km^3. The overburden pressure was assumed to be 10^6 Pa and the temperature boundary in the hole was assumed to be 1000°C with conduction as the only heat transfer mechanism. The minimum tensile yield strength was assumed to be 10^6 Pa and the tensile yield strength in the perpendicular direction was assumed to be 10^7 Pa.

The temperature distribution and the overburden pressure result in a stress distribution about the hole. Figure 7 shows the region where cracking will occur as a function of the direction of minimum yield strength.

While only the loading strength has been examined, there exist several other thermomechanical properties of coal which may be significant. These include (1) anisotropic thermal conductivity, (2) anisotropic Young's modulus, and (3) the temperature dependence of the structural properties. In a real test all of these properties will play a role in determining the manner in which a test progresses.

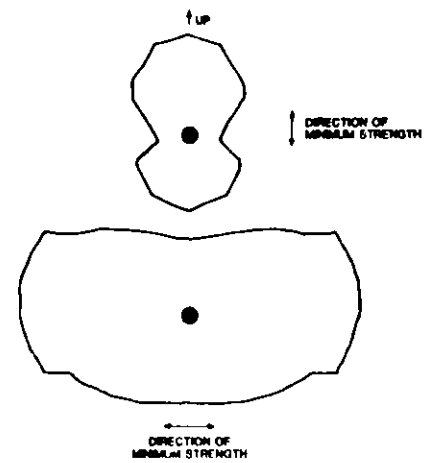

Figure 7. Region Where Cracking Occurs as a Function of the Direction of Minimum Yield Strength.

CONCLUSIONS

The results of field tests and modeling efforts show several site specific parameters that can determine the degree to which any UCG test will be successful. These can be identified broadly as the flow and mechanical properties of the seam. Specifically the following characteristics have been shown to be important: (1) permeability structures and mobile water play a crucial role in determining air flow paths, (2) an enhanced permeability zone at the bottom of the seam may inhibit the proper flow of air if mobile water is present, (3) high permeability zones at midseam and above will act as the primary air flow path, (4) the spacing of injection and production wells can be varied to enhance the chance of keeping the air flow paths low in the seam, (5) completion of the process wells in a manner that minimizes neighboring permeability inhibits the chance of override, (6) the orthotropic permeabilities of coal improve UCG test results, (7) the thermomechanical properties of coal are important with respect to the manner of combustion front propagation, and (8) heating will result in stress distributions in the coal with resulting cracking dependent on the anisotropic strength characteristics of the coal.

While this discussion has centered on the flow and mechanical properties of the coal, there are other properties characteristic of a given coal which may also prove to be important to the process. These include the petrographic constituents of the coal, the chemistry of combustion, and the in situ stress distribution. All of these factors point to the importance of carefully characterizing future UCG sites to determine the role these parameters play in the process. This will then lead to the establishment of criteria for selecting UCG sites with a high probability of efficient use of the resource.

NOMENCLATURE

E = Young's Modulus
K = thermal conductivity
ρc = product of mass density and specific heat
ν = Poisson's Ratio

REFERENCES

1. Covell, J. R., L. F. Wojdac, F. A. Barbour, G. W. Gardner, R. E. Glass, P. J. Hommert, "Results of the Fourth Hanna Field Test", Proceedings of the Sixth Underground Coal Conversion Symposium, July 13-17, 1980.

2. Brandenburg, C. F., D. D. Fischer, D. A. Northrop, L. A. Schrider, "Results and Status of the Second Hanna In Situ Coal Gasification Experiment", Proceedings of the Second Underground Coal Conversion Symposium, August 10-12, 1976.

3. Hommert, P. J. and G. S. Beard, "Descriptions of Reverse Combustion Linkage and Forward Gasification During Underground Coal Gasification", SAND 76-9317, February 1977.

4. Bartke, T. C., L. Dockter, T. E. Sterner, J. E. Virgona, L. F. Wojdac, "Status Report on the Hanna III and Hanna IV Underground Coal Gasification Experiments", Proceedings of the Fourth Underground Coal Conversion Symposium, July 17-20, 1978.

5. Bartel, L. C., "Instrumentation and Process Control Development for In Situ Coal Gasifiction Sixteenth Quarterly Report: September 1978 - November 1978", SAND 79-0706, April 1979.

6. Bartel, L. C., "Site Selection and Characterization for an Underground Coal Gasification Process", Proceedings of the Fifth Underground Coal Conversion Symposium, June 18-21, 1979.

7. Hill, R. W., C. B. Thorsness, R. J. Cena, W. R. Aiman, D. R. Stephens, "Results From the Third LLL Underground Coal Gasification Experiment at Hoe Creek", Proceedings of the Sixth Underground Coal Conversion Symposium, July 13-17, 1980.

8. Shannon, M. J., C. B. Thorsness, R. W. Hill, "Early Cavity Growth During Forward Burn", Proceedings of the Sixth Underground Coal Conversion Symposium, July 13-17, 1980.

9. Glass, R. R., "Applications of Reservoir Simulation to In Situ Coal Gasification", SAND 80-2579, February 1981.

10. Fulton, P. F., and A. A. Reznik, "The Measurement of the Flow Properties and Capillary Pressure Relationships of Certain Coals Pertaining to Underground Coal Gasification Final Report, September 1976 November 1977", Contract No. EY-76-5-02-4129, December 1977.

11. Shoemaker, H. E., "Mechanical Properties of the Pittsburgh Coal at Elevated Temperature", Doctoral Dissertation, West Virginia University, 1976.

12. Klaus-Jurgen Bathe, "ADINAT A Finite Element Program for Automatic Dynamic Incremental Nonlinear Analysis of Temperature", May 1977 (Rev. Dec. 1978) Massachusetts Institute of Technology, Rept. 82448-5.

13. Klaus-Jurgen Bathe, "ADINA A Finite Element Program for Automatic Dynamic Incremental Nonlinear Analysis", September 1975 (Rev. Dec. 1978) Massachusetts Institute of Technology, Rept. 82448-1.

14. Berenbaum, R., and I. Brodie, "Tensile Strength of Coal", J. Inst. Fuel, 1959, Vol 32, pp 320-327.

Wednesday Morning, June 10, 1981

Session B - PROCESS CONTROL - Part 3

REMOTE ACOUSTIC AND ELECTROMAGNETIC DIAGNOSTICS FOR OIL SHALE PROCESSING

Joel DuBow,* Tom Mraz, Krishnan Rajeshwar and Sang Hong
Electrical Engineering Dept.
Colorado State University
Fort Collins, Colorado 80523
(303)491-8235

ABSTRACT A055

Indirect measurements of fossil fuel processes offer the advantages of spatial averaging over the process bed and no contact with the severe conditions inside the process zone. Thus localized conditions or boundary layer effects near vessel walls are less likely to lead to erroneous readings and radial gradients can be more readily detected. However, accurately interpreting data obtained in both forward (system assumed) and inverse (input and output assumed) operating modes is essential to the successful application of these techniques. Data interpretation is critically dependent on the accuracy of forward wave propagation models since no inverse model can resolve features that aren't described in the forward model. The forward model, in turn, is critically dependent on accurate knowledge of the thermophysical properties of the feedstock.

The acoustical and electromagnetic properties of oil shale and tar sands exhibit significant and systematic variation with temperature, pressure, organic content, moisture content and packing of the process bed. These variations are reviewed, as well as properties models of the heterogeneous packed beds encountered in above and below ground processes. Acoustic and electromagnetic wave propagation calculations using average or "effective" constitutive properties for the bed will be compared to these using experimentally determined bed properties. These results will be discussed in view of evaluating the feasibility and information content obtainable from acoustic and electromagnetic diagnostics of oil shale and other fossil fuels.

*Presenting Author

THE USE OF LABORATORY AND PILOT SCALE DATA IN THE DESIGN AND CONTROL OF COAL PREPARATION FACILITIES

David J. Akers
William H. Buttermore
Coal Research Bureau
College of Mineral and Energy Resources
West Virginia University

INTRODUCTION

The operation of a conventional coal cleaning plant poses many difficult control problems. These problems have two related sources. First, the feed coal to the plant will vary greatly in terms of both its physical and chemical characteristics. This variation may be caused by the need to process coals from several different mines within a single plant; however, the cleaning characteristics of coal from various sections of the same mine may be significantly different. The second problem source relates to the lack of instrumentation to provide a constant and immediate knowledge of the performance of a cleaning unit operation. It is possible to characterize both the feed and product coal chemically by, for example, the new methods of on-line nuclear analysis. The separation being performed is, however, a physical separation rather than a chemical process and the relationship between the chemical analysis of a coal and its cleaning characteristics is tenuous at best.

Most conventional coal cleaning unit operations have been in use for many years and are often operated by various rule of thumb procedures. These procedures are generally effective, but may not be highly efficient in terms of fuel value lost with the refuse or in handling difficult cleaning situations.

The Coal Research Bureau, College of Mineral and Energy Resources of West Virginia University has responded to these problems by developing an extensive facility for research in coal preparation using both laboratory and pilot scale coal cleaing equipment. This paper contains a discussion of the design of this facility, current research projects, and methods of applying data produced at a laboratory of this type to real world coal cleaning situations.

LABORATORY AND EQUIPMENT DESIGN

The design of the coal preparation laboratory at West Virginia University is based on the use of each piece of equipment as a unit operation. Effects of each cleaning, sizing, or classification operation can be easily monitored in this way; and since most of the equipment is portable it can be stored in a relatively small area when not in use.

A 40 x 60 foot building houses the majority of the pilot scale cleaning, sizing, and crushing equipment as well as providing space for sample processing and storage. Some operations such as sample container preparation, flotation testing, and fine sieve analyses are performed elsewhere.

In the center of the building, 600 square feet of floor space enclosed on either end by a loading door facilitates the processing of bulk samples of coal. It is normally necessary to process 4,000 to 5,000 pounds of raw coal to provide representative samples for pilot scale evaluation. Crushing equipment is located adjacent to the central processing area and includes a toothed double-roll crusher, single roll crusher, jaw crusher, and cone crusher to handle coal of any size.

Also, a working sample storage area of 800 square feet is provided to store the different processed size fractions of coal to be evaluated. On one end of the building an overhead loft of 150 square feet is used to store empty sample containers; on the other end of the building water for various unit operations is fed from a 200 gallon capacity head tank fourteen feet above floor level. Aisle space sufficient for fork lift access is maintained throughout the facility.

Through the years laboratory and pilot scale coal cleaning equipment have been procured by the Coal Research Bureau for research efforts. Recently, under contract with the Department of Energy to investigate the effects of minerals on coal beneficiation processes, this equipment was assembled at a pilot plant facility in Westover, West Virginia. Two cleaning circuits were created for the evaluation of coal samples. The first, a water-only circuit, includes a pilot scale jig and table and a bench scale froth flotation unit. The single compartment, three-cell baum type jig (Figure 1) was built in 1949 by McNally-Horton and is the only one of its size known to exist today. Feed to the jig (about 1000 lbs/hr.) is limited to the 1" to 3/16" size range. Pulsion and suction effects are regulated by water flow and air pressure to each of the three cells. Coarse refuse is conveyed from the bottom of the bed through a float controlled gate to the bucket elevator and out the refuse chute. A screw in the bottom of the hutch conveys anything that passes the 3/16" holes in the plate which supports the coal bed into the sump and out the bucket elevator with the coarse refuse. Careful sizing of the feed coal minimizes the loss of fuel value with the refuse.

For 3/16" x 100 mesh coals, a small Diester concentrating table (Figure 2) is used. This unit is fed through a distributor tank where a 30% slurry concentration is maintained. The small ridges on the table are called riffles, and gradually decrease in height from approximately 1/4" on the drive end to nothing on the refuse end of the table. Water fed onto the table is adjusted to carry particles of coal across the riffles as they are stratified by the horizontal reciprocating motion of the deck. The end result is a concentration of coarse coal near the feed end of the table grading to finer coal mixed with some refuse at the corner. Refuse is discharged from the end of the table, the finest refuse reporting to the end on the feed or higher side of the deck. The angle of the deck in the plane of the main water flow can be varied from horizontal to about 20 degrees; the angle from drive to discharge usually is sloped upward one or two degrees. Water flow rate, and amplitude and frequency of stroke complete the operating adjustments on the table. The table must be adjusted separately by hand and eye to produce the desired separation for each coal cleaned. Cleaned

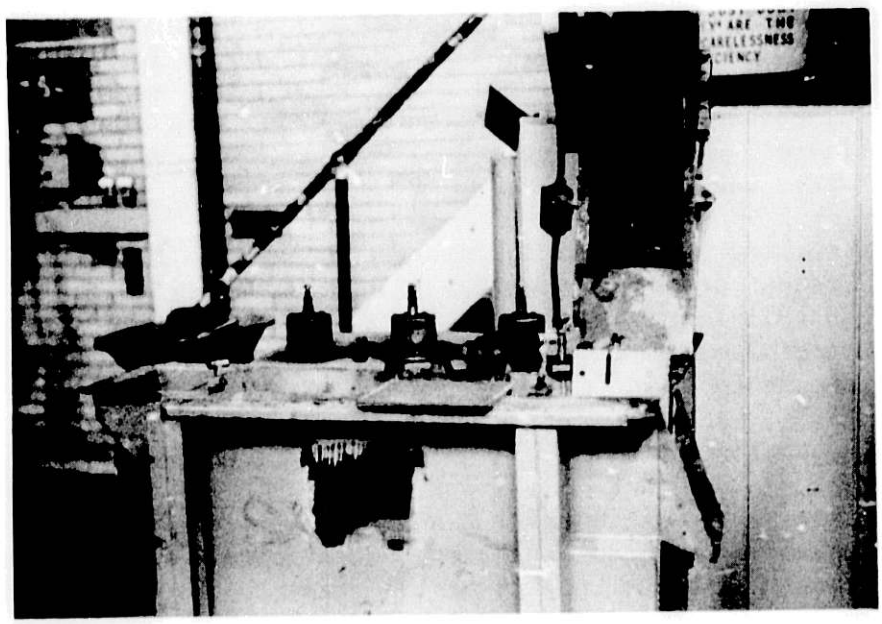

Figure 1 - Baum Type Jig

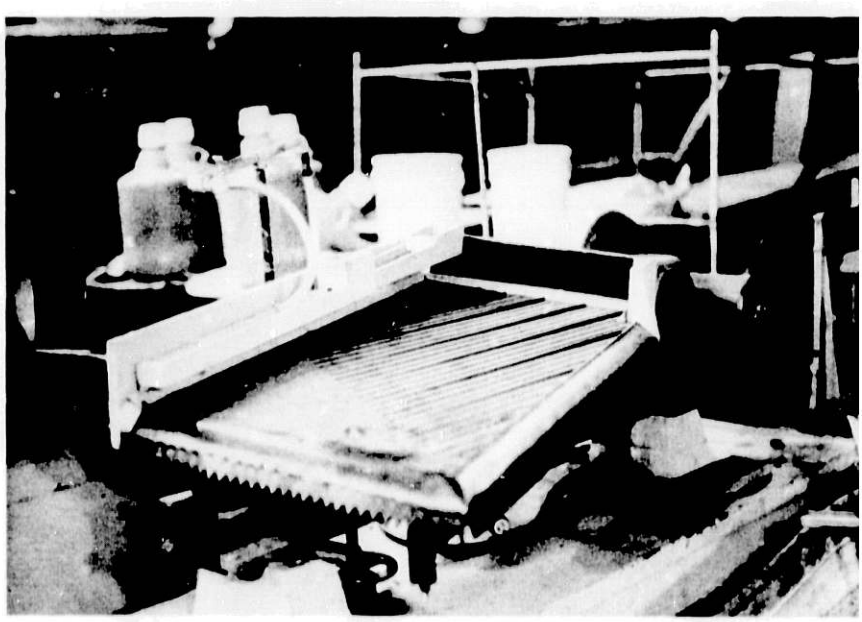

Figure 2 - Diester Concentrating Table

coal is collected in gutters along the front and side of the table. Partitions in the gutters allow control of middling product (coal mixed with refuse) for each sample tested.

Completing the water-only circuit is froth flotation. Froth flotation is used to clean the -100 mesh fraction of raw coal. For bench testing, a representative sample is separated from the raw coal. Methyl isobutyl carbinol and kerosene are normally added in a small quantity to the slurry to enhance the flotation of coal from the refuse. In this process coal particles attach themselves to small air bubbles introduced in the bottom of the agitated slurry and are subsequently carried to the surface to form an easily removed froth of fine coal leaving the refuse behind in the bottom of the cell as tailings. As in tabling and jigging, operating parameters, which include slurry density, agitation speed, and reagent quantity and type must all be tailored to the coal being cleaned.

The second part of the pilot plant is the dense media circuit and includes a 200 gallon sump and pump, a Wemco dense media drum separator, and a Heyl Patterson three-inch dense media cyclone. The Wemco separator (Figure 3) is used to clean coals in the 1" to 10 mesh size range. A slurry of the desired density is first prepared by mixing grade "B" magnetite (90% - 325 mesh) with water. A double propellor mixer keeps the slurry uniform and a variable speed pump feeds the drum. Welded along the interior of the drum are refuse shelves which remove the heavier material that has fallen to the bottom of the dense media as the drum rotates. As the shelves approach the top position of their revolution, the refuse drops into a chute, the top of which is water fed to assist in the removal of refuse. The refuse chute passes through a hole in the end plate which is smaller than the product discharge end to force the product out with the media overflow. Operating controls include drum speed, specific gravity of media, and feed rate. Both refuse and product (which exit on opposite ends of the machine) are passed over a drain and rinse screen to recover the magnetite and clean the product. This unit operation is fed pre-wet coal manually and has been shown to produce results similar to values predicted by coal washability data.

For dense media cleaning of fine coals (10 mesh by 100 mesh) a three inch Heyl Patterson dense media cyclone is used. This unit is portable and includes its own sump, pump, feed control and by-pass valves. Adjustment is made by varying the pressure of the feed pump. The cyclone will operate at inlet pressures as low as 8 psi, but the reduction of impurities in the product coal is improved at higher pressures. The cyclone consists of a three inch diameter cylindrical section above a conical section as shown in Figure 4. The mixture of media and raw coal enters tangentially near the top of the cyclone and forms a strong vortical flow. Centrifugal force speeds the movement of the refuse through the dense media to the wall of the cyclone where it is discharged through an orifice at the bottom. The coal moves toward the center of the cyclone where it enters the ascending vortex and is discharged through an outlet at the top. Drain and rinse screens are used to recover the magnetite.

CURRENT RESEARCH PROJECTS

Conventional coal cleaning technology commonly exploits a difference in

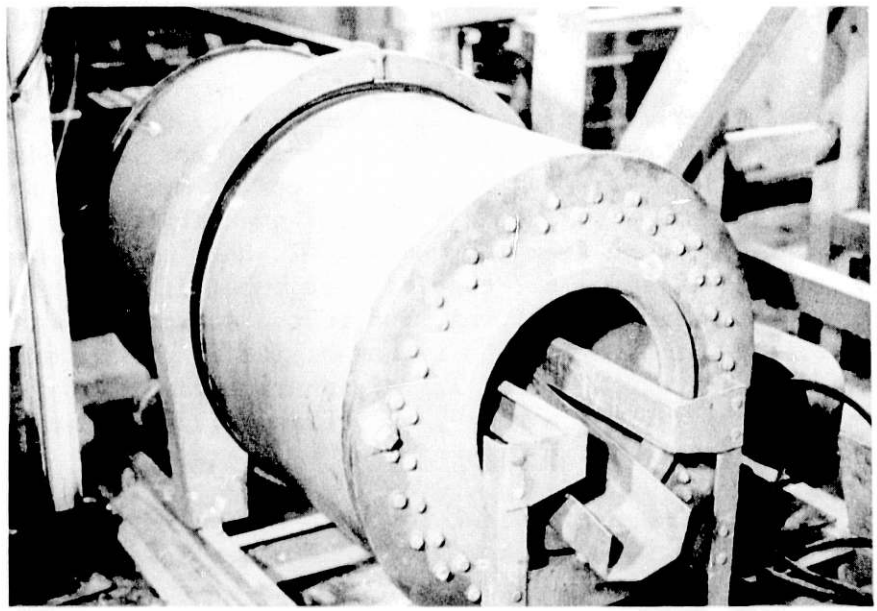

Figure 3 - Wemco Dense Media Drum

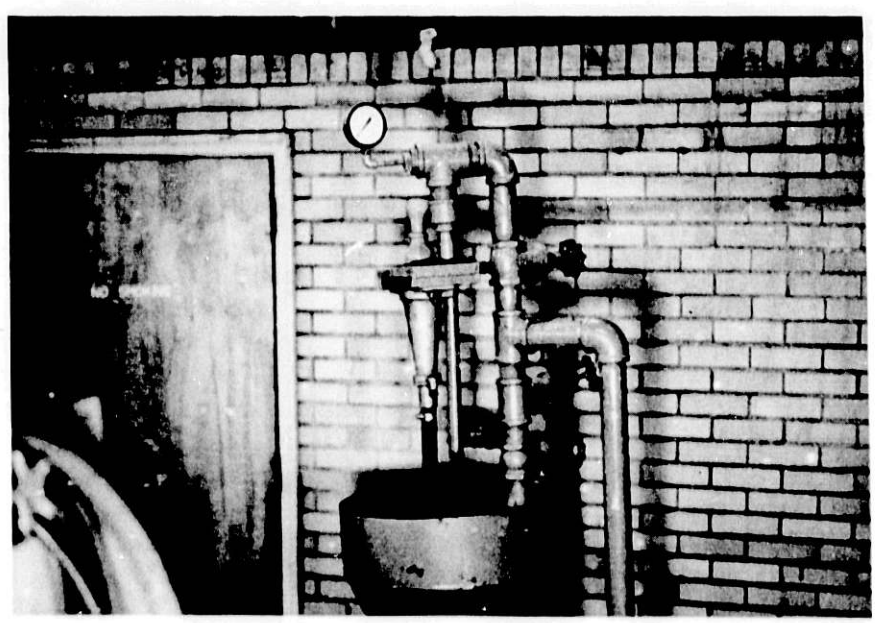

Figure 4 - Heyl Patterson Dense Media Cyclone

specific gravity to effect a separation. This emphasis on specific gravity is reflected in the common reliance on laboratory washability tests which measure the specific gravity distribution of a coal sample. There are, however, other variables including particle settling characteristics which affect preparation plant performance.

The movement of regularly shaped particles through fluids has been investigated in some detail. Theoretical treatments of the movement of coal particles in fluids assume regular shapes, generally spherical. The movement of irregularly shaped coal particles through a fluid has only received passing attention because of the complexity of the problem. The Coal Research Bureau, operating on funds provided by the West Virginia University Energy Research Center, has been involved in a project designed to develop practical methods of evaluating coal and coal waste particle settling characteristics and to apply the information gained to the development of improved methods of preparation plant design and control. The present area of research emphasis involves the use of a density gradient column to measure the specific gravity of coal particles and to determine their settling characteristics at various media temperatures. While this paper is not intended to provide detailed information about a single project, a sample of the type of information to be gained from this work may be helpful for the purpose of illustration. Some coal particles have been found, for example, to follow a helical (spiral) path during settling in a fluid. The percent of coal particles which commonly follow this path is at present unknown; however, preliminary evidence indicated that a significant number (1 to 10%) do follow a helical path. Particles which follow a helical path during free settling (type h particles) will be prevented from doing so during hindered settling by the presence of other particles. However, type h particles still tend to develop a significant velocity at some angle to the vertical even during hindered settling, resulting in a number of collisions between type h and other particles. It appears that the "interference effect" of type h particles on the settling rate of a mass of coal particles is higher than would be projected by consideration of number of type h particles only. Coals which contain large numbers of type h particles are then perhaps more likely to create operational problems, especially in all water cleaning processes, than are coals which do not.

A second current research project, funded by the Department of Energy, concerns in part the determination of the effects of beneficiation processes on the minerals in coal. Representative samples of raw coal from preparation plants cleaning three major coal seams were analyzed for major mineral distributions. These coals were run through each piece of pilot scale equipment to determine how the distribution and concentration of minerals were affected. Jig tests on Pittsburgh seam coal revealed, for example, that the concentration of illite in the product coal was reduced significantly while the concentration of kaolinite was significantly increased. This information implies that jigging is less effective in removing kaolinite from Pittsburgh seam coal than it is in removing illite. The research phase of this project has been completed and the final report is now being prepared.

APPLICATION OF RESEARCH DATA

In order to indicate how data from a coal cleaning research facility

can be used to correct control problems in existing coal cleaning plants, two examples are presented. These examples are not true case histories, but are intended to represent the types of problems encountered over a number of years of research experience and to illustrate how laboratory and pilot scale data may be applied in their control.

In the first case difficulty was encountered at a coal preparation plant relating to fluctuations in product quality. Routine analysis of product coal sometimes revealed coal of unacceptable quality, although generally the product met the contractual specifications. Blending of product coal to eliminate the problem of periodic low quality was not considered feasible because the periods of quality decrease appeared to be random and constant monitoring of the product stream was not practical.

Initially, ultimate and proximate analysis were made on stop belt samples of both the plant feed and the product coal allowing a time lag between samples equivalent to the retention time of the coal in the plant. The results of this analysis did not detect any change in feed coal chemical parameters which could be used to explain the variations in the quality of the product. Next, stop belt samples were taken of the run-of-mine coal from each of the working sections in the mine. In addition to ultimate and proximate analysis of these samples, a standard washability test was performed on the coal from each section. The coal from one section was found to contain approximately 20 percent near gravity material, enough to create a large amount of misplaced material in an all water cleaning plant. In the other sections of the mine, the amount of near gravity material was normally less than 10 percent. The problems with the product coal occurred during periods in which, because of operational problems or delays in the other sections, the feed to the preparation plant was predominantly coal from the section with a high near gravity content. Two options were available to deal with this problem. The first option involved isolating the coal from the problem section and treating it separately under different operational parameters. While this option would be difficult to manage from a control standpoint, it would provide for an increased yield from the problem coal. The option which was taken involved the construction of surge bins for each section controlled such that the problem coal was blended roughly with the other coals on the main belt to produce a more uniform plant feed. This solution was augmented by an increased awareness by production personnel of the need for careful scheduling of anticipated operational delays in each section. The creation of a more uniform plant feed did not decrease the total amount of misplaced material during cleaning, but did allow the production of a clean coal of uniform quality.

In the second case a plant employing a dense media static vessel as a primary coal cleaning unit operation was experiencing problems with a lowered quality of product coal. Examination of the plant, conventional washability analysis, and screen analysis detected no obvious problems. Pilot scale testing of the coal in a Wemco dense media drum initially indicated no problem. The product and refuse material from the drum approximated the composition predicted by the washability analysis; however, during the course of the testing, the quality of the product began to deteriorate. This deterioration could not be explained by examination of the dense media drum's operational parameters. It was noted that after the first course of

tests, the coal would produce a great deal of black water upon being rinsed on a screen. Some of the black water was caused by residual magnetite, but many of the particles in suspension were found to be non-magnetic. A sample of the non-magnetic portion of the suspension was examined with an optical microscope and by S.E.M. and found to be primarily kaolin type clay along with some very fine coal particles. The kaolin type clay was not released from the coal matrix until the coal had been first wetted and then subjected to some attrition during handling. The effect of the fine clay particles on the dense media operation was primarily to increase the viscosity of the media and thereby reduce settling rates. This reduction in settling rate created a situation in which refuse material fairly near the gravity of separation would be discharged with the product coal, resulting in increased ash and sulfur content of the product.

This problem was solved by a two-fold approach. First, the coal was wet screened before entering the dense media circuit to liberate and then remove the clays. Second, after the coal had passed through the dense media bath and entered the magnetite recovery circuit, the underflow from the rinsing screen was processed to prevent any fines created during cleaning from being recycled with the magnetite. This underflow was first passed between two magnets to promote flocculation and then to a thickener. The thickener underflow was passed under two magnetic separators to remove and recycle the magnetite and the non-magnetic particles were discharged into the refuse circuit.

SUMMARY

Conventional coal cleaning processes are often difficult to regulate because of variations in feed coal characteristics and the lack of sophisticated control instrumentation enjoyed by many industrial processes. In order to compensate for these problems, extensive laboratory and pilot scale testing is required. Also, research of a basic nature which would lead to improved control technology is needed. The Coal Research Bureau is involved in both basic and pilot scale research with the goal of providing the coal industry with improved methods of coal cleaning process control.

MICROCOMPUTER CONTROL OF A CONSOLIDATION/INVERTER SYSTEM FOR COMBINED CYCLE MHD POWER GENERATION

R. Johnson, K. Marcotte, K. Crisafulli, and B. Jordan
Department of Electrical Engineering and Computer Science
Montana State University
Bozeman, Montana 59717

ABSTRACT

Coal-fired MHD/steam combined-cycle power plants possess potential for significant efficiency improvements in comparison to conventional coal-fired steam power plants. MHD (magnetohydrodynamic) topping cycles produce d.c. (direct current) power which must be converted to a.c. (alternating current) power for use in utility distribution systems. In order that the number of d.c. to a.c. converters (inverters) be minimized it is also necessary to consolidate many MHD d.c. electrode power output before inversion to a.c. power.

This paper describes a distributed microcomputer control system for dynamic control of a model MHD consolidation/three-phase a.c. inverter system which is presently under study. All facets of the operation of the consolidation/inverter are under computer control including the characteristics of a MHD generator simulator (four programmable power supplies) and a programmable load bank. The paper describes in detail the operation of the system and the implications for real-time control of the consolidation network, power factor, maintenance of MHD generator arc suppression, and higher order harmonic suppression.

INTRODUCTION

Montana State University, under DOE contract* is studying various consolidation/inverter system designs for use in MHD/steam power plants. The process of collecting the multielectrode current outputs of an MHD Faraday connected generator into a single d.c. source is called consolidation. The process of converting a d.c. source of energy to single or three-phase a.c. is called inversion.

Since a MHD/steam power plant produces a.c. power both from the MHD inverted topping cycle and a conventional steam driven generator bottoming cycle, the system requirements for generator integrity control and load regulation are quite different from the usual d.c. to a.c. systems in use on high voltage d.c. transmission lines. In particular, it is desired that an MHD consolidation/inverter system should provide as many of the following features as desireable: (1) the ability to work at different power input levels and generator impedance levels at relatively high efficiency, (2) the ability to aide in the clearing of inverter and power grid induced faults on the system for maximum generator integrity, (3) the ability to provide some output voltage and frequency control, and (4) the ability to provide

*DOE Contract No. DE AC07-78-ET-10816

VAR adjustment or power factor control.

One type of system which accomplishes many of these capabilities is a Rosa[1] type consolidation system followed by a force-commutated three-phase inverter system; an experimental 18KW system of this type has been built at MSU and is shown in Figure 1. Figure 2 shows a block diagram of the major components of the system including the microcomputers utilized for control of the system. The MHD Faraday voltage in the system is simulated by a set of four programmable power supplies which are controlled by a LSI 11/03 microcomputer. This permits the simulation of interelectrode noise voltages as well as gas-to-electrode arcs. A Hall voltage also exists between adjacent electrode pairs and this is simulated using storage batteries with series diodes to block circulating currents. The figure also indicates measurement transducers connected between the power supplies and the computer; an actual MHD system may have total end-to-end Hall voltage of several thousand volts so that the computer system is optically isolated from the inverter system. The resistance shown in series with the power supplies serve the dual purpose of permitting the measurement of current and the adjustment of the internal power supply impedance so that load line characteristics are representative of an actual MHD generator. The particular MHD system chosen for simulation is the Stanford University High Temperature Gas Dynamic Laboratory low field generator on which the consolidation/inverter system will be tested in July.

A programmable load is also included in the system; this permits the study of power grid induced transients on the system.

THE CONSOLIDATION SYSTEM

Figure 3 shows the consolidation circuit. This circuit uses the mutual inductance of autotransformers (T1, T2) along with a commutation capacitor C to equalize the Hall voltages between adjacent electrodes so that the currents can be combined. The frequency of commutation is in the range of 12 to 20 KHz and is load dependent. Ignition frequency of the SCR's (A,B,C,D) is controlled by a Z80 microcomputer. The optimum number N of electrodes to consolidate per inverter is not known but will depend on the cost of inverters in comparison with the risk of single interelectrode fault disabling all of the electrodes in a consolidation group. It is expected to lie in the range of 4-to-16 electrode pairs. The electrode interconnection shown provides zero average flux in the transformer cores. The polarized connection of the various transformer windings causes the flux generated by one half-cycle to be cancelled by the flux generated by the alternate half-cycle. This prevents the cores from saturating which would cause the inductance to become very small and force the electrode currents to diverge significantly.

THE INVERTER SYSTEM

Typical inverter systems used for the d.c. to a.c. conversion process at the receiving end of a high voltage transmission line are of the natural or line commutated configuration; the natural extinction of the SCR current as the voltage becomes negative permits the SCR control gate to

open the SCR. Such inverter systems always possess lagging power factor characteristics with the resultant necessity of power factor correction using large static capacitor banks. By the incorporation of a suitable LC commutating circuit of the McMurray type[2] as shown in Figure 4 it is possible to open the SCR's at nearly arbitrary values of current with a resultant gain in power factor control. It is possible, with suitable design, to operate this inverter system in a leading power factor mode which reduces the capital cost and increases the power capacity of the transmission system to which it is connected. The forced-commutated system also provides load voltage control, rapid response to either power grid or channel disturbances, and control of inverter generated harmonic voltages.

The inverters used are a slightly modified version of the standard McMurray inverter circuit. The standard McMurray inverter requires the input power source to supply large commutation transient currents which appear throughout the system. Diodes DA and DB along with capacitors CA and CB were added to reduce the interaction of these transient commutation currents with the power source. The three-phase inverter system constructed consist of three parallel connected inverters that drive a delta-delta connected transformer bank as shown in Figure 5.

Three Z80 microcomputers are used to provide the timing of the SCR firing signals to the three single-phase inverters that make up the three-phase system. The use of these microcomputers (see Figure 6) makes it possible to control the frequency of the a.c. output in a much more flexible method than presently possible with conventional rotating generators.

The program space in each Z80 is divided into two areas: a programmable-read-only-memory (PROM) space containing the overall monitor or operating system program for the Z80 and, a random access read-write memory (RAM) which contains the actual timing algorithm for the SCR's firing control. This subdivision was implemented in order to decrease the program development time on the system. The operating systems of each Z80 are identical and never needs changing whereas the timing and control algorithms are constantly being revised. All of the source programs for the Z80 are kept on the LSI 11/03 disk and may be edited and crossassembled on the LSI 11/03 for downloading into Z80 RAM if revisions are necessary. This greatly accelerates the program development process.

All of the microcomputers that provide inverter SCR firing signals are synchronized by interrupt signals generated by comparator circuits and a clock reference-counter (see Figure 7). The clock reference circuit can be synchronized to a system standard frequency clock. In addition, because each Z80 only needs to control a single phase of the inverter system, it possesses sufficient speed to permit notch filtering of the power output.

The computer controlled inverter output waveform is shown in Figure 8. This notch waveform was selected to remove the fifth and seventh harmonics while maintaining a symmetrical output. A typical set of unfiltered output load voltage waveforms for phase A,B, and C respectively are shown in Figure 9. The symmetry of the notch waveform yields even order harmonic removal. The delta-delta connected transformers bank provides cancellation of the third harmonic and multiples of the third harmonic. A linear amplitude

frequency spectrum through the 13th harmonic is shown in Figure 10. The three spectral peaks are related to the fundamental (60 Hz), 11th and 13th harmonics respectively. Note the absence of the second through tenth harmonic components. Figure 11 is a logarithmic presentation of the output spectrum through the 47th harmonic. In a commercial system, a low pass filter system cutting off all frequencies above the tenth harmonic would be utilized.

CONCLUSIONS

A distributed computer controlled consolidation/inverter system has been constructed. The system can be programmed to control a.c. output frequency, voltage output level, power factor, and to provide some selective higher harmonic suppression. Additional fault control management capability is being studied.

REFERENCES

1. R. Rosa, "Voltage Consolidation and Control Circuits for Multiple-Electrode MHD Generators," 15th Symposium Engineering Aspects of Magnetohydrodynamics, Philadelphia, 1976.

2. B. D. Bedford, and R. G. Hoft, "Principles of Inverter Circuits," John Wiley and Sons, Inc., 1964.

Figure 1. Consolidation/Inverter System

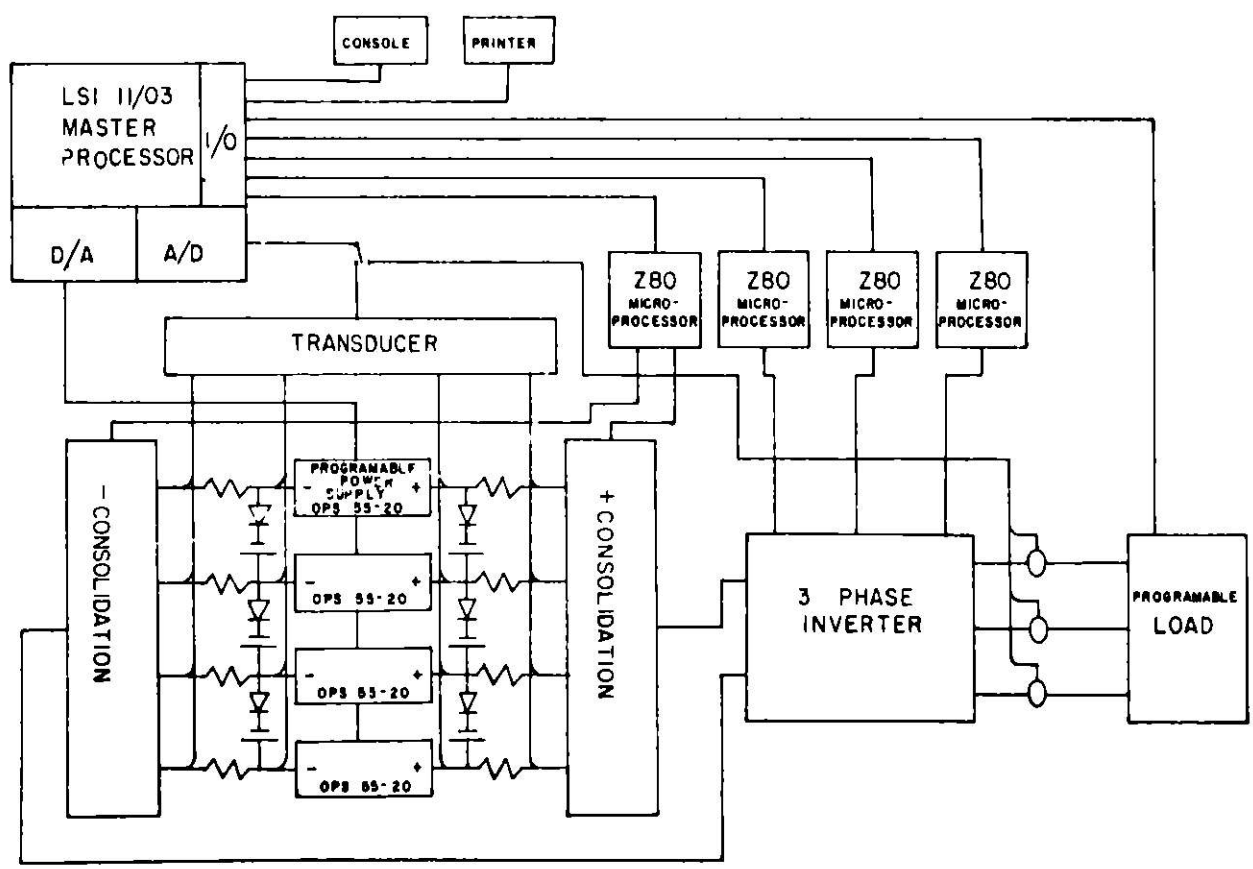

Figure 2. System Block Diagram

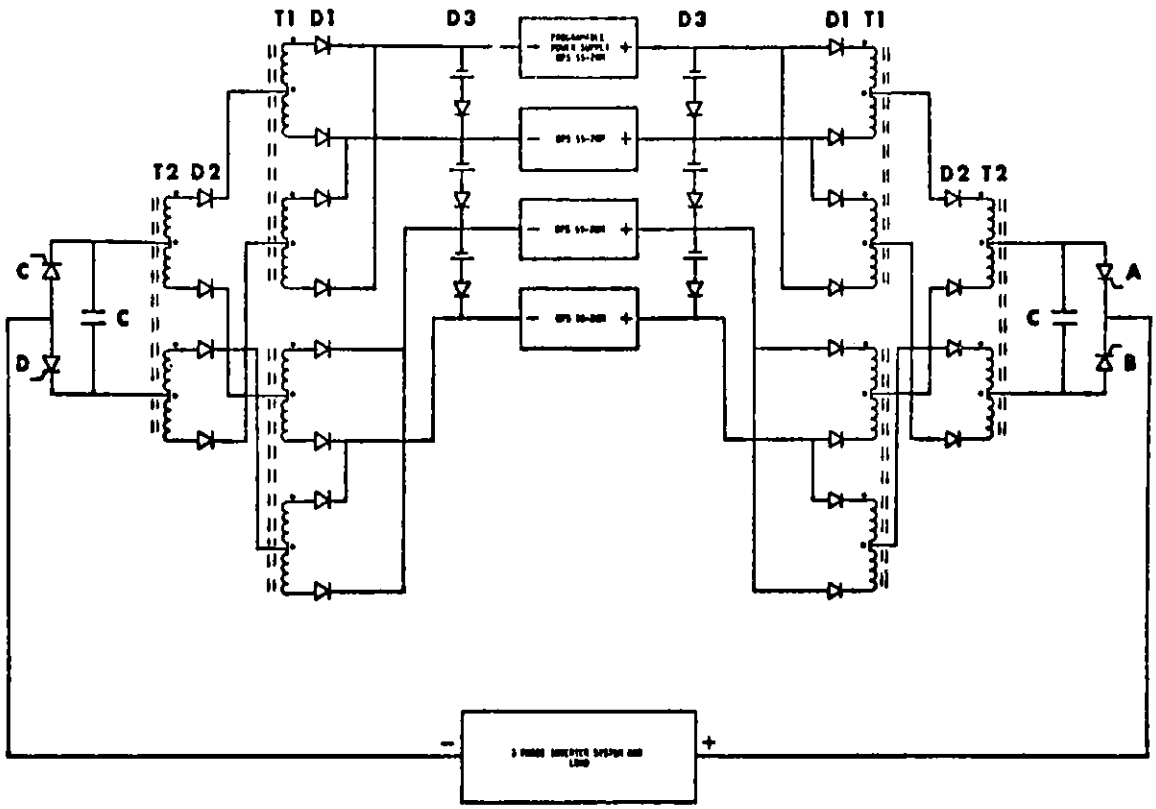

Figure 3. Four-Electrode Pair Consolidation Circuit

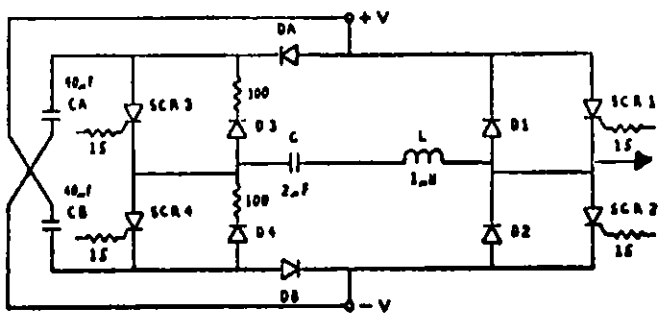

Figure 4. Modified McMurray Inverter

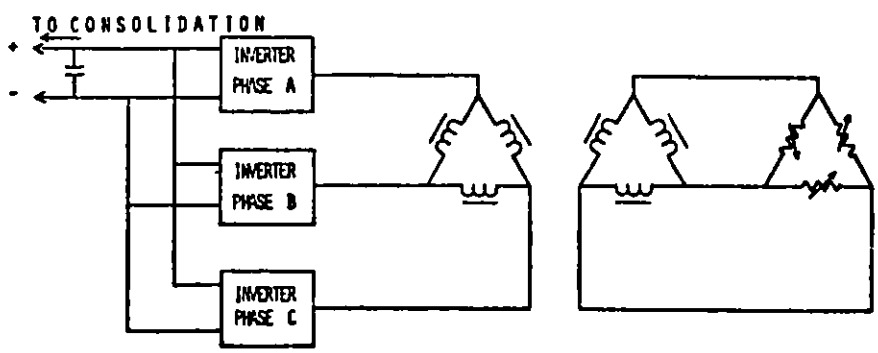

Figure 5. Three-Phase Inverter System

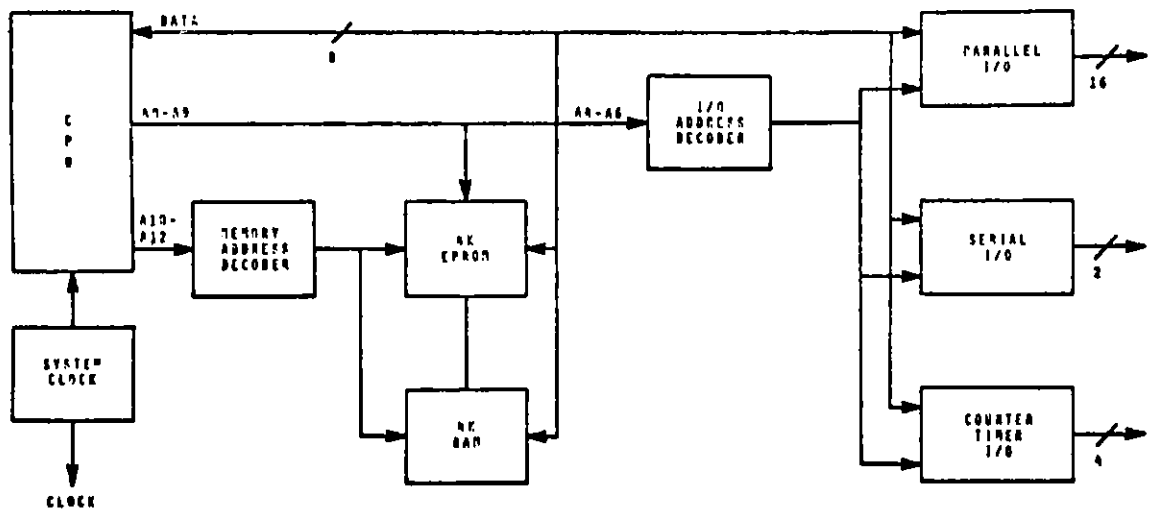

Figure 6. Z80 Microcomputer Block Diagram

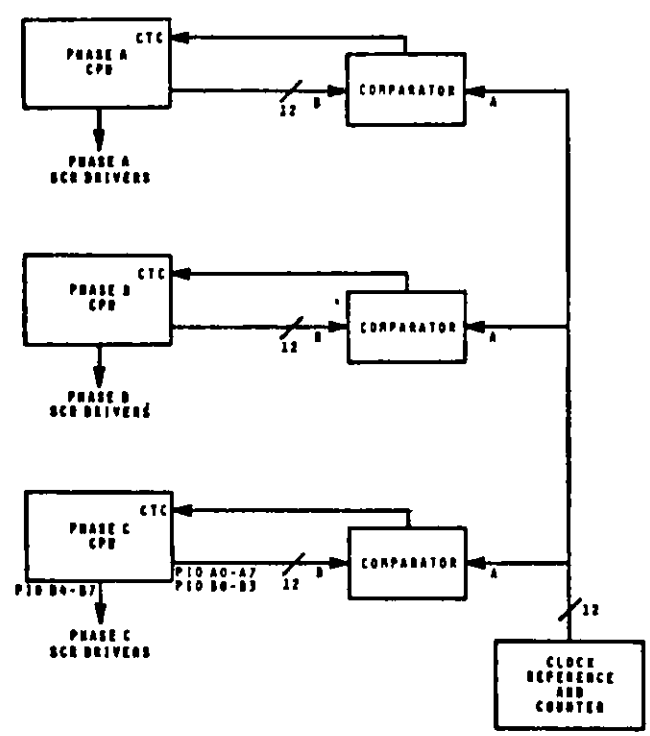

Figure 7. Timing-Synchronization Block Diagram

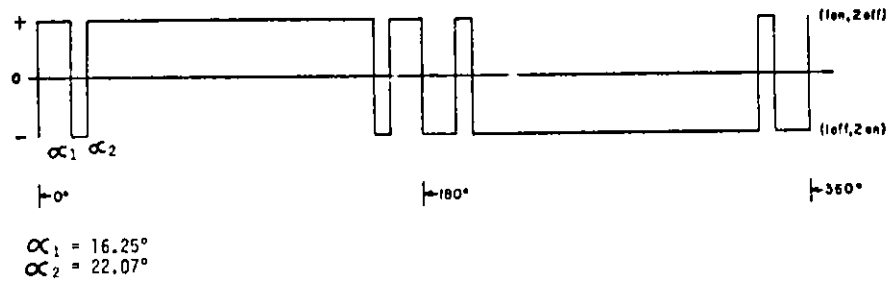

Figure 8. Theoretical Single Inverter Output

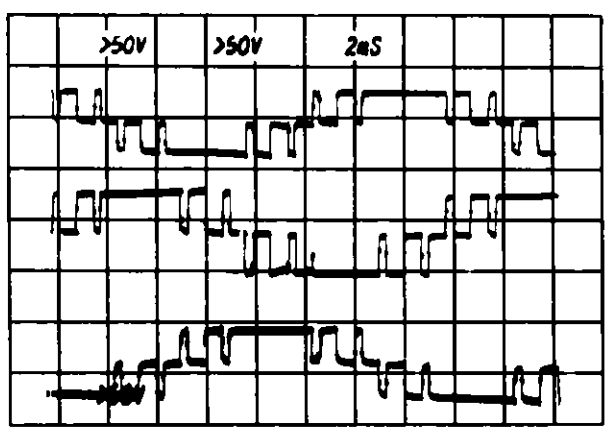

Figure 9. Three-phase Unfiltered Output Voltage

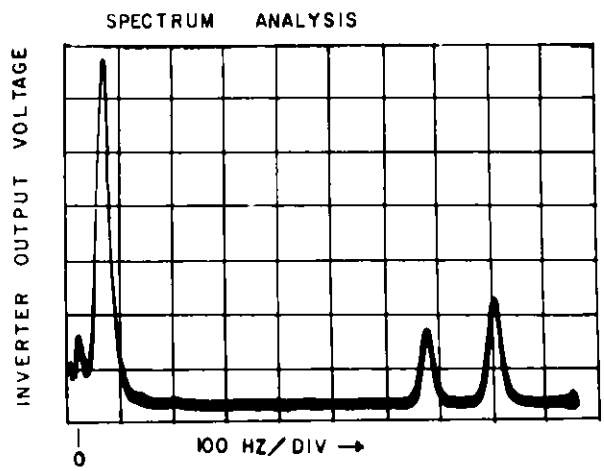

Figure 10. Unfiltered Output Spectrum

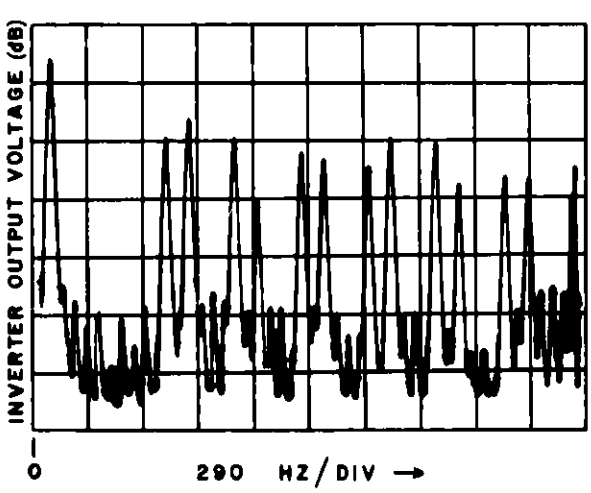

Figure 11. Unfiltered Output Spectrum

AN ALKALI METAL VAPOR DETECTOR FOR USE IN FLUIDIZED BED COMBUSTOR EFFLUENT STREAMS

A.S. Zarchy
Corporate Research and Development
General Electric Company

INTRODUCTION

The pressurized fluidized bed (PFB) combined cycle is an advanced power generation system that appears to offer many advantages over current technology. In addition to the advantage of using coal rather than oil, the PFB combined cycle technology offers lower installation and lower operating costs than current generating plants as well as the ability to exceed current air quality standards[1]. The effluent from a PFB combustor is ladden with particulate carryover and contains high levels of vapor phase alkali compounds. It is recognized that the current bottleneck in the development of the PFB combined cycle is the high temperature high pressure clean up necessary to interface the PFB with the gas turbine. While fairly conventional techniques can be used to characterize the particulate content of the stream and hence to evaluate different clean up concepts, quantification of the alkali concentration requires new analytical and sampling techniques.

The alkali contained in a PFB effluent stream is found in both the vapor phase and as a constituent of the particulate material entrained in the stream. Thermodynamic calculations demonstrate[2] that the quantity and nature of the vapor phase species is a very strong function of temperature. Calculations[3] and experimental data[4] suggests that the velocity of the evaporation and equilibration reactions involved is of the same order as the gas transit time from combustor to turbine. Hence, the alkali vapor-particulate split follows a complicated function of time and temperature history. In-situ measurement techniques provide a convenient means for eliminating the complicating effects.

The specifications for alkali material in a fuel gas stream is 20 ppb at the turbine inlet and is generally given as (Na + K) level. It is not necessary to know the exact chemical composition of the alkali level, but simply the total level. Given this fact, it was apparent that an approach would be to select a property which is common to all alkali material, and use it as the basis for a detector. The property selected was the low ionization potential found almost exclusively in alkali metals. Once the alkali metal is ionized, the ions can easily be collected by proper focusing of

electrical fields, and measured with an ammeter. The signal obtained is proportional to the alkali metal level in the monitored stream.

This report describes the principles, calibration and operation of a detector for in-situ measurement of alkali concentration in PFB effluent streams. The detector described represents an extension of the low temperature device presented at the Fourth Annual Symposium on Instrumentation and Control for Fossil Energy Processes[5].

PRINCIPLES OF SURFACE IONIZATION

Table 1 lists the ionization potential of the alkali metals. It should be noted that these values are substantially below the ionization potentials of all other elements of concern. Thus, alkalis can be identified by monitoring all compounds with an ionization potential equal to or below 5.4 eV.

TABLE 1
IONIZATION POTENTIAL OF ALKALI METALS

	eV
Li	5.4
Na	5.1
K	4.3
Rb	4.2
Cs	3.9

Most methods for ionization of neutrals utilize large energy excesses, and, hence, show little specificity in ion production. It has been known for some time that when an atom having an ionization potential, I, comes in contact with a metal of work function, Φ, if Φ is greater than I, the atom can undergo ionization. This phenomenon, termed surface ionization, has been described successfully with the modified Saha-Langmuir equation:[6]

$$\frac{n_+}{n_o} = \exp \frac{(\Phi - I)}{kT} \qquad (1)$$

where: n_+ = number of ions evaporating from a surface

n_o = number of atoms evaporating from a surface

Figure 1a[7] and 1b[8] are plots of ionization efficiency vs. temperature for various alkali and alkali halide compounds on tungsten and platinum surfaces, and are presented because they typify the wealth of surface ionization data. In general, ionization begins at a temperature of approximately 1000°K and rises extremely

rapidly to a peak typically around 1100°K. In this region ionization efficiency is governed by the kinetics of the charging reaction on the surface. There have been few attempts to characterize the surface ionization behavior in this regime.

Above 1100°K the fractional ionization decreases slowly with temperature. In this region the fractional ionization is governed by the local equilibrium. The Saha-Langmuir equation is a thermodynamic calculation based on equilibrium of a mixture of ideal atomic, ionic and electronic gases on a metal surface.

Platinum has a work function of 5.5 eV, and is inert enough to withstand the hostile conditions found in a PFB effluent stream. Thus, platinum has been identified as a material suitable for use as an alkali ionizing element under PFB conditions.

HIGH TEMPERATURE ALKALI METAL DETECTOR (HT-SIAMD)

The ability to measure alkali metal vapor concentrations at the high temperature found in PFB effluent stream will play an important role in the understanding of alkali related phenomena in gas turbines. Additionally, this detector will be of considerable value in the understanding of proposed alkali metal vapor cleanup schemes.

Surface Ionization Detector - Description

Figure 2 is a schematic diagram of the basic components of a surface ionization detector. A filament is supported between two electrodes and heated to the temperature necessary for alkali vaporization by use of a controlled power supply. This ionization surface is biased at a high positive voltage. The bias voltage serves as a repellant for all positive ions which are formed on the active platinum surface. Surrounding this filament is a collection grid which is grounded through a sensitive electrometer. The current measured on the electrometer is in direct proportion to the arrival rate of alkali atoms onto the surface of the grid -- one electron per atom. The arrival rate can be related directly to the concentration of alkali-containing materials in the gas phase. This relation will be discussed in Calibration Section.

Surface Ionization Detector - Hardware

One practical requirement in the construction of an alkali metal detector is that the ionizer probe and the collection surface have sufficient electrical isolation. Typically the bias voltage needed is of the order of 600 volts, and a reasonable signal is of the order of 10^{-10} amps. It is necessary to ensure that the leakage current from the 600-volt ionizer through the collector and ammeter be maintained at a level

sufficiently below that of the 10^{-10} amp signal. From Ohm's law it is seen that the required resistance could be quite high. In order to divert this leakage current from the collection probe a concentric conductor/insulator arrangement was utilized. The assembly is connected to the detector case via the outer ring and the central ring is then grounded. This arrangement effectively isolates the collector from the case provided the resistance of the insulators is adequate. Normally this arrangement provides an adequate safety factor; however, ceramic insulators become sufficiently conductive at PFB temperatures that even in this configuration leakage currents remain a problem. This problem was eliminated by cooling the insulator.

A photograph of the HT-SIAMD is shown in Figure 3. The detector base was constructed from a standard flange so that the device could be easily attached to or removed from the system. Channels were cut internally through this flange so that water could provide the necessary cooling of the insulator. Two standard electrical feed throughs were used to insulate the two 1/16" stainless steel filament supports. A 1.75" gap was left between the supports between which a 0.005" platinum filament was strung. The filament was attached to each support with a threaded collar.

A 2.0" long x 0.75" diameter collection cylinder was fabricated of stainless steel screen (¼" grid) and was fastened to the 1/16" stainless rod support with threaded collars. The rod was connected to the triaxial insulator with silver solder. This insulator was a standard triaxial insulator supplied by the Ceramaseal Corp.

A constant resistance power supply was used to maintain the filament at a constant temperature. This power supply which was obtained from Thermo Systems Inc., was a modified hot wire anemometer supply. The filament temperature was normally set at 1000°C. As noted from the electrical schematic (Figure 2) the entire heater supply circuit had to be floated at a high voltage above ground. To accomplish this "float", it was necessary to construct a plexiglass cage for the heater chassis to isolate the circuit from human contact and from ground. The grounding lug of the circuit was then biased at 600V above ground with a Hewlett Packard 6515A power supply. Current from the detector was monitored with a Keithly 410 picoammeter. For the purposes of this experiment a separate detector vessel was constructed which was heated to 900°C with a tube furnace. In other applications the detector might "T" into the gas stream in question. The sample stream entered the detector chamber through the port labeled gas inlet over the detector and out the exit port on the bottom of the detector chamber.

HT-SIAMD OPERATION

In order to use the HT-SIAMD as an analytical instrument it was necessary to calibrate the output of the detector against a known source. An analytical calibration utilizing basic principles of mass transfer was first performed. Then an experimental calibration was performed by measuring the detector output against a wide variety of alkali compounds and concentrations.

Initial Procedure

1. Filament bakeout. Initially when a new filament is put into service a very high background current is observed. At the start, this level is so high that meaningful readings are impossible. This level gradually drops to a low background level over the course of a week. This phenomena has been observed before in vacuum type ionization detectors, and it appears to be caused by the high level of alkali contaminants in the virgin platinum metal, which diffuse to the surface during this startup period and are then expelled.

To eliminate this spurious background, the filament was operated for one week at a temperature of 1100^{o}C. After this time the temperature was reduced to the normal operating point of 1000^{o}C.

2. Temperature Control. The filament is heated with a power supply capable of maintaining a fixed voltage to current ratio. A calibration chart was prepared from tables of platinum resistivity vs. temperature and the known length and diameter of the filament. Then, the temperature of the filament could be controlled by selecting and setting the power supply to the appropriate resistance.

3. Bias voltage. A bias voltage is applied to the filament to "push" positive ions formed there onto the collector grid. Clearly, the electrical field provided must be sufficient to provide the ion with enough energy to overcome the viscous forces imposed by the gas medium. This required voltage was determined by making plateau current measurements. A plot of collected current vs. voltage was made. As the voltage was raised from 0 to some large value, the collected current rose from 0 and then leveled off at some saturation value. This value corresponds to 100% collection. A convenient voltage can be chosen somewhere above the knee in the curve. For the detector it was found that a convenient voltage was 600V.

Calibration

1. Analytical

A calibration for vapor phase alkali at high temperatures has been prepared. In modeling the current generated from the detector it was assumed that; 1) alkali was

present in the form of vapor phase molecules, 2) these species are transported to the filament surface in a manner consistent with the local fluid mechanics, 3) species that are contacted with the surface are charged according to the Saha-Langmuir relation as if they were atomic species, and 4) bias voltage is sufficient such that all charged species are collected and measured with the ammeter. To generate a calibration curve for our sample assembly which includes the detector mounted parallel to the flow, it was necessary to obtain a correlation for the mass transfer coefficient in a similar flow arrangement. This correlation was given in a variety of standard engineering handbooks, Perry's[9], for example. Physical property data was estimated when necessary from correlations also found in the handbooks. For sodium chloride at 900°C this correlation has been calculated to be 0.9 μA/ppm.

2. Experimental

A schematic of the apparatus used to calibrate the detector is shown in Figure 4. A constant output atomizer is used to generate a well characterized aerosol from a solution of the salt in question. The carrier gas stream containing the aerosol flows through the detector chamber and exits through a port on the bottom of the chamber. This particular atomizer generated 5 cc of solution per hour. The median diameter of these droplets is 0.3 μm. Based on the liquid entrainment rate of 5 cc/hr and the known carrier gas flow of 47 scch, it was possible to calculate solution concentrations necessary to produce the equivalent of 0.1 ppm to 50 ppm of a given salt in the carrier stream. For example, sodium chloride solutions of 4.24 mg/l to 2.12 g/l were used to cover this range. After evaporation of the water from the droplet the residual salt particles range between 44 Å and 350 Å.

The mean evaporation time for these residual particles at 900°C has been calculated. Based on the evaporation of a spherical drop in a stagnent gas the evaporation time was calculated to be on the range of nano seconds to a micro second. This short time indicates that the alkali should be entirely evaporated inside the detector chamber.

The calibration apparatus was then run with a number of concentrations of alkali containing compounds. The results of this calibration are shown in Figure 5. The most notable feature of this calibration is that very little variation in the signal is noted when either cation or anion is substituted. This demonstrates that the detector is performing the desired function, that of producing a signal which is only dependent on alkali concentration. Secondly, the signal monitored is approximately first order in alkali concentration, thus indicating that the signal generated is in proportion to the arrival rate of alkali atoms to the surface of the filament.

It is instructive to compare this calibration curve to the curve generated for the low temperature calibration curve which was generated in a similar manner as the HT-SIAMD. The difference between these two cases is that the salt crystals generated for the low temperature case remain as crystals. Thus, detection of the crystals depends on the aerodynamic capture of the individual crystals on the filament, while detection of the vapor depends on the diffusion of the vapor to the filament surface. A composite plot of the two curves is shown in Figure 6. This comparison indicates that the overall mass transfer of alkali vapor to the filament at 900^{o}C is approximately 20 times as great as the collection of particles on the filament at low temperatures. As the particle collection is not expected to be a large function of temperature, this indicates that the high temperature detector will preferentially respond to vapor rather than particles in the high temperature mode. Thus, this detector provides the means for monitoring alkali vapor concentration in a high temperature environment.

APPLICATION

The high temperature alkali metal detector was used as a means of evaluating the viability of an electrostatic alkali metal vapor scrubbing device. The detector was placed in-situ just downstream of the scrubber. The alkali vapor pressure measured at this position was a reliable indication of the effectiveness of the scrubber operation. Shown in Figure 7 is some typical output from one of these scrubbing experiments. The dip in signal level corresponds to a specific "on" condition in the alkali scrubber. The magnitude of the reduction in signal indicates a reduction in alkali vapor pressure of approximately 30%.

The use of the detector in these experiments has provided a great experimental convenience not otherwise available. The more conventional approach is to take grab samples of the streams in question, and analyze those samples by wet chemistry or atomic absorption. These conventional methods generally impose inconvenient lower concentration limits and long sampling and turn around times. The use of the detector provided immediate results which meant that a great variety of experimental conditions could be examined in a short time.

CONCLUSIONS

Surface ionization detection has been shown to be a viable technique for on-line in-situ measurement of alkali vapor pressure in a high temperature carrier gas. The high temperature detector with a filament ionizer is an effective means for monitoring only that signal which is due to vapor phase alkali.

The surface ionization alkali metal detector is a straight forward approach to on-line alkali metal monitoring in fuel gas streams. In comparison to other competitive technologies the device is simple and inexpensive, requiring very little peripheral equipment. Although this device does not provide an absolute signal, it is calibratable over wide ranges of conditions. Since the detector can be mounted in situ, the readings are uncomplicated by sampling errors. Thus, surface ionization should be a top choice as the basis for alkali metal detection.

REFERENCES

1. Corman, J.C., "Energy Conversion Alternatives Study", NASA-CR-134949.
2. Spacil, H.S. & Luthra, K.L., "Thermochemistry of a PFB Coal Combustor/Gas Turbine Combined Cycle", General Electric Company, 80CRD238.
3. General Electric Co., Combustion Chemistry: DOE Report No. Fe-2357-40, 8/78.
4. National Research Development Corporation, R&D Report No. 85, "Pressurized Fluidized Bed Combustion," OCR Contract No. 14-32-001-1511, July 1974, London.
5. Zarchy, A.S., "A Surface Ionization Detector for Alakli Metal Measurements in Gas Streams, Proc. Symp. on Inst. & Control for Fossil Energy Process, June 9-11, 1980, Virginia Beach, Virginia.
6. Hughes, V.W., ed., Methods of Experimental Physics, Volume 4, p. 395, Academic Press, NY 1967.
7. Ionov, N.I., J. Tech. Phys. (U.S.S.R.) 26, 2200 (1956).
8. Datz, G. and Taylor, E.H., J. Chem. Phys. 25, 389, (1956).
9. Perry, J.H., ed., Chemical Engineers Handbook, Fourth Edition, McGraw Hill Book Company, New York, 1963.

FIGURE TITLES

1. Typical Data Demonstrating Surface Ionization Phenomena
2. Basic Components of a Surface Ionization Detector
3. Photograph of the HT-SIAMD
4. Detector Calibration Apparatus
5. Calibration Curve for the HT-SIAMD
6. Comparison of the High and Low Temperature Calibration Curves
7. Typical HT-SIAMD Output from Alkali Scrubber Monitoring

ACKNOWLEDGEMENTS

This work was partially supported by DOE Contract # DE-AC21-79ET15490.

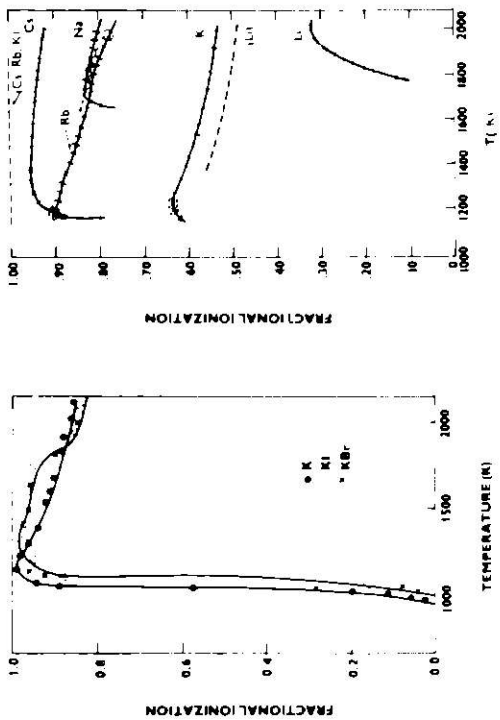

FIGURE 1

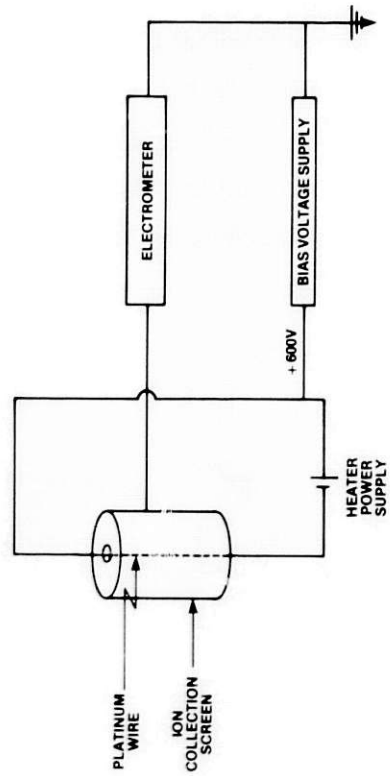

FIGURE 2

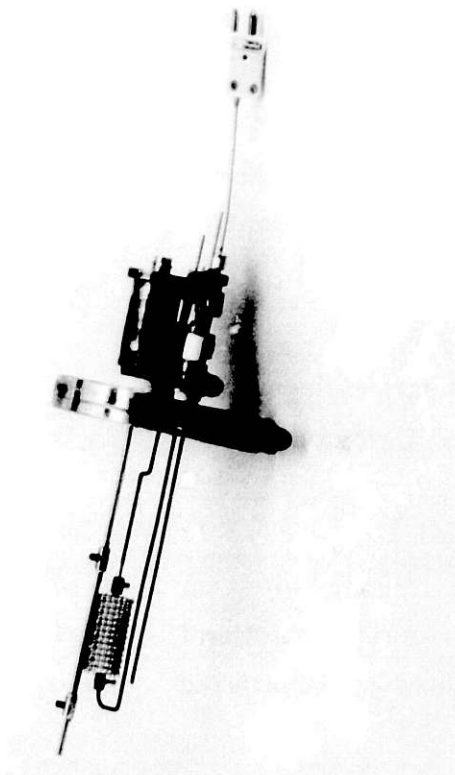

FIGURE 3

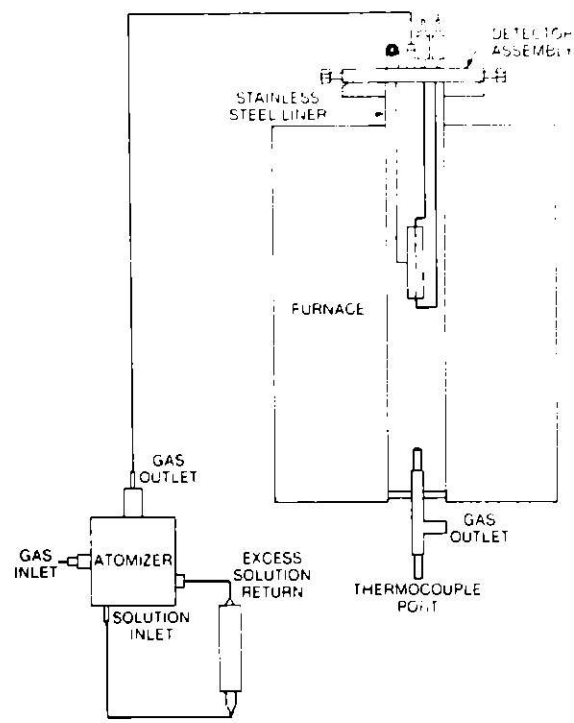

FIGURE 4

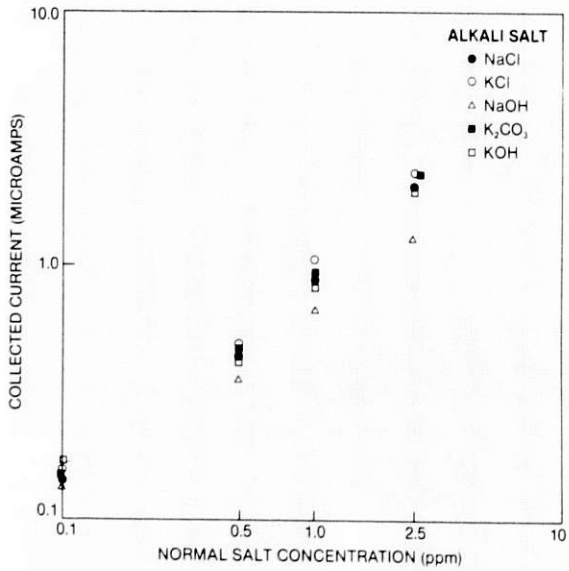

FIGURE 5

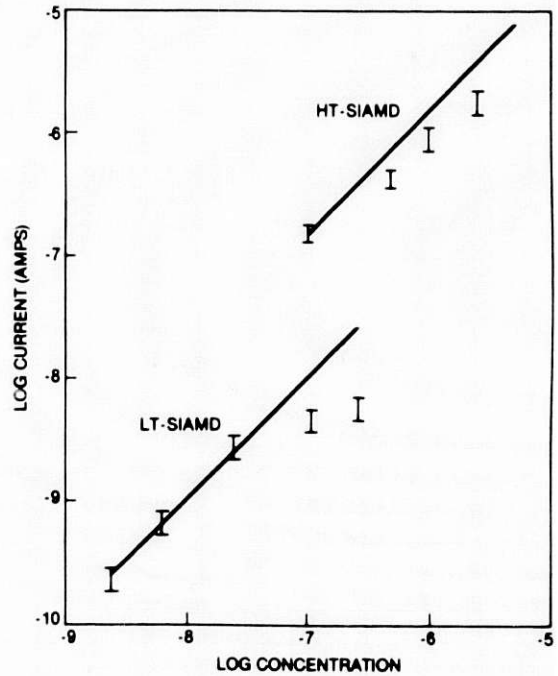

FIGURE 6

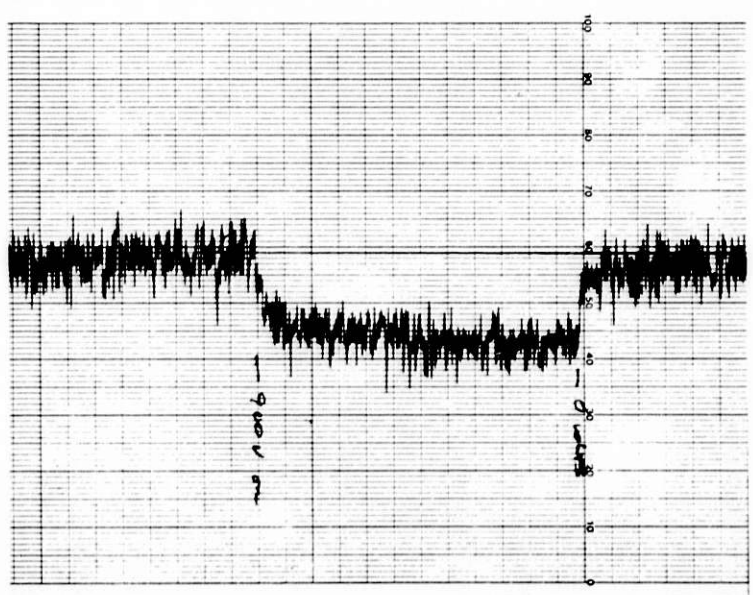

FIGURE 7

ON-LINE MEASUREMENT OF ALKALI METAL SULFATE DEW POINT IN A PFBC FLUE GAS

J. E. Helt and Irving Johnson

Argonne National Laboratory
Chemical Engineering Division
9700 South Cass Avenue
Argonne, Illinois 60439

ABSTRACT

High-temperature corrosion of gas turbine parts due to the presence of alkali metal compounds in the hot flue gas is a potential problem in the commercialization of pressurized fluidized-bed combustion (PFBC) of coal. Most suggested corrosion mechanisms state that the corrosion reactions take place at an appreciable rate only in the presence of the molten alkali metal sulfates (Na_2SO_4 and K_2SO_4). Therefore, on-line measurement of the alkali metal sulfate dew points in the flue gas offers a basis for anticipating hot corrosion conditions in the gas turbine.

Two methods of dew point measurement, electrical conductivity and remote optical techniques, have been identified as having potential for this application. This paper discusses the feasibility of such instrumentation in the light of preiminary experiments and analyses.

I. INTRODUCTION AND BACKGROUND

Hot corrosion is, in general, the accelerated oxidation of nickel, cobalt, and iron-base alloys which occurs in combustion systems in the presence of small amounts of impurities--notably, sodium, sulfur, chlorine, and vanadium. There is no real consensus on which mechanisms are primarily responsible for high-temperature corrosion. One point generally accepted, however, is that a liquid phase is necessary for corrosion reactions to take place at an appreciable rate.

When coal is the fuel for combustion, hot corrosion may occur in the form of accelerated sulfidation. It is generally agreed by investigators that molten alkali metal sulfates (Na_2SO_4 and K_2SO_4) are the principal agents responsible for the occurrence of sulfidation. Although molten sodium sulfate by itself appears to have little or no effect on the corrosion of metal alloys, its presence may increase the accessibility of the bare metal surface to the external atmosphere.

In the commercialization of pressurized fluidized-bed combustion (PFBC) of coal, the flue gas is passed directly through gas turbines. The presence of alkali metal salts in the hot PFBC flue gas may drastically reduce the expected life of the turbine blades. It is well documented that deposition of molten Na_2SO_4 (K_2SO_4) on turbine blades greatly enhances corrosion of the turbine blade materials.[1-7]

II. WHY DEW POINT MEASUREMENT

The overall reaction which represents Na_2SO_4 deposition from the flue gas is as follows:

$$2NaCl(g) + H_2O(g) + 1/2\ O_2(g) + SO_2(g) \rightleftarrows Na_2SO_4(g) \downarrow + 2HCl(g) \qquad (1)$$

Equation 1 states that the formation of Na_2SO_4 in the flue gas is a gas phase reaction. If the sulfate is formed but remains in the vapor state, it seems to have no detrimental effect on the turbine. Only when the sulfate condenses on the turbine surfaces does it promote serious corrosion. Therefore, to anticipate hot corrosion of the gas turbine, it is not sufficient to know the sulfate concentration in the flue gas since the deposition of sulfate on the cooler turbine parts is a "dew point" phenomenon. What is of interest is to monitor the gas just upstream from the turbine. From measurements of the Na_2SO_4 dew point of this stream, it will be possible to predict the extent of alkali metal sulfate condensation on the turbine blades.

For practical application of such a technique, it is apparent that because of the sensitivity of the instrumentation required and the kinetics of the sulfate condensed on the surface, direct measurement of the dew point may not be possible. It may be more practical to measure the growth rate of a liquid film and, thereby, the deposition rate on a cooled surface at several different degrees of supercooling. This data would yield a plot of deposition rate versus surface temperature. Then, to obtain a "dew point" for the flue gas, the curve could be extrapolated to find the surface temperature that would give a zero deposition rate.

III. TECHNIQUES FOR MEASUREMENT OF DEW POINT AND FILM DEPOSITON RATE

A. Optical Techniques

At least two general techniques of remote optical measurement might be useful: interferometry and ellipsometry. In the interference technique, a beam of monochromatic light is reflected off a test surface. The light has a wavelength which is absorbed by Na_2SO_4. When condensation begins, the intensity of the reflected light decreases sharply. The growth rate of the sulfate layer can also be calculated by use of the interference technique. Light is reflected alternately from the film surface and the metal surface, resulting in a modulated intensity of the collected beam. The film growth rate can be calculated from the spacing between intensity maxima.

Ellipsometry[8,9] is an optical technique for the observation of events at an interface (or film) between two media and is based on utilizing the polarization transformation that occurs when a beam of polarized light is reflected from or transmitted through the interface (or film). The technique has very good sensitivity and is essentially nonperturbing when the wavelength and intensity of the light beam are properly chosen. The procedure for making growth rate measurements with ellipsometry is very similar to that

used for interference techniques. Light reflected off the growing film undergoes changes in intensity due to changes in polarization. The growth rate can be calculated from the transient intensity patterns recorded.

B. Electrical Conductivity

Monitoring of surface electrical conductivity also has potential as a technique for measuring the Na_2SO_4 dew point. Electrodes can be embedded in the surface of an inert substrate. The formation and growth of a sulfate film on the substrate surface would result in a changing electrical conductivity which could be measured by an electrical circuit connected to the electrodes.

There are precedents for using conductivity to measure dew points. Johnstone[10] developed and used such a device in his research work on the reactions of sulfur. Johnstone's instrument used two platinum electrodes sealed in the outer surface of a glass thimble and measured the changing conductivity due to a condensed film of sulfuric acid.

A team of researchers at the British Coal Utilization Research Association (BCURA)[11-14] developed a dew point meter similar in principle to Johnstone's. The BCURA meter, which used platinum electrodes and an embedded thermocouple in a controlled-temperature glass surface, was intended to show the temperature at which a liquid film could first be detected upon cooling. It was found that on a laboratory scale, the meter could distinguish between condensed films of water, sulfuric acid, and alkali metal salts.

IV. EXPERIMENTAL EQUIPMENT AND PROCEDURE TO VERIFY THE USEFULNESS OF THE ELECTRICAL CONDUCTIVITY TECHNIQUE

Of the two methods identified as having a potential for dew point measurement, surface electrical conductivity measurement appears to be preferable from a practical standpoint for an operating PFBC system.[15] Preiminary experiments are being performed to test the feasibility of using electrical conductivity as a technique.

A schematic of the experimental equipment is shown in Fig. 1. This unit is capable of providing a simulated PFBC flue gas environment, and the induction heating unit can be utilized to vaporize alkali metal salts.

A test specimen (disk) made of 99.5% Al_2O_3 with platinum electrodes has been designed. This is mounted on the end of a pipe to form a probe (see Fig. 2). The probe is a concentric tube-within-a-tube arrangement which was designed to provide air cooling to the back side of the specimen surface. Air cooling allows the test surface to be cooled 50-100°C below the temperature of the hot gas stream striking it.

In the experimental tests, alkali metal salt was evaporated from the platinum sample pan into a nitrogen carrier gas. This gas was then passed over the cooled surface of the test probe. As the test surface was cooled, the thermocouple measured the surface temperature; also, the electrical resistance between the two surface electrodes was monitored. When the alumina surface was cooled sufficiently to produce a supersaturated condition,

Sketch of Experimental Equipment

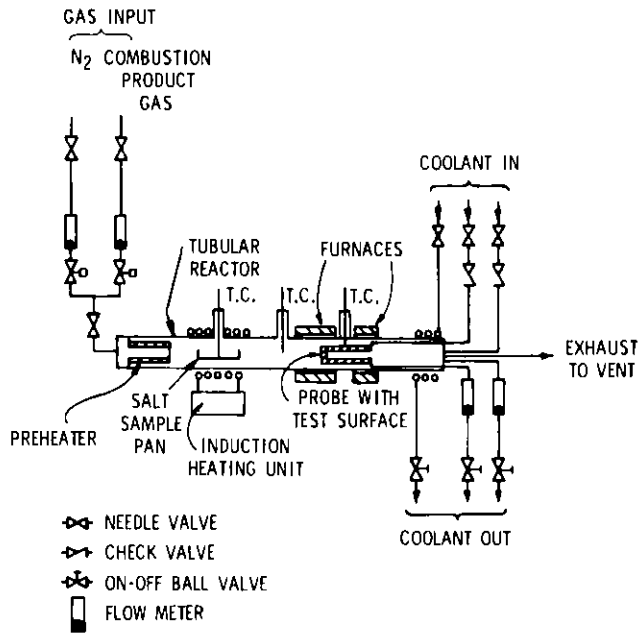

Fig. 1

Sketch of Possible Electrical Resistivity Probe

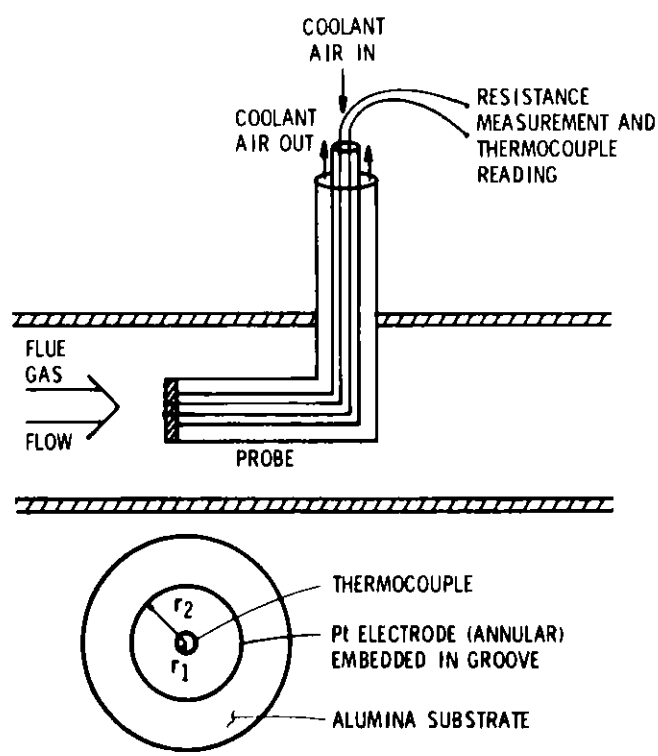

Fig. 2

the alkali metal salt condensed on the surface. Deposition of salt and the subsequent growth of a liquid film caused the electrical resistance measured between the two electrodes to decrease.

The resistance of a film between two concentric electrodes is given by:

$$R = (\rho/h)\,\frac{\ln(r_2/r_1)}{2\pi} \tag{2}$$

where h = thickness or height of film in cm
ρ = electrical resistivity of liquid film (ohm-cm)
R = equivalent electrical resistance (ohm)
r_1 = radius of center electrode
r_2 = radius of outer electrode

The film growth rate can then be calculated from the change in resistance with time:

$$\frac{dh}{dt} = -\frac{\rho}{R^2}\,\frac{\ln(r_2/r_1)}{2\pi}\,\frac{dR}{dt} \tag{3}$$

V. EXPERIMENTS WITH NaCl

The initial tests were made using NaCl. In all of these initial runs, the probe surface was kept between 800 and 815°C and the NaCl was vaporized at 900–1050°C. The resultant film growth rates, as shown in Fig. 3, were on the order of 0.015 pm/s to 0.15 pm/s.

In these experiments, the partial pressure of NaCl in the vapor phase was calculated from the weight loss of salt in the platinum sample pan and the nitrogen flow rate to be 50 Pa, which is approximately the vapor pressure of NaCl at 800°C. Previously reported work[16,17] suggests that condensation of NaCl from a hot gas stream requires as much as 100°C of supercooling. If this is the case, the probe surface temperatures used in these experiments were much too high.

An additional experiment was completed using a higher partial pressure of NaCl (obtained by lowering the bulk N_2 flow and increasing the temperature of the vaporizing NaCl). The partial pressure of NaCl was approximately 270 Pa, and the calculated film growth rate was 2.8 pm/s.

Problems arose in trying to use NaCl to verify the technique because of its high melting point. To keep any deposited NaCl film in the liquid state required that the surface temperature of the collector be above 800°C. To get deposition on a 800°C surface, the NaCl must be vaporized at a very high temperature to achieve sufficient supersaturation. With a temperature of 1000°C at the point of vaporization, the level of supersaturation at a 800°C surface is still very low. To help overcome this problem, NaOH, which has a melting point of 318°C, was used to demonstrate the technique.

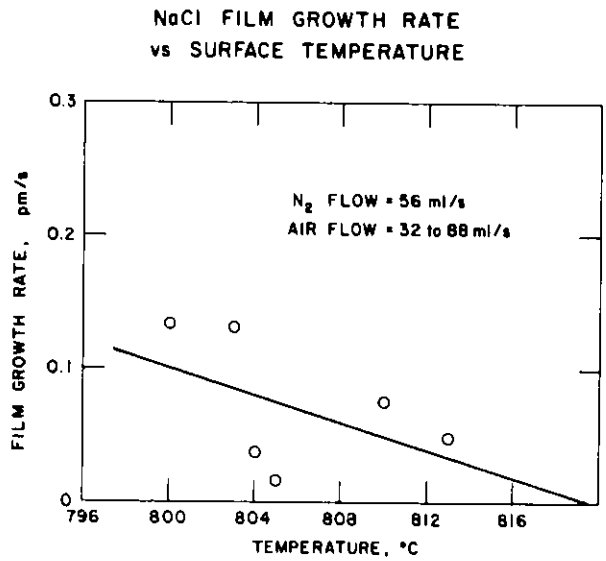

Fig. 3

VI. EXPERIMENTS WITH NaOH

In the experimental runs using NaOH, the sampling surface was kept at 300-400°C and the vaporization temperature was 700-800°C (heat was provided by the induction heater). At 800°C, the vapor pressure of the hydroxide is approximately 1 kPa; at 400°C it is 2.7 Pa. Even with losses and condensation on other parts of the equipment, this provides ample supersaturation for deposition of the salt on the cooled sampling surface. In the experimental runs, there was evidence of film formation on the surface, accompanied by a rapid drop in the measured resistance values. When the surface was reheated, the R value returned very rapidly to an off-scale value (that is, >2000 Mohms).

During cooling, the response rate was on an order of magnitude drop in R value in 10-20 min. There is a change in resistance which is more than that associated with a temperature change of the alumina substrate. Also, this resistance change is in the opposite direction--the electrical resistivity of aluminum oxide increases with decreasing temperature by a factor of 2-3 for every 25°C.[18]

Several experimental runs were completed using NaOH. The experimental parameters varied during the experiments were carrier gas (N_2) flow rate, coolant gas (air) flow rate, and surface temperature of the test surface. In all of the experiments the temperature of the vaporizing salt in the crucible was maintained at 825°C $\pm$25°C.

VII. DISCUSSION

In the probe design used for these experiments, the air coolant tube was not a closed system. After the coolant air hit the back side of the test specimen, it was free to mix with the carrier gas. In fact, the coolant gas exited from the system with the carrier gas. When the coolant air flow was very low relative to the carrier gas flow, no problems were expected because all mixing (and therefore dilution) would take place downstream from the test specimen. However, when the air coolant flow was increased, the likelihood that significant dilution would occur adjacent to the test surface increased. That is, as the air coolant flow rate was increased, two changes had to be considered. First, the surface temperature of the test specimen was decreased, which would be expected to result in an increased deposition rate of the salt. Secondly, some dilution of the carrier gas might occur, decreasing the partial pressure of the salt and resulting in a lower deposition rate. (Actually, a third change might have been important at low deposition rates. Since the deposition rate was calculated from the change in resistance, the resistivity versus temperature relationship for the alumina substrate might have had an important effect during thermal transients occurring when the air coolant flow rate was changed. This would not happen once a steady state surface temperature was achieved.)

A net change in salt deposition rate is a result of the relative magnitudes of the individual changes due to surface temperature and gas dilution. Since the surface temperature can be varied not only by the air coolant flow rate, but also by changing other experimental parameters (e.g., temperatures of the tube furnaces and temperature of carrier gas stream), the same surface temperature may be obtained at different air coolant flows. Likewise, the partial pressure of the salt is directly related to the nitrogen flow rate and not just to dilution by the air coolant. It is probably best, therefore, to plot the results as a family of curves using the following parameters: N_2 flow rate, air coolant flow rate, and surface temperature. Such plots are shown in Figs. 4-10.

Figure 4 gives the NaOH film growth rate at a constant N_2 (carrier gas) flow rate and a variety of air (coolant) flows. As the coolant flow increases, the dew point temperature decreases. This indicates that significant dilution of the carrier gas by the air coolant has occurred.

In conjunction with Fig. 4, Figs. 5 and 6 show that as the N_2 flow is decreased, and the stream becomes more concentrated in the alkali metal salt, the dew point temperature increases.

Figures 7-10 are at a higher N_2 flow of 125 mL/s. In viewing the four figures as a group, the general trends are reinforced. For a comparable air coolant flow rate at a lower carrier gas flow rate (i.e., those in Fig. 4), the dew points are all lower. The higher N_2 flow rate (125 mL/s versus 93 mL/s), with a constant vaporization rate of NaOH, yields a lower salt concentration in the carrier gas stream. Also, as the coolant flow increases from 0.0 mL/s to 32 mL/s (shown in Figs. 7-10), the dew point is decreased. This indicates again that the coolant flow is diluting the carrier gas stream. However, the decrease in dew point is not as great as that evidenced at the lower N_2 flow rates. This is as expected since the relative dilution would be less.

NaOH FILM GROWTH RATE
vs SURFACE TEMPERATURE

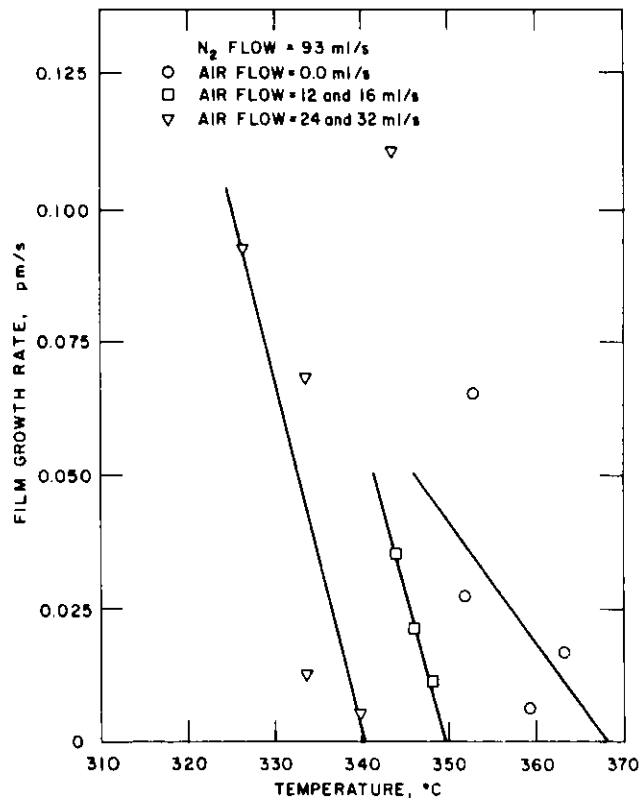

Fig. 4

NaOH FILM GROWTH RATE
vs SURFACE TEMPERATURE

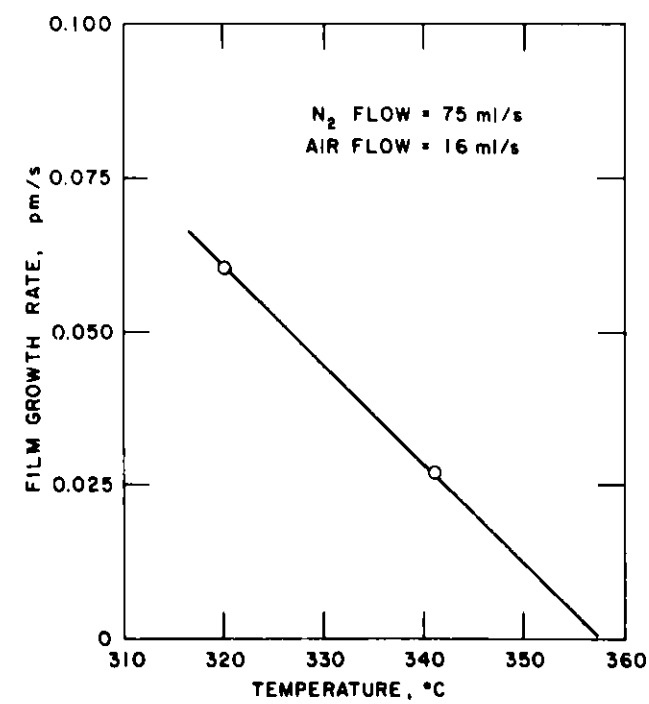

Fig. 5

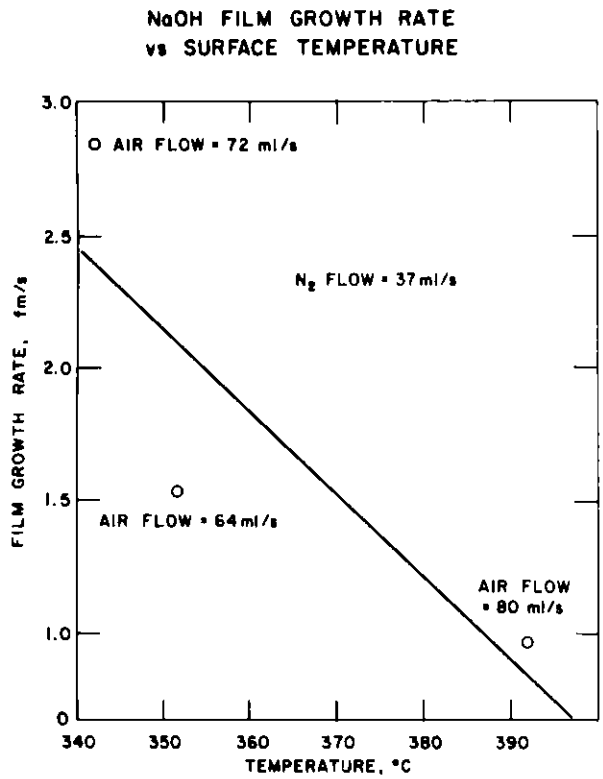

Fig. 6

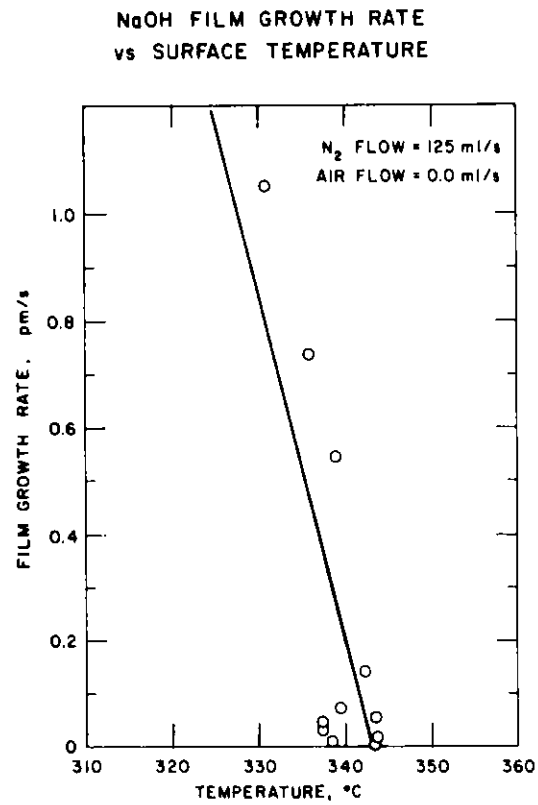

Fig. 7

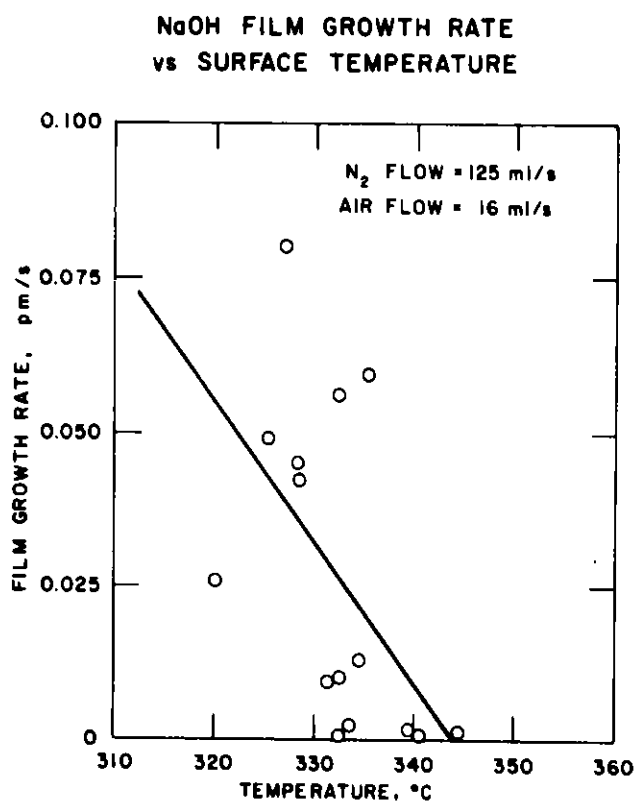

Fig. 8

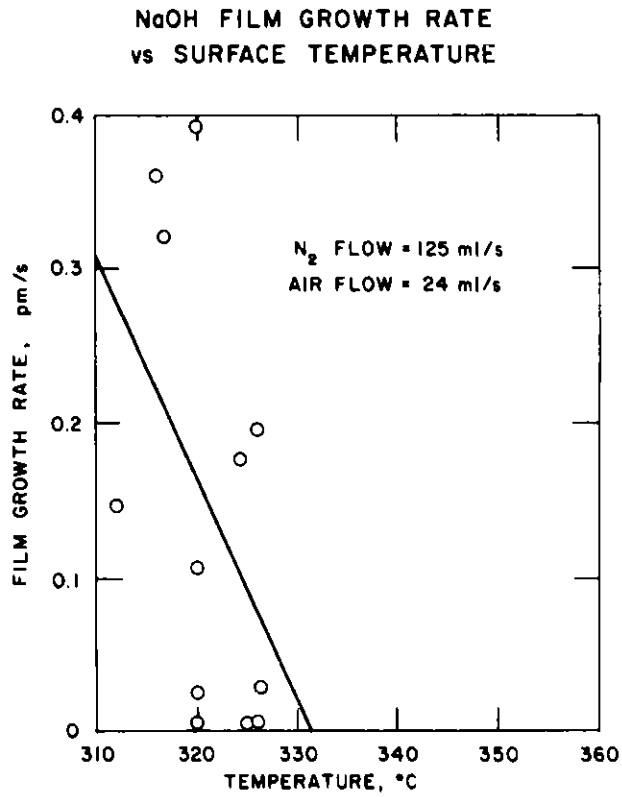
NaOH FILM GROWTH RATE
vs SURFACE TEMPERATURE
FILM GROWTH RATE, pm/s
0.4
0.3
0.2
0.1
0
N_2 FLOW = 125 ml/s
AIR FLOW = 24 ml/s
310
320
330
340
350
360
TEMPERATURE, °C

Fig. 9

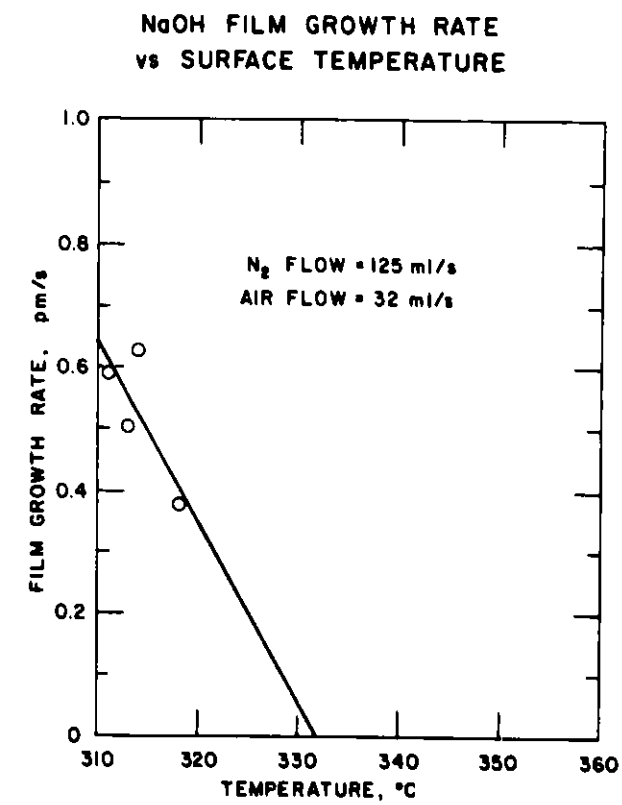
NaOH FILM GROWTH RATE
vs SURFACE TEMPERATURE
FILM GROWTH RATE, pm/s
1.0
0.8
0.6
0.4
0.2
0
N_2 FLOW = 125 ml/s
AIR FLOW = 32 ml/s
310
320
330
340
350
360
TEMPERATURE, °C

Fig. 10

VIII. CONCLUSIONS

The preliminary experiments with NaCl and NaOH have demonstrated the potential usefulness of the electrical conductivity technique. Alkali metal salt-deposition rates from a hot gas stream can be measured in situ.

The present probe design does need improvement. A new air-coolant tube and test surface have been designed. In this design, the coolant air passes through a closed loop. The coolant blows on the back of the test surface but then exits from the system without mixing with and diluting the carrier gas. Initial testing of this new design is presently under way.

Initial experiments have been done with a "clean" carrier gas. Additional tests with a simulated flue gas, and eventually in a PDU, will be necessary. Further refinement and design changes will undoubtedly be made, but the basis for practical instrumentation is now available.

IX. ACKNOWLEDGMENTS

This work is supported by the U.S. Department of Energy. The authors wish to thank A. A. Jonke, ANL Director of Fossil Energy Program; Leslie Burris, Director of the Chemical Engineering Division; and D. S. Webster, the Deputy Director of the Chemical Engineering Division, for their administrative support and encouragement. We also extend our thanks to F. G. Teats for helping with the experimental work.

X. REFERENCES

1. J. Stringer, Hot Corrosion in Gas Turbines, Corrosion Problems in Energy Conversion and Generation, The Electrochemical Society, Princeton, N.J., pp. 79-101 (1974).

2. M. A. DeCrescente and N. S. Bornstein, Formation and Reactivity Thermodynamics of Sodium Sulfate with Gas Turbine Alloys, Corrosion 24(5), 127-133 (1968).

3. W. T. Reid, External Corrosion and Deposits, Elsevier, New York (1971).

4. J. Stringer, Hot Corrosion of High-Temperature Alloys, Ann. Rev. Mater. Sci. 7, 477-509 (1977).

5. E. Raask, Reactions of Coal Impurities During Combustion and Deposition of Ash Constituents on Cooled Surfaces, The Mechanism of Corrosion by Fuel Impurities, H. R. Johnson and D. J. Littler, Eds., Butterworths, London, pp. 145-154 (1963).

6. J. A. Goebel and F. S. Pettit, Alloy-Molten Slag Reactions Associated with Hot Corrosion of Alloys, Metal-Slag-Gas Reaction and Process, Smeltzer and Foroulis, Eds., Intern. Symp. of Electrochem. Soc., Toronto, Canada, May 11-16, 1975, pp. 693-710.

7. R. F. Reising, Molten Sodium Sulfate Induced Corrosion of Nickel Alloys, Metal-Slag-Gas Reaction and Process, Smeltzer and Fouroulis, Eds., Intern. Symp. of Electrochem. Soc., Toronto, Canada, May 11-16, 1975, pp. 747-761.

8. R. M. A. Azzam and N. H. Bashara, Ellipsometry and Polarized Light, North Holland, Amsterdam (1977).

9. R. H. Muller, Principles of Ellipsometry, Adv. Electrochem. Eng., R. H. Muller, Ed., 9, 167-226 (1973).

10. H. F. Johnstone, Univ. Illinois Bull. 27, No. 13 (1929).

11. D. Flint, The Investigation of Dew Point and Related Condensation Phenomenon in Flue Gases, J. Inst. Fuel 21, 248 (1948).

12. P. F. Corbett, D. Flint, and R. F. Littlejohn, Development in the B.C.U.R.A. Dew Point Meter, for the Measurement of the Rate of Acid Build-up on Cooled Surfaces Exposed to Flue Gases, J. Inst. Fuel 25, 246 (1952).

13. P. F. Corbett, The Determination of SO_2 and SO_3 in Flue Gases, J. Inst. Fuel 24, 247 (1951).

14. G. G. Thurlow, An Air-Cooled Metal Probe for the Investigation of the Corrosive Nature of Boiler Flue Gases, J. Inst. Fuel 25, 252 (1952).

15. J. E. Helt, Evaluation of Alkali Metal Sulfate Dew Point Measurement for Detection of Hot Corrosion Conditions in PFBC Flue Gas, Argonne National Laboratory Report, ANL/CEN/FE-80-12, 1980.

16. R. J. Bishop, J. Inst. Fuel 41, 55-65, 1968.

17. P. J. Jackson and H. C. Duffin, C.E.G.B. Conf. Mechanism of Corrosion by Fuel Impurities, Butterworths, London, pp. 427-442 (1963).

18. Y. S. Touloukian, Ed., Thermophysical Properties of High Temperature Solid Materials, Vol. 4, Part 1, MacMillan, New York (1967).

AUTOMATED ON-LINE DETERMINATION OF PPB LEVELS OF SODIUM AND POTASSIUM IN LOW-BTU COAL GAS AND FLUIDIZED BED COMBUSTOR EXHAUST BY ATOMIC EMISSION SPECTROMETRY

W. J. Haas, Jr., D. E. Eckels, R. N. Kniseley, and V. A. Fassel
Ames Laboratory, Iowa State University, Ames, Iowa 50011

ABSTRACT

The Morgantown Energy Technology Center (METC), U. S. Department of Energy, is involved in the development of processes and equipment for production of low-BTU gas from coal and for fluidized bed combustion of coal. The ultimate objective is large scale production of electricity using high temperature gas turbines. Such turbines, however, are susceptible to accelerated corrosion and self-destruction when relatively low concentrations of sodium and potassium are present in the driving gas streams. Knowledge and control of the concentrations of those elements, at part per billion levels, are critical to the success of both the gas cleanup procedures that are being investigated and the overall energy conversion processes. This presentation describes instrumentation and procedures developed at the Ames Laboratory for application to the problems outlined above and results that have been obtained so far at METC. The first Ames instruments, which feature an automated, dual channel flame atomic emission spectrometer, perform the sodium and potassium determinations simultaneously, repetitively, and automatically every two to three minutes by atomizing and exciting a fraction of the subject gas sample stream in either an oxyhydrogen flame or a nitrous oxide-acetylene flame. The analytical results are printed and can be transmitted simultaneously to a process control center.

INTRODUCTION

Coal gasification/combustion and fluidized bed combustion of coal, when employed with combined cycle (gas turbine/steam turbine) electrical generation, are attractive approaches for the production of electricity from coal. Both approaches offer important possibilities for control of sulfur and nitrogen oxide emissions, within acceptable environmental limits.

Other constituents of coal can also influence the economics, process chemistry, and/or environmental acceptability of gasification/combustion and fluidized bed combustion. The presence of trace quantities of Na and K in fuels for gas turbine applications has been implicated in accelerated turbine materials corrosion and failure (1). Also, elements such as As, Be, Cd, Pb, Se, and V are toxic, and emissions of such elements from large scale power facilities are either already regulated or might be expected to come under regulation in the future.

Because of the need for knowledge and control of the elemental composition of the turbine driving gases, the Ames Laboratory has been involved in a series of projects, all funded by METC, for development of analytical instruments and procedures for on-line determination of alkali and other trace elements in coal-gas and in fluidized bed combustion process streams. Table 1 contains brief descriptions of the first two instruments and methods

included in the development program.

Table 1. Instrumentation Development for Alkali Monitoring

	INSTRUMENT/(METHOD)	APPLICATION
1.	Alkali Monitor (Flame Emission Spectrometry with a premix slot burner and oxyhydrogen flame)	Determination of total Na and total K in cleaned gasifier product.
2.	FBC Modification of Instrument 1. (Flame Emission Spectrometry with a specially designed circular-slot burner, nitrous oxide - acetylene flame, and axial introduction of the sample stream)	Determination of total Na and total K in hot, scalped FBC gas streams (maximum particulate size ≤ 10 μm).

The instruments listed in Table 1 are real-time, computer-controlled analysis systems, designed to take a continuous sample flow in the range of 1 L/min. to 10 L/min. They are capable of detecting ng/g or fractional ng/g levels of the alkali elements, and they are capable of performing the necessary concentration determinations on-line, with a maximum automatic repetition rate greater than one analysis per minute. The instruments are capable of logging the analytical results on removable computer-readable media and can simultaneously transmit the results to a process control center or to a remote process control computer.

INSTRUMENTATION AND PROCEDURES

Figure 1 shows the spectroscopic equipment that is common to both the Alkali Monitor and the FBC Modification.

Burners

The Alkali Monitor uses a linear-slot premix burner (2), and the sample gas stream is mixed with oxygen and hydrogen before combustion. This burner and the operating conditions indicated in Table 2 were selected to maximize the detection power of the system for the ultra-low Na and K concentrations expected for the cleaned coal-gas stream.

Table 2. Description and operating conditions for the linear-slot premix burner

SLOT	76.2 mm X 0.127 mm
COMBUSTION GASES	
Hydrogen	40.5 L/min
Oxygen	9.6 L/min
SAMPLE GAS STREAM	1 to 10 L/min
OBSERVATION HEIGHT	20 mm above slot

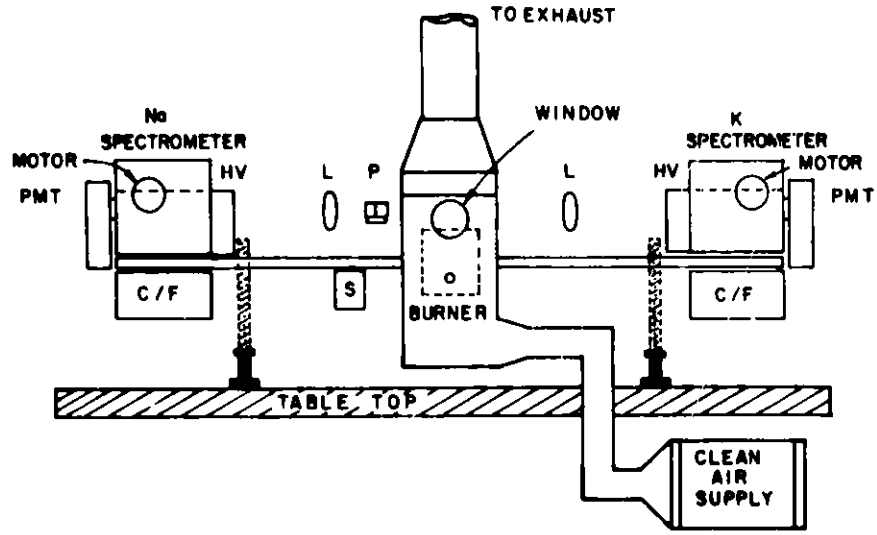

Figure 1. Spectroscopic equipment arrangement for Alkali Monitor and FBC Modification.

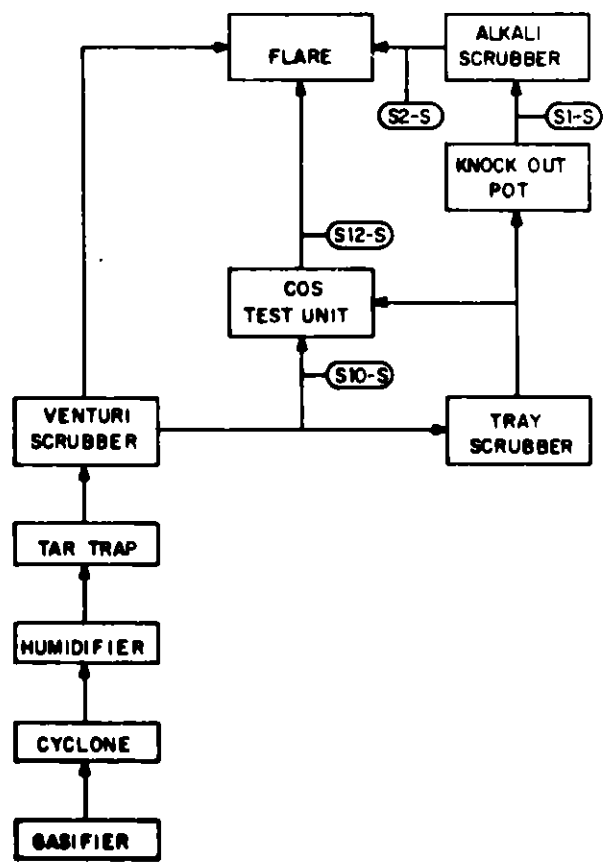

Figure 2. Process stream configuration and sampling points for METC gasifier run #94.

The FBC Modification uses a water-cooled, circular-slot burner, specially designed for introduction of a hot, particulate-laden gas sample stream along the central axis of the burner and the flame. This mode of sample introduction and the burner operating conditions given in Table 3 were chosen (1) to avoid the loss of particulates that would be expected to occur in a conventional linear-slot burner, and (2) to provide the high temperature and long flame residence time required for vaporization of the particulates. Under the conditions indicated, the nitrous oxide-acetylene flame provides a temperature of approximately 2700 K, and a residence time in the range of 1 to 10 msec. Other aspects of the design and operation of the circular-slot burner have been described previously (3).

Table 3. Description and operating conditions for the circular-slot burner.

SLOT	25.4 mm dia. X 0.127 mm
COMBUSTION GASES	
Acetylene	3.3 L/min
Nitrous Oxide	16.6 L/min
STABILIZING GAS	
Argon	2 L/min
SAMPLE GAS STREAM	1 to 10 L/min
Introduction tube	3.5 mm i.d.
OBSERVATION HEIGHT	40 mm above slot

Spectrometric Measurements

Both the Alkali Monitor and the FBC Modification employ one spectrometer for measurement of emission from Na atoms present in the flame and a second spectrometer for simultaneous measurement of the emission from K atoms. The wavelength of the radiation measured in each spectrometer (588.995 nm for Na, and 766.490 nm for K) is determined by the grating angle of incidence, and the latter is determined, independently for each spectrometer, by a computer-driven stepping motor. The two spectrometers employ standard photomultiplier detectors, and the photocurrent measurements are performed with current-to-frequency converters.

Enclosures

The purpose of the water-cooled burner enclosure and HEPA-filtered air supply is to prevent ambient airborne particulates from entering the flame. In early field trials without the enclosure, the Na and K emission caused by such particulates was often several orders of magnitude greater than the emission caused by Na and K in the coal-gas. Because such high blank levels were clearly unacceptable, the enclosure and clean air supply have been employed for all subsequent analyses of the coal-gas stream. They have been effective in reducing the blank to concentration levels of well below 1 ng/g. The enclosure and clean air supply have not been required, so far, for measurements with the FBC Modification, because the Na and K content of the FBC gas stream is much higher than that of the cleaned coal-gas stream.

The use of light-path enclosures to prevent ambient light from entering the two spectrometers is a second practice that, so far, has only been required for the Alkali Monitor. The purpose of the latter enclosures is to exclude light from the high pressure Na lamps used for general illumination of the coal-gasifier work areas at METC. The light-path enclosures (not shown in Figure 1) are constructed of black acrylic plastic and their inner surfaces are painted flat black. They completely enclose the light path between the burner enclosure and the entrance slits of the two spectrometers.

COMPUTER CONTROL AND WAVELENGTH ALIGNMENT

The instrument computer (Digital Equipment Corp., Model PDP-11/03) controls the spectrometer stepping motors, acquires the photocurrent measurement results from the current-to-frequency converters, averages the results for the measurement period selected by the analyst, and controls the operation of three solenoids. Two of the solenoids operate valves that select either the sample gas stream or a synthetic gas stream for introduction into the burner. (As will be described below, the synthetic stream is used for calibration of the instrument.) The third (rotary) solenoid is used to swing two right angle prisms into the optical line of sight between the entrance slits of the two spectrometers. When in that position, the prisms deflect light from a Na and K hollow cathode lamp into the two spectrometers. The hollow cathode lamp (not shown in Figure 1) is located behind the burner enclosure. Light from the hollow cathode lamp is used as the reference for determination of the optimum wavelength settings for the spectrometers. For that determination, each spectrometer is scanned through a small wavelength region around the emission line of interest. The data obtained are then examined to determine the wavelength settings that yielded maximum Na emission intensity and maximum K emission intensity. The computer sets the spectrometers to those wavelengths automatically at the conclusion of this "wavelength alignment" procedure. The entire wavelength alignment procedure is performed by the computer, with no assistance from an operator, and can be executed either at the operator's command or, automatically, after each n analyses, where n is a software parameter value entered by the analyst. The wavelength alignment feature provides a certain degree of immunity from drift that might otherwise occur because of the wide ambient temperature range often experienced in coal gasification and combustion facilities.

Calibration

Both the Alkali Monitor and the FBC Modification can be calibrated in the field. The instruments are calibrated using measurements of the emission intensities observed when a known flow rate of a synthetic gas stream, containing known amounts of Na and K, is introduced into the flame. Aqueous reference solutions that contain known amounts of Na and K salts are pumped to an ultrasonic nebulizer at a known rate; the nebulizer transforms the solutions into finely dispersed aerosol in a synthetic gas stream that has been prepared beforehand with a composition that approximates the composition of the sample stream of interest (i.e., the coal-gas stream or the FBC sample stream). Water from the aerosol droplets is vaporized and removed from the stream as it passes through a desolvation apparatus. The synthetic gas stream, as introduced into the burner, contains Na and K in the form of dry, alkali-containing particulates. The facilities used for addition of the alkali elements to the synthetic gas stream are described in References 3 and 4.

Both instruments employ least squares fitting calculations to establish a calibration equation of the type

$$c_i = \sum_{j=0}^{m} a_j I_i^j \qquad (1)$$

for each analyte. The values of the coefficients a_j are determined in the least squares calculation, c_i is the calculated concentration of the analyte in the ith reference solution, and I_i is the analyte emission intensity observed for the ith reference solution. The number of terms in each calibration equation (m+1) is specified by the analyst. The most frequently used values are m+1=2 and 3, corresponding to linear or quadratic calibration equations, respectively. The analyte emission intensity is determined by subtracting the intensity of the background emission, I_b, from the intensity of the analyte plus background emission, I_i+I_b. The latter quantity is the total intensity measured at the specified analysis line wavelength. I_b can be measured at a wavelength slightly less or slightly greater than the analysis line wavelength, or at two such offset wavelengths. If background measurements are made at two offset wavelengths, linear interpolation is employed for estimation of the background emission at the analysis line wavelength. The background correction procedure for Na can differ from that employed for K. A typical calibration procedure employs 4 or 5 reference solutions, covering a concentration range of two orders of magnitude; the calibration equations obtained are very nearly linear.

The relationship between the concentration of the analyte in solution and the concentration of analyte in the sample gas stream is given by

$$c_{gas} = \left(\frac{re}{Vd}\right) c_{soln} \qquad (2)$$

Here r is the rate at which the solution is delivered to the nebulizer, e is the efficiency of nebulization, i.e., the fraction of dissolved analyte that is nebulized and introduced into the flame, V is the volume flow rate of the sample gas stream, and d is its density. The computer interface module has provisions for accepting binary input of the volume flow rate during the course of the intensity measurements. For determination of the concentration of Na and K in the sample gas stream, the equipment measures the analyte emission intensities and uses the previously determined values of the calibration coefficients to compute the solution concentrations that would yield those intensities. The concentrations of the analytes in the sample gas stream are then determined by application of Equation (2), above.

EXPERIMENTAL RESULTS

Alkali Monitor

The first measurements with the Alkali Monitor were conducted on the gasifier sidestream cleanup system at METC in December, 1979. Table 4 gives a summary of results for gas obtained from various sampling points, and under various cleanup conditions employed during that run. Figure 2 shows the process stream configuration and identifies the sampling points. The limit of detection was approximately 0.1 ng/g for both Na and K.

Table 4. Summary of sodium and potassium concentration results for sidestream cleanup product from METC gasifier run #94, December, 1979.

Sampling Point	Date	Time Period	Average Sampling Rate (L/min)	Total Sample Volume (L)	SODIUM		POTASSIUM	
					Greatest Concentration (ng/g)	Mean Concentration (ng/g)	Greatest Concentration (ng/g)	Mean Concentration (ng/g)
S1-S	12/3	1142-1835	5.1	2106	12	2	61	10
	12/4	1122-1635	7.0	2191	n.d.	n.d.	6	0.8
	12/5	1106-1501	6.9	1622	0.5	0.1	13	1.4
	12/6	1641-1710	7.6	220	n.d.	n.d.	0.5	0.3
	12/7	1104-1604	7.1	2130	0.9	0.1	8	1.6
S2-S	12/5	1515-1709	8.4	958	n.d.	n.d.	0.3	0.1
S10-S	12/6	0047-0241	5.8	661	2	0.4	12	1.7
S12-S	12/5	2113-0040	4.4	911	10	1.3	50	6.1

n.d.=not detected

The Alkali Monitor was also used in September, 1980, for analysis of the product from the METC full-stream cleanup system. No Na or K were detected in the gas from that run, even though our tests of the Alkali Monitor showed that the instrument was working perfectly.

For both of the occasions mentioned above, the results obtained with the Alkali Monitor were checked by independent analyses performed by METC personnel. The latter analyses were performed by an impinger method (3). Within the limitations of the impinger method, the results verified those obtained with the Alkali Monitor.

FBC

The first application of the FBC Modification of the Alkali Monitor was conducted in January, 1981, using a hot sample stream from the METC 6-inch diameter, laboratory scale, atmospheric fluidized bed combustor. The sample gas stream for analysis was taken from the output of a small cyclone located within the freeboard of the FBC. The instrumentation for alkali monitoring was located directly above the top of the FBC. The hot gas sample line and valve, and the instrument calibration line were heat traced and maintained at the freeboard temperature. The total length of the sample line was approximately four feet. A complete description of the sampling arrangement and the mass loading and particule size characteristics of the sample stream are contained in References 3 and 5.

Because of its small size, the freeboard cyclone required blowdown at frequent intervals. Similarly, the operational requirements of the gas analysis instrumentation (SO_2, NO, NO_x, etc.) necessitated another frequent blowdown procedure. Generally, both blowdown procedures were performed prior to each series of 10 to 15 consecutive alkali measurements, i.e., when the sample line to the circular-slot burner was closed and the wavelength alignment procedure was being executed. During the course of the alkali measurements, it was noted that a simple blowdown with high pressure air was not always sufficient for cleaning the freeboard cyclone. Therefore, a variety of other cleanout and blowdown procedures, including insertion of a cleaning rod into the bottom of the cyclone, were applied for some of the measurements. The various cleanout and blowdown procedures employed for different series of measurements obviously differed in their effectiveness, as will be seen below.

Figure 3 shows the analytical results that were obtained when the FBC was operated with Tymochtee dolomite as the bed material and propane as the fuel. (The bed probably contained some coal ash residue as well, because the same bed had been used for burning coal during the previous day's work.) The principal conclusions from the dolomite plus propane results are given below.

(1) The concentrations of Na and K in the FBC sample stream were approximately 0.2 to 0.4 ppm and 1 to 2 ppm by weight, respectively.

(2) The first one or two alkali concentration values obtained after the closing and opening of the sample stream valve at the beginning of each of the three measurement series were probably not representative of the concentrations that prevailed later in each series, after a more stable sampling situation had been established. Particulate hangup on the closed ball valve and/or on the sample line walls when the valve was closed, and subsequent

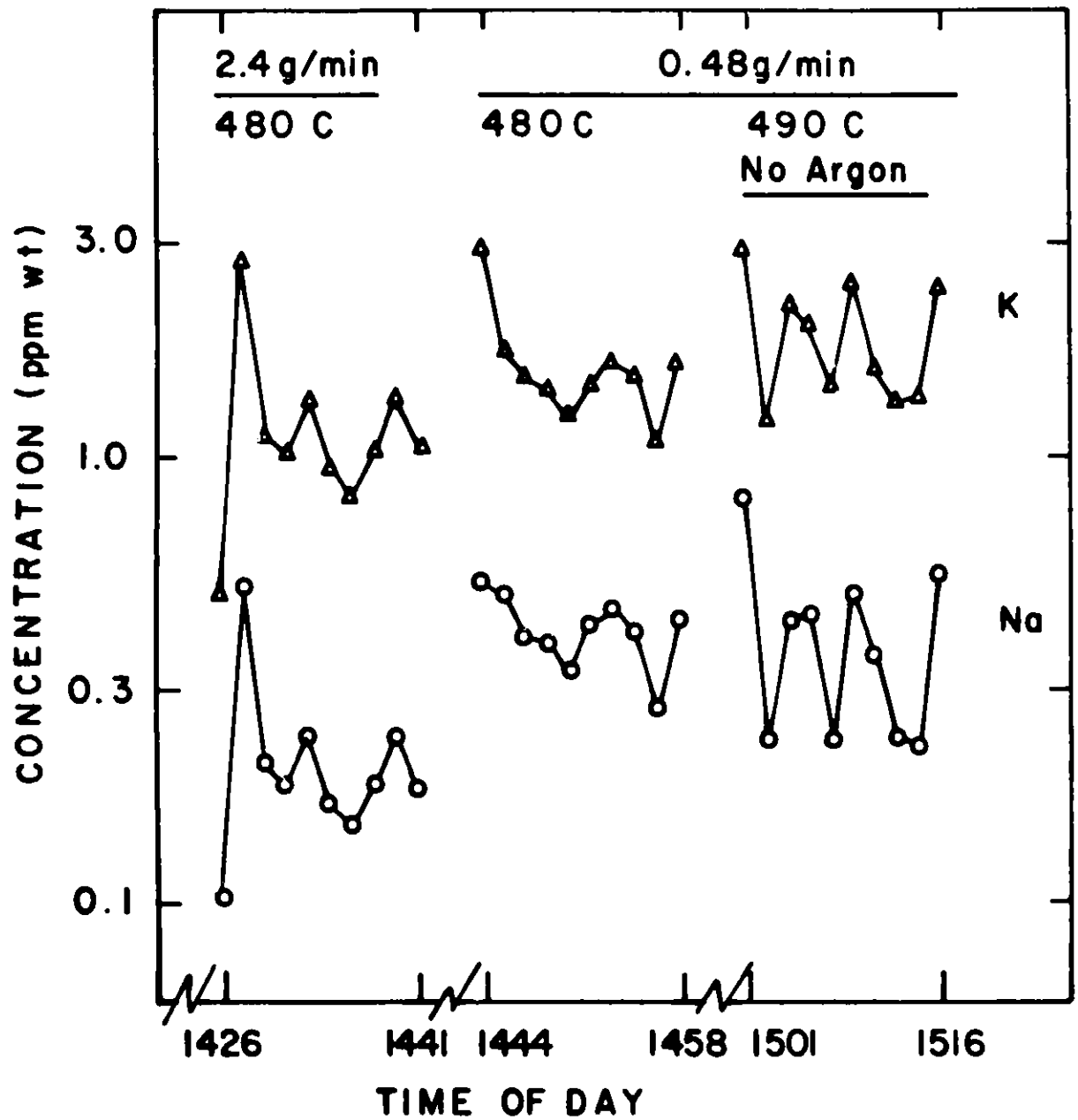

Figure 3. Alkali content of the FBC hot gas sample stream for the case: bed material = Tymochtee dolomite; fuel = propane. The data averaging time for each background and analyte line intensity measurement was 30 sec. The mass flow rate and temperature of the sample stream for the various measurement times are indicated at the top of the Figure. The notation "No Argon" above the results for the third series of measurements means that the flow of "Stabilizing Gas" was turned off for that series (Please see Ref. 3). Prior to each of the three series of measurements, the sample stream was turned off, the wavelength alignment procedure was performed, and then the sample stream was turned back on again.

non-reproducible reentrainment of those particulates when the valve was reopened is one possible explanation for the divergence of the first results in each series.

(3) The ratio of the concentration observed for K at time t_i to that observed for Na at the same time was approximately constant ($3.5 \leq \text{ratio} \leq 6$) for all of the measurements shown in Figure 3. This is the type of behavior expected for time-averaged measurements on a sample stream whose constituents are derived from a fluidized bed that is composed of relatively stable and uniform material, and whose total mass is large compared to the content of the sample stream.

(4) The presence or absence of the stabilizing gas flow had no significant effect on the observed alkali concentration levels.

Figure 4 shows the analytical results for the case in which the FBC was operated with Tymochtee dolomite as the bed material and Pittswick coal as the fuel. Only coal was fed during the period shown. As before, the sample stream valve was closed, the wavelength alignment procedure was executed, and then the valve was reopened, prior to each of the six series of measurements. Also, as mentioned above, various cleanout and blowdown procedures were performed prior to each series of measurements. The principal features of the results were as follows.

(1) The lowest alkali concentrations observed for this case were approximately ten times greater than for the dolomite plus propane case.

(2) The alkali concentrations in the sample stream appeared to increase with time during each series of measurements, i.e., after each cleaning of the freeboard cyclone. Apparently, the lowest alkali concentration levels were observed just after execution of those cleaning procedures that were most effective for restoring the particle separation capability of the cyclone. The particle separation capability appeared to degrade most rapidly after the most effective cleanings.

(3) The observed K/Na concentration ratios were relatively constant ($2 \leq \text{ratio} \leq 3.5$), as in the dolomite plus propane case.

(4) The Na and K concentration values obtained when substantially higher flows of N_2O and C_2H_2 were employed (without recalibration of the instrument) were approximately twice as large as those obtained with the normal flows for those gases. The apparent concentration increases are not attributed to an increase in the efficiency of particulate vaporization. On the contrary, as the flows of N_2O and C_2H_2 are increased, the temperature of the flame at the spectroscopic observation height actually decreases as compared to the low flow case. The lower temperature causes relatively small decreases in the concentrations of alkali ions in the flame, but relatively large increases in the concentrations of alkali atoms. Because the instrument measures emission from alkali atoms, it sees the larger relative changes. If the instrument had been calibrated for use at the high flow rates as well as for the low flow case, it is likely that alkali measurements conducted under the two different sets of conditions would have yielded nearly identical results.

Figure 5 shows the alkali concentrations for the case in which the FBC was operated with simultaneous feeding of both coal and dolomite. As before,

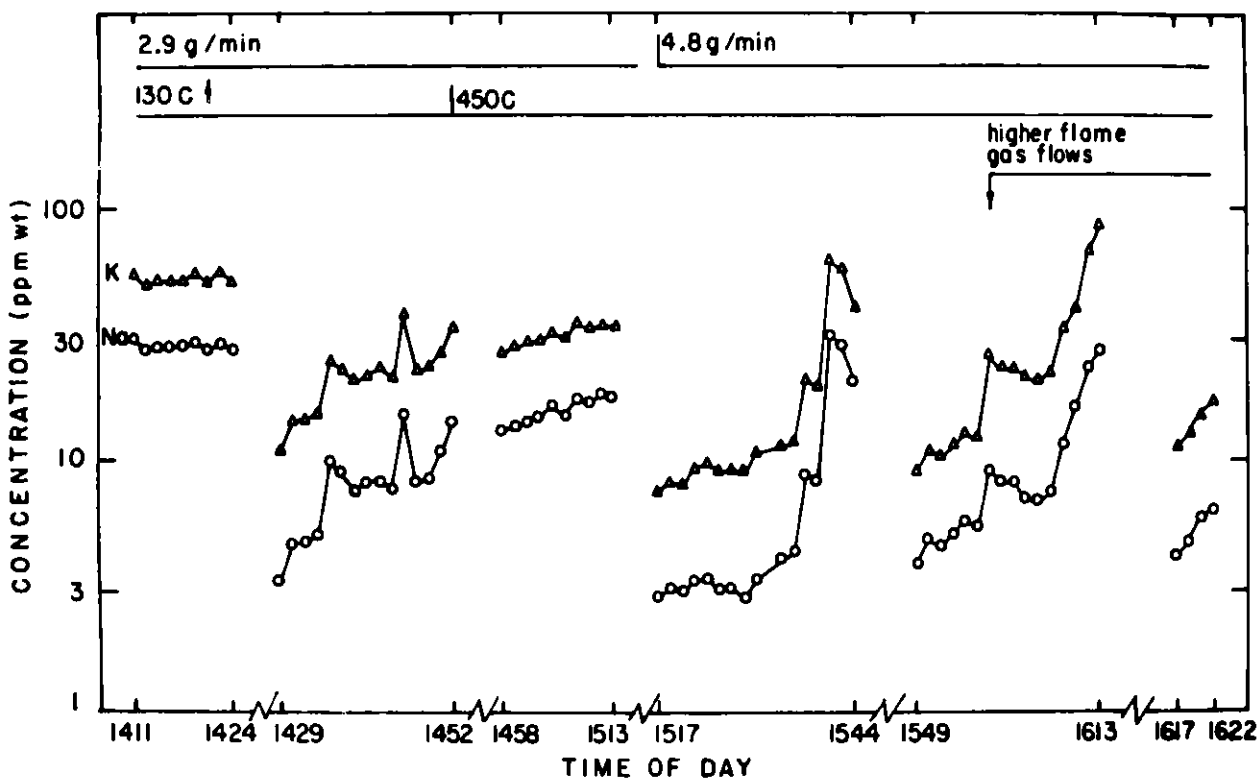

Figure 4. Alakli content of the FBC hot gas sample stream for the case: bed = Tymochtee dolomite; fuel = Pittswick coal (2.2 lbs/hr). Data averaging time = 30 sec. The sample stream flow rates and temperatures are indicated at the top of the Figure. The notation 130 ↑ means that the sample stream temperature was being increased from 130°C at time = 1411 to 450°C at time = 1452. The flows of N_2O and C_2H_2 were increased to 19.9 and 4.7 L/min, respectively, for the measurements indicated at the right hand side of the Figure.

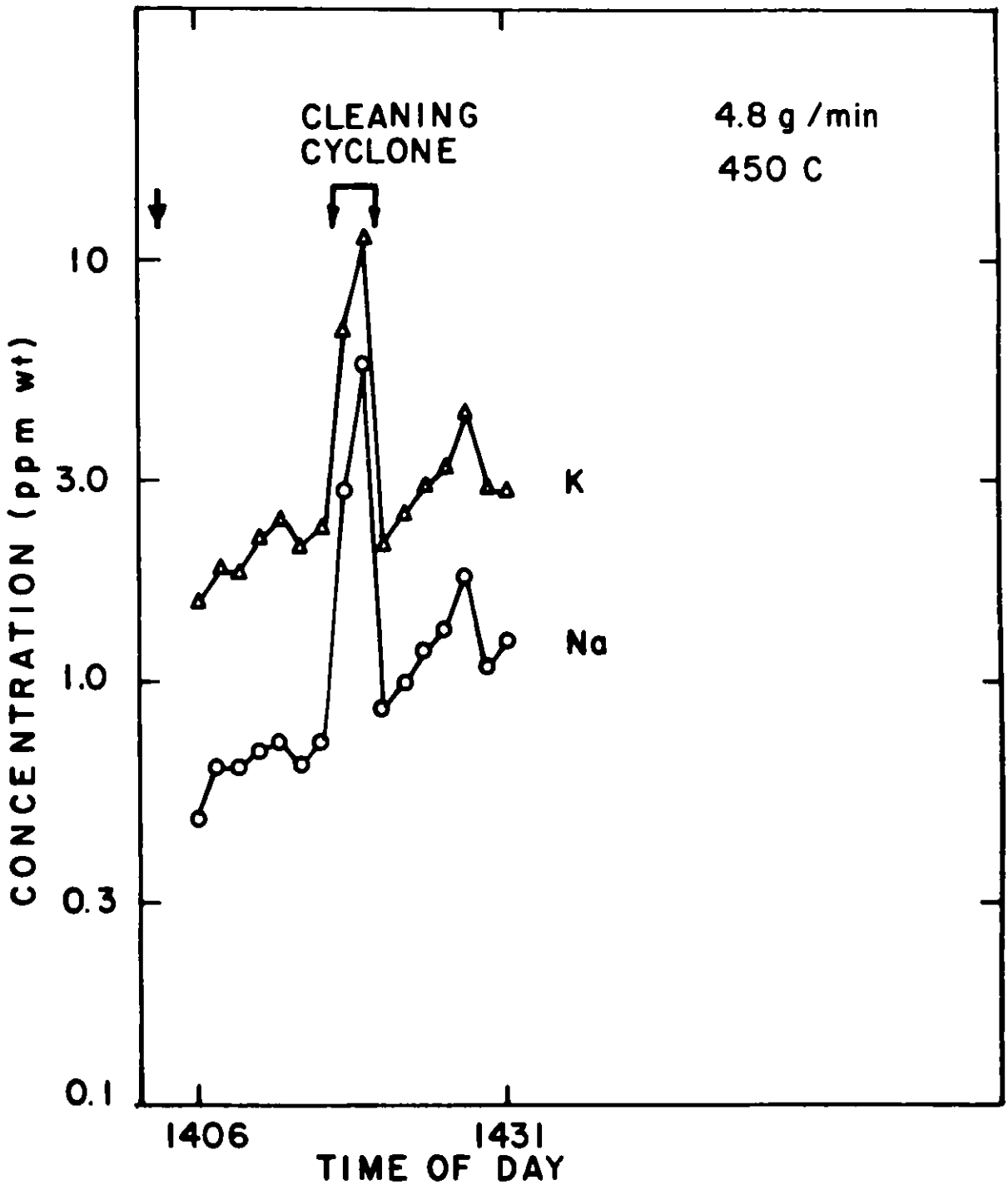

Figure 5. Alkali content of the FBC hot gas sample stream for the case: bed = Tymochtee dolomite (0.81 lbs/hr); fuel = Pittswick coal (2.2 lbs/hr). Data averaging time = 30 sec. The sample stream temperature and flow rate are indicated.

the freeboard cyclone was cleaned just before the start of the measurement series. The sample line valve was closed during this initial cleaning period and it was reopened just before the first measurements. After seven pairs of measurements were completed, the cyclone was cleaned again, but this time without interruption of the sample flow or the measurement sequence. The approximately 10-fold higher apparent alkali concentrations observed during the second cyclone cleaning are consistent with the much higher flow of sample gas and the increased level of particulate transport that occurred during the cleanout period. (The apparent concentrations during the second cleanout were not corrected for the larger sample flow rate.) Remarkably, the concentrations reported in Figure 5 were five to ten times lower than for the case in which only coal was fed. Apart from the possibility that the particular cyclone cleaning procedure employed before these measurements may have been more effective than previous procedures, we can offer no plausible explanation for the lower concentration levels. The results for the case in which both coal and dolomite were fed exhibited the same trend toward higher concentrations after cylcone cleanings as were found for the coal feed only case. As noted earlier, we believe this increase is caused by rather rapid degradation of the performance of the cyclone after each cleaning.

The total particulate loading of the sample stream for the coal plus dolomite case was 615 ppmw. That measurement was made by passing the sample stream through a glass fiber filter and determining the weight gain. The sample line heater was turned off for the mass loading measurement.

We had hoped to determine the alkali content of the material collected on the filter and thus obtain an independent measure of the alkali concentrations in the hot gas sample stream. Unfortunately, this proved to be impossible because of the large Na and K blank contributed by the filter itself. As an alternative, we calculated the ranges of the Na and K concentrations that would be expected if the particulates in the sample stream had the same composition as those collected in the two large cyclones and final filter on the main FBC exhaust line. The ranges of the concentrations calculated in this way were 2.7 to 12 ppmw for Na, and 8.9 to 25 ppmw for K. The ratios of the Na and K concentrations measured with the Alkali Monitor were in agreement with the values expected from the calculations, but the absolute values were considerably lower than expected. Nevertheless, the measured values were not inconsistent with the results obtained from chemical analysis of cyclone dust samples in the NCB-CURL 1000-hr PFBC test program (6).

CONCLUSION

The results obtained in the first field trials of the Alkali Monitor and FBC Modification of that instrument indicate that the instrumentation and analytical procedures described herein can provide valid on-line determinations of the total Na and total K content of coal-gas and hot FBC process streams. The principal problem that surfaced during the first field trials was the apparent difficulty in providing and maintaining a stable, representative sample stream in the FBC case.

ACKNOWLEDGEMENTS

We are grateful to John Kovach, Bob Romanosky, Ulrich Grimm, and Rodney

Anderson of METC, all of whom made important contributions to the work described here.

This work was supported by the Morgantown Energy Technology Center under U. S. Department of Energy Contract No. EY-77-21-0694.

REFERENCES

1. "Hot Corrosion of High Temperature Alloys", John Stringer, in Proceedings of the Symposium on Properties of High-Temperature Alloys, Z. A. Foroulis and F. S. Pettit (eds.), (Electrochemical Society, Princeton, NJ, 1976) 513.

2. J. A. Fiorino, R. N. Kniseley, and V. A. Fassel, Spectrochim. Acta 23B, 413 (1968).

3. "Development of Alkali and Trace Heavy Metal Monitors for Coal Conversion Process Streams", W. J. Haas, Jr., D. E. Eckels, R. N. Kniseley, and V. A. Fassel, in High Temperature, High Pressure Particulate and Alkali Control in Coal Combustion Process Streams, Proceedings of U. S. Department of Energy Contractor's Meeting, Feburary 3-5, 1981, Morgantown WV. (Available from the Morgantown Energy Technology Center, Collins Ferry Road, Morgantown, WV).

4. K. W. Olson, W. J. Haas, Jr., and V. A. Fassel, Anal. Chem. 49. 632 (1977).

5. "High Temperature Measurements of Alkali Levels in an Experimental 6-Inch AFBC", U. Grimm, R. J. Anderson, and R. R. Romanosky, in High Temperature, High Pressure Particulate and Alkali Control in Coal Combustion Process Streams, Proceedings of U. S. Department of Energy Contractor's Meeting, Feburary 3-5, 1981, Morgantown, WV. (Availability as in Ref. 3).

6. K. K. Pillai and P. Wood, Fluidized Bed Combustion, 1000 Hour Test Programme in a Pressurized Fluidized Bed Combustion Facility, Final Report, Vol. III - Combustor Emissions and Hot Gas Cleanup, U. S. Department of Energy Report No. FE-3121-15c.

LASER-INDUCED BREAKDOWN SPECTROSCOPY: DETECTING SODIUM AND POTASSIUM IN COAL GASIFIERS

T. R. Loree and L. J. Radziemski
University of California, Los Alamos National Laboratory
P. O. Box 1663, Los Alamos, New Mexico 87545

INTRODUCTION

One of the classic techniques for the detection of atomic species is the analysis of optical spectra emitted from an excited sample. In general, emission spectroscopy requires a method of exciting the medium of interest, a light gathering system, a spectral resolver, and a photon detector. We are investigating a variant of emission spectroscopy called LIBS, an acronym for laser-induced breakdown spectroscopy. While conventional in the detection methods, this approach excites the sample materials by the breakdown that occurs in the focal spot of a high-powered laser beam.

The breakdown generates a plasma[1] of excited atoms, ions (singly-ionized under our conditions), and electrons, all of which radiate brightly. The laser pulse is quite short (tens of nanoseconds) but the plasma lasts for tens of microseconds. The initiation of the breakdown requires a reasonable mass of material in the focal volume; that mass can be in the form of a gas, entrained particles in a gas, or a solid surface. For studies of coal gasification we are concerned with mixtures of gaseous compounds and entrained ash particles. Whatever the composition of the parent medium, the plasma contains only the constituent atomic species, with molecules and radicals appearing in recombination as the plasma cools.

LIBS EXPERIMENTS

Since the LIBS technique requires only optical access, and not physical intrusion, it is well suited to sampling hostile environments. A representative apparatus is shown in Fig. 1, a schematic of the setup used in our gasifier field tests. The laser beam enters from the left, is focused into the product stream, and causes breakdown there. The emitted light is gathered from a viewing port, dispersed by a spectrometer, and detected and recorded by an optical multichannel analyzer. An analysis of the recorded spectra then identifies the atomic makeup of the product gas. Both detection and analysis can be carried out at various levels of complexity, to the limits of one's finances and time. In our gasifier tests, we limited our efforts to the degree required to detect and unambiguously identify sodium and potassium. Detailed information pertinent to Fig. 1 is contained in Appendix A.

The coal gasifier/combuster used in the field tests was a laboratory-scale device built under the leadership of Prof. Paul Hedman in the Chemical Engineering Department of Brigham Young University. The conditions in the test section are detailed in Appendix B. The field testing was preceded by six months of intensive experimentation, establishing the necessary background information on gases and particulate spectra, including samples of powdered BYU coal.

An example of the survey spectra obtained from the gasifier is given in Fig. 2. The dominant spectral line is the hydrogen alpha at 656.3 nm. The next strongest spectral line comes from oxygen, followed by characteristic lines of sodium and potassium. The identifications were not made from these rough spectra; in Figs. 3 and 4 we show the medium-resolution spectra in the regions of the sodium and potassium lines, along with calibration lines from a standard neon lamp. The sodium doublet was further pursued to higher resolutions, where the observed splitting confirmed identification.

We thus achieved the goals of the field testing, which was to simply detect sodium and potassium in the field, and in real time. These spectra required 25 seconds of collection time (256 laser shots) for valid statistics, but the spectral lines were observable in a single shot. Since there is some line broadening and an increase in white light at higher pressures, it was to our advantage that the gasifier was running at atmospheric pressure. These problems, however, may be ameliorated by an extension of the LIBS technique, called TRELIBS (for time-resolved LIBS).

TRELIBS DEVELOPMENT

Subsequent to the LIBS field test, we tried adding time resolution to the detector section. This was done by using either a time-gated optical multichannel analyzer, or gating the signal from a photomultiplier. In the latter case, the spectral resolver was either a scanning monochromator or a narrow-band transmission filter.

It was immediately clear that with LIBS we had been integrating quite a bit of optical history, which with TRELIBS was resolvable into its various components. This is shown in Fig. 5, a series of TRELIBS spectra for a sample of oxygen at STP conditions. The spectra are not corrected for the wavelength sensitivity of the diode array, and thus are relative, but it is clear that the early spectra contain ionic lines superimposed on a strong continuum, while the late-time spectra contain only neutral atomic lines, with very little background. The improved signal-to-noise and detectability at late times were unintentionally demonstrated in this example by the appearance of hydrogen lines from an unsuspected impurity in the oxygen sample.

As the strongest sodium and potassium spectral lines (Figs. 3 and 4) are neutral atom emissions, one should gain in detectability for these elements by going to late-time TRELIBS. This is illustrated in Fig. 6, which contrasts early and late-time spectra from NaCl in air. The early spectrum is essentially that of air, with no detectable sodium emission from the NaCl particles. In the late spectrum, however, the sodium D lines dominate the air contribution, and the white light background is negligible.

TRELIBS is also of use in avoiding the line-broadening effects that can be seen in LIBS spectra at high pressures. This is shown in Fig. 7, which compares LIBS spectra of 1 and 10-atm helium and a delayed 10-atm TRELIBS spectrum. The delayed spectrum is, as expected, composed only of sharp neutral lines; the delay time required to develop these is shorter than at 1 atm.

We are engaged in an effort to obtain absolute calibrations that will enable us to derive sample concentrations from observed signal amplitudes. The apparatus being used in the first round of testing is shown in Fig. 8. A known solution of NaCl is aspirated by a nebulizer into a known gas flow. This is heated before passing into the experimental optical cell, so that the laser focus takes place in a region of known NaCl concentration. From the focal volume, one can derive the actual mass of sodium being sampled. Figure 9 shows the solium doublet observed with 85 pg in the plasma on each shot, taken after a delay of 5 μs. In this case the detection system consisted of a 1/2-m scanning monochromator and a photomultiplier. From the signal-to-noise ratio of this trace, one would estimate that one could detect 20 pg (2 mg/m^3) of sodium with this particular apparatus. This is by no means intended to represent a limit of detectability for sodium by TRELIBS, since the apparatus under discussion is far from an optimum embodiment. Using a narrow-band transmission filter and photomultiplier detection system (instead of the more general monochromator/photomultiplier) would allow collection of several orders of magnitude more signal. The present focal volume can also be increased, which for a fixed detectable mass would increase the concentration sensitivity. The critical issue will be the influence of such changes on the signal-to-noise ratio.

CONCLUSIONS

The goal of this research program is the eventual development of a real-time monitor of trace quantities of elements present in hostile environments such as coal gasifier process streams. With LIBS, we have demonstrated the ability to probe a real process stream and achieve appropriate levels of detectability for sodium and potassium with real-time response. TRELIBS will extend the capabilities of this form of emission spectroscopy to both better sensitivity and higher pressure environments. The difficult problem of quantification is being investigated.

APPENDIX A

The laser was a Quanta-Ray Nd:YAG unit running on the fundamental 1.06 μm wavelength. The pulse length was 80 ns, and the output was 1.0 J (for the coal studies). This resulted in a focused power density in the range 10^8-10^9 W/cm^2, well above the required threshold for breakdown.

The lightgathering lens was only used for the high-resolution work, in which the spectrometer was a 1/2-m instrument with a 1200-line grating. With this spectrometer, only film was used for detection. This level of resolution was required to resolve the sodium D-line doublet, and was also used in a general search for molecular lines and faint atomic lines. The range of the film extended farther into the uv than the diode array. The film results were the basis for the reported species listed in Table I.

Two configurations of 1/4-m spectrometer were used, both with the diode array detection. This was a 1024-element silicon diode array, followed by a Tracor-Northern multichannel analyzer and processor. Hard copies of the data were made on a x-y recorder. Survey spectra, such as Fig. 2, were taken with a 150-line grating and covered the entire wavelength range visible to the diodes. For more detailed spectra, as in Figs. 3 and 4, a 600-line grating was used in the same 1/4-m instrument.

With a 50-μm slit about 25 cm from the breakdown, only about 10^{-6} of the emitted light was collected for these data.

APPENDIX B

The BYU gasifier experiments were carried out in a Los Alamos-designed optical test section[2] which was preceded in the flow stream by a cyclone particle separator. The particle density measured in the test section was 1.3×10^5 particles/cm^3; the particle size distribution peaked at 20 μm diameter. At this particle density the product stream was opaque, requiring that the breakdown spot be positioned at the edge nearest the observation window, as shown in Fig. 1.

The lower breakdown threshold of the particles (relative to any gas) also made it difficult to get the laser focal spot far enough into the stream to observe, since the particles caused breakdown to occur in the converging beam well before the focus was reached. The laser had to be turned up to its maximum output (1 J) to get an observable focal region, although with gas only in the cell, the focal spot was well established with about 0.2 J of laser output.

From the mass density of the entrained particles, and the estimated focal volume, the actual mass of the sodium and potassium detected may be calculated in an upper limit. The focal volume in the gas was measured to be 25×10^{-3}cm^3, so about 2500 particles were contained in that volume. For 20-μm diameter particles of density 2 g/cm^3, the mass of each particle was 10^{-8}g, and the total mass in the plasma was 25 μg. We shall assume that all of the particles were completely vaporized and contributed to the optical signal. We know from an analysis of the ash[3] that the particles contained 4.5% Na_2O and 0.6% K_2O. We conclude that at most, we detected samples of sodium of 0.8 μg, and potassium masses of 0.1 μg. This was with a very inefficient optical system, so that the detection limits are clearly orders of magnitude lower than these worst-case numbers.

TABLE I
SPECIES DETECTED IN BYU FIELD TESTS

Atomic
Na I, K I, H, O I, O II, C I, C II, C III, Ca I, Ca II, Si I, Mg II

Molecular
CN, N_2, CO, O_2

REFERENCES

1. Y. P. Raizer, Laser-Induced Discharge Phenomena, (Consultants Bureau, New York, 1977).

2. E. O. Ballard, "Purged Window Development for Laser Beam Insertion and Signal Retrieval from Coal Gasification Product Streams," unpublished report, Los Alamos National Laboratory.

3. Coal ash analysis by U. S. Geological Survey.

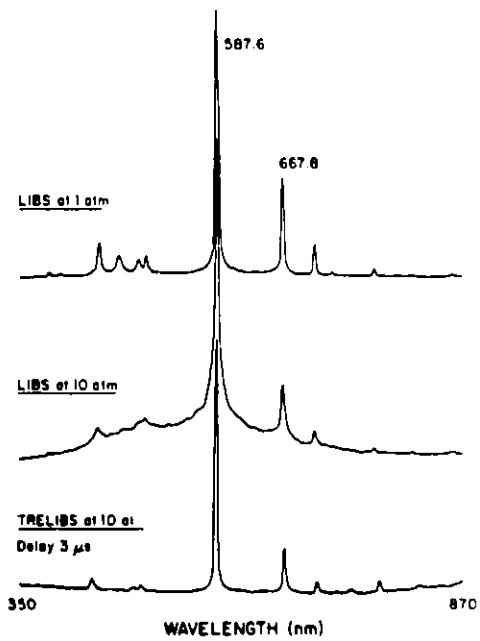

Fig. 7. Pressure broadening of the LIBS spectrum of helium at 10 atm, and its elimination in a 10-atm TRELIBS spectrum of 3 μs delay.

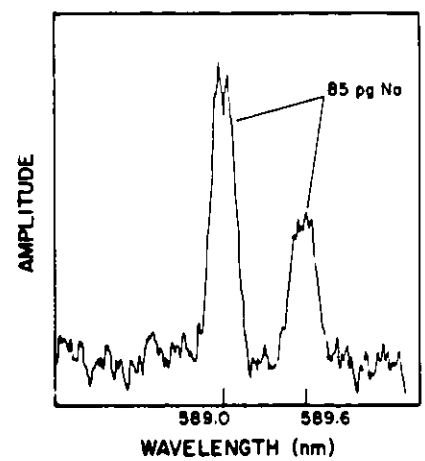

Fig. 9. A representative sodium trace taken with the apparatus of Fig. 8. As the signal-to-noise ratio is about 8, this would suggest that the particular detection system in use at that time could be used to detect 20 pg of sodium in the focal spot.

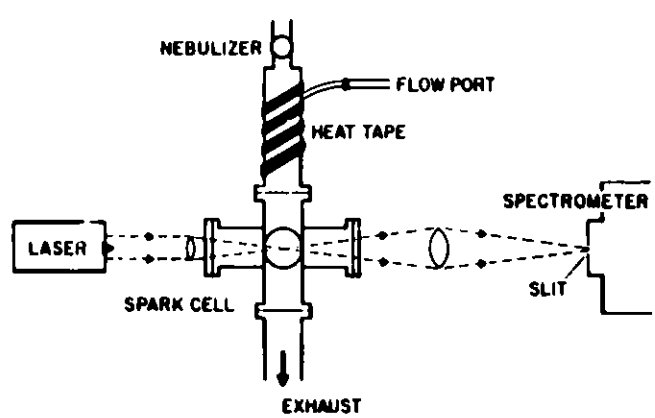

Fig. 8. A calibration apparatus for producing samples of known concentration in the laser focus. A known solution of the species of interest is aspirated by a nebulizer into a measured flow of carrier gas. This is vaporized in a heated tube and flows into the optical cell, where LIBS or TRELIBS can be carried out in the normal manner.

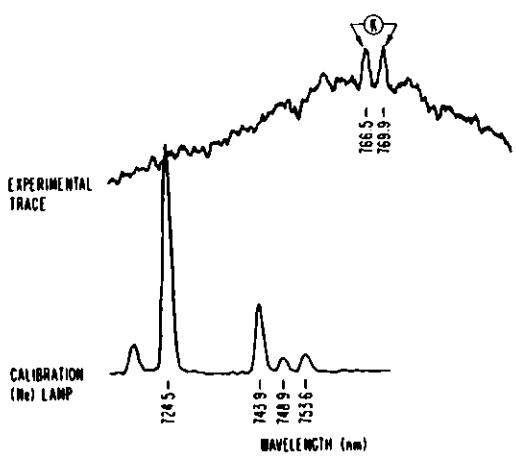

Fig. 4. The potassium doublet from the gasifier product stream, resolved and calibrated at medium resolution.

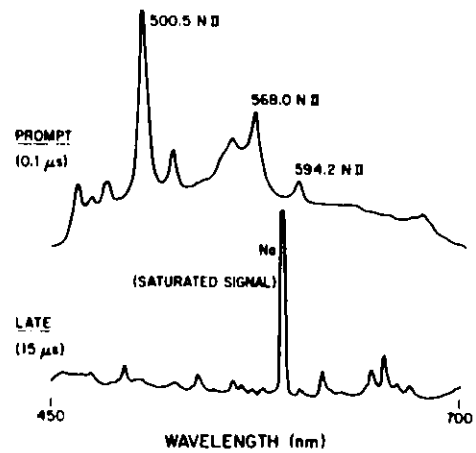

Fig 6. An illustration of the improved detectability of sodium with late-time TRELIBS. The air background changes are due to the change from ionized lines to neutrals. The early white light is also gone in the late-time spectrum.

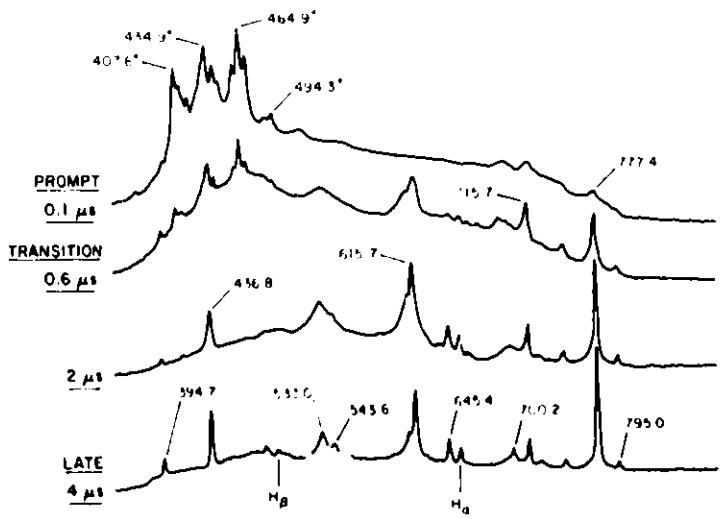

Fig. 5. The TRELIBS time development of the oxygen spectrum at 0.6 atm, not corrected for the diode array wavelength response. The relative differences show that at early times, the spectrum is the sum of a large white light component and (singly) ionic lines, while at late times only neutral lines can be seen. This improves the signal-to-noise at late times, as demonstrated by the development of lines from a hydrogen impurity.

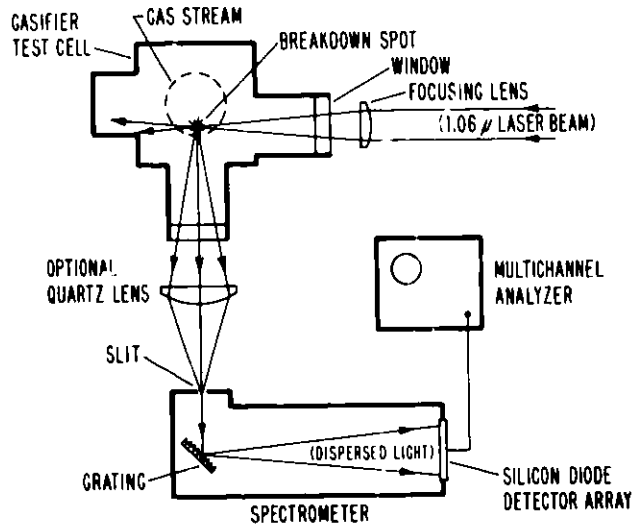

Fig. 1. A schematic view of the apparatus used in our gasifier field tests. The laser beam (entering from the left) breaks down a sample of the product stream. The light from the plasma is dispersed by a spectrometer and detected by a silicon-diode array coupled to a Tracor Northern optical multichannel analyzer. Film detection was also used with a larger spectrometer.

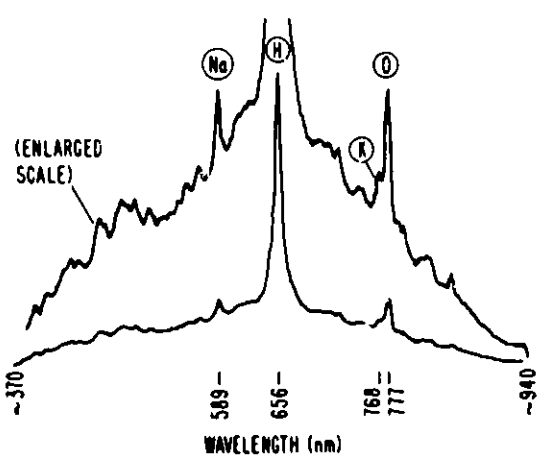

Fig. 2. A low-resolution spectrum from the gasifier, covering the wavelength range detectable with the diode array. The dominant hydrogen line made the breakdown appear pink.

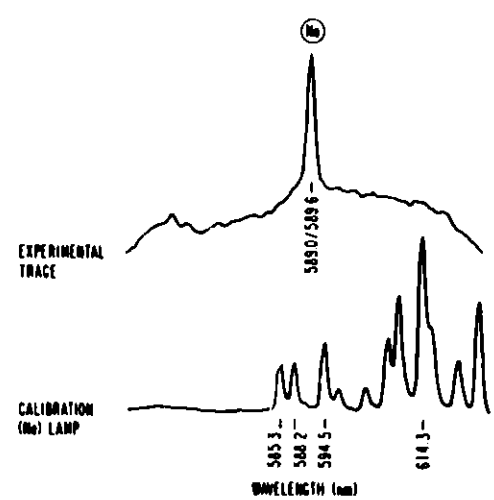

Fig. 3. A medium-resolution spectrum from the gasifier, made for the identification of the sodium doublet. This assignment was verified by high-resolution spectra that resolved the doublet and confirmed the proper doublet spacing.

Wednesday Morning, June 10, 1981

Session C - Alkalis

THE DETERMINATION OF COMBUSTION EFFICIENCY AND CALCIUM UTILIZATION OF A FLUIDIZED BED COMBUSTION FURNACE

R. L. Fyans*, and R. F. Culmo
The Perkin-Elmer Corporation
Main Avenue
M/S 131
Norwalk, Connecticut 06856
Phone: (203) 762-6915

ABSTRACT A091

The use of coal is projected to triple in the next twenty years and sixty five percent of our domestic increase in energy output will come from coal. With this increased usage of coal as an energy source, the problem of environmental emissions will be of great concern. The U.S. is abundant in coal. Its known reserves alone could satisfy the energy needs of the world for at least forty years. Stated another way, at the present rate of consumption, the known coal reserves in the U.S. could last for three hundred years! Unfortunately, the majority of these reserves are high in sulfur content. This sulfur must be removed either before combustion by a method such as solvent refining or "scrubbed" during the combustion process. One of the most successful methods of treating coal used for fluidized bed combustion is by mixing limestone with the coal. This treatment removes sulfur from the stack emissions through an in situ combustion retention approach. During combustion, the limestone decomposes to calcium oxide which reacts with the sulfur oxides. Analysis of the combustion products (i.e. flue gas, fly ash, and bed ash) determines the scrubbing and combustion efficiency of the fluidized bed combustion furnace. The flue gas analysis will determine the extent to which the sulfur oxides have been removed while the ash analysis for organic carbon, calcium carbonate and calcium oxide will determine the combustion efficiency and proper balance of limestone to coal. Since excess limestone will reduce the combustion efficiency and insufficient limestone will reduce scrubbing efficiency, its natural balance is critical in the combustion process.

This paper will desdribe a thermogravimetric (TG) method that has been developed to determine the optimum balance of the limestone-coal fluidized bed combustion furnace. Using the Perkin-Elmer Model TGS-2 and System 4 microcomputer, retained water, unreacted calcium carbonate, calcium oxide and organic carbon contents can be rapidly determined from a single sample. Details of the method and actual results will be presented.

*Presenting author.

FLAME RADIATION CONTROL IN HIGH TEMPERATURE FURNACES

Tomio Suzuki, Kotaro Morimoto,
Toru Abe, Kazuo Ikeda

Mechanical Engineering Research Laboratory,
Kobe Steel, Ltd. JAPAN
3-18, 1-chome, Wakinohama-cho, Chuo-ku,
Kobe, Japan
Phone: Kobe (078) 251-1551
Telex: 5622-177 (KOBESTEEL KOB)

1. ABSTRACT

Radiation from flames in high temperature furnaces was investigated for saving energy.

Fuels used in this experiment were kerosene, C heavy (No.6) oil, coal-oil mixture (COM), coke oven gas and butane gas.

The states of combustion basically fall into slow (de.layed) combustion, ordinary combustion and rapid combustion. A soft (long) flame was formed in slow combustion and a hard (short) flame was formed in rapid combustion by changing mixing of fuel and air, or fuel droplets size.

Results are as follows.

(1) Radiation from the soft flame is larger than that from the hard flame, because of its high flame emissivity and large area of the flame surface.

(2) Effects of fuel types on radiation agree with the data obtained by I.F. R.F. except for COM.

(3) A COM firing flame represents lower radiation than an oil firing flame. Because flame radiation from the oil firing flame is originally high, the effect of increasing flame radiation by addition of solid carbon to oil is not observed.

(4) There is an optimum range of the amount of atomizing agent for increasing heat transfer in the furnaces.

(5) Control of excess air, fuel injection position and the ratio of fuel injection velocity to air velocity are very important for saving energy and decreasing NOx emission.

(6) The fuel consumption of our new combustion method in soaking pits, heating furnaces and melting furnaces is 5 - 15% less than that of prior combustion methods.

2. INTRODUCTION

The heat transfer mechanism in industrial furnaces consists of the radiation heat transfer among the flame (combustion gas), the furnace wall and the material to be heated in the furnace, and the convection heat transfer by the combustion gas. In high temperature furnaces such as soaking pit and heating furnace for iron and steel, the heat transfer by radiation accounts for about 90% of the total heat transfer[1]; the heat transfer by radiation is dominant.

It seems therefore useful, as an energy saving combustion technique, to investigate the radiation characteristics of the flame in high temperature furnaces so as to optimize the radiation, to improve soaking and heating performances of the furnaces.

The types of the flame radiation can be roughly divided into the nonluminous gas radiation and the luminous flame radiation. The former nonluminous gas radiation is mainly composed of the radiation of H_2O, CO_2, CO, etc. Numerous experimental and theoretical studies on it such as those of Hottel et al.[2], Schack[3] and Leckner[4] have been made and their results have been widely applied in industrial fields.

The latter luminous flame radiation is the heat radiation of a mass of solid particles such as carbon, liberated and floated in the high temperature combustion gas. On this radiation, reports of IFRF[5], Kunitomo et al.[6] and Holliday et al.[7] are available. For example, IFRF carried out large-scale combustion experiments to investigate the effects of the fuel, combustion air, the combustion chamber construction and the burner construction, on the radiation from the flames; the flame temperature, the soot concentration in the flame, and the emissivity were quantitatively indicated.

The results of these studies, however, seem to be difficult to be applied to high temperature furnaces, since the experiments were made in furnaces of a low furnace temperature with little furnace wall radiation, or the luminous flame radiation was related to the formation of soot and coke and the results are applicable to the specific flames used in the experiments only.

In this study, a combustion test furnace was used to burn C heavy oil, kerosene, coke oven gas (COG), butane gas and coal-oil mixture (COM), and the radiation characteristics of flames in high temperature furnaces were clarified. The study also investigated on correlation between the flame radiation

characteristics, and the temperature distribution in the furnace and the NOx formation.

The application of the results of the study to soaking pits and heating furnaces could reduce the fuel consumption rates by from 5 to 15%.

3. EXPERIMENTAL APPARATUS AND METHOD

The combustion test furnace is shown in Fig. 1. The combustion test furnace is a horizontal cylindrical type refractory wall furnace measuring 1,000 mm in diameter and 4,000 mm in length. Many sight holes and sampling holes are provided in the furnace in its circumferential and lengthwise directions.

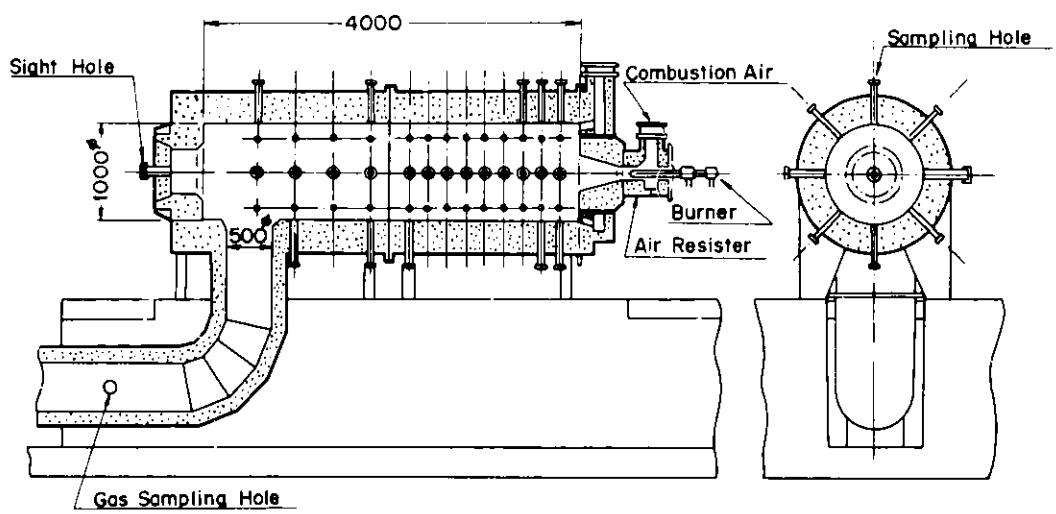

Fig. 1 Combustion Test Furnace

The experiment was carried out under the following standard combustion conditions:

Standard Combustion Conditions

Rate of heat input: 40×10^4 kcal/hour, Furnace temperature: 1,300°C, Secondary air temperature: 320°C, Excess air ratio: 1.16 (excess O_2 concentration, 3%), Fuel: Kerosene, C heavy (No.6) oil, butane gas and COM (Coal-Oil Mixture), Burner: Fuel injection direction ..... Straight, conical, slant[8], swirl, (diffusion combustion type), Oil burner ..... Internal mixing type, Burner tile: Straight, conical 30°, and swirl.

For the temperature measurement, a ø0.5 PR thermocouple was used. Temperature compensation for radiation, etc. was not made. (When COM was burnt,

a recrystallized-alumina-protective-tube sheathed thermocouple was used. When other fuels were used, a naked thermocouple was used.)

For measuring radiant heat flux, a thin foil type radiometer, of which the visual angle is 7° and spectral sensitivity range is from 0.3 to 6.5 μ, was used.

As for the gas analysis, the combustion gas was sampled in the flue at a point 3 m down-stream from the outlet of the test furnace by a water-cooled probe, and the sample gases were analyzed by a chemiluminescence type NOx continuous analyzer and/or a magnetic type O_2 continuous analyzer. For all of the NOx values, 11% O_2 corrected values were used.

4. EXPERIMENTAL RESULTS AND DISCUSSION

4-1) Effects of Type of Fuel

The relation between the fuel type and the flame radiation in the ordinary combustion method is shown in Fig. 2. The radiant heat flux distribution of the gas fuels and kerosene is flat. For C heavy oil, the radiant heat flux is high near the burner and low in the post-flame stream, and the difference is large. The order of radiation levels in the flame-present-zone of which L/D is not exceeding about 1.5 is C heavy oil > kerosene > COG ≧ butane gas.

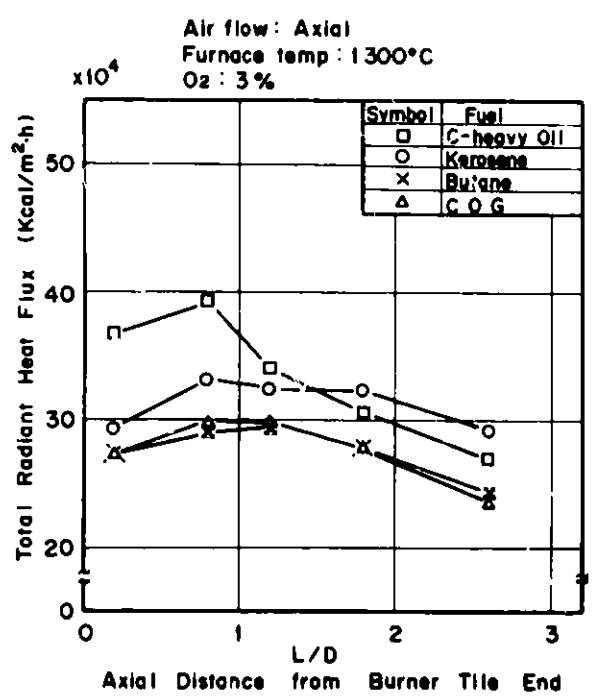

Fig. 2 Relation between Fuel Type and Flame Radiation (Ordinary Combustion Method)

When the C/H (weight) ratio of each fuel is computed from the fuel components, their order is C heavy oil (7.07) > kerosene (5.73) > butane gas (4.80) > COG (2.28), and this order almost agrees with the order of the flame radiant heat flux levels.

Holiday and Thring[7] proposed the following equation for the flame emissivity in small experimental furnaces:

$$\varepsilon_{av} = 0.282\ell n \frac{(C/H) - 5.0}{4} + 0.002(T - 200) + 0.484 \qquad (1)$$

Since the combustion method, the excess air ratio, etc. actually produce strong effects on the flame emissivity, the equation has some problems to solve for its practical application. However, the higher the C/H ratio, the higher the radiation emissivity ε_{av} of the fuel, and the higher the boiling point, the higher the radiation emissivity.

In this way, when the C/H ratio becomes larger, the formation of soot will be increased. As the solid radiation of soot and coke particles increases, the flame radiant heat flux increases.

The flame radiation and the temperature distribution in the furnace buring COM are shown in Fig. 3 and Fig. 4 respectively.

The flame radiation of coal-oil mixture combustion, when compared with C heavy oil combustion, is low in the flame-present-zone near the burner, but no noticeable difference can be seen in the post-flame stream. The flame radiation of coke & C heavy oil COM combustion is low all over. As for the temperature distribution in the furnace, the C heavy oil combustion has the widest high temperature zone and shows the highest temperature, and the coke & C heavy oil COM combustion shows the widest low temperature zone.

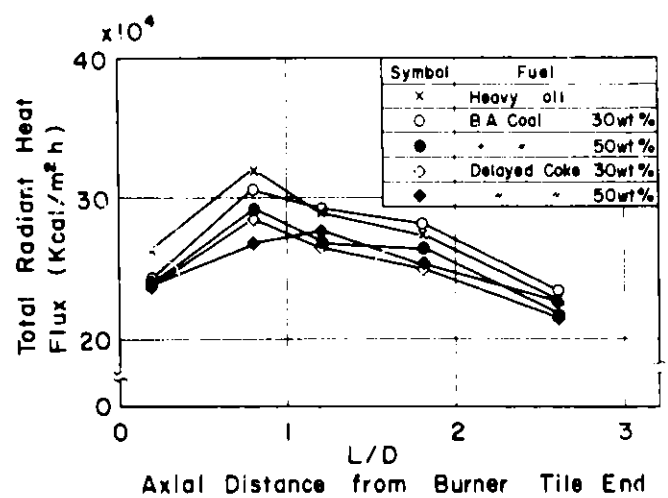

Fig. 3 Flame Radiation in COM Combustion

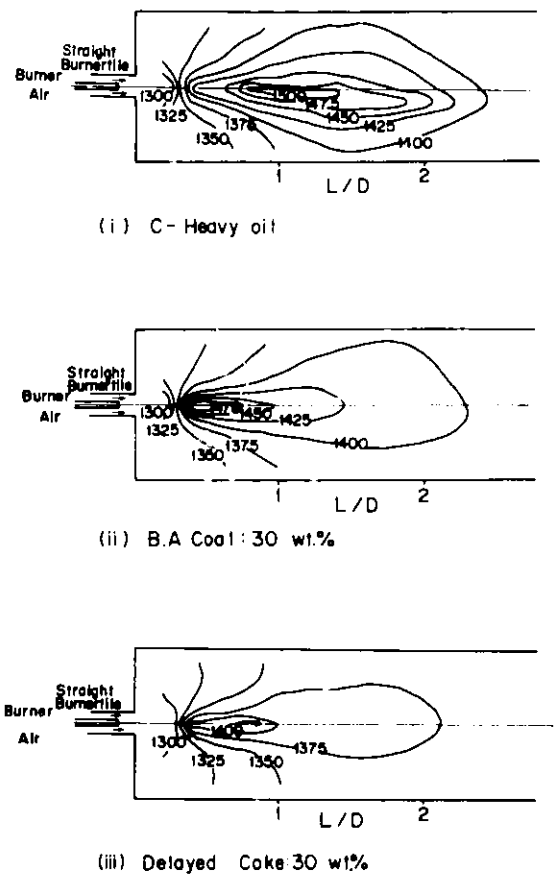

Fig. 4 Temperature Distribution in Furnace in COM Combustion

According to the results of IFRF, when COG was mixed with oil or pitch and burnt, the flame radiation increased locally by from 5 to 7 times. In our experiment, when C heavy oil, of which flame radiant heat flux is originally high, was mixed with solid carbon and burnt, the luminous flame radiant heat flux did not increase sharply. It is thought that the flame radiant heat flux is rather determined by the flame temperature. In other words, since liquid fuels are more combustible than solid fuels, and among solid fuels, the more the fuel has volatile matter, the more combustible it is, it is considered that the flame temperature becomes higher and, in turn, the flame radiation increases.

The nonluminous gas emissivity εg was obtained from the Schack's equation and the Hottel's correction diagram.

$$\text{For } CO_2,\ \varepsilon\ CO_2 = \frac{3.5}{4.88} \cdot \frac{(P\ CO_2 \cdot L)^{1/3}}{(T/100)^{1/2}} \qquad (2)$$

$$\text{For } H_2O,\ \varepsilon\ H_2O = \frac{34.5}{4.88} \cdot \frac{(P\ H_2O \cdot L)^{0.8}}{(T/100)} \qquad (3)$$

The radiation of these CO_2 and H_2O accounts most of the gas radiation. As their spectral bands overlap with each other in some places, the correction should be given, then we get the equation:

$$\varepsilon g = \varepsilon\ CO_2 + \varepsilon\ H_2O - \Delta\varepsilon \qquad (4)$$

Where, $\varepsilon\ CO_2$: emissivity of carbon dioxide, $P\ CO_2$: partial pressure of carbon dioxide [atm], $\varepsilon\ H_2O$: emissivity of steam, $P\ H_2O$: partial pressure of steam [atm], $\Delta\varepsilon$: correction term, L: gas effective thickness [m], εg: emissivity of combustion gas, T: gas temperature [°K].

When the combustion gas temperature is the same, the order of the nonluminous gas emissivity of each fuel is COG > butane gas > kerosene > C heavy oil, and this is the reverse order of the C/H one.

4-2) Effects of Combustion Method

The effects of the combustion method on the flame emissivity in butane gas combustion are shown in Fig. 5.

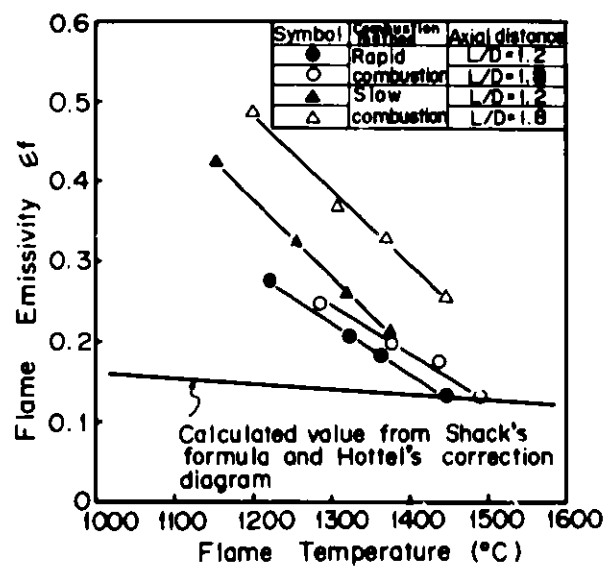

Fig. 5 Effects of Combustion Method in Butane Gas Combustion

In Fig. 5, at the same flame temperature, the flame emissivity of the slow combustion method is higher than that of the rapid combustion method. Further, the lower the flame temperature is, the higher the flame emissivity is. The temperature dependency is greater than that of the nonluminous gas emissivity.

When the gaseous fuel is burnt by the slow combustion method, the early mixing of the fuel and the air for combustion is suppressed. Through the processes of dehydrogenation of hydrocarbon, thermal decomposition, polymerization, formation of unsaturated bond, and formation of aromatic ring, soot of the gas-phase-separating-out type, of which the particle size is very small, from 0.03 to 0.05 μ, is generated to increase the luminous flame radiation. Therefore, it is considered that, in the slow combustion method, the flame emissivity becomes high due to the rise of the luminous flame emissivity. When the furnace temperature is low, or when the temperature of the air for combustion is low, the flame temperature will become low. In this case, the flame tends to become a luminous one, and as the luminous flame emissivity increases, the flame emissivity increases, too.

4-3) Effects of Excess Air Ratio

The effects of excess air ratio on the flame radiation in butane gas combustion is shown in Fig. 6. The low excess air ratio combustion can reduce the quantity of flue gas and reduce the heat loss. In addition, it can be said that it also works for promoting the heat transfer by radiation.

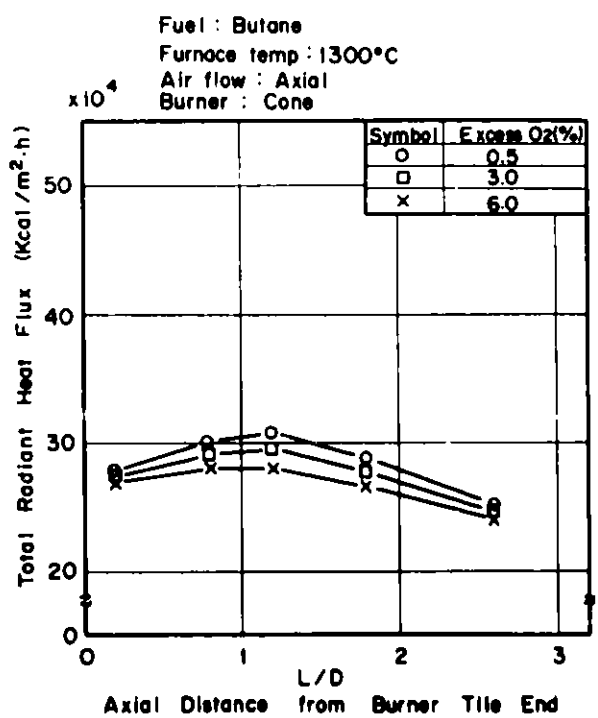

Fig. 6 Effects of Excess Air Ratio in Butane Gas Combustion

4-4) Effects of Fuel Jet Velocity

The effects of the fuel jet velocity on the flame radiation in butane

gas combustion is shown in Fig. 7. In Fig. 7, the upper diagram indicates the effects of the fuel jet velocity on NOx formation, and all the symbols used are the same as those used in the figure below, which indicates the flame emissivity distribution. As clearly seen in the diagram, the flame emissivity becomes high when the ratio of the fuel jet velocity to the air flow velocity is 1 or 2. Further, the NOx formation reaches the minimum under the same condition, and this agrees well with our results previously reported.[9]

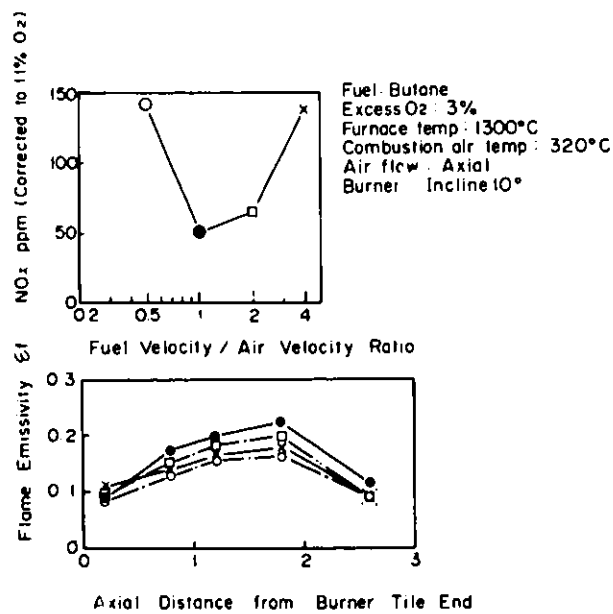

Fig. 7 Effects of Fuel Jet Velocity in Butane Gas Combustion

As explained above, since the fuel jet velocity governs the mixing process of the fuel and the air for combustion, it is considered to be an important factor for saving energy and suppressing NOx formation.

4-5) Effects of Atomizing Quantity

The effects of the atomizing quantity on the flame radiation in C heavy oil combustion are shown in Fig. 8, and the effects of the atomizing quantity on the temperature distribution in the furnace are shown in Fig. 9. When the steam atomizing quantity relative to the C heavy oil quantity is reduced gradually, the radiation from the flame will increase gradually, and it will reach the maximum when the steam atomizing quantity is in the range of from 0.13 to 0.20 kg/litre of fuel. If the atomizing quantity is reduced further, the radiation will be reduced.

As for the temperature distribution in the furnace, the high temperature zone will move away from the burner and the size of the zone will be reduced as the atomizing quantity is reduced. The maximum temperature also drops.

The combustion flue gas temperature and the NOx concentration drops, in contrast with the effects on the flame radiation, as the atomizing quantity is reduced down to the above-mentioned range. It is needless to say that reducing the atomizing quantity extremely is not desirable since it will make the fuel droplets coarse resulting in smoke generation.

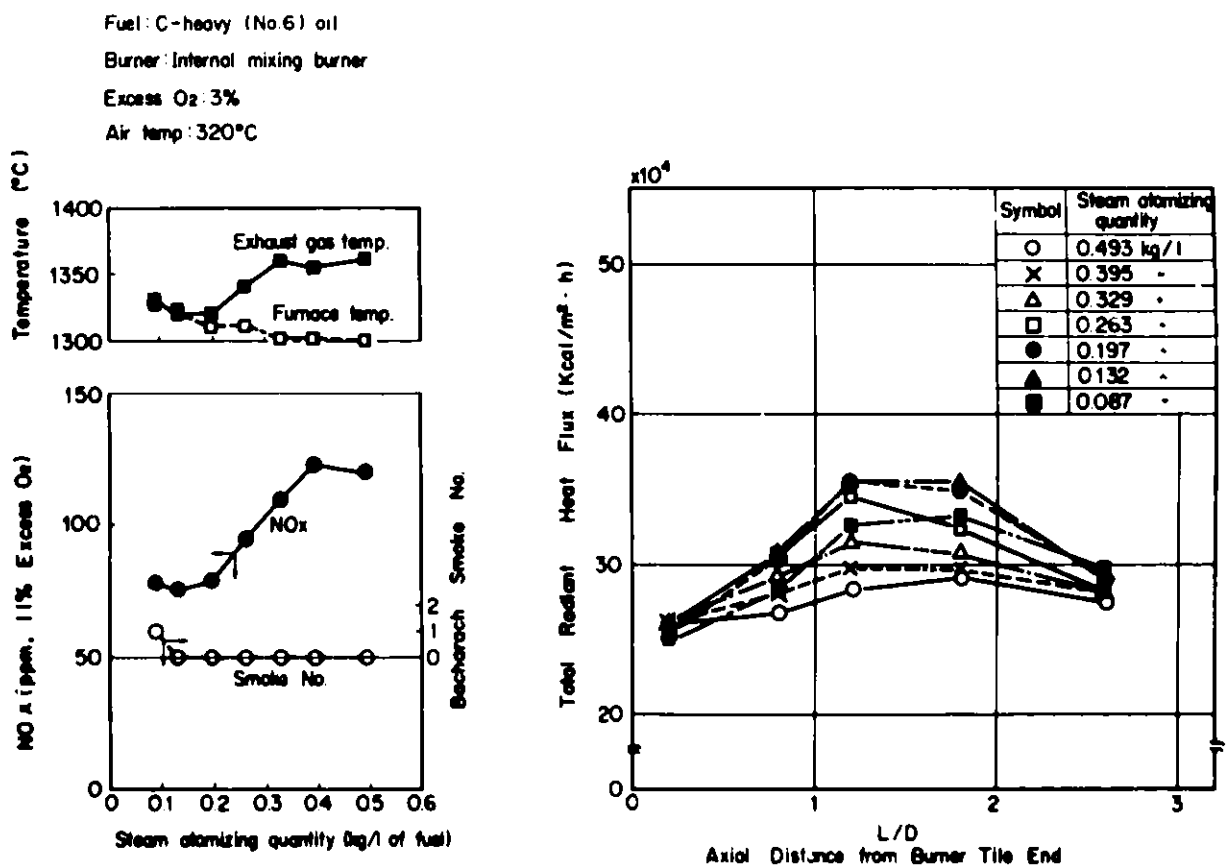

Fig. 8 Effects of Atomizing Quantity in C Heavy Oil Combustion

In other words, when the atomizing quantity is reduced to the optimal value to increase the flame radiation, the heat transfer in the furnace will be promoted, and as the result, the temperature of the exhaust gas will drop. This, in turn, will suppress the formation of thermal NOx.

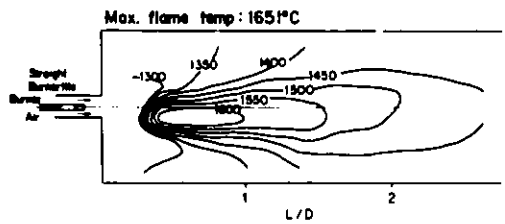

(i) Steam atomizing quantity : 0.395 kg/l of fuel(150%)

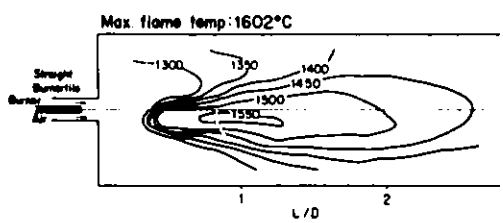

(ii) Steam atomizing quantity : 0.263kg/l of fuel (100%)

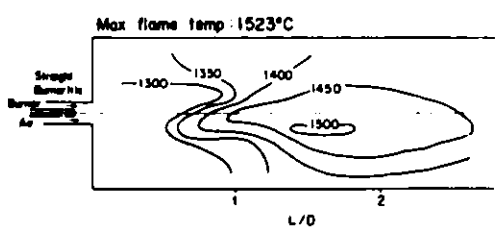

(iii) Steam atomizing quantity : 0.132kg/l of fuel (50%)

Fig. 9 Temperature Distribution in Furnace
in C Heavy Oil Combustion

As explained above, a simple measure of optimizing the atomixing quantity is considered to be effective in improving the heating characteristics and lowering the NOx formation.

5. APPLICATION TO ACTUAL FURNACES

The examination and analysis of the flame radiation characteristics in high temperature furnaces, using a combustion test furnace, revealed the optimal combustion method for saving energy and lowering NOx formation, applicable to each furnace.

When these research results were applied to soaking pits, heating furnaces and melting furnaces, it was confirmed that they were effective in lowering the fuel consumption rate. These actual examples are explained below.

5-1) Application to Soaking Pit

Examples of heat raising characteristics and heat pattern of a top one way soaking pit (COG, heavy oil) are shown in Fig. 10 and Fig. 11 respectively.

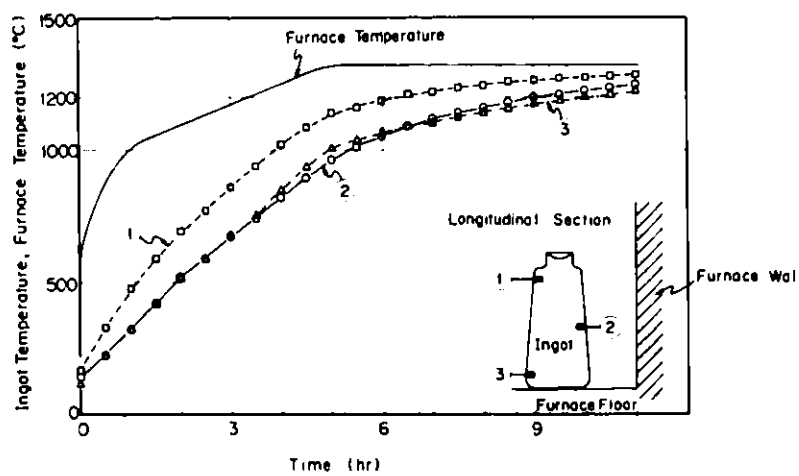

Fig. 10 Steel Ingot Temperature Raising Characteristics (COG Combustion)

In Fig. 10, the temperature of the top portion of the ingot attains the highest value, and the temperature raising of the bottom portion lags behind. This is caused by the fact that the flame is located at the top and the shape factor differs in each portion of the steel ingot, that there is a heat loss on the furnace floor and on the furnace wall, and also by the combustion gas flow, etc.

Accordingly, for lowering the fuel consumption rate, it is important to reduce the temperature differences inside the steel ingots so as to quickly raise the lowest temperature portion's temperature to the required value.

Fig. 11 shows an example of converting the ordinary combustion method to the rapid combustion method in a top one way soaking pit (fuel: C heavy oil). In this example, the radiation from the flame was reduced and the high temperature gas was made to circulate over the bottom portion of steel ingots.

With these measures, the differences in temperature in the steel ingots were improved, and the temperature raising speed of the bottom portion could

be increased. As clearly seen in the diagrams, the time required for reaching the soaking stage was shortened and the time of staying in the furnace could also be reduced. As the result, the fuel consumption rate could be reduced by about 1 ℓ/T.

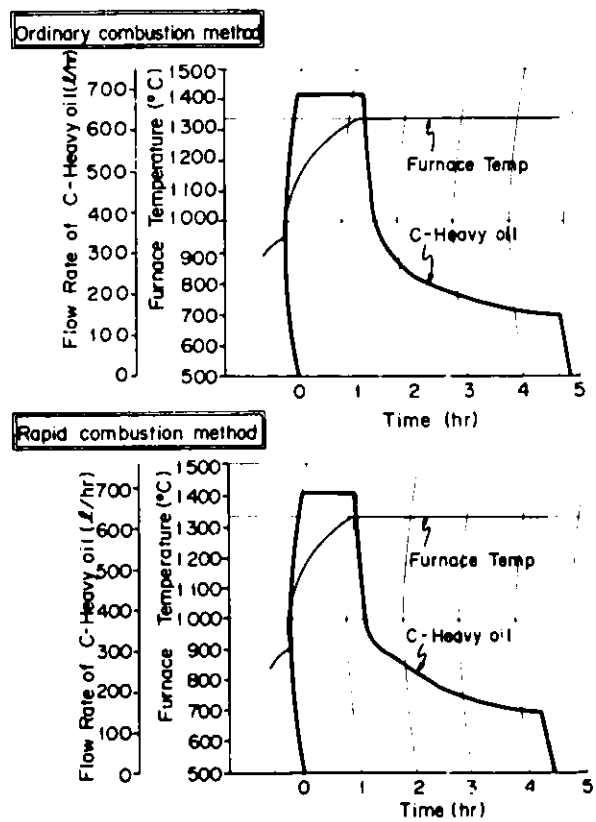

Fig. 11 Relation Between Combustion Method and Heat Pattern (Oil Combustion)

5-2) Application to Continuous Heating Furnace

An example of application to 25T/H walking-beam type furnace burning C heavy oil is shown in Figs. 12 through 14.

Fig. 12 indicates the relation between the atomizing quantity and the flame shape in the heating zone.

If the atomizing quantity is large, the flame becomes a relatively short one, and the combustion becomes a rapid one. On the other hand, if the atomizing quantity is reduced, the flame will stretch, and the combustion will become a slow one. If the atomizing quantity is reduced to an extreme extent, for example, down to AQ = 0.12 Nm^3/ℓ, the flame will go out of the heating

zone into the preheating zone.

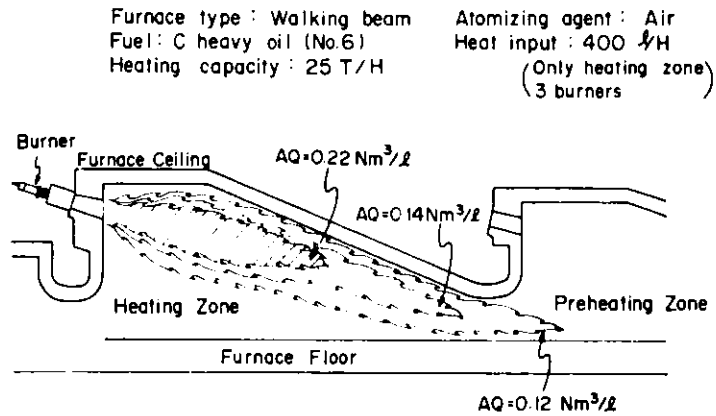

Fig. 12 Relation Between Atomizing Quantity and Flame Shape

Fig. 13 shows the relation between the atomizing quantity and the flame radiation in the heating zone, and Fig. 14 shows the relation between the atomizing quantity and the flue gas heat loss rate at the end of the furnace.

As clarified by the experiments on the fundamentals of combustion, when the atomizing quantity is extremely reduced, the flame radiation will drop. As this increases the flue gas heat loss rate, it is not desirable. Hence, there is an optimal atomizing quantity which maximizes the heat transfer inside the furnace.

In this furnace, when the fuel rate was 580 ℓ/H, the atomizing quantity was kept in the range of from 0.14 to 0.15 Nm^3/ℓ (fuel), and when the fuel rate was smaller, the atomizing quantity was set higher than the above-mentioned range. With these arrangements, the fuel consumption rate could be reduced.

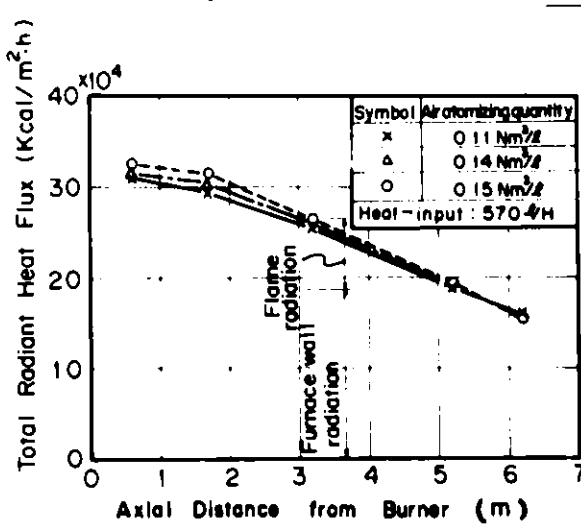

Fig. 13 Relation Between Atomizing Quantity and Flame Radiation

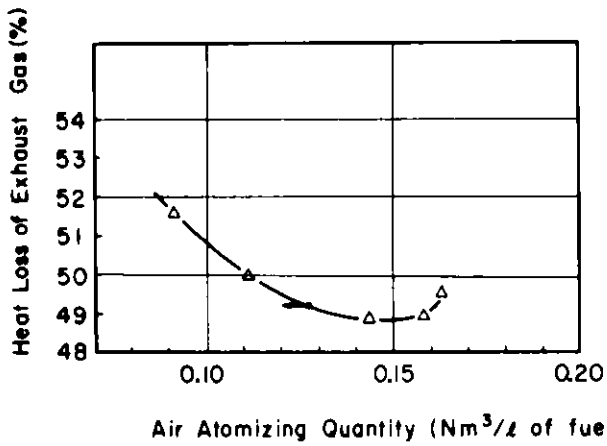

Fig. 14 Relation Between Atomizing Quantity and Flue Gas Heat Loss

6. CONCLUSION

The radiation characteristics of radiation in high temperature furnaces such as soaking pits and heating furnaces for iron and steel have been clarified, and the optimal combustion technique for each furnace has been established.

In particular, the effectiveness of achieving the optimal combustion by making slow combustion and increasing the luminous flame radiation in saving energy has been experimentally and theoretically clarified. As its effectiveness in suppressing NOx formation has already been recognized, it can be called an energy-saving and low-pollution combustion technique.

This optimal combustion technique has already been applied to many of our industrial furnaces. Since the fuel consumption rate has been reduced by from 5 to 15% and the NOx formation has been reduced, the effectiveness of the technique has been confirmed.

REFERENCES

(1) Kitamura, Hirose, Suzuki et al., Journal of The Iron and Steel Institute of Japan No.8, Vol.65 (1979), A153.
(2) Hottel et al., "Heat Transmission" 3rd ed. McGraw-Hill (1954) Chapter 4, Trans. A. I. Ch. E., 31, 517 (1035), Trans. A.S.M.E., 57, 463 (1935), Trans. A.I. Ch. E., 38, 531 (1942).
(3) Schack, "Arch. Eisenhut tenwesen", 241 (1939).
(4) Leckner, B., Combustion and flame, 19 (1972), 33.
(5) IFRF, J. Inst. Fuel, 29 (1956) 23, Riviere, J. Inst. Fuel, 30 (1957) 556, Hubbard, J. Inst. Fuel, 30 (1957) 564.
(6) Kunitomo et al., Journal of Japan Society of Mechanical Engineers, Vol. 32, No. 234 (1969, Feb.), Vol. 35, No. 270 (1972, Feb.) 384, Vol. 37,

No. 304 (1974, Dec.), 232.
(7) Holliday et al., J. Inst. Fuel, 30 (1957), 127.
(8) T. Suzuki et al., IFRF Document nr. F29/1a/15 (1979).
(9) T. Suzuki et al., IFRF Document nr. F29/1a/7 (1978).

POSTER DISPLAY - REAR OF RALSTON ROOM

PURGED WINDOW DEVELOPMENT FOR LASER BEAM INSERTION AND SIGNAL RETRIEVAL FROM COAL GASIFICATION PRODUCT STREAMS*

E. O. Ballard
University of California
Los Alamos Scientific Laboratory
P.O. Box 1663, MS-566
Los Alamos, New Mexico 87545
Phone: (505) 667-7395

POSTER DISPLAY ABSTRACT

Development of window assemblies purged with heated nitrogen was undertaken to permit laser beam insertion into and signal retrieval from a small test section attached to the Brigham Young University (BYU) entrained flow coal gasifier. This gasifier was used to provide an atmospheric pressure, 500°F, gas stream to the test section. The window assemblies were developed to allow for laser beam interrogation of the gas stream as a subtask of a larger effort to develop laser instrumentation for detection of minority contaminant species, sodium and postassium, using a Laser Induced Breakdown Spectroscopy (LIBS) technique.

The development of window assemblies to maintain clean windows during gasifier operation evolved, after testing several different concepts, to a configuration where heated (150°F) nitrogen purge gas was directed onto the inside window surface. The purge gas then flowed through a tapered section into the test section. The tapered section accelerated the purge gas flow, thus providing an effective buffer zone between the gasifier product gas and the interior window surface. The quartz windows remained clean throughout each gasifier run enabling data to be taken without degradation of the emitted signal to the detector.

*Work performed under the auspices of the Morgantown Energy Technology Center (METC).

MASS FLOW MEASUREMENTS BY ACTIVE ACOUSTIC CROSS-CORRELATION TECHNIQUES

A. C. Raptis and S. H. Sheen
Argonne National Laboratory

Abstract

The application of ultrasonic techniques to the measurement of coal concentration and flow velocity of coal slurries was investigated at the HYGAS pilot plant. It was found that the sound attenuation in a coal slurry is linearly dependent on coal concentration and provides a direct measurement of coal concentration with an uncertainty of 5%. An active cross-correlation technique using an amplitude-demodulation scheme can be used to measure the flow velocity of the coal slurry with a resolution of 3%. Demodulated signals from transducers spaced at 12.7-cm intervals contain frequencies primarily in the range of 20-50 Hz as a result of flow disturbance in the coal slurry. Based on the results of this investigation, an on-line ultrasonic mass flowmeter is proposed which would measure: (1) the coal concentration based on the sound attenuation in the coal slurry, and (2) the flow velocity by means of an active cross-correlation technique.

INTRODUCTION

The analysis and design of acoustic flowmeters are based on the sonar equation, which states that "a received signal level is equal to the noise background level plus a measurement requirement." This equation considers such terms as the source level, the processing gain of the instrumentation, the directivity gain of the transducers, the transmission loss through the medium, and the noise background level. The first three depend on the choice of transducers and instrumentation and, therefore, are known quantities. The last two quantities (transmission loss through the medium and noise background level) have to be determined experimentally.

In this paper, experimental values on the sound attenuation in coal/oil slurries and noise background levels at the low pressure slurry line of the HYGAS pilot plant will be presented. These results will be used to design an active acoustic cross-correlation flowmeter for coal/oil slurries.[1,2,3,4] The measurements were obtained by making use of the test section shown in Fig. 1. The test section was installed in the low pressure slurry line of the HYGAS pilot plant and it is 182.82 cm (72 in.) long with six transducer housings along its length. An important feature of the test section is the isolation of the transducer housings from the abrasive properties of the Toluene-Benzene-coal slurry and the pipe vibration. This is accomplished by using (1) a concave acoustic window structure made of Teflon to fit the pipe contour, thus isolating the transducers from the slurry, and (2) Viton gaskets to isolate the transducers from the pipe vibration.

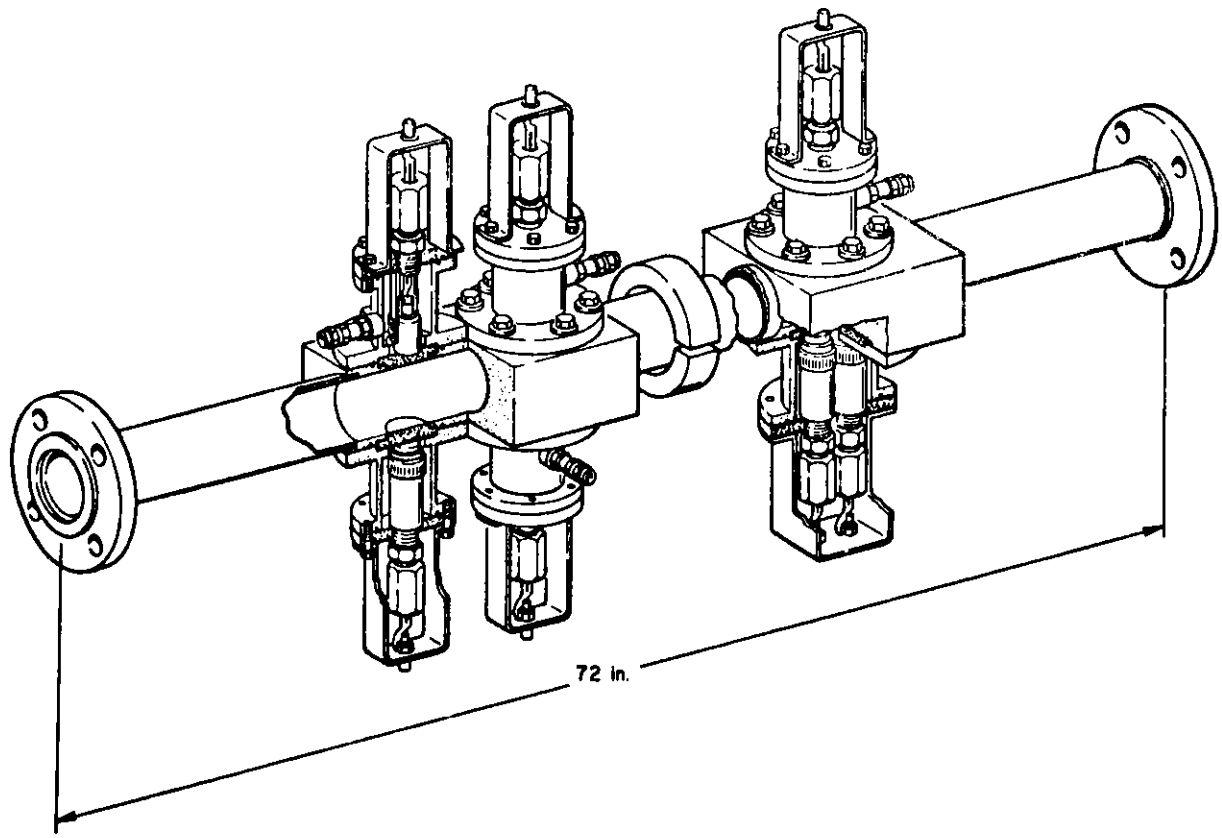

Fig. 1 Ultrasonic test section.

EXPERIMENTAL RESULTS

To obtain the necessary measurements for noise background, sound attenuation and test the active acoustic cross-correlation concept, HYGAS provided us with a special experiment, where the flow velocity and concentration of coal in the slurry line were varied. Three coal concentrations (5, 15, and 20 wt %) and two flow rates for the 5- and 15-wt % concentrations were achieved in the test.

Figure 2 displays a schematic diagram of the instrumentation, data acquisition system and the transducer arrangement on the test section. In the active mode of operation, namely the sound attenuation and active cross-correlation, transducers one to three were pulsed with continuous sine waves, which were generated by a function generator. The pressure waves were transmitted through the coal slurry and then received by similar transducers across the 5.0-cm-dia pipe. The received signals were further conditioned with ac differential amplifiers and all signals were recorded on direct channels of a wide-band tape recorder. For the noise background measurements, transducers one to three were used as listening devices and their outputs after amplification were also recorded.

The recorded data was later processed by using the data processing system shown in Fig. 3. Using this data processing system acoustic noise background was analyzed for its frequency contents up to 400 kHz and the results are shown in Fig. 4. It was observed that the magnitude of the

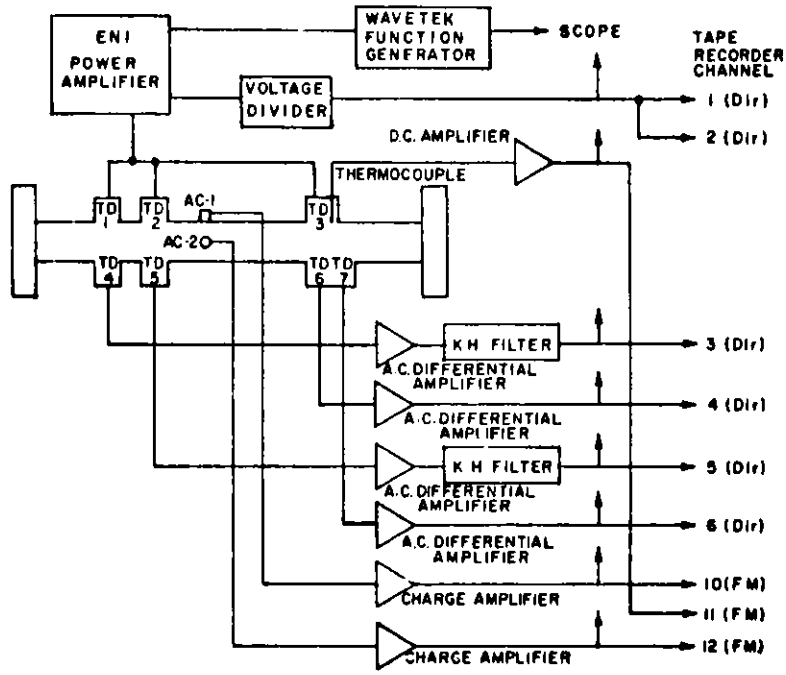

Fig. 2 Data acquisition system.

noise background decreases as coal concentration is increased. This observation implies that the coal concentration in the slurry line may be obtained by measuring the RMS value of the noise background. This observation, however, needs additional experiments for further validation.

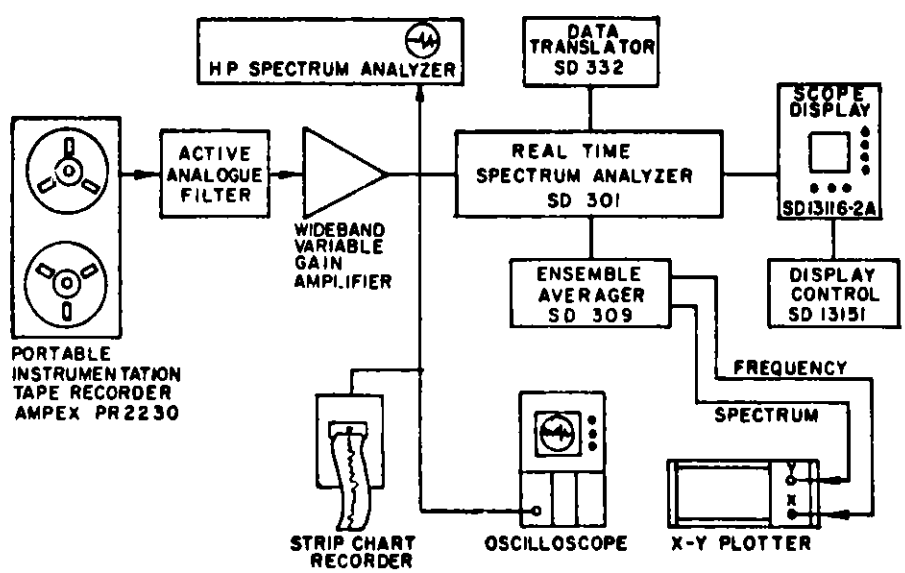

Fig. 3 Data processing system.

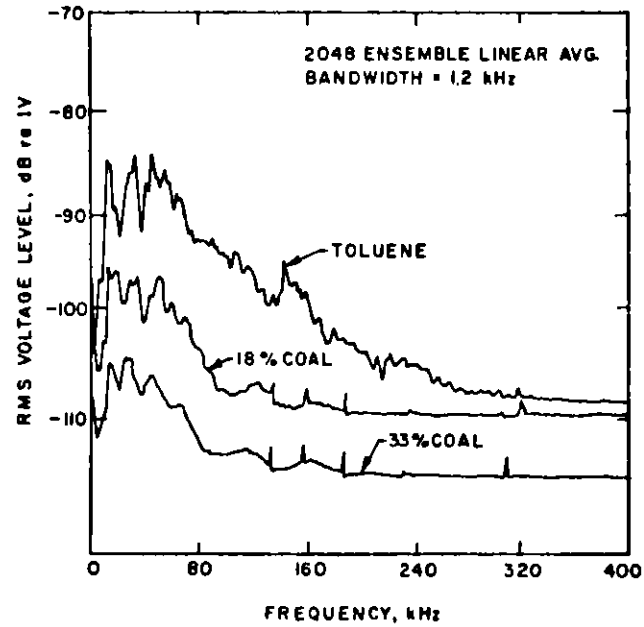

Fig. 4 Noise background for three coal concentrations at HYGAS

Figure 5 presents the relative attenuation as a function of frequency for 5, 15, and 20%-wt coal slurries. In general, the attenuation increases as the sound frequency increases. At low concentrations, e.g., the increase in attenuation is not obvious until the frequency becomes high enough that the sound wavelength is compatible with the coal particle size. The most interesting fact of the attenuation results is the concentration

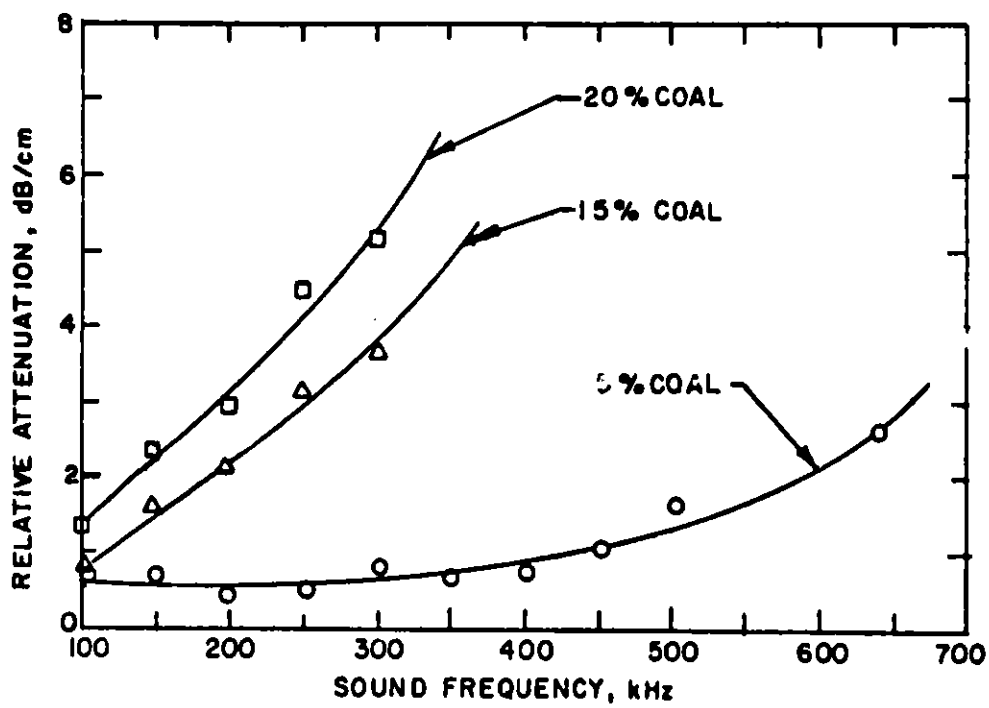

Fig. 5 Relative attenuation versus frequency in coal slurries.

dependence shown in Fig. 6. Linear dependence can be approximated up to the test limit of 35 wt % coal concentration. The dependence of attenuation on coal concentration can be used to determine the density in slurries. This measurement, of course, will depend on particle size distribution in the slurry. For example, at 200 kHz the change in attenuation is about 0.16 dB/cm in a 2 in. pipe per 2 percent change in concentration. Another uncertainty in the concentration measurement based on sound attenuation may arise from the fluctuation of the flow velocity. Figure 7 shows the relative attenuation for two given coal concentrations at two flow rates. In general, the change in attenuation due to the flowrate change is rather small. For example, at 200 kHz the variation in attenuation is about 0.3% per 1% flow velocity change. Under the normal steady-state operation of a coal plant, the attenuation change due to the fluctuation of the flow velocity is probably insignificant. Therefore, the sound attenuation measurement can provide an estimate of the coal concentration accurate to within 5 per cent of the actual reading.

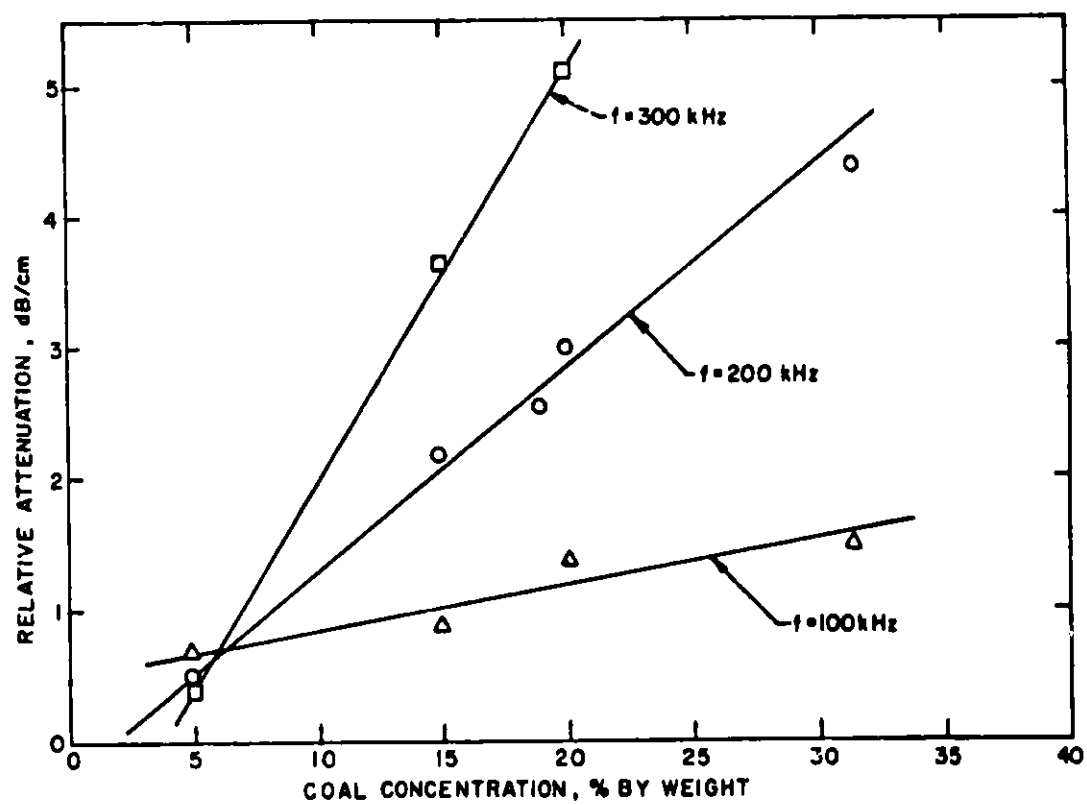

Fig. 6 Relative attenuation versus coal concentration for three sound frequency.

The active cross-correlation technique for flow monitoring requires sending a pressure wave into the medium. The medium, in turn, modulates the pressure wave with the local disturbances. Such disturbances might be caused by the flow turbulence near the pipe wall and the boundaries of the coal particles. The flow modulated waves require demodulation and band-pass filtering before they are used for cross-correlation.

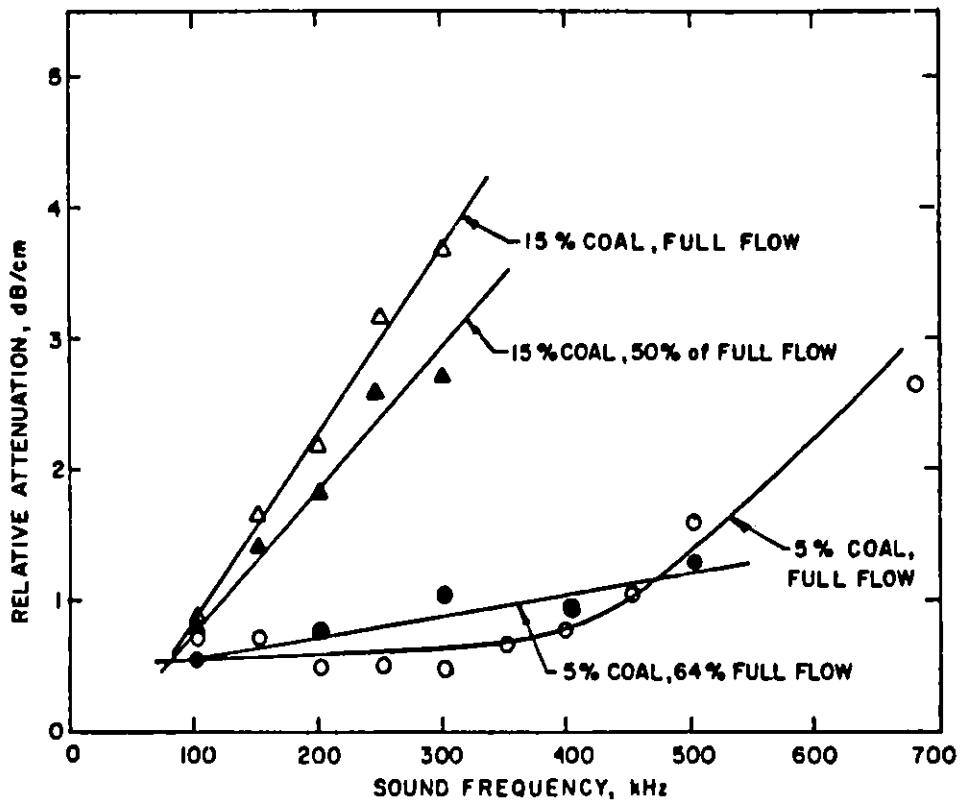

Fig. 7 Relative sound attenuation versus sound frequency at different flow velocities for two coal concentrations.

Figure 8 displays the cross-correlation function at 20-wt % coal concentration and three carrier frequencies, while Fig. 9 displays cross-correlation functions of two flow velocities in 5-wt % coal concentration. From this and additional data at other concentrations, it was observed that the full-flow velocities for three coal concentrations were consistent within 1 percent; i.e., the increase in coal concentration introduces a very small change in flow velocity.

Based on the above results, an on-line ultrasonic mass flowmeter is proposed, its schematic diagram is shown in Fig. 10. Two pairs of transducers are installed in transducer housings, which are separated from the coal slurry by Teflon windows. The main features of the data-processing system are AM demodulators with built-in filters and a low-frequency cross-correlator. The coal concentration is indicated by the RMS value of the transmitted signal, and the flow velocity is derived from the peak position of the cross-correlation function. Finally, the product of the flow velocity and coal concentration gives the mass flow rate of the coal slurry.

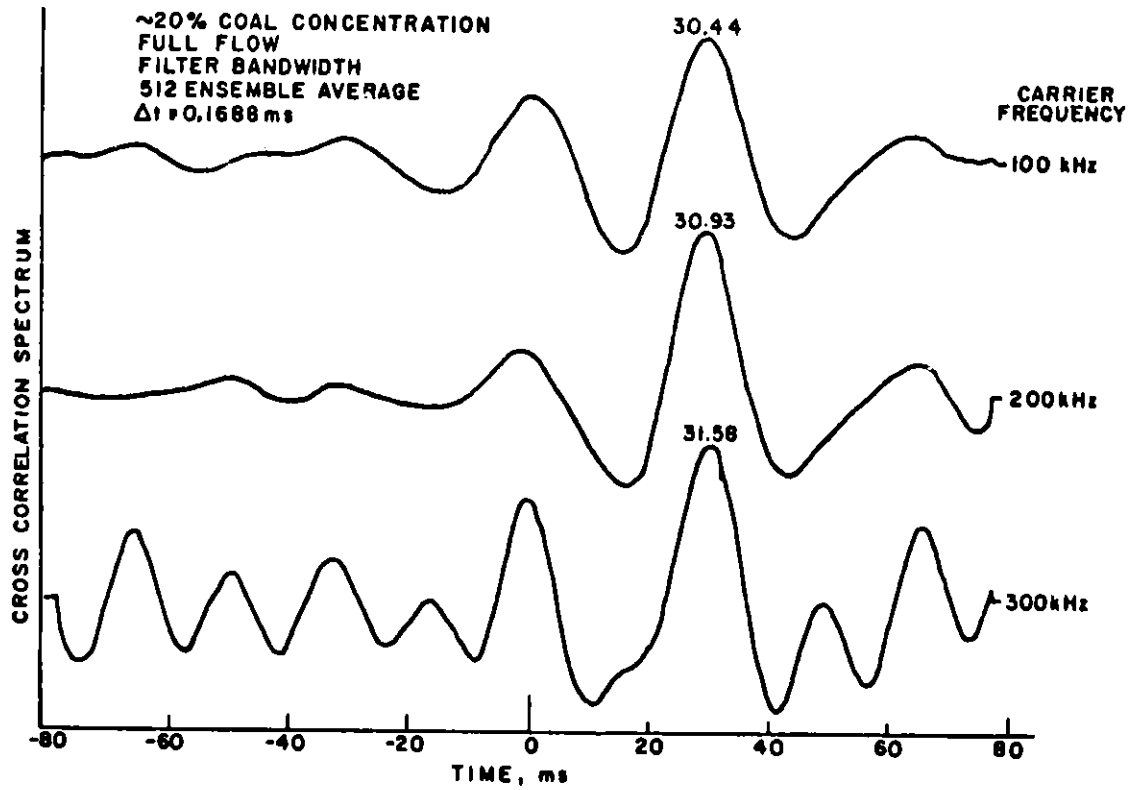

Fig. 8 Cross-correlation function at 20 % coal concentration and three carrier frequencies.

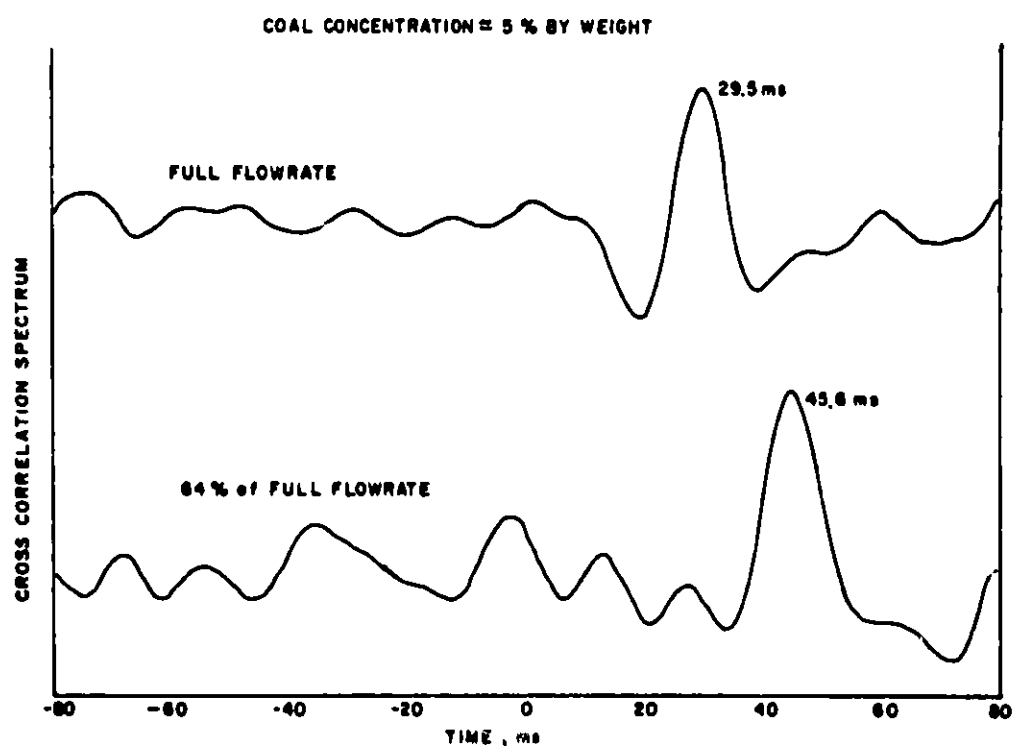

Fig. 9 Cross-correlation functions of two flow velocities in 5-wt % coal concentration.

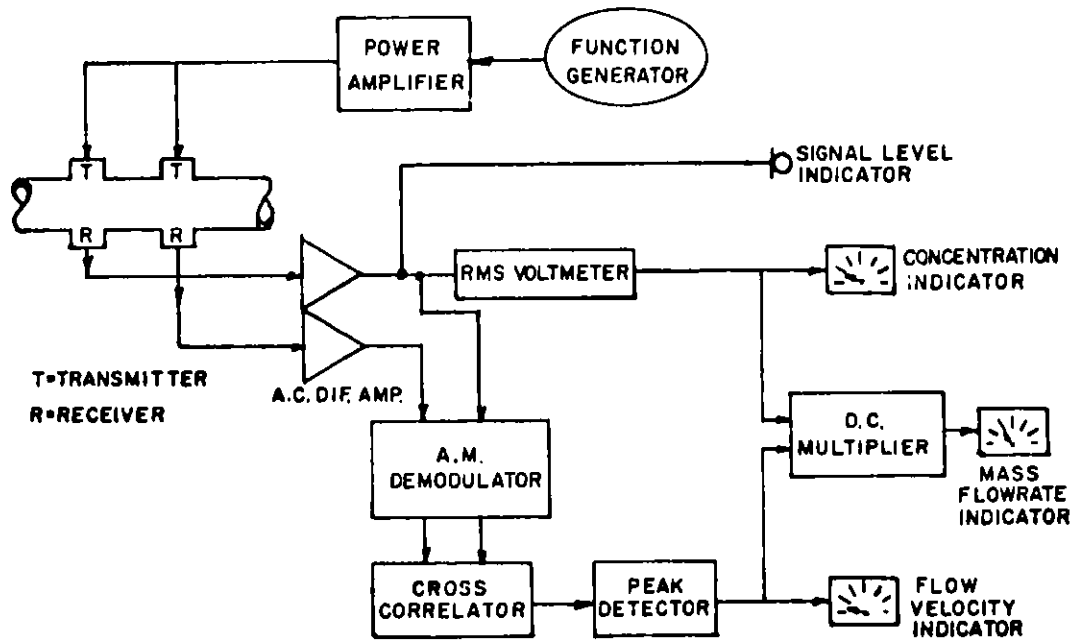

Fig. 10 Schmetic diagram of an on-line cross-correlation ultrasonic mass flowmeter.

CONCLUSIONS

To improve and optimize the design and capability of the proposed mass flowmeter, the following areas require further investigation: (1) the effects of flow-velocity and coal-concentration measurements due to the coal particle size distribuiton, (2) the upper and lower limits of the flow-velocity that can be measured with a given transducer separation; (3) the effects on the flow-velocity measurement of a change in transducer separation; and (4) the limitations in the mass-flow measurement when transducers are directly clamped on the pipe wall. Finally, for any future measurements, direct mass-flow measurement without the use of a tape recorder, is recommended.

ACKNOWLEDGMENT

The authors wish to thank T. K. Lau (DOE), R. S. Zeno, G. S. Rosenberg, T. P. Mulcahey, and N. M. O'Fallon for their support of this project. We also thank Nancy Heeg for the typing of the paper.

REFERENCES

1. A. C. Raptis, et al.. "Measurements of Noise Background and Attenuation in Coal Toluene Slurries," Proc. 1978 Ultrasonics Sym, IEEE cat. #78CH1344-ISU.

2. A. C. Raptis, et al., "Acoustic Noise Background and Sound Transmission Tests in a Slurry Line at the HYGAS Pilot Plant," ANL-FE-49622-TM04, Jan. 1979.

3. S. H. Sheen and A. C. Raptis, "HYGAS Coal-Slurry-Mass-Flow Measurement Using Ultrasonic Cross-correlation," ANL-FE-49622-TM07, Sept. 1979.

4. A. C. Raptis and S. H. Sheen, "Ultrasonic Properties of Coal Slurries and Flow Measurements by Cross Correlation," IEEE Trans. on Sonics and Ultrasonics, Vol. SU-28, No. 4, July 1981.

Density-Measurement Studies at the BI-GAS Pilot Plant

S. H. Sheen and A. C. Raptis
Argonne National Laboratory

ABSTRACT

Argonne National Laboratory has developed and tested an acoustic flow/no-flow monitor (or indicator) for the char return line of the BI-GAS pilot plant. The indicator has operated successfully for the last three years. It has been observed that the strength of the noise signal was affected by the amount of char in the line. In a recent experiment at BI-GAS this observation was further explored, and it was found that the signal is related to the char valve opening, particularly in the frequency range of 1-20 kHz. This is a clear indication that the flow/no-flow indicator can be upgraded to a density meter and consequently to a true mass flowmeter. This can be done by installing another flow/no-flow indicator upstream or downstream of the existing one and cross-correlating the two signals.

INTRODUCTION

In 1976 the BI-GAS coal-gasification pilot plant at Homer City, PA, urgently requested that a flowmeter, or at least a flow monitor, be developed for monitoring char flow to the gasifier Because an undetected flow stoppage can very quickly cause a dangerous temperature excursion in the gasifier. Argonne National Laboratory (ANL) responded to the request by developing, installing, and successfully testing acoustic flow monitors, which give rapid indication of blockages or other flow perturbations in the char lines.[1,2] These flow monitors have been operating at BI-GAS for the last three years and have greatly contributed to the safe operation of the plant.

After the successful implementation of the flow/no-flow monitors, ANL proposed to upgrade them to mass flowmeters by first installing another flow/no-flow monitor upstream or downstream of the existing one to measure flow velocity via cross-correlation and, second, using the observation that the attenuation of the noise signal is directly proportional to char concentration in the line to measure density. The proposal, however, was not funded, and the necessary development work was not carried out. On November 17-19, 1980, BI-GAS ran a char-flow test during which ANL verified the observation that the attenuation of the noise signal is proportional to the char density in the line.

This paper presents the results of this special test. In doing so, it will be essential to summarize some of the previous work on the flow/no-flow monitors presented in references 1 and 2.

FLOW/NO-FLOW MONITOR

The BI-GAS coal-conversion process is being developed by Bituminous Coal Research, Inc., at its pilot plant in Homer City, PA. The process involves two-stage high-pressure coal gasification in an entrained bed-

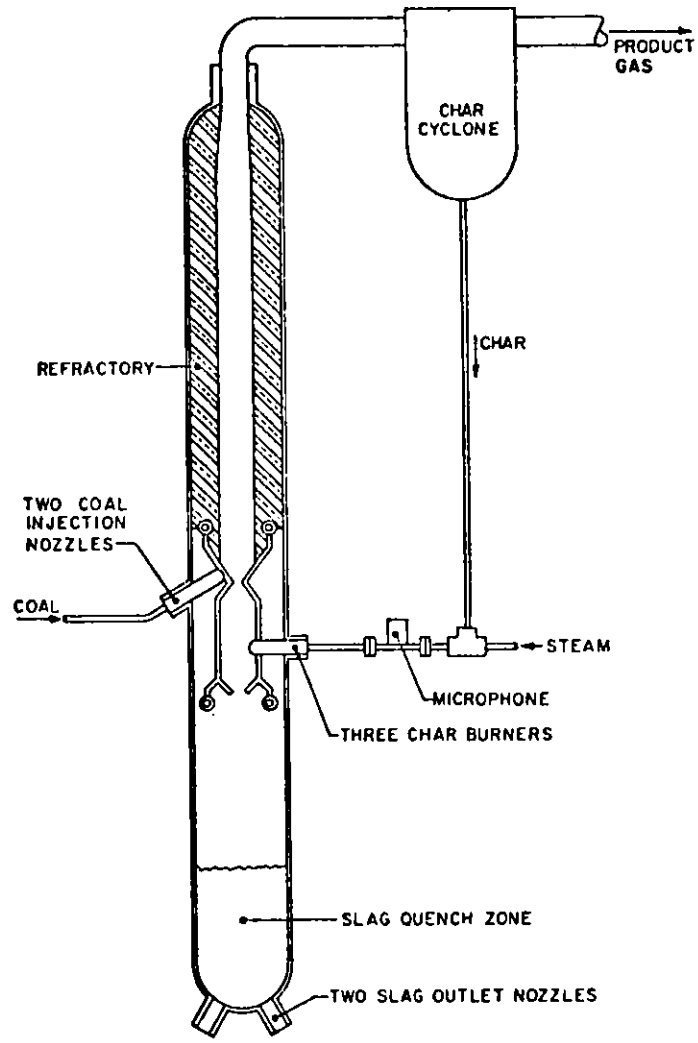

Fig. 1 Schematic Diagram of BI-GAS Reactor

type reactor, shown schematically in Fig. 1. Powdered coal is fed to an initial (upper) stage, where it is devolatilized and partly gasified as it contacts the hot gases rising from the lower stage. The gas and char (partly reacted coal) are separated in a char cyclone, and the char is reintroduced into the gasifier in the lower stage. In this stage, the char reacts with steam and oxygen under much hotter conditions (1380-1650°C, 2500-3000°F). The residue, or slag, is molten at this temperature and flows to the water-cooled quench zone, while the hot gases rise to the upper section of the gasifier. After passing through the char cyclone, the gases go to a shift reactor and fluidized-bed methanator to produce a high-Btu pipeline-quality gas.

Of particular concern at the BI-GAS pilot plant is monitoring the char flow. Blockage of the char feed lines between the char cyclone and the char burners has been a recurrent problem. The char first drops approximately 16 meters by gravity feed from the cyclone to a steam eductor, where high-pressure steam is added to the char. The char and

steam then move horizontally about 3 meters to the nozzle of the char burner. Blockage of the char in either the vertical or horizontal section can cause a very serious perturbation of the gasifier operation and can quickly lead to a hazardous temperature excursion in the gasifier.[3] The safety aspects of this problem made the need for a flow monitor very urgent, but no commercially available unit was known that could do the job. The design operating conditions in the char line are a temperature of 430°C (800°F) and pressure of 11.4 MPa (1650 psi). The char particles are quite abrasive and also tend to plug orifices and to foul moving parts.

A high-temperature microphone developed by ANL and presently commercially available from Kaman Nuclear was placed in the char return line as shown in Fig. 1. The microphone supported by a blind Grayloc hub is placed in a Tee section in such a way that its lower edge is positioned flush with the inner surface of the char line in a hole that was machined in the pipe wall. A steam eductor, shown in Fig. 1, is used to inject char into the line to the burner. This steam eductor provides a constant broadband noise source for the pipe section (attenuation path) between it and the microphone.

With steam-only flow, the microphone located as shown in Fig. 1 produced a strong, broadband signal associated with the steam flow. This meant that the presence of char can be judged in two different ways: first, by looking at the reduction of the steam signal (attenuation model) caused by scattering from the char particles,[4] and second, by looking at noise added by the char flow caused by impingement of particles on the microphone. The presence of the char particles in the attenuation path will cause absorption and scattering of the acoustic energy generated by the steam eductor, causing a decrease in the observed microphone signal. The amount of this decrease is an indication of the amount of char present in the line. Thus, the apparatus not only indicates whether char is flowing, but also indicates the amount that is flowing. Thus it can be used as a measure of the density of the char in the line.

An instrument to process the microphone signal and provide flow/no-flow indication has been built. The block diagram of this instrument is shown in Fig. 2. The microphone signal is first amplified in an external charge amplifier and then is sent to the flow monitor, where it is analyzed into three different frequency bands by bandpass filters. The rms detectors and log-ratio converters generate a dc voltage proportional to the log of the ratios of the amplitudes in the frequency band A, B, or C. The A signal is the lowest-frequency component and is least attenuated by the char, so this signal is taken as the amplitude reference. The other two signals are then normalized to this reference, the result being fed to a voltmeter for the intermediate band and to a voltage comparator for the high-frequency band. The high frequencies are most sensitive to the presence of char, and this signal (signal C) is used for the flow/no-flow indication. Whenever the high-frequency signal drops below a certain level relative to the low-frequency band, the CHAR FLOW light turns on.

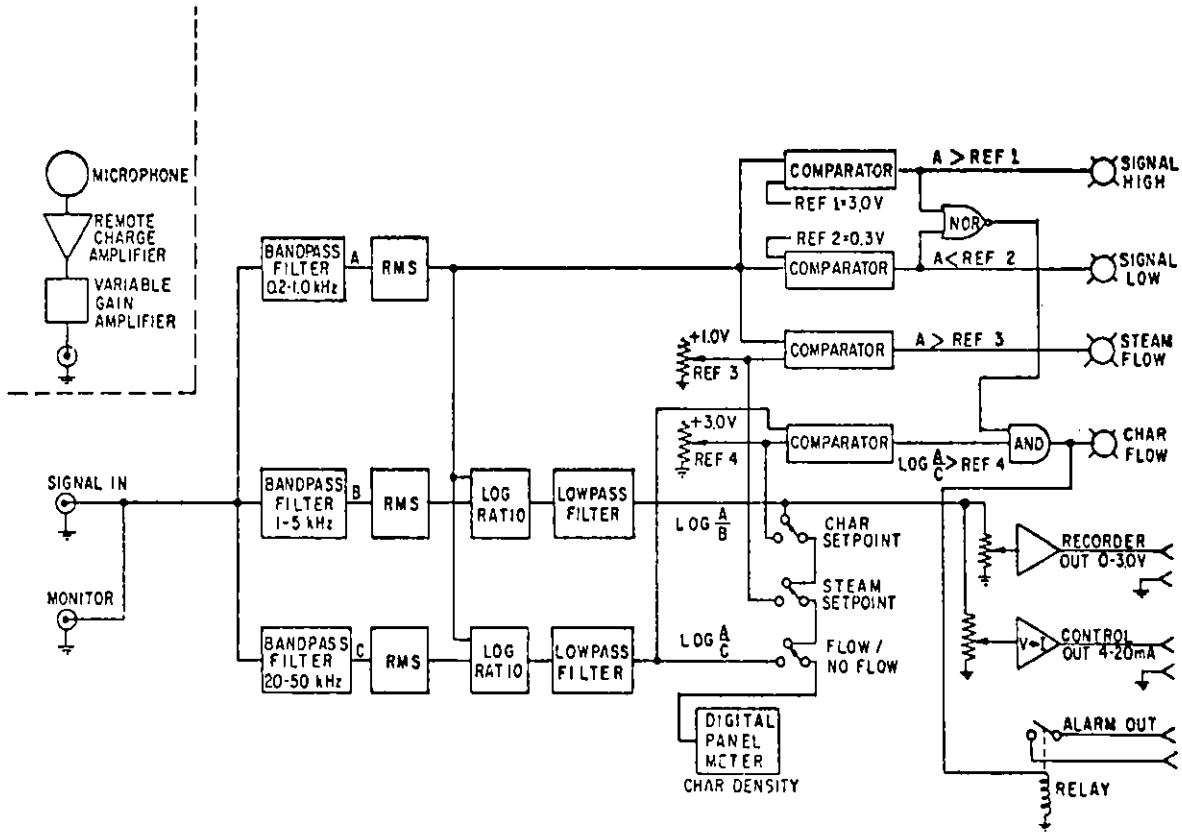

Fig. 2 Block Diagram of Flow Monitor

As mentioned earlier, this flow/no-flow indicator has operated at the BI-GAS pilot plant very successfully for the last three years. The observation that the attenuation of the noise signal is proportional to the amount of char in the line can be used as a density indicator. This observation is examined further in this report. This study is based on a char-flow test at BI-GAS on November 17-19, 1980.

CHAR-DENSITY MEASUREMENTS AT BI-GAS

When char is flowing in the line, two factors affect the overall spectrum of the signal: (a) the attenuation loss, which is more pronounced at higher frequencies and is directly proportional to the volumetric fraction of the char particles and in principle will be used to measure the char density in the char feed line, and (b) the increase of low-frequency noise resulting from the particle impingement on the microphone. This second observation should be further investigated for char particle counting. Whether or not the spectrum can be used efficiently in determining the char density is the subject of this section.

This section contains the analysis results of a BI-GAS char-flow test. The test provided several char densities in two char return legs (legs A and C). The schematic of Fig. 1 shows only one of the three legs. There was no direct measurement of char density during the test. Instead, the char density was monitored by the valve opening position, and therefore the results are presented in terms of the valve opening position.

Experiment

Table I summarizes the results of the char density test conducted at BI-GAS. The test was consisted of, (a) an experiment on steam-pressure change and (b) variations of valve opening, that is, changes in char feed for legs A and C. Leg B was experiencing difficulty in char feed; therefore no experiment was performed for that leg. The purpose of the steam pressure experiment was to examine the effect of steam pressure on the steam-only signal. Three steam pressures were made available. For each pressure a closed valve position and a 50%-open valve position were provided.

The experimental setup for this test was very simple. Signals from the microphone were conditioned by a remote charge converter and amplified by a charge amplifier. This setup is shown in the upper left corner of Fig. 2. The amplified signals were recorded on an FM channel of a tape recorder or analyzed by a 0-50-kHz spectrum analyzer.

Results of the Experiment

Acoustic noise from the steam pressure test was analyzed over the frequency range of 0-5 kHz with a 300-Hz bandwidth. No significant change in the spectrum was detected between the closed and 50%-open states of the valve with no char in the line. But increase of noise level was observed when the steam pressure was increased. Table II shows the relative spectrum levels for the three steam pressures tested. Also shown in the table is the output of the flow/no-flow indicator (Log A/B column) for the three steam-pressure settings. No change in the A/B ratio was detected.

All the char-density (more appropriately the valve opening) tests were conducted under 1350 psig in steam pressure. Five valve openings were tested for each leg (A and C). When the leg A or C valve opening was tested, leg C or A valve was set at a fixed opening. Recorded acoustic noise signals were analyzed for the frequency ranges of 0-50 and 0-10 kHz. Figure 3 shows the power spectrum up to 50 kHz for the test on leg A. The figure displays the steam-only noise-signal spectra and spectra of three valve openings. It is clearly shown in the figure that

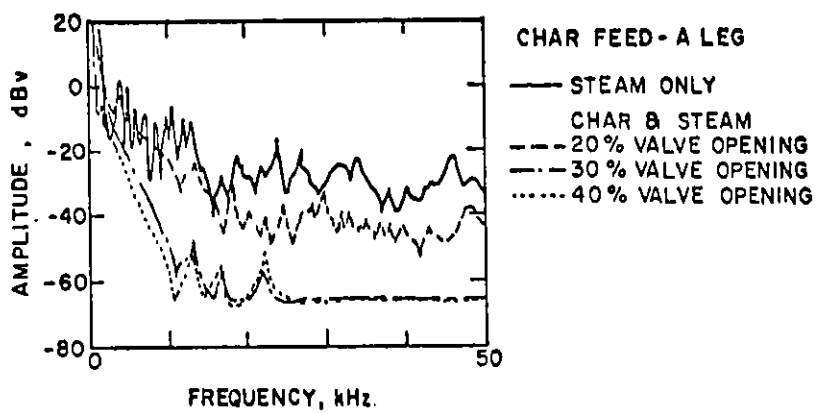

Fig. 3 Power Spectra versus Frequency for the Background Noise from Leg A at Three Valve Openings, (0050 kHz)

Table I. BI-GAS Char-Density Test Summary

Date	Time	Steam		Valve Opening (%)	
		Pressure (psig)	Temperature (°F)	Leg A	Leg C
11-17-80	1225	1350	~ 675	50	50
11-17-80	1324	1350	~ 675	0	0
11-17-80	1340	1425	~ 675	50	50
11-17-80	1354	1425	~ 675	0	0
11-17-80	1405	1500	~ 675	50	50
11-17-80	1422	1500	~ 675	0	0
11-19-80	1215	1350	676	45	51
11-19-80	1230	1350	675	40	54
11-19-80	1245	1350	677	35	57
11-19-80	1300	1350	677	30	63
11-19-80	1315	1350	677	20	68
11-19-80	1333	1350	678	62	70
11-19-80	1346	1350	680	66	60
11-19-80	1355	1350	681	65	50
11-19-80	1410	1350	683	66	40
11-19-80	1424	1350	680	66	30

Table II. Results on Steam-Only Test From Leg A

Steam Pressure (psig)	Valve Opening (%)	Log A/B	Relative Spectrum in 20-50 kHz (dB)
1500	50	0.99	0
1425	50	1.0	-2
1350	50	0.98	-6

the signal level decreases as the valve opening increases. The difference in signal level, however, between 30 and 40% valve opening is not obvious, particularly for frequencies greater than 10 kHz. For frequencies less than 10 kHz, the spectra are still clearly separated for different valve openings as shown in Fig. 4. Another distinct feature shown in Fig. 4 is that the spectra in this range are linear in nature and the slope of the spectrum becomes steeper as the valve opening increases. Physically, this change in slope may be due to a combined effect of the signal attenuation at high frequencies and the particle-impingement noise increase at low frequencies.

In a similar manner to Figs. 3 and 4, Figs. 5 and 6 display the power spectra for different valve openings for the char-feed leg C. Again spectra in the frequency range of 0-10 kHz are seen to have higher sensitivity in responding to valve opening.

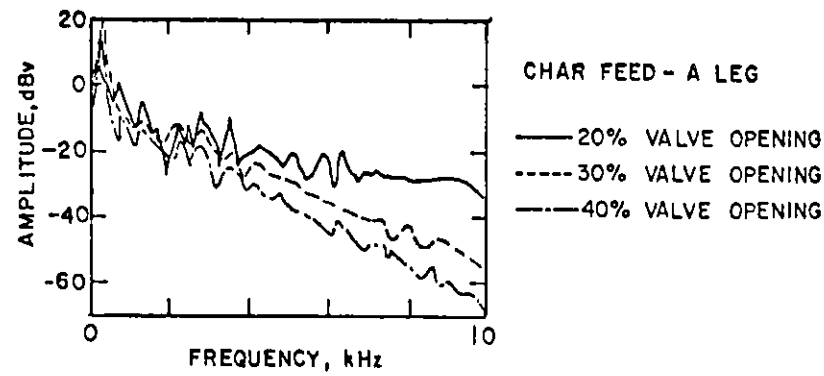

Fig. 4 Power Spectra versus Frequency for the Background Noise from Leg A at Three Valve Openings, (0-10 kHz)

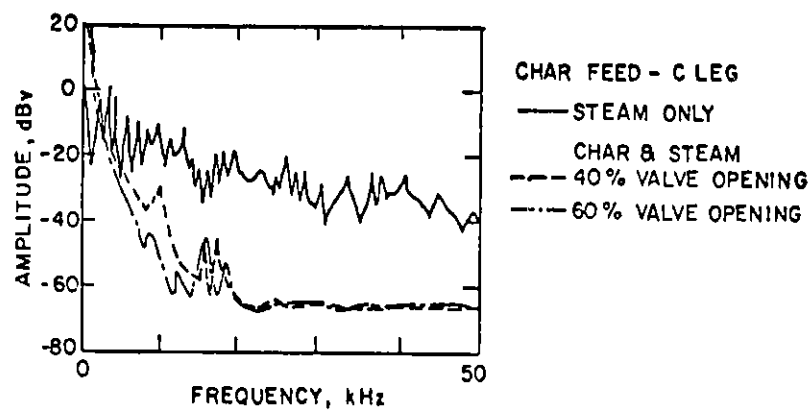

Fig. 5 Power Spectra versus Frequency for the Background Noise from Leg C at Two Valve Openings, (0-50 kHz)

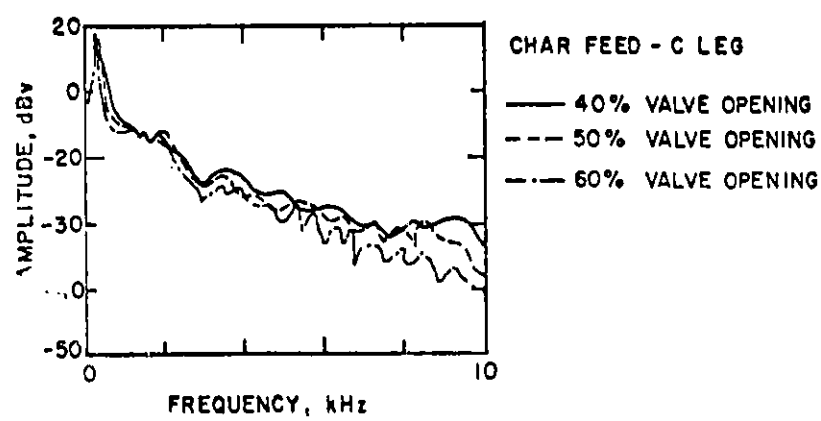

Fig. 6 Power Spectra versus Frequency for the Background Noise from Leg C at Three Valve Openings, (0-10 kHz)

CONCLUSIONS

The present signal arrangement of the flow/no-flow monitor cannot provide a quantitative measure of char particle density in the stream, because the frequency ranges chosen for the circuit design, 0.2-1, 1-5, and 20-50 kHz, are rather insensitive to the valve opening or char density. The best frequency range responding to valve opening was determined in this test to be 1-10 kHz. The spectra in this frequency range show a linear characteristic. The slope of such a spectrum was found to be directly related to the valve opening, and therefore it can be used to monitor the valve opening or the char density.

To measure the char density in the feed line, the present flow/no-flow monitor requires some simple modifications. Two approaches may be used: (a) to change the present frequency range of 1-5 to 1-20 kHz and (b) to design a circuit to measure the slope of the spectrum in the frequency range of 1-10 kHz. Since it is uncertain at present how the char density is related to the valve opening, the test results given in this paper cannot indicate the precision of this instrument in char-density measurements.

The results, however, indicate that a calibration char-density test is needed. If the test is done at BI-GAS, some relationship of the char feed and valve opening must be found. It is possible, however, that the Solid/Gas Test Facility at ANL can be used to calibrate this instrument. It will require some modifications in the existing setup in order to create the BI-GAS situation. In conclusion, the results of this test are encouraging and the present flow/no-flow indicator can be upgraded to a mass flowmeter by obtaining density as discussed above and obtaining velocity through cross-correlation.

REFERENCES

1. P. D. Roach and A. C. Raptis, "A Preliminary Report on the Flow/No-Flow Indicator for the BI-GAS Char Line," Argonne National Laboratory Technical Memorandum ANL-FE-49622-TM02, July 1978.

2. P. D. Roach and A. C. Raptis, "An Acoustic Char Flow Monitor for the BI-GAS Pilot Plant," Argonne National Laboratory Technical Memorandum ANL-FE-49622-TM08, July 1979.

3. J. W. Zink and L. P. Delsasso, "Attenuation and Dispersion of Sound by Solid Particles Suspended in Gas," J. Acoust. Soc. Am. 30(8), 765-771, August 1958.

4. L. D. Mullins, W. F. Baldwin and P. M. Berry, "How Detectors Measure Flowline Sand," Oil and Gas Journal, p. 101, February 3, 1975.

POSTER DISPLAY - REAR OF RALSON ROOM

DYNAMIC ANALYSIS: A USEFUL TOOL FOR PREDICTING THE PERFORMANCE OF COAL PREPARATION PROCESS CONTROLS[+]

W. R. Hamel, G. O. Allgood,
C. H. Brown, Jr., and G. S. Canright
Oak Ridge National Laboratory
P.O. Box X
Oak Ridge, Tennessee 37830
Phone: (615) 574-6824
FTS 624-6824

POSTER DISPLAY ABSTRACT

The basic steps in using dynamic analysis to compare manual control with one form of automatic control of a typical froth flotation circuit are presented. The essential features of the analysis are shown by summarizing: (1) the specific application data, (2) the dynamic mathematical equations for the flotation and filtration processes, (3) the manual and automatic control models, and (4) the computer solution method. Results of a comparison between manual operator control and automatic feedforward control are presented in terms of transient response characteristics and cost-saving potential.

[+]Research sponsored by the Pittsburgh Mining Operation, Coal Preparation Division, U.S. Department of Energy under contract W-7405-eng-26 with the Union Carbide Corporation.

A LOW-ORDER, SYSTEM-LEVEL DYNAMIC MODEL OF A FLUIDIZED-BED GASIFIER

D. Laird, M. Ringham, and S. Ubhayakar

JAYCOR, 11011 Torreyana Road, San Diego, California 92122

ABSTRACT

A lumped-parameter dynamic computer model has been developed by JAYCOR to simulate a fluidized-bed coal gasifier. Finite heterogeneous chemical reaction rates provide for a realistic representation of processes which occur on time scales near the response times of instruments and controls. Thus, the model predicts time-dependent gasifier responses to transient perturbations in operating parameters, and is suited for practical problems in process control. Computation times as low as 1/100 of real time are obtained, and the model provides remarkably detailed insight into process dynamics in spite of the simplicity of its underlying assumptions.

MODEL DEVELOPMENT

The underlying assumptions for the fluidized-bed gasifier dynamic model are:

1. The interior of the gasifier is lumped into an isothermal, isobaric zone and treated as a well stirred reactor.
2. Reacting gases are assumed in thermochemical equilibrium.
3. Coal is assumed to devolatilize instantly within the gasifier. In devolatilization, it is assumed that nitrogen and sulfur are released as N_2 and H_2S, respectively. Methane, N_2, and H_2S are treated as inert products of devolatilization.
4. Gasification of carbon in the char is governed by the combustion reaction (with O_2), the Boudouard reaction (with CO_2), and the water-gas reaction (with H_2O). Each of these reactions proceeds at a finite rate determined by a global kinetic expression, with displacement from equilibrium as the driving force for reaction. Hydrogasification (with H_2) reaction is neglected because of its relatively slow rate compared to the other three. The composition and thermodynamics of graphite are attributed to char.

5. The gas exit stream is assumed free from solid particulates.
6. The only solids exiting the system are assumed to be agglomerates, comprised of 100% ash and flowing at a rate equal to ash carried in by the coal.

Five chemically reactive gas-phase species (O_2, CO, CO_2, H_2, and H_2O) are considered. Their partial pressures are determined by water-gas shift and H_2 oxidation equilibria:

$$K_{WG}(T) = \frac{P_{H_2O} P_{CO}}{P_{H_2} P_{CO_2}} , \tag{1}$$

$$K_H(T) = \frac{P_{H_2O}}{P_{H_2} P_{O_2}^{0.5}} = \frac{Y_{H_2O}}{Y_{H_2} Y_{O_2}^{0.5} P^{0.5}} = \frac{M_{H_2O}}{M_{H_2} M_{O_2}^{0.5} \left(\frac{P}{M_g}\right)^{0.5}} , \tag{2}$$

along with the conservation of the elements C, H, and O. See glossary for variable definitions and units.

$$M_C = M_{CO} + M_{CO_2} , \tag{3}$$

$$M_H = 2M_{H_2} + 2M_{H_2O} , \tag{4}$$

$$M_O = M_{CO} + 2M_{CO_2} + M_{H_2O} + 2M_{O_2} , \tag{5}$$

and the ideal gas law

$$\frac{P}{M_g} = \frac{RT}{V_g} , \tag{6}$$

where the volume currently occupied by solid is deducted to obtain gas volume:

$$V_g = V_T - \frac{M_C}{\rho_C} - \frac{M_A}{\rho_A} . \tag{7}$$

Thus, M_{CO}, M_{CO2}, M_{O2}, M_{H2}, AND M_{H2O} are algebraic functions of K_{WG}, K_H, M_{SA}, M_{SC}, M_C, M_H, M_O, and T. The latter five variables are determined by solution of differential mole and energy balances.

Methane, N_2, and H_2S produced in the devolatilization of coal are lumped into an equivalent species, M_{NON}, defined by the mole balance

$$\frac{dM_{NON}}{dt} = v\, F_{COAL} - Y_{NON}\, F_{OUT} \cdot \tag{8}$$

Gasification of the carbon char is assumed to be governed by three rate mechanisms; combustion described by

$$C + \frac{1}{2}\, O_2 \rightleftarrows CO$$

occurs at a rate defined functionally by the expression

$$R_{O_2} = \frac{P_{C_2} - [P_{CO_2}/K_O(T)]^2}{P_{O_2} + k_1} \exp\left(A_{O_2} - \frac{\Delta E_{2O}}{RT}\right) , \tag{9}$$

the heterogeneous CO_2 reaction

$$C + CO_2 \rightleftarrows 2CO$$

occurs at a rate defined by

$$R_{CO_2} = \frac{P_{CO_2} - P_{CO}^2/K_{CO_2}(T)}{P_{CO_2} + k_3} \exp\left(A_{CO_2} - \frac{\Delta E_{CO_2}}{RT}\right) \tag{10}$$

and the heterogeneous H_2O reaction

$$C + H_2O \rightleftarrows CO + H_2$$

occurs with rate R_{H_2O} defined functionally as

$$R_{H_2O} = \frac{P_{H_2O} - P_{H_2} P_{CO}/K_{H_2O})\, \exp\left(A_1 - \frac{\Delta E_1}{RT}\right)}{1 + k_3\, P_{H_2} + P_{H_2O} \exp\left(A_2 - \frac{\Delta E_2}{RT}\right)} \cdot \tag{11}$$

The elemental conservation equation for solid char is written as

$$\frac{dM_{SC}}{dt} = \beta\, F_{COAL} - \left(2R_{O_2} + R_{CO_2} + R_{H_2O}\right)\, SM_{SC} \cdot$$

The amount of ash M_A is currently held constant.

Elemental balances on the number of atoms of carbon M_C, hydrogen M_H, and oxygen M_O in the gas phase are written as

$$\frac{dM_C}{dt} = (x - \beta)\, F_{COAL} + \left(2R_{O_2} + R_{CO_2} + R_{H_2O}\right) SM_{SC} - \left(Y_{CO} + Y_{CO_2} + Y_{CH_4}\right) F_{OUT} ,$$

$$\frac{dM_H}{dt} = y\, F_{COAL} + 2F_{H_2O} - 2\left(Y_{H_2O} + Y_{H_2}\right) F_{OUT} ,$$

$$\frac{dM_O}{dt} = z\, F_{COAL} + F_{H_2O} + 2F_{O_2} - \left(2Y_{O_2} + 2Y_{CO_2} + Y_{H_2O} + Y_{CO}\right) F_{OUT} .$$

The lumped energy conservation for the reactor is first expressed as

$$\frac{d}{dt}\left[M_{SC}H_{SC}(T) + M_{SA}H_{SA}(T) + \sum_i M_i H_i(T)\right] = F_{COAL}\, H_{COAL}\,(T_{COAL}) + F_{H_2O}\, H_{H_2O}\,(T_{H_2O}) + F_{O_2}\, H_{O_2}\,(T_{O_2}) - F_{OUT} \sum Y_i H_i(T) = A ,$$

where $i = 1, \ldots, 6$ corresponds to the five interacting and the single non-reacting equivalent gas species, and is then reduced to

$$\frac{dT}{dt} = \left(A - H_{SC}\frac{dM_{SC}}{dt}\right)\Big/\left(M_C C_{pC} + M_A C_{pA} + \sum_i M_i C_{pi}\right) .$$

The $H_{()}(T)$ terms are the total specific enthalpies expressed as

$$H_{()}(T) = \Delta H^{o}_{f,()} + \int_{T_0}^{T} C_{p,()}\,dT = \Delta H_{f,()} + C_{p,()}(T - T_0) ,$$

assuming constant specific heats.

The flow rate of output gas is determined by the flow resistance posed by the downstream system. It is assumed that the back pressure regulator (BPR) incurs the most significant pressure drop and that the output flow rate is determined predominantly by this regulator. Treating the regulator as an orifice, we have

$$F_{OUT} = (\text{constant})(A_V)\sqrt{P(P - P_1)/(W_{OUT}\, T_{OUT})} , \qquad (12)$$

where A_V is the orifice area which is assumed to vary as a linear first-order log on controller demand with a time constant of 1 second.

DISCUSSION

Figure 1 illustrates model response to a 100% reduction in coal feed. Interruption of coal feed to the gasifier immediately deprives the gas of species sources due to devolatilization. Consequently, there is a rapid readjustment of gas species distribution as devolatilization products are displaced by products of gasification and combustion. This short-lived transient is accompanied by a quick temperature increase due to the heat no longer required for devolatilization of coal and heating of its products.

Following this short-term transient is a period of near-constant gas concentration and gradually increasing temperature. The predominant heterogeneous reaction is CO_2 gasification. Incoming oxygen is entirely consumed by combustion with gasification product CO and with H_2 from the water-gas shift. During this phase, the chemical mechanism could be regarded as indirect quasi-steady-state combustion of char, with CO and H_2 as reactive intermediates. The rate controlling gasification reaction accelerates with increasing temperature, but this happens to be nearly counterbalanced by reduction in the char inventory, so that gas distribution and production stays nearly constant.

There is a change in chemistry as char residue nears exhaustion. Gasification reactions no longer keep pace with incoming oxygen, so that H_2 and CO rapidly decline. There is a dramatic increase in temperature due to heat no longer consumed in endothermic gasification reactions, coupled with the reduced thermal inertia of the bed. Direct combustion of carbon residue is sufficiently rapid to keep O_2 concentration very low until the char is entirely consumed.

With char oxidation complete, there is no longer a fuel source for chemical reaction. Carbon-containing gases are quickly displaced by feed O_2 and H_2O, which also transfer sensible heat away from residual ash.

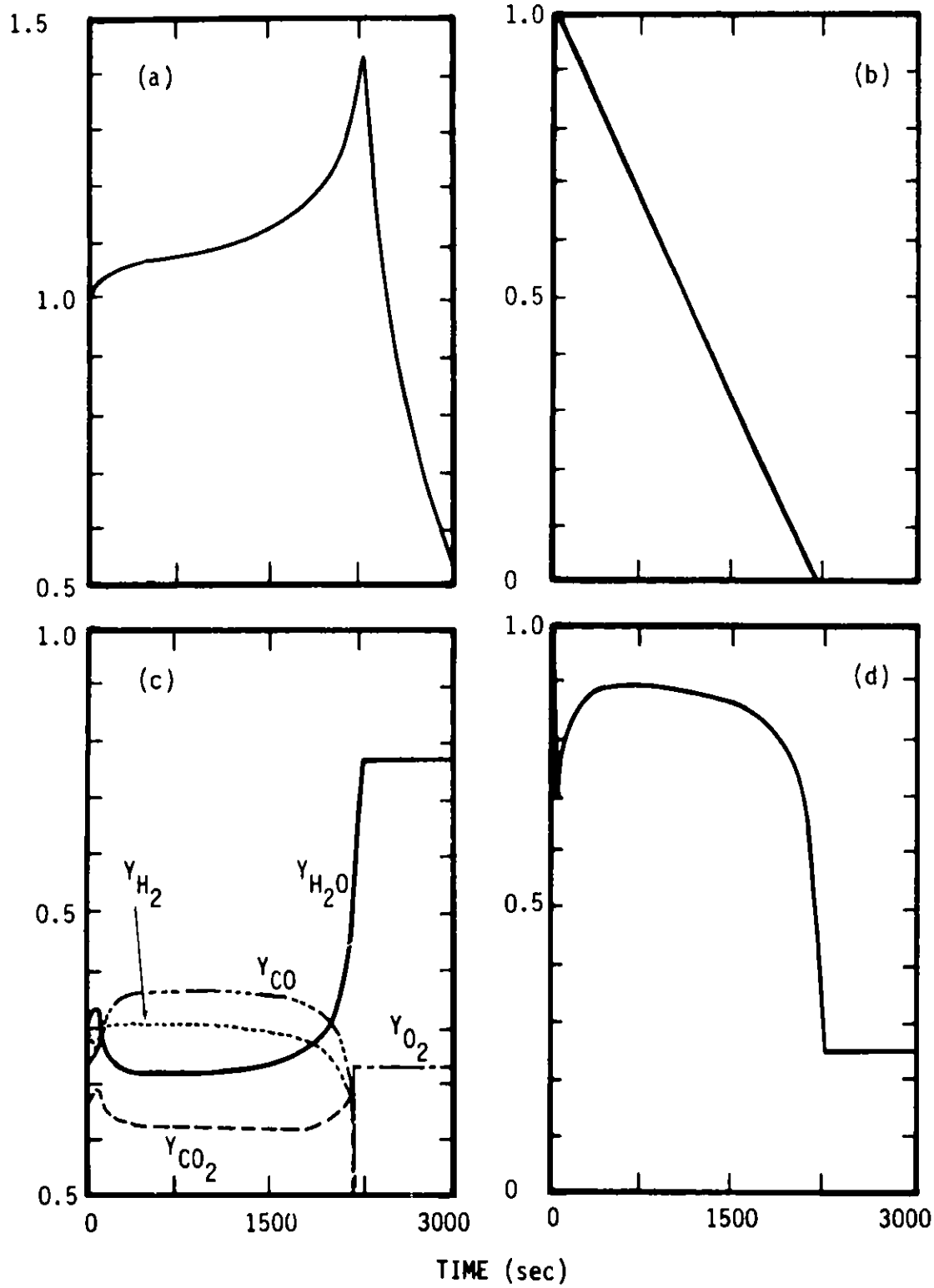

Figure 1. Transient response to interruption of coal feed

(a) Absolute temperature relative to steady state
(b) Char mass holdup relative to steady state
(c) Gas species mole fractions
(d) Gas molar production relative to steady state

GLOSSARY

C_p = Specific heat at constant pressure (Btu/lb-mole°F)

F = Flow rate (lb-moles/sec)

H = Total enthalpy per lb-mole (Btu/lb-mole)

K(T) = Equilibrium constant (units of psia, as appropriate)

M = Total lb-atoms or lb-moles in gasifier (lb-atoms or lb-moles)

P = Reactor gas pressure (psia)

R = Universal gas constant [(ft^3-psia)/lb-mole°R)]

$R_{()}$ = Reaction rate (lb-ataom/lb-atom char)

T = Temperature (°F)

V = Volume (ft^3)

W = Molecular weight (lb/lb-mole)

Y = Mole fraction of gas species

x = Carbon-to-ash atom ratio in bulk char

v,y,z = Nonreacting, hydrogen, oxygen-to-ash atom ratios in bulk char

β = Carbon-to-ash atom ratio in devolatilized char

ΔH_f° = Heat of formation at reference temperature T_0 (Btu/lb-mole)

ρ = Density (lb/ft^3)

PROCESS CLINIC LIST OF PARTICIPANTS

William Miller Ashland Synthetic Fuels, Inc.	Chairman
T. K. Lau U.S. Department of Energy	Alternate
George H. Quentin Project Manager Clean Gaseous Fuels Program Electric Power Research Institute	Panelist
Thomas Carroll Principal Engineer Foster Wheeler Energy Corporation	Panelist
Frank G. Mesich Assistant Vice President Radian Corporation	Panelist
Herbert C. March Principal Instrument Engineer Procon, Inc.	Panelist
Walter F. Podolski Leader, FBC Process Evaluation Group Argonne National Laboratory	Panelist
Harold E. Hendler Industry Marketing Manager Industrial Energy Processes Taylor Instruments	Panelist
David L. Murphree Director, MHD Energy Center Mississippi State University	Panelist

EXHIBITORS

R. L. Beery
The Bendix Corporation
Lewisburg, West Virginia

Don Bowlin
Cameron Iron Works
Houston, Texas

Mr. Flandreau
Perkin-Elmer Corporation
Norwalk, Connecticut

Brad Gehring
Rosemount, Inc.
Eden Prairie, Minnesota

Roseann Geyer
The McIlvaine Company
Northbrook, Illinois

Brooke M. Hinds
Barnes Engineering Company
Stamford, Connecticut

Herb Kaplan
Society for Control and
Instrumentation of Energy Processes
Norwalk, Connecticut

Robert Kaufman
Mogas Machine Works, Inc.
Houston, Texas

P. Kindersley
Kamyr Valves, Inc.
Glen Falls, New York

L. L. Landskov
Delavan Electronics, Inc.
Scottsdale, Arizona

Richard F. Leftwich
Irtronics, Inc.
Stamford, Connecticut

Tom McCall
MANCO
Santa Clara, California

Urie McCleary, Jr.
Perkin-Elmer Corporation
Pomona, California

Lawrence B. Shovelton
Gentran, Inc.
Sunnyvale, California

R. Sielemann
Carl Zeiss, Inc.
New York, New York

David Snyder
Validyne Engineering Corporation
Northridge, California

John Sozio
Taylor Instruments
Rochester, New York

Seymour Steinberg
ARI Industries, Inc.
Franklin Park, Illinois

Ron Weisen
Land Instruments, Inc.
Tullytown, Pennsylvania

Harold Weiss
Analog Devices, Inc.
Huntington Beach, California

Grant N. Wetzel
Hach Company
Anaheim, California

List of Attendees

Robert F. Adamowicz
Avco Everett Research Laboratory, Inc., Everett, MA

A. K. Agarwal
Monsanto Research Corporation, Miamisburg, OH

Johannes J. Albrecht
Lurgi Kohle und Mineralotechnik, Frankfurt, Germany

Peter Alexander
TRW Energy Systems, Lakewood, CO

Harold B. Arsem
Chevron Research Company, Richmond, CA

Irina Auerbach
Chevron USA, San Francisco, CA

E. O. Ballard
Los Alamos National Laboratory, Los Alamos, NM

Robert F. Barber
The Ralph M. Parsons Company, Pasadena, CA

Leslie E. Bauman
Mississippi State University, Starkville, MS

Donald G. Beason
Lawrence Livermore National Laboratory, Livermore, CA

Maurice Sidney Beck
University of Manchester, Manchester, England

Ray G. Bedford
Lawrence Livermore National Laboratory, Livermore, CA

Bonnie Lee Bell
Stanford Medical Center, Stanford, CA

Joseph F. Bencini
Gulf Research and Development Company, Pittsburgh, PA

Pompilio Bermudez
Fisher Controls Company, Marshalltown, IA

Peter F. Berry
Texas Nuclear Corporation, Austin, TX

Corey A. Bertelsen
Chevron Research Company, Richmond, CA

Peter J. Blok
H.R.I. R&D Center, Lawrenceville, NJ

J. H. Bochinski
Enviro Control, Inc., Rockville, MD

Anthony A. Boiarski
Battelle Columbus Labs, Columbus, OH

Neil D. Bond
Ashland Synthetic Fuels, Inc., Ashland, KY

Hadi Bozorgmanesh
Science Applications, Inc., Sunnyvale, CA

Clifton H. Brown, Jr.
Oak Ridge National Laboratory, Oak Ridge, TN

D. R. Brown
Science Applications, Inc., Sunnyvale, CA

David Brown
Koninklijke/Shell-Laboratorium, Amsterdam, The Netherlands

William H. Brumage
Louisiana Tech University, Ruston, LA

Wojciech Stanistaw Brzozowski
Institute of Nuclear Research, Swierk, Poland

Eugene A. Burns
Systems, Science, and Software, La Jolla, CA

G. Burns
National Bureau of Standards, Washington, D.C.

William H. Bushnell
Solvent Refined Coal International, Inc., Englewood, CO

William H. Buttermore
West Virginia University, Morgantown, WV

Geoffrey S. Canright
Oak Ridge National Laboratory, Oak Ridge, TN

Peter K. Carlson
Union Carbide Corporation, Oak Ridge, TN

Ken Carr
Oak Ridge National Laboratory, Oak Ridge, TN

C. T. Carroll
Foster Wheeler Energy Corporation, Livingston, NJ

Gloria M. Caton
Oak Ridge National Laboratory, Oak Ridge, TN

Tom J. Cebulla
Honeywell, Inc., Roseville, MN

Phil Celli
Leeds & Northrup Company, Largo, FL

George W. Charboneau
University of Tennessee Space Institute, Tullahoma, TN

Alex N. Chen
Standard Oil Company of California, San Francisco, CA

David Frank Ciliberti
Westinghouse R&D, Pittsburgh, PA

James John Colyar
Cogas Development Company, Princeton, NJ

H. R. Cooper
H. R. Cooper Systems, Inc., Salt Lake City, UT

Jack George Crump
Kay Ray, Inc., Arlington Heights, IL

Clayton T. Crowe
Washington State University, Pullman, WA

Robert F. Culmo
Perkin-Elmer Corp., Norwalk, CT

Donald E. Davis
Rockwell International Corporation, Canoga Park, CA

Robert H. Davis
Florida State University, Tallahassee, FL

Fred J. Deadrick
Lawrence Livermore Laboratory, Livermore, CA

Sam DeBose
Foster Wheeler Energy Corporation, Livingston, NJ

Herbert Deich
MDH Industries, Inc., Monrovia, CA

Clyde B. Dennis
Argonne National Laboratory, Argonne, IL

F. E. Diebold
Montana College of Mineral Science & Technology, Butte, MT

Richard W. Doering
Argonne National Laboratory, Argonne, IL

Paul Dunne
Monsanto Research Corporation, Miamisburg, OH

Bernard J. Eastlund
The BDM Corporation, McLean, VA

Paul J. Ebert
U.S. Department of Energy, Washington, D.C

William E. Farthing
Southern Research Institute, Birmingham, AL

Gunter Fauth
Bergbau-Forschung GmbH, West Germany

Howard Feldstein
Taylor Instrument Company, Rochester, NY

Gerd Wolfgang Felgener
Rheinische Braunkohlenwerke AG, Germany

Paul D. Fetherland
Texaco, Inc., Montebello, CA

Robert C. Figel
System Development Corporation, El Segundo, CA

Carlos Figueroa
Lawrence Berkeley Laboratory, Berkeley, CA

Francis T. Finch
Los Alamos National Laboratory, Los Alamos, NM

David O. Fleming
Exxon Research and Engineering Company, Florham Park, NJ

William L. Flower
Sandia National Laboratory, Livermore, CA

Michael Robert Fuchs
Radian Corporation, Austin, TX

Walter Fuchs
Pittsburgh Energy Technology Center, Pittsburgh, PA

Jerzy Galka
U.S. Department of Energy, Morgantown, WV

Bradley P. Gehring
Rosemount, Inc., Eden Prairie, MN

Ken D. Gehring
Alberta Research Council, Edmonton, Alberta, Canada

John H. George
University of Wyoming, Laramie, WY

Bernd Gerlach
Halterner Strabe 125, Dorsten, Germany

Thomas V. Giel, Jr.
University of Tennessee Space Institute, Tullahoma, TN

Guy D. Gimson
International Coal Refining Company, Allentown, PA

Robert E. Glass
Sandia National Laboratories, Albuquerque, NM

Ira B. Goldberg
Rockwell International Science Center, Thousand Oaks, CA

N. Gopalsami
Argonne National Laboratory, Argonne, IL

Terry L. Greenlee
JAYCOR, San Diego, CA

W. P. Gulledge
Pittsburgh Energy Technology Center, Pittsburgh, PA

R. J. Gylys
Standard Oil of California, San Francisco, CA

William J. Haas, Jr.
Ames Laboratory, Ames, IA

Richard A. Handschumacher
ITT Grinnell Valve Co., Inc., Providence, RI

Bernard R. Hao
Mechanical Technology, Inc., Fairfax, VA

Don Hardesty
Sandia National Laboratories, Livermore, CA

Dan Hartley
Sandia National Laboratories, Livermore, CA

Abu R. Hasan
University of North Dakota, Grand Forks, ND

Jim E. Helt
Argonne National Laboratory, Argonne, IL

Harold E. Hendler
Taylor Instrument Company, Rochester, NY

John A. Herbst
University of Utah, Salt Lake City, UT

Jose R. Hernandez
M. W. Kellogg Company, Houston, TX

Leroy E. Herr
Kieley & Mueller, Inc., Middletown, NY

Caroline L. Herzenberg
Argonne National Laboratory, Argonne, IL

Wolfgang Herzog
Staatl. Materialprufungsamt NW, Federal Republic of Germany

Alberta R. Hibbs
Jet Propulsion Laboratory, Pasadena, CA

Guy Hines
Motherwell Control Systems, Inc., Minnetonka, MN

R. F. Holland
Los Alamos National Laboratory, Los Alamos, NM

Donald J. Holve
Sandia National Laboratories, Livermore, CA

B. R. Hoover
Armco, Inc., Middletown, OH

H. M. Horowitz
IBM Corporation, Bethesda, MD

J. Hsu
KTI Corporation, Pasadena, CA

Jack S. Hubacher
Mechanical Technology, Inc., Fairfax, VA

Elton B. Hunt
Amoco Production Research, Tulsa, OK

John E. Huntington
Tosco Corporation, Golden, CO

John E. Janssen
Honeywell, Inc., Roseville, MN

Robert L. Jeffcoat
Foster-Miller Associates, Inc., Waltham, MA

Kay Ann Jenkins
Stanford Medical Center, Stanford, CA

J. D. Jobe
Shell Development Company, Houston, TX

Roy M. Johnson
Montana State University, Bozeman, MT

Robert R. J. Jungerhans
KTI Corporation, Pasadena, CA

H. Kaplan
Crest Energy Systems, Inc., Norwalk, CT

Muhammad N. Karim
Colorado State University, Fort Collins, CO

Fred V. Karlson
Electric Power Research Institute, Palo Alto, CA

Henry B. Karplus
Argonne National Laboratory, Argonne, IL

Dennis M. Kelly
Stearns-Roger Engineering Corporation, Homer City, PA

Peter J. King
Tosco Corporation, Los Angeles, CA

Fred A. Kirsten
Lawrence Berkeley Laboratory, Berkeley, CA

Fred E. Kiviat
Gulf Research & Development Co., Pittsburgh, PA

Tadeusz Kozlowski
Institute of Nuclear Research, Swierk, Poland

Chester L. Krcil
Conoco Coal Development Company, Library, PA

Manfred Kurth
Institut fur Eisenhuttenkunde, West Germany

Richard Kwiatkowski
Mine Safety Appliances Company, Evans City, PA

Ying-San Lai
Dresser Industries, Inc. Alexandria, LA

Tom M. Lastrapes
Bendix Epid, Lewisburg, WV

T. K. Lau
U.S. Department of Energy, Washington, D.C.

Swenam R. Lee
U.S. Department of Energy, Pittsburgh, PA

A. M. Leonardi-Cattolica
Shell Development Company, Houston, TX

Emil Lepsch
Motherwell Control Systems, Inc., Minnetonka, MN

Allan R. Levin
Cameron Iron Works, Inc., Houston, TX

Donald W. Lewis
Jet Propulsion Laboratory, Pasadena, CA

Myron R. Lewis
White Consolidated Industries, Inc., Burlington, MA

Michael D. Liquori
Foster Wheeler, Livingston, NJ

Donald J. L. Lin
Forney Engineering Company, Addison, TX

Ralph W. Lindeman
Bailey Controls Company, Wickliffe, OH

Ivan R. Linscott
NASA-Ames Research Center, Ames, IA

Thomas E. Lippert
Westinghouse R&D, Pittsburgh, PA

E. A. Lloyd
Hydrocarbon Research, Inc., McLean, VA

Billy W. Loo
Lawrence Berkeley Laboratory, Berkeley, CA

Thomas R. Loree
Los Alamos National Laboratory, Los Alamos, NM

Dale Kendall Lyle
Fisher Controls Company, Marshalltown, IA

John B. McDaniel
Honeywell, Inc., Phoenix, AZ

Joseph E. Macko
Westinghouse Electric Corporation, Madison, PA

William W. Managan
Technology for Energy Corporation, Knoxville, TN

Herbert Charles March
Procon, Inc., Des Plaines, IL

John E. Marion
Sandia National Laboratories, Livermore, CA

Robert L. Markoja
Acurex Corporation, Mountain View, CA

Robert Martin
Jet Propulsion Laboratory, Pasadena, CA

Rommel R. Martinez
Bechtel Power Corporation, San Francisco, CA

Mahendra P. Mathur
U.S. Department of Energy, Pittsburgh, PA

Doug Merrick
Dow Chemical, Plaquemine, LA

Frank G. Mesich
Radian Corporation, McLean, VA

Howard S. Meyer
Gas Research Institute, Chicago, IL

Emmett R. Miller
Shell Oil Company, Martinez, CA

Mike Miller
Mountain States Energy, Butte, MT

William R. Miller
Ashland Synthetic Fuels, Inc., Ashland, KY

William C. Mines
ITT Barton Instruments, City of Industry, CA

Hideo Mitsuyasu
Yokogawa Electric Works, Shinjuku-Ku, Tokyo, Japan

Dennis F. Moore
Laramie Energy Technology Center, Laramie, WY

Larry Louis Moresco
Combustion Power Company, Menlo Park, CA

Thomas E. Morris
Leeds & Northrup, Tarpon Springs, FL

Pat B. Moseley
Louisiana Tech University, Ruston, LA

Thomas P. Mulcahey
Argonne National Laboratory, Argonne, IL

David Murphree
Mississippi State University, Mississippi State, MS

Taki Negas
National Bureau of Standards, Washington, D.C.

H. Newman
Ashland Synthetic Fuels, Inc., Ashland, KY

Roy O. Nicholson
Monsanto Research Corporation, Miamisburg, OH

Murray C. Nixon
Perkin-Elmer Corporation, Norwalk, CT

John E. Notestein
U.S. Department of Energy, Morgantown, WV

Ron Oda
Conoco, Inc., Ponca City, OK

Nancy M. O'Fallon
Argonne National Laboratory, Argonne, IL

Thomas Patrick O'Shea
Electric Power Research Institute, Cupertino, CA

George E. Oswald
Oak Ridge National Laboratory, Oak Ridge, TN

Joe P. Parris
Cameron Iron Works, Inc., Houston, TX

Allen L. Payne
Washington State University, Pullman, WA

Alexandra Perandinou
Bechtel Power Corporation, San Francisco, CA

Richard M. Phillippi
U.S. Army, Harry Diamond Labs, Adelphi, MD

Robert A. Piccirelli
Available Energy, Inc., Detroit, MI

Jim Pitrak
Amoco Oil Company, Naperville, IL

John S. Platou
Cameron Iron Works, Inc., Houston, TX

Robert J. Platt
Exxon Engineering, Florham Park, NJ

Walter F. Podolski
Argonne National Laboratory, Argonne, IL

Karl Porges
Argonne National Laboratory, Argonne, IL

George H. Quentin
Electric Power Research Institute, Palo Alto, CA

Kuppuswamy Rajamani
University of Utah, Salt Lake City, UT

Apostolos Raptis
Argonne National Laboratory, Argonne, IL

Claude Reed
Argonne National Laboratory, Argonne, IL

Arthur H. Renault
Koppers Company, Inc., Burlingame, CA

Larry J. Ricci
Chemical Engineering Magazine, New York, NY

John W. Richardson
Dresser Industries, Inc., Alexandria, LA

William H. Roach
EG&G/Idaho, Idaho Falls, ID

John J. Roberts
Argonne National Laboratory, Argonne, IL

Michael Rogers
Chevron Research Company, Richmond, CA

Robert R. Romanoski
Morgantown Energy Technology Center, Morgantown, WV

Joe J. Ronchetto
Lawrence Livermore Laboratory, Livermore, CA

Gerald S. Rosenberg
Argonne National Laboratory, Argonne, IL

Donald A. Rudberg,
Montana State University, Bozeman, MT

Frank A. Ruiz
Dow Chemical Company, Plaquemine, LA

D. G. Sample
Sandia National Laboratories, Albuquerque, NM

Myrrl J. Santy
TRW Energy Systems, Redondo Beach, CA

Toshio Satori
Hokushin Electric Works, Minato-ku, Tokyo, Japan

Roy O. Scandrol
Conoco Coal Development Company, Library, PA

John Scarafiotti
Lawrence Livermore Laboratory, Livermore, CA

T. R. Schmidt
Shell Development Company, Houston, TX

Robert F. Schnurstein
ETEC/Rockwell International, Canoga Park, CA

Mary Anne Scott
University of Tennessee Space Institute, Tullahoma, TN

P. W. Seabaugh
Monsanto Research Corporation Mound Facility, Miamisburg, OH

George Sedgwick
Alberta Research Council, Edmonton, Alberta, Canada

Sidney A. Self
Stanford University, Stanford, CA

George Selgin
Rolfite Company, Stamford, CT

Wayne E. Shannon
Synthetic Oil Corporation, Cupertino, CA

Kelly Sievers
Turbine Metal Technology, Burbank, CA

David S. Smith
Chevron Research Co., Richmond, CA

Randy L. Snyder
Leeds & Northrup Company, Largo, FL

John R. Southan
Motherwell Control Systems, Inc., Minnetonka, MN

Robert W. Stansfield
Stearns-Roger, Inc., Homer City, PA

Seymour Steinberg
ARI Industries, Inc., Franklin Park, IL

C. R. Stewart
Honeywell, Inc., Roseville, MN

David B. Stickler
Avco Everett Research Laboratory, Inc., Everett, MA

John W. Stumm
Occidental Research Corporation, Irvine, CA

Wen S. Su
Stearns-Roger Engineering Corporation, Homer City, PA

Mark M. Sutton
Hydrocarbon Research, Inc., Lawrenceville, NJ

Tomio Suzuki
Kobe Steel, Fukiai-Ku, Kobe, Japan

Owen J. Tassicker
Electric Power Research Institute, Palo Alto, CA

D. R. Telesca
Enviro Control, Inc., Rockville, MD

Gordon R. Thompson
Syncrude Canada Ltd., Edmonton, Alberta, Canada

Daniel A. Tichenor
Sandia National Laboratories, Freemont, CA

Marsha W. Timmerman
Air Products & Chemicals, Inc., Allentown, PA

John C. Trisler
Louisiana Tech University, Ruston, LA

Thomas H. Tsai
Tenneco, Inc., Houston, TX

Thomas F. Turner
Laramie Energy Technology Center, Laramie, WY

Elzbieta Tyrkiel
Institute of Nuclear Research, Swierk, Poland

Victor S. Underkoffler
Gilbert/Commonwealth, Inc., Reading, PA

Nicholas Vagelatos
IRT Corporation, San Diego, CA

Th. J. van Beek
Shell International, The Hague, The Netherlands

Ernest S. Van Valkenburg
Leeds & Northrup Company, North Wales, PA

Stephen N. Vaughn
Exxon Research and Engineering Co., Baytown, TX

Geary R. Voots
Texas Nuclear Corporation, Austin, TX

John Wallace
Denver Research Institute, Denver, CO

P. Henrik Wallman
Chevron Research Company, Richmond, CA

John V. Walsh
Jet Propulsion Laboratory, Pasadena, CA

J. C. F. Wang
Sandia National Laboratories, Livermore, CA

Teresa L. Webster
Cameron Iron Works, Inc., Houston, TX

Mathew Werner
Washington State University, Pullman, WA

Paul A. Westcott
TRW, Lakewood, CO

Hans R. Wilde
Staatliches Materialprufungsamt, West Germany

Stan J. Wohadlo
Institute of Gas Technology, Chicago, IL

Thomas R. Wood
Bechtel, San Francisco, CA

Carl L. Wright
Sandia National Laboratories, Livermore, CA

Edward L. Wright
Exxon Research & Engineering Co., Florham Park, NJ

Frederick J. Wyant
Westinghouse Electric Corporation, Madison, PA

Frederick J. Wyant
Westinghouse Electric Corporation, Madison, PA

Hsunwei Lawrence Yang
Texaco, Inc., Montebello, CA

Gerald E. Youngblood
MERDI, Butte, MT

Johnny O. Younghanse
Union Carbide Corporation, Oak Ridge, TN

Kamel S. Youssef
U.S. Department of Energy, Washington, D.C.

Huey K. Zang
Texaco, Inc., Beacon, NY

Andrew S. Zarchy
General Electric, Schenectady, NY

L. P. Zestar
Chevron Research Company, Richmond, CA

Ronald E. Zielinski
Monsanto Research Corporation, Miamisburg, OH

August H. Zoll
Curtiss-Wright Corporation, Wood Ridge, NJ

James F. Zumberge
MDH Industries, Inc., Monrovia, CA

F. M. Zweibaum
Barnes Engineering Company, Stamford, CT

Paul S. Zygielbaum
Electric Power Research Institute, Palo Alto, CA

Exhibitors

R. L. Beery
The Bendix Corporation, Lewisburg, WV

Don Bowlin
Cameron Iron Works, Houston, TX

Mr. Flandreau
Perkin-Elmer Corporation, Norwalk, CT

Brad Gehring
Rosemount, Inc., Eden Prairie, MN

Roseann Geyer
The McIlvaine Co., Northbrook, IL

Brooke M. Hinds
Barnes Engineering Company, Stamford, CT

Herb Kaplan
Society for Control & Instrumentation of Energy Processes, Norwalk, CT

Robert Kaufman
Mogas Machine Works, Inc., Houston, TX

P. Kindersley
Kamyr Valves, Inc., Glens Falls, NY

L. L. Landskov
Delavan Electronics, Inc., Scottsdale, AZ

Richard F. Leftwich
Irtronics, Inc., Stamford, CT

Tom McCall
MANCO, Santa Clara, CA

Urie McCleary, Jr.
Perkin-Elmer Corporation, Pomona, CA

Lawrence B. Shovelton
Gentran, Inc., Sunnyvale, CA

R. Sielemann
Carl Zeiss, Inc., New York, NY

David Snyder
Validyne Engineering Corporation, Northridge, CA

John Sozio
Taylor Instruments, Rochester, NY

Seymour Steinberg
ARI Industries, Inc., Franklin Park, IL

Ron Weisen
Land Instruments, Inc., Tullytown, PA

Harold Weiss
Analog Devices, Inc., Huntington Beach, CA

Grant N. Wetzel
Hach Company, Anaheim, CA